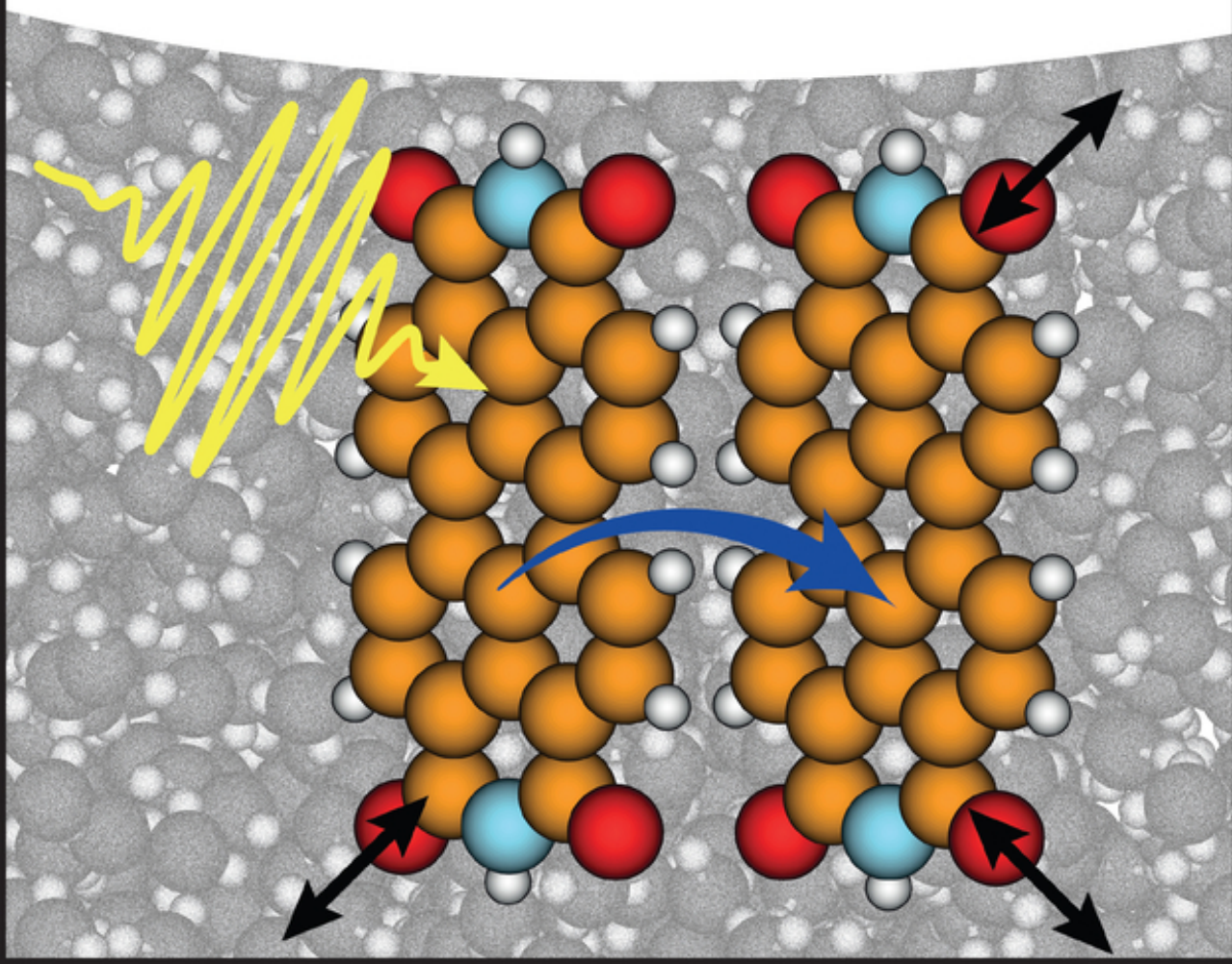Volkhard May and Oliver Kühn

Charge and Energy Transfer Dynamics in Molecular Systems

Fourth Edition

Charge and Energy Transfer Dynamics in Molecular Systems

Charge and Energy Transfer Dynamics in Molecular Systems

Fourth Edition

Volkhard May and Oliver Kühn

WILEY-VCH

Authors

Dr. Volkhard May
Humboldt-Universität zu Berlin
Institut für Physik, Newtonstraße 15
12489 Berlin
Germany

Prof. Dr. Oliver Kühn
Universität Rostock
Institut für Physik
Albert-Einstein-Str. 23-24
18059 Rostock
Germany

Cover Image: Figure courtesy of Oliver
    Kühn

Contents

Preface to the Fourth Edition

The third edition of this book has been published more than 10 years ago. During this time, the field of molecular charge- and energy-transfer processes evolved tremendously. Therefore, we consider it timely to provide an update of our 2011 edition. Among the most important developments in quantum dissipative dynamics has been the further elaboration of nonperturbative and non-Markovian approaches such as the hierarchy equation of motion (HEOM) method. Although already known at the time of the publication of the third edition, the past decade has witnessed not only numerous applications but also a broader development of methods being based on the hierarchy idea. For the common system-reservoir models it provides a feasible numerical exact reference such that HEOM can be considered a game changer. The derivation of the HEOM and applications are covered in this fourth edition. In this context, the discussion of spectral density models has also been considerably enhanced. A second method that has matured to a versatile tool for studying various transfer processes is two-dimensional spectroscopy. In the expanded Chapter 4, we provide an introduction into the formulation of two-dimensional spectroscopy in terms of dipole correlation functions, knowing that a full account of this fascinating method is far beyond the scope of this book. Besides these two mentioned additions, we have included many minor modifications introducing up-to-date material in terms of both methodology and applications. We have also replaced some of the older examples from the literature by more recent ones.

Each chapter contains a section entitled "Further Reading", which should serve as a starting point to explore the original literature. Additionally, at the end of each chapter, the reader will find a brief list of references pointing to the sources of the given examples and to the origins of those fundamental concepts that have been directly integrated into the text. As in previous editions, we emphasize that these lists are by no means exhaustive. It is not the purpose of this book to review all relevant literature on molecular charge and energy transfer dynamics.

Among the recent developments that are not covered in this book, we would like to mention the fields of Attosecond Physics and X-ray Spectroscopy. While femtochemistry successfully explored nuclear dynamics over the past three decades, Attosecond Physics has the focus on the dynamics of electronic degrees of freedom on time scales where the nuclei are essentially frozen. In contrast to, for instance, Marcus theory of electron transfer where the electron motion is intimately

connected to nuclear rearrangement, the driving forces of attosecond electron dynamics are different. They originate, for instance, in electron correlations or spin–orbit coupling. X-ray science has a long tradition, but it is the availability of novel light sources offering, for instance, intense X-ray flashes that enable time-resolved studies of charge and energy transfer. In contrast to optical spectroscopy of valence transitions, core-level excitation by X-ray radiation is element specific, thus providing a complementary local view on electronic structure changes. The recent development in these two areas has already been impressive, but many exciting insights into the dynamics of charge- and energy-transfer processes are yet to come. A number of concepts and methods introduced in this book, such as the correlation function description of transfer rates, can be adopted to serve these fields. However, in particular, phenomena due to the interaction of molecular systems with strong external fields require a different theoretical framework.

Volkhard May and Oliver Kühn
Berlin and Rostock, December 2022

Preface to the Third Edition

The continued interest in our book since its first publication in 2000 and its second edition in 2004 triggered the idea to prepare a third edition in order to account for more recent developments in the field of molecular charge- and energy-transfer research.

Following the concept of the previous editions, we start by providing some general background on gas- and condensed-phase interaction potentials and Hamiltonians, now including a discussion of quantum mechanics/molecular mechanics hybrid methods for the explicit treatment of condensed-phase environments. The methodologically oriented Chapter 3 on the dynamics of quantum systems has been extended in several respects. Most notable is an exposition on the calculation of transfer rates within the Liouville space approach. Here, special emphasis is put on the fourth-order rates that are crucial for an understanding of the more involved electron- and excitation energy-transfer processes. Further, we give an account on the multiconfiguration time-dependent Hartree method that in recent years has been proven to be a versatile tool for the numerically exact treatment of the quantum dynamics of thousands of degrees of freedom.

The introduction to basic theoretical concepts has been expanded by a new Chapter 4 devoted to some general aspects of the interaction between light and molecular systems. This comprises a derivation of the interaction Hamiltonian in dipole approximation, an introduction to field quantization for the description of emissions, and an outline of the basics of linear and nonlinear spectroscopy. In the second edition, laser control was covered in a separate chapter. For the present edition, we have incorporated a discussion of the topic into the text, which reflects the development of laser control into an almost routine tool for the investigation of molecular dynamics phenomena. The theoretical foundations and, in particular, optimal control theory are now part of Chapter 4, while the various applications are covered in Chapters 7–9.

The applications start with Chapter 5, where the discussion of vibrational dynamics has been expanded to include quantum-classical approaches to the calculation of pure dephasing-induced line broadening. Chapter 6, focusing on intramolecular electronic transitions, now contains a section on pump–probe spectroscopy and its role in interrogating molecular dynamics in the condensed phase. Major changes in Chapter 7 on electron transfer include the incorporation of heterogeneous electron

transfer at surfaces as well as of single-molecule electron transfer in the context of molecular electronics. The quantum dynamics treatment of proton-transfer reactions has flourished recently due to the development of time-dependent multiconfiguration approaches, as mentioned above; an example is discussed in Chapter 8. Finally, Chapter 9, on excitation energy (Frenkel exciton) transfer, has been substantially rewritten. Topics that have been added include Dexter transfer and two-electron-assisted as well as photon-mediated exciton transfer.

The "Suggested Reading" section of the previous editions, which served to give a systematic starting point to explore the original literature, has been merged into the main text to become a list of "Further Reading" suggestions at the end of each chapter. As before, we would like to emphasize that these lists are by no means exhaustive; that is, it is not the purpose of this book to review all the relevant literature on the title subject.

While working on the manuscript of this third edition, we enjoyed the inspiring atmosphere of the Berlin Collaborative Research Center (Sfb450) "Analysis and Control of Ultrafast Photoinduced Reactions" and the Rostock Sfb652 "Strong Correlations and Collective Effects in Radiation Fields."

Finally, we wish to thank E. Petrov (Bogolyubov Institute for Theoretical Physics, Kiev) and L. Wang (University of Science and Technology, Beijing) for reading parts of the new manuscript and K. Mishima (University of Tokyo) for drawing our attention to corrections required for the second edition.

Volkhard May and Oliver Kühn
Berlin and Rostock, October 2010

Preface to the Second Edition

The positive response to the First Edition of this text has encouraged us to prepare the present Revised and Enlarged Second Edition. All chapters have been expanded to include new examples and figures and also to cover more recent developments in the field. The reader of the First Edition will notice that many of the topics that were addressed in its "Concluding Remarks" section have now been integrated into the different chapters.

The introduction to dissipative quantum dynamics in Chapter 3 now gives a broader view on the subject. Particularly, we elaborated on the discussion of hybrid quantum-classical techniques that promise to be able to incorporate microscopic information about the interaction of some quantum system with a classical bath beyond the weak coupling limit. In Chapter 4, we give a brief account on the state-space approach to intramolecular vibrational energy and the models for treating the intermediate time scale dynamics, where the decay of the survival probability is nonexponential. Chapter 5 now compares different methodologies to compute the linear absorption spectrum of a molecule in a condensed-phase environment. Furthermore, the basic aspects of nonlinear optical spectroscopy have been included to characterize a primary tool for the experimental investigation of molecular transfer processes. Bridge-mediated electron transfer is now described in detail in Chapter 6 also including a number of new examples. Chapter 7 on proton transfer has been supplemented by a discussion of the tunneling splitting and its modification due to the strong coupling between the proton-transfer coordinate and other intramolecular vibrational modes. Chapter 8 dealing with exciton dynamics has been considerably rearranged and includes now a discussion of two-exciton states.

Finally, we have added a new Chapter 9, which introduces some of the fundamental concepts of laser field control of transfer processes. This is a rapidly developing field which is stimulated mostly by the possibility to generate ultrafast laser pulse of almost any shape and spectral content. Although there are only few studies on molecular transfer processes so far, this research field has an enormous potential not only for a more detailed investigation of the dynamics but also with respect to applications, for instance, in molecular-based electronics.

Following the lines of the First Edition, we avoided to make extensive use of abbreviations. Nevertheless, the following abbreviations are occasionally used: DOF (degrees of freedom), ET (electron transfer), IVR (intramolecular vibrational

redistribution), PES (potential energy surface), PT (proton transfer), QME (quantum master equation), RDM (reduced density matrix), RDO (reduced density operator), VER (vibrational energy relaxation), and XT (exciton transfer).

We have also expanded the "Suggested Reading" section which should give a systematic starting point to explore the original literature and also to become familiar with alternative views on the topics. Additionally, at the end of each chapter, the reader will find a brief list of references. Here, we included the information about the sources of the given examples and refer to the origin of those fundamental concepts and theoretical approaches that have been directly integrated into the text. We would like to emphasize, however, that these lists are by no means exhaustive. In fact, given the broad scope of this text, a complete list of references would have expanded the book's volume enormously, without necessarily serving its envisaged purpose.

<div align="right">

Volkhard May and Oliver Kühn
Berlin, September 2003

</div>

Preface to the First Edition

The investigation of the stationary and dynamical properties of molecular systems has a long history extending over the whole century. Considering the past decade only, one observes two tendencies: First, it became possible to study molecules on their natural scales, that is, with a spatial resolution of some Ångström (10^{-10} m) and on a time scale down to some femtoseconds (10^{-15} s). And second, one is able to detect and manipulate the properties of single molecules. This progress comes along with a steadily growing number of theoretical and experimental efforts crossing the traditional borderlines between chemistry, biology, and physics. In particular, the study of molecular transfer processes involving the motion of electrons, protons, small molecules, and intramolecular excitation energy resulted in a deeper understanding of such diverse phenomena as the photoinduced dynamics in large molecules showing vibrational energy redistribution or conformational changes, the catalysis at surfaces, and the microscopic mechanisms of charge and energy transfer in biological systems. The latter are of considerable importance for unraveling the functionality of proteins and all related processes such as the primary steps of photosynthesis, the enzymatic activity, and the details of the repair mechanisms in DNA strands, to mention just a few examples. In a more general context, molecular electronics, that is, the storage and processing of information in molecular structures on a nanometer length scale, has also triggered enormous efforts. Finally, with the increasing sophistication of laser sources, first steps toward the control of chemical reaction dynamics have been taken.

The ever-growing precision of the experiments requires on the theoretical side to have microscopic models for simulating the measured data. For example, the interpretation of optical spectroscopies in a time region of some tenths of femtoseconds demands for an appropriate simulation of the molecular dynamics for the considered system. Or, understanding the characteristics of the current flowing through a single molecule in the context of scanning tunneling microscopy needs detailed knowledge of the electronic level structure of the molecule as well as the role of its vibrational degrees of freedom. These few examples already demonstrate that advanced theoretical concepts and numerical simulation techniques are required, which are the combination of methods known from general quantum mechanics, quantum chemistry, molecular reaction dynamics, solid-state theory, nonlinear optics, and nonequilibrium statistical physics.

Such a broad approach is usually beyond the theoretical education of chemists and biologists. On the other hand, quantum chemistry and chemical reaction dynamics are quite often not on the curriculum of physics students. We believe that this discrepancy quite naturally does not facilitate communication between scientists having different backgrounds. Therefore, it is one of the main intentions of the present book to provide a common language for bridging this gap.

The book starts with an introduction and general overview of different concepts in Chapter 1. The essentials of theoretical chemical physics are then covered in Chapter 2. For chemistry students this will be mostly a repetition of quantum chemistry and in particular the theory of electronic and vibrational spectra. It is by no means a complete introduction into this subject but intended to provide some background mainly for physics students. The prerequisites from theoretical physics for the description of dynamical phenomena in molecular systems are presented in Chapter 3. Here, we give a detailed discussion of some general aspects of the dynamics in open and closed quantum systems, focusing on transfer processes in the condensed phase.

The combination of qualitative arguments, simple rate equations, and the powerful formalism of the reduced statistical operator constitutes the backbone of the second part of the book. We start in Chapter 4 with a discussion of intramolecular transfer of vibrational energy that takes place in a given adiabatic electronic state. Here, we cover the limits of isolated large polyatomic molecules, small molecules in a matrix environment, up to polyatomics in solution. In Chapter 5, we then turn to processes that involve a transition between different electronic states. Special emphasis is put on the discussion of optical absorption, which is considered to be a reference example for more involved electron-vibrational transfer phenomena such as internal conversion, which is also presented in this chapter. Chapter 6 then outlines the theoretical frame of electron-transfer reactions, focusing mainly on intramolecular processes. Here, we develop the well-known Marcus theory of electron transfer, describe nuclear tunneling and superexchange electron transfer, and discuss the influence of polar solvents. In Chapter 7, it will be shown that, even though proton transfer has many unique aspects, it can be described by adapting various concepts from electron-transfer theory. The intermolecular excitation energy transfer in molecular aggregates is considered in Chapter 8. In particular, the motion of Frenkel excitons coupled to vibrational modes of the aggregate will be discussed. In the limit of ordinary rate equations, this leads us to the well-known Förster expression for the transfer rate in terms of emission and absorption characteristics of the donor and acceptor molecules, respectively.

By presenting a variety of theoretical models that exist for different types of transfer processes on a common formal background, we hope that the underlying fundamental concepts are becoming visible. This insight may prepare the reader to take up one of the many challenging problems provided by this fascinating field of research. Some personal reflections on the current and possible future developments are given in Chapter 9.

The idea for writing this book emerged from lectures given by the authors at the Humboldt University Berlin, the Free University Berlin, and at the Johannes

Gutenberg University Mainz during the past decade. These courses have been addressed to theoretically and experimentally oriented undergraduate and graduate students of Molecular Physics, Theoretical Chemistry, Physical Chemistry, and Biophysics, being interested in the fast developing field of transfer phenomena. The book is self-contained and includes detailed derivations of the most important results. However, the reader is expected to be familiar with basic quantum mechanics. Most of the chapters contain a supplementary part where more involved derivations as well as special topics are presented. At the end of the main text, we also give some comments on selected literature, which should complement the study of this book.

Of course, this book would not have been possible without the help, the critical comments, and the fruitful discussions with many students and colleagues. In this respect, it is a pleasure for us to thank I. Barvik, N. P. Ernsting, W. Gans, L. González, O. Linden, H. Naundorf, J. Manz, S. Mukamel, A. E. Orel, T. Pullerits, R. Scheller, and D. Schirrmeister. We are also grateful for continuous financial support that has been provided by the Deutsche Forschungsgemeinschaft, in particular through the Sonderforschungsbereich 450 "Analysis and Control of Ultrafast Photoinduced Reactions."

Volkhard May and Oliver Kühn
Berlin, September 1999

1

Introduction

The understanding of transfer phenomena in *molecular systems* calls for a unified theoretical treatment that should have its foundation in a microscopic definition of the constituent parts and their interactions. There are three important questions that need to be answered in this regard. *First*, what is the appropriate theoretical description of the molecular system? *Second*, what is the form of the dynamical equations that describe the transfer process? And *third*, how can the computed results be related to experimental observations?

In what follows the term "molecular system" will cover single molecules and simple molecular aggregates as well as larger arrangements of molecules such as supramolecular complexes. In particular, molecules embedded in different types of environments will be of interest. Here, the scope ranges from molecules in solution to biological macromolecules such as membrane-bound protein complexes. The common link between these molecular systems is that they show *transfer processes*. By "transfer process," we understand the flow of vibrational energy and the dynamics of electrons, protons, and electronic excitation energy.

From a general point of view, quantum mechanics gives the framework for all phenomena occurring in molecular systems. Given the broad scope of transfer processes to be discussed, it is clear that an exact quantum mechanical treatment is impossible if we go beyond the level of simple model systems. Therefore, it is a particular challenge for theory to develop versatile models that provide answers to the initially raised three questions.

Chapter 2 addresses the first question discussing the steps that lead us from the formally exact to some approximate molecular Hamilton operator. Given a molecule in gas phase (vacuum) as shown in Figure 1.1a, the *Born–Oppenheimer separation* of nuclear and electronic motions can be performed. Here, the molecular wave function is split up into an electronic and a nuclear part, a procedure that is justified by the large mass difference between both types of particles. This results in a Schrödinger equation for the electronic wave function alone, for given fixed positions of the nuclei. Calculating the electronic energy spectrum for different positions of the nuclei, one obtains *potential energy surfaces* that govern the motion of the nuclei. These potential energy surfaces are at the heart of our understanding of stationary molecular spectra and molecular dynamics. If nuclear and electronic

Molecule in gas phase

Molecule in environment

Potential energy curve
for nuclear motion

Energy

Bond distance

(a)

(b)
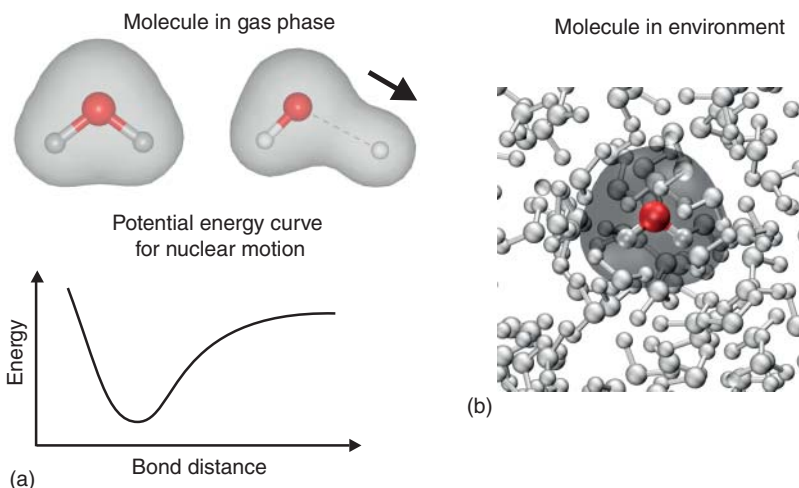
Figure 1.1 The problem of the interaction between electrons and nuclei is transformed to some tractable level by employing the Born–Oppenheimer separation of their motions. (a) Three-atomic molecule (H_2O) with the electron density shown for the equilibrium distance (left) as well as for a stretched bond (right). The electron density adjusts instantaneously to the configuration of the nuclei. As a result, a potential energy curve is formed determining the dynamics of the bond distance coordinate. (b) If the molecule is taken from the gas into the condensed phase, its stationary and dynamic properties have to take into account the interaction with the surrounding molecules. This may give rise, for instance, to a change in equilibrium geometry and electron density (figure courtesy of Ashour Ahmed).

motion are adiabatically separable, that is if the coupling between different electronic states is negligible, one can carry out the Born–Oppenheimer approximation. Under certain conditions, however, the so-called nonadiabatic transitions between different electronic states as a consequence of the nuclear motions take place.

If we move from the gas to the condensed phase as shown in Figure 1.1b, the effect of the molecule–environment interaction has to be taken into account. The simplest way to do this is to add an additional external potential to the molecular Hamiltonian. Often, the environment can be described as a macroscopic dielectric, and its influence can be judged from its dielectric properties.

Having discussed the stationary molecular properties, we turn in Chapter 3 to the second question related to *molecular dynamics*. Here, the reader will become familiar with the concepts ranging from incoherent to coherent transfer events. The connection between these limits is provided by the relevant time scales; of particular importance is the relation between intramolecular relaxation and intermolecular transfer times. In view of experimental advances in ultrafast spectroscopy, our treatment reflects the historical evolution of knowledge about molecular dynamics from simple transfer rates to quantum mechanical wave packet dynamics.

An important ingredient for the theoretical modeling is the concept of an *open molecular system S* interacting with its *environment* (reservoir) *R* by collision processes or via other means of energy exchange. A schematic illustration of this
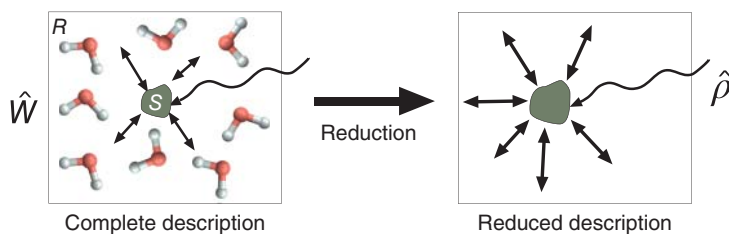
Figure 1.2 The total system consisting of a relevant system (*S*) interacting with a reservoir (*R*) is completely described by the quantum-statistical operator $\hat{W}$. By means of a reduction procedure, one can focus on the relevant system using the reduced statistical operator $\hat{\rho}$. Effects of the *S*–*R* interaction are still accounted for. In addition, the system may be influenced by external fields (wiggly line).

situation is given in Figure 1.2. The *relevant* system *S* may represent any type of molecule, but it may also comprise selected so-called active degrees of freedom of a particular molecule.

The most general description of the total system, *S* plus *R*, is given by the quantum-statistical operator $\hat{W}$, as indicated in the left-hand part of Figure 1.2. This operator is based on the concept of a *mixed* quantum state formed by *S* and its macroscopic environment. However, the operator $\hat{W}$ contains much more information than will ever be needed, for instance, to simulate a particular experiment. Indeed, it is the relevant system *S* whose properties we are interested in. Making use of a reduction procedure, we obtain a *reduced statistical operator* $\hat{\rho}$ that contains the information on the dynamics of *S* only but including the influence of the environment *R* (right-hand part of Figure 1.2). When deriving equations of motion for the reduced statistical operator, the so-called quantum master equations, a number of approximations have to be invoked. Most fundamental in this respect will be the assumption of a weak interaction between the system *S* and the reservoir *R*, which in practice requires a proper separation into relevant and environmental coordinates for the molecular system at hand. Under certain conditions, however, a numerical exact description of the dynamics of the relevant system becomes possible. If there is no interaction at all, the quantum master equation is equivalent to the time-dependent Schrödinger equation. This is the regime of *coherent* dynamics. If the interaction is not negligible, however, the system dynamics gradually changes with increasing coupling strength from a *partially coherent* one to an *incoherent* one. The incoherent motion of a quantum system is commonly described using ordinary rate equations that are based on the *Golden Rule* rate expression of quantum mechanics.

The concept of the statistical operator provides a *quantum-statistical* description of *S* and *R*. However, in many situations it is sufficient to describe *R* by means of classical mechanics. Then, *S* can be characterized by a wave function Ψ, and the dynamics of the environmental degrees of freedom is governed by Newton's equations. Often, the dynamics is split up in such a way that the classical particles move in the mean field of the quantum particle. This situation is visualized in Figure 1.3.

The overwhelming amount of data on transfer processes in molecular systems is obtained by spectroscopic techniques working in the infrared, the visible to
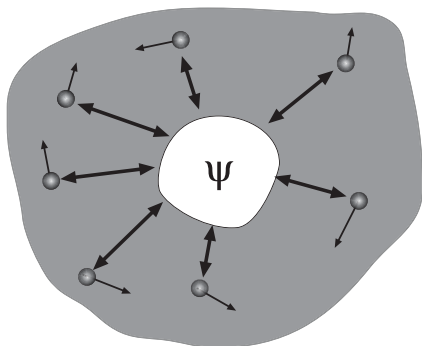
Figure 1.3 Mixed quantum–classical description of condensed phase dynamics. The classical particles move in the mean field generated by the quantum particle described by the wave function Ψ.

ultraviolet, and, more recently, also in the X-ray region. We will discuss the third question related to experimental observation mostly in the context of spectroscopy, with focus on the infrared to ultraviolet domain. As a means of preparation, Chapter 4 gives a brief account on the general theoretical concepts of the interaction of molecular systems with the electromagnetic radiation field. Further, a formulation of linear and nonlinear spectroscopy in terms of correlation functions will be introduced.

The general concepts presented in Chapters 2–4 are then applied to describe different transfer phenomena. In principle, transfer processes can be classified according to the type of transferred particle. In addition, one can distinguish between intra- and intermolecular particle transfer. The common frame is provided by the molecular Schrödinger equation together with the Born–Oppenheimer separation of electronic and nuclear motions as mentioned above.

The coupled nuclear dynamics in polyatomic molecules that might be immersed in some condensed phase environment is treated in Chapter 5. We show how an initially prepared vibrational state decays while its excitation energy is distributed over all possible environmental modes, as illustrated in the left-hand part of Figure 1.4. For small polyatomic molecules, the energy flow out of the initial state is called *intramolecular vibrational energy redistribution*. For condensed phase situations, the dissipation of energy into the environment is called *vibrational energy relaxation*. In both cases, the transferred objects are the quanta of vibrational energy.

The preparation of the initial state can be due to an optical transition between two electronic states as a consequence of the interaction between the molecular system and an external electromagnetic field (cf. Figure 1.4). In Chapter 6, we discuss the processes of photon absorption and emission sketched in Figure 1.4. It will be shown that the coupled electron-vibrational dynamics responsible for the absorption line shape can be described by a combined density of states that is the Fourier transform of some correlation function. This theoretical result will turn out to be quite general. In particular, we show that different types of transfer processes can be accommodated in such a framework. For example, the *internal conversion* dynamics of nonadiabatically coupled electronic states (right-hand part of Figure 1.4) can, in the incoherent limit, be described by a combined density of states.

The external field interaction, on the other hand, provides the means for preparing nonequilibrium initial states that can act as a donor in a photoinduced
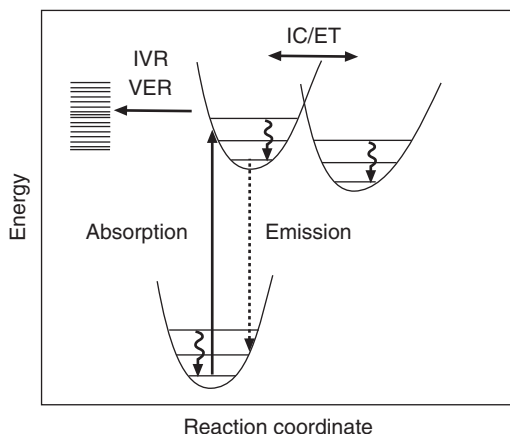
Figure 1.4 Scheme of molecular potential energy surfaces including the levels of the quantized motion of some reaction coordinate. After optical preparation of an electronically and vibrationally excited initial state (absorption), different transfer processes can occur. If the electronic state is not changed, but there is a coupling to some manifold of vibrational states, intramolecular vibrational energy redistribution (IVR) or vibrational energy relaxation (VER) can be observed. If there is some coupling to another electronic state, intramolecular internal conversion (IC), or electron transfer (ET) takes place. At the same time, one has VER as indicated by the wiggly lines. In addition, the system may return to the ground state by emitting a photon.

electron-transfer reaction, which is discussed in Chapter 7. The concerted electron-vibrational dynamics accompanying electron-transfer reactions can often be modeled in the so-called curve-crossing picture of two coupled potential energy surfaces representing two electronic states along a *reaction coordinate* (right-hand part of Figure 1.4). Generalizations of this picture to larger molecular systems and to the case where the molecule is in contact with metal electrodes and a voltage is applied will also be discussed.

In contrast, the proton or hydrogen atom transfer investigated in Chapter 8 usually does not involve electronic transitions. In Figure 1.5, we have sketched a typical situation for intramolecular proton transfer that is realized as an isomerization reaction in the adiabatic electronic ground state. Since the proton has a rather small mass, tunneling processes may play an important role for proton transfer. The small mass ratio between the proton and the other heavy atoms provides the background for

Figure 1.5 Hydrogen bonding, which governs the proton transfer (PT) dynamics, often leads to a double minimum potential along a reaction coordinate. The interaction between the proton and some environment may cause vibrational relaxation (wiggly lines).
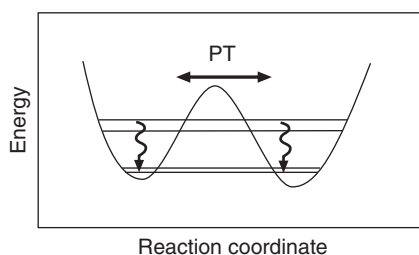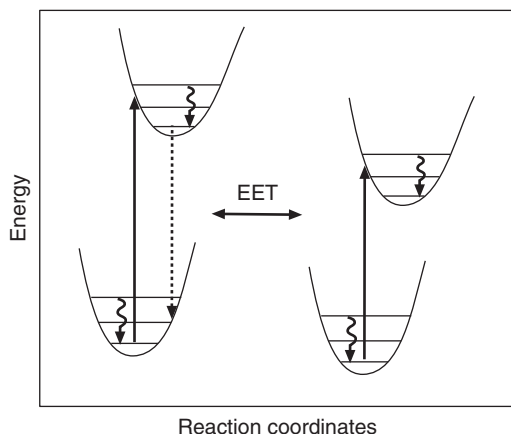
Figure 1.6 Excitation energy transfer (EET), which occurs after optical preparation of an electronically and vibrationally excited initial state (donor, left). The Coulomb interaction is responsible for deexcitation of the donor and excitation of the acceptor (right). The nuclear dynamics may be subject to relaxation processes (wiggly lines). Often, two independent nuclear (reaction) coordinates are used for the donor and the acceptor molecules.

the introduction of a second Born–Oppenheimer separation. This will enable us to adapt most of the concepts of electron-transfer theory to the case of proton transfer.

In Chapter 9, we discuss excitation energy transfer or the so-called exciton transfer in molecular aggregates as another example of coupled electron-vibrational motion. In Figure 1.6, the mechanism of excitation energy transfer in the limit of localized excitations is shown. The donor (left) is initially excited, for example, by an external field. As a consequence of the Coulomb interaction, excitation energy is transferred between the excited molecule and some acceptor molecule (right). Often, donors and acceptors retain their chemical identity upon aggregation and, therefore, are usually described by different sets of nuclear (reaction) coordinates. In the incoherent limit, the rate of the process can be expressed in terms of an overlap integral between donor emission and acceptor absorption spectra. If the Coulomb interaction between different molecules becomes large enough, then excitation energy transfer has to be discussed by introducing quantum mechanical superposition states of all excited molecules, the so-called Frenkel excitons. Their introduction gives a new view on excitation energy transfer via the motion of spatially delocalized states. A rigorous nonequilibrium quantum-statistical model can describe both the incoherent and the coherent limits.

2

Electronic and Vibrational Molecular States

This chapter provides the background material for the subsequent development of a microscopic description of charge- and energy-transfer processes in molecular systems. After introducing the molecular Hamilton operator, we discuss the Born–Oppenheimer separation of electronic and nuclear motions as the key to the solution of the molecular Schrödinger equation. Next, the Hartree–Fock method, which is a simple yet very successful approach to the solution of the ground state electronic structure problem, is explained. It enables us to obtain, for instance the potential energy surface for nuclear motions. To prepare for the treatment of condensed-phase situations, we further introduce the dielectric continuum model as a means for incorporating static solvent polarization effects into the electronic structure calculations.

The topology of the potential energy surface can be explored by calculating the first and second derivatives with respect to the nuclear coordinates. Of particular interest are the stationary points on a potential energy surface that may correspond to stable conformations of the molecule. In the vicinity of a local minimum it is often possible to analyze nuclear motions in terms of small amplitude normal mode vibrations. If one wants to model chemical reaction dynamics, however, the shape of the potential energy surface away from the stationary points is required as an input. We present two different approaches in this respect: the minimum energy reaction path and the Cartesian reaction surface model. Particularly, the latter will provide the microscopic justification for the generic Hamiltonians used later on to simulate molecular systems embedded in some environment. Finally, we discuss the diabatic and the adiabatic representations of the molecular Hamiltonian.

2.1 Introduction

The development of quantum theory in the 1920s was to a considerable extent triggered by the desire to understand the properties of atoms and molecules. It was soon appreciated that the Schrödinger equation together with the probabilistic

interpretation of its solutions provides a powerful tool for tackling a variety of questions in physics and chemistry. The mathematical description of the hydrogen atom's spectral lines could be given and developed to a textbook example of the success of quantum mechanics. Stepping into the molecular realm, one faces a complicated many-body problem involving the interactions of all electrons and all nuclei of the considered molecule. Its solution can be approached using the fact that nuclei and electrons have quite different masses, allowing their motion to be adiabatically separated. This concept was first introduced by Born and Oppenheimer in 1927. Within the Born–Oppenheimer adiabatic approximation, the simplest molecule, the hydrogen molecule ion, H_2^+, can be treated.

From the electronic point of view, the appearance of one more electron, for instance in H_2, necessitates the incorporation of the repulsive electronic interaction. Moreover, since one deals with two identical electrons, care has to be taken that the wave function has the proper symmetry with respect to an exchange of any two particle labels. In a straightforward way this is accomplished by the *self-consistent field method* according to Hartree, Fock, and Slater. Despite its deficiencies Hartree–Fock theory has played an enormous role in the process of exploring the electronic structure of molecules. It still serves as the basis for many of the more advanced approaches used nowadays. In terms of practical applications to large systems, Density Functional Theory has emerged as the method of choice during the past decades.

However, it is not only the electronic structure at the equilibrium configuration of the nuclei that is of interest, the form of the potential energy hypersurfaces obtained upon varying the positions of the nuclei also proves crucial for the understanding of the vibrational and rotational structures of molecular spectra. Moreover, it provides the key to chemical reaction dynamics. While the adiabatic Born–Oppenheimer ansatz is an excellent approximation in the vicinity of the ground state equilibrium configuration, nonadiabatic couplings leading to transitions between electronic states become an ubiquitous phenomenon if the nuclei are exploring their potential surface in processes such as photodissociation and electron-transfer reactions, for example.

This chapter introduces the concepts behind the keywords given so far and sets up the stage for the following chapters. Having this intention it is obvious that we present a rather selective discussion of a broad field. We first introduce the molecular Hamiltonian and the respective solutions of the stationary Schrödinger equation in Section 2.2. This leads us directly to the Born–Oppenheimer separation of electronic and nuclear motions in Section 2.3. A brief account of electronic structure theory for polyatomic molecules is given next (Section 2.4). This is followed by a short summary of the dielectric continuum model in Section 2.7.1, which allows for incorporation of solvent effects into electronic structure calculations. On this basis we continue in Section 2.5 to discuss the potential energy surfaces (PESs) and the related concepts of harmonic vibrations and reaction paths. In Section 2.6 we focus attention to the problem of nonadiabatic couplings, which are neglected in the Born–Oppenheimer adiabatic approximation. Finally, the issue of diabatic versus adiabatic pictures that

emerges from this discussion is explained, and alternative representations of the molecular Hamiltonian are given.

2.2 Molecular Schrödinger Equation

In what follows we will be interested in situations where atoms made of interacting point-like nuclei and electrons are forming of stable molecules. Let us consider such a molecule composed of N_{nuc} atoms having atomic numbers $z_1, \ldots, z_{N_{\text{nuc}}}$. The Cartesian coordinates and conjugate momenta for the N_{el} electrons are denoted $\boldsymbol{r}_j$ and $\boldsymbol{p}_j$, respectively. For the N_{nuc} nuclei, we use $\boldsymbol{R}_n$ and $\boldsymbol{P}_n$. The Hamiltonian operator of the molecule has the general form

$$H_{\text{mol}} = T_{\text{el}} + V_{\text{el–nuc}} + V_{\text{el–el}} + T_{\text{nuc}} + V_{\text{nuc–nuc}}. \tag{2.1}$$

Here, the kinetic energy of the electrons is given by (m_{el} is the electron mass)

$$T_{\text{el}} = \sum_{j=1}^{N_{\text{el}}} \frac{\boldsymbol{p}_j^2}{2m_{\text{el}}}, \tag{2.2}$$

and for the nuclei, it is

$$T_{\text{nuc}} = \sum_{n=1}^{N_{\text{nuc}}} \frac{\boldsymbol{P}_n^2}{2M_n}, \tag{2.3}$$

with M_n being the mass of the nth nucleus.[1] Since both kinds of particles are charged, they interact via Coulomb forces. The repulsive Coulomb pair interaction between electrons is

$$V_{\text{el–el}} = \frac{1}{2} \sum_{i \neq j} \frac{e^2}{|\boldsymbol{r}_i - \boldsymbol{r}_j|}, \tag{2.4}$$

and for the nuclei, we have

$$V_{\text{nuc–nuc}} = \frac{1}{2} \sum_{m \neq n} \frac{z_m z_n e^2}{|\boldsymbol{R}_m - \boldsymbol{R}_n|}. \tag{2.5}$$

(Note that the factor $1/2$ compensates for double counting.) The attractive interaction between electrons and nuclei is given by

$$V_{\text{el–nuc}} = -\sum_{j,n} \frac{z_n e^2}{|\boldsymbol{r}_j - \boldsymbol{R}_n|}. \tag{2.6}$$

Since there are N_{el} electrons and N_{nuc} nuclei, the molecule has $3(N_{\text{el}} + N_{\text{nuc}})$ spatial degrees of freedoms (DOFs). Each electron is assigned an additional quantum number σ_j to account for its spin. The purely quantum mechanical (QM) concept of electron spin was introduced to explain the fine structure of certain atomic spectra

---

1) In the following discussion, we will skip the summation bounds unless it is required by the specific context.

by Uhlenbeck and Goudsmit in 1925. Later, its theoretical foundation was laid in the relativistic extension of quantum mechanics developed by Dirac in 1928. When using the nonrelativistic Hamiltonian equation (2.1) we have no means to rigorously introduce spin operators and to derive the interaction potential between coordinate and spin variables (spin–orbit coupling). Therefore, the existence of spin operators is usually postulated, and their action on spin functions defined. We will not consider relativistic effects in this text and therefore carry the spin variable along with the electron coordinate only in the formal considerations of Section 2.4.

All QM information about the stationary properties of the molecular system defined so far is contained in the solutions of the time-independent nonrelativistic Schrödinger equation,

$$H_{\text{mol}} \Psi(r, \sigma; R) = \mathcal{E} \Psi(r, \sigma; R). \tag{2.7}$$

Here and in the following equations we will combine the set of electronic Cartesian coordinates in the multi-index $r = (\boldsymbol{r}_1, \boldsymbol{r}_2, \dots, \boldsymbol{r}_{N_{\text{el}}})$. A similar notation is introduced for the nuclear Cartesian coordinates, $R = (\boldsymbol{R}_1, \boldsymbol{R}_2, \dots, \boldsymbol{R}_{N_{\text{nuc}}})$. In addition, we will frequently use the more convenient notation $(\boldsymbol{R}_1, \boldsymbol{R}_2, \dots, \boldsymbol{R}_{N_{\text{nuc}}}) \to (R_1, \dots, R_{3N_{\text{nuc}}}) = R$. Momenta and masses of the nuclei will be written in the same way. (In this notation, $M_1 = M_2 = M_3$ is the mass of nucleus number 1, etc.) For the spin we use the notation $\sigma = (\sigma_1, \sigma_2, \dots, \sigma_{N_{\text{el}}})$.

As it stands, Eq. (2.7) does not tell much about what we are aiming at, namely electronic excitation spectra and equilibrium geometries. However, some general points can be made immediately: first, the solution of Eq. (2.7) will provide us with an energy spectrum $\mathcal{E}_\lambda$ and the corresponding eigenfunctions, $\Psi_\lambda(r, \sigma; R)$. The energetically lowest state $\mathcal{E}_0$ is called the ground state. If $\mathcal{E}_\lambda$ is negative, the molecule is in a stable bound state. Note that in what follows we will also make use of the more formal notation where the eigenstates of the molecular Hamiltonian are denoted by the state vector $|\Psi_\lambda\rangle$. The wave function is obtained by switching to the $(r, \sigma; R)$ representation: $\Psi_\lambda(r, \sigma; R) = \langle r, \sigma; R | \Psi_\lambda \rangle$.

Second, owing to the *Pauli principle*, which states that the wave function of a system of electrons has to be antisymmetric with respect to the interchange of any two electronic indices, $\Psi(r, \sigma; R)$ will be antisymmetric in electronic Cartesian plus spin coordinates. The fact that there can be identical nuclei as well is frequently neglected when setting up the exchange symmetry of the total wave function. This is justified since the nuclear wave function is usually much more localized as compared with the electronic wave function, and the indistinguishability is not an issue. Exceptions may occur in systems containing, for example several hydrogen atoms.

Third, the probability density distribution, $|\Psi_\lambda(r, \sigma; R)|^2$, contains the information on the distribution of electrons as well as on the arrangement of the nuclei. Having this quantity at hand, one can calculate, for example the charge density distribution $\rho_\lambda(\boldsymbol{x})$ for a particular molecular state at some spatial point $\boldsymbol{x}$. The expression due to classical physics,

$$\rho(\boldsymbol{x}) = -e \sum_j \delta(\boldsymbol{x} - \boldsymbol{r}_j) + e \sum_n z_n \delta(\boldsymbol{x} - \boldsymbol{R}_n), \tag{2.8}$$

is quantized by replacing the coordinates by the respective operators. Taking the matrix elements of the resulting charge density operator with respect to the state $\Psi_\lambda(r, \sigma; R)$, we get

$$\rho_\lambda(\boldsymbol{x}) = -e \sum_j \sum_\sigma \int dr\, dR\, \delta(\boldsymbol{r}_j - \boldsymbol{x}) |\Psi_\lambda(r, \sigma; R)|^2$$
$$+ \sum_n e z_n \sum_\sigma \int dr\, dR\, \delta(\boldsymbol{R}_n - \boldsymbol{x}) |\Psi_\lambda(r, \sigma; R)|^2. \tag{2.9}$$

Finally, since the Hamiltonian does not depend on spin, the solution of Eq. (2.7) can be separated according to

$$\Psi(r, \sigma; R) = \psi(r; R)\, \zeta(\sigma). \tag{2.10}$$

Here, $\zeta(\sigma)$ is the electronic spin function, which is obtained by projecting the molecule's spin state vector $|\zeta\rangle$ onto the spin states of the individual electrons, $\zeta(\sigma) = (\langle\sigma_1| \langle\sigma_2| \dots \langle\sigma_{N_{el}}|) |\zeta\rangle$. The individual spin states, $|\sigma_i\rangle$, describe electrons whose spin is parallel (spin up) or antiparallel (spin down) with respect to some spatial direction.

2.3 Born–Oppenheimer Separation

The practical solution of Eq. (2.7) makes use of the fact that due to the large mass difference ($m_{el}/M_n < 10^{-3}$), on average electrons can be expected to move much faster than nuclei. Therefore, in many situations the electronic DOFs can be considered to respond instantaneously to any changes in the nuclear configuration, that is their wave function corresponds always to a stationary state. This is called adiabatic regime in which the motion of the nuclei does not cause transitions between different stationary electronic states. Thus, it is reasonable to define an electronic Hamiltonian that carries a parametric dependence on the nuclear coordinates:

$$H_{el}(R) = T_{el} + V_{el-nuc} + V_{el-el}. \tag{2.11}$$

As a consequence, the solutions of the time-independent electronic Schrödinger equation describing the state of the electrons in the electrostatic field of the fixed nuclei (leaving aside the electron's spin),

$$H_{el}(R)\, \phi_a(r; R) = E_a(R)\, \phi_a(r; R), \tag{2.12}$$

will parametrically depend on the set of nuclear coordinates as well. Here, the index a labels the different electronic states. The *adiabatic* electronic wave functions $\phi_a(r; R) = \langle r; R |\phi_a\rangle$ define a complete basis in the electronic Hilbert space. Hence, given the solutions to Eq. (2.12), the spatial part of the molecular wave function can be expanded in this basis set as follows:

$$\psi(r; R) = \sum_a \chi_a(R)\, \phi_a(r; R). \tag{2.13}$$

The expansion coefficients in Eq. (2.13), $\chi_a(R)$, depend on the configuration of the nuclei. It is possible to derive an equation for their determination after inserting Eq. (2.13) into Eq. (2.7). One obtains

$$
\begin{aligned}
H_{\mathrm{mol}}\psi(r;R) &= (H_{\mathrm{el}}(R) + T_{\mathrm{nuc}} + V_{\mathrm{nuc-nuc}})\sum_a \chi_a(R)\,\phi_a(r;R) \\
&= \sum_a [E_a(R) + V_{\mathrm{nuc-nuc}}]\,\chi_a(R)\,\phi_a(r;R) \\
&\quad + \sum_a T_{\mathrm{nuc}}\chi_a(R)\,\phi_a(r;R) \\
&= \mathcal{E}\sum_a \chi_a(R)\,\phi_a(r;R).
\end{aligned}
\tag{2.14}
$$

Multiplication of Eq. (2.14) by $\phi_b^*(r;R)$ from the left and integration over all electronic coordinates yields the following equation for the expansion coefficients $\chi_a(R)$ (using the orthogonality of the adiabatic basis):

$$
\begin{aligned}
\int dr\,\phi_b^*(r;R)\,H_{\mathrm{mol}}\,\psi(r;R) &= [E_b(R) + V_{\mathrm{nuc-nuc}}]\chi_b(R) \\
&\quad + \sum_a \int dr\,\phi_b^*(r;R)\,T_{\mathrm{nuc}}\,\phi_a(r;R)\chi_a(R) \\
&= \mathcal{E}\,\chi_b(R).
\end{aligned}
\tag{2.15}
$$

Since the electronic wave functions depend on the nuclear coordinates, we have, using $\boldsymbol{P}_n = -i\hbar\boldsymbol{\nabla}_n$ and the product rule for differentiation,

$$
\begin{aligned}
T_{\mathrm{nuc}}\,\phi_a(r;R)\,\chi_a(R) = \sum_n \frac{1}{2M_n} &\left\{ [\boldsymbol{P}_n^2\phi_a(r;R)]\,\chi_a(R) \right. \\
&+ 2\left[\boldsymbol{P}_n\phi_a(r;R)\right]\,\boldsymbol{P}_n\chi_a(R) \\
&\left. + \phi_a(r;R)\,\boldsymbol{P}_n^2\,\chi_a(R) \right\}.
\end{aligned}
\tag{2.16}
$$

The last term is simply the kinetic energy operator acting on $\chi_a(R)$. The other terms can be comprised into the so-called *nonadiabaticity* operator,

$$
\begin{aligned}
\Theta_{ab} = &\int dr\,\phi_a(r;R)\,T_{\mathrm{nuc}}\,\phi_b(r;R) \\
&+ \sum_n \frac{1}{M_n}\left[\int dr\,\phi_a(r;R)\boldsymbol{P}_n\phi_b(r;R)\right]\boldsymbol{P}_n.
\end{aligned}
\tag{2.17}
$$

Thus, we obtain from Eq. (2.15) an equation for the coefficients $\chi_a(R)$ that reads

$$
\left(T_{\mathrm{nuc}} + E_a(R) + V_{\mathrm{nuc-nuc}} + \Theta_{aa} - \mathcal{E}\right)\chi_a(R) = -\sum_{b\neq a}\Theta_{ab}\chi_b(R).
\tag{2.18}
$$

This result can be interpreted as the stationary Schrödinger equation for the motion of nuclei, with the $\chi_a(R)$ being the respective wave functions. The solution of Eq. (2.18), which is still exact, requires knowledge of the electronic spectrum for all configurations of the nuclei that are covered during their motion. Transitions between individual adiabatic electronic states become possible due to the electronic *nonadiabatic coupling* operator, Θ_{ab}. This is a consequence of the motion of the nuclei as expressed by the fact that their momenta enter Eq. (2.17). The diagonal

part of the nonadiabaticity operator, Θ_{aa}, is usually only a small perturbation to the nuclear dynamics in a given electronic state.

Looking at Eq. (2.18), we realize that it will be convenient to introduce the following effective potential for nuclear motion if the electronic system is in its adiabatic state $|\phi_a\rangle$:

$$U_a(R) = E_a(R) + V_{\text{nuc-nuc}}(R) + \Theta_{aa}. \tag{2.19}$$

This function defines a hypersurface in the space of nuclear coordinates, the *PES*, which will be discussed in more detail in Section 2.5. Its exceptional importance for a microscopic understanding of molecular dynamics phenomena will become evident in Chapters 5–9.

The solution to Eq. (2.18) is given by $\chi_{aM}(R) = \langle R | \chi_{aM} \rangle$. The index M denotes the (set of) *vibrational* quantum numbers. The molecular wave function is

$$\psi_M(r, R) = \sum_a \chi_{aM}(R) \, \phi_a(rR). \tag{2.20}$$

By virtue of the expansion (2.20) it is clear that the vibrational quantum number M in general is related to the *total* electronic spectrum and not to an individual electronic state.

2.3.1 Born–Oppenheimer Approximation

Solving the coupled equations (2.18) for the expansion coefficients in Eq. (2.20) appears to be a challenging task. However, in practice, it is often possible to neglect the nonadiabatic couplings altogether or take into account the couplings between certain adiabatic electronic states only. In order to investigate this possibility let us consider Figure 2.1. Here, we have plotted different adiabatic electronic states for a diatomic molecule as a function of the bond distance. Without going further into the details of the different states, we realize that there is one state, the electronic ground state $|\phi_0\rangle$, which particularly close to its minimum is well separated from the other states $|\phi_{a>0}\rangle$. Intuitively, we would expect the nonadiabatic couplings, Θ_{0a}, to be rather small in this region. In such situations it might be well justified to neglect the nonadiabatic couplings, that is we can safely set $\Theta_{0a} = 0$ in Eq. (2.18). The nuclear Schrödinger equation then simplifies considerably. Consider the general case $\Theta_{ab} = 0$,

$$H_a(R)\chi_a(R) = \left(T_{\text{nuc}} + U_a(R)\right)\chi_a(R) = \mathcal{E}\chi_a(R), \tag{2.21}$$

where $H_a(R)$ defines the *nuclear Hamiltonian* for the state $|\phi_a\rangle$. Thus, the nuclei can be considered to move in an effective potential $U_a(R)$ generated by their mutual Coulomb interaction and the interaction with the electronic charge distribution corresponding to the state $|\phi_a\rangle$ and the actual configuration R. The solutions of Eq. (2.21) are again labeled by M, but this quantum number is now related to the *individual* adiabatic electronic states. The total *adiabatic* wave function becomes

$$\psi_{aM}^{(\text{adia})}(r, R) = \chi_{aM}(R)\phi_a(r; R). \tag{2.22}$$
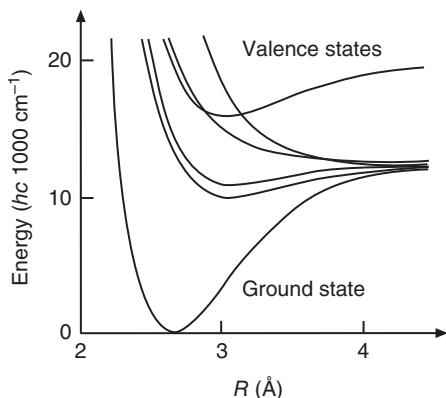
Figure 2.1 Potential energy curves $U_a(R)$ for different adiabatic electronic states $|\phi_a\rangle$ along the bond distance R of a diatomic molecule (ground and valence states of I_2).

The neglect of the nonadiabatic couplings leading to the wave function (2.22) is called the *Born–Oppenheimer approximation.*[2]

Going back to Figure 2.1, it is clear, however, that in particular for excited electronic states one might encounter situations where different potential curves are very close to each other. If Θ_{ab} does not vanish for symmetry reasons, it can no longer be neglected. The physical picture is that electronic and nuclear motions are no longer adiabatically separable, that is the change of the nuclear configuration from R to some $R + \Delta R$ causes an electronic transition.

In order to estimate the magnitude of this effect, we consider a perturbation expansion of the energy with respect to the nonadiabaticity operator. The second-order correction to the adiabatic energies $\mathcal{E}_{aM}^{(\text{adia})}$ is obtained as

$$\mathcal{E}_{aM}^{(2)} = \mathcal{E}_{aM}^{(\text{adia})} + \sum_{bN} \frac{\left|\left\langle \chi_{aM}\right| \Theta_{ab} \left|\chi_{bN}\right\rangle\right|^2}{\mathcal{E}_{aM}^{(\text{adia})} - \mathcal{E}_{bN}^{(\text{adia})}}, \tag{2.23}$$

where the $\chi_{aM}(R) = \langle R | \chi_{aM}\rangle$ are the Born–Oppenheimer nuclear wave functions. Apparently, the matrix elements $\langle \chi_{aM}| \Theta_{ab} |\chi_{bN}\rangle$ have to be small compared to the energy difference $|\mathcal{E}_{aM}^{(\text{adia})} - \mathcal{E}_{bN}^{(\text{adia})}|$ in order to validate the adiabatic Born–Oppenheimer approximation. Looking at the definition of Θ_{ab}, it is clear that this operator will be a small perturbation whenever the character of the electronic wave function does not change appreciably with R. On the other hand, the denominator in Eq. (2.23) will become small if two electronic states approach each other. Thus, knowledge about the adiabatic states is necessary to estimate the effect of nonadiabatic couplings. The actual calculation of Θ_{ab} is possible but often cumbersome, and an alternative representation of the Hamiltonian will be discussed in Section 2.6.

---

2) Note that neglecting only the off-diagonal elements of Θ_{ab} is referred to as the adiabatic approximation.

2.4   **Electronic Structure Methods**

Our knowledge about the microscopic origin of properties of molecules, their stable configurations, and their ability to break and make chemical bonds derives to a large extent from the progress made in electronic structure theory in recent decades. Nowadays, modern quantum chemical methods routinely achieve almost quantitative agreement with experimental data, for example for transition energies between the lowest electronic states of small- and medium-sized molecules. With increasing number of electrons the computational resources limit the applicability of the so-called ab initio methods (that is, based on fundamental principles and not on experimental data), and alternatives have to be exploited. Semiempirical methods simplify the exact ab initio procedure in a way that gives results consistent with the experimental data. On the other hand, ongoing developments in Density Functional Theory shift the attention to this more accurate method. Switching to situations of molecules in the condensed phase, for example in solution, requires more approximate methods as given, for example by the reduction of the solvent to a dielectric continuum surrounding the solute[3]) (see Section 2.7.1).

In what follows we will outline a tool for the practical solution of the electronic Schrödinger equation (2.12) for fixed nuclei. For simplicity, our discussion will mostly be restricted to the electronic ground state $E_0(R)$. Specifically, we will discuss the Hartree–Fock self-consistent field procedure in some detail. It is the working horse of most more advanced ab initio methods which also include the effect of electronic correlations missing in the Hartree–Fock approach. While these methods are based on the electronic wave function, Density Functional Theory (discussed afterward) builds on the electron density function. We note in caution that this section by no means presents a complete treatment of the field of electronic structure theory. The intention is rather to provide a background for the following discussions. The reader interested in a more comprehensive overview of the state of the art is referred to the literature quoted at the end of the book.

Let us start with the situation in which the Coulomb interaction between the electrons is switched off. Then, the electronic Hamiltonian (2.11) becomes a sum of *single-particle* Hamiltonians, $H_{el}(R) = \sum_j h_{el}(\boldsymbol{r}_j)$, containing the kinetic energy of the jth electron and the Coulomb energy due to its interaction with the static nuclei. Note that in the following discussion we will drop the parametric dependence on the nuclear coordinates. The stationary Schrödinger equation for $h_{el}(\boldsymbol{r}_i)$ is solved by the single-particle wave function $\varphi_{\alpha_j}(\boldsymbol{r}_j, \sigma_j)$,

$$
\begin{aligned}
h_{el}(\boldsymbol{r}_j)\varphi_{\alpha_j}(\boldsymbol{r}_j, \sigma_j) &= [T_{el}(j) + V_{el-nuc}(\boldsymbol{r}_j)]\varphi_{\alpha_j}(\boldsymbol{r}_j, \sigma_j) \\
&= \epsilon_{\alpha_j}\varphi_{\alpha_j}(\boldsymbol{r}_j, \sigma_j).
\end{aligned} \tag{2.24}
$$

---

3) Throughout, we will use the terms solute and solvent to describe a molecule (solute) embedded in a medium (solvent), no matter whether the latter is really a solvent in the usual sense or, for instance a solid-state matrix.

Here, the index α_i runs over all possible single-particle states (including spin) of the N_{el}-electron system, which have the energy ϵ_{α_j}. The single-particle functions $\varphi_{\alpha_j}(\boldsymbol{r}_j, \sigma_j)$ are called *spin orbitals*.

There are several points to make concerning the solutions of Eq. (2.24): First, since we are dealing with identical particles, the single-particle spectrum ϵ_{α_j} is the same for all electrons. Second, for the spin-independent Hamiltonian we use here, the spin function can be separated from the spatial orbital in the single-particle wave function according to $\varphi_{\alpha_j}(\boldsymbol{r}_j, \sigma_j) = \varphi_{a_j}(\boldsymbol{r}_j)\zeta_{a_j}(\sigma_j)$ and $\alpha_j = (a_j, \sigma_j)$. As mentioned above, the orthogonal spin functions $\zeta_{a_j}(\sigma_j)$ describe spin-up or spin-down electrons. Therefore, for N_{el} spatial orbitals $\varphi_{a_j}(\boldsymbol{r}_j)$, there will be $2N_{el}$ possible spin orbitals $\varphi_{\alpha_j}(\boldsymbol{r}_j, \sigma_j)$. Thus, given N_{el} electrons, the electronic ground state would correspond to the situation where we fill in electrons in the different spin orbitals starting from the one with the lowest energy. Of course, we must be mindful of the *Pauli principle*, that is each electron must have a distinct set of quantum numbers. In the present case, this implies that each spatial orbital may be occupied by two electrons having spin up and spin down, respectively. The result of the distribution of electrons over the available spin orbitals is referred to as an *electronic configuration*.

Depending on whether there is an even number of electrons in the ground state (*closed-shell* configuration) or an odd number (*open-shell* configuration), all electrons will be paired or not, respectively. For simplicity, we focus in what follows on the electronic ground state of closed-shell systems only. Here, N_{el} spin orbitals are occupied. One can further require the spatial orbitals to be identical for spin-up and spin-down electrons so that there will be $N_{el}/2$ doubly-occupied spatial orbitals in the ground state. The total spin of this many-electron system is zero. A closed-shell situation is shown for the water molecule in Figure 2.2.

The Pauli principle, which we invoked above, can be traced back to a fundamental property of the total wave function of a many-electron system. First, we observe that
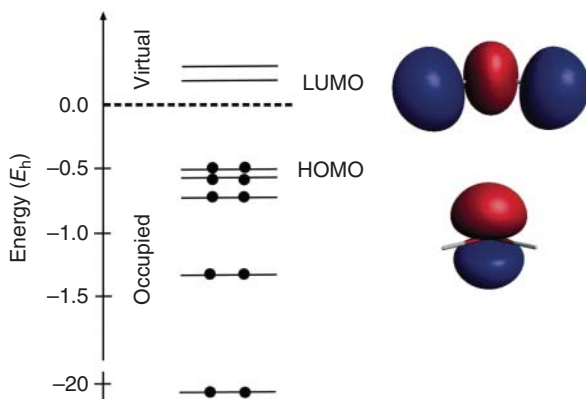
Figure 2.2 Orbital diagram for water calculated using Hartree–Fock theory (the energy is given in atomic units ($E_h = \hbar^2/(ea_0^2)$). There are $N_{el}/2 = 5$ doubly-occupied orbitals; the empty orbitals are called virtual. The highest occupied molecular orbital (HOMO) and the lowest unoccupied molecular orbital (LUMO) are assigned and shown on the right (different colors correspond to positive and negative values).

in contrast to classical mechanics, in quantum mechanics the electrons described by a wave function are not distinguishable. This means that the total probability distribution, $|\phi(r, \sigma)|^2$, should be invariant with respect to the exchange of any two particle indices. The permutation of the particle indices is conveniently written using a permutation operator $\mathcal{P}$ which, when acting on a many-particle wave function, exchanges the indices of any two particles. After the application of $\mathcal{P}$ the wave function can change at most by a constant factor ξ (of modulus 1). Therefore, applying $\mathcal{P}$ twice one should recover the original wave function, that is we have $\xi^2 = 1$ or $\xi = \pm 1$. For spin 1/2 particles like electrons, it turns out that $\xi = -1$, and therefore, the total wave function has to be antisymmetric with respect to the exchange of any two electron indices.

If we go back to the single-particle spin orbitals defined by Eq. (2.24), it is clear now that even in the absence of the electron interaction the so-called *Hartree product* ansatz,

$$\phi^{\mathrm{HP}}_{\{\alpha_j\}}(r, \sigma) = \prod_{j=1}^{N_{\mathrm{el}}} \varphi_{\alpha_j}(\boldsymbol{r}_j, \sigma_j), \tag{2.25}$$

cannot be correct since it does not have the required antisymmetry ($\{\alpha_j\}$ comprises the set of quantum numbers α_j). However, Eq. (2.25) can be used to generate an antisymmetric wave function. To this end, we make use of the permutation operator $\mathcal{P}$. Keeping track of the number of permutations, p, which have been performed, one obtains an antisymmetric wave function by the prescription

$$\phi(r, \sigma) = \frac{1}{\sqrt{N_{\mathrm{el}}!}} \sum_{\mathrm{perm}} (-1)^p \mathcal{P} \left[\phi^{\mathrm{HP}}_{\{\alpha_j\}}(r, \sigma) \right]. \tag{2.26}$$

Here, the summation is carried out over all $N_{\mathrm{el}}!$ possible permutations of the electron indices $(\boldsymbol{r}_j, \sigma_j)$ ($j = 1, \ldots, N_{\mathrm{el}}$) in the Hartree product. Alternatively, Eq. (2.26) can be written in the form of a determinant, the so-called *Slater determinant*, where the rows contain the single-particle spin orbitals for a given state and all possible electron coordinates, and the different electronic states for a given coordinate are recorded in the columns. The elementary properties of determinants then guarantee the antisymmetry of the ansatz for the total electronic wave function.

2.4.1 The Hartree–Fock Equations

So far we have not considered the effect of the Coulomb interaction between the electrons. Within Hartree–Fock theory this is usually done by starting from the antisymmetric ansatz (2.26) for the wave function. Then, the goal is to optimize the single-particle spin orbitals such that the total energy is minimized. This can be achieved by invoking the calculus of variation. Consider a Slater determinant $\phi(r, \sigma)$, which will be a function of some parameters. In practice, the spatial orbitals are expanded in terms of some fixed basis set, and the expansion coefficients then take the role of the parameters (linear variational problem). The basis set is usually chosen to consist of functions that are centered at the different atoms in the molecule (linear combination of atomic orbitals, LCAO).

The expectation value of the energy is then given by

$$\langle H_{el} \rangle = \int dr \sum_{\sigma} \phi^*(r, \sigma) \left[\sum_{j=1}^{N_{el}} h_{el}(\boldsymbol{r}_j) + \frac{1}{2} \sum_{i,j=1}^{N_{el}} V_{el-el}(\boldsymbol{r}_i, \boldsymbol{r}_j) \right] \phi(r, \sigma).$$
(2.27)

The first term denotes the single-particle Hamiltonian including the electron–nuclei Coulomb interaction, Eq. (2.24), and the second term describes the electron–electron repulsion, Eq. (2.4). The variational optimization of Eq. (2.27) leads to the following so-called Hartree–Fock integrodifferential equations for determination of the optimal orbitals for a closed-shell configuration

$$\left[h_{el}(\boldsymbol{x}) + \sum_{b}^{N_{el}/2} [2J_b(\boldsymbol{x}) - K_b(\boldsymbol{x})] \right] \varphi_a(\boldsymbol{x}) = \varepsilon_a \varphi_a(\boldsymbol{x}).$$
(2.28)

Here, ε_a is the energy associated with the spatial orbital $\varphi_a(\boldsymbol{x})$.[4] Further, the operator on the left hand side is called the *Fock operator*; it is an *effective* one-electron operator.

Without the electron–electron interaction and wave function antisymmetrization the Fock operator reduces to the single-electron Hamiltonian, $h_{el}(\boldsymbol{x})$. Different spatial orbitals are coupled by means of the Coulomb operator

$$J_b(\boldsymbol{x}) = \int d^3 \boldsymbol{x}' |\varphi_b(\boldsymbol{x}')|^2 \, V(\boldsymbol{x}', \boldsymbol{x})$$
(2.29)

and the exchange operator

$$K_b(\boldsymbol{x}) \varphi_a(\boldsymbol{x}) = \left[\int d^3 \boldsymbol{x}' \varphi_b^*(\boldsymbol{x}') \, V(\boldsymbol{x}, \boldsymbol{x}') \, \varphi_a(\boldsymbol{x}') \right] \varphi_b(\boldsymbol{x}).$$
(2.30)

The Coulomb operator represents the average local potential of an electron in orbital $\varphi_b(\boldsymbol{x})$ felt by the electron in $\varphi_a(\boldsymbol{x})$. Thus, the exact two-particle Coulomb interaction is replaced by an effective one-electron potential. The fact that each electron only experiences the *mean field* generated by all other electrons is a basic characteristic of the Hartree–Fock approach. Of course, in this way, the interaction between electrons becomes blurred, and correlations between their individual motions are lost.

For electrons having parallel spins there is a particular correlation introduced by the antisymmetric ansatz for the wave function. This effect is contained in the exchange operator. However, the action of $K_b(\boldsymbol{x})$ on the orbital $\varphi_a(\boldsymbol{x})$ obviously cannot be viewed in terms of a local potential for the electron in $\varphi_a(\boldsymbol{x})$. In fact, it is the exchange operator that makes the Fock operator *nonlocal* in space.

The Hartree–Fock equations are nonlinear since the Fock operator itself depends on the orbitals $\varphi_a(\boldsymbol{x})$. Their numerical solution can be obtained by iteration. Starting from some trial orbitals, one first constructs the Fock operator and then uses it to obtain improved orbitals that are the input for a new Fock operator. This iterative procedure is continued until the operators $J_a(\boldsymbol{x})$ and $K_a(\boldsymbol{x})$ are consistent with the solutions for the orbitals. Therefore, the approach is usually termed Hartree–Fock *self-consistent field* method.

---

4) Note the use of the general electron coordinate $\boldsymbol{x}$.

Given the solution of the Hartree–Fock equations, one has at hand the ground state energy as well as the ground state adiabatic electronic wave function, which follows from a *single* Slater determinant built up by the optimal molecular orbitals. For the common LCAO basis, a given number of atomic orbitals yields M spin orbitals. Usually, $N_{el} < M$, and one distinguishes the N_{el} occupied spin orbitals from the $M - N_{el}$ unoccupied (the so-called virtual) spin orbitals (cf. Figure 2.2). Orbitals and their energies are functions of the nuclear coordinates; by exploring the possible nuclear configurations, the ground state Hartree–Fock PESs can be constructed according to Eq. (2.19). However, if, for instance the bond in a diatomic molecule is stretched toward dissociation, the character of the electronic state will change considerably, for example from a closed-shell to an open-shell system. This effect of having contributions from different electronic configurations cannot be described by a single Slater determinant, Eq. (2.26); the predicted potential energy curve will be qualitatively incorrect. The effect of the simultaneous presence of different electronic configurations, which is also an ubiquitous phenomenon for electronically excited states in the region where potential curves intersect (cf. Figure 2.1), is called static correlation. It has to be distinguished from dynamic correlations, which are related to that part of the electron–electron interaction that is not accounted for by the mean-field approximation based on a single Slater determinant.

Conceptually, the simplest approach to account for such correlations is the configuration interaction (CI) method. Here, one starts with the Hartree–Fock ground state and generates a basis for expanding the total electronic wave function by forming all possible Slater determinants that result from promoting different numbers of electrons from the occupied to the unoccupied orbitals, that is

$$|\phi^{(CI)}\rangle = C_0|\phi^{(0)}\rangle + C_1|\phi^{(1)}\rangle + C_2|\phi^{(2)}\rangle + \dots . \tag{2.31}$$

Here, $|\phi^{(0)}\rangle$ stands for the Hartree–Fock ground state, and $|\phi^{(1)}\rangle$ and $|\phi^{(2)}\rangle$ comprise all possible single and double excitations, respectively, starting from the ground state. The coefficients C_i give the weight for these configurations. Upon diagonalization of the electronic Hamiltonian in this basis set the expansion coefficients are obtained, and the problem of electron correlations is solved in principle. In practice, the number of possible excitations increases rapidly[5], and the approach has to be restricted, for instance to include at most double excitations. Several alternatives to the CI method have been developed, and the reader is referred to the literature list at the end of the chapter for more details.

2.4.2 Density Functional Theory

The methods discussed so far have been based on the electronic wave function; that is, the Hartree–Fock ground state energy was assumed to be a functional of the wave function, and variational minimization has been applied. A different strategy

---

5) Given M spin–orbitals, there are $\binom{M}{N_{el}}$ possibilities for the distribution of N_{el} electrons.

is followed in Density Functional Theory where the one-electron probability density,[6]

$$\rho(\boldsymbol{x}) = N_{el} \sum_{\sigma} \int dr \, \delta(\boldsymbol{x} - \boldsymbol{r}_1) \, |\phi(r,\sigma)|^2 \tag{2.32}$$

is the central object of interest. The foundation of Density Functional Theory is laid by the Hohenberg–Kohn theorems. They state that for a given electron–nuclear interaction potential,[7] the full many-particle ground state energy, E_0, is a unique functional of the electronic density, and that any density $\rho(\boldsymbol{x})$ other than the ground state density $\rho_0(\boldsymbol{x})$ will give an energy higher than the ground state energy, that is $E[\rho] \geq E[\rho_0] \equiv E_0$, implying that a variational principle can be applied.

The energy functional can be decomposed as follows:

$$E[\rho] = e \int d^3\boldsymbol{x} \, V_{el-nuc}(\boldsymbol{x}) \, \rho(\boldsymbol{x}) + T_{el}[\rho] + \frac{e^2}{2} \int d^3\boldsymbol{x} \, d^3\boldsymbol{x}' \, \frac{\rho(\boldsymbol{x})\rho(\boldsymbol{x}')}{|\boldsymbol{x}-\boldsymbol{x}'|} + E_{XC}[\rho]. \tag{2.33}$$

The different terms correspond to the interaction between electrons and nuclei, the kinetic energy of the electrons,[8] the classical electron–electron interaction energy, and the nonclassical contribution from the electron–electron interaction due to exchange and correlation effects. It should be noted that apart from the first term all contributions to the energy functional (2.33) are universal, that is not molecule specific. They are comprised in what is called the Hohenberg–Kohn functional and depend only on the properties of the electronic DOFs.

The practical calculation of the electron density starts from the variational principle. Here, the stationarity condition for the energy $\delta E[\rho]/\delta\rho = 0$ has to be fulfilled subject to the constraint that the system must contain a fixed number of electrons. The variational freedom is provided by expressing the density in terms of the so-called Kohn–Sham orbitals $\varphi_\alpha^{KS}(\boldsymbol{x})$, that is $\rho(\boldsymbol{x}) = \sum_\alpha |\varphi_\alpha^{KS}(\boldsymbol{x})|^2$. This leads to the Kohn–Sham equations

$$\left[T_{el} + V_{el-nuc} + e \int d^3\boldsymbol{x}' \, \frac{\rho(\boldsymbol{x}')}{|\boldsymbol{x}-\boldsymbol{x}'|} + V_{XC}(\boldsymbol{x}) \right] \varphi_\alpha^{KS}(\boldsymbol{x}) = \varepsilon_\alpha^{KS} \varphi_\alpha^{KS}(\boldsymbol{x}), \tag{2.34}$$

which can be used to determine the Kohn–Sham orbitals as well as the respective orbital energies ε_α^{KS}, which are determined in a self-consistent manner. Apart from the exchange-correlation potential, here, $V_{XC}(\boldsymbol{x}) = \delta E_{XC}[\rho(\boldsymbol{x})]/\delta\rho(\boldsymbol{x})$, Eq. (2.34) resembles the Hartree–Fock equations (2.28). However, it is important to emphasize that upon adding V_{XC} the Kohn–Sham equations become formally exact.

---

6) Note that in order to obtain this equation from the first term on the right-hand side of Eq. (2.9), one has to make use of the exchange symmetry of the electronic wave function with respect to the electronic coordinates. This gives the factor N_{el}.

7) In fact, the first Hohenberg–Kohn theorem holds for an arbitrary external potential for the electron motion.

8) Note that $T_{el}[\rho]$ refers to the kinetic energy of some noninteracting reference system which has the same density as the real system. The difference between the real and the reference kinetic energy is assumed to be part of the unknown exchange-correlation energy.

Moreover, V_{XC} and therefore the Kohn–Sham equations are local in space.[9] This has to be contrasted with the Hartree–Fock equations where the exchange operator introduces a nonlocal spatial dependence of the orbitals.

But, unfortunately, the form of the exchange-correlation functional is not specified by the Hohenberg–Kohn theorems, and in fact it is not known. In practice, this problem is approached by developing approximate functionals that may incorporate sum rules, asymptotic properties of the electron density, information from approximations to the electron density, and fits to exact numerical results available for some test systems. A simple form for the exchange-correlation energy is given, for example by the so-called local density approximation,

$$E_{XC}^{LDA}[\rho] = \int d^3\boldsymbol{x} \ \rho(\boldsymbol{x}) \ \varepsilon_{XC}[\rho(\boldsymbol{x})], \tag{2.35}$$

where $\varepsilon_{XC}[\rho(\boldsymbol{x})]$ is the known exchange-correlation energy per particle for a homogeneous electron gas moving on a positive background charge density. This model works rather well, for example for perfect metals. For molecules, the electron density is far from being uniform, and hence, the local density approximation in general does not show a reasonable performance. A substantial improvement is achieved by including in addition the gradient of the density as well a portion of the exact Hartree–Fock exchange. This leads to a number of popular functionals, with the Becke three-parameter Lee–Yang–Parr (B3LYP) functional being the most successful one. For more information on Density Functional Theory, we refer the reader to the literature list given at the end of this chapter.

Despite this fundamental deficiency of an unknown $E_{XC}[\rho]$, in practical applications modern Density Functional Theory often outperforms the Hartree–Fock method, for example when predicting barrier heights for chemical reactions, because it includes correlation effects at least approximately. Compared to high-level wave function-based methods, it is numerically much less expensive, making it a tool for studying larger molecules.

2.5 Potential Energy Surfaces

In the previous sections it was indicated that the potential energy hypersurface defined by Eq. (2.19) is the key quantity when it comes to investigate chemical reaction dynamics or, more generally, nuclear motions. In the following discussion, we will consider some properties of the adiabatic Born–Oppenheimer PES ($\Theta_{ab} = 0$) for a particular electronic state,

$$U_a(R) = E_a(R) + V_{nuc-nuc}(R). \tag{2.36}$$

In general, $U_a(R)$ is a function of all the $3N_{nuc}$ nuclear coordinates R (recall the notation $R = (R_1, \dots, R_{3N_{nuc}})$). Since the energy is independent of the overall translations and rotations of the molecule, there are actually only $3N_{nuc} - 6$ coordinates

---

9) This does not imply that the actual dependence of V_{XC} on the density or its coordinate dependence itself is simple.

necessary to completely specify the energy of the molecule in the configuration space of the nuclear coordinates (for linear molecules, there are only $3N_{nuc} - 5$ independent coordinates).

Let us assume for the moment that we have obtained $U_a(R)$. Then, we are in a position to draw several conclusions, for example on the nature of the bonding as well as on the dynamical behavior to be expected in the considered system. To this end we define the gradient of the potential as

$$\nabla U_a(R) = \{\partial U_a(R)/\partial R_1, \dots, \partial U_a(R)/\partial R_{3N_{nuc}}\}. \tag{2.37}$$

This vector points along the direction of the steepest rise of the potential, and its negative is just the force acting along that particular direction in the configuration space. Another quantity of great importance is the $3N_{nuc} \times 3N_{nuc}$ force constant matrix or *Hessian matrix* whose elements are defined as

$$\kappa_{mn}^{(a)} = \frac{\partial^2 U_a(R)}{\partial R_m \partial R_n} \quad (m, n = 1, \dots, 3N_{nuc}). \tag{2.38}$$

The points in configuration space for which the gradient of the potential vanishes,

$$\nabla U_a(R) = 0, \tag{2.39}$$

are called *stationary* points. Suppose that we have located a stationary point at the equilibrium configuration $R^{(a)}$. The nature of the PES in the vicinity of this stationary point can then be investigated by looking at the eigenvalues of the Hessian matrix. In general, there will be six eigenvalues equal to zero reflecting the fact that there are only $3N_{nuc} - 6$ independent coordinates necessary to determine the energy (see below). If the remaining eigenvalues of the Hessian matrix are all positive, we are at a minimum of the PES. In Figure 2.3, this situation is plotted for a diatomic molecule where R is the bond length. The minimum of $U(R)$ at $R = R_{eq}$ gives the equilibrium distance between the two atoms. As a consequence of QM zero-point motion, the lowest possible energy eigenvalue is above the bottom of the potential minimum (solid line in Figure 2.3). The molecule is said to be stable if the difference between this zero-point energy and the energy it takes to separate the atoms, $U(R \to \infty)$, is finite (dissociation energy, D_0 in Figure 2.3).

Figure 2.3 corresponds to the situation where $U(R)$ only has a single global minimum. In fact, there are many systems that support multiple minima in the potential energy landscape. In Figure 2.4, we have plotted a potential showing two equivalent minima. These minima in $U(R)$ may correspond to different isomers of the molecule.
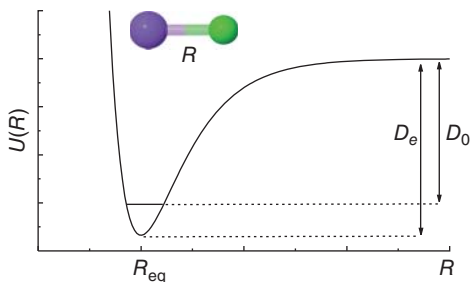
Figure 2.3 Schematic view of a typical potential energy curve of a diatomic molecule. Here, R_{eq} denotes the equilibrium bond length, and D_0 (D_e) the dissociation energy which does (does not) take into account the quantum mechanical zero-point energy.

Figure 2.4 Schematic view of a potential energy curve typical for isomerization reactions. Reactants and products are separated by a reaction barrier of height E_B along the reaction coordinate R.
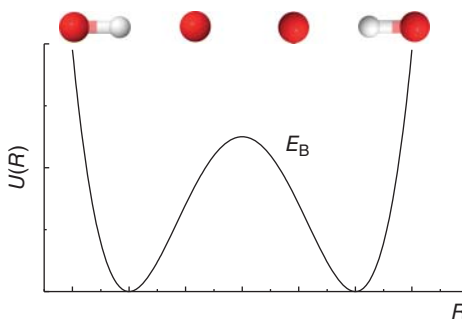
Figure 2.5 Schematic view of typical ground and excited state potential energy curves of diatomic molecules. If the molecule is promoted to the excited state, for example by means of an external field, dissociation will occur.
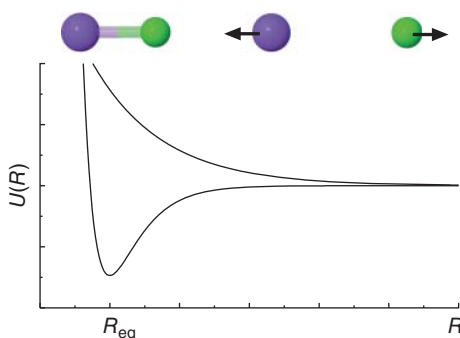
Such situations occur, for example in systems showing intramolecular hydrogen transfer. Another standard example is the umbrella vibration of NH_3. In the course of isomerization the system has to pass a maximum of the potential curve that corresponds to a saddle point of $U(R)$. At such a simple saddle point the Hessian matrix will have one negative eigenvalue.

Finally, we consider a case one typically encounters in excited states. In Figure 2.5, we plotted potential energy curves for the adiabatic ground and excited states of a diatomic molecule. Apparently, the excited state potential has no minimum. This implies that an electronically excited molecule will experience a force, $-\partial U / \partial R$, leading to dissociation as indicated in the figure.

For larger molecules it is no longer possible to plot the potential energy as a function of all coordinates. It goes without saying that in addition the calculation of these PES becomes computationally very demanding. Fortunately, quite often, one has to deal with situations where only few coordinates are important for a reaction. Then, it becomes possible to describe this reaction by taking into account only the motion along a single so-called *reaction coordinate* while keeping the remaining coordinates fixed at their equilibrium positions. Consider, for instance the dissociation of the A––B bond of a triatomic molecule ABC. If the internal excitation of the BC fragment during the cleavage of the A––B bond is negligible, BC can be treated as an entity characterized by its center of mass. Before discussing the more advanced concepts (applicable for polyatomic molecules) in Section 2.5.3, we focus on the nuclear dynamics in the vicinity of stationary points.

2.5.1 Harmonic Approximation and Normal Mode Analysis

Having discussed some general aspects of adiabatic PES, we turn to the problem of solving the nuclear Schrödinger equation. Let us assume that we have located a stationary point $R^{(a)}$ in the configuration space corresponding to a global minimum of $U_a(R)$. Restricting our discussion to small deviations, $\Delta R_n^{(a)} = R_n - R_n^{(a)}$ ($n = 1, \ldots, 3N_{\text{nuc}}$), from the stationary point the potential can be approximated by a second-order Taylor expansion with respect to $R^{(a)}$,

$$U_a(R) = U_a(R^{(a)}) + \sum_{m,n=1}^{3N_{\text{nuc}}} \frac{1}{2} \kappa_{mn}^{(a)} \Delta R_m^{(a)} \Delta R_n^{(a)}. \tag{2.40}$$

Here, the Hessian matrix has to be taken at the point $R^{(a)}$. Note that at the stationary point the first derivatives vanish because of the condition (2.39). According to Eq. (2.21), the Hamiltonian for the nuclear DOFs in the adiabatic approximation reads

$$H_a = U_a(R^{(a)}) + \sum_{n=1}^{3N_{\text{nuc}}} \frac{P_n^2}{2M_n} + \sum_{m,n=1}^{3N_{\text{nuc}}} \frac{1}{2} \kappa_{mn}^{(a)} \Delta R_m^{(a)} \Delta R_n^{(a)}. \tag{2.41}$$

The linear transformation,

$$\Delta R_n^{(a)} = \sum_{\xi} M_n^{-1/2} A_{n\xi}^{(a)} q_{a\xi}, \tag{2.42}$$

can be used to diagonalize the potential energy operator, whereas the kinetic energy operator remains in diagonal form due to the Cartesian character of the displacements. Expressed in the so-called *normal mode coordinates* $q_{a\xi}$, Eq. (2.41) becomes (note that the normal mode coordinates are mass weighted)

$$H_a = U_a(q_{a\xi} = 0) + H_a^{(\text{nm})}, \tag{2.43}$$

with the normal mode Hamiltonian defined as

$$H_a^{(\text{nm})} = \frac{1}{2} \sum_{\xi} \left(p_\xi^2 + \omega_{a\xi}^2 q_{a\xi}^2 \right). \tag{2.44}$$

Here, the normal mode frequencies $\omega_{a\xi}$ have been introduced, with $\omega_{a\xi}^2$ being the nonzero eigenvalues of the Hessian matrix.

The nuclear motions according to Eq. (2.44) can be understood as a superposition of independent harmonic vibrations around the equilibrium configuration $R^{(a)}$, which corresponds to $q_{a\xi} = 0$. It is noteworthy that the harmonic oscillations of the *individual* atoms within a normal mode have all the same frequency, $\omega_{a\xi}$, but different amplitudes determined by their masses (cf. Eq. (2.42)). In Figure 2.6, we show
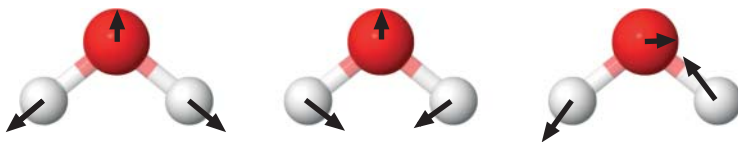
Figure 2.6 The displacement vectors for the three normal modes of water. The different amplitudes are determined by the atomic masses (cf. Eq. (2.42)).

as an example the displacement vectors for the three normal modes of water. The different amplitudes are represented by arrows of different lengths. It should be noted that the normal mode vibrations do not lead to any translations or rotations of the molecules as a whole, that is linear and angular momenta are conserved. In addition to the $3N_{nuc} - 6$ normal mode frequencies, the diagonalization of the Hessian will result in six eigenvalues which are equal to zero. In terms of the PES, this means that there is no restoring force along these zero-frequency normal mode displacements. Thus, it is clear that the eigenvectors obtained for the zero eigenvalues must correspond to the free translation and rotation of the molecule.

Having specified the vibrational Hamiltonian for the adiabatic electronic state $|\phi_a\rangle$ in Eq. (2.44), the nuclear Schrödinger equation can be solved by making a factorization ansatz with respect to the normal modes for the wave function. Using the standard textbook solution for harmonic oscillators, we have (q comprises all normal mode coordinates)

$$H_a^{(nm)} \chi_{aN}^{(adia)}(q) = \mathcal{E}_{aN} \chi_{aN}^{(adia)}(q), \tag{2.45}$$

with

$$\chi_{aN}^{(adia)}(q) = \prod_\xi \chi_{aN_\xi}(q_{a\xi}). \tag{2.46}$$

Here, the set of quantum numbers is written as $N = \{N_1, N_2, \dots\}$, and the eigenfunctions for mode ξ are given by

$$\chi_{aN_\xi}(q_{a\xi}) = \frac{\lambda_{a\xi}}{\sqrt{\sqrt{\pi}\, 2^{N_\xi}\, N_\xi!}} \exp\left(-\frac{1}{2}\lambda_{a\xi}^2 q_{a\xi}^2\right)\, H_{N_\xi}(\lambda_{a\xi}\, q_{a\xi}), \tag{2.47}$$

with $\lambda_{a\xi}^2 = \omega_{a\xi}/\hbar$. The H_{N_ξ} in Eq. (2.47) are the Hermite polynomials. The eigenenergies in Eq. (2.45) read

$$\mathcal{E}_{aN} = \sum_\xi \hbar\omega_{a\xi}(N_\xi + \frac{1}{2}), \tag{2.48}$$

with the vibrational quantum numbers for mode ξ being $N_\xi = 0, 1, 2, \dots$

In Figure 2.7, we have plotted the oscillator potential for a single mode together with the eigenfunctions corresponding to the lowest eigenenergies. Note that in contrast to classical mechanics, the lowest possible state has finite energy due to QM zero-point motion (see Eq. (2.48)). Having solved the electronic and the

Figure 2.7 Harmonic oscillator potential together with the eigenfunctions for the lowest energy eigenstates along the normal mode coordinate q.
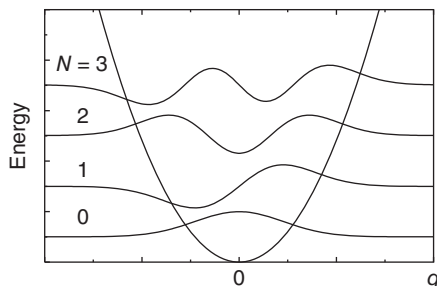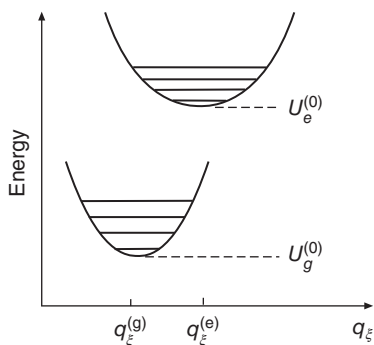
Figure 2.8 Shifted harmonic oscillator potential surfaces for two electronic states described by the same normal coordinate q_ξ. Here, we have used the notation $U_a^{(0)} = U_a(q_\xi^{(a)})$.

nuclear problems separately, we are in a position to give the solutions, $\Psi_N^{(\text{adia})}(r, \sigma; R)$ (Eq. (2.22)), to the molecular Schrödinger equation (2.7) within the adiabatic Born–Oppenheimer approximation.

In preparation of the following chapters, we now address the issue of the relation between normal modes belonging to different electronic states. Suppose that we have made a normal mode analysis for the electronic ground state PES, $U_{a=g}(R)$, which had a stationary point at $R^{(g)}$. We then proceed by searching for the minima in some excited state PES $U_{a=e}(R)$. This excited state will be selected, for instance because it is accessible from the ground state via an optical transition (see Chapter 6). Let us assume that we found a stationary point for the configuration $R^{(e)}$. Assuming further the harmonic approximation to the PES in the vicinity of $R^{(e)}$ to be valid, we can write

$$U_e(R) = U_e(R^{(e)}) + \sum_{m,n=1}^{3N_{\text{nuc}}} \frac{1}{2} \kappa_{mn}^{(e)} \, \Delta R_m^{(e)} \, \Delta R_n^{(e)}. \tag{2.49}$$

According to Eq. (2.42), the normal modes are obtained by a linear transformation of the Cartesian displacements. We can relate the displacement vectors for the excited state to those for the ground state via

$$\Delta R_n^{(e)} = R_n - R_n^{(g)} - (R_n^{(e)} - R_n^{(g)}) = \sum_\xi M_n^{-1/2} A_{n\xi}^{(g)}(q_{g\xi} - \Delta q_{e\xi}). \tag{2.50}$$

Here, the $\Delta q_{e\xi}$ are defined by the deviations between the ground and excited state minima. This situation is illustrated in Figure 2.8 for a single normal mode.

In the general case, the shape of the PES may be different in different electronic states. This would imply that the normal mode transformation does not bring the Hamiltonian for the ground and the excited states into diagonal form simultaneously.[10] Thus, the Hessian $\kappa_{mn}^{(e)}$ is not diagonalized by the transformation matrix of the ground state, $A_{n\xi}^{(g)}$. In what follows, we will assume for simplicity that the ground and excited states can be described by the *same* normal mode coordinates. We allow, however, for state-dependent normal mode frequencies, $\omega_{a\xi}$. With this restriction, we can write the Hamiltonian for the excited state as

$$H_e = U_e(q_\xi = q_\xi^{(e)}) + \frac{1}{2} \sum_\xi \left(p_\xi^2 + \omega_{e\xi}^2 (q_\xi - q_\xi^{(e)})^2 \right). \tag{2.51}$$

---

10) The resulting mixing between the ground and the excited state normal modes is called Duschinsky rotation.

Here, and in what follows, we will drop the electronic state index at the normal coordinates, $q_{g\xi} = q_{e\xi} = q_\xi$, and introduce the abbreviation $q_\xi^{(e)} = \Delta q_{e\xi}$. Typical PESs along some normal coordinate valid for the ground and the excited states are plotted in Figure 2.8. The solutions of the stationary Schrödinger equation for the excited state Hamiltonian, (2.51), are now shifted oscillator states, which read for mode ξ

$$\chi_{eN_\xi}(q_\xi - q_\xi^{(e)}) = \frac{\lambda_{e\xi}}{\sqrt{\sqrt{\pi}\, 2^{N_\xi}\, N_\xi!}} \exp\!\left(-\frac{1}{2}\lambda_{e\xi}^2(q_\xi - q_\xi^{(e)})^2\right) H_{N_\xi}(\lambda_{e\xi}(q_\xi - q_\xi^{(e)})).$$

(2.52)

This procedure is easily generalized to incorporate any excited electronic state that can be described by the normal modes of the electronic ground state. The displacement $q_\xi^{(e)}$ gives a measure for the strength of the coupling of a particular mode on the electronic transition. This allows for a classification of modes into active and passive ones (see also Chapters 5 and 6).

2.5.2 Operator Representation of the Normal Mode Hamiltonian

The properties of harmonic oscillators are conveniently derived using the so-called creation and annihilation operators of second quantization. We define the annihilation operator (dropping the electronic state index, which is unnecessary if the frequency is state independent as will be assumed in the following discussion).[11]

$$C_\xi = \sqrt{\frac{\omega_\xi}{2\hbar}}\, \hat{q}_\xi + i\frac{1}{\sqrt{2\hbar\omega_\xi}}\, \hat{p}_\xi.$$

(2.53)

Its Hermitian conjugate C_ξ^+ is called the creation operator. Then, the coordinate and momentum operators can be expressed by means of these operators as

$$\hat{q}_\xi = \sqrt{\frac{\hbar}{2\omega_\xi}}(C_\xi + C_\xi^+)$$

(2.54)

and

$$\hat{p}_\xi = -i\sqrt{\frac{\hbar\omega_\xi}{2}}(C_\xi - C_\xi^+).$$

(2.55)

Frequently, we also use dimensionless coordinates that are defined according to

$$\hat{Q}_\xi = \hat{q}_\xi\sqrt{\frac{2\omega_\xi}{\hbar}} = C_\xi + C_\xi^+,$$

(2.56)

and dimensionless momenta

$$\hat{P}_\xi = \hat{p}_\xi\sqrt{\frac{2}{\hbar\omega_\xi}} = -i(C_\xi - C_\xi^+).$$

(2.57)

---

11) In what follows, $\hat{p}_\xi$ and $\hat{q}_\xi$ denote abstract operators in Hilbert space spanned by the vectors $|\chi_N\rangle$.

The action of creation and annihilation operators is conveniently described using the occupation number representation. For a general f-dimensional wave function like Eq. (2.46), this corresponds to the following change (skipping the electronic state index):

$$\left| \chi_{N_1}, \dots, \chi_{N_f} \right\rangle \equiv |N_1, \dots, N_f\rangle, \tag{2.58}$$

that is the f-dimensional state is completely characterized by the quantum numbers N_ξ. For the present case of bosons, these so-called *occupation numbers* can have values $N_\xi = 0, 1, 2, \dots$. The effect of the action of the annihilation operator on an occupation number state is to decrease that occupation number by 1, that is

$$C_\xi \, |N_\xi\rangle = \sqrt{N_\xi} \, |N_\xi - 1\rangle \tag{2.59}$$

and

$$C_\xi \, |0_\xi\rangle = 0. \tag{2.60}$$

The creation operator, C_ξ^+, increases the occupation number in mode ξ by 1

$$C_\xi^+ \, |N_\xi\rangle = \sqrt{N_\xi + 1} \, |N_\xi + 1\rangle. \tag{2.61}$$

These operators obey the boson commutation relation

$$[C_\xi, C_{\xi'}^+] = C_\xi C_{\xi'}^+ - C_{\xi'}^+ C_\xi = \delta_{\xi\xi'}. \tag{2.62}$$

Using these relations the normal mode Hamiltonian (2.44) takes the simple form

$$H^{(\text{nm})} = \sum_\xi \hbar \omega_\xi \left(C_\xi^+ C_\xi + \frac{1}{2} \right). \tag{2.63}$$

The operator $C_\xi^+ C_\xi = \hat{N}_\xi$ is the so-called occupation number operator whose eigenvalue equation is $\hat{N}_\xi |N_\xi\rangle = N_\xi |N_\xi\rangle$. All eigenstates $|N_\xi\rangle$ of Eq. (2.63) can be obtained by successive application of the creation operator C_ξ^+ on the ground state $|0_\xi\rangle$

$$|N_\xi\rangle = \frac{1}{\sqrt{N_\xi!}} (C_\xi^+)^{N_\xi} |0_\xi\rangle. \tag{2.64}$$

Of course, the eigenenergies do not change, that is they are given by Eq. (2.48).

In the previous section we learned that the nuclear motion in two different electronic states can – under certain conditions – be described using the same normal mode coordinates. The different equilibrium positions of the normal mode oscillators are then accounted for by shifting the equilibrium position of the potential and the respective oscillator wave function by $q_\xi^{(a)}$. Introducing dimensionless coordinates according to Eq. (2.56), the Hamiltonian for the shifted oscillator, (2.51), becomes

$$H_a^{(\text{nm})} = U_a^{(0)} + \sum_\xi \hbar \omega_\xi \left(C_\xi^+ C_\xi + \frac{1}{2} \right)$$
$$+ \sum_\xi \hbar \omega_\xi [g_a(\xi)(C_\xi^+ + C_\xi) + g_a^2(\xi)]. \tag{2.65}$$

Here, we introduced the dimensionless shift of the PES belonging to state a as

$$g_a(\xi) = -\sqrt{\frac{\omega_\xi}{2\hbar}}\, q_\xi^{(a)}. \tag{2.66}$$

The respective energy offset has been abbreviated as $U_a^{(0)} = U_a(q_\xi^{(a)})$. In order to find a suitable representation of the shifted oscillator functions (2.52) in terms of occupation number states, we introduce the so-called displacement operator. Suppose that we expand the wave function $\chi_{aN_\xi}(q_\xi - q_\xi^{(a)})$ (Eq. (2.52)) in powers of the displacement according to

$$\chi_{aN_\xi}(q_\xi - q_\xi^{(a)}) = \sum_{n=0}^{\infty} \frac{(-q_\xi^{(a)})^n}{n!} \frac{d^n}{dq_\xi^n} \chi_{aN_\xi}(q_\xi)$$

$$= \exp\left\{ -\frac{i}{\hbar} q_\xi^{(a)} p_\xi \right\} \chi_{aN_\xi}(q_\xi), \tag{2.67}$$

where we have used the coordinate representation of the momentum operator for mode ξ, $\hat{p}_\xi = -i\hbar d/dq_\xi$. Using Eqs. (2.55) and (2.66), the exponent can be written in operator form as

$$-\frac{i}{\hbar} q_\xi^{(a)} \hat{p}_\xi = g_a(\xi)(C_\xi - C_\xi^+). \tag{2.68}$$

This suggests the introduction of the displacement operator according to

$$D^+(g_a(\xi)) = \exp\left\{ g_a(\xi)(C_\xi - C_\xi^+) \right\}. \tag{2.69}$$

Thus, if $|N_\xi\rangle$ corresponds to an eigenstate of some nonshifted reference oscillator Hamiltonian, the eigenstates of the shifted oscillator Hamiltonian can be generated as follows:

$$\left| N_\xi^{(a)} \right\rangle = \frac{1}{\sqrt{N_\xi!}} D^+(g_a(\xi))\, (C_\xi^+)^{N_\xi}\, \left| 0_\xi \right\rangle$$

$$= D^+(g_a(\xi))\, |N_\xi\rangle. \tag{2.70}$$

The displacement operator is unitary, that is

$$D^+(g_a(\xi)) = D(-g_a(\xi)) = D^{-1}(g_a(\xi)). \tag{2.71}$$

Further, the following useful property can be derived by expanding the displacement operator in a power series:

$$D(g_a(\xi))\, C_\xi^+\, D^+(g_a(\xi)) = [D(g_a(\xi))\, C_\xi\, D^+(g_a(\xi))]^+ = C_\xi^+ - g_a(\xi). \tag{2.72}$$

Changing from $g_a(\xi)$ to $-g_a(\xi)$, we directly conclude that

$$D^+(g_a(\xi))\, C_\xi^+\, D(g_a(\xi)) = C_\xi^+ + g_a(\xi). \tag{2.73}$$

Then, we can rewrite the vibrational Hamiltonian, (2.51), in the form

$$H_a^{(nm)} = U_a^{(0)} + \sum_\xi \hbar\omega_\xi \left[(C_\xi^+ + g_a(\xi))\, (C_\xi + g_a(\xi)) + \frac{1}{2} \right]$$

$$= U_a^{(0)} + \sum_\xi \hbar\omega_\xi \left[D^+(g_a(\xi))\, C_\xi^+ C_\xi\, D(g_a(\xi)) + \frac{1}{2} \right], \tag{2.74}$$

where we used the unitarity of the displacement operator.

Comparing Eqs. (2.74) and (2.51), we realize that the introduction of the displacement operator yields a very compact notation for the Hamiltonian of a set of harmonic oscillators whose equilibrium positions are displaced with respect to each other. We will encounter this situation in Chapters 6 and 7. There, the overlap integral between two shifted oscillator states will play an important role. Assuming $|\chi_{aM}\rangle$ and $|\chi_{bN}\rangle$ to be two normal mode eigenstates for a particular mode belonging to the electronic states a and b, respectively, the overlap integral can be written as (skipping the mode index)

$$\langle \chi_{aM} | \chi_{bN} \rangle = \langle M | D(g_a) D^+(g_b) | N \rangle. \tag{2.75}$$

In order to rewrite the product of the two displacement operators, we make use of the operator identity

$$e^{\alpha(A+B)} = e^{\alpha A} e^{\alpha B} e^{-\alpha^2 [A,B]/2}, \tag{2.76}$$

which holds if $[A, B]$ commutes with A and B. Here, α is some parameter. For the displacement operators, we obtain with the help of Eq. (2.62),

$$D(g_a) D^+(g_b) = D(\Delta g_{ab})$$
$$= e^{\Delta g_{ab} C^+} e^{-\Delta g_{ab} C} e^{-\Delta g_{ab}^2/2}, \tag{2.77}$$

with $\Delta g_{ab} = g_a - g_b$. The action of the exponential operator on the oscillator states is calculated using a Taylor expansion

$$e^{-\Delta g_{ab} C} |N\rangle = \sum_{n=0}^{N} \frac{(-\Delta g_{ab})^n}{n!} C^n |N\rangle$$
$$= \sum_{n=0}^{N} \frac{(-\Delta g_{ab})^n}{n!} \sqrt{\frac{N!}{(N-n)!}} |N - n\rangle, \tag{2.78}$$

where we made use of the properties (2.59) and (2.60). Applying the same expansion to the bra vector, we obtain for the matrix elements

$$\langle \chi_{aM} | \chi_{bN} \rangle = e^{-(\Delta g_{ab})^2/2} \sum_{m=0}^{M} \sum_{n=0}^{N} \frac{(-1)^n (\Delta g_{ab})^{m+n}}{m! n!}$$
$$\times \sqrt{\frac{M! N!}{(M-m)!(N-n)!}} \delta_{M-m, N-n}. \tag{2.79}$$

This overlap expression is called the *Franck–Condon factor* (see Chapter 6). The most apparent property of this overlap expression, Eq. (2.79), is certainly the fact that, due to the exponential prefactor, for any given pair of states, the overlap decreases upon increasing the shift between the two PESs. The elements of Eq. (2.79), which are diagonal in the vibrational quantum number, can be further simplified. Since $\delta_{N-m, N-n} = \delta_{mn}$, we have

$$\langle \chi_{aN} | \chi_{bN} \rangle = e^{-(\Delta g_{ab})^2/2} \sum_{n=0}^{N} \frac{(-1)^n (\Delta g_{ab})^{2n}}{n!^2} \frac{N!}{(N-n)!}$$
$$= e^{-(\Delta g_{ab})^2/2} L_N((\Delta g_{ab})^2), \tag{2.80}$$

where $L_N(x)$ is a Laguerre polynomial. We will discuss Franck–Condon factors in Chapter 6. A generalization to the case of different frequencies as well as a numerical recipe for an efficient calculation is given in Section 2.8.1.

2.5.3 Construction of System–Bath Models

Chemical reaction dynamics can be understood in terms of the adiabatic Born–Oppenheimer PES for nuclear motion.[12] Let us consider the simple example of a PES for an isomerization reaction shown in Figure 2.4. Suppose that initially the positions of the nuclei correspond to a reactant configuration (left minimum). The properties of nuclear motion in the vicinity of this minimum (equilibrium configuration) were considered in the previous section. In order to understand how the nuclei move to the right minimum corresponding to the product state, it is necessary to explore the properties of the PES away from the stationary points. For this purpose, we return to the general Hamiltonian

$$H_{\text{nuc}} = \sum_{n=1}^{3N_{\text{nuc}}} \frac{P_n^2}{2M_n} + U(R_1, \dots, R_{3N_{\text{nuc}}}). \tag{2.81}$$

This expression poses a serious problem for polyatomic molecules since the numerical calculation of a full $3N_{\text{nuc}}$–6-dimensional PES becomes prohibitive with increasing N_{nuc}. In practice, however, the case that all DOFs move appreciably during a reaction is rather unlikely. This observation suggests to separate all DOFs into *active* and *spectator* or *substrate* coordinates. This concept can be realized in several ways that differ in the way the substrate DOFs are treated and in the choice of the coordinate system.

First, let us consider the standard approach of quantum chemistry. Suppose that we have performed a search for stationary points and transitions states on the multidimensional PES (geometry optimization). For simplicity, we assume that there are two minima separated by a single transition state as shown in Figure 2.9.

This situation may correspond to an isomerization reaction occurring, for example in the course of intramolecular proton transfer (cf. Chapter 8). In order to learn more about the way the reaction takes from the reactant to the product well via the transition state, one can follow the so-called *minimum energy path*. This path is obtained by starting from the transition state configuration[13] and following the steepest descent path to the reactant and product well minima (see the solid line in Figure 2.9).[14]

------

12) As discussed in Section 2.3, in the general case it might be necessary to include the nonadiabatic coupling between PESs belonging to different electronic states.
13) In principle, one could also start at a minimum and follow the shallowest ascent path to the transition states. However, it is numerically very difficult to reach to transition state this way, because at a minimum the potential energy increases in *all* directions; at a transition state, there is only one downward path.
14) In practice, one follows the steepest descent path defined in mass-weighted coordinates, which can be viewed as the path taken by a particle of unit mass sliding down at high friction.
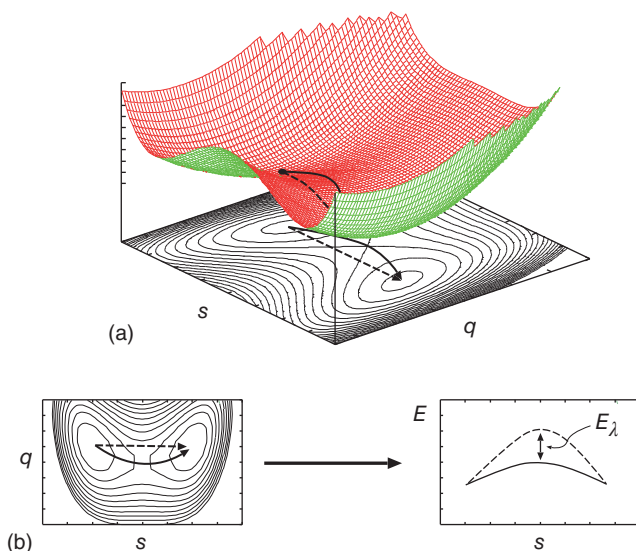
Figure 2.9 (a) Schematic plot of a two-dimensional PES. The coordinate *s* is a reaction coordinate, while *q* describes a harmonic vibration orthogonal to the reaction coordinate. Also shown is the minimum energy path (solid line) as well as a straight line path (dashed line) connecting the reactant and the product wells. In (b), we show the contour view (left) together with a cut along the straight line path where $q = 0$ (right). The energetic difference between both paths is the reorganization energy of the oscillator coordinate (see Eq. (2.91)) (figure courtesy of H. Naundorf).

The $3N_{\mathrm{nuc}}$-dimensional vector $R^{(p)}$, which points to the minimum energy path, defines a curve in the $3N_{\mathrm{nuc}}$-dimensional space of the nuclear coordinates. This curve $s = s(R^{(p)})$, which is the arc length along the minimum energy path, can be considered as the one-dimensional *reaction coordinate*. This one-dimensional description provides a valuable framework for the understanding of many reaction mechanisms. Looking at Figure 2.9 it becomes clear, however, that restricting the reaction *dynamics* to take place on the minimum energy path only may be a rather crude approximation. In many cases, the minimum energy path will be considerably curved in full $3N_{\mathrm{nuc}}$-dimensional space. Let us imagine a (classical) ball starting at the transition state with some very small velocity. It is clear that unless the ball moves very slowly down into the reactant/product valley, the trajectory of the ball will not follow the minimum energy path if this path is curved. This implies that a one-dimensional description of the dynamics is not adequate.

There are several ways to account for the motion away from the minimum energy path. In the following discussion we will outline a strategy leading to a Hamiltonian that is particularly suited for large molecules or condensed-phase situations as will be encountered in later chapters.[15] The first step consists in the identification of those Cartesian coordinates, which describe large displacements, $\boldsymbol{s} = (s_1, \ldots, s_{N_{\mathrm{rc}}})$.

---

15) For an alternative formulation, which is based on the minimum energy path and harmonic vibrations perpendicular to it, see Miller et al. [1].

These are the *active coordinates*. Typical choices are atomic coordinates or certain collective coordinates that span the relevant part of the PES. They are separated from the remaining $3N_{nuc} - N_{rc}$ *substrate coordinates* Z. The key assumption is that the substrate coordinates stay close to their equilibrium configurations $Z^{(0)}(s)$ during the reaction. As indicated, this equilibrium configuration may depend on the positions of the reaction coordinates s. As an example, consider the transfer of a light atom A between two heavy fragments B and C, that is B−A $\cdots$ C → B $\cdots$ A−C. Such a situation is typical for intramolecular hydrogen-transfer reactions, for instance (see Chapter 8). Proper choice of the coordinate system allows a one-dimensional treatment of the A atom motion along the coordinate s_1. The coordinates describing the fragments are then comprised into the vector Z.

Since the substrate atoms perform only small-amplitude motion around their equilibrium Positions, $U(R) = U(s, Z)$ can be expanded in terms of the deviations $\Delta Z(s) = (Z - Z^{(0)}(s))$ as follows:

$$U(R) \approx U(s, Z^{(0)}(s)) + \left(\frac{\partial U(s, Z)}{\partial Z} \right)_{Z=Z^{(0)}(s)} \Delta Z(s)$$
$$+ \frac{1}{2} \Delta Z(s) \left(\frac{\partial^2 U(s, Z)}{\partial Z \partial Z} \right)_{Z=Z^{(0)}(s)} \Delta Z(s). \tag{2.82}$$

The different terms have a straightforward interpretation: $U(s, Z^{(0)}(s))$ is the potential energy on the (in general multidimensional) Cartesian reaction surface, with the spectator DOFs frozen at some reference geometry. This can be, for example the equilibrium geometry of the spectator atoms at a given value of the reaction coordinates. The second term in Eq. (2.82) contains the forces exerted on the substrate atoms due to the motion of the important DOFs away from their equilibrium positions:

$$f(s) = - \left(\frac{\partial U(s, Z)}{\partial Z} \right)_{Z=Z^{(0)}(s)}. \tag{2.83}$$

Finally, the third term describes the Hessian matrix

$$\kappa(s) = \left(\frac{\partial^2 U(s, Z)}{\partial Z \partial Z} \right)_{Z=Z^{(0)}(s)} \tag{2.84}$$

(and thus of the vibrational frequencies) due to the motion along s.

Since the substrate atoms are assumed to perform small-amplitude harmonic motions, we can introduce normal modes. Note that the normal modes have to be defined with respect to some fixed reference configuration $Z^{(0)}(s_{ref})$ to preserve the decoupling from the external motions (rotations and translation). Thus, we have

$$\Delta Z(s) = Z - Z^{(0)}(s_{ref}) + Z^{(0)}(s_{ref}) - Z^{(0)}(s)$$
$$= M^{-1/2} A q + Z^{(0)}(s_{ref}) - Z^{(0)}(s), \tag{2.85}$$

where M is the diagonal matrix containing the atom masses, and A is the normal mode transformation matrix (see also Eq. (2.42)). Straightforward application of this transformation to the Hamiltonian with the potential equation (2.82) gives the

all-Cartesian form[16)]

$$H = T_s + U(s, Z^{(0)}(s)) + U_{\text{add}}(s, Z^{(0)}(s))$$
$$+ T_q + \frac{1}{2} q K(s) q - F(s) q. \tag{2.86}$$

Here, T_s and T_q are the diagonal kinetic energy operator for the reaction coordinates and the substrate modes, respectively, and the transformed Hessian is given by $K(s) = A^+ M^{-1/2} \kappa(s) M^{-1/2} A$. Note that it includes a coupling between different substrate modes due to the motion of the reaction coordinates away from the reference configuration s_{ref}. Since this motion is not restricted to some minimum energy path, there is also a force acting on the substrate modes

$$F(s) = \left[f(s) - (Z^{(0)}(s_{\text{ref}}) - Z^{(0)}(s)) \kappa(s) \right] M^{-1/2} A. \tag{2.87}$$

Finally, the special choice of the reference configuration for the definition of the normal modes leads to an additional potential defined by

$$U_{\text{add}}(s, Z^{(0)}(s)) = -f(s)(Z^{(0)}(s_{\text{ref}}) - Z^{(0)}(s))$$
$$+ \frac{1}{2} (Z^{(0)}(s_{\text{ref}}) - Z^{(0)}(s)) \kappa(s) (Z^{(0)}(s_{\text{ref}}) - Z^{(0)}(s)).. \tag{2.88}$$

Of course, not all substrate modes will couple strongly to the reaction coordinates. A convenient measure for this coupling is the substrate oscillator's displacement from their equilibrium value of zero taken at the reference geometry $Z^{(0)}(s_{\text{ref}})$, that is

$$q^{(0)}(s) = -[K(s)]^{-1} F(s). \tag{2.89}$$

Introducing this quantity into Eq. (2.86) yields after some rearrangement

$$H = T_s + U(s, Z^{(0)}(s)) + U_{\text{add}}(s, Z^{(0)}(s)) - E_\lambda(s)$$
$$+ T_q + \frac{1}{2} (q - q^{(0)}(s)) K(s) (q - q^{(0)}(s)). \tag{2.90}$$

Here, we introduced the so-called *reorganization energy* defined as

$$E_\lambda(s) = \frac{1}{2} q^{(0)}(s) K(s) q^{(0)}(s). \tag{2.91}$$

The interpretation of the substrate mode part of Eq. (2.90) (second line) is straightforward. It is the Hamiltonian for a set of shifted oscillators whose equilibrium positions depend on the coupling to the reaction coordinates. In our considerations of PESs for different electronic excited states we have already met this type of Hamiltonian. There, the shift of the PES was due to different electronic charge distributions in the considered electronic states. In the present case, the shift is a consequence of the motion of the reaction coordinates s away from a stationary point on the PES. This

---

16) Note that an arbitrary displacement of some active atom in general does not conserve linear and angular momenta of the total system. Strictly speaking, a rigorous treatment of the molecule's rotation would require the use of curvilinear coordinates and therefore destroy the all-Cartesian character of the Hamiltonian. However, since we focus on a description of large molecules or even condensed-phase reactions, rotation/translation does not play an important role. In the numerical implementation of this approach it is accounted for approximately by projecting out infinitesimal rotations and translations of the substrate atoms from the Hessian before performing the normal mode transformation (for details see Ruf and Miller [2]).

can be rationalized by looking at the two-dimensional case shown in Figure 2.9. Let us further assume that the configuration of the left minimum has served as a reference for the expansion in Eq. (2.82). Therefore, at this minimum, the force on the substrate oscillator is zero. Now, we move the reaction coordinate on a straight line toward the right potential well (dashed line). This force is trying to push the oscillator back to the minimum energy path (solid line). Restoring the equilibrium position of the substrate oscillator requires the reorganization energy $E_\lambda(\boldsymbol{s})$ as indicated in the lower right panel of Figure 2.9.

Keeping track of the dependence of the reference geometry for the spectator modes on the value of the reaction coordinates is important whenever one wishes to describe a reaction where reactants and products have quite different geometries and atomic reaction coordinates have been chosen. This is due to the fact that complex molecular rearrangements cannot be described effectively in terms of the change of just a few atomic coordinates, and the molecular skeleton has to be adjusted accordingly. On the other hand, collective reaction coordinates might be able to capture most of the rearrangements such that the references geometry for the harmonic expansion can be fixed, thus simplifying the resulting Hamiltonian (the additional potential as well as the second term in the force equation (2.87) vanish). A convenient choice for symmetric reactions such as isomerizations (cf. Figure 2.9) are the so-called reaction plane coordinates.[17] Suppose that we denote the $3N_{\mathrm{nuc}}$ vector pointing to the left and right minimum as well as to the transition state geometry by $\boldsymbol{R}^{(\mathrm{L})}$, $\boldsymbol{R}^{(\mathrm{R})}$, and $\boldsymbol{R}^{(\mathrm{TS})}$, respectively. Then, the following two vectors span a two-dimensional reaction plane:[18]

$$\boldsymbol{d}_1 = \frac{\boldsymbol{R}^{(\mathrm{R})} - \boldsymbol{R}^{(\mathrm{L})}}{|\boldsymbol{R}^{(\mathrm{R})} - \boldsymbol{R}^{(\mathrm{L})}|}, \tag{2.92}$$

$$\boldsymbol{d}_2 = \frac{\boldsymbol{R}^{(\mathrm{C})} - \boldsymbol{R}^{(\mathrm{TS})}}{|\boldsymbol{R}^{(\mathrm{C})} - \boldsymbol{R}^{(\mathrm{TS})}|}. \tag{2.93}$$

Here, we defined the center geometry $\boldsymbol{R}^{(\mathrm{C})} = (\boldsymbol{R}^{(\mathrm{R})} + \boldsymbol{R}^{(\mathrm{L})})/2$. The interpretation of these collective coordinates becomes clear by the inspection of the example in Figure 2.10. Here, hydrogen atom transfer in tropolon is described by a coordinate d_1 that essentially gives the hydrogen atom motion in transfer direction and a coordinate d_2 that accounts for the deformation of the skeleton, which takes place upon passing the transition state (cf. generic example in Figure 2.9).

Finally, we simplify the reaction surface Hamiltonian equation (2.90) to establish the contact with a widely used system-reservoir Hamiltonian. To this end, we neglect the change of the reference geometry as well as the coupling between different substrate modes. Furthermore, the normal mode frequencies are assumed to be independent of the reaction coordinate, that is we have $K_{\xi\xi'}(\boldsymbol{s}) \approx \delta_{\xi\xi'}\omega_\xi^2$. Then, the Hamiltonian can be written as $H = H_{\mathrm{S}} + H_{\mathrm{R}} + H_{\mathrm{S-R}}$, with H_{S} and H_{R} describing the motion of the system ($\boldsymbol{s}$) and bath (q_ξ) DOFs, respectively. $H_{\mathrm{S-R}}$ contains the

---

17) For the formulation and application to proton tunneling, see also Takada and Nakamura [3].
18) Note that $\boldsymbol{R}^{(\mathrm{L})}$ and $\boldsymbol{R}^{(\mathrm{R})}$ are unique only up to an arbitrary rotation. This arbitrariness can be removed by minimizing the distance $|\boldsymbol{R}^{(\mathrm{R})} - \boldsymbol{R}^{(\mathrm{L})}|$; likewise, $|\boldsymbol{R}^{(\mathrm{C})} - \boldsymbol{R}^{(\mathrm{TS})}|$ is minimized.
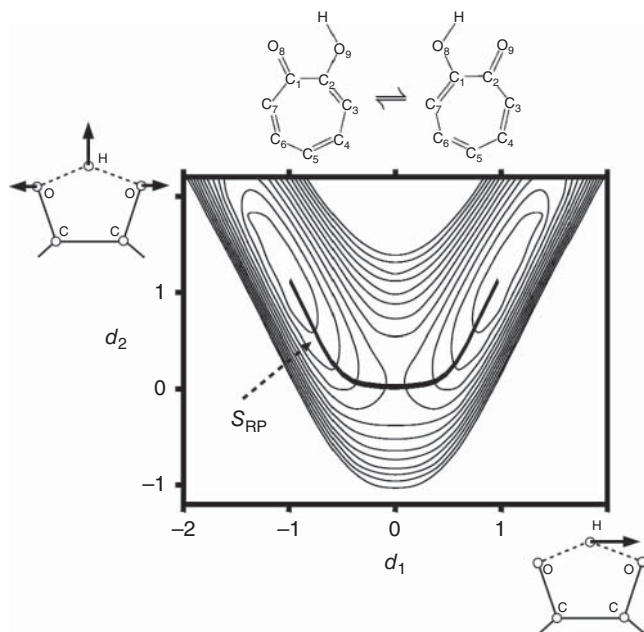
Figure 2.10 Two-dimensional Cartesian reaction plane for the hydrogen atom transfer in tropolon. The coordinates $d_{1/2}$ spanning the reaction plane are shown next to the axes. The solid line corresponds to the projection of the minimum energy path onto the reaction plane (coordinate units $a_0(a.m.u.)^{1/2}$, contour spacing is 500 cm^{-1}, and maximum contour at 6000 cm^{-1}) (figure courtesy of K. Giese).

interaction between both subsystems:

$$H_R + H_{S-R} = \frac{1}{2} \sum_{\xi=1}^{3N_{nuc}-N_{rc}-6} \left[p_\xi^2 + \omega_\xi^2 \left(q_\xi - \frac{F_\xi(s)}{\omega_\xi^2} \right)^2 \right], \tag{2.94}$$

where we used $q_\xi^{(0)}(s) = -F_\xi(s)/\omega_\xi^2$. With the reorganization energy given by $E_\lambda(s) = \sum_{\xi=1}^{3N_{nuc}-N_{rc}-6} F_\xi^2(s)/2\omega_\xi^2$, the renormalized system Hamiltonian becomes

$$H_S = \sum_{n=1}^{N_{rc}} \frac{p_n^2}{2M_n} + U(s, Z^{(0)}) - E_\lambda(s). \tag{2.95}$$

2.6 Adiabatic versus Diabatic Representation of the Molecular Hamiltonian

2.6.1 Adiabatic Picture

In Section 2.3, we gave the general form of the molecular wave function as (cf. Eq. (2.20))

$$\psi_M(r, R) = \sum_a \chi_{aM}(R) \, \phi_a(r; R). \tag{2.96}$$

In principle, the summation has to be carried out over the complete set of adiabatic electronic states. These states are possibly coupled through the nonadiabaticity operator (Eq. (2.17)). Fortunately, in practice, reasonable results are often obtained by including only a finite number of states in the actual calculation. This happens, for example if one is interested in the electronic excitation spectrum of a molecule, or if one wants to model photodissociation dynamics occurring upon irradiation by a laser having a certain fixed wavelength (see, for example Figure 2.1).

Let us suppose that we have obtained the adiabatic electronic wave function $\phi_a(r; R) = \langle r; R | \phi_a \rangle$. The representation of the molecular Hamiltonian in this electronic basis is then obtained as (using the definitions (2.17) and (2.21))

$$H_{\text{mol}}^{(\text{adia})} = \sum_{ab} \left(\delta_{ab} H_a(R) + (1 - \delta_{ab}) \Theta_{ab} \right) |\phi_a\rangle \langle\phi_b| . \tag{2.97}$$

Note that $H_a(R)$ and Θ_{ab} are still operators with respect to the nuclear coordinates. We can go one step further and write down the molecular Hamiltonian in the matrix representation of the adiabatic states $|\psi_{aM}\rangle = |\phi_a\rangle |\chi_{aM}\rangle$, which define the Born–Oppenheimer wave function (2.22), $\psi_{aM}^{(\text{adiab})}(r, R) = \langle r, R | \psi_{aM}\rangle$. We have

$$H_{\text{mol}}^{(\text{adia})} = \sum_{aM} \mathcal{E}_{aM} |\psi_{aM}\rangle \langle\psi_{aN}| + \sum_{aM,bN} \Theta_{aM,bN} |\psi_{aM}\rangle \langle\psi_{bN}| , \tag{2.98}$$

where we introduced

$$\Theta_{aM,bN} = \int dR \chi_{aM}^*(R) \left[\langle\phi_a| T_{\text{nuc}} |\phi_b\rangle \right. $$
$$\left. - \sum_n \frac{\hbar^2}{M_n} \langle\phi_a| \boldsymbol{\nabla}_n |\phi_b\rangle \boldsymbol{\nabla}_n \right] \chi_{bN}(R). \tag{2.99}$$

We note that the coupling is mediated by the momentum operator $\boldsymbol{P}_n = -i\hbar\boldsymbol{\nabla}_n$. It is therefore referred to as *dynamic coupling*, and its calculation requires knowledge of the first and second derivatives of the electronic wave function. This poses a computational challenge, especially for polyatomics. Further, the second term in Θ_{ab} is often rather sharply peaked if not singular, indicating that the character of the electronic wave function changes rapidly within a narrow range of configuration space (see Figure 2.11). Such a behavior of the coupling may cause numerical problems, for example in a quantum dynamical calculation based on the Hamiltonian (2.98) and using the methods which will be introduced in Chapter 3. On the other hand, since the adiabatic electronic states contain information on the instantaneous nuclear configuration, it can be expected that they will lead to a very compact representation of the molecular wave function.

2.6.2 Diabatic Picture

In what follows we will present an alternative to the adiabatic representation of the Hamiltonian. Let us consider an electronic basis $\phi_a(r; R^{(0)})$, where the positions of the nuclei are *fixed* at some point $R^{(0)}$ in configuration space. A typical choice for $R^{(0)}$ could be, for instance some local minimum of the PES in the electronic state
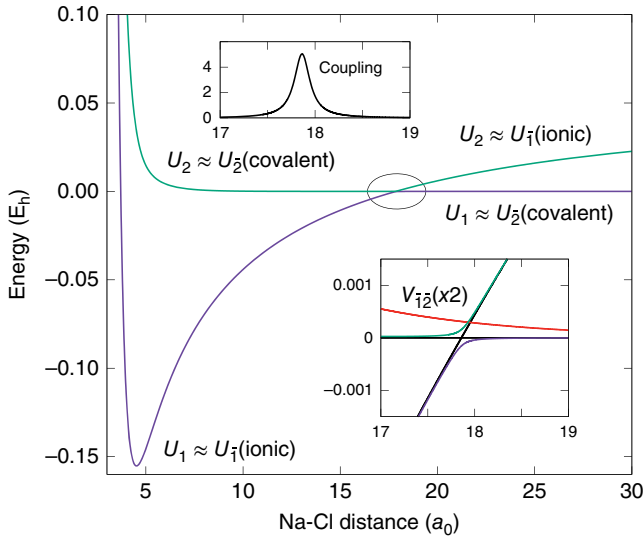
Figure 2.11 Potential energy curves for the ground and the lowest excited states of NaCl. In the vicinity of the ground state equilibrium bond length, the ground and the excited adiabatic states are of ionic and covalent characters, respectively. In the asymptotic region this energetic order is reversed. The nature of the electronic states changes in the region around 17.9 a_0. As a consequence, the nonadiabatic coupling $\propto \left\langle \phi_1 | \nabla_n | \phi_2 \right\rangle$ takes large values (upper inset), and there is an avoided crossing between the adiabatic curves (lower inset). The diabatic potential curves essentially coincide with the adiabatic ones, except in the crossing region. Here, the diabatic curves (black lines) cross, and their coupling is given by $V_{\overline{12}}$ (lower inset) (Reproduced with permission from Persico and Granucci [4]/Springer Nature).

a. Of course, $\phi_a(r; R^{(0)})$ is no longer an eigenfunction of H_{el} except at $R^{(0)}$. Defining $H_{el}(R^{(0)}) = H^{(0)}$, the electronic Hamiltonian can be written as

$$H_{el}(R) = H^{(0)}(R^{(0)}) + V(R, R^{(0)}), \tag{2.100}$$

with the potential coupling given by

$$V(R, R^{(0)}) = H_{el}(R) - H^{(0)}(R^{(0)}). \tag{2.101}$$

The molecular wave function expanded in this so-called *diabatic* basis set[19] reads

$$\psi(r, R) = \sum_{\bar{a}} \chi_{\bar{a}}(R) \, \phi_{\bar{a}}(r; R^{(0)}), \tag{2.102}$$

where we have used the quantum number $\bar{a}$ to distinguish diabatic states from adiabatic ones.

Suppose that the diabatic basis is complete, and the summations in Eqs. (2.96) and (2.102) are carried out with respect to the whole set of quantum numbers; both representations will give identical results. In practice, however, one is interested only in a certain subset of the electronic state manifold in order to model some property of the

———

19) Note that the special choice of $\phi_a(r; R^{(0)})$ as a diabatic basis is sometimes also called crude adiabatic basis.

molecule. Since $\phi_{\bar{a}}(r; R^{(0)})$ does not account for the change in nuclear configuration, it can in general be assumed that the diabatic representation is not as compact as the adiabatic one. Thus, more terms in the expansion (2.102) may be needed to represent some feature of the molecular wave function. On the other hand, all matrix elements of the nonadiabaticity operator vanish because the diabatic basis functions are not R-dependent. The coupling between different electronic states is now due to $V(R; R^{(0)})$ defined in Eq. (2.101); the respective matrix elements are $V_{\bar{a}\bar{b}}(R; R^{(0)}) = \left\langle \phi_{\bar{a}} \right| V(R, R^{(0)}) \left| \phi_{\bar{b}} \right\rangle$. Thus, the representation of the molecular Hamiltonian in terms of the diabatic electronic states is

$$H_{\text{mol}}^{(\text{diab})} = \sum_{\bar{a}\bar{b}} \left(\delta_{\bar{a}\bar{b}} H_{\bar{a}} + (1 - \delta_{\bar{a}\bar{b}}) V_{\bar{a}\bar{b}} \right) \left| \phi_{\bar{a}} \right\rangle \left\langle \phi_{\bar{b}} \right|. \tag{2.103}$$

Here, we introduced the Hamiltonian for the motion of the nuclei in the diabatic electronic state $\left| \phi_{\bar{a}} \right\rangle$ as

$$H_{\bar{a}}(R) = T_{\text{nuc}} + U_{\bar{a}}(R), \tag{2.104}$$

with

$$U_{\bar{a}}(R) = E_{\bar{a}}(R^{(0)}) + V_{\text{nuc-nuc}} + V_{\bar{a}\bar{a}}(R, R^{(0)}) \tag{2.105}$$

being the diabatic PES. The $E_{\bar{a}}(R^{(0)})$ are the diabatic electronic energies according to $H^{(0)}$. The shift of the electronic state coupling from the kinetic to the potential energy operator is the general feature for a diabatic basis as compared to the adiabatic basis.

It is straightforward to derive the equation for the expansion coefficients in (2.102), that is the diabatic nuclear wave functions, along the lines outlined in Section 2.3. One obtains

$$(H_{\bar{a}}(R) - \mathcal{E}) \chi_{\bar{a}}(R) = -\sum_{\bar{b} \neq \bar{a}} V_{\bar{a}\bar{b}}(R, R^{(0)}) \chi_{\bar{b}}(R) \tag{2.106}$$

Neglecting the coupling between different states, we get

$$H_{\bar{a}}(R) \chi_{\bar{a}M}(R) = \mathcal{E}_{\bar{a}M} \chi_{\bar{a}M}(R). \tag{2.107}$$

The solutions of this equation, $\chi_{\bar{a}M}(R)$, together with the diabatic electronic states can be used to define the molecular Hamiltonian in the diabatic representation $(\left| \psi_{\bar{a}M} \right\rangle = \left| \phi_{\bar{a}} \right\rangle \left| \chi_{\bar{a}M} \right\rangle)$,

$$H_{\text{mol}}^{(\text{diab})} = \sum_{\bar{a}M} \mathcal{E}_{\bar{a}M} \left| \psi_{\bar{a}M} \right\rangle \left\langle \psi_{\bar{a}M} \right| + \sum_{\bar{a}M, \bar{b}N} V_{\bar{a}M, \bar{b}N} \left| \psi_{\bar{a}M} \right\rangle \left\langle \psi_{\bar{b}N} \right|. \tag{2.108}$$

Here, $E_{\bar{a}M}$ are the eigenvalues following from Eq. (2.107) and

$$V_{\bar{a}M, \bar{b}N} = \int dR \; \chi_{\bar{a}M}^*(R) V_{\bar{a}\bar{b}}(R, R^{(0)}) \chi_{\bar{b}N}(R). \tag{2.109}$$

In contrast to the adiabatic representation, the Hamiltonian matrix contains only coupling terms between different electronic states, which stem from the potential energy operator. To distinguish this from the dynamic coupling, the potential coupling is called *static*. Static couplings are usually not as sharply peaked as dynamic ones and in general easier to treat in numerical applications (see Figures 2.11).

But, as already pointed out for a choice such as the crude adiabatic basis, it may be required to take into account many terms in the expansion of the total wave function. Thus, the dimension of the diabatic Hamiltonian matrix in this case is likely to be higher than that of the adiabatic matrix.

Quantum chemical ab initio calculations usually provide adiabatic PESs and wave functions. Thus, the question arises whether it is possible to construct a diabatic basis that provides a compact representation of the molecular wave function.

Having a broad definition of a diabatic representation, it should be clear that the crude adiabatic basis, $\phi_{\bar{a}}(r; R^{(0)})$, is not the only possible choice of a diabatic basis. In general, one can argue that any complete basis set is suited that solves the stationary Schrödinger equation for a part of the Hamiltonian and yields negligibly small matrix elements of the nonadiabaticity operator. The potential coupling term has to be properly adjusted for each case. A typical situation will be encountered in Chapter 7, where electron transfer in donor–acceptor complexes is considered. In this case, one can define the local electronic states with respect to the donor and acceptor groups.

An alternative can be developed by starting from a diabatic basis which is constructed in a way that certain properties such as the dipole moments of the molecule behave smoothly. A related constraint is that the electronic wave function should not change appreciably when moving in the configuration space of the nuclear coordinates. Thus, diabatic wave functions for neighboring points should overlap considerably. The simplest approach in this respect is certainly to use some parameterized form for the diabatic potential surface, the static coupling, and if necessary also for other quantities such as the dipole moment. The parameters are then chosen to make observables, for example those relevant for dynamic processes, agree with the experiment.

2.6.3 Two-State Case

In this section, we focus on the adiabatic-to-diabatic transformation and the resulting shapes of the PES for the case of two electronic states and a single nuclear coordinate R (cf. Figure 2.11). Thereby, we will make use of the results for the diagonalization of a coupled two-state Hamiltonian derived in Section 2.8.2. Labeling the adiabatic states as $a = \pm$, Eq. (2.97) becomes in matrix notation (assuming $\Theta_{aa} = 0$)

$$H_{\text{mol}}^{(\text{adia})} = \begin{pmatrix} T_{\text{nuc}} & \Theta_{+-} \\ \Theta_{+-} & T_{\text{nuc}} \end{pmatrix} + \begin{pmatrix} U_+(R) & 0 \\ 0 & U_-(R) \end{pmatrix}. \tag{2.110}$$

For the diabatic states denoted as $\bar{a} = 1,2$, Eq. (2.103) becomes

$$H_{\text{mol}}^{(\text{diab})} = \begin{pmatrix} T_{\text{nuc}} & 0 \\ 0 & T_{\text{nuc}} \end{pmatrix} + \begin{pmatrix} U_1(R) & V_{12}(R) \\ V_{12}(R) & U_2(R) \end{pmatrix}. \tag{2.111}$$

The two representations are related by an orthogonal transformation; for instance, we can express the adiabatic states in terms of the diabatic states:

$$|\phi_\pm\rangle = \sum_{\bar{a}=1,2} C_\pm(\bar{a}) \, |\phi_{\bar{a}}\rangle. \tag{2.112}$$

The coefficients $C_a(\bar{a})$ were determined in Section 2.8.2 (cf. Eqs. (2.171) and (2.172), for instance). They depend on the so-called *mixing angle*, Eq. (2.170), which in the present case will depend on the coordinate R, that is

$$\gamma(R) = \frac{1}{2} \arctan \left(\frac{2|V_{12}(R)|}{|U_1(R) - U_2(R)|} \right). \tag{2.113}$$

The adiabatic potentials following from the diabatic ones upon including the coupling reads (Eq. (2.153))

$$U_{\pm}(R) = \frac{1}{2} \left(U_1(R) + U_2(R) \pm \sqrt{[U_1(R) - U_2(R)]^2 + 4|V_{12}(R)|^2} \right). \tag{2.114}$$

In Figure 2.12, diabatic and adiabatic potentials as well as expansion coefficients are shown for the case where the diabatic states are described by two shifted harmonic oscillator potentials. For the coupling $V_{12}(R)$, a Gaussian form centered at the crossing point, $R = R_c = 0$, has been chosen. While the diabatic potentials cross at R_c, the adiabatic ones show a splitting of $2|V_{12}(R_c)|$. This can be rationalized as follows: The crossing condition for the diabatic potentials, $U_1(R) = U_2(R)$, can in principle be fulfilled for any R. For the adiabatic ones, according to Eq. (2.114), the conditions $U_1(R) = U_2(R)$ *and* $V_{12}(R) = 0$ should be fulfilled simultaneously to obtain a crossing. Thus, unless $V_{12}(R)$ vanishes due to the symmetry of the diabatic wave functions, the crossing of the diabatic potentials is replaced by an *avoided crossing* of the adiabatic ones. The case $V_{12}(R) = 0$ usually occurs if the symmetry of the two diabatic
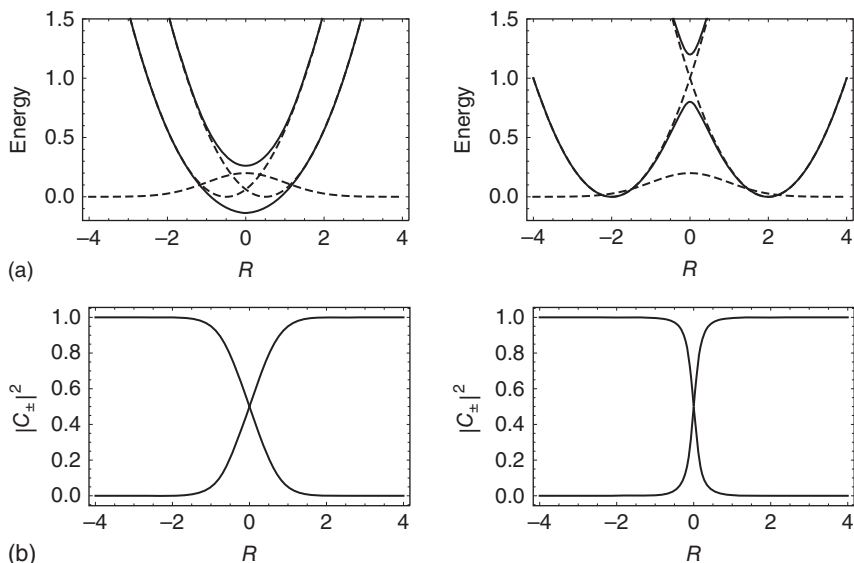
Figure 2.12 (a) Diabatic (dashed) and adiabatic (solid) potential energy curves for two shifted diabatic oscillator potentials coupled by a diabatic coupling V_{12} (dashed). (b) Coordinate-dependent expansion coefficients, Eq. (2.112). The two columns correspond to two different values of the displacement between the coupled diabatic oscillator potentials.

states is different. Because diabatic and adiabatic Hamiltonians describe the same molecular system, adiabatic potential curves of states having the same symmetry will not cross, which is called the *noncrossing rule*.

Returning to Figure 2.12, we further notice that the change in the character of the wave function is restricted to a range around the crossing where $V_{12}(R)$ takes values comparable to the energy gap. Comparing the left and right columns it becomes clear that the actual shape of the adiabatic potentials, for instance single versus double well, is dictated by the form of the diabatic potential curves.

The situation is different in polyatomic molecules. Here, the crossing conditions $U_1(R) = U_2(R)$ and $V_{12}(R) = 0$ can be simultaneously fulfilled even for states having the same symmetry. However, for an N-dimensional PES these are only two conditions, that is the crossing will only be in $N - 2$ dimensions (if $V_{12}(R) = 0$ due to symmetry, the crossing is in $N - 1$ dimensions only). For instance, in the two-dimensional case, the PES of two electronic states of the same symmetry will intersect in a single point ($N - 2 = 0$). The topography of the PES in the vicinity of this point is that of a double cone and usually called a *conical intersection* (this was first introduced by E. Teller in 1937). A numerical example is shown in Figure 2.13. A frequently used model Hamiltonian describing this situation will be discussed in Section 6.6.2.

2.7 Condensed-phase Approaches

In the previous sections we were concerned with the electronic structure of poly-atomic molecules and their parametric dependence on the positions of the nuclei. The numerical effort for calculating ground state energies or PES clearly prohibits an application to systems of hundreds of interacting molecules or to macroscopic systems such as molecules in solution.

A straightforward but approximate solution of this problem is the inclusion of a few solvent molecules or, if possible, the first solvation shell into the quantum chemical calculation. This so-called supermolecule approach has the advantage that short-range interactions between solute and solvent molecules are reasonably accounted for. Thus, one can learn about the local structure of the solvent around the solute. Such a treatment is necessary, for instance to describe the formation of hydrogen bonds that may occur if the solvent is water.

The long-range electrostatic interactions are, of course, not included in the super-molecule approach. They are, however, accounted for in the so-called continuum models, which are in turn applicable whenever short-range interactions are negligible. The model implies that we discard the discrete nature of the solvent and treat it as a homogeneous entity fully characterized by its macroscopic properties. This approach will be discussed in Section 2.7.1. Indeed, it is flexible enough to accommodate the supermolecule approach yielding a mixed description that may distinguish between the first solvation shell and the rest of the solvent. Another strategy is followed in the so-called Quantum Mechanics/Molecular Mechanics (QM/MM) approach, where a quantum chemical calculation of the solute or an active site is
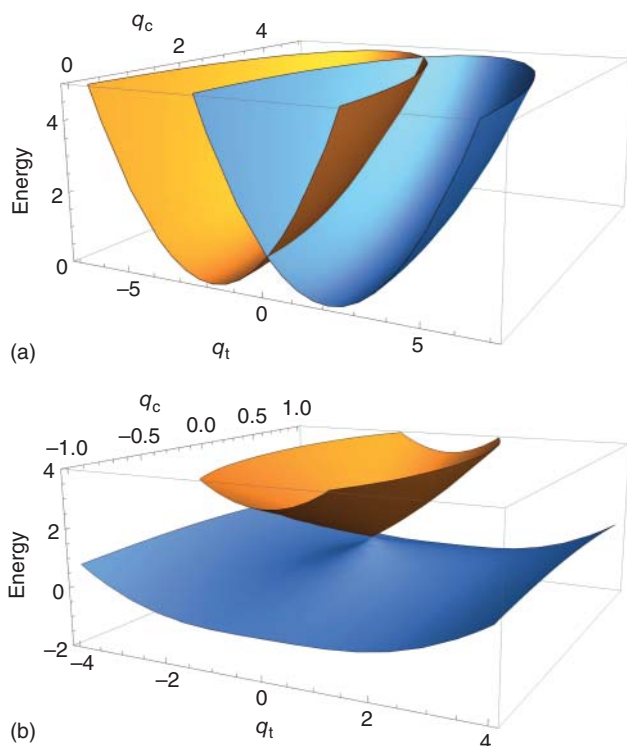
Figure 2.13 (a) Two intersection diabatic harmonic PESs along the so-called tuning and coupling coordinates q_t and q_c, respectively. (b) Adiabatic PES obtained by including a coupling of the form $V_{12} \propto q_c$.

combined with point charges resulting from a classical but atomistic treatment of the environment. The QM/MM approach will be addressed in Eq. (2.138).

2.7.1 Dielectric Continuum Model

In the following section, we give a brief summary of some concepts of classical electrostatics. The selection will provide a background for the reaction field approach discussed in Section 2.7.1.2 as well as for the elaboration of electron-transfer theory in Chapter 7.

2.7.1.1 Medium Electrostatics

Consider a solvent in a container whose dimension is such that the effects due to the walls can be neglected. If there are no free charges, the solvent is a *dielectric*. The mth solvent molecule can be characterized by its charge density distribution $\rho_m(\boldsymbol{x})$. Using the definition of Section 2.2, the classical expression for $\rho_m(\boldsymbol{x})$ reads

$$\rho_m(\boldsymbol{x}) = -e \sum_{j=1}^{N_{\text{el}}^{(m)}} \delta(\boldsymbol{x} - \boldsymbol{r}_j^{(m)}) + e \sum_{n=1}^{N_{\text{nuc}}^{(m)}} z_n^{(m)} \delta(\boldsymbol{x} - \boldsymbol{R}_n^{(m)}), \tag{2.115}$$

where the additional index m is used to label the respective molecule here and in what follows.

For the present electrostatic considerations, it suffices to consider the stationary version of Maxwell's equations $\nabla E(x) = 4\pi\rho(x)$ and $\nabla \times E(x) = 0$, which enables one to compute the electric field $E(x)$ induced by the complete molecular charge distribution

$$\rho(x) = \sum_m \rho_m(x). \tag{2.116}$$

The field is related to the scalar potential by $E(x) = -\nabla\Phi(x)$. The scalar potential can be obtained from the Poisson equation $\Delta\Phi(x) = -4\pi\rho(x)$, which gives

$$\Phi(x) = \int d^3x' \frac{\rho(x')}{|x - x'|}. \tag{2.117}$$

Often, the complete information on the microscopic electric field contained in these expressions is of little practical use. In many experiments, one is only interested in macroscopic quantities, which are *averaged* with respect to their microscopic contributions. This averaging is equivalent to the elimination of the short-range part of the field from all expressions.

In order to explore this point further, let us assume that we have divided the macroscopic probe volume into smaller volumes $\Delta V(x_s)$ that still contain a large number of molecules. Here, x_s is a vector pointing to the sth small volume (see Figure 2.14). Replacing the total integration of Eq. (2.117) by integrations with respect to the $\Delta V(x_s)$, we get

$$\Phi(x) = \sum_s \int_{\Delta V(x_s)} d^3x' \frac{\rho(x')}{|x - x'|}. \tag{2.118}$$

We are only interested in the long-range contributions of the charges located in $\Delta V(x_s)$ to the potential. Therefore, we take x to be far away from x_s such that $|x - x_s| \gg |x' - x_s|$. This inequality enables us to expand the factor $|x - x'|^{-1}$ into a Taylor series with respect to $x' - x_s$. Keeping only the first two terms, we get

$$\frac{1}{|x - x_s - (x' - x_s)|} \approx \frac{1}{|x - x_s|} - (x' - x_s)\nabla_x \frac{1}{|x - x_s|}. \tag{2.119}$$

Inserting this into Eq. (2.118), one obtains the first two contributions of the so-called *multipole expansion* of $\Phi(x_s)$. The monopole term

$$\Phi_{\mathrm{mp}}(x) = \sum_s \frac{1}{|x - x_s|} \int_{\Delta V(x_s)} d^3x' \, \rho(x') \tag{2.120}$$

corresponds to the potential of a point charge located at $x = x_s$. If there is no net charge in $\Delta V(x_s)$ this contribution vanishes. Introducing the *dipole moment* of $\Delta V(x_s)$ as

$$d_s = \int_{\Delta V(x_s)} d^3x' \, (x' - x_s)\rho(x'), \tag{2.121}$$

the second term in the above expansion can be written as

$$\Phi_{dp}(\boldsymbol{x}) = \sum_s \boldsymbol{d}_s \frac{\boldsymbol{x} - \boldsymbol{x}_s}{|\boldsymbol{x} - \boldsymbol{x}_s|^3}. \tag{2.122}$$

The dipole moment is the quantity we will be concerned with in the following discussion of dielectric media. In the spirit of the Taylor expansion (2.119), the contribution of higher-order multipole moments is usually small compared to the dipole term. An important exception occurs if the dipole moment vanishes for symmetry reasons.

The dipole moment of the small volume element $\boldsymbol{d}_s$ can of course be traced to the individual molecular dipole moments. We have

$$\boldsymbol{d}_s = \sum_{m \in \Delta V(\boldsymbol{x}_s)} \boldsymbol{d}_m, \tag{2.123}$$

with

$$\boldsymbol{d}_m = \int d^3\boldsymbol{x}' \boldsymbol{x}' \rho_m(\boldsymbol{x}'). \tag{2.124}$$

Apparently, whether a molecule has a permanent dipole moment or not is determined by its symmetry. Systems such as CCl_4 or diatomics such as H_2 or N_2 do not have a permanent dipole; the dielectric is nonpolar. However, application of an external field can lead to a distortion of the molecular charge density and in this way induce a dipole moment. On the other hand, H_2O and NH_3, for instance, do have a permanent dipole and form polar dielectrics (see Figure 2.14).

For the description of the behavior of the dielectric in some external field, for example, it is customary to introduce the dipole density or the *polarization*, which is defined as

$$\boldsymbol{P}(\boldsymbol{x}_s) = \frac{\boldsymbol{d}_s}{\Delta V(\boldsymbol{x}_s)}. \tag{2.125}$$

Suppose that the discrete nature of our subdivision into the $\Delta V(\boldsymbol{x}_s)$ can be neglected. Then, $\boldsymbol{x}_s$ becomes a continuous quantity, and we can write the macroscopic potential in dipole approximation and under the assumption of charge neutrality as

$$\begin{aligned}
\Phi_{mac}(\boldsymbol{x}) &= \sum_s \boldsymbol{d}_s \frac{\boldsymbol{x} - \boldsymbol{x}_s}{|\boldsymbol{x} - \boldsymbol{x}_s|^3} \approx \int d^3\boldsymbol{x}' \, \boldsymbol{P}(\boldsymbol{x}') \frac{\boldsymbol{x} - \boldsymbol{x}'}{|\boldsymbol{x} - \boldsymbol{x}'|^3} \\
&= \int d^3\boldsymbol{x}' \, \boldsymbol{P}(\boldsymbol{x}') \nabla_{\boldsymbol{x}'} \frac{1}{|\boldsymbol{x} - \boldsymbol{x}'|} = -\int d^3\boldsymbol{x}' \frac{\nabla_{\boldsymbol{x}'} \boldsymbol{P}(\boldsymbol{x}')}{|\boldsymbol{x} - \boldsymbol{x}'|}.
\end{aligned} \tag{2.126}$$

(a)   (b)
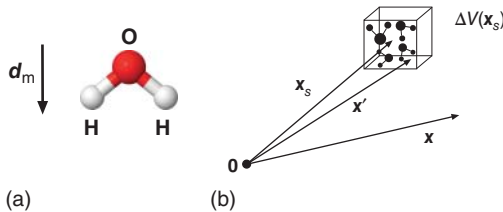
Figure 2.14 (a) Dipole moment of H_2O (left). (b) Macroscopic electrostatic quantities are obtained by averaging over the volume elements $\Delta V(\boldsymbol{x}_s)$. The $\Delta V(\boldsymbol{x}_s)$ contain a large number of individual molecules but have a dimension small enough to neglect the discrete nature of the vector $\boldsymbol{x}_s$ pointing to it. The distance $|\boldsymbol{x} - \boldsymbol{x}_s|$ should be large.

Here, the integration is with respect to the entire probe volume. Furthermore, the last line has been obtained by making use of the Gauss theorem.

Comparison of this expression with Eq. (2.118) suggests the interpretation of $-\nabla P$ as a charge density. Specifically, we can define the (macroscopic) polarization charge density

$$\rho_P(\boldsymbol{x}) = -\nabla \boldsymbol{P}(\boldsymbol{x}). \tag{2.127}$$

Besides this density, an additional externally controlled charge density ρ_{ext} may be present. By this, we mean, for example, the charge density is introduced in a dielectric if a solute molecule is placed into it (see below). Note that we are only interested in the long-range contribution of the solute to the electric field. The equation for the macroscopic electric field in the medium is then given by

$$\nabla \boldsymbol{E}_{\text{mac}}(\boldsymbol{x}) = 4\pi(\rho_{\text{ext}}(\boldsymbol{x}) + \rho_P(\boldsymbol{x})). \tag{2.128}$$

Defining the dielectric displacement vector as

$$\boldsymbol{D} = \boldsymbol{E}_{\text{mac}} + 4\pi \boldsymbol{P}, \tag{2.129}$$

the macroscopic source equation becomes

$$\nabla \boldsymbol{D}(\boldsymbol{x}) = 4\pi \rho_{\text{ext}}(\boldsymbol{x}). \tag{2.130}$$

According to this relation, the dielectric displacement field can be interpreted as the *external* field.

So far, we discussed how a given charge distribution of the medium results in an electric field. But one can also ask the question: how an external field leads to a change in the medium charge distribution? Within the present approach, the answer to this question is that the polarization of the medium will be an unknown functional of the total macroscopic electric field, $\boldsymbol{P} = \boldsymbol{P}[\boldsymbol{E}_{\text{mac}}]$. If we assume that the perturbation of the medium due to the electric field is weak, a Taylor expansion of the polarization in terms of $\boldsymbol{E}_{\text{mac}}$ is justified. In linear approximation, the relation between the electric field and the polarization is expressed in terms of the so-called linear *susceptibility* χ as

$$\boldsymbol{P}(\boldsymbol{x}) = \chi \boldsymbol{E}_{\text{mac}}(\boldsymbol{x}). \tag{2.131}$$

Here, we assumed that the medium is homogeneous and isotropic. In general, however, the susceptibility is a tensor, that is the vectors of the polarization and the electric field do not have to be parallel. Further, for an inhomogeneous medium, the relation between polarization and electric field may be nonlocal in space. One can introduce the dielectric constant

$$\varepsilon = 1 + 4\pi \chi \tag{2.132}$$

and write

$$\boldsymbol{E}_{\text{mac}}(\boldsymbol{x}) = \varepsilon^{-1} \boldsymbol{D}(\boldsymbol{x}). \tag{2.133}$$

This expression shows that the total macroscopic field $\boldsymbol{E}_{\text{mac}}(\boldsymbol{x})$ results from the response of the medium to the external field. The response properties of the medium are contained in the inverse dielectric function.

Finally, we give the expression for the potential energy of a charge distribution:

$$W = \frac{1}{2} \int d^3\boldsymbol{x}\, \rho(\boldsymbol{x})\Phi(\boldsymbol{x}). \tag{2.134}$$

2.7.1.2 Reaction Field Model

In this section we address the influence a continuously distributed solvent has on the solute's electronic properties. In principle, we expect the following behavior: The solute's electrons and nuclei feel the charge of the solvent molecules and vice versa. As a result, the charge distribution in the solute changes and, consequently, its electronic spectrum. But at the same time, the charge distribution of the solvent is rearranged too.

In what follows, this situation will be discussed using a model where the solute is treated by its electronic Schrödinger equation, and the solvent enters through its macroscopic dielectric properties. The solute molecule is placed inside a *cavity* (V_{cav} with dielectric constant equal to 1 (vacuum)) within the dielectric (V_{sol}). We will assume for simplicity that the solvent is homogeneous and isotropic, that is we can characterize it by a dielectric constant ε_{sol}. This neglects, for instance the effects coming from a locally inhomogeneous distribution of the solvent molecules in the first solvation shell.

The first important step is the definition of the size and the shape of the cavity. Various cavity shapes are possible, which should in the ideal case give a reasonable approximation to the molecular charge distribution. The simplest and most approximate model is that of a spherical cavity. More elaborate calculations could be based, for instance on the union of overlapping spheres centered at the different nuclei (see Figure 2.15). The size of the cavity is also an important parameter. In particular, one must be aware that serious errors can be expected if the cavity size is too small to accommodate most of the charge distribution as described by the molecular wave function. Thus, we assume that the solute's charge distribution, $\rho_{mol}(\boldsymbol{x})$, is confined inside V_{cav}.
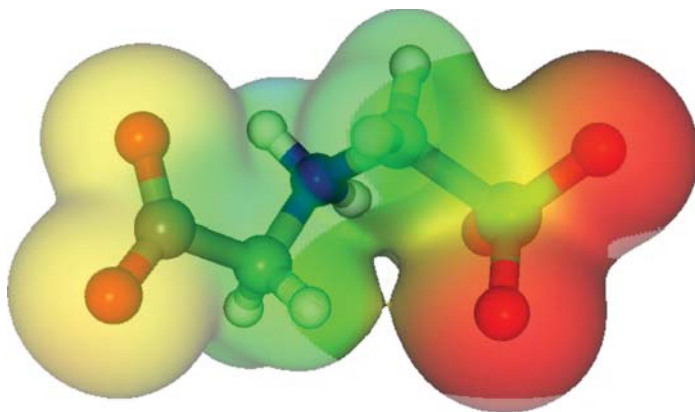
Figure 2.15 Molecule (doubly-charged glyphosate) and cavity within a dielectric continuum (water). The gray scale on the surface of the enclosing cavity is drawn to illustrate the variation of the electrostatic potential $\Phi_{pol}(\boldsymbol{x})$ (figure courtesy of A. Ahmed).

Provided that the molecular charge distribution $\rho_{mol}(\boldsymbol{x})$ is given and the size and the shape of the cavity have been defined, we still have to account for the coupling between solvent and solute. In the spirit of the dielectric continuum description of the solvent, the exact microscopic Coulomb interaction (cf. Eq. (2.1)) is approximated by the respective expressions for a dielectric discussed in Section 2.7.1.1.

We first note that the solute's charge distribution generates an electrostatic potential which is obtained from $\Delta\Phi(\boldsymbol{x}) = -4\pi\rho_{mol}(\boldsymbol{x})$ inside the cavity and from $\Delta\Phi(\boldsymbol{x}) = 0$ within V_{sol}. The boundary conditions at the cavity surface are given by $\Phi(\boldsymbol{x} \in V_{cav}) = \Phi(\boldsymbol{x} \in V_{sol})$ and $\partial\Phi(\boldsymbol{x} \in V_{cav})/\partial\boldsymbol{n} = \varepsilon_{sol}\partial\Phi(\boldsymbol{x} \in V_{sol})/\partial\boldsymbol{n}$. Here, $\boldsymbol{n}$ is a unit vector on cavity surface pointing outward.

The potential of the solute's charge density induces a polarization of the dielectric. This polarization gives rise to a potential $\Phi_{pol}(\boldsymbol{x})$. In the present case, $\Phi_{pol}(\boldsymbol{x})$ depends on the polarization charge densities that are induced at the cavity surface. The total electrostatic potential inside V_{cav} is therefore $\Phi_{pol}(\boldsymbol{x}) + \Phi(\boldsymbol{x})$. According to Eq. (2.134), we can calculate the interaction energy (polarization energy) between the solute's charge distribution and the induced so-called *reaction field* as follows:

$$W_{pol} = \frac{1}{2} \int d^3\boldsymbol{x} \, \rho_{mol}(\boldsymbol{x})\Phi_{pol}(\boldsymbol{x}). \tag{2.135}$$

In a next step, the electrostatic problem has to be linked to the QM treatment of the solute molecule. This is straightforwardly done by replacing the discrete classical charge distribution in Eq. (2.135) by the QM expectation value of the respective charge density operator: $\rho_{mol}(\boldsymbol{x}) \rightarrow \left\langle \hat{\rho}_{mol}(\boldsymbol{x}) \right\rangle$. It is customary to stay with a classical description of the nuclei such that $\left\langle \hat{\rho}_{mol}(\boldsymbol{x}) \right\rangle = \rho_{nuc}(\boldsymbol{x}) + \left\langle \hat{\rho}_{el}(\boldsymbol{x}) \right\rangle$. Here, the nuclear and the electronic parts are given by the second term in Eq. (2.8) and the first term in Eq. (2.9), respectively. Using the Born–Oppenheimer separation of electronic and nuclear motions, the integration in (2.9) is performed with respect to an adiabatic electronic state for a fixed nuclear configuration. In order to incorporate the effect of the continuous dielectric on the solute's electronic properties, we have to interpret W_{pol} as the expectation value of the single-particle operator

$$\hat{V}_{int} = \frac{1}{2} \int d^3\boldsymbol{x}\hat{\rho}_{mol}(\boldsymbol{x})\Phi_{pol}(\boldsymbol{x}). \tag{2.136}$$

Within Hartree–Fock theory, this operator is simply added to the single-particle Hamiltonian in the Fock operator in Eq. (2.28).

At this point, it is important to notice that $\Phi_{pol}(\boldsymbol{x})$ itself depends on the molecular charge distribution. This makes the determination of the electronic states of the solute a nonlinear problem which has to be solved *iteratively*: starting from some initial guess for the reaction field potential, one first calculates the charge distribution of the molecule. The resulting potential is then used to generate a new $\Phi_{pol}(\boldsymbol{x})$. This procedure is repeated until some convergence criteria are fulfilled. Finally, one obtains the electronic energies and the respective wave functions for the molecule inside the cavity.

The reaction field method has found various applications. In particular, one is frequently interested in knowing the energy required to adjust the solvent molecules

(in the present case, their dipole moments) in response to the introduction of a solute (solvation energy). This solvation energy, for example often is responsible for the stabilization of certain isomers of the solute.

In preparation of the following Chapter 3, we point out that the reaction field approach has also a dynamical aspect. In order to appreciate this, we have to recall that it is the (quantum mechanically) *averaged* charge distribution of the solute that is "seen" by the solvent. The time scale for electronic motion is typically of the order of 10^{-15}–10^{-16} seconds. Thus, for the solvent to experience only the *mean field* due to the solute's electrons, it is necessary to assume that the time scale required for building up a polarization in the solvent is much longer than that of the electronic motion. If we consider, for example rotational motion of the solvent molecules on a time scale of about 10^{-12} seconds (orientational polarization), this reasoning is certainly valid. However, if the polarization is of electronic character, the description in terms of a static dielectric constant is likely to fail.

2.7.2 Explicit Quantum-classical Solvent Model

In Section 2.7.1 we have adopted the point of view that the environment can be described by means of a dielectric continuum model, implying that its molecular structure does not matter for the process under consideration. As mentioned before, this idea can be extended by explicitly including, for example a solvation shell within a supermolecule approach. However, there are situations where a continuum description might fail. Consider, for example cases of long-range structural correlations as they occur in proteins whose structures and functions are often not only determined by local properties, but an explicit account of the full atomistic details is also required.

Keeping in mind the explicit description of many DOFs prohibits the use of QM approaches for the generation of the forces that act on the nuclei as outlined in Section 2.4. Most of the interaction potentials between different atoms, groups of atoms within a molecule, or molecules can ultimately be traced back to the Coulomb interaction between electronic and nuclear charges (see Section 2.2). Instead of taking into account the Coulomb interactions on an ab initio level, it is customary to use parameterized *empirical* potentials (Molecular Mechanics [MM] force fields) whose parameters are chosen in a way to obtain agreement with experimental results, for example for thermodynamic properties of the solvent. These empirical interaction potentials are usually partitioned into parts involving only a single atom (for instance, potentials describing external fields or container walls), pairs of atoms (bonding or repulsive interaction), three atoms (for instance, bending motions), four atoms (for instance, dihedral motions), etc. A prominent pair potential is the so-called *Lennard-Jones potential*

$$V_{\text{LJ}}(|\boldsymbol{R}_m - \boldsymbol{R}_n|) = 4\epsilon_{mn}\left(\left(\frac{\sigma_{mn}}{|\boldsymbol{R}_m - \boldsymbol{R}_n|}\right)^{12} - \left(\frac{\sigma_{mn}}{|\boldsymbol{R}_m - \boldsymbol{R}_n|}\right)^{6}\right).$$

$$(2.137)$$

It has a steeply rising repulsive wall for interparticle separations less than σ_{mn} (effective particle diameter due to nonbonding interactions in the region of wave function overlap, which is specific to the type of atoms), a negative well of depth ϵ_{mn}, and a long-range attractive r^{-6} tail (van der Waals interaction, for instance due to the so-called dispersion interactions originating from the correlated electronic motion in different molecules). We would like to stress that this effective pair potential should account for the effect of complicated many-body interactions in an averaged way. Further, it should be noted that for situations where electrostatic interactions are important (for example, if the system contains ions), the Lennard-Jones potential is not sufficient, and the classical Coulomb interaction has to be taken into account explicitly.

However, the QM character of the electronic DOFs cannot always be neglected, for example if the bond-making and -breaking processes need to be described accurately. This calls for a combination of QM and MM force calculations, which is achieved in the QM/MM approach. Here, the total system is separated into a QM and an MM part

$$H_{\text{total}} = H_{\text{QM}} + H_{\text{MM}} + V_{\text{QM/MM}}, \tag{2.138}$$

where $V_{\text{QM/MM}}$ is the interaction potential between the two regions. Separation schemes can be distinguished according to whether or not the QM/MM boundary cuts through molecular bonds. Bonds are cut, for instance in cases where only the active site, for instance of an enzyme, is treated quantum mechanically, and all other atoms including the solvent are taken into the MM part. There are different ways of dealing with this situation such as capping the dangling bonds with link atoms such as hydrogen. In the simpler case where, for example a solute is treated quantum mechanically and embedded in a classical solvent such that there is negligible overlap of electron densities in the boundary region, one can proceed as follows. For the QM part, one takes the full Hamiltonian, Eq. (2.1), whereas the classical part is composed of empirical force fields such as Eq. (2.137) as well as bonding and Coulomb terms. For the interaction Hamiltonian, one includes a Lennard-Jones potential for the nonbonded interaction as well as a Coulomb term for the interaction between QM electrons (first term) as well as nuclei (second term) with the classical environment as follows:

$$V_{\text{QM/MM}} = \sum_{m \in \text{QM}} \sum_{n \in \text{MM}} V_{\text{LJ}}(|\boldsymbol{R}_m - \boldsymbol{R}_n|) + \sum_{i \in \text{QM}} \sum_{n \in \text{MM}} \frac{e q_n}{|\boldsymbol{r}_i - \boldsymbol{R}_n|}$$
$$+ \sum_{m \in \text{QM}} \sum_{n \in \text{MM}} \frac{e z_m q_n}{|\boldsymbol{R}_m - \boldsymbol{R}_n|}. \tag{2.139}$$

Here, q_m are the partial charges assigned to the molecules in the classical MM force field.[20] For the solution of the electronic Schrödinger equation, only the first term of this expression is of relevance since it contains the electronic position operator of the QM part. However, we notice that this is merely a one-electron operator (such

---

[20] Note that in general the charges do not have to be multiples of *e* and are not restricted to atomic positions. Further, one distinguishes electronic and polarizable embedding, depending on whether or not the MM force field contains fixed or polarizable charges.

as $V_{\text{el-nuc}}$), which can be included, for example into the Hartree–Fock scheme in a straightforward manner, thereby allowing one to treat the effect of an explicit atomistic environment on the electronic structure of the solute.

2.8 Supplement

2.8.1 Franck–Condon Factors

In Section 2.5.2, we have discussed the Franck–Condon factors that describe the overlap between wave functions of different PESs. The expression equation (2.79) is limited to the case of two harmonic potentials of *equal* curvature. If the curvatures are different, the resulting expressions become more complicated. In terms of the numerical implementation, however, it is much more convenient to express the Franck–Condon factors via recursion relations. Their derivation for the general case of different curvatures will be outlined as follows.

Using the operator notation introduced in Section 2.5.2, the Franck–Condon factor reads

$$\langle \chi_{aM} | \chi_{bN} \rangle = \langle 0_a | \frac{(C_a)^M}{\sqrt{M!}} D(g_a) D^+(g_b) \frac{(C_b^+)^N}{\sqrt{N!}} | 0_b \rangle , \qquad (2.140)$$

where we skipped the normal mode index but accounted for the fact that the operators and the vacuum states depend on the index of the PES because of the different frequencies. To proceed, we have to reformulate Eq. (2.140) into a state vector product that only contains one type of oscillator operator, for example C_a, and one type of vacuum, $| 0_a \rangle$. This is possible if we use the so-called squeezing operator

$$S_b^+(z) = \exp(z(C_b^2 - C_b^{+2})/2) \qquad (2.141)$$

to write

$$C_a = S_b^+(z_{ab}) \, C_b \, S_b(z_{ab}) \qquad (2.142)$$

with $z_{ab} = \ln(\omega_a/\omega_b)/2$. After some algebra, one finds the following expression for the Franck–Condon factor:

$$\langle \chi_{aM} | \chi_{bN} \rangle = \langle 0 | \frac{C^M}{\sqrt{M!}} D(g) \, S(z) \frac{C^{+N}}{\sqrt{N!}} | 0 \rangle. \qquad (2.143)$$

Here, we have introduced $g = g_a - g_b \sqrt{\epsilon}$, $\epsilon = \omega_a/\omega_b$, $C = C_a$, $|0\rangle = |0_a\rangle$, and $z = z_{ab} = (\ln \epsilon)/2$. Starting with the interchange of one annihilation operator from the left to the right in Eq. (2.143), a recursion relation for the Franck–Condon factor can be derived. One obtains

$$\langle \chi_{aM} | \chi_{bN} \rangle = \sqrt{\frac{N-1}{N}} \frac{1-\epsilon}{1+\epsilon} \langle \chi_{aM} | \chi_{bN-2} \rangle - \frac{2g\sqrt{\epsilon}}{\sqrt{N}(1+\epsilon)} \langle \chi_{aM} | \chi_{bN-1} \rangle$$

$$+ \sqrt{\frac{M\epsilon}{N}} \frac{2}{1+\epsilon} \langle \chi_{aM-1} | \chi_{bN-1} \rangle \qquad (2.144)$$

and

$$\langle \chi_{aM} | \chi_{bN} \rangle = -\sqrt{\frac{M-1}{M}} \frac{1-\epsilon}{1+\epsilon} \langle \chi_{aM-2} | \chi_{bN} \rangle + \frac{2g}{\sqrt{M}(1+\epsilon)} \langle \chi_{aM-1} | \chi_{bN} \rangle$$

$$+ \sqrt{\frac{N\epsilon}{M}} \frac{2}{1+\epsilon} \langle \chi_{aM-1} | \chi_{bN-1} \rangle . \tag{2.145}$$

Notice that terms with "negative" quantum numbers have to be set equal to zero. The initial value for the recursion relations can be simply calculated in the coordinate representation, which gives

$$\langle \chi_{a0} | \chi_{b0} \rangle = \frac{\sqrt{2\sqrt{\epsilon}}}{\sqrt{1+\epsilon}} \exp\left(-\frac{g^2}{1+\epsilon}\right) . \tag{2.146}$$

Equations (2.144)–(2.146) together with the relation $\langle \chi_{aM} | \chi_{bN} \rangle = \left(\langle \chi_{bN} | \chi_{aM} \rangle\right)^*$ allow for a numerically stable determination of the Franck–Condon overlap integrals.

2.8.2 The Two-level System

There are many situations where the relevant molecular system can be modeled as an effective two-level system. A prominent example is given by the one-dimensional double minimum potential shown in Figure 2.16. This type of potential describes isomerization reactions such as intramolecular proton transfer. Provided the temperature is low enough such that thermal occupation of higher states is negligible, the dynamics for the situation of Figure 2.16 is readily described in terms of the two lowest states. In the following discussion we will study the eigenstates as well as the population dynamics of a generic two-level system. This exactly solvable model will provide a reference case for the subsequent discussions.

The Hamiltonian for a two-level system can be written in two alternative ways. First, we can assume that we know the eigenstates $|\pm\rangle$ and eigenenergies $\mathcal{E}_\pm$, for instance of the model potential shown in Figure 2.16. Then, we can write

$$H = \sum_{\kappa=\pm} \mathcal{E}_\kappa |\kappa\rangle\langle\kappa| . \tag{2.147}$$
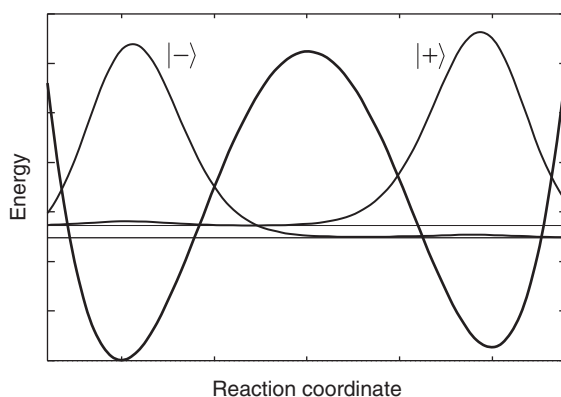
Figure 2.16 Potential energy surface along a reaction coordinate describing the intramolecular proton transfer in asymmetrically substituted malonaldehyde. The potential supports two below barrier states whose probability density is plotted here with a vertical offset corresponding to the respective eigenenergies (figure courtesy of H. Naundorf).

If we do not know the eigenstates but some zeroth-order states $|1\rangle$ and $|2\rangle$ that correspond to a situation where, for instance the coupling between the left and the right well in Figure 2.16 is switched off, the Hamiltonian reads

$$\overline{H} = \varepsilon_1 |1\rangle\langle 1| + \varepsilon_2 |2\rangle\langle 2| + V|1\rangle\langle 2| + V^* |2\rangle\langle 1|. \tag{2.148}$$

Here, the level energies of the zeroth-order states are denoted $\varepsilon_{a=1,2}$, and the coupling between these states is given by V. Independent of the specific situation, the Hamiltonian (2.148) can be transformed to take the form (2.147). In what follows, we outline how this diagonalization of (2.148) is achieved.

In a first step, we determine the eigenvalues and eigenstates that follow from the stationary Schrödinger equation

$$H|\Psi\rangle = \mathcal{E}|\Psi\rangle. \tag{2.149}$$

We expand the state vector with respect to the states $|a = 1,2\rangle$,

$$|\Psi\rangle = C(1)|1\rangle + C(2)|2\rangle, \tag{2.150}$$

which leads to a matrix equation for the expansion coefficients $C(a = 1,2)$,

$$\begin{pmatrix} \varepsilon_1 & V \\ V^* & \varepsilon_2 \end{pmatrix} \begin{pmatrix} C(1) \\ C(2) \end{pmatrix} = \mathcal{E} \begin{pmatrix} C(1) \\ C(2) \end{pmatrix}. \tag{2.151}$$

The eigenvalues are obtained from the secular equation,

$$(\mathcal{E} - \varepsilon_1)(\mathcal{E} - \varepsilon_2) - |V|^2 = 0. \tag{2.152}$$

Solving this quadratic equation gives

$$\mathcal{E}_{\kappa=\pm} = \frac{1}{2} \left\{ \varepsilon_1 + \varepsilon_2 \pm \sqrt{(\varepsilon_1 - \varepsilon_2)^2 + 4|V|^2} \right\}. \tag{2.153}$$

To determine the expansion coefficients, and thus the eigenstates, the $\mathcal{E}_{\kappa=\pm}$ are inserted into the eigenvalue equation (2.151),

$$\begin{pmatrix} \mathcal{E}_\kappa - \varepsilon_1 & -V \\ -V^* & \mathcal{E}_\kappa - \varepsilon_2 \end{pmatrix} \begin{pmatrix} C_\kappa(1) \\ C_\kappa(2) \end{pmatrix} = 0. \tag{2.154}$$

Note that the expansion coefficients $C(m)$ have been labeled by the quantum numbers $\kappa = \pm$. If we make use of the normalization condition

$$\sum_m |C_\kappa(m)|^2 = 1, \tag{2.155}$$

we obtain

$$|C_\kappa(1)|^2 = \frac{(\mathcal{E}_\kappa - \varepsilon_2)^2}{(\mathcal{E}_\kappa - \varepsilon_2)^2 + |V|^2}. \tag{2.156}$$

From Eq. (2.153), we get the relations

$$(\mathcal{E}_\kappa - \varepsilon_1)(\mathcal{E}_\kappa - \varepsilon_2) = |V|^2 \tag{2.157}$$

and

$$\mathcal{E}_+ + \mathcal{E}_- = \varepsilon_1 + \varepsilon_2, \tag{2.158}$$

which, if inserted into (2.156), gives

$$\left|C_{\kappa}(1)\right|^2 = \frac{(\mathcal{E}_{\kappa} - \varepsilon_2)^2}{(\mathcal{E}_{\kappa} - \varepsilon_2)^2 + (\mathcal{E}_{\kappa} - \varepsilon_1)(\mathcal{E}_{\kappa} - \varepsilon_2)} = \frac{\mathcal{E}_{\kappa} - \varepsilon_2}{\mathcal{E}_{\kappa} - \varepsilon_2 + \mathcal{E}_{\kappa} - \varepsilon_1}$$

$$= \frac{\mathcal{E}_{\kappa} - \varepsilon_2}{\mathcal{E}_{\kappa} - \mathcal{E}_{\overline{\kappa}}}. \tag{2.159}$$

To have compact notation, we introduced $\overline{\kappa} = \pm$, if $\kappa = \mp$. The complex expansion coefficient itself reads

$$C_{\kappa}(1) = \sqrt{\frac{\mathcal{E}_{\kappa} - \varepsilon_2}{\mathcal{E}_{\kappa} - \mathcal{E}_{\overline{\kappa}}}} \, e^{i\chi_1(\kappa)}, \tag{2.160}$$

where the phase $\chi_1(\kappa)$ remains open at this point. In a similar manner, we can derive

$$|C_{\kappa}(2)| = \sqrt{\frac{\mathcal{E}_{\kappa} - \varepsilon_1}{\mathcal{E}_{\kappa} - \mathcal{E}_{\overline{\kappa}}}}. \tag{2.161}$$

However, the phase of $C_{\kappa}(2)$ is not free but has to be determined from

$$C_{\kappa}(2) = |C_{\kappa}(2)| e^{i\chi_2(\kappa)} = \frac{|V| e^{-i\arg(V)}}{\mathcal{E}_{\kappa} - \varepsilon_2} \sqrt{\frac{\mathcal{E}_{\kappa} - \varepsilon_2}{\mathcal{E}_{\kappa} - \mathcal{E}_{\overline{\kappa}}}} \, e^{i\chi_1(\kappa)}. \tag{2.162}$$

We note that for $\kappa = +$, it is $\mathcal{E}_{\kappa} > \varepsilon_2$, and for $\kappa = -$, one has $\mathcal{E}_{\kappa} < \varepsilon_2$. Consequently, the phase $\chi_2(\kappa)$ is given by $\chi_2(+) = \chi_1(+) - \arg(V)$ and $\chi_2(-) = \chi_1(-) - \arg(V) + \pi$.

There exist alternative formulas for $\left|C_{\kappa}(1)\right|^2$ and $\left|C_{\kappa}(2)\right|^2$. Before presenting them we note that $|C_{\overline{\kappa}}(1)| = |C_{\kappa}(2)|$, which is easily demonstrated using, for example Eq. (2.158). To get the first alternative to Eqs. (2.160) and (2.162), one introduces

$$\Delta E = \mathcal{E}_{-} - \varepsilon_2 \equiv \frac{1}{2} \left\{ \varepsilon_1 - \varepsilon_2 + \sqrt{(\varepsilon_1 - \varepsilon_2)^2 + 4|V|^2} \right\}. \tag{2.163}$$

Using the abbreviation

$$\eta = \frac{\Delta E}{|V|}, \tag{2.164}$$

it follows that

$$\left|C_{+}(1)\right|^2 = \left|C_{-}(2)\right|^2 = \frac{\eta^2}{1 + \eta^2} \tag{2.165}$$

and

$$\left|C_{-}(1)\right|^2 = \left|C_{+}(2)\right|^2 = \frac{1}{1 + \eta^2}. \tag{2.166}$$

To arrive at another alternative notation, one defines the ratio

$$\lambda = \frac{2|V|}{|\Delta\varepsilon|}, \tag{2.167}$$

with $\Delta\varepsilon = \varepsilon_1 - \varepsilon_2$. We obtain for the expansion coefficients ("sgn" is the sign function)

$$\left|C_{\kappa}(1)\right|^2 = \frac{1}{2} \left(1 + \kappa \frac{\text{sgn}(\Delta\varepsilon)}{\sqrt{1 + \lambda^2}} \right). \tag{2.168}$$

Next, we use the trigonometric relation

$$\cos^2\gamma = \frac{1}{2}\left(1 + \frac{1}{\sqrt{1 + \tan^2(2\gamma)}}\right), \tag{2.169}$$

which is also valid for the sine function after replacing the plus sign in the bracket on the right-hand side by a minus sign. We identify

$$\gamma = \frac{1}{2}\arctan\frac{2|V|}{|\Delta\varepsilon|} \tag{2.170}$$

and obtain from Eq. (2.168) the expressions

$$\left|C_+(1)\right|^2 = \left|C_-(2)\right|^2 = \cos^2\left(\gamma + \frac{\pi}{4}[1 - \mathrm{sgn}(\Delta\varepsilon)]\right) \tag{2.171}$$

and

$$\left|C_-(1)\right|^2 = \left|C_+(2)\right|^2 = \sin^2\left(\gamma - \frac{\pi}{4}[1 - \mathrm{sgn}(\Delta\varepsilon)]\right). \tag{2.172}$$

The quantity γ is the so-called *mixing angle*. Finally, we point out that the coefficients fulfill the condition

$$\sum_\kappa C_\kappa^*(m)C_\kappa(n) = \delta_{mn}, \tag{2.173}$$

which is obtained by expanding the orthogonal zeroth-order states in terms of the eigenstates.

2.8.3 The Linear Molecular Chain and the Molecular Ring

The linear molecular chain represents a simple model system for studying the transfer phenomena as well as the behavior of energy spectra in dependence on the system size. In different contexts it is also known as the *tight-binding* or the *Hückel* model. We will encounter this model when discussing electron and excitation energy transfer in Chapters 7 and 9, respectively. In the present section, we focus on the most simple setup consisting of an arrangement of N identical quantum states at energy ε_0 and being coupled via the matrix element $V_{m,m+1} = V_{m-1,m} = V$; that is, only nearest-neighbor couplings are assumed. This situation might describe, for example the diabatic states $|\varphi_m\rangle$ of different parts of an electron-transfer system (donor, bridge, and acceptor, see Chapter 7). The potential coupling between these diabatic electronic states is then given by V (see also Eq. (2.103)).

This results in the following Hamiltonian:

$$H_{\mathrm{chain}} = \sum_{m=1}^{N}\varepsilon_0\left|\varphi_m\right\rangle\left\langle\varphi_m\right| + \sum_{m=1}^{N-1}\left(V\left|\varphi_{m+1}\right\rangle\left\langle\varphi_m\right| + \mathrm{H.\,c.}\right). \tag{2.174}$$

In a first step, we determine the eigenstates $|\Psi_a\rangle$ of the chain by solving the stationary Schrödinger equation

$$H_{\mathrm{chain}}\left|\Psi_a\right\rangle = \mathcal{E}_a\left|\Psi_a\right\rangle. \tag{2.175}$$

Since the states $|\varphi_m\rangle$ are supposed to be known, we can expand the $|\Psi_a\rangle$ in this basis:

$$|\Psi_a\rangle = \sum_m C_a(m) |\varphi_m\rangle. \tag{2.176}$$

Inserting Eq. (2.176) into Eq. (2.175) and using Eq. (2.174), we obtain the equation for the expansion coefficients $C_a(m)$:

$$(\mathcal{E}_a - \varepsilon_0)C_a(m) = V[C_a(m+1) + C_a(m-1)], \tag{2.177}$$

which is valid for $1 < m < N$. For $m = 1$ and $m = N$, we have to take into account the finite structure of the chain. This gives two additional equations:

$$(\mathcal{E}_a - \varepsilon_0)C_a(1) = VC_a(2) \tag{2.178}$$

and

$$(\mathcal{E}_a - \varepsilon_0)C_a(N) = VC_a(N-1). \tag{2.179}$$

The set of Eqs. (2.177), (2.178), and (2.179) can be solved using the following ansatz:

$$C_a(m) = C \, \sin(am), \tag{2.180}$$

where C is a real constant. Inserting Eq. (2.180) into Eq. (2.177) gives

$$(\mathcal{E}_a - \varepsilon_0) \sin(am) = V \left(\sin(a[m+1]) + \sin(a[m-1]) \right). \tag{2.181}$$

With the help of some theorems for trigonometric functions, this equation can be transformed into

$$\mathcal{E}_a = \varepsilon_0 + 2V \cos a. \tag{2.182}$$

This expression tells us how the energy spectrum depends on the yet unknown quantum number a; the same result is obtained from Eq. (2.178). Equation (2.179), however, gives the condition

$$(\mathcal{E}_a - \varepsilon_0) \sin(aN) = V \sin(a[N-1]), \tag{2.183}$$

which can be rewritten as

$$\left((\mathcal{E}_a - \varepsilon_0) - 2V \cos a \right) \sin(aN) = -V \left(\sin(aN) \cos a + \cos(aN) \sin a \right)$$
$$= 0, \tag{2.184}$$

where the second line follows from Eq. (2.182). Rearranging the right-hand side of Eq. (2.184) gives the condition for the eigenvalues

$$\sin\left(a(N+1) \right) = 0, \tag{2.185}$$

which is solved by

$$a = \frac{\pi j}{N+1} \quad (j = 0, \pm 1, \pm 2, \ldots). \tag{2.186}$$

Thus, the energy spectrum becomes

$$\mathcal{E}_a = \varepsilon_0 + 2V \cos\left(\frac{\pi j}{N+1} \right). \tag{2.187}$$

The normalization constant C appearing in Eq. (2.180) is obtained from the relation:

$$\sum_{m=1}^{N} \left| C_a(m) \right|^2 = C^2 \sum_{m} \sin^2(am) = 1. \tag{2.188}$$

Using the tabulated result for the sum, one arrives at

$$C = \sqrt{\frac{2}{N+1}}. \tag{2.189}$$

If one considers the expansion coefficients, Eq. (2.180), it is obvious that they are identical to zero for $j = 0$ and for multiples of $N + 1$. Furthermore, an inspection of Eqs. (2.187) and (2.180) shows that identical results are obtained for j being in the interval $1, \ldots, N$ and for all other $\bar{j}$ which differ from j by multiples of N. Therefore, j has to be restricted to the interval $1, \ldots, N$.

In the remaining part of this section we discuss the model of a molecular ring. Such a system we will encounter, for instance in Chapter 9. To arrive at a Hamiltonian for a molecular ring, that is a circular and regular arrangement of identical molecules, the following specification of the model for the chain becomes necessary. The first molecule of the chain is connected with the last one in a way that the coupling strength between both takes the value V, which is the strength of the nearest-neighbor couplings between all other molecules too. For this model, we may use the ansatz, Eq. (2.176), but the expansion coefficients have to fulfill $C_a(m) = C_a(m + \nu N)$ (where ν is an integer). This requirement can be satisfied by choosing

$$C_a(m) = C \exp(iam), \tag{2.190}$$

with $a = 2\pi j/N$ ($j = 0, \ldots, N_{\text{mol}} - 1$). Since $\left| C_a(m) \right|^2 = |C|^2$, one easily verifies that $C = 1/\sqrt{N}$. Inserting the expansion coefficients into Eq. (2.177) (Eqs. (2.178) and (2.177) are dispensable), it again follows Eq. (2.187) for the eigenvalues E_a, but now with a modified definition of the quantum numbers a as given above.

References

1 W. H. Miller et al., J. Chem. Phys. **72**, 99 (1980).

2 B. A. Ruf and W. H. Miller, J. Chem. Soc., Faraday Trans. 2 **84**, 1523 (1988).

3 S. Takada and H. Nakamura, J. Chem. Phys. **102**, 3977 (1995).

4 M. Persico and G. Granucci, *Photochemistry. A Modern Theoretical Perspective*, (Springer International Publishing AG, Cham, 2018).

Further Reading

- Theoretical concepts and basic experiments of Molecular Physics:
  H. Haken and H. C. Wolf, *Molecular Physics and Elements of Quantum Chemistry*, (Springer-Verlag, Berlin, 2004).

- Electronic structure theory and Computational Chemistry:

   F. Jensen, *Introduction to Computational Chemistry*, (Wiley, Chichester, 2017).

   W. Koch and M. C. Holthausen, *A Chemist's Guide to Density Functional Theory*, (Wiley-VCH, Weinheim, 2001).

   A. Szabo and N. S. Ostlund, *Modern Quantum Chemistry*, (Dover, New York, 1996).

- Nonadiabatic PES and Photochemistry:

   M. Baer, *Beyond Born–Oppenheimer*, (Wiley–Interscience, Hoboken, NJ, 2006).

   K. Takatsuka, T. Yonehara, K. Hanasaki, and Y. Arasaki, *Chemical Theory Beyond the Born–Oppenheimer Paradigm*, (World Scientific, Hoboken, New Jersey, 2015).

3

Dynamics of Isolated and Open Quantum Systems

A quantum mechanical description of time-dependent phenomena in two types of molecular systems is given. First, we consider small systems that are isolated from their surroundings. This situation can be modeled using the time-dependent Schrödinger equation. Some basic properties of the time-evolution operator are discussed, and the concept of the scattering operator is introduced, which can serve as a starting point of a perturbation expansion. Further the multiconfiguration time–dependent Hartree method is presented, which allows to treat high–dimensional wave packet propagation. It is shown that with increasing dimensionality of the considered system, the treatment of transitions between different manifolds of quantum states can be replaced by a rate description based on the Golden Rule of quantum mechanics.

To go beyond a description of the system by a single wave function, the density operator (statistical operator) is introduced. This concept, when specified to the reduced density operator, is used to treat the dynamics of the system when interacting with some macroscopic environment. The interaction can be systematically incorporated using the projection operator formalism. The latter is shown to provide a means to develop a perturbation theory in line with a reduction scheme onto the state space of the small system. Restricting ourselves to the second order of the perturbation expansion, we derive a generalized master equation, which is the basic equation for the considered system–reservoir situation.

The approach is contrasted with a generalized rate theory that focusses on the computation of diagonal matrix elements of the density operator taken with respect to some basis. The rate expressions of the Golden Rule type are obtained, as are the higher order extensions.

Finally, we give a brief introduction into nonperturbative methods for dealing with condensed-phase dynamics. In particular, we discuss the path integral representation of the reduced density operator, the hierarchy equation of motion method, and the quantum–classical hybrid approach.

3.1 Introduction

In the development of quantum theory, the focus has been on simple systems such as the harmonic oscillator or the hydrogen atom assuming them to be isolated from the rest of the universe. The dynamics of such isolated quantum systems is completely described by the time-dependent Schrödinger equation for the wave function $\Psi(x, t)$,

$$i\hbar \frac{\partial}{\partial t} \Psi(x, t) = H\Psi(x, t). \tag{3.1}$$

Here, x comprises some set of degrees of freedoms (DOFs). An unambiguous solution of this first-order differential equation is obtained by fixing an initial wave function $\Psi(x, t_0)$. Provided Eq. (3.1) has been solved for a particular Hamilton operator H, the time dependence of physical observables of the system is given by the expectation values of the associated Hermitian operators, $\hat{O}$, with respect to the time-dependent wave function, $O(t) = \langle \Psi(t) | \hat{O} | \Psi(t) \rangle$.[1]

However, the model of an isolated system is an oversimplification, and different perturbations from the environment have to be taken into account. One may ask the question how the dynamics of the quantum system of interest (the system S) is influenced by some environment. Of course, the answer depends on the actual type of environment and in particular on its coupling strength to the system. If the environment comprises only a small number of DOFs, one can attempt to solve the time-dependent Schrödinger equation, but now for the system plus the small environment. A typical example are small clusters embedding a diatomic molecule. Such an approach is impossible if the environment is large and forms a macroscopic system R (see Figure 3.1). If the environment stays in thermal equilibrium at temperature T as it is the case for many applications, it represents a *heat bath* for the system S, and one has to resort to statistical methods as we will see below.

Any coupling to external DOFs results in energy exchange between the system S and its environment. If initially energy is deposited into S, it will be transferred to the reservoir over the course of time. The DOFs of the reservoir accept the energy and distribute it among themselves. If the environment is a macroscopic system, the energy is distributed over its huge number of DOFs. At the end of this process, the environment does not "feel" this negligibly small increase in its internal energy. If the environment stays in thermal equilibrium, S will eventually relax into a state of thermal equilibrium with R. The situation is different for the case of a small environment. Here, all DOFs may become noticeably excited, and it may be possible that the energy moves back into the system S. This phenomenon is known as *recurrence*. The energy transfer from S to its surroundings (possibly followed by a recurrence) is termed relaxation. If there is no chance for the energy to move back into S, the unidirectional energy flow into the environment is called dissipation. Obviously, on short time scales, the distinction between relaxation and dissipation is likely to be blurred. Hence, there is often no strict discrimination between the two terms in the literature.

---

1) Note that whenever the context requires to distinguish operators from observables, we use a "hat" to mark the operator.
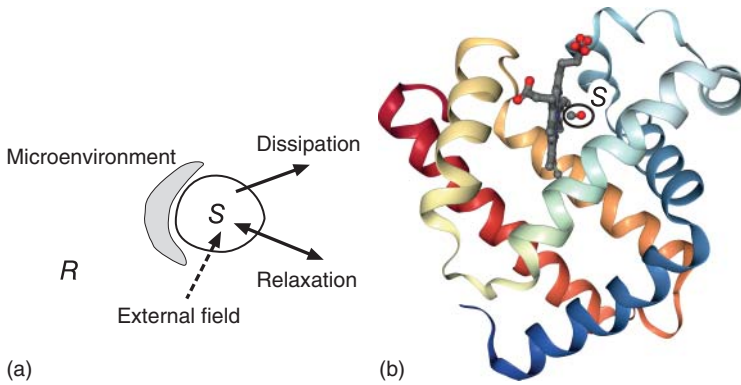
Figure 3.1 (a) Schematic view of a typical situation encountered in condensed-phase dynamics. A small system interacting with its surroundings (thermal reservoir or microenvironment) is investigated by means of an externally applied field. The system–reservoir interaction leads to unidirectional dissipation or bidirectional relaxation of energy initially deposited into the system. (b) Illustration of system–reservoir partitioning using the example of the myoglobin protein in the carbon monoxide-ligated state. Here, the CO molecule can be considered as the relevant system, interacting with its microenvironment (heme complex) as well as with the surrounding protein; for protein structure, see Kachalova et al. [1].

In the short time limit, it is possible that one enters a regime where the interaction of S with its surroundings is negligible. An upper limit for this time scale would be given, for example by the mean time between two scattering events of the molecule of interest with the surrounding molecules. In this time range, the time-dependent Schrödinger equation for the system S alone may provide an adequate description. This means that for a short time there exists a time-dependent wave function that, however, will be strongly disturbed in its evolution at later times. To indicate the existence of a quantum mechanical wave function during this early state of the time evolution of S, the motion is called *coherent*. If the coupling to the environment becomes predominant, the motion changes to an *incoherent* one.

The incoherent motion can be described by time-dependent occupation probabilities, $P_a(t)$, of certain quantum states of the system, $|a\rangle$. The $P_a(t)$ are obtained as the solution of rate equations of the type

$$\frac{\partial}{\partial t} P_a = -\sum_b \left(k_{a\to b} P_a - k_{b\to a} P_b \right). \tag{3.2}$$

This equation contains the rates of probability transfer per unit time, $k_{a\to b}$, for the transition from $|a\rangle$ to $|b\rangle$. In the first term on the right-hand side, the decrease in P_a with time due to probability transfer from $|a\rangle$ to all other states is given. The reverse process is described by the second term which contains the transfer from all other states $|b\rangle$ into the state $|a\rangle$. Equation (3.2) was "intuitively derived" by W. Pauli in 1928. It is frequently called *Pauli master equation* or just *master equation*. It is already obvious at this point that a method is required that allows to connect the description of *coherent* and *incoherent* motions. Before dealing with this problem, we give a more general characterization of the quantum system interacting with an environment.

There are an impressive number of different experiments that are of the type that rather small systems are studied under the influence of a thermal environment using external electromagnetic fields. A typical example is optical spectroscopy of dye molecules (the system *S*) in solution (the reservoir *R*). Studying electronic and vibrational transitions in these molecules, which are induced by the absorption of photons, one simultaneously detects the influence of the solvent molecules. This influence is often given by a random sequence of scattering events between the dye and the solvent molecules.[2] As a consequence, there is a stochastic modulation of the initial and final states involved in the optical transition. A closer look at this example provides us with some general aspects of condensed-phase dynamics.

First, experimentalists seek to arrange their setup in such a manner that the external field exclusively acts on the dye molecule (solute), without directly influencing the solvent molecules. This situation demands a theoretical description that is focused on the DOFs of the molecular system but does not a priori neglect the influence of the environment. In terms of the probabilistic aspect inherent in quantum mechanics, this means that *reduced probabilities* valid only for the molecular system *S* have to be introduced.

Second, if molecular properties are sensitive to the so-called *microenvironment*, that is if energy levels and other intramolecular quantities change their values with a change in the molecular structure in close proximity to the studied molecule, a careful description of the system–reservoir coupling has to be carried out, or *S* is supplemented by the microenvironment. An example for a microenvironment is the first solvation shell of molecules in solution or the rest of a molecule if *S* refers to one of its DOFs (see Figure 3.1).

Third, experiments can be performed on single molecules. The standard scheme of spectroscopy deals with a large number of molecules excited simultaneously by the external field. Therefore, an *averaging* with respect to this *ensemble* has to be carried out in the theoretical description. According to statistical physics, the ensemble average can be replaced by an average taken with respect to the possible states of the environment *R*, provided all molecules are identical. The standard example is a thermal environment where this averaging is done using the canonical distribution function for a given temperature *T*.

Fourth, one often studies a system of identical molecules. But, it is very likely that every molecule feels a somewhat different environment, and as a result, molecular properties such as the electronic energy spectrum, vibrational frequencies, and dipole moments may differ from molecule to molecule. In this case, we have some static *disorder* in the system, and an additional averaging over the different possible values of, for example the transition frequencies is necessary. This particular situation may lead to a broad absorption band in the linear optical spectroscopy of the respective transition. Since this broadening is caused by different values of the transition frequency found for different molecules located at different points in the probed sample, it is called *inhomogeneous broadening*. In contrast, the line broadening caused by the rapid stochastic fluctuations of the molecular properties is called *homogeneous*.

----

2) Note that a polar solvent may also act on the dye via long-range electrostatic forces.

And finally, if the reservoir is noticeably disturbed by the dynamics of the molecular system, the state of the microenvironment may be driven away from equilibrium, and a description in terms of a thermal equilibrium distribution of the whole reservoir becomes invalid.

The *density matrix* formalism is the key to the theoretical description of condensed-phase experiments. It was introduced by L. Landau and J. von Neumann in 1927. Before looking at the concept of density matrices in more detail, we introduce some useful definitions. In what follows, we refer to the molecular system of interest or more specifically to all those DOFs of a molecule that actively participate in a particular experiment as the *relevant system* or *active system S*. All other DOFs form the irrelevant part of the system. For nearly all applications discussed below, this irrelevant part forms a macroscopic *reservoir R* and is assumed to stay in thermal equilibrium at some temperature *T*; that is, it can be considered as a *heat bath* (see Figure 3.1).

Usually, the relevant quantum system *S* consists of a small number of DOFs ($< 10^3$) and has a relatively simple energy spectrum. It is the aim of the theory explained in the following to study the dynamic properties of *S* on a microscopic basis. In contrast, the reservoir *R* consists of a large number of DOFs ($10^3 \ldots 10^{23}$) and may form a macroscopic system. Since the reservoir does not participate in an active manner in the dynamics initiated, for example by an externally applied field, we do not aim at its detailed description. As a matter of fact, statistical physics tells us that such a detailed knowledge is not only impossible but useless as well. Instead, a formulation in terms of quantum statistics, classical statistics, or of stochastic concepts is appropriate. Here, the choice of the approach is dictated by the problem at hand. For instance, most liquid-phase environments are very likely to behave classically.

One basic question that will be answered by the theory introduced in this chapter is: How do the equilibrated reservoir DOFs influence the externally induced dynamics of the relevant system? Our starting point for developing the formalism is the general Hamiltonian

$$H = H_S + H_{S-R} + H_R. \tag{3.3}$$

It is composed of the Hamiltonian H_S of the relevant system, the Hamiltonian H_R of the reservoir, and the interaction H_{S-R} between them. For the moment, let the system be characterized by the set of coordinates $s = \{s_j\}$ and their conjugate momenta $p = \{p_j\}$. The reservoir coordinates and momenta are $Z = \{Z_\xi\}$ and $P = \{P_\xi\}$, respectively. Note that this type of Hamiltonian has already been considered in Section 2.5.3. There, however, isolated polyatomics were discussed. We will see in Chapter 5 how the concept of a Taylor expansion of the global PES around some stable equilibrium configurations leads to Hamiltonians of the type (3.3) even in the context of condensed-phase problems. Chapters 6–9 will also present different variants of this *system–reservoir* Hamiltonian. Here, we only quote a generic example that is based on the picture of a reservoir, which carries out small vibrations around some equilibrium configuration; that is, it can be characterized by normal-mode oscillations. Thus, we have

$$H_R = \frac{1}{2} \sum_\xi \left(P_\xi^2 + \omega_\xi^2 Z_\xi^2 \right). \tag{3.4}$$

The Hamiltonian of the relevant part can be simply taken as $H_S = T(p) + V(s)$ with the kinetic and potential energy contributions $T(p)$ and $V(s)$, respectively. Concerning the coupling part in Eq. (3.3), we notice the small amplitude vibrations of the reservoir coordinates and restrict H_{S-R} to a linear expansion with respect to the various Z_ξ:

$$H_{S-R} = \sum_\xi K_\xi(s) Z_\xi. \tag{3.5}$$

The expansion coefficients $K_\xi(s)$ are just functions of the system coordinates. If a linearization with respect to these coordinates is also included, we arrive at the frequently used *bilinear* system–reservoir coupling model (Caldeira–Leggett model), see Eq. (2.94).

Since S and R are coupled by means of H_{S-R}, it is impossible to introduce a wave function of the system or the reservoir alone. There only exists the total wave function, $\Psi(s, Z)$, which does not factorize into a system part $\Phi_S(s)$ and a reservoir part $\chi_R(Z)$,

$$\Psi(s, Z) \neq \Phi_S(s)\, \chi_R(Z), \tag{3.6}$$

unless the coupling between S and R vanishes.

To accomplish the aim of the present approach, that is to treat the system dynamics without an explicit consideration of the reservoir dynamics, one could attempt to reduce the wave function $\Psi(s, Z)$ to a part depending on the system coordinates s alone. But, in quantum mechanics, we have a probabilistic interpretation of the *square* of the wave function. Thus, the only reduced quantity that can be introduced is the reduced probability density following from an integration of $|\Psi(s, Z)|^2$ with respect to all reservoir coordinates Z.

We encounter a generalization of this reduced probability distribution if we try to define the expectation value of an observable described by the Hermitian operator $O = O(s)$, which acts in the state space of S only. (A dependence on the momenta p is possible but does not change any conclusion given below.) The expectation value reads

$$\langle O \rangle = \int ds\, dZ\ \Psi^*(s, Z) O(s) \Psi(s, Z). \tag{3.7}$$

If we introduce

$$\rho(s, \bar{s}) = \int dZ\ \Psi(s, Z)\Psi^*(\bar{s}, Z), \tag{3.8}$$

Equation (3.7) can be rewritten as

$$\langle O \rangle = \int ds \big[O(s)\rho(s, \bar{s}) \big]_{s=\bar{s}}. \tag{3.9}$$

In this notation, the averaging with respect to the large number of reservoir coordinates is absorbed in the definition of $\rho(s, \bar{s})$. Changing from the coordinate representation to a representation with respect to some discrete system quantum numbers $a, b, \ldots$, the name *density matrix* introduced for ρ_{ab} becomes obvious. The density matrix $\rho(s, \bar{s})$ or ρ_{ab} will be more precisely called *reduced density matrix*

(RDM) since it is the result of a reduction in the total probability density onto the state space of the relevant system. If there is no coupling between the system and the reservoir, that is if $H_{S-R} = 0$, the density matrix is given as a product of wave functions

$$\rho(s, \bar{s}) = \Phi_S(s)\Phi_S^*(\bar{s}). \tag{3.10}$$

Since this expression contains no more information than the wave function itself, it should be clear that in the case of a quantum system isolated from its environment, the characterization by a wave function should be sufficient.

In order to get some first insight into the time evolution of the density matrix, the total wave function (at time $t = 0$) is expanded with respect to a complete basis set ϕ_a of the system state space:

$$\Psi(s, Z; t = 0) = \sum_a \phi_a(s)\chi_a(Z). \tag{3.11}$$

The χ_a are wave functions defined in the reservoir state space and follow from

$$\chi_a(Z) = \int ds \, \phi_a^*(s)\Psi(s, Z; t = 0). \tag{3.12}$$

The expansion (3.11) reflects Eq. (3.6), and the summation over the various χ_a can be interpreted as a manifestation of system–reservoir correlations.

The time evolution of the total wave function is determined by the related time-dependent Schrödinger equation, and the expansion similar to that at $t = 0$ reads

$$\Psi(s, Z; t) = \sum_a \phi_a(s)\chi_a(Z, t), \tag{3.13}$$

now including the time-dependent reservoir wave functions. Since the total wave function Ψ is normalized, we may deduce

$$1 = \sum_a \langle \chi_a(t)|\chi_a(t)\rangle \equiv \sum_a P_a(t), \tag{3.14}$$

with $P_a(t) = \langle \chi_a(t)|\chi_a(t)\rangle = \int dZ \, \chi_a(Z, t)\chi_a^*(Z, t)$. This quantity gives the probability that a particular system state ϕ_a is realized at time t. Noting Eq. (3.8), we may introduce the time-dependent density matrix using the expansion (3.13). It follows that

$$\begin{aligned}\rho(s, \bar{s}; t) &= \sum_{a,b} \langle \chi_b(t)|\chi_a(t)\rangle \phi_a(s)\phi_b^*(s) \\ &= \sum_a P_a(t)\phi_a(s)\phi_a^*(s) + \sum_{\substack{a,b \\ a\neq b}} \langle \chi_b(t)|\chi_a(t)\rangle \phi_a(s)\phi_b^*(s).\end{aligned} \tag{3.15}$$

The first part of the density matrix proportional to the $P_a(t)$ is different from zero at all times. However, the second part determined by the overlap expressions $\langle \chi_b(t)|\chi_a(t)\rangle$ of reservoir wave functions belonging to different system states typically decays in time as $\langle \chi_b(t)|\chi_a(t)\rangle \sim \exp(-\gamma_{ab}t^r)$ ($r = 1, 2$) due to the different time evolution with respect to the two states. This phenomenon is known as *decoherence*. In other words, while the probabilities P_a to have the system state

ϕ_a always sum up to 1, interrelations between different system states ϕ_a and ϕ_b expressed by the part of the sum in Eq. (3.15) with $a \neq b$ decay.

Often, the decay of the off-diagonal elements of the density matrix is called *dephasing*, which is rather a statement about the effect and not the underlying mechanism. In this sense, decoherence could be a particular cause for dephasing. However, going from a single system to an ensemble decoherence is complemented by the destructive interference among observables belonging to different members of the ensemble in the course of the time evolution. This would also lead to a decay of the off-diagonal elements of the density matrix, but it is not related to quantum properties of the individual systems. In addition, experiments can be designed where this type of dephasing is compensated such that a rephasing occurs.

Besides the convenience of notation, density matrices offer a systematic way to describe the dynamics of the reduced quantum system embedded in a thermal reservoir. This theme will be explored in the remainder of this chapter. In Section 3.2, we start with reviewing some fundamental aspects of time-dependent quantum mechanics as based on the Schrödinger equation. This will lead us to the important result of the Golden Rule description of quantum transitions in the relevant system. In Section 3.4, the density matrix formalism will be introduced in detail. Equations of motion for the reduced density operator (RDO) are derived whose approximate treatment is considered in Sections 3.5–3.8. Further methods for describing the quantum dynamics in a molecular system are given in Sections 3.13 and 3.14.

3.2 Time-dependent Schrödinger Equation

3.2.1 Wave Packets

The time-dependent Schrödinger equation given in Eq. (3.1) in the coordinate representation will be discussed without using a particular representation in what follows. To this end, the state vector $|\Psi\rangle$ is introduced, which is related to the wave function $\Psi(x)$ through $\langle x|\Psi\rangle$ ($|x\rangle$ comprises the eigenstates of the system coordinate operator). Using the state vector notation, Eq. (3.1) becomes

$$i\hbar \frac{\partial}{\partial t}|\Psi(t)\rangle = H|\Psi(t)\rangle, \tag{3.16}$$

and the initial value of the state vector is $|\Psi_0\rangle \equiv |\Psi(t_0)\rangle$. If the Hamiltonian is time independent, a formal solution of Eq. (3.16) is given by

$$|\Psi(t)\rangle = e^{-iH(t-t_0)/\hbar}|\Psi_0\rangle. \tag{3.17}$$

The exponential function that contains the Hamiltonian is defined via a Taylor expansion: $\exp\{-iHt/\hbar\} = 1 - iHt/\hbar + \dots$. This expression is conveniently written by introducing the time-evolution operator

$$U(t, t_0) \equiv U(t - t_0) = e^{-iH(t-t_0)/\hbar}. \tag{3.18}$$

Note that in the case of a time-dependent Hamiltonian, $U(t, t_0) \neq U(t - t_0)$ (see below). The operator $U(t, t_0)$ is unitary and obeys the following equation of motion:

$$i\hbar \frac{\partial}{\partial t} U(t, t_0) = HU(t, t_0), \tag{3.19}$$

with the initial condition $U(t_0, t_0) = 1$. The time-evolution operator has the important property that it can be decomposed as

$$U(t, t_0) = U(t, t_{N-1}) U(t_{N-1}, t_{N-2}) \ldots U(t_2, t_1) U(t_1, t_0), \tag{3.20}$$

where $t_1 \leq t_2 \ldots \leq t_{N-1}$ are arbitrary times in the interval $[t_0, t]$. Note that Eqs. (3.19)–(3.20) are also valid if the Hamiltonian depends explicitly on time (see below).

If the solution of the stationary Schrödinger equation

$$H|a\rangle = E_a |a\rangle \tag{3.21}$$

with eigenstates $|a\rangle$ and eigenvalues E_a is known, it is straightforward to solve the time-dependent Schrödinger equation (3.16). To do this we expand the state vector with respect to the states $|a\rangle$ that form a complete basis. We have

$$|\Psi(t)\rangle = \sum_a c_a(t)|a\rangle. \tag{3.22}$$

Since the state vector is time dependent, the expansion coefficients $c_a(t) = \langle a|\Psi(t)\rangle$ are time dependent as well. Using Eq. (3.17) and the eigenvalue equation (3.21), we may write

$$c_a(t) = \langle a|e^{-iE_a(t-t_0)/\hbar}|\Psi_0\rangle = e^{-iE_a(t-t_0)/\hbar} c_a(t_0), \tag{3.23}$$

and the solution of the time-dependent Schrödinger equation is obtained as a superposition of oscillatory terms[3]

$$|\Psi(t)\rangle = \sum_a c_a(t_0) e^{-iE_a(t-t_0)/\hbar}|a\rangle. \tag{3.24}$$

Which oscillations are present is determined by the expansion coefficients $c_a(t_0) = \langle a|\Psi(t_0)\rangle$ of the state vector's initial value. As an instructive example, Section 3.12 gives a detailed discussion of the dynamics of a simple yet nontrivial case, the coupled two-level system.

The superposition state equation (3.24) is known as a *wave packet*. This name has its origin in the fact that such a superposition of state vectors may correspond to a localized probability distribution if it is transformed into the coordinate representation. Since the state vector $|\Psi(t)\rangle$ is given here as a superposition of (time-dependent) states $c_a(t)|a\rangle$, it is alternatively called *coherent* superposition state. This coherent superposition is phase sensitive, and the so-called *quantum beats* in the time evolution of the occupation probability of eigenstates can occur (see Figure 3.2).

If we choose the initial state for the solution of the time-dependent Schrödinger equation according to $|\Psi_0\rangle = |a\rangle$, we get $|\Psi(t)\rangle = \exp(-iE_a(t - t_0)/\hbar)|a\rangle$. Here, the

---

3) If the Hamiltonian also has a continuous spectrum, the sum over the states has to be extended by an integral with respect to the continuous energy.

initial state is multiplied by a time-dependent phase factor that cancels when calculating probabilities, $|\Psi(t)|^2$. Hence, we can state that time-dependent phenomena such as quantum beats in an isolated quantum system can only be expected if a noneigenstate, that is a superposition of eigenstates, is initially prepared.

Let us calculate the time-dependent expectation value of the operator $\hat{O}$:

$$O(t) = \langle \Psi(t)|\hat{O}|\Psi(t)\rangle = \sum_{a,b} c_b^*(t_0)c_a(t_0)\langle b|\hat{O}|a\rangle e^{-i(E_a - E_b)(t-t_0)/\hbar}. \tag{3.25}$$

The different time-dependent contributions are determined by *transition frequencies* $\omega_{ab} = (E_a - E_b)/\hbar$, which follow from combinations of the eigenvalues of the Hamiltonian H. The time-dependent expectation value, Eq. (3.25), can be rewritten using the time-evolution operator, Eq. (3.18), as

$$O(t) = \langle \Psi(t_0)|U^+(t,t_0)\hat{O}U(t,t_0)|\Psi(t_0)\rangle. \tag{3.26}$$

By means of this relation, the time dependence of the state vector can be transferred to the operator. This yields the so-called *Heisenberg* picture where time-dependent operators are defined as

$$\hat{O}^{(\mathrm{H})}(t) = U^+(t,t_0)\hat{O}U(t,t_0), \tag{3.27}$$

and the state vector is time independent.

In the case where the states $|a\rangle$ are also eigenstates of $\hat{O}$ with eigenvalues o_a, Eq. (3.25) simplifies to

$$O(t) = \sum_a |c_a(t_0)|^2 o_a, \tag{3.28}$$

that is, the expectation value becomes time independent. If $\hat{O}$ is the Hamiltonian itself, this relation reflects energy conservation during the time evolution of a wave function which is not an eigenstate of the system Hamiltonian.

If $\hat{O}$ is the projector $|\Psi_0\rangle\langle\Psi_0|$ on the initial State, we obtain (note $t_0 = 0$)

$$P_{\mathrm{surv}}(t) = \langle \Psi(t)|\Psi_0\rangle\langle\Psi_0|\Psi(t)\rangle = \sum_{a,b} |c_a(0)\, c_b(0)|^2 e^{-i\omega_{ab}t}. \tag{3.29}$$

The expression is called *survival probability* since $\langle\Psi_0|\Psi(t)\rangle$ gives the probability amplitude for the initial state to be present in the actual state $|\Psi(t)\rangle$ at time t. $P_{\mathrm{surv}}(t)$ has a time-independent part given by all terms with $a = b$. The summation over the different terms with $a \neq b$ that oscillate with time give rise to a decay of survival probability. Since this is due to the fact that the different terms are running out of phase, one speaks about a *dephasing* at this point.[4] Depending on the number of eigenstates, a *rephasing* triggering a recurrence peak in $P_{\mathrm{surv}}(t)$ may occur during a later stage of the evolution.

In order to illustrate dephasing, we show in Figure 3.2 the survival probability for a system with N eigenstates whose energy spectrum is given by that of a linear molecular chain (cf. Section 2.8.3). To get a pronounced behavior, we take as the initial state an equal distribution of probability ($c_a(0) = 1/\sqrt{N}$). It is evident from

---

4) Notice that following the discussion in the introductory part of this chapter, it would be more appropriate to speak about decoherence.
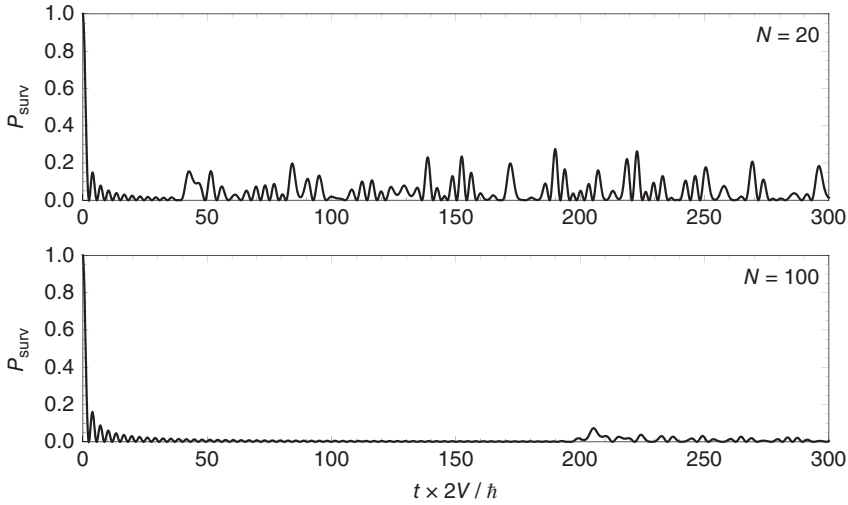
Figure 3.2 Survival probability for a system with N eigenstates ($N = 20, 100$). The energy spectrum is that of a linear regular chain according to Eq. (2.182), and the initial values $c_a(0)$ have been set equal to $1/\sqrt{N}$.

this figure that with increasing N, the structured behavior of $P_{\text{surv}}(t)$ seen for $N = 20$ disappears in the considered time interval. Note that for $N = 100$, there is some indication of a partial rephasing after about 200 fs.

We notice that even when there is complete dephasing, the survival amplitude does not decay to zero but to the time-independent limit $P_{\text{surv}}(t \gg 0) = \sum_a |c_a(0)|^4$. Since the coefficients are normalized, the asymptotic value $P_{\text{surv}}(t \gg 0)$ will be proportional to the inverse number of basis states $|a\rangle$ present in the initial state $|\Psi_0\rangle$. Thus, only in the case of an infinite number of eigenstates participating in the dynamics is it possible that the survival amplitude vanishes completely.

3.2.2 The Interaction Representation

If the Hamiltonian H of the system under consideration can be decomposed as $H = H_0 + V$, where V represents a small perturbation of the dynamics given by H_0, an expansion with respect to V can be performed. Usually, one will attempt to separate H such that the eigenvalue problem of H_0 can be solved analytically or by means of numerical diagonalization. Provided such a separation can be made, the time-dependent state vector

$$|\Psi(t)\rangle = U(t, t_0)|\Psi(t_0)\rangle \tag{3.30}$$

is conveniently written as

$$|\Psi(t)\rangle = U_0(t, t_0)|\Psi^{(\text{I})}(t)\rangle. \tag{3.31}$$

This representation makes use of the formal solution that is available for the unperturbed time-dependent Schrödinger equation for H_0, Eq. (3.17), that is

$$U_0(t, t_0) = e^{-iH_0(t-t_0)/\hbar}. \tag{3.32}$$

The new state vector $|\Psi^{(\mathrm{I})}(t)\rangle$ is called the state vector in the interaction representation. Since $U(t_0, t_0) = 1$, we have

$$|\Psi^{(\mathrm{I})}(t_0)\rangle = |\Psi(t_0)\rangle. \tag{3.33}$$

The equation of motion for the state vector in the interaction representation follows directly from the original time-dependent Schrödinger equation,

$$i\hbar \frac{\partial}{\partial t}|\Psi(t)\rangle = U_0(t, t_0)\left(H_0|\Psi^{(\mathrm{I})}(t)\rangle + i\hbar\frac{\partial}{\partial t}|\Psi^{(\mathrm{I})}(t)\rangle\right) = H|\Psi(t)\rangle. \tag{3.34}$$

After some rearrangement, we get (note that $U_0^{-1} = U_0^+$)

$$i\hbar \frac{\partial}{\partial t}|\Psi^{(\mathrm{I})}(t)\rangle = U_0^+(t, t_0)VU_0(t, t_0)|\Psi^{(\mathrm{I})}(t)\rangle \equiv V^{(\mathrm{I})}(t)|\Psi^{(\mathrm{I})}(t)\rangle. \tag{3.35}$$

The quantity $V^{(\mathrm{I})}(t)$ is the interaction representation of the perturbational part of the Hamiltonian. This representation is defined for an arbitrary operator $\hat{O}$ as

$$\hat{O}^{(\mathrm{I})}(t) = U_0^+(t, t_0)\hat{O}U_0(t, t_0). \tag{3.36}$$

The formal solution of Eq. (3.35) is obtained by introducing the so-called *S-operator* (the scattering operator) defined via

$$|\Psi^{(\mathrm{I})}(t)\rangle = S(t, t_0)|\Psi^{(\mathrm{I})}(t_0)\rangle \equiv S(t, t_0)|\Psi(t_0)\rangle, \tag{3.37}$$

where we made use of Eq. (3.33). Comparison with Eq. (3.31) yields

$$U(t, t_0) = U_0(t, t_0)S(t, t_0). \tag{3.38}$$

The *S*-operator can be determined by the iterative solution of the equation of motion (3.35) for $|\Psi^{(\mathrm{I})}\rangle$. The formal time integration gives

$$|\Psi^{(\mathrm{I})}(t)\rangle = |\Psi^{(\mathrm{I})}(t_0)\rangle - \frac{i}{\hbar}\int_{t_0}^{t} d\tau V^{(\mathrm{I})}(\tau)|\Psi^{(\mathrm{I})}(\tau)\rangle. \tag{3.39}$$

This equation is suited to develop a perturbation expansion with respect to $V^{(\mathrm{I})}$. If there is no interaction, one gets

$$|\Psi^{(\mathrm{I},0)}(t)\rangle = |\Psi^{(\mathrm{I})}(t_0)\rangle. \tag{3.40}$$

If we insert this result into the right-hand side of Eq. (3.39), we get the state vector in the interaction representation, which is the first-order correction to $|\Psi^{(\mathrm{I},0)}(t)\rangle$ in the presence of a perturbation,

$$|\Psi^{(\mathrm{I},1)}(t)\rangle = -\frac{i}{\hbar}\int_{t_0}^{t} d\tau_1 V^{(\mathrm{I})}(\tau_1)|\Psi^{(\mathrm{I},0)}(\tau_1)\rangle. \tag{3.41}$$

Upon further iteration of this procedure, one obtains the *n*th-order correction as

$$|\Psi^{(\mathrm{I},n)}(t)\rangle = -\frac{i}{\hbar}\int_{t_0}^{t} d\tau_n V^{(\mathrm{I})}(\tau_n)|\Psi^{(\mathrm{I},n-1)}(\tau_n)\rangle. \tag{3.42}$$

Thus, the total formally exact state vector in the interaction representation is

$$|\Psi^{(\mathrm{I})}(t)\rangle = \sum_{n=0}^{\infty}|\Psi^{(\mathrm{I},n)}(t)\rangle. \tag{3.43}$$

Let us consider the total wave function containing the effect of the interaction up to the order n. This function is obtained by explicit insertion of all orders into the right-hand side of Eq. (3.42)

$$|\Psi^{(I,n)}(t)\rangle = \left(-\frac{i}{\hbar}\right)^n \int_{t_0}^{t} d\tau_n V^{(I)}(\tau_n) \int_{t_0}^{\tau_n} d\tau_{n-1} V^{(I)}(\tau_{n-1}) \times$$

$$\cdots \times \int_{t_0}^{\tau_2} d\tau_1 V^{(I)}(\tau_1)|\Psi^{(I)}(t_0)\rangle$$

$$= \left(-\frac{i}{\hbar}\right)^n \frac{1}{n!} \hat{T} \int_{t_0}^{t} d\tau_n \cdots d\tau_1 V^{(I)}(\tau_n) \cdots V^{(I)}(\tau_1)|\Psi^{(I)}(t_0)\rangle. \qquad (3.44)$$

In the last part of this expression, all integrals are carried out to the upper limit t. Double counting is compensated for by the factor $1/n!$. In order to account for the fact that the time-dependent operators $V^{(I)}$ do not commute for different time arguments, the *time-ordering operator* $\hat{T}$ has been introduced. It orders time-dependent operators from the right to the left with increasing time arguments; that is, if $t_1 > t_2$, $\hat{T}[V^{(I)}(t_2)V^{(I)}(t_1)] = V^{(I)}(t_1)V^{(I)}(t_2)$. This formal rearrangement enables us to write for the exact state vector in the interaction representation

$$|\Psi^{(I)}(t)\rangle = \hat{T} \sum_{n=0}^{\infty} \frac{1}{n!} \prod_{k=1}^{n} \left(-\frac{i}{\hbar} \int_{t_0}^{t} d\tau_k V^{(I)}(\tau_k)\right)|\Psi^{(I)}(t_0)\rangle. \qquad (3.45)$$

The summation on the right-hand side is formally identical to the expansion of the exponential function. Comparing this expression with Eq. (3.37), we see that the S-operator can be written as a *time-ordered exponential function*

$$S(t,t_0) = \hat{T} \exp\left\{-\frac{i}{\hbar} \int_{t_0}^{t} d\tau V^{(I)}(\tau)\right\}. \qquad (3.46)$$

This expression is an example for a compact notation of a resumed perturbation expansion which is very useful when doing formal manipulations with the time-evolution operator. Nevertheless, for any specific calculation, it is necessary to go back to the expansion equation (3.44).[5]

3.2.3 Multidimensional Wave Packet Dynamics

Before discussing density matrix theory which can account for the dynamics of a few relevant DOFs embedded in a macroscopic environment at finite temperature, we briefly review a method for the solution of the multidimensional time-dependent Schrödinger equation. While being of interest on its own, it may also serve as a

---

[5] Note also that the derived expression may serve as the time-evolution operator, Eq. (3.18), for the case of a time-dependent Hamiltonian $H(t)$ (therefore, $V^{(I)}(\tau)$ has to be replaced by $H(\tau)$).

reference for judging approximations in condensed-phase dynamics. Such type of comparative studies became possible with the development of the multiconfiguration time-dependent Hartree (MCTDH) approach. It enables one to treat typical system–reservoir Hamiltonians on the basis of discretized bath DOFs but approaching the continuous limit.

In what follows we consider the time-dependent Schrödinger equation, Eq. (3.1), for f-coupled DOFs $s = \{s_1, \ldots, s_f\}$. In order to derive working equations for its solution, we use the time-dependent Dirac–Frenkel variational principle,

$$\langle \delta\Psi | H(t) - i\hbar \frac{\partial}{\partial t} | \Psi \rangle = 0, \tag{3.47}$$

where $\delta\Psi$ denotes the variation of the wave function. A straightforward generalization of Eq. (3.22) starts from an expansion of the wave packet into a product basis set of known wave functions for the different DOFs, $\overline{\chi}_{j_\kappa}(s_\kappa)$,

$$\Psi(s_1, \ldots s_f, t) = \sum_{j_1=1}^{N_1} \cdots \sum_{j_f=1}^{N_f} c_{j_1 \ldots j_f}(t) \, \overline{\chi}_{j_1}(s_1) \cdots \overline{\chi}_{j_f}(s_f). \tag{3.48}$$

Here, N_κ denotes the number of basis functions employed for the κth DOF. From the variational principle, Eq. (3.47), we obtain a set of coupled first-order differential equations

$$i\hbar \frac{\partial}{\partial t} c_{j_1, \ldots, j_f}(t) = \sum_{k_1, \ldots, k_f} \langle \overline{\chi}_{j_1} \cdots \overline{\chi}_{j_f} | H | \overline{\chi}_{k_1} \cdots \overline{\chi}_{k_f} \rangle c_{k_1, \ldots, k_f}(t). \tag{3.49}$$

The numerical solution of this set of equations becomes unfeasible due to the exponential scaling of the number of configurations that have to be considered on the right-hand side of Eq. (3.48) with increasing dimensionality. However, the large number of configurations derives from the fact that a *fixed* basis set has to accommodate a *moving* wave packet during the whole time interval of the dynamics. It can be expected that a more compact representation of the wave packet can be achieved using *time-dependent* basis functions. The simplest ansatz would consist of just a single Hartree product of time-dependent basis functions, which are called single-particle functions (SPFs), that is[6]

$$\Psi(s_1, \ldots, s_f, t) = A(t) \, \chi_1(s_1, t) \ldots \chi_f(s_f, t). \tag{3.50}$$

The SPFs are expanded into a static basis as before, that is

$$\chi_{j_\kappa}(s_\kappa, t) = \sum_{i_\kappa=1}^{N_\kappa} c_{i_\kappa}(t) \overline{\chi}_{i_\kappa}(s_\kappa). \tag{3.51}$$

In analogy to electronic structure theory, this is called time-dependent Hartree (TDH) ansatz. Notice that this ansatz is not unique since every function can be multiplied by some factor if another one is divided by the same factor. This arbitrariness is distributed by the redundant factor $A(t)$, but at the same time one

---

6) Note that the basis functions for the κth DOF will also be abbreviated by $\chi^{(\kappa)}$.

has to introduce some constraints such as $i\langle \chi^{(\kappa)} \mid \partial \chi^{(\kappa)}/\partial t \rangle = 0^{7)}$ for each DOF to fix these free factors.

Using the Dirac–Frenkel variational principle, Eq. (3.47), one gets upon variation with respect to $A(t)$

$$\left(E(t)A(t) - i\hbar \frac{\partial}{\partial t}A(t) \right) \delta A(t) = 0, \tag{3.52}$$

where we introduced the expectation value of the Hamiltonian

$$E(t) = \langle \chi^{(1)} \cdots \chi^{(f)} \mid H \mid \chi^{(1)} \cdots \chi^{(f)} \rangle. \tag{3.53}$$

Equation (3.52) gives immediately

$$i\hbar \frac{\partial}{\partial t}A(t) = E(t)A(t), \tag{3.54}$$

which can readily be integrated to give

$$A(t) = A(0) \exp\left(-\frac{i}{\hbar} \int\limits_{0}^{t} d\tau E(\tau) \right). \tag{3.55}$$

Variation with respect to $\chi^{(\kappa)}$ yields using Eq. (3.54)

$$
\begin{aligned}
0 = A^*(t) &\left(A(t)\langle \chi^{(1)} \cdots \chi^{(\kappa-1)} \chi^{(\kappa+1)} \cdots \chi^{(f)} \mid H \mid \chi^{(1)} \cdots \chi^{(f)} \rangle \right. \\
&\left. - i\hbar \frac{\partial}{\partial t}(A(t)|\chi^{(\kappa)}\rangle) \right) \delta\chi^{(\kappa)} \\
= |A(0)|^2 &\left(\left[H^{(\kappa)} - E(t) - i\hbar \frac{\partial}{\partial t} \right] |\chi^{(\kappa)}\rangle \right) \delta\chi^{(\kappa)}. \tag{3.56}
\end{aligned}
$$

Here, we introduced the so-called mean-field Hamiltonian which is an operator in the space of the κth DOF

$$H^{(\kappa)} = \langle \chi^{(1)} \cdots \chi^{(\kappa-1)} \chi^{(\kappa+1)} \cdots \chi^{(f)} \mid H \mid \chi^{(1)} \cdots \chi^{(\kappa-1)} \chi^{(\kappa+1)} \cdots \chi^{(f)} \rangle. \tag{3.57}$$

Note that mean-field expressions of this type will appear later on, for example when considering the equation of motion for the density matrix treating the interaction between system and environment in first-order perturbation theory (cf. Section 3.5.3).

We can rewrite Eq. (3.56) using $E|\chi^{(\kappa)}\rangle = |\chi^{(\kappa)}\rangle\langle \chi^{(\kappa)}|H^{(\kappa)}|\chi^{(\kappa)}\rangle$ and obtain the following equation of motion:

$$i\hbar \frac{\partial}{\partial t}|\chi^{(\kappa)}\rangle = (1 - |\chi^{(\kappa)}\rangle\langle \chi^{(\kappa)}|)H^{(\kappa)}|\chi^{(\kappa)}\rangle \qquad \kappa = 1, \dots, f. \tag{3.58}$$

Notice that the projection operator on the right-hand side of Eq. (3.58) ensures that the change of a certain basis function is orthogonal to the space already spanned by this function. This triggers the exploration of new regions of space according to the wave packet dynamics.

Equation (3.58) reveals that the f-dimensional quantum problem has been separated into f one-dimensional problems. However, underlying the use of the TDH method is the assumption that the interaction between the different DOFs can

---

7) Note that, in general, any real function can appear on the right-hand side of this equation.

be reasonably described by their mean fields. In order to go beyond the mean-field description, Eq. (3.50) has to be extended to include more than just a single Hartree product. This is achieved in the MCTDH method which combines the standard ansatz, Eq. (3.48), with the TDH idea of time-dependent basis functions, that is

$$\Psi(s_1, \ldots s_f, t) = \sum_{j_1=1}^{n_1} \cdots \sum_{j_f=1}^{n_f} A_{j_1 \ldots j_f}(t) \; \chi_{j_1}(s_1, t) \ldots \chi_{j_f}(s_f, t). \tag{3.59}$$

First, we notice that in the limit where $n_\kappa = 1$ we recover the TDH ansatz, Eq. (3.50). On the other hand, if we choose $n_\kappa = N_\kappa$ we have the numerically exact wave packet of Eq. (3.48) in the reduced Hilbert space, and the expansion basis will be time independent (see below). The actual advantage comes if $n_\kappa < N_\kappa$; that is, if compared with the fixed basis, less time-dependent basis function can be used to describe the moving wave packet. Equations of motion can be obtained again from the Dirac–Frenkel principle. For the expansion coefficient one derives an equation similar to Eq. (3.49) (although in the present case the Hamiltonian matrix is time dependent), whereas the basis functions follow from

$$i\hbar \frac{\partial}{\partial t} |\boldsymbol{\chi}^{(\kappa)}\rangle = (1 - \mathcal{P}^{(\kappa)})(\boldsymbol{\rho}^{(\kappa)})^{-1} \boldsymbol{H}^{(\kappa)} |\boldsymbol{\chi}^{(\kappa)}\rangle. \tag{3.60}$$

Here, $\boldsymbol{\chi}^{(\kappa)} = (\chi_1, \ldots, \chi_{n_\kappa})^{\mathrm{T}}$ is a vector containing all basis functions for the κth DOF. Further, $\boldsymbol{H}^{(\kappa)}$ is the matrix of mean-field operators acting on the κth DOF. It has the dimension $n_\kappa \times n_\kappa$ and is formed with respect to the basis functions $\boldsymbol{\chi}^{(\kappa)}$.

Similar to Eq. (3.58), a projection operator onto the space spanned by the κth DOF

$$\mathcal{P}^{(\kappa)} = \sum_{j_\kappa=1}^{n_\kappa} |\chi_{j_\kappa}\rangle\langle\chi_{j_\kappa}| \tag{3.61}$$

appears ensuring the exploration of configuration space according to the wave packet motion. Note that, in the complete basis set limit, the right-hand side of this equations becomes equal to the unit operator, and the expansion functions will not change in time according to Eq. (3.60). Additionally, a density matrix enters Eq. (3.60), which is defined as

$$\rho_{jl}^{(\kappa)}(t) = \sum_{j_1} \cdots \sum_{j_{\kappa-1}} \sum_{j_{\kappa+1}} \cdots \sum_{j_f} A^*_{j_1 \ldots j_{\kappa-1} j j_{\kappa+1} \ldots j_f}(t) A_{j_1 \ldots j_{\kappa-1} l j_{\kappa+1} \ldots j_f}(t). \tag{3.62}$$

The equation for the expansion coefficients and Eq. (3.60) constitute a set of nonlinear equations that need to be solved numerically. The range of applicability strongly depends on the type of system and in particular on the number of strongly coupled DOFs. Systems with some thousands of DOFs become accessible upon further structuring the time-dependent wave packet. Strongly coupled DOFs can be combined into multidimensional SPFs. The time dependence of the latter is not obtained via an expansion into a static basis as in Eq. (3.51) but using again the MCTDH ansatz equation (3.59). This procedure is repeated until one reaches the level of Eq. (3.51). The resulting approach is called multilayer MCTDH. A method for incorporating effects due to finite temperature into wave packet propagation is outlined in the supplementary Section 3.15.1. Applications of the MCTDH method will be discussed in Chapters 8 and 9.

3.3 The Golden Rule of Quantum Mechanics

The Golden Rule rate formula (also called Fermi's Golden Rule) is certainly one of the most important and widely used expressions of quantum mechanics. It offers a simple way to determine the transition rate between different quantum states of some zeroth-order Hamiltonians in the presence of a small coupling. Therefore, the formula enables one to calculate the change in probability of some initial state due to transition events as a function of time. The basic assumption is that these transitions are irreversible. As discussed earlier (cf. Sections 3.1 and 3.2), such a behavior can be found whenever the transition proceeds into a macroscopic number of final states forming an energetic continuum. In such a situation, the mutual interferences among the final states and with the initial state preclude any recurrence of probability back into the initial state. The recurrences are additionally suppressed when the coupling between the initial and final states is sufficiently weak. Such an irreversible transition can also be found if a fast relaxation from the final state to further additional states is possible. Here, the final state itself may be discrete, but there is a coupling to another continuum of states.

There exist different situations that lead to a description by the Golden Rule formula. In what follows we present alternatives before we embed the formalism into a more general framework in Section 3.4.5.

3.3.1 Transition from a Single State into a Continuum

Let us consider quantum transitions between some state $|0\rangle$ with energy E_0 and a continuum of states $|\alpha\rangle$ with energies E_α. The state $|0\rangle$ is supposed to be initially populated, and the transitions into the states $|\alpha\rangle$ are due to some interstate coupling expressed by $V_{0\alpha}$. The situation is sketched in Figure 3.3. The total system is described by the Hamiltonian[8]

$$H = E_0|0\rangle\langle 0| + \sum_\alpha \left(E_\alpha|\alpha\rangle\langle\alpha| + V_{0\alpha}|0\rangle\langle\alpha| + V_{\alpha 0}|\alpha\rangle\langle 0| \right). \tag{3.63}$$

Our goal is to obtain an expression that tells us how the initially prepared state $|0\rangle$ decays into the set of states $|\alpha\rangle$. This transfer of occupation probability can be characterized by looking at the population of state $|0\rangle$, which reads

$$P_0(t) = |\langle 0|U(t)|0\rangle|^2. \tag{3.64}$$

Figure 3.3 Coupling of the single-state $|0\rangle$ to the manifold of states $|\alpha\rangle$ as described by the Hamiltonian (3.63).

$E_0 \;\rule[0.5ex]{1em}{0.4pt}\; \longleftarrow\; V_{0\alpha}\; \longrightarrow\; \equiv E_\alpha$

---
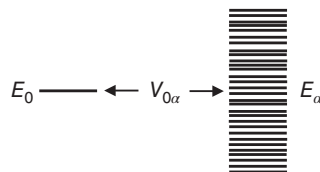
8) This setup is similar to a system of two adiabatic states where $|0\rangle$ denotes an initial electron-vibrational state, and the set $|\alpha\rangle$ contains the vibrational states belonging to the final electronic state.

$U(t)$ is the time-evolution operator, already introduced in Eq. (3.18), and defined here by the Hamiltonian equation (3.63). Note that $P_0(t)$ is a survival probability as introduced in Eq. (3.29).

Provided that one would know the eigenstates of the Hamiltonian (3.63), the survival amplitude would take the form (3.29). Of course, introducing the eigenstates of (3.63) is not the appropriate way to compute, for example the decay time since a large Hamiltonian has to be diagonalized.

As an alternative, let us derive equations of motion for the matrix elements of the time-evolution operator

$$A_{\nu\mu}(t) = \theta(t)\langle\nu|U(t)|\mu\rangle. \tag{3.65}$$

The quantum numbers μ and ν represent the states $|0\rangle$ and $|\alpha\rangle$, and the unit-step function $\theta(t)$ has been introduced to restrict the definition of $A_{\nu\mu}(t)$ to times larger than zero. The quantity $A_{\nu\mu}(t)$ is called *transition amplitude* and tells us how the state $|\nu\rangle$ is contained in the propagated state $U(t)|\mu\rangle$ at time t if at time $t = 0$ the system was in the state $|\mu\rangle$. The survival amplitude, $P_0(t)$, is equal to $|A_{00}(t)|^2$.

The equations of motion for the transition amplitudes read[9]

$$i\hbar\frac{d}{dt}A_{\nu\mu} = i\hbar\delta(t)\,\delta_{\nu\mu} + \sum_\kappa \langle\nu|H|\kappa\rangle A_{\kappa\mu}. \tag{3.66}$$

In order to solve Eq. (3.66), we introduce the Fourier transform of the transition amplitudes

$$A_{\nu\mu}(\omega) = \int dt\, e^{i\omega t} A_{\nu\mu}(t). \tag{3.67}$$

Taking the Fourier transform of Eq. (3.66), we obtain for the transition amplitudes the following equations:

$$\hbar\omega A_{\nu\mu}(\omega) = i\hbar\,\delta_{\nu\mu} + \sum_\kappa \langle\nu|H|\kappa\rangle A_{\kappa\mu}(\omega). \tag{3.68}$$

In particular, for $\nu = \mu = 0$, this gives

$$\hbar\omega A_{00}(\omega) = i\hbar + E_0 A_{00}(\omega) + \sum_\alpha V_{0\alpha} A_{\alpha 0}(\omega). \tag{3.69}$$

The off-diagonal elements, $A_{\alpha 0}(\omega)$, can be obtained from

$$\hbar\omega A_{\alpha 0}(\omega) = E_\alpha A_{\alpha 0}(\omega) + V_{\alpha 0} A_{00}(\omega). \tag{3.70}$$

Inserting the solution of this equation into the equation for A_{00} yields a closed equation for the latter quantity, which can be solved to give

$$A_{00}(\omega) = i\hbar \left(\hbar\omega - E_0 - \sum_\alpha \frac{|V_{0\alpha}|^2}{\hbar\omega - E_\alpha + i\varepsilon} + i\varepsilon \right)^{-1}. \tag{3.71}$$

Here, ε has to be understood as a small and positive number that we will let go to zero at the end of the calculation. It guarantees that $A_{00}(\omega)$ is an analytical function in the upper part of the complex frequency plane, and consequently, that the

---

9) Note that Dirac's delta function appears on the right-hand side since the time derivative of the unit-step function is given by $d\theta(t)/dt = \delta(t)$.

inverse Fourier transform becomes proportional to $\theta(t)$. Carrying out the backtransformation into the time domain, we obtain the desired occupation probability as $P_0(t) = |A_{00}(t)|^2$.

The contributions in the denominator of $A_{00}(\omega)$, which are proportional to the square of the coupling matrix, result in a complicated frequency dependence of $A_{00}(\omega)$. One effect is apparent: the coupling to the continuum shifts the energy E_0 of the initial state to a new value. This shift, which is in general a complex quantity, is commonly called *self-energy*

$$\Sigma(\omega) = \sum_\alpha \frac{|V_{0\alpha}|^2}{\hbar\omega - E_\alpha + i\varepsilon}. \tag{3.72}$$

The separation into a real and imaginary part gives[10]

$$\Sigma(\omega) \equiv \hbar\Delta\Omega(\omega) - i\hbar\Gamma(\omega) = \sum_\alpha \mathcal{P} \frac{|V_{0\alpha}|^2}{\hbar\omega - E_\alpha} - i\pi \sum_\alpha |V_{0\alpha}|^2 \delta(\hbar\omega - E_\alpha). \tag{3.73}$$

If the energies E_α form a continuum, the summation with respect to α has to be replaced by an integration. In this case, and provided that the coupling constant has no strong dependence on the quantum number α, the variation in the self-energy in the region where $\hbar\omega \approx E_0$ can be expected to be rather weak. This means that the frequency dependence of $A_{00}(\omega)$ is dominated by the resonance at $\hbar\omega = E_0$. Since this will give the major contribution to the inverse Fourier transform, we can approximately replace $\hbar\omega$ in $\Sigma(\omega)$ by E_0. In contrast, if the levels E_α were discrete, $\Sigma(\omega)$ would go to infinity at $\hbar\omega = E_\alpha$, and the frequency dependence of the self-energy can no longer be neglected.

To carry out the inverse Fourier transformation, we replace the quantity $\Sigma(\omega)$ by the frequency-independent value $\Sigma(E_0/\hbar)$ and obtain the desired state population $P_0(t)$ as

$$P_0(t) = \left| \int \frac{d\omega}{2\pi} e^{-i\omega t} \frac{i\hbar}{\hbar\omega - (E_0 + \hbar\Delta\Omega(E_0/\hbar)) + i\hbar\Gamma(E_0/\hbar)} \right|^2$$
$$= \theta(t) \, e^{-2\Gamma(E_0/\hbar)t}. \tag{3.74}$$

The integral has been calculated using the residue theorem of the theory of complex functions. As expected, the occupation probability of the initially occupied state $|0\rangle$ decreases in time due to transitions into the manifold of states $|\alpha\rangle$. For the time evolution of P_0, one gets from Eq. (3.74) the simple equation

$$\frac{d}{dt} P_0(t) = -2\Gamma P_0(t), \tag{3.75}$$

which is a particular example for Eq. (3.2).[11] Following Eq. (3.2), the rate of change of the survival probability is called k. It is defined as

$$k = 2\Gamma = \frac{2\pi}{\hbar} \sum_\alpha |V_{0\alpha}|^2 \, \delta(E_0 - E_\alpha). \tag{3.76}$$

---

10) Here, we used the Dirac identity, which states that expressions $\propto 1/(\hbar\omega + i\varepsilon)$ appearing in a frequency integral can be rewritten as $\mathcal{P} \, 1/\hbar\omega - i\pi\delta(\hbar\omega)$, where $\mathcal{P}$ denotes the principal part evaluation of the integral.

11) Note that, in principle, the right-hand side of the equation has to be supplemented by the term $\delta(t)P_0(0)$ which stems from the time derivate of the unit-step function.

This type of expression is known as the *Golden Rule* of quantum mechanics. It was first discussed by P. A. M. Dirac and E. Fermi. According to Eq. (3.76), the Golden Rule allows the determination of the rate for occupation probability transfer from some initial state $|0\rangle$ into the manifold of final states $|\alpha\rangle$. The delta function appearing in the rate expression can be interpreted as the energy conservation law for the transition. Only those transitions from $|0\rangle$ to $|\alpha\rangle$ are possible for which the energy of the initial state E_0 matches some energy E_α of the final states. The rate is proportional to the square of the interstate coupling $V_{0\alpha}$. This is a direct consequence of replacing the variable energy argument of the self-energy, $\hbar\omega$, by E_0. Otherwise, higher order approximations with respect to the coupling would have been obtained. Furthermore, it should be taken into account that the derivation assumed an initial population of the discrete state $|0\rangle$, which is not an eigenstate of the complete system. Therefore, Eq. (3.76) is only justified for the case of a weak coupling matrix $V_{0\alpha}$. For cases with stronger coupling, the Golden Rule expression for the transition rate would be valid at best for times less than the recurrence time.

3.3.2 Transition Rate for a Thermal Ensemble

Let us extend the considerations of the preceding section in two respects. We introduce a manifold of initial states labeled by $|a\rangle$ that is coupled to some final states $|\beta\rangle$ (see Figure 3.4; to have a clear notation, the final state manifold quantum numbers α have been replaced by β). Moreover, we change from the consideration of a single system to an ensemble of N independent but identical systems that are in thermal contact to a reservoir. The generalization of the Hamiltonian (3.63) reads

$$H = \sum_a E_a |a\rangle\langle a| + \sum_\beta E_\beta |\beta\rangle\langle\beta| + \sum_{a,\beta} \left(V_{a\beta} |a\rangle\langle\beta| + \text{h.c.} \right). \tag{3.77}$$

The situation described by this Hamiltonian is typical, for example for the nonadiabatic coupling between two electronic states in a molecule where the manifolds $\{|a\rangle\}$ and $\{|\beta\rangle\}$ take the role of the different vibrational states. Various realizations of this scenario are discussed in the forthcoming chapters.

Since we consider an ensemble of systems, where the initially prepared state $|a\rangle$ may be different for each member of the ensemble, we count the different systems by the index m. The population $P_{ma}(t)$ gives the probability that the system m is in the particular state $|a\rangle$. Its time dependence follows as

$$P_{ma}(t) = \theta(t) e^{-k_a t} P_{ma}(0), \tag{3.78}$$
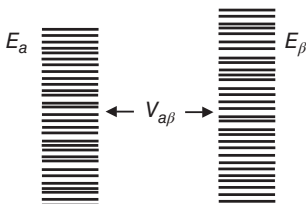
Figure 3.4 Coupling of the manifold of initial states $\{|a\rangle\}$ to the manifold of final states $\{|\beta\rangle\}$ as described by the Hamiltonian (3.77).

where $P_{ma}(0)$ defines the probability to have system m initially in the particular state $|a\rangle$. The transition rate characterizing the population decay of this state is

$$k_a = \frac{2\pi}{\hbar} \sum_\beta |V_{a\beta}|^2 \delta(E_a - E_\beta). \tag{3.79}$$

Since different systems are in different states, the quantity $P_m(t) = \sum_a P_{ma}(t)$ gives the probability to have system m in the initial manifold independent of the actual state. Therefore, $P_m(t)$ represents a *reduced probability*. Often, observables measured in the experiment are only determined by such a reduced quantity. We assume that initially all considered systems have been prepared in one of the states $|a\rangle$. Then, we get $\sum_m P_m(0) = N$. It is suitable to introduce the probability to have the state $|a\rangle$ realized in the ensemble. This probability takes the form

$$P_a(t) = \frac{1}{N} \sum_m P_{ma}(t). \tag{3.80}$$

The overall probability to have the initial state manifold populated follows as $P_i(t) = \sum_a P_a(t)$. Since we assumed that the ensemble stays initially in thermal equilibrium with some environment at temperature T, we can write

$$P_a(0) = f_a, \tag{3.81}$$

where we introduced the quantum statistical equilibrium distribution

$$f_a = \frac{\exp(-E_a/k_B T)}{\sum_{a'} \exp(-E_{a'}/k_B T)}. \tag{3.82}$$

To discuss the actual situation where a finite coupling to the environment is present, two characteristic times will be introduced. First, we have the time scale τ_{S-R}, which characterizes the coupling of the different members of the ensemble to the thermal reservoir. For example, τ_{S-R} could be the collision time of the system of interest with the atoms or molecules forming the reservoir. Second, the interstate coupling introduces a time scale given by $1/k_a$. Now, we can distinguish the cases $\tau_{S-R} \gg 1/k_a$ (slow thermalization compared to the transition), $\tau_{S-R} \ll 1/k_a$ (fast thermalization), and $\tau_{S-R} \approx 1/k_a$ (intermediate case).

Case $\tau_{S-R} \gg 1/k_a$:
We suppose that the interaction with an external field promotes the ensemble into the state manifold $\{|a\rangle\}$, where each state occurs N_a times in the ensemble. Since the interaction with the environment is weak compared to the state coupling, the overall initial state manifold population will evolve according to $P_i(t) = \sum_a N_a/N \times \exp(-k_a t)$ (absence of thermalization on the time scale of the transfer).

Case $\tau_{S-R} \ll 1/k_a$:
Here, thermalization proceeds at every time step of the transfer, and we may set $P_a(t) = f_a P_i(t)$. It remains to determine $P_i(t)$. To derive the appropriate equation, let us introduce the time step $\Delta t \approx \tau_{S-R}$. Usually, we will be interested in the time evolution of the system on time scales much longer than Δt. Therefore, we can consider Δt to be a continuous quantity on the time scale of observation (*coarse graining*

of the time axis). We obtain for $t + \Delta t$:

$$P_a(t + \Delta t) \approx (1 - k_a \Delta t) f_a P_i(t). \tag{3.83}$$

The total initial state population follows as

$$P_i(t + \Delta t) \approx P_i(t) - \sum_a k_a f_a P_i(t) \Delta t. \tag{3.84}$$

Because Δt has been assumed to be very small, we can rewrite the expression as

$$\frac{P_i(t + \Delta t) - P_i(t)}{\Delta t} \approx \frac{d}{dt} P_i(t) = -k_{i \to f} P_i(t), \tag{3.85}$$

where we introduced the rate for transitions from a thermalized state manifold

$$k_{i \to f} = \sum_a f_a k_a = \frac{2\pi}{\hbar} \sum_{a,\beta} f_a |V_{a\beta}|^2 \ \delta(E_a - E_\beta). \tag{3.86}$$

The strong coupling of the system of interest to a thermal reservoir results in a rate expression which is the thermal average of the transition rate k_a, Eq. (3.79).

Case $\tau_{\text{S-R}} \approx 1/k_a$:
In this case, one can no longer make a separation of time scales, and the reasoning used in the previous two cases breaks down. A more general description of the simultaneous influence of the interstate coupling and the coupling to the reservoir is necessary; this more general approach is offered by the *density matrix theory*.

Up to now our discussion has been concentrated on the transitions from the states $|a\rangle$ (the initial states) to the states $|\beta\rangle$ (the final states). Of course, one can also consider the reverse process along the same line of arguments. We expect that the rate $k_{i \to f}$ of the forward transition from the initial to the final state manifold and the population P_i have counterparts, which are the reverse rate $k_{f \to i}$ and the final state population P_f, respectively. $k_{f \to i}$ follows from Eq. (3.86) by interchanging f_a with the thermal distribution f_β (transfer starts from the thermalized distribution at the state manifold $|\beta\rangle$)

$$k_{f \to i} = \frac{2\pi}{\hbar} \sum_{\beta,a} f_\beta |V_{\beta a}|^2 \delta(E_\beta - E_a). \tag{3.87}$$

Instead of a single rate equation for $P_i(t)$, one obtains the *Pauli master equations* already discussed in Section 3.1

$$\frac{d}{dt} P_i(t) = -k_{i \to f} P_i(t) + k_{f \to i} P_f(t), \tag{3.88}$$

$$\frac{d}{dt} P_f(t) = -k_{f \to i} P_f(t) + k_{i \to f} P_i(t). \tag{3.89}$$

The population P_i decreases due to transitions into the final state manifold. However, it increases by the reverse process. The same holds for the population P_f (a more rigorous derivation will be offered in Sections 3.4.5 and 3.14).

The possible transfer forth and back between the state manifolds $\{|a\rangle\}$ and $\{|\beta\rangle\}$ needs comments. It seems as if recurrences (as a result of constructive wave function interference) are incorporated. However, on a much shorter time scale and resulting from the coupling to the reservoir, any phase relation among the states $|a\rangle$ has been destroyed. We can therefore state that a completely *incoherent* transfer takes place.

It is easy to find the solution of the above given coupled rate equations. Because conservation of probability $P_i(t) + P_f(t) = 1$ holds, the two equations can be transformed to a single one for $P_i(t) - P_f(t)$. Taking as the initial condition $P_i(0) = 1$, the solutions read (note $K = k_{i \to f} + k_{f \to i}$)

$$P_i(t) = \frac{1}{K} \left(k_{i \to f} e^{-Kt} + k_{f \to i} \right) , \qquad P_f(t) = \frac{k_{i \to f}}{K} \left(1 - e^{-Kt} \right) . \tag{3.90}$$

It is instructive to put both solutions ($\kappa = i, f$) into the form

$$P_\kappa(t) = P_\kappa(\infty) + \left(P_\kappa(0) - P_\kappa(\infty) \right) e^{-Kt}, \tag{3.91}$$

with $P_i(\infty) = k_{f \to i}/K$ and $P_f(\infty) = k_{i \to f}/K$. As it has to be expected, the result indicates a complete depletion of the initial state if there is no backtransfer ($k_{f \to i} = 0$). Otherwise, both manifolds remain populated.

A generalization of the Pauli master equation to a larger set of different states is straightforward. As an example, one may consider adiabatic Born–Oppenheimer states, where each state manifold would represent the vibrational eigenstate for a particular electronic state. To obtain a general solution of Eq. (3.2), we denote the right-hand side as $-\sum_b K_{ab} P_b$ with the general rate-matrix $K_{ab} = \delta_{ab} \sum_{c \neq a} k_{a \to c} - (1 - \delta_{ab}) k_{b \to a}$. Given the eigenvalues $\kappa(\eta)$ and (normalized) eigenvectors $e_a(\eta)$ of K_{ab}, the general solution for the population of state $|a\rangle$ reads as $P_a(t) = \sum_\eta c(\eta) e_a(\eta) \exp(-\kappa(\eta)t)$ (η counts the rate matrix eigenvalues). The additional factors $c(\eta)$ are determined from the initial conditions. The decay of the various populations is multiexponential. Since the smallest $\kappa(\eta)$ equals zero, the respective term in $P_a(t)$ fixes $P_a(\infty)$. It is obvious that the given solution (except for some special examples) can be only achieved by numerical computations.

The Pauli master equation has found numerous applications, and we will return to it in the subsequent chapters. However, the basic assumptions are those leading to the Golden Rule for the transition rates, which are not always fulfilled (see above). In order to go beyond this level of description, a more flexible theory for open quantum systems has to be introduced. This will be done in the following section where we discuss the density matrix approach. It goes without saying that the Pauli master equation will be recovered as a limiting case of the more general quantum master equation which is derived below.

3.3.3 Green's Function Approach

The computation scheme used in the foregoing section to calculate the transition rate from level $|0\rangle$ into the manifold of levels $|\alpha\rangle$ can be casted into a more formal frame. Instead of working with time-evolution operator matrix elements of the type given in Eq. (3.65), we introduce

$$\hat{G}(t) = -i\theta(t)e^{-iHt/\hbar}. \tag{3.92}$$

This quantity is known as the *Green's operator* defined by the Hamiltonian H, Eq. (3.63). Let us write the Hamiltonian as

$$H = H_0 + H_1 + V, \tag{3.93}$$

where H_0 corresponds to level $|0\rangle$, H_1 covers all levels $|\alpha\rangle$, and the coupling between them is V. The equation of motion for $\hat{G}(t)$ simply reads

$$i\hbar\frac{\partial}{\partial t}\hat{G}(t) = \hbar\delta(t) + H\hat{G}(t). \tag{3.94}$$

Introducing the Fourier transform

$$\hat{G}(\omega) = \int dt\, e^{i\omega t}\hat{G}(t) \tag{3.95}$$

translates the equation of motion into

$$(\omega - H/\hbar)\hat{G}(\omega) = 1. \tag{3.96}$$

We may also compute the Fourier-transformed Green's operator directly, which gives

$$\hat{G}(\omega) = -i\int\limits_0^\infty dt\, e^{i\omega t}e^{-iHt/\hbar} = \frac{1}{\omega - H/\hbar + i\varepsilon}. \tag{3.97}$$

The obtained expression has to be understood as the inverse of the operator $\omega - H/\hbar$ with a small imaginary contribution $i\varepsilon$ indicating the form of the solution of Eq. (3.96) for $\hat{G}(\omega)$ (it should have a pole below the real axis in the complex frequency plane).

To get the time dependence of the population of level $|0\rangle$, Eq. (3.64), we have to compute

$$P_0(t) = |\langle 0|\hat{G}(t)|0\rangle|^2. \tag{3.98}$$

The respective matrix elements of the Green's operator are deduced from its equation of motion by introducing projection operators. The operator

$$\hat{\Pi}_0 = |0\rangle\langle 0| \tag{3.99}$$

projects on the single-state $|0\rangle$, and the operator

$$\hat{\Pi}_1 = \sum_\alpha |\alpha\rangle\langle\alpha| \tag{3.100}$$

on the manifold of states $|\alpha\rangle$. Both projection operators enter the completeness relation

$$\hat{\Pi}_0 + \hat{\Pi}_1 = 1, \tag{3.101}$$

which can be used, for example to write $\hat{\Pi}_1 = 1 - \hat{\Pi}_0$.

The goal of the following derivation is to obtain an explicit expression for the population, Eq. (3.98). First, we determine the reduced Green's operator

$$\hat{G}_0(t) = \hat{\Pi}_0\hat{G}(t)\hat{\Pi}_0 \tag{3.102}$$

instead of directly focusing on its matrix element with state $|0\rangle$. Using the equation of motion for the Fourier-transformed Green's operator $\hat{G}(\omega)$, we may derive an equation for $\hat{G}_0(\omega)$. By applying $\hat{\Pi}_0$ to Eq. (3.96) from the left and from the right, we get

$$\hat{\Pi}_0(\omega - H/\hbar)\left(\hat{\Pi}_0 + \hat{\Pi}_1\right)\hat{G}(\omega)\hat{\Pi}_0 = \hat{\Pi}_0. \tag{3.103}$$

For further computations, we note that $\hat{\Pi}_0 H \hat{\Pi}_0 = H_0$, $\hat{\Pi}_1 H \hat{\Pi}_1 = H_1$, and $\hat{\Pi}_0 H \hat{\Pi}_1 = \hat{\Pi}_0 V \hat{\Pi}_1$ (cf. Eq. (3.93)). It gives

$$(\omega - H_0/\hbar)\hat{G}_0 - \hat{\Pi}_0 (V/\hbar)\hat{\Pi}_1 \times \hat{\Pi}_1 \hat{G}(\omega)\hat{\Pi}_0 = \hat{\Pi}_0. \tag{3.104}$$

The new quantity $\hat{\Pi}_1 \hat{G}(\omega)\hat{\Pi}_0$ obeys

$$\hat{\Pi}_1 (\omega - H/\hbar)\left(\hat{\Pi}_0 + \hat{\Pi}_1\right) \hat{G}(\omega)\hat{\Pi}_0 = \hat{\Pi}_1 \hat{\Pi}_0 = 0 \tag{3.105}$$

or

$$-\hat{\Pi}_1 V/\hbar \hat{\Pi}_0 \hat{G}_0(\omega) + (\omega - H_1/\hbar)\hat{\Pi}_1 \hat{G}(\omega)\hat{\Pi}_0 = 0. \tag{3.106}$$

We define

$$[\hat{G}_1^{(0)}(\omega)]^{-1} = \omega - H_1/\hbar, \tag{3.107}$$

which represents the inverse of a zeroth-order Green's operator (it is defined without the coupling V). Then, the equation for $\hat{\Pi}_1 \hat{G}(\omega)\hat{\Pi}_0$ can be rewritten as

$$\hat{\Pi}_1 \hat{G}(\omega)\hat{\Pi}_0 = \hat{G}_1^{(0)}(\omega)\hat{\Pi}_1 (V/\hbar)\hat{\Pi}_0 \hat{G}_0(\omega). \tag{3.108}$$

If inserted into the equation for $\hat{G}_0$, we obtain

$$\left(\omega - H_0/\hbar - \hat{\Pi}_0 (V/\hbar)\hat{\Pi}_1 \hat{G}_1^{(0)}(\omega)\hat{\Pi}_1 (V/\hbar)\hat{\Pi}_0\right) \hat{G}_0 = \hat{\Pi}_0. \tag{3.109}$$

We analyze the extra term, which depends on V, and get

$$\hat{\Pi}_0 (V/\hbar)\hat{\Pi}_1 \hat{G}_1^{(0)}(\omega)\hat{\Pi}_1 (V/\hbar)\hat{\Pi}_0 = \frac{1}{\hbar^2} \sum_\alpha \frac{V_{0\alpha} V_{\alpha 0}}{\omega - E_\alpha/\hbar + i\varepsilon}\hat{\Pi}_0$$

$$\equiv \hat{\Sigma}(\omega)/\hbar. \tag{3.110}$$

The operator $\hat{\Sigma}$ is the self-energy operator. It represents the operator version of Eq. (3.72), and its introduction gives for the reduced Green's operator

$$\hat{G}_0(\omega) = \frac{\hat{\Pi}_0}{\omega - H_0/\hbar - \hat{\Sigma}(\omega)/\hbar + i\varepsilon}. \tag{3.111}$$

Let us separate the self-energy operator into a Hermitian and an anti-Hermitian part

$$\hat{\Sigma}(\omega) = \frac{1}{2}\left(\hat{\Sigma}(\omega) + \hat{\Sigma}^+(\omega)\right) + \frac{1}{2}\left(\hat{\Sigma}(\omega) - \hat{\Sigma}^+(\omega)\right) \equiv \Delta H(\omega) - i\pi\hbar\hat{\Gamma}(\omega). \tag{3.112}$$

Noting Eq. (3.73), we can identify the Hermitian part as

$$\Delta H(\omega) = \hbar\Delta\Omega(\omega)\hat{\Pi}_0, \tag{3.113}$$

and the anti-Hermitian part as

$$\hat{\Gamma}(\omega) = \Gamma(\omega)\hat{\Pi}_0. \tag{3.114}$$

Inserting Eq. (3.111) for $\hat{G}_0$ into the above given expression for the level population $P_0(t)$, we reproduce Eq. (3.74). At first glance, the derivation of known results may seem as a useless exercise. However, the Green's operator approach will show its advantages later on if more complex quantum systems are considered.

3.4 The Nonequilibrium Statistical Operator and the Density Matrix

3.4.1 The Density Operator

According to quantum mechanics, a *complete description* of a system is only possible if a set of observables exists from which all physical quantities can be measured simultaneously. This situation is described by a set of commuting operators $\{\hat{A}_\alpha\}$; that is, the relation

$$\left[\hat{A}_\alpha, \hat{A}_{\alpha'}\right]_- = \hat{A}_\alpha \hat{A}_{\alpha'} - \hat{A}_{\alpha'} \hat{A}_\alpha = 0 \tag{3.115}$$

has to be fulfilled for all possible pairs of indices. If for the considered system the maximal number of such operators is known, a complete description can be accomplished.

The measurement of some set of observables corresponds to the application of the respective operators $\hat{A}_\alpha$ on the state vector $|\Psi\rangle$. If this exclusively gives the eigenvalues a_α; that is, if

$$\hat{A}_\alpha |\Psi\rangle = a_\alpha |\Psi\rangle, \tag{3.116}$$

the state $|\Psi\rangle$ is called a *pure* state. Alternatively, one can say that a pure state is prepared if a measurement of all observables belonging to the operators $\hat{A}_\alpha$ has been carried out (complete measurement). The expectation value of any operator $\hat{O}$ can be determined as

$$\langle \hat{O} \rangle = \langle \Psi | \hat{O} | \Psi \rangle. \tag{3.117}$$

The choice of a complete set of observables is not unique. There may exist another complete set $\{\hat{B}_\beta\}$, independent of the set $\{\hat{A}_\alpha\}$. The respective pure states are denoted as $|\Phi_\nu\rangle$. Then, the *superposition principle* of quantum mechanics states that the superposition of all pure states related to the complete set $\{\hat{B}_\beta\}$ reproduces *any* pure state $|\Psi\rangle$:

$$|\Psi\rangle = \sum_\nu c_\nu |\Phi_\nu\rangle. \tag{3.118}$$

If the complete measurement of all $\hat{A}_\alpha$ has not been carried out, for example because the complete set of observables is principally unknown, only an incomplete description of a quantum system is possible (incomplete preparation or measurement of the system). In this case, the state of the quantum system has to be described as a *statistical mixture* of pure states $|\Psi_\nu\rangle$. The probability of a single state to be in the mixture will be denoted as w_ν. The states $|\Psi_\nu\rangle$ are assumed to be normalized, and therefore, the w_ν must satisfy the relation

$$\sum_\nu w_\nu = 1. \tag{3.119}$$

Although it is not necessary to demand that the states $|\Psi_\nu\rangle$ form an orthonormal set, it is convenient to do so in what follows. Hence, we require in addition that

$$\langle \Psi_\mu | \Psi_\nu \rangle = \delta_{\mu\nu}. \tag{3.120}$$

According to this characterization of a mixture of pure states, the expectation value of an observable becomes

$$\langle \hat{O} \rangle = \sum_\nu w_\nu \langle \Psi_\nu | \hat{O} | \Psi_\nu \rangle. \tag{3.121}$$

This expression provides the idea of the *density operator* (the statistical operator), which will be defined as

$$\hat{W} = \sum_\nu w_\nu | \Psi_\nu \rangle \langle \Psi_\nu |. \tag{3.122}$$

It is a summation of projection operators on the states $|\Psi_\nu\rangle$ weighted by the probabilities w_ν. This definition allows a simple notation of the expectation value of any observable using the *trace formula*

$$\langle \hat{O} \rangle = \text{tr}\{\hat{W}\hat{O}\}. \tag{3.123}$$

The abbreviation "tr" is defined as the trace with respect to the matrix formed by all matrix elements that are determined in a complete orthonormal basis $|a\rangle$

$$\text{tr}\{\dots\} = \sum_a \langle a | \dots | a \rangle. \tag{3.124}$$

If $\hat{O}$ and $\hat{P}$ are two operators acting in the Hilbert space spanned by the basis set $|a\rangle$, we have

$$\text{tr}(\hat{O}\hat{P}) = \sum_\alpha \langle a|\hat{O}\hat{P}|a\rangle = \sum_{a,b} \langle a|\hat{O}|b\rangle \langle b|\hat{P}|a\rangle$$
$$= \sum_{a,b} \langle b|\hat{P}|a\rangle \langle a|\hat{O}|b\rangle = \text{tr}(\hat{P}\hat{O}). \tag{3.125}$$

This property is called *cyclic invariance* of the operator arrangement in a trace expression (it is also valid if three or more operators are involved). The density operator is normalized such that $\text{tr}\{\hat{W}\} = 1$. If this is not the case it can always be achieved by replacing $\hat{W}$ with $\hat{W}/\text{tr}\{\hat{W}\}$. Furthermore, we mention that the density operator is Hermitian, $\hat{W} = \hat{W}^+$, which follows from Eq. (3.122).

As an example we give the canonical density operator for the thermal equilibrium

$$\hat{W}_{\text{eq}} = \frac{1}{\mathcal{Z}} e^{-H/k_\text{B}T} = \frac{1}{\mathcal{Z}} \sum_\alpha e^{-E_\alpha/k_\text{B}T} |\alpha\rangle\langle\alpha|. \tag{3.126}$$

Here, $\mathcal{Z}$ is the partition function $\text{tr}[\exp\{-H/k_\text{B}T\}]$ ensuring proper normalization of $\hat{W}_{\text{eq}}$. The second part of Eq. (3.126) is obtained using the eigenenergies E_α and eigenstates $|\alpha\rangle$ of the Hamiltonian H.

Further, we quote the density operator of a pure state $|\Psi\rangle$, which is defined via the operator projecting onto the pure state

$$\hat{W}_{\text{pure}} = |\Psi\rangle\langle\Psi| = \hat{\Pi}_\Psi. \tag{3.127}$$

Comparing this expression with the general definition of the density operator equation (3.122), it is obvious that $\hat{W}_{\text{pure}}$ corresponds to the special case where all probabilities w_ν are equal to zero except the one related to the state vector $|\Psi\rangle$.

Suppose that we expand the state vector $|\Psi\rangle$ with respect to the complete orthogonal basis $|\alpha\rangle$,

$$|\Psi\rangle = \sum_\alpha c_\alpha |\alpha\rangle. \tag{3.128}$$

Introducing this expansion into the expression for the pure state density operator, one obtains

$$\hat{W}_{\text{pure}} = \sum_{\alpha,\overline{\alpha}} c_\alpha c_{\overline{\alpha}}^* |\alpha\rangle\langle\overline{\alpha}| \neq \sum_\alpha |c_\alpha|^2 |\alpha\rangle\langle\alpha|. \tag{3.129}$$

The last part of this equation indicates that this expansion does not result in projections onto the basis states $|\alpha\rangle$. Instead, the flip operators $|\alpha\rangle\langle\overline{\alpha}|$ introduce a mixture of states $|\alpha\rangle$ and $|\overline{\alpha}\rangle$, which results in nonvanishing off-diagonal elements of the matrix $(c_\alpha^* \, c_{\overline{\alpha}})$. This is typical for pure states expanded in a particular basis set.

There exists a measure that tells us whether the state is a pure state or not. This measure is called the *degree of coherence* and is defined as

$$C = \text{tr}\{\hat{W}^2\}. \tag{3.130}$$

It takes the value 1 for pure states since the statistical operator in this case is a projector

$$C_{\text{pure}} = \text{tr}\{\hat{W}_{\text{pure}}^2\} = \text{tr}\{\hat{\Pi}_\Psi^2\} = \text{tr}\{\hat{\Pi}_\Psi\} = \text{tr}\{\hat{W}_{\text{pure}}\} = 1, \tag{3.131}$$

where the projector property $\hat{\Pi}_\Psi^2 = \hat{\Pi}_\Psi$ has been used. For a mixed state, it follows that

$$
\begin{aligned}
C_{\text{mixed}} = \text{tr}\{\hat{W}^2\} &= \sum_{\mu,\nu} w_\mu w_\nu \, \text{tr}\left\{\hat{\Pi}_{\Psi_\mu} \hat{\Pi}_{\Psi_\nu}\right\} \\
&= \sum_{\mu,\nu} \sum_\alpha w_\mu w_\nu \langle\alpha|\Psi_\mu\rangle\langle\Psi_\mu|\Psi_\nu\rangle\langle\Psi_\nu|\alpha\rangle \\
&= \sum_\mu \sum_\alpha w_\mu^2 \langle\Psi_\mu|\alpha\rangle\langle\alpha|\Psi_\mu\rangle = \sum_\mu w_\mu^2 < 1.
\end{aligned}
\tag{3.132}
$$

Hence, the degree of coherence becomes less than 1. If one studies this quantity for time-dependent density operators, the decrease in C indicates the loss of coherence during the time evolution, which is caused by the interaction of the relevant system with the reservoir.

3.4.2 The Density Matrix

In Section 3.1, the concept of the density matrix has been introduced. In order to discuss the density matrix formalism in more detail, we consider a complete orthogonal basis of states $|a\rangle$. Using the completeness relation, the density operator can be expanded as

$$\hat{W} = \sum_{a,b} \langle a|\hat{W}|b\rangle \, |a\rangle\langle b|. \tag{3.133}$$

The expansion coefficients are called *density matrix* and denoted by

$$\rho_{ab} = \langle a|\hat{W}|b\rangle. \tag{3.134}$$

Alternatively, we may use the flip operator $|b\rangle\langle a|$ to write the density matrix as the quantum statistical average of this operator

$$\rho_{ab} = \text{tr}\left\{\hat{W}|b\rangle\langle a|\right\}. \tag{3.135}$$

Since the density operator $\hat{W}$ is Hermitian, the density matrix fulfills the relation

$$\rho_{ab} = \rho_{ba}^*, \tag{3.136}$$

from which one simply deduces

$$\text{Re } \rho_{ab} = \text{Re } \rho_{ba}, \qquad \text{Im } \rho_{ab} = -\text{Im } \rho_{ba}. \tag{3.137}$$

In particular, it follows from this expression that the diagonal elements of the density matrix are real:

$$\rho_{aa} = \text{Re } \rho_{aa}. \tag{3.138}$$

Alternatively, one can use the definition (3.122) of the density operator to write

$$\rho_{aa} = \langle a|\hat{W}|a\rangle = \sum_\nu \langle a|w_\nu|\Psi_\nu\rangle\langle\Psi_\nu|a\rangle$$
$$= \sum_\nu w_\nu |\langle a|\Psi_\nu\rangle|^2, \tag{3.139}$$

which also yields the real diagonal elements. Additionally, it shows that ρ_{aa} gives us the probability for the state $|a\rangle$ being contained in the statistical mixture described by $\hat{W}$. And indeed, $\rho_{aa} \geq 0$, since w_ν and $|\langle a|\Psi_\nu\rangle|^2$ are larger than 0. Taking the off-diagonal matrix elements of the density operator, it follows that

$$\rho_{ab} = \sum_\nu w_\nu c_a(\nu) c_b^*(\nu), \tag{3.140}$$

with the expansion coefficients $c_a(\nu) = \langle a|\Psi_\nu\rangle$. Apparently, the density matrix ρ_{ab} describes an *incoherent* superposition of contributions from different pure states. Depending on the basis set $\{|a\rangle\}$, the different terms on the right-hand side of Eq. (3.140) can cancel each other or give a finite ρ_{ab}. The off-diagonal density matrices are also called *coherences*.

Since the definition of the density matrix, Eq. (3.133), represents a quadratic form, the Schwarz inequality,

$$\rho_{aa}\rho_{bb} \geq |\rho_{ab}|^2, \tag{3.141}$$

holds. Equation (3.141) is particularly useful for checking the quality of any numerical or analytical approximation to the density matrix.

The representation of the statistical operator equation (3.133) via the density matrix introduced in Eq. (3.134) is frequently termed *state representation*. If eigenstates of some Hamiltonian are used, it is also called *energy representation*. Alternatively, it is possible to use, for example *eigenstates* of the coordinate operator

$$|s\rangle = \prod_j |s_j\rangle \tag{3.142}$$

or the momentum operator

$$|p\rangle = \prod_j |p_j\rangle, \tag{3.143}$$

with coordinate $|s_j\rangle$ and momentum states $|p_j\rangle$ for the jth DOF of the system, respectively. Consequently, the *coordinate representation* of the statistical operator (density matrix in the coordinate representation) reads

$$\rho(s, \bar{s}) = \langle s|\hat{W}|\bar{s}\rangle. \tag{3.144}$$

In the same way, the *momentum representation* can be introduced. This allows us to define the respective probability distribution $\rho(s, s)$ in coordinate space and the distribution $\rho(p, p)$ in momentum space.

Both types of density matrices cannot straightforwardly be related to the *classical* distribution function in phase space. This limit is conveniently approached using the so-called *Wigner* representation, which is defined as

$$\rho(x, p) = \int dr \, e^{-ipr/\hbar} \, \rho(x + r/2, x - r/2). \tag{3.145}$$

To simplify the notation, we first concentrate on the case of a single coordinate. The arguments of the density matrix in the coordinate representation, $\rho(s, \bar{s})$, have been transformed to a difference coordinate $r = s - \bar{s}$ and to a sum coordinate $x = (s + \bar{s})/2$. The dependence on the momentum p enters via a Fourier transformation with respect to the difference coordinate. Apparently, $\rho(x, p)$ is a *phase space* representation of the density operator. Its generalization to the case of many coordinates requires the introduction of difference and sum coordinates for every DOF. Given $\rho(x, p)$, the probability distribution with respect to the coordinate x and the momentum p can be obtained by integration over p and x, respectively. The advantage of this representation is that in the classical limit ($\hbar \to 0$), the density matrix $\rho(x, p)$ can be directly related to the phase space distribution of classical statistical physics (Section 3.4.4).

3.4.3 Equation of Motion for the Density Operator

According to the definition of the density operator $\hat{W}$, Eq. (3.122), the probabilities w_ν represent our reduced knowledge about the state of the system. Furthermore, we note that the state vectors $|\Psi_\nu(t)\rangle$ of the mixed state evolve in time, of course, according to the time-dependent Schrödinger equation

$$i\hbar \frac{\partial}{\partial t}|\Psi_\nu(t)\rangle = H|\Psi_\nu(t)\rangle. \tag{3.146}$$

Although any individual state of the mixture changes in time, there is no change whatsoever in our knowledge about the system. In particular, the probabilities w_ν weighting the contribution of the different states $|\Psi_\nu\rangle$ to the mixed state are constant ($w_\nu \neq w_\nu(t)$). The only exception occurs if a measurement has been done on the system. It is known from the basics of quantum mechanics that the result of a measurement process is a reduction in the state of the system onto an eigenstate of the operator corresponding to the observable that has been measured. This means that the mixed state collapses into a pure state. If the pure state is, for example $|\Psi_{\nu_0}\rangle$, all w_ν will be zero except the one related to the final pure state, which is equal to unity: $w_\nu = \delta_{\nu\nu_0}$.

According to this reasoning, the time-dependent density operator has the following form:

$$\hat{W}(t) = \sum_\nu w_\nu |\Psi_\nu(t)\rangle\langle\Psi_\nu(t)|. \tag{3.147}$$

In order to derive an equation of motion, we write the solution of the time-dependent Schrödinger equation by means of the time-evolution operator, Eq. (3.18), $|\Psi_\nu(t)\rangle = U(t, t_0)|\Psi_\nu(t_0)\rangle$. Then, we obtain for the density operator

$$\hat{W}(t) = \sum_\nu w_\nu U(t, t_0)|\Psi_\nu(t_0)\rangle\langle\Psi_\nu(t_0)|U^+(t, t_0)$$

$$= U(t, t_0)\hat{W}(t_0)U^+(t, t_0). \tag{3.148}$$

Taking the time derivative of this expression, it follows

$$\frac{\partial}{\partial t}\hat{W}(t) = -\frac{i}{\hbar}\left(H\hat{W}(t) - \hat{W}(t)H\right) \equiv -\frac{i}{\hbar}\left[H, \hat{W}(t)\right]_-. \tag{3.149}$$

This is the equation of motion for the density operator $\hat{W}$. It is called *Liouville–von Neumann* or *quantum Liouville* equation because of its formal analogy to the equation for the classical statistical distribution function.[12] The advantage of the Liouville–von Neumann equation is its capability to directly propagate mixed states without reference to the underlying time-dependent Schrödinger equations. It is also obvious from Eq. (3.149) that any density operator which is given by a mixture of *eigenstates* of the respective Hamiltonian remains stationary. For a concrete example, we refer to the canonical density operator, Eq. (3.126).

Next, we give the Liouville–von Neumann equation (3.149) in the state representation, Eq. (3.134). One easily derives:

$$\frac{\partial}{\partial t}\rho_{ab} = -i\frac{H_{aa} - H_{bb}}{\hbar}\rho_{ab} - \frac{i}{\hbar}\sum_{c\neq a}H_{ac}\rho_{cb} + \frac{i}{\hbar}\sum_{c\neq b}H_{cb}\rho_{ac}. \tag{3.150}$$

The difference of the diagonal matrix elements of the Hamiltonian defines the transition frequency $\omega_{ab} = (H_{aa} - H_{bb})/\hbar$, whereas the off-diagonal matrix elements describe the interstate coupling.

There exists an alternative notation of the Liouville–von Neumann equation that has its origin in the so-called Liouville space formulation of quantum statistical dynamics. The Liouville space is a linear vector space whose elements are the ordinary operators of the Hilbert space. An operator acting in Liouville space is called a *superoperator*. We will not make full use of this concept here but introduce superoperators as a convenient shorthand notation. The most important example for a superoperator is the *Liouville superoperator* defined via the commutator with the Hamiltonian:

$$\mathcal{L}\ldots = \frac{1}{\hbar}[H, \ldots]_-. \tag{3.151}$$

We see immediately that the Liouville–von Neumann equation can be written as

$$\frac{\partial}{\partial t}\hat{W}(t) = -i\mathcal{L}\hat{W}(t), \tag{3.152}$$

---

12) The classical distribution function depends on all coordinates and momenta and is defined in the so-called phase space spanned by all coordinates and momenta.

with the solution

$$\hat{W}(t) = e^{-i\mathcal{L}(t-t_0)} \, \hat{W}(t_0).$$ (3.153)

The exponential function of the superoperator is defined via the respective power expansion. In analogy to Eq. (3.18), one can introduce the time-evolution superoperator as follows:

$$\mathcal{U}(t, t_0) = e^{-i\mathcal{L}(t-t_0)}.$$ (3.154)

Comparing Eqs. (3.153) and (3.148), we see that $\mathcal{U}(t, t_0)$ is acting on some operator from the left *and* the right, that is

$$\hat{W}(t) = \mathcal{U}(t, t_0)\hat{W}(t_0) = U(t, t_0)\hat{W}(t_0)U^+(t, t_0).$$ (3.155)

This is, of course, a consequence of the definition of $\mathcal{L}$ in terms of a commutator.

3.4.4 Wigner Representation of the Density Operator

In Section 3.4.2 it was discussed that the matrix elements of the density operator can be considered in the coordinate representation, momentum representation, and also in a mixture of both, which is the Wigner representation $\rho(x, p)$, Eq. (3.145). Here, we derive the Liouville–von Neumann equation for the density operator in the Wigner representation. As we will see, for instance in Section 3.9, it is not only of conceptional but also of great practical interest to carry out the classical limit, giving the classical phase space distribution.

Inspecting Eq. (3.149), it is clear that one needs to find the Wigner representation of some operator product $\hat{Z} = \hat{X}\hat{Y}$. First, we introduce the coordinate representation of $\hat{Z}$

$$Z(s, \bar{s}) = \int ds' \, X(s, s') \, Y(s', \bar{s}).$$ (3.156)

As in Eq. (3.145), we concentrate on the case of a single coordinate and obtain the Wigner representation for $Z(s, \bar{s})$ as

$$Z(x, p) = \int dr \, ds' \, e^{-ipr/\hbar} X(x + r/2, s') \, Y(s', x - r/2).$$ (3.157)

This expression is not yet satisfactory since it contains the coordinate representation of $\hat{X}$ and $\hat{Y}$ on the right-hand side. We introduce the Wigner representation for these functions by using the inverse of Eq. (3.145) and obtain the expression

$$
\begin{aligned}
Z(x, p) = \frac{1}{(2\pi\hbar)^2} &\int dr \, ds' \, dp' dp'' \\
&\times \exp\left\{\frac{i}{\hbar}\left(-pr + (x + r/2 - s')p' + (s' - x + r/2)p''\right)\right\} \\
&\times X((x + r/2 + s')/2, p') \, Y((s' + x - r/2)/2, p'').
\end{aligned}
$$ (3.158)

In what follows, the quantities X and Y have to be written as functions of the single coordinate argument x only; that is, the r and s' dependence has to be eliminated.

We achieve this using the shift operator introduced in Eq. (2.67). For example, for X, it gives

$$X((x + r/2 + s')/2, p') = X(x - (x - r/2 - s')/2, p')$$

$$= \exp\left\{ -\frac{x - r/2 - s'}{2}\frac{\partial}{\partial x} \right\} X(x, p'). \tag{3.159}$$

Inserting this result and the similar one for the function Y into Eq. (3.158), one obtains

$$Z(x, p) = \frac{1}{(2\pi\hbar)^2} \int dr\, ds'\, dp'dp''$$

$$\times \exp\left(\frac{i}{\hbar}\left(-rp + (x + r/2 - s')p' - (x - r/2 - s')p'' \right) \right)$$

$$\times \left\{ \exp\left(-\frac{x - r/2 - s'}{2}\frac{\partial}{\partial x'} - \frac{x + r/2 - s'}{2}\frac{\partial}{\partial x''} \right) \right.$$

$$\left. \times X(x', p')Y(x'', p'') \right\}_{x'=x''=x} . \tag{3.160}$$

A more compact notation is obtained if we take into account that the prefactors of the coordinate derivatives in the shift operators appear again in the first exponential function. Therefore, we write the integrand in Eq. (3.160) as

$$Z(x, p) = \frac{1}{(2\pi\hbar)^2} \int dr\, ds'\, dp'dp''$$

$$\times \left\{ \left\{ \exp\left[-\frac{i\hbar}{2}\frac{\partial}{\partial \overline{p}''}\frac{\partial}{\partial x'} + \frac{i\hbar}{2}\frac{\partial}{\partial \overline{p}'}\frac{\partial}{\partial x''} \right] \right.$$

$$\left. \times \exp\left[\frac{i}{\hbar}(x + r/2 - s')\overline{p}' - \frac{i}{\hbar}(x - r/2 - s')\overline{p}'' \right] \right\}_{\substack{|\overline{p}'=p' \\ |\overline{p}''=p''}}$$

$$\times X(x', p')Y(x'', p'') \right\}_{x'=x''=x} . \tag{3.161}$$

This notation enables us to carry out all four integrations. To do this, we order the terms with respect to s', x, and r. The integration with respect to s' results in the delta function $\delta(p' - p'')$. At the same time, the term proportional to x in the exponent and the p''-integration vanishes. Finally, the integration with respect to r leads to $p = p'$, which removes the p'-integration. The final result can be put into a compact notation if one introduces the operator

$$\hat{\Theta} = \frac{\partial}{\partial x}\frac{\partial}{\partial p'} - \frac{\partial}{\partial x'}\frac{\partial}{\partial p}. \tag{3.162}$$

It results in the Wigner representation of the operator product $\hat{Z} = \hat{X}\hat{Y}$ as

$$Z(x, p) = \left\{ e^{i\hbar\hat{\Theta}/2}X(x, p)Y(x', p') \right\}_{\substack{|x=x' \\ |p=p'}} . \tag{3.163}$$

Frequently, the operator equation (3.162) is also written as

$$\hat{\Theta} = \frac{\overleftarrow{\partial}}{\partial x}\frac{\overrightarrow{\partial}}{\partial p} - \frac{\overleftarrow{\partial}}{\partial x}\frac{\overrightarrow{\partial}}{\partial p}, \tag{3.164}$$

where the arrows indicate the direction of the action of the derivative. Using this notation, Eq. (3.163) can be written as

$$Z(x, p) = X(x, p)e^{i\hbar\hat{\Theta}/2}Y(x, p) = Y(x, p)e^{-i\hbar\hat{\Theta}/2}X(x, p). \tag{3.165}$$

Although exact, this compact expression for the Wigner transformation can only be handled after expanding the exponential function. Since this corresponds to an expansion in powers of $\hbar$, it can be used to obtain the classical limit.

To introduce the Wigner representation of the Liouville–von Neumann equation, we consider from now on the case where any coordinate argument x and any momentum argument p have to be understood as a set of coordinates and momenta, $x = \{x_j\}$ and $p = \{p_j\}$, respectively. This requires generalizing Eq. (3.162) to an expression where a summation with respect to all derivatives has to be taken. Additionally, we take into account that the Wigner representation of an operator exclusively defined via the coordinate operator or the momentum operator is a function depending on the coordinate or the momentum, respectively, alone. Therefore, one obtains for the potential operator the Wigner representation $U(x)$, and for kinetic energy $T(p)$. Let us start with the following form of the Liouville–von Neumann equation:

$$\frac{\partial\rho(x, p; t)}{\partial t} = -\frac{i}{\hbar} \int dr \, e^{-ipr/\hbar} \, \langle x + r/2|\left[H, \hat{W}(t)\right]_-|x - r/2\rangle. \tag{3.166}$$

To obtain the classical limit, $\hbar \to 0$, Eq. (3.165) has to be expanded up to the first order in the $\hat{\Theta}$-operator:

$$\frac{\partial\rho(x, p; t)}{\partial t} = -\frac{i}{\hbar} \left\{ \left[1 + \frac{i\hbar}{2}\hat{\Theta}\right] \left[H(x, p)\rho(x', p'; t) - \rho(x, p; t)H(x', p')\right] \right\}_{\substack{|x=x' \\ |p=p'}}. \tag{3.167}$$

The zero-order contribution vanishes, and the classical limit results in

$$\frac{\partial\rho(x, p; t)}{\partial t} = \mathcal{L}_{cl}\rho(x, p; t)$$

$$= \sum_j \left\{ \frac{\partial U(x)}{\partial x_j} \frac{\partial}{\partial p_j}\rho(x, p; t) - \frac{\partial T(p)}{\partial p_j} \frac{\partial}{\partial x_j}\rho(x, p; t) \right\}. \tag{3.168}$$

This relation is known from classical statistical mechanics as the *Liouville equation*, and $\mathcal{L}_{cl}$ is the classical Liouville operator. It describes the reversible time evolution of the phase space probability distribution. To determine $\rho(x, p; t)$, one has to fix an initial distribution $\rho_0(x, p)$. Then, one can solve the partial differential equation (3.168). The solution can be written as

$$\rho(x, p; t) = \int d\bar{x}d\bar{p} \, \delta\big(x - x(\bar{x}, \bar{p}; t)\big) \, \delta\big(p - p(\bar{x}, \bar{p}; t)\big) \, \rho_0(\bar{x}, \bar{p}), \tag{3.169}$$

where $x(\bar{x}, \bar{p}; t)$ and $p(\bar{x}, \bar{p}; t)$ denote the solution of the classical equations of motion for the coordinates and momenta, respectively, following from the initial values $\bar{x}$ and $\bar{p}$. The $\bar{x}, \bar{p}$-integral accounts for all those initial values that constitute the initial distribution $\rho_0(\bar{x}, \bar{p})$.

3.4.5 Dynamics of Coupled Multilevel Systems in a Heat Bath

As a first application of the density operator method, we consider two coupled multilevel systems as already introduced in Eq. (3.77). It is not the aim here to derive new results, rather we would like to give an alternative derivation of what has been introduced in Section 3.3.2. In particular, a number of approximations are introduced, which we will discuss again later on in Section 3.6.1. Following Section 3.3.2, each multilevel system is described by the energies E_a and E_β, respectively, and the coupling between them is due to the matrix element $V_{a\beta}$ of the coupling operator V. For both quantum numbers, a and β, we again use the running indices μ, ν, etc. Accordingly, the Hamiltonian equation (3.77) can be expressed by the common energies E_μ and coupling matrices $V_{\mu\nu}$ (of course, $V_{aa'} = V_{\beta\beta'} = 0$). The density matrix relevant for this system is $\rho_{\mu\nu}(t) = \langle \mu | \hat{W}(t) | \nu \rangle$, and it obeys an equation of motion of the type given in Eq. (3.150) with the transition frequencies $\omega_{\mu\nu} = (E_\mu - E_\nu)/\hbar$.

   As in Section 3.3, the subject of the following consideration is to derive a closed set of equations of motion for the total population of the state manifold $\{|a\rangle\}$ (the initial state manifold)

$$P_i(t) = \sum_a \rho_{aa}(t) \equiv \sum_a P_a(t), \tag{3.170}$$

and the total population of the manifold $\{|\beta\rangle\}$ (the final state manifold)

$$P_f(t) = \sum_\beta \rho_{\beta\beta}(t) \equiv \sum_\beta P_\beta(t). \tag{3.171}$$

The coupling of the two multilevel systems to the heat bath will not be specified any further here. The only assumption we will make is that this coupling is much stronger than the interstate coupling $V_{a\beta}$ (this is identical to the assumption of Section 3.3.2). Thus, the rates for transitions within the two manifolds, $k_{a\to a'}$ and $k_{\beta\to\beta'}$, are supposed to be much larger than those for interstate probability transfer. As a consequence, the populations of the initial and final states can be assumed to be thermalized within the two manifolds on the time scale of the intermanifold transfer. Accordingly, the populations are written as

$$P_a(t) = P_i(t) f_a , \qquad P_\beta(t) = P_f(t) f_\beta. \tag{3.172}$$

Recall that this ansatz corresponds to a coarse graining of the time axis, which has already been introduced in Section 3.3.2. Within this framework, we search for equations of motion obeyed by the total populations P_i and P_f, which are based on Eq. (3.150). Since the coupling matrix element should be small, a perturbational treatment is appropriate. We start with an equation of motion for the diagonal elements of the density matrix, $\rho_{\mu\mu} = P_\mu$, and get from Eq. (3.150), assuming $V_{\mu\mu} = 0$,

$$\frac{\partial}{\partial t} P_\mu = -\frac{i}{\hbar} \sum_\kappa \left(V_{\mu\kappa} \rho_{\kappa\mu} - V_{\kappa\mu} \rho_{\mu\kappa} \right) \equiv \frac{2}{\hbar} \mathrm{Im} \sum_\kappa V_{\mu\kappa} \rho_{\kappa\mu}. \tag{3.173}$$

The off-diagonal density matrix elements that appear on the right-hand side have to be determined too. They obey

$$\frac{\partial}{\partial t}\rho_{\kappa\mu} = -i\omega_{\kappa\mu}\rho_{\kappa\mu} - \frac{i}{\hbar}\sum_{\lambda}\left(V_{\kappa\lambda}\rho_{\lambda\mu} - V_{\lambda\mu}\rho_{\kappa\lambda}\right)$$

$$\approx -i\omega_{\kappa\mu}\rho_{\kappa\mu} - \frac{i}{\hbar}V_{\kappa\mu}\left(\rho_{\mu\mu} - \rho_{\kappa\kappa}\right). \tag{3.174}$$

Since we are looking for the lowest order approximation in $V_{\mu\nu}$, off-diagonal density matrix elements have been neglected in the second line. Fixing the initial condition as $\rho_{\alpha\beta}(0) = 0$ (absence of a superposition state between both subsystems) or more generally $\rho_{\mu\nu} = 0$ for $\mu \neq \nu$, we can solve Eq. (3.174) by formal integration and obtain

$$\rho_{\kappa\mu}(t) = -\frac{i}{\hbar}\,V_{\kappa\mu}\int_{0}^{t}d\bar{t}\;e^{-i\omega_{\kappa\mu}\,(t-\bar{t})}\,[P_{\mu}(\bar{t}) - P_{\kappa}(\bar{t})]. \tag{3.175}$$

Inserting the result into Eq. (3.173) yields (note the replacement of $\bar{t}$ by $t - \tau$)

$$\frac{\partial}{\partial t}P_{\mu} = -\frac{1}{\hbar^2}\sum_{\kappa}|V_{\mu\kappa}|^2\,2\mathrm{Re}\int_{0}^{t}d\tau\;e^{-i\omega_{\kappa\mu}\,\tau}\,[P_{\mu}(t-\tau) - P_{\kappa}(t-\tau)]. \tag{3.176}$$

The total state populations P_i and P_f are obtained by making use of the thermalization condition, Eq. (3.172). If these expressions are introduced into Eq. (3.176), we get

$$\frac{\partial}{\partial t}P_i = -\int_{0}^{t}d\tau\,[K_{i\to f}(\tau)\,P_i(t-\tau) - K_{f\to i}(\tau)\,P_f(t-\tau)], \tag{3.177}$$

with the integral kernel given by

$$K_{i\to f}(\tau) = \frac{2}{\hbar^2}\sum_{a,\beta}|V_{a\beta}|^2\,f_a\;\cos(\omega_{a\beta}\tau). \tag{3.178}$$

The kernel referring to the inverse transition is obtained in replacing f_a by f_β. Interchanging i and f leads to the equation for $P_f(t)$. The quantity $K_{i\to f}(\tau)$ is usually named *memory kernel* since it reflects that Eq. (3.177) is not an ordinary rate equation as Eq. (3.2). As a consequence of the time integral, the state populations enter the equation at a time τ earlier than t. In other words, the system retains the *memory* of its past dynamics. Master equations, such as Eq. (3.177), that include memory effects are called *generalized master equations* (GMEs).

The time dependence of the memory kernel is determined by the structure of the energy spectrum related to the initial and the final states. If these spectra are dense, $K_{i\to f}(\tau)$ would decay in a certain time interval τ_{mem} due to destructive interference (cf. Section 3.2). If τ_{mem} is short compared to the characteristic time where the populations P_i and P_f change, the variation in both quantities within the interval $[t - \tau_{\mathrm{mem}}, t]$ can be neglected, and we can replace $P_i(t-\tau)$ and $P_f(t-\tau)$ by $P_i(t)$ and $P_f(t)$, respectively, in the integrand. Note that this corresponds to a further coarse graining of the time axis. According to both coarse graining approximations, the populations P_i and P_f are only valid for times much larger than τ_{mem}. Therefore,

the result of the integration does not change if the upper limit is put to infinity, and we arrive at the ordinary rate equation

$$\frac{\partial}{\partial t} P_i = -k_{i\to f} \, P_i(t) + k_{f\to i} \, P_f(t), \tag{3.179}$$

where the transition rates take the form

$$k_{i\to f} = \int\limits_0^\infty d\tau \, K_{i\to f}(\tau) = \frac{2}{\hbar^2} \sum_{a,\beta} |V_{a\beta}|^2 f_a \, \mathrm{Re} \int\limits_0^\infty d\tau \, \exp(i\omega_{a\beta}\tau). \tag{3.180}$$

We note that $\mathrm{Re}\,z = (z + z^*)/2$ (where z is an arbitrary complex number) and replace the integral by one along the total time axis. Using the Fourier representation of the δ-function

$$\delta(\omega) = \frac{1}{2\pi} \int\limits_{-\infty}^\infty dt \, e^{i\omega t}, \tag{3.181}$$

we get

$$k_{i\to f} = \frac{2\pi}{\hbar} \sum_{a,\beta} f_a \, |V_{a\beta}|^2 \, \delta(E_a - E_\beta). \tag{3.182}$$

The derived rate formula is identical to the *Golden Rule* expression of the transition rates of Eq. (3.87). Of course, this is not surprising since our derivation of Eq. (3.182) followed the same arguments. A strong coupling to the reservoir is assumed to give fast thermalization, and a quasi-continuous final-state energy spectrum is required to prevent probability revivals from the final to the initial states. Note that the demand for a quasi-continuous energy spectrum was found to correspond to a short memory time of the kernel entering the GME.

It is instructive to view the transition rates from a different perspective. Let us go back to Eq. (3.178) and write

$$\begin{aligned} K_{i\to f}(t) &= \frac{2}{\hbar^2} \, \mathrm{Re} \sum_{a,\beta} |V_{a\beta}|^2 f_a \, e^{i(E_a - E_\beta)t/\hbar} \\ &= \frac{2}{\hbar^2} \, \mathrm{Re} \sum_{a,\beta} f_a \langle a| e^{iE_a t/\hbar} V e^{-iE_\beta t/\hbar} |\beta\rangle\langle\beta|V|a\rangle. \end{aligned} \tag{3.183}$$

Introducing the part $H_0 = \sum_a E_a |a\rangle\langle a| + \sum_\beta E_\beta |\beta\rangle\langle\beta|$ of the total Hamiltonian, Eq. (3.77), we can replace the energies E_a and E_β by H_0 (the coupling part of the Hamiltonian, Eq. (3.77), is denoted by V). Using the completeness relation with respect to the state manifold $|\beta\rangle$ gives

$$\begin{aligned} K_{i\to f}(t) &= \frac{2}{\hbar^2} \mathrm{Re} \sum_a \langle a| \hat{W}_{\mathrm{eq}}^{(i)} e^{iH_0 t/\hbar} V e^{-iH_0 t/\hbar} V |a\rangle \\ &= 2\mathrm{Re} \, C_{i\to f}(t). \end{aligned} \tag{3.184}$$

Here, the distribution f_a has been replaced by the equilibrium density operator of the initial state $\hat{W}_{\mathrm{eq}}^{(i)}$, Eq. (3.126), and we introduced the correlation function $C_{i\to f}(t)$, which can also be written as

$$C_{i\to f}(t) = \frac{1}{\hbar^2} \, \mathrm{tr}_i \{ \hat{W}_{\mathrm{eq}}^{(i)} V^{(I)}(t) V^{(I)}(0) \}. \tag{3.185}$$

This represents an *autocorrelation function* of the interstate coupling $V^{(I)}(t)$ written in the interaction representation and taken with respect to the thermal equilibrium ($\mathrm{tr}_i\{\cdots\}$ abbreviates $\sum_a \langle a|\cdots|a\rangle$). Thus, the memory kernel turns out to be proportional to the autocorrelation function of the interstate coupling. A short memory time thus implies a rapid decay of this correlation function. The fact that rate expressions such as (3.182) in general can be written in terms of correlation functions of the perturbational part of the Hamiltonian is of great importance for the understanding as well as the numerical modeling of condensed-phase processes. We will frequently return to this point in the following considerations.

3.5 The Reduced Density Operator and the Reduced Density Matrix

3.5.1 The Reduced Density Operator

Having discussed the concept of the density operator, we are ready to put the idea of the RDM introduced in Section 3.1 into a more rigorous framework. The starting point will be a Hamiltonian H that is separable into a system part H_S, a reservoir part H_R, and the system–reservoir interaction H_{S-R} (cf. Eq. (3.3))

$$H = H_S + H_{S-R} + H_R. \tag{3.186}$$

First, as in Section 3.1, we introduce the density matrix in the coordinate representation, Eq. (3.144), using the states equation (3.142) separated now into

$$|s\rangle = \prod_j |s_j\rangle, \tag{3.187}$$

defined in the state space of the relevant system, and into the states

$$|Z\rangle = \prod_\xi |Z_\xi\rangle, \tag{3.188}$$

defined in the state space of the reservoir. According to the general form of the time-dependent density operator $\hat{W}(t)$, Eq. (3.147), the density matrix in the coordinate representation reads

$$\begin{aligned}
\rho(s, Z; s', Z'; t) &= \langle s| \langle Z| \hat{W}(t) |Z'\rangle |s'\rangle \\
&= \sum_\nu w_\nu \Psi_\nu(s, Z; t) \Psi_\nu^*(s', Z'; t),
\end{aligned} \tag{3.189}$$

with $\Psi_\nu(s, Z; t) = \langle s|\langle Z|\Psi_\nu(t)\rangle$. Following the reasoning of Section 3.1, we introduce the RDM defined in the state space of the relevant system only. This quantity is obtained by carrying out an integration with respect to the set of reservoir coordinates Z, that is,

$$\rho(s, s'; t) = \int dZ \, \langle s|\langle Z| \hat{W}(t) |Z\rangle|s'\rangle = \langle s|\hat{\rho}(t)|s'\rangle, \tag{3.190}$$

where the RDO of the relevant system

$$\hat{\rho}(t) = \int dZ \, \langle Z|\hat{W}(t)|Z\rangle \tag{3.191}$$

has been introduced. It is defined by taking the trace of the total density operator with respect to a particular basis in the reservoir state space. Instead of the coordinate states $|Z\rangle$, any basis $|\alpha\rangle$ in the reservoir state space may be chosen,

$$\hat{\rho}(t) = \sum_\alpha \langle\alpha|\hat{W}(t)|\alpha\rangle = \text{tr}_\text{R}\left\{\hat{W}(t)\right\}, \tag{3.192}$$

that is, the trace with respect to the reservoir states reduces the total density operator $\hat{W}$ to the RDO $\hat{\rho}$.

Besides the coordinate representation of the density matrix equation (3.190), any basis $|a\rangle$ in the state space of the system can be used to define the RDM

$$\rho_{ab}(t) = \langle a|\hat{\rho}(t)|b\rangle. \tag{3.193}$$

As in the case of the total density operator, we expect the following relation to be fulfilled:

$$\text{tr}_\text{S}\{\hat{\rho}(t)\} \equiv \sum_a \rho_{aa}(t) = 1. \tag{3.194}$$

The relation is easily confirmed if we note that $\hat{W}(t)$ entering Eq. (3.192) obeys $\text{tr}\{\hat{W}(t)\} = 1$.

3.5.2 Equation of Motion for the Reduced Density Operator

An equation of motion for the RDM is derived by starting from the respective operator equation for the RDO. From the Liouville–von Neumann equation (3.149), we obtain

$$\frac{\partial}{\partial t}\hat{\rho}(t) = \text{tr}_\text{R}\left\{\frac{\partial}{\partial t}\hat{W}(t)\right\} = -\frac{i}{\hbar}\,\text{tr}_\text{R}\left\{\left[H_\text{S} + H_{\text{S-R}} + H_\text{R}, \hat{W}(t)\right]_-\right\}$$

$$= -\frac{i}{\hbar}\left[H_\text{S}, \hat{\rho}(t)\right]_- - \frac{i}{\hbar}\,\text{tr}_\text{R}\left\{\left[H_{\text{S-R}} + H_\text{R}, \hat{W}(t)\right]_-\right\}. \tag{3.195}$$

In the first part of this equation, we used the fact that the basis that defines the trace in the reservoir space state is time independent. Then, we took into account that the system Hamiltonian H_S is not influenced by the reservoir trace. Therefore, it is possible to introduce the commutator of H_S with respect to the RDO directly. Indeed, we could have anticipated such a contribution since for $H_{\text{S-R}} = 0$, the equation for the RDO should reduce to the Liouville–von Neumann equation (3.149).

The commutator notation for the RDO is not possible for the contributions proportional to $H_{\text{S-R}}$ and H_R. To calculate the commutator with H_R, we take into account Eq. (3.125). The cyclic interchange of operators can be carried out here since H_R exclusively acts in the state space of the reservoir. As a result, the term proportional to H_R vanishes, and the equation of motion for the RDO follows as

$$\frac{\partial}{\partial t}\hat{\rho}(t) = -\frac{i}{\hbar}\left[H_\text{S}, \hat{\rho}(t)\right]_- - \frac{i}{\hbar}\,\text{tr}_\text{R}\left\{\left[H_{\text{S-R}}, \hat{W}(t)\right]_-\right\}. \tag{3.196}$$

Before dealing with the case $H_{\text{S-R}} \neq 0$, we note that the type of equation (3.149) is recovered if $H_{\text{S-R}}$ is neglected. But this Liouville–von Neumann equation is defined by H_S instead of the full Hamiltonian H, and it describes the isolated time evolution of the relevant quantum system. As already pointed out in Section 3.1, the density matrix description of coherent dynamics contains some redundancy, and a wave

function formulation is more appropriate in this case. However, if the RDO describes a mixed state of the isolated system, a generalization of the ordinary time-dependent Schrödinger equation has been achieved. Changing to the more interesting case of the presence of $H_{\text{S-R}}$, we realize that Eq. (3.196) is not yet a closed equation for the RDO. Because of the appearance of $H_{\text{S-R}}$ in the commutator on the right-hand side, it still contains the total density operator. It will be the main task of the following sections to develop approximations that yield the second term in Eq. (3.196) as a functional of the RDO only, such that one has a closed equation for the RDO.

3.5.3 Mean-field Approximation

In a first attempt to close Eq. (3.196), we take the most simple route. Since the total density operator appears on the right-hand side of Eq. (3.196), which includes $H_{\text{S-R}}$ in all orders (according to the given time dependence of $\hat{W}(t)$), we expect that a perturbation theory with respect to $H_{\text{S-R}}$ can be developed. Let us start with the first-order approximation, which is obtained if we replace the total density operator by its $H_{\text{S-R}} \to 0$ limit. In this limit, there are no interactions between the two subsystems. $\hat{W}(t)$ factorizes into $\hat{\rho}(t)$ and an operator $\hat{R}(t)$ that is defined only in the Hilbert space of the reservoir and which obeys $\text{tr}_{\text{R}}\{\hat{R}\} = 1$.

According to our assumptions, the approximated equation of motion for the RDO becomes

$$\frac{\partial}{\partial t}\hat{\rho}(t) = -\frac{i}{\hbar}\left[H_{\text{S}} + \text{tr}_{\text{R}}\{H_{\text{S-R}}\hat{R}(t)\}, \hat{\rho}(t)\right]_{-}. \tag{3.197}$$

This equation is of the type of a Liouville–von Neumann equation for the RDO, but with the only difference here that H_{S} has been supplemented by $\text{tr}_{\text{R}}\{H_{\text{S-R}}\hat{R}(t)\}$. The additional term is the expectation value of the system–reservoir coupling taken with respect to the actual state of the reservoir. (Note that $H_{\text{S-R}}$ and $\hat{R}(t)$ can be interchanged under the trace giving the compact notation of Eq. (3.197)). Since the bath part of $H_{\text{S-R}}$ has been replaced by an expectation value, the result is called *mean-field approximation*[13]. The meaning becomes more obvious if we assume that the system–reservoir interaction Hamiltonian can be factorized into system parts $K_u = K_u(s)$ and into reservoir parts $\Phi_u = \Phi_u(Z)$, that is,

$$H_{\text{S-R}} = \sum_u K_u \Phi_u. \tag{3.198}$$

The index u counts the different contributions that may follow from a particular microscopic model for the coupling of the system to the reservoir. Note that it is not necessary that the single operator K_u or Φ_u is Hermitian. Only the complete coupling Hamiltonian needs to be Hermitian. Since no further restriction has been introduced with respect to these two functions, Eq. (3.198) is sufficiently general to

---

13) The term mean-field approximation indicates that quantum fluctuations are not considered, and that the quantum mechanical operators act only via the "mean field" given by their expectation values. Such a type of approximation has been already considered in Section 2.4 in the framework of the derivation of the Hartree–Fock equations. Therefore, the mean-field approximation is often also called Hartree approximation.

comprise all cases of practical importance. In the subsequent chapters, we discuss several examples supporting this point of view.

Taking the factorized form of $H_{\text{S-R}}$, Eq. (3.197) becomes

$$\frac{\partial}{\partial t}\hat{\rho}(t) = -\frac{i}{\hbar}\left[H_{\text{S}} + \sum_u K_u \, \text{tr}_{\text{R}}\{\Phi_u \hat{R}(t)\}, \hat{\rho}(t)\right]_- . \tag{3.199}$$

For further use, we define the mean-field Hamiltonian

$$H_{\text{mf}} = \sum_u K_u \, \text{tr}_{\text{R}}\{\Phi_u \hat{R}(t)\}. \tag{3.200}$$

Because the time dependence of the reservoir density operator is not known, the equation for the RDO is not closed. But taking an equilibrium assumption for the reservoir and replacing $\hat{R}(t)$ by

$$\hat{R}_{\text{eq}} = e^{-H_{\text{R}}/k_{\text{B}}T}/\text{tr}_{\text{R}}\{e^{-H_{\text{R}}/k_{\text{B}}T}\}, \tag{3.201}$$

Equation (3.199) defines a closed equation. As a convenient abbreviation, we introduce here and for what follows

$$\text{tr}_{\text{R}}\{\hat{R}_{\text{eq}} \ldots\} = \langle \cdots \rangle_{\text{R}}. \tag{3.202}$$

The effect of $\langle\Phi_u\rangle_{\text{R}}$, and thus of the mean-field term, is a shift of the energy scale; that is, it does not give the relaxation behavior discussed in the context of the Golden Rule approach. As we will see below, relaxation is caused by *fluctuations*, $\Phi_u - \langle\Phi_u\rangle_{\text{R}}$, around the mean-field energies. In order to take these into account, we need to go one step further in our perturbation expansion.

But before doing this, we consider the more general case where the mean-field term remains time dependent. In such a situation, we have to set up an additional equation for $\hat{R}(t)$. Understanding it as the RDO of the reservoir and setting

$$\hat{R}(t) = \text{tr}_{\text{S}}\{\hat{W}(t)\}, \tag{3.203}$$

we can repeat the derivation, which leads us to Eq. (3.197) (or Eq. (3.199)), and obtain

$$\frac{\partial}{\partial t}\hat{R}(t) = -\frac{i}{\hbar}\left[H_{\text{R}} + \sum_u \Phi_u \text{tr}_{\text{S}}\{K_u \hat{\rho}(t)\}, \hat{R}(t)\right]_- . \tag{3.204}$$

This equation together with Eq. (3.199) represents a closed set to determine the coupled evolution of the relevant system and the reservoir once respective initial conditions for both types of RDO have been set up. Because the solution of Eq. (3.204) for a macroscopic reservoir becomes impossible, the approach is not suited to describe energy dissipation out of the relevant system. An application of the coupled set of Eqs. (3.199) and (3.204) only makes sense when both subsystems are sufficiently small.

3.5.4 The Interaction Representation of the Reduced Density Operator

In the foregoing section, an equation of motion for the RDO has been derived, which is of first order in $H_{\text{S-R}}$. In the following section, we apply a projection operator

technique. It allows to handle separately the projection of the operator equation onto the subspace of the relevant system and the formulation of a perturbation theory with respect to the system–reservoir coupling H_{S-R}. The latter is conveniently developed by changing to the interaction representation as explained in what follows.

Recall that the formal solution of the Liouville–von Neumann equation can be written as (Eq. (3.148))

$$\hat{W}(t) = U(t - t_0)\hat{W}(t_0)U^+(t - t_0), \tag{3.205}$$

where the time-evolution operator $U(t - t_0)$ is defined with respect to the total Hamiltonian H. One can separate this operator into the "free" time-evolution operator

$$U_0(t - t_0) = \exp\left(-\frac{i}{\hbar}H_S(t - t_0)\right) \exp\left(-\frac{i}{\hbar}H_R(t - t_0)\right)$$
$$\equiv U_S(t - t_0) \, U_R(t - t_0) \tag{3.206}$$

(note that H_S and H_R commute with each other) and the related S-operator (cf. Section 3.2.2)

$$S(t, t_0) = T \exp\left(-\frac{i}{\hbar}\int_{t_0}^{t} d\tau H_{S-R}^{(I)}(\tau)\right). \tag{3.207}$$

This expression contains the system–reservoir coupling Hamiltonian in the interaction representation

$$H_{S-R}^{(I)}(t) = U_0^+(t - t_0)H_{S-R}U_0(t - t_0). \tag{3.208}$$

For the total density operator, we can write

$$\hat{W}(t) = U_0(t - t_0)\hat{W}^{(I)}(t)U_0^+(t - t_0), \tag{3.209}$$

where the density operator in the interaction representation reads

$$\hat{W}^{(I)}(t) = U_0^+(t - t_0)\hat{W}(t)U_0(t - t_0) = S(t, t_0)\hat{W}(t_0)S^+(t, t_0). \tag{3.210}$$

Using this equation, the time derivative of Eq. (3.209) can be written as

$$\frac{\partial}{\partial t}\hat{W}(t) = -\frac{i}{\hbar}[H_0, \hat{W}(t)]_- + U_0(t - t_0)\frac{\partial}{\partial t}\hat{W}^{(I)}(t)U_0^+(t - t_0). \tag{3.211}$$

If we set this expression equal to the right-hand side of the Liouville–von Neumann equation, $-i[H, \hat{W}(t)]_-/\hbar$, we get after some rearrangement

$$\frac{\partial}{\partial t}\hat{W}^{(I)}(t) = -\frac{i}{\hbar}[H_{S-R}^{(I)}(t), \hat{W}^{(I)}(t)]_-. \tag{3.212}$$

Notice that this equation can be viewed as the generalization of Eq. (3.35) to the case of a density operator. Next, we transform the RDO into the interaction representation (using Eq. (3.206))

$$\hat{\rho}(t) = \text{tr}_R\{\hat{W}(t)\} = \text{tr}_R\left\{U_0(t - t_0)\hat{W}^{(I)}(t)U_0^+(t - t_0)\right\}$$
$$= U_S(t - t_0)\text{tr}_R\left\{U_R(t - t_0)\hat{W}^{(I)}(t)U_R^+(t - t_0)\right\} U_S^+(t - t_0). \tag{3.213}$$

Using the cyclic invariance of the trace, we can write

$$\hat{\rho}(t) = U_S(t - t_0)\hat{\rho}^{(I)}(t)U_S^+(t - t_0), \tag{3.214}$$

with the RDO in the interaction representation defined as

$$\hat{\rho}^{(I)}(t) = \text{tr}_R \left\{ \hat{W}^{(I)}(t) \right\}. \tag{3.215}$$

With these definitions, the equation of motion for $\rho^{(I)}(t)$ follows from Eq. (3.212) as

$$\frac{\partial}{\partial t} \hat{\rho}^{(I)}(t) = -\frac{i}{\hbar} \text{tr}_R \left\{ \left[H_{S-R}^{(I)}(t), \hat{W}^{(I)}(t) \right]_- \right\}. \tag{3.216}$$

3.5.5 The Nakajima–Zwanzig Equation

The generation of equations for the RDO of higher order in the system–reservoir coupling requires the combination of a perturbation theory with a scheme for restricting the operator equations to the state space of the relevant system. Suppose that $\hat{O}$ is an operator acting in the space of the system and the reservoir states. Let us consider the quantity $\mathcal{P}$ that acts on $\hat{O}$ as follows

$$\mathcal{P}\hat{O} = \hat{R}\,\text{tr}_R\{\hat{O}\}. \tag{3.217}$$

By definition, $\mathcal{P}$ separates $\hat{O}$ defined in the full space into the part $\text{tr}_R\{\hat{O}\}$ acting only in the system space and an operator $\hat{R}$ which by definition exclusively acts in the state space of the reservoir. In other words, $\mathcal{P}$ factorizes any operator into a system part and into a reservoir part. Since $\mathcal{P}$ is not an operator acting on a wave function, but manipulates operators by itself, it is another example of a superoperator.

If we apply $\mathcal{P}$ to the full density operator, we obtain by definition the RDO $\hat{\rho}$ and some reservoir operator

$$\mathcal{P}\hat{W}(t) = \hat{R}\,\hat{\rho}(t). \tag{3.218}$$

If $\text{tr}_R\{\hat{R}\} = 1$, which we will assume in what follows, the superoperator $\mathcal{P}$ is a projector or more precisely a *projection superoperator*, that is, $\mathcal{P}^2 = \mathcal{P}$, as can be easily proved

$$\mathcal{P}^2\hat{O} = \hat{R}\,\text{tr}_R\{\hat{R}\,\text{tr}_R\{\hat{O}\}\} = \hat{R}\,\text{tr}_R\{\hat{R}\}\,\text{tr}_R\{\hat{O}\} = \mathcal{P}\hat{O}. \tag{3.219}$$

Since $\hat{R}$ has a trace equal to unity, it can be interpreted as a statistical operator restricted to the state space of the reservoir. Although in principle, a time dependence is possible, we take $\hat{R}$ as the (time-independent) equilibrium density operator of the reservoir; that is, we define

$$\mathcal{P}\ldots = \hat{R}_{eq}\,\text{tr}_R\{\cdots\}. \tag{3.220}$$

It is useful to introduce in addition to $\mathcal{P}$ its orthogonal complement

$$\mathcal{Q} = 1 - \mathcal{P}. \tag{3.221}$$

The operator $\mathcal{Q}$ is a projection superoperator as well, and by construction, we have

$$\mathcal{Q}\mathcal{P} = \mathcal{P}\mathcal{Q} = 0. \tag{3.222}$$

The action of Q on the total density operator leads to

$$Q\hat{W}(t) = \hat{W}(t) - \hat{\rho}(t)\hat{R}_{\text{eq}}. \tag{3.223}$$

This is often called the irrelevant part of the statistical operator.

Both projectors, $\mathcal{P}$ and $\mathcal{Q}$, can be used to systematically develop a perturbation expansion with respect to $H_{\text{S–R}}$ in the equation of motion for the RDO. To achieve this goal, we start our considerations in the interaction representation. We have

$$\mathcal{P}\hat{W}^{(\text{I})}(t) = \hat{R}_{\text{eq}}\text{tr}_{\text{R}}\{\hat{W}^{(\text{I})}(t)\} = \hat{R}_{\text{eq}}\hat{\rho}^{(\text{I})}(t). \tag{3.224}$$

Using the identity $\hat{W}^{(\text{I})}(t) = \mathcal{P}\hat{W}^{(\text{I})}(t) + \mathcal{Q}\hat{W}^{(\text{I})}(t)$, the Liouville–von Neumann equation (3.149) can be split into two coupled equations. First, we have

$$\mathcal{P}\frac{\partial}{\partial t}\hat{W}^{(\text{I})}(t) = -\frac{i}{\hbar}\mathcal{P}\left[H_{\text{S–R}}^{(\text{I})}(t), \mathcal{P}\hat{W}^{(\text{I})}(t) + \mathcal{Q}\hat{W}^{(\text{I})}(t)\right]_{-}. \tag{3.225}$$

Taking the trace with respect to the reservoir states, it follows that

$$\begin{aligned}
\text{tr}_{\text{R}}\left\{\mathcal{P}\frac{\partial}{\partial t}\hat{W}^{(\text{I})}(t)\right\} &= \frac{\partial}{\partial t}\hat{\rho}^{(\text{I})}(t) \\
&= -\frac{i}{\hbar}\text{tr}_{\text{R}}\left\{\left[H_{\text{S–R}}^{(\text{I})}(t), \hat{R}_{\text{eq}}\hat{\rho}^{(\text{I})}(t) + \mathcal{Q}\hat{W}^{(\text{I})}(t)\right]_{-}\right\}.
\end{aligned} \tag{3.226}$$

In a similar manner, one obtains the equation of motion for $\mathcal{Q}\hat{W}^{(\text{I})}$ as

$$\frac{\partial}{\partial t}\mathcal{Q}\hat{W}^{(\text{I})}(t) = -\frac{i}{\hbar}\mathcal{Q}\left[H_{\text{S–R}}^{(\text{I})}(t), \hat{R}_{\text{eq}}\hat{\rho}^{(\text{I})}(t) + \mathcal{Q}\hat{W}^{(\text{I})}(t)\right]_{-}. \tag{3.227}$$

By means of these formal manipulations, we have been able to reduce the equation of motion for $\hat{W}^{(\text{I})}$ to a coupled set of equations for $\hat{\rho}^{(\text{I})}$ and $\mathcal{Q}\hat{W}^{(\text{I})}$.

Next, we show that a solution of Eq. (3.227) allows to generate a perturbation expansion with respect to $H_{\text{S–R}}$ on the right-hand side of Eq. (3.226). If we neglect $\mathcal{Q}\hat{W}^{(\text{I})}$ altogether, we recover the result of the previous section; that is, we obtain the mean-field correction to the system dynamics which is of first order in $H_{\text{S–R}}$ (see Eq. (3.197)). The second-order contribution is calculated by inserting a solution of Eq. (3.227) which is of first order in $H_{\text{S–R}}$. The commutator structure of the right-hand side of Eq. (3.226) then results in second-order terms. The formal first-order solution of the equation for $\mathcal{Q}\hat{W}^{(\text{I})}$ is obtained by neglecting $\mathcal{Q}\hat{W}^{(\text{I})}$ on the right-hand side of Eq. (3.227). One obtains

$$Q\hat{W}^{(\text{I})}(t) = Q\hat{W}^{(\text{I})}(t_0) - \frac{i}{\hbar}\int_{t_0}^{t} d\tau\, Q\left[H_{\text{S–R}}^{(\text{I})}(\tau), \hat{R}_{\text{eq}}\hat{\rho}^{(\text{I})}(\tau)\right]_{-}. \tag{3.228}$$

Here, the first part on the right-hand side tells us whether or not $\hat{W}^{(\text{I})}$ initially factorizes into a system and a reservoir part. It is easy to verify that this term vanishes if the total density operator factorizes at $t = t_0$, $\hat{W}(t_0) \to \rho(t_0)\hat{R}_{\text{eq}}$. If such a factorization is not possible, the so-called *initial correlations* between the relevant system and the reservoir have to be taken into account. The time scale for the decay of these initial correlations depends on the details of the system–reservoir coupling. For simplicity, we will not consider this effect in what follows; that is, we assume that $Q\hat{W}^{(\text{I})}(t_0) = 0$.

The third-order contribution to Eq. (3.226) can be obtained by inserting Eq. (3.228) into the right-hand side of Eq. (3.227). The formal solution of the resulting equation is then used in Eq. (3.226). This iteration procedure can be continued to generate all orders of the perturbation expansion. However, one of the advantages of the projection operator approach is that a formal exact summation of the perturbation series is possible. To this end, we start again with Eqs. (3.226) and (3.227). To have a more compact notation, the commutator with the interaction Hamiltonian $H_{\text{S--R}}^{(\text{I})}$ is replaced by the interaction Liouville superoperator $\mathcal{L}_{\text{S--R}}^{(\text{I})}$ defined as

$$\mathcal{L}_{\text{S--R}}^{(\text{I})} \ldots = \frac{1}{\hbar} [H_{\text{S--R}}^{(\text{I})}, \ldots]_{-}. \tag{3.229}$$

We introduce this notation into Eq. (3.227) and obtain the solution of the inhomogeneous differential equation as

$$Q\hat{W}^{(\text{I})}(t) = S_Q(t, t_0)Q\hat{W}^{(\text{I})}(t_0) - i \int\limits_{t_0}^{t} d\bar{t} \, S_Q(t, \bar{t})Q\mathcal{L}_{\text{S--R}}^{(\text{I})}(\bar{t})\hat{R}_{\text{eq}}\hat{\rho}^{(\text{I})}(\bar{t}). \tag{3.230}$$

Here, the time-ordered superoperator

$$S_Q(t, \bar{t}) = \mathcal{T} \exp\left\{ -i \int\limits_{\bar{t}}^{t} d\tau \, Q\mathcal{L}_{\text{S--R}}^{(\text{I})}(\tau) \right\} \tag{3.231}$$

is introduced. It solves the homogeneous part of Eq. (3.230). As all other types of *S*-operators, Eq. (3.231) is defined via the Taylor expansion of the exponential function.[14]

Since we are not interested in the problem of initial correlations, the first term on the right-hand side of Eq. (3.230) will be neglected by assuming that at time t_0, the density operator of the total system factorizes into the density operator of the relevant system and the reservoir, $W(t_0) = \hat{\rho}(t_0)\hat{R}_{\text{eq}}$.

Inserting Eq. (3.230) into Eq. (3.226), we get an equation of motion that allows an *exact* determination of the reduced statistical operator of the relevant system. This so-called *Nakajima–Zwanzig equation* reads

$$\frac{\partial}{\partial t}\hat{\rho}^{(\text{I})}(t) = -i \, \text{tr}_{\text{R}}\{\mathcal{L}_{\text{S--R}}^{(\text{I})}(t)\hat{R}_{\text{eq}}\}\hat{\rho}^{(\text{I})}(t)$$

$$- \int\limits_{t_0}^{t} d\bar{t} \, \text{tr}_{\text{R}}\{\mathcal{L}_{\text{S--R}}^{(\text{I})}(t)S_Q(t, \bar{t})Q\mathcal{L}_{\text{S--R}}^{(\text{I})}(\bar{t})\hat{R}_{\text{eq}}\}\hat{\rho}^{(\text{I})}(\bar{t}). \tag{3.232}$$

Since according to Eq. (3.231), $\mathcal{L}_{\text{S--R}}$ is contained in the time-ordered exponential operator, the system–reservoir interaction enters the right-hand side of Eq. (3.232)

---

14) The expansion of $S_Q\hat{O}$ in powers of $Q\mathcal{L}_{\text{S--R}}^{(\text{I})}(\tau)$ introduces multiple commutators with $H_{\text{S--R}}^{(\text{I})}$ (the quantity $\hat{O}$ is an arbitrary operator). Those $H_{\text{S--R}}^{(\text{I})}$ appearing left from $\hat{O}$ are ordered with increasing time from right to left, while the $H_{\text{S--R}}^{(\text{I})}$ appearing right from $\hat{O}$ are arranged in the reverse manner. These two different types of time ordering have been abbreviated by the symbol $\mathcal{T}$.

in *infinite* order. In other words, the whole perturbation series with respect to H_{S-R} is summed up in Eq. (3.232). A more compact notation of the Nakajima–Zwanzig equation is given by

$$\frac{\partial}{\partial t}\hat{\rho}^{(I)}(t) = -i\,\langle\mathcal{L}_{S-R}^{(I)}(t)\rangle_R\,\hat{\rho}^{(I)}(t) - \int_{t_0}^{t} d\bar{t}\,\mathcal{M}^{(I)}(t,\bar{t})\hat{\rho}^{(I)}(\bar{t}). \tag{3.233}$$

Here, we used the short-hand notation, Eq. (3.202), for the averaging with respect to the reservoir equilibrium density operator: $\langle\cdots\rangle_R = \text{tr}_R\{\dots\hat{R}_{eq}\}$. The first term in (3.233) can easily be identified as the mean-field contribution (cf. Section 3.5.3). In the second term of Eq. (3.233), we have introduced the memory kernel superoperator (in the interaction representation)

$$\mathcal{M}^{(I)}(t,\bar{t}) = \langle\mathcal{L}_{S-R}^{(I)}(t)S_Q(t,\bar{t})Q\mathcal{L}_{S-R}^{(I)}(\bar{t})\rangle_R. \tag{3.234}$$

According to the definition of the kernel, we have $t > \bar{t}$, and additionally, any expansion of the S-superoperator guarantees time-ordered expressions. Therefore, the approach leading to the Nakajima–Zwanzig equation is often named *chronological time-ordering prescription* (COP). In most practical cases, it is impossible to derive a closed expression for this memory kernel even if we restrict ourselves to a partial summation only. However, the formal exact Nakajima–Zwanzig equation is well suited for the development of approximation schemes to the propagation for the RDO. For example, the quantum master equation (QME) (3.237) is easily recovered if the S_Q-operator is treated in zeroth order with respect to the system–reservoir coupling.

Finally, it is important to note here that the special choice equation (3.220) for the projection operator does not imply that the reservoir stays in equilibrium in the course of the time evolution of the relevant system. Instead, a time dependence of the RDO of the reservoir can be expected. This nonequilibrium behavior is induced by the coupling to the relevant system. Let us define the RDO for the *reservoir* as

$$\hat{R}^{(I)}(t) = \text{tr}_S\{\hat{W}^{(I)}(t)\} \equiv \text{tr}_S\{\mathcal{P}\hat{W}^{(I)}(t) + Q\hat{W}^{(I)}(t)\}. \tag{3.235}$$

Using the definition of the projection operator $\mathcal{P}$ and Eq. (3.230), we may write

$$\hat{R}^{(I)}(t) = \hat{R}_{eq} - i\int_{t_0}^{t} d\bar{t}\,\text{tr}_S\{S_Q(t,\bar{t})Q\mathcal{L}_{S-R}^{(I)}(\bar{t})\hat{R}_{eq}\hat{\rho}^{(I)}(\bar{t})\}. \tag{3.236}$$

Since it is only the equilibrium density operator $\hat{R}_{eq}$ that enters the Nakajima–Zwanzig equation (3.232), the time dependence of $\hat{R}^{(I)}(t)$ does not affect $\hat{\rho}^{(I)}(t)$ directly. It is only indirectly accounted for via $\mathcal{L}_{S-R}^{(I)}$, which is contained in the S-superoperator equation (3.231).

In the following section, we focus on the second-order contribution to the equations of motion of the RDO.

3.5.6 Second-order Equation of Motion for the Reduced Density Operator

Inserting Eq. (3.228) into Eq. (3.226), we obtain the equation of motion for the RDO, which is of second order with respect to $H_{\text{S–R}}$, as

$$
\frac{\partial}{\partial t}\hat{\rho}^{(\text{I})}(t) = -\frac{i}{\hbar}\text{tr}_{\text{R}}\left\{\hat{R}_{\text{eq}}1\left[H_{\text{S–R}}^{(\text{I})}(t),\hat{\rho}^{(\text{I})}(t)\right]_{-}\right\}
$$
$$
-\frac{1}{\hbar^2}\int\limits_{t_0}^{t}d\tau\;\text{tr}_{\text{R}}\left\{\left[H_{\text{S–R}}^{(\text{I})}(t),(1-\mathcal{P})\left[H_{\text{S–R}}^{(\text{I})}(\tau),\hat{R}_{\text{eq}}\hat{\rho}^{(\text{I})}(\tau)\right]_{-}\right]_{-}\right\}.
$$

(3.237)

In what follows, we discuss this equation for the factorized form equation (3.198) of the system–reservoir coupling. The first-order term on the right-hand side corresponds to that in Eq. (3.197). In order to show this, one has to use the cyclic invariance of the trace, Eq. (3.125), in the space of the reservoir states. The mean-field contribution (in the interaction representation) to the dynamics of the relevant system results as

$$
\text{tr}_{\text{R}}\{\hat{R}_{\text{eq}}\left[H_{\text{S–R}}^{(\text{I})}(t),\hat{\rho}^{(\text{I})}(t)\right]_{-}\} = \sum_{u}\left[K_u^{(\text{I})}(t)\langle\Phi_u\rangle_{\text{R}},\hat{\rho}^{(\text{I})}(t)\right]_{-}
$$
$$
\equiv \left[H_{\text{mf}}^{(\text{I})}(t),\hat{\rho}^{(\text{I})}(t)\right]_{-}.
$$

(3.238)

The general form of the mean-field Hamiltonian H_{mf} was introduced in Eq. (3.200). Here, the expectation value has to be taken with the equilibrium reservoir density operator (cf. Eq. (3.202)).

Next, the second term in Eq. (3.237) is considered in more detail. Due to the factor $(1-\mathcal{P})$, there are altogether eight terms, where those containing the factor $\mathcal{P}$ include two trace operations. We consider the four terms corresponding to the unit operator "1" of $(1-\mathcal{P})$ and write

$$
\mathcal{M}_1 = \text{tr}_{\text{R}}\left\{\left[H_{\text{S–R}}^{(\text{I})}(t),\left[H_{\text{S–R}}^{(\text{I})}(\tau),\hat{R}_{\text{eq}}\rho^{(\text{I})}(\tau)\right]_{-}\right]_{-}\right\},
$$

(3.239)

or in more detail

$$
\mathcal{M}_1 = \sum_{u,v}\Big(\text{tr}_{\text{R}}\left\{\Phi_u^{(\text{I})}(t)\Phi_v^{(\text{I})}(\tau)\hat{R}_{\text{eq}}\right\}\;K_u^{(\text{I})}(t)K_v^{(\text{I})}(\tau)\hat{\rho}^{(\text{I})}(\tau)
$$
$$
-\text{tr}_{\text{R}}\left\{\Phi_u^{(\text{I})}(t)\hat{R}_{\text{eq}}\Phi_v^{(\text{I})}(\tau)\right\}\;K_u^{(\text{I})}(t)\hat{\rho}^{(\text{I})}(\tau)K_v^{(\text{I})}(\tau)
$$
$$
-\text{tr}_{\text{R}}\left\{\Phi_v^{(\text{I})}(\tau)\hat{R}_{\text{eq}}\Phi_u^{(\text{I})}(t)\right\}\;K_v^{(\text{I})}(\tau)\hat{\rho}^{(\text{I})}(\tau)K_u^{(\text{I})}(t)
$$
$$
+\text{tr}_{\text{R}}\left\{\hat{R}_{\text{eq}}\Phi_v^{(\text{I})}(\tau)\Phi_u^{(\text{I})}(t)\right\}\;\hat{\rho}^{(\text{I})}(\tau)K_v^{(\text{I})}(\tau)K_u^{(\text{I})}(t)\Big).
$$

(3.240)

For the second term proportional to $\mathcal{P}$, we write

$$
\mathcal{M}_2 = \text{tr}_{\text{R}}\left\{\left[H_{\text{S–R}}^{(\text{I})}(t),\hat{R}_{\text{eq}}\text{tr}_{\text{R}}\left\{\left[H_{\text{S–R}}^{(\text{I})}(\tau),\hat{R}_{\text{eq}}\hat{\rho}^{(\text{I})}(\tau)\right]_{-}\right\}\right]_{-}\right\},
$$

(3.241)

which leads to

$$
\mathcal{M}_2 = \sum_{u,v}\langle\Phi_u\rangle_{\text{R}}\langle\Phi_v\rangle_{\text{R}}\left[K_u^{(\text{I})}(t),\left[K_v^{(\text{I})}(\tau),\hat{\rho}^{(\text{I})}(\tau)\right]_{-}\right]_{-}.
$$

(3.242)

Next, we apply the results of Section 3.5.3 to rewrite the expectation values of the reservoir part of $H_{\text{S--R}}$ as follows (first term in Eq. (3.240)):

$$\text{tr}_{\text{R}} \left\{ \Phi_u^{(\text{I})}(t) \Phi_v^{(\text{I})}(\tau) \hat{R}_{\text{eq}} \right\} = \text{tr}_{\text{R}} \left\{ \hat{R}_{\text{eq}} U_{\text{R}}^+(t - \tau) \Phi_u U_{\text{R}}(t - \tau) \Phi_v \right\}$$

$$= \langle \Phi_u^{(\text{I})}(t - \tau) \Phi_v^{(\text{I})}(0) \rangle_{\text{R}}. \tag{3.243}$$

Using similar steps, we obtain for the remaining terms in Eq. (3.239)

$$\text{tr}_{\text{R}} \left\{ \Phi_u^{(\text{I})}(\tau) \hat{R}_{\text{eq}} \Phi_v^{(\text{I})}(t) \right\} = \langle \Phi_v^{(\text{I})}(0) \Phi_u^{(\text{I})}(t - \tau) \rangle_{\text{R}}, \tag{3.244}$$

$$\text{tr}_{\text{R}} \left\{ \Phi_v^{(\text{I})}(t) \hat{R}_{\text{eq}} \Phi_u^{(\text{I})}(\tau) \right\} = \langle \Phi_u^{(\text{I})}(t - \tau) \Phi_v^{(\text{I})}(0) \rangle_{\text{R}}, \tag{3.245}$$

and

$$\text{tr}_{\text{R}} \left\{ \hat{R}_{\text{eq}} \Phi_v^{(\text{I})}(\tau) \Phi_u^{(\text{I})}(t) \right\} = \langle \Phi_v^{(\text{I})}(0) \Phi_u^{(\text{I})}(t - \tau) \rangle_{\text{R}}. \tag{3.246}$$

Apparently, the integrand of Eq. (3.237) can be cast into a form that has only four terms, each containing the following type of function (the superscript I on the bath operators will be suppressed in what follows)

$$C_{uv}(t) = \frac{1}{\hbar^2} \langle \Phi_u(t) \Phi_v(0) \rangle_{\text{R}} - \frac{1}{\hbar^2} \langle \Phi_u \rangle_{\text{R}} \langle \Phi_v \rangle_{\text{R}} = \frac{1}{\hbar^2} \langle \Delta \Phi_u(t) \Delta \Phi_v(0) \rangle_{\text{R}}. \tag{3.247}$$

Here, we combined the reservoir operators with their expectation values to the operator

$$\Delta \Phi_u(t) = \Phi_u(t) - \langle \Phi_u \rangle_{\text{R}}. \tag{3.248}$$

This operator describes the *fluctuations* of the reservoir part of $H_{\text{S--R}}$ with respect to its average value. The function $C_{uv}(t)$ in Eq. (3.247) which is called *reservoir correlation function* therefore establishes a connection between the fluctuations of the operators Φ_v and Φ_u at different times (see also Section 3.4.5, a detailed discussion of the correlation functions can be found in the following section). For most systems, the correlations of the fluctuations decay after a certain *correlation time* τ_{c}. Note that these fluctuations do *not* change the quantum mechanical state of the reservoir, which is still described by the canonical density operator.

If Φ_u is a Hermitian operator, we have

$$\langle \Phi_v(0) \Phi_u(t) \rangle_{\text{R}} = \left[\langle \Phi_u(t) \Phi_v(0) \rangle_{\text{R}} \right]^* = \langle \Phi_v(-t) \Phi_u(0) \rangle_{\text{R}}, \tag{3.249}$$

from which we get the important property

$$C_{uv}^*(t) = C_{vu}(-t). \tag{3.250}$$

Using the definition of the correlation function, the equation of motion for the RDO finally follows as

$$\frac{\partial}{\partial t} \hat{\rho}^{(I)}(t) = -\frac{i}{\hbar} \sum_u \langle \Phi_u \rangle_{\text{R}} \left[K_u^{(I)}, \hat{\rho}^{(I)}(t) \right]_-$$

$$- \sum_{u,v} \int_{t_0}^t d\tau \ \left(C_{uv}(t - \tau) \left[K_u^{(I)}(t), K_v^{(I)}(\tau) \hat{\rho}^{(I)}(\tau) \right]_- \right.$$

$$\left. - C_{vu}(-t + \tau) \left[K_u^{(I)}(t), \hat{\rho}^{(I)}(\tau) K_v^{(I)}(\tau) \right]_- \right). \tag{3.251}$$

This equation is valid for non-Hermitian operators K_u and Φ_u. If the reservoir operators Φ_u are Hermitian, then $C_{vu}(-t + \tau)$ can be replaced by $C_{uv}^*(t - \tau)$. Since every term on the right-hand side of Eq. (3.251) is given by a commutator, it is easy to demonstrate that the RDO equation ensures conservation of total probability, that is $\mathrm{tr}_S\{\partial\hat{\rho}(t)/\partial t\} = 0$. Furthermore, by computing the Hermitian conjugated of the right-hand side of Eq. (3.251), one may demonstrate that the Hermiticity of $\hat{\rho}^{(I)}$ is assured for all times (note that in the case of non-Hermitian operators K_u and Φ_u, the whole u, v-summation realizes Hermitian operators).

Equation (3.251) is frequently called *QME* since it generalizes ordinary rate equations (master equations) of the type given in Eq. (3.2) to the quantum case (represented by the RDO). Alternatively, the term *density matrix equation in the second Born approximation* is common. Here, one refers to the second-order perturbation theory applied to the system–reservoir coupling.

The right-hand side of this equation reveals that the change over time of the RDO is not only determined by its actual value but by the history of its own time dependence. Therefore, Eq. (3.251) is specified as the QME with memory effects. This type of memory effect has been already encountered in our introductory example in Section 3.4.5. In the present case, the memory time τ_{mem} is obviously determined by the reservoir correlation function but is not necessarily identical to the correlation time τ_{c}. Before we concentrate on the properties of the reservoir correlation function, the QME will be discussed in more detail in the following section.

3.6 Quantum Master Equation

So far, we have derived the QME in the interaction representation. For a number of applications it may be useful to stay in the interaction representation. Often, however, it is more appropriate to go back to the Schrödinger representation. Following Section 3.5.3, the equation of motion for the RDO can be transformed from the interaction representation into the Schrödinger representation according to

$$
\begin{aligned}
\frac{\partial}{\partial t}\hat{\rho}(t) &= \frac{\partial}{\partial t}\left[U_S(t - t_0)\hat{\rho}^{(I)}U_S^+(t - t_0)\right]_- \\
&= -\frac{i}{\hbar}\left[H_S, \hat{\rho}(t)\right]_- + U_S(t - t_0)\frac{\partial}{\partial t}\hat{\rho}^{(I)}(t)U_S^+(t - t_0).
\end{aligned}
\tag{3.252}
$$

For Eq. (3.251), this gives

$$
\begin{aligned}
\frac{\partial}{\partial t}\hat{\rho}(t) = &-\frac{i}{\hbar}\left[H_S + \sum_u \langle\Phi_u\rangle_R K_u, \hat{\rho}(t)\right]_- - U_S(t - t_0) \\
&\times \sum_{u,v}\int_{t_0}^t d\bar{t}\,\Big\{C_{uv}(t - \bar{t})\left[U_S^+(t - t_0)K_u U_S(t - t_0),\right. \\
&\qquad\left. U_S^+(\bar{t} - t_0)K_v U_S(\bar{t} - t_0)U_S^+(\bar{t} - t_0)\hat{\rho}(\bar{t})U_S(\bar{t} - t_0)\right]_- \\
&\qquad - C_{vu}(-t + \bar{t})\left[U_S^+(t - t_0)K_u U_S(t - t_0),\right. \\
&\qquad\left. U_S^+(\bar{t} - t_0)\hat{\rho}(\bar{t})U_S(\bar{t} - t_0)U_S^+(\bar{t} - t_0)K_v U_S(\bar{t} - t_0)\right]_-\Big\} \\
&\times U_S^+(t - t_0).
\end{aligned}
\tag{3.253}
$$

Combining the products of time-evolution operators and replacing $t - \bar{t}$ by τ, we obtain the QME in the Schrödinger representation

$$
\frac{\partial}{\partial t} \hat{\rho} = -\frac{i}{\hbar} \left[H_S + \sum_u \langle \Phi_u \rangle_R K_u, \hat{\rho} \right]_-
$$

$$
- \sum_{u,v} \int_0^{t-t_0} d\tau \left(C_{uv}(\tau) \left[K_u, U_S(\tau) K_v \hat{\rho}(t-\tau) U_S^+(\tau) \right]_- \right.
$$

$$
\left. - C_{vu}(-\tau) \left[K_u, U_S(\tau) \hat{\rho}(t-\tau) K_v U_S^+(\tau) \right]_- \right). \tag{3.254}
$$

Before discussing the details of this equation, we estimate the range of validity for the second-order perturbation theory. Let us assume that the integrand in Eq. (3.251) is constant within the memory time. Then, the contribution of the integral to the right-hand side of the QME is of the order of $\tau_{\text{mem}} \langle H_{S-R} \rangle^2 / \hbar^2$. In order to justify the perturbation expansion, this quantity (which has the dimension of a rate) has to be small compared to the first term on the right-hand side of Eq. (3.254), $\langle H_S \rangle / \hbar$.

The term $\sim \langle \Phi_u \rangle_R$ on the right-hand side of Eq. (3.254) is already known from Section 3.5.3. It contains the mean-field contribution to the system dynamics, which is of first order in the system–reservoir interaction. The dynamics including this mean-field term is reversible. The second term on the right-hand side, which depends on the complex-valued correlation function $C_{uv}(t)$, leads to a quite different behavior. This can be rationalized by neglecting the time integration for a moment and considering only the diagonal elements of the density operator (in an arbitrary representation), which are real. In this case, the resulting differential equation is of the type $\partial f(t) / \partial t = -k f(t)$, where k is proportional to the real part of the correlation function. The solution of this type of equation will decay exponentially in time, indicating an irreversible flow of probability in the system. It will be shown in more detail below that the second term in Eq. (3.254) is responsible for energy dissipation from the relevant system into the reservoir. Finally, as already discussed at the end of Section 3.5.6, Eq. (3.254) also guarantees hermiticity of $\hat{\rho}$ and conservation of total probability.

In the QME (3.254), the RDO $\hat{\rho}$ appears with a retarded time argument, $t - \tau$, in the integrand. This means that the actual change of probabilistic information in time (that is, the right-hand side of Eq. (3.254)) is determined by the probabilistic information not only at the same time t but also by that of earlier times $t - \tau$. This type of equation is known from probabilistic theory as a *non-Markovian* equation. It is encountered whenever time-local equations of motion are reduced to equations that only describe a part of the original set of DOFs. In the present case, we changed from the Liouville–von Neumann equation (3.149) for the full density operator, which is Markovian, to the non-Markovian QME for the RDO. In Section 3.6.1, we show under which conditions the right-hand side only depends on $\hat{\rho}(t)$ and the dynamics becomes Markovian again.

The characteristic feature of non-Markovian behavior is the appearance of *memory* effects in the determination of the time dependence of the RDO. The time span for this memory is mostly determined by the reservoir correlation functions $C_{uv}(t)$. The

time dependence of $C_{uv}(t)$ can often be characterized by a single or a set of *correlation times*, τ_c; more details will be discussed in Section 3.7.

For illustration, let us assume that this correlation time is short compared to any other characteristic time scale of the considered system. This allows us to write

$$C_{uv}(t) \approx \delta(t)\, c(u, v). \tag{3.255}$$

Inserting Eq. (3.255) into the non-Markovian QME (3.254), it becomes Markovian, and the dissipative part reads

$$\left(\frac{\partial \hat{\rho}}{\partial t} \right)_{\text{diss}} = -\sum_{u,v} \left\{ c(u,v) \left[K_u, K_v \hat{\rho} \right]_- - c^*(u,v) \left[K_u, \hat{\rho} K_v \right]_- \right\}. \tag{3.256}$$

If the $c(uv)$ are real and diagonal, this expression reduces to[15]

$$\left(\frac{\partial \hat{\rho}}{\partial t} \right)_{\text{diss}} = -\sum_u c(u,u) \left\{ \left[K_u^2, \hat{\rho} \right]_+ - 2 K_u \hat{\rho} K_u \right\}. \tag{3.257}$$

This is the so-called Lindblad form of dissipation (for another example, see Section 3.8.4). Quite often in practical calculations, one starts from the rather general expression (3.257) without making any particular model for the system–reservoir interaction operator. In this case, the choice of the operators K_u as well as of the prefactor $c(u, u)$ has to be guided by intuition.

The QME (3.254) is a fundamental result of the relaxation theory. It has found many applications in different areas of physics, mainly in quantum optics, nuclear magnetic resonance, and solid state and molecular physics. When using a QME, however, one should keep in mind that the perturbative treatment of the system–reservoir coupling restricts its applicability and demands for a careful separation of the full system at hand. In Chapters 5–9, we will discuss several examples in this respect.

3.6.1 Markov Approximation

In what follows, we explain in detail the transition from the non-Markovian QME (3.254) to a Markovian equation. Let us assume that a characteristic time τ_{mem} (*memory time*) exists that characterizes the time span of memory effects. Now, if the RDO $\hat{\rho}$ (that is any of its matrix elements) does not change substantially on the time scale given by τ_{mem}, the memory effects will be negligible. In this case, one can invoke the *Markov approximation*, which amounts to setting

$$\hat{\rho}(t - \tau) \approx \hat{\rho}(t) \tag{3.258}$$

in the time integral equation (3.254).

An alternative view is provided, if we suppose that within the Markov approximation the minimum time step, Δt, for which information on the RDM is obtainable is restricted by the memory time, that is $\Delta t > \tau_{\text{mem}}$. In case that the continuous time

---

[15] If the $c(u, v)$ are not diagonal, we can diagonalize the complete matrix to get a similar result as in Eq. (3.257).

axis is *coarse grained* with a mesh size dictated by τ_{mem}, memory effects do not play any role for the dissipative dynamics of the system. Due to this requirement, the upper limit of the integration in Eq. (3.254) exceeds the time interval where the integrand is finite. Thus, we can increase this limit without changing the value of the integral; that is, we will set $t - t_0 \to \infty$ in what follows.

In order to discuss in more detail the consequences of the assumption that the RDO does not change on the time scale of τ_{mem}, we change to the representation of $\hat{\rho}(t)$ in the eigenstates of H_{S}, Eq. (3.193). Without any coupling to the reservoir, the solution for ρ_{ab} can be directly deduced from Eq. (3.150) as

$$\rho_{ab}(t) = e^{-i\omega_{ab}(t-t_0)}\rho_{ab}(t_0). \tag{3.259}$$

The diagonal elements are time independent, but the off-diagonal elements may be rapidly oscillating functions. If $1/\omega_{ab} \ll \tau_{\text{mem}}$, the above given reasoning leading to the Markov approximation breaks down. Thus, it is advisable to split off the oscillatory factor $e^{-i\omega_{ab}t}$ from the RDM and invoke the Markov approximation for the remaining slowly varying envelope. Therefore, we carry out the following replacement:

$$\begin{aligned} \rho_{ab}(t - \tau) &= e^{-i\omega_{ab}(t-\tau-t_0)}\tilde{\rho}_{ab}(t - \tau) \\ &\approx e^{-i\omega_{ab}(t-\tau-t_0)}\tilde{\rho}_{ab}(t) = e^{i\omega_{ab}\tau}\rho_{ab}(t), \end{aligned} \tag{3.260}$$

where the tilde denotes the envelope part of the RDM. This approximation scheme is equivalent to perform the Markov approximation in the interaction representation since

$$\begin{aligned} \rho_{ab}(t) &= \langle a|e^{-iH_{\text{S}}(t-t_0)/\hbar}\hat{\rho}^{(\text{I})}(t)e^{iH_{\text{S}}(t-t_0)/\hbar}|b\rangle \\ &= e^{-i\omega_{ab}(t-t_0)}\langle a|\hat{\rho}^{(\text{I})}(t)|b\rangle. \end{aligned} \tag{3.261}$$

Thus, the general prescription is that first we have to change to the interaction Representation, and only then, the Markov approximation is made:

$$\begin{aligned} \hat{\rho}(t - \tau) &= U_{\text{S}}(t - \tau - t_0)\hat{\rho}^{(\text{I})}(t - \tau)U_{\text{S}}^+(t - \tau - t_0) \\ &\approx U_{\text{S}}(-\tau)U_{\text{S}}(t - t_0)\hat{\rho}^{(\text{I})}(t)U_{\text{S}}^+(t - t_0)U_{\text{S}}^+(-\tau) \\ &= U_{\text{S}}^+(\tau)\hat{\rho}(t)U_{\text{S}}(\tau). \end{aligned} \tag{3.262}$$

Using this approximation, the dissipative part of the QME (3.254) becomes

$$\begin{aligned} \left(\frac{\partial\hat{\rho}}{\partial t}\right)_{\text{diss}} = -\sum_{u,v}\int_0^\infty d\tau \Big\{ &C_{uv}(\tau)\Big[K_u, K_v^{(\text{I})}(-\tau)\hat{\rho}(t)\Big]_- \\ &- C_{vu}(-\tau)\Big[K_u, \hat{\rho}(t)K_v^{(\text{I})}(-\tau)\Big]_- \Big\}, \end{aligned} \tag{3.263}$$

where $K_v^{(\text{I})}(-\tau) = U_{\text{S}}(\tau)K_v U_{\text{S}}^+(\tau)$. A more compact form of this equation is obtained after introduction of the operator

$$\Lambda_u = \sum_v \int_0^\infty d\tau\, C_{uv}(\tau)K_v^{(\text{I})}(-\tau) \tag{3.264}$$

and the operator $\Lambda_u^{(+)}$ following from Λ_u upon replacing $C_{uv}(\tau)$ by $C_{vu}(-\tau)$ (if any term of $H_{\text{S-R}}$ is Hermitian, then $\Lambda_u^{(+)} = \Lambda_u^+$). With this definition, Eq. (3.263) can be written as

$$\left(\frac{\partial\hat{\rho}}{\partial t}\right)_{\text{diss}} = -\sum_u \left[K_u, \Lambda_u\hat{\rho}(t) - \hat{\rho}(t)\Lambda_u^{(+)}\right]_-. \tag{3.265}$$

Carrying out the commutator, the resulting expression suggests supplementing the system Hamiltonian by non-Hermitian contributions that are proportional to $K_u\Lambda_u$. Therefore, we introduce the effective non-Hermitian system Hamiltonian

$$H_{\text{S}}^{(\text{eff})} = H_{\text{S}} + \sum_u K_u \left[\langle\Phi_u\rangle - i\hbar\Lambda_u\right]. \tag{3.266}$$

Note that for convenience we included the first-order mean-field term in the definition of the effective Hamiltonian as well. Using Eq. (3.266), we obtain for the QME in the Markov approximation the final result ($H_{\text{S}}^{(\text{eff})\,+}$ has to be understood as the Hermitian conjugated of $H^{(\text{eff})}$ except that all Λ_u have been replaced by $\Lambda_u^{(+)}$)

$$\frac{\partial}{\partial t}\hat{\rho}(t) = -\frac{i}{\hbar}\left(H_{\text{S}}^{(\text{eff})}\hat{\rho}(t) - \hat{\rho}(t)H_{\text{S}}^{(\text{eff})\,+}\right)$$
$$+ \sum_u \left(K_u\hat{\rho}(t)\Lambda_u^{(+)} + \Lambda_u\hat{\rho}(t)K_u\right). \tag{3.267}$$

This equation can be interpreted as follows. We first note that the part of the dissipative contributions acting exclusively from the left or from the right on the RDO could be comprised to a non-Hermitian Hamiltonian. According to the general structure of the density operator, Eq. (3.122), this action can be understood as changing of the state vector norm. However, the remaining dissipative part acting on the RDO from the left and the right simultaneously compensates for this normalization change. As a result, the condition $\text{tr}_S\{\hat{\rho}\} = 1$ is fulfilled (together, of course, with conservation of total probability).

We conclude the discussion of this section by giving an alternative notation of the QME, Eq. (3.267), based on the superoperator formulation in Liouville space which has already been introduced in connection with the Liouville–von Neumann equation in Section 3.4.3. In the present case, a Liouville superoperator can only be introduced for the reversible part of the QME. We set $\mathcal{L}_{\text{S}} \ldots = [H_{\text{S}}, \ldots]_-/\hbar$ and obtain from Eq. (3.265):

$$\frac{\partial}{\partial t}\hat{\rho}(t) = -i\mathcal{L}_{\text{S}}\hat{\rho}(t) - \mathcal{D}\hat{\rho}(t). \tag{3.268}$$

In contrast to the first term on the right-hand side, the second one cannot be given via a Liouville superoperator abbreviating a simple commutator. Instead, the so-called dissipative (or relaxation) superoperator $\mathcal{D}$ has been introduced. Its concrete action on the RDO can be obtained from the right-hand side of Eq. (3.265). Sometimes, it is useful to introduce the formal solution of Eq. (3.268) as

$$\hat{\rho}(t) = \mathcal{U}(t - t_0)\hat{\rho}(t_0), \tag{3.269}$$

with the time-evolution superoperator

$$\mathcal{U}(t - t_0) = \exp\left(-i(\mathcal{L}_{\text{S}} - i\mathcal{D})(t - t_0)\right). \tag{3.270}$$

The action of D can be characterized by considering the change in the internal energy of the relevant system $E_S = \text{tr}_S\{\hat{\rho}(t)H_S\}$. Using Eq. (3.268), one immediately obtains

$$\frac{\partial}{\partial t}E_S = -\text{tr}_S\{H_S D\hat{\rho}(t)\} = -\sum_u \text{tr}_S\{[H_S, K_u]_- \left(\Lambda_u\hat{\rho}(t) - \hat{\rho}(t)\Lambda_u^{(+)}\right)\}. \qquad (3.271)$$

The second part of the right-hand side follows if D is introduced according to Eq. (3.265). The resulting expression shows that for cases where the commutator of the system Hamiltonian with every operator K_u vanishes, dissipation does not alter the internal energy. This may be interpreted as an action of the environment reduced to elastic scattering processes, which do not change the system energy but probably the phase of the system. Because of this particular property, dissipative processes that do not change the system energy are related to what is known as *pure dephasing*. Assuming that the $|a\rangle$ are *eigenstates* of H_S, the coupling operator $K_u = |a\rangle\langle a|$ represents an example for a system–reservoir coupling, which guarantees the conservation of the internal energy E_S. This has to be expected since the system part K_u of the system–reservoir coupling does not change the system state. To be complete, we also emphasize that the internal energy remains constant if the dissipation is of such a type that the second term in the trace expression of Eq. (3.271) vanishes. We will discuss this case in more detail in Section 3.8.2

3.7   The Reservoir Correlation Function

3.7.1   General Properties of $C_{uv}(t)$

The importance of the reservoir correlation function for the dynamics of a relevant system interacting with a reservoir is apparent from the QME (3.251) and the discussion in the previous section. Before turning to specific models for $C_{uv}(t)$, we discuss some of the more general properties of this function as well as of its Fourier transform

$$C_{uv}(\omega) = \int dt\, e^{i\omega t} C_{uv}(t). \qquad (3.272)$$

If Eq. (3.250) holds, that is Φ_u is hermitian, it follows immediately that

$$C_{vu}(-\omega) = \int dt\, e^{i\omega t} C_{uv}^*(t), \qquad (3.273)$$

and that $C_{uv}^*(\omega) = C_{vu}(\omega)$. It will further be convenient to introduce symmetric and antisymmetric correlation functions

$$C_{uv}^{(+)}(t) = C_{uv}(t) + C_{uv}^*(t), \qquad C_{uv}^{(-)}(t) = C_{uv}(t) - C_{uv}^*(t), \qquad (3.274)$$

respectively. Note that $C_{uv}^{(+)}(t)$ is a real function, while $C_{uv}^{(-)}(t)$ is imaginary. Moreover, $C_{uv}^{(+)}(-t) = C_{vu}^{(+)}(t)$ as well as $C_{uv}^{(-)}(-t) = -C_{vu}^{(-)}(t)$ holds.

Another fundamental property of $C_{uv}(\omega)$ can be derived if one starts from the definition (3.247) and introduces eigenstates $|\alpha\rangle$ and eigenvalues E_α of the reservoir

Hamiltonian. Using these eigenstates to perform the trace operation, we obtain

$$C_{uv}(\omega) = \frac{1}{\hbar^2} \int dt\, e^{i\omega t} \sum_{\alpha,\beta} \langle\alpha|\hat{R}_{eq} e^{iH_R t/\hbar} \Delta\Phi_u e^{-iH_R t/\hbar}|\beta\rangle\langle\beta|\Delta\Phi_v|\alpha\rangle$$

$$= \frac{1}{\hbar^2} \sum_{\alpha,\beta} \int dt\, e^{i(\omega-\omega_{\beta\alpha})t} f_\alpha \langle\alpha|\Delta\Phi_u|\beta\rangle\langle\beta|\Delta\Phi_v|\alpha\rangle. \tag{3.275}$$

The $\omega_{\beta\alpha} = (E_\beta - E_\alpha)/\hbar$ are the transition frequencies between the reservoir energy levels, and

$$f_\alpha \equiv \langle\alpha|\hat{R}_{eq}|\alpha\rangle = \exp(-E_\alpha/k_B T)/\sum_\beta \exp(-E_\beta/k_B T) \tag{3.276}$$

denotes the thermal distribution function with respect to the reservoir states. The time integration of the exponential function produces the delta function (Eq. (3.181)); that is, we obtain

$$C_{uv}(\omega) = \frac{2\pi}{\hbar^2} \sum_{\alpha,\beta} f_\alpha \langle\alpha|\Delta\Phi_u|\beta\rangle\langle\beta|\Delta\Phi_v|\alpha\rangle \delta(\omega - \omega_{\beta\alpha}). \tag{3.277}$$

Now we consider the Fourier transform of the correlation function where the indices u and v are interchanged. Interchanging also α and β gives

$$C_{vu}(\omega) = \frac{2\pi}{\hbar^2} \sum_{\alpha,\beta} f_\beta \langle\alpha|\Delta\Phi_u|\beta\rangle\langle\beta|\Delta\Phi_v|\alpha\rangle \delta(\omega - \omega_{\alpha\beta}). \tag{3.278}$$

According to the identity

$$\exp\left\{-\frac{E_\beta}{k_B T}\right\} \delta(\omega - \omega_{\alpha\beta}) = \exp\left\{-\frac{E_\alpha - \hbar\omega}{k_B T}\right\} \delta(\omega + \omega_{\beta\alpha}), \tag{3.279}$$

we arrive at the important result

$$C_{uv}(\omega) = \exp\left\{\frac{\hbar\omega}{k_B T}\right\} C_{vu}(-\omega), \tag{3.280}$$

which relates the correlation function with frequency argument ω to the one with the negative argument. Note that Eq. (3.280) builds upon the definition of $C_{uv}(\omega)$ with respect to the thermal equilibrium of the reservoir.

Using Eq. (3.274), the Fourier transform of the symmetric and antisymmetric parts of the correlation function can be written as

$$C_{uv}^{(\pm)}(\omega) = C_{uv}(\omega) \pm C_{vu}(-\omega). \tag{3.281}$$

If we replace $C_{vu}(-\omega)$ in Eq. (3.281) by the result of Eq. (3.280), it follows that

$$C_{uv}(\omega) = \frac{C_{uv}^{(\pm)}(\omega)}{1 \pm \exp\{-\hbar\omega/k_B T\}} \equiv (1 + n(\omega))\, C_{uv}^{(-)}(\omega). \tag{3.282}$$

Here, the Bose–Einstein distribution function

$$n(\omega) = \frac{1}{\exp\{\hbar\omega/k_B T\} - 1} \tag{3.283}$$

has been used to rewrite the expression for C_{uv}. Combining the two parts of Eq. (3.282), we get a relation between the Fourier transforms of the symmetric and antisymmetric parts of the correlation function, which reads

$$C_{uv}^{(+)}(\omega) = \coth\left(\frac{\hbar\omega}{2k_B T}\right) C_{uv}^{(-)}(\omega). \tag{3.284}$$

Now, it is easy to express $C_{uv}(t)$ by $C_{uv}^{(-)}(\omega)$. The inverse Fourier transform can then be written in terms of the half-sided Fourier integral

$$
\begin{aligned}
C_{uv}(t) &= \int\limits_{-\infty}^{\infty} \frac{d\omega}{2\pi} \; e^{-i\omega t}[1 + n(\omega)]C_{uv}^{(-)}(\omega) \\
&= \int\limits_{0}^{\infty} \frac{d\omega}{2\pi} \; \left(e^{-i\omega t}[1 + n(\omega)]C_{uv}^{(-)}(\omega) + e^{i\omega t}n(\omega)C_{vu}^{(-)}(\omega) \right).
\end{aligned}
\tag{3.285}
$$

To summarize, it is possible to express the reservoir correlation function either by its symmetric or antisymmetric part. This freedom of choice will be particularly useful in the context of classical simulations of the reservoir as we will see in Section 3.7.5.

3.7.2 Harmonic Oscillator Reservoir

The explicit quantum mechanical calculation of $C_{uv}(t)$ is not feasible in practice since there is no way to calculate the states of a general macroscopic reservoir such as a solvent surrounding some solute molecule. To overcome this difficulty, several models for the reservoir and its interaction with the system have been developed.

In the case of a reservoir that is characterized by a stable crystalline structure, the correlation function can readily be calculated using the following reasoning: In many of such systems where the atoms (or molecules) form a regular lattice with high symmetry, lattice vibrations only appear as small oscillations around the equilibrium positions at sufficiently low temperature. In this case, a harmonic approximation is possible; that is, the force driving the atoms back to their equilibrium position can be taken to be proportional to the deviation from this equilibrium position. In Section 2.5.1, we have seen that a harmonic approximation to some global PES allows to introduce normal mode vibrations whose quantum counterparts in the case of a crystalline structure are called (lattice) *phonons.* As the main result of the introduction of normal mode oscillations, the individual atom coordinates are mapped on a set of harmonic oscillator coordinates that are independent of each other.

It should be remarked that this situation is not the rule: For example, in low-temperature solutions, the solvent is essentially frozen into a disordered solid. Here, it is more difficult to calculate $C_{uv}(t)$ because the solute is likely to interact with system-specific localized vibrational modes of its immediate surroundings. If the temperature is increased such that the reservoir becomes a liquid, the notion of normal modes as small amplitude motions around stable structures loses its meaning. In such situations, one has to resort to classical simulations of the reservoir. This approach will be discussed in Section 3.13. In fact, as we will see in Section 5.3 on ultrashort time scales, it is often possible to introduce instantaneous normal modes. Furthermore, assuming that anharmonicities of the PES are negligible, even reservoirs such as proteins can be described in harmonic approximation.

Having in mind the important concept of a normal mode bath, we adapt the correlation function to this situation now. In a first step, we introduce a more specific

structure of the coupling Hamiltonian, H_{S-R}. Let us assume that we have performed a Taylor expansion of H_{S-R} with respect to the reservoir coordinates. If we focus on the lowest order contribution only, H_{S-R} will become linear with respect to the harmonic oscillator reservoir coordinates $Z = \{Z_\xi\}$. Further, H_{S-R} given in Eq. (3.198) is assumed to contain a single term only. This restriction is made basically to simplify the notation. The extension to more general expressions for the coupling Hamiltonian is straightforward. Dropping the index u, we can write (cf. also Eq. (3.5))

$$H_{S-R} = K(s) \sum_\xi \hbar \gamma_\xi Z_\xi. \tag{3.286}$$

Here, s comprises the coordinates of the system, and γ_ξ is the system–reservoir coupling constant. The given expression for H_{S-R}, if compared with Eq. (3.198), corresponds to a reservoir part $\Phi = \sum_\xi \hbar \gamma_\xi Z_\xi$. Note that $\langle Z_\xi \rangle_R = 0$; that is, the thermal fluctuations of the reservoir coordinates are taking place symmetrically around $Z_\xi = 0$. Since we are dealing with decoupled normal mode oscillators, the reservoir Hamiltonian can be written as $H_R = \sum_\xi H_\xi^{(R)}$. Here, the single-mode Hamiltonian is given by $H_\xi^{(R)} = \hbar \omega_\xi (C_\xi^+ C_\xi + 1/2)$, where C_ξ^+ and C_ξ denote the normal mode oscillator creation and annihilation operators (cf. Section 2.5.2). In terms of the creation and annihilation operators, the reservoir coordinates are written as $Z_\xi = \sqrt{\hbar/2\omega_\xi} \times (C_\xi + C_\xi^+)$ (see Eq. (2.54)). Further, ω_ξ is the normal mode frequency, and the harmonic oscillator eigenstates, $|N_\xi\rangle = (C_\xi^+)^{N_\xi} |0_\xi\rangle / \sqrt{N_\xi!}$, will be labeled by the oscillator quantum number N_ξ. For the subsequent derivation, it is more suitable to define Φ in terms of $Q_\xi = C_\xi + C_\xi^+$ simply writing

$$\Phi = \hbar \sum_\xi \omega_\xi g_\xi Q_\xi, \tag{3.287}$$

with $g_\xi = \gamma_\xi \sqrt{\hbar/2\omega_\xi^3}$. To get the Fourier transformed correlation function $C(\omega)$, we may use directly Eq. (3.277). Its determination becomes somewhat easier if we start from the time-dependent version, Eq. (3.247), which takes the following form for the present situation:

$$C(t) = \sum_{\xi,\xi'} \omega_\xi g_\xi \, \omega_{\xi'} g_{\xi'} \, \text{tr}_R \{\hat{R}_{eq} Q_\xi(t) Q_{\xi'}\}. \tag{3.288}$$

The time dependence of Q_ξ results in operators C_ξ and C_ξ^+ carrying a phase with frequency ω_ξ. To go on the trace is specified as the summation with respect to the product of the normal-mode harmonic oscillator states weighted by the respective thermal distributions $f_{N_\xi} = 1/\mathcal{Z} \times \exp(-N_\xi \hbar \omega_\xi / k_B T)$ (note the use of the mode index ζ):

$$\text{tr}_R \{\hat{R}_{eq} Q_\xi(t) Q_{\xi'}\} = \sum_{\{N_\zeta\}} \left(\prod_\zeta f_{N_\zeta} \langle N_\zeta | \right) Q_\xi(t) Q_{\xi'} \left(\prod_{\zeta'} f_{N_\zeta} | N_\zeta \rangle \right). \tag{3.289}$$

Since only operators are concerned with mode indices ξ and ξ', the trace reduces to $f_{N_\xi} f_{N_{\xi'}} \langle N_\xi | \langle N_{\xi'} | Q_\xi(t) Q_{\xi'} | N_\xi \rangle | N_{\xi'} \rangle$ (the remaining parts of $\sum_{\{N_\zeta\}}$ always give 1).

We note that, for example $\langle N_{\xi'}|Q_{\xi'}|N_{\xi'}\rangle = 0$, and see that only the case $\xi = \xi'$ contributes. Accordingly, the correlation function reads

$$
\begin{aligned}
C(t) &= \sum_{\xi} \omega_{\xi}^2 g_{\xi}^2 \sum_{N_{\xi}} f_{N_{\xi}} \langle N_{\xi}|[C_{\xi}e^{-i\omega_{\xi}t} + C_{\xi}^+ e^{i\omega_{\xi}t}][C_{\xi} + C_{\xi}^+]|N_{\xi}\rangle \\
&= \sum_{\xi} \omega_{\xi}^2 g_{\xi}^2 \sum_{N_{\xi}} f_{N_{\xi}} \left([1 + N_{\xi}]e^{-i\omega_{\xi}t} + e^{-i\omega_{\xi}t}N_{\xi}\right).
\end{aligned}
\tag{3.290}
$$

In the second part of this expression, it has been shown that only the operator combinations $C_{\xi}^+ C_{\xi}$ and $C_{\xi} C_{\xi}^+$ contribute. Finally, they have been replaced by the respective occupation number N_{ξ} according to Eq. (2.63). The summations with respect to the oscillator quantum numbers can be removed by introducing the mean occupation number of a harmonic oscillator mode (Bose–Einstein distribution, see Eq. (3.283))

$$
\sum_{N_{\xi}} N_{\xi} f_{N_{\xi}} = n(\omega_{\xi}).
\tag{3.291}
$$

With the help of this expression, we obtain

$$
C(t) = \sum_{\xi} (\omega_{\xi} g_{\xi})^2 \left([1 + n(\omega_{\xi})]e^{-i\omega_{\xi}t} + n(\omega_{\xi})e^{i\omega_{\xi}t}\right).
\tag{3.292}
$$

The Fourier transformed version follows as

$$
C(\omega) = 2\pi \sum_{\xi} (\omega_{\xi} g_{\xi})^2 \left([1 + n(\omega_{\xi})]\delta(\omega - \omega_{\xi}) + n(\omega_{\xi})\delta(\omega + \omega_{\xi})\right).
\tag{3.293}
$$

In principle, correlation functions that are of higher order with respect to the oscillator coordinate could be obtained along the same lines.

3.7.3 The Spectral Density

To have a compact notation of the Fourier transformed correlation function, Eq. (3.293), at hand, we introduce a new quantity $J(\omega)$ called *spectral density*, which is defined as

$$
J(\omega) = \sum_{\xi} g_{\xi}^2 \delta(\omega - \omega_{\xi}).
\tag{3.294}
$$

Before proceeding, we point out that in the general case where $H_{\text{S–R}}$ has the form (3.198), we arrive at a spectral density that depends on the same indices u and v as the reservoir correlation function; that is, $J(\omega)$ is replaced by $J_{uv}(\omega)$. The dependence of the coupling on some additional index could occur, for example if we consider several electronic states that are characterized by different coupling strengths to the environment. This point will be further discussed in Chapters 7 and 9.

With the help of (3.294), the correlation function (3.293) can be written as[16]

$$
C(\omega) = 2\pi\, \omega^2 [1 + n(\omega)]\, [J(\omega) - J(-\omega)].
\tag{3.295}
$$

---

16) It is important to note that in the literature, the factor ω^2 in (3.295) is often included into the definition of the spectral density. However, the present notation will be more convenient in the following chapters since g_{ξ} is directly related to the dimensionless shift between PES belonging to different electronic states (cf. Eq. (2.66)).

This notation points out the significance of the spectral density, which contains the specific information about the reservoir and its interaction with the relevant system. We emphasize that for the case that the reservoir can be modeled as a set of harmonic oscillators in thermal equilibrium that are linearly coupled to the system DOFs, the reservoir correlation function is described by a *single* function $J(\omega)$, which does not depend on temperature.

The strength of the system–reservoir coupling is often characterized by the bath's reorganization energy defined as

$$E_\lambda = \hbar \int d\omega \, \omega J(\omega). \tag{3.296}$$

If there exists an unambiguous relation between the mode index ξ and the mode frequency ω_ξ, the quantity g_ξ can be defined as a frequency-dependent function. Using the abbreviation $\kappa(\omega_\xi) = g_\xi^2$, it is then possible to rewrite the spectral density by introducing the *density of states* (DOS) of the reservoir oscillators

$$\mathcal{N}_R(\omega) = \sum_\xi \delta(\omega - \omega_\xi). \tag{3.297}$$

We will meet such a quantity several times in the subsequent sections. Here, it gives the number of oscillators in the reservoir one finds in the frequency interval $\Delta\omega$. It follows the relation

$$J(\omega) = \kappa(\omega)\mathcal{N}_R(\omega), \tag{3.298}$$

which highlights that the spectral density can be viewed as the reservoir oscillator DOS, which is weighted by the coupling strength between the system and reservoir coordinates.

For a given $J(\omega)$, the time-dependent correlation function $C(t)$ can be calculated using Eq. (3.285) together with the relation (which can be obtained from Eq. (3.282))

$$C^{(-)}(\omega) = 2\pi \, \omega^2 \left[J(\omega) - J(-\omega) \right]. \tag{3.299}$$

The obtained expression can be separated into a real and an imaginary part:[17],[18]

$$C(t) = \int_0^\infty d\omega \left(\cos(\omega t) \coth\left(\frac{\hbar\omega}{2k_B T} \right) - i \sin(\omega t) \right) \omega^2 J(\omega). \tag{3.300}$$

Although the spectral density, Eq. (3.294), is defined in terms of a sum of delta functions, any macroscopic system will in practice have a continuous spectral density. There exist different models for $J(\omega)$ that are adapted to particular system–environment situations. They are often characterized by a frequency dependence showing a power law rise for small frequencies that turns, after reaching a cut-off frequency ω_c, into an exponential decay for large frequencies:

$$\omega^2 J(\omega) = \theta(\omega) \, j_0 \, \omega^p \, e^{-\omega/\omega_c}. \tag{3.301}$$

---

17) Here, we used $\coth(\hbar\omega/2k_B T) = 1 + 2n(\omega)$.
18) It should benoted that often $C(t)$ is defined with a prefactor $1/\pi$. This prefactor is then compensated by defining $J(\omega)$ accordingly.

The unit-step function guarantees that $J = 0$ for $\omega < 0$, and j_0 is a normalization factor, which can be expressed in terms of the reorganization energy as $j_0 = E_\lambda / \omega_c^p \Gamma(p)$ ($\Gamma(p)$ is the Euler Gamma function). For $p = 1$ and a cut-off frequency ω_c, which is much larger than the relevant frequencies of the considered system, we obtain the *Ohmic* form of the spectral density, $\omega^2 J(\omega) \propto \omega$. This expression has to be used with caution, since a real system cannot have oscillator modes at arbitrarily high frequencies.

A different frequency dependence is given by the so-called Debye spectral density

$$\omega^2 J(\omega) = \theta(\omega) \; \frac{j_0 \omega}{\omega^2 + \omega_D^2}, \tag{3.302}$$

which is typically used to characterize the coupling between a solute and a polar solvent. The frequency, ω_D, appearing in Eq. (3.302) is called the Debye frequency. Further, the normalization factor can be expressed as $j_0 = E_\lambda 2\omega_D / \pi\hbar$. Note that this spectral density also reduces to the Ohmic case mentioned above if the Debye frequency is assumed to be large.

A third example for a spectral density is related to the so-called *Brownian oscillator model*. This model describes a harmonic system coordinate bilinearly coupled to a harmonic bath. Typical applications are found in optical spectroscopy, where the system coordinate corresponds to some high-frequency intramolecular vibrational mode, while the surrounding solvent is described by the harmonic bath (Section 6.2.6). The Brownian oscillator spectral density is defined as

$$\omega^2 J(\omega) = \theta(\omega) \, j_0 \frac{\omega \omega_0^2 \gamma_0}{(\omega^2 - \omega_0^2)^2 + \omega^2 \gamma_0^2}. \tag{3.303}$$

Here, ω_0 is the frequency of the system oscillator, and γ_0 its damping.[19] The normalization factor can be specified for the particular applications, see, for example Section 6.2.6. All three spectral densities are illustrated in Figure 3.5.

Given a spectral density, the correlation function $C(t)$, Eq. (3.300), can be calculated. This will be done for a decomposition into real (symmetric) and imaginary (antisymmetric) parts according to

$$C(t) = \frac{1}{2}[C^{(+)}(t) + C^{(-)}(t)]. \tag{3.304}$$

Using complex contour integration, it is more convenient to start from Eqs. (3.285) and (3.299). The real part of the correlation function is obtained as

$$C^{(+)}(t) = \int_{-\infty}^{\infty} d\omega \; e^{-i\omega t} \coth\left(\frac{\hbar\omega}{2k_B T}\right) \omega^2 [J(\omega) - J(-\omega)], \tag{3.305}$$

and the imaginary part as

$$C^{(-)}(t) = \int_{-\infty}^{\infty} d\omega \; e^{-i\omega t} \omega^2 [J(\omega) - J(-\omega)]. \tag{3.306}$$

---

19) Note that, in general, γ_0 could be a function of ω according to the spectral density of the bath modes, which couple to the harmonic system mode. The present limit of a constant γ_0 is called Ohmic dissipation limit.
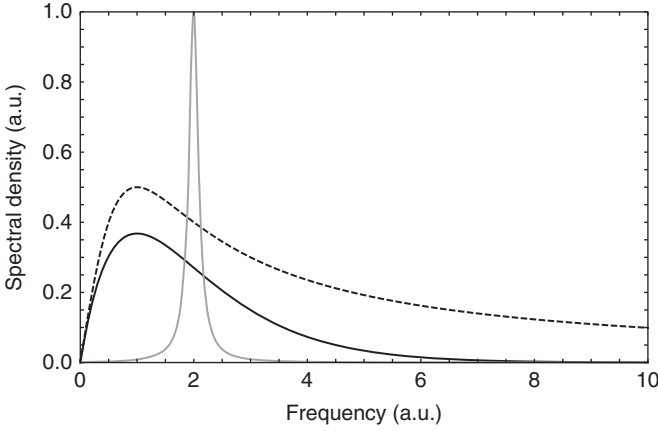
Figure 3.5 Ohmic spectral density with cut-off (dashed line), Eq. (3.301), with $\omega_c = 1$ and $p = 1$; Debye spectral density (solid line), Eq. (3.302), for $\omega_D = 1$; and Brownian oscillator spectral density (gray line), Eq. (3.303), for $\omega_0 = 2$ and $\gamma_0 = \omega_0/10$.

The integrations can be performed using the residue theorem. For $C^{(-)}(t)$, one obtains

$$C^{(-)}(t) = 2\pi i \sum_{\{\omega_k\}} \text{Res}_{\{\omega_k\}}[\omega^2 J(\omega)] e^{-i\omega_k t}, \tag{3.307}$$

with $\{\omega_k\}$ being the poles of $\omega^2 J(\omega)$. For $C^{(+)}(t)$, one usually assumes that the poles of $\omega^2 J(\omega)$ and $\coth\left(\hbar\omega/2k_B T\right)$ (labeled $\{\omega_l\}$) do not coincide. This allows to write

$$C^{(+)}(t) = 2\pi i \sum_{\{\omega_k\}} \text{Res}_{\{\omega_k\}}[\omega^2 J(\omega)] \coth\left(\frac{\hbar\omega_k}{2k_B T}\right) e^{-i\omega_k t}$$
$$+ 2\pi i \sum_{\{\omega_l\}} \text{Res}_{\{\omega_l\}}\left[\coth\left(\frac{\hbar\omega}{2k_B T}\right)\right] \omega_l^2 J(\omega_l) e^{-i\omega_l t}. \tag{3.308}$$

The contribution due to the residues of the $\coth\left(\hbar\omega/2k_B T\right)$ term can be obtained using the Matsubara decomposition technique that yields poles at $i\omega_l$ with the Matsubara frequencies $\omega_l = 2\pi l k_B T/\hbar$.[20],[21]

Using Eqs. (3.307) and (3.308), correlation functions for particular spectral density models can be obtained. First, the case of the Debye spectral density introduced in Eq. (3.302) will be considered. The poles of the spectral density are at $\{\omega_k\} = \{i\omega_D, -i\omega_D\}$. For $t > 0$, the integration contour is closed in the lower part of the complex plane, whereas for $t < 0$, it is closed in the upper plane. Thus, Eq. (3.307) can be written as

$$C^{(-)}(t) = -i\pi j_0 \text{sgn}(t) e^{-\omega_D |t|}. \tag{3.309}$$

---

20) The Matsubara method rests on the series expansion of the meromorphic function $\coth(x)$ in terms of its poles and the residues at these poles; that is, $\coth\left(\hbar\omega/2k_B T\right) = (2k_B T/\hbar)$ $\sum_{l=-\infty}^{+\infty} [\omega - i\omega_l]^{-1}$.

21) Note that, in practice, the Matsubara decomposition shows a slow convergence behavior, and more convenient schemes, for example based on a Padé approximation have been developed, see Hu et al. [2].

Concerning the first term of $C^{(+)}(t)$, we note that $\coth(\pm ix) = \mp i\cot(x)$ and write

$$C^{(+)}(t) = \pi j_0 \cot\left(\frac{\hbar\omega_D}{2k_B T}\right) e^{-\omega_D|t|}$$
$$+ \frac{4\pi j_0 k_B T}{\hbar} \sum_{l=1}^{\infty} \frac{\omega_l}{\omega_l^2 - \omega_D^2} e^{-\omega_l|t|}. \tag{3.310}$$

In the high-temperature limit, the Matsubara summation can be neglected, and one can approximate $\cot\left(\hbar\omega_D/2k_B T\right) \approx 2k_B T/\hbar\omega_D$. Thus, the total correlation function becomes

$$C(t) \approx \frac{\pi j_0}{2\hbar\omega_D}\left(2k_B T - i\hbar\omega_D\mathrm{sgn}(t)\right) e^{-\omega_D|t|}. \tag{3.311}$$

It decays with a time constant τ_c determined by the inverse of ω_D. Notice that $C(t)$ is defined by bath operators; that is, the correlation time can be considered as a reservoir property. If the Debye frequency is assumed to be large, the spectral density (3.302) has an Ohmic behavior, and the correlation time goes to zero, that is $C(t) \approx \delta(t)$; this is the *Markovian* limit.

Second, the correlation function for the Brownian oscillator model, Eq. (3.303), is calculated. For $t > 0$, one has to consider the two poles $\{\omega_k\} = \{-i\Omega_0^{(+)}, -i\Omega_0^{(-)}\}$ with $\Omega_0^{(\pm)} = \gamma_0/2 \pm i\Omega_0$ and $\Omega_0 = \sqrt{\omega_0^2 - \gamma_0^2/4}$. For $t < 0$, the relevant poles are at $\{\omega_k\} = \{i\Omega_0^{(+)}, i\Omega_0^{(-)}\}$. The residues are $\pm ij_0\omega_0^2/4\Omega_0$ and $\mp ij_0\omega_0^2/4\Omega_0$, respectively. Hence, one obtains for the antisymmetric correlation function a damped oscillation behavior

$$C^{(-)}(t) = -i\frac{\pi j_0\omega_0^2}{\Omega_0} e^{-\gamma_0|t|/2}\mathrm{sgn}(t)\sin(\Omega_0|t|). \tag{3.312}$$

The symmetric part of the correlation function is given by

$$C^{(+)}(t) = -\frac{\pi j_0\omega_0^2}{2\Omega_0}\left[\coth\left(\frac{i\hbar\Omega_0^{(+)}}{2k_B T}\right)e^{-i\Omega_0|t|} - \coth\left(\frac{i\hbar\Omega_0^{(-)}}{2k_B T}\right)e^{i\Omega_0|t|}\right]$$
$$\times e^{-\gamma_0|t|/2}$$
$$- \frac{4\pi j_0\omega_0^2\gamma_0 k_B T}{\hbar}\sum_{l=1}^{\infty}\frac{\omega_l}{(\omega_l^2 + \omega_0^2)^2 - \omega_l^2\gamma_0^2}e^{-\omega_l|t|}. \tag{3.313}$$

In the high-temperature limit, where $\coth(i\hbar\Omega_0^{(\pm)}/2k_B T) \approx -i2k_B T/\hbar\Omega_0^{(\pm)}$, this expression can be written as

$$C^{(+)}(t) = -\frac{\pi j_0\omega_0^2 k_B T}{\hbar\Omega_0}2\mathrm{Im}\left(\frac{e^{-i\Omega_0|t|}}{\Omega_0^{(+)}}\right)e^{-\gamma_0|t|/2}. \tag{3.314}$$

Applications of the Brownian oscillator model to absorption spectroscopy will be discussed in Section 6.2.6.

3.7.4 Linear Response Theory for the Reservoir

In Section 3.5.6, we have seen that the correlation functions $C_{uv}(t)$ automatically enter the QME as a result of the second-order approximation with respect to the

system–reservoir coupling. In what follows, we demonstrate how these functions, which are exclusively defined by reservoir quantities, can be introduced in an alternative way. For this reason, we change the point of view taken so far. We will not ask in what manner the system is influenced by the reservoir but how the reservoir dynamics is modified by the system's motion. To answer this question, it will be sufficient to describe the action of the system on the reservoir via classical time-dependent fields $K_u(t)$. Therefore, we replace H_{S-R} by

$$H_{\text{ext}}(t) = \sum_u K_u(t)\Phi_u. \qquad (3.315)$$

The Φ_u are the various reservoir operators. The bath Hamiltonian becomes time-dependent too and is denoted by

$$\mathcal{H}(t) = H_{\text{R}} + H_{\text{ext}}(t). \qquad (3.316)$$

As a consequence of the action of the fields $K_u(t)$, the reservoir will be driven out of equilibrium. In the case where the actual nonequilibrium state deviates only slightly from the equilibrium, this deviation can be linearized with respect to the external perturbations. We argue that in this limit the expectation value of the reservoir operator Φ_u obeys the relation

$$\langle \Phi_u(t) \rangle = \sum_v \int_{t_0}^{t} d\bar{t} \; \chi_{uv}(t, \bar{t}) K_u(\bar{t}). \qquad (3.317)$$

The functions $\chi_{uv}(t, \bar{t})$ are called *linear response functions* or *generalized linear susceptibilities*. In order to derive an expression for χ_{uv}, we start with the definition of the expectation value $\langle \Phi_u(t) \rangle$, which reads (cf. Eq. (3.123))

$$\langle \Phi_u(t) \rangle = \text{tr}_{\text{R}}\{U(t + t_0)\hat{R}_{\text{eq}}U^+(t + t_0)\Phi_u\}, \qquad (3.318)$$

where the time evolution of the reservoir statistical operator starting with the reservoir equilibrium density operator $\hat{R}_{\text{eq}}$ has been explicitly indicated. The time-evolution operator $U(t, t_0)$ does not depend on $t - t_0$ since the Hamiltonian $\mathcal{H}(t)$, Eq. (3.316), is time dependent. A rearrangement of the time-evolution operators shows that the expectation value is identical with $\langle \Phi_u(t) \rangle_{\text{R}}$ as introduced in Eq. (3.202). To linearize this expression with respect to the external fields, $U(t, t_0)$ is first separated into the free part $U_{\text{R}}(t - t_0)$ defined by H_{R}, and the S-operator (cf. Section 3.2.2), which reads

$$S(t, t_0) = \hat{T} \exp\left(-\frac{i}{\hbar}\int_{t_0}^{t} d\bar{t} \; U_{\text{R}}^+(\bar{t} - t_0)H_{\text{ext}}(\bar{t})U_{\text{R}}(\bar{t} - t_0)\right). \qquad (3.319)$$

In a second step, the S-operator is expanded up to first order in $H_{\text{ext}}(\tau)$. The result is inserted into Eq. (3.318), and we obtain

$$\langle \Phi_u(t) \rangle_{\text{R}} \approx \text{tr}_{\text{R}}\left\{\hat{R}_{\text{eq}}\Phi_u^{(\text{I})}(t)\right\} - \frac{i}{\hbar}\int_{t_0}^{t} d\bar{t} \; \text{tr}_{\text{R}}\left\{\hat{R}_{\text{eq}}\left[\Phi_u^{(\text{I})}(t), \Phi_v^{(\text{I})}(\bar{t})\right]_-\right\} K_v(\bar{t}). \qquad (3.320)$$

Here, the time dependence of the reservoir operators $\Phi_u^{(I)}(t)$ is given in the interaction representation. Comparing Eq. (3.320) with Eq. (3.317), the linear response function can be identified as[22]

$$\chi_{uv}(t, \bar{t}) = -\frac{i}{\hbar} \left\langle \left[\Phi_u^{(I)}(t), \Phi_v^{(I)}(\bar{t}) \right]_- \right\rangle_R. \tag{3.321}$$

First, we notice that the right-hand side depends on the time difference $t - \bar{t}$ only (cf. Eq. (3.243)), that is $\chi_{uv}(t, \bar{t}) = \chi_{uv}(t - \bar{t})$. Second, a comparison with Eq. (3.274) shows that $\chi_{uv}(t) = -i\hbar C_{uv}^{(-)}(t)$. The important point is that if there exists an experimental setup to measure the various $\langle \Phi_u(t) \rangle$, one is able to deduce $\chi_{uv}(t)$ if the K_v can be changed in the measurement. Thus, the response functions $\chi_{uv}(t)$ are quantities that can be experimentally determined at least in principle. In contrast, the correlation functions $C_{uv}(t)$ which are needed to study dissipation into the reservoir are not directly related to an experiment. However, using Eq. (3.285), one can compute $C_{uv}(t)$ if $\chi_{uv}(t)$ is known.[23]

Next, we consider how the internal energy of the reservoir changes via the influence of the external fields $K_u(t)$. We obtain the internal energy as

$$E_R(t) = \langle U^+(t + t_0)\mathcal{H}(t)U(t + t_0) \rangle_R. \tag{3.322}$$

The change in time follows as

$$\begin{aligned}
\frac{\partial}{\partial t} E_R = &\left\langle \frac{i}{\hbar}\mathcal{H}(t)U^+(t, t_0)\mathcal{H}(t)U(t, t_0) \right\rangle_R \\
&- \left\langle U^+(t, t_0)\mathcal{H}(t)\frac{i}{\hbar}\mathcal{H}(t)U(t, t_0) \right\rangle_R \\
&+ \left\langle U^+(t, t_0)\left(\frac{\partial}{\partial t}\mathcal{H}(t) \right)U(t, t_0) \right\rangle_R.
\end{aligned} \tag{3.323}$$

The first two terms compensate each other, and one finally gets

$$\frac{\partial}{\partial t} E_R = \sum_u \langle \Phi_u(t) \rangle_R \frac{\partial}{\partial t} K_u(t). \tag{3.324}$$

If the disturbance of the reservoir equilibrium state is weak enough, we can insert the linear susceptibility, Eq. (3.317), and obtain the change in internal energy expressed by the correlation function $C_{uv}^{(-)}(t)$. The latter describes fluctuations of certain operators of the reservoir, whereas the change in internal energy is a measure of energy dissipation. Therefore, the relation is called *fluctuation–dissipation theorem*.

Finally, it should be noted that this discussion is not restricted to the present situation. Whenever some system under the influence of a weak external field is considered, its response can be described in the lowest order using an appropriate linear response function. The latter is completely defined by an equilibrium correlation function of some system operators (cf. also Chapter 4).

3.7.5 Classical Description of $C_{uv}(t)$

As long as the reservoir can be described by independent harmonic oscillators, one can compute the correlation functions C_{uv} using spectral densities, as has

---

22) Here, we assume that the equilibrium expectation values of $\hat{\Phi}_u$ vanish.
23) Note that the use of Eq. (3.285) requires in a first step according to Eq. (3.321) the determination of $C_{uv}^{(-)}(\omega)$ from $\chi_{uv}(t)$.

been shown in Section 3.7.2. If this is not possible, one can go back to a classical description via molecular dynamics simulations using the Hamilton function $H_R(P, Z)$ (which is defined by the sets $P = \{P_\xi\}$ and $Z = \{Z_\xi\}$ of momenta and coordinates, respectively). In such a case, one has to clarify how the quantum statistical correlation functions discussed so far have to be expressed via the results of the classical molecular dynamic simulations. Let us denote the classical correlation functions by

$$\zeta_{uv}(t) = \langle \Phi_u(t)\Phi_v \rangle_{\text{cl}}. \tag{3.325}$$

Here, the $\Phi_u(t)$ are functions $\Phi_u(P(t), Z(t))$ of the canonically conjugated variables, and the classical average is performed with respect to the sets $P_0 \equiv \{P_\xi^{(0)}\}$ and $Z_0 \equiv \{Z_\xi^{(0)}\}$ of initial momenta and coordinates corresponding to the thermal equilibrium distribution, $f(P, Z) = \exp(-H_R(P, Z)/k_B T)/\mathcal{Z}$ ($\mathcal{Z}$ is the partition function). Thus, we have

$$\zeta_{uv}(t) = \int dP_0 dZ_0 \, f(P_0, Z_0)\Phi_u\left(P(t), Z(t)\right)\Phi_v\left(P_0, Z_0\right). \tag{3.326}$$

The classical correlation function is a real quantity that can be determined by a molecular dynamics simulation of the reservoir equilibrium. The problem is that it does not fulfill a relation as $C_{uv}(t) = C_{vu}^*(-t)$. Upward and downward relaxation become equally probable since the relation $C_{uv}(\omega)/C_{vu}(-\omega) = \exp\{-\hbar\omega/k_B T\}$ does not exist (see Eq. (3.280)). In order to solve this problem, one identifies $\zeta_{uv}(t)$ with half of the symmetric correlation function $C_{uv}^{(+)}$, Eq. (3.274). For the Fourier transform $\zeta_{uv}(\omega)$, we use Eq. (3.282) and obtain

$$C_{uv}(\omega) = 2\left(1 + \exp\left\{-\frac{\hbar\omega}{k_B T}\right\}\right)^{-1}\zeta_{uv}(\omega) \tag{3.327}$$

and

$$C_{vu}(-\omega) = 2\left(1 + \exp\left\{\frac{\hbar\omega}{k_B T}\right\}\right)^{-1}\zeta_{uv}(\omega). \tag{3.328}$$

Due to the temperature-dependent prefactor, detailed balance is guaranteed by these expressions. However, note that, for an arbitrary system, the replacement of the symmetrized quantum correlation function by the classical correlation function represents only an approximation.[24]

3.8 Reduced Density Matrix in Energy Representation

3.8.1 The Quantum Master Equation in Energy Representation

In what follows, we transform the QME (3.254) into the energy (state) representation with respect to the system Hamiltonian. Suppose that we have solved the eigenvalue problem for H_S,

$$H_S|a\rangle = E_a|a\rangle. \tag{3.329}$$

---

24) For a systematic investigation of quantum corrections to classical correlation functions, see Egorov et al. [3].

Then, the RDM is given by $\rho_{ab}(t) = \langle a|\hat{\rho}(t)|b\rangle$ (cf. Eq. (3.193)). Furthermore, we introduce the matrix elements of the system part of the system–reservoir coupling according to

$$\langle a|K_u|b\rangle = K_{ab}^{(u)}. \tag{3.330}$$

It should be pointed out that even though any other choice of a complete basis set for representing the density matrix is possible, the energy representation offers the advantage that

$$U_S(\tau)|a\rangle = e^{-iE_a\tau/\hbar}|a\rangle, \tag{3.331}$$

which simplifies the description of the coherent system dynamics. Taking the respective matrix element of the QME (3.254), we obtain after some rearrangement on the right-hand side the following equation of motion for the RDM ($\omega_{ab} = (E_a - E_b)/\hbar$):

$$\frac{\partial}{\partial t}\rho_{ab} = -i\omega_{ab}\rho_{ab} + \frac{i}{\hbar}\sum_c\sum_u\langle\Phi_u\rangle_R\left(K_{cb}^{(u)}\rho_{ac} - K_{ac}^{(u)}\rho_{cb}\right)$$

$$- \sum_{c,d}\sum_{u,v}\int_0^{t-t_0} d\tau\left(C_{vu}(-\tau)K_{db}^{(u)}K_{cd}^{(v)}e^{i\omega_{da}\tau}\rho_{ac}(t-\tau)\right.$$

$$+ C_{uv}(\tau)K_{ac}^{(u)}K_{cd}^{(v)}e^{i\omega_{bc}\tau}\rho_{db}(t-\tau)$$

$$- \left\{C_{vu}(-\tau)K_{ac}^{(u)}K_{db}^{(v)}e^{i\omega_{bc}\tau}\right.$$

$$\left.\left. + C_{uv}(\tau)K_{db}^{(u)}K_{ac}^{(v)}e^{i\omega_{da}\tau}\right\}\rho_{cd}(t-\tau)\right). \tag{3.332}$$

A more compact notation of this equation is achieved by introducing the tetradic matrix

$$M_{ab,cd}(t) = \sum_{u,v}C_{uv}(t)K_{ab}^{(u)}K_{cd}^{(v)}, \tag{3.333}$$

which satisfies the relation[25]

$$M_{ab,cd}^*(t) = \sum_{u,v}C_{vu}(-t)K_{ba}^{(u)}K_{dc}^{(v)} = M_{dc,ba}(-t). \tag{3.334}$$

Apparently, $M_{ab,cd}(t)$ determines the time span for correlations. For this reason, it will be called *memory matrix* or *memory function*. Using this notation, we can write the dissipative part of the non-Markovian density matrix equation (3.332) as

$$\left(\frac{\partial\rho_{ab}}{\partial t}\right)_{diss} = -\sum_{c,d}\int_0^{t-t_0} d\tau\left(M_{cd,db}(-\tau)e^{i\omega_{da}\tau}\rho_{ac}(t-\tau)\right.$$

$$+ M_{ac,cd}(\tau)e^{i\omega_{bc}\tau}\rho_{db}(t-\tau)$$

$$\left. - \left[M_{db,ac}(-\tau)e^{i\omega_{bc}\tau} + M_{db,ac}(\tau)e^{i\omega_{da}\tau}\right]\rho_{cd}(t-\tau)\right). \tag{3.335}$$

In what follows, let us discuss two important properties of the solutions of the QME in the energy representation. The first one concerns the normalization condition for

---

25) The expression requires the Hermiticity of H_{S-R} and not necessarily that of the individual K_u and Φ_u.

the RDM, Eq. (3.194), which expresses the fact that the total occupation probability of the different eigenstates of H_S is conserved, that is $\sum_a \partial \rho_{aa}/\partial t = 0$. It should be noted here that the basic property of a probability to be positive, that is $\rho_{aa} \geq 0$, cannot be proven in the general case. This requires careful analysis when carrying out the numerical calculation.

As a further property we expect that the stationary solution of the equations of motion for ρ_{ab} must correspond to a state that is in equilibrium with the reservoir. Since the reservoir is at temperature T, we demand for the density matrix the limiting behavior

$$\lim_{t \to \infty} \rho_{ab}(t) = \delta_{ab} e^{-E_a/k_B T} / \sum_c e^{-E_c/k_B T}. \tag{3.336}$$

To verify this relation, we demonstrate that its right-hand side is an asymptotic solution of the QME (3.332). This means that the right-hand side of the QME should vanish in the stationary limit, $\lim_{t \to \infty} \partial \rho_{aa}/\partial t = 0$. In the first step of the proof, we introduce the limit $t \to \infty$ in the time integral in Eq. (3.335). Since the reservoir correlation time τ_c is finite, we can replace the time-dependent RDM $\rho_{ab}(t - \tau)$ in the integrand by its asymptotic expression $\rho_{ab}(\infty)$. For $\rho_{ab}(\infty)$, we substitute Eq. (3.336) (omitting the normalization constant), which is supposed to be the correct solution. It follows that

$$0 = \frac{i}{\hbar} \sum_c \sum_u \langle \Phi_u \rangle_R (K_{ca}^{(u)} \delta_{ac} - K_{ac}^{(u)} \delta_{ca}) e^{-E_a/k_B T}$$

$$- \sum_{c,d} \int_0^\infty d\tau \left[\{ M_{cd,da}(-\tau) e^{i\omega_{da}\tau} \delta_{ac} + M_{ac,cd}(\tau) e^{i\omega_{ac}\tau} \delta_{da} \} e^{-E_a/k_B T} \right.$$

$$\left. - \{ M_{da,ac}(-\tau) e^{i\omega_{ac}\tau} + M_{da,ac}(\tau) e^{i\omega_{da}\tau} \} \delta_{cd} e^{-E_c/k_B T} \right]. \tag{3.337}$$

Next, we use the properties of the memory matrix and combine various terms of the dissipative part. Afterward, the Fourier transform of the correlation function $C_{uv}(\omega)$ will be introduced

$$0 = - \sum_c \int_0^\infty d\tau \left(\{ M_{ac,ca}(-\tau) e^{i\omega_{ca}\tau} + M_{ac,ca}(\tau) e^{i\omega_{ac}\tau} \} e^{-E_a/k_B T} \right.$$

$$\left. - \{ M_{ca,ac}(-\tau) e^{i\omega_{ac}\tau} + M_{ca,ac}(\tau) e^{i\omega_{ca}\tau} \} e^{-E_c/k_B T} \right)$$

$$= - \sum_c \int_{-\infty}^\infty d\tau \left(M_{ac,ca}(\tau) e^{i\omega_{ac}\tau} e^{-E_a/k_B T} - M_{ca,ac}(\tau) e^{i\omega_{ca}\tau} e^{-E_c/k_B T} \right)$$

$$= - \sum_c \sum_{u,v} \left(C_{uv}(\omega_{ac}) K_{ac}^{(u)} K_{ca}^{(v)} e^{-E_a/k_B T} - C_{uv}(\omega_{ca}) K_{ca}^{(u)} K_{ac}^{(v)} e^{-E_c/k_B T} \right). \tag{3.338}$$

To see that the last part vanishes, we use relation (3.280). Introducing it into Eq. (3.337) gives

$$\sum_c \sum_{u,v} \left(C_{uv}(\omega_{ac}) K_{ac}^{(u)} K_{ca}^{(v)} - C_{vu}(-\omega_{ca}) K_{ca}^{(u)} K_{ac}^{(v)} \right) = 0. \tag{3.339}$$

The final result is obtained after an interchange of u and v in the second term. Thus, the above given reasoning demonstrates that the asymptotic form of the RDO determined by the QME reads

$$\lim_{t \to \infty} \hat{\rho}(t) = \frac{1}{\mathcal{Z}} e^{-H_S/k_B T}. \tag{3.340}$$

The asymptotic form of the RDO, which is the equilibrium density operator of the relevant system, was obtained as a result of the second-order perturbational treatment of the system–reservoir coupling H_{S-R}. Including all orders in a nonperturbative treatment, the exact asymptotic form of the RDO has to be derived from the equilibrium density operator of the total system with the Hamiltonian H. This is achieved by restricting it to the state space of the relevant system according to $\text{tr}_R \{\exp(-H/k_B T)\}$.

3.8.2 Multilevel Redfield Equations

After having introduced the energy (state) representation of the RDO, let us discuss the Markov limit. Equation (3.335) gives the dissipative part of the RDM equations of motion. Carrying out the Markov approximation, that is using Eq. (3.260) and shifting the upper bound of the time integral to infinity, we obtain

$$\left(\frac{\partial \rho_{ab}}{\partial t}\right)_{\text{diss}} = -\sum_{c,d} \int_0^\infty d\tau \left(M_{cd,db}(-\tau)e^{i\omega_{dc}\tau}\rho_{ac}(t) + M_{ac,cd}(\tau)e^{i\omega_{dc}\tau}\rho_{db}(t)\right.$$
$$\left. - [M_{db,ac}(-\tau)e^{i\omega_{bd}\tau} + M_{db,ac}(\tau)e^{i\omega_{ca}\tau}]\rho_{cd}(t)\right). \tag{3.341}$$

(Note that we could have started from the operator equation (3.267) as well.) The time integrals can be viewed as half-sided Fourier transforms of the memory functions. These complex quantities define the dissipative part of the QME in the Markov approximation. Their real part describes an irreversible redistribution of the amplitudes contained in the various parts of RDM. The imaginary part introduces terms that can be interpreted as a modification of the transition frequencies and the respective mean-field matrix elements. These frequency shifts often give no qualitative new contribution to the RDM equations. They can in these cases be accounted for by changing the energy scale or adjusting the transition frequencies. Therefore, we restrict ourselves to the discussion of the real part only, leading to the following (damping) matrix:

$$\Gamma_{ab,cd}(\omega) = \text{Re} \int_0^\infty d\tau \, e^{i\omega\tau} M_{ab,cd}(\tau) = \text{Re} \sum_{u,v} K_{ab}^{(u)} K_{cd}^{(v)} \int_0^\infty d\tau \, e^{i\omega\tau} C_{uv}(\tau). \tag{3.342}$$

In the second part, we introduced Eq. (3.333) indicating that the damping matrix is mainly determined by the half-sided Fourier transform of the reservoir correlation functions. To establish the connection to the operator equation (3.267) derived in the previous section, we note that the damping matrix can be written in the alternative form

$$\Gamma_{ab,cd}(\omega_{dc}) = \text{Re} \sum_u \langle a|K_u|b\rangle\langle c|\Lambda_u|d\rangle. \tag{3.343}$$

(Note that the actual frequency argument of $\Gamma_{ab,cd}(\omega)$ is fixed by the matrix elements of $\langle c|K_v^{(I)}(-\tau)|d\rangle$ in Eq. (3.264).) Using Eq. (3.342), the dissipative part of the QME in the state representation, Eq. (3.341), becomes

$$\left(\frac{\partial\rho_{ab}}{\partial t}\right)_{\text{diss}} = -\sum_{c,d}\left(\Gamma_{bd,dc}(\omega_{cd})\rho_{ac}(t) + \Gamma_{ac,cd}(\omega_{dc})\rho_{db}(t)\right.$$
$$\left. -[\Gamma_{ca,bd}(\omega_{db}) + \Gamma_{db,ac}(\omega_{ca})]\rho_{cd}(t)\right). \tag{3.344}$$

If we further introduce the *relaxation matrix*

$$R_{ab,cd} = \delta_{ac}\sum_e\Gamma_{be,ed}(\omega_{de}) + \delta_{bd}\sum_e\Gamma_{ae,ec}(\omega_{ce})$$
$$-\Gamma_{ca,bd}(\omega_{db}) - \Gamma_{db,ac}(\omega_{ca}), \tag{3.345}$$

the dissipative contribution to the RDM equations of motion can be finally written as

$$\left(\frac{\partial\rho_{ab}}{\partial t}\right)_{\text{diss}} = -\sum_{c,d}R_{ab,cd}\rho_{cd}(t). \tag{3.346}$$

It should be noted that in the literature the tetradic relaxation matrix, Eq. (3.345), is frequently termed the *Redfield* tensor after A. G. Redfield who introduced it in the theory of nuclear magnetic resonance spectroscopy in the early 1960s.[26]

Let us discuss in more detail the Redfield tensor and its effect on the dynamics of the RDM $\rho_{ab}(t)$. Since the density matrix elements can be distinguished as populations ($a = b$) and coherences ($a \neq b$), it is reasonable to discuss $R_{ab,cd}$ according to its effect on the dynamics of ρ_{aa} and ρ_{ab}.

3.8.2.1 Population Transfer: $a = b, c = d$

Using Eq. (3.345), the respective matrix elements of the Redfield tensor can be written as

$$R_{aa,cc} = 2\delta_{ac}\sum_e\Gamma_{ae,ea}(\omega_{ae}) - 2\Gamma_{ca,ac}(\omega_{ca})$$
$$= \delta_{ac}\sum_e k_{a\to e} - k_{c\to a}. \tag{3.347}$$

Here, we introduced the rate $k_{a\to b}$ for the transition from state $|a\rangle$ to state $|b\rangle$ according to

$$k_{a\to b} = 2\Gamma_{ab,ba}(\omega_{ab}) = 2\text{Re}\int_0^\infty d\tau e^{i\omega_{ab}\tau}M_{ab,ba}(\tau)$$
$$= \int_0^\infty d\tau e^{i\omega_{ab}\tau}M_{ab,ba}(\tau) + \int_0^\infty d\tau e^{-i\omega_{ab}\tau}M_{ab,ba}^*(\tau). \tag{3.348}$$

The two terms on the last line can be combined to give

$$k_{a\to b} = \int d\tau\, e^{i\omega_{ab}\tau}M_{ab,ba}(\tau) \equiv M_{ab,ba}(\omega_{ab}). \tag{3.349}$$

---

26) The original publication can be found in Redfield [4].

From Eq. (3.347), we see that $R_{aa,cc}$ combines the rates for transitions between different system eigenstates. The first term in Eq. (3.347) corresponds to transitions from the state $|a\rangle$ into all other system states $|e\rangle$, thus decreasing the occupation probability of the state $|a\rangle$. Conservation of probability is established, then, by the second term in Eq. (3.347), which represents transitions from all other states into the state $|a\rangle$.

Equation (3.349) shows that the transfer rate can also be written in terms of the Fourier-transformed memory matrix at the transition frequency ω_{ab}. Using Eq. (3.333) for the memory matrix gives the following alternative expression for the energy relaxation rates:

$$k_{a \to b} = \sum_{u,v} C_{uv}(\omega_{ab}) K_{ab}^{(u)} K_{ba}^{(v)}. \tag{3.350}$$

The amplitude of the rate for a particular transition is determined by the matrix elements of the operators K_u and by the value of the correlation function taken at the respective transition frequency, $C_{uv}(\omega = \omega_{ab})$. This last dependence can be viewed as a "probing" of the spectral density at this frequency (cf. Figure 3.6). In terms of the harmonic reservoir model this implies that there has to be a reservoir oscillator mode which can absorb or emit a reservoir quantum at the transition frequency of the system. Since the transitions between the system states are therefore accompanied by energy dissipation into the reservoir, the rates (3.349) are also called *energy relaxation* rates.

We can use Eq. (3.280) for $C_{uv}(\omega)$ to relate the forward rate for the transition from $|a\rangle$ to $|b\rangle$ to the respective backward rate. Interchanging the summation indices u and v in Eq. (3.350) yields

$$\begin{aligned} k_{a \to b} &= \sum_{u,v} C_{vu}(\omega_{ab}) K_{ab}^{(v)} K_{ba}^{(u)} = e^{\hbar\omega_{ab}/k_{\mathrm{B}}T} \sum_{u,v} C_{uv}(\omega_{ba}) K_{ba}^{(u)} K_{ab}^{(v)} \\ &= e^{\hbar\omega_{ab}/k_{\mathrm{B}}T} k_{b \to a}. \end{aligned} \tag{3.351}$$

This result, which is a direct consequence of Eq. (3.280), guarantees the proper relation between excitations and deexcitation of the system's quantum states yielding the equilibrium according to Eq. (3.336). Equation (3.351) is also known as the *principle of detailed balance*.
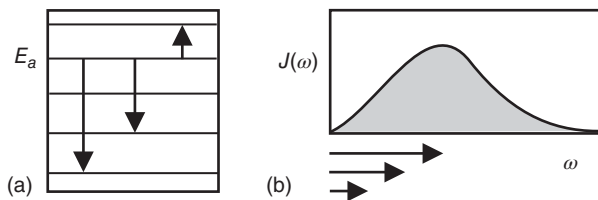
Figure 3.6 Transitions among five different quantum states $|a\rangle$ of the relevant system with energies E_a ($a = 1, 2, \ldots, 5$) (a). The transitions are induced by the interaction with the reservoir, which is characterized by the spectral density $J(\omega)$ (b). The magnitude of the rate is proportional to the value of the spectral density at the respective transition energy.

3.8.2.2 Coherence Dephasing: $a \neq b, a = c, b = d$

In this case, we have according to Eq. (3.345)

$$R_{ab,ab} \equiv \gamma_{ab} = \sum_e \left(\Gamma_{ae,ea}(\omega_{ae}) + \Gamma_{be,eb}(\omega_{be}) \right) - \Gamma_{aa,bb}(0) - \Gamma_{bb,aa}(0). \qquad (3.352)$$

The expression determines the damping of the off-diagonal elements of the reduced density matrix $\rho_{ab}(t)$. As already indicated, these are called *coherences* since they represent phase relations between different states (here, eigenstates of H_S). Consequently, the decay of coherences is known as the *dephasing* process, and the γ_{ab} are called *dephasing rates*. We notice that the first part of the dephasing rate can be written as $\gamma_a + \gamma_b$, where γ_a and γ_b equal half of the relaxation rates, Eq. (3.349), for the transitions out of the states $|a\rangle$ and $|b\rangle$, respectively. Thus, within the present model, energy relaxation is a source of coherence dephasing. The second part of Eq. (3.352) denoted by $\gamma_{ab}^{(pd)}$ is defined by the reservoir correlation function at zero frequency; that is, it represents an elastic type of collision where no energy is exchanged between the system and the reservoir. These rates are usually named *pure dephasing* rates , and we write

$$\gamma_{ab} = \frac{1}{2} \sum_e k_{a \to e} + \frac{1}{2} \sum_e k_{b \to e} + \gamma_{ab}^{(pd)}, \qquad (3.353)$$

with

$$\gamma_{ab}^{(pd)} = -\sum_{u,v} K_{aa}^{(u)} K_{bb}^{(v)} C_{uv}(\omega = 0). \qquad (3.354)$$

However, the presence of pure dephasing not only requires nonzero correlation functions at zero frequency but also nonvanishing diagonal matrix elements of the operators K_u. We already met this requirement at the end of Section 3.6.1 where we discussed types of dissipation that do not change the internal energy.

Traditionally, the relation $1/T_2 = 1/2T_1 + 1/T_2^*$ is used to indicate the different contributions to the dephasing rate. Here, the total dephasing time T_2 is called the transverse relaxation time. (The term "transverse" is connected with its early use in the field of magnetic resonance experiments where only two-level systems with a single relaxation time have to be considered.) $1/T_2$ has to be identified with γ_{ab} for a particular pair of levels, and the pure dephasing rate $\gamma_{ab}^{(pd)}$ with $1/T_2^*$. Moreover, T_1 is called longitudinal relaxation time and corresponds to the lifetime $2/\sum_e k_{ae}$ and the lifetime $2/\sum_e k_{be}$. It is important to note that we have related the different relaxation times, which often serve as phenomenological parameters, to a particular microscopic model for the system–reservoir interaction.

3.8.2.3 Remaining Elements of $R_{ab,cd}$

The remaining elements of the Redfield tensor do not have a simple interpretation in terms of energy relaxation and coherence dephasing rates. However, we can distinguish the following transitions induced by $R_{ab,cd}$. First, coherences can be transferred between different pairs of states: $\rho_{ab} \to \rho_{cd}$ ($R_{ab,cd}$). Second, populations can change to coherences: $\rho_{aa} \to \rho_{cd}$ ($R_{aa,cd}$). And finally, the coherences can be transformed into populations: $\rho_{ab} \to \rho_{cc}$ ($R_{ab,cc}$). As a consequence, there is a mixing between different

types of RDM elements. The conditions under which this reservoir induced mixing of populations and coherences is negligible will be discussed in the following section.

Before doing this, we underline that the multilevel Redfield equations also guarantee that the equilibrium density matrix equation (3.336) is a stationary solution. The demand immediately leads to $0 = \sum_c R_{aa,cc} \exp(-E_c/k_B T)$. Noting Eq. (3.347) and the principle of detailed balance, Eq. (3.351), it becomes obvious that the required relation is fulfilled.

3.8.3   The Secular Approximation

The present form of the dissipative contribution to the QME in the state representation, Eq. (3.346), mixes diagonal and off-diagonal elements of the RDM, as pointed out at the end of the previous section. In order to see under what conditions this mixing between population and coherence-type density matrix elements can be neglected, consider Eq. (3.346) in the interaction representation with respect to the system Hamiltonian (see also Eq. (3.261)):

$$\left(\frac{\partial \rho_{ab}^{(I)}}{\partial t}\right)_{\text{diss}} = -\sum_{c,d} R_{ab,cd}\, e^{i(\omega_{ab}-\omega_{cd})(t-t_0)} \rho_{cd}^{(I)}(t). \tag{3.355}$$

The right-hand side contains various contributions that oscillate with the combined frequency $\omega_{ab} - \omega_{cd}$. All contributions to the equations of motion where $1/|\omega_{ab} - \omega_{cd}|$ is much smaller than the time increment Δt for which the QME is solved will cancel each other upon integration of the equations of motion due to destructive interference. Let us suppose that we can neglect all those contributions to the dissipative part for which the condition $1/|\omega_{ab} - \omega_{cd}| \ll \Delta t$ is fulfilled. There are at first glance two types of contributions that cannot be neglected since $|\omega_{ab} - \omega_{cd}| = 0$ holds. These are related to those elements of $R_{ab,cd}$ that were discussed as cases 1 and 2 in the previous section. However, for systems with degenerate transition frequencies such as a harmonic oscillator, $|\omega_{ab} - \omega_{cd}| = 0$ can be fulfilled even if $R_{ab,cd}$ belongs to the category 3 of the previous section. In general, the approximation that builds upon the consideration of only those terms in the dissipative part of the QME (3.346) for which $|\omega_{ab} - \omega_{cd}| = 0$ holds is called *secular approximation*.[27]

Note that within the Markov approximation, the smallest possible time step, Δt, is determined by the memory time τ_{mem}. If, however, in systems with nearly degenerate transition frequencies, the condition $1/|\omega_{ab} - \omega_{cd}| > \tau_{\text{mem}}$ is realized, the secular approximation determines the *coarse graining* of the time axis and therefore imposes a lower limit on the time resolution of the RDM. On the other hand, even in anharmonic systems, the condition $|\omega_{ab} - \omega_{cd}| = 0$ can also be fulfilled accidentally. In other words, in practice, one should always carefully examine the system at hand and its time scales before using the secular approximation. All contributions to the QME that are beyond the secular approximation will be called *nonsecular* in what follows.

---

27) The approximation is often also termed *rotating wave approximation*.

Thus, we have seen that even in the secular approximation, there is a chance that populations and coherences are coupled via $R_{ab,cd}$. If we neglect this coupling, that is if we suppose that $|\omega_{ab} - \omega_{cd}| = 0$ holds only in the cases 1 and 2 of the previous section, we are at the level of the so-called *Bloch model*. This type of approximation is likely to be good in rather anharmonic systems. Within the Bloch model, the right-hand side of Eq. (3.355) can be separately written down for the diagonal part of the RDM, $\rho_{aa}^{(I)} \equiv \rho_{aa} = P_a$, and the off-diagonal part. We obtain for the former using $a = b$ and $c = d$

$$\left(\frac{\partial P_a}{\partial t}\right)_{\text{diss}} = -\sum_c R_{aa,cc} P_c(t) \tag{3.356}$$

Next, we consider the off-diagonal part of Eq. (3.355), that is $a \neq b$. Assuming within the Bloch model that all transition frequencies are different, we obtain from the secular condition $\omega_{ab} = \omega_{cd}$ the relations $a = c$ and $b = d$, *that is* case 2 of the previous section. Changing from the interaction representation of the RDM to the Schrödinger representation, the off-diagonal part becomes

$$\left(\frac{\partial \rho_{ab}}{\partial t}\right)_{\text{diss}} = -(1 - \delta_{ab})R_{ab,ab}\rho_{ab}. \tag{3.357}$$

Inspecting Eqs. (3.356) and (3.357), we find that these elements of the Redfield tensor do not mix the diagonal and off-diagonal elements of the RDM as desired. This means that we can consider the equations for the populations and the coherences separately. The influence of the reservoir on these two types of RDM elements is characterized by the energy relaxation and coherence dephasing rates introduced in the foregoing section (Eqs. (3.350) and (3.350), respectively).

3.8.4   State Expansion of the System–Reservoir Coupling

To illustrate the formulas presented for the damping matrix in Section 3.8.2, we introduce an expansion of $H_{\text{S-R}}$ in the eigenstates of H_{S}:

$$H_{\text{S-R}} = \sum_{a,b} \langle a|H_{\text{S-R}}|b\rangle \, |a\rangle\langle b|. \tag{3.358}$$

This expansion is very fundamental, and we will meet different versions of it in the following sections. However, Eq. (3.358) is also a special version of the factorized ansatz, Eq. (3.198), for the system–reservoir interaction Hamiltonian. This conclusion is obvious when identifying the index u with (ab), K_u with $|a\rangle\langle b|$ (that is $K_{cd}^{(u)} = \delta_{ca}\delta_{db}$), and Φ_u with $\langle a|H_{\text{S-R}}|b\rangle$. We also stress the fact that the K_u-operators do not represent Hermitian operators. In a first step and in specifying Eq. (3.286), we set $\langle a|H_{\text{S-R}}|b\rangle \equiv \Phi_{ab} = \sum_\xi \hbar\omega_\xi g_{ab}(\xi)Q_\xi$. From Eq. (3.350), the (energy) relaxation rates are obtained as

$$k_{a \to b} = C_{ab,ba}(\omega_{ab}). \tag{3.359}$$

In accordance with Eq. (3.295), we get for the correlation function

$$C_{ab,cd}(\omega) = 2\pi\omega^2[1 + n(\omega)] \left[J_{ab,cd}(\omega) - J_{ab,cd}(-\omega)\right], \tag{3.360}$$

where we introduced the generalized spectral density

$$J_{ab,cd}(\omega) = \sum_{\xi} g_{ab}(\xi) g_{cd}(\xi) \delta(\omega - \omega_{\xi}). \tag{3.361}$$

The relaxation rates follow as (using $-n(-\omega) = 1 + n(\omega)$)

$$k_{a \to b} = 2\pi\omega_{ab}^2 \left([1 + n(\omega_{ab})] J_{ab,ba}(\omega_{ab}) + n(\omega_{ba}) J_{ab,ba}(\omega_{ba}) \right), \tag{3.362}$$

and the dephasing rates γ_{ab} can be derived from Eq. (3.353). The pure dephasing contribution may vanish if the correlation function equals zero for $\omega = 0$.

Finally, we demonstrate that in the case of the Bloch model as introduced in Section 3.8.3, it is possible to change back from the energy representation to an operator notation of the QME. One immediately arrives at

$$\left(\frac{\partial \hat{\rho}(t)}{\partial t} \right)_{\text{diss}} = - \sum_{a,b} \left\{ \frac{1}{2} \left[k_{a \to b} |a\rangle\langle a|, \hat{\rho}(t) \right]_+ - k_{a \to b} |b\rangle\langle a|\hat{\rho}(t)|a\rangle\langle b| \right\}$$
$$- \sum_{a,b} \gamma_{ab}^{(\text{pd})} |a\rangle\langle a|\hat{\rho}(t)|b\rangle\langle b|. \tag{3.363}$$

The first sum including an anticommutator is exclusively determined by the energy relaxation rate $k_{a \to b}$, whereas the second sum incorporates the pure dephasing part $\gamma_{ab}^{(\text{pd})}$, Eq. (3.354).

Once pure dephasing vanishes, the whole dissipative part resembles what is often called the *Lindblad form*, cf. Eq. (3.257). It is possible to derive this type of dissipative contribution to the equation of motion of the RDO in a more formal way starting from the assumption that the diagonal elements of the RDO have to be greater or equal to zero in any basis set. This has been shown by Lindblad in the 1970s. The advantage of Eq. (3.363) is that the condition $\rho_{aa}(t) \geq 0$ is guaranteed by construction in contrast to the case of the QME.

Using the Lindblad form of dissipation (or the Bloch model), which guarantees positivity of the density matrix, one has to pay attention not to overinterpret the results. In contrast to the multilevel Redfield theory, one may increase the system reservoir coupling strength without obtaining results that apparently behave in a wrong way. Nevertheless, one has already left the region of applicability of the whole approach, which is of second order in the system reservoir coupling, and obtained formally meaningless results.

3.8.4.1 Some Estimates

After Eq. (3.254), we already discussed the range of validity of the QME. Using the energy representation introduced in this section, a more detailed account is possible. To do this, we concentrate on the energy representation of the Markovian version of Eq. (3.254) with the dissipative part given by Eq. (3.346). A necessary criterion for the validity of the QME would be that the absolute value of any transition frequency ω_{ab} is larger than the respective level broadening determined by the dephasing rates γ_{ab}, Eq. (3.353). Using the expression for $H_{\text{S-R}}$ introduced in Eq. (3.358) and noting the absence of pure dephasing, we have to compare $|\omega_{ab}|$ with the dephasing rates

following from Eqs. (3.350) and (3.360). Since every term stemming from Eq. (3.360) has to be small and assuming zero temperature, we get $|\omega_{ab}| > \omega_{ae}^2 J_{ae,ea}(\omega_{ae}) + \omega_{be}^2 J_{be,eb}(\omega_{be})$. If $\omega_{ab} \approx \omega_{ae}, \omega_{be}$, the respective values of the spectral densities have to be small compared to ω_{ab}^{-1}. This restriction can be relaxed whenever the cut-off frequencies of the spectral densities are smaller than ω_{ae}, ω_{be}. If ω_{ab} is much larger than ω_{ae}, ω_{be}, then the spectral densities have to be small compared to $\omega_{ab}/\omega_{ae}^2$. This latter case imposes to the spectral density a much stronger constraint of smallness as the foregoing relations. The discussion indicates that the concrete structure of the spectrum of the relevant system decides on the extent to which the system–reservoir coupling can be increased such that the QME is still valid.

3.9 Coordinate and Wigner Representation of the Reduced Density Matrix

In the preceding parts of this section, we concentrated on the energy representation of the density matrix. There may be situations where the eigenstates of the Hamiltonian are not easily available, for example for problems involving dissociation. In this case, the coordinate representation may offer a convenient alternative. In what follows, we derive the coordinate representation of the QME in the Markov approximation, Eq. (3.267).

As in Section 3.1, we assume that the total system has been separated into a relevant part and a reservoir. The relevant system will be described by the set of coordinates $s \equiv \{s_j\}$. Then, according to Eq. (3.190), the density matrix in the coordinate representation follows as $\rho(s, \bar{s}; t) = \langle s|\hat{\rho}(t)|\bar{s}\rangle$; that is, the matrix elements of the RDO are taken with the eigenstates $|s\rangle$ of the coordinate operators. In contrast to the energy representation, the RDM introduced here is a *continuous* function of the coordinates s_j.

The equation of motion for $\rho(s, \bar{s}; t)$ is obtained by taking the respective matrix elements of the Markovian QME, Eq. (3.267). First, we have to calculate the matrix elements of the system Hamiltonian, $\langle s|H_S|\bar{s}\rangle$. It is well known from quantum mechanics that these matrix elements follow as $H_S(s, p)\delta(s - \bar{s})$ (here and in what follows the δ-function stands for a product of the single coordinate expressions $\delta(s_j - \bar{s}_j)$). The momentum operators in H_S are given by $p_j = -i\hbar\partial/\partial s_j$. The notation $H_S(s, p) = T(p) + U(s)$ used in the following equation indicates the coordinate representation of the system Hamiltonian with its kinetic energy part $T(p)$ and the potential energy $U(s)$.

The QME in the Markov approximation follows as

$$\frac{\partial}{\partial t}\rho(s, \bar{s}; t) = -\frac{i}{\hbar}\left(H_S(s, p) - H_S(\bar{s}, \bar{p})\right)\rho(s, \bar{s}; t) + \langle s|\left(\frac{\partial\hat{\rho}}{\partial t}\right)_{\text{diss}}|\bar{s}\rangle. \qquad (3.364)$$

The mean-field contribution is not considered explicitly. It is supposed to be included into the definition of H_S (see Eq. (3.266)). The dissipative part can be rewritten as a nonlocal (integral) operator. For the present purpose, it is sufficient to assume that

the operators K_u in Eq. (3.198) only depend on the coordinates s. Thus, we have $\langle s|K_u|\bar{s}\rangle = \delta(s - \bar{s})K_u(s)$, and the dissipative part reads

$$\langle s|\left(\frac{\partial \hat{\rho}}{\partial t}\right)_{\text{diss}}|\bar{s}\rangle = -\sum_u \left(K_u(s) - K_u(\bar{s})\right)$$
$$\times \int ds' \left(\langle s|\Lambda_u|s'\rangle \rho(s', \bar{s}; t) - \rho(s, s'; t)\langle s'|\Lambda_u^{(+)}|\bar{s}\rangle\right).$$
(3.365)

Note that $\int ds'$ abbreviates the multidimensional integration with respect to all coordinates $\{s'_j\}$.

To establish the relation to the approximations discussed in Section 3.8.2, we compute the coordinate matrix elements of the Λ-operator Eq. (3.264). In doing so, it is necessary to determine $\langle s|K_v^{(I)}(-\tau)|\bar{s}\rangle$, which will have nonvanishing off-diagonal elements for $\tau > 0$. All elements are easily calculated if one uses the eigenstates $\varphi_a(s)$ of H_S. Inserting the result into the matrix elements of the Λ-operator gives (for the matrix elements of the operators K_v see Eq. (3.330))

$$\langle s|\Lambda_u|\bar{s}\rangle = \sum_{a,b} \varphi_a(s)\varphi_b^*(\bar{s}) \sum_v \int_0^\infty d\tau \, C_{uv}(\tau)e^{-i\omega_{ab}\tau} K_{ab}^{(v)}.$$
(3.366)

As in Section 3.8.2, we would like to relate the given description to the concept of the spectral density, Eq. (3.294), of a harmonic oscillator environment. Therefore, the system–reservoir coupling of Eq. (3.286) is used, resulting in a single K-operator and a single correlation function $C(t)$. The approximation made in Section 3.8.2, which takes into account only the real expression $\Gamma_{ab,cd}(\omega)$, Eq. (3.342), is in the present context equivalent to the replacement of the half-sided Fourier transform of $C(t)$ by half of the fully transformed expression $C(\omega)$.[28] Therefore, Eq. (3.366) is expressed by $C(-\omega_{ab})$. Noting Eq. (3.295), which relates $C(\omega)$ to $J(\omega)$, we finally obtain

$$\langle s|\Lambda_u|\bar{s}\rangle = \sum_{a,b} \varphi_a(s)\varphi_b^*(s') K_{ab} \, \pi\omega_{ab}^2 \left(1 + n(\omega_{ba})\right)\left(J(\omega_{ba}) - J(\omega_{ab})\right).$$
(3.367)

Let us discuss a case where this expression reduces to a local one ($\sim \delta(s - \bar{s})$). First, we concentrate on the high-temperature limit where $n(\omega) \approx k_B T/\hbar\omega$ holds. If one takes the Debye spectral density, Eq. (3.302), the ω_{ba} stemming from $n(\omega_{ba})$ and those coming from the spectral density cancel each other. Moreover, we assume that $\omega_{ba} \ll \omega_D$. If $K_{aa} = 0$, there is no need to care about the case $a = b$, and the a, b-summation gives $\langle s|K(s)|s'\rangle = \delta(s - s')K(s)$. According to Eq. (3.365), we obtain the dissipative part of the QME in the coordinate representation as

$$\left(\frac{\partial \rho(s, \bar{s}; t)}{\partial t}\right)_{\text{diss}} = -\frac{2\pi k_B T j_0}{\hbar\omega_D^2}\left(K(s) - K(\bar{s})\right)^2 \rho(s, \bar{s}; t).$$
(3.368)

---

28) The half-sided Fourier transform if expressed by the complete Fourier-transformed correlation function reads $\hat{C}(\omega) = \int_0^\infty dt \exp(i\omega t) \int d\overline{\omega}/2\pi \times \exp(-i\overline{\omega}t)C(\overline{\omega})$. A rearrangement of the integrations leads to $\int_0^\infty dt \exp(i\Delta\omega t)$ where we introduced $\Delta\omega = \omega - \overline{\omega}$. The integral gives $i/(\Delta\omega + i\varepsilon)$ (with $\varepsilon \to +0$). As a result, we obtain $\hat{C}(\omega) = -\int d\overline{\omega}/2\pi i \times C(\overline{\omega})/(\Delta\omega + i\varepsilon)$. Since $C(\overline{\omega})$ is a real function (cf. Section 3.7.1), the separation of $\hat{C}(\omega)$ results in a principal-value integral and a δ-function from which the relation $\text{Re}\hat{C}(\omega) = C(\omega)/2$ can be verified.

The $s, \bar{s}$-dependence of the right-hand side nicely reflects the destruction of coherences contained in the off-diagonal elements of the RDM. However, the present derivation does not include contributions that describe energy dissipation.[29]

Next, we use the coordinate representation of the RDO to introduce the respective Wigner representation. For simplicity, we consider the case of a single coordinate and a coupling function to the reservoir $K(s) = s$ (that is, the so-called bilinear system–reservoir coupling is used). In Section 3.4.4, the change in the Wigner representation has been demonstrated for the total density operator, putting emphasis on the relation to classical statistical mechanics. This will be repeated here for the RDO but including the dissipative part. Following Section 3.4.4, we can directly adopt Eq. (3.168) to transform the reversible part of the QME. One obtains

$$\left(\frac{\partial \rho(x, p; t)}{\partial t} \right)_{\text{rev}} = \frac{\partial U(x)}{\partial x} \frac{\partial}{\partial p} \rho(x, p; t) - \frac{\partial T(p)}{\partial p} \frac{\partial}{\partial x} \rho(x, p; t). \tag{3.369}$$

Next, we determine the dissipative part of the QME in the Wigner representation using expression (3.368). To compute the respective Wigner representation, we introduce sum and difference coordinates and take into account that

$$\int dr\ e^{-ipr/\hbar}\ r^2 \rho(x, r; t) = -\hbar^2 \frac{\partial^2}{\partial p^2} \rho(x, p; t). \tag{3.370}$$

This gives directly

$$\left(\frac{\partial \rho(s, p; t)}{\partial t} \right)_{\text{diss}} = \frac{2\pi k_{\text{B}} T \hbar j_0}{\omega_{\text{D}}^2} \frac{\partial^2}{\partial p^2} \rho(x, p; t). \tag{3.371}$$

Combining this expression with Eq. (3.369), we obtain the Markovian QME in the Wigner representation as follows:

$$\left(\frac{\partial}{\partial t} - \frac{\partial U(x)}{\partial x} \frac{\partial}{\partial p} + \frac{\partial T(p)}{\partial p} \frac{\partial}{\partial x} - \frac{2\pi k_{\text{B}} T \hbar j_0}{\omega_{\text{D}}^2} \frac{\partial^2}{\partial p^2} \right) \rho(x, p; t) = 0. \tag{3.372}$$

As required for a classical limit, Eq. (3.372) is of zeroth order in $\hbar$. Equation (3.372) is also known as the *Fokker–Planck equation* (note that it is common to replace $2\pi \hbar j_0/\omega_{\text{D}}^2$ by the friction constant η).

3.10 The Path Integral Representation of the Density Matrix

The second-order perturbational treatment of the system–reservoir coupling and the Markov approximation are restrictions inherent to the density matrix theory presented particularly in Section 3.8.2. If we focus on harmonic oscillator reservoirs, it is

---

29) Using a slightly different derivation, terms proportional to derivatives of $\rho(s, \bar{s}; t)$ with respect to the coordinates may also appear. Now, one focuses on $K(s) = s$, where s is a single coordinate. Moreover, one uses again the Debye spectral density equation (3.302) but accounts for the full complex correlation function. And, when calculating $\langle s|\Lambda_u|\bar{s}\rangle$, one stays with $\langle s|s^{(\text{I})}(\tau)|\bar{s}\rangle$ (cf. Eq. (3.264)). The use of a short-time approximation $s^{(\text{I})}(\tau) \approx s - i[H_{\text{S}}, s]_-\tau/\hbar \equiv s - p\tau/m$ then reproduces Eq. (3.368) together with the additional coordinate derivative terms.

possible to derive an exact, that is nonperturbative and non-Markovian, expression for the RDM within the framework of Feynman's path integral approach to quantum dynamics. This will be demonstrated in the present section.

In order to illustrate the basic idea, we go back to Section 3.4.3, where the time evolution of the total density operator is given in Eq. (3.148). Let us suppose that we slice the time interval $[t_0, t = t_N]$ into N pieces of length $\Delta t = (t_N - t_0)/N$, that is $t_j = t_0 + j\Delta t$ $(j = 0, \dots, N)$. If we use the decomposition property of the time-evolution operator, Eq. (3.20), the matrix elements of this operator with respect to the coordinate representation become

$$\langle x_N | U(t_N, t_0) | x_0 \rangle = \langle x_N | U(t_N, t_{N-1}) U(t_{N-1}, t_{N-2}) \dots \times U(t_2, t_1) U(t_1, t_0) | x_0 \rangle. \tag{3.373}$$

In a next step, we insert the identity $1 = \int dx_j |x_j\rangle\langle x_j|$ between all operator products in Eq. (3.373). This gives

$$\langle x_N | U(t_N, t_0) | x_0 \rangle = \prod_{j=1}^{N-1} \left[\int dx_j \right] \prod_{j=1}^{N} \langle x_j | U(t_j, t_{j-1}) | x_{j-1} \rangle. \tag{3.374}$$

Within this representation, the matrix elements of the time-evolution operator, that is the transition amplitudes for the particle for going from point x_0 to point x_N in the time interval $[t_0, t_N]$, have a simple interpretation, illustrated in Figure 3.7.

The vertical axis in this figure represents the coordinate, and the horizontal one is the discretized time. Starting from a particular x_0, the system explores *all* possible paths that lead to x_N in the interval $[t_0, t_N]$, because at each intermediate time step t_j, Eq. (3.374) demands for an integration with respect to the coordinate x_j. Within this intuitive picture, the action of the time-evolution operator presented in the previous sections is replaced by a high-dimensional integration in coordinate space.

A fundamental property of the representation (3.374) can be derived starting for simplicity from the single particle Hamiltonian $H = T(\hat{p}) + V(\hat{x})$. We further suppose that the time step Δt is small enough to justify the decomposition

$$e^{-iH\Delta t/\hbar} \approx e^{-iV(\hat{x})\Delta t/\hbar} e^{-iT(\hat{p})\Delta t/\hbar}. \tag{3.375}$$
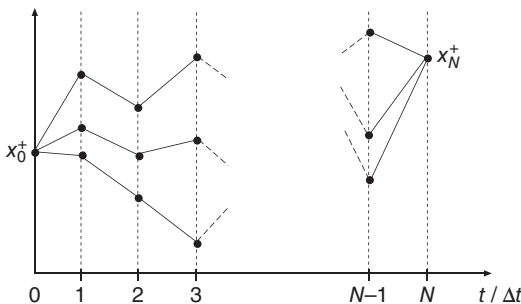
Figure 3.7 Visualization of different time-sliced paths leading from x_0^+ to x_N^+ in the time interval $[t_0, t_N]$.

According to Eq. (2.76), the error here will be of the order $\Delta t^2[V(\hat{x}), T(\hat{p})]_-$. For the matrix elements of the time-evolution operator in Eq. (3.374), we can then write

$$
\langle x_j|U(t_j, t_{j-1})|x_{j-1}\rangle \approx \langle x_j|e^{-iV(\hat{x})\Delta t/\hbar}e^{-iT(\hat{p})\Delta t/\hbar}|x_{j-1}\rangle
$$

$$
= \int dx \int \frac{dp}{2\pi\hbar} \int \frac{dp_j}{2\pi\hbar} \langle x_j|e^{-iV(\hat{x})\Delta t/\hbar}|x\rangle
$$

$$
\times \langle x|p_j\rangle\langle p_j|e^{-iT(\hat{p})\Delta t/\hbar}|p\rangle\langle p|x_{j-1}\rangle
$$

$$
= \int \frac{dp_j}{2\pi\hbar} e^{-iV(x_j)\Delta t/\hbar} e^{ip_j(x_j-x_{j-1})/\hbar} e^{-iT(p_j)\Delta t/\hbar},
$$

(3.376)

where we used $\langle x_j|V(\hat{x})|x\rangle = V(x_j)\delta(x_j - x)$, $\langle x|p_j\rangle = \exp\{ip_jx/\hbar\}/\sqrt{2\pi\hbar}$, and $\langle p_j|T(\hat{p})|p\rangle = T(p_j)\delta(p_j - p)$. Inserting this expression into Eq. (3.374), we have

$$
\langle x_N|U(t_N, t_0)|x_0\rangle = \prod_{j=1}^{N-1}\left[\int dx_j\right]\prod_{j=1}^{N}\left[\int \frac{dp_j}{2\pi\hbar}\right]
$$

$$
\times \exp\left\{\frac{i}{\hbar}\sum_{j=1}^{N}\left[p_j(x_j - x_{j-1}) - \Delta t[T(p_j) + V(x_i)]\right]\right\}.
$$

(3.377)

The momentum integrals can be performed analytically if the kinetic energy operator has the form $T = p^2/2m$. One obtains

$$
\langle x_N|U(t_N, t_0)|x_0\rangle = \frac{1}{\sqrt{2\pi\hbar i\Delta t/m}}\prod_{j=1}^{N-1}\left[\int \frac{dx_j}{\sqrt{2\pi\hbar i\Delta t/m}}\right]
$$

$$
\times \exp\left\{\frac{i}{\hbar}\Delta t\left[\sum_{j=1}^{N}\frac{m}{2}\left(\frac{x_j - x_{j-1}}{\Delta t}\right)^2 - V(x_j)\right]\right\}.
$$

(3.378)

If we now take the continuum limit, $\Delta t \to 0$, the sum in the exponent becomes an integral over time in the interval $[t_0, t_N]$. Since $(x_j - x_{j-1})/\Delta t \to \dot{x}(t)$, the integrand turns into the Lagrange function known from classical mechanics. Introducing the symbol $\mathcal{D}x$ for the $\Delta t \to 0$ limit of the integration over the different intermediate points along the time sliced path, the matrix elements of the time-evolution operator can be written as

$$
\langle x_N|U(t_N, t_0)|x_0\rangle = \int \mathcal{D}x \exp\left\{\frac{i}{\hbar}\int_{t_0}^{t_N} dt\, L(x, \dot{x}, t)\right\}.
$$

(3.379)

The exponent is just the classical action corresponding to the Lagrangian $L(x, \dot{x}, t) = m\dot{x}^2/2 - V(x, t)$. (Note that we have tacitly assumed a general time-dependent potential here for which the derivation proceeds along the same lines.) Since $\int \mathcal{D}x$ denotes the integration over all possible paths leading from x_0 to x_N, the interpretation of (3.379) is as follows: The transition amplitude for going from x_0 to x_N during the time interval $[t_0, t_N]$ is obtained by summing all different paths and assigning a *phase* to each path, which corresponds to $i/\hbar$ times the classical action. The exponent in Eq. (3.379) is of course a rapidly oscillating function on a scale given by Planck's constant. Thus, most of the terms in this sum will interfere in such a way that their net contributions are small. The main

contribution is likely to come, however, from the classical path, which makes the action stationary. This offers the intriguing possibility to understand quantum mechanical transition amplitudes in terms of classical paths supplemented by fluctuations around these paths that are responsible for quantum effects.

We now turn to the density matrix. Here, we have to account for the time evolution of the bra and ket vectors. Going back to Eq. (3.205), we can write for the total density operator using Eq. (3.379) ($\int dx_0^{\pm}$ abbreviates the integration with respect to x_0^+ and x_0^-, and $\mathcal{D}x^{\pm}$ stands for $\mathcal{D}x^+\mathcal{D}x^-$.)

$$
W(x_N^+, x_N^-; t_N) = \int dx_0^{\pm} \langle x_N^+ | U(t_N, t_0) | x_0^+ \rangle \langle x_0^+ | W(t_0) | x_0^- \rangle \langle x_0^- | U^+(t_N, t_0) | x_N^- \rangle
$$

$$
= \int dx_0^{\pm} \int \mathcal{D}x^{\pm} \exp\left\{ \frac{i}{\hbar} \int_{t_0}^{t_N} dt L(x^+, \dot{x}^+, t) \right\}
$$

$$
\times \langle x_0^+ | W(t_0) | x_0^- \rangle \exp\left\{ -\frac{i}{\hbar} \int_{t_0}^{t_N} dt L(x^-, \dot{x}^-, t) \right\}. \tag{3.380}
$$

This path integral expression for the total system's density matrix shows that the bra and the ket parts of the density operator have to be propagated forward and backward, respectively. Thereby, all paths $x^{\pm}(t)$ connecting x_0^+ with x_N^+ and x_0^- with x_N^-, respectively, in the interval $[t_0, t_N]$ have to be explored. The initial points are subject to an additional integration.

For the purpose of illustration, we develop the expression for the RDM of a one-dimensional system (s) embedded in a harmonic bath ($Z = \{Z_\xi\}$). We start with the Lagrangian corresponding to the generic bilinear system–reservoir Hamiltonian (cf. Sections 2.5.3, 3.1, and 3.7.2)

$$
L = \frac{m_s \dot{s}^2}{2} - V(s) + \sum_\xi \left(\frac{\dot{Z}_\xi^2}{2} - \frac{\omega_\xi^2}{2}\left(Z_\xi - \frac{\hbar \gamma_\xi s}{\omega_\xi^2} \right)^2 \right). \tag{3.381}
$$

Apparently, this Lagrangian is of the form $L = L_S + L_R + L_{S-R}$. Using Eqs. (3.381) and (3.380) with $x = (s, Z)$, we obtain for the RDM

$$
\rho(s_N^+, s_N^-; t_N) = \int dZ_N W(s_N^+, Z_N, s_N^-, Z_N; t_N) \tag{3.382}
$$

the expression

$$
\rho(s_N^+, s_N^-; t_N) = \int ds_0^{\pm} dZ_0^{\pm} dZ_N \int \mathcal{D}s^{\pm} \mathcal{D}Z^{\pm} W(s_0^+, Z_0^+, s_0^-, Z_0^-; t_0)
$$

$$
\times \exp\left\{ \frac{i}{\hbar} \int_{t_0}^{t_N} dt\, [L_S(s^+, \dot{s}^+, t) - L_S(s^-, \dot{s}^-, t)] \right\}
$$

$$
\times \exp\left\{ \frac{i}{\hbar} \int_{t_0}^{t_N} dt\, [L_R(Z^+, \dot{Z}^+, t) - L_R(Z^-, \dot{Z}^-, t)] \right\}
$$

$$
\times \exp\left\{ \frac{i}{\hbar} \int_{t_0}^{t_N} dt\, [L_{S-R}(s^+, \dot{s}^+, Z^+, \dot{Z}^+, t) \right.
$$

$$
\left. - L_{S-R}(s^-, \dot{s}^-, Z^-, \dot{Z}^-, t)] \right\}. \tag{3.383}
$$

Note that, due to the trace operation with respect to the reservoir DOFs, the endpoints for the forward and backward reservoir paths are identical (Z_N). For

simplicity, let us assume that the density matrix factorizes initially according to

$$W(s_0^+, Z_0^+, s_0^-, Z_0^-; t_0) = \rho(s_0^+, s_0^-; t_0) R_{\text{eq}}(Z_0^+, Z_0^-; t_0).$$
(3.384)

Then, Eq. (3.383) can be written as

$$\rho(s_N^+, s_N^-; t_N) = \int ds_0^\pm \int Ds^\pm \, \rho(s_0^+, s_0^-; t_0)$$
$$\times \exp\left\{\frac{i}{\hbar} S_S(s^+, t_N)\right\} \mathcal{F}(s^\pm) \exp\left\{-\frac{i}{\hbar} S_S(s^-, t_N)\right\}.$$
(3.385)

Here, we have introduced the classical action of the system part $S_S(s, t) = \int_{t_0}^t dt' L_S(s, \dot{s}, t')$. The structure of the equation is such that all the influence of the environment on the system dynamics is contained in the so-called *Feynman–Vernon influence functional*, which is defined as

$$\mathcal{F}(s^\pm) = \mathcal{F}[s^+(t), s^-(t)] = \int dZ_0^\pm dZ_N \int DZ^\pm$$

$$\times \exp\left\{\frac{i}{\hbar} \int_{t_0}^{t_N} dt \, (L_R(Z^+, \dot{Z}^+, t) - L_R(Z^-, \dot{Z}^-, t))\right\} R_{\text{eq}}(Z_0^+, Z_0^-; t_0)$$

$$\times \exp\left\{\frac{i}{\hbar} \int_{t_0}^{t_N} dt \, (L_{S-R}(s^+, \dot{s}^+, Z^+, \dot{Z}^+, t) - L_{S-R}(s^-, \dot{s}^-, Z^-, \dot{Z}^-, t))\right\}.$$
(3.386)

Even though we arrived at Eqs. (3.385) and (3.386) in a rather straightforward manner, the physical content of these expressions is remarkable. The system's density matrix evolution is given as a path integral over all paths $s^+(t)$, connecting s_0^+ with s_N^+ (forward time evolution), and all paths $s^-(t)$, connecting s_0^- with s_N^- (backward time evolution). The free system dynamics is modified by the interaction with the environment introduced by the influence functional $\mathcal{F}(s^\pm)$. Inspecting Eq. (3.386), we realize immediately that $\mathcal{F}(s^\pm)$ contains interactions that are *nonlocal* in time and span, in principle, the whole time interval of the density matrix evolution. This is just another way of saying that Eq. (3.385) contains all memory effects. Further, we notice that L_{S-R} can be interpreted as an extra potential for the environmental oscillators; they experience a force that changes along the system paths. For the Lagrangian (3.381), it is possible to obtain an analytical expression for the influence functional. It reads

$$\mathcal{F}(s^\pm) = \exp\left\{-\frac{1}{\hbar} \int_{t_0}^{t_N} dt' \int_{t_0}^{t'} dt'' \, [s^+(t') - s^-(t')]\right.$$

$$\times \left. [C(t' - t'')s^+(t'') - C^*(t' - t'')s^-(t'')]\right\}$$

$$\times \exp\left\{-\frac{i}{\hbar} \int_{t_0}^{t_N} dt' \sum_\xi \frac{(\hbar\gamma_\xi)^2}{2\omega_\xi^2} [s^+(t')^2 - s^-(t')^2]\right\}.$$
(3.387)

Here, $C(t)$ is the correlation function for the harmonic oscillator reservoir coordinates, discussed in Section 3.7.2. The second exponent contains the so-called counter term.

Equations (3.385) and (3.386) represent an *exact* analytical solution to the problem of the time evolution of the RDM for a one-dimensional system in a harmonic oscillator bath. However, the bottleneck for its straightforward numerical implementation is the multidimensional integration of a highly oscillatory function. Since the time step and the number of integrations are directly related (cf. Eqs. (3.373)–(3.375)), one would expect that only the short-time dynamics is accessible by this method. However, in a typical condensed-phase situation, the memory time of the bath DOFs does not extend over arbitrarily large time intervals. Stated in another way, the spectral density of the environment is often a rather smooth function in the spectral range of interest. Thus, the correlation function $C(t)$ can be expected to decay rather rapidly. Note that the extreme limit $C(t) \propto \delta(t)$ leads directly to the Markov approximation. Here, the interactions introduced by the influence functional become local in time, and the time evolution of the density matrix can be solved in an iterative fashion. Needless to say, that this does not yet correspond to the level of theory adopted in Section 3.6.1; the system–reservoir interaction is still treated nonperturbatively. Along these lines it is possible now to develop a systematic procedure for incorporation of finite memory effects. A limitation of the approach outlined so far is its restriction to harmonic oscillator reservoirs. A generalization to arbitrary reservoirs is possible, however, only at the expense of additional assumptions.

3.11 Hierarchy Equations of Motion Approach

There is an alternative formulation of the equations of motion for the RDM that provides for a certain class of spectral densities a numerical protocol for obtaining the dynamics in the nonperturbative and non-Markovian regime. The derivation builds on the path integral representation introduced in the previous section.[30] For simplicity, we will not consider the counter term, and the system bath coupling will be taken to be of the form

$$H_{S–R} = \sum_u K_u(s)\Phi_u(Z). \tag{3.388}$$

The reservoir part is assumed to consist of harmonic oscillators. For this model, the influence functional, Eq. (3.387), can be written as (setting $t_N = t$)

$$\mathcal{F}(s^{\pm}) = \exp\left\{ -\int_{t_0}^{t} dt' \sum_{u,v} \Delta_u[s^{\pm}(t')]A_{uv}[s^{\pm}(t')] \right\}. \tag{3.389}$$

Here, we have introduced the functions

$$\Delta_u[s^{\pm}(t)] = \frac{1}{\hbar}(K_u[s^{+}(t)] - K_u[s^{-}(t)]) \tag{3.390}$$

---

30) Note that the following derivation can be generalized to cases where the system operator K_u is not given in the coordinate representation.

and

$$A_{uv}[s^\pm(t)] = \int_{t_0}^{t} d\tau \{C_{uv}(t-\tau)K_v[s^+(\tau)] - C^*_{uv}(t-\tau)K_v[s^-(\tau)]\}, \qquad (3.391)$$

with $C_{uv}(t)$ being the correlation function of the bath operator $\Phi_u(Z)$. In the present notation, the time evolution of the RDM can be written as

$$\rho(s^\pm, t) = \int ds_0^\pm \; \mathcal{U}(s^\pm, t, s_0^\pm, t_0)\rho(s_0^\pm, t_0), \qquad (3.392)$$

with the time-evolution operator given by

$$\mathcal{U}(s^\pm, t, s_0^\pm, t_0) = \int_{s^\pm(t_0)}^{s^\pm(t)} Ds^\pm \exp\left\{\frac{i}{\hbar}S_S(s^+, t)\right\} \mathcal{F}(s^\pm) \exp\left\{-\frac{i}{\hbar}S_S(s^-, t)\right\}. \qquad (3.393)$$

To obtain the equation of motion, the time derivate of the evolution operator needs to be calculated. For the influence functional, we obtain

$$\frac{\partial}{\partial t}\mathcal{F}(s^\pm) = -\sum_{u,v} \Delta_u[s^\pm(t)]A_{uv}[s^\pm(t)]\mathcal{F}(s^\pm)$$

$$= -i\sum_{u,v} \Delta_u[s^\pm(t)]\mathcal{F}_{uv}(s^\pm), \qquad (3.394)$$

with the auxiliary influence functional

$$\mathcal{F}_{uv}(s^\pm) = -iA_{uv}[s^\pm(t)]\mathcal{F}(s^\pm). \qquad (3.395)$$

Next, an equation of motion is derived for this auxiliary influence functional, that is

$$\frac{\partial}{\partial t}\mathcal{F}_{uv}(s^\pm) = -i\left(\frac{\partial}{\partial t}A_{uv}[s^\pm(t)]\right)\mathcal{F}(s^\pm) - iA_{uv}[s^\pm(t)]\frac{\partial}{\partial t}\mathcal{F}(s^\pm)$$

$$= -i\left(\frac{\partial}{\partial t}A_{uv}[s^\pm(t)]\right)\mathcal{F}(s^\pm) - i\sum_{u',v'} \Delta_{u'}[s^\pm(t)]\mathcal{F}_{uv,u'v'}(s^\pm), \qquad (3.396)$$

with

$$\mathcal{F}_{uv,u'v'}(s^\pm) = -iA_{uv}[s^\pm(t)]\mathcal{F}_{u'v'}(s^\pm)$$

$$= (-iA_{uv}[s^\pm(t)])(-iA_{u'v'}[s^\pm(t)])\mathcal{F}(s^\pm). \qquad (3.397)$$

Obviously, this procedure can be continued by deriving an equation of motion for $\mathcal{F}_{uv,u'v'}(s^\pm)$ and so on. Whether this set of coupled equations can be closed depends on the properties of $A_{uv}[s^\pm(t)]$. Taking its time derivative yields

$$\frac{\partial}{\partial t}A_{uv}[s^\pm(t)] = C_{uv}(t_0)K_v[s^+(t)] - C^*_{uv}(t_0)K_v[s^-(t)]$$

$$+ \int_{t_0}^{t} d\tau \left\{\frac{\partial C_{uv}(t-\tau)}{\partial t}K_v[s^+(\tau)] - \frac{\partial C^*_{uv}(t-\tau)}{\partial t}K_v[s^-(\tau)]\right\}. \qquad (3.398)$$

Assuming that the bath correlation function can be written as a sum of exponential terms, the integral can be explicitly evaluated. That is, we suppose that for $t \geq 0$ $C_{uv}(t)$ can be written as

$$C_{uv}(t) = \sum_k \eta_{uv,k} e^{-\Omega_{uv,k}t} \qquad (3.399)$$

where $\eta_{uv,k}$ and $\Omega_{uv,k}$ are complex parameters. Examples for model spectral densities have been given in Section 3.7.3. For illustration, let us consider the case of a Debye spectral density generalized to correlated bath modes (cf. Eq. (3.311))

$$C_{uv}(t) = \eta_{uv}e^{-\gamma_{uv}t}, \tag{3.400}$$

where we have $\partial C_{uv}(t)/\partial t = -\gamma_{uv}C_{uv}(t)$. Hence, we obtain

$$\frac{\partial}{\partial t}A_{uv}[s^{\pm}(t)] = \eta_{uv}K_v[s^+(t)] - \eta_{uv}^*K_v[s^-(t)] - \gamma_{uv}A_{uv}[s^{\pm}(t)]. \tag{3.401}$$

Equation (3.396) can now be rewritten as

$$\frac{\partial}{\partial t}\mathcal{F}_{uv}(s^{\pm}) = B_{uv}[s^{\pm}(t)]\mathcal{F}(s^{\pm}) - \gamma_{uv}\mathcal{F}_{uv}(s^{\pm}) - i\sum_{u',v'}\Delta_{u'}[s^{\pm}(t)]\mathcal{F}_{uv,u'v'}(s^{\pm}), \tag{3.402}$$

with

$$B_{uv}[s^{\pm}(t)] = -i(\eta_{uv}K_v[s^+(t)] - \eta_{uv}^*K_v[s^-(t)]). \tag{3.403}$$

In order to arrive at the general structure of the equations of motion, the composite indices $\mathbf{u} = (u,v)$ and $\mathbf{n} = (n_{\mathbf{u}}, n_{\mathbf{u}'}, \ldots)$ with $n_{\mathbf{u}} \geq 0$ are introduced. The auxiliary influence functional can then be written as (skipping the path argument)

$$\mathcal{F}_{\mathbf{n}} = \left[(-iA_{\mathbf{u}})^{n_{\mathbf{u}}}(-iA_{\mathbf{u}'})^{n_{\mathbf{u}'}} \times \ldots\right]\mathcal{F} = \left[\prod_{\mathbf{u}}(-iA_{\mathbf{u}})^{n_{\mathbf{u}}}\right]\mathcal{F}, \tag{3.404}$$

and the equations of motion follow as

$$\frac{\partial}{\partial t}\mathcal{F}_{\mathbf{n}} = -\left(\sum_{\mathbf{u}}n_{\mathbf{u}}\gamma_{\mathbf{u}}\right)\mathcal{F}_{\mathbf{n}} + \sum_{\mathbf{u}}\left(n_{\mathbf{u}}B_{\mathbf{u}}\mathcal{F}_{\mathbf{n}_{\mathbf{u}}^-} - i\Delta_u\mathcal{F}_{\mathbf{n}_{\mathbf{u}}^+}\right). \tag{3.405}$$

Here, $\mathbf{n}_{\mathbf{u}}^{\pm}$ implies that the index $n_{\mathbf{u}}$ within the multiindex $\mathbf{n}$ is shifted to $n_{\mathbf{u}} \pm 1$. From the complete time evolution can now be expressed via the (auxiliary) influence functionals as $\rho_{\mathbf{n}}(t) = \mathcal{U}_{\mathbf{n}}(t,t_0)\rho(t_0)$. Using

$$\frac{\partial}{\partial t}\exp\left\{\pm\frac{i}{\hbar}S_S(s,t)\right\} = \mp\frac{i}{\hbar}H_S\exp\left\{\pm\frac{i}{\hbar}S_S(s,t)\right\}, \tag{3.406}$$

which follows from the Hamilton–Jacobi equation, we obtain[31]

$$\frac{\partial}{\partial t}\rho_{\mathbf{n}} = -\left(i\mathcal{L}_S + \sum_{\mathbf{u}}n_{\mathbf{u}}\gamma_{\mathbf{u}}\right)\rho_{\mathbf{n}} + \sum_{\mathbf{u}}\left(n_{\mathbf{u}}B_{\mathbf{u}}\rho_{\mathbf{n}_{\mathbf{u}}^-} - i\Delta_u\rho_{\mathbf{n}_{\mathbf{u}}^+}\right). \tag{3.407}$$

These equations constitute an infinite hierarchy, which upon solution contains all orders of perturbation theory. According to Eq. (3.392), the physical RDO is given by $\rho_{0,0,\ldots}(t)$. For practical applications, the hierarchy of equations needs to be truncated at a particular order; for a discussion, see suggested reading at the end of this chapter. Finally, we note that there is an alternative, wave function-based, formulation of hierarchical equations starting from a stochastic unraveling of the Feynman–Vernon expression equation (3.385). This so-called hierarchy of pure states approach is outlined in the supplementary Section 3.15.2.

---

31) Note that in general one could have a summation of terms containing exponential factors according to the decomposition Eqs. (3.307) and (3.308). In this case the dimension of the index array for the multiindex $\mathbf{n}$ increases according to the number of terms in the summation.

3.12 Coherent to Dissipative Dynamics of a Two-level System

In what follows, we discuss the dynamics of a coupled two-level system using the methods developed in Sections 3.2, 3.8.2, and 3.11. It should be noted that despite its simplicity, the model of a two-level system provides an important reference for understanding the dynamics in complicated condensed-phase situations. We start by solving the time-dependent Schrödinger equation for the two-level system. Afterward, the density matrix theory based on the QME in the Markov approximation and using the hierarchy equations of motion will be applied.

3.12.1 Coherent Dynamics

In Section 2.8.2, we obtained the eigenvalues $\mathcal{E}_{\kappa=\pm}$ and eigenvectors $|\kappa = \pm\rangle$ for a system consisting of two zeroth-order states $|m = 1,2\rangle$ with energies $\varepsilon_{m=1,2}$ coupled by some interaction V (cf. Eq. (2.148)). The time-evolution operator for the isolated two-level system $U(t) = e^{-iHt/\hbar}$ is conveniently expressed in terms of the eigenstates $|\kappa = \pm\rangle$. One obtains

$$U(t) = \sum_{\kappa,\lambda=\pm} \langle \kappa|U(t)|\lambda\rangle \, |\kappa\rangle\langle\lambda| = \sum_{\kappa=\pm} e^{-i\mathcal{E}_\kappa t/\hbar}|\kappa\rangle\langle\kappa|. \tag{3.408}$$

This expression can be used to determine, for instance how the initially prepared zeroth-order state $|1\rangle$ evolves in time. To this end, we calculate the probability for transitions between $|1\rangle$ and $|2\rangle$, which is defined as

$$P_{1\to2}(t) = |\langle 2|U(t)|1\rangle|^2. \tag{3.409}$$

Once this quantity is known, the survival probability is obtained as $P_{1\to1}(t) = 1 - P_{1\to2}(t)$. Using Eqs. (2.160) and (2.162), we get ($\hat{\kappa} = \mp$, if $\kappa = \pm$)

$$\langle 2|U(t)|1\rangle = \sum_{\kappa=\pm} e^{-i\mathcal{E}_\kappa t/\hbar}\langle 2|\kappa\rangle\langle\kappa|1\rangle = \sum_{\kappa=\pm} e^{-i\mathcal{E}_\kappa t/\hbar} \, C_\kappa(2) \, C_\kappa^*(1)$$

$$= \sum_{\kappa=\pm} e^{-i\mathcal{E}_\kappa t/\hbar}\left(\frac{\mathcal{E}_\kappa - \varepsilon_2}{\mathcal{E}_\kappa - \mathcal{E}_{\hat\kappa}} \, \frac{\mathcal{E}_\kappa - \varepsilon_1}{\mathcal{E}_\kappa - \mathcal{E}_{\hat\kappa}}\right)^{\frac{1}{2}} e^{i(\chi_2(\kappa)-\chi_1(\kappa))}$$

$$= e^{-i\arg(V)}\frac{|V|}{\mathcal{E}_+ - \mathcal{E}_-}\left(e^{-i\mathcal{E}_+ t/\hbar} - e^{-i\mathcal{E}_- t/\hbar}\right). \tag{3.410}$$

This gives for the transition probability

$$P_{1\to2}(t) = \frac{|V|^2}{(\hbar\Omega)^2}\left|e^{-i\mathcal{E}_- t/\hbar}\{e^{-i\Omega t} - 1\}\right|^2$$

$$= \frac{|V|^2}{(\hbar\Omega)^2}\left([\cos(\Omega t) - 1]^2 + \sin^2(\Omega t)\right), \tag{3.411}$$

where we introduced

$$\hbar\Omega = \mathcal{E}_+ - \mathcal{E}_- \equiv \sqrt{(\varepsilon_1 - \varepsilon_2)^2 + 4|V|^2}. \tag{3.412}$$
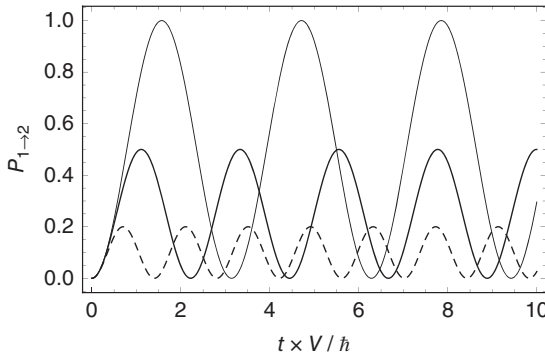
Figure 3.8 Transition amplitude $P_{1\rightarrow 2}(t)$ following from Eq. (3.414) for different (rescaled) detunings $|\varepsilon_1 - \varepsilon_2|/2|V| = 0$ (thin solid), 1 (thick solid), and 2 (dashed), plotted versus (scaled) time.

Using

$$[\cos(\Omega t) - 1]^2 + \sin^2(\Omega t) = 2\,(1 - \cos(\Omega t)) = 4\sin^2\frac{\Omega t}{2}, \qquad (3.413)$$

we finally get

$$P_{1\rightarrow 2}(t) = \frac{4|V|^2}{(\hbar\Omega)^2}\sin^2(\Omega t/2). \qquad (3.414)$$

For the case that the zeroth-order states have the same energy, this expression simplifies to

$$P_{1\rightarrow 2}(t) = \sin^2\left(|V|t/\hbar\right). \qquad (3.415)$$

The time dependence of the transition probability is shown in Figure 3.8 for different detunings, $|\varepsilon_1 - \varepsilon_2|/2|V|$, between the zeroth-order states. From (3.414), we realize that $P_{1\rightarrow 2}(t)$ will oscillate with frequency $\Omega/2$, which depends on the detuning. Given a constant coupling V, the oscillation frequency will increase with increasing detuning. At the same time, due to the prefactor in Eq. (3.414), the transfer will be less complete. A complete population switching occurs only if the two zeroth-order states are degenerate. The oscillation frequency is then $V/\hbar$, and according to Eq. (3.415), a complete transfer is realized for the condition $t = (2N + 1)\pi\hbar/2|V|$, where N is an integer.

We would like to point out that this simple result reflects the general statement made earlier, namely that time-dependent phenomena in a closed quantum system appear whenever a noneigenstate, that is a superposition of eigenstates, has been prepared initially. In the present case, the initial preparation of state $|1\rangle$ corresponds to a particular superposition of the two eigenstates $|+\rangle$ and $|-\rangle$.

3.12.2 Dissipative Dynamics Using Eigenstates

The dissipative dynamics of the two-level system will be described using the density matrix in the state representation. Here, in principle, we have two possibilities: In a situation where some zeroth-order initial state has been prepared, one is often interested in the survival amplitude related to this initial state, which is given by $\rho_{mm}(t)$ (cf. Section 3.2.1). On the other hand, one could also use the representation

in terms of the eigenstates: $\rho_{\kappa\lambda}$. It seems as if there were no difference between these two representations because we can relate them via

$$\rho_{mn}(t) = \sum_{\kappa,\lambda} C_\kappa(m)C_\lambda^*(n) \; \rho_{\kappa\lambda}(t). \tag{3.416}$$

However, we should recall that in Section 3.6 and Eq. (3.267), the equations of motion for the RDM have been derived in the *eigenstate* representation. As a consequence, all approximations (Markovian dynamics and secular approximation) make reference to the spectrum of the *full* Hamiltonian (2.147) and not only to the zeroth-order states. In what follows, we show that simulations using either eigenstates or zeroth-order states can yield different results.

Let us start by specifying the coupling of the two-level system to its environment. We assume that the latter can be described by uncoupled harmonic oscillators with coordinates $Z = \{Z_\xi\}$. To account for energy dissipation from the two-level system into the reservoir, we consider the simplest version of the coupling Hamiltonian (cf. the final part of Section 3.8.2). Using the general notation, Eq. (3.198), we take the system part to be

$$K_u = |m\rangle\langle n|. \tag{3.417}$$

The index u in Eq. (3.198) has to be identified with the pair (m, n), and the reservoir part of Eq. (3.198) is written as a linear expression in the reservoir coordinates:

$$\Phi_u \equiv \Phi_{mn} = \sum_\xi \hbar\omega_\xi g_{mn}(\xi) \; Q_\xi. \tag{3.418}$$

Here, we have introduced the dimensionless coupling constant $g_{mn}(\xi)$, which has already been used in Section 3.7.2. Concentrating on energy exchange with the environment via transitions between both the zeroth-order system states, we assume that $g_{mn}(\xi)$ has only off-diagonal elements.

The definition of the system–environment coupling in terms of the zeroth-order states will often have practical reasons. For instance, in Chapter 7, we discuss the electron transfer between a donor and an acceptor state (that is, in an electronic two-level system). Since the electronic donor and acceptor states are well defined, it may be more straightforward to model their interaction with the environment *separately*, that is without taking into account their mutual interaction.

The eigenstate representation of the system–reservoir coupling Hamiltonian $H_{\text{S--R}}$ is easily obtained. For the system part, we have

$$K_u = |\kappa\rangle\langle\lambda| \tag{3.419}$$

($u \equiv (\kappa, \lambda)$ in Eq. (3.198)). The reservoir part has diagonal and off-diagonal contributions

$$\Phi_u \equiv \Phi_{\kappa\lambda} = \sum_\xi \hbar\omega_\xi \; g_{\kappa\lambda}(\xi) \; Q_\xi \tag{3.420}$$

where the coupling matrix is now given by

$$g_{\kappa\lambda}(\xi) = \sum_{m,n} C_\kappa^*(m)g_{mn}(\xi)C_\lambda(n). \tag{3.421}$$

The density matrix equations in the eigenstate representation are directly obtained from the QME (3.344). Restricting ourselves to the secular approximation (cf. Section 3.8.3), we get for the state populations the equation of motion

$$\frac{\partial}{\partial t}\rho_{++} = -k_{+\to-}\,\rho_{++} + k_{-\to+}\,\rho_{--}. \tag{3.422}$$

Due to the secular approximation, this equation is decoupled from the equation for the coherence, which reads ($\Omega = (\mathcal{E}_+ - \mathcal{E}_-)/\hbar$):

$$\frac{\partial}{\partial t}\rho_{+-} = -i(\Omega - i\gamma)\rho_{+-}. \tag{3.423}$$

(The other two matrix elements follow from $\rho_{--} = 1 - \rho_{++}$ and $\rho_{-+} = \rho_{+-}^*$.) The transition rates can be directly adapted from Eq. (3.362). We obtain for the particular rate from state $|+\rangle$ to state $|-\rangle$ (note $\Omega > 0$),

$$k_{+\to-} = 2\pi\Omega^2[1 + n(\Omega)]J_{+-}(\Omega), \tag{3.424}$$

and for the reverse process

$$k_{-\to+} = 2\pi\Omega^2 n(\Omega)J_{+-}(\Omega). \tag{3.425}$$

The definition of the spectral density in Eq. (3.362) has been specified here to

$$J_{+-}(\omega) = \sum_{\xi}|g_{+-}|^2(\xi)\,\delta(\omega - \omega_{\xi}). \tag{3.426}$$

The dephasing rate follows from Eq. (3.353) as

$$\gamma = \frac{1}{2}(k_{+\to-} + k_{-\to+}) + \gamma^{(\mathrm{pd})}. \tag{3.427}$$

In the low-temperature limit, $k_{\mathrm{B}}T \ll \hbar\Omega$, we can neglect $n(\Omega)$, and the rate for upward transitions $k_{-\to+}$ vanishes.

The solutions for the equations of motion, (3.422) and (3.423), can be given right away. Considering the low-temperature limit for simplicity, we obtain

$$\rho_{++}(t) = \rho_{++}(0)\,e^{-k_{+\to-}t} \tag{3.428}$$

and

$$\rho_{+-}(t) = \rho_{+-}(0)\,e^{-i(\Omega - i\gamma)t}. \tag{3.429}$$

Thus, nonequilibrium populations of the eigenstates decay exponentially, while the coherences will oscillate with the transition frequency Ω. The amplitude of this oscillation will decrease exponentially, too; that is, any initial coherence between the two eigenstates is destroyed.

This time dependence can be easily translated into the picture of the zeroth-order states using Eq. (3.416). For illustration, let us consider the case of an initially prepared zeroth-order state, that is $\rho_{mn}(t = 0) = \delta_{mn}\delta_{m1}$. Since the transformation (3.416) couples populations and coherences in the different representations, the respective initial density matrix in the eigenstate representation will have nonzero diagonal and off-diagonal elements. In Figure 3.9, we show the subsequent time evolution of the density matrix in both representations. Notice that the dynamics of the zeroth-order state population reflects the oscillatory behavior obtained for the
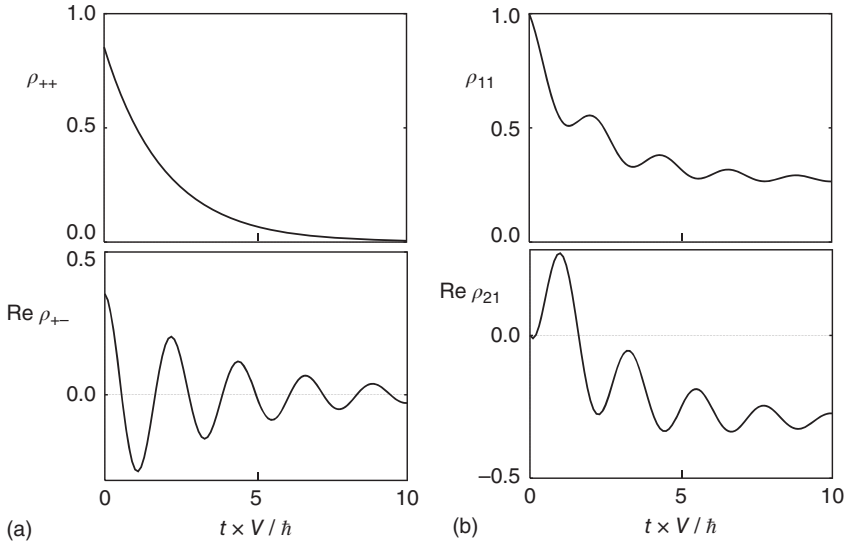
Figure 3.9 Dissipative dynamics in a coupled two-level system as obtained from the eigenstate representation (a) and the zeroth-order state representation (b). The parameters are: detuning, $|\varepsilon_1 - \varepsilon_2|/2|V| = 1$; relaxation rate, $k_{+\to-} = 0.5|V|/\hbar$; and initial state, $|1\rangle$ (figure courtesy of H. Naundorf).

coherent regime in Figure 3.8. Further, the off-diagonal elements ρ_{12} do not vanish at long times. This reflects the fact that the eigenstate $|-\rangle$, which is populated in the stationary limit, is a superposition state with respect to the zeroth-order states $|1\rangle$ and $|2\rangle$ (cf. Eq. (2.150)).

Figure 3.10 compares the perturbative and Markovian QME dynamics with numerical exact hierarchy equation of motion results for the Debye spectral density, Eq. (3.302). In panels (a,c), $\omega_D = 8\Omega$ such that in the weak coupling limit (a) the correlation time exceeds the relaxation time and the system is in the Markovian regime, that is both curves agree approximately. Increasing the system–reservoir coupling strength (panel (c)) yields a faster relaxation, and hence, the Markov approximation breaks down. In addition, higher order effects contribute to the difference between QME and exact results. In panels (b,d), $\omega_D = 0.4\Omega$, that is even in the weak coupling case (panel (b)), non-Markovian effects play a role. Once additional higher order contributions come into play (panel (d)), QME and exact results differ markedly. As a note in caution, we emphasize that despite the failure of the QME, the population dynamics does not look suspicious.

3.12.3 Dissipative Dynamics Using Zeroth-order States

Let us compare the eigenstate formulation of the QME with its zeroth-order version. In this case, the equations of motion read

$$\frac{\partial}{\partial t}\rho_{11} = \frac{2}{\hbar}\text{Im}(V\rho_{21}) - k_{1\to2}\rho_{11} + k_{2\to1}\rho_{22} \tag{3.430}$$
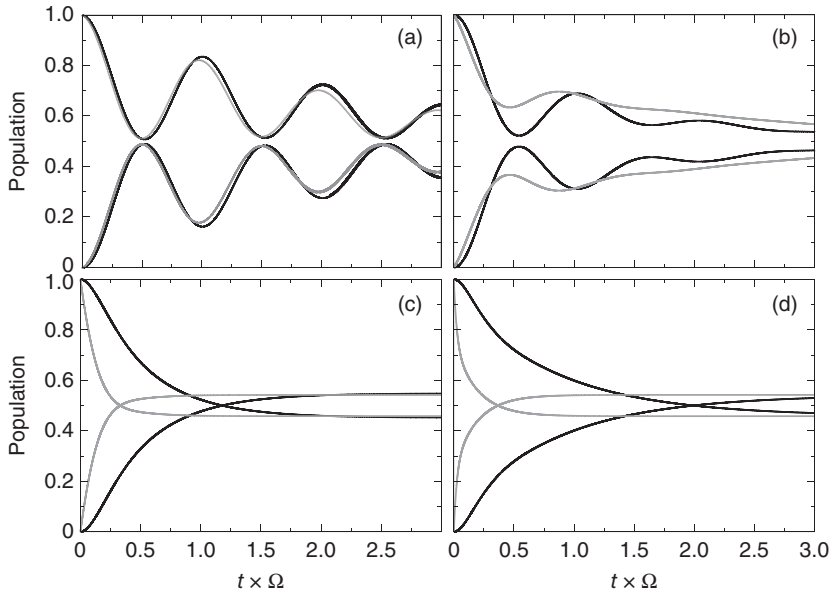
Figure 3.10 Dissipative dynamics in a coupled two-level system as obtained from the hierarchy equations of motion (black) and Redfield (gray) approach. The detuning has been set to $|\varepsilon_1 - \varepsilon_2|/2|V| = 1$ such that $\Omega = 50$ cm^{-1} (cf. Eq. (3.412)). For the system–reservoir coupling, a Debye spectral density, Eq. (3.302), has been chosen. In panels (a,c) $\omega_D = 400$ cm^{-1}, whereas in panels (b,d) $\omega_D = 20$ cm^{-1}. The coupling strength j_0 has been adjusted such as to have $C(\Omega) = 2.3$ and 36.9 in panels (a,b) and (c,d), respectively (figure courtesy of J. Seibt).

and (note $\hbar\omega_{21} = \varepsilon_2 - \varepsilon_1$)

$$\frac{\partial}{\partial t}\rho_{21} = -i[\omega_{21} - i(\gamma_2 + \gamma_1)]\,\rho_{21} - \frac{i}{\hbar}V\,(\rho_{11} - \rho_{22}). \qquad (3.431)$$

Suppose that we consider a problem that involves many zeroth-order states such that the diagonalization of the Hamiltonian may be rather time consuming. In this case, it would be tempting to formulate the rates in the zeroth-order states only, that is

$$k_{m\to n} = 2\pi\omega_{mn}^2[1 + n(\omega_{mn})]\left(J_{mn}(\omega_{mn}) - J_{mn}(-\omega_{mn})\right), \qquad (3.432)$$

with the spectral density now given by

$$J_{mn}(\omega) = \sum_{\xi} g_{mn}^2(\xi)\,\delta(\omega - \omega_\xi). \qquad (3.433)$$

At first glance, there appears to be nothing wrong with this expression. However, writing down the detailed balance condition, which follows from Eq. (3.432) (cf. Eq. (3.351)),

$$k_{2\to 1} = e^{\hbar\omega_{21}/k_B T}k_{1\to 2}, \qquad (3.434)$$

we realize that this will guide the system to an equilibrium distribution with respect to the *zeroth-order* states; that is, the coupling V is not accounted for. In order to understand the reason for this behavior, we have to go back to Section 3.6.1.

There, we had introduced the operators Λ_u in Eq. (3.264), which contain the information about the system–reservoir interaction. In particular, they include the operators K_u defined in the interaction representation with respect to H_S. Let us inspect the matrix elements of the operator Λ_u with respect to the zeroth-order basis ($u \equiv (mn)$),

$$\langle \overline{m}|\Lambda_{mn}|\overline{n}\rangle = \sum_{k,l} \int\limits_0^\infty d\tau \, C_{mn,kl}(\tau) \langle \overline{m}|K_{kl}^{(\mathrm{I})}(-\tau)|\overline{n}\rangle. \tag{3.435}$$

Strictly speaking, the calculation of $\langle \overline{m}|K_{kl}^{(\mathrm{I})}(-\tau)|\overline{n}\rangle$ would require to use the eigenstates. This would result in the expression

$$\langle \overline{m}|K_{kl}^{(\mathrm{I})}(-\tau)|\overline{n}\rangle = \sum_{\kappa,\lambda} e^{-i(\mathcal{E}_\kappa - \mathcal{E}_\lambda)\tau/\hbar} \, C_\kappa(\overline{m})C_\kappa^*(k)C_\lambda(l)C_\lambda^*(\overline{n}). \tag{3.436}$$

Inserting this into Eq (3.435) gives

$$\langle \overline{m}|\Lambda_{mn}|\overline{n}\rangle = \sum_{k,l}\sum_{\kappa,\lambda} C_\kappa(\overline{m})C_\kappa^*(k)C_\lambda(l)C_\lambda^*(\overline{n}) \int\limits_0^\infty d\tau \, e^{-i(\mathcal{E}_\kappa - \mathcal{E}_\lambda)\tau/\hbar} C_{mn,kl}(\tau). \tag{3.437}$$

On the other hand, neglecting the coupling V in Eq. (3.436), one gets

$$\langle \overline{m}|K_{kl}^{(\mathrm{I})}(-\tau)|\overline{n}\rangle = \delta_{\overline{m}k}\delta_{l\overline{n}} e^{-i\omega_{kl}\tau}. \tag{3.438}$$

Whether the half-sided Fourier transform of the correlation function $C_{mn,cd}(t)$ is taken with respect to $(\mathcal{E}_\kappa - \mathcal{E}_\lambda)/\hbar$ or ω_{kl} determines the frequency argument in the Bose–Einstein distribution function. This in turn fixes the detailed balance condition to the respective spectrum.

Finally, we point out that the quality of the approximation that neglects the detailed structure of the spectrum and only takes into account some zeroth-order states depends, of course, on the strength of the coupling. Moreover, if one is only interested in the short-time behavior and not in the stationary solutions of the equations of motion, a formulation of the relaxation rates in terms of zeroth-order states may be acceptable. We return to this point in the context of electron (Section 7.9) and exciton (Section 9.6) transfer.

3.13 Trajectory-based Methods

3.13.1 The Mean-field Approach

The theoretical description of condensed-phase dynamics given so far has been focused on situations where the reservoir DOFs can be modeled by a collection of harmonic oscillators. Of course, in many cases, for example in a liquid environment, this will be an oversimplification. Here, one can often resort to a description of the reservoir (the solvent) in terms of classical mechanics. For the solute, however, quantum effects may be important, and a quantum approach is necessary. In what

follows, we introduce some basic concepts behind such a *quantum-classical hybrid* description, often also called *mixed quantum classical* approach.

In a first step, let us consider an approach based on the time-dependent Schrödinger equation. We start with the Hamiltonian (3.186). The quantum coordinates will be labeled by s, and the classical reservoir coordinates and momenta are denoted $Z = \{Z_\xi\}$ and $P = \{P_\xi\}$, respectively. As before, we assume that $H_{\text{S-R}} = H_{\text{S-R}}(s, Z)$, where s is the coordinate (set of coordinates) of the relevant quantum system. $H_{\text{S-R}}$ can be considered as an external potential acting on the relevant quantum system, and the Schrödinger equation for the quantum system reads

$$i\hbar \frac{\partial}{\partial t} \Psi(s, t) = \left(H_{\text{S}} + H_{\text{S-R}}(s, Z(t)) \right) \Psi(s, t). \tag{3.439}$$

It describes the quantum part of the coupled quantum mechanical and classical dynamics of the full system. $H_{\text{S-R}}(s, Z(t))$ is now time dependent, where the time dependence is induced by the classical reservoir coordinates.

Let us take now the perspective of the classical reservoir. If the coupling among both subsystems vanishes; that is, if we have $H_{\text{S-R}} = 0$, the reservoir coordinates Z_ξ and momenta P_ξ satisfy the canonical equations of motion

$$\frac{\partial Z_\xi}{\partial t} = \frac{\partial H_{\text{R}}}{\partial P_\xi} \,, \qquad \frac{\partial P_\xi}{\partial t} = -\frac{\partial H_{\text{R}}}{\partial Z_\xi}. \tag{3.440}$$

If the coupling is taken into account, we would expect to have an additional potential on the right-hand side of Eq. (3.440). In order to link classical and quantum mechanics, this potential is taken as the quantum mechanical expectation value of the system–reservoir coupling according to the instantaneous values of the classical coordinates and the wave function of the quantum DOFs

$$\langle H_{\text{S-R}}(Z, t) \rangle_{\text{S}} = \int ds \, \Psi^*(s, t) H_{\text{S-R}}(s, Z) \Psi(s, t). \tag{3.441}$$

The canonical equations are then given by Eq. (3.440), where H_{R} has to be replaced by $H_{\text{R}} + \langle H_{\text{S-R}}(Z, t) \rangle_{\text{S}}$. This leads to an additional force,

$$F_\xi(t) = -\frac{\partial}{\partial Z_\xi} \int ds \, \Psi^*(s, t) \, H_{\text{S-R}}(s, Z) \, \Psi(s, t), \tag{3.442}$$

on the classical coordinates Z.

The coupled equations of motion (3.439) and (3.440) are solved simultaneously by imposing appropriate initial conditions such as

$$\Psi(s, t = 0) = \Psi_0(s) \,,$$
$$Z_\xi(t = 0) = Z_\xi^{(0)} \,, \qquad P_\xi(t = 0) = P_\xi^{(0)}. \tag{3.443}$$

The set of Eqs. (3.439) and (3.440) (extended by the system–reservoir coupling) determines the quantum dynamics of the relevant quantum system coupled to the reservoir, which is described by classical mechanics. While the presence of the classical DOFs is an additional potential for the motion of the quantum system, the classical reservoir feels the quantum mechanically averaged force of the relevant

quantum system. This method is named after P. Ehrenfest and represents just another example for a *mean-field* approach.

Within this description it is possible to determine how the small quantum system is influenced by the macroscopic reservoir. In many applications the reservoir is in thermal equilibrium characterized by a temperature T. Then, the quantum system is influenced by external forces that change with time due to the sampling of the thermal equilibrium state of the reservoir. We also note that besides the action of the reservoir on the system dynamics, it is also possible that the system dynamics drives the reservoir out of the equilibrium. In this case, a nonequilibrium state of the reservoir influences the system dynamics. This can also be viewed as a backreaction of the system dynamics on itself by means of the nonequilibrium state of the reservoir. Such a behavior may be observed for strong system–reservoir couplings. In the case of a sufficiently weak coupling, it is appropriate to study the system dynamics under the influence of a reservoir staying in thermal equilibrium.

To describe the coupling between the thermal reservoir and the quantum system within the hybrid approach, classical molecular dynamics simulations for the reservoir have to be performed. Although the concept of a thermal reservoir is not applied directly, a temperature can be introduced by choosing the initial conditions for the reservoir according to a thermal distribution. To this end, we introduce a set of different initial conditions $(Z^{(0,i)}, P^{(0,i)})$ with $i = 1 \, \ldots \, N$ for which the coupled equations (3.439) and (3.440) have to be solved. The initial conditions are taken from the related thermal distribution; that is, they have to fulfill

$$f(Z^{(0,i)}, P^{(0,i)}) = \frac{1}{\mathcal{Z}_{\mathrm{R}}} e^{-H_{\mathrm{R}}(Z^{(0,i)}, P^{(0,i)})/k_{\mathrm{B}}T}, \tag{3.444}$$

where $\mathcal{Z}_{\mathrm{R}}$ is the reservoir partition function. The solutions of the time-dependent Schrödinger equation can then be labeled by the specific initial condition,

$$\Psi_i(s, t) = \Psi(s, t; Z^{(0,i)}, P^{(0,i)}). \tag{3.445}$$

Calculating the expectation value of a system operator $\hat{O}$, we have to introduce an additional averaging with respect to the distribution of the initial values of the reservoir coordinates

$$\langle\langle \hat{O} \rangle_{\mathrm{S}} \rangle_{\mathrm{R}} = \sum_{i=1}^{N} f(Z^{(0,i)}, P^{(0,i)}) \int ds \, \Psi_i^*(s, t) \, \hat{O} \, \Psi_i(s, t). \tag{3.446}$$

The performance of a numerical implementation of this approach depends on the proper choice of representative initial values $(Z^{(0,i)}, P^{(0,i)})$ such that N does not become too large. Here, the thermal distribution function can be used, as it gives a weight to the different $(Z^{(0,i)}, P^{(0,i)})$.

There are some characteristics of the hybrid approach that we would like to point out: First, the dynamics is obtained starting with a specific initial state of the reservoir; that is, no thermal averaged equation of motion is introduced. Any averaging with respect to the reservoir can be carried out after solving the coupled equations of motion (see Eq. (3.446)). Second, the approach does not contain any approximation with respect to the coupling between S and R, and any type of complex reservoir dynamics can be introduced. Third, it is necessary to note that

the simulation of a thermal reservoir acting on a quantum system assumes that there are no *initial correlations* between the system and the reservoir. Any coupling between S and R in the initial state of the correlated dynamics has been removed by choosing the initial reservoir state from a distribution defined by the reservoir Hamiltonian function $H_R(P, Z)$ alone. Finally, a clear disadvantage of the described method is the fact that the reservoir coordinates move only under the influence of the quantum mechanically averaged system–reservoir coupling. This is very different from the quantum dynamics where the reservoir wave function would "feel" a concrete system–reservoir coupling Hamiltonian (as it is the case for a dependence on the electronic states of the system). The method outlined in the following section is designed such as to compensate for this disadvantage.

3.13.2 The Surface Hopping Method

In the previous section, we did not elaborate on the solution of the time-dependent Schrödinger equation (3.439), which has to be determined simultaneously with the classical propagation of the coordinates Z. For condensed-phase systems, this is a tremendous task. Therefore, most applications focus on the special case of a light particle (electron and proton) in a heavy atom environment. To solve Eq. (3.439), one can define *adiabatic* basis functions in the spirit of the Born–Oppenheimer ansatz (introduced in Section 2.3 to solve the electron–nuclear Schrödinger equation). These basis functions follow as solutions of the stationary Schrödinger equation

$$\left(H_S(s) + H_{S-R}(s, Z)\right) \phi_a(s; Z) = E_a(Z)\phi_a(s; Z). \tag{3.447}$$

This includes the influence of the classical coordinates via H_{S-R}. In analogy to Eq. (2.12), the eigenstates as well as the eigenvalues of Eq. (3.447) depend parametrically on the reservoir coordinates Z. The solution of the time-dependent Schrödinger equation (3.439) can then be obtained by expanding $\Psi(s, t)$ with respect to $\phi_a(s, Z)$:

$$\Psi(s, t) = \sum_a c_a(t)\phi_a(s, Z). \tag{3.448}$$

Inserting the expansion into Eq. (3.439), one may derive an equation of motion for the $c_a(t)$. However, we have to be aware that the basis functions become time dependent according to the time dependence of the reservoir coordinates. It follows that

$$i\hbar \frac{\partial}{\partial t} c_a(t) = E_a\left(Z(t)\right) c_a(t) - i\hbar \sum_b \langle \phi_a\left(Z(t)\right) | \frac{\partial}{\partial t} |\phi_b\left(Z(t)\right)\rangle c_b(t). \tag{3.449}$$

The matrix elements that couple different adiabatic basis states read

$$\langle \phi_a\left(Z(t)\right) | \frac{\partial}{\partial t} |\phi_b\left(Z(t)\right)\rangle = \int ds\, \phi_a^*(s, Z(t)) \frac{\partial}{\partial t} \phi_b(s, Z(t))$$

$$= \sum_\xi \langle \phi_a\left(Z(t)\right) | \frac{\partial}{\partial Z_\xi} |\phi_b\left(Z(t)\right)\rangle \frac{\partial Z_\xi}{\partial t}. \tag{3.450}$$

This coupling is a consequence of the fact that the reservoir coordinates Z change with time so that there will be an overlap between state ϕ_a and the time derivative of state ϕ_b. Consequently, the coupling is of the *nonadiabatic* type. Notice that

according to the correspondence principle, we have $-i\hbar\partial Z_\xi/\partial t \rightarrow \hbar^2/M_\xi^2\nabla_\xi$. Thus, the type of coupling between different adiabatic states in Eq. (3.450) corresponds to the second contribution to the nonadiabaticity operator in Eq. (2.17). The first terms in Eq. (2.17), that is the matrix elements of the kinetic energy operator, do not appear.

If one computes the expectation value, Eq. (3.441),

$$\langle H_{\text{S-R}}(Z,t)\rangle_{\text{S}} = \sum_{a,b} c_a^*(t)c_b(t) \int ds \, \phi_a^*(s,Z(t))H_{\text{S-R}}(s,Z(t))\phi_b(s,Z(t)), \quad (3.451)$$

it appears to be a sum of diagonal as well as off-diagonal contributions with respect to the basis states. Thus, in principle, Eq. (3.451) contains the information on the forces, which are specific for a given adiabatic state of the quantum system. Moreover, there is a contribution from nonadiabatic transitions between these states. However, this information has to be disentangled in order to go beyond the mean-field treatment of the previous section. A recipe for turning this concept into a practical scheme is the surface hopping approach, which is sketched in what follows.

Let us assume that there is some initial set of classical reservoir coordinates $Z^{(0)}$ for which the Schrödinger equation (3.448) has been solved. Suppose that the quantum system is initially in the state $\phi_i(s,Z^{(0)})$ such that $c_a(0) = \delta_{ai}$ in Eq. (3.449). Thus, only the initial state contributes the expectation value $\langle\phi_i|H_{\text{S-R}}|\phi_i\rangle$ to Eq. (3.451). The forces (3.442) are calculated, and the classical DOFs are propagated for one time step Δt. For the new configuration, Eq. (3.447) is solved, and the new expansion coefficients are obtained from Eq. (3.449). Due to the nonadiabatic couplings entering Eq. (3.449), other states $|\phi_{a\neq i}\rangle$ may become populated at time Δt.

The information about these population changes can now be used to decide whether the adiabatic state for calculating the expectation value of $H_{\text{S-R}}$, that is the forces in Eq. (3.442), is switched during the propagation of the classical trajectory.

Let us consider two adiabatic states for simplicity. Suppose that we have calculated the coefficients as $|c_i(t+\Delta t)|^2 < |c_i(t)|^2$ and $|c_a(t+\Delta t)|^2 > |c_a(t)|^2$; that is, a transition from $|\phi_i\rangle$ to $|\phi_a\rangle$ occurred. The quantum mechanical probability $p_{i\rightarrow a}(t, t+\Delta t)$ for switching from $|\phi_i\rangle$ to $|\phi_a\rangle$ within the time step Δt is therefore equal to

$$p_{i\rightarrow a}(t, t+\Delta t) = \frac{|c_i(t)|^2 - |c_i(t+\Delta t)|^2}{|c_i(t)|^2}. \quad (3.452)$$

Whether the potential for the actual trajectory is really changed is decided by drawing a random number δ in between 0 and 1; if $p_{i\rightarrow a}(t, t+\Delta t) < \delta$, the potential for the trajectory is changed; otherwise, it stays the same during the next propagation step. If the state is changed, the trajectory is interrupted and continues to move according to the potential $\langle\phi_a|H_{\text{S-R}}|\phi_a\rangle$. Energy conservation is introduced by rescaling the momenta P_ξ such as to accommodate the change in potential energy. This procedure is repeated for every time step, and it introduces a discontinuous classical dynamics, which mimics the population changes of the quantum states. Notice, however, that these interruptions are influencing the time evolution of the expansion coefficients as well since Eq. (3.449) also depends on $Z(t)$. Moreover, it should be clear that along a trajectory many jumps between different quantum states are possible, which introduces some averaging with respect to the random choice of
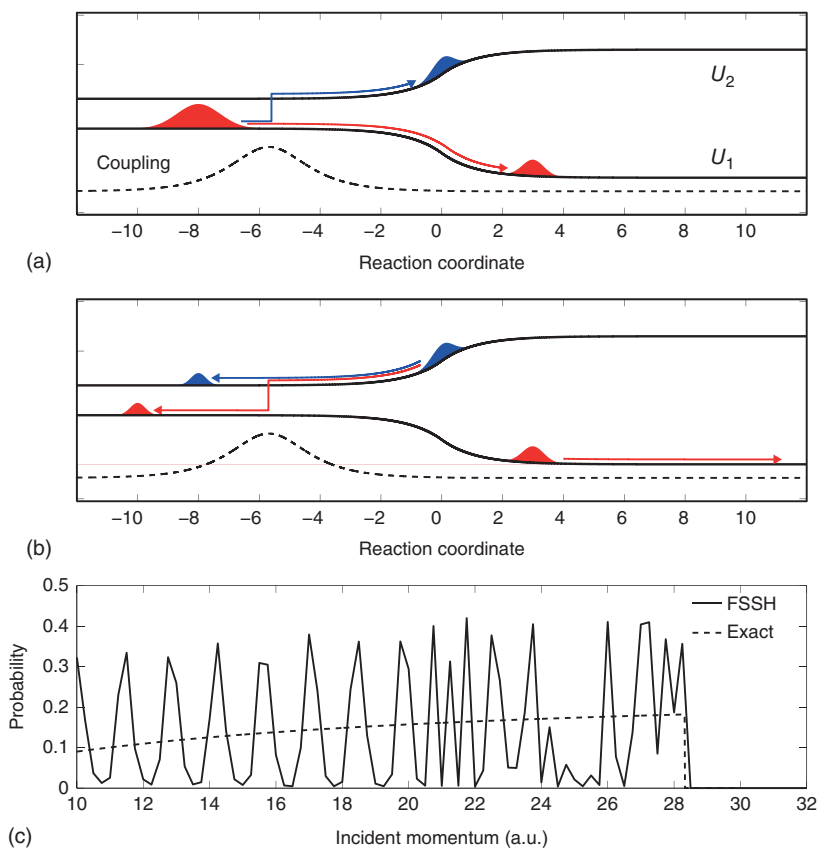
Figure 3.11 Surface hopping (FSSH) versus exact description of wave packet reflection at two coupled adiabatic PES. (a) Wave packet entering the coupling region on the lower adiabatic PES leading to a bifurcation. (b) Reflection of the wave packet on the upper PES. (c) Probability of reflection on the lower PES as a function of the incoming momentum (exact [dashed line] and FSSH [solid line]) (figure courtesy of J. E. Subotnik; for more information, see also Subotnik et al. [6]).

the parameter δ at every time step. Finally, the whole procedure has to be repeated for an ensemble of classical trajectories starting from different initial conditions.

Since the method introduces jumps from one potential $\langle \phi_a | H_{S-R} | \phi_a \rangle$ to another potential (PES) $\langle \phi_b | H_{S-R} | \phi_b \rangle$, it is frequently called *surface hopping method*.[32] It is important to emphasize that the quantum jumps are introduced in an *ad hoc* fashion; that is, the method has no strict theoretical foundation. There are numerous studies of the performance of surface hopping that enable one to appreciate its advantages and shortcomings (cf. Figure 3.11). A particular challenge is provided by the so-called overcoherence error. In condensed-phase dynamics, according to Eq. (3.15), decoherence between two system states emerges from the decay of

---

32) Note that the procedure has been suggested in Tully [7]. The prescription for state changes yields the minimum number of hops and, therefore, is also called *fewest switches surface hopping* (FSSH).

the overlap between the reservoir wave functions. In surface hopping, the reservoir is described by classical point particles. Their trajectories are independent of each other, and the Schrödinger equation (3.449) is propagated fully coherent along each individual trajectory. This causes spurious effects such as the oscillations as seen in Figure 3.11c. Various schemes for introducing decoherence have been developed, see suggested reading.

3.14 Generalized Rate Equations: The Liouville Space Approach

In Sections 3.6 and 3.8, we have focused on a second-order perturbational treatment of the system–reservoir coupling. This approach is particularly useful if it can be combined with a normal-mode description of the reservoir. Of course, second-order perturbation theory may not always be appropriate, even if we did our best to separate the total system into active and spectator DOFs. Including higher order perturbation terms is, of course, a way for improvement, but the resulting expressions become very soon rather cumbersome. In Sections 3.10–3.13, we introduced approaches that may overcome the second-order treatment of the system–reservoir coupling, either within a full quantum description or using a quantum–classical approach. The present section is devoted to a derivation of generalized rate equations that are also going beyond a perturbational treatment of the system–reservoir coupling.

The approach focuses on the derivation of generalized rate equations (or GMEs) for the populations $P_a(t)$ of the system eigenstates (an elementary version of what will follow here we already encountered in Section 3.4.5). Once such equations have been established, one can easily extract the transition rates that are valid in any order of perturbation theory. To this end, we use the projection operator technique. Since the projection operator $\mathcal{P}$ is a superoperator acting in the Liouville space formed by the usual operators, we refer to the following treatment as the *Liouville space approach*. But before introducing the projection operator $\mathcal{P}$, we separate the total Hamiltonian, Eq. (3.3), into a zeroth-order and coupling term. This separation starts from the expansion of H_{S-R} with respect to the system eigenstates (cf. Section 3.8.4.1). Here, we assume that the diagonal elements of $\Phi_{ab} = \langle a|H_{S-R}|b\rangle$ are much larger than the off-diagonal ones. Therefore, a different treatment of the two types of couplings is reasonable. In particular, a perturbational description of the off-diagonal elements might be possible. But the diagonal elements should be so large that they cannot be handled in a perturbation theory. (Such a situation, for example is typical for nonadiabatic electron transfer and will be discussed in greater detail in Sections 7.4, 7.5, and 7.6.)

We write the system–reservoir Hamiltonian as follows:

$$H = H_0 + \hat{V}, \tag{3.453}$$

where the "zeroth-order" part is given by

$$H_0 = H_S + \sum_a \Phi_{aa}(Z)|a\rangle\langle a| + H_R \equiv \sum_a \left(E_a + H_R + \Phi_{aa}(Z)\right)|a\rangle\langle a|. \tag{3.454}$$

The second part suggests that we can introduce the vibrational Hamiltonian

$$H_a = E_a + H_R + \Phi_{aa}(Z),\tag{3.455}$$

which describes the reservoir coordinate motion when the system is in its eigenstate $|a\rangle$. The perturbation $\hat{V}$ accounts for the off-diagonal elements of $\Phi_{ab}(Z)$ and reads

$$\hat{V} = \sum_{a,b} (1 - \delta_{ab})\Phi_{ab}(Z)|a\rangle\langle b|.\tag{3.456}$$

Once the diagonal matrix elements Φ_{aa} can be accounted for exactly, a nonperturbative description of the system–reservoir coupling has been achieved.

3.14.1 Projection Operator Technique

In order to establish a nonperturbative description of the system–reservoir coupling, let us introduce an appropriate projection operator. Since a simultaneous description of various states $|a\rangle$ is necessary, we generalize the projection operator $\mathcal{P}$ introduced in Section 3.5.5. If the latter acts on an arbitrary operator $\hat{O}$, it reads

$$\mathcal{P}\hat{O} = \hat{R}_{eq}\mathrm{tr}_R\{\hat{O}\} \equiv \hat{R}_{eq}\sum_{a,b}\mathrm{tr}_R\{\langle a|\hat{O}|b\rangle\}|a\rangle\langle b|.\tag{3.457}$$

This projector is constructed in such a way as to introduce a common equilibrium state of the reservoir modes represented by $\hat{R}_{eq}$. In contrast, the new projection operator takes the form

$$\tilde{\mathcal{P}}\hat{O} = \sum_a \hat{R}_a\ \mathrm{tr}_R\{\langle a|\hat{O}|a\rangle\}|a\rangle\langle a|.\tag{3.458}$$

Instead of including the full state space related to the system Hamiltonian as it would be the case for the projection operator $\mathcal{P}$, the new quantity $\tilde{\mathcal{P}}$ projects on the diagonal system states matrix element. And every system state is characterized by a separate reservoir equilibrium statistical operator

$$\hat{R}_a = \frac{\exp(-H_a/k_B T)}{\mathrm{tr}_R\{\exp(-H_a/k_B T)\}}.\tag{3.459}$$

The introduction of the vibrational Hamiltonians H_a, Eq. (3.455), consequently results in such equilibrium statistical operators. For further use, we introduce the projector $\hat{\Pi}_a = |a\rangle\langle a|$ and the combined system–reservoir equilibrium statistical operator

$$\hat{W}_a = \hat{R}_a\hat{\Pi}_a.\tag{3.460}$$

If $\tilde{\mathcal{P}}$ acts on the complete statistical operator, we obtain

$$\tilde{\mathcal{P}}\hat{W}(t) = \sum_a P_a(t)\hat{W}_a.\tag{3.461}$$

The expression indicates a specification to the various reservoir equilibrium states (with statistical operators $\hat{R}_a$) controlled by the actual population of the respective system states. The state populations are extracted if we take the diagonal system state matrix element and the trace with respect to the reservoir state space

$$P_a(t) = \mathrm{tr}_R\{\langle a|\tilde{\mathcal{P}}\hat{W}(t)|a\rangle\}.\tag{3.462}$$

3.14.2 Generalized Rate Equations

We start with the Liouville–von Neumann equation[33]

$$\frac{\partial}{\partial t}\hat{W}(t) = -i\mathcal{L}\hat{W}(t), \tag{3.463}$$

where $\mathcal{L}\dots = [H,\dots]_-/\hbar$. Introducing the orthogonal complement, $\tilde{\mathcal{Q}} = 1 - \tilde{\mathcal{P}}$, a separation into two orthogonal parts yields

$$\frac{\partial}{\partial t}\tilde{\mathcal{P}}\hat{W}(t) = -i\tilde{\mathcal{P}}\mathcal{L}\left(\tilde{\mathcal{P}}\hat{W}(t) + \tilde{\mathcal{Q}}\hat{W}(t)\right) \tag{3.464}$$

and

$$\frac{\partial}{\partial t}\tilde{\mathcal{Q}}\hat{W}(t) = -i\tilde{\mathcal{Q}}\mathcal{L}\left(\tilde{\mathcal{P}}\hat{W}(t) + \tilde{\mathcal{Q}}\hat{W}(t)\right). \tag{3.465}$$

The solution of the equation for $\tilde{\mathcal{Q}}\hat{W}$, including the assumption $\tilde{\mathcal{Q}}\hat{W}(t_0) = 0$, can be written as follows:

$$\tilde{\mathcal{Q}}\hat{W}(t) = -i\int_{t_0}^{t} d\bar{t}\ \mathcal{U}_{\tilde{\mathcal{Q}}}(t-\bar{t})\tilde{\mathcal{Q}}\mathcal{L}\tilde{\mathcal{P}}\hat{W}(\bar{t}), \tag{3.466}$$

where the time-propagation superoperator,

$$\mathcal{U}_{\tilde{\mathcal{Q}}}(t) = \exp\left\{-i\tilde{\mathcal{Q}}\mathcal{L}t\right\}, \tag{3.467}$$

has been introduced. The resulting equation for $\tilde{\mathcal{P}}\hat{W}$ (the Nakjima–Zwanzig equation, Eq. (3.232)) is a closed equation with respect to $\tilde{\mathcal{P}}\hat{W}$ and reads

$$\frac{\partial}{\partial t}\tilde{\mathcal{P}}\hat{W}(t) = -i\tilde{\mathcal{P}}\mathcal{L}\tilde{\mathcal{P}}\hat{W}(t) - \int_{t_0}^{t} d\bar{t}\ \tilde{\mathcal{P}}\mathcal{L}\ \mathcal{U}_{\tilde{\mathcal{Q}}}(t-\bar{t})\tilde{\mathcal{Q}}\mathcal{L}\ \tilde{\mathcal{P}}\hat{W}(\bar{t}). \tag{3.468}$$

Using Eq. (3.462), it is possible to derive the related equations of motion for the state populations. In order to do this, we consider the general expressions

$$\text{tr}_{\text{R}}\left\{\langle a|\tilde{\mathcal{P}}\mathcal{L}\hat{O}|a\rangle\right\} \equiv \text{tr}_{\text{R}}\left\{\langle a|\mathcal{L}\hat{O}|a\rangle\right\}. \tag{3.469}$$

$\hat{O}$ may take the form

$$\hat{O}_1 = \tilde{\mathcal{P}}\hat{W}(t) \tag{3.470}$$

as well as

$$\hat{O}_2 = \mathcal{U}_{\tilde{\mathcal{Q}}}(t-\bar{t})\tilde{\mathcal{Q}}\mathcal{L}\tilde{\mathcal{P}}\hat{W}(\bar{t}). \tag{3.471}$$

If we insert $\hat{O}_1$ into Eq. (3.469), we easily verify that the resulting expression vanishes. The term with $\hat{O}_2$ suggests the definition of the so-called memory kernels K_{ab} of the related GME. First, we get

$$\text{tr}_{\text{R}}\left\{\langle a|\mathcal{L}\hat{O}_2|a\rangle\right\} = \sum_b \text{tr}_{\text{R}}\left\{\langle a|\left(\mathcal{L}\mathcal{U}_{\tilde{\mathcal{Q}}}(t-\bar{t})\tilde{\mathcal{Q}}\mathcal{L}\hat{W}_b\right)|a\rangle\right\}P_b(\bar{t}). \tag{3.472}$$

---

33) In what follows, we do not change to the interaction representation as it had been done, for example in Section 3.5.6. Instead, we stay in the Schrödinger representation, which has the technical advantage that we can avoid the introduction of a time-ordered S-superoperator (compare Eq. (3.231)). However, the basic idea to arrive at a closed equation for $\tilde{\mathcal{P}}\hat{W}$ is the same.

To arrive at the memory kernel, we multiply the trace expression by -1 and the unit-step function $\theta(t - \bar{t})$ and obtain

$$K_{ab}(t - \bar{t}) = -\theta(t - \bar{t})\, \mathrm{tr}_{\mathrm{R}} \left\{ \langle a| \left(\mathcal{L}\mathcal{U}_{\tilde{Q}}(t - \bar{t})\tilde{Q}\mathcal{L}\hat{W}_b \right) |a\rangle \right\}. \tag{3.473}$$

To set up the GME, we change to $\tau = t - \bar{t}$ and obtain from Eq. (3.468) the following compact relation:

$$\frac{\partial}{\partial t}P_a(t) = \sum_b \int_{-\infty}^{t-t_0} d\tau \; K_{ab}(\tau)P_b(t - \tau). \tag{3.474}$$

The time t_0 can be moved to $-\infty$ if we directly account for the initial time in the definition of the populations ($P_a \sim \theta(t - t_0)$).

A closer inspection of the memory kernels leads to some simplifications. First, we note that the introduction of the projector $\hat{\Pi}_a$ allows to replace the trace with respect to the reservoir states by a complete trace. Moreover, we introduce the Green's super-operator

$$\mathcal{G}_{\tilde{Q}}(\tau) = -i\theta(\tau)\mathcal{U}_{\tilde{Q}}(\tau) \tag{3.475}$$

and may write

$$K_{ab}(\tau) = -i\mathrm{tr}\{\hat{\Pi}_a\mathcal{L}\mathcal{G}_{\tilde{Q}}(\tau)\tilde{Q}\mathcal{L}\hat{W}_b\}. \tag{3.476}$$

For a further simplification, we separate $\mathcal{L}$ into the zeroth-order part $\mathcal{L}_0 \ldots = [H_0, \ldots]_-/\hbar$ as well as into the coupling $\mathcal{L}_V \ldots = [\hat{V}, \ldots]_-/\hbar$ and arrive at

$$\tilde{P}\mathcal{L}_0 = \mathcal{L}_0\tilde{P} = 0. \tag{3.477}$$

These relations are easily verified when being applied to an arbitrary operator $\hat{O}$. In the same way, we may deduce

$$\tilde{P}\mathcal{L}_V\tilde{P} = 0. \tag{3.478}$$

Using these identities and replacing $\hat{\Pi}_a\mathcal{L}$ in Eq. (3.476) again by $\hat{\Pi}_a\tilde{P}\mathcal{L}$, we have $\tilde{P}\mathcal{L}\mathcal{G}_{\tilde{Q}}(t) = \tilde{P}\mathcal{L}_V\mathcal{G}_{\tilde{Q}}(t)$. Moreover, we note that $\tilde{Q}\mathcal{L}\hat{W}_b = \tilde{Q}\mathcal{L}\tilde{P}\hat{W}_b = \mathcal{L}_V\hat{W}_b$, resulting in the following notation of the memory kernels:

$$K_{ab}(\tau) = -i\mathrm{tr}\{\hat{\Pi}_a\mathcal{L}_V\mathcal{G}_{\tilde{Q}}(\tau)\mathcal{L}_V\hat{W}_b\} \equiv \mathrm{tr}\{\hat{\Pi}_a\mathcal{T}(\tau)\hat{W}_b\}. \tag{3.479}$$

In the last expression, we introduced the transfer superoperator

$$\mathcal{T}(\tau) = -i\mathcal{L}_V\mathcal{G}_{\tilde{Q}}(\tau)\mathcal{L}_V. \tag{3.480}$$

It offers a suitable interpretation of the memory kernel as describing probability transfer from state b to state a via time evolution of the statistical operator $\hat{W}_b = \hat{R}_b\hat{\Pi}_b$. The time evolution starts at $\tau = 0$ and proceeds to $\tau > 0$ as specified by the transfer superoperator $\mathcal{T}(\tau)$. The reservoir state-space trace and the diagonal state matrix element $\langle a| \cdots |a\rangle$ give the memory kernel.

Finally, we notice the existence of a particular sum rule for the memory kernels:

$$\sum_a K_{ab}(\tau) = \sum_a \mathrm{tr}\{\hat{\Pi}_a\mathcal{T}(\tau)\hat{W}_b\} = \mathrm{tr}\{\mathcal{T}(\tau)\hat{W}_b\} = 0. \tag{3.481}$$

The result follows if we take into consideration that $\mathcal{T}(\tau)\hat{W}_b$ can be written as $\mathcal{L}_V$ acting on $-i\mathcal{G}_{\tilde{Q}}(\tau)\mathcal{L}_V\hat{W}_b$. This results in the trace of a commutator, which likewise vanishes.

3.14.3 Rate Equations

Before further dealing with the $K_{ab}(\tau)$, we briefly explain their relation to ordinary transition rates. Suppose that the kernels in Eq. (3.474) change fast compared to the time dependence of the populations. Then, we can neglect memory effects and may write

$$\int d\tau \, K_{ab}(\tau) P_b(t - \tau) \approx \int d\tau \, K_{ab}(\tau) P_b(t). \tag{3.482}$$

We introduce the Fourier-transformed kernels

$$K_{ab}(\omega) = \int d\tau \, e^{i\omega\tau} K_{ab}(\tau) \tag{3.483}$$

and set

$$k_{ab} = K_{ab}(\omega = 0). \tag{3.484}$$

Then, Eq. (3.474) changes to an ordinary rate equation

$$\frac{\partial}{\partial t} P_a(t) = \sum_b k_{ab} P_b(t). \tag{3.485}$$

The rates are interpreted as the zero-frequency part of the Fourier-transformed kernels. To demonstrate the conservation of total probability

$$\sum_a \frac{\partial}{\partial t} P_a(t) = 0. \tag{3.486}$$

The conservation is guaranteed because of the memory kernel sum rule, Eq. (3.481), which apparently remains valid after Fourier transformation

$$0 = \sum_a k_{ab}. \tag{3.487}$$

This relation also yields

$$k_{bb} = -\sum_{a \neq b} k_{ab}. \tag{3.488}$$

We introduce transition rates for $a \neq b$

$$k_{ab} = k_{b \to a} \tag{3.489}$$

and obtain rate equations in their standard form:

$$\frac{\partial}{\partial t} P_a = -\sum_b (k_{a \to b} P_a - k_{b \to a} P_b). \tag{3.490}$$

3.14.4 The Memory Kernels

For calculating rate expressions, it is important to replace the Green's superoperator $\mathcal{G}_{\tilde{Q}}$ by an expression that does not contain the projector $\tilde{Q}$. In order to do this, we first introduce the Fourier-transformed Green's superoperator

$$\mathcal{G}_{\tilde{Q}}(\omega) = \int dt \, e^{i\omega t} \, \mathcal{G}_{\tilde{Q}}(t) = \left(\omega - \tilde{Q}\mathcal{L} + i\varepsilon \right)^{-1}. \tag{3.491}$$

The Fourier-transformed version of the kernel, Eq. (3.479), may be written as

$$K_{ab}(\omega) = -i\mathrm{tr}\{\hat{\Pi}_a \mathcal{L}_V \mathcal{G}_{\tilde{Q}}(\omega)\mathcal{L}_V \hat{W}_b\}. \tag{3.492}$$

The Green's superoperator, which should replace $\mathcal{G}_{\tilde{Q}}(\omega)$ and which should be independent on the projector $\tilde{Q}$, takes the form

$$\mathcal{G}(\omega) = (\omega - \mathcal{L} + i\varepsilon)^{-1}. \tag{3.493}$$

We note the identity

$$1 = \mathcal{G}_{\tilde{Q}}^{-1}(\omega)\mathcal{G}_{\tilde{Q}}(\omega) = \left(\mathcal{G}^{-1}(\omega) + \tilde{P}\mathcal{L}_V\right)\mathcal{G}_{\tilde{Q}}(\omega) \tag{3.494}$$

and obtain after multiplying with $\mathcal{G}$ from the left

$$\mathcal{G}_{\tilde{Q}}(\omega) = \mathcal{G}(\omega) - \mathcal{G}(\omega)\tilde{P}\mathcal{L}_V \mathcal{G}_{\tilde{Q}}(\omega). \tag{3.495}$$

If this relation is inserted into the rate expression, we arrive at

$$K_{ab}(\omega) = -i\mathrm{tr}\{\hat{\Pi}_a \mathcal{L}_V \mathcal{G}(\omega)\mathcal{L}_V \hat{W}_b\} + i\mathrm{tr}\{\hat{\Pi}_a \mathcal{L}_V \mathcal{G}(\omega)\tilde{P}\mathcal{L}_V \mathcal{G}_{\tilde{Q}}(\omega)\mathcal{L}_V \hat{W}_b\}. \tag{3.496}$$

Noting the definition of $\tilde{P}$, Eq. (3.458), the second trace on the right-hand side can be rewritten as

$$\begin{aligned} &\mathrm{tr}\{\hat{\Pi}_a \mathcal{L}_V \mathcal{G}(\omega)\tilde{P}\mathcal{L}_V \mathcal{G}_{\tilde{Q}}(\omega)\mathcal{L}_V \hat{W}_b\} \\ &= \sum_c \mathrm{tr}\{\hat{\Pi}_a \mathcal{L}_V \mathcal{G}(\omega)\hat{W}_c\}\,\mathrm{tr}\{\hat{\Pi}_c \mathcal{L}_V \mathcal{G}_{\tilde{Q}}(\omega)\mathcal{L}_V \hat{W}_b\}. \end{aligned} \tag{3.497}$$

The second trace in the c-sum is identical to $iK_{ca}(\omega)$. To rewrite the first trace in the c-sum, we introduce the zeroth-order Green's superoperator

$$\mathcal{G}_0(\omega) = \left(\omega - \mathcal{L}_0 + i\varepsilon\right)^{-1}. \tag{3.498}$$

This allows us to set up the relations

$$\mathcal{G}(\omega) = \mathcal{G}_0(\omega) + \mathcal{G}_0(\omega)\mathcal{L}_V \mathcal{G}(\omega) \tag{3.499}$$

and

$$\mathcal{G}(\omega) = \mathcal{G}_0(\omega) + \mathcal{G}(\omega)\mathcal{L}_V \mathcal{G}_0(\omega). \tag{3.500}$$

Both equations are a version of the ubiquitous *Dyson equation*. Then, we can rearrange the first trace expression on the right-hand side of Eq. (3.497) as

$$\begin{aligned} \mathrm{tr}\{\hat{\Pi}_a \mathcal{L}_V \mathcal{G}(\omega)\hat{W}_c\} &= \mathrm{tr}\{\hat{\Pi}_a \mathcal{L}_V \mathcal{G}_0(\omega)\hat{W}_c\} + \mathrm{tr}\{\hat{\Pi}_a \mathcal{L}_V \mathcal{G}(\omega)\mathcal{L}_V \mathcal{G}_0(\omega)\hat{W}_c\} \\ &= \frac{1}{\omega + i\varepsilon}\mathrm{tr}\{\hat{\Pi}_a \mathcal{L}_V \mathcal{G}(\omega)\mathcal{L}_V \hat{W}_c\}. \end{aligned} \tag{3.501}$$

The last line follows from the fact that trace expressions of first order in $\mathcal{L}_V$ Vanish, and that $\mathcal{G}_0(\omega)$ applied to $\hat{W}_c$ simply produces a frequency denominator. We denote the kernel, which does not depend on the projector $\tilde{Q}$, by

$$L_{ab}(\omega) = -i\mathrm{tr}\{\hat{\Pi}_a \mathcal{L}_V \mathcal{G}(\omega)\mathcal{L}_V \hat{W}_b\} \tag{3.502}$$

and arrive at the following equation, which relates the two types of kernels to each other:

$$K_{ab}(\omega) = L_{ab}(\omega) - \frac{i}{\omega + i\varepsilon} \sum_c L_{ac}(\omega) K_{cb}(\omega). \tag{3.503}$$

Once all L_{ab} have been determined, the rates K_{ab} entering the rate equations can be computed according to this equation.

Let us consider a perturbation expansion of L_{ab} in powers of the coupling $\hat{V}$, Eq. (3.456). This expansion would be of even order in $\hat{V}$ and can be generated by a respective expansion of Eq. (3.499) or Eq. (3.500). We count the orders with respect to $\hat{V}$ by m, n, and n' and get a recursion relation

$$\sum_{m=1}^{\infty} K_{ab}^{(2m)}(\omega) = \sum_{m=1}^{\infty} L_{ab}^{(2m)}(\omega) - \frac{i}{\omega + i\varepsilon} \sum_c \sum_{n=1}^{\infty} \sum_{n'=1}^{\infty} L_{ac}^{(2n)}(\omega) K_{cb}^{(2n')}(\omega). \tag{3.504}$$

In particular, the relation indicates that (note also the replacement of $\mathcal{G}$ by $\mathcal{G}_0$ in Eq. (3.502))

$$K_{ab}^{(2)}(\omega) \equiv L_{ab}^{(2)}(\omega) = -i\mathrm{tr}\{\hat{\Pi}_a \mathcal{L}_V \mathcal{G}_0(\omega) \mathcal{L}_V \hat{W}_b\}. \tag{3.505}$$

However, all higher order contributions $K^{(2m)}$ are determined not only by $L^{(2m)}$ but also by products of lower order rates. When solving, for example rate equations such as Eq. (3.490) including rates up to a particular order m, and computing related state populations, the combination of $L^{(2n)}$ with $K^{(2n')}$ ($n, n' < m$) avoids multiple counting of the lower order rates (an application can be found in Section 7.6).

3.14.5 Second-order Rate Expressions

In what follows, we specify the formal results of the foregoing discussion to the second-order rate, Eq. (3.505). In doing so, we expect a zero-frequency expression that is identical to the *Golden Rule* rate already computed in Sections 3.3.2 and 3.4.5. Noting the definition of $\mathcal{G}_0(\omega)$, we may write for the second-order rate

$$K_{ba}^{(2)}(\omega) = -\int_0^{\infty} dt \, e^{i\omega t} \mathrm{tr}_R\{\langle b|(\mathcal{L}_V \mathcal{U}_0(t) \mathcal{L}_V \hat{W}_a)|b\rangle\}. \tag{3.506}$$

In the trace expression under the time integral, the action of the coupling Liouvillian $\mathcal{L}_V$ is combined with that of the time-evolution superoperator. Starting with $\hat{W}_a$, the operator $\hat{V}$ acts either from the left or the right. The resulting two expressions are propagated from time zero to time t according to $U_0(t) \cdots U_0^+(t)$. After calculating the commutator with $\hat{V}$, the matrix element with respect to $|b\rangle$ is taken. Finally, the trace concerning the reservoir coordinate states has to be carried out. The parenthesis guarantees that the matrix elements are calculated after the sequence of superoperators has affected $\hat{W}_a$.

The whole procedure seems to be easy in the case of second-order rates but becomes much more involved when considering fourth-order rate expression. Therefore, it is already useful in the case of second-order rates to introduce a graphical scheme for rate computation as displayed in Figure 3.12. To distinguish
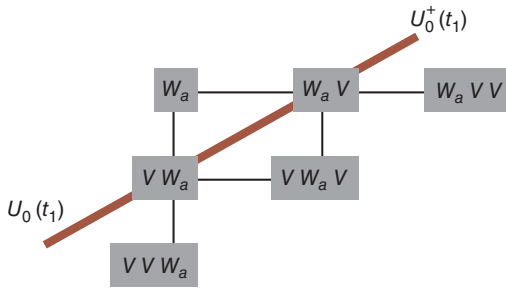
Figure 3.12 Graphical scheme for second-order rate computation. The diagonal line indicates an embedding of the operator products that are crossed by this line into the action of time-evolution operators according to $U_0(t_1) \cdots U_0^+(t_1)$ (note the sign rule, which results in the appearance of a minus sign for every action of $\hat{V}$ from the right; for more details, see text).

the two possible actions of $\hat{V}$, we move downward to the next row of the scheme if $\hat{V}$ acts from the left and rightward to the next column if $\hat{V}$ acts from the right. (Here, we have to note the sign rule, which results in the appearance of a minus sign for every action of $\hat{V}$ from the right.) The first action of this type is followed by an application of the time-evolution operator. It is indicated by the gray line and labeled by the time-evolution operators with the actual time argument. As also visible from Figure 3.12, there result three different types of arranging two $\hat{V}$ around $\hat{W}_a$. The different ways to reach these arrangements in the scheme of Figure 3.12 are known as *Liouville space pathways*. Of interest here are only those two pathways leading to the symmetric arrangement VW_aV. Since the matrix element with respect to the state $|b\rangle$, which is different from $|a\rangle$, only has to be calculated, the operator arrangements VVW_a and W_aVV do not contribute (to indicate the formal character of this notation, we removed the operator hat). Consequently, we may write

$$K_{ba}^{(2)}(\omega) = \int\limits_0^\infty dt\, e^{i\omega t}\left(C_{ba}(t) + \text{c.c.}\right), \tag{3.507}$$

where the correlation function is formed by the trace expression (U_a^+ and U_b are time-evolution operators defined by the vibrational Hamiltonians, Eq. (3.455))

$$
\begin{aligned}
C_{ba}(t) &= \frac{1}{\hbar^2}\text{tr}_\text{R}\{\langle b|U(t)\hat{V}\hat{W}_a U^+(t)\hat{V}|b\rangle\} \\
&= \frac{1}{\hbar^2}\text{tr}_\text{R}\{U_b(t)\Phi_{ba}\hat{R}_a U_a^+(t)\Phi_{ab}\} \\
&= \frac{1}{\hbar^2}\text{tr}_\text{R}\{\hat{R}_a U_a^+(t)\Phi_{ab}U_b(t)\Phi_{ba}\}.
\end{aligned}
\tag{3.508}
$$

This expression is complemented by the complex conjugated trace when determining the rate, Eq. (3.507). We note that

$$
\begin{aligned}
C_{ba}^*(t) &= \frac{1}{\hbar^2}\text{tr}_\text{R}\{\Phi_{ab}U_b(-t)\Phi_{ba}U_a^+(-t)\hat{R}_a\} \\
&= \frac{1}{\hbar^2}\text{tr}_\text{R}\{\hat{R}_a U_a^+(-t)\Phi_{ab}U_b(-t)\Phi_{ba}\} = C_{ba}(-t)
\end{aligned}
\tag{3.509}
$$

and obtain

$$K_{ba}^{(2)}(\omega) = \int\limits_{0}^{\infty} dt \, e^{i\omega t} \left(C_{ba}(t) + C_{ba}(-t) \right). \tag{3.510}$$

It is also of interest to introduce the Fourier-transformed correlation function

$$C_{ba}(\omega) = \int dt \, e^{i\omega t} C_{ba}(t). \tag{3.511}$$

Its zero-frequency expression as well as that of $K_{ba}^{(2)}$ gives the transition rate

$$k_{a\to b} = C_{ba}(\omega = 0) = K_{ba}^{(2)}(\omega = 0). \tag{3.512}$$

A similar expression has been already derived in Section 3.4.5.

We analyze $C_{ba}(\omega)$ in more detail by introducing the eigenstates (eigenvalues) $\chi_{a\mu}$ ($\chi_{b\nu}$) and $\omega_{a\mu}(\omega_{b\nu})$ of the Hamiltonians H_a and H_b, respectively (cf. Eq. (3.455)). We, first, get

$$C_{ba}(t) = \frac{1}{\hbar^2} \sum_{\mu,\nu} f_{a\mu} |\langle \chi_{a\mu} | \Phi_{ab} | \chi_{b\nu} \rangle|^2 e^{i(\omega_{a\mu} - \omega_{b\nu})t}, \tag{3.513}$$

which immediately results in

$$C_{ba}(\omega) = \frac{2\pi}{\hbar^2} \sum_{\mu,\nu} f_{a\mu} |\langle \chi_{a\mu} | \Phi_{ab} | \chi_{b\nu} \rangle|^2 \delta(\omega + \omega_{a\mu} - \omega_{b\nu}). \tag{3.514}$$

This expression indicates that it is a real and positive function of frequency. The equilibrium distribution $f_{a\mu}$ takes the form $\exp(-\hbar\omega_{a\mu}/k_B T)/Z_a$ (Z_a is the state sum). The zero-frequency limit reproduces the Golden Rule rate formula already derived in Section 3.3.2.

To relate the (forward) rate $k_{a\to b}$ to that of the reverse process (backward rate) $k_{b\to a}$, we consider

$$C_{ab}(\omega) = \frac{2\pi}{\hbar^2} \sum_{\nu,\mu} f_{b\nu} |\langle \chi_{b\nu} | \Phi_{ba} | \chi_{a\mu} \rangle|^2 \delta(\omega + \omega_{b\nu} - \omega_{a\mu}). \tag{3.515}$$

It is related to C_{ba} by noting that $f_{b\nu}\delta(\omega + \omega_{b\nu} - \omega_{a\mu})$ equals $f_{a\mu}\delta(-\omega + \omega_{b\nu} - \omega_{a\mu})$ multiplied by $\mathcal{Z}_a/\mathcal{Z}_b \times \exp(-\hbar\omega/k_B T)$, thus arriving at

$$C_{ab}(\omega) = \frac{\mathcal{Z}_a}{\mathcal{Z}_b} e^{\hbar\omega/k_B T} C_{ba}(-\omega). \tag{3.516}$$

The type of correlation function, Eq. (3.508), is of interest whenever the dependence of the coupling matrices Φ on the reservoir coordinates is included. Otherwise, the Φ can be removed from the trace. For this case and separating the Hamiltonian H_a into the reference energy $E_a = \hbar\omega_a$ (at the minimum of the respective PES) and a remaining vibrational Hamiltonian h_a, we obtain the correlation function, Eq. (3.508), as

$$C_{ba}(t) = \frac{|\Phi_{ab}|^2}{\hbar^2} e^{i\omega_{ab}t} \text{tr}_R \{ \hat{R}_a e^{ih_a t/\hbar} e^{-ih_b t/\hbar} \} + \text{c.c.} \tag{3.517}$$

3.14.6 Fourth-order Rate Expressions

According to Eq. (3.504), the fourth-order (frequency-dependent) rate expression takes the form

$$K_{ba}^{(4)}(\omega) = L_{ba}^{(4)}(\omega) - \frac{i}{\omega + i\varepsilon} \sum_c K_{bc}^{(2)}(\omega) K_{ca}^{(2)}(\omega). \tag{3.518}$$

The fourth-order frequency-dependent rate $L_{ba}^{(4)}$ forms the total rate $K_{ba}^{(4)}$ after subtracting the products of the two second-order rates. Those describe transitions from the initial state $|a\rangle$ to all intermediate states $|c\rangle$ and, afterward, from these intermediate states to the final state $|b\rangle$. The possible divergence of the prefactor $1/(\omega + i\varepsilon)$ in the zero-frequency limit indicates the need for a careful analysis. One expects a cancellation of the factorized part $\sum_c K_{bc}^{(2)} K_{ca}^{(2)}$ by parts of $L_{ba}^{(4)}$ to arrive at a finite overall fourth-order rate.

The second-order rates have been already presented in Eq. (3.506). To obtain an expression for $L_{ba}^{(4)}(\omega)$, we note the general form of $L_{ba}(\omega)$, Eq. (3.502). It indicates that the fourth order in $\hat{V}$ is obtained if we compute the Green's superoperator up to the second order

$$\mathcal{G}(\omega) \approx \mathcal{G}_0(\omega) + \mathcal{G}_0(\omega)\mathcal{L}_V\mathcal{G}_0(\omega) + \mathcal{G}_0(\omega)\mathcal{L}_V\mathcal{G}_0(\omega)\mathcal{L}_V\mathcal{G}_0(\omega). \tag{3.519}$$

Inserting this expression into $L_{ba}(\omega)$ gives the fourth-order rate

$$L_{ba}^{(4)}(\omega) = -i\mathrm{tr}\{\hat{\Pi}_b \mathcal{L}_V\mathcal{G}_0(\omega)\mathcal{L}_V\mathcal{G}_0(\omega)\mathcal{L}_V\mathcal{G}_0(\omega)\mathcal{L}_V \hat{W}_a\}. \tag{3.520}$$

Noting the definition of $\mathcal{G}_0(\omega)$, we may write

$$L_{ba}^{(4)}(\omega) = \int_0^\infty dt_3 \; dt_2 \; dt_1 \; e^{i\omega(t_3 + t_2 + t_1)}$$
$$\times \mathrm{tr}_{\mathrm{R}}\{\langle b|(\mathcal{L}_V\mathcal{U}_0(t_3)\mathcal{L}_V\mathcal{U}_0(t_2)\mathcal{L}_V\mathcal{U}_0(t_1)\mathcal{L}_V\hat{W}_a)|b\rangle\}. \tag{3.521}$$

As in the case of the second-order rate expression, the trace combines the action of the coupling Liouvillian and that of the time-evolution superoperator. However, this combined action is applied here three times. Obviously, the whole procedure results in eight different terms. Finally, and again in similarity to the foregoing section, the commutator with $\hat{V}$ has to be calculated. Afterward, the matrix element with respect to $|b\rangle$ and the trace concerning the reservoir coordinate states have to be taken. Figure 3.13 gives a graphical representation according to the rules already explained in relation to Figure 3.12. Now, there result five different types of arranging four $\hat{V}$s around $\hat{W}_a$. The arrangements $W_a VVVV$ and $VVVV W_a$ appear each once. Again, since $L_{ba}^{(4)}$ also has to be calculated for $b \neq a$ only, these arrangements do not contribute. The arrangements $VW_a VVV$ and $VVV W_a V$ appear four times, and the symmetric arrangement $VV W_a VV$ six times. Compared to the foregoing section, the present number of different arrangements of $\hat{W}_a$ with respect to the four $\hat{V}$s, that is the number of different Liouville space pathways in the scheme of Figure 3.13, is much larger. It reflects the different possibilities to include the three types of time-evolution operators (with time argument t_1, t_2, and t_3). Which paths really contribute depends on the mutual level position and coupling. The most simple case is considered in the following section.
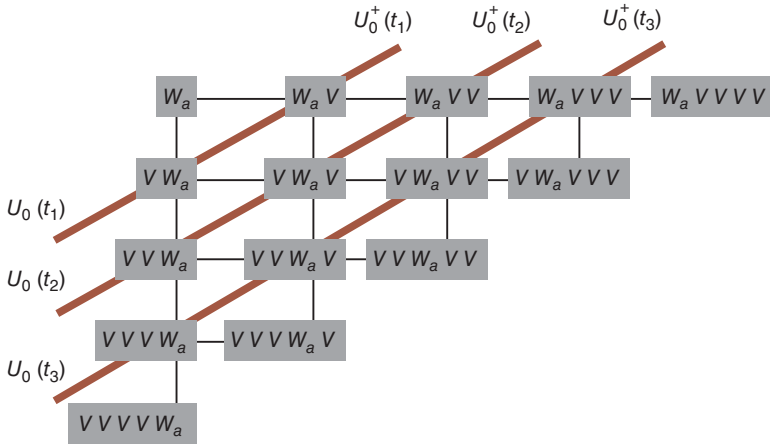
Figure 3.13 Graphical scheme for fourth-order rate computation. The three diagonal lines indicate an embedding into the action of time-evolution operators according to $U_0(t) \cdots U_0^+(t)$ at the three different times t_1, t_2, and t_3 (note the sign rule, which results in the appearance of a minus sign for every action of $\hat{V}$ from the right; for more details, see text).

Denoting the trace expression under the triple time integral in Eq. (3.521) as $C(t_3, t_2, t_1) + C^*(t_3, t_2, t_1)$, we may write the transition rate (for transitions from a to b) as

$$k_{a\to b} = K^{(4)}_{ba}(\omega = 0) = \int_0^\infty dt_3 \, dt_2 \, dt_1 \, \left\{ \left(C_{ba}(t_3, t_2, t_1) + C^*_{ba}(t_3, t_2, t_1) \right) \right.$$

$$\left. - \sum_c \left(C_{bc}(t_3) + C^*_{bc}(t_3) \right) \left(C_{ca}(t_1) + C^*_{ca}(t_1) \right) \right\}. \quad (3.522)$$

This formula does not require us to carry out the zero-frequency limit. It again indicates, however, the need to achieve partial compensation between the fourth-order correlation functions $C_{ba} + C^*_{ba}$ and the products C_{bc} and C_{ca} of the second-order ones. This becomes necessary since the divergent t_2-integral in the second part has to be removed.

3.14.6.1 Three-level System with Sequential Coupling

As an application of the fourth-order rate theory of the preceding section, we discuss a three-level system $a = 1, 2, 3$ with a coupling Φ_{12} connecting the first to the second level and a coupling Φ_{23} that relates the second to the third level (see also the examples in Sections 7.6, 9.10.2, and 9.8). The direct coupling between the first and the third levels does not exist. This sequential type of coupling initiates transfer from the first to the third level exclusively via the second level. It can proceed stepwise via second-order rates or directly via a fourth-order rate. Because of the structure of the level coupling, we get for VW_aVVV the contributions $\Phi_{21}W_1\Phi_{12}\Phi_{23}\Phi_{32}$ and $\Phi_{21}W_1\Phi_{12}\Phi_{21}\Phi_{12}$. They represent transition rates from the first to the second state
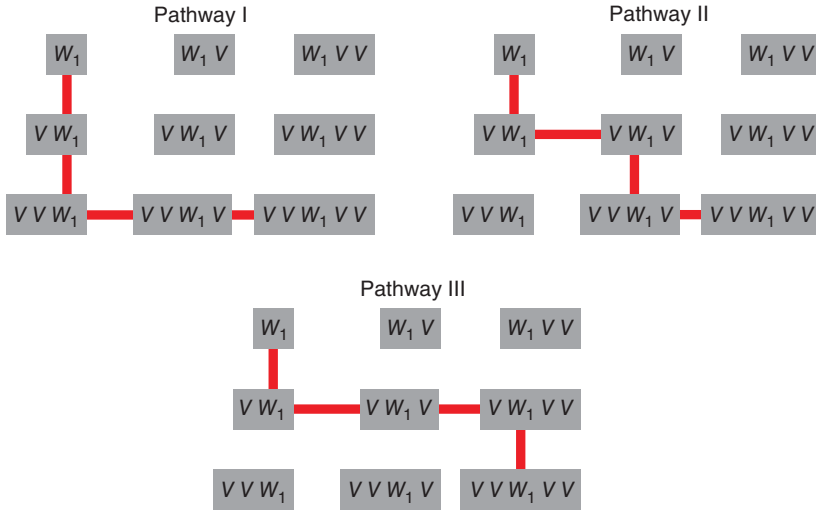
Figure 3.14 Three different pathways in the graphical scheme of the fourth-order rate computation contributing to the transition rate of the three-level system with sequential coupling.

but do not contribute to the rate from the first to the third state (this is also valid for contributions from $VVVW_aV$). There remain the six different terms corresponding to the arrangement VVW_aVV. They are pairwise complex conjugated. The three different terms if included into the trace expression are labeled by the number of the paths shown in Figure 3.14, that is we may write

$$C_{31}(t_3, t_2, t_1) = C_{31}^{(\mathrm{I})}(t_3, t_2, t_1) + C_{31}^{(\mathrm{II})}(t_3, t_2, t_1) + C_{31}^{(\mathrm{III})}(t_3, t_2, t_1). \tag{3.523}$$

The different parts read in detail

$$
\begin{aligned}
&C_{31}^{(\mathrm{I})}(t_3, t_2, t_1) \\
&= \frac{1}{\hbar^4} \mathrm{tr}_{\mathrm{R}}\{\langle 3|U(t_3 + t_2)\hat{V}U(t_1)\hat{V}\hat{W}_1 U^+(t_1 + t_2)\hat{V}U^+(t_3)\hat{V}|3\rangle\},
\end{aligned} \tag{3.524}
$$

$$
\begin{aligned}
&C_{31}^{(\mathrm{II})}(t_3, t_2, t_1) \\
&= \frac{1}{\hbar^4} \mathrm{tr}_{\mathrm{R}}\{\langle 3|U(t_3)\hat{V}U(t_2 + t_1)\hat{V}\hat{W}_1 U^+(t_1)\hat{V}U^+(t_2 + t_3)\hat{V}|3\rangle\},
\end{aligned} \tag{3.525}
$$

and

$$
\begin{aligned}
&C_{31}^{(\mathrm{III})}(t_3, t_2, t_1) \\
&= \frac{1}{\hbar^4} \mathrm{tr}_{\mathrm{R}}\{\langle 3|\hat{V}U(t_3 + t_2 + t_1)\hat{V}\hat{W}_1 U^+(t_1)\hat{V}U^+(t_2)\hat{V}U^+(t_3)|3\rangle\}.
\end{aligned} \tag{3.526}
$$

We specify $\hat{V}$ and obtain

$$
\begin{aligned}
&C_{31}^{(\mathrm{I})}(t_3, t_2, t_1) \\
&= \frac{1}{\hbar^4} \mathrm{tr}_{\mathrm{R}}\{U_3(t_3 + t_2)\Phi_{32}U_2(t_1)\Phi_{21}\hat{R}_1 U_1^+(t_1 + t_2)\Phi_{12}U_2^+(t_3)\Phi_{23}\} \\
&= \frac{1}{\hbar^4} \mathrm{tr}_{\mathrm{R}}\{\hat{R}_1 U_1^+(t_1 + t_2)\Phi_{12}U_2^+(t_3)\Phi_{23}U_3(t_3 + t_2)\Phi_{32}U_2(t_1)\Phi_{21}\},
\end{aligned} \tag{3.527}
$$

$$C_{31}^{(II)}(t_3, t_2, t_1)$$

$$= \frac{1}{\hbar^4} \mathrm{tr}_R \{ U_3(t_3) \Phi_{32} U_2(t_2 + t_1) \Phi_{21} \hat{R}_1 U_1^+(t_1) \Phi_{12} U_2^+(t_2 + t_3) \Phi_{23} \}$$

$$= \frac{1}{\hbar^4} \mathrm{tr}_R \{ \hat{R}_1 U_1^+(t_1) \Phi_{12} U_2^+(t_2 + t_3) \Phi_{23} U_3(t_3) \Phi_{32} U_2(t_2 + t_1) \Phi_{21} \}, \qquad (3.528)$$

and

$$C_{31}^{(III)}(t_3, t_2, t_1)$$

$$= \frac{1}{\hbar^4} \mathrm{tr}_R \{ \Phi_{32} U_2(t_3 + t_2 + t_1) \Phi_{21} \hat{R}_1 U_1^+(t_1) \Phi_{12} U_2^+(t_2) \Phi_{23} U_3^+(t_3) \}$$

$$= \frac{1}{\hbar^4} \mathrm{tr}_R \{ \hat{R}_1 U_1^+(t_1) \Phi_{12} U_2^+(t_2) \Phi_{23} U_3^+(t_3) \Phi_{32} U_2(t_3 + t_2 + t_1) \Phi_{21} \}. \qquad (3.529)$$

The derived expressions will be used later in Sections 7.6, 9.10.2, and 9.8. In order to take a closer look on the fourth-order rate expression, we consider a simple example where only the discrete energies $\hbar\omega_a$ ($a = 1, 2, 3$) contribute and a respective reservoir coordinate dependence is neglected (the Hamiltonians H_a are replaced by $\hbar\omega_a$). This yields

$$C_{31}^{(I)}(t_3, t_2, t_1) = \frac{|\Phi_{12}\Phi_{23}|^2}{\hbar^4} \exp\left(i\omega_{12}t_1 + i\omega_{13}t_2 + i\omega_{23}t_3 \right), \qquad (3.530)$$

$$C_{31}^{(II)}(t_3, t_2, t_1) = \frac{|\Phi_{12}\Phi_{23}|^2}{\hbar^4} \exp\left(i\omega_{12}t_1 + i\omega_{23}t_3 \right), \qquad (3.531)$$

and

$$C_{31}^{(III)}(t_3, t_2, t_1) = \frac{|\Phi_{12}\Phi_{23}|^2}{\hbar^4} \exp\left(i\omega_{12}t_1 + i\omega_{32}t_3 \right). \qquad (3.532)$$

Be aware of the fact that $C_{31}^{(I)}$ depends on t_2, but $C_{31}^{(II)}$ and $C_{31}^{(III)}$ do not. This indicates a possible factorization in a t_1-dependent and a t_3-dependent part and a resulting compensation by the product of two second-order correlation functions (depending either on t_1 or t_3, cf. Eq. (3.522)). It can also be interpreted as a transition from level 1 to level 3 but interrupted by level 2 (the extent of this interruption depends on the used model).

We use these expressions to compute $K_{31}^{(4)}(\omega)$. The respective approximation for the second-order rate takes the form (see Eqs. (3.510) and (3.517) and note the abbreviation $\tilde{\omega} = \omega + i\varepsilon$)

$$K_{ba}^{(2)}(\omega) = -\frac{|\Phi_{ab}|^2}{\hbar^2} \left(\frac{i}{\tilde{\omega} + \omega_{ab}} + \frac{i}{\tilde{\omega} - \omega_{ab}} \right). \qquad (3.533)$$

Accordingly, we get the fourth-order expression as

$$K_{31}^{(4)}(\omega) = L_{31}^{(4)}(\omega) - \frac{i}{\tilde{\omega}} K_{32}^{(2)}(\omega) K_{21}^{(2)}(\omega) = -i\frac{|\Phi_{12}\Phi_{23}|^2}{\hbar^4}$$

$$\times \left(\frac{1}{(\tilde{\omega} + \omega_{12})(\tilde{\omega} + \omega_{13})(\tilde{\omega} + \omega_{23})} \right.$$

$$+ \frac{1}{(\tilde{\omega} - \omega_{12})(\tilde{\omega} - \omega_{13})(\tilde{\omega} - \omega_{23})}$$

$$+ \frac{1}{(\tilde{\omega} + \omega_{12})\tilde{\omega}(\tilde{\omega} + \omega_{23})} + \frac{1}{(\tilde{\omega} - \omega_{12})\tilde{\omega}(\tilde{\omega} - \omega_{23})}$$

$$+ \frac{1}{(\tilde{\omega} + \omega_{12})\tilde{\omega}(\tilde{\omega} + \omega_{32})} + \frac{1}{(\tilde{\omega} - \omega_{12})\tilde{\omega}(\tilde{\omega} - \omega_{32})}$$
$$- \frac{1}{\tilde{\omega}} \left[\frac{1}{\tilde{\omega} - \omega_{23}} + \frac{1}{\tilde{\omega} + \omega_{23}} \right] \left[\frac{1}{\tilde{\omega} - \omega_{12}} + \frac{1}{\tilde{\omega} + \omega_{12}} \right] \Bigg). \tag{3.534}$$

One easily verifies that only the first two terms contribute (corresponding to the first Liouville space pathway I of Figure 3.14). Thus, the fourth-order rate due to pathways II and III is completely compensated by the factorized part of the rate. This will not be the case if more sophisticated energy level schemes are considered. Note also that in the $\omega \to 0$-limit, the mentioned terms vanish independently. Accordingly, we obtain the ordinary rate expression as

$$k_{1\to 3}^{(4)} = \frac{2|\Phi_{12}\Phi_{23}|^2}{\hbar^4} \mathrm{Im} \left(\frac{1}{(\omega_{12} + i\varepsilon)(\omega_{13} + i\varepsilon)(\omega_{23} + i\varepsilon)} \right)$$
$$= \frac{2\pi|\Phi_{12}\Phi_{23}|^2}{\hbar^4} \left(\frac{\delta(\omega_{13})}{\varepsilon_{12}^2} - \frac{\delta(\omega_{23})}{\varepsilon_{12}^2} - \frac{\delta(\omega_{12})}{\varepsilon_{23}^2} + \pi^2 \delta(\omega_{13})\delta(\omega_{23})\delta(\omega_{12}) \right). \tag{3.535}$$

We assume that $\omega_{12} \neq 0$ and $\omega_{32} \neq 0$ and arrive at

$$k_{1\to 3}^{(4)} = \frac{2\pi}{\hbar} \left| \frac{\Phi_{12}\Phi_{23}}{\hbar\omega_{12}} \right|^2 \delta(\hbar\omega_{13}), \tag{3.536}$$

which is the standard formula used whenever transfer processes are studied that are mediated by an intermediate (bridge level). The present discussion demonstrates, however, that the intermediate level has to be off-resonant to the initial and final levels. If this is not the case, the more general expression has to be used.

Finally, we use Eq. (3.522) to directly calculate the fourth-order rate circumventing the introduction of frequency-dependent rates

$$k_{1\to 3} = \frac{|\Phi_{12}\Phi_{23}|^2}{\hbar^4} \int_0^\infty dt_3 \, dt_2 \, dt_1 \left(\left(e^{i\omega_{12}t_1 + i\omega_{13}t_2 + i\omega_{23}t_3} \right. \right.$$
$$\left. + e^{i\omega_{12}t_1 + i\omega_{23}t_3} + e^{i\omega_{12}t_1 + i\omega_{32}t_3} + \mathrm{c.c.} \right) - \left(e^{i\omega_{23}t_3} + \mathrm{c.c.} \right) \left(e^{i\omega_{12}t_1} + \mathrm{c.c.} \right) \Big)$$
$$= \frac{|\Phi_{12}\Phi_{23}|^2}{\hbar^4} \int_0^\infty dt_3 \, dt_2 \, dt_1 \left(e^{i\omega_{12}t_1 + i\omega_{13}t_2 + i\omega_{23}t_3} + \mathrm{c.c.} \right). \tag{3.537}$$

The derivation again displays a complete cancellation of the second and third Liouville space pathway contributions by the factorized part. A modification of these formulas including interstate dephasing is introduced in Section 9.8.

3.15 Supplement

3.15.1 Thermofield Dynamics

In Section 3.2.3, we have introduced the MCTDH method as a powerful tool to solve the time-dependent Schrödinger equation for many DOFs. The question arises if temperature effects can be accounted for in wave packet propagations. In what follows, we sketch thermofield dynamics as one possible approach that serves this

task. Given a system in thermal equilibrium according to the canonical ensemble, thermal expectation values of an operator $\hat{O}$ are calculated according to Eq. (3.123) with the statistical operator given by Eq. (3.126). The goal of thermofield dynamics is to formulate the trace expression in terms of an expectation value with respect to a temperature-dependent vacuum state $|0_T\rangle$, that is

$$\langle\hat{O}\rangle = \frac{1}{\mathcal{Z}}\mathrm{tr}\{e^{-H/k_{\mathrm{B}}T}\hat{O}\} = \frac{1}{\mathcal{Z}}\sum_\alpha e^{-E_\alpha/k_{\mathrm{B}}T}O_{\alpha\alpha}$$

$$= \langle 0_T|\hat{O}|0_T\rangle \tag{3.538}$$

(with $H|\alpha\rangle = E_\alpha|\alpha\rangle$). The correspondence can be achieved if one augments the original physical Hilbert space with a so-called *tilde space*; that is, the new states are $|\alpha\tilde{\alpha}\rangle = |\alpha\rangle|\tilde{\alpha}\rangle$. The states $|\tilde{\alpha}\rangle$ are eigenstates of a tilde Hamiltonian

$$\tilde{H}|\tilde{\alpha}\rangle = E_\alpha|\tilde{\alpha}\rangle. \tag{3.539}$$

Note that by definition, $\tilde{H}$ has the same eigenvalues as H, and it holds that $\langle\tilde{\beta}|\tilde{\alpha}\rangle = \delta_{\tilde{\alpha}\tilde{\beta}}$. Further, for an operator in physical space, one has the relation

$$\langle\tilde{\alpha}'\alpha|\hat{O}|\beta\tilde{\beta}'\rangle = \langle\alpha|\hat{O}|\beta\rangle\delta_{\alpha'\beta'}. \tag{3.540}$$

Using these rules and defining

$$|0_T\rangle = \frac{1}{\mathcal{Z}^{1/2}}\sum_\alpha e^{-E_\alpha/2k_{\mathrm{B}}T}|\alpha\tilde{\alpha}\rangle, \tag{3.541}$$

Eq. (3.538) holds, since due to Eq. (3.540), we have

$$\langle 0_T|\hat{O}|0_T\rangle = \frac{1}{\mathcal{Z}}\sum_{\alpha,\beta}e^{-E_\alpha/2k_{\mathrm{B}}T}e^{-E_\beta/2k_{\mathrm{B}}T}\langle\tilde{\alpha}\alpha|\hat{O}|\beta\tilde{\beta}\rangle$$

$$= \frac{1}{\mathcal{Z}}\sum_{\alpha,\beta}e^{-E_\alpha/2k_{\mathrm{B}}T}e^{-E_\beta/2k_{\mathrm{B}}T}\langle\alpha|\hat{O}|\beta\rangle\delta_{\alpha\beta}$$

$$= \frac{1}{\mathcal{Z}}\sum_\alpha e^{-E_\alpha/k_{\mathrm{B}}T}O_{\alpha\alpha}. \tag{3.542}$$

This approach can be extended to time-dependent expectation values

$$\langle\hat{O}\rangle(t) = \mathrm{tr}\{\hat{W}(t)\hat{O}\} = \langle\Psi_T(t)|\hat{O}|\Psi_T(t)\rangle, \tag{3.543}$$

where

$$|\Psi_T(t)\rangle = \hat{W}^{1/2}(t)\sum_\alpha|\alpha\tilde{\alpha}\rangle. \tag{3.544}$$

The Hamiltonian entering the Schrödinger equation in the augmented Hilbert space is defined as[34]

$$\overline{H} = H - \tilde{H}, \tag{3.545}$$

such that

$$i\hbar\frac{\partial}{\partial t}|\Psi_T(t)\rangle = \overline{H}|\Psi_T(t)\rangle. \tag{3.546}$$

For an initial state in a thermal ensemble, this equation is solved subject to the initial condition $|\Psi_T(0)\rangle = |0_T\rangle$. Indeed, since physical and tilde operators act in

---

34) Note that in a more general formulation, one can introduce a so-called tilde conjugation. Here, it holds that $(c\hat{O})\tilde{} = c^*\tilde{O}$. The choice of Eq. (3.545) guarantees that the time-evolution operator is invariant with respect to tilde conjugation.

different spaces and thus commute, using the time-evolution operators corresponding to Eq. (3.546), we have

$$\langle\Psi_T(t)|\hat{O}|\Psi_T(t)\rangle = \langle\Psi_T(0)|e^{i(H-\tilde{H})t/\hbar}\hat{O}e^{-i(H-\tilde{H})t/\hbar}|\Psi_T(0)\rangle$$

$$= \langle\Psi_T(0)|e^{iHt/\hbar}\hat{O}e^{-iHt/\hbar}|\Psi_T(0)\rangle. \tag{3.547}$$

Inserting Eq. (3.544) yields the proper expectation value. The actual implementation of this approach depends on the quantum statistical properties of the considered system. Since harmonic oscillator Hamiltonians play a central role in the theoretical description of charge and energy transfer processes, we focus on these bosonic systems and use the second quantization introduced in Section 2.5.2. In order to simplify the notation, we consider a single mode only and neglect the zero-point energy; that is, we have instead of Eq. (2.63)

$$H = \hbar\omega\, C^+C. \tag{3.548}$$

The tilde-space Hamiltonian then reads[35]

$$\tilde{H} = \hbar\omega\, \tilde{C}^+\tilde{C}. \tag{3.549}$$

The extension of Eq. (3.550) to the augmented space is given by

$$|N\tilde{N}\rangle = \frac{1}{N!}(C^+)^N(\tilde{C}^+)^N|0\tilde{0}\rangle. \tag{3.550}$$

With this definition, Eq. (3.541) can be written as

$$|0_T\rangle = \frac{1}{\mathcal{Z}^{1/2}}\sum_N e^{-N\hbar\omega/2k_BT}\frac{1}{N!}(C^+)^N(\tilde{C}^+)^N|0\tilde{0}\rangle$$

$$= [1 - \exp(-\hbar\omega/k_BT)]^{1/2}\exp\left\{C^+\tilde{C}^+e^{-\hbar\omega/2k_BT}\right\}|0\tilde{0}\rangle$$

$$= e^{-iG_T}|0\tilde{0}\rangle, \tag{3.551}$$

where the argument of the square root is the inverse of the harmonic oscillator partition function (without zero-point energy). In the last line, we introduced the thermal Bogoliubov transformation with the operator

$$G_T = G_T^+ = -i\theta_T(C\tilde{C} - C^+\tilde{C}^+), \tag{3.552}$$

where

$$\theta_T = \ln(u_T + v_T), \tag{3.553}$$

and using the Bose–Einstein distribution equation (3.283),

$$u_T = [1 - \exp(-\hbar\omega/k_BT)]^{-1/2} = [1 + n(\omega)]^{1/2}, \tag{3.554}$$

$$v_T = [\exp(\hbar\omega/k_BT) - 1]^{-1/2} = [n(\omega)]^{1/2}. \tag{3.555}$$

Alternatively, one can write

$$u_T = \cosh(\theta), \tag{3.556}$$

$$v_T = \sinh(\theta). \tag{3.557}$$

---

35) The tilde-space operators $\tilde{C}^+$ and $\tilde{C}$ obey the bosonic commutation rules. Physical and tilde operators do commute.

Using this transformation, the Schrödinger equation (3.546) can be written as

$$i\hbar\frac{\partial}{\partial t}|\Psi_\theta(t)\rangle = \overline{H}_\theta|\Psi_\theta(t)\rangle, \tag{3.558}$$

where we introduced the backtransformed state vector $|\Psi_\theta(t)\rangle = \exp(iG_T)|\Psi_T(t)\rangle$ and the Hamiltonian

$$\overline{H}_\theta = e^{iG_T}\overline{H}e^{-iG_T}. \tag{3.559}$$

Equation (3.558) has to be solved subject to the initial condition $|\Psi_\theta(0)\rangle = |0\tilde{0}\rangle$.

To achieve the unitary transformation of the Hamiltonian $\overline{H}$, we first inspect the creation and annihilation operators. For instance, we have[36]

$$e^{iG_T}Ce^{-iG_T} = C\cosh(\theta_T) - \tilde{C}^+\sinh(\theta_T). \tag{3.560}$$

Thus, for products of two operators as in the vibrational Hamiltonian, Eq. (3.548), we have (using $\sinh^2(\theta_T) - \cosh^2(\theta_T) = 1$)

$$e^{iG_T}(C^+C - \tilde{C}^+\tilde{C})e^{-iG_T} = C^+C - \tilde{C}^+\tilde{C}. \tag{3.561}$$

It follows that

$$\overline{H}_\theta = \hbar\omega(C^+C - \tilde{C}^+\tilde{C}). \tag{3.562}$$

Applications of harmonic oscillator models to charge and energy transfer processes often rest on the shifted oscillator Hamiltonian, Eq. (2.65). Its transformation is readily performed; that is, we define for a single mode

$$\overline{H}_a = \hbar\omega(C^+C - \tilde{C}^+\tilde{C}) + \hbar\omega g_a(C^+ + C) \tag{3.563}$$

and obtain

$$\overline{H}_{a,\theta} = \hbar\omega(C^+C - \tilde{C}^+\tilde{C})$$
$$+ \hbar\omega g_a[(C^+ + C)\cosh(\theta_T) - (\tilde{C}^+ + \tilde{C})\sinh(\theta_T)]. \tag{3.564}$$

The extension to an arbitrary number of normal modes is straightforward. Treating systems with different electronic states (for instance, the electronic excitation between the ground and some excited states), thermal population of electronic excited states is usually negligible. This allows to introduce the tilde states for the vibrational subspace only and treat the electronic states in the physical Hilbert space. This has been the motivation for subtracting the ground state vibrational tilde Hamiltonian only in Eq. (3.563).

From the solution of the time-dependent Schrödinger equation (3.558), one obtains expectation values taking temperature effects into account. This comes at the price of doubling the number of DOFs. Using methods such as multilayer MCTDH introduced in Section 3.2.3, such simulations are possible even for high-dimensional systems. For instance, the MCTDH wave packet dynamics simulation shown in Figure 9.18 has also been performed at finite temperature using the approach outlined in this section; see Further Reading.

---

36) This can be shown using the relation $\exp(a\hat{A})\hat{B}\exp(-a\hat{A}) = \sum_{n=0}^{\infty}\frac{a^n}{n!}[\hat{A},\hat{B}]_n$, with $[\hat{A},\hat{B}]_0 = \hat{B}$ and $[\hat{A},\hat{B}]_{n>0} = [\hat{A},[\hat{A},\hat{B}]_{n-1}]$, which follows from the Baker–Campbell–Hausdorff formulae, cf. also Eq. (2.76).

3.15.2 Stochastic Schrödinger Equation

In Sections 3.10 and 3.11, the dynamics of the RDM was expressed in terms of the Feynman–Vernon influence functional. The closed-form expression for $\mathcal{F}(s^\pm)$ could be obtained for the common case of a relevant system coordinate s coupled to a harmonic oscillator reservoir. In Section 3.11, we have shown that for a bath correlation function that can be expressed as a sum of exponential terms, a nonperturbative and non-Markovian HEOM for the RDM can be derived. Suppose that the relevant system has N states, the dimension of the RDM is $N \times N$. In what follows, we address the question whether the information contained in the RDM can also be obtained by propagation of an N-dimensional state vector.

To simplify the notation, we consider a system–reservoir coupling, Eq. (3.198), having a single term only, that is[37]

$$H_{\text{S-R}} = K(s)\Phi(Z) = s\sum_\xi \hbar\gamma_\xi Z_\xi. \tag{3.565}$$

Note that we do not take into account the counter term in Eq. (3.381). Setting $t_N = t$, $t_0 = 0$, and recalling that $\mathcal{F}[s^+(t), s^-(t)] = \mathcal{F}(s^\pm)$, Eq. (3.387) can be written as

$$\mathcal{F}(s^\pm) = \exp\left\{ -\frac{1}{\hbar}\int_0^t dt'\int_0^{t'} dt''\ [s^+(t') - s^-(t')] \right.$$

$$\left. \times [C(t'-t'')s^+(t'') - C^*(t'-t'')s^-(t'')] \right\}$$

$$= \exp\left\{ -\frac{1}{\hbar}\int_0^t dt'\int_0^{t'} dt''\ [s^+(t')C(t'-t'')s^+(t'') \right.$$

$$\left. + s^-(t')C^*(t'-t'')s^-(t'')] \right\}$$

$$\times \exp\left\{ \frac{1}{\hbar}\int_0^t dt'\int_0^{t'} dt''\ [s^+(t')C^*(t'-t'')s^-(t'') \right.$$

$$\left. + s^-(t')C(t'-t'')s^+(t'')] \right\}. \tag{3.566}$$

Here, $C(t)$ is the harmonic oscillator correlation function (cf. Section 3.7.2). Further, $\mathcal{F}(s^\pm)$ has been rewritten such as to reveal the coupling between the paths $s^+(t)$ and $s^-(t)$ due to the second exponential factor. Interchanging the integration variables, this expression can be rewritten as

$$\exp\left\{ \frac{1}{\hbar}\int_0^t dt'\int_0^{t'} dt''\ [s^+(t')C^*(t'-t'')s^-(t'') + s^-(t')C(t'-t'')s^+(t'')] \right\}$$

$$= \exp\left\{ \frac{1}{\hbar}\int_0^t dt'\int_0^t dt''\ [s^+(t')C^*(t'-t'')s^-(t'')] \right\}. \tag{3.567}$$

---

37) Note that a formulation in terms of a general system operator $K(s)$ as in Section 3.11 is straightforward. Here, we use $K(s) = s$ to compare with the standard Feynman–Vernon path integral expression given in Section 3.10.

Next, we define a complex Gaussian stochastic process $\zeta(t)$ with the following properties:

$$\langle\langle \zeta(t) \rangle\rangle = 0, \tag{3.568}$$

$$\langle\langle \zeta(t)\zeta(t') \rangle\rangle = 0, \tag{3.569}$$

$$\langle\langle \zeta(t)\zeta^*(t') \rangle\rangle = C^*(t - t'), \tag{3.570}$$

$$\langle\langle \zeta^*(t')\zeta(t) \rangle\rangle = C(t' - t) . \tag{3.571}$$

where $\langle\langle \ldots \rangle\rangle$ denotes the classical ensemble average with respect to the stochastic process. With the help of these definitions, the exponential function in Eq. (3.567) can be written as

$$\exp\left\{ \frac{1}{\hbar} \int_0^t dt' \int_0^t dt'' \ [s^+(t')C^*(t' - t'')s^-(t'')] \right\}$$
$$= \left\langle\left\langle \exp\left\{ \frac{i}{\hbar} \int_0^t dt'[s^+(t')\zeta(t') - s^-(t')\zeta^*(t')] \right\} \right\rangle\right\rangle. \tag{3.572}$$

This equality can be verified using the cumulant expansion method that will be explained in detail in Section 4.3.4. What has been achieved with the introduction of the stochastic variables is a decoupling of the paths $s^+(t)$ and $s^-(t)$. Inspecting the time-evolution superoperator in path integral representation entering Eq. (3.392), that is

$$\mathcal{U}(s^\pm, t, s_0^\pm, 0) = \int_{s_0^\pm}^{s^\pm(t)} \mathcal{D}s^\pm \exp\left\{ \frac{i}{\hbar} S_S(s^+, t) \right\} \mathcal{F}(s^\pm) \exp\left\{ -\frac{i}{\hbar} S_S(s^-, t) \right\}, \tag{3.573}$$

we notice that upon introduction of the stochastic variables, it can be written in terms of two *independent* time-evolution operators

$$\mathcal{U}(s^\pm, t, s_0^\pm, 0) = \left\langle\left\langle U_\zeta(s^+, t, s_0^+, 0) \ U_\zeta^*(s^-, t, s_0^-, 0) \right\rangle\right\rangle, \tag{3.574}$$

with the path integral expression

$$U_\zeta(s, t, s_0, 0) = \int_{s_0}^{s(t)} \mathcal{D}s \ \exp\left\{ \frac{i}{\hbar} S_S(s, t) + \frac{i}{\hbar} \int_0^t dt' s(t')\zeta(t') \right.$$
$$\left. - \frac{1}{\hbar} \int_0^t dt' \int_0^{t'} dt'' \ s(t')C(t' - t'')s(t'') \right\}. \tag{3.575}$$

Hence, given some initial state vector $|\Psi_0\rangle$, its time evolution can be written as (recall the definition in Eq. (3.379))

$$|\Psi_\zeta(t)\rangle = U_\zeta(t, 0)|\Psi_0\rangle. \tag{3.576}$$

It is important to note that this equation gives the relevant system's state vector for a single stochastic trajectory $\zeta(t)$. The RDO in this pure state case is obtained by the ensemble average, that is

$$\hat{\rho}(t) = \langle\langle |\Psi_\zeta(t)\rangle\langle\Psi_\zeta(t)| \rangle\rangle. \tag{3.577}$$

For mixed states, the conditions must be adjusted accordingly (cf. Section 3.4.1). We conclude that the sketched procedure decouples bra and ket state evolution of the RDO, while being exact for the model Hamiltonian that has been used in the derivation of the influence functional. The method is also called stochastic unraveling of the influence functional.

In what follows, we derive the equation of motion for $|\Psi_\zeta(t)\rangle$. Using Eqs. (3.575) and (3.576), the time derivative is given by

$$\frac{\partial}{\partial t}|\Psi_\zeta(t)\rangle = -\frac{i}{\hbar}[H_S - s(t)\zeta(t)]|\Psi_\zeta(t)\rangle$$
$$-\frac{1}{\hbar}s(t)\int_0^t dt' \ C(t-t')s(t')|\Psi_\zeta(t)\rangle. \tag{3.578}$$

Considering the last term of this equation, one needs to take care of the fact that the state vector is actually a functional of the stochastic variable, that is $|\Psi[\zeta(t)]\rangle$. The functional derivative of $U_\zeta(t,0)$ with respect to $\zeta(t')$ is given by

$$\frac{\delta U_\zeta(t,0)}{\delta\zeta(t')} = \frac{i}{\hbar}s(t')U_\zeta(t,0) \ . \tag{3.579}$$

Using this expression, Eq. (3.581) can be rewritten, and we obtain the stochastic Schrödinger equation,

$$\frac{\partial}{\partial t}|\Psi_\zeta(t)\rangle = -\frac{i}{\hbar}[H_S - s\zeta(t)]|\Psi_\zeta(t)\rangle$$
$$-\frac{i}{\hbar}s(t)\int_0^t dt' \ C(t-t')\frac{\delta|\Psi_\zeta(t)\rangle}{\delta\zeta(t')}. \tag{3.580}$$

The appearance of the time integral on the right-hand side indicates the non-Markovian nature of this equation. The Markov limit is obtained by setting $C(t) \propto \delta(t)$, which renders the equation to become local in time.

In order to account for the non-Markovian time evolution, one follows an idea, which reminds on the derivation of the HEOM method in Section 3.11. Let us define the operator

$$A(t) = \int_{-\infty}^{+\infty} dt' \ C(t-t')\frac{\delta}{\delta\zeta(t')} \tag{3.581}$$

and introduce the auxiliary state vector

$$A(t)|\Psi_\zeta(t)\rangle = |\Psi_\zeta^{(1)}(t)\rangle. \tag{3.582}$$

Equation (3.580) thus becomes[38]

$$\frac{\partial}{\partial t}|\Psi_\zeta(t)\rangle = -\frac{i}{\hbar}[H_S - s\zeta(t)]|\Psi_\zeta(t)\rangle - \frac{i}{\hbar}s|\Psi_\zeta^{(1)}(t)\rangle. \tag{3.583}$$

To proceed, one needs to derive an equation of motion for the auxiliary state vector $|\Psi_\zeta^{(1)}(t)\rangle$, that is

$$\frac{\partial}{\partial t}|\Psi_\zeta^{(1)}(t)\rangle = \left(\frac{\partial}{\partial t}A(t)\right)|\Psi_\zeta(t)\rangle + A(t)\left(\frac{\partial}{\partial t}|\Psi_\zeta(t)\rangle\right). \tag{3.584}$$

The time derivative of the operator $A(t)$ is given by

$$\left(\frac{\partial}{\partial t}A(t)\right)|\Psi_\zeta(t)\rangle = \int_0^t dt' \frac{\partial C(t-t')}{\partial t}\frac{\delta|\Psi_\zeta(t)\rangle}{\delta\zeta(t')}. \tag{3.585}$$

---

38) Note that as compared to Eq. (3.580), the integration in $A(t)$ has been extended over the whole time axis. This is possible since system and reservoir are assumed to be initially uncorrelated such that $\delta|\Psi_\zeta(t=0)\rangle/\delta\zeta(t') = 0$ for $t' \in \mathbb{R}$. This makes the state vector at time t independent of the trajectory $\zeta(t')$ for $t' \notin [0,t]$.

Similar to the case of the HEOM method, a closed set of equations can be obtained if the correlation function has a sum-of-exponentials form, Eq. (3.399). To keep the notation simple, let us assume that there is only one term

$$C(t) = \eta e^{-\Omega t}. \tag{3.586}$$

As already noted in Section 3.11, η and Ω can be complex-valued. Using this expression as well as Eq. (3.580), one has

$$\frac{\partial}{\partial t}|\Psi_\zeta^{(1)}(t)\rangle = -\Omega|\Psi_\zeta^{(1)}(t)\rangle$$
$$+ A(t)\left(-\frac{i}{\hbar}[H_S - s\zeta(t)]|\Psi_\zeta(t)\rangle - \frac{i}{\hbar}s|\Psi_\zeta^{(1)}(t)\rangle\right). \tag{3.587}$$

Note that $A(t)$ commutes with the operators of the relevant system but not with the stochastic variable. For the latter, it holds that $[A(t), \zeta(t')]_- = C(t - t')$ such that we can write

$$\frac{\partial}{\partial t}|\Psi_\zeta^{(1)}(t)\rangle = \left(-\frac{i}{\hbar}H_S - \Omega + s\zeta(t)\right)|\Psi_\zeta^{(1)}(t)\rangle + sC(0)|\Psi_\zeta(t)\rangle$$
$$- \frac{i}{\hbar}sA(t)|\Psi_\zeta^{(1)}(t)\rangle. \tag{3.588}$$

Introducing $|\Psi_\zeta^{(0)}(t)\rangle = |\Psi_\zeta(t)\rangle$ and $|\Psi_\zeta^{(2)}(t)\rangle = A(t)|\Psi_\zeta^{(1)}(t)\rangle$, we have

$$\frac{\partial}{\partial t}|\Psi_\zeta^{(1)}(t)\rangle = \left(-\frac{i}{\hbar}H_S - \Omega + s\zeta(t)\right)|\Psi_\zeta^{(1)}(t)\rangle + sC(0)|\Psi_\zeta^{(0)}(t)\rangle$$
$$- \frac{i}{\hbar}s|\Psi_\zeta^{(2)}(t)\rangle. \tag{3.589}$$

One can proceed by deriving an equation of motion for $|\Psi_\zeta^{(2)}(t)\rangle$ and so on. Eventually, one obtains the hierarchy of pure states (HOPS) equations

$$\frac{\partial}{\partial t}|\Psi_\zeta^{(k)}(t)\rangle = \left(-\frac{i}{\hbar}H_S - k\Omega + s\zeta(t)\right)|\Psi_\zeta^{(k)}(t)\rangle$$
$$+ skC(0)|\Psi_\zeta^{(k-1)}(t)\rangle - \frac{i}{\hbar}s|\Psi_\zeta^{(k+1)}(t)\rangle. \tag{3.590}$$

This is a formally exact equation of motion for the physical state $|\Psi_\zeta^{(0)}(t)\rangle$, which is coupled to the auxiliary states $|\Psi_\zeta^{(k>0)}(t)\rangle$. It has to be solved subject to the initial conditions $|\Psi_\zeta^{(0)}(t)\rangle = |\Psi(0)\rangle$ and $|\Psi_\zeta^{(k>0)}(0)\rangle = 0$. Of course, in practice, one needs to truncate the hierarchy of equations such that it does not influence the resulting physical state evolution. Using the solution of the HOPS equations for an ensemble of stochastic trajectories expectation values are obtained using Eq (3.577). In numerical applications, Eq. (3.590) is used only after transformation to a form that enables better sampling when calculating the ensemble average. For more details and applications, see Further Reading.

References

1 G. S. Kachalova et al., Science **284**, 473 (1999).

2 J. Hu et al., J. Chem. Phys. **133**, 101106 (2010).

3 S. A. Egorov et al., J. Phys. Chem. A **103**, 9494 (1999).

4 A. G. Redfield, Adv. Magn. Res. **1**, 1 (1965).

5 R.-X. Xu and Y. Yan, Phys. Rev. E **75**, 031107 (2007).

6 J. E. Subotnik et al., Annu. Rev. Phys. Chem. **67**, 387 (2016).

7 J. C. Tully, J. Chem. Phys. **93**, 1061 (1990).

Further Reading

- General time–dependent view on quantum mechanics
  D. J. Tannor, *Introduction to Quantum Mechanics: A Time–Dependent Perspective*, (University Science Books, Sausalito, CA, USA, 2018).
- General relaxation theory:
  K. Blum, *Density Matrix Theory and Applications*, (Springer-Verlag, Berlin, 2012).
  H.-P. Breuer and F. Petruccione, *The Theory of Open Quantum Systems*, (Oxford University Press, Oxford, 2006).
- Superoperator approach to dissipative dynamics:
  E. Fick and G. Sauermann, *The Quantum Statistics of Dynamic Processes*, (Springer-Verlag, Berlin, 1990).
- Various topics in the theory of dissipative quantum dynamics:
  A. Nitzan, *Chemical Dynamics in Condensed Phases*, (Oxford University Press, Oxford, 2014).
  U. Weiss, *Quantum Dissipative Systems*, (World Scientific, Singapore, 2012).
- Chemical perspective on rate theory:
  B. Peters, *Reaction Rate Theory and Rare Events*, (Elsevier, Amsterdam, 2017).
- Numerical path integral methodology
  N. Makri, J. Phys. Chem. A **102**, 4414 (1998).
- Hierarchy of equations of motion approach
  Y. Tanimura, J. Chem. Phys. **153**, 020901 (2020).
  R.-X. Xu and Y. Yan, Phys. Rev. E **75**, 031107 (2007).
- Hierarchy of open pure states approach
  D. Suess, A. Eisfeld, and W. Strunz, Phys. Rev. Lett. **113**, 150403 (2014).
- Thermofield dynamics theory and applications
  R. Borrelli and M. F. Gelin, Sci. Rep. **7**, 9127 (2017).
  Y. Takahashi and H. Umezawa, Int. J. Mod. Phys. B **10**, 1755 (1996).
- MCTDH theory and applications
  F. Gatti, B. Lasorne, H.-D. Meyer, and A. Nauts, *Applications of Quantum Dynamics in Chemistry*, (Springer International Publishing AG, 2017).
- Surface hopping
  L. Wang, J. Qiu, X. Bai, and J. Xu, WIREs: Comput. Mol. Sci. e1435 (2019).

4

Interaction of Molecular Systems with Radiation Fields

Charge and energy transfer processes can be investigated by means of laser spectroscopy. This gives access not only to the properties of stationary states but also to the real-time nonequilibrium dynamics. In this chapter, we review some fundamental aspects of the interaction between molecular systems and radiation fields. First, we present the interaction Hamiltonian in dipole approximation, which can be derived from the minimal coupling Hamiltonian describing the coupled system of interacting charges and the radiation field. The considerations will be extended to dielectrics, and the polarization field will be introduced, which depends on the dynamics of the molecules driven by the external electric field.

Next, the linear absorption coefficient will be derived on the basis of Beer's law. It will be shown that it can be written as the Fourier transform of the autocorrelation function of the molecular dipole operator. Further, we address the rate of spontaneous emission, which requires to consider a quantized description of the radiation field.

Nonlinear response functions are introduced starting from a systematic representation of the polarization field in powers of the electric field strength combined with time-dependent perturbation theory. Explicit expressions are given for a three-level model with weak system–bath coupling, and for a two-level model with strong coupling to vibrational degrees of freedom. The third-order polarization is discussed, and its relation to different experimental techniques is established. Here, pump–probe and two-dimensional spectroscopy are discussed in some detail. We also give a brief account on nonperturbative methods for obtaining the polarization by wave packet propagation under explicit inclusion of the electric field.

4.1 Introduction

In what follows we give a brief review of classical electrodynamics. The starting point are the Maxwell equations, which read

$$\nabla \times \boldsymbol{E}(\boldsymbol{r}, t) = -\frac{1}{c} \frac{\partial \boldsymbol{B}(\boldsymbol{r}, t)}{\partial t}, \tag{4.1}$$

$$\nabla \times \boldsymbol{B}(\boldsymbol{r}, t) = \frac{1}{c} \frac{\partial \boldsymbol{E}(\boldsymbol{r}, t)}{\partial t} + \frac{4\pi}{c} \boldsymbol{j}(\boldsymbol{r}, t), \tag{4.2}$$

$$\nabla \cdot \boldsymbol{E}(\boldsymbol{r}, t) = 4\pi \rho(\boldsymbol{r}, t), \tag{4.3}$$

$$\nabla \cdot \boldsymbol{B}(\boldsymbol{r}, t) = 0, \tag{4.4}$$

where $\boldsymbol{E}$ and $\boldsymbol{B}$ are the electric and magnetic fields, respectively. Further, we have the charge density $\rho(\boldsymbol{r}, t)$ and the current density $\boldsymbol{j}(\boldsymbol{r}, t)$. The latter two quantities are used to characterize the motion of electrons and nuclei in the considered material system.

Instead of the physical fields, one usually introduces a vector and a scalar potential $\boldsymbol{A}(\boldsymbol{r}, t)$ and $U(\boldsymbol{r}, t)$, respectively, which are related to the fields via

$$\boldsymbol{B}(\boldsymbol{r}, t) = \nabla \times \boldsymbol{A}(\boldsymbol{r}, t), \tag{4.5}$$

$$\boldsymbol{E}(\boldsymbol{r}, t) = -\frac{1}{c} \frac{\partial \boldsymbol{A}(\boldsymbol{r}, t)}{\partial t} - \nabla U(\boldsymbol{r}, t). \tag{4.6}$$

The ambiguity with respect to gauge transformations can be removed by requiring (Coulomb gauge)

$$\nabla \cdot \boldsymbol{A}(\boldsymbol{r}, t) = 0. \tag{4.7}$$

Note that this condition makes the vector potential a transverse vector field $\boldsymbol{A} = \boldsymbol{A}^{\perp}$.[1] Furthermore, this vector field can be supplemented by a contribution of an *externally* applied field to account for the interaction of the particle system, e.g. with a laser field. The Hamiltonian in the Coulomb gauge is given by (minimal coupling Hamiltonian)

$$H = \sum_u \frac{1}{2m_u} \left[\boldsymbol{p}_u - \frac{q_u}{c} \boldsymbol{A}(\boldsymbol{x}_u, t) \right]^2 + \frac{1}{2} \sum_{u \neq v} \frac{q_u q_v}{|\boldsymbol{x}_u - \boldsymbol{x}_v|} + H_{\text{field}}. \tag{4.8}$$

The expression corresponds to an abbreviated notation of the molecular Hamiltonian, Eq. (2.1), with u and v counting electrons and nuclei simultaneously (m_u are the respective masses, $\boldsymbol{x}_u$ the coordinates, $\boldsymbol{p}_u$ the momenta, and q_u the charges). The Hamiltonian of the free radiation field is given by the transverse electric field and the magnetic field according to

$$H_{\text{field}} = \frac{1}{8\pi} \int dr [\boldsymbol{E}^{\perp 2}(\boldsymbol{r}) + \boldsymbol{B}^2(\boldsymbol{r})]. \tag{4.9}$$

----

1) If the field is expanded with respect to plane waves $\sim \exp(i\boldsymbol{k}\boldsymbol{r})$, the transversal part of the field is given by that contribution where all expansion coefficients are perpendicular to the actual wavevector $\boldsymbol{k}$, here $\boldsymbol{k}\boldsymbol{A}^{\perp}(\boldsymbol{k}) = 0$.

For molecular systems it is usually a good approximation to account for the Coulomb interaction between the charges only and to consider the coupling between particles and the transverse external field, i.e. $\boldsymbol{A} = \boldsymbol{A}^{\text{ext}}$. Further, the contribution of H_{field} to the total Hamiltonian is neglected. Another simplification arises upon restriction to wavelengths of the external field that exceed the spatial extension of the molecular system (long wavelength approximation). In this case, the canonical momentum becomes $\boldsymbol{p}_u - q_u\boldsymbol{A}(\boldsymbol{X}_m, t)/c$, where $\boldsymbol{X}_m$ is a representative point for the mth molecule (for example, the center of mass). Note that Eq. (4.8) contains two radiation–matter interaction terms, i.e. $\propto \boldsymbol{p}_u \cdot \boldsymbol{A}$ and $\propto \boldsymbol{A}^2$. Within the long wavelength approximation a simplification arises upon using the time-dependent unitary transformation (displacement operator, cf. Section 2.5.2)

$$
\begin{aligned}
D(t) &= \exp\left\{ -\frac{i}{\hbar c}\sum_u q_u \boldsymbol{x}_u \boldsymbol{A}(\boldsymbol{X}_m, t) \right\} \\
&= \exp\left\{ -\frac{i}{\hbar c}\hat{\boldsymbol{\mu}}_m \boldsymbol{A}(\boldsymbol{X}_m, t) \right\},
\end{aligned}
\tag{4.10}
$$

where we introduced the dipole operator for the mth molecule $\hat{\boldsymbol{\mu}}_m = \sum_u q_u \boldsymbol{x}_u$. Application of the transformation to the momentum operator gives

$$
D(t)\boldsymbol{p}_u D^+(t) = \boldsymbol{p}_u + \frac{q_u}{c}\boldsymbol{A}(\boldsymbol{X}_m, t).
\tag{4.11}
$$

Since the transformation operator is time dependent, the unitary transformation of the Hamiltonian reads as

$$
\tilde{H}(t) = D(t)HD^+(t) + i\hbar\left(\frac{\partial D(t)}{\partial t}\right)D^+(t).
\tag{4.12}
$$

Using Eq. (4.6), we have

$$
\begin{aligned}
i\hbar\left(\frac{\partial D(t)}{\partial t}\right)D^+(t) &= \frac{1}{c}\hat{\boldsymbol{\mu}}_m\frac{\partial \boldsymbol{A}(\boldsymbol{X}_m, t)}{\partial t} \\
&= -\hat{\boldsymbol{\mu}}_m \boldsymbol{E}(\boldsymbol{X}_m, t).
\end{aligned}
\tag{4.13}
$$

Thus, the transformed Hamiltonian becomes

$$
\tilde{H}(t) = \sum_u \frac{1}{2m_u}\boldsymbol{p}_u^2 + \frac{1}{2}\sum_{u \neq v}\frac{q_u q_v}{|\boldsymbol{x}_u - \boldsymbol{x}_v|} - \hat{\boldsymbol{\mu}}_m \boldsymbol{E}(\boldsymbol{X}_m, t).
\tag{4.14}
$$

The first two terms reproduce the molecular Hamiltonian H_{mol}, Eq. (2.1), and the last term represents the interaction of the dipole moment $\hat{\boldsymbol{\mu}}_m$ of molecule m with the electric field at the chosen point $\boldsymbol{X}_m$. It gives the dipole approximation of the molecule–field interaction and is written in what follows as

$$
H_{\text{field}}^{(m)}(t) = -\boldsymbol{E}(\boldsymbol{X}_m, t)\,\hat{\boldsymbol{\mu}}_m.
\tag{4.15}
$$

So far, we have considered the case of individual molecules. In order to proceed to condensed phase situations, we will make several assumptions: (i) We will not be concerned with magnetization effects in the medium, and the respective contributions that are proportional to the magnetic field will be skipped. (ii) We adopt the point of view that molecules in the condensed phase form a dielectric medium with electronically polarizable units that are sufficiently described as dipoles

(cf. Section 2.7.1). (iii) There are *no* free charges giving rise to respective densities and currents. (iv) Only those spectroscopic experiments are considered that probe macroscopic properties of the matter so that one can use Maxwell's macroscopic electrodynamics for dielectrics.

The term *macroscopic* indicates that the description does not account for those parts of the electromagnetic field varying on a microscopic length scale of some nanometers. These parts are not measurable in those experiments where the spectrometer is far away from the illuminated sample. In other words, only the so-called *far field* is of interest, and any near-field contribution is eliminated from the theory.[2] To include the far field only, we proceed as in Section 2.7.1 and carry out an averaging of the field with respect to a volume element ΔV. This volume element should contain a sufficiently large number of molecules. In particular, ΔV has to be large in comparison to the size of the molecules. Furthermore, the externally applied field should vary weakly inside ΔV. Then, we can discretize the sample volume by the elements ΔV and label every element by the spatial vector $\boldsymbol{x}$. These vectors are discrete on the length scale of the volume elements, but from a macroscopic point of view, they can be considered as continuous quantities.

The key quantity of the electrostatics as well as of the electrodynamics of dielectrics is the *macroscopic* polarization field vector $\boldsymbol{P}(\boldsymbol{x}, t)$ that, according to our assumption, corresponds to the dipole density of the medium. As a macroscopic vector field its definition must contain the averaging with respect to the volume elements ΔV. This has already been done in Eq. (2.125), which can be generalized from the static to the dynamic case as follows:

$$\boldsymbol{P}(\boldsymbol{x}, t) = \frac{1}{\Delta V(\boldsymbol{x})} \sum_{m \in \Delta V(\boldsymbol{x})} \boldsymbol{d}_m(t). \tag{4.16}$$

It gives the polarization as the sum of molecular dipole moments $\boldsymbol{d}_m(t)$ contained in the volume element $\Delta V(\boldsymbol{x})$ in the neighborhood of the point $\boldsymbol{x}$ versus ΔV (dipole density). Since molecules are treated quantum mechanically, $\boldsymbol{d}_m(t)$ is the time-dependent expectation value of the molecular (electric) dipole operator $\hat{\boldsymbol{\mu}}_m$ given by

$$\hat{\boldsymbol{\mu}}_m = \sum_{u \in m} q_u \boldsymbol{x}_u = -\sum_j e \boldsymbol{r}_j^{(m)} + \sum_n e z_n^{(m)} \boldsymbol{R}_n^{(m)}. \tag{4.17}$$

With the help of this operator the interaction Hamiltonian follows from Eq. (4.15) as

$$H_{\text{int}}(t) = \sum_m H_{\text{field}}^{(m)}(t) = -\sum_m \boldsymbol{E}(\boldsymbol{X}_m, t) \, \hat{\boldsymbol{\mu}}_m. \tag{4.18}$$

This expression is often termed the semiclassical molecule–field interaction Hamiltonian. This Hamiltonian of light–matter interaction supplements the Hamiltonian of the molecular system. In contrast to the subsequent chapters we have neglected molecule–molecule interactions responsible for charge and energy transfer here.

---

2) The situation is different in near-field spectroscopy where the near field on a subwavelength scale is measured.

Therefore, the Hamiltonian of all molecules in the sample can be written as a sum of individual molecular contributions.[3]

Neglecting intermolecular interactions the macroscopic optical properties of the material system are calculated by determining the interaction of a single molecule with the radiation field first. In a second step all individual molecular contributions are summed to give the macroscopic response.

The time-dependent expectation value of the dipole operator entering Eq. (4.16) can be written in two ways:

$$\boldsymbol{d}_m(t) = \mathrm{tr}\{\hat{W}_{\mathrm{eq}}U^+(t,t_0)\hat{\boldsymbol{\mu}}_m U(t,t_0)\} \equiv \mathrm{tr}\{\hat{W}(t)\hat{\boldsymbol{\mu}}_m\}. \tag{4.19}$$

In the first expression, $\hat{W}_{\mathrm{eq}} = \exp\{-H_{\mathrm{mol}}/k_{\mathrm{B}}T\}/\mathcal{Z}$ is the equilibrium statistical operator in the absence of an external field. The time dependence of the dipole operator is given by the Hamiltonian, which includes the external electric field via $H_{\mathrm{field}}^{(m)}(t)$ (see Eq. (4.15)). In the second part of Eq. (4.19), the time evolution has been transferred to the statistical operator to give $\hat{W}(t) = U(t,t_0)\hat{W}_{\mathrm{eq}}U^+(t,t_0)$. Both variants to compute $\boldsymbol{d}_m(t)$ will be used in what follows.

Introducing an expansion with respect to the (adiabatic) electronic states of the mth molecule $|\phi_{ma}\rangle$ as

$$\hat{\boldsymbol{\mu}}_m = \sum_{a,b} \langle \phi_{ma}| \hat{\boldsymbol{\mu}}_m |\phi_{mb}\rangle |\phi_{ma}\rangle \langle \phi_{mb}|, \tag{4.20}$$

it is straightforward to select all those electronic states involved in a particular experiment and to exclude all unimportant states from the summation. For example, if the molecules do not possess a permanent dipole moment, it suffices to use off-diagonal matrix elements only, leading to the *transition dipole moments* (transition matrix elements)

$$\boldsymbol{d}_{ab}^{(m)} = \langle \phi_{ma}| \hat{\boldsymbol{\mu}}_m |\phi_{mb}\rangle. \tag{4.21}$$

A special case arises when the ensemble of molecular systems does not show the phenomenon of inhomogeneous broadening. In such a situation, all molecules within the volume element $\Delta V(\boldsymbol{x})$ around point $\boldsymbol{x}$ are identical, and we may replace the summation with respect to the various dipole moments in Eq. (4.16) by a representative dipole moment at $\boldsymbol{x}$ times the volume density n_{mol} of molecules in the sample volume:

$$\boldsymbol{P}(\boldsymbol{x};t) = n_{\mathrm{mol}}\boldsymbol{d}(\boldsymbol{x};t). \tag{4.22}$$

Note that in the present case the spatial variation of $\boldsymbol{d}$ is exclusively determined by the spatial dependence of the radiation field. In order to discuss this issue in more detail, we recall Maxwell's macroscopic equations for dielectric media under the assumption of vanishing free charges and nonmagnetic systems

---

3) This noninteracting single-molecule concept is extended in the so-called *local field approximation* to include the effect of the averaged field of all other molecules on a particular molecule. While this approach is reasonable for weakly to moderately interacting molecules, it cannot account for many effects that occur in strongly interacting molecular aggregates (see Chapter 9).

$$\nabla \times \boldsymbol{E} = -\frac{1}{c} \frac{\partial \boldsymbol{B}}{\partial t}, \tag{4.23}$$

$$\nabla \times \boldsymbol{B} = \frac{1}{c} \frac{\partial \boldsymbol{D}}{\partial t}, \tag{4.24}$$

$$\nabla \cdot \boldsymbol{D} = 0, \tag{4.25}$$

$$\nabla \cdot \boldsymbol{B} = 0, \tag{4.26}$$

where the dielectric displacement vector $\boldsymbol{D} = \boldsymbol{E} + 4\pi\boldsymbol{P}$ has been introduced.

According to Eq. (4.19), the determination of $\boldsymbol{P}$ requires the solution of the dynamical equations for the molecule under the action of the field, that is the time-dependent Schrödinger equation or the density operator equation. If this has been accomplished, the response of the molecules is available. Further the polarization introduced in Eq. (4.16) is known as a function (functional) $\boldsymbol{P}[\boldsymbol{E}]$ of the electric field strength. Taking the curl of the equation for $\nabla \times \boldsymbol{E}$, one obtains a closed equation for the electric field strength

$$\left(\frac{\partial^2}{\partial t^2} - c^2 \Delta \right) \boldsymbol{E} = -4\pi \frac{\partial^2}{\partial t^2} \boldsymbol{P}[\boldsymbol{E}]. \tag{4.27}$$

Since this equation contains again the polarization which is obtained from the dynamical equations of the molecular system, a self-consistent solution of this closed set of equations is required.

In general, the polarization $\boldsymbol{P}$ will be a nonlinear functional of the electric field $\boldsymbol{E}$. In the following section we will discuss the simplest case of a linear relationship, that is $\boldsymbol{P} = \chi\boldsymbol{E}$ (cf. Section 2.7.1.1), where the response of the molecular system is completely determined by the linear electric susceptibility χ. The nonlinear response will be considered in Section 4.3.

4.2 Absorption of Light

4.2.1 Linear Absorption Coefficient

If the polarization depends linearly on the external field, Eq. (4.27) is solved by a plane wave ansatz for the electric field,

$$\boldsymbol{E}(\boldsymbol{x}, t) = \boldsymbol{n}E_0 \exp\{i(\boldsymbol{k}\boldsymbol{x} - \omega t)\} + \text{c.c.} \tag{4.28}$$

Here, $\boldsymbol{n}$ and E_0 are the polarization vector and field amplitude, respectively. Further, the field is assumed to be monochromatic with carrier frequency ω and wavevector $\boldsymbol{k}$.

For the determination of the linear absorption coefficient α, we consider a platelet of a dielectric medium of thickness d extending into the z-direction. In the x and y directions (lateral directions), there should be no geometric restriction. The strictly monochromatic light is supposed to propagate in the z-direction with perpendicular incidence on the platelet. For simplicity, we let the platelet thickness d go to infinity, $d \to \infty$, such that there is a single reflecting boundary between the dielectric

and the vacuum (dielectric half-space). Thus, the electric field strength along the propagation direction can be written as

$$\mathbf{E}(z,t) = \mathbf{n}\, e^{-i\omega t}\left(\theta(-z)\{E_0 e^{ik_{\text{vac}}z} + E_r e^{-ik_{\text{vac}}z}\} + \theta(z)E_t e^{ik_{\text{med}}z}\right) + \text{c.c.} \qquad (4.29)$$

The unit-step function $\theta(z)$ has been used to discriminate between the part in the medium (transmitted part) with amplitude E_t and wavenumber $k_{\text{med}} = \omega\sqrt{\varepsilon}/c$ in the z-direction and the field in the vacuum. The latter contains the incoming part with amplitude E_0 and the reflected part with amplitude E_r, both with wavenumber $k_{\text{vac}} = \omega/c$. The unit vector $\mathbf{n}$ defines the polarization direction of the field. The different field components are determined via the boundary conditions.

In general, the dielectric function $\varepsilon(\omega)$ is complex. The decay of the field intensity inside the medium is determined by the imaginary part of k_{med} according to Beer's law

$$I(z) = I(0)\, e^{-\alpha z}, \qquad (4.30)$$

where the absorption coefficient $\alpha(\omega) = 2\text{Im}(k_{\text{med}}) = 2\omega\,\text{Im}\sqrt{\varepsilon(\omega)}/c$ depends on the frequency of the light wave traveling through the platelet. Usually one has $\text{Re}(\varepsilon) \gg \text{Im}(\varepsilon)$, so that $\text{Im}\sqrt{\varepsilon} \approx \text{Im}(\varepsilon)/2\sqrt{\text{Re}(\varepsilon)}$. Assuming a frequency-independent index of refraction $n = \sqrt{\text{Re}(\varepsilon)}$, we obtain

$$\alpha(\omega) = \frac{4\pi\omega}{nc}\,\text{Im}\chi(\omega), \qquad (4.31)$$

where $\chi(\omega) = (\varepsilon(\omega) - 1)/4\pi$ is the linear dielectric susceptibility. The actual frequency dependence of the absorption coefficient is determined by the properties of the molecules.

Provided that the rate of absorption k_{abs} of a certain molecule is known, the absorption coefficient $\alpha(\omega)$ can be obtained as follows. Consider a macroscopic sample volume V containing N_{mol} noninteracting molecules absorbing light at frequency ω. The sample volume should have a surface cross section of area A where the light goes through perpendicularly. We take a small section of length dz and volume Adz and determine the change in the radiation field energy dE if absorption takes place. It is given during the time interval dt as

$$dE = -N_{\text{mol}}\frac{Adz}{V}\hbar\omega\, k_{\text{abs}}\, dt. \qquad (4.32)$$

Here, $N_{\text{mol}}Adz/V$ gives the fraction of molecules inside the considered segment, and $\hbar\omega k_{\text{abs}}dt$ is the mean energy absorbed by a single molecule in the time interval dt. Since the field energy decreases, the minus sign has been introduced.

Instead of dE, we can calculate the change in the field energy density $du = dE/Adz$. Given the volume density $n_{\text{mol}} = N_{\text{mol}}/V$ of the absorbing molecules, the change in energy density per time follows as

$$\frac{du}{dt} = -n_{\text{mol}}\,\hbar\omega\, k_{\text{abs}}. \qquad (4.33)$$

The continuity equation $du/dt = dI/dz$, which is a direct consequence of Maxwell's equations, allows to change from the energy density to the field intensity I. We further note that $I = c\,E_0^2/2\pi$, which is valid for a monochromatic field, and get

$$\frac{dI}{dz} = -\frac{2\pi n_{\text{mol}}}{c\,E_0^2}\,\hbar\omega\,k_{\text{abs}}. \tag{4.34}$$

Comparing this expression with the definition of the absorption coefficient α according to $dI/dz = -\alpha I$ (cf. Eq. (4.30)) enables us to identify the frequency-dependent absorption coefficient as

$$\alpha(\omega) = \frac{2\pi n_{\text{mol}}}{c\,E_0^2}\,\hbar\omega\,k_{\text{abs}}. \tag{4.35}$$

Comparing Eqs. (4.31) and (4.35), we notice the relation between $\text{Im}\,\chi(\omega)$ and k_{abs}. The absorption rate can be determined either from the knowledge of the system's eigenstates (Golden Rule) or using the time correlation functions ($\text{Im}\,\chi(\omega)$). In the following section, a correlation function expression will be derived. The relation to the Golden Rule will be discussed in Chapter 6.

4.2.2 Dipole–Dipole Correlation Function

Our objective is to obtain a formula for the absorption coefficient that does not rely on a particular representation of the Hamiltonian but is based on a general prescription of Eq. (4.19).

For simplicity, let us focus on a homogeneous sample and therefore start with Eq. (4.22) for the macroscopic polarization including Eq. (4.19) for the time-dependent expectation value of the dipole operator. In order to carry out a perturbation expansion with respect to $H_{\text{field}}(t)$ (index m skipped), that is in powers of the electric field strength, we separate $U(t, t_0)$ in Eq. (4.19) into the molecular part $U_{\text{mol}}(t - t_0) = \exp(-iH_{\text{mol}}(t - t_0)/\hbar)$ and into the S-operator (cf. Section 3.2.2)

$$S(t, t_0) = \hat{T}\exp\left(-\frac{i}{\hbar}\int_{t_0}^{t} dt'\,H_{\text{field}}^{(I)}(t')\right). \tag{4.36}$$

The coupling Hamiltonian in the interaction representation reads $H_{\text{field}}^{(I)}(t) = U_{\text{mol}}^{+}(t - t_0)H_{\text{field}}(t)\,U_{\text{mol}}(t - t_0)$. Accordingly, Eq. (4.19) becomes[4]

$$\boldsymbol{d}(\boldsymbol{x}; t) = \text{tr}\{\hat{W}_{\text{eq}}S^{+}(t, t_0)\hat{\boldsymbol{\mu}}^{(I)}(t)S(t, t_0)\}. \tag{4.37}$$

The different contributions in powers of the field strength are obtained by a series expansion of $S(t, t_0)$. Here, we concentrate on the first-order contribution (higher order terms have to be considered in the case of nonlinear spectroscopy, cf. Section 4.3). The expansion up to the first order in the field strength gives (the zeroth-order

---

4) We remind here on the fact that the operator $\hat{\boldsymbol{\mu}}^{(I)}(t)$ is independent of the spatial position $\boldsymbol{x}$ since the sample's heterogeneity has been neglected. However, the electric field depends on $\boldsymbol{x}$ due to the plane wave factor, and just this dependence enters the expectation value via the S-operator.

term does not contribute because of the assumed absence of a macroscopic dipole density in the equilibrium)

$$\boldsymbol{d}(\boldsymbol{x};t) \approx \mathrm{tr}\left\{\hat{W}_{\mathrm{eq}}\left[1 + S^{(1)+}(t,t_0)\right]\hat{\boldsymbol{\mu}}^{(I)}(t)\left[1 + S^{(1)}(t,t_0)\right]\right\}. \tag{4.38}$$

Here, $S^{(1)}$ denotes the first-order term of the S-operator expansion, Eq. (4.36), with respect to the electric field strength

$$S^{(1)}(t,t_0) = \frac{i}{\hbar}\int_{t_0}^{t} d\tau \; \boldsymbol{E}(\tau)\hat{\boldsymbol{\mu}}^{(I)}(\tau). \tag{4.39}$$

Collecting the terms that are linear in the field, one obtains the linear polarization from Eqs. (4.22) and (4.38) as follows (using $t_0 \to -\infty$):

$$\boldsymbol{P}^{(1)}(\boldsymbol{x},t) = \int_{0}^{\infty} dt_1 \; R^{(1)}(t_1)\boldsymbol{E}(\boldsymbol{x},t-t_1). \tag{4.40}$$

Here, $R^{(1)}(t)$ is the linear response function, which is a second rank tensor according to

$$R^{(1)}(t) = \frac{i}{\hbar}\theta(t)n_{\mathrm{mol}}\mathrm{tr}\left\{\hat{W}_{\mathrm{eq}}\left[\hat{\boldsymbol{\mu}}^{(I)}(t),\hat{\boldsymbol{\mu}}^{(I)}(0)\right]_{-}\right\}. \tag{4.41}$$

The right-hand side of this equation contains the *dipole–dipole correlation function*

$$C_{jj'}^{(\mathrm{d-d})}(t) = \mathrm{tr}\left\{\hat{W}_{\mathrm{eq}}\left[\hat{\mu}_{j}^{(I)}(t),\hat{\mu}_{j'}^{(I)}(0)\right]_{-}\right\}. \tag{4.42}$$

In the following equation, we only consider the case of randomly oriented molecules where it is sufficient to use

$$C_{\mathrm{d-d}}(t) = \sum_{j} C_{jj}^{(\mathrm{d-d})}(t). \tag{4.43}$$

In order to establish the relation to Eq. (4.31), we introduce the Fourier transform of the polarization $\boldsymbol{P}^{(1)}(\boldsymbol{x},\omega)$. Due to the θ-function in Eq. (4.41), the lower limit of the integral in Eq. (4.40) can be extended to $-\infty$, and the convolution-type integral gives

$$\boldsymbol{P}^{(1)}(\boldsymbol{x},\omega) = \chi(\omega)\boldsymbol{E}(\boldsymbol{x},\omega), \tag{4.44}$$

where the linear dielectric susceptibility is defined as

$$\chi(\omega) = \int_{-\infty}^{\infty} dt \; e^{i\omega t} \; R^{(1)}(t). \tag{4.45}$$

Combining Eqs. (4.31), (4.42), and (4.45), the absorption coefficient can be expressed in terms of the Fourier transform of the dipole–dipole correlation function,

$$\alpha(\omega) = \frac{4\pi\omega n_{\mathrm{mol}}}{3\hbar c}\mathrm{Re}\int_{0}^{\infty} dt \; e^{i\omega t} \; C_{\mathrm{d-d}}(t). \tag{4.46}$$

Finally, we emphasize that in the derivation we did not refer to any specific form of the molecular Hamiltonian. It can in principle describe any

type of PES but can also contain contributions from an environment. Thus, Eq. (4.46) is suitable for computation of the absorption spectrum of molecular systems in the condensed phase.

4.3 Nonlinear Optical Response

4.3.1 Nonlinear Polarization

The field of nonlinear optics is of a diversity that goes far beyond the scope of this book. Therefore, we will only outline some basic concepts that provide the background for the understanding of the methods for detecting the elementary charge and the energy transfer processes. For a more detailed discussion, we refer the reader to the various textbooks existing on the different facets of this field (see Further Reading).

Extending the treatment of Section 4.2.1, the polarization field can be expanded in powers of the electric field strength according to

$$\boldsymbol{P}(\boldsymbol{x};t) = \boldsymbol{P}^{(1)}(\boldsymbol{x};t) + \boldsymbol{P}^{(2)}(\boldsymbol{x};t) + \boldsymbol{P}^{(3)}(\boldsymbol{x};t) + \dots$$
$$= \boldsymbol{P}^{(1)}(\boldsymbol{x};t) + \boldsymbol{P}^{(\mathrm{NL})}(\boldsymbol{x};t). \tag{4.47}$$

Here, $\boldsymbol{P}^{(n)}$ ($n = 1, 2, \dots$) is the nth-order polarization, that is it is of the nth order in the field strength $\boldsymbol{E}$ (a zeroth-order contribution does not appear since we assumed the absence of a permanent polarization). Inserting Eq. (4.47) into Eq. (4.27), one has

$$\Delta \boldsymbol{E} - \frac{1}{c^2} \frac{\partial^2}{\partial t^2} \left(\boldsymbol{E} + 4\pi \boldsymbol{P}^{(1)} \right) = \frac{4\pi}{c^2} \frac{\partial^2}{\partial t^2} \boldsymbol{P}^{(\mathrm{NL})}. \tag{4.48}$$

Assuming that the nonlinear experiment is performed such that losses due to linear absorption can be neglected, and that the index of refraction n_{r} is not frequency dependent, one obtains (note Eq. (4.44))

$$\Delta \boldsymbol{E} - \frac{n_{\mathrm{r}}^2}{c^2} \frac{\partial^2}{\partial t^2} \boldsymbol{E} = \frac{4\pi}{c^2} \frac{\partial^2}{\partial t^2} \boldsymbol{P}^{(\mathrm{NL})}. \tag{4.49}$$

The right-hand side expresses the fact that the nonlinear interaction of the incoming fields with the molecular system leads to a nonlinear polarization field that is the source of the generated signal field.

In general, the incoming fields can be written as

$$\boldsymbol{E}(\boldsymbol{x}, t) = \sum_{p=1}^{N} \boldsymbol{n}_p E_p(t) \exp\{i(\boldsymbol{k}_p \boldsymbol{x} - \omega_p t)\} + \mathrm{c.c.} \tag{4.50}$$

Here, N different partial waves (counted by p) with polarization unit vector $\boldsymbol{n}_p$, envelope E_p, wavevector $\boldsymbol{k}_p$, and frequency ω_p form the total field. These partial waves may interfere or may be separated in time to give different independent pulses (see Figure 4.1).

The polarization field, Eq. (4.22), given by the time-dependent expectation value of the dipole operator according to Eq. (4.37) is obtained as a function of the electric field strength. This can be appreciated by recalling the expression of the expectation
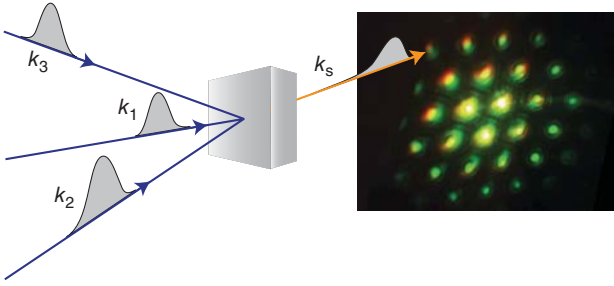
Figure 4.1 Scheme of a three-pulse experiment with the different pulses $p = 1, 2, 3$ with wavevector $\mathbf{k}_p$, frequency ω_p. After, the sample signal fields are propagating into different phase-matching directions $\mathbf{k}_s$ (only one shown). In the right part, a view of a screen placed after the sample is given. It shows various spots corresponding to directly transmitted incoming fields as well as to the phase-matched signal field (right panel, figure courtesy of T. Pullerits).

value of the molecular dipole operator in terms of the field-dependent S-operator, Eq. (4.36). Once the S-operator has been expanded in powers of $H^{(\mathrm{I})}_{\mathrm{field}}(t)$, we have, at the same time, an expansion in powers of the field strength $\mathbf{E}(\mathbf{x}, t)$ (cf. discussion in previous section). The resulting expression will contain all powers of the electric field strength, and every partial wave of the total electric field, Eq. (4.50), should appear with any power. Therefore, we expect the following form of the polarization field:

$$\mathbf{P}(\mathbf{x}, t) = \sum_{n_1 = -\infty}^{\infty} \cdots \sum_{n_N = -\infty}^{\infty} \mathbf{e}(n) P(n, t) \exp\{i(\mathbf{K}(n)\mathbf{x} - \Omega(n)t)\}. \tag{4.51}$$

Note that n abbreviates the whole set $\{n_1, \ldots, n_N\}$ of numbers counting the power at which the respective partial wave appears in the actual part of the total polarization field. The multiples of the wavevector and the frequency are abbreviated by $\mathbf{K}(n) = \sum_p n_p \mathbf{k}_p$ and by $\Omega(n) = \sum_p n_p \omega_p$, respectively. The resulting polarization direction $\mathbf{e}(n)$ depends on the field combination as well.

According to Eq. (4.49), the polarization generates a signal field $\mathbf{E}_s(\mathbf{x}, t)$, which can be decomposed analogous to Eq. (4.51). Thus, in total, there are $N + 1$ fields that mix while propagating through the sample (the so-called $N + 1$ wave mixing process). The problem of $N + 1$ coupled propagating fields is usually linearized by assuming that the signal field is much weaker than the incoming fields such that the latter are unaffected by the wave mixing. Thus, the signal field whose intensity is measured is given by the solution of Eq. (4.49). It propagates along the so-called phase-matching directions $\mathbf{K}(n)$, expressing momentum conservation. The signal and polarization field components for this direction are proportional to each other and phase-shifted by $\pi/2$, that is $E_s(n, t) \propto i\Omega(n)P(n, t)$.[5] In homodyne detection, the signal is proportional to the absolute square of the respective field component $E_s(n, t)$. In heterodyne detection, a so-called local oscillator field copropagates with the signal field. At the

---

5) This dependence is obtained by solving the linearized wave equation in one dimension under the slowly varying envelope approximation, i.e. $|\partial P(n, t)/\partial t| \ll |\Omega(n)P(n, t)|$ and similar for $E_s(n, t)$ (for details, see Mukamel [1]).

detector, the intensity of the superposition of the signal and the local oscillator field is measured. It has a contribution that is proportional to the signal field component itself, which enhances sensitivity as compared to the quadratic homodyne case.

Two basic ways to characterize the optical response of an ensemble of molecular systems can be distinguished. On the one hand, one can solve the time-dependent Schrödinger equation (or the density operator equation) including explicitly the radiation–matter coupling, Eq. (4.18). As a result, one obtains the polarization field according to Eq. (4.51) without resorting to any type of perturbation theory. The information on the signal field that is radiated in a particular spatial direction is then contained in the function $P(n, t)$, which has to be extracted numerically from $\boldsymbol{P}(\boldsymbol{x}, t)$. However, often such a rigorous treatment is unnecessary since the field is weak enough that an expansion of the polarization field in powers of the field strength is sufficient. This leads to the response function formalism, which will be outlined in Section 4.3.2.

However, we start with a general discussion of Eq. (4.51). In a first step of our analysis, we consider the case that the total electric field is given by a single wave (case $N = 1$). As a result, we obtain $\Omega(n) \equiv \Omega(n_1) = \omega_1, 2\omega_1, 3\omega_3, \ldots$ (negative frequencies appear too). Here, the nth multiple of ω_1 corresponds to the nth-order nonlinear response of the molecular system (generation of the nth-order harmonic). Apart from the linear response, there may appear frequency doubling as the quadratic response and frequency triplication as the third-order nonlinear response (two- and three-photon absorption, respectively). Besides the frequency of the polarization field, we have to consider the wavevector $\boldsymbol{K}(n)$. It contains multiples of $\boldsymbol{k}_1$ but all having the same direction, which indicates that the field corresponding to the nonlinear response propagates in the same direction as the incoming field.

Changing to the case of two partial waves with frequency ω_1 and ω_2, the resulting frequencies of the polarization $\Omega(n) \equiv \Omega(n_1, n_2)$ may take the following values: ω_1, $\omega_1 \pm \omega_2$, $\omega_1 \pm 2\omega_2$, etc. as well as $\omega_2, \omega_2 \pm \omega_1, \omega_2 \pm 2\omega_1$, etc. These frequency combinations may be of the first, second, and third orders in the field strength, respectively, but may also contain higher orders. This is due to the fact that the combination of the positive and the negative frequency parts of every partial wave, that is $\exp(-i\omega_p t)$ $\times \exp(i\omega_p t)$, results in a vanishing contribution to the total frequency. For example, we have $\omega_1 = \omega_1 + \omega_2 - \omega_2$ indicating that it may belong to a third-order process. This type of process is of basic importance for the pump–probe spectroscopy, which will be discussed in more detail in Section 4.3.6.

Considering, however, frequency doubling with $\Omega(n_1 = 1, n_2 = 1) = \omega_1 + \omega_2$, in the general case, the respective wavevector $\boldsymbol{k}_1 + \boldsymbol{k}_2$ shows neither into the direction of partial wave 1 nor in that of partial wave 2. This is also valid for the case with $\Omega(n_1 = 2, n_2 = -1) = 2\omega_1 - \omega_2$, where the wavevector is given by $2\boldsymbol{k}_1 - \boldsymbol{k}_2$. If the magnitude of both frequencies is comparable, the *mixed* frequency $2\omega_1 - \omega_2$ lies in the same region. Thus, this type of nonlinear response does not include frequency multiplication, but it forms a type of response that propagates in the direction $2\boldsymbol{k}_1 - \boldsymbol{k}_2$ and that is known as the *photon echo* (if subpulse 1 corresponding to partial wave 1 and subpulse 2 corresponding to partial wave 2 are clearly separated in

time, and pulse 2 comes first) and the *transient grating* technique (pulse 1 comes first).

When studying the case of the three partial waves $N = 3$, the situation becomes even more complex, and we will restrict ourselves to some selected examples (cf. Figure 4.1). First of all, a new frequency $\Omega(n_1 = 1, n_2 = 2, n_3 = 3) = \omega_1 + \omega_2 + \omega_3$ may be generated that has to be considered as a generalization of the third-order harmonic generation. Furthermore, we may introduce $\Omega(n_1 = 1, n_2 = 2, n_3 = -1) = -\omega_1 + \omega_2 + \omega_3$. If all three basic frequencies lie in the same spectral region, this is also valid for the mixed frequency $\Omega(-1,1,1)$ as well all other combinations $\Omega(1, -1,1)$ and $\Omega(1,1, -1)$. However, the wavevector $-\boldsymbol{k}_1 + \boldsymbol{k}_2 + \boldsymbol{k}_3$ as well as the two other combinations may define directions different from that of $\boldsymbol{k}_1$, $\boldsymbol{k}_2$, and $\boldsymbol{k}_3$, in which all these third-order response signal fields propagate. These four-wave mixing signals are usually classified to be of rephasing, $\boldsymbol{k}_R = -\boldsymbol{k}_1 + \boldsymbol{k}_2 + \boldsymbol{k}_3$, and nonrephasing, $\boldsymbol{k}_{NR} = \boldsymbol{k}_1 - \boldsymbol{k}_2 + \boldsymbol{k}_3$, types. The *three-pulse photon echo* is an example for a rephasing signal. In *two-dimensional spectroscopy*, a broader perspective on these signals is provided. It will be discussed in Section 4.3.7.

Apparently, the extent to which higher order processes become important essentially depends on the considered molecular system. To obtain a more detailed understanding we have to carry out an expansion with respect to the field strength.

4.3.2 Nonlinear Response Functions

In what follows we will consider the third-order nonlinear response only, which accounts for the most frequently used spectroscopic techniques. Extending the treatment of Section 4.2.2, the *S*-operator entering the expectation value of the dipole operator is expanded up to third order in the field strength

$$\boldsymbol{d}(t) = \mathrm{tr}\{\hat{W}_{\mathrm{eq}} \left[1 + S^{(1)+}(t, t_0) + S^{(2)+}(t, t_0) + S^{(3)+}(t, t_0)\right] \hat{\boldsymbol{\mu}}^{(I)}(t)$$

$$\times \left[1 + S^{(1)}(t, t_0) + S^{(2)}(t, t_0) + S^{(3)}(t, t_0)\right]\}. \tag{4.52}$$

The first-order part has been given in Eq. (4.39), and the other contributions read

$$S^{(2)}(t, t_0) = \left(\frac{i}{\hbar}\right)^2 \int\limits_{t_0}^{t} d\tau_1 \int\limits_{t_0}^{\tau_1} d\tau_2 \, \boldsymbol{E}(\boldsymbol{x}, \tau_1)\hat{\boldsymbol{\mu}}^{(I)}(\tau_1) \, \boldsymbol{E}(\boldsymbol{x}, \tau_2)\hat{\boldsymbol{\mu}}^{(I)}(\tau_2) \tag{4.53}$$

and

$$S^{(3)}(t, t_0) = \left(\frac{i}{\hbar}\right)^3 \int\limits_{t_0}^{t} d\tau_1 \int\limits_{t_0}^{\tau_1} d\tau_2 \int\limits_{t_0}^{\tau_2} d\tau_3$$

$$\times \boldsymbol{E}(\boldsymbol{x}, \tau_1)\hat{\boldsymbol{\mu}}^{(I)}(\tau_1) \, \boldsymbol{E}(\boldsymbol{x}, \tau_2)\hat{\boldsymbol{\mu}}^{(I)}(\tau_2) \, \boldsymbol{E}(\boldsymbol{x}, \tau_3)\hat{\boldsymbol{\mu}}^{(I)}(\tau_3). \tag{4.54}$$

After insertion into Eq. (4.52) and keeping only those terms, which are of third order in the field, the third-order polarization can be written in terms of the third-order

response function $R^{(3)}$ in analogy to Eq. (4.40) as follows:[6]

$$
\boldsymbol{P}^{(3)}(\boldsymbol{x}, t) = \int_0^\infty dt_3 dt_2 dt_1 \ R^{(3)}(t_3, t_2, t_1)
$$
$$
\times \boldsymbol{E}(\boldsymbol{x}, t - t_3)\boldsymbol{E}(\boldsymbol{x}, t - t_3 - t_2)\boldsymbol{E}(\boldsymbol{x}, t - t_3 - t_2 - t_1). \tag{4.55}
$$

Here, we have introduced the time arguments $t_1 = \tau_2 - \tau_1$, $t_2 = \tau_3 - \tau_2$, and $t_3 = t - \tau_3$. Note that in comparison with Eq. (4.51), we select only a particular term of the general nonperturbative expression. Due to the vector character of the dipole moment operator, the response function is a tensor of rank 4 given by

$$
R^{(3)}(t_3, t_2, t_1) = \left(\frac{i}{\hbar}\right)^3 \theta(t_3)\theta(t_2)\theta(t_1)n_{\text{mol}}
$$
$$
\times \text{tr}\left\{\hat{W}_{\text{eq}}\left[\left[\left[\hat{\boldsymbol{\mu}}^{(\text{I})}(t_3 + t_2 + t_1)\right]_-, \hat{\boldsymbol{\mu}}^{(\text{I})}(t_2 + t_1)\right]_-, \hat{\boldsymbol{\mu}}^{(\text{I})}(t_1)\right]_-, \hat{\boldsymbol{\mu}}^{(\text{I})}(0)\right]_-\right\}. \tag{4.56}
$$

The threefold commutator structure of $R^{(3)}$ results in eight different terms contributing to the third-order nonlinear response.[7] These multitime correlation functions of the dipole operator can be expressed as[8]

$$
R^{(3)}(t_3, t_2, t_1) = n_{\text{mol}}\left(\frac{i}{\hbar}\right)^3 \theta(t_3)\theta(t_2)\theta(t_1) \sum_{i=1}^{8} R_i(t_3, t_2, t_1), \tag{4.57}
$$

with

$$
R_1(t_3, t_2, t_1) = \text{tr}\left\{\hat{W}_{\text{eq}}\hat{\mu}^{(\text{I})}(t_1)\hat{\mu}^{(\text{I})}(t_2 + t_1)\hat{\mu}^{(\text{I})}(t_3 + t_2 + t_1)\hat{\mu}^{(\text{I})}(0)\right\},
$$
$$
R_2(t_3, t_2, t_1) = \text{tr}\left\{\hat{W}_{\text{eq}}\hat{\mu}^{(\text{I})}(0)\hat{\mu}^{(\text{I})}(t_2 + t_1)\hat{\mu}^{(\text{I})}(t_3 + t_2 + t_1)\hat{\mu}^{(\text{I})}(t_1)\right\},
$$
$$
R_3(t_3, t_2, t_1) = \text{tr}\left\{\hat{W}_{\text{eq}}\hat{\mu}^{(\text{I})}(0)\hat{\mu}^{(\text{I})}(t_1)\hat{\mu}^{(\text{I})}(t_3 + t_2 + t_1)\hat{\mu}^{(\text{I})}(t_2 + t_1)\right\},
$$
$$
R_4(t_3, t_2, t_1) = \text{tr}\left\{\hat{W}_{\text{eq}}\hat{\mu}^{(\text{I})}(t_3 + t_2 + t_1)\hat{\mu}^{(\text{I})}(t_2 + t_1)\hat{\mu}^{(\text{I})}(t_1)\hat{\mu}^{(\text{I})}(0)\right\},
$$
$$
R_i(t_3, t_2, t_1) = -R_{i-4}^*(t_3, t_2, t_1) \quad i = 5, \dots, 8. \tag{4.58}
$$

These representation-free expressions contain the information about possible third-order nonlinear spectroscopic techniques. Be aware of the relation to the fourth-order rates discussed in Section 3.14.6. In the following sections, we first specify the response functions to the cases of a multilevel system weakly coupled to a bath and to an electronic two-level system strongly coupled to vibrational DOFs. Subsequently, two different nonlinear spectroscopic techniques will be discussed in more detail.

---

6) The present perturbation expansion treats the bra and ket evolutions of the density matrix separately. In principle, this type of perturbation theory can also be formulated using a time-evolution superoperator. While the resulting expressions are identical, the superoperator formulation gives Eq. (4.55) directly, whereas the present case requires some rearrangement of the time integrals.

7) Note that in analogy to the linear case, one can introduce a third-order nonlinear susceptibility after switching to the frequency domain.

8) In the following equations, we will skip the vector notation which is important for experiments only where explicit use of the laser field polarization is made.

4.3.3 Eigenstate Expansion of the Response Functions

In order to illustrate the structure of the linear and nonlinear response functions, Eqs. (4.41) and (4.58), we consider an electronic three-level system with states ϕ_a and energies E_a $(a = g, e, f)$. It is assumed that the dipole operator allows for transitions between ϕ_g and ϕ_e and ϕ_e and ϕ_f only; that is, neglecting the vector character, we have

$$\hat{\mu} = d_{eg} |\phi_e\rangle \langle \phi_g| + d_{fe} |\phi_f\rangle \langle \phi_e| + \text{h.c.} \tag{4.59}$$

Further, the transition frequencies $\omega_{eg} = (E_e - E_g)/\hbar$ and $\omega_{fe} = (E_f - E_e)/\hbar$ shall be comparable, that is $\omega_{eg} \approx \omega_{fe}$. Initially, the system is in its ground state ϕ_g, and the reservoir in thermal equilibrium (density operator $\hat{R}_g$), that is $\hat{W}_{\text{eq}} = \hat{R}_g |\phi_g\rangle\langle\phi_g|$. Here, the equilibrium statistical operator for the reservoir in the electronic ground state is given by

$$\hat{R}_g = \frac{e^{-H_g/k_{\text{B}}T}}{\text{tr}_{\text{vib}}\{e^{-H_g/k_{\text{B}}T}\}}. \tag{4.60}$$

According to Eq. (3.269), the time evolution of the reduced density matrix is obtained by taking the appropriate matrix elements of $\hat{\rho}(t) = \mathcal{U}(t - t_0)\hat{\rho}(t_0)$, with $\mathcal{U}(t)$ describing the evolution of the three-level system subject to the interaction with the reservoir vibrations. For the purpose of illustration, we use a simplified Bloch model (Section 3.8.3).[9] Within the Bloch model, the dynamics of coherences and populations is decoupled. Using Eqs. (3.353) and (3.357), we can write for $a \neq b$

$$\rho_{ab}(t) = I_{ab}(t)\rho_{ab}(0), \tag{4.61}$$

with

$$I_{ab}(t) = e^{-(i\omega_{ab} + \gamma_{ab})t}. \tag{4.62}$$

For the population decay, we assume that it proceeds into states different from those of the relevant three-level system. For the ground state there should be no decay, whereas the two excited states should have a finite lifetime. Using Eq. (3.347) together with the relation $\gamma_{aa}^{(\text{pd})} = 0$, one notices that the time evolution of the diagonal elements can as well be given in the form of Eqs. (4.61) and (4.62).

The linear response function, Eq. (4.41), can be written as follows:

$$R^{(1)}(t) = \frac{i}{\hbar}\theta(t)n_{\text{mol}}\left(\text{tr}\left\{\hat{W}_{\text{eq}} U_{\text{mol}}^+(t)\hat{\mu}\ U_{\text{mol}}(t)\hat{\mu}\right\} - \text{c.c.}\right) \tag{4.63}$$

Note that the trace still contains the time evolution of the total system, that is three-level system plus reservoir. Performing the trace with respect to the reservoir DOFs gives the dissipative time-evolution superoperator $\mathcal{U}(t)$, and the response function becomes

$$R^{(1)}(t) = \frac{i}{\hbar}\theta(t)n_{\text{mol}}\left(\text{tr}_{\text{S}}\left\{\hat{\mu}\ \mathcal{U}(t)\hat{\mu}\left|\phi_g\right\rangle\left\langle\phi_g\right|\right\} - \text{c.c.}\right) \tag{4.64}$$

---

9) Note that going beyond the Bloch model is straightforward, but the resulting expressions are less transparent and therefore not suitable for the present discussion.

The trace contains the dissipative time evolution of the operator $\hat{\mu} \left| \phi_g \right\rangle \left\langle \phi_g \right| = d_{eg} \left| \phi_e \right\rangle \left\langle \phi_g \right|$ (cf. discussion in Section 6.3.2). Taking the trace yields $\left| d_{eg} \right|^2 \rho_{eg}(t)$ such that

$$R^{(1)}(t) = \frac{i}{\hbar} \theta(t) n_{\mathrm{mol}} \left(\left| d_{eg} \right|^2 I_{eg}(t) - \mathrm{c.c.} \right) \tag{4.65}$$

For this model, the linear susceptibility is readily obtained according to Eq. (4.45). Performing the integration, one has

$$\chi(\omega) = -\frac{\left| d_{eg} \right|^2 n_{\mathrm{mol}}}{\hbar} \left\{ \frac{1}{\omega - \omega_{eg} + i\gamma_{eg}} - \frac{1}{\omega + \omega_{eg} + i\gamma_{eg}} \right\}. \tag{4.66}$$

For $\omega \approx \omega_{eg} > 0$, the second term can be neglected. Viewed from the perspective of the Fourier transform, it corresponds to a rapidly oscillating term $\propto e^{i(\omega + \omega_{eg})t}$, which yields a vanishing time integral (rotating wave approximation, cf. Section 4.3.5). The linear susceptibility can be split into real (dispersive) and imaginary (absorptive) parts as follows:

$$\chi(\omega) = \frac{\left| d_{eg} \right|^2 n_{\mathrm{mol}}}{\hbar} \frac{\omega_{eg} - \omega + i\gamma_{eg}}{(\omega - \omega_{eg})^2 + \gamma_{eg}^2}. \tag{4.67}$$

According to Eq. (4.31), the imaginary part is proportional to the absorption coefficient. Thus, for the present model, one obtains a Lorentzian lineshape centered at ω_{eg} and having the width γ_{eg}.

Next, we focus on the third-order response functions. As an exemplary case, let us consider $R_1(t_3, t_2, t_1)$, Eq. (4.58), which can be written as

$$\begin{aligned} R_1(t_3, t_2, t_1) &= \mathrm{tr} \left\{ \hat{W}_{\mathrm{eq}} U_{\mathrm{mol}}^+(t_1) \hat{\mu} U_{\mathrm{mol}}(t_1) U_0^+(t_1 + t_2) \hat{\mu} U_{\mathrm{mol}}(t_1 + t_2) \right. \\ &\quad \left. \times U_{\mathrm{mol}}^+(t_1 + t_2 + t_3) \hat{\mu} U_{\mathrm{mol}}(t_1 + t_2 + t_3) \hat{\mu} \right\} \\ &= \mathrm{tr} \left\{ U_{\mathrm{mol}}^+(t_1) \hat{\mu} U_{\mathrm{mol}}^+(t_2) \hat{\mu} U_{\mathrm{mol}}^+(t_3) \hat{\mu} U_{\mathrm{mol}}(t_1 + t_2 + t_3) \hat{\mu} \hat{W}_{\mathrm{eq}} \right\} \\ &= \mathrm{tr} \left\{ \hat{\mu} U_{\mathrm{mol}}(t_1 + t_2 + t_3) \hat{\mu} \hat{W}_{\mathrm{eq}} U_{\mathrm{mol}}^+(t_1) \hat{\mu} U_{\mathrm{mol}}^+(t_2) \hat{\mu} U_{\mathrm{mol}}^+(t_3) \right\}. \end{aligned} \tag{4.68}$$

The result of this rearrangement is an expression containing all time evolution operators $U_{\mathrm{mol}}(t)$ on the left of the initial state, that is acting on its ket vector, whereas all time evolution operators $U_{\mathrm{mol}}^+(t)$ are on the right of the initial state, that is acting on its bra vector.[10]

Similar to the linear response function in Eq. (4.64), Eq. (4.68) still contains the time evolution of the total system. In order to obtain an expression in terms of the time-evolution superoperator for the three-level system in the three time intervals, $\mathcal{U}(t_i)$ ($i = 1, 2, 3$), one has to make an additional assumption. Specifically, one has to write the trace with respect to the reservoir in terms of separate traces for the different time intervals. This requires that the reservoir correlation time is ultrashort

---

10) Note that this particular form provides the starting point for the development of a diagrammatic representation of the response functions in terms of the so-called double-sided Feynman diagrams (see Further Reading).

such that correlations of the reservoir DOFs between different time intervals t_i can be neglected. In other words, the bath trace with respect to the whole time evolution separates into a product of averaged time evolutions for the different time intervals. This gives the response function (note that the superoperators act on the operators inside the brackets only)

$$R_1(t_3, t_2, t_1) = \text{tr}_S \left\{ \hat{\mu} \, \mathcal{U}(t_3) \left[\mathcal{U}(t_2) \left[\mathcal{U}(t_1) \left[\hat{\mu} \left| \phi_g \right\rangle \left\langle \phi_g \right| \right] \hat{\mu} \right] \hat{\mu} \right] \right\}. \tag{4.69}$$

Inserting Eq. (4.59) and taking the trace gives two terms:

$$R_1(t_3, t_2, t_1) = \left| d_{eg} \right|^4 I_{eg}(t_3) I_{ee}(t_2) I_{eg}(t_1)$$
$$+ \left| d_{eg} \right|^2 \left| d_{fe} \right|^2 I_{ef}(t_3) I_{ee}(t_2) I_{eg}(t_1). \tag{4.70}$$

The interpretation of this expression in terms of the time evolution of the electronic density matrix is as follows: Initially, the system is in the electronic ground state when the interaction with the field promotes it into a coherence $I_{eg}(t_1)$ where it propagates during t_1. The second interaction (on the bra side) generates an electronic population evolving during t_2, $I_{ee}(t_2)$. A third interaction with the field on the bra side yields again an electronic coherence during t_3. For the three-level system, this coherence is between the first excited state and either the ground, $I_{eg}(t_2)$, or the second excited state, $I_{ef}(t_3)$. A further action of the dipole moment operator (coming from the definition of the polarization, Eq. (4.22)) closes the trace.

The other response functions in Eq. (4.58) can be derived along the same lines, and one obtains

$$R_2(t_3, t_2, t_1) = \text{tr}_S \left\{ \hat{\mu} \, \mathcal{U}(t_3) \left[\mathcal{U}(t_2) \left[\hat{\mu} \, \mathcal{U}(t_1) \left[\left| \phi_g \right\rangle \left\langle \phi_g \right| \hat{\mu} \right] \right] \hat{\mu} \right] \right\}$$
$$= \left| d_{eg} \right|^4 I_{eg}(t_3) I_{ee}(t_2) I_{ge}(t_1)$$
$$+ \left| d_{eg} \right|^2 \left| d_{fe} \right|^2 I_{ef}(t_3) I_{ee}(t_2) I_{eg}(t_1), \tag{4.71}$$

$$R_3(t_3, t_2, t_1) = \text{tr}_S \left\{ \hat{\mu} \, \mathcal{U}(t_3) \left[\hat{\mu} \, \mathcal{U}(t_2) \left[\mathcal{U}(t_1) \left[\left| \phi_g \right\rangle \left\langle \phi_g \right| \hat{\mu} \right] \hat{\mu} \right] \right] \right\}$$
$$= \left| d_{eg} \right|^4 I_{eg}(t_3) I_{gg}(t_2) I_{ge}(t_1)$$
$$+ \left| d_{eg} \right|^2 \left| d_{fe} \right|^2 I_{ef}(t_3) I_{gf}(t_2) I_{ge}(t_1), \tag{4.72}$$

$$R_4(t_3, t_2, t_1) = \text{tr}_S \left\{ \hat{\mu} \, \mathcal{U}(t_3) \left[\hat{\mu} \, \mathcal{U}(t_2) \left[\hat{\mu} \, \mathcal{U}(t_1) \left[\hat{\mu} \left| \phi_g \right\rangle \left\langle \phi_g \right| \right] \right] \right] \right\}$$
$$= \left| d_{eg} \right|^4 I_{eg}(t_3) I_{gg}(t_2) I_{eg}(t_1)$$
$$+ \left| d_{eg} \right|^2 \left| d_{fe} \right|^2 I_{ef}(t_3) I_{fg}(t_2) I_{eg}(t_1). \tag{4.73}$$

The respective expressions for $R_{i=5-8}$ can be obtained using the relation given in Eq. (4.58). Compared to R_1, we notice that R_3 and R_4 contain $I_{gg}(t_2)$; that is, after two interactions with the field, the system is in a ground state population; note that for the present simple model, there is actually no time evolution in state ϕ_g. Overall, the expressions can be distinguished by the phase factors of the

different time intervals, for instance $R_1(t_3, t_2, t_1) \propto \exp(-i\omega_{eg}(t_1 + t_3))$, whereas $R_2(t_3, t_2, t_1) \propto \exp(i\omega_{eg}(t_1 - t_3))$. This will be important for the classification according to the phase-matching directions as given in Section 4.3.7.

4.3.4 Cumulant Expansion of the Response Functions

In what follows, an alternative to the simple three-level model with Bloch-type relaxation will be introduced. It does not make use of the perturbation theory for the system–reservoir coupling and takes into account the full system–reservoir correlations when calculating the traces in Eqs. (4.41) and (4.58). It can be applied to coupled electron-vibrational dynamics (Chapter 6) as well as to the dynamics of high-frequency vibrations coupled to a low-frequency vibrational reservoir (Chapter 5). Further, it is an eigenstate-free approach, that is it does not require knowledge of the vibrational (reservoir) states of the considered system. It is based on a method known from probability theory as the *cumulant expansion*. In what follows, the cumulant expansion will be illustrated for the case of an electronic two-level system, coupled to a not-further-specified number of vibrational DOFs, q. The molecular Hamiltonian reads

$$H = \sum_{g,e} H_a(q) |\phi_a\rangle \langle\phi_a|, \tag{4.74}$$

and the dipole operator is given by

$$\hat{\mu} = d_{eg} |\phi_e\rangle \langle\phi_g| + d_{ge} |\phi_g\rangle \langle\phi_e|. \tag{4.75}$$

Often, the dependence of the transition dipole matrix elements on the vibrational coordinates is weak and can be neglected. This so-called Condon approximation will be used in the following derivation. Further, we assume that the system is initially in the electronic ground state with the equilibrium statistical operator $\hat{W}_{eq} = \hat{R}_g |\phi_g\rangle \langle\phi_g|$; $\hat{R}_g$ is given in Eq. (4.60), with $H_g = H_g(q)$.

Taking the trace with respect to the electronic states and using the Condon approximation, the linear response function, Eq. (4.41), can be written as

$$R^{(1)}(t) = \frac{i}{\hbar} \theta(t) n_{\text{mol}} \left(\left| d_{eg} \right|^2 \text{tr}_{\text{vib}} \left\{ \hat{R}_g U_g^+(t) U_e(t) \right\} - \text{c.c.} \right) \tag{4.76}$$

Next, we introduce $\Delta H_{eg} = H_e - H_g - \Delta_{eg}$ and rewrite the time-evolution operator for H_e as follows:

$$U_e(t) = e^{-iH_e t/\hbar} = e^{-i\Delta_{eg}t} e^{-i(H_g + \Delta H_{eg})t/\hbar}$$
$$= e^{-i\Delta_{eg}t\hbar} U_g(t) S_{eg}(t, 0), \tag{4.77}$$

with $U_g(t) = \exp(-iH_g t/\hbar)$ and the real constant Δ_{eg}. The S-operator has the form

$$S_{eg}(t, 0) = \hat{T} \exp \left\{ -\frac{i}{\hbar} \int_0^t d\bar{t} \, \Delta H_{eg}^{(g)}(\bar{t}) \right\}, \tag{4.78}$$

where the abbreviation $\Delta H_{eg}^{(g)}(\bar{t}) = U_g^+(\bar{t}) \Delta H_{eg} U_g(\bar{t})$ has been introduced.

Since $U_g^+(t)U_g(t) = 1$, the trace expression in Eq. (4.76) becomes

$$\text{tr}_{\text{vib}}\{\hat{R}_g S_{eg}(t,0)\} = \langle S_{eg}(t,0)\rangle_g = 1 - \frac{i}{\hbar}\int_0^t d\bar{t}_1 \langle \Delta H_{eg}^{(g)}(\bar{t}_1)\rangle_g$$

$$+ \left(\frac{i}{\hbar}\right)^2 \int_0^t d\bar{t}_1 \int_0^{\bar{t}_1} d\bar{t}_2 \left\langle \Delta H_{eg}^{(g)}(\bar{t}_1)\Delta H_{eg}^{(g)}(\bar{t}_2)\right\rangle_g + \dots . \quad (4.79)$$

In the cumulant expansion method, the following ansatz is used:

$$\left\langle S_{eg}(t,0)\right\rangle_g = e^{\Gamma(t)}, \quad (4.80)$$

where $\Gamma(t)$ has still to be computed. To this end, let us introduce a power expansion with respect to $\Delta H_{eg}^{(g)}$ such as

$$\Gamma(t) = \Gamma_1(t) + \Gamma_2(t) + \Gamma_3(t) + \dots, \quad (4.81)$$

where $\Gamma_n(t)$ is of the nth order in $\Delta H_{eg}^{(g)}$. It is reasonable that this expansion exists because it exists for $\left\langle S_{eg}(t,0)\right\rangle_g$. Since the exponent of the (time-ordered) S-operator is of the first order with respect to $\Delta H_{eg}^{(g)}$, there is no zeroth-order contribution in Eq. (4.81). In order to compare the present approach with the direct expansion of $\left\langle S_{eg}(t,0)\right\rangle_g$ in Eq. (4.79), we expand Eq. (4.80) and insert Eq. (4.81). This gives

$$e^{\Gamma(t)} = 1 + \left(\Gamma_1(t) + \Gamma_2(t) + \Gamma_3(t) + \dots\right)$$

$$+ \frac{1}{2}\left(\Gamma_1(t) + \Gamma_2(t) + \Gamma_3(t) + \dots\right)^2 + \dots . \quad (4.82)$$

Restricting ourselves to terms up to the second order with respect to $\Delta H_{eg}^{(g)}$ yields

$$e^{\Gamma(t)} \approx 1 + \left(\Gamma_1(t) + \Gamma_2(t)\right) + \frac{1}{2}\left(\Gamma_1(t) + \Gamma_2(t)\right)^2 + \dots$$

$$\approx 1 + \Gamma_1(t) + \left(\Gamma_2(t) + \frac{1}{2}\Gamma_1^2(t)\right). \quad (4.83)$$

A direct comparison with Eq. (4.79) gives

$$\Gamma_1(t) = -\frac{i}{\hbar}\int_0^t dt_1 \langle \Delta H_{eg}^{(g)}(t_1)\rangle_g \quad (4.84)$$

and

$$\Gamma_2(t) = -\frac{1}{\hbar^2}\int_0^t dt_1 \int_0^{t_1} dt_2 \langle \delta H_{eg}^{(g)}(t_1)\Delta H_{eg}^{(g)}(t_2)\rangle_g + \frac{1}{2}\Gamma_1^2(t)$$

$$= -\frac{1}{\hbar^2}\int_0^t dt_1 \int_0^{t_1} dt_2 \langle \Delta H_{eg}^{(g)}(t_2)\Delta H_{eg}^{(g)}(0)\rangle_g + \frac{1}{2}\Gamma_1^2(t). \quad (4.85)$$

The cumulant expansion provides a partial resummation of the perturbation series. Clearly, even if only some low-order contributions such as Γ_1 or Γ_2 would be known, we would have $\langle S_{eg}(t,0)\rangle_g$ for any order in $\Delta H_{eg}^{(g)}$. However, in general, retaining

only low-order terms in $\Gamma(t)$ would not give the exact expression for $\langle S_{eg}(t, 0)\rangle_g$. In the present case, including Γ_1 and Γ_2 only would be called second-order cumulant approximation. In Chapter 6, the example of harmonic vibrational DOFs will be discussed. Here, the second-order cumulant expansion is exact (cf. Section 6.2.5).

The constant Δ_{eg} has not yet been specified. The choice

$$\Delta_{eg} = \langle H_e - H_g\rangle_g \tag{4.86}$$

is of particular advantage since in this case, one has

$$\Delta H_{eg}^{(g)}(t) = U_g^+(t)(H_e - H_g)U_g(t) - \langle H_e - H_g\rangle_g \tag{4.87}$$

and $\langle\Delta H_{eg}^{(g)}(t)\rangle_g = 0$. In other words, the first-order cumulant vanishes, $\Gamma_1(t) = 0$, and the response function can be written as

$$R^{(1)}(t) = \frac{i}{\hbar}\theta(t)n_{mol}\left(\left|d_{eg}\right|^2 e^{-i\Delta_{eg}t/\hbar}e^{\Gamma_2(t)} - \text{c.c.}\right) \tag{4.88}$$

Thus, the response function is determined by $\Gamma_2(t)$, which contains the autocorrelation function of the thermal fluctuation of the energy gap between the two electronic states.

Using the cumulant expansion technique, the higher-order response functions can be expressed in terms of $\Gamma_2(t)$ as well. This can be shown by considering the general four-time dipole correlation function

$$C(\tau_4, \tau_3, \tau_2, \tau_1) = \text{tr}\left\{\hat{W}_{eq}\hat{\mu}^{(I)}(\tau_4)\hat{\mu}^{(I)}(\tau_3)\hat{\mu}^{(I)}(\tau_2)\hat{\mu}^{(I)}(\tau_1)\right\}. \tag{4.89}$$

For the purpose of illustration, we consider the same two-level system as before, Eqs. (4.74) and (4.75).[11] Taking the trace with respect to the electronic states and using the Condon approximation, one obtains

$$\begin{aligned}
C(\tau_1, \tau_2, \tau_3, \tau_4) &= \left|d_{eg}\right|^4 \text{tr}\left\{\hat{R}_g U_g^+(\tau_1)U_e(\tau_1)U_e^+(\tau_2)U_g(\tau_2)U_g^+(\tau_3)U_e(\tau_3)\right.\\
&\qquad \times \left. U_e^+(\tau_4)U_g(\tau_4)\right\}\\
&= \left|d_{eg}\right|^4 e^{-i\Delta_{eg}(\tau_1-\tau_2+\tau_3-\tau_4)/\hbar}\\
&\qquad \times\left\langle S_{eg}(\tau_1, 0)S_{eg}^+(\tau_2, 0)S_{eg}(\tau_3, 0)S_{eg}^+(\tau_4, 0)\right\rangle_g.
\end{aligned} \tag{4.90}$$

Next, one expands all time-order exponentials according to Eq. (4.79) and reorders the different terms to compare with the cumulant expansion equation (4.82). Assuming the choice Eq. (4.86), the correlation function Eq. (4.90) can be cast into the form

$$\begin{aligned}
C(\tau_1, \tau_2, \tau_3, \tau_4) &= \left|d_{eg}\right|^4 e^{-i\Delta_{eg}(\tau_1-\tau_2+\tau_3-\tau_4)/\hbar}\\
&\quad \times e^{\Gamma_2(\tau_1-\tau_2)-\Gamma_2(\tau_1-\tau_3)+\Gamma_2(\tau_2-\tau_3)}\\
&\quad \times e^{\Gamma_2(\tau_1-\tau_4)-\Gamma_2(\tau_2-\tau_4)+\Gamma_2(\tau_3-\tau_4)}.
\end{aligned} \tag{4.91}$$

---

11) Note that along the same lines, the inclusion of a higher excited state, which enables excited state absorption, is straightforward.

The third-order response functions follow as:

$$R_1(t_3, t_2, t_1) = C(t_1, t_1 + t_2, t_1 + t_2 + t_3, 0), \tag{4.92}$$

$$R_2(t_3, t_2, t_1) = C(0, t_1 + t_2, t_1 + t_2 + t_3, t_1), \tag{4.93}$$

$$R_3(t_3, t_2, t_1) = C(0, t_1, t_1 + t_2 + t_3, t_1 + t_2), \tag{4.94}$$

$$R_4(t_3, t_2, t_1) = C(t_1 + t_2 + t_3, t_1 + t_2, t_1, 0). \tag{4.95}$$

These second-order cumulant expressions are valid for arbitrary strong coupling between the electronic and vibrational coordinates. They are often used together with model spectral densities to obtain analytical expressions for the response functions (cf. Chapter 6). However, one should note that they describe gap fluctuations only; that is, effects due to population relaxation between the electronic states are not taken into account. Thus, the obtained line broadening is due to pure dephasing only.[12]

4.3.5 Rotating Wave Approximation

In what follows we determine the polarization component, $P(n, t)$, using the response functions for the case of three well-separated pulses acting sequentially with the system. Neglecting the vector character of the field, we have

$$E(\boldsymbol{x}, t) = E_1(t + T + \tau)e^{i(\boldsymbol{k}_1\boldsymbol{x} - \omega_1(t + T + \tau))} + E_2(t + T)e^{i(\boldsymbol{k}_2\boldsymbol{x} - \omega_2(t + T))}$$
$$+ E_3(t)e^{i(\boldsymbol{k}_3\boldsymbol{x} - \omega_3 t)} + \text{c.c.} \tag{4.96}$$

Thus, the pulses are centered at $t = -T - \tau$, $t = -T$, and $t = 0$. Further, for the field frequencies, we assume that $\omega_p \approx \omega_{eg}$, with ω_{eg} being a characteristic transition frequency of the system. The polarization itself is given by Eq. (4.55). According to the general discussion of wave mixing in Section 4.3.1, the combination fields give rise to a resultant wavevector $\boldsymbol{K}(n)$ and frequency $\Omega(n)$, with $n = (n_1, n_2, n_3)$.

In principle, the product of the three fields in Eq. (4.55) gives 6^3 terms. In addition, the response function consists of eight terms. However, not all of the resulting integrals are equally important. First, in the phase-matching direction, we are looking for those combinations of fields that contribute a plane wave factor $e^{i\boldsymbol{K}(n)\boldsymbol{x}}$. Second, as already mentioned in Section 4.3.3, the response functions in Eqs. (4.70)–(4.73) (and their complex conjugates, cf. Eq. (4.58)) each have a distinct combination of phase factors. Within the so-called rotating wave approximation only those field combinations are kept where the phase factors coming from the fields match those of the response functions. For example, we have $R_1(t_3, t_2, t_1) \propto e^{-i\omega_{eg}(t_1 + t_3)}$, that is the respective factor from the fields would be $\propto e^{i(\omega_1 t_1 + \omega_3 t_3)}$. Terms without such a match yield,

---

12) For the present two-level system, population relaxation is likely to play a minor role on the time scales of ultrafast spectroscopic experiments due to the large energy gap. If several excited states are present, nonadiabatic coupling could lead to population flow between these states. Such effects can be taken into account using perturbation theory; for details, see, for instance Mukamel and Abramavicius [2].

for example a factor $\propto e^{-i(\omega_{eg}+\omega_1)t_1}$. It is highly oscillatory and will give a vanishing contribution upon time integration.

For well-separated pulses and combining Eqs. (4.55) and (4.96), the polarization field envelope can be written in rotating wave approximation as

$$P(n, t) = e^{-i\Omega(n)t - i(n_1\omega_1 + n_2\omega_2)T - in_1\omega_1\tau} \int_0^\infty dt_3 dt_2 dt_1 \ R_n^{(3)}(t_3, t_2, t_1)$$

$$\times \ e^{i\Omega(n)t_3 + i(n_1\omega_1 + n_2\omega_2)t_2 + in_1\omega_1 t_1} \ E_3(t - t_3)$$

$$\times E_2(t - t_3 - t_2 + T)E_1(t - t_3 - t_2 - t_1 + T + \tau). \tag{4.97}$$

Here, $R_n^{(3)}(t_3, t_2, t_1)$ is the rotating wave approximation contribution of the response function in the phase-matching direction $\boldsymbol{K}(n)$. In what follows, this expression will be specified to the cases of pump–probe and two-dimensional spectroscopy.

4.3.6 Pump–Probe Spectroscopy

Pump–probe spectroscopy is a widely applied method for the investigation of molecular dynamics. In particular, charge and energy transfer processes can be followed on their natural time scale. The method appeals to the intuitive picture where a pump pulse, $E_1(t + T)$, prepares the system in a nonequilibrium state whose dynamics is followed by monitoring the spectral changes experienced by a time-delayed probe pulse, $E_2(t)$, passing through the sample. Specifying Eq. (4.96) to the present case, we have

$$E(\boldsymbol{x}, t) = E_1(t + T)e^{i(\boldsymbol{k}_1\boldsymbol{x} - \omega_1(t+T))} + E_2(t)e^{i(\boldsymbol{k}_2\boldsymbol{x} - \omega_2 t)} + \text{c.c.} \tag{4.98}$$

A schematic view of the setup is given in Figure 4.2. With the wavevectors $\boldsymbol{k}_1$ and $\boldsymbol{k}_2$, the resulting wavevector of the relevant polarization field component in Eq. (4.51)

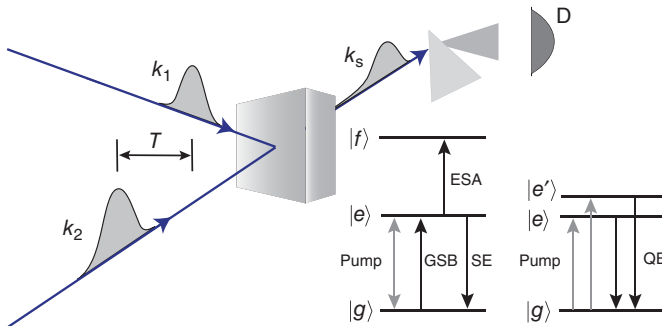**Figure 4.2** Scheme of a pump–probe experiment with the pump and probe pulse being characterized by the wavevectors $\boldsymbol{k}_1$ and $\boldsymbol{k}_2$, respectively. The delay between both pulses (pulse maxima) is given by T. The field intensity for a given delay time along the direction $\boldsymbol{k}_s = \boldsymbol{k}_2$ is measured at the detector D. To obtain spectral information, the signal field can be dispersed, for example using a prism. The level schemes on the right show different situations and the corresponding contributions to the pump–probe signal. First, for a three-level system with $\omega_{eg} \approx \omega_{fe}$, one has ground state bleach (GSB), stimulated emission (SE), and excited state absorption (ESA). If $\omega_{eg} \approx \omega_{e'g}$, quantum beats (QBs) can be observed.

will be

$$k_{PP} = K(-1,1,1) = K(1,-1,1) = k_2, \qquad (4.99)$$

and likewise, $\Omega(-1,1,1) = \Omega(1,-1,1) = \omega_{PP} = \omega_2$. Thus, the signal field travels in the probe field direction, and the probe field acts simultaneously as a heterodyne field. The respective polarization field component will be called $P(n,t) = P_{PP}(t)$ in what follows.

In this so-called self-heterodyned detection, the total intensity of the local oscillator (here, the probe field $E_2(t)$) plus signal ($E_{PP}(t)$) fields is given by $I_{total}(t) = (n_r(\omega_{PP})c/4\pi)|E_2(t) + E_{PP}(t)|^2$. Here, $n_r(\omega_{PP})$ is the index of refraction at the signal field frequency. Eliminating the known probe field intensity and assuming that the bare signal field intensity is negligible, the intensity of the self-heterodyned pump–probe signal is given by

$$I_{PP}(t) = \frac{n_r(\omega_{PP})c}{4\pi} \text{Re}[E_2^*(t)E_{PP}(t)]. \qquad (4.100)$$

As pointed out in Section 4.3.1, the signal and polarization fields are proportional, that is $E_{PP}(t) \propto i\omega_{PP}P_{PP}(t)$. Inserting this relation into Eq. (4.100) and assuming a constant index of refraction across the spectrum of the probe pulse, the time-integrated pump–probe signal is given by (skipping the constant prefactors and indicating the delay time dependence of the polarization)[13]

$$S_{PP}(\omega_2, T) = \omega_2 \int_{-\infty}^{\infty} dt \, \text{Im}[E_2(t)P_{PP}^*(t,T)]. \qquad (4.101)$$

Note that $P_{PP}^*(t,T)$ refers to the third-order polarization only, whereas in general, there would also be a contribution of the first order in the probe field along the direction k_2. In the actual experiment, this separation is realized by subtracting the signal obtained without a pump field from the total signal.

Using a Fourier decomposition of $E_2(t)$ and $P_{PP}(t,T)$, Eq. (4.101) can be written as

$$S_{PP}(\omega_2, T) = \omega_2 \int_{-\infty}^{\infty} \frac{d\omega}{2\pi} \, \text{Im}[E_2(\omega)P_{PP}^*(\omega,T)]. \qquad (4.102)$$

The integrand defines the so-called dispersed pump–probe signal,

$$S_{disp}(\omega, T) = \text{Im}[E_2(\omega)P_{PP}^*(\omega,T)]. \qquad (4.103)$$

It can be obtained after passing the signal through a monochromator (cf. Figure 4.2). Notice that apart from the effects due to the finite spectral width of the probe pulse ($E_2(\omega)$), the dispersed signal carries the same information as the time-integrated signal, if for the latter the probe pulse frequency is varied.

The polarization field component, Eq. (4.97), can be specified to the present case. Note that one has to take into account that according to Eq. (4.99) there are two

—————
13) Note that experimental signals are often normalized with respect to the total incoming intensity $(n_r(\omega_2)c/4\pi) \int dt |E_2(t)|^2$.

possibilities to obtain $\boldsymbol{k}_{PP}$. They differ in the order of the first two field interactions. This results in (note that the field envelopes are assumed to be real-valued functions)

$$
P_{PP}(t, T) = -i\frac{n_{mol}}{\hbar^3}e^{-i\omega_2 t}\int_0^\infty dt_3 dt_2 dt_1
$$
$$
\times E_2(t - t_3)E_1(t - t_3 - t_2 + T)E_1(t - t_3 - t_2 - t_1 + T)
$$
$$
\times \left\{e^{-i\omega_1 t_1 + i\omega_2 t_3}R_R(t_3, t_2, t_1) + e^{i\omega_1 t_1 + i\omega_2 t_3}R_{NR}(t_3, t_2, t_1)\right\}.
$$
(4.104)

Here, we introduced the so-called rephasing,

$$
R_R(t_3, t_2, t_1) = R_2(t_3, t_2, t_1) + R_3(t_3, t_2, t_1) + R_5(t_3, t_2, t_1),
$$
(4.105)

and nonrephasing,

$$
R_{NR}(t_3, t_2, t_1) = R_1(t_3, t_2, t_1) + R_4(t_3, t_2, t_1) + R_6(t_3, t_2, t_1),
$$
(4.106)

response functions. Equation (4.104) can be used to calculate either the time-integrated, Eq. (4.101), or the dispersed, Eq. (4.103), signal. However, due to the multiple convolution of the response functions with the fields, this provides little physical insight. Time-resolved experiments are often performed for situations where the so-called impulsive limit applies. Here, the pulses are much shorter than the typical molecular dynamics time scales but longer than the optical period. In this limit, the pulse envelopes can be approximated by delta functions, and the time integrations can be performed. Notice, however, that such pulses will be spectrally extremely broad such that no frequency resolution is available. For the detection, this problem is circumvented by spectrally dispersing the signal.

Applying this limit to the pump pulse, one notices that the two pulse actions coincide such that only $t_1 = 0$ contributes to the integral, that is $E_1(t - t_3 - t_2 + T)E_1(t - t_3 - t_2 - t_1 + T) \approx A_1^2\delta(t_1)\delta(t - t_3 - t_2 + T)$, where A_1 is the field amplitude. For the probe field, we have $E_2(t - t_3) \approx A_2\delta(t - t_3)$. Hence, in the impulsive limit, Eq. (4.104) becomes

$$
P_{PP}(t, T) = -i\frac{n_{mol}}{\hbar^3}A_1^2 A_2\theta(t)\left\{R_R(t, T, 0) + R_{NR}(t, T, 0)\right\}.
$$
(4.107)

For illustration, let us consider the three-level system ϕ_g, ϕ_e, ϕ_f sketched in Figure 4.2. In the Bloch-type limit, the relevant response functions, Eqs. (4.70)–(4.73), take the following form:

$$
R_{i=1,2}(t, T, 0) = \left|d_{eg}\right|^4 I_{eg}(t)I_{ee}(T),
$$
(4.108)

$$
R_{i=3,4}(t, T, 0) = \left|d_{eg}\right|^4 I_{eg}(t)I_{gg}(T),
$$
(4.109)

$$
R_{i=5,6}(t, T, 0) = -\left|d_{eg}\right|^2\left|d_{fe}\right|^2 I_{fe}(t)I_{ee}(T).
$$
(4.110)

These expressions show that after the pump pulse action, the system is in a population state either with respect to the ground state ϕ_g or the first excited state ϕ_e. There, it evolves during the delay time T before the probe pulse converts the population into a coherence $I_{eg}(t)$ or $I_{fe}(t)$.

The dispersed pump–probe signal, Eq. (4.103), becomes (using $\gamma_{gg} = 0$ for the ground state ϕ_g and $E_2(\omega) \approx A_2$ for the impulsive limit)

$$
\begin{aligned}
S_{\text{disp}}(\omega, T) = {}& 2A_1^2 A_2^2 \frac{n_{\text{mol}}}{\hbar^3} \text{Re} \int_0^\infty dt\, e^{i\omega t} \\
& \times \left\{ R_1(t, T, 0) + R_3(t, T, 0) + R_5(t, T, 0) \right\} \\
= {}& 2A_1^2 A_2^2 \frac{n_{\text{mol}}}{\hbar^3} \left\{ \frac{\left| d_{eg} \right|^4 \gamma_{eg} (e^{-\gamma_{ee} T} + 1)}{(\omega - \omega_{eg})^2 + \gamma_{eg}^2} - \frac{\left| d_{eg} \right|^2 \left| d_{fe} \right|^2 \gamma_{fe} e^{-\gamma_{ee} T}}{(\omega - \omega_{fe})^2 + \gamma_{fe}^2} \right\}.
\end{aligned}
$$

$$(4.111)$$

The signal consists of three contributions as shown in Figure 4.2: (i) stimulated emission (SE) from the state ϕ_e prepared by the pump pulse (R_1), (ii) ground state bleaching (GSB) where the system is in the ground state ϕ_g after the pump pulse interactions,[14] and (iii) excited state absorption (ESA) between the excited state prepared by the pump pulse, ϕ_e, and the second excited state, ϕ_f. Compared to the linear absorption, GSB and SE cause a reduction, whereas ESA gives an increase in the signal around ω_{eg} and ω_{fe}, respectively.[15] With increasing delay time T, the signal will diminish. In fact, if the system relaxes back to the ground state, we have in equilibrium $S_{\text{disp}}(\omega, T \to \infty) = 0$. The present simple relaxation model does not capture this behavior, and a more elaborate treatment, for example according to the Redfield model, is needed. The application of pump–probe spectroscopy to the relaxation of a high-frequency vibrational mode is given in Figure 5.12, and the pump–probe signal of a solvated dye molecule is shown in Figure 6.3.

In cases where there is a third state, $\phi_{e'}$, with $\omega_{eg} \approx \omega_{e'g}$, a new type of contribution can be expected besides SE and GSB. As sketched in Figure 4.2, the two interactions with the pump pulse can prepare a coherence between states ϕ_e and $\phi_{e'}$, leading to a time evolution $I_{e'e}(t_2)$ (and $I_{ee'}(t_2)$) in the response function R_1. Using the same approximations as for Eq. (4.111), this contribution to the response function reads

$$
\begin{aligned}
R_1(t, T, 0) &= \left| d_{eg} \right|^2 \left| d_{e'g} \right|^2 I_{e'g}(t) I_{e'e}(T) \\
&= \left| d_{eg} \right|^2 \left| d_{e'g} \right|^2 e^{-i\omega_{e'g} t - \gamma_{e'g} t} e^{-i\omega_{e'e} T - \gamma_{e'e} T}.
\end{aligned}
$$

$$(4.112)$$

Therefore, there is an oscillatory behavior of the signal with frequency $\omega_{e'e}$ (the so-called quantum beats [QBs]) as a function of the delay time T.

Pump–probe spectroscopy has the drawback that time and excitation–frequency resolution are interdependent. The impulsive limit used for illustration provides optimal resolution with respect to the delay time dependence. But, such an excitation will be spectrally very broad, which reduces the spectral resolution. Conversely, a spectrally narrow pump pulse will be broad in time domain, thus diminishing the

---

14) The name GSB derives from the fact that due to the pump pulse interaction there are fewer molecules in their ground state. Since the pump–probe signal is taken as the difference with respect to the nonexcited case, the ground state appears to be bleached, that is there is less absorption.
15) Note that experimental data are often shown with a different sign, that is GSB/SE are taken negative, and ESA positive.

time resolution (see also the discussion in Section 6.5). Hence, there will be some optimum concerning the separation of transitions and time scales of dynamics as far as the observation with pump–probe spectroscopy is concerned. It is important to note that using the frequency-dispersed signal detection, this problem is resolved as far as the probe pulse is concerned. Here, according to Eq. (4.103), a spectrally very broad probe field is even desirable to recover the full spectral information contained in the signal field.

4.3.7 Two-dimensional Spectroscopy

The response function $R^{(3)}(t_3, t_2, t_1)$ depends on three time intervals. Pump–probe spectroscopy makes use of two of these intervals only, that is the time before, t_2, and after, t_3, the interaction of the probe pulse. The full information contained in $R^{(3)}$ can be explored using three distinct pulses according to Eq. (4.96). The signal is detected in the heterodyne mode with the additional local oscillator field having the envelope $E_{LO}(t - t_{LO})$. Hence, the signal becomes (neglecting prefactors)

$$S_s(t_{LO}, T, \tau) = \int_{-\infty}^{\infty} dt \, \mathrm{Im}[E_{LO}(t - t_{LO})P_s^*(t, T, \tau)]. \tag{4.113}$$

The two-dimensional spectrum is obtained by taking the Fourier transform with respect to t_{LO} and τ, that is

$$S_s(\Omega_d, \Omega_e, T) = \int_0^{\infty} dt_{LO} \int_0^{\infty} d\tau \, e^{i\Omega_d t_{LO}} e^{i\Omega_e \tau} S_{2D}(t_{LO}, T, \tau). \tag{4.114}$$

As far as the detection of the signal field is concerned, this is analogous to pump–probe spectroscopy. However, by scanning the pulse separation variable τ and performing a Fourier transformation of the signal with respect to this variable, one circumvents the time–frequency interdependence and obtains a frequency-resolved signal using excitation pulses with a very broad spectrum. In fact, all pulses can be taken in the impulsive limit, and still, spectral resolution is obtained. In this limit, the three time arguments of S_{2D} in Eq. (4.114) correspond to the delay times between the four pulses. In terms of the response functions, we have $(t_1, t_2, t_3) = (t_{LO}, T, \tau)$. Two-dimensional spectra are presented in the plane of the excitation, Ω_e, and detection, Ω_d, frequencies as a function of the delay time T.

In two-dimensional spectroscopy, one distinguishes three phase-matching directions given by the following conditions for the wavevector $\boldsymbol{K}(n_1, n_2, n_3)$:

$$\boldsymbol{k}_R = \boldsymbol{K}(-1, 1, 1) = -\boldsymbol{k}_1 + \boldsymbol{k}_2 + \boldsymbol{k}_3, \tag{4.115}$$

$$\boldsymbol{k}_{NR} = \boldsymbol{K}(1, -1, 1) = \boldsymbol{k}_1 - \boldsymbol{k}_2 + \boldsymbol{k}_3, \tag{4.116}$$

$$\boldsymbol{k}_{DQ} = \boldsymbol{K}(1, 1, -1) = \boldsymbol{k}_1 + \boldsymbol{k}_2 - \boldsymbol{k}_3, \tag{4.117}$$

and accordingly for the frequencies $\Omega(n_1, n_2, n_3)$. The respective contributions are called rephasing, $\boldsymbol{k}_R$, nonrephasing, $\boldsymbol{k}_{NR}$, and double-quantum coherence, $\boldsymbol{k}_{DQ}$, signals. The related polarization components are readily obtained from Eq. (4.97) within the rotating wave approximation.

The rephasing, $R_R(t_3, t_2, t_1)$, and nonrephasing, $R_{NR}(t_3, t_2, t_1)$, response functions have already been defined in Eqs. (4.105) and (4.106), respectively. The double-quantum coherence response function is given by

$$R_{DQ}^{(3)}(t_3, t_2, t_1) = R_4(t_3, t_2, t_1) + R_7(t_3, t_2, t_1). \tag{4.118}$$

In what follows we specify these contributions for a three-level system ϕ_g, ϕ_e, ϕ_f sketched in Figure 4.2 with the simple relaxation model, according to Eqs. (4.70)–(4.73). For the rephasing contribution, we obtain

$$\begin{aligned} R_R^{(3)}(t_3, t_2, t_1) = &\left|d_{eg}\right|^4 I_{eg}(t_3) I_{ee}(t_2) I_{ge}(t_1) \\ &+ \left|d_{eg}\right|^4 I_{eg}(t_3) I_{gg}(t_2) I_{ge}(t_1) \\ &- \left|d_{eg}\right|^2 \left|d_{fe}\right|^2 I_{fe}(t_3) I_{ee}(t_2) I_{ge}(t_1). \end{aligned} \tag{4.119}$$

For the nonrephasing contribution, we have

$$\begin{aligned} R_{NR}^{(3)}(t_3, t_2, t_1) = &\left|d_{eg}\right|^4 I_{eg}(t_3) I_{ee}(t_2) I_{eg}(t_1) \\ &+ \left|d_{eg}\right|^4 I_{eg}(t_3) I_{gg}(t_2) I_{eg}(t_1) \\ &- \left|d_{eg}\right|^2 \left|d_{fe}\right|^2 I_{fe}(t_3) I_{fe}(t_2) I_{eg}(t_1). \end{aligned} \tag{4.120}$$

Inspecting these two expressions, we notice that the rephasing contributions have a phase dependence $\propto e^{-i\omega_{eg}(t_1 - t_3)}$, whereas for the nonrephasing contributions, it is $\propto e^{-i\omega_{eg}(t_1 + t_3)}$. Thus, for the rephasing contribution, the phase cancels for $t_1 = t_3$. This fact is not only responsible for the name, but it is also explored in photon echo experiments (see Further Reading).

Finally, we have for the double-quantum coherence contribution:

$$\begin{aligned} R_{DQ}^{(3)}(t_3, t_2, t_1) = &\left|d_{eg}\right|^2 \left|d_{fe}\right|^2 I_{eg}(t_3) I_{fg}(t_2) I_{eg}(t_1) \\ &- \left|d_{eg}\right|^2 \left|d_{fe}\right|^2 I_{fe}(t_3) I_{fg}(t_2) I_{eg}(t_1), \end{aligned} \tag{4.121}$$

which is not observed for a two-level system.

Two-dimensional spectroscopy is an ideal time-domain experiment such that the impulsive limit can be taken for all fields. This allows to perform all four time integrations in Eq. (4.113) to obtain for the signal in a particular phase-matching direction (A_i are the field amplitudes)

$$S_s(t_{LO}, T, \tau) = A_{LO} A_3 A_2 A_1 \frac{n_{mol}}{\hbar^3} \mathrm{Re}[R_s(t_{LO}, T, \tau)], \tag{4.122}$$

with s = (R, NR, DQ). For the purpose of illustration let us discuss the rephasing and nonrephasing signals for the case where $T = 0$, that is there is no evolution during the population time. This implies that $R_2 = R_3$ and $R_1 = R_4$ in Eqs. (4.119) and (4.120), respectively. For the rephasing signal, we have

$$
\begin{aligned}
S_R(\Omega_d, \Omega_e, 0) = A_{LO} A_3 A_2 A_1 \frac{n_{mol}}{2\hbar^3} & \left\{ \frac{2|d_{eg}|^4}{[i(\Omega_e + \omega_{eg}) - \gamma_{eg}][i(\Omega_d - \omega_{eg}) - \gamma_{eg}]} \right. \\
& + \frac{|d_{eg}|^4}{[i(\Omega_e - \omega_{eg}) - \gamma_{eg}][i(\Omega_d + \omega_{eg}) - \gamma_{eg}]} \\
& - \frac{|d_{fe}|^2 |d_{eg}|^2}{[i(\Omega_e + \omega_{eg}) - \gamma_{eg}][i(\Omega_d - \omega_{fe}) - \gamma_{fe}]} \\
& \left. - \frac{|d_{fe}|^2 |d_{eg}|^2}{[i(\Omega_e - \omega_{eg}) - \gamma_{eg}][i(\Omega_d + \omega_{fe}) - \gamma_{fe}]} \right\},
\end{aligned}
\tag{4.123}
$$

and for the nonrephasing signal, we obtain

$$
\begin{aligned}
S_{NR}(\Omega_d, \Omega_e, 0) = A_{LO} A_3 A_2 A_1 \frac{n_{mol}}{2\hbar^3} & \left\{ \frac{2|d_{eg}|^4}{[i(\Omega_e - \omega_{eg}) - \gamma_{eg}][i(\Omega_d - \omega_{eg}) - \gamma_{eg}]} \right. \\
& + \frac{2|d_{eg}|^4}{[i(\Omega_e + \omega_{eg}) - \gamma_{eg}][i(\Omega_d + \omega_{eg}) - \gamma_{eg}]} \\
& - \frac{|d_{fe}|^2 |d_{eg}|^2}{[i(\Omega_e - \omega_{eg}) - \gamma_{eg}][i(\Omega_d - \omega_{fe}) - \gamma_{fe}]} \\
& \left. - \frac{|d_{fe}|^2 |d_{eg}|^2}{[i(\Omega_e + \omega_{eg}) - \gamma_{eg}][i(\Omega_d + \omega_{fe}) - \gamma_{fe}]} \right\}.
\end{aligned}
\tag{4.124}
$$

Inspecting these expressions, we first notice that rephasing and nonrephasing spectra will be observed in different quadrants of the (Ω_e, Ω_d) plane. That is, for rephasing, one has $(-, +)$ and $(+, -)$, whereas for nonrephasing, the quadrants are $(+, +)$ and $(-, -)$. Often, one assumes $\Omega_d > 0$ such that half of the terms in Eqs. (4.123) and (4.124) can be neglected.

Second, the Fourier transform yields a complex signal where each dimension, Ω_d and Ω_e, contains a real and an imaginary part being called absorptive and dispersive contributions, respectively (cf. Eq. (4.67)). In the two-dimensional spectrum, both contributions are overlaid such that by taking the real part of Eqs. (4.123) and (4.124) one does not obtain a purely absorptive spectrum but rather a mixture of the individual absorptive and dispersive components. This circumstance complicates the

overall shape of the spectrum, which for multilevel systems renders the analysis to become a difficult task. To cope with this situation, one can extract the absorptive part of the two-dimensional signal by adding rephasing and nonrephasing contributions according to

$$S_{\text{abs}}(\Omega_d, \Omega_e, 0) = \text{Re}\big\{ S_R(\Omega_d, -\Omega_e, 0) + S_{\text{NR}}(\Omega_d, \Omega_e, 0) \big\}$$

$$= A_{\text{LO}} A_3 A_2 A_1 \frac{n_{\text{mol}}}{\hbar^3} \left\{ \frac{2|d_{eg}|^4 \gamma_{eg}^2}{[(\Omega_e - \omega_{eg})^2 + \gamma_{eg}^2][(\Omega_d - \omega_{eg})^2 + \gamma_{eg}^2]} \right.$$

$$\left. - \frac{d_{eg}|^2|d_{fe}|^2 \gamma_{eg}\gamma_{fe}}{[(\Omega_e - \omega_{eg})^2 + \gamma_{eg}^2][(\Omega_d - \omega_{fe})^2 + \gamma_{fe}^2]} \right\}. \tag{4.125}$$

Different situations are sketched in Figure 4.3. In panel (a), the case of a two-level system is plotted (that is, only the first term of Eq. (4.125)). Adding a third level (panel (b)) yields ESA for excitation at ω_{eg} and detection at ω_{fe}. For level schemes having coupled transitions, the so-called cross-peaks appear for $\Omega_e \neq \Omega_d$ (panel (c)).
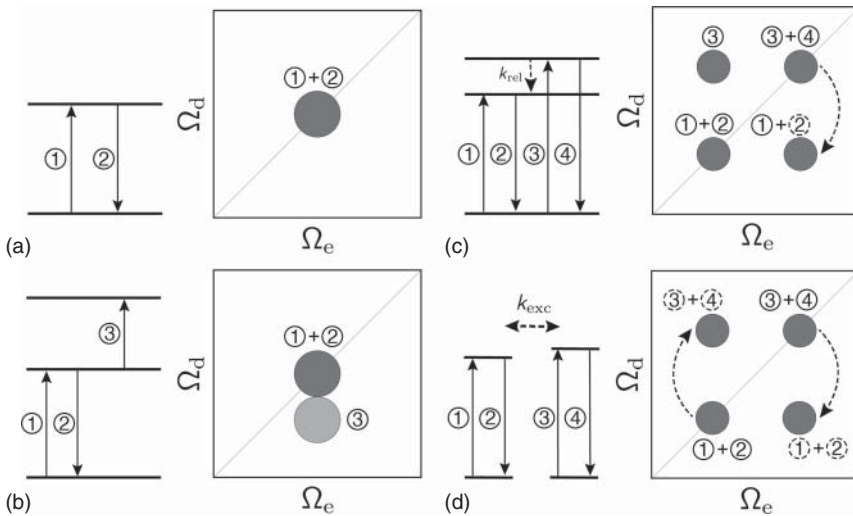
Figure 4.3 Schematic view of different scenarios of two-dimensional spectroscopy. The signal is shown as a function of excitation, Ω_e, and detection, Ω_d, frequencies with the diagonal ($\Omega_e = \Omega_d$) being marked by the line (cf. Eq. (4.125)). (a) For a two-level system, one observes a peak on the diagonal due to GSB (1) and SE (2) processes. (b) For a three-level system, one has in addition a peak due to ESA (3), which has a different sign. (c) For a three-level system with close-lying excited states (in the observation window), there are peaks due to GSB/SE on the diagonal. If both transitions share the same ground state as is the case for interacting systems, there appear cross-peaks off the diagonal. For example, (1) for excitation of the higher transition but detection at the lower transition where GSB is observed. If population relaxation is included with rate k_{rel}, the intensities of the peaks change, and new contributions become possible such as SE (2) below the diagonal. (d) Chemical exchange spectroscopy measures the interconversion of two species in equilibrium by tagging a transition with the excitation pulses. With increasing population time, cross-peaks appear, allowing to extract the exchange rate k_{exc}.

They provide information, for example on the existence and strength of the coupling (an example is given in Figure 5.16).

Taking into account the population relaxation, redistribution of intensity between peaks and appearance of new peaks can be observed. This is shown in Figure 4.3c, where population relaxation between the two excited states leads, for instance, to a redistribution of intensity from the upper diagonal peak to the peak below the diagonal due to the stimulated emission channel (an example is given in Figure 9.4).[16]

Two-dimensional spectroscopy can also be used to investigate the so-called chemical exchange, that is the interconversion between species, for instance, due to isomerization (cf. Figure 2.4) in equilibrium. Here, a transition of one species is initially tagged by the excitation pulses. If the lifetime of this excitation exceeds the time scale for interconversion, the emergence of the new species having a different transition frequency can be observed in the cross-peak region, as shown in Figure 4.3d (for an application, see Figure 8.4).

4.4 Field Quantization and Spontaneous Emission of Light

If an excited electronic state has been prepared as a result of a photoabsorption process in the molecule, this state has a finite lifetime. It is a consequence of spontaneous transitions to the electronic ground state accompanied by a photoemission process. The radiative decay results from the coupling of the molecule to the vacuum state of the electromagnetic field. The appropriate description therefore demands for a quantization of the radiation field. Here, we only give an intuitive picture and present some formulas for further use in Chapter 9.

Since the radiation field can be considered as a reservoir coupled to the molecular electronic states, the spontaneous emission of a photon is described in analogy to the transition processes resulting from system–reservoir coupling discussed in Chapter 3. The specific point here, of course, is the form of the coupling operator H_{int} between the electronic states and the quantized radiation field. One usually starts with the minimal coupling Hamiltonian, Eq. (4.8). However, instead of treating the radiation field classically, a quantum description is introduced. In doing so, we assume that the radiation field is of low intensity such that the term $\propto \boldsymbol{A}^2$ can be neglected as compared with the one $\propto \boldsymbol{p}_j \boldsymbol{A}$. Specifying our consideration to electronic transitions only, the interaction Hamiltonian follows as[17]

$$H_{\text{int}} = -\frac{e}{m_{\text{el}}c}\sum_j \boldsymbol{p}_j \boldsymbol{A}(\boldsymbol{r}_j). \tag{4.126}$$

Field quantization can be achieved by expanding the vector potential $\boldsymbol{A}(\boldsymbol{r})$ in terms of plane waves, with wavevectors $\boldsymbol{k}$ pointing in the propagation direction. Usually,

---

16) Population relaxation effects can be accounted for using, for instance, a response function formulation in terms of direct propagations, see Further Reading.

17) Note that, in principle, both terms of the minimal coupling Hamiltonian can be accounted for by applying a unitary transformation similar to Eq. (4.10). For the calculation of the emission rate, it suffices to stay with the linear term alone (see also Section 9.10.2).

this is done assuming that the radiation field is contained in a volume L^3 (box with lengths L, quantization volume). This gives

$$A(\boldsymbol{r}) = \sum_{\lambda,\boldsymbol{k}} N_{\boldsymbol{k}} \boldsymbol{n}_{\lambda\boldsymbol{k}} \left[\hat{a}_{\lambda\boldsymbol{k}} e^{i\boldsymbol{kr}} + \text{h.c.} \right]. \tag{4.127}$$

The vector potential is a transverse field, and every partial wave can be characterized by two (linear independent) transverse ($\boldsymbol{kn}_{\lambda\boldsymbol{k}} = 0$) polarization directions with unity vectors $\boldsymbol{n}_{\lambda\boldsymbol{k}}$ ($\lambda = 1,2$). Further, we introduced the normalization constant $N_{\boldsymbol{k}} = (2\pi\hbar c^2/L^3\omega_{\boldsymbol{k}})^{1/2}$ as well as the photon dispersion relation $\omega_{\boldsymbol{k}} = c|\boldsymbol{k}|$. Finally, we have the photon creation and annihilation operators, $\hat{a}_{\lambda\boldsymbol{k}}^+$ and $\hat{a}_{\lambda\boldsymbol{k}}$, respectively, which fulfill the commutation relations of the harmonic oscillator operators (cf. Section 2.5.2). With the help of these operators, the energy of the photon field can be written as[18]

$$H_{\text{phot}} = \sum_{\lambda,\boldsymbol{k}} \hbar\omega_{\boldsymbol{k}}(a_{\lambda\boldsymbol{k}}^+ a_{\lambda\boldsymbol{k}} + 1/2). \tag{4.128}$$

Returning to Eq. (4.126), we arrive at the following interaction Hamiltonian:

$$H_{\text{int}} = -\frac{e}{m_{\text{el}}c} \sum_{j} \sum_{\lambda,\boldsymbol{k}} N_{\boldsymbol{k}} \boldsymbol{p}_j \boldsymbol{n}_{\lambda\boldsymbol{k}} \left[\hat{a}_{\lambda\boldsymbol{k}} e^{i\boldsymbol{kr}_j} + \text{h.c.} \right]. \tag{4.129}$$

In the remaining part of this section, this interaction Hamiltonian will be used to calculated the rate $k_{e\to g}$ for transitions from the excited electronic state $|\phi_e\rangle$ to the ground state $|\phi_g\rangle$ accompanied by the spontaneous emission of a photon with energy $\hbar\omega_{\boldsymbol{k}}$ and polarization λ. In doing so, we take the continuum limit for the quantization volume ($L^3 \to \infty$) and use $\sum_{\boldsymbol{k}} \to (L/2\pi)^3 \int d\boldsymbol{k}$. This gives

$$k_{e\to g} = \frac{2\pi}{\hbar} \sum_{\lambda} \frac{L^3}{(2\pi)^3} \int d^3\boldsymbol{k} \sum_{M,N} f_{eM} \left| \langle 0 | \langle \phi_e | \langle \chi_{eM} | H_{\text{int}} | \chi_{gN} \rangle | \phi_g \rangle | \lambda\boldsymbol{k} \rangle \right|^2$$
$$\times \delta(E_{eM} - \hbar\omega_{\boldsymbol{k}} - E_{gN}). \tag{4.130}$$

The excited electron-vibrational state with energy E_{eM} and with zero photons (vacuum state $|0\rangle$) decays into the state, with the energy E_{gN} of the electronic ground state releasing a photon in state $|\lambda\boldsymbol{k}\rangle$ and of energy $\hbar\omega_{\boldsymbol{k}}$. The initial population of the vibrational levels of the excited electronic states has been described by the thermal distribution f_{eM}, and a summation with respect to all vibrational levels of the final state is performed. Inserting the expression for the interaction Hamiltonian, one obtains

$$k_{e\to g} = \frac{e^2}{2\pi m_{\text{el}}^2 c^3} \sum_{\lambda} \int do \int_0^\infty d\omega_{\boldsymbol{k}} \, \omega_{\boldsymbol{k}} \sum_{M,N} f_{eM}$$
$$\times \sum_{j} |\langle \phi_e | \langle \chi_{eM} | e^{i\boldsymbol{kr}_j} \boldsymbol{n}_{\lambda\boldsymbol{k}} \boldsymbol{p}_j | \chi_{gN} \rangle | \phi_g \rangle|^2 \, \delta(E_{eM} - E_{gN} - \hbar\omega_{\boldsymbol{k}}). \tag{4.131}$$

Here, the three-dimensional wavevector integral has been rewritten by introducing spherical coordinates and, afterward, by replacing the $|\boldsymbol{k}|$-integral by a frequency integral. The integration with respect to the unit sphere in $\boldsymbol{k}$-space gives $\int d\Omega/2\pi$.

---

[18] In order to derive this expression, one has to start from Eq. (4.9) and use the relations (4.5) and (4.6) to obtain the quantized form of the physical fields.

The long-wavelength approximation can be used to simplify this expression, that is employing that $\boldsymbol{k}\boldsymbol{r}_j \approx \boldsymbol{k}\boldsymbol{X}_m$ is a small quantity to replace the exponential function in the matrix element by 1. This corresponds to the dipole approximation since one can replace the electronic matrix element of the momentum operator by the transition dipole moment. To show this, we start with the equation of motion for the electronic coordinate operator $\boldsymbol{r}_j$ given by

$$i\hbar \frac{\partial}{\partial t}\boldsymbol{r}_j = [\boldsymbol{r}_j, H_{\text{el}}]_- = i\hbar \frac{\boldsymbol{p}_j}{m_{\text{el}}}. \tag{4.132}$$

Thus, the matrix elements of the momentum operator can be written as

$$\langle \phi_e | \sum_j \boldsymbol{n}_{\lambda k}\boldsymbol{p}_j|\phi_g\rangle = -i\frac{m_{\text{el}}}{\hbar}\boldsymbol{n}_{\lambda k}\sum_j \langle \phi_e|(\boldsymbol{r}_j H_{\text{el}} - H_{\text{el}}\,\boldsymbol{r}_j)|\phi_g\rangle$$

$$= -i\frac{m_{\text{el}}}{\hbar}\boldsymbol{n}_{\lambda k}(E_g - E_e)\sum_j \langle \phi_e|\boldsymbol{r}_j|\phi_g\rangle$$

$$= i\frac{m_{\text{el}}}{\hbar e}(E_e - E_g)\boldsymbol{n}_{\lambda k}\boldsymbol{d}_{eg}. \tag{4.133}$$

Here, $\boldsymbol{d}_{eg}$ is the transition dipole matrix element (which should be independent of the nuclear coordinates), and E_e and E_g are the electronic energy levels. To get the final formula used in Section 6.4 to calculate the emission spectrum related to the transition between two electronic states coupled to nuclear DOFs, we have to compute $\sum_\lambda \int do\, |\boldsymbol{n}_{\lambda k}\boldsymbol{d}_{eg}|^2$. In order to do this, we note that an arbitrary vector $\boldsymbol{A}$ if expanded in the basis that is spanned by the two transversal polarization unit vectors $\boldsymbol{n}_{\lambda k}$ and the longitudinal unit vector $\boldsymbol{k}/|\boldsymbol{k}|$ is written as $\boldsymbol{A} = [\boldsymbol{k}\boldsymbol{A}]\boldsymbol{k}/k^2 + \sum_\lambda[\boldsymbol{n}_{\lambda k}\boldsymbol{A}]\boldsymbol{n}_{\lambda k}$. Thus, we may write for the expression including the transition dipole moment $\sum_\lambda|\boldsymbol{n}_{\lambda k}\boldsymbol{d}_{eg}|^2 = |\boldsymbol{d}_{eg}|^2 - |\boldsymbol{d}_{eg}\boldsymbol{k}|^2/k^2$. Carrying out the solid angle integration $\int do$, we obtain $8\pi|\boldsymbol{d}_{eg}|^2/3$ and the rate results as (note $\omega_k \to \omega$ and $|\boldsymbol{d}_{eg}|^2 \to |d_{eg}|^2$)

$$k_{e\to g} = \int\limits_0^\infty d\omega\, \frac{4\omega^3\left|d_{eg}\right|^2}{3c^3}\sum_{M,N}f_{eM}|\langle\chi_{eM}|\chi_{gN}\rangle|^2\,\delta(E_{eM} - E_{gN} - \hbar\omega). \tag{4.134}$$

Since the frequency integration is restricted by the δ-function, we replaced $E_e - E_g$ by $\hbar\omega$.

References

1 S. Mukamel, *Principles of Nonlinear Optical Spectroscopy*, (Oxford University Press, Oxford, 2000).

2 S. Mukamel and D. Abramavicius, Chem. Rev. **104**, 2073 (2004).

Further Reading

- Introduction into the theory of nonlinear optical spectroscopy:

  S. Mukamel, *Principles of Nonlinear Optical Spectroscopy*, (Oxford University Press, Oxford, 2000).

  P. E. Powers, *Fundamentals of Nonlinear Optics*, (CRC Press, Boca Raton, FL, 2011).

- Two–dimensional spectroscopy:

  M. Cho, *Two–Dimensional Optical Spectroscopy*, (CRC Press, Boca Raton, FL, 2009).

  F.D. Fuller and J.P. Ogilvie, *Experimental Implementations of Two–Dimensional Fourier Transform Electronic Spectroscopy*, Ann. Rev. Phys. Chem. **66**, 667 (2015).

  A. Gelzinis, R. Augulis, V. Butkus, B. Robert, and L. Valkunas, *Two–Dimensional Spectroscopy for Nonspecialists*, Biochim. Biophys. Acta B **1860**, 271 (2019).

  P. Hamm and M. Zanni, *Concepts and Methods of 2D Infrared Spectroscopy*, (Cambridge University Press, Cambridge, 2011).

- Numerical methods for nonlinear spectroscopy

  M.F. Gelin, L. Chen, and W. Domcke, *Equation-of-Motion Methods for the Calculation of Femtosecond Time-Resolved 4-Wave-Mixing and N-Wave-Mixing Signals*, Chem. Rev. **122**, 17339–17396 (2022).

- Applications of time–resolved spectroscopy:

  O. Kühn and L. Wöste (eds.), *Analysis and Control of Ultrafast Photoinduced Reactions*, Springer Series in Chemical Physics Vol. **87**, (Springer–Verlag, Heidelberg, 2007).

5

Vibrational Dynamics: Energy Redistribution, Relaxation, and Dephasing

In Chapter 3, we introduced some fundamental concepts for the description of quantum dynamics ranging from the coherent (Schrödinger equation) to the incoherent (Pauli master equation) regime. Density matrix theory was shown to provide a versatile tool for all types of dynamics, thus establishing the link between these two limits. The type of dynamics realized in an actual system, of course, depends on the Hamiltonian describing the way active and reservoir DOFs interact with each other. The definition of active coordinates is closely related to the type of preparation of the initial state, for instance due to photon absorption.

In the present chapter, we discuss different scenarios for vibrational dynamics in systems ranging from simple diatomic molecules in solution to large polyatomic molecules in the gas or condensed phase. The key to the derivation of vibrational energy transfer rates for inter- and intramolecular vibrational energy flow within a given adiabatic electronic state is provided by a low-order expansion of the respective interaction Hamiltonian. This approach allows to define the parameters entering the system–reservoir Hamiltonian on a microscopic level. For the specific case of the Caldeira–Leggett model, a generalized Langevin equation for the dynamics of an active coordinate under the influence of dissipative and stochastic forces is derived. It provides a route to the calculation of spectral densities. Finally, a quantum-classical approach is introduced, where the quantized active coordinate is coupled to a classical bath. It is particularly well suited for the calculation of stationary and time-resolved infrared spectra.

5.1 Introduction

The investigation of vibrational energy flow in polyatomic molecules is of pivotal importance for the understanding of chemical reaction dynamics. In Section 2.5.3, it was pointed out that the definition of reaction coordinates comes along with the incorporation of a large number of environmental DOFs. If the latter are only weakly coupled, they still might cause energy dissipation out of the reaction coordinate. If there is a stronger coupling to specific environmental motions, this

might provide a means, for instance to accelerate the reaction dynamics by helping to overcome potential barriers. These two examples already indicate that the type of dynamics may cover the whole range from the incoherent to the coherent regime.

The starting point for the description of vibrational energy flow will be a situation in which energy is contained in specific vibrational modes of a molecule. Such a state could have been prepared, for example by an external laser field (cf. Section 6.5). Taking a time-dependent point of view, this initial state often can be thought of as a *superposition* of eigenstates of the vibrational Hamiltonian (cf. Eq. (6.104)). Then, the subsequent dynamics of the system as characterized, for example by the survival amplitude equation (3.29), will show a behavior similar to the ones depicted in Figure 3.2. An experimental example is given in Figure 5.1, where results are shown for the creation and observation of a superposition state composed of a so-called Fermi resonance pair of states (cf. Section 5.2.1 and Figure 5.3).

For large polyatomics, knowledge of these eigenstates is, however, hardly available. Therefore, the interpretation of experiments conveniently starts with some *zeroth-order states* chosen according to the preparation conditions. For an excitation with a laser field, for instance, this leads to a definition of the zeroth-order states in close relation to the classification into optically (or infrared) *bright* and *dark* states, depending on whether there is some oscillator strength for the transition to the considered state. Typical choices for the zeroth-order states are derived from, for example normal modes or localized vibrational modes along particular internal coordinates. In terms of the vibrational Hamiltonian, this approach could imply a Taylor expansion of the adiabatic PES allowing the specification of the zeroth-order states and the couplings between them. In more general terms, the PES can be written using the following correlation expansion (here for N coupled DOFs, not necessarily normal-mode coordinates):

$$V(q_1, \ldots, q_N) = \sum_{n=0}^{N} V^{(n)}(q_1, \ldots, q_N). \tag{5.1}$$

Here, $V^{(0)} = V(\{q_j = 0\})$ is the energetic off-set, the one-mode potential is given by $V^{(1)}(q_1, \ldots, q_N) = \sum_i V(\{q_{j \neq i} = 0\}, q_i)$, the two-mode correlation potential is $V^{(2)}(q_1, \ldots, q_N) = \sum_{i<j} V(\{q_{k \neq i,j} = 0\}, q_i, q_j) - (N-2)V^{(1)}(q_1, \ldots, q_N)$, and so on.

While this concept is straightforwardly applied to polyatomics in the gas phase, under certain conditions, it can be transferred to the condensed phase as well where, for instance the system and the reservoir part of the Hamiltonian are coupled by a potential due to a correlation expansion. The relaxation of energy from an initially excited state into other vibrational DOFs of a polyatomic molecule is called *intramolecular vibrational redistribution* (IVR). IVR will be on focus in Section 5.2 where we consider collision-free polyatomic molecules being observable in a molecular beam, for instance. Neglecting radiative couplings leading to emission also, it is clear from the outset that the total energy of the molecule is conserved. Depending on the number of DOFs and the couplings between them, the vibrational dynamics as observed in time-domain spectroscopy can cover a broad range of regimes. It may extend from a damped oscillation to an exponential decay at early times and to
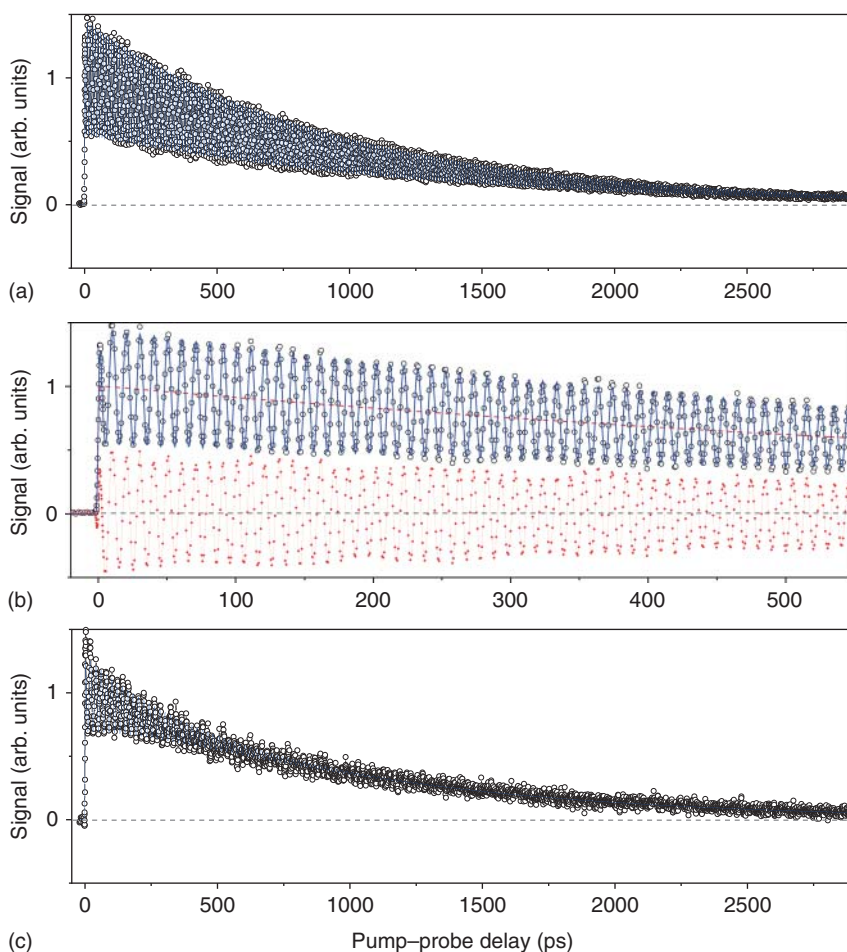
Figure 5.1 Pump–probe signal corresponding to the $[C_6H_5OH]^+$ ion yield after excitation of a pair of vibrational states (so-called Fermi resonance, cf. Figure 5.3) in the S_1 electronic state of phenol. In the signal, the population of one of the zeroth-order states is projected out, that is it is proportional to $P_{surv}(t)$ (see Eq. (3.29)). The overall decay of the signal is caused by H atom abstraction due to tunneling. Panels (a) and (c) correspond to different pairs having different initial vibrational energies. While in (a) IVR can be neglected, in panel (c) it causes a dephasing of the regular oscillations. Panel (b) shows the initial behavior of (a), with the red lines giving the result of a decomposition into decaying (dashed line) and oscillatory (thin line) contributions (figure courtesy of Kyung Chul Woo, for more details see also Woo and Kim [1]).

a power law decay at intermediate times before a stationary value is reached. In Section 5.2, how these different regimes can be rationalized will be discussed. Golden Rule-type approaches to IVR apparently cannot account for such a rich dynamics. However, going beyond the simple Golden Rule requires knowledge of the molecule's Hamiltonian, which is not easily obtained for larger systems. The useful concepts of the tier model and the state space approach will be introduced in Section 5.2.

The simplest condensed-phase situation one can study is the vibrational dynamics of a single diatomic solute molecule in an atomic solvent (infinite dilution limit). Here, the interaction between both subsystems will lead to energy dissipation into the solvent, where it is stored as translational motion. The irreversible energy transfer between the solute and the solvent is termed *vibrational energy relaxation* (VER) and will be on focus in Section 5.3.[1] An example for the case that the solvent is a rare gas matrix is shown in Figure 5.2.

The dynamics will of course become more complex if we go to molecular solvents. However, as will be shown in Section 5.3, the theoretical framework for modeling
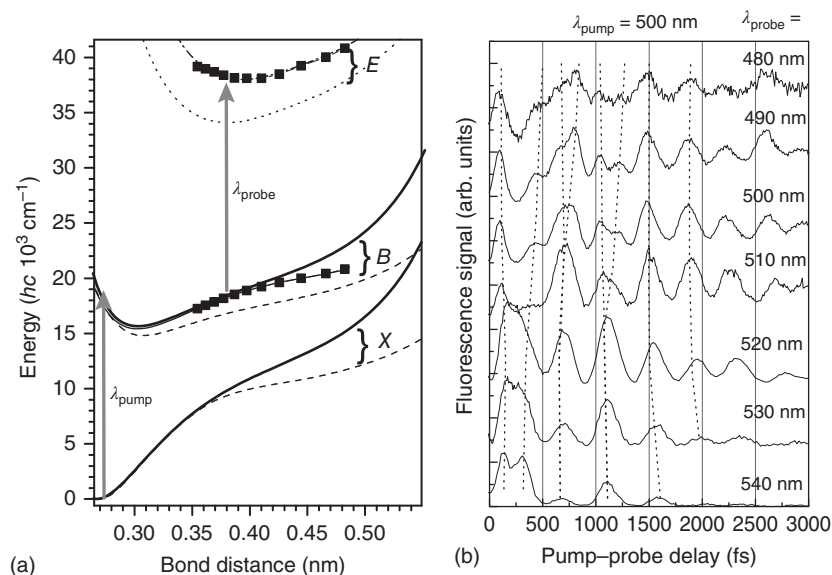
Figure 5.2 Pump–probe spectroscopy of the vibrational dynamics of a diatomic molecule (I_2) in a rare gas lattice (Kr). (a) Potential energy curves of the ground state *X*, the valence *B* state, and an ionic *E* state of I_2 if embedded in the Kr lattice. The solid lines correspond to calculations where the Kr lattice is relaxed to its minimum configuration for a given I_2 bond distance *R*. In contrast, the dashed lines display results for the Kr lattice frozen at its equilibrium configuration (in the absence of the guest molecule). The dotted ionic state curve corresponds to a fixed lattice as well. (b) Pump–probe spectra (the signal is measured in terms of the fluorescence from the ionic states) for pumping at 500 nm (transition from the *X* to the *B* state) and probing at different wavelengths (from the *B* to the *E* state, cf. the arrows in (a)). Shown are the probe beam absorption spectra versus the delay time between the pump and the probe pulse and for different probe wavelengths (numbers at the curves in (b)). Upon increasing the probe wavelength, the wave packet dynamics is tested at different energies and thus the bond lengths in the *B* state. The phase and frequency of the oscillations due to coherent I_2 bond vibration change as does the decay time of the oscillatory signal. This information from different pump–probe measurements can be used to construct an effective potential, which is shown with solid squares in (a) (Bargheer [2] – Reproduced by permission of the PCCP Owner Societies).

---

1) Note that according to our classification, this type of energy transfer would be of the dissipative type. Using the term "VER" in this chapter, we follow the convention which is widely adopted.

VER dynamics is rather generic, provided that the abovementioned low-order expansion of the total PES can be performed. This is most straightforward if the solvent is, for instance a low-temperature solid-state matrix. Here, the atoms perform only small amplitude motions around their equilibrium positions (Section 5.3). In the case of a solvent at liquid-state temperatures, a low-order expansion of the interaction potential leads to relaxation rates that are determined by the equilibrium correlation function of the force which is exerted by the solvent on the static solute (Section 5.3). Often, the decay of these types of correlation functions takes place on a rather short time scale. This allows for a modeling of the solvent in terms of collective harmonic oscillators in the vicinity of instantaneous configurations, even though the liquid's dynamics is inherently anharmonic on longer time scales (Section 5.3).

The most general situation of a polyatomic molecule in solution will be treated in Section 5.4. Here, it is shown how the system–reservoir concept can be applied resulting in relaxation rates that enter the density matrix equations of motion discussed in Section 3.6. Since energy conservation constrains relaxation dynamics, different types of multiple quantum transitions will become important, in particular for the relaxation of high-frequency modes.

There are various motivations for studying vibrational energy flow besides its general importance for reaction dynamics mentioned in the beginning of this section. On a fundamental level, the understanding of such processes requires knowledge about the molecular Hamiltonian, and in particular of the PES for nuclear motions as well as a sophisticated treatment of the dynamics. Thus, combining experimental observations with theoretical predictions provides an excellent testing ground for theoretical models in this respect. On the more practical side, one can imagine, for instance that vibrational energy has been deposited into a particular mode in order to trigger a chemical reaction. In such a case, it would be desirable to know to what extent this energy is lost, for example due to the release of heat into the surrounding solvent.

5.2 Intramolecular Vibrational Energy Redistribution

5.2.1 Zeroth-order Basis and State Mixing

In this section, we consider the case of isolated polyatomic molecules in a single adiabatic electronic state. We are interested in the redistribution of vibrational energy after it has been deposited into a certain vibrational state, for example by means of an electronic or infrared laser excitation.[2] The central question concerns the microscopic origins and mechanism of IVR. Let us recall that in Section 2.5.1 we learned about the normal mode expansion of the vibrational Hamiltonian obtained from the Born–Oppenheimer separation of electronic and nuclear DOFs. This description

---

2) We do not take into account the effect of rotations in the following discussion. While the overall rotation of large molecules can be safely neglected on the time scale of interest here (< 1 ns), internal rotations will have an effect on the density of states.

was based on the harmonic approximation to the PES in the vicinity of stationary points. Away from these stationary points, with increasing vibrational energy, the harmonic approximation breaks down, and anharmonic effects have to be included. An empirical anharmonic one-dimensional potential is given by the Morse potential shown in Figure 2.3. In more general terms, the PES can be expanded with respect to the (mass-weighted) normal-mode coordinates, $\{q_\xi\} = (q_{\xi_1}, q_{\xi_2}, \dots, q_{\xi_N})$, to obtain the N-dimensional vibrational Hamiltonian

$$
\begin{aligned}
H_{\text{vib}} = \frac{1}{2}\sum_\xi \left(p_\xi^2 + \omega_\xi^2 q_\xi^2 \right) + \sum_{\xi_i \xi_j \xi_k} K_{\xi_i \xi_j \xi_k} \; q_{\xi_i} q_{\xi_j} q_{\xi_k} \\
+ \sum_{\xi_i \xi_j \xi_k \xi_l} K_{\xi_i \xi_j \xi_k \xi_l} \; q_{\xi_i} q_{\xi_j} q_{\xi_k} q_{\xi_l} + \dots
\end{aligned}
\tag{5.2}
$$

Here, $K_{\xi_i \dots}$ are the anharmonic coupling constants, that is the derivatives of the PES with respect to the normal-mode coordinates.[3]

It should be emphasized that the usually collective normal-mode coordinates are not the only choice for a representation of the vibrational Hamiltonian. Alternatively, we could have used, for instance local modes pertaining to individual bonds. Then, the Hamiltonian contains couplings between these local modes, in general, due to potential and kinetic energy operators. Furthermore, anharmonicity can be accounted for by representing the n-mode potentials in Eq. (5.1) on a numerical grid. A combination of grid potentials and potentials from anharmonic coupling constants is possible as well.

An eigenstate of the harmonic part of H_{vib} in Eq. (5.2) can be classified according to the quanta contained in the different normal modes, that is

$$
\left| M_{\xi_1}, M_{\xi_2}, \dots, M_{\xi_N} \right\rangle = \left| M_{\xi_1} \right\rangle \dots \left| M_{\xi_N} \right\rangle \quad (M_{\xi_i} = 0, 1, \dots).
\tag{5.3}
$$

Given that the anharmonic coupling constants are small, Eq. (5.3) provides a reasonable choice for a zeroth-order basis. Concerning the anharmonic terms in Eq. (5.2), one distinguishes diagonal (all indices are equal, for instance $K_{\xi_i \xi_i \xi_i}$) and off-diagonal contributions. While the former lead to anharmonic dynamics of a particular mode, the latter couple different modes.

The effect of anharmonic mode coupling can be illustrated using the example of a so-called Fermi resonance interaction, which is typical for the coupling between a hydrogenic vibrational stretching ($q_{\xi_1} = q_1$) fundamental and a bending ($q_{\xi_2} = q_2$) overtone transition. For this example, the harmonic frequencies are $\omega_1 \approx 2\omega_2$, the relevant coupling term is $K_{122} q_1 q_2^2$, and the state space is composed of the zeroth-order states $|0, 0\rangle$, $|0, 1\rangle, |0, 2\rangle$, $|1, 0\rangle$, and so on (see Figure 5.3). In order to obtain a matrix representation of the vibrational Hamiltonian in this basis, one needs the matrix elements of the type

$$
\langle M_1, M_2 | q_1 q_2^2 | N_1, N_2 \rangle = \langle M_1 | q_1 | N_1 \rangle \langle M_2 | q_2^2 | N_{\xi_2} \rangle.
\tag{5.4}
$$

---

3) To simplify the notation, the factor $1/n!$ due to the nth order Taylor expansion has been included into the definition of the $K_{\xi_i \dots}$
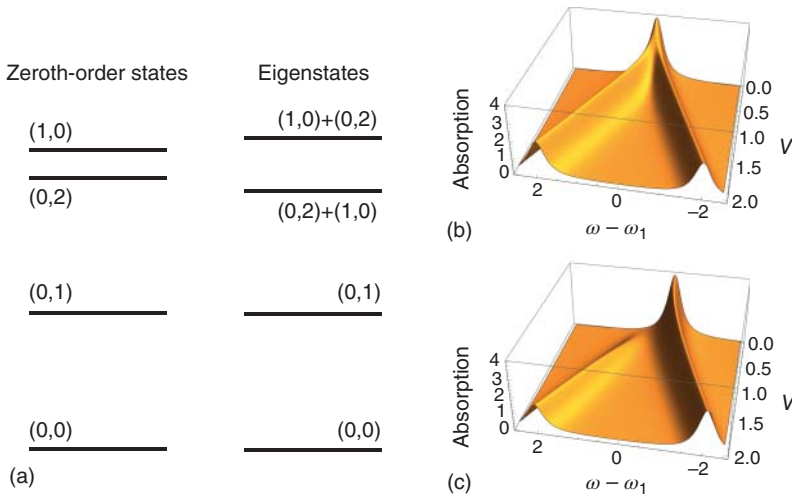
Figure 5.3 Mixing of zeroth-order vibrational states due to a Fermi resonance anharmonic coupling. (a) Zeroth-order harmonic oscillator states with quantum numbers (M_1, M_2) for a two-mode model where the second excited state of mode q_2, $(0, 2)$, is close to resonance with the first excited state of mode q_1, $(1, 0)$. The anharmonic coupling $\propto K_{122} q_1 q_2^2$ leads to the formation of eigenstates with mixed character. (b,c) Infrared absorption spectrum in dependence on the coupling strength for $\omega_1 - 2\omega_2 = 0$ (b) and $\omega_1 - 2\omega_2 = 1$ (c). The distribution of oscillator strengths is according to Eq. (5.8) with explicit expressions for the coefficients as given in Section 2.8.2.

Using the results of Section 2.5.2, one has

$$\langle M_1 | q_1 | N_1 \rangle = \frac{1}{\sqrt{2}\lambda_1} \left(\delta_{M_1, N_1 - 1} \sqrt{N_1} + \delta_{M_1, N_1 + 1} \sqrt{N_1 + 1} \right) \tag{5.5}$$

and

$$\langle M_2 | q_2^2 | N_2 \rangle = \frac{1}{2\lambda_2^2} \left(\delta_{M_2, N_2}(2N_2 + 1) + \delta_{M_2, N_2 - 2} \sqrt{N_2(N_2 - 1)} \right.$$
$$\left. + \delta_{M_2, N_2 + 2} \sqrt{(N_2 + 1)(N_2 + 2)} \right). \tag{5.6}$$

Restricting ourselves to the coupling between the states $|0, 2\rangle$ and $|1, 0\rangle$, we obtain a two-level Hamiltonian with diagonal entries $\varepsilon_1 = \omega_1$ and $\varepsilon_2 = 2\omega_2$ and the off-diagonal term $V = K_{112}/\lambda_1 \lambda_2^2$. The respective eigenvalue problem was solved in Section 2.8.2. The eigenstates can be written in terms of the zeroth-order states as follows:

$$|\kappa = \pm\rangle = \sum_{M_1, M_2} C_\kappa(M_1, M_2) |M_1, M_2\rangle$$
$$= C_\kappa(1, 0) |1, 0\rangle + C_\kappa(0, 2) |0, 2\rangle, \tag{5.7}$$

and the eigenenergies are given by Eq. (2.153).

It is instructive to discuss the mixing of zeroth-order states according to Eq. (5.7) in terms of the infrared absorption spectrum. For simplicity, we consider the simple Lorentzian lineshape model leading to Eq. (4.67). The dipole moment will depend

linearly on the vibrational coordinates, that is $\hat{\mu} = \mu_1 q_1 + \mu_2 q_2$. If the system is initially in its ground state, $|0, 0\rangle$, the strength of a transition to the eigenstate $|\kappa\rangle$ is given by the absolute square of the respective dipole matrix element. Using Eqs. (5.5) and (5.6), one obtains

$$\left| \langle \pm | \hat{\mu} | 0, 0 \rangle \right|^2 = \left| C_\pm^*(1, 0) \langle 0, 1 | \mu_1 q_1 | 0, 0 \rangle + C_\pm^*(0, 2) \langle 2, 0 | \mu_2 q_2 | 0, 0 \rangle \right|^2$$

$$= \frac{|\mu_1|^2}{2\lambda_1^2} \left| C_\pm(1, 0) \right|^2. \tag{5.8}$$

Notice that both transitions obtain their oscillator strength from the bright q_1 mode. In Figure 5.3, the effect of Fermi resonance coupling on the infrared spectrum is illustrated for the cases of a perfect resonance $\omega_1 = 2\omega_2$ and a mismatch $\Delta\varepsilon$. According to Section 2.8.2, Eqs. (2.171) and (2.172), for the perfect resonance it holds that $\left| C_\pm(1, 0) \right|^2 = \left| C_\pm(0, 2) \right|^2 = 1/2$. Thus, each eigenstate is composed of equal contributions from the two zeroth-order states. Since a transition having no oscillator strength (dark q_2 overtone) contributes to a bright state of the anharmonically coupled system, the dark transition is said to "borrow" oscillator strength from the bright one.

In principle, there are different possibilities for the so-called *zeroth-order* basis, and the best choice will depend on the experimental situation at hand. For example, using the normal mode Hamiltonian (5.2), the presence of, for instance a strong Fermi resonance between two DOFs leaves the question whether or not to diagonalize the Hamiltonian in the subspace of these two modes and work with the respective eigenstates whose residual coupling to the remaining modes, of course, would be modified. At this point, the type of preparation of the initial state plays an important role as shown in Figure 5.3. Let us assume that the excitation is due to an infrared laser having a narrow spectral bandwidth. In this case, the prepared state will be close to an eigenstate of the full Hamiltonian. Therefore, a prediagonalization of the Fermi resonance interaction might be suitable, that is the zeroth-order basis set would include the strongest anharmonic coupling. On the other hand, if the excitation is due to an ultrafast broadband laser infrared pulse, a coherent superposition state is prepared, which could be of more local character (cf. Section 6.5); that is, in our example, it could be closer to the fundamental stretching transition. In this case, the use of the normal mode basis would be appropriate.

Let us assume that we would be able to obtain the eigenstates of the *full* Hamiltonian, Eq. (5.2), although this is, of course, impossible for larger systems. In terms of high-resolution frequency-domain spectra, this gives the means to reproduce the numerous spectral lines that upon increasing the excitation energy merge into a quasi-continuum. However, unless these eigenstates are expressed as superposition states of, for instance harmonic oscillator states, there would be little insight gained into the nature of the eigenstates and the resulting transitions. In time-domain experiments, the initially prepared wave packet will be a complicated superposition of many eigenstates. However, as in our Fermi-resonance example, only the choice of a suitable basis that captures the nature of the initially excited state enables a straightforward analysis of the vibrational dynamics, see also Figure 5.3.

Figure 5.4 Preparation of bright (zeroth-order) states (for example, by laser light absorption, cf. Chapter 6) starting from some set of initial states. The subsequent dynamics will be influenced by the coupling between the bright and the dark states. In the lower right part, the structure of the Hamiltonian is sketched for the case of a single bright state $|0\rangle$ (E_0, black) and a large number of dark states $|\alpha\rangle$ (E_α, light gray). The residual couplings $V_{0\alpha}$ ($V_{\beta 0}$) are shown as dark gray areas.
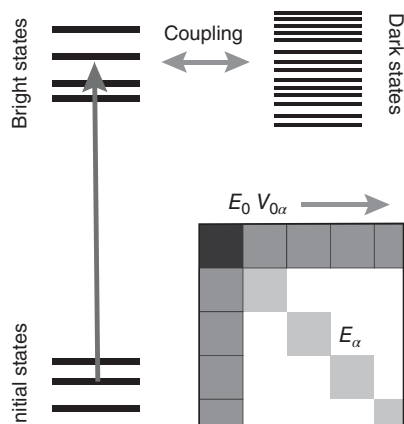
This discussion reflects the influence of selection rules and the initial state preparation time scale on the choice of the zeroth-order basis for the description of the IVR process. In any case, there will be a residual coupling between the initially excited bright states and the usually large number of dark states. This situation, which comprises the essential theme of IVR dynamics, is illustrated in Figure 5.4.

5.2.2 Golden Rule and Beyond

The zeroth-order bright state basis that is shown in Figure 5.4 recalls the discussion of the Golden Rule in Section 3.3. In the context of IVR, the Golden Rule description has been given by Bixon and Jortner in the 1960s.[4] In order to emphasize the basic idea, let us assume that there is initially only a single bright state appreciably populated. For simplicity, we suppose that the vibrational Hamiltonian has been *prediagonalized* with the single bright state $|0\rangle$, with energy E_0 projected out. Let E_α denote the energy of the prediagonalized bath (dark) states, and $V_{0\alpha}$ the coupling of the bright state to the prediagonalized bath (cf. Figure 5.4). If we further assume that the bath has a quasi-continuous spectrum, we recover the Hamiltonian equation (3.63), and the Golden Rule rate for IVR is according to Eq. (3.76) given by

$$k_{\text{IVR}} = \frac{2\pi}{\hbar} \sum_\alpha |V_{0\alpha}|^2 \delta(E_0 - E_\alpha). \tag{5.9}$$

First, we should recall that Eq. (5.9) is a result that is valid in second-order perturbation theory; that is, $|V_{0\alpha}|^2$ has to be sufficiently small. This assumption is reasonable since upon prediagonalization of the bath the anharmonic coupling strengths are redistributed over many bath eigenstates. It is important to remember, however, that the coupling has to be much larger than the mean level spacing of the bath in order to validate the Golden Rule description. In a next step, we replace the coupling matrix by its root mean square value across the bath spectrum, V_{rms}^2. In other words, we throw away all details of this coupling such as its energy dependence and

---

4) The original reference is Bixon and Jortner [3].

correlations between different couplings. Replacing the sum over the delta functions by the *global* density of states,

$$\mathcal{N}(E) = \sum_{\alpha=1}^{N_\alpha} \delta(E - E_\alpha), \tag{5.10}$$

we obtain the Bixon–Jortner rate for IVR,

$$k_{\text{IVR}} = \frac{2\pi}{\hbar} V_{\text{rms}}^2 \, \mathcal{N}(E_0). \tag{5.11}$$

Equation (5.11) expresses the IVR rate in terms of the quantities, V_{rms}^2 and $\mathcal{N}(E)$, that are experimentally available from an analysis of the positions and relative intensities of spectral lines in high-resolution frequency domain vibrational spectroscopy. Thus, provided that we have obtained these values, and the conditions leading to the Golden Rule expression are fulfilled, the IVR rate will by construction match the experimentally observed rate. But one should be aware at this point that there is no direct link between V_{rms} and the anharmonic coupling constants entering Eq. (5.2).

So far, we have assumed that there is an infinite number of accessible bath states. However, at not too high energies, the number of accessible states, N_{IVR}, in polyatomic molecules may be rather large but still finite. This fact is characterized by the so-called dilution factor $\sigma = \bar{P}_{\text{surv}}(t \to \infty)$, that is the time-averaged long-time survival probability. Assuming that all states are equally populated, the latter is proportional to N_{IVR}^{-1} and experimentally accessible (Figure 5.6), compare the discussion of Figure 3.2. Taking this into account, the decay of the survival probability should be characterized by the function:

$$P_{\text{surv}}(t) \equiv |\langle 0(t)| \, 0 \rangle|^2 = (1 - \sigma)e^{-k_{\text{IVR}}t} + \sigma. \tag{5.12}$$

There are many examples where this Golden Rule approach has been successfully applied. In the following discussion, we concentrate, however, on situations where the dynamics cannot be described by a single exponential decay. In Figure 5.1, we show experimental data indicating a quantum beat-type behavior with and without disturbance by IVR. The possibility of such dynamics has already been discussed in more general terms in Section 3.3. In principle, the existence of a finite dilution factor already indicates that there is the possibility for a revival of the survival amplitude after a finite time. In the context of IVR, there are more points that need to be addressed.

First, given an initial bright state, one can imagine that it is not equally coupled to all energetically possible dark states, in contrast to the assumption that led to Eq. (5.11). Thus, there will be a certain finite set of dark states coupled to the initial state $|0\rangle$. This can be seen as a direct consequence of the local character of chemical bonding. This reasoning can be extended to the first set of strongly coupled dark states; that is, they in turn will be strongly coupled to another finite set of dark states only. This leads to the so-called *tier* model of IVR, which is illustrated in Figure 5.5. Given a normal-mode expansion of the vibrational Hamiltonian, the partitioning of the dark states into different tiers can proceed, for instance using a classification with respect to the order of the anharmonic coupling. However, one has to keep in mind that resonance conditions have to be considered as well when judging efficient
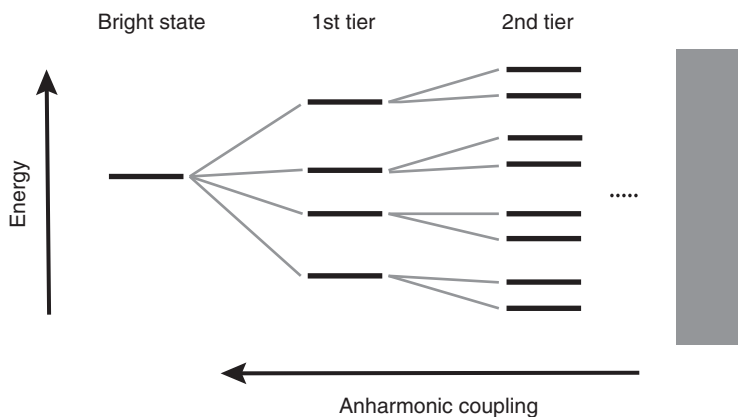
Figure 5.5 Hierarchical structure of IVR as described by the tier model. A single bright state is strongly coupled only to a finite set of dark states constituting the first tier. The first tier is then coupled to another set of dark states in the second tier and so on. With increasing tier number, the density of states increases, but the anharmonic coupling strength decreases.

IVR pathways. For instance, it is possible that high-order couplings dominate when the respective dark states are in better resonance than those coupled via low-order anharmonicities.

The tier model is in fact a two-dimensional projection of the *vibrational state space* model. Here, the energy flow is considered in the space spanned, for example by the N-dimensional harmonic oscillator vectors $\left| M_{\xi_1}, M_{\xi_2}, \ldots, M_{\xi_N} \right\rangle$. This is illustrated in Figure 5.6 where we also see another important feature of IVR, namely its energy dependence. For a given state $|0\rangle$, there is a certain threshold below which this state will be effectively isolated from the rest of the state space. Upon increasing the energy of the initial state, the average number of dark states increases, and so does the average strength of anharmonic couplings. Figure 5.6a–c schematically shows three different cases realized when moving across the *IVR threshold*. They correspond to a situation of small, moderate, and large couplings. Clearly, the number of relevant couplings indicated by thick lines increases with energy such that from some initial state $|0\rangle$ an increasing number of states becomes accessible. Notice, however, that the IVR threshold is not a strictly defined quantity but reflects the averaged structure of state space.

In the tier model, these possible pathways are projected onto a single axis. In terms of the observed light absorption, the increasing number of couplings results in a spectrum that becomes more and more structured as seen in the right panels of Figure 5.6a–c. In other words, due to the coupling, the zeroth-order states share oscillator strength and appear as pairs (see also Figure 5.3). Still not all states are equally accessible, and one has to state that it is *not* the total but the *local* density of states that is responsible for the energy flow. Furthermore, Figure 5.6 illustrates that there are likely to exist correlations between different couplings. In other words, the basic assumption made in the derivation of the Golden Rule expression Eq. (5.11) is not fulfilled here.
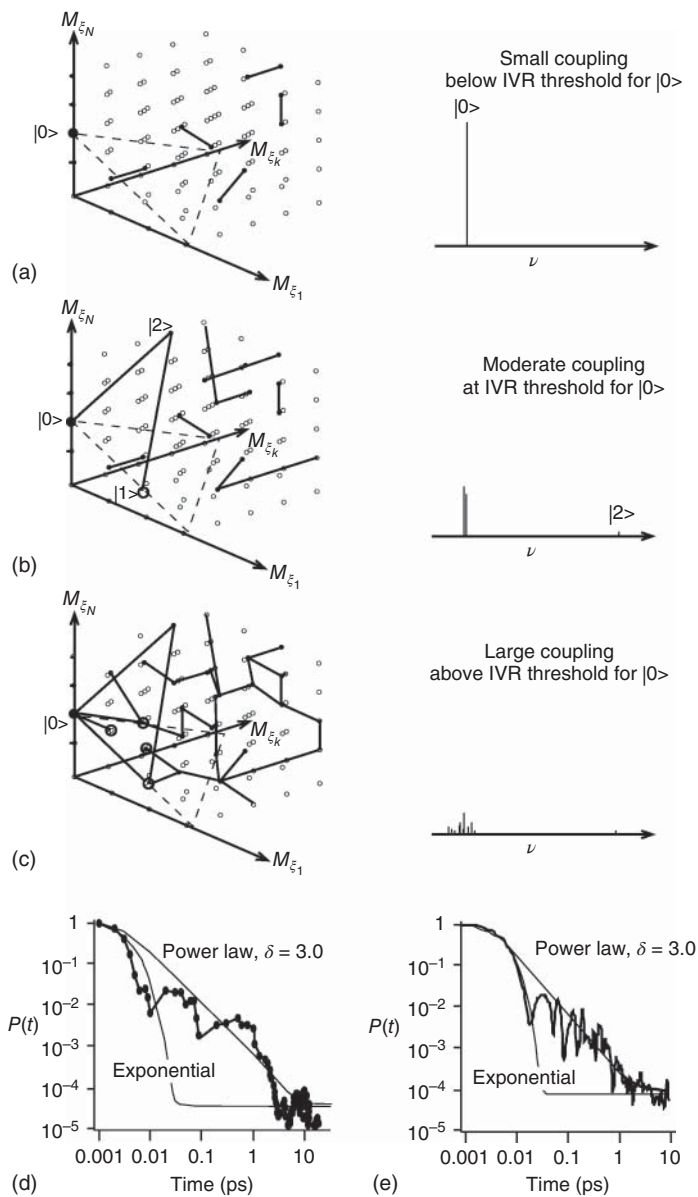
Figure 5.6 IVR in a polyatomic system. (a)–(c) The IVR process in a three-dimensional section of the space of quantum numbers ($M_{\xi_1}, M_{\xi_2}, \ldots, M_{\xi_N}$) (shown as open circles; thick solid lines connect strongly coupled states; and the dashed triangle is a surface of constant vibrational energy). The position corresponding to some initial state $|0\rangle$ is indicated by a full circle. The coupling strength of $|0\rangle$ to other states increases from (a) to (c) (depending on the energetic position relative to the IVR threshold). The related (infrared) absorption lines (right panels) show an increasing splitting. In (d) and (e), the decay of the survival probability is shown for $SCCl_2$ as obtained from experiment (fluorescence and stimulated emission pumping) and quantum dynamics simulation, respectively. Exponential (Eq. (5.12)) and power law (Eq. (5.13)) fits of the decay are shown as thin lines (figure courtesy of M. Gruebele; for more details see also Gruebele [4]).

How is this reflected in the behavior of the survival probability? Once the state is at the IVR threshold, there might be a few other states (denoted $|1\rangle$ and $|2\rangle$ in Figure 5.6b) that dominate the coupling and lead to quantum beats (cf. also Figure 5.1). Going beyond this threshold, the number of possible zeroth-order states for energy transfer increases, and P_{surv} will decay almost exponentially. During a certain time interval the decay is reasonably reproduced by a single exponential function. After a characteristic time, however, the energy flow will become dominated by the details of the local density of states and the local anharmonic couplings for a given point in state space. It was found that in this intermediate time range, the decay of P_{surv} will no longer be exponential, and it is better described by a power law:

$$P_{surv}(t) \sim (1 - \sigma)t^{-\delta/2} + \sigma. \tag{5.13}$$

Here, the exponent δ is a parameter that reflects the local dimensionality of IVR; usually one finds $\delta \ll N$ (cf. Figure 5.6d,e). This period of power law decay is considerably longer than the initial exponential decay. Finally, P_{surv} will fluctuate around the value of the dilution factor, which is a manifestation of the finite size of the state space.

5.3 Intermolecular Vibrational Energy Relaxation

In the previous section, we considered the *intra*molecular energy flow in large polyatomic molecules. The latter were assumed to be isolated from any environment such that *inter*molecular processes could be neglected. The IVR dynamics already indicated that large polyatomics may form a reservoir on their own. In the following sections we extend the scope and add an additional external reservoir that is provided by a solid-state matrix, a protein, or a solvent. On general grounds, it is to be expected that this will considerably enhance the density of states for vibrational energy flow such that for an appropriate separation of relevant and bath DOFs, one may recover rate dynamics. To set the stage, we start with the discussion of a *single relevant coordinate* coupled to some reservoir before focusing on the combined effect of inter- and intramolecular energy flow in Section 5.4.

5.3.1 The System–Reservoir Hamiltonian

The simplest setup for studying vibrational relaxation is certainly the situation of a single diatomic molecule in a monoatomic solid-state environment. Typical examples are dihalogens such as I_2 and Br_2, for instance built into a rare gas matrix at low temperatures, as shown in Figure 5.7 (cf. also Figure 5.2). The separation into system and reservoir DOFs in the sense of Chapter 3 strongly depends on the considered dynamics. If, for instance the diatomic molecule is photoexcited onto a PES that is dissociative in the gas phase, the fragments might be able to escape the matrix cage. However, if their energy is not sufficient, they will recombine after collision with the nearest matrix atoms, as shown in Figure 5.7 (cage effect). This process will be accompanied by a nonadiabatic transition, for example back
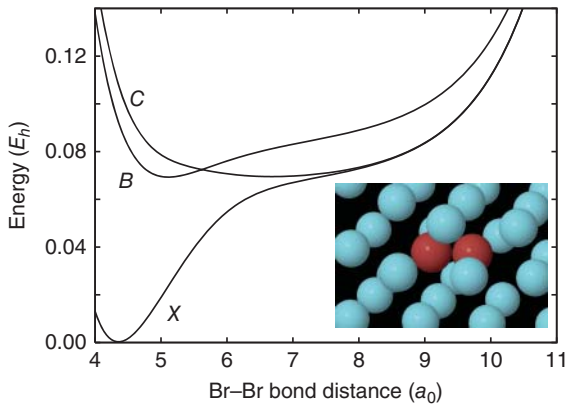
Figure 5.7 Photodissociation of a diatomic molecule (Br_2) in a rare gas lattice (Ar), see inset. The potential energy curves correspond to the lowest singlet states (X and C) as well as a triplet state (B). Upon $X \rightarrow C$ photoexcitation, the Br_2 bond elongates, and there is a certain probability for a transition to the B state, triggered by spin–orbit coupling. In the Ar lattice, the atoms recombine after collision with the lattice atoms (figure courtesy of A. Borowski).

onto the electronic ground state. Here, the vibrationally hot diatomic bond will relax into thermal equilibrium as a consequence of the interaction with the matrix environment. Clearly, the theoretical modeling of the collision process requires to take into account the solvent cage explicitly. On the other hand, for the vibrational relaxation in the electronic ground state, the matrix acts merely as a heat bath. It is the latter process of vibrational relaxation that we discuss in what follows. It also occurs, for example upon infrared excitation of a normal-mode vibration of a solvated molecule and subsequent energy dissipation into the solvent. Here, the relevant DOF is selected, for instance by the frequency of the excitation light.

In what follows, the one-dimensional coordinate of the relevant system will be labeled by s, and the remaining coordinates of the reservoir by $Z \equiv \{Z_k\}$. The Hamiltonian can therefore be written in the standard form:

$$H = H_{\text{S}} + H_{\text{R}} + H_{\text{S–R}}, \tag{5.14}$$

where

$$H_{\text{S}} = \frac{p^2}{2\mu_{\text{s}}} + V_{\text{S}}(s), \tag{5.15}$$

$$H_{\text{R}} = \sum_k \frac{P_k^2}{2M_k} + V_{\text{R}}(Z), \tag{5.16}$$

and

$$H_{\text{S–R}} = V(s, Z). \tag{5.17}$$

To simplify our considerations, we restrict ourselves to the case where the relevant system (for instance, the diatomic guest molecule) does not appreciably disturb the dynamics of the reservoir (for instance, the host lattice of rare gas atoms).

Usually, this will imply only small amplitude motion with respect to the equilibrium positions. Concerning the reservoir DOFs, it is customary to map the small amplitude vibrations of the coordinates Z with respect to their equilibrium values to collective normal modes $q = \{q_\xi\}$ (Section 2.5.1). In the case of a solid-state matrix, this amounts to the introduction of lattice phonons. Concepts applicable to other environments will be discussed below. Thus, the reservoir Hamiltonian becomes a sum of decoupled harmonic oscillators (cf. Eq. (2.44)):

$$H_R = \frac{1}{2} \sum_\xi \left(p_\xi^2 + \omega_\xi^2 q_\xi^2 \right). \tag{5.18}$$

The interaction potential in Eq. (5.17) is written in terms of the introduced normal-mode coordinates, $V(s, \{q_\xi\})$. Suppose that we expand this potential with respect to the equilibrium configuration ($s = 0$, $\{q_\xi\} = 0$); the lowest order nontrivial term is of first order with respect to both types of coordinates

$$\begin{aligned} V(s, \{q_\xi\}) &= \frac{1}{2} \sum_\xi \left. \frac{\partial^2 V(s, \{q_\xi\})}{\partial s \partial q_\xi} \right|_{s=0, \{q_\xi\}=0} s\, q_\xi \\ &= s \sum_\xi c_\xi q_\xi. \end{aligned} \tag{5.19}$$

Note that we will frequently assume that the trivial zeroth-order term $V(s = 0, \{q_\xi\} = 0)$ has been included in the definition of either the system or the bath Hamiltonian. Further, we assume that the Taylor expansion is performed around a minimum of the total PES, where first-order derivatives vanish. In the last line of Eq. (5.19), we introduced the coupling constant c_ξ, thus transforming the interaction Hamiltonian into the form of Eq. (3.286), which was discussed in Section 3.7.2. Note that in Section 3.7.2, the system part $K(s)$ of the interaction Hamiltonian was chosen to be dimensionless. This can be achieved by proper scaling for the system at hand.

The resulting system–reservoir Hamiltonian resembles the Cartesian reaction surface Hamiltonian derived in Section 2.5.3, provided that the force is linear in the system coordinate. Although derived here having in mind the special case of a diatomic in a rare gas environment, it has found wide applications as a model for studying dissipative dynamics of nuclear DOFs. We stress that this also includes situations where, for example the system describes a single bond or normal-mode vibration of a solvated polyatomic molecule. Since $V(s, \{q_\xi\})$ is linear in the system coordinate, the system itself moves in an effective potential, which can be substantially distorted. Often, one is interested in the effect of dissipation only, neglecting the renormalization of the system potential. This is achieved by adding a counter term, that is the reorganization energy introduced in Eq. (2.94), to the system–reservoir coupling. It gives the system–reservoir Hamiltonian in Caldeira–Leggett form[5]

$$H = \frac{p^2}{2\mu_s} + V_S(s) + \frac{1}{2} \sum_\xi \left[p_\xi^2 + \omega_\xi^2 \left(q_\xi - \frac{c_\xi s}{\omega_\xi^2} \right)^2 \right]. \tag{5.20}$$

---

5) Strictly speaking, it would have been necessary to subtract the reorganization energy from the system potential (cf. Eq. (2.95)), which is usually not done if the Hamiltonian is taken as a model only.

General application of this Hamiltonian raises the question whether a real system can be mapped onto the Caldeira–Leggett form. For the considered case of diatomics in low-temperature rare gas environments, such a mapping is most reasonable. However, in general, the validity of this mapping has to be checked carefully for the case at hand.[6] An approximate mapping can be achieved using the concept of instantaneous normal modes introduced in the following section.

5.3.2 Instantaneous Normal Modes

Solvent autocorrelation functions, for instance of the velocity or the position, are often characterized by a rapid initial decay stage. Focusing on this short-term dynamics of the solvent, the *instantaneous normal-mode* approach maps the motions of the solvent molecules onto the dynamics of independent collective oscillators that interact with the solute. This results in a microscopically defined system–reservoir Hamiltonian.

Suppose that we have chosen some initial configuration for the solute and solvent coordinates, $(s(0), Z(0))$, from the classical equilibrium distribution function as given in Eq. (3.326). For short enough times it is possible to expand the potential energy in terms of the deviation from this initial configuration, $\Delta s(t) = s(t) - s(0)$ and $\Delta Z(t) = Z(t) - Z(0)$. Considering, for example the solvent potential in Eq. (5.16), one can write

$$V_R(Z(t)) = V_R(Z(0)) + \sum_k \left. \frac{\partial V_R(Z)}{\partial Z_k} \right|_{Z=Z(0)} \Delta Z_k(t)$$

$$+ \frac{1}{2} \sum_{kl} \left. \frac{\partial^2 V_R(Z)}{\partial Z_k \partial Z_l} \right|_{Z=Z(0)} \Delta Z_k(t) \Delta Z_l(t). \tag{5.21}$$

Of course, the time range where this expansion applies is intimately connected to the specific situation, that is to the form of the potential, the masses of the particles, and so on. With this type of potential, the Hamiltonian (5.16) is readily diagonalized by a linear normal-mode transformation (see Eq. (2.42)), $\Delta Z_k(t) = \sum_\xi M_k^{-1/2} A_{k\xi}(Z(0)) \, q_\xi(t)$, leading to the time-dependent collective (mass-weighted) reservoir coordinates $q_\xi(t)$. The reservoir potential then becomes

$$V_R(q_\xi(t)) = V_R(Z(0)) - \sum_\xi \left(F_\xi(Z(0)) \, q_\xi(t) + \frac{1}{2} \omega_\xi^2(Z(0)) \, q_\xi^2(t) \right). \tag{5.22}$$

Here, the frequencies are resulting from the diagonalization of the (mass-weighted) Hessian matrix (see Section 2.5.1) at the initial configuration, and the forces for this configuration are

$$F_\xi(Z(0)) = -\sum_k M_k^{-1/2} \left. \frac{\partial V_R(Z)}{\partial Z_k} \right|_{Z=Z(0)} A_{k\xi}(Z(0)). \tag{5.23}$$

---

6) For a protocol based on the generalized Langevin equation introduced in Section 5.3.3, see Gottwald [5].

Figure 5.8 Instantaneous normal-mode density of states for an Ar$_{13}$ cluster at 10 K (a) and 40 K (b) (Reproduced with permission from Stratt [6]; copyright (1995)/American Chemical Society).
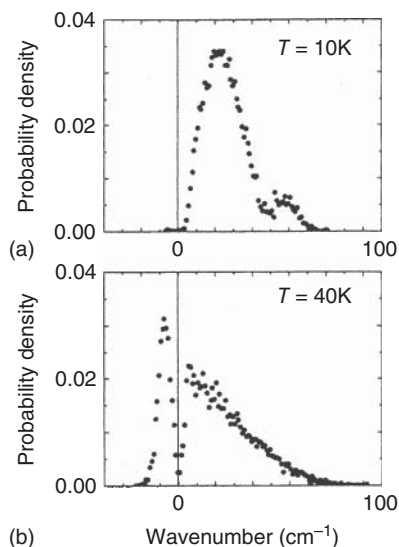
Let us neglect the presence of the solute for a moment. In this case, the spectral distribution of the instantaneous eigenvalues of the Hessian gives important information about the solvent. To discuss the instantaneous density of states for the liquid normal modes it is appropriate to use the following quantity:

$$\mathcal{N}_{\text{INM}}(\omega) = \left\langle \sum_{\xi} \delta(\omega - \omega_{\xi}(Z(0))) \right\rangle_{Z(0)}, \tag{5.24}$$

which contains the average with respect to different initial configurations. In Figure 5.8, we show the instantaneous normal-mode density of states for a small Argon cluster at different temperatures. Within the instantaneous normal-mode approach, it is typical that the Hessian also has negative eigenvalues, $\omega_{\xi}^2(Z(0)) < 0$, implying "imaginary" frequencies. This indicates that the chosen initial configuration is not a minimum in all directions of the PES as it is reasonable for liquids. Notice, however, that upon decreasing the temperature, the cluster is frozen, and the negative frequency contributions disappear, as shown in the example of Figure 5.8.

We now return to the solute–solvent system and consider the interaction Hamiltonian (5.17). Assuming that the same type of short-term expansion is valid, we can write after introducing the solvent normal modes

$$V_{\text{S-R}}(s, Z) = V_{\text{S-R}}(s(0), Z(0)) + \Delta s(t) \sum_{\xi} c_{\xi}(s(0), Z(0)) \, q_{\xi}(t). \tag{5.25}$$

Here, we have retained the bilinear term only (cf. Eq. (5.19)), and the solvent–solute coupling constant is given by

$$c_{\xi}(s(0), Z(0)) = \sum_{k} A_{k\xi}(s(0), Z(0)) M_k^{-1/2} \left. \frac{\partial V_{\text{S-R}}(s, Z)}{\partial Z_k \partial s} \right|_{s=s(0), Z=Z(0)}. \tag{5.26}$$

Comparing Eq. (5.25) with (3.286), we realize that we have obtained the classical system–reservoir Hamiltonian function in the generic form with all parameters microscopically well defined. Therefore, the results of Section 3.7 can readily be adapted to the present case. In Particular, one can define a spectral density within the instantaneous normal-mode approach.[7]

Despite the fact that a liquid is inherently unstable as compared with a solid-state environment, the idea of extracting information on the solute–solvent dynamics from the short-term behavior of classical trajectories has proven to give valuable insight. In addition, from the conceptually desirable link between the formal system–reservoir Hamiltonian and the actual microscopic dynamics, the analysis of instantaneous normal modes provides the key to the understanding of energy relaxation processes in terms of *collective* solvent motions. In contrast, within standard molecular dynamics simulations, the collective character of the solvent response is usually hidden in the correlation functions.

5.3.3 Generalized Langevin Equation

For the system–reservoir Hamiltonian of the Caldeira–Leggett form, one can derive equations of motion for the system's coordinate and momentum under the influence of the system–reservoir interaction. The Heisenberg equations of motion for system operators read

$$\dot{s} = -\frac{i}{\hbar}[s, H]_- = \frac{p_s}{\mu_s}, \tag{5.27}$$

$$\dot{p}_s = -\frac{i}{\hbar}[p_s, H]_- = F_s + \sum_\xi c_\xi \left(q_\xi - \frac{c_\xi s}{\omega_\xi^2} \right), \tag{5.28}$$

with $F_s - \frac{\partial V_S}{\partial s}$. For the bath operators, we have

$$\dot{q}_\xi = p_\xi, \tag{5.29}$$

$$\dot{p}_\xi = -\omega_\xi^2 \left(q_\xi - \frac{c_\xi s}{\omega_\xi^2} \right). \tag{5.30}$$

The last two equations can be combined to a second-order inhomogeneous differential equation for q_ξ having the general solution

$$q_\xi(t) = q_\xi^{(H)}(t) + c_\xi \int_0^t d\tau \, \frac{\sin(\omega_\xi(t-\tau))}{\omega_\xi} s(\tau), \tag{5.31}$$

with the homogeneous solution

$$q_\xi^{(H)}(t) = q_\xi(0)\cos(\omega_\xi t) + p_\xi(0)\frac{\sin(\omega_\xi t)}{\omega_\xi}. \tag{5.32}$$

---

7) The connection between instantaneous normal modes and spectral densities can be found in Goodyear and Stratt [7].

The integral coming from the particular solution of the inhomogeneous equation can be rewritten using integration by parts. This yields

$$q_\xi(t) - \frac{c_\xi s(t)}{\omega_\xi^2} = q_\xi^{(H)}(t) - \frac{c_\xi s(0)}{\omega_\xi^2} \cos(\omega_\xi t)$$

$$- c_\xi \int_0^t d\tau \, \cos(\omega_\xi(t - \tau)) \frac{p_s(\tau)}{\mu_s}. \tag{5.33}$$

Inserting this expression into Eq. 5.28, one obtains the Generalized Langevin Equation (GLE)

$$\mu_s \ddot{s} = F_s - \int_0^t d\tau \, K(t - \tau) \dot{s}(\tau) + R(t), \tag{5.34}$$

with the dissipative memory kernel

$$K(t) = \sum_\xi \frac{c_\xi^2}{\omega_\xi^2} \cos(\omega_\xi t). \tag{5.35}$$

The memory kernel can be expressed in terms of a spectral density,

$$K(t) = \int d\omega J_{GLE}(\omega) \cos(\omega t), \tag{5.36}$$

with[8]

$$J_{GLE}(\omega) = \sum_\xi \frac{c_\xi^2}{\omega_\xi^2} \delta(\omega - \omega_\xi). \tag{5.37}$$

We notice that $K(t)$ has a structure similar to Eq. (3.178). Following our previous argument, for a dense spectrum of reservoir oscillators, $K(t)$ will decay on the time scale of the memory time τ_{mem}. If this time scale is short as compared to the system evolution, $K(t - \tau)$ can be approximated by a delta function, and one obtains the Markovian Langevin equation. In terms of the spectral density entering Eq. (5.36), this implies $J_{GLE}(\omega) \approx \text{const.}$

The last term in Eq. (5.34) is given by

$$R(t) = \sum_\xi c_\xi q_\xi^{(H)}(t) - \sum_\xi \frac{c_\xi^2}{\omega_\xi^2} s(0) \cos(\omega_\xi t)$$

$$= \sum_\xi c_\xi \left(q_\xi(0) - \frac{c_\xi s(0)}{\omega_\xi^2} \right) \cos(\omega_\xi t) + \sum_\xi c_\xi \frac{p_\xi(0)}{\omega_\xi} \sin(\omega_\xi t). \tag{5.38}$$

In a macroscopic condensed-phase system, the initial state of the reservoir is uncertain but characterized by a thermal distribution. Hence, $R(t)$ is defined by a sum of essentially random variables, and it is just a random force acting on the system coordinate s. This function is usually characterized by its average and autocorrelation function. Here, care has to be taken when defining the reservoir Hamiltonian

---

8) To establish the connection to the spectral density defined in Eq. (3.294), one should be aware of the different forms of the bath part of the system–reservoir interaction in Eq. (3.287), with the relation $c_\xi^2 / \omega_\xi^2 = 2\hbar \omega_\xi g_\xi^2$.

that enters the equilibrium statistical operator $\hat{R}_{eq}$ in Eq. (3.202). According to Eq. (5.20), the reservoir equilibrium is shifted due to the interaction with the system. In $R(t)$, this appears as a shift of $q_\xi(0)$ according to the initial value of the system coordinate $s(0)$. At this point, one usually assumes that initially, the reservoir has been equilibrated according to some fixed position of the system coordinate; that is, the Hamiltonian entering Eq. (3.202) is given by

$$H'_R = \frac{1}{2}\sum_\xi \left[p_\xi^2 + \omega_\xi^2 \left(q_\xi - \frac{c_\xi s(0)}{\omega_\xi^2} \right)^2 \right]. \tag{5.39}$$

In this case, it follows immediately that (cf. Section 3.7.2)

$$\langle R(t) \rangle_R = 0 \tag{5.40}$$

and

$$\begin{aligned}
\langle R(t)R(0) \rangle_R &= \sum_\xi c_\xi^2 \left[\left\langle \left(q_\xi(0) - \frac{c_\xi s(0)}{\omega_\xi^2} \right)^2 \right\rangle_R \cos(\omega_\xi t) \right. \\
&\quad \left. + \frac{1}{\omega_\xi} \left\langle p_\xi(0) \left(q_\xi(0) - \frac{c_\xi s(0)}{\omega_\xi^2} \right) \right\rangle_R \sin(\omega_\xi t) \right] \\
&= \sum_\xi c_\xi^2 \left[\coth\left(\frac{\hbar\omega_\xi}{2k_B T} \right) \cos(\omega_\xi t) - \frac{i}{\omega_\xi} \sin(\omega_\xi t) \right]. \tag{5.41}
\end{aligned}$$

It is instructive to consider the symmetrized correlation function of the random force (cf. Eq. (3.274))

$$\begin{aligned}
\langle R(t)R(0) \rangle_R + \langle R(t)R(0) \rangle_R^* &= \sum_\xi A_\xi^{(+)}(t) \\
&= 2\sum_\xi c_\xi^2 \coth\left(\frac{\hbar\omega_\xi}{2k_B T} \right) \cos(\omega_\xi t). \tag{5.42}
\end{aligned}$$

Comparison with Eq. (5.36) yields the relation

$$K(t) = \sum_\xi A_\xi^{(+)}(t) \frac{1}{\omega_\xi} \tanh\left(\frac{\hbar\omega_\xi}{2k_B T} \right). \tag{5.43}$$

Since this expression connects the dissipative memory kernel with the correlation function of the thermal noise, it is also called quantum fluctuation–dissipation theorem (see also Section 3.7.4). We note that this is an exact relation for the system–reservoir Hamiltonian Eq. (5.20).

An important feature of the Caldeira–Leggett model is that quantum and classical GLE have the same form, Eq. (5.34). However, the classical fluctuation–dissipation theorem differs from Eq. (5.43). Calculating the noise autocorrelation function according to a classical phase space average (cf. Eq. (3.326)), the integrals with respect to the Gaussian distributions can be performed straightforwardly (note that the second term in Eq. (5.41) vanishes due to symmetry), and one obtains

$$\langle R(t)R(0) \rangle_{cl,R} = k_B T \sum_\xi \frac{c_\xi^2}{\omega_\xi^2} \cos(\omega_\xi t). \tag{5.44}$$

Comparison with Eq. (5.35) yields the classical fluctuation–dissipation theorem[9]

$$\langle R(t)R(0)\rangle_{\text{cl,R}} = k_{\text{B}}TK(t).\tag{5.45}$$

The classical GLE provides a means for calculation of the spectral density using classical molecular dynamics provided that the total system can be described by the Caldeira–Leggett model. According to Eq. (5.36), the spectral density can be expressed via the one-sided Fourier transform (denoted by the tilde) of the memory kernel according to

$$J_{\text{GLE}}(\omega) = \frac{2}{\pi}\text{Re}\,\tilde{K}(\omega) = \frac{2}{\pi}\text{Re}\int_0^\infty dt e^{i\omega t}K(t).\tag{5.46}$$

In order to obtain a protocol solely based on correlation functions, first, the GLE is expressed in terms of the system's momentum. Next, both sides are multiplied by $p_{\text{s}}(0)$, and a canonical average with respect to the total system is performed. This gives

$$\dot{C}_{\text{pp}}(t) = C_{\text{pF}}(t) - \int_0^t d\tau K(t-\tau)C_{\text{pp}}(\tau),\tag{5.47}$$

with $C_{\text{pp}}(t) = \langle p_{\text{s}}(t)p_{\text{s}}(0)\rangle_{\text{cl}}$, $C_{\text{pF}}(t) = \langle F_{\text{s}}(t)p_{\text{s}}(0)\rangle_{\text{cl}}$, and the initial momenta and noise being uncorrelated. Taking the one-sided Fourier transform, one obtains

$$-i\omega\tilde{C}_{\text{pp}}(\omega) - C_{\text{pp}}(t=0) = \tilde{C}_{\text{pF}}(\omega) - \tilde{K}(\omega)\tilde{C}_{\text{pp}}(\omega),\tag{5.48}$$

which can be rearranged to

$$\tilde{K}(\omega) = \frac{C_{\text{pp}}(t=0) + \tilde{C}_{\text{pF}}(\omega)}{\tilde{C}_{\text{pp}}(\omega)} + i\omega.\tag{5.49}$$

Calculating $C_{\text{pp}}(t)$ and $C_{\text{pF}}(t)$ using classical molecular dynamics simulations, one thus obtains the memory kernel that, according to Eq. (5.46), gives the spectral density of the Caldeira–Leggett model. Two examples are shown in Figure 5.9.

5.3.4 Classical Force–Force Correlation Functions

The introduction of normal modes for the bath in Eq. (5.18) assumes an environment that performs only small oscillations around its equilibrium configuration or an approximate treatment, for instance in terms of instantaneous normal modes. In what follows we aim at a more general description of the bath dynamics in terms of classical molecular dynamics. It makes use of the availability of empirical force fields as discussed in Section 2.7.2. Hence, for the following equation, we assume that the potentials for the interaction between the solvent molecules and between solvent and solute, $V(s, Z)$, are known. Here, $Z = \{Z_k\}$ is the respective set of the

---

9) Notice that often this fluctuation–dissipation theorem is used in the sense that for a given $K(t)$, the noise $R(t)$ entering the GLE is generated as a stochastic zero-centered Gaussian process fulfilling this theorem.
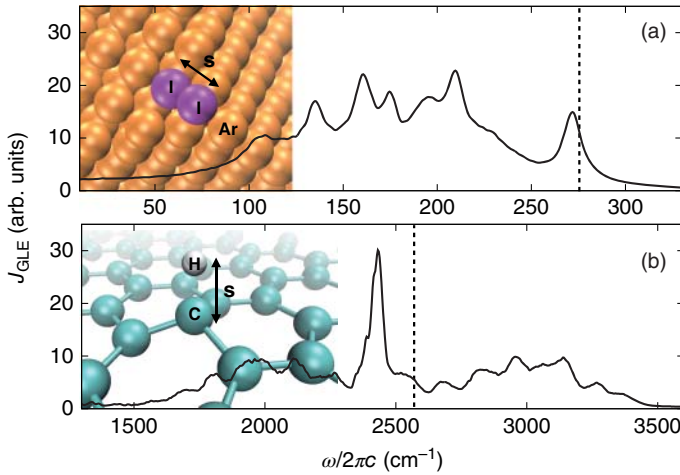
Figure 5.9 Spectral densities obtained using GLE-based simulation according to Eq. (5.49). (a) The spectral density for the I_2 bond vibration in an Ar crystal and (b) the spectral density for the C–H stretching vibration of an H atom on a graphene surface. The dashed line marks the frequency of the considered stretching vibrations (figure courtesy of F. Gottwald, for more details see also Gottwald [8]).

nuclear solvent molecule coordinates. In a first step, we suppose that this potential can be expanded in terms of the relevant system coordinate s as follows:

$$V(s, Z) = V(s = 0, Z) + \left. \frac{\partial V(s, Z)}{\partial s} \right|_{s=0} s + \ldots \tag{5.50}$$

The first term is a potential for the bath coordinates if the system coordinate is kept fixed at its equilibrium value, $s = 0$. It can be incorporated into the reservoir Hamiltonian H_R. The second part is the force of the solvent acting on the relevant coordinate that is kept fixed at its equilibrium position. This term is the system–reservoir coupling we are looking for, and we write

$$H_{S-R} = s \left. \frac{\partial V(s, Z)}{\partial s} \right|_{s=0} = -sF(Z). \tag{5.51}$$

Notice that this form would reduce to the Caldeira–Leggett model for $F = -\sum_\xi c_\xi q_\xi$ (Eq. (5.19)). Following the discussion of the GLE in the previous section, it provides the random force $R(t)$ acting on the system coordinate. At this point, F is still an operator. Its autocorrelation function $\langle F(t)F(0) \rangle_R$ is the reservoir correlation function whose Fourier transform, according to Eq. (3.350), enters the desired relaxation rates. Since we are aiming at a classical description of the reservoir, the quantum correlation function has to be replaced by its classical counterpart given in Eq. (3.325) ($\Phi_u = \Phi_v = F$). As explained in Section 3.7.5, the detailed balance can be fulfilled despite the time reversal symmetry of the classical correlation function, if we identify $\langle F(t)F(0) \rangle_{cl,R}$ with the symmetrized quantum correlation function $C^{(+)}(t)$.

Suppose that the eigenvalue problem, $H_S |M\rangle = E_M |M\rangle$, for the system part of the Hamiltonian has been solved, the relaxation rates are obtained from Eq. (3.350) as ($\hbar\Omega_{MN} = E_M - E_N$)

$$k_{MN} = \frac{|s_{MN}|^2}{1 + \exp(-\hbar\Omega_{MN}/k_B T)} \int_{-\infty}^{\infty} dt\, e^{i\Omega_{MN}t}\, C^{(+)}(t)$$

$$= \frac{2|s_{MN}|^2}{1 + \exp(-\hbar\Omega_{MN}/k_B T)} \int_0^{\infty} dt\, \cos(\Omega_{MN}t)\, \langle F(t)F(0)\rangle_{\text{cl,R}}$$

$$= \frac{2|s_{MN}|^2\, c(\Omega_{MN})}{1 + \exp(-\hbar\Omega_{MN}/k_B T)}. \tag{5.52}$$

Here, $c(\Omega_{MN})$ is the Fourier cosine transform of the classical force–force autocorrelation function, which is obtained within the present model using classical *equilibrium* molecular dynamics simulations. Since the system coordinate is fixed in this approach, it is also called *rigid bond method*. In the limit that the system is harmonic, we can calculate the matrix elements s_{MN} and obtain for the relaxation rate between the first excited state and the ground state $k_{1\to 0} = (\hbar/\mu_s\Omega_s)c(\Omega_s)/(1 + \exp(-\hbar\Omega_s/k_B T))$.

In Figure 5.10a, we plot as an example the correlation function of the force an ethanol solvent exerts on the bond of HgI, which is obtained as a fragment in the photodissociation of HgI_2. The force of the solvent projected onto the HgI bond is given by

$$F(t) = M_{\text{red}} \boldsymbol{n}_{12} \left[\frac{\boldsymbol{F}_1(t)}{M_1} - \frac{\boldsymbol{F}_1(t)}{M_1} \right], \tag{5.53}$$

with $\boldsymbol{F}_k$ and M_k being the force vector and mass, respectively, for atom k, M_{red} is the reduced mass of the atom pair, and $\boldsymbol{n}_{12}$ is the unit vector pointing from atom 1 to atom 2.
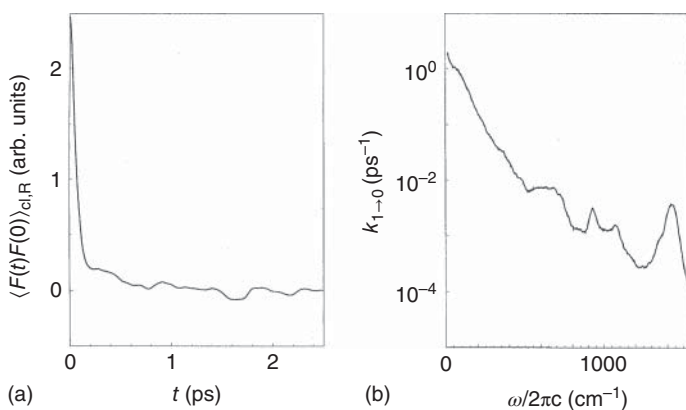
Figure 5.10 Molecular dynamics simulations of HgI in ethanol solution. (a) Classical autocorrelation function of the force acting along the HgI bond, and (b) the respective Landau–Teller relaxation rate. In the actual experiment, the diatomic molecule is produced as a fragment in the photodissociation of HgI_2 (Reproduced with permission from Gnanakaran and Hochstrasser [9]/ AIP Publishing).

There are two regimes easily discernible in Figure 5.10a. First, there is a rapid decay on a time scale of about 60–100 fs, which is rationalized as follows. Given some initial configuration chosen from an equilibrium ensemble (see Eq. (3.326)), the molecules perform inertial motions up to a point where collisions with neighboring molecules set in. After such collisions, the forces get randomized. Thus, the decay time of the correlation function represents the average time between two collision events; that is, it reflects mostly the short-range part of the interaction potential. After this initial phase, the correlation function does not decay to zero in the time window shown in Figure 5.10. Instead, the decay rate slows done appreciably. In this regime, the long-range forces give the major contributions to the correlation function. There appears to be also some oscillatory behavior that can be traced back to the internal vibrations of the solvent. The vibrational relaxation rate is shown in Figure 5.10b. In order to see what types of motions of the solvent are responsible for the relaxation of the HgI bond vibration in the harmonic approximation, one has to analyze the spectrum at the vibrational frequency, which is 130 cm^{-1}. This leads to the conclusion that mostly the Lennard-Jones-type collisions are responsible for the relaxation in this system. The high-frequency peaks (>900 cm^{-1}), which are due to the internal modes of the ethanol, have no influence on the relaxation of HgI.

Finally, we would like to point out that there is a limitation involved in the calculation of the relaxation rates we have outlined so far. Remember that the system coordinate has been fixed at its equilibrium value. For the symmetric oscillator potential this can be viewed as if the environment only sees the time-averaged position of the system oscillator. Any type of backreaction, where the reservoir notices the actual position of the system coordinate whose dynamics it influences, would be beyond the QME treatment. In the spirit of an adiabatic separation of system and bath motions, the rigid bond approximation should be particularly good for high-frequency system oscillators coupled to a low-frequency bath.[10]

5.3.5 Dissipative Dynamics of a Harmonic Oscillator

In order to illustrate the vibrational relaxation dynamics, we consider the case of a harmonic system with the potential

$$V_{S}(s) = \frac{\mu_{s}\Omega_{s}^{2}}{2}s^{2}. \tag{5.54}$$

Here, μ_{s} is the reduced mass, and Ω_{s} the vibrational frequency. In this case, the eigenfunctions and -energies of H_{S} are given by Eqs. (2.47) and (2.48), respectively. The interaction between the relevant system and the reservoir is taken according to Eq. (5.19). To obtain a dimensionless system part, the following scaling can be used $K(s) = s\sqrt{2\mu_{s}\Omega_{s}/\hbar}$. Accordingly, the reservoir part of the interaction Hamiltonian is given by $\Phi(q) = \sqrt{\hbar/2\mu_{s}\Omega_{s}}\sum_{\xi}c_{\xi}q_{\xi}$.

The dynamics will be described using the QME in the representation of the relevant system's eigenstates $\{|N\rangle\}$. Further, we invoke the Markov approximation and

---

10) A detailed study of the validity of both the Caldeira–Leggett model and the rigid bong method can be found in Gottwald [10].

for simplicity also the secular approximation. Thus, the equations of motion given in Section 3.8.3 can be straightforwardly adapted to the present situation. We obtain the expression

$$
\frac{\partial}{\partial t}\rho_{MN} = -\delta_{MN}\sum_K \left(k_{MK}\rho_{MM} - k_{KM}\rho_{KK} \right)
$$
$$
-(1 - \delta_{MN})\,(i\Omega_s(M - N) + \gamma_M + \gamma_N)\rho_{MN}. \tag{5.55}
$$

According to Eq. (3.350), the energy relaxation rates, $k_{MN} = k_{M\to N}$, are given by

$$
k_{MN} = |\langle M|\, K(s)\, |N\rangle|^2\; C(\omega_{MN}). \tag{5.56}
$$

Assuming that $C(0) = 0$ holds, we have for the dephasing rates $\gamma_M = \sum_N k_{MN}/2$. The correlation function $C(\omega)$ has been given in Eq. (3.295). The transition rates can be calculated straightforwardly for the interaction Hamiltonian given in Eq. (5.19). We obtain for the matrix elements of the system part (cf. Eq. (5.5))

$$
\langle M|\, K(s)\, |N\rangle = \left(\sqrt{N}\,\delta_{M,N-1} + \sqrt{N+1}\,\delta_{M,N+1} \right). \tag{5.57}
$$

Using this result, the rate for the vibrational transition between the states $|M\rangle$ and $|N\rangle$, Eq. (3.350), becomes

$$
k_{MN} = \left(\delta_{M,N-1}(M+1)C(-\Omega_s) + \delta_{M,N+1}MC(\Omega_s) \right). \tag{5.58}
$$

For the oscillator reservoir, the Fourier transform of the correlation function was given in Eq. (3.293). Inspecting this rate, one can draw a number of conclusions as visualized in Figure 5.11:

First, only transitions between neighboring system oscillator states are possible if H_{S-R} is linear in the system coordinate s. Second, the relaxation rates grow linearly with the quantum number of the excited state. If we define the inverse lifetime of the state $|M\rangle$, τ_M^{-1}, in terms of all possibilities for making transitions out of this state, we obtain

$$
\tau_M^{-1} = \sum_N k_{MN} = \left((M+1)C(-\Omega_s) + MC(\Omega_s) \right). \tag{5.59}
$$

Thus, with increasing quantum number, the lifetime decreases as $1/M$.

Third, according to Eq. (3.295), the correlation function $C(\omega)$ is proportional to the spectral density of the reservoir. From Eq. (5.58), we see that the spectral density is "probed" only at the system's oscillator frequency Ω_s (cf. Section 3.8.2).

Figure 5.11 Schematic view of vibrational relaxation out of the harmonic oscillator state with quantum number M due to the coupling to some environment, characterized by the spectral density $J(\omega)$.
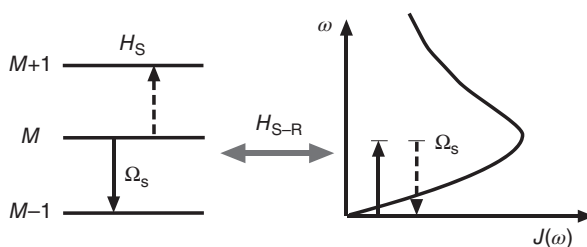
Finally, for the bilinear coupling, upward transitions from $|M\rangle$ to $|M+1\rangle$ require that there be a bath mode at frequency Ω_s that is also thermally accessible according to the distribution function $n(\Omega_s)$ (see Eq. (3.295)). Downward transitions release energy into the bath and occur due to the factor $1 + n(\Omega_s)$ even if the temperature goes to zero. They also require a bath mode having the same frequency. Thus, in both cases, energy conservation is fulfilled.

The above treatment is readily extended to anharmonic system potentials. In such cases, the eigenstates and matrix elements have to be obtained numerically. In any case, connecting the dynamics in eigenstate representation to wave packet dynamics such as shown in Figure 5.2, a transformation to the probability distribution for the system coordinate has to be performed as follows:

$$P(s, t) \equiv \rho(s, s; t) = \sum_{M,N} \chi_M(s) \chi_N^*(s) \rho_{MN}(t). \tag{5.60}$$

Experimentally, vibrational relaxation can be monitored using time-resolved infrared pump–probe spectroscopy (cf. Section 4.3.6). According to Eq. (4.111), the dispersed pump–probe signal consists of contributions from ground state bleach (GSB) and stimulated emission (SE) due to transitions between states $|M = 0\rangle$ and $|M = 1\rangle$ as well as from excited state absorption (ESA) due to a transition from state $|M = 1\rangle$ to state $|M = 2\rangle$. For an anharmonic system, $\omega_{10} > \omega_{21}$; that is, the ESA spectrum is shifted to lower frequencies as compared with the GSB/SE spectrum; recall that GSB/SE and ESA contributions differ in sign. Initially, the pump pulse prepares the system in a nonequilibrium state. The relaxation back to equilibrium is observed by the probe pulse as a function of the delay time. This gives access to the associated relaxation rate. An example demonstrating vibrational relaxation of an azide ion in liquid water is given in Figure 5.12.
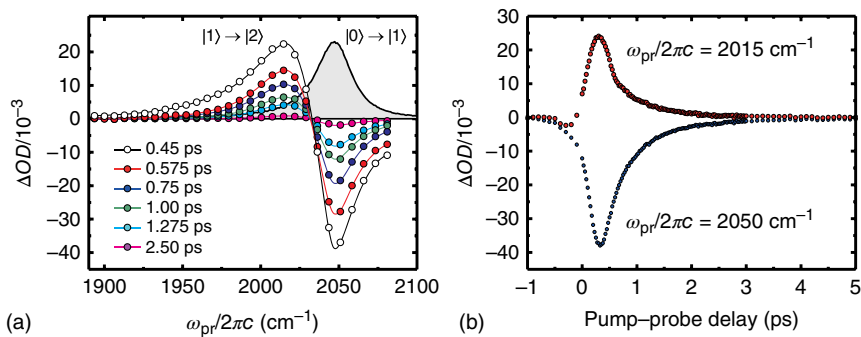
Figure 5.12 Infrared pump–probe signal showing the vibrational relaxation of the asymmetric stretching vibration of azide ions in liquid water at a pressure of 500 bar and a temperature of 333 K. The signal is given as a difference in optical density $\Delta OD = OD$(pump on)$–OD$(pump off) at the probe frequency ω_{pr}. The vibrational lifetime was determined to be 650 fs. (a) Dispersed signal for different delay times showing ESA and GSB/SE contributions. Also shown is the linear absorption spectrum (gray-shaded area). (b) Time traces of signal at different probe frequencies (figure courtesy of P. Vöhringer, for more details see Olschewski [11]).

5.4   Polyatomic Molecules in Solution

5.4.1   System–Reservoir Hamiltonian

Having discussed the aspects of intramolecular vibrational dynamics of isolated polyatomics as well as VER of a single relevant DOF in solution, we are now in the position to address the general situation of a polyatomic solute in a polyatomic solvent. On the one hand, we know that the intramolecular motions can be adequately described in terms of zeroth-order states such as given by the normal-mode expansion. On the other hand, we have seen that even the complex dynamics of a polyatomic solvent can be mapped onto a set of collective harmonic oscillators, provided one is interested in the short-time behavior of solvent correlation functions, for instance. Given this information, there appears to be still some freedom in the choice of the zeroth-order states for the solute plus the solvent. The most frequently used approach to this problem is as follows. Assume that we have identified a bright state of the solute corresponding, for example to a local vibrational mode. In this case, the system Hamiltonian is given by

$$H_{\text{S}} = \frac{p^2}{2\mu_{\text{s}}} + V_S(s),$$ (5.61)

with $V_S(s)$ being the system potential along the considered mode, which in the general case may be anharmonic. The remaining DOFs, that is the intramolecular as well as the solvent DOFs, are then treated within the harmonic approximation. If the corresponding normal-mode coordinates, $\{q_\xi\}$, are introduced, H_{R} is given by Eq. (5.16). For the solvent, this may imply, for instance the introduction of instantaneous normal modes. Since it is assumed that the bath has been diagonalized without the system DOF, there will be a coupling between both subsystems

$$H_{\text{S–R}}^{\text{I}} = V_{\text{S–R}}(s, \{q_\xi\}) \equiv V_{\text{S–R}}(s, q).$$ (5.62)

In the next step, we introduce a Taylor expansion of this interaction potential with respect to both types of coordinates. We write

$$\begin{aligned} V_{\text{S–R}}(s, q) = {}& V_{\text{S–R}}(s = 0, q = 0) \\ & + \left.\frac{\partial V_{\text{S–R}}(s, 0)}{\partial s}\right|_{s=0} s + \sum_{\xi} \left.\frac{\partial V_{\text{S–R}}(0, q)}{\partial q_\xi}\right|_{q=0} q_\xi \\ & + \frac{1}{2} \left.\frac{\partial^2 V_{\text{S–R}}(s, q)}{\partial s^2}\right|_{s=0} s^2 + \frac{1}{2} \sum_{\xi_1 \xi_2} \left.\frac{\partial^2 V_{\text{S–R}}(s, q)}{\partial q_{\xi_1} \partial q_{\xi_2}}\right|_{q=0} q_{\xi_1} q_{\xi_2} \\ & + \sum_{\xi} \left.\frac{\partial^2 V_{\text{S–R}}(s, q)}{\partial s \partial q_\xi}\right|_{s=0, q=0} s q_\xi + \dots \end{aligned}$$ (5.63)

Note that this expansion illustrates the appropriateness of the *ansatz* we made for $H_{\text{S–R}}$ in Eq. (3.198) since it is a sum of terms that can be factorized into a system part ($K(s)$) and a reservoir part ($\Phi(q)$). This is in accord with another statement made in Section 3.5.3; that is, the factorized system–reservoir interaction Hamiltonian provides sufficient flexibility to model dissipative quantum dynamics. Taking into account only the bilinear term $\propto s q_\xi$, one recovers the Caldeira–Leggett model,

Eq. (5.20). Its dynamics can be described by the GLE, Eq. (5.34). Assuming that the Caldeira–Leggett model provides a valid description, spectral densities can be extracted from molecular dynamics simulations according to Eq. (5.49). An example is given in Figure 5.9.

Before continuing, it is useful to compare this approach with an alternative one that assumes that the normal modes of *all* DOFs, denoted here as $\{\tilde{q}_\xi\}$ to distinguish them from the set $\{q_\xi\}$, are used as a zeroth-order basis. For simplicity, suppose that we are able to identify the bright mode mentioned above as $\tilde{q}_{\xi_1}$. Let us further assume that the Hamiltonian has been expanded in these normal modes according to Eq. (5.2). Then, we can partition the Hamiltonian to fourth order as follows:

$$H_{\mathrm{S}} = \frac{1}{2}\left(\tilde{p}_{\xi_1}^2 + \omega_{\xi_1}^2 \tilde{q}_{\xi_1}^2\right) + K_{\xi_1\xi_1\xi_1}\tilde{q}_{\xi_1}^3 + K_{\xi_1\xi_1\xi_1\xi_1}\tilde{q}_{\xi_1}^4, \tag{5.64}$$

$$H_{\mathrm{R}} = \frac{1}{2}\sum_{\xi_2\neq\xi_1}\left(\tilde{p}_{\xi_2}^2 + \omega_{\xi_2}^2\tilde{q}_{\xi_2}^2\right) + \sum_{\xi_2\xi_3\xi_4\neq\xi_1}K_{\xi_2\xi_3\xi_4}\tilde{q}_{\xi_2}\tilde{q}_{\xi_3}\tilde{q}_{\xi_4}$$
$$+ \sum_{\xi_2\xi_3\xi_4\xi_5\neq\xi_1}K_{\xi_2\xi_3\xi_4\xi_5}\tilde{q}_{\xi_2}\tilde{q}_{\xi_3}\tilde{q}_{\xi_4}\tilde{q}_{\xi_5}, \tag{5.65}$$

and

$$H_{\mathrm{S-R}}^{\mathrm{II}} = \tilde{q}_{\xi_1}\left(\sum_{\xi_2\xi_3\neq\xi_1}K_{\xi_1\xi_2\xi_3}\tilde{q}_{\xi_2}\tilde{q}_{\xi_3} + \sum_{\xi_2\xi_3\xi_4\neq\xi_1}K_{\xi_1\xi_2\xi_3\xi_4}\tilde{q}_{\xi_2}\tilde{q}_{\xi_3}\tilde{q}_{\xi_4}\right)$$
$$+ \tilde{q}_{\xi_1}^2\left(\sum_{\xi_2\neq\xi_1}K_{\xi_1\xi_1\xi_2}\tilde{q}_{\xi_2} + \sum_{\xi_2\xi_3\neq\xi_1}K_{\xi_1\xi_1\xi_2\xi_3}\tilde{q}_{\xi_2}\tilde{q}_{\xi_3}\right)$$
$$+ \tilde{q}_{\xi_1}^3\sum_{\xi_2\neq\xi_1}K_{\xi_1\xi_1\xi_1\xi_2}\tilde{q}_{\xi_2}. \tag{5.66}$$

For a large polyatomic molecule in a complex solvent, exact microscopic knowledge about the individual anharmonic couplings is hardly available. So, one may as well assume that the $K_{\xi_1\xi_2\xi_3}$, $K_{\xi_1\xi_1\xi_2}$, $K_{\xi_1\xi_1\xi_1\xi_2}$, etc. factorize into a system and a bath part. If we treat the bath in harmonic approximation, we are back to the level of approximation of Eq. (5.63). Note that the coupling constants are defined differently because of the different basis sets used. Comparing $H_{\mathrm{S-R}}^{\mathrm{I}}$ and $H_{\mathrm{S-R}}^{\mathrm{II}}$, however, we notice that there is no bilinear term in $H_{\mathrm{S-R}}^{\mathrm{II}}$ since we have assumed a normal-mode expansion with respect to *all* DOFs around a minimum of the *total* PES.

This consideration can be viewed as a variation on the theme of which basis should be used for actual calculations. Depending on the choice, that is here zeroth-order system and bath Hamiltonian plus coupling versus expansion of the total Hamiltonian and subsequent partitioning into system and bath, different types of transitions between the considered system and bath states due to the coupling may occur. For a comparable level of approximation, both representations should give the same results for experimental observable quantities such as relaxation rates.

5.4.2 Higher Order Multiquantum Relaxation

In what follows, we focus on the effect of higher order terms in the normal-mode expansion Eq. (5.63); that is, we use the interaction Hamiltonian $H_{\mathrm{S-R}}^{\mathrm{I}}$ (the superscript

will be omitted). For simplicity, we will take a single contribution $K(s)\Phi(q)$ of the complete expansion of $V_{S-R}(s, q)$. Which part of the expansion we take, that is the concrete structure of $K(s)$ and $\Phi(q)$, will be specified below. In Section 3.8.2, we saw that the transition rates between the vibrational states $|M\rangle$ and $|N\rangle$ of the relevant system ($H_S |N\rangle = E_N |N\rangle$) could be written as

$$
k_{MN} = \frac{1}{\hbar^2} |\langle M| K(s) |N\rangle|^2 \int_{-\infty}^{+\infty} dt \, e^{i\omega_{MN}t} \langle \Delta\Phi^{(I)}(q, t)\Delta\Phi^{(I)}(q, 0)\rangle_R
$$

$$
= |\langle M| K(s) |N\rangle|^2 C(\omega_{MN}). \tag{5.67}
$$

It has also been shown that this is just a particular element of the damping matrix $\Gamma_{KL,MN}$, which can be calculated by the same procedure we follow now. The rates for the bilinear form of the interaction Hamiltonian were already discussed after Eq. (5.58) (we just have to keep in mind that the coupling constant entering the spectral density is defined differently in the present case).

In connection with Eq. (5.58), we have highlighted the role of energy conservation in the relaxation process. A particularly interesting case in this respect is the relaxation of an intramolecular high-frequency mode. If we assume that intramolecular and solvent modes do not mix appreciably, there are two possibilities: Either there is another intramolecular mode in this frequency range, or the solvent normal-mode spectrum supports such a high-frequency mode. Usually, the collective solvent modes are of rather low frequency (see Figure 5.14). Thus, vibrational energy acceptors in the solvent can only be specific intramolecular modes of the solvent molecules in the surrounding of the solute or of the solute itself. From these restricting conditions, it is clear that relaxation of high-frequency vibrations due to the bilinear coupling term is not always possible since this implies a one-quantum transition.

As an example, we mention the studies of the CO asymmetric stretch relaxation of tungsten hexacarbonyl ($W(CO)_6$) in chloroform ($CHCl_3$). Here, the 1976 cm^{-1} CO mode cannot relax via a mechanism involving a single transition in the bath only. The next $W(CO)_6$ vibrational normal mode is at 580 cm^{-1}, and $CHCl_3$ supports a mode at 1250 cm^{-1}, both out of reach for the CO stretch. Therefore, a quartic process is most likely to be responsible for the relaxation behavior. Changing the solvent to carbon tetrachloride (highest frequency mode 780 cm^{-1}) even led to the conclusion that a quintic order process might be involved.[11]

This is where the higher order terms in the expansion of H_{S-R} in Eq. (5.63) come into play. Here, the relaxation proceeds with the participation of different bath modes; that is, multiquantum transitions occur in the bath. For a given order in the system coordinate s, we have to identify the bath part of H_{S-R} in Eq. (5.63) with $\Phi(Q_\xi = q_\xi \sqrt{\hbar/2\omega_\xi})$, which will contain a product of harmonic bath coordinates. The calculation of the rates in Eq. (5.67) requires us to determine the multitime correlation function of these bath coordinates:

$$
\langle \Delta\Phi^{(I)}(q, t)\Delta\Phi^{(I)}(q, 0)\rangle_R = \sum_{m,n} \sum_{\xi,\bar{\xi}} g_\xi^{(m)} g_{\bar{\xi}}^{(n)} \, C_{\xi,\bar{\xi}}^{(m,n)}(t), \tag{5.68}
$$

---

11) Details of the experimental investigation can be found in Tokmakoff [12].

with

$$C_{\xi,\bar{\xi}}^{(m,n)}(t) = \langle Q_{\xi_1}(t) \dots Q_{\xi_m}(t) Q_{\bar{\xi}_1} \dots Q_{\bar{\xi}_n} \rangle_{\mathrm{R}}, \tag{5.69}$$

and $\xi = (\xi_1, \xi_2, \dots, \xi_m)$ and $\bar{\xi} = (\bar{\xi}_1, \bar{\xi}_2, \dots, \bar{\xi}_n)$. The coupling constant $g_{\xi}^{(m)}$ comprises the mth derivative of the coupling with respect to the bath coordinates as well as the factor $\prod_{i=1}^{m} \sqrt{\hbar/2\omega_{\xi_i}}$.[12]

In order to illustrate the principal effect of the higher order system–reservoir interactions, let us consider the term linear in the system coordinate but quadratic in the bath normal-mode coordinates. This requires the calculation of the bath correlation function $C_{\xi,\bar{\xi}}^{(2,2)}(t)$, which is straightforward for harmonic oscillators.[13] Collecting the different contributions, we obtain

$$\langle \Delta\Phi^{(\mathrm{I})}(q,t)\Delta\Phi^{(\mathrm{I})}(q,0)\rangle_{\mathrm{R}} = 2\sum_{\xi_1,\xi_2}[g_{\xi_1,\xi_2}^{(2)}]^2$$
$$\times [(1 + n(\omega_{\xi_1}))e^{-i\omega_{\xi_1}t} + n(\omega_{\xi_1})e^{i\omega_{\xi_1}t}]$$
$$\times [(1 + n(\omega_{\xi_2}))e^{-i\omega_{\xi_2}t} + n(\omega_{\xi_2})e^{i\omega_{\xi_2}t}]. \tag{5.70}$$

The frequency–domain correlation function entering Eq. (5.67) can be written as

$$C(\Omega) = 4\pi \sum_{\xi_1,\xi_2}[g_{\xi_1,\xi_2}^{(2)}]^2 \left[\delta(\Omega - \omega_{\xi_1} - \omega_{\xi_2})(1 + n(\omega_{\xi_1}))(1 + n(\omega_{\xi_2})) \right.$$
$$+ \delta(\Omega - \omega_{\xi_1} + \omega_{\xi_2})(1 + n(\omega_{\xi_1}))n(\omega_{\xi_2})$$
$$+ \delta(\Omega + \omega_{\xi_1} - \omega_{\xi_2})n(\omega_{\xi_1})(1 + n(\omega_{\xi_2}))$$
$$\left. + \delta(\Omega + \omega_{\xi_1} + \omega_{\xi_2})n(\omega_{\xi_1})n(\omega_{\xi_2}) \right]. \tag{5.71}$$

If the system is harmonic with frequency Ω_{s}, we have upward and downward transitions with rates proportional to $C(\Omega_{\mathrm{s}})$ (see Eq. (5.58)). For illustration of the transitions that are possible according to Eq. (5.71), let us consider *downward* relaxation. Note that all transitions are weighted with the proper thermal equilibrium distribution for the environmental modes. In Figure 5.13, we show diagrams visualizing the different terms in Eq. (5.71). The first term (a) corresponds to an excitation of two vibrational modes of the environment, while the second (b) and the third (c) terms incorporate excitation as well as deexcitation. The last term (d) represents the simultaneous deexcitation of the system *and* the environment. This last process is very unlikely and is usually neglected within the rotating wave approximation. However, if we considered upward transitions, this process of deexcitation of two bath modes and simultaneous excitation of the system mode in principle could give a contribution.

The *exact* resonance conditions will be hardly met in any realistic solute–solvent system taking into account only high-frequency intramolecular modes. However, we have not yet discussed the low-frequency collective modes of the solvent. Often, they

---

12) Notice that in the present model, the coupling constants do not depend on the system coordinate. This is a consequence of the fact that in Eq. (5.63) the derivatives are taken at the minimum of the PES.
13) A general prescription can be found in May and Kühn [13], Sect. 3.6.3.
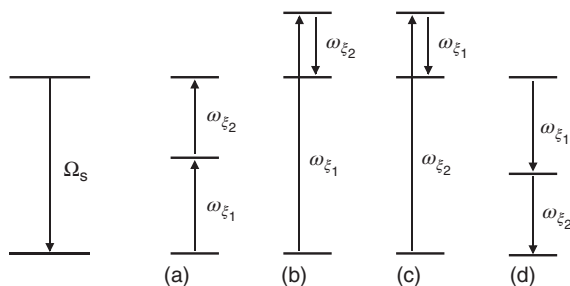
Figure 5.13 Multiquantum relaxation processes in a two-level system. Downward relaxation of the system mode (left) can be accompanied by different transitions in the reservoir if the system–reservoir coupling is quadratic in the reservoir coordinates. Diagrams (a)–(d) correspond to the four terms of the right-hand side of Eq. (5.71).

will provide the continuum of states, which is necessary to ensure energy conservation (Figure 5.14). To be specific, suppose that the modes with index η belong to the low-frequency solvent continuum of states; the intramolecular high-frequency modes are labeled σ. Let us further assume that the coupling matrix factorizes with respect to the oscillators having quite different origin such that we can use $[g_{\eta,\sigma}^{(2)}]^2 \to c_\eta^2 c_\sigma^2$. If we then introduce the spectral density of the low-frequency solvent modes as

$$J_{\mathrm{lf}}(\omega) = \sum_\eta c_\eta^2 \delta(\omega - \omega_\eta), \tag{5.72}$$

we can cast the correlation function into the form:[14]

$$
\begin{aligned}
C(\Omega) = 4\pi \sum_\sigma c_\sigma^2 \Big[&(1 + n(\omega_\sigma))(1 + n(\Omega - \omega_\sigma))J_{\mathrm{lf}}(\Omega - \omega_\sigma) \\
&- (1 + n(\omega_\sigma))(1 + n(\Omega - \omega_\sigma))J_{\mathrm{lf}}(-\Omega + \omega_\sigma) \\
&+ n(\omega_\sigma)(1 + n(\Omega + \omega_\sigma))J_{\mathrm{lf}}(\Omega + \omega_\sigma) \\
&- n(\omega_\sigma)(1 + n(\Omega + \omega_\sigma))J_{\mathrm{lf}}(-\Omega - \omega_\sigma) \Big].
\end{aligned}
\tag{5.73}
$$

If we think of the mode σ as a high-frequency mode of the solute itself or of the neighboring solvent molecules whose frequency we know, the transfer rates can be immediately calculated, provided we have knowledge about the spectral density, for instance derived from full force–force autocorrelation functions. An example for solvent-assisted intramolecular relaxation is given in Figure 5.14.

Generalizing the results we have obtained for the case of a system–reservoir interaction quadratic in the bath normal modes, we want to point out that of course the next (cubic) term gives rise to three-quantum transitions in the bath and so on. Even though the coupling might at first glance seem to be rather weak compared to the low-order terms in the Taylor expansion, energy conservation can take over such that higher order quantum transitions provide the only relaxation channel.

Up to this point we have considered the situation typical for the relaxation of a high-frequency solute mode, which is basically a transition between the first excited

---

14) Here, we have taken only those contributions into account that mix low- and high–frequency modes.

$\nu_{OH} = 3034 \text{ cm}^{-1}$ $\delta_{OH} = 1455 \text{ cm}^{-1}$

$\gamma_{OH1} = 800 \text{ cm}^{-1}$ $\gamma_{OH2} = 690 \text{ cm}^{-1}$

$\nu_{HB} = 65 \text{ cm}^{-1}$

(a) (b) Q_{HB} (a_0 (a.m.u.)$^{1/2}$)

(c) Time (ps) (d) Energy (hc cm^{-1})
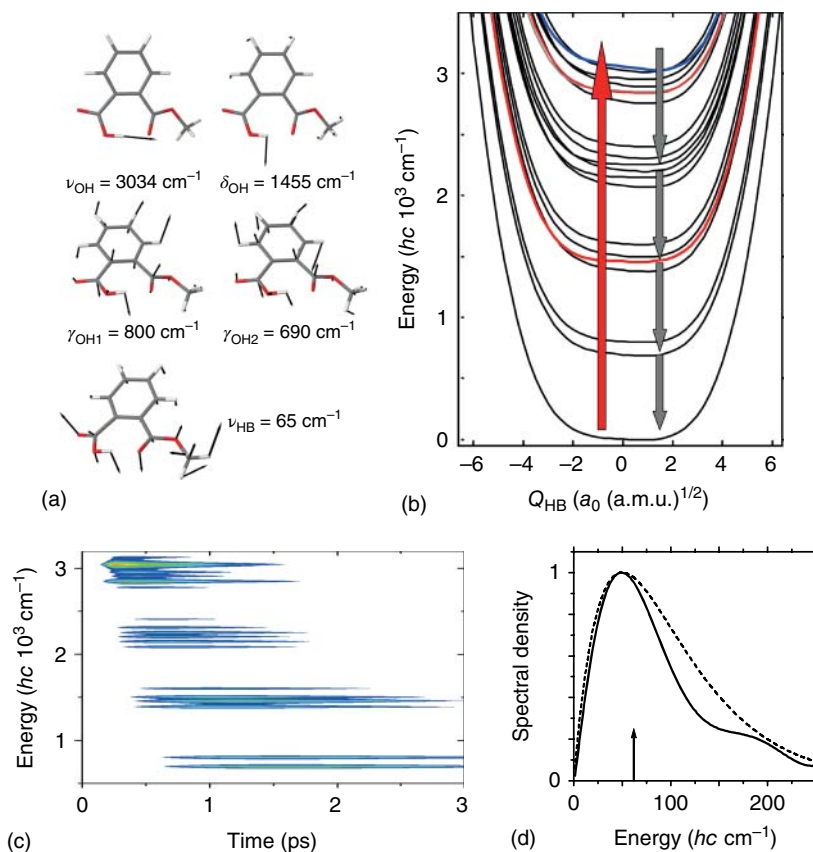
Figure 5.14 Solvent-assisted vibrational energy cascading after excitation of the OH-stretching vibration in the intramolecular hydrogen bond in phthalic acid monomethyl ester in CCl$_4$ solution. In panel (a), normal-mode displacements of the five-dimensional intramolecular relevant system are shown. Panel (b) gives the diabatic potential curves along mode ν_{HB} for fundamental, combination, and overtone transitions of the high-frequency modes. The relevant system is coupled quadratically to another intramolecular mode as well as to the solvent. This leads to a cascaded vibrational energy relaxation as indicated by the arrows and quantified by the populations of the different high-frequency states in panel (c) (populations range from 0.05 to 0.001). The (normalized) spectral density for the coupling of the solvent to mode ν_{HB} (solid line – simulation, dashed line – Ohmic fit, Eq. (3.301), arrow marks – frequency of ν_{HB}) is shown in panel (d). For more details on the model and the experiment, see Heyne [14].

state and the ground vibrational state of that mode. In the following we would like to discuss the relaxation of a mode having some intermediate frequency. The initial condition might be provided by an excitation of an electronic transition. In the electronically excited state, we suppose an excitation along a vibrational mode involving high quantum number states (see also Chapter 6). In the bilinear model, the relaxation would proceed via relaxation down the vibrational ladder step by step. What happens if we include the next higher order, that is the term quadratic in

the system coordinate? For simplicity, we assume that the environment provides a dense spectrum, and all relaxation takes place via single quantum transition in the bath. The system coordinate is assumed to describe a harmonic oscillator with frequency Ω_s. The quadratic contribution to the interaction Hamiltonian can be written in dimensionless form as $K(s) = s^2 2\Omega_s \mu_s / \hbar$. The respective transition rate is given by

$$k_{MN} = |\langle M| K(s) |N\rangle|^2 C(\omega_{MN}), \qquad (5.74)$$

with $C(\omega)$ according to Eq. (3.295). The matrix elements have been given in Eq. (5.6), and we obtain

$$\begin{aligned} k_{MN} = \big[&\delta_{MN}(2M+1)^2 + \delta_{M,N+2}M(M-1) \\ &+ \delta_{M,N-2}(M+1)(M+2) \big] \, C(\Omega_{MN}). \end{aligned} \qquad (5.75)$$

As to be expected, two-quantum transitions become possible at this point. Provided that the spectral density is flat such that $J(\Omega_s) \approx J(2\Omega_s)$, the difference between the one-quantum and two-quantum transitions comes from the thermal prefactor. Thus, the rates for downward transitions behave like $(1 + n(\Omega_s))/(1 + n(2\Omega_s)) = (1 + \exp(-\Omega_s/k_B T))$, and for upward transitions, we have $n(\Omega_s)/n(2\Omega_s) = (1 + \exp(\Omega_s/k_B T))$. Therefore, for moderate temperatures in particular, the two-quantum upward transitions will be much less probable than the respective one-quantum transitions. In general, however, estimating the relative importance of one- and two-quantum transitions, one has to take into account the form of the spectral density. There is another term in Eq. (5.75) which is proportional to δ_{MN}. This term is nothing but energy conserving *pure dephasing*.

5.5 Quantum–Classical Approaches to Relaxation and Dephasing

Classical molecular dynamics simulations have the advantage that realistic condensed-phase situations can be described using forces that are determined on the fly from molecular mechanics force fields or quantum chemical calculations. However, often, one needs to account for the quantum nature of high-frequency vibrations, and therefore, hybrid quantum–classical approaches are used (see also Section 3.13). Since in vibrational problems, the relevant system, that is the vibrational coordinate is not appreciably displaced from its equilibrium value, the feedback of the quantum to the classical system can often be neglected. Furthermore, the relevant system Hamiltonian and the system–reservoir coupling are comprised into a system Hamiltonian that depends on the classical solvent coordinates $Z = \{Z_\xi\}$, that is $H_S + H_{S-R} = H_S(Z(t))$. Hence, the quantum states of the relevant system are to be defined for a given solvent configuration. Here, a straightforward method is to generate a PES for the relevant system along the molecular dynamics trajectory (the so-called snapshot potentials where the reservoir DOFs are
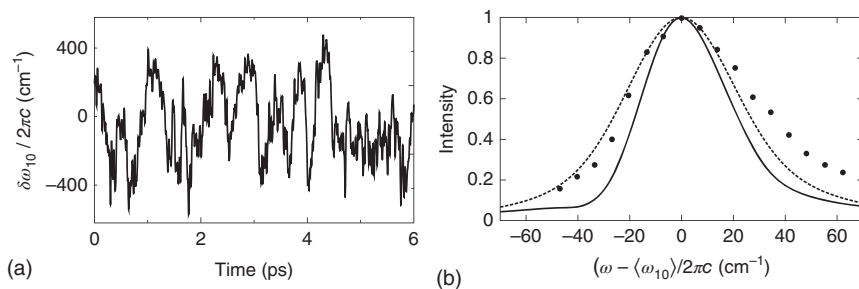
Figure 5.15 (a) Fluctuations of the fundamental transition frequency of the N–H vibration in an adenine–uracil base pair in deuterochloroform solution as obtained from snapshot potentials within a QM/MM simulation. (b) The related IR absorption spectrum is shown according to Eq. (5.77) (solid) as well as within a second-order cumulant expansion (dashed, see Section 4.3.4). The experimental result (bullets) is taken from Woutersen and Cristalli [15] (figure courtesy of Y. Yan).

fixed) and diagonalize the respective Hamiltonian to obtain the vibrational eigenstates, see Eq. (3.447). A numerically less-expensive approach is to employ certain mapping relations. In hydrogen-bonded systems, for instance, the frequency of the hydrogen motion within a hydrogen bond depends on the length of that bond (see Chapter 8), and simple empirical relations have been established from experimental data.

A more accurate procedure employs the fact that by virtue of the Stark effect the vibrational energy levels of some high-frequency vibration depend on the local electric field due to the surrounding solvent. Employing gas-phase simulation of the relevant system in an electric field, a mapping between the system Hamiltonian and the field parameters (for example, field plus field gradient) can be established. Extensions to include, for instance, dispersive interactions are possible. This so-called *vibrational spectroscopy map* approach enables one to assign the system Hamiltonian based on the field, which is obtained along the molecular dynamics trajectory in the condensed phase. This approach has the advantage that using ab initio quantum chemical methods in the gas phase, one circumvents the problem that classical force fields are usually designed to reproduce structural and thermodynamic properties but not vibrational spectra. On the other hand, it is limited to purely electrostatic effects, not accounting for, for instance covalent bonding. This approach has been widely used for the investigation of water and peptide dynamics.

Pure vibrational dephasing and its effect on the lineshape of the infrared absorption spectrum is readily discussed within a quantum–classical approach. Let us consider the two lowest states of a high-frequency mode, $|0\rangle$ and $|1\rangle$, with transition frequency ω_{10} and dipole operator (in Condon approximation and neglecting the vector character) $\hat{\mu} = \mu_{10} |1\rangle \langle 0| + \text{h.c.}$ An expression for the absorption spectrum in terms of the dipole–dipole correlation function is given in Eq. (4.46). For the present model, we can use the results of Section 4.3.4. This implies that we assume $H_0(Z)$ and $H_1(Z)$ being the Hamiltonian operators for the Z DOFs in the ground and excited states, respectively. Next, we introduce the fluctuation operator $\Delta H_{10}^{(0)}(t) = H_1(t) - H_0(t) - \Delta_{10}$, with $\Delta_{10} = \langle \hbar\omega_{10} \rangle$ and the thermal average taken with respect

to the equilibrium statistical operator for the Z DOFs, $\hat{R}_0(Z)$. The S-operator in Eq. (4.78) takes the form

$$S_{10}(t,0) = \hat{T} \exp\left\{ -\frac{i}{\hbar} \int_0^t d\bar{t}\, \Delta H_{10}^{(0)}(\bar{t}) \right\}. \tag{5.76}$$

Instead of performing a cumulant expansion as in Section 4.3.4, the classical approximation is taken for the Z DOFs.[15] In this case, the time ordering in the S-operator can be neglected, and the average is performed with respect to a classical ensemble. The absorption spectrum becomes (cf. Section 4.2.2)

$$\alpha(\omega) = \frac{4\pi\omega n_{mol}}{3\hbar c}\,\mathrm{Re} \int_0^\infty dt\, e^{i(\omega - \Delta_{10}^{(cl)}/\hbar)t} \left\langle \exp\left\{ -i \int_0^t d\bar{t}\, \delta\omega_{10}(\bar{t}) \right\} \right\rangle_{cl,R}. \tag{5.77}$$

Here, we introduce the gap fluctuation function $\delta\omega_{10}(t)$ as the time-dependent deviation of the transition energy from its average value, $\Delta_{10}^{(cl)}/\hbar$, due to the classical motion of the Z DOFs. Notice that the classical equilibrium dynamics of the Z DOFs takes place with respect to the ground state of the high-frequency mode, which is a consequence of the partitioning in Eq. (4.77). Alternatively, the excited state could have taken as a reference, which, however, would imply to adapt molecular dynamics force fields. An example is given in Figure 5.15. Note that the line width according to Eq. (5.77) is not necessarily Lorentzian; that is, in general, the simple Bloch model of dephasing does not apply. Nevertheless, a pure dephasing time T_2^* is often estimated on the basis of a fitting to a Lorentzian lineshape.

The classical approximation can also be applied to the nonlinear response functions introduced in Section 4.3.2, Eqs. (4.92)–(4.95). For example, for $R_1(t_3, t_2, t_1)$, we obtain for the present two-level system the expression

$$R_1(t_3, t_2, t_1) = |d_{10}|^4 e^{-i\Delta_{10}^{(cl)}(t_1+t_3)\hbar}$$

$$\times \left\langle \exp\left\{ -i \int_0^{t_1} d\bar{t}\, \delta\omega_{10}(\bar{t}) - i \int_{t_1+t_2}^{t_1+t_2+t_3} d\bar{t}\, \delta\omega_{10}(\bar{t}) \right\} \right\rangle_{cl,R}. \tag{5.78}$$

Hence, provided that the gap correlation function has been calculated, linear and nonlinear spectroscopic signals can be determined as far as the contributions due to pure dephasing are concerned. In Figure 5.16, results of the classical simulations of the two-dimensional IR spectrum of an adenine–uracil base pair in deuterochloroform solution are shown (cf. Figure 5.15). The spectrum can be analyzed in terms of features discussed in Figure 4.3. Peaks I and I′ on the diagonal ($\Omega_e = \Omega_d$) correspond to the response of the N–H$\cdots$N (I) and N–H$\cdots$O vibrations. The corresponding ESA signals due to vibrational anharmonicity are marked by II and II′.

---

15) Note that the expression still contains $\hbar$ and therefore is formally not a classical limit in the strict sense.
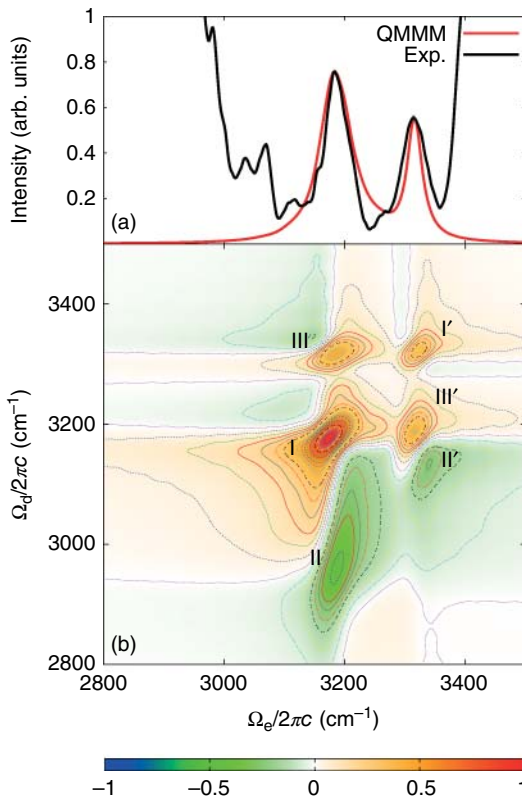
Figure 5.16 (a) IR absorption spectrum of N–H···N and N–H···O vibrations in an adenine–uracil base pair in deuterochloroform solution (cf. Figure 5.15). (b) Two-dimensional IR spectrum, $S_s(\Omega_d, \Omega_e, T = 0)$, Eq. (4.114), in classical approximation, based on gap fluctuations shown in Figure 5.15a. The labels mark the diagonal peaks (I, I′), ESA (II, II′), and cross-peaks (III, III′); for a discussion, see text (figure courtesy of Y. Yan, for more information see Yan and Kühn [16]).

Two cross-peaks, III and III′, are also visible, indicating the coupling between the two vibrations.

In order to describe population dynamics, one makes use of the assumption that the relevant quantum system does not react back onto the classical bath. This system part is defined with parameters depending on the actual position of the bath coordinates obtained using a vibrational spectroscopy map. To be specific, we consider the example of a system formed by two DOFs coupled via a Fermi resonance (cf. Section 5.2.1), that is

$$H_S(Z(t)) = \frac{1}{2} \sum_{\xi=1,2} \left(p_\xi^2 + \omega_\xi^2(Z(t)) q_\xi^2 \right) + K_{122}(Z(t)) \, q_1 q_2^2. \tag{5.79}$$

Using an expansion into a basis set such as harmonic oscillator states, one obtains a set of differential equations for the expansion coefficients that can be solved numerically including a sampling of the bath fluctuations, for instance along a molecular dynamics trajectory (cf. Eq. (3.449) where, however, an eigenstate expansion had been used). As a result, the population dynamics as well as spectroscopic signals can be investigated. One should be aware, however, that as a consequence of the neglected backreaction of the system to the reservoir, this approach cannot describe thermalization to the proper equilibrium.

References

1 K. C. Woo and S. K. Kim, J. Phys. Chem. Lett. **11**, 161 (2020).
2 M. Bargheer et al., Phys. Chem. Chem. Phys. **4**, 75 (2002).
3 M. Bixon and J. Jortner, J. Chem. Phys. **48**, 715 (1968).
4 M. Gruebele, Theor. Chem. Acc. **109**, 53 (2003).
5 F. Gottwald et al., J. Phys. Chem. Lett. **6**, 2722 (2015).
6 R. M. Stratt, Acc. Chem. Res. **28**, 201 (1995).
7 G. Goodyear and R. M. Stratt, J. Chem. Phys. **105**, 10050 (1996).
8 F. Gottwald et al., J. Chem. Phys. **144**, 164102 (2016).
9 S. Gnanakaran and R. M. Hochstrasser, J. Chem. Phys. **105**, 3486 (1996).
10 F. Gottwald et al., J. Chem. Phys. **142**, 244110 (2015).
11 M. Olschewski et al., J. Chem. Phys. **134**, 214504 (2011).
12 A. Tokmakoff et al., J. Chem. Phys. **100**, 9035 (1994).
13 V. May and O. Kühn, *Charge and Energy Transfer Dynamics in Molecular Systems* 2nd Ed., (Wiley–VCH, Weinheim, 2004).
14 K. Heyne et al., J. Phys. Chem. A **108**, 6083 (2004).
15 S. Woutersen and G. Cristalli, J. Chem. Phys. **121**, 5381 (2004).
16 Y. Yan and O. Kühn, J. Phys. Chem. B **115**, 5254 (2011).

Further Reading

- Reviews on vibrational energy flow:
  S. C. Farantos, R. Schinke, H. Guo, and M. Joyeux, Chem. Rev. **109**, 4248 (2009).
  M. Gruebele and R. Bigwood, Int. Rev. Phys. Chem. **17**, 91 (1998).
- Vibrational energy flow and chemical dynamics:
  C. G. Elles and F. F. Crim, Annu. Rev. Phys. Chem. **57**, 273 (2006).
- Generalized Langevin equation:
  R. Zwanzig, *Nonequilibrium Statistical Mechanics*, (Oxford University Press, New York, 2001).
- Vibrational spectroscopic maps:
  C.R. Baiz, B. Błasiak, J. Bredenbeck, M. Cho et al., Chem. Rev. **120**, 7152 (2020).
- Two–dimensional vibrational spectroscopy:
  T. la Cour Jansen, S. Saito, J. Jeon, and M. Cho, J. Chem. Phys. **150**, 100901 (2019).

6

Intramolecular Electronic Transitions

Photoinduced intramolecular electronic transitions as well as transitions caused by intramolecular state couplings will be discussed below. In contrast to more complex transfer reactions, which we will encounter in later chapters, these processes exclusively take place in a single molecule where an electron is promoted from an initial electronic state $|\phi_i\rangle$ to a final electronic state $|\phi_f\rangle$. We explain in detail that the interplay of the dynamics of the electronic transition and the accompanying vibrational motion is at the heart of such transitions.

If the vibrational relaxation within the considered potential energy surface is fast compared to the electronic transition, a simple perturbational treatment with respect to the electronic coupling between the states $|\phi_i\rangle$ and $|\phi_f\rangle$ becomes possible. As an important example for such a transition, linear optical absorption is discussed. Here, the state coupling is due to an external electromagnetic field. Different ways for calculating the absorption spectrum are introduced that highlight particular aspects of the coupled electronic and nuclear motions during the transition event and demonstrate different types of approximations. Nonlinear optical processes are also briefly addressed.

On the basis of this discussion, we are in the position to describe the internal conversion process, which is an intramolecular electronic transition that results from the nonadiabatic coupling between different adiabatic electronic states. Here, we focus on the cases of slow and fast vibrational relaxation as compared to the electronic transition rate.

6.1 Introduction

Adiabatic electronic states are approximate solutions of the stationary electronic Schrödinger equation for the molecule (cf. Section 2.3). Since they are *not eigenstates* of the molecular Hamiltonian, there exists a residual interaction between adiabatic states. Different situations can be identified where this nonadiabatic coupling has to be taken into account. For example, if bound electronic states are considered, an overlap of the related PES indicates that nonadiabatic transitions may be important. If a molecule is initially prepared in a particular excited adiabatic state, a spontaneous transition to the electronic ground state will take place. In the

general case, this may involve a sequence of transitions via intermediate electronic states. Such a type of transition is called *internal conversion* (IC). It is characterized by the conservation of the total molecular spin. Hence, starting in an excited singlet state S_n, IC proceeds down to the singlet ground state S_0. Normally, the transitions down to the first excited singlet state, S_1, are rather rapid (so-called Kasha rule). However, the nonradiative transition $S_1 \rightarrow S_0$ is so slow that it competes with possible radiative transitions (luminescence). IC processes are also observed within the manifold of triplet (or higher spin) states, whereas singlet–triplet transitions (and vice versa) are known as *intersystem crossing* processes.

The equilibrium configuration of the nuclei depends on the electronic state (see Section 2.19). This is why the dynamics of intramolecular electronic transitions may strongly depend on the coupling between electronic and nuclear DOFs. Let us consider transitions between two adiabatic electronic states, $|\phi_i\rangle$ (initial state) and $|\phi_f\rangle$ (final state). If the relaxation of the nuclear DOFs in these two electronic states (for instance, due to the coupling to a reservoir) is fast compared to the time needed for a transition between these two states, the process is electronically incoherent. Electronic coherences between the two states can exist if the nuclear motion is comparable or slow in relation to the electronic dynamics. Then, a time-dependent wave function is formed that is a superposition of the initial and final states. In general, intramolecular electronic transitions are not necessarily induced by internal couplings, such as nonadiabatic or spin–orbit couplings. Scattering processes of the considered molecule with other molecules as well as the interaction with external electromagnetic fields can cause electronic transitions, too. The most common example is the absorption of light energy via an electronic transition from the ground state of the molecule to a particular excited state. This process conserves the total spin; it is a transition from the singlet ground state S_0 to an excited singlet state S_n $(n = 1, 2, \ldots)$.[1] We expect many similarities between externally induced electronic transitions and those induced by internal perturbations. In particular, this holds when the coupling is weak, which allows for a perturbational treatment. This provides the motivation to discuss the theoretical description of optical absorption in some detail. Many of the relations we introduce here will also be valid for other types of transfer processes to be treated in the following chapters.

6.1.1 Optical Transitions

We start with some qualitative considerations of optical absorption; details on the theoretical background of molecule radiation field interaction have been already presented in Chapter 4. Let us focus on the simple case of a diatomic molecule. The ground state will be characterized by the PES $U_g(R)$, whereas the excited state PES is given by $U_e(R)$. R denotes the relative distance between the two atoms, and rotational motion will be neglected. Both PESs are assumed to have a single minimum at R_a $(a = g, e)$. Usually, $R_e > R_g$, since an electronic excitation results in a weakening

---

1) Notice that, of course, the electronic ground state could have a higher multiplicity as well.
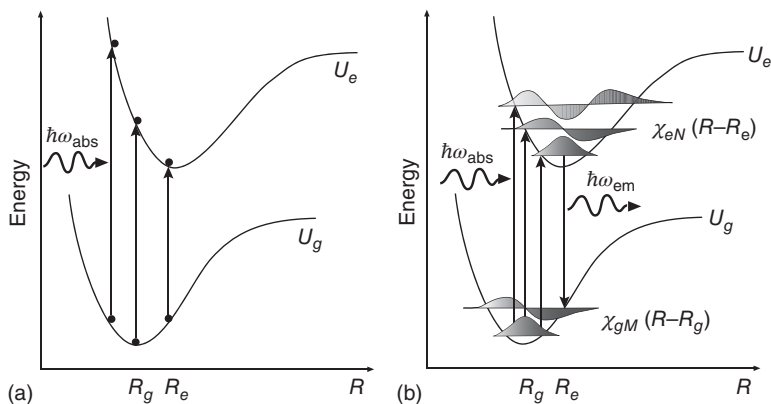
Figure 6.1 Ground and excited state PESs of a diatomic molecule versus bond distance R with exemplary transitions for absorption at energy $\hbar\omega_{abs}$ and emission at $\hbar\omega_{em}$. (a) Different vertical transitions are shown that correspond to different relative positions in the sense of classical physics. (b) Different vibrational states in both electronic states together with the respective wave function are sketched. Transitions to and from the excited electronic state are possible for different values of the bond length R.

of the bond. The electronic transition can be considered to take place on a time scale that is fast compared to the relative motion of both nuclei (bond vibration).[2] Therefore, we can disregard the nuclear motion during the electronic transition. In the picture of PES, this means that the electronic transition is *vertical*, and the nuclei are frozen during the transition, as shown in Figure 6.1. This scheme for optical transitions in molecules is known as the *Franck–Condon principle*.

Next, we discuss how this principle affects the details of the absorption spectra. We start with a *classical* description of the relative motion of the two nuclei. Although the nuclear motion in molecules is of quantum nature, the classical description is appropriate if the energy of a characteristic vibrational quantum $\hbar\omega_{vib}$ is much smaller than a characteristic mean energy of the vibrational motion, for example smaller than the thermal energy $k_B T$.

According to the classical description, the state of the lowest energy in the electronic ground state PES U_g corresponds to $R = R_g$; that is, the bond distance takes its equilibrium value. After the optical excitation the electronic state has been changed to the excited state without any change in R. Optical absorption is possible whenever the photon energy $\hbar\omega$ equals $U_e(R_g) - U_g(R_g)$. This results in a sharp absorption line at this photon energy. Usually we have $R = R_g < R_e$, and the bond is elongated according to the new equilibrium length R_e. As a consequence, following the excitation, there will be vibrational motion with respect to R_e.

If collisions with other molecules take place, for example in a condensed phase environment (solvent), R may deviate from R_g in the initial state, and absorption becomes possible at photon energies different from $U_e(R_g) - U_g(R_g)$.

---

2) Although this picture is useful, we remind the reader on the fact that quantum mechanics does make any statement neither concerning the actual time nor on the duration of the electronic transition. We exclusively get information on the change of the particle wave function with time (cf. Section 6.5).

Since the experiments we have in mind are done with a macroscopically large number of molecules, a multitude of transitions become possible at photon energy $\hbar\omega = U_e(R) - U_g(R)$, with values of R being determined by the type and the strength of the collision processes.[3] If system and environment are in thermal equilibrium with temperature T, we can use statistical mechanics to determine the possible values of R from the thermal distribution

$$f(R) = \frac{1}{\mathcal{Z}} \, e^{-U_g(R)/k_{\mathrm{B}}T}, \tag{6.1}$$

with the partition function $\mathcal{Z} = \int dR \exp(-U_g(R)/k_{\mathrm{B}}T)$. As a consequence of the thermal distribution of bond lengths, the measured absorption spectrum will be broadened so that it has a width approximately equal to $k_{\mathrm{B}}T$. Since $R = R_g$ occurs with highest probability, the maximum of the absorption spectrum is located at the photon energy $U_e(R_g) - U_g(R_g)$ (vertical transition).

Next, we assume that $k_{\mathrm{B}}T < \hbar\omega_{\mathrm{vib}}$ and change to a quantum description as illustrated in Figure 6.1b. In this case, the vibrational motion is characterized by discrete vibrational levels E_{gM} and E_{eN} of the electronic ground and excited states, respectively. Consequently, (one-photon) absorption processes of a monochromatic radiation field take place only if the energy $\hbar\omega$ of a photon equals a possible transition energy $E_{eN} - E_{gM}$. Let us again make use of the Franck–Condon principle to understand the details of these transitions. For simplicity, we assume that only the vibrational ground state, $\chi_{gM=0}(R)$, is populated before the absorption process. The description in terms of a wave function implies that the coordinate R does not possess the sharp value R_g but is distributed around it. As a consequence, vertical transitions to the excited state are also possible for $R \neq R_g$. The mentioned coordinate distribution is also valid for the vibrational states, $\chi_{eN}(R)$, of the PES U_e. Here, $\chi_{eN}(R)$ determines the possible values of R in the excited state. To what extent these vibrational states are excited follows from the overlap between the initial wave function $\chi_{g0}(R)$ and the final state wave functions $\chi_{eN}(R)$:

$$\int dR \, \chi_{eN}^*(R)\chi_{g0}(R) \equiv \langle \chi_{eN} | \chi_{g0} \rangle. \tag{6.2}$$

These overlap matrix elements are called *Franck–Condon factors*. The square of these Franck–Condon factors is proportional to the respective transition strength (see below); the individual spectral lines will be sharp in the simple one-dimensional model considered here. If excited vibrational states in the electronic ground state are thermally occupied, additional transitions to the excited electronic state are possible. Considering a large number of molecules in thermal equilibrium with a particular environment, every transition is weighted by the probability,

$$f_{gM} = \frac{\exp(-E_{gM}/k_{\mathrm{B}}T)}{\sum\limits_{N} \exp(-E_{gN}/k_{\mathrm{B}}T)}, \tag{6.3}$$

that a molecule of the thermal ensemble is in the initial state $|\chi_{gM}\rangle$.

---

3) In such a situation one has to include the kinetic energy T_{vib} of the nuclear motion resulting in the energy $T_{\mathrm{vib}} + U_g(R)$ of the initial state and the energy $T_{\mathrm{vib}} + U_e(R)$ of the final state of the transition. However, the difference again amounts to $U_e(R) - U_g(R)$.

So far, we have assumed that the spectrum can be calculated from the knowledge of the eigenstates of the relevant system. In a condensed phase environment, however, one has to account for the interaction between the relevant system and the reservoir (for example, the solvent). Without adopting a specific model for the reservoir and its interaction with the system, we can discuss two principal effects. To this end, we assign a certain time scale to the modulation of the system's properties (for example, the transition energies) by the reservoir. If this time scale is long compared with some characteristic time for the experiment (typically given by the optical pulse length, which can be nanoseconds for absorption measurements), the effect of the environment is to introduce *static disorder*. This means that there will be a static distribution of transition energies. This induces a broadening of the molecular absorption caused by the fact that the absorption spectra of individual molecules are not identical. Usually, it is referred to as *inhomogeneous broadening* of absorption lines (cf. Section 6.7). In contrast, if the modulation of molecular properties by the environment is fast with respect to the time of the measurement, we have *dynamic disorder*. It results in the so-called *homogeneous broadening*, which can be rationalized in terms of dephasing rates, which have to be added to the transition energies in Eq. (6.17). In Section 6.2.4, these two limits will emerge from a particular model for a spectral density that can be introduced Section 3.7.3. Figure 6.3 shows the broadened absorption spectrum of a perylene bisimide dye molecule.

Having discussed the optical process where a single photon is absorbed by the molecule, we now turn to the case of higher intensities of the incoming radiation or multiple fields. The resulting nonlinear absorption processes are used in nonlinear spectroscopies such as pump–probe spectroscopy. Pump–probe spectroscopy has been introduced in Section 4.3.6. Adapting the level scheme in Figure 4.2 to the present case, one arrives at the picture of shifted PES. Here, the pump–pulse excites a wave packet on state $|\phi_e\rangle$ whose dynamics can be probed by a second pulse, for instance by excited state absorption (ESA) to a higher bound state, $|\phi_f\rangle$, as in Figure 5.2 or by photoionization as illustrated in Figure 6.2.

If the molecule is in condensed phase, the interaction with the environment will lead to vibrational energy relaxation and equilibration in the excited state. Provided that the lifetime of the electronic state is long, the pump–probe spectrum (transient absorption) gives valuable information about the properties of the excited state PES, such as electronic energy differences and relative shifts of the PES. An example is given in Figure 6.3.

In the preceding discussion we concentrated on the absorption of photons, but the reverse process is also possible. Optical recombination, that is emission, is simply the inversion of the optical absorption process, as shown in Figure 6.1b. Since the lifetime of the first excited singlet state is in most cases large compared to the characteristic times of the vibrational motion and relaxation, a thermal equilibrium is established of the vibrational motion in the excited electronic state before recombination. Therefore, the initial state of this process has to be characterized by a thermal distribution function as in Eq. (6.3) but related to the first excited state. Emission from this equilibrium distribution in the excited electronic state takes place to different excited vibrational states belonging to the electronic ground
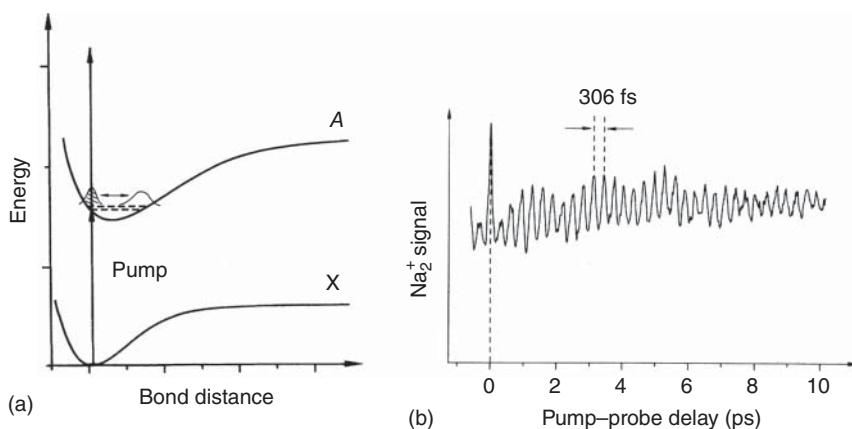
Figure 6.2 Pump–probe spectroscopy of wave packet dynamics. (a) Wave packet motion of Na_2 after preparation of a nonstationary state in the electronic state $A^1\Sigma_u^+$ by means of a pump pulse. The subsequent probe pulse ionizes the molecule such that the observed signal shown in (b) corresponds to the ion yield as a function of the delay time between the pump and probe pulses. The oscillation time of 306 fs corresponds to the oscillation period of the evolving wave packet (Reproduced with permission from Baumert et al. [1]/American Physical Society).
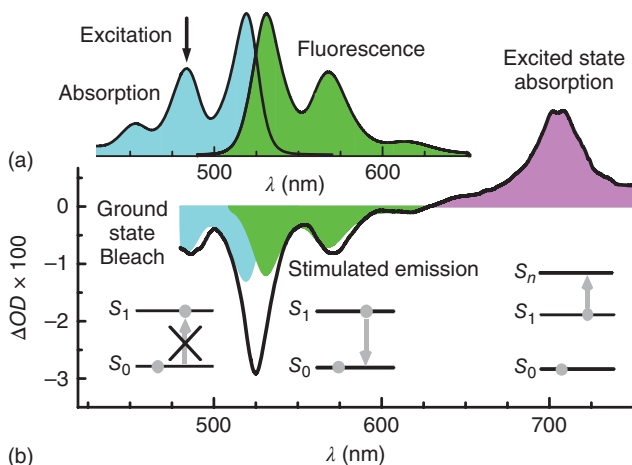
Figure 6.3 Steady-state absorption and fluorescence spectrum (a) of a perylene bisimide dye (in chloroform). Both spectra exhibit a broadened vibrational or Franck–Condon progression. The transient absorption spectrum (dispersed pump–probe spectrum, Eq. (4.103), given as change in optical density [OD]) is shown in (b) 5 ps after excitation at 480 nm. The spectrum is decomposed according to the contributions coming from ground state bleaching, stimulated emission, and excited state absorption to a higher electronic state (S_n); see also Figure 4.2 (figure courtesy of S. Lochbrunner).

Figure 6.4 Internal conversion of the population of electronic levels with energy E_{1M} into a population of electronic levels with energy E_{2N}. Every vibrational level loses its population via transitions induced by the nonadiabatic coupling. If the nonadiabatic transition is fast compared to vibrational relaxation, recurrences of population become possible. In the contrary case, the transfer is irreversible, and the energetic degeneracy between the levels of state 1 and state 2 is a necessary condition for the transition.
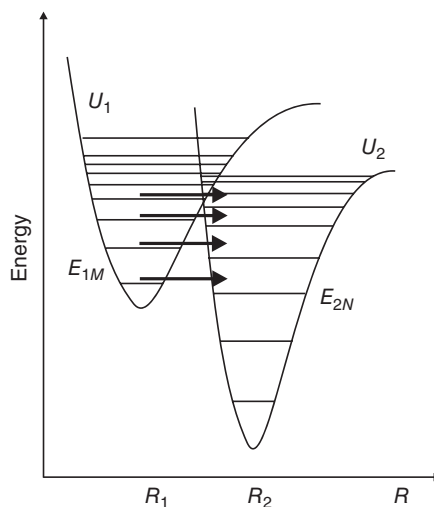
state. Finally, we note that emission can take place as a spontaneous as well as a stimulated process (cf. Figure 6.3).

6.1.2 Internal Conversion Processes

A possible scheme for IC processes is given in Figure 6.4, indicating the transition from the adiabatic electron–vibrational states E_{1M} to the states E_{2N}. If the nonadiabatic coupling is weak so that the characteristic time for the transition is long compared to the time vibrational relaxation needs to establish thermal equilibrium, the IC process starts from such a thermal distribution among the vibrational levels E_{1M}. However, if the transition is also fast, vibrational relaxation is accompanied by transitions to the vibrational levels E_{2N}. Of course, the details of this process are not only determined by the strength of the nonadiabatic coupling, there is also a considerable influence of the initial state preparation. For instance, if the preparation time is long compared to the time of the nonadiabatic transition, any detail of the IC process may be smeared out (for more details on the problem of state preparation, see Section 6.5).

6.2 The Optical Absorption Coefficient

6.2.1 Golden Rule Formulation

We start our discussion of the absorption coefficient by deriving the expression for the rate $k_{g\to e}$ of transitions between the electronic ground state $|\phi_g\rangle$ and some excited state $|\phi_e\rangle$ due to the absorption of a single photon. During this process, energy of the electromagnetic field is converted into molecular excitation energy. For the molecular Hamiltonian, the representation in terms of the electron–vibrational states $|\phi_a\rangle|\chi_{aN}\rangle$ will be used (cf. Section 2.6). The interaction with the field is
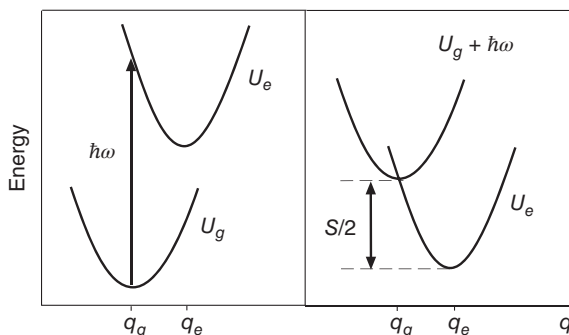
Figure 6.5 Description of optical absorption as a curve-crossing problem with initial state PES $\hbar\omega + U_g$ and final state PES U_e. The type of curve crossing determines the degree of the initial and final state vibrational wave function overlap. (S is the Stokes shift parameter.)

accounted for in the semiclassical approximation discussed in Section 4.1. Note that describing electronic transitions in a system of two electronic states with the Golden Rule formula implies that the coupling between both states is weak, and that any coherence between the initial and final states is suppressed.

It will be the main aim of the following considerations to determine the transition rate for a single molecule using a point of view that establishes a relation between optical absorption and other types of electronic transitions induced by *intramolecular* perturbations. Therefore, the absorption process is viewed as the transition from the initial state $|\phi_g\rangle|\chi_{gM}\rangle$ with energy levels $\hbar\omega + E_{gM}$ to the final states $|\phi_e\rangle|\chi_{eN}\rangle$ in the excited electronic state with energy levels E_{eN}. In other words, the energy of the absorbed photon $\hbar\omega$ is incorporated by defining the PES for the initial state as $U_g + \hbar\omega$ (cf. Figure 6.5). We consider situations where this PES overlaps with the final state PES U_e. Then, the optical absorption can be interpreted as a charge transfer between PESs belonging to different adiabatic electronic states. Such an arrangement of two overlapping PESs is usually called a *curve-crossing system*.

First, the concept of the energetically shifted electronic ground state PES is introduced into the molecular Hamiltonian (two-level version of Eq. (2.98) with the neglect of nonadiabatic couplings). Including the external field also, the Hamiltonian reads (cf. Eq. (4.15))

$$H(t) = \sum_{a=g,e} H_a(q)|\phi_a\rangle\langle\phi_a| - \boldsymbol{E}(t)\left(\boldsymbol{d}_{eg}|\phi_e\rangle\langle\phi_g| + \text{h.c.}\right). \tag{6.4}$$

Here, q comprises the relevant nuclear coordinates of the molecule. The external field is taken to be monochromatic: $\boldsymbol{E}(t) = \boldsymbol{E}_0 \exp(-i\omega t) + \text{c.c.}$ Let us rearrange the Hamiltonian according to

$$H(t) = \mathcal{H}_0 + \mathcal{H}_1(t), \tag{6.5}$$

with $\mathcal{H}_0 = -\hbar\omega|\phi_g\rangle\langle\phi_g|$. The remaining part gives the Hamiltonian with the shifted electronic ground state spectrum

$$\mathcal{H}_1(t) = \left(H_g(q) + \hbar\omega\right)|\phi_g\rangle\langle\phi_g| + H_e(q)|\phi_e\rangle\langle\phi_e|$$
$$-\boldsymbol{E}(t)\left(\boldsymbol{d}_{eg}|\phi_e\rangle\langle\phi_g| + \text{h.c.}\right). \tag{6.6}$$

Next, we use this particular representation to calculate the transition rate $k_{ge} \equiv k_{g\to e}$. To do so, we follow the approach presented in Section 3.3, where the Golden Rule

formula has been derived. The manifold of initial states $|a\rangle$ is identified with the adiabatic electron–vibrational states $|\phi_g\rangle|\chi_{gM}\rangle$, whereas the final states $|\beta\rangle$ are the excited electron–vibrational states $|\phi_e\rangle|\chi_{eN}\rangle$.

To apply the results of Section 3.3, we have to specify the time-evolution operator. This is done here by taking the (zeroth-order) time-evolution operator $U_0(t) = \exp\{-i\mathcal{H}_0 t/\hbar\}$ and changing to the interaction picture with respect to the (zeroth-order) Hamiltonian $\mathcal{H}_0$. According to Section 3.2.2, the total time-evolution operator reads $U(t) = U_0(t)S(t,0)$. The S-operator is defined as the time-ordered exponential of $\mathcal{H}_1(t)$ taken in the interaction picture

$$S(t,0) = \hat{T} \exp\left(-\frac{i}{\hbar} \int_0^t dt'\; \mathcal{H}_1^{(\mathrm{I})}(t') \right), \tag{6.7}$$

with $\mathcal{H}_1^{(\mathrm{I})}(t) = U_0^+(t)\mathcal{H}_1(t)U_0(t)$. One easily verifies that

$$U_0(t)|\phi_g\rangle = e^{i\omega t}|\phi_g\rangle\,, \quad U_0^+(t)|\phi_g\rangle = e^{-i\omega t}|\phi_g\rangle\,, \quad U_0(t)|\phi_e\rangle = |\phi_e\rangle. \tag{6.8}$$

Applying these results, we get

$$\begin{aligned}
\mathcal{H}_1^{(\mathrm{I})}(t) = {} & \left(H_g(q) + \hbar\omega \right)\; e^{-i\omega t}|\phi_g\rangle\langle\phi_g|e^{i\omega t} + H_e(q)|\phi_e\rangle\langle\phi_e| \\
& -\boldsymbol{E}_0 e^{-i\omega t} \left(\boldsymbol{d}_{eg}|\phi_e\rangle\langle\phi_g|e^{i\omega t} + \boldsymbol{d}_{eg}^* e^{-i\omega t}|\phi_g\rangle\langle\phi_e| \right) \\
& -\boldsymbol{E}_0^* e^{i\omega t} \left(\boldsymbol{d}_{eg}|\phi_e\rangle\langle\phi_g|e^{i\omega t} + \boldsymbol{d}_{eg}^* e^{-i\omega t}|\phi_g\rangle\langle\phi_e| \right).
\end{aligned} \tag{6.9}$$

This transformed Hamiltonian contains a *time-independent* part,

$$\begin{aligned}
\mathcal{H}_{\mathrm{rw}}^{(\mathrm{I})} = {} & \left(H_g(q) + \hbar\omega \right) |\phi_g\rangle\langle\phi_g| + H_e(q)|\phi_e\rangle\langle\phi_e| \\
& -\boldsymbol{E}_0 \boldsymbol{d}_{eg}|\phi_e\rangle\langle\phi_g| - \boldsymbol{E}_0^* \boldsymbol{d}_{eg}^*|\phi_g\rangle\langle\phi_e|,
\end{aligned} \tag{6.10}$$

and a part oscillating at twice the field frequency ω. If one neglects these high-frequency oscillations, the interaction picture introduced in this way leads to a time-independent Hamiltonian $\mathcal{H}_{\mathrm{rw}}^{(\mathrm{I})}$. This is known as the Hamiltonian in the *rotating wave approximation*.[4]

Accepting the time-independent Hamiltonian as a good approximation for $\mathcal{H}_1^{(\mathrm{I})}(t)$, the S-operator becomes very simple since no time ordering is necessary. We obtain the complete time-evolution operator as

$$U(t) = \exp\{i\omega t|\phi_g\rangle\langle\phi_g|\}\; \exp\{i\mathcal{H}_{\mathrm{rw}}^{(\mathrm{I})}t/\hbar\}. \tag{6.11}$$

Following the derivation of the Golden Rule formula in Section 3.3, we introduce the transition amplitude, Eq. (3.65), $A_{gM,eN}(t) = \theta(t)\, \langle\phi_g|\langle\chi_{gM}|U(t)|\phi_e\rangle|\chi_{eN}\rangle$, which simplifies to $A_{gM,eN}(t) = \theta(t)\,\exp(i\omega t)\langle\phi_g|\langle\chi_{gM}|\exp\{i\mathcal{H}_{\mathrm{rw}}^{(\mathrm{I})}t/\hbar\}\,|\phi_e\rangle\,|\chi_{eN}\rangle$. Except for the unimportant time-dependent phase factor, the transition amplitude is identical to that discussed in Sections 3.3.1 and 3.86. We identify the Hamiltonian, Eq. (6.10), with that of Eq. (3.63) and get from Eq. (3.87) the desired transition rate:

$$k_{g\to e} = \frac{2\pi}{\hbar} \sum_{M,N} f_{gM} |\langle\chi_{gM}|\boldsymbol{E}_0^* \boldsymbol{d}_{eg}^*|\chi_{eN}\rangle|^2\; \delta(\hbar\omega + E_{gM} - E_{eN}). \tag{6.12}$$

---

4) Since $\mathcal{H}_{\mathrm{rw}}^{(\mathrm{I})}$ is time independent, one can imagine that it has been defined in a frame rotating with the frequency of the externally applied light field.

Using Eq. (6.12) together with Eq. (4.35), we obtain the absorption coefficient (here and in the following c has to be understood as the medium velocity of light nc_{vacuum})

$$\alpha(\omega) = \frac{4\pi^2 \omega n_{\text{mol}}}{c} \sum_{MN} f_{gM} |\langle \chi_{gM} | d_{eg} | \chi_{eN} \rangle|^2 \delta(\hbar\omega + E_{gM} - E_{eN}). \tag{6.13}$$

This result assumes that the molecular transition matrix elements $\boldsymbol{d}_{eg}$ of the non-interacting single molecules are identical, and that all molecules possess the same spatial orientation. Then, the scalar product $\boldsymbol{d}_{eg}\boldsymbol{E}_0$ can be calculated. The quantity d_{eg} in Eq. (6.13) is the component of the vector $\boldsymbol{d}_{eg}$ along the direction of the field vector.[5] Often, one simplifies the matrix element $\langle \chi_{gM} | d_{eg} | \chi_{eN} \rangle$ to the expression $d_{eg} \langle \chi_{gM} | \chi_{eN} \rangle$. This approximation is known as the *Condon approximation*, which replaces the exact matrix element by the pure electronic matrix element d_{eg} of the dipole operator and the Franck–Condon factor $\langle \chi_{gM} | \chi_{eN} \rangle$. The simplification is possible whenever the dependence of d_{eg} on the nuclear DOFs (via the parametric dependence of the electronic wave functions $\phi_a(r; R)$, cf. Section 2.3) is sufficiently weak to be negligible.

6.2.2 The Density of States

The obtained result for the absorption coefficient will be transformed into a more compact form by introducing the *lineshape function* $\mathcal{D}_{\text{abs}}$. We assume that the Condon approximation can be used and get for a sample of randomly oriented molecules

$$\alpha(\omega) = \frac{4\pi^2 \omega n_{\text{mol}}}{3c} |d_{eg}|^2 \, \mathcal{D}_{\text{abs}}(\omega - \omega_{eg}), \tag{6.14}$$

with

$$\mathcal{D}_{\text{abs}}(\omega - \omega_{eg}) = \sum_{N,M} f_{gM} |\langle \chi_{eN} | \chi_{gM} \rangle|^2 \, \delta\left(\hbar\omega - (E_{eN} - E_{gM})\right). \tag{6.15}$$

For convenience, the transition frequency,

$$\hbar\omega_{eg} = U_e^{(0)} - U_g^{(0)}, \tag{6.16}$$

defined via the values of the PES at the respective vibrational equilibrium configuration has been introduced.

The lineshape function can be understood as a density of states (DOS) that combines two electronic states, the ground state and the considered excited state. Therefore, it is often called *Franck–Condon weighted and thermally averaged combined density of states*. The actual calculation of $\mathcal{D}_{\text{abs}}(\omega - \omega_{eg})$ and thus of the absorption coefficient requires the detailed knowledge of the vibrational energy spectrum for both PESs. This knowledge may be attained for small systems in the gas phase, or whenever only a small number of vibrational DOFs is coupled to an electronic transition. However, Eq. (6.15) is inadequate for more complex systems or for systems in the condensed phase. Therefore, our aim is to formulate $\mathcal{D}_{\text{abs}}(\omega - \omega_{eg})$ without

---

5) In the case of random orientations, an additional factor $1/3$ appears on the right-hand side of Eq. (6.13) as a consequence of orientational averaging.

making use of any eigenstates of the system. For this purpose, $\mathcal{D}_{\text{abs}}$ will be written in an alternative way after introduction of the Fourier representation of the delta function. Then, it follows from Eq. (6.15) that

$$\mathcal{D}_{\text{abs}}(\omega - \omega_{eg}) = \frac{1}{2\pi\hbar} \sum_{N,M} \int dt \, f_{gM} \, |\langle \chi_{eN} | \chi_{gM} \rangle|^2 \, e^{i(\omega - (E_{eN} - E_{gM})/\hbar)t}. \tag{6.17}$$

This expression is better suited even though at first glance the replacement of the delta function may appear as a formal mathematical trick. However, we should recall that in Section 3.4.5, where the Golden Rule had been derived via the Liouville–von Neumann equation of the statistical operator, this type of time integration emerged in a natural way. In Section 6.3, we discuss such a *time-dependent* formulation for the absorption coefficient. Here, we only derive some general relations used later in this chapter.

Let us follow Section 3.4.5 and eliminate the vibrational energy spectra using the vibrational eigenvalue equations $H_a | \chi_{aN} \rangle = E_{aN} | \chi_{aN} \rangle$. We obtain

$$|\langle \chi_{eN} | \chi_{gM} \rangle|^2 \, e^{i(E_{eN} - E_{gM})t/\hbar} = \langle \chi_{gM} | e^{iE_{gM}t/\hbar} e^{-iE_{eN}t/\hbar} | \chi_{eN} \rangle \langle \chi_{eN} | \chi_{gM} \rangle$$

$$= \langle \chi_{gM} | e^{iH_g t/\hbar} e^{-iH_e t/\hbar} | \chi_{eN} \rangle \langle \chi_{eN} | \chi_{gM} \rangle. \tag{6.18}$$

If we introduce this result into $\mathcal{D}_{\text{abs}}(\omega - \omega_{eg})$ and use the completeness relation for the vibrational states, it follows that

$$\mathcal{D}_{\text{abs}}(\omega - \omega_{eg}) = \frac{1}{2\pi\hbar} \int dt \, e^{i\omega t} \sum_M \langle \chi_{gM} | \hat{R}_g \, e^{iH_g t/\hbar} \, e^{-iH_e t/\hbar} | \chi_{gM} \rangle$$

$$= \frac{1}{2\pi\hbar} \int dt \, e^{i\omega t} \, \text{tr}_{\text{vib}} \{ \hat{R}_g \, e^{iH_g t/\hbar} \, e^{-iH_e t/\hbar} \}. \tag{6.19}$$

Here, we inserted the equilibrium statistical operator for the vibrational motion in the electronic ground state, Eq. (4.60). This way the DOS (lineshape function) has been obtained as a Fourier-transformed correlation function, which relates the vibrational motion in the electronic ground state PES to the motion in the excited state PES. The averaging has to be taken with respect to the vibrational equilibrium statistical operator for the electronic ground state.

For later use, we give an alternative notation of Eq. (6.19) that connects the present results to the response functions introduced in Chapter 4 (cf. Section 4.3.4). It is based on the separation of an S operator in analogy to Eq. (4.78). In the present case, we introduce $\Delta H_{eg} = H_e - H_g - \hbar\omega_{eg}$ and rewrite the time-evolution operator for H_e as follows:

$$U_e(t) = e^{-iH_e t/\hbar} = e^{-i\omega_{eg}t} e^{-i(H_g + \Delta H_{eg})t/\hbar}$$

$$= e^{-i\omega_{eg}t} U_g(t) S_{eg}(t, 0), \tag{6.20}$$

with $U_g(t) = \exp(-iH_g t/\hbar)$. The S-operator has the form

$$S_{eg}(t, 0) = \hat{T} \exp \left\{ -\frac{i}{\hbar} \int_0^t d\bar{t} \, \Delta H_{eg}^{(g)}(\bar{t}) \right\}, \tag{6.21}$$

where the abbreviation $\Delta H_{eg}^{(g)}(\bar{t}) = U_g^+(\bar{t})\Delta H_{eg}U_g(\bar{t})$ has been introduced. Using this notation, the lineshape function is obtained in the compact form:

$$\mathcal{D}_{\text{abs}}(\omega - \omega_{eg}) = \frac{1}{2\pi\hbar} \int dt\, e^{i(\omega-\omega_{eg})t} \operatorname{tr}_{\text{vib}}\{\hat{R}_g S_{eg}(t,0)\}. \tag{6.22}$$

The existence of the time integral requires that the trace expression vanishes if t goes to $\pm\infty$. In the most simple case, the trace expression may become proportional to $\exp(-|t|/\tau)$ at $t \to \pm\infty$. The time constant τ is known as the dephasing time. It describes the temporal decay of correlations between the electronic ground and excited state vibrational dynamics (cf. Eq. 6.19). In particular, it determines the broadening of the transition from the vibrational ground state level E_{g0} in the electronic ground state to the vibrational ground state level E_{e0} in the excited electronic states (so-called zero-phonon transition).

Although Eqs. (6.19) and (6.22) do not require any knowledge about the system's eigenstates, the determination of the correlation function is still a formidable task. The best strategy depends on the details of the system under consideration. For systems with a few number of vibrational DOFs, the time-dependent Schrödinger equation subject to particular initial conditions can be solved, as will be presented in Section 6.3.1. For larger systems, a direct solution of the Schrödinger equation (either time dependent or stationary) is impossible. Instead, approximations have to be introduced. One possibility we have already encountered in Section 4.3.4 is the cumulant expansion. Further, an approximate description of the vibrational DOFs as a thermal reservoir in the spirit of the QME can be used (cf. Section 6.3.2 for this approach to the absorption spectrum). A classical description of the vibrational coordinates (or a part of it) is given in Section 6.3.3. In the case that the vibrational motion can be described in the harmonic approximation such that it can be mapped onto those of independent harmonic oscillators (via a normal-mode analysis, see Section 2.5.1), an analytical computation of the correlation function in Eq. (6.19) becomes possible.

6.2.3 Absorption Coefficient for Harmonic Potential Energy Surfaces

In the case where the vibrations are described by independent harmonic oscillators, an analytical expression for Eq. (6.19) can be derived starting from the vibrational Hamiltonian introduced in Eq. (2.51). The various vibrational frequencies should be independent of the electronic state, but both PESs are shifted relative to each other along the different normal-mode coordinates. The related dimensionless displacements $g_a(\xi)$ are given in Eq. (2.66). Within this model, we obtain the lineshape function as (for details see the supplementary Section 6.7.1)

$$\mathcal{D}_{\text{abs}}(\omega - \omega_{eg}) = \frac{1}{2\pi\hbar} \int dt\, e^{i(\omega-\omega_{eg})t - G(0) + G(t)}, \tag{6.23}$$

with the transition frequency introduced in Eq. (6.16). The time-dependent function in the exponent of Eq. (6.23) reads

$$G(t) = \sum_{\xi} \left(g_e(\xi) - g_g(\xi)\right)^2 \left[(1 + n(\omega_\xi))e^{-i\omega_\xi t} + n(\omega_\xi)e^{i\omega_\xi t}\right]. \tag{6.24}$$

This expression includes the dimensionless relative displacement $g_e(\xi) - g_g(\xi)$ between both PESs. The ω_ξ denote the frequencies of the normal-mode oscillators, and $n(\omega)$ is the Bose–Einstein distribution, which introduces the temperature dependence. Obviously, the function $G(t)$ carries the complete information on the influence of the nuclear DOFs. Neglecting $G(t)$, the absorption profile reduces to a sharp line at $\omega = \omega_{eg}$. The time-independent part,

$$G(0) = \sum_\xi (g_e(\xi) - g_g(\xi))^2 (1 + 2n(\omega_\xi)), \tag{6.25}$$

includes the so-called *Huang–Rhys factor* $\sum_\xi (g_e(\xi) - g_g(\xi))^2$. It is related to the expression

$$S = 2\hbar \sum_\xi \omega_\xi \left(g_e(\xi) - g_g(\xi)\right)^2, \tag{6.26}$$

which is known as the *Stokes shift* (cf. Figure 6.5).

Starting with the Golden Rule expression, Eq. (6.15), where the thermal averaging with respect to the initial vibrational eigenstates has to be carried out directly, the final result includes thermally averaged quantities in the exponent. This can be formally rationalized by means of the cumulant expansion as shown in Section 6.2.5. Once the function $G(t)$ is given, a single time integration generates the complete absorption spectrum according to

$$\alpha(\omega) = \frac{2\pi\omega n_{\mathrm{mol}}}{3\hbar c} |d_{eg}|^2 e^{-G(0)} \int dt \, e^{i(\omega - \omega_{eg})t + G(t)}. \tag{6.27}$$

The general character of this expression becomes obvious when discussing the limiting cases for $G(t)$. We start in considering the limit where only a *single* vibrational mode with frequency ω_{vib} couples to the electronic transition. From Eq. (6.24) it follows that $(\Delta g = g_e - g_g)$

$$G(t) = \Delta g^2 \left(e^{-i\omega_{\mathrm{vib}}t}(1 + n(\omega_{\mathrm{vib}})) + e^{i\omega_{\mathrm{vib}}t}n(\omega_{\mathrm{vib}})\right). \tag{6.28}$$

Expanding the exponential function in Eq. (6.23) yields

$$\exp\{G(t)\} = \sum_{M=0}^{\infty} \frac{1}{M!} \left[\Delta g^2(1 + n(\omega_{\mathrm{vib}}))\right]^M e^{-iM\omega_{\mathrm{vib}}t}$$
$$\times \sum_{N=0}^{\infty} \frac{1}{N!} \left[\Delta g^2 \, n(\omega_{\mathrm{vib}})\right]^N e^{iN\omega_{\mathrm{vib}}t}. \tag{6.29}$$

Inserting this result into the expression of the combined DOS allows to carry out the time integration for every contribution in the double sum. It simply gives

$$\mathcal{D}_{\mathrm{abs}}(\omega - \omega_{eg}) = \frac{1}{\hbar} e^{-\Delta g^2(1 + 2n(\omega_{\mathrm{vib}}))} \sum_{M,N=0}^{\infty} \frac{1}{M!} \left[\Delta g^2(1 + n(\omega_{\mathrm{vib}}))\right]^M$$
$$\times \frac{1}{N!} \left[\Delta g^2 n(\omega_{\mathrm{vib}})\right]^N \delta(\omega - \omega_{eg} - (M - N)\omega_{\mathrm{vib}}). \tag{6.30}$$

Using this expression, the absorption coefficient, Eq. (6.14), becomes a collection of sharp lines corresponding to transitions at frequencies $\omega_{eg} - (M - N)\,\omega_{\mathrm{vib}}$ (vibrational or Franck–Condon progression). In contrast to Eq. (6.15), the Franck–Condon
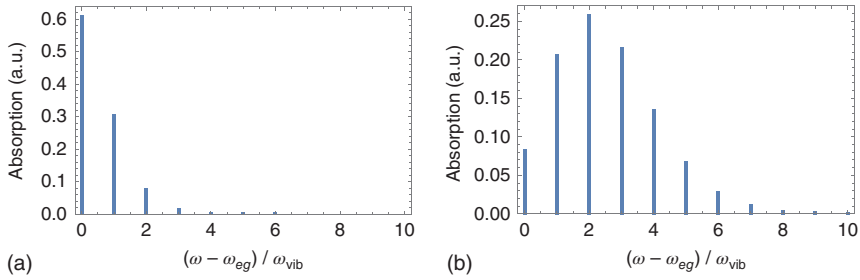
Figure 6.6 Stick spectrum of the absorption described by Eq. (6.31). The weighting factors, Eq. (6.32), are plotted versus frequency: (a) $\Delta g^2 = 0.5$ and (b) $\Delta g^2 = 2.5$.

factor and the thermal distribution have been replaced by powers of Δg and $n(\omega_{\rm vib})$, respectively.

Before discussing this result further, we consider the zero-temperature case ($n(\omega_{\rm vib}) = 0$):

$$\mathcal{D}_{\rm abs}(\omega - \omega_{eg})|_{T=0} = \frac{1}{\hbar} e^{-\Delta g^2} \sum_{M=0}^{\infty} \frac{\Delta g^{2M}}{M!} \delta(\omega - \omega_{eg} - M\omega_{\rm vib}). \tag{6.31}$$

The absorption spectrum is a sequence of sharp lines (see Figure 6.6) at frequencies $\omega_{eg} + M\omega_{\rm vib}$ with weighting factors

$$w_M = e^{-\Delta g^2} \frac{\Delta g^{2M}}{M!}. \tag{6.32}$$

Thus, these weighting factors follow from the *Poisson distribution*. They become maximal at $M \approx \Delta g^2$ or, in terms of energies, at $M\hbar\omega_{\rm vib} \approx \hbar\omega_{\rm vib}\Delta g^2$. Note that the vibrational quantum number at which the absorption reaches its maximum is given by the difference $U_e(q = q_g) - U_e(q = q_e) = \hbar\omega_{\rm vib}\Delta g^2 = S/2$. This corresponds to a vertical transition which is in accord with the Franck–Condon principle introduced at the beginning of this chapter. The shape of the spectrum following from Eq. (6.31) is illustrated in Figure 6.6.

At finite temperatures, we have to consider the double summation in Eq. (6.30). Nevertheless, a more compact expression can be derived. If $M > N$, we introduce $K = M - N$ and $N = L$, where L and K run from 0 to ∞. In case that $M < N$, we set $M = L$, which again runs from 0 to ∞, but K is in between the interval from 0 to $-\infty$. Rearranging the combined DOS gives

$$\mathcal{D}_{\rm abs}(\omega - \omega_{eg}) = \frac{1}{\hbar} \sum_{K=-\infty}^{\infty} \left(\frac{n(\omega_{\rm vib})}{1 + n(\omega_{\rm vib})} \right)^{|K|/2} \delta(\omega - \omega_{eg} - K\omega_{\rm vib})$$

$$\times \sum_{L=0}^{\infty} \frac{1}{L!(L + |K|)!} (\Delta g^4 n(\omega_{\rm vib})[1 + n(\omega_{\rm vib})]/4)^{L+|K|/2}. \tag{6.33}$$

Using the definition of the modified Bessel function

$$I_K(z) = \sum_{L=0}^{\infty} \frac{1}{L!(L + |K|)!} (z^2/4)^{L+|K|/2}, \tag{6.34}$$

we get

$$
D_{\text{abs}}(\omega - \omega_{eg}) = \frac{1}{\hbar} \sum_{K=-\infty}^{\infty} I_K \left(\Delta g^2 \sqrt{n(\omega_{\text{vib}})[1 + n(\omega_{\text{vib}})]} \right)
$$
$$
\times \left(\frac{n(\omega_{\text{vib}})}{1 + n(\omega_{\text{vib}})} \right)^{|K|/2} \delta(\omega - \omega_{eg} - K\omega_{\text{vib}}). \tag{6.35}
$$

This compact expression contains only a single sum with respect to the difference in vibrational quanta between the electronic ground and the excited states. It gives the temperature-dependent intensity of transitions between the two electronic states.

6.2.4 Absorption Lineshape and Spectral Density

If many intramolecular vibrational modes couple to the electronic transition, or if additionally there is a coupling to modes of a reservoir, we expect a quasi-continuous spectrum of vibrational frequencies. In such a case, it is convenient to introduce the *spectral density* into Eq. (6.24). This can be done in complete analogy to Section 3.7.3, Eq. (3.294). Here, we define

$$
J_{eg}(\omega) = \sum_{\xi} \left(g_e(\xi) - g_g(\xi) \right)^2 \delta(\omega - \omega_{\xi}). \tag{6.36}
$$

The spectral density enables us to write Eq. (6.24) as follows:

$$
G(t) = \int_0^\infty d\omega \left[(1 + n(\omega))e^{-i\omega t} + n(\omega)e^{i\omega t} \right] J_{eg}(\omega). \tag{6.37}
$$

Furthermore, we can use the spectral density to write the Stokes shift introduced in Eq. (6.26) as

$$
S = 2\hbar \int_0^\infty d\omega \, \omega J_{eg}(\omega). \tag{6.38}
$$

It is convenient to introduce the real and imaginary parts of the function $G(t)$, Eq. (6.37),

$$
G(t) = G_1(t) - iG_2(t), \tag{6.39}
$$

where

$$
G_1(t) = \int_0^\infty d\omega \, \cos(\omega t)[1 + 2n(\omega)]J_{eg}(\omega), \tag{6.40}
$$

and

$$
G_2(t) = \int_0^\infty d\omega \, \sin(\omega t)J_{eg}(\omega). \tag{6.41}
$$

Note that the imaginary part is temperature independent, whereas the real part includes all temperature effects. Apparently, the real and imaginary parts of

$G(t)$, Eq. (6.37), have to obey $G_1(t) = G_1(-t)$ and $G_2(t) = -G_2(-t)$, respectively. In particular, these properties have to be fulfilled if both functions are calculated from the model spectral density.

According to this separation of $G(t)$, the DOS equation (6.23) reads

$$\mathcal{D}_{\text{abs}}(\omega - \omega_{eg}) = \frac{1}{2\pi\hbar} e^{-G_1(0)} \int dt \, e^{i[(\omega-\omega_{eg})t - G_2(t)] + G_1(t)}. \tag{6.42}$$

The imaginary part of $G(t)$ introduces a shift of the electronic transition frequency ω_{eg}, whereas the real part leads to an exponential decay of the integrand in Eq. (6.42). We expect that this exponential decay is reflected in the broadening of the absorption lines.

It is instructive to compare the expressions in Eqs. (6.37) and (6.38) with the results obtained for the reservoir correlation function in Section 3.7. The system–reservoir coupling, Eqs. (3.286) and (3.287), and the shifted oscillator Hamiltonian, Eq. (2.65), involve the same linear coupling of the system and electronic transitions, respectively, to a set of oscillator coordinates. The reservoir correlation function $C(t)$ in Eq. (3.300) differs from $G(t)$ insofar as $\omega^2 J(\omega)$ instead of $J_{eg}(\omega)$ appears in the integrand. This is a consequence of the definition of $G(t)$ via the S-operator (cf. Eq. (6.22)), which becomes apparent in the cumulant approach discussed in the following section. As has been mentioned in Section 3.7.2, in condensed phase dynamics, the factor ω^2 is often included into the definition of the spectral density. The current definition solely in terms of the dimensionless coupling constant is more convenient for describing processes related to electronic transitions. Finally, we would like to point out that the Stokes shift in Eq. (6.38) corresponds to twice the reorganization energy, E_λ, of the system bath model in Eq. (3.296).

6.2.5 Cumulant Expansion of the Absorption Coefficient

In Section 4.3.4, the cumulant expansion of the response functions for a two-level system has been discussed. In principle, it applies to arbitrary, that is anharmonic PES. In what follows, we connect the cumulant expansion to the results of the previous section by showing that in the limit of harmonic PES identical results are obtained for the absorption coefficient. In particular, we demonstrate that the second-order cumulant expansion (up to $\Gamma_2(t)$, see Eq. (4.85)) is exact for harmonic vibrations.

We prove this statement by reproducing Eq. (6.23) in what follows and start with a calculation of $\Delta H_{eg}^{(g)}(t)$ entering Eq. (4.79). Within the model of shifted harmonic potentials, the vibrational Hamiltonians H_e and H_g take the form, Eq. (2.74), and we obtain $\Delta H_{eg} = D_e^+ H_{\text{vib}} D_e - D_g^+ H_{\text{vib}} D_g$. It follows that

$$\begin{aligned}
\Delta H_{eg}^{(g)}(t) &= D_g^+ U_{\text{vib}}^+(t) D_g \Delta H_{eg} D_g^+ U_{\text{vib}}(t) D_g \\
&= D_g^+ U_{\text{vib}}^+(t) \left(D_{eg}^+ H_{\text{vib}} D_{eg} - H_{\text{vib}} \right) U_{\text{vib}}(t) D_g.
\end{aligned} \tag{6.43}$$

Here, D_{eg} stands for $D_e D_g^+$. The Hamiltonian H_{vib} defines a fictitious reference oscillator system introduced in Eq. (2.74). Inserting the explicit expressions for the Hamiltonians yields finally (note the application of the displacement operator and the

abbreviation $g_{eg}(\xi) = g_e(\xi) - g_g(\xi)$)

$$\Delta H_{eg}^{(g)}(t) = D_g^+ \sum_\xi \hbar\omega_\xi \left(Q_\xi(t) + g_{eg}(\xi) \right) g_{eg}(\xi) D_g. \tag{6.44}$$

The time dependence of the dimensionless oscillator coordinate $Q_\xi(t)$ is determined by H_{vib} and reads $Q_\xi(t) = C_\xi \exp(-i\omega_\xi t) + C_\xi^+ \exp(i\omega_\xi t)$. The trace operation necessary to calculate the different correlation functions of $\Delta H_{eg}^{(g)}(t)$ will be rewritten in terms of the nondisplaced vibrational states of the oscillator Hamiltonian H_{vib} as $\langle \cdots \rangle_g \equiv \text{tr}_{\text{vib}}\{\hat{R}_{\text{vib}} D_g \ldots D_g^+\}$, with $\hat{R}_{\text{vib}} = \exp(-H_{\text{vib}}/k_BT)/\mathcal{Z}$.

Now we can determine the two expectation values entering Γ_1 and Γ_2, Eqs. (4.84) and (4.85), respectively. The expression

$$\langle \Delta H_{eg}^{(g)}(t) \rangle_g = \text{tr}_{\text{vib}} \left\{ \hat{R}_{\text{vib}} \sum_\xi \hbar\omega_\xi \left(Q_\xi(t) + g_{eg}(\xi) \right) g_{eg}(\xi) \right\}$$

$$= \sum_\xi \hbar\omega_\xi g_{eg}^2(\xi) \equiv \frac{S}{2} \tag{6.45}$$

becomes time independent. Here, we took into account that the equilibrium expectation values of C_ξ and C_ξ^+ vanish. Further, we recovered the expression for the *Stokes shift* already introduced in Eq. (6.38). In a similar manner, we obtain

$$\langle \Delta H_{eg}^{(g)}(t) \Delta H_{eg}^{(g)}(\bar{t}) \rangle_g = \text{tr}_{\text{vib}} \left\{ \hat{R}_{\text{vib}} \sum_{\xi,\bar{\xi}} \hbar\omega_\xi \hbar\omega_{\bar{\xi}} \left(Q_\xi(t) + g_{eg}(\xi) \right) \right.$$

$$\left. \times g_{eg}(\xi) \left(Q_{\bar{\xi}}(\bar{t}) + g_{eg}(\bar{\xi}) \right) g_{eg}(\bar{\xi}) \right\}$$

$$= \sum_\xi \left(\hbar\omega_\xi g_{eg}(\xi) \right)^2 \text{tr}_{\text{vib}}\{\hat{R}_{\text{vib}} Q_\xi(t) Q_{\bar{\xi}}(\bar{t})\} + S^2/4. \tag{6.46}$$

The trace with respect to the dimensionless oscillator coordinate vanishes for $\xi \neq \bar{\xi}$ and reads (cf. Section 3.7.2)

$$\text{tr}_{\text{vib}}\{\hat{R}_{\text{vib}} Q_\xi(t) Q_\xi(\bar{t})\} = \left(1 + n(\omega_\xi) \right) e^{-i\omega_\xi(t-\bar{t})} + n(\omega_\xi) e^{i\omega_\xi(t-\bar{t})}. \tag{6.47}$$

Now, it is easy to determine Γ_1 and Γ_2. It follows directly from Eqs. (4.84) and (6.45) that $\Gamma_1(t) = -iSt/2\hbar$. To obtain Γ_2, some additional calculations have to be carried out. First, we note that the double time integration necessary to get Γ_2 gives the contribution $(St/\hbar)^2/2$. This follows directly from the part of Eq. (6.46) containing S^2. It can be written as $-\Gamma_1^2(t)/2$. With this result and according to Eq. (4.85), Γ_2 can be reduced to

$$\Gamma_2(t) = \sum_\xi (\omega_\xi g_{eg}(\xi))^2$$

$$\times \int_0^t dt_1 \int_0^{t_1} dt_2 \left\{ \left(1 + n(\omega_\xi) \right) e^{-i\omega_\xi(t_1-t_2)} + n(\omega_\xi) e^{i\omega_\xi(t_1-t_2)} \right\}. \tag{6.48}$$

The calculation of the time integrals gives $\Gamma_2(t) = \Gamma_1(t) + G(t)$, with the function $G(t)$ introduced in Eq. (6.24). Thus, we get as the final result

$$\Gamma_1(t) + \Gamma_2(t) = -G(0) + G(t) \tag{6.49}$$

and reproduced the expression (6.23) for the combined DOS $\mathcal{D}_{abs}(\omega)$. Since Eq. (6.23) gives the exact result for the combined DOS, the cumulant expansion only contains contributions up to the second-order cumulant Γ_2. Cumulants of type Γ_3 and higher are not necessary to calculate $\langle S_{eg}(t, 0)\rangle_g$ within the model of shifted harmonic oscillator PESs.

Finally, we note that for the present case of linearly shifted oscillators, $\Gamma_2(t)$ can be expressed in terms of the reservoir correlation function introduced in Eq. (3.292), that is

$$\Gamma_2(t) = -\int_0^t dt_1 \int_0^{t_1} dt_2 \, C(t_1 - t_2). \tag{6.50}$$

This connection between the shifted oscillator model and the system–reservoir model of Section 3.7 was already discussed in the previous section.

6.2.6 Absorption Coefficient for Model Spectral Densities

To be more specific, let us discuss the absorption in terms of model spectral densities introduced in Section 3.7.3. Since these spectral densities describe harmonic oscillator reservoirs, the connection to spectroscopy can immediately be established using the second-order cumulant expansion and Eq. (6.49). Specifically, we can use the relation (6.50) together with the correlation functions calculated in Section 3.7.3.

The *Debye spectral density* was already introduced in Eq. (3.302). Adopting the notation common in spectroscopy, it reads (note that $E_\lambda = S/2$)

$$J_{eg}(\omega) = \theta(\omega) \frac{S\omega_D}{\pi\hbar} \frac{1}{\omega} \frac{1}{\omega^2 + \omega_D^2}. \tag{6.51}$$

In the context of spectroscopy, it is often used to describe the response of low-frequency reservoir modes to the change in the electron density upon optical excitation (for example, reorientation of the solvation shell or collective protein vibration in photosynthetic complexes). In the following equation we only consider the high-temperature limit ($k_B T \gg \hbar\omega_D$) and use the correlation function given in Eq. (3.311). Inserting this expression into Eq. (6.50) and performing the integrations yields

$$\Gamma_2(t) = -\frac{S}{2(\hbar\omega_D)^2}(2k_B T - i\hbar\omega_D)\left(e^{-\omega_D t} + \omega_D t - 1\right). \tag{6.52}$$

With the help of $\Gamma_2(t)$ and $\Gamma_1(t) = -iSt/2\hbar$, one can identify

$$G_1(t) = -\frac{k_B T S}{(\hbar\omega_D)^2}(e^{-\omega_D t} + \omega_D t - 1) \tag{6.53}$$

and

$$G_2(t) = \frac{S}{2\hbar\omega_D}(1 - e^{-\omega_D t}). \tag{6.54}$$

The frequency-dependent combined DOS is obtained after the time integration in Eq. (6.42) has been carried out.

In order to discuss this result we introduce two time scales. First, the time scale for vibrational motion characterized by $T_{\text{vib}} \approx 1/\omega_{\text{D}}$. The second time scale is related to the strength of the coupling between electronic and nuclear motions (S). We have $T_{\text{fluc}} = \hbar/\sqrt{k_{\text{B}}TS}$, where the square root contains the mean energy of thermal motion and nuclear displacement upon excitation (both quantities result in energy gap fluctuations).

We can distinguish two limits reflecting in distinct absorption lineshapes. In the limit of *slow nuclear motion*, we suppose that $T_{\text{vib}} \gg T_{\text{fluc}}$ such that it is possible to perform a short-time expansion of $G(t)$ with respect to $\omega_{\text{D}}t$. One obtains

$$
\begin{aligned}
\mathcal{D}_{\text{abs}}(\omega - \omega_{eg}) &= \frac{1}{2\pi\hbar} \int dt \, \exp\left\{ i(\omega - \omega_{eg} - S/2\hbar)t - \frac{1}{2}\left(\frac{t}{T_{\text{fluc}}}\right)^2 \right\} \\
&= \frac{T_{\text{fluc}}}{\sqrt{2\pi}\,\hbar} \exp\left\{ -\frac{1}{2}\left(T_{\text{fluc}}(\omega - \omega_{eg} - S/2\hbar) \right)^2 \right\}.
\end{aligned} \tag{6.55}
$$

This case is known as the limit of *inhomogeneous broadening*, where the time scale for nuclear motion is such that the nuclei can be considered to be frozen. We have a Gaussian absorption lineshape centered around the vertical Franck–Condon transition $\omega = \omega_{eg} + S/2$ (cf. Figure 6.5).

In the *fast nuclear motion* limit, we have $T_{\text{vib}} \ll T_{\text{fluc}}$, and the exponential factors in $G(t)$ can be neglected. Setting $\omega_{\text{D}}t - 1 \approx \omega_{\text{D}}t$ and neglecting $G_2(t)$, which is of the order of $(T_{\text{vib}}/T_{\text{fluc}})^2 \hbar\omega_{\text{D}}/k_{\text{B}}T$, one arrives at $G(t) \approx T_{\text{vib}}|t|/T_{\text{fluc}}^2$. The absorption lineshape follows as a Lorentzian

$$
\begin{aligned}
\mathcal{D}_{\text{abs}}(\omega - \omega_{eg}) &= \frac{1}{2\pi\hbar} \int dt \, \exp\left\{ (i(\omega - \omega_{eg})t - T_{\text{vib}}|t|/T_{\text{fluc}}^2 \right\} \\
&= \frac{1}{\pi\hbar} \frac{\gamma}{(\omega - \omega_{eg})^2 - \gamma^2}.
\end{aligned} \tag{6.56}
$$

The linewidth is given by $\gamma = T_{\text{vib}}/T_{\text{fluc}}^2$. This is the limit of *homogeneous broadening*. Note that the absorption is now centered at the electronic transition frequency, and the Stokes shift does not appear. This can be rationalized by the fact that the nuclear motion is so fast that only the electronic transition, which is averaged with respect to the nuclear dynamics, is detected in the experiment.

Finally, we point out that the transition between the limits of inhomogeneous and homogeneous broadening can be observed upon changing the temperature. While at low temperature the nuclear motions are frozen and the lineshape is Gaussian, at higher temperature, it becomes Lorentzian. This phenomenon is also known as motional line narrowing.

As a second example we discuss the *Brownian oscillator model* introduced in Eq. (3.303). In the context of spectroscopy it describes a single active vibrational coordinate bilinearly coupled to further vibrations being either of intramolecular character or due to solvent motions (reservoir). The single active coordinate is characterized by a strong coupling to an electronic transition such that it leads to a vibrational progression in the absorption spectrum as shown, for instance in Figure 6.6. The

coupling to the reservoir causes a broadening of the sharp absorption lines as seen in Figure 6.3.

The related Hamiltonian represents a particular example for the generic system–reservoir Hamiltonian, Eq. (3.3). The system part, H_S, is identical with the molecular part of Eq. 6.4 (here restricted to a single vibration with frequency ω_0, although the extension to many active coordinates is straightforward), that is

$$H_S = \sum_{a=g,e} \left[U_a(q = q^{(a)}) + \frac{1}{2} \left(p^2 + \omega_0^2 (q - q^{(a)})^2 \right) \right] |\phi_a\rangle\langle\phi_a|. \tag{6.57}$$

The system–reservoir coupling is of Caldeira–Leggett form, Eq. (5.20), and reads

$$H_{S+R} + H_R = \frac{1}{2} \sum_{\xi} \left[p_\xi^2 + \omega_\xi^2 \left(q_\xi - \frac{c_\xi q}{\omega_\xi^2} \right)^2 \right]. \tag{6.58}$$

This model can be described by the spectral density given in Eq. (3.303). Specification to the notation commonly used in spectroscopy gives

$$J_{eg}(\omega) = \theta(\omega) \frac{S}{\pi\hbar} \frac{1}{\omega} \frac{\omega_0^2 \gamma_0}{(\omega^2 - \omega_0^2)^2 + \omega^2 \gamma_0^2}. \tag{6.59}$$

The correlation function for this model was calculated in Section 3.7.3, Eqs. (3.312) and (3.314). Employing the high-temperature limit ($k_B T \gg \hbar\omega_0$), one obtains

$$C(t) = \frac{S\omega_0^2}{4\hbar\Omega_0} \left[\left(1 + i\frac{2k_B T}{\hbar\Omega_0^{(+)}} \right) e^{-\Omega_0^{(+)}t} - \left(1 + i\frac{2k_B T}{\hbar\Omega_0^{(-)}} \right) e^{-\Omega_0^{(-)}t} \right]. \tag{6.60}$$

Since $\Omega_0^{(\pm)} = \gamma_0/2 \pm i\Omega_0$, the correlation function decays as $\exp(-\gamma_0 t/2)$, which is a consequence of the dephasing due to the system–reservoir interaction. From $C(t)$, the second-order cumulant can readily be obtained according to Eq. (6.50). In Figure 6.7, we give an example for a spectrum in case of weak damping. As compared to Figure 6.6, the lines are broadened. In addition, the thermal population of higher vibrational states in the electronic ground state leads to the appearance of peaks at frequencies smaller than the electronic transition frequency ω_{eg}.
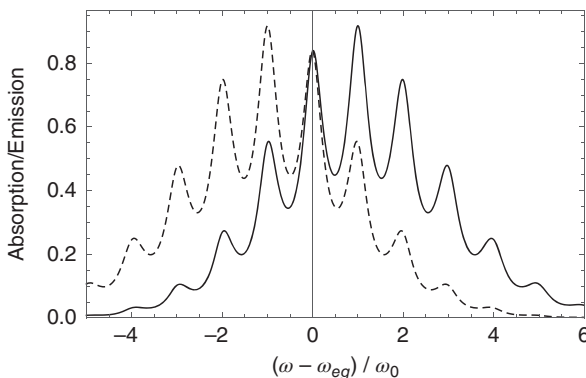
Figure 6.7 Absorption (solid line) and emission (dashed line) spectrum (in arbitrary units) of a single harmonic mode bilinearly coupled to a harmonic oscillator reservoir (Brownian oscillator model in high-temperature limit). The mode frequency is ω_0, the Stokes shift $S = 2\hbar\omega_0$, the damping $\gamma_0 = 0.05\omega_0$, and temperature $k_B T = 2\hbar\omega_0$.

6.3 Absorption Coefficient and Dipole–Dipole Correlation Function

In Section 4.2.2, the frequency-dependent linear absorption coefficient was expressed by the time-dependent dipole–dipole correlation function, Eq. (4.42). In the following equations, different derivations of the latter quantity will be given based on the solution of dynamic equations for the respective time-dependent wave functions or density matrices. The basic idea behind these approaches has already been encountered in Section 6.2.2, where the absorption coefficient was expressed in terms of a Fourier transform of a particular correlation function (see Eq. (6.19)). Having different ways of calculating correlation functions is of great importance not only to get the linear absorption coefficient but to compute different types of transfer rates in molecular systems. In particular, it will be a goal of the following sections to provide a means for the description of systems beyond the harmonic oscillator model. The actual numerical wave packet propagations can be performed, for instance using the method outlined in Section 3.2.3.

In order to keep the connection with the previous section, we adopt the same electronic two-level model for our discussion. The time-dependent description of the stationary absorption will also enable us to bridge the gap between the fast intramolecular dynamic phenomena, that is phenomena in the time domain, and properties observed in the frequency domain.

6.3.1 Absorption Coefficient and Wave Packet Propagation

Starting from Eq. (4.42), one can derive an expression for the dipole–dipole correlation function based on the time evolution of a particular statistical operator. To this end, Eq. (4.42) is rewritten as (note that the Cartesian index on both dipole operators has been omitted since the scalar product of the orientation unit vectors just gives a number)

$$C_{d-d}(t) = \text{tr}\{\hat{\mu} U_{\text{mol}}(t) \, [\hat{\mu}, \hat{W}_{\text{eq}}]_- \, U_{\text{mol}}^+(t)\} \equiv \text{tr}\{\hat{\mu}\hat{\sigma}(t)\}. \tag{6.61}$$

This formula results from a simple rearrangement of the various operators under the trace in Eq. (4.42), and we introduced $\hat{\sigma}(t) = U_{\text{mol}}(t) \, [\hat{\mu}, \hat{W}_{\text{eq}}]_- \, U_{\text{mol}}^+(t)$. Now, we may calculate the correlation function via a propagation of the commutator of the equilibrium statistical operator with the dipole operator (which induces the transitions according to the coupling with the radiation field).

This statement can be put into a more transparent formula if one changes from the propagation of mixed states to that of pure states. Such a situation is encountered in the gas phase, where any environmental influence is absent. Hence, we replace $\hat{W}_{\text{eq}}$ by $|\Psi\rangle\langle\Psi|$, where $|\Psi\rangle$ is an eigenstate of H_{mol} with energy $\mathcal{E}$. Using $U_{\text{mol}}(t)|\Psi\rangle = \exp(-i\mathcal{E}t/\hbar)|\Psi\rangle$, we obtain for the dipole–dipole correlation function

$$C_{d-d}(t) = \text{tr}\{\hat{\mu} \left(U_{\text{mol}}(t)\hat{\mu}|\Psi\rangle\langle\Psi|e^{i\mathcal{E}t/\hbar} - e^{-i\mathcal{E}t/\hbar}|\Psi\rangle\langle\Psi|\hat{\mu}U_{\text{mol}}^+(t) \right)\}. \tag{6.62}$$

Next, we rearrange the matrix elements formed by the pure state vector $|\Psi\rangle$ and those states used to calculate the trace. We can profit from the completeness relation for

the state vectors defining the trace formula and obtain

$$C_{d-d}(t) = e^{i\mathcal{E}t/\hbar} \langle \Psi | \hat{\mu} U_{mol}(t) \ \hat{\mu} | \Psi \rangle - \text{c.c.} \tag{6.63}$$

The interpretation of Eq. (6.63) is straightforward: the dipole operator induces a transition from the initial state $|\Psi\rangle$ to the state $\hat{\mu}|\Psi\rangle$. This is usually not an eigenstate of H_{mol}. Therefore, one can expect wave packet motion to take place. At time t, the propagated state $U_{mol}(t)\hat{\mu}|\Psi\rangle$ is multiplied by $\langle\Psi|\hat{\mu}$ to give the *dipole autocorrelation* function $\langle\Psi|\hat{\mu}U_{mol}(t)\hat{\mu}|\Psi\rangle$. Its half-sided Fourier transform determines the absorption according to Eq. (4.46). The first term on the right-hand side of Eq. (6.63) gives resonant contributions to the absorption coefficient, Eq. (4.46). We expect that $U_{mol}(t)\hat{\mu}|\Psi\rangle$ will oscillate with different excited state energies $\mathcal{E}_{exc}$. Therefore, the absorption coefficient will have a frequency dependence of the type $\omega - (\mathcal{E}_{exc} - \mathcal{E})/\hbar$. These resonances at positive frequencies are absent in the second term on the right-hand side of Eq. (6.63) (labeled by "c.c."). It is therefore often called *antiresonant* contribution.

In the specific case of an electronic two-level system, the state $|\Psi\rangle$ is replaced by the vibrational ground state in the electronic ground state, $|\phi_g\rangle|\chi_{g0}\rangle$. Provided that the Condon approximation is valid, we obtain $\hat{\mu}|\phi_g\rangle|\chi_{g0}\rangle = d_{eg}|\phi_e\rangle|\chi_{g0}\rangle$. Therefore, due to the action of the dipole operator, the vibrational state $|\chi_{g0}\rangle$ of the electronic ground state PES has been promoted to the excited electronic state $|\phi_e\rangle$. The resulting time dependence reads

$$U_{mol}(t)\hat{\mu}|\phi_g\rangle|\chi_{g0}\rangle = d_{eg}|\phi_e\rangle e^{-iH_e t/\hbar}|\chi_{g0}\rangle. \tag{6.64}$$

The vibrational state $|\chi_{g0}\rangle$ propagates under the action of the vibrational Hamiltonian of the excited electronic state, where $|\chi_{g0}\rangle$ is not an eigenstate of H_e.

We neglect the antiresonant contribution and get the absorption coefficient as

$$\alpha(\omega) = \frac{4\pi\omega n_{mol}}{3\hbar c} |d_{eg}|^2 \text{Re} \int_0^\infty dt \ e^{i(\omega + E_{g0}/\hbar)t} \ \langle \chi_{g0} | \chi_{g0}^{(e)}(t) \rangle. \tag{6.65}$$

Thus, the absorption coefficient is obtained by solving the time-dependent Schrödinger equation for nuclear motion on the electronic excited PES (indicated by the superscript "e" at $\chi_{g0}^{(e)}$). The initial condition is given by $|\chi_{g0}^{(e)}(t=0)\rangle = |\chi_{g0}\rangle$. At each time, the overlap integral between the propagated and the initial wave function has to be calculated to get the absorption spectrum. In Figure 6.8, wave packet dynamics, autocorrelation function, and absorption spectrum are shown for the example of a Morse oscillator potential.

The wave packet description of absorption is particularly useful if the excited electronic state $|\phi_e\rangle$ is dissociative. Because no reference is made to eigenstates, there is no need to calculate the continuous energy spectrum. Instead, one solves the Schrödinger equation in the coordinate representation. Additionally, Eq. (6.65) combines a frequency domain quantity, $\alpha(\omega)$, with a time domain quantity, $\chi_{g0}^{(e)}(R, t)$. Therefore, the approach enables one to draw conclusions on the molecular system, both in the frequency and in the time domain.[6]

----

6) As a note in caution, we point out that in principle only the *full* time propagation of the wave packet up to $t \to \infty$ gives the absorption coefficient. In practice, an additional factor $\exp(-\gamma t)$ is
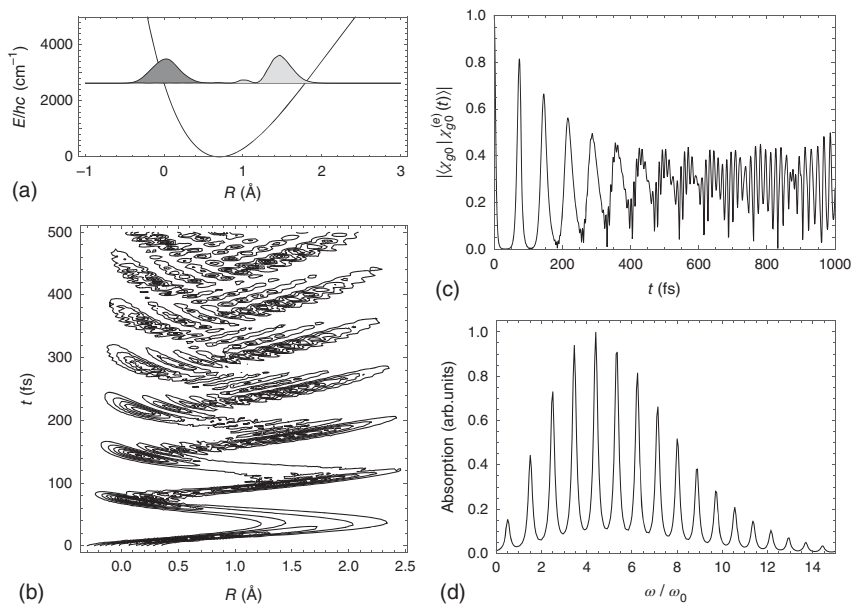
Figure 6.8 From wave packet motion to the absorption spectrum of a Morse oscillator potential surface (cf. Figure 2.3). (a) Excited state potential, initial state according to a vertical transition from the electronic ground state (dark gray) and wave packet after 100 fs (light gray). (b) Contour plot of wave packet dynamics ($|\chi_{g0}^{(e)}(R,t)|^2$). (c) Autocorrelation function $|\langle\chi_{g0}|\chi_{g0}^{(e)}(t)\rangle|$ (normalized). (d) Absorption spectrum according to Eq. (6.65) with an exponential damping of the correlation function of $\gamma = 0.01$ 1/fs (ω_0 is the transition frequency between the two lowest vibrational states).

In Figure 6.9, we show the results of a numerical wave packet simulation of the $S_0 - S_1$ absorption spectrum of the three-atomic molecule FNO. The initial wave packet on the excited state is given according to $\chi_{g0}^{(e)}(R_{\mathrm{N-O}}, R_{\mathrm{F-NO}}; t = 0) = \chi_{g0}(R_{\mathrm{N-O}}, R_{\mathrm{F-NO}})$ (cf. Figure 6.9a). The subsequent dynamics is characterized by an oscillatory motion in the bound region of the potential and a simultaneous dissociation indicated by those parts of the wave packet that leave along the exit channel $R_{\mathrm{F-NO}} \to \infty$. The interplay between bond vibration and dissociation is reflected in the damped oscillations of the correlation function shown in the lower part of Figure 6.9b. Consequently, the Fourier transform of this correlation function, which gives the absorption spectrum, is quite structured (Figure 6.9c).

It is easy to extend the considerations carried out so far to the case where the absorption process starts from a mixed state (as already included in Eq. (6.61)). We may generalize Eq. (6.65) using for the equilibrium statistical operator in Eq. (6.61) $\hat{W}_{\mathrm{eq}} = \sum_M f_{gM} |\chi_{gM}\rangle\langle\chi_{gM}|$; that is, we assume a thermal distribution over the vibrational levels of the electronic ground state. Since every (pure) state in this mixtures

---

often introduced to mimic, for instance the effect of system–reservoir coupling in terms of absorption line broadening. It also provides a cut-off for the upper integration boundary.
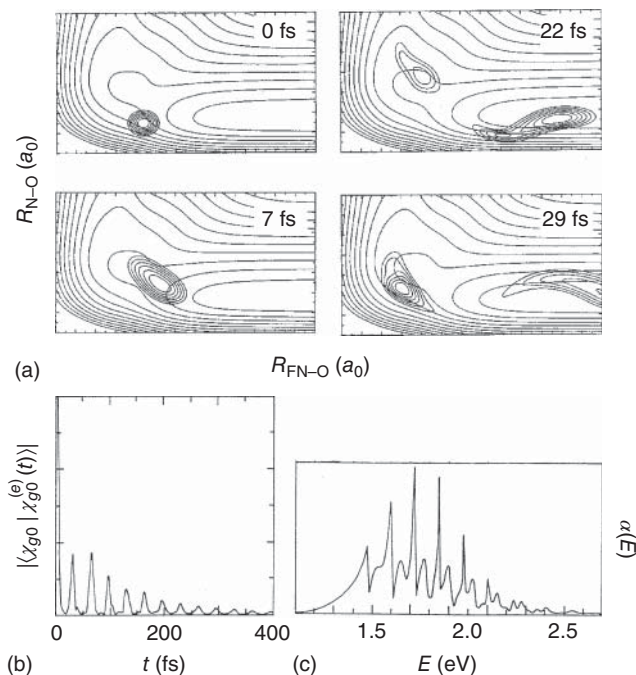
Figure 6.9 Numerical results for the $S_0 - S_1$ absorption spectrum of FNO obtained using the wave packet propagation method. (a) The dynamics has been restricted to two dimensions, that is the NO bond distance R_{N-O} (from 1.8 to 3.2 Å) and the distance between F and the center of mass of the NO fragment R_{F-NO} (from 2.5 to 5 Å). (b and c) The correlation function $|\langle \chi_{g0} | \chi_{g0}^{(e)}(t)\rangle|$ and the linear absorption spectrum, respectively (Reproduced with permission from Suter et al. [2]/AIP Publishing).

enters the formula for the absorption coefficient independently, we directly obtain

$$\alpha(\omega) = \frac{4\pi\omega n_{\text{mol}}}{3\hbar c} \, |d_{eg}|^2 \sum_M f_{gM} \, \text{Re} \int_0^\infty dt \, e^{i(\omega + E_{gM}/\hbar)t} \, \langle \chi_{gM} | \chi_{gM}^{(e)}(t)\rangle. \quad (6.66)$$

Instead of a single wave function overlap as in Eq. (6.65), we now have multiple overlaps $\langle \chi_{gM} | \chi_{gM}^{(e)}(t)\rangle$ between the vibrational wave functions χ_{gM} and its time-dependent form propagated on the excited state PES. Moreover, every term is weighted by the thermal distribution function.

A complication appears if several coupled electronic states become accessible after photon Absorption, and nonadiabatic dynamics has to be taken into account. Let us consider the case of two coupled states $|\phi_e\rangle$ and $|\phi_f\rangle$. Here, the excited state cannot be described by the single vibrational Hamiltonian H_e but by the Hamiltonians H_e and H_f coupled via the operator V_{fe} (here, we use the diabatic picture). This is another example for a *curve-crossing* problem. The coupling has to be accounted for in the numerical solution of the Schrödinger equation for the wave function determining the correlation function in Eq. (6.65). As a consequence of the nonadiabatic coupling, the spectrum changes; that is, the positions of the transitions are modified,
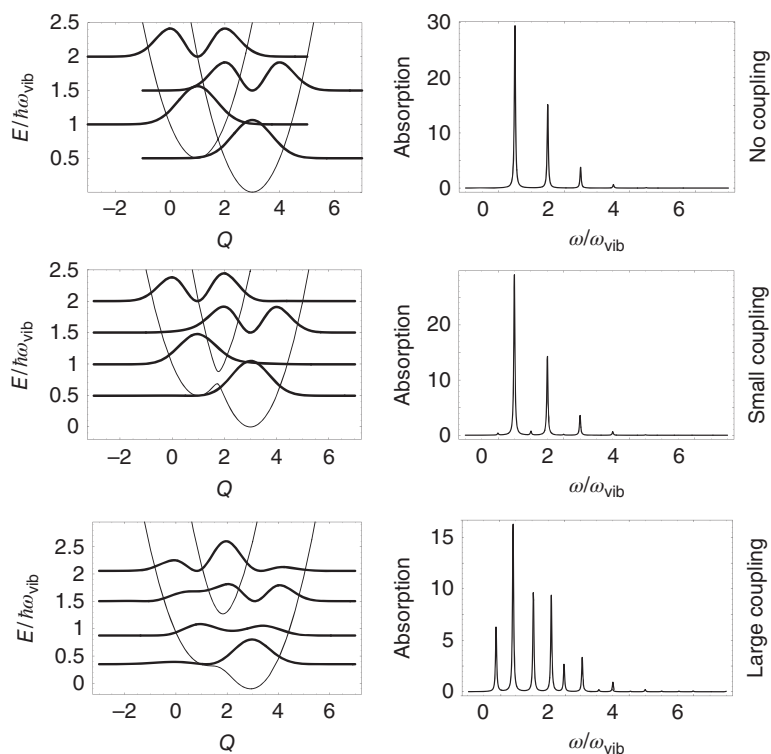
Figure 6.10 Linear absorption spectrum for a curve crossing system (states $|\phi_e\rangle$ and $|\phi_f\rangle$) along a one-dimensional reaction coordinate Q (dimensionless oscillator coordinate). The ground state is at $Q = 0$, and the transition dipole moment is assumed to be constant; that is, only the Franck–Condon factors between the ground state wave function and the eigenstates of the coupled excited states determine the spectrum. The left column shows the adiabatic potential curves and the coordinate probability distribution for the lowest eigenstates (the detuning between the diabatic potentials is $0.5\hbar\omega_{vib}$). The right column shows the absorption spectrum (in arbitrary units) for the case of no ($V_{ef} = 0$), weak ($V_{ef} = 0.1$), and strong ($V_{ef} = 0.5$) interstate coupling. Upon increasing the interstate coupling, new peaks appear, and the spectrum is shifted.

and new transitions appear (cf. Figure 6.10). We will return to the dynamics within coupled PES in more detail in Section 6.6 as well as in Chapter 7.

6.3.2 Absorption Coefficient and Reduced Density Operator Propagation

In the foregoing section, we used the rearrangement Eq. (6.61) of the dipole–dipole correlation function to give an interpretation of the absorption coefficient in terms of a wave packet propagation, which holds if the initial state of the transition is a pure or a mixed state. Here, we briefly demonstrate how to proceed if the system that undergoes the optical transition is in a condensed phase environment and is characterized by an RDO. To be more specific, we assume that the vibrational DOFs

described in the preceding section by the states χ_{aM} $(a = g, e)$ are coupled to a solvent that acts as a thermal bath in the sense of Section 3.6. As a result, every state χ_{aM} has a finite lifetime because of transitions accompanied by the emission or absorption of environmental quanta.

The simplest example for such a situation would be a diatomic molecule in a solvent where the bond distance coordinate is linearly coupled to some solvent coordinates (cf. Section 5.3.3). If both types of coordinates are assumed to move in parabolic PES, the bilinear coupling allows to introduce common harmonic coordinates, and the whole system can be described exactly as outlined in Section 6.2.3. It is the advantage of the following treatment that it is also valid in the case of a general coupling to the condensed phase environment. Nevertheless, the treatment of the system–reservoir coupling is still approximately according to the use of the QME.

To obtain the dipole–dipole correlation function in the present case, we again have to start from Eq. (4.22) for the polarization and have to introduce its linearized version with respect to the radiation field. However, if the radiation field only affects the (active) molecular system and does not induce optical transitions in the environment, Eq. (4.19) for the dipole operator expectation value can be written as

$$\boldsymbol{d}(t) = \mathrm{tr}_S\{\hat{\mu}\hat{\rho}(t)\}. \tag{6.67}$$

Here, the trace is taken with respect to the state space of the active molecular system responsible for the absorption processes. $\hat{\rho}(t)$ denotes the RDO, which is propagated under the action of the external field starting with the equilibrium value $\hat{\rho}_{\mathrm{eq}}$. The environment enters the expression via the time evolution of $\hat{\rho}(t)$. In a next step, we linearize Eq. (6.67) with respect to the electric field strength to find the generalization of Eq. (6.61) for the dipole–dipole correlation function:

$$C_{\mathrm{d-d}}(t) = \mathrm{tr}_S\left\{\hat{\mu}\hat{\sigma}(t)\right\}. \tag{6.68}$$

The operator $\hat{\sigma}(t)$ has to be propagated according to the respective QME master equation (without the external field) and with the initial value $[\hat{\mu}, \hat{\rho}_{\mathrm{eq}}]_-$ (at $t = 0$). Therefore, we may write $\hat{\sigma}(t) = \mathcal{U}(t)[\hat{\mu}, \hat{\rho}_{\mathrm{eq}}]_-$, where $\mathcal{U}(t)$ denotes the dissipative time-evolution superoperator (cf. Eq. (3.269)).

To obtain a deeper insight into the expression for the dipole–dipole correlation function, we again specify it to a system with two electronic states (ϕ_g and ϕ_e) already used in the preceding sections. Introducing an expansion with respect to these electronic states and using $\hat{\rho}_{\mathrm{eq}} = \hat{R}_g|\phi_g\rangle\langle\phi_g|$, where $\hat{R}_g$ is the vibrational equilibrium statistical operator of the electronic ground state, we get from Eq. (6.68)

$$C_{\mathrm{d-d}}(t) = \mathrm{tr}_{\mathrm{vib}}\left\{\boldsymbol{d}_{ge}\langle\phi_e|\hat{\sigma}(t)|\phi_g\rangle + \boldsymbol{d}_{eg}\langle\phi_g|\hat{\sigma}(t)|\phi_e\rangle\right\}. \tag{6.69}$$

This expression allows to generalize Eq. (6.65) to the condensed phase situation. The propagation of the electronic ground state vibrational wave functions on the excited state PES (cf. Eq. (6.65)) has been replaced by a propagation of the off-diagonal electronic matrix elements of the density operator $\hat{\sigma}$.

If the equation of motion for the density matrix elements follows, for example from the Bloch approximation (Section 3.8.3), an analytical expression for the linear absorption coefficient may be derived. The Bloch approximation has the advantage

that the propagation of the off-diagonal density matrix elements is separated from that of the diagonal elements. We introduce the electron-vibrational energy representation $\sigma_{aN,bM}(t) = \langle \chi_{aN} | \langle \phi_a | \hat{\sigma}(t) | \phi_g \rangle | \chi_{bM} \rangle$ and obtain for $a \neq b$:

$$\frac{\partial}{\partial t} \sigma_{aN,bM}(t) = -i \left(\omega_{aN,bM} - i\gamma_{aN,bM} \right) \sigma_{aN,bM}(t). \tag{6.70}$$

The $\omega_{aN,bM}$ are the transition frequencies, and the $\gamma_{aN,bM}$ describe the dephasing rates (cf. Eqs. (3.352), (3.353), and (3.357)). After specifying the initial conditions, $\sigma_{eN,gM}(0) = \boldsymbol{d}_{eg} \langle \chi_{eN} | \chi_{gM} \rangle f_{gM}$, the time dependence of $\sigma_{aN,bM}$ is simply obtained as a damped oscillation. A Fourier transformation as in Eq. (4.46) results in the final expression for the absorption coefficient. If $\sigma_{eN,gM}(t)$ is Fourier transformed, there appears the exponent $\omega - \omega_{eN,gM}$, which describes the resonant transitions. In contrast, $\sigma_{gN,eM}(t)$ results in the exponent $\omega - \omega_{gN,eM}$, which is completely off-resonant. These contributions can be neglected (cf. Eq. (6.65)), and we only consider $\sigma_{eN,gM}(t)$. Then, the trace formula in Eq. (6.69) can be specified as follows:

$$\mathrm{tr}_{\mathrm{vib}} \{ \langle \phi_e | \hat{\sigma}(t) | \phi_g \rangle \} = \sum_M \langle \chi_{gM} | \langle \phi_e | \hat{\sigma}(t) | \chi_{gM} \rangle | \phi_g \rangle$$
$$= \sum_{M,N} \langle \chi_{gM} | \chi_{eN} \rangle \, \sigma_{eN,gM}(t), \tag{6.71}$$

where in the last part the complete set of vibrational states belonging to the excited electronic state has been introduced. The final expression for the absorption coefficient reads

$$\alpha(\omega) = \frac{4\pi\omega n_{\mathrm{mol}}}{3\hbar c} |d_{ge}|^2 \sum_{M,N} f_{gM} |\langle \chi_{gM} | \chi_{eN} \rangle|^2 \frac{\gamma_{eN,gM}}{(\omega - \omega_{eN,gM})^2 + \gamma_{eN,gM}^2}. \tag{6.72}$$

This expression is a direct generalization of Eq. (6.13) since the various sharp transitions (described by a δ-function) are broadened here to a Lorentzian-like lineshape (note the use of frequency instead of energy arguments here). The amount of broadening is determined by the dephasing rates $\gamma_{eN,gM}$. Pure dephasing, which was introduced in Section 6.2.2, is described here by the line-broadening $\gamma_{e0,g0}$ corresponding to a transition between the vibrational ground states of both the considered electronic levels. Whether $\gamma_{e0,g0}$ gives a contribution or not depends on the concrete model of the system–reservoir coupling.

6.3.3 Mixed Quantum–Classical Computation of the Absorption Coefficient

We complete our considerations of different ways to compute the linear absorption spectrum of a molecular system by an approach that accounts for the vibrational DOFs (either of an intramolecular nature or of the surrounding solvent) using classical mechanics. Again, we demonstrate this for a transition including an electronic excitation.

The easiest way to achieve this goal is based on Eq. (6.22), where the S-operator is obtained by a classical quantity that is not time ordered and where the trace has been replaced by the phase space integral over initial vibrational coordinates q_0

and momenta p_0 weighted by the thermal distribution f_g (defined by the vibrational Hamilton function $H_g(q, p)$):

$$\text{tr}_{\text{vib}}\{\hat{R}_g S_{eg}(t, 0)\} \rightarrow \int dq_0 dp_0 \, f_g(q_0, p_0) \exp\left\{-\frac{i}{\hbar} \int_0^t d\bar{t} \, U_{eg}\left(q(\bar{t})\right)\right\}. \quad (6.73)$$

This approximation, which is known as the *dynamical classical limit* (DCL), includes the PES difference (cf. Section 5.5):

$$U_{eg}\left(q(\bar{t})\right) = U_e\left(q(\bar{t}; q_0, p_0)\right) - U_g\left(q(\bar{t}; q_0, p_0)\right). \quad (6.74)$$

It replaces the difference Hamiltonian $\Delta H_{eg}^{(g)}(\bar{t})$ appearing in the exact formula, Eq. (6.22). The nuclear kinetic energy contributions cancel each other, and the $q(\bar{t}; q_0, p_0)$ are understood as solutions of Newton's equations obtained with the initial coordinates and momenta q_0 and p_0, respectively (note the similarity to the Ehrenfest theory introduced in Section 3.13.1). As indicated, the latter quantities are subject to a thermal averaging procedure. Thus, the DCL determines the absorption coefficient via the fluctuating PES difference (energy gap function), which is sampled by a trajectory in the electronic ground state (cf. discussion in Section 5.5). How this approximation compares to the exact behavior of the absorption coefficient is shown in Figure 6.11. Although the DCL approximation cannot reproduce the sharp absorption lines at low temperature (or weaker coupling to the secondary oscillators), it gives a satisfactory reproduction of the spectrum and the correct position of the various lines in the overall spectrum.

In the following equation, we invoke the classical (as well as quasi-classical) description of the vibrational dynamics when calculating the absorption coefficient in a more rigorous way. This is achieved by changing to a partial Wigner representation of the statistical operator $\hat{\sigma}$ entering Eq. (6.61) for the dipole–dipole correlation function. Taking the Wigner transformation partially, that is only with respect to the nuclear DOFs, allows to treat them classically, while the electronic DOFs are still considered quantum mechanically (cf. Section 3.4.4). As in Eq. (6.69) and after specifying the trace with respect to the vibrational states to coordinate operator eigenstates, we write

$$C_{\text{d–d}}(t) = \int dq \, \{\boldsymbol{d}_{ge}\langle\phi_e|\langle q|\hat{\sigma}(t)|q\rangle|\phi_g\rangle - \boldsymbol{d}_{eg}\langle\phi_g|\langle q|\hat{\sigma}(t)|q\rangle|\phi_e\rangle\}. \quad (6.75)$$

Here, $q \equiv \{q_\xi\}$ denotes the $\mathcal{N}$ vibrational coordinates, $|q\rangle$ is the product of the respective eigenstates of the coordinate operators, and $\hat{\sigma}(t)$ is given by $U_{\text{mol}}(t)$ $[\hat{\mu}, \hat{R}_g|\phi_g\rangle\langle\phi_g|]_-U_{\text{mol}}^+(t)$. The introduction of the partial Wigner representation of $\hat{\sigma}(t)$ results in the quantity $\hat{\sigma}(x, p; t)$, which is an operator in the electronic state space. The equation of motion for $\hat{\sigma}(t)$ yields upon Wigner transformation (using the definition Eq. (3.164))

$$\frac{\partial}{\partial t}\hat{\sigma}(x, p; t) = -\frac{i}{\hbar}\left[H_{\text{mol}}(x, p)e^{i\hbar\hat{\Theta}/2}\hat{\sigma}(x, p; t)\right.$$
$$\left. -\hat{\sigma}(x, p; t)e^{i\hbar\hat{\Theta}/2}H_{\text{mol}}(x, p)\right]. \quad (6.76)$$
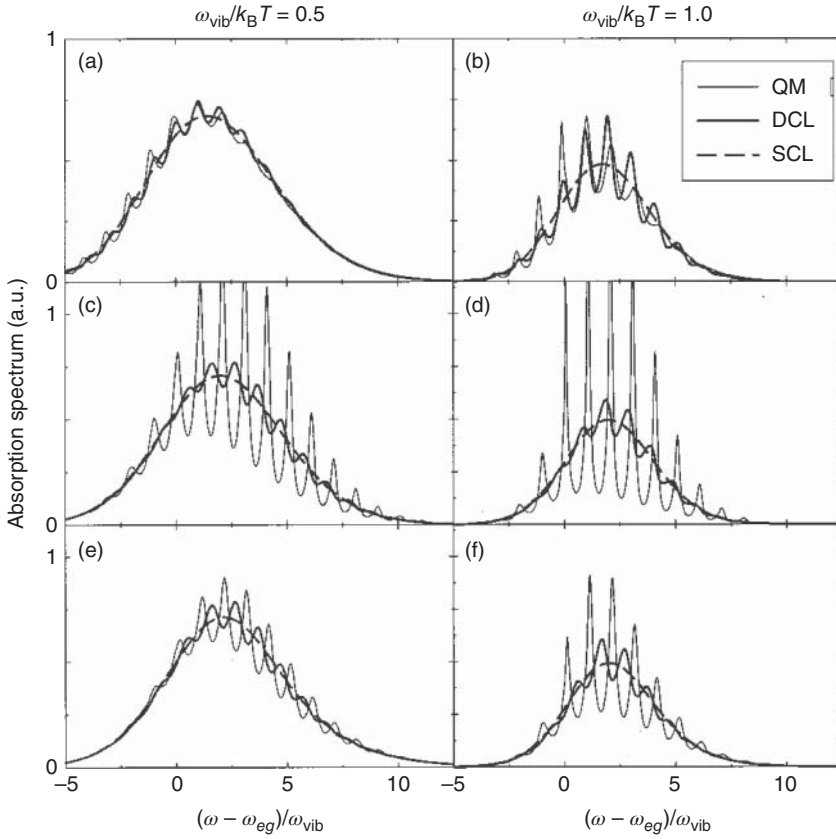
Figure 6.11 Linear absorption coefficient for an MBO model, Eqs. (6.57) and (6.58), incorporating a single harmonic coordinate ($\Delta g = -4$) coupled to 100 reservoir modes, with a coupling derived from a discretized spectral density of type Eq. (3.301), with different coupling strengths in the ground and excited electronic states ($J_a = \eta_a J, a = g, e$, with $\eta_g = 0.05$, $\eta_e = 0.125$ ((a) and (b)); $\eta_g = 0.0625$, $\eta_e = 0.025$ ((c) and (d)); and $\eta_g = 0.125$, $\eta_e = 0.05$ ((e) and (f))). The two columns correspond to two different temperatures as indicated. The quantum mechanical (QM) results are contrasted to the DCL and SCL limits (Reproduced with permission from Egorov et al. [3]/AIP Publishing).

The classical limit for the vibrational DOFs is obtained by expanding the exponential, $\exp(i\hbar\hat{\Theta}/2)$, to first order (cf. Eq. (3.167)), which gives

$$
\frac{\partial}{\partial t}\hat{\sigma}(x, p; t) = -\frac{i}{\hbar}\left[H_{\mathrm{mol}}(x, p), \hat{\sigma}(x, p; t)\right]_{-}
$$
$$
+ \frac{1}{2}\left[H_{\mathrm{mol}}(x, p)\hat{\Theta}\hat{\sigma}(x, p; t) - \hat{\sigma}(x, p; t)\hat{\Theta}H_{\mathrm{mol}}(x, p)\right]. \tag{6.77}
$$

As it is the case for $\hat{\sigma}$, the Hamiltonian H_{mol} depends on the classical coordinates and momenta but remains an operator in the electronic state space. Therefore, Planck's constant also appears in Eq. (6.77). Let us neglect for a moment the second term on the right-hand side. Then, the remaining equation is solved by

$$
\hat{\sigma}(x, p; t) = U_{\mathrm{mol}}(x, p; t)\hat{\sigma}(x, p; 0)U_{\mathrm{mol}}^{+}(x, p; t). \tag{6.78}
$$

The time-evolution operators have been defined by H_{mol}, and therefore, they depend on the classical coordinates and momenta, too. Moreover, we note the initial condition $\hat{\sigma}(0) = [\hat{\mu}, \hat{R}_g |\phi_g\rangle\langle\phi_g|]_-$. In the classical limit, this leads to the Wigner representation as $\hat{\sigma}(x, p; 0) = \boldsymbol{d}_{eg}f_g(x, p) |\phi_e\rangle\langle\phi_g| -\text{h.c.}$ Then, after taking the electronic matrix elements, it follows for $\hat{\sigma}(x, p; t)$ (as in the foregoing Section 6.3.2 we concentrate on the resonant contribution)

$$\langle\phi_e|\hat{\sigma}(x, p; t)|\phi_g\rangle = \langle\phi_e|U_{\text{mol}}(x, p; t)\boldsymbol{d}_{eg}f_g|\phi_e\rangle\langle\phi_g|U_{\text{mol}}^+(x, p; t)|\phi_g\rangle$$

$$= \boldsymbol{d}_{eg}f_g(x, p) \exp\left(-\frac{i}{\hbar}U_{eg}(x)t\right). \tag{6.79}$$

Since the time-evolution operators are defined in terms of the classical vibrational Hamiltonians $H_g(x, p)$ and $H_e(x, p)$, the exponent in the last part only contains the difference $U_{eg}(x) = U_e(x) - U_g(x)$ of the related PES. If we insert Eq. (6.79) into Eq. (6.75) for the dipole–dipole correlation function, the absorption coefficient is obtained as

$$\alpha(\omega) = \frac{4\pi\omega n_{\text{mol}}}{3\hbar c}|d_{eg}|^2 \text{Re} \int_0^\infty dt\, e^{i\omega t} \int dx \frac{dp}{(2\pi\hbar)^{\mathcal{N}}} f_g(x, p) e^{-iU_{eg}(x)t/\hbar}$$

$$= \frac{4\pi^2\omega n_{\text{mol}}}{3c}|d_{eg}|^2 \int dx f_g(x)\delta\left(\hbar\omega - (U_e(x) - U_g(x))\right). \tag{6.80}$$

In the final expression, the momentum integration has been carried out, leading to the reduced distribution function $f_g(x) \sim \exp(-U_g(x)/k_B T)$. The δ-function follows from the time integral. The result for the linear absorption coefficient reflects the qualitative discussion carried out in Section 6.1 in connection with Figure 6.1a. The absorption of a photon becomes possible if its energy $\hbar\omega$ equals the difference, $U_e(x) - U_g(x)$, between the PES of the ground and the excited electronic states (vertical transitions). This is also the essence of Eq. (6.80).

Assuming parabolic PES, the x-integration in Eq. (6.80) can be carried out. This will be demonstrated in detail in Section 7.4.1, where the electron transfer between two states is discussed (see calculations following Eq. (7.62)). Here, we use only the result (cf. Eq. (7.71)) adopted to the case of the absorption coefficient

$$\alpha(\omega) = \frac{4\pi^2\omega n_{\text{mol}}}{3c}|d_{eg}|^2 \sqrt{\frac{1}{2\pi k_B TS}} \exp\left\{-\frac{\left[\hbar(\omega - \omega_{eg}) - S/2\right]^2}{2Sk_B T}\right\}. \tag{6.81}$$

Note the introduction of the transition frequency ω_{eg} according to Eq. (6.16) and of the Stokes shift, Eq. (6.26). In Section 6.2.4, this type of expression was derived for the case of slow nuclear motion (cf. Eq. (6.55)). This can be brought into a different perspective; that is, the neglect of any dynamic corrections to the solution, Eq. (6.79), of the density operator equation in the Wigner representation (Eq. (6.77)) results in a *static approximation* (static classical limit [SCL]). In other words, during the absorption process, there is no classical vibrational motion. Because the static approximation is of fundamental character, we will come across it again at various places in the later chapters.

Next, we consider the effect of the second term in Eq. (6.77). Taking the electronic matrix elements, one obtains using Eq. (3.165)

$$
\frac{\partial}{\partial t} \langle \phi_e | \hat{\sigma}(x, p; t) | \phi_g \rangle = -\frac{i}{\hbar} U_{eg}(x) \, \langle \phi_e | \hat{\sigma}(x, p; t) | \phi_g \rangle
$$
$$
+ \frac{1}{2} [H_e(x, p) + H_g(x, p)] \, \hat{\Theta} \, \langle \phi_e | \hat{\sigma}(x, p; t) | \phi_g \rangle. \qquad (6.82)
$$

The second term contains the classical Liouvillian for the evolution with respect to the average of ground and excited state Hamiltonians, $\overline{\mathcal{L}}_{cl} = [H_e(x, p) + H_g(x, p)] \, \hat{\Theta}/2$. The formal solution of Eq. (6.82) can be written in Condon approximation as

$$
\langle \phi_e | \hat{\sigma}(x, p; t) | \phi_g \rangle = \exp \left\{ \frac{i}{\hbar} \int_{-t}^{0} d\bar{t} \, \bar{U}_{eg}(\bar{t}) \right\} e^{-\overline{\mathcal{L}}_{cl} t} \langle \phi_e | \hat{\sigma}(x, p; 0) | \phi_g \rangle
$$
$$
= \boldsymbol{d}_{eg} \exp \left\{ \frac{i}{\hbar} \int_{-t}^{0} d\bar{t} \, \bar{U}_{eg}(\bar{t}) \right\} e^{-\overline{\mathcal{L}}_{cl} t} f_g(x, p), \qquad (6.83)
$$

with $e^{\overline{\mathcal{L}}_{cl} t} U_{eg}(x) = \bar{U}_{eg}(t)$. Notice that $f_g(x, p) = \exp(-H_g(x, p)/k_B T)/\mathcal{Z}_g$ is not stationary if propagated with the average Liouvillian $\overline{\mathcal{L}}_{cl}$. However, we can write

$$
f_g(x, p) = \frac{\mathcal{Z}_{av}}{\mathcal{Z}_g} e^{U_{eg}(x)/2k_B T} f_{av}(x, p), \qquad (6.84)
$$

where f_{av} and $\mathcal{Z}_{av}$ are defined with respect to the average Hamiltonian $(H_e + H_g)/2$.

In order to obtain the absorption spectrum, a phase space average has to be performed with respect to the distribution $f_{av}(x, p)$. Due to the time invariance of this equilibrium average, one can shift the time arguments in the exponential functions by t. This yields, using Eq. (6.84), the absorption spectrum

$$
\alpha(\omega) = \frac{4\pi \omega n_{mol}}{3\hbar c} |d_{eg}|^2 \, \mathrm{Re} \int_0^\infty dt \, e^{i\omega t}
$$
$$
\times \int dx \frac{dp}{(2\pi\hbar)^{\mathcal{N}}} \exp \left\{ \frac{i}{\hbar} \int_0^t d\bar{t} \, \bar{U}_{eg}(\bar{t}) \right\} f_g(x, p). \qquad (6.85)
$$

In contrast to Eq. (6.80), the energy gap $U_{eg}(x)$ is propagated with the average Hamiltonian, $(H_e + H_g)/2$, instead of H_g. Therefore, this approximation is also called the *averaged classical limit* (ACL).[7]

In Figure 6.11, the DCL and SCL approximations are compared to the exact quantum mechanical (QM) results for a discretized MBO model, Eqs. (6.57) and (6.58). The QM absorption spectrum shows a pronounced Franck–Condon progression that is broadened with increasing temperature. The SCL spectra are structureless but

---

7) For a discussion of this approximation in the context of nonlinear spectroscopy, see Shemetulskis and Loring [4].

wrap the more exact spectra. The DCL approximation presents an improvement as compared with the SCL case but without being able to reproduce the correct positions of the peaks. The ACL approximations are essentially indistinguishable from the exact results (not shown).[8]

6.4 The Emission Spectrum

The rate of spontaneous emission of a photon by a molecule via a transition from an excited electronic state to the ground state has been derived in Section 4.4. Here, we discuss the respective frequency-resolved emission spectrum $I(\omega)$ in some detail. $I(\omega)$ is obtained by introducing the radiative lifetime τ_{rad} of the excited electronic state. The latter quantity follows from the inverse of the transition rate $k_{e \to g}$. We write

$$k_{e \to g} \equiv \frac{1}{\tau_{\mathrm{rad}}} = \int_0^\infty d\omega \, I(\omega), \tag{6.86}$$

where the emission spectrum $I(\omega)$ gives the photon emission rate per frequency interval. According to Eq. (4.134), one obtains for the emission spectrum

$$I(\omega) = \frac{4\omega^3 |d_{eg}|^2}{3c^3} \sum_{M,N} f_{eM} |\langle \chi_{eM} | \chi_{gN} \rangle|^2 \delta(E_{eM} - E_{gN} - \hbar\omega). \tag{6.87}$$

This expression will be encountered in Chapter 9 in the context of the Förster theory of resonance energy transfer in molecular aggregates. It is obvious from the general structure that the emission spectrum can be calculated in complete analogy to the absorption coefficient. Following Section 6.2.1, we obtain

$$I(\omega) = \frac{4\omega^3 |d_{eg}|^2}{3c^3} \mathcal{D}_{\mathrm{em}}(\omega - \omega_{eg}), \tag{6.88}$$

where the combined DOS $\mathcal{D}_{\mathrm{em}}$ characterizes the emission process. In analogy to Eq. (6.19), we may write

$$\mathcal{D}_{\mathrm{em}}(\omega - \omega_{eg}) = \sum_{M,N} f_{eM} |\langle \chi_{eM} | \chi_{gN} \rangle|^2 \delta(E_{eM} - E_{gN} - \hbar\omega). \tag{6.89}$$

This expression differs in two respects from the DOS characterizing the absorption process, Eq. (6.19). First, the electronic quantum numbers g and e have been interchanged (resulting in a replacement of f_{gM} by f_{eM}), and second, ω has been replaced by $-\omega$. Thus, we obtain ($\hat{R}_e$ is the vibrational equilibrium statistical operator referring to the excited electronic state)

$$\mathcal{D}_{\mathrm{em}}(\omega - \omega_{eg}) = \frac{1}{2\pi\hbar} \int dt \, e^{-i\omega t} \, \mathrm{tr}_{\mathrm{vib}} \{ \hat{R}_e \, e^{iH_e t/\hbar} \, e^{-iH_g t/\hbar} \}. \tag{6.90}$$

---

8) For a comprehensive comparison of the different trajectory-based approaches to the absorption spectra, see Karsten et al. [5].

Reducing this expression to the case of harmonic PES as demonstrated in Section 6.2.3, we have

$$\mathcal{D}_{\mathrm{em}}(\omega - \omega_{eg}) = \frac{1}{2\pi\hbar} \int dt \, e^{-i(\omega-\omega_{eg})t - G(0) + G(t)}, \tag{6.91}$$

directly demonstrating the property $\mathcal{D}_{\mathrm{em}}(\omega - \omega_{eg}) = \mathcal{D}_{\mathrm{abs}}(-\omega + \omega_{eg})$. This shows that for harmonic oscillator PES (with the same curvature in the ground as well as the excited state), the absorption and emission spectra are mirror symmetric with respect to $\omega = \omega_{eg}$, as shown in Figure 6.7. The difference between the absorption and emission maxima is equal to the Stokes shift S. Notice that in condensed phase experiments, there is an additional contribution to the Stokes shift, which is due to the reorganization energy required to adjust, for instance the solvation shell to the respective electronic state (cf. the main peak separation of the absorption and emission spectra in Figure 6.3). This effect can be described, for instance by a Debye-type spectral density.

6.5 Optical Preparation of an Excited Electronic State

The following considerations will focus on the temporal behavior of molecular excitation due to the interaction with an external field. In particular, we consider the preparation of an excited electronic state via an optical transition from the electronic ground state. A detailed understanding of such a transition is of great importance for the study of photoinduced transfer phenomena starting from an excited electronic state. This goes beyond the linear absorption and, thus, linear optics since the preparation, and possible detection, of the excited state dynamics includes the field in higher than the first order. Before studying the preparation in the general frame of the density matrix theory, a simpler approach will be given, which is based on the solution of the time-dependent Schrödinger equation.

6.5.1 Wave Function Formulation

Let us consider again the two-state Hamiltonian equation 6.4; however, instead of a strictly monochromatic electromagnetic field, a *pulsed field* (laser pulse) will be assumed. It has the form

$$\boldsymbol{E}(t) = \boldsymbol{n}E(t)e^{-i\omega t} + \text{c.c.} \tag{6.92}$$

The vector $\boldsymbol{n}$ defines the polarization of the field, and ω is the carrier frequency (center frequency of the pulse spectrum). $E(t) \equiv Af(t)$ denotes the pulse envelope with the pulse amplitude A and the normalized pulse envelope $f(t)$ ($\int dt f(t) = 1$). The pulse duration is fixed by the pulse envelope. Frequently, a Gaussian pulse shape centered at $t = t_p$ is used:

$$f(t) = \frac{1}{\sqrt{2\pi\tau_p^2}} \exp\left\{ -\frac{(t - t_p)^2}{2\tau_p^2} \right\}. \tag{6.93}$$

The time integral of this envelope is normalized to unity and contains τ_p as the pulse duration.[9] To solve the time-dependent Schrödinger equation,

$$\frac{\partial}{\partial t}|\Psi(t)\rangle = -\frac{i}{\hbar}H(t)|\Psi(t)\rangle, \tag{6.94}$$

defined by the time-dependent Hamiltonian, Eq. 6.4, and the initial condition $|\Psi(t_0)\rangle$, we change to the interaction representation (compare Section 3.2.2). The unperturbed Hamiltonian is given by the molecular part $H_{\text{mol}} = \sum_{a=g,e} H_a(q)|\phi_a\rangle\langle\phi_a|$ of Eq. 6.4, whereas the perturbation is represented by the external-field contribution $H_{\text{field}}(t) = -\boldsymbol{E}(t)\boldsymbol{d}_{eg}|\phi_e\rangle\langle\phi_g| + $ h.c. Consequently, the state vector in the interaction representation reads $|\Psi^{(\text{I})}(t)\rangle = U_{\text{mol}}^+(t - t_0)|\Psi(t)\rangle$, with the time-evolution operator U_{mol} defined via H_{mol}. The determination of $|\Psi^{(\text{I})}(t)\rangle$ can be reduced to the solution of an integral equation of type (3.43). Here, we concentrate on the first-order correction with respect to the external field and obtain

$$|\Psi^{(\text{I})}(t)\rangle \approx |\Psi(t_0)\rangle - \frac{i}{\hbar}\int_{t_0}^{t} d\bar{t}\, H_{\text{field}}^{(\text{I})}(\bar{t})\,|\Psi^{(\text{I})}(t_0)\rangle. \tag{6.95}$$

After switching back to the Schrödinger representation, the complete state vector including the first-order correction reads[10]

$$|\Psi(t)\rangle = |\Psi^{(0)}(t)\rangle + |\Psi^{(1)}(t)\rangle = U_{\text{mol}}(t - t_0)|\Psi(t_0)\rangle$$
$$- \frac{i}{\hbar}\int_{t_0}^{t} d\bar{t}\, U_{\text{mol}}(t - t_0)U_{\text{mol}}^+(\bar{t} - t_0)H_{\text{field}}(\bar{t})U_{\text{mol}}(\bar{t} - t_0)|\Psi(t_0)\rangle. \tag{6.96}$$

The initial condition will be specified to

$$|\Psi(t_0)\rangle = \delta_{ag}|\phi_g\rangle|\chi_{g0}\rangle, \tag{6.97}$$

thus assuming that the system is in the vibrational ground state of the electronic ground state. In a next step, we take into account that

$$U_{\text{mol}}(t) = \sum_a e^{-iH_a t/\hbar}|\phi_a\rangle\langle\phi_a| \tag{6.98}$$

and expand the time-dependent state vector, Eq. (6.96), with respect to the electronic basis. The zeroth-order part $|\Psi^{(0)}(t)\rangle$ corresponds to a stationary vibrational state on the electronic ground state PES. The expansion of the first-order contribution with respect to the excited electronic state gives the related state vector for vibrational motion:

---

9) Gaussian pulse envelopes are also characterized by the full width at half maximum, which is $\sqrt{8\ln 2}\,\tau_p$.

10) Note that as long as we concentrate on a strict linearization with respect to the external field, a normalization of the state vector is not necessary since it gives terms that are of higher order in the field.

$$|\chi_e(t)\rangle = \langle \phi_e | \Psi^{(1)}(t)\rangle$$

$$= -\frac{i}{\hbar} \int_{t_0}^{t} d\bar{t}\; e^{-iH_e(t-\bar{t})/\hbar} \left(-\boldsymbol{d}_{eg}\boldsymbol{E}(\bar{t}) \right) e^{-iH_g(\bar{t}-t_0)/\hbar} |\chi_{g0}\rangle. \tag{6.99}$$

This expression suggests a simple picture of the excitation process. From the initial time t_0 up to time $\bar{t}$, the initial vibrational state $|\chi_{g0}\rangle$ is propagated on the electronic ground state PES (t_0 has to be taken well before the pulse acts). Since the initial state is an eigenstate of H_g, one obtains the phase factor $\exp\{-iE_{g0}(\bar{t}-t_0)/\hbar\}$. The dynamics on the excited state PES starts at $\bar{t}$ and proceeds up to the actual time t. Note that the transition occurs *instantaneously*, which supports the picture of vertical transitions discussed in the introduction to this chapter. But the moment of transition to the excited state is not fixed; instead, an integration over all possible times $\bar{t}$ has to be performed. In which way the time $\bar{t}$ contributes depends on the amplitude of the pulse envelope. If the time t lies in the region where the pulse is present, Eq. (6.99) describes the preparation process. For larger times it shows how the optically prepared state develops further in the absence of the field.

To determine the $\bar{t}$-dependence of the integrand in Eq. (6.99), we switch to the representation given by the eigenstates $|\chi_{eM}\rangle$ of the excited state Hamiltonian H_e. The expansion of $|\chi_e(t)\rangle$ gives an example for a wave packet (see Eq. (3.24))

$$|\chi_e(t)\rangle = \sum_M c_{eM}(t) |\chi_{eM}\rangle. \tag{6.100}$$

The expansion coefficients are obtained as ($\omega_{aM} = E_{aM}/\hbar$)

$$c_{eM}(t) = \langle \chi_{eM} | \chi_e(t) \rangle$$

$$= i\frac{\boldsymbol{n}\boldsymbol{d}_{eg}A}{\hbar}\; e^{-i\omega_{eM}t} \int_{t_0}^{t} d\bar{t}\; e^{i(\omega_{eM}-\omega_{g0}-\omega)\bar{t}}\, f(\bar{t})$$

$$\times e^{i\omega_{g0}t_0} \langle \chi_{eM} | \chi_{g0} \rangle. \tag{6.101}$$

The magnitude of the expansion coefficients is determined by the Franck–Condon factors $\langle \chi_{eM} | \chi_{g0} \rangle$ and by a certain time integral. If we let $t_0 \to -\infty$ and take t at a time at which the pulse has already passed through the sample ($t \gg t_p$), the time integral reduces to the Fourier-transformed pulse envelope $f(\Omega)$, with $\Omega = \omega_{eM} - \omega_{g0} - \omega$. Thus, the different vibrational states $|\chi_{eM}\rangle$ of the expansion, (6.100) are weighted according to the form of the Fourier-transformed pulse envelope. For the Gaussian-shaped envelope, Eq. (6.93), we get

$$f(\Omega) = \int_{-\infty}^{+\infty} d\bar{t}\; e^{i\Omega\bar{t}} \frac{1}{\sqrt{2\pi\tau_p^2}} \exp\left\{ -\frac{(\bar{t}-t_p)^2}{2\tau_p^2} \right\} = e^{-\Omega^2\tau_p^2/2}\; e^{i\Omega t_p}. \tag{6.102}$$

This function becomes maximal for $\Omega \approx \omega_{eM} - \omega_{g0}$ (vertical Franck–Condon transition) and goes to zero for values of Ω that are larger than the inverse pulse duration $1/\tau_p$. Apparently, the shorter the pulse duration, the larger its spectral width.

6.5.1.1   Case of Short Pulse Duration

In order to populate vibrational levels away from the vertical Franck–Condon transition, the inverse pulse duration $1/\tau_p$ has to cover the respective frequency difference on the excited state PES. If a sufficient range of vibrational levels is covered, a transfer of the complete ground state wave function $\chi_{g0}(q)$ to the excited electronic state becomes possible. This picture can be idealized in the limit of impulsive excitation ($\tau_p \to 0$), where one replaces the pulse envelope by a delta function. Then, the expansion coefficients introduced in Eq. (6.101) read ($t > t_p$)

$$c_{eM}(t) = i\frac{\boldsymbol{nd}_{eg}A}{\hbar}\, e^{-i\omega_{eM}(t-t_p)}\, e^{-i\omega t_p}\, e^{-i\omega_{g0}(t_p-t_0)}\, \langle \chi_{eM}|\chi_{g0}\rangle. \tag{6.103}$$

A vibrational wave packet is formed on the excited state PES, which results from a projection of the initial state $|\chi_{g0}\rangle$ onto the excited state PES at time t_p. The related population of the vibrational levels is exclusively determined by the Franck–Condon factors,

$$P_{eM}(t) = |c_{eM}(t)|^2 = \theta(t-t_p)\frac{1}{\hbar^2}|\boldsymbol{nd}_{eg}A|^2\, |\langle \chi_{eM}|\chi_{g0}\rangle|^2. \tag{6.104}$$

It is also of interest to obtain the total electronic occupation probability, $P_e(t)$, transferred to the excited state. It can be calculated from Eq. (6.104) or directly from Eq. (6.99) as $P_e(t) = \langle\Psi^{(1)}(t)|\phi_e\rangle\langle\phi_e|\Psi^{(1)}(t)\rangle$. According to the case of impulsive excitation, one gets

$$P_e(t) = \sum_M |c_{eM}(t)|^2 = \frac{\theta(t-t_p)}{\hbar^2}|\boldsymbol{d}_{eg}\boldsymbol{E}(t_p)\tau_p|^2. \tag{6.105}$$

Note that we wrote $\boldsymbol{E}(t_p)\tau_p$ instead of using the amplitude A. This corresponds to the more realistic case of a finite but still short pulse duration. The expression shows the dependence on the field intensity via the factor $|\boldsymbol{E}|^2$. Note that $|\boldsymbol{E}|^2$ has to be small enough to guarantee that $P_e \ll 1$ as required for the perturbational treatment.

6.5.1.2   Case of Long Pulse Duration

Upon increasing τ_p, the Fourier-transformed envelope $f(\Omega)$ concentrates around the vertical Franck–Condon transition region, and for a very long pulse ($\tau_p \to \infty$), we obtain $f(\Omega) = \sqrt{2\pi}\tau_p\delta(\Omega)$. An optical excitation is only possible for $\omega = \omega_{eM} - \omega_{g0}$, which corresponds to the condition found in the previous section for stationary linear absorption.

6.5.2   Density Matrix Formulation

In this section, we generalize the results of the previous section and formulate the optical preparation of an excited state via the density matrix, $\rho_{aM,bN}(t)$, given in a representation with respect to the electron–vibrational states. In the preceding section, we obtained a nonvanishing excited state population, P_e, indicating that density matrix elements *diagonal* in the excited state electronic quantum numbers and proportional to the field intensity have to be considered. Concerning the vibrational quantum numbers, however, diagonal as well as off-diagonal elements may appear (Figure 6.12).

Figure 6.12 Population of an excited state PES via an ultrashort laser pulse. In the Franck–Condon transition region, the wave packet is shown for the case of an impulsive preparation. The distribution $f(\Omega)$, Eq. (6.102), is drawn on the right versus the frequency around the Franck–Condon transition region. The cases of a shorter laser pulse (full line) and longer pulse (dashed line) are given. Note that the actual excitation probability also depends on the Franck–Condon factors.
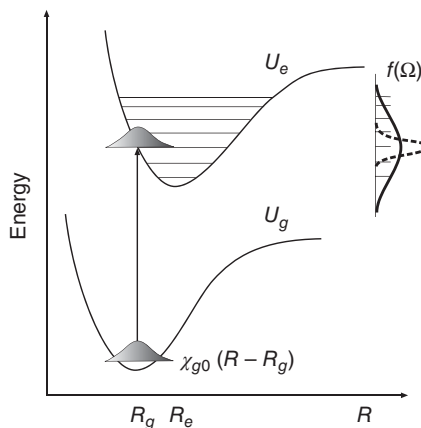
Let us consider the density matrix taken with respect to electronic states only,

$$\hat{W}_{ab}(t) = \langle \phi_a | \hat{W}(t) | \phi_b \rangle, \tag{6.106}$$

which is still an operator in the state space of the vibrational DOFs. The equations of motion obtained from the general equation (3.149) reads

$$\frac{\partial}{\partial t} \hat{W}_{ab} = -\frac{i}{\hbar}(H_a \hat{W}_{ab} - \hat{W}_{ab} H_b)$$
$$+ \frac{i}{\hbar} \sum_c \left(\boldsymbol{d}_{ac} \boldsymbol{E}(t) \hat{W}_{cb} - \boldsymbol{d}_{cb} \boldsymbol{E}(t) \hat{W}_{ac} \right). \tag{6.107}$$

Writing down the equation of motion for the desired density operator elements $\hat{W}_{ee}$ gives a contribution linear in $\boldsymbol{E}(t)$, which is also proportional to $\hat{W}_{eg}$ (and the hermitian conjugate expression). The solution reads (the U_a denote the time-evolution operators defined by the vibrational Hamiltonian H_a, and we assume that $\hat{W}_{ee}(t_0) = 0$)

$$\hat{W}_{ee}(t) = -\frac{i}{\hbar} \int\limits_{t_0}^{t} d\bar{t} \left(\boldsymbol{d}_{ge} \boldsymbol{E}(\bar{t}) U_e(t - \bar{t}) \hat{W}_{eg}(\bar{t}) U_e^+(t - \bar{t}) - \text{h.c.} \right). \tag{6.108}$$

The equation for $\hat{W}_{eg}$ gives again contributions linear in the electric field strength, but now proportional to both types of diagonal density operators, that is $\hat{W}_{ee}$ *and* $\hat{W}_{gg}$. Since we are interested in the second order of perturbation theory with respect to $\boldsymbol{E}(t)$, we can use the zeroth-order approximation for these diagonal density operators. Thus, $\hat{W}_{ee} = 0$, and $\hat{W}_{gg} = \hat{R}_g$. The last quantity defines the thermal equilibrium of the vibrational coordinates in the electronic ground state (cf. Eq. (4.60)). Consequently, the electronic off-diagonal density operator reads

$$\hat{W}_{eg}(t) = \frac{i}{\hbar} \int\limits_{t_0}^{t} d\bar{t} \, \boldsymbol{d}_{eg} \boldsymbol{E}(\bar{t}) U_e(t - \bar{t}) \hat{R}_g U_g^+(t - \bar{t}). \tag{6.109}$$

If we insert this expression into Eq. (6.108), the excited state population linearized in the field intensity can be determined. In general, this requires the solution of a

double time integral. However, in the impulsive limit, the integrations can be performed analytically. We obtain the optically prepared electronic density matrix as

$$\hat{W}_{ee}(t_p) = \frac{1}{\hbar^2} |\boldsymbol{d}_{eg} \boldsymbol{E}(t_p) \tau_p|^2 \hat{R}_g. \tag{6.110}$$

Resulting from the impulsive excitation, the vibrational state in the electronic ground state, as represented by the ground state equilibrium density operator $\hat{R}_g$, is *instantaneously* transferred onto the excited electronic state. Therefore, Eq. (6.110) is a mixed-state generalization of Eq. (6.104). This becomes obvious if we note that $\hat{R}_g \propto \sum_M \exp\{-E_{gM}/k_B T\} |\chi_{gM}\rangle\langle\chi_{gM}|$. At low temperatures, it corresponds to the transfer of the ground state vibrational wave function to the excited state.

The initially prepared wave packet will move on the excited state PES. Provided that the time resolution in a pump–probe experiment is comparable to the time scale of this motion, the latter can be investigated in real time. This is illustrated in Figure 6.2, where the time evolution of the bond vibration of a diatomic molecule was observed after it has been prepared on an electronically excited state. Often, wave packet dynamics on electronically excited PES is influenced by nonadiabatic couplings. The resulting internal conversion dynamics is addressed in the following section.

6.6 Internal Conversion Dynamics

In Section 6.2.1, we already stressed the similarity of optical absorption and intramolecular electronic transitions induced by the nonadiabatic coupling (internal conversion). We focus on the latter in more detail now. If a higher lying singlet state S_n ($n > 1$) is excited, it is the internal conversion process that induces transitions to lower electronic states. Within this process the electronic excitation energy is distributed among the different vibrational DOFs. Since the radiation field does not take part in this type of transition, it is also called *radiationless*.[11]

If the internal conversion is slow compared to the time scale of vibrational relaxation within an electronic state, it can be characterized by a transition rate. This is the situation where the Golden Rule formula introduced in Chapter 3 can be applied. The respective rate will be calculated in the following section. If the nonadiabatic coupling becomes stronger, one cannot assume complete vibrational equilibrium for every step of the transition. In case that vibrational relaxation can be completely neglected, a description of ultrafast internal conversion in terms of wave functions becomes possible, as shown in Section 6.6.2. The intermediate case needs a more involved description. However, having followed the present discussion and in anticipation of Chapter 7 dealing with electron transfer, one realizes a number of similarities. Therefore, the subject of internal conversion dynamics is outlined only very briefly. More involved questions related to charge transfer dynamics will be discussed in the context of electron transfer reactions in Chapter 7.

---

11) *Kasha's rule* states that because of dominant internal conversion processes, any appreciable fluorescence from S_n states ($n > 1$) is absent in polyatomic molecules. However, even fluorescence from the S_1 state can be reduced by radiationless transitions to the ground state.

6.6.1 The Internal Conversion Rate

In order to describe internal conversion via a rate expression such as $k_{a \to b}^{(IC)}$, the characteristic time for the transition process $1/k_{a \to b}^{(IC)}$ must be long compared to any vibrational relaxation time scale (in the initial as well as in the final state of the transition, also compare the similar discussion on electron transfer reactions in Section 7.3). If this condition implies that the nonadiabatic coupling can be considered as a weak perturbation, we can follow the argument of Section 6.2.1. In analogy to Eq. (6.12), the rate of nonadiabatic transitions from state $|\phi_a\rangle$ to state $|\phi_b\rangle$ can be determined by a Golden rule expression. Before doing this, we briefly recall the Hamiltonian describing the system that undergoes an internal conversion process. In Chapter 2, we introduced the following notation for the molecular Hamiltonian (compare Eq. (2.97)):

$$H_{\text{mol}} = \sum_{a,b} (\delta_{ab} H_a + (1 - \delta_{ab}) \Theta_{ab}) |\phi_a\rangle\langle\phi_b|. \tag{6.111}$$

Here, H_a denotes the vibrational Hamiltonian for the adiabatic electronic state $|\phi_a\rangle$. The nonadiabatic coupling between different states is described by the nonadiabaticity operator Θ_{ab} acting on the nuclear coordinates. The Hamiltonian is similar to expression 6.4 but with Θ_{ab} replacing the interaction term, $-\boldsymbol{E}(t)\boldsymbol{d}_{ab}$.

According to the form of the molecular Hamiltonian, the internal conversion rate follows as

$$k_{a \to b}^{(IC)} = \frac{2\pi}{\hbar} \sum_{M,N} f_{aM} |\langle \chi_{aM} | \Theta_{ab} | \chi_{bN} \rangle|^2 \ \delta(E_{aM} - E_{bN}). \tag{6.112}$$

As indicated in Figure 6.4, the internal conversion process is a transition from an initial manifold E_{aM} of vibrational levels into the final manifold E_{bN}. Since there is no time-dependent external field involved, the argument in the delta function of Eq. (6.112) contains only the *bare* molecular transition frequencies (cf. Eq. (6.12)). For optical transitions, one often neglects the nuclear coordinate dependence of the electronic transition dipole moment (Condon approximation). A similar approximation, which replaces the operator Θ_{ab} by a constant (or by a certain averaged value $\overline{\Theta}_{ab}$ with respect to the nuclear coordinates), results here in the replacement of the full matrix element by the simpler expression $\overline{\Theta}_{ab}\langle\chi_{aM}|\chi_{bN}\rangle$. Introducing the zero-frequency DOS (see Eq. (6.15))

$$\mathcal{D}_{ab}(0) = \sum_{M,N} f_{aM} \ |\langle \chi_{aN} | \chi_{bM} \rangle|^2 \ \delta(E_{aM} - E_{bN}), \tag{6.113}$$

we can write

$$k_{a \to b}^{(IC)} = \frac{2\pi}{\hbar} |\overline{\Theta}_{ab}|^2 \mathcal{D}_{ab}(0). \tag{6.114}$$

As in the case of the absorption coefficient, the result for the zero-frequency DOS can be put into a more specific form if the model of parabolic PES is used. Then, we obtain (cf. Eq. (6.23))

$$\mathcal{D}_{ab}(0) = \frac{1}{2\pi\hbar} \int dt \, e^{i\omega_{ab}t + G_{ab}(t) - G_{ab}(0)}. \tag{6.115}$$

The function $G_{ab}(t)$ has been introduced in Eq. (6.24). The index "ab" indicates for which states the displacements enter in Eq. (6.24). This clearly demonstrates the formal analogy between the different transition processes as stressed above.

For illustration, let us consider the $T = 0$ K case. Here, we can use the result for the harmonic oscillator given in Eq. (6.31). For the present case, it reads ($\Delta g = g_b - g_a$)

$$D_{ab}(0) = e^{-\Delta g^2} \sum_{N=0}^{\infty} \frac{\Delta g^{2N}}{N!} \delta(\hbar(\omega_{ab} - N\omega_{\text{vib}})). \tag{6.116}$$

Next, we introduce $\overline{N} = \text{int}[\omega_{ab}/\omega_{\text{vib}}]$ as a measure for electronic energy gap and perform the summation. We obtain

$$D_{ab}(0) \approx \frac{1}{\hbar\omega_{\text{vib}}} e^{-\Delta g^2} \frac{\Delta g^{2\overline{N}}}{\overline{N}!}. \tag{6.117}$$

Provided that $\overline{N} \gg 1$, one can use Stirling's formula, that is

$$\overline{N}! \approx \sqrt{2\pi\overline{N}} \left(\frac{\overline{N}}{e}\right)^{\overline{N}} = \sqrt{2\pi\overline{N}} \exp[\overline{N}(\ln(\overline{N}) - 1)]. \tag{6.118}$$

Thus, we obtain the following expression for the DOS:

$$D_{ab}(0) \approx \frac{1}{\hbar\omega_{\text{vib}}\sqrt{2\pi\overline{N}}} e^{-\Delta g^2} \exp\{-\overline{N}[\ln(\overline{N}/\Delta g^2) - 1]\}. \tag{6.119}$$

For $\ln(\overline{N}/\Delta g^2) > 1$, a condition that is usually fulfilled, the DOS, and thus the rate $k_{a\to b}^{(\text{IC})}$, is an exponentially decaying function of the electronic energy gap ω_{ab}. This is called the *energy gap law*. It is the decisive factor in the competition between radiative and nonradiative deactivation processes of electronically excited states; an example is given in Figure 6.13.

6.6.2 Ultrafast Internal Conversion

In many organic molecules, the internal conversion process after photoexcitation proceeds on a time scale that is much shorter than any vibrational relaxation time. As already pointed out, it is possible to neglect in this ultrafast limit any vibrational energy dissipation and to describe the internal conversion process by the solution of the respective time-dependent Schrödinger equation. For the treatment of high-dimensional quantum dynamics on coupled electronic states the multiconfiguration time–dependent Hartree (MCTDH) method introduced in Section 3.2.3 provides an efficient and flexible tool. To accommodate the electronic state coupling, the total state vector is expanded as follows:

$$|\Psi(t)\rangle = \sum_a |\chi_a(t)\rangle|\phi_a\rangle. \tag{6.120}$$

For the vibrational wave functions on the electronic state $|\phi_a\rangle$, $\chi_a(q,t) = \langle q|\chi_a(t)\rangle$, an MCTDH ansatz can be made according to Eq. (3.59). From the MCTDH propagation, one then obtains, for instance $|\chi_a(t)\rangle$ and thus the electronic state population as

$$P_a(t) = \langle \chi_a(t)|\chi_a(t)\rangle. \tag{6.121}$$
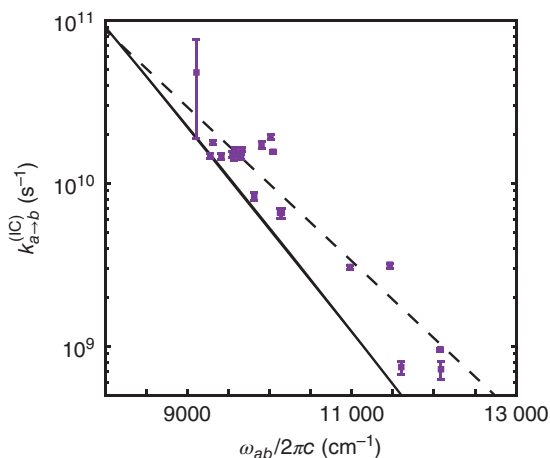
Figure 6.13 Experimental verification of the energy gap law, Eq. (6.119). The IC rate is shown as a function of the energy gap (semilogarithmic scale) for a series of chromophores (flavylium and chromenylium heptamethine and pentamethine fluorophores as well as two laser dyes). The dashed line gives a linear fit according to the energy gap law. The solid line corresponds to the case of a vibrational mode at 3000 cm^{-1}, indicating that high-frequency modes beyond 3000 cm^{-1} are dominating the IC process (figure courtesy of J.R. Caram, for more details, see also Friedman et al. [6]).

MCTDH quantum dynamics calculations according to Section 3.2.3 require the *a priori* knowledge of PES. Here, the diabatic representation is commonly used. According to Eq. (2.103), the molecular Hamiltonian in diabatic representation can be written as (skipping the "overbar notation")

$$H_{\text{mol}} = \sum_{ab} \left(\delta_{ab} H_a(q) + (1 - \delta_{ab}) V_{ab}(q) \right) |\phi_a\rangle\langle\phi_b|. \tag{6.122}$$

Following the discussion of this section, we assume that the diabatic PESs are harmonic with state-independent frequencies. It is customary to approximate the diagonal part as follows:

$$H_a(Q) = T_{\text{nuc}} + U_a(q_\xi = 0) + \frac{1}{2} \sum_\xi \omega_\xi^2 q_\xi^2 + \sum_\xi \kappa_{a,\xi} q_\xi + \dots \tag{6.123}$$

Here, the normal-mode Hamiltonian, Eq. (2.43), is supplemented by an electronic state-dependent Taylor expansion of the PES in terms of normal mode coordinates. The coupling parameter $\kappa_{a,\xi}$ is given by the derivative of the PES with respect to q_ξ, taken at $q_\xi = 0$ (ground state equilibrium configuration).[12]

The diabatic state coupling $V_{ab}(q)$ is also expanded in terms of the normal mode coordinates, that is

$$V_{ab}(q) = V_{ab}^{(0)} + \sum_\xi \lambda_{ab,\xi} q_\xi + \dots \tag{6.124}$$

----

12) Notice that in linear order this expression is identical to Eq. (2.51). This holds because for the model of shifted oscillators, the vertical excitation energy in Eq. (6.123) and the adiabatic excitation energy in Eq. (2.51) are related via $U_a(q_\xi = 0) = U_a(q_\xi^{(a)}) + (1/2)\sum_\xi \omega_\xi^2 q_\xi^{(a)\,2}$.

Here, $V_{ab}^{(0)} = V_{ab}(q_\xi = 0)$ is a constant coupling, and the parameter $\lambda_{ab,\xi}$ is given by the derivative of V_{ab} with respect to q_ξ, taken at $q_\xi = 0$. Equation (6.122) with H_a and V_{ab} approximated in linear order with respect to q_ξ defines the *linear vibronic coupling* (LVC) Hamiltonian. The modes leading to a displacement of the PES and thus to a modification of the energy gap between electronic states ($\kappa_{a,\xi} \neq 0$) are called *tuning modes*. Modes triggering diabatic state coupling ($\lambda_{ab,\xi} \neq 0$) are called *coupling modes*. In case of molecules having a certain symmetry, tuning and coupling modes are totally and nontotally symmetric, respectively. For two coupled states, the adiabatic PESs of the LVC model along a tuning and a coupling mode form a conical intersection (cf. Figure 2.13).

In cases where a low-order expansion of the PES is not appropriate (for instance, for dissociation or isomerization reactions) and also for larger molecules or molecules embedded in some environment, quantum dynamics simulations become unfeasible, and one has to resort to methods based on classical trajectories such as surface hopping (see Section 3.13.2). Surface hopping simulations are performed in the adiabatic representation and do not require an *a priori* determination of the PES.

Figure 6.14 shows a comparison of results of MCTDH and surface hopping simulations for the same three electronic state plus nine vibrational modes model of pyrazine. Initially, the system is prepared in the B_{2u} state. The population of this state rapidly decays within the first 50 fs via transfer to the A_{1u} and, to a lesser extent, to the B_{3u} state. The latter two states show a population exchange that reminds of the two-state dynamics in Figure 3.8. This sequence of events is determined by the location of the potential curve crossings ($\kappa_{a,\xi}$) and state couplings $\lambda_{ab,\xi}$; cuts of the PES along the tuning modes are given in Figure 6.14a–d. For this model, MCTDH and surface hopping simulations give rather similar results.

6.7 Supplement

6.7.1 Absorption Coefficient for Displaced Harmonic Oscillators

In this section, we show how to simplify expression (6.19) for the lineshape function $D_{\text{abs}}(\omega)$ of linear absorption, if the two vibrational Hamiltonians H_g and H_e describe independent harmonic oscillators (normal mode vibrations). The derivation will be particularly illuminating since the model is exactly solvable. For simplicity, the normal mode oscillators should not change their vibrational frequencies if the electronic state changes but merely attain a new equilibrium position (see Section 2.5.1 and Figure 2.8). Using the displacement operator (cf. Eq. (2.69))

$$D_a^+ = \exp\left\{ \sum_\xi g_a(\xi)(C_\xi - C_\xi^+) \right\} \equiv \prod_\xi D_\xi^+(g_a(\xi)), \tag{6.125}$$

the two vibrational Hamiltonians can be generated from the Hamiltonian of a non-shifted oscillator,

$$H_a = U_a^{(0)} + D_a^+ H_{\text{vib}} D_a. \tag{6.126}$$
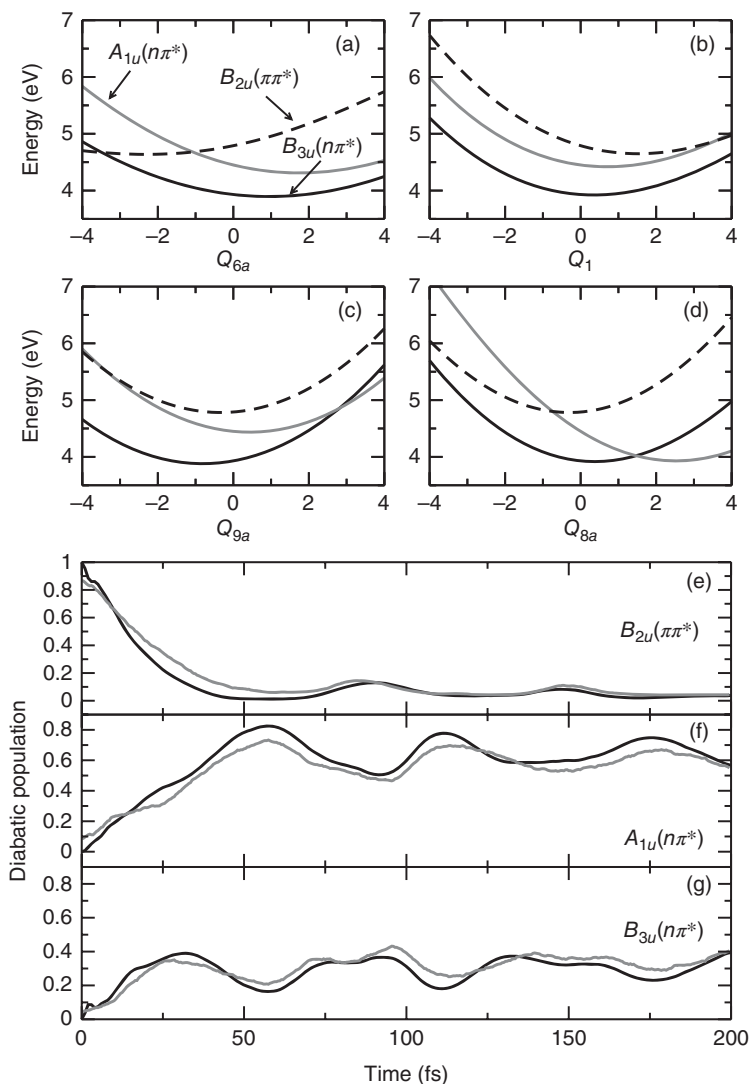
Figure 6.14 Ultrafast internal conversion dynamics in a three electronic state plus nine vibrational modes model of pyrazine. (a–d) Cuts of the diabatic PES along the four totally symmetric tuning modes. The five nontotally symmetric coupling modes (not shown) lead to conical intersections of the adiabatic PES in analogy to Figure 2.13. (e–g) Population dynamics after initial excitation of the B_{2u} state, calculated using MCTDH (black line) and trajectory surface hopping (gray line) as introduced in Sections 3.2.3 and 3.13.2, respectively (figure courtesy of N. Došˇ lić; for more details, see also Xie et al. [7]).

Here,

$$H_{\text{vib}} = \sum_{\xi} \hbar\omega_{\xi}(C_{\xi}^{+}C_{\xi} + 1/2) \tag{6.127}$$

denotes the *reference* vibrational Hamiltonian. Accordingly, the trace formula introduced in Eq. (6.19) can be rewritten as (the statistical operator $\hat{R}_g$ is given in Eq. (4.60))

$$\text{tr}_g\{\hat{R}_g \ e^{iH_g t/\hbar} \ e^{-iH_e t/\hbar}\} = e^{-i\omega_{eg}t} \ \text{tr}_{\text{vib}}\{D_g \ D_g^+ \ \hat{R}_{\text{vib}} \ D_g \ D_g^+ \ e^{iH_{\text{vib}}t/\hbar}$$

$$\times D_g \ D_e^+ e^{-iH_{\text{vib}}t/\hbar} D_e \ D_g^+\}$$

$$= e^{-i\omega_{eg}t}$$

$$\times \text{tr}_{\text{vib}}\{\hat{R}_{\text{vib}} \ e^{iH_{\text{vib}}t/\hbar} \ D_g D_e^+ e^{-iH_{\text{vib}}t/\hbar} D_e D_g^+\}$$

$$= e^{-i\omega_{eg}t} \ \text{tr}_{\text{vib}}\{\hat{R}_{\text{vib}} \ e^{iH_{\text{vib}}t/\hbar} \ D_{ge} e^{-iH_{\text{vib}}t/\hbar} D_{ge}^+\}. \tag{6.128}$$

Here, we have used the notations tr_g and tr_{vib} to distinguish between the trace taken with respect to the electronic ground state vibrations and the eigenstates $|N\rangle$ of the *nondisplaced* reference Hamiltonian H_{vib}, respectively. Additionally, we introduced $\hbar\omega_{eg} = U_e^{(0)} - U_g^{(0)}$,

$$\hat{R}_{\text{vib}} = \frac{\exp\{-H_{\text{vib}}/k_B T\}}{\text{tr}\{\exp() - H_{\text{vib}}/k_B T)\}} \equiv \frac{1}{\mathcal{Z}} e^{-H_{\text{vib}}/k_B T}, \tag{6.129}$$

and the combined displacement operator

$$D_{ge} = D_g D_e^+. \tag{6.130}$$

Using the Heisenberg representation of D_{ge}, which is given by

$$D_{ge}(t) = e^{iH_{\text{vib}}t/\hbar} \ D_{ge} e^{-iH_{\text{vib}}t/\hbar}, \tag{6.131}$$

the trace formula becomes

$$T(t) = \text{tr}_g\{\hat{R}_g \ e^{iH_g t/\hbar} \ e^{-iH_e t/\hbar}\} = e^{-i\omega_{eg}t} \ \text{tr}_{\text{vib}}\{\hat{R}_{\text{vib}} \ D_{ge}(t)D_{ge}^+(0)\}. \tag{6.132}$$

This is the autocorrelation function of the combined displacement operators taken with respect to the equilibrium of the nondisplaced reference oscillators.

Since we are dealing with normal mode oscillators, there is no coupling among the modes. The vibrational Hamiltonian H_{vib} is additive with respect to the mode index ξ, and the vibrational state $|N\rangle$ factorizes into the single oscillator states $|N_\xi\rangle$. As a result, the trace in Eq. (6.132) factorizes into single-mode traces

$$T(t) = \prod_\xi T_\xi(t). \tag{6.133}$$

Therefore, we can deal in what follows with a single-mode contribution $T_\xi(t)$ to the complete trace. To simplify the notation, the mode index ξ will be dropped, and ω_ξ is replaced by ω_{vib}. First, we note that

$$D_{ge} = D(g_g) \ D^+(g_e) = D(g_g - g_e) = D(\Delta g), \tag{6.134}$$

where $\Delta g = g_g - g_e$. The time-dependent displacement operator appearing in Eq. (6.132) (the single-mode contribution to it) can be written as

$$D_{ge}(t) = D(\Delta g; t) = e^{i\omega_{\text{vib}} C^+ C t} \ D(\Delta g) \ e^{-i\omega_{\text{vib}} \ C^+ C t}$$

$$= \exp\{-\Delta g(Ce^{-i\omega_{\text{vib}}t} - C^+ e^{i\omega_{\text{vib}}t})\}. \tag{6.135}$$

Consequently, the single-mode contribution to the trace reads ($\mathcal{Z}$ is the single-mode partition function)

$$T_\xi(t) = \frac{1}{\mathcal{Z}_\xi}\sum_N \langle N| \ e^{-\hbar\omega_{\text{vib}}N/k_B T} \ D(\Delta g; t) \ D^+(\Delta g; 0)|N\rangle. \tag{6.136}$$

For the further treatment of this expression, we make use of Eq. (2.76)) and utilize the relation

$$\mathcal{M}(N) = \langle N|D(\Delta g; t)\, D^+(\Delta g; 0)\, |N\rangle$$
$$= \langle N|e^{-\alpha(t)C + \alpha^*(t)C^+}\, e^{\alpha(0)C - \alpha^*(0)C^+}|N\rangle, \tag{6.137}$$

with $\alpha(t) = \Delta g \exp(-i\omega_{\mathrm{vib}} t)$. We can write

$$\mathcal{M}(N) = \langle N|e^{-|\alpha(t)|^2/2}\, e^{\alpha^*(t)\, C^+}\, e^{-\alpha(t)\, C}\, e^{-|\alpha(0)|^2/2}\, e^{-\alpha^*(0)\, C^+}\, e^{\alpha(0)\, C}|N\rangle$$
$$= e^{-\frac{1}{2}(|\alpha(t)|^2 + |\alpha(0)|^2)}$$
$$\times \langle N|e^{\alpha^*(t)\, C^+}\, e^{\alpha(t)\, \alpha^*(0)}\, e^{-\alpha^*(0)\, C^+}\, e^{-\alpha(t)\, C}\, e^{\alpha(0)\, C}\, |N\rangle$$
$$= e^{-\frac{1}{2}(|\alpha(t)|^2 + |\alpha(0)|^2 - 2\alpha(t)\alpha^*(0))}$$
$$\times \langle N|e^{(\alpha^*(t) - \alpha^*(0))C^+}\, e^{-(\alpha(t) - \alpha(0))C}\, |N\rangle. \tag{6.138}$$

Next, we introduce the abbreviation $\Delta\alpha(t) = \alpha(t) - \alpha(0) = \Delta g(\exp(-i\omega_{\mathrm{vib}} t) - 1)$ and take into account that

$$|\alpha(t)|^2 + |\alpha(0)|^2 - 2\alpha(t)\,\alpha^*(0) = |\Delta\alpha(t)|^2 - 2\,i\,\mathrm{Im}(\alpha(t)\,\alpha^*(0)). \tag{6.139}$$

Then, we obtain the normal ordering of the original matrix elements in the trace formula as

$$\langle N|D(\Delta g; t)\, D^+(\Delta g; 0)|N\rangle = \exp\left\{-|\Delta\alpha|^2/2 - i\,\mathrm{Im}(\alpha^*(t)\,\alpha(0))\right\}$$
$$\times \langle N|e^{\Delta\alpha^* C^+}\, e^{-\Delta\alpha C}|N\rangle. \tag{6.140}$$

To determine the oscillator matrix elements, we use Eqs. (2.78)–(2.80) and obtain for Eq. (6.136)

$$T_\xi(t) = (1 - e^{-\hbar\omega_{\mathrm{vib}}/k_{\mathrm{B}} T})\, e^{-z/2 - i\mathrm{Im}\,(\alpha^*(t)\alpha(0))} \sum_{N=0}^{\infty} e^{-\hbar\omega_{\mathrm{vib}} N/k_{\mathrm{B}} T}\, L_N(z). \tag{6.141}$$

Note the introduction of $z = |\Delta\alpha(t)|^2$ and of the Laguerre polynomial $L_N(z)$ of order N (cf. Eq. (2.80)). The relation between the Laguerre polynomials and their generating function,

$$\sum_{N=0}^{\infty} \lambda^N\, L_N(z) = \frac{1}{1 - \lambda}\, e^{-\lambda z/(1-\lambda)} \qquad (|\lambda| < 1), \tag{6.142}$$

results in $T_\xi(t) = \exp\{E_\xi(t)\}$, with

$$E_\xi(t) = -z/2 - i\mathrm{Im}(\alpha^*(t)\,\alpha(0)) - \frac{e^{-\hbar\omega_{\mathrm{vib}}/k_{\mathrm{B}} T}}{1 - e^{-\hbar\omega_{\mathrm{vib}}/k_{\mathrm{B}} T}} z. \tag{6.143}$$

The Bose–Einstein distribution $n(\omega_{\mathrm{vib}})$ (cf. Section 3.7.1) allows us to rewrite the last term of the exponent. The final result for $T_\xi(t)$ will be obtained if the exponent is rearranged with respect to $\Delta\alpha(t)$ and $\Delta\alpha^*(t)$ according to

$$E_\xi(t) = -z/2 - i\,\mathrm{Im}\,\alpha^*(t)\alpha(0) - n(\omega_{\mathrm{vib}})z$$
$$= -\frac{1}{2}\left(1 + 2n(\omega_{\mathrm{vib}})\right)\Delta g^2(2 - e^{i\omega_{\mathrm{vib}} t} - e^{-i\omega_{\mathrm{vib}} t})$$

$$-\frac{1}{2}\Delta g^2 \left(e^{i\omega_{\text{vib}}t} - e^{-i\omega_{\text{vib}}t}\right)$$

$$= \frac{\Delta g^2}{2} \left(2\left(1 + n(\omega_{\text{vib}})\right)(e^{-i\omega_{\text{vib}}t} - 1) + 2n(\omega_{\text{vib}})(e^{i\omega_{\text{vib}}t} - 1)\right). \tag{6.144}$$

The result contains two terms $E_\xi(t) = -G_\xi(0) + G_\xi(t)$, with

$$G_\xi(t) = \Delta g^2(\xi) \left[e^{-i\omega_\xi t}(1 + n(\omega_\xi)) + e^{i\omega_\xi t}n(\omega_\xi)\right]. \tag{6.145}$$

The complete trace is the product with respect to the various single-mode contributions $T_\xi(t)$; hence, the total exponent is determined by

$$G(t) = \sum_\xi G_\xi(t). \tag{6.146}$$

This *exact* result is used in the definition of the DOS, Eq. (6.23).

References

1 T. Baumert et al., Phys. Rev. Lett. **67**, 3753 (1991).

2 H. U. Suter et al., J. Chem. Phys. **96**, 6727 (1992).

3 S. A. Egorov et al., J. Chem. Phys. **108**, 1407 (1998).

4 N. E. Shemetulskis and R. F. Loring, J. Chem. Phys. **97**, 1217 (1992).

5 S. Karsten et al., J. Chem. Phys. **148**, 102337 (2018).

6 H. C. Friedman et al., Chem **7**, 1 (2021).

7 W. Xie et al., J. Chem. Phys. **150**, 154119 (2019).

Further Reading

- Wave packet motion and linear spectroscopy of small molecules:
  R. Schinke, *Photodissociation Dynamics*, (Cambridge University Press, Cambridge, 1993).
- Electronic structure and dynamics of electronically excited states:
  L. González and R. Lindh (eds.), *Quantum Chemistry and Dynamics of Excited States: Methods and Applications*, (John Wiley & Sons, Hoboken, NJ, 2021).
  M. Persico and G. Granucci, *Photochemistry*, (Springer Nature, 2018).
- Application of semiclassical theory to spectroscopy:
  E. J. Heller, *The Semiclassical Way to Dynamics and Spectroscopy*, (Princeton University Press, Princeton, NJ, 2018).
- Nonadiabatic dynamics in chemical reactions:
  K. Takatsuka, T. Yonehara, K. Hanasaki, and Y. Arasaki, *Chemical Theory Beyond the Born–Oppenheimer Paradigm*, (World Scientific, Hoboken, New Jersey, 2015).
  D. R. Yarkony, W. Domcke, and H. Köppel (eds.), *Conical Intersections. Theory, Computations, and Experiment*, (World Scientific, Teaneck, 2011).

7

Electron Transfer

Spatial electronic charge redistribution in single molecules as well as in molecular complexes will be described. The charge transfer process occurs as a spontaneous transition from a metastable initial state to a stable final state. The initial state is prepared either by photoabsorption or charge injection from external sources. The electronic transition can be understood as a tunneling process through barriers separating different localization centers of the moving electron. This causes a modification of the electrostatic field in the molecule, which leads to a change in the nuclear equilibrium configuration. To develop an understanding for the interplay between electron transfer and the accompanying nuclear rearrangement is the principal aim of electron transfer theories.
Different transfer regimes will be discussed, which are distinguished by the time scales for electronic and nuclear motion. The limits of classical and quantum mechanical descriptions of the nuclear dynamics are described, and appropriate rate expressions will be derived. The specialty of heterogeneous electron transfer is explained where charge exchange between a molecule and a metal or semiconductor surface to which the molecule has been attached is of interest. Here, current formation through a molecule is explained, which is contacted by two nanoelectrodes and subject to an applied voltage. Finally, ultrafast photoinduced electron transfer is introduced as a phenomenon whose theoretical description is beyond a simple rate equation.

7.1 Classification of Electron Transfer Reactions

Electron transfer (ET) is one of the basic types of chemical processes. It represents the initial step of a number of reactions such as the making and breaking of chemical bonds and the change in molecular conformations (Figure 7.1). In all fields of inorganic, organic, and biochemistry, ET reactions are common. For example, corrosion is caused by the ET between a metal surface and oxygen. ET is also an important part of many photocatalytic reactions such as those leading to water splitting (Figure 7.2). In biological systems, ET reactions are a basic step of enzymatic activity in the living cells of bacteria, plants, and animals. ET in proteins or protein

$$\text{Na} + \langle\bigcirc\rangle\text{-CH}_2\text{-Br} \longrightarrow \text{Na}^+ + \langle\bigcirc\rangle\text{-CH}_2^{\bullet} + \text{Br}$$
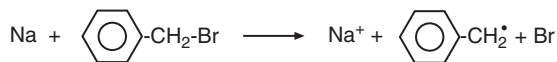
Figure 7.1 ET from sodium to benzyl halide resulting in bond breaking and benzyl halide radical formation.
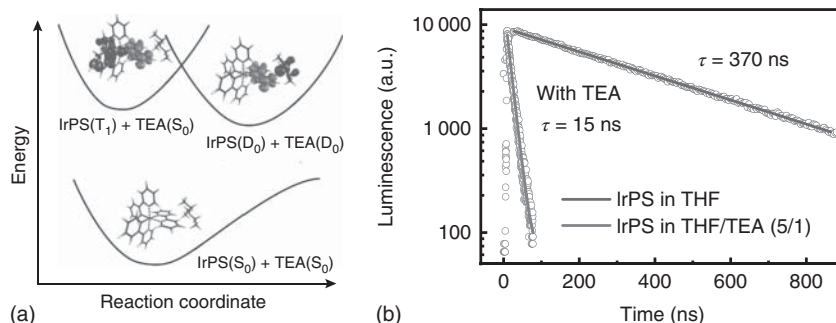
Figure 7.2 Photoinduced ET from triethylamine (TEA) to IrPS ([Ir(ppy)$_2$(bpy)]$^+$), which form an encounter complex in tetrahydrofuran solution. IrPS acts as a photosensitizer within an iron-based photocatalytic system. (a) Initially, IrPS is photoexcited into a charge-separated triplet state (the difference electron density of this metal to ligand charge transfer state is shown with respect to the ground state density). The hole at the metal center is filled by ET from TEA. (b) ET leads to a reduction in the photoluminescence lifetime τ in dependence on the TEA concentration (for further details, see Neubauer et al. [1]).

complexes plays an important role in the cell metabolism and energy balance. ATP, for instance, is produced in oxidative phosphorylation where NADH releases electrons.[1] These are captured by dioxygen to form water; the total process generates a large amount of excess energy. Another prominent example is given by the electron transferring system of photosynthesis. Here, a transmembrane potential is created that supports a proton pump to produce ATP. ET in the reaction center of purple bacteria has been unraveled on an atomic length scale and a time scale down to the femtosecond region (Figure 7.3).

To give a working definition of ET, we characterize it as a *spontaneous* charge redistribution between an initially prepared reactant state and a well-defined product state. ET reactions proceed in such a manner that the transferred electron remains in a bound state with respect to the particular molecule or molecular system. In other words, the electron is *not* activated above the ionization threshold and in this way transferred to a different region of the molecular complex. This means that ET reactions occur as *tunneling processes*; the reaction barriers, which the moving electron experiences, are penetrated via tunneling.[2]

---

1) ATP is the abbreviation for adenosine triphosphate, the compound that acts as an energy storage in any living system. NADH stands for nicotinamide adenine dinucleotide, which plays an important role in respiration.
2) This definition of ET excludes processes in biological systems where special enzymes act as charge carriers transporting electrons over large spatial distances.

Figure 7.3 Chromophores of the photosynthetic bacterial reaction center (side group capped) of *Rhodobacter sphaeroides*. After excitation of the special pair of coupled bacteriochlorophyll molecules (P), ET proceeds along the left branch via bacteriochlorophyll B_A, bacteriopheophytin H_A, and ubiquinone Q_A to Q_B. The initial two-step charge separation to form $P^+H_A^-$ is nearly 100% efficient and takes less than 10 ps (Figure courtesy of A. Ahmed; adapted from Protein Data Bank, 1PCR).
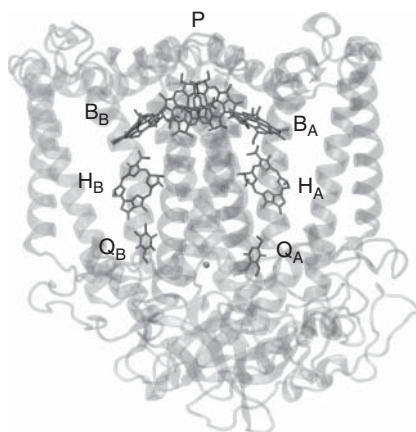
In this respect, it is important to note that the motion of the considered electron does *not* take place while the configuration of the other electrons is fixed. Instead, the electronic wave function changes from that describing the reactant state (ϕ_{rea}) to that of the product state (ϕ_{pro}), cf. Figure 7.2. According to the ansatz, (2.26) introduced in Section 2.4, we may say that in principle all molecular orbitals (MOs) of the system will be modified during this transition. This change can be characterized by the electronic charge density ($a = $ rea, pro)

$$\varrho_a^{(\text{el})}(\boldsymbol{r}) = eN_{\text{el}}\left(\prod_{r_j \neq r} \int d^3\boldsymbol{r}_j\right)|\phi_a(\{\boldsymbol{r}_j\})|^2, \tag{7.1}$$

which is the probability distribution for the N_{el} electrons reduced to a *single*-particle density. Although the whole electronic wave function changes in the course of the ET, in many reactions the change in the electronic charge density corresponds to the change induced by a single electron. Therefore, it is often sufficient to discuss ET as the result of the transition of a *single* electron from an initial MO (*donor* state) to the MO of the final state (*acceptor* state).

Due to the change in the electronic charge distribution during an ET reaction, the internal electrostatic field of the molecular complex is modified. This in turn causes new equilibrium positions of the nuclei. First, when mentioning the nuclei, we have in mind those of the considered molecule. If the environment is polarizable as it is the case for a polar solvent, a polarization and rearrangement of the solvent molecules may take place too. Hence, an ET reaction (as any other change in the electronic state of the molecule) is accompanied by a change in the equilibrium configuration of the nuclei. This process may be viewed as the motion of the electron carrying along a polarization cloud with respect to the surrounding molecular structure.

There is some apparent similarity between intramolecular electronic transitions, induced by the radiation field or by the nonadiabatic coupling, discussed in Chapter 6, and the ET reaction. Therefore, one expects that in the case of ET also there exists a coupling between the reactant and the product state. If this interstate
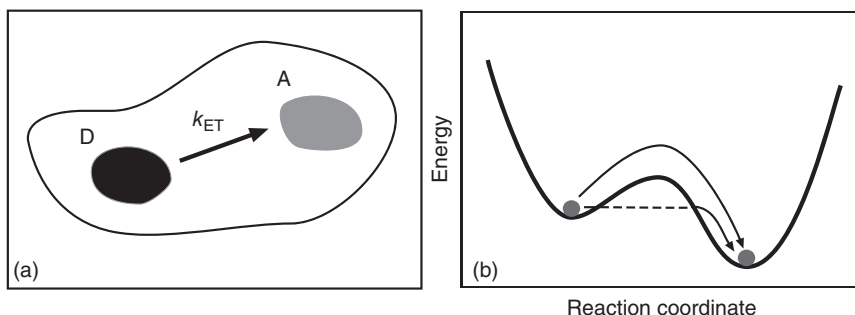
Figure 7.4 (a) ET in a schematically drawn DA complex. The initial and final spatial localizations of the electron are shown by the hatched areas (k_{ET} denotes the transfer rate). (b) Double-well potential versus reaction coordinate, which can be some collective nuclear coordinate triggering the adiabatic ET. In the initial state of the ET reaction the system is localized in the left metastable well. It can reach the right stable state by crossing the barrier (full line) or by tunneling through the barrier (broken line).

coupling V is small, one is in the limit of *nonadiabatic* ET. The opposite case is called *adiabatic* transfer. These terms, and also the meaning of a small or large coupling, will be explained in more detail below. At the moment, we only state that in most cases nonadiabatic ET can be understood as a particular type of *spatial* charge redistribution, as shown in Figure 7.4a.

In the reactant state, the transferred electron is localized at the electron donor part of the molecular system (it occupies the donor MO). From the donor it moves to the acceptor region, where it is in some spatially localized acceptor MO (product state).

In contrast, the adiabatic ET is *not* connected with a characteristic spatial redistribution of charge. It is usually described in terms of chemical reaction kinetics for which the double-well potential provides a good model (Figure 7.4b). In this approach, the internal energy of the reaction (or if entropic effects are important, the free energy) is considered in dependence on a reaction coordinate, which is a particularly chosen collective coordinate for the nuclei (cf. Section 2.5.3). The metastable initial (reactant) state and the stable final (product) state are separated by a potential barrier along this reaction coordinate. To overcome this barrier the reaction requires thermal activation. Alternatively, a tunneling transition through the barrier is possible. This is in contrast to the electron motion, which occurs exclusively via a tunneling process.

Given the definition of the donor (D) and acceptor (A) states of a molecular system, the ET reaction is most simply characterized by the following scheme:

$$D^- A \rightarrow DA^-. \tag{7.2}$$

D^- means that in the reactant state there is a so-called *excess* electron localized at the donor. After the electron has moved to the acceptor, the product state is formed.

This basic event can occur in different variants, and numerous generalizations are possible. First, we have to distinguish whether or not the donor and the acceptor belong to the same molecule. In the first case, the reaction is called *intramolecular* ET or alternatively *unimolecular* ET. In contrast, if at least two distinct molecules are

Figure 7.5 ET reaction of an excess electron in a HOMO–LUMO scheme of a DA complex with spatial donor position x_D and acceptor position x_A. The reactant state electron configuration is shown. The curved arrow indicates the pathway the transferred electron takes toward the product state.
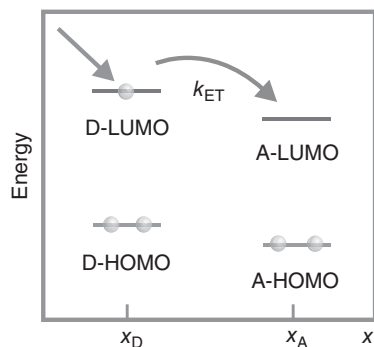
involved, the reaction is called *intermolecular* ET or *bimolecular* ET. Independent of this distinction, the common structure formed by the donor and the acceptor that enables the ET is called donor–acceptor (DA) *complex*.

In Figure 7.5, the energy level diagram is shown for the ET reaction according to Scheme (7.2). We concentrate on the highest occupied molecular orbital (HOMO) (cf. Section 2.4) as well as the lowest unoccupied molecular orbital (LUMO) of the DA complex (remember that these states have to be computed in a self-consistent way, as explained in Section 2.4). The excess electron initially occupies the LUMO of the donor (donor state) and then moves to the LUMO of the acceptor (acceptor state). The excess electron can be injected into the DA complex, for example from a metal electrode to which the complex is attached, a redox compound contained in the solution where DA complex has been dissolved, or via an electron beam. Alternatively, the transferred electron may come from the donor itself. This is the case if the ET reaction involves an excited electron:

$$D^*A \rightarrow D^+A^-. \tag{7.3}$$

The excitation of the donor may be the result of a scattering process with another molecule, or it may be introduced via excitation energy transfer (exciton transfer, see Chapter 9). The excitation can also be achieved via optical absorption, as discussed in Chapter 6.

After optical excitation, an electron of the donor is placed into the LUMO, $D \rightarrow D^*$, where D^* indicates the excited state of the donor. Then, the ET proceeds between the donor and the acceptor LUMOs, as shown in Figure 7.6a. This type of ET is usually called a *photoinduced* reaction. After the transfer event there is an electron missing at the donor, which becomes positively charged. Accordingly, the acceptor is negatively charged, resulting in the formation of a dipole moment in the DA complex.

Figure 7.6a suggests the possibility of a backreaction where the transferred electron moves directly from the acceptor LUMO into the empty donor HOMO. In most cases, this backreaction is much slower than the forward ET, which makes it possible to clearly describe the reaction displayed in Figure 7.6a as an ET.

Alternatively to the transfer of the excited electron from the donor LUMO to the acceptor LUMO, an unexcited electron may move in the opposite direction from the acceptor HOMO to the donor HOMO:

$$D^*A \rightarrow D^-A^+. \tag{7.4}$$
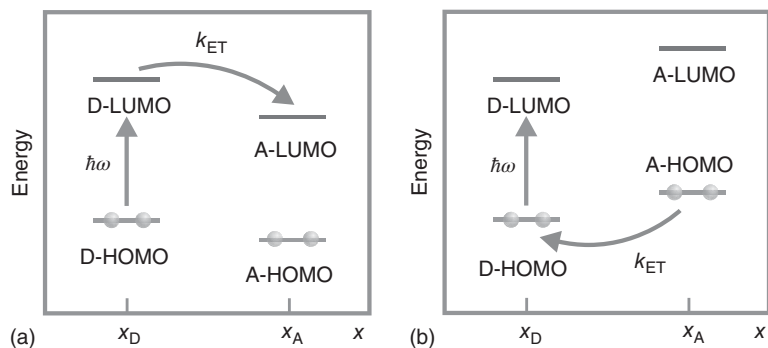
Figure 7.6 Photoinduced ET (a) and hole transfer (b) reaction in a HOMO–LUMO scheme of a DA complex (for further details, compare Figure 7.5).
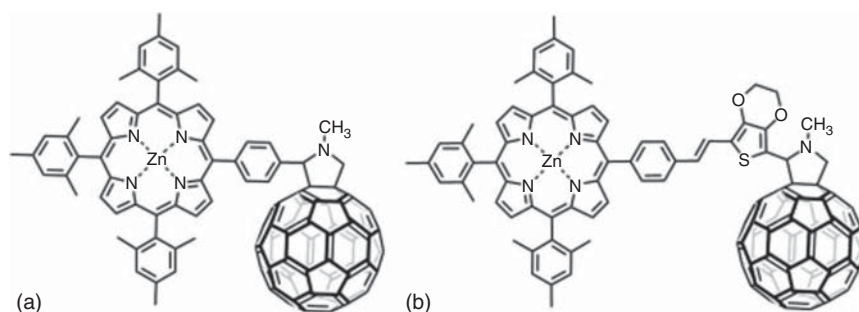
Figure 7.7 Porphyrin (D)–fullerene (A) dyads with a phenyl (a) and an additional 3,4-ethylenedioxythienylvinylene (b) spacer. In benzonitrile solution, ET from the photoexcited state D*A in case (a) proceeds via an intermediate excited state of the whole complex, (AD) *. This intermediate state does not form when increasing the spacer length and thus reducing the electronic coupling between D and A in case (b). In this case, the electronic excitation energy is first transferred to the fullerene forming A*D, before charge separation occurs as a hole transfer to give A⁻D⁺ (Pelado et al. [2]/John Wiley & Sons).

Figure 7.6b shows this so-called *hole transfer*. The name has been introduced since the reaction can be alternatively understood as the motion of a missing electron (hole) from the donor to the acceptor. Figure 7.7 shows the example of porphyrin–fullerene dyads, where ET versus hole transfer can be tuned by a spacer unit.

Let us turn to the discussion of bimolecular ET as it occurs for an intermolecular reaction in solution. If we suppose that initially the donor as well as the acceptor molecules are moving randomly (see also Figure 7.2), any reasonable description should include the mechanism that leads to the *formation* of the DA complex. For this purpose, it is also necessary to assess the probability at which the two molecules meet to form the so-called *encounter complex*. Within this encounter complex, the donor and the acceptor are close together, allowing for the ET to proceed. Afterward, the encounter complex is destroyed, and the donor and the acceptor molecules move again independently. The following scheme displays the complete

reaction assuming that the side groups R and R′ of the individual molecules are relevant for the formation of the encounter complex:

$$D^- - R + R' - A \rightarrow D^- - R \cdots R' - A \rightarrow D - R \cdots R' - A^-$$
$$\rightarrow D - R + R' - A^-. \tag{7.5}$$
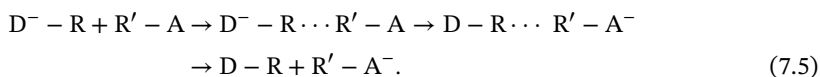
As already indicated, those ET reactions that occur in polar solvents are of particular significance. Here, every solvent molecule carries a permanent dipole moment that will be sensitive to the change in the charge distribution taking place in the DA complex upon ET. If the ET is not too fast, the solvent molecules react via the formation of a polarization cloud with an extension that is large compared to that of the DA complex. Then, the macroscopic dielectric properties of the solvent comprised in the dielectric function can be used to characterize the solvent influence on the ET. If the ET is influenced mainly by solvent molecules, it is of an *outer-sphere* type. On the other hand, it is of an *inner-sphere* type whenever intramolecular nuclear motions are dominant.

The intramolecular ET reactions discussed above for a simple two-state DA complex may also take place in this more difficult framework. From Scheme (7.5), it is obvious that a particular bimolecular ET reaction can be realized at various geometries and orientations of the donor and the acceptor parts of the complex. Therefore, an experimental investigation of an ensemble of encounter complexes will include an averaging with respect to these different realizations. (Note the similarity to inhomogeneous broadening of optical lineshapes introduced in Chapter 6.) An additional complication arises if one takes into account that in the experiment the actual charge transfer act is masked by the random sequence of formation and destruction of the encounter complex. In view of these difficulties, it is of great advantage to focus on ET in systems with *fixed* DA distance. Such experiments can be carried out, for example in frozen solutions or in other types of solid carrier matrices such as polymer layers. But if the ET proceeds as a bimolecular reaction, the DA distance still enters as a random quantity. In order to avoid all these complications, we focus on the simpler case of intramolecular ET reactions in the following discussion.

Next, we focus on ET reactions that are beyond the two-state model used so far for the DA complex. For instance, various types of molecules or molecular building blocks can bridge the donor and the acceptor. If the ET proceeds directly from the donor to the acceptor, although some bridging units are separating them, the process is called *through-space* transfer. If some LUMOs of the bridge participate in the ET, the reaction is called *through-bond* transfer. The through-space transfer is only possible for DA distances less than 20 Å. (We will see below that this value is mainly determined by the overlap of the wave functions of the transferred electron in the reactant and the product states.) The ET distance can become larger in the case of the through-bond transfer. This long-range ET is typical for conducting polymers or for the ET in proteins. Through-bond ET is alternative named *bridge-assisted* ET (Figure 7.8):

$$D^- \, BA \rightarrow DB^- A \rightarrow DBA^-. \tag{7.6}$$
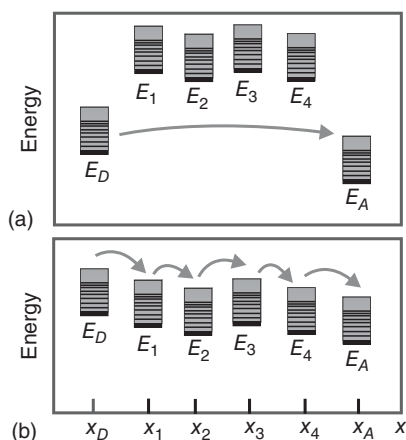
Figure 7.8 Bridge-mediated ET between a donor and an acceptor level connected by a linear chain of bridging units. To underline the importance of vibrational levels, we incorporated them here (thick lines – electronic levels and thin lines – vibrational levels). (a) The bridge levels are energetically well separated from the donor and the acceptor levels. (b) A situation where the energy levels of the donor and the acceptor are approximately resonant with the bridge levels.

The electron moves from the donor to the acceptor via different bridge molecules (denoted here by the symbol B). Often, these bridging molecules are called *spacers* since they fix the donor and the acceptor at a particular distance from one another (this term is also common if the bridging molecules do not participate in the ET). Note that in contrast to the bimolecular ET, in the encounter complex, the properties of the bridge, B, are rather well defined as compared to $R \cdots R'$.

There are two distinct mechanisms for bridge-mediated ET as shown in Figure 7.8. The LUMOs of donor and acceptor may be either resonant or off-resonant with respect to the bridge levels. In the latter case, it is reasonable to assume that there will be only a very small probability for population of these levels by the transferred electron.[3] This situation is called *superexchange* ET (Figure 7.8a). Here, the most important function of the bridge units is to provide a means for delocalization of the donor state wave function across the whole bridge. In the case of ET, the charge jumps stepwise from one part to the other of the whole DBA chain (Figure 7.8b). This process is often called *sequential* or *hopping* transfer. Obviously, superexchange and sequential ET are through-bond transfer reactions. If the different bridge molecules are not positioned in a linear arrangement but form a three-dimensional network, the electron may move on different *pathways* from the donor to the acceptor. Examples of bridge-mediated ET are further discussed in Section 7.5.

At the end of our introductory discussion, we focus on ET processes where solid-state systems are involved. These ET reactions are known as *heterogeneous electron transfer* (HET). They take place between a molecule and a solid-state system to whose surface the molecule is attached. The former may be either a metal or semiconductor (Figure 7.9). Depending on the direction of charge transfer (from the molecule to the solid-state system or reverse), the solid with its huge number of available electronic levels functions as the acceptor or as the donor. The participation of a continuum of donor or acceptor levels distinguishes HET from the ET reactions introduced earlier. As in the case of bimolecular ET, molecular states are involved, which are positively or negatively charged.

---

3) Often, one characterizes this very small population of the bridge state as being a virtual one.
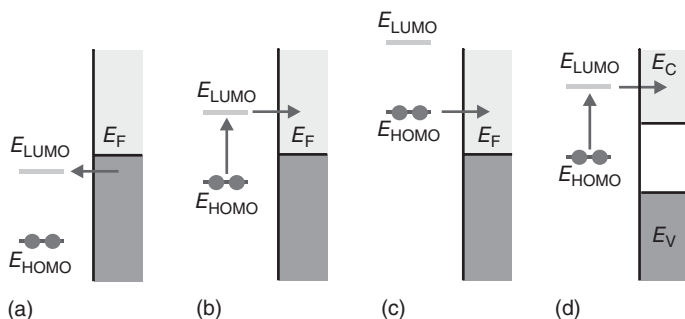
Figure 7.9 (a–c) Possible HET reactions between a molecule represented in a HOMO–LUMO scheme and a metal with a single band filled by electrons up to the Fermi level E_F (dark gray). (a) $E_{LUMO} < E_F$: charge injection proceeds from the Fermi sea into the LUMO level, (b) $E_{LUMO} > E_F$ but $E_{HOMO} < E_F$: charge injection into empty band state above the Fermi edge (light gray) becomes possible after photoexcitation of an electron from the HOMO to the LUMO, (c) $E_{HOMO} > E_F$: an electron can be transferred from the LUMO into an empty band state. (d) HET reactions between a molecule represented in a HOMO–LUMO scheme and a semiconductor with a filled valence band with energies E_V (dark gray) and an empty conduction band with energies (E_C, light gray). Both band edges are separated by the band gap (white).

We first consider HET between a molecule and a metal. Figure 7.9a–c gives an overview of the possible reactions, either photoinduced or not. A simple HOMO–LUMO scheme for the molecule and a band continuum scheme for the metal has been introduced. The continuum is separated into occupied states below the Fermi energy E_F and empty states above E_F. At finite temperatures, the transition between the occupied and unoccupied states is continuous and regulated by the Fermi distribution of electrons. The concrete type of reaction depends on the position of the HOMO and LUMO levels relative to the Fermi energy. Charge transfer from the metal into the molecule results in the formation of a molecular anion. The reverse process forms a molecular cation.

Turning to the HET between a molecule and a semiconductor, we have to note the specificity of the electron distribution in the latter (Figure 7.9d). On the one hand, it includes the valence band with states completely occupied by electrons. This band is separated via the band gap from the conduction band with empty states. If the HOMO and LUMO lie entirely in the range of the valence band, the situation is similar to Figure 7.9a. If both molecular levels cover the range of the conduction band, the situation corresponds to Figure 7.9c. What is of particular interest for HET involving a semiconductor is shown in Figure 7.9d. The HOMO is positioned in the band gap, and the LUMO lies above the lower conduction band edge. Now, HET becomes possible if an electron is promoted by photoabsorption to the LUMO since it is degenerated with conduction band energies. A particular example of photoinduced HET is given in Figure 7.10.

If the molecule–solid coupling is strong enough, HET may proceed on a sub-picosecond time scale. Such ultrafast photoinduced HET became of particular interest in relation to the photovoltaic devices known as Grätzel cells. As a basic
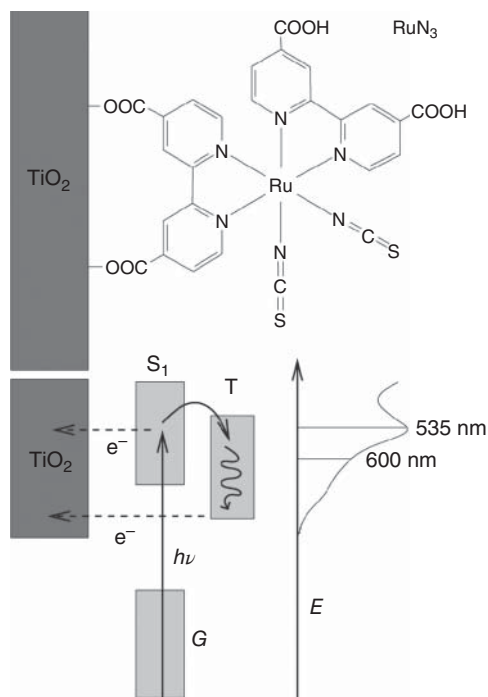
Figure 7.10 Ultrafast HET between an Ru(2,2′-bipyridyl-4,4′-dicarboxylic acid)$_2$(NCS)$_2$ (RuN$_3$) molecule and a nanocrystalline TiO$_2$ film; 60% of the initial population of the excited singlet state (S$_1$) is quenched before thermalization via hot electron injection (it proceeds within 100 fs), and 40% of the S$_1$ state population is transferred to the triplet state (T). To indicate the two used excitation frequencies, the absorption spectrum is also drawn (Reproduced with permission from Brueggemann et al. [3]/American Physical Society).

part, it contains nanoparticles of the semiconductor TiO$_2$ to which surface chromophores such as perylene and others are attached (a so-called *dye-sensitized solar cell* is formed, cf. also Figure 7.10). Photoinduced HET from the dye to the nanoparticle may finally lead to a macroscopic current in the whole device.

A rather novel route of applying the concept of HET concerns charge transmission through single molecules. This combines HET as well as long-range and bridge-mediated ET and is related to the long-standing dream to achieve a replacement of traditional semiconductor-based microelectronics by a *Molecular Electronics*. Various molecular schemes have been suggested to realize the molecular pendant to a solid state-based transistor (Figure 7.11). Transistor-like behavior became possible by contacting individual molecules with metal electrodes. Such a contact requires the creation of a nanoelectrode. The tip of a scanning tunneling microscope could form one contact to the molecule, while the other contact is given by the conduction layer on which the molecule has been placed (Figure 7.30). Contacts (leads) could also be formed using a tiny metal (gold) wire, which breaks after careful stretching, thereby forming a so-called break junction. If one applies a voltage across the molecule that is connected to two leads, the basic measured quantity is the respective stationary current. Having a current induced by an applied voltage, the so-called current voltage (IV) characteristics is the quantity of interest. This is different from the ET in molecular DA complexes, which is discussed in terms of transition rates.
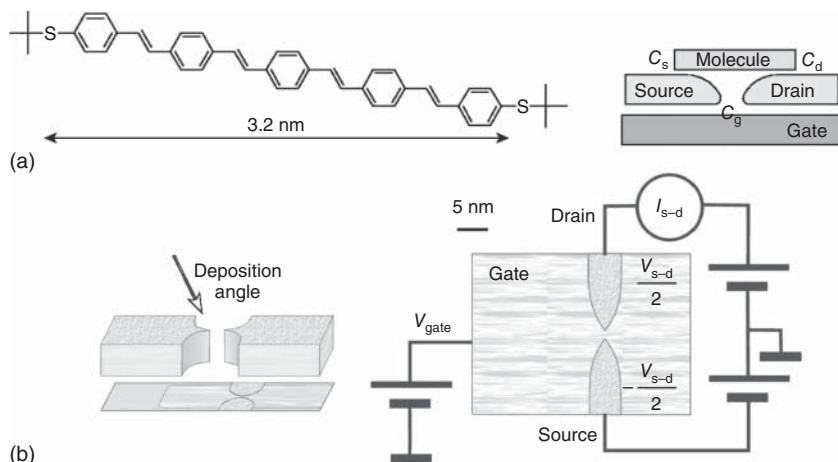
Figure 7.11 Single-molecule transistor including different charging states of the molecule OPV5 ((*E,E*)-1,4-bis4-(*E*)-4-(*tert*-butylthio)styrylbenzene, see left upper panel). Also shown is the field-effect transistor arrangement with source, drain, and gate electrode as well as the device preparation procedure (first and second rows) (Reproduced with permission from Kubatkin et al. [4]/Springer Nature).

7.2 Theoretical Models for Electron Transfer Systems

The derivation of the ET Hamiltonian proceeds in close analogy to the reasoning that led to the molecular Schrödinger equation in Section 2.3. The problem is split up into an electronic part for frozen nuclear configuration and a nuclear part. However, since there are a number of approximations that are special to the ET problem, we explain in some detail how to arrive at the electron–vibrational Hamiltonian governing the transfer of a single electron through a DA complex. The electronic Hamiltonian of the DA complex including possible bridging units will be denoted as $H_{\mathrm{el}}^{(\mathrm{DBA})}$, whereas the full Hamiltonian, including vibrational contributions, is written as H_{DBA}.

7.2.1 The Electron Transfer Hamiltonian

Although ET comes along with the modification of many MOs, and thus has to be considered as a process in which different electrons take part, we proceed here with a simple and intuitive picture. It is based on the notion of a single *excess* electron injected from the outside into the DA complex. The transfer of this excess electron will be described by introducing an effective potential experienced by the excess electron after entering the DA complex

$$V(\boldsymbol{r}) = \sum_m V_m(\boldsymbol{r}). \tag{7.7}$$
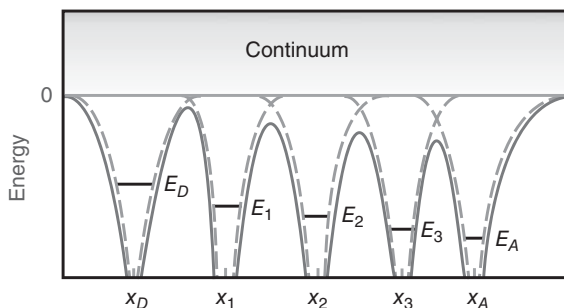
Figure 7.12 One-dimensional sketch of the pseudopotential $V(r)$, introduced in Eq. (7.7) (full line). x_D, x_1, etc. mark the spatial positions of the different units of the ET system. The pseudopotentials $V_m(r)$ of the individual molecular units (broken lines) and the levels E_m occupied by the excess electron are also shown. The motion of the excess electron among the various energy levels proceeds as a tunneling process through the barriers separating different potential wells.

The individual contributions $V_m(\boldsymbol{r})$ belong to the donor, the acceptor, or to some bridging molecules. (In what follows, the bridging units are counted by $m = 1, \dots, N_B$, starting at the donor site, whereas the donor and acceptor are labeled by $m = D$ and A, respectively; see Figure 7.12.)

The introduction of the effective potential $V(\boldsymbol{r})$ appears to be reasonable, even though there is no unique way of separating it into the various $V_m(\boldsymbol{r})$. Only in the case of bimolecular ET reactions, where independent molecules are involved, is the separation scheme obvious. For unimolecular ET, one would relate the $V_m(\boldsymbol{r})$ to those fragments of the DA complex on which the excess electron is localized for an appreciable time.

Each contribution $V_m(\boldsymbol{r})$ can be understood as a so-called *pseudopotential* that mimics the action of the total electronic system of the molecular fragment on the excess electron. Within this picture all exchange and correlation effects among the excess electron and the electrons of the molecule are replaced by a simple single-particle potential that is local in space. The techniques and approximation schemes for establishing these pseudopotentials are provided by the theory of many-particle systems. Here, we define the various $V_m(\boldsymbol{r})$ by demanding that their ground state energy level E_m should coincide with the electronic ground state of the isolated molecular unit *plus* the excess electron. The mentioned approach is *not* identical to a single-particle model, which neglects any charge relaxation in the course of the excess electron motion. The excess electron does not move through an arrangement of frozen MOs. It is taken into account that the *full* many-electron wave function adjusts itself during the ET reaction. But this is done by reducing the many-particle dynamics to the action of an *effective* local single-particle potential.

Independent of the specific definition of the localized states, the single-level treatment is only a good approximation if the next unoccupied orbital has a much higher energy. Otherwise, the number of unoccupied orbitals per pseudopotential $V_m(\boldsymbol{r})$ has to be adjusted. The pseudopotential $V_m(\boldsymbol{r})$ enters the single-electron

Schrödinger equation, which determines the single-particle energies E_m and wave functions $\varphi_m(\boldsymbol{r})$:

$$\left(T_{\mathrm{el}} + V_m(\boldsymbol{r})\right) \varphi_m(\boldsymbol{r}) = E_m \varphi_m(\boldsymbol{r}). \tag{7.8}$$

Again, only the lowest eigenvalue E_m is of interest in the following discussion, although higher energetic solutions may exist. Since the energies E_m correspond to different sites in the complex, they are usually called *site energies*. The states φ_m are reminiscent of the diabatic states introduced in Section 2.6. Hence, using these states as an expansion basis, a *diabatic representation* is provided. According to its definition, the set of states φ_m does not form a normalized and orthogonal basis, that is nonvanishing *overlap integrals* exist: $\langle \varphi_m | \varphi_n \rangle \neq \delta_{mn}$.

In order to construct the ET Hamiltonian, we consider the electronic Schrödinger equation for the total DA complex. Since we assume spin degeneracy of the considered excess electron states, spin quantum numbers do not appear in what follows. The total DA Schrödinger equation reads

$$(T_{\mathrm{el}} + V)|\phi\rangle = \mathcal{E}|\phi\rangle. \tag{7.9}$$

Let us expand this equation with respect to the basis set $|\varphi_m\rangle$:

$$|\phi\rangle = \sum_m c_m |\varphi_m\rangle\,. \tag{7.10}$$

Inserting this into Eq. (7.9) and multiplying by $\langle \varphi_n |$ from the left gives

$$\langle \varphi_n | T_{\mathrm{el}} + \sum_k V_k |\phi\rangle = \mathcal{E}\langle \varphi_n|\phi\rangle \tag{7.11}$$

or

$$\sum_m c_m \left(E_m \langle \varphi_n|\varphi_m\rangle + \sum_{k \neq m} \langle \varphi_n|V_k|\varphi_m\rangle \right) = \mathcal{E} \sum_m c_m \langle \varphi_n|\varphi_m\rangle. \tag{7.12}$$

This set of equations contains the overlap integrals and the *three-center integrals* $\langle \varphi_n|V_k|\varphi_m\rangle$.[4]

Although a more general description is possible, in what follows, we introduce two approximations. First, we assume that the two-center overlap integrals can be neglected; that is, we set $\langle \varphi_n|\varphi_m\rangle \approx \delta_{nm}$. Within this approximation, the set of states φ_m forms an orthogonal basis.[5] Second, because of their smallness compared to the two-center integrals, all three-center integrals are neglected. We only take into account one- and two-center integrals. The latter contain terms of the type $\langle \varphi_m|V_k|\varphi_m\rangle$, which introduce a shift of the site energies E_m due to the presence of the pseudopotential V_k at site k. The other two-center integrals are of the type $\langle \varphi_n|V_n|\varphi_m\rangle$. This expression couples the state $|\varphi_m\rangle$ to the state $|\varphi_n\rangle$ via the tail of the potential V_n at site m.

---

4) The integrand has contributions from sites n, k, and m, that is from three different spatial positions.
5) Of course, a transformation to a new set of states may remove the overlap integrals. But in this case, the intuitive picture of the states $|\varphi_m\rangle$ is lost.

An expansion of the electronic part of the DA Hamiltonian gives

$$H_{\mathrm{el}}^{\mathrm{(DBA)}} = \sum_{m,n} \langle \varphi_m | H_{\mathrm{el}}^{\mathrm{(DBA)}} | \varphi_n \rangle | \varphi_m \rangle \langle \varphi_n |, \tag{7.13}$$

with the matrix elements of the Hamiltonian given by

$$\langle \varphi_m | H_{\mathrm{el}}^{\mathrm{(DBA)}} | \varphi_n \rangle = \delta_{mn} \left(E_m + \sum_{k \neq m} \langle \varphi_m | V_k | \varphi_m \rangle \right)$$
$$+ (1 - \delta_{mn}) \langle \varphi_m | T_{\mathrm{el}} + V_m + V_n | \varphi_n \rangle. \tag{7.14}$$

The off-diagonal part can be rewritten in different forms. We use the eigenvalue Eq. (7.8) and get

$$\langle \varphi_m | T_{\mathrm{el}} + V_m + V_n | \varphi_n \rangle = \frac{1}{2} \langle \varphi_m | (T_{\mathrm{el}} + V_m) + (T_{\mathrm{el}} + V_n) + (V_m + V_n) | \varphi_n \rangle$$
$$= \frac{1}{2} \langle \varphi_m | E_m + E_n + (V_m + V_n) | \varphi_n \rangle$$
$$= \frac{1}{2} \langle \varphi_m | V_m + V_n | \varphi_n \rangle = V_{mn}. \tag{7.15}$$

The final expression V_{mn} is usually called *transfer integral* or, alternatively, *interstate coupling*. Since the motion of the electron through the DA complex proceeds via tunneling processes, the term *tunneling* matrix element is also common. Alternatively to Eq. (7.15), one can also write V_{mn} $(m \neq n)$ in terms of the matrix elements of the kinetic energy operator:

$$V_{mn} = \langle \varphi_m | T_{\mathrm{el}} + V_m + T_{\mathrm{el}} + V_n - T_{\mathrm{el}} | \varphi_n \rangle$$
$$= \langle \varphi_m | E_m + E_n - T_{\mathrm{el}} | \varphi_n \rangle = -\langle \varphi_m | T_{\mathrm{el}} | \varphi_n \rangle. \tag{7.16}$$

The complete electronic Hamiltonian for the DA complex reads

$$H_{\mathrm{el}}^{\mathrm{(DBA)}} = \sum_m E_m | \varphi_m \rangle \langle \varphi_m | + \sum_{m,n} V_{mn} | \varphi_m \rangle \langle \varphi_n |. \tag{7.17}$$

Here, we included the diagonal matrix elements of the pseudopotentials into the definition of the site energies E_m (note also the convention $V_{mm} = 0$). If convenient, we will write in the following $|D\rangle$, $|B\rangle$, and $|A\rangle$ instead of $|\varphi_D\rangle$, $|\varphi_m\rangle$, and $|\varphi_A\rangle$, respectively (here, $|B\rangle$ stands for a particular bridge state).[6]

The construction of the Hamiltonian, Eq. (7.17), was mainly based on the concept of a single excess electron moving in a particular spatial arrangement of pseudopotentials that refer to the donor, the bridge, and the acceptor. But a derivation would also be possible if a many-electron generalization of the wave functions for the excess electron $\varphi_m(\mathbf{r})$ could be achieved. Let $\Phi(r, \sigma)$ be the full many-electron wave function of the neutral DA complex in its ground state (with the set of spatial and spin coordinates r and σ, respectively). Then, we assume the existence of the wave function $\Phi_m^{(-)}(r, \sigma; \mathbf{r}_{\mathrm{exc}}, \sigma_{\mathrm{exc}})$ referring to the DA complex *plus* the excess electron that is in a diabatic state localized at site m. The expansion of some suitable many-electron

---

6) In the solid-state-physics literature, the electronic part of the full DA complex Hamiltonian (7.17) is often called *tight-binding* Hamiltonian.

generalization of the DA Hamiltonian $H_{el}^{(DBA)}$ (whose definition starts from the general expressions of Section 2.2) then gives the respective diabatic energies E_m in the diagonal parts.

Although this many-electron extension seems to be simple, it essentially depends on the proper definition of the states $\Phi_m^{(-)}(r, \sigma; \boldsymbol{r}_{exc}, \sigma_{exc})$. In particular, one has to clarify how to define these states as diabatic states of the total DA complex, as well as how to separate the DA complex into isolated units and to define the localized excess electron states for these units. We will not further comment on these more involved issues but refer the reader to the literature listed in the section "Further Reading".

In a similar way, it becomes possible to construct the Hamiltonian that describes photoinduced ET (cf. Figure 7.6). Here, we have to assume the existence of the many-electron wave functions $\Phi_m(r, \sigma)$ that correspond to the excited donor state as well as the presence of the transferred electron at the bridge units and the acceptor. One may argue that for those states where the electron already left the donor the Coulomb interaction should be accounted for between the donor without one electron (D^+) and the other parts of the DA complex with an additional electron (e.g. A^-). But often, one interprets the states Φ_m (and the related energies E_m) as constructed in such a manner that this Coulomb interaction is already contained in their definition. Of course, all these states are not eigenstates of the electronic part of the molecular Hamiltonian. They describe spatial charge localization in the DA complex and should be coupled weakly one to another. (If this latter restriction is not fulfilled, the introduction of the Φ_m becomes meaningless.) Expanding the electronic part $H_{el}^{(DBA)}$ of the DA Hamiltonian with respect to these states Φ_m, we again arrive at an expression as given by Eq. (7.17). This indicates the universal form of the ET Hamiltonian, Eq. (7.17). Only the actual interpretation of the involved matrix elements and expansion states specifies $H_{el}^{(DBA)}$ to a concrete type of ET reaction.

The derivation of Eq. (7.17) provides the conceptional framework of the DBA Hamiltonian. To conclude this section, we address the question: how the energies E_m and interstate couplings V_{mn} can be computed for a given molecular system? The states $|\varphi_m\rangle$ form a diabatic basis, describing the localized charge densities. However, starting with the electronic Schrödinger equation of the total DBA system, one will obtain the adiabatic electronic states $|\varphi_a\rangle$. The two representations are related by a linear transformation as outlined in Section 2.6 for a general two-state problem. In the present situation, this transformation can be obtained using physical arguments as follows. Since the electronic states are localized on different parts of the DBA complex, it is assumed that the matrix elements of the dipole moment operator connecting different diabatic states vanish. Provided that one has calculated the dipole matrix in the adiabatic basis, that is $\boldsymbol{\mu}^{(adia)}$ with matrix elements $\boldsymbol{d}_{ab}$, the transformation $\mathbf{C}^{(\mu)}$ is chosen such as to bring this adiabatic dipole matrix into diagonal form, that is

$$\mathbf{C}^{(\mu)T}\boldsymbol{\mu}^{(adia)}\mathbf{C}^{(\mu)} = \boldsymbol{\mu}^{(diag)}, \tag{7.18}$$

with the diagonal matrix $\boldsymbol{\mu}^{(\text{diag})}$, which is identified with the dipole matrix in diabatic representation under the assumption that due to diabatic state localization, the off-diagonal dipole matrix elements vanish. The vector character of the dipole is incorporated by projection onto the direction of the difference vector between the expectation values of the dipole moment for the initial and final adiabatic states (in the case of more than two states, the average is taken). The diabatic representation in Eq. (7.17) is obtained by transformation of the (diagonal) adiabatic Hamiltonian with $\mathbf{C}^{(\mu)}$. To obtain an analytic expression, we consider a two-state DA system, with the adiabatic transition dipole vector pointing along the difference vector between the two adiabatic state dipoles, and use the following transformation matrix (cf. Section 2.8.2):

$$\mathbf{C}^{(\mu)} = \begin{pmatrix} \cos\gamma & -\sin\gamma \\ \sin\gamma & \cos\gamma \end{pmatrix}. \tag{7.19}$$

Performing the matrix multiplications on the right-hand side of Eq. (7.18) and demanding that the off-diagonal elements of the resulting matrix vanish, one obtains

$$\gamma = \frac{1}{2}\arctan\left(\frac{2d_{12}}{|\boldsymbol{d}_{11} - \boldsymbol{d}_{22}|}\right), \tag{7.20}$$

where d_{12} is the projection along $(\boldsymbol{d}_{11} - \boldsymbol{d}_{22})/(|\boldsymbol{d}_{11} - \boldsymbol{d}_{22}|)$. Applying the transformation to the diagonal Hamiltonian matrix with energies $\mathcal{E}_{\alpha=1,2}$ yields the coupling matrix elements:

$$V_{12} = \frac{1}{2}(\mathcal{E}_2 - \mathcal{E}_1)\sin(2\gamma). \tag{7.21}$$

Inserting the expression for γ, one gets the interstate coupling (usually written in terms of its absolute value)

$$|V_{12}| = \frac{|\mathcal{E}_2 - \mathcal{E}_1||d_{12}|}{\sqrt{|\boldsymbol{d}_{11} - \boldsymbol{d}_{22}|^2 + 4d_{12}^2}}. \tag{7.22}$$

Thus, the interstate coupling can be expressed solely in terms of adiabatic quantities, that is the electronic energy difference and dipole matrix elements. Note that this procedure does not make any assumption concerning the method by which the adiabatic states have been obtained. In other words, they may contain many body correlation effects. This approach is known as generalized Mulliken–Hush method. An example is given in Figure 7.35.

7.2.2 The Electron–Vibrational Hamiltonian of a Donor–Acceptor Complex

In general, one should distinguish between intra- and intermolecular nuclear DOFs. While the former are more important for unimolecular ET, the latter play a prominent role in bimolecular ET, although also in that case there will be intramolecular vibrations for the separate D and A molecules. The following derivation is more suitable for intramolecular ET. The case of separate sets of vibrational DOFs will

be discussed in Section 7.4.2. The vibrational DOFs may couple in two different ways to the transferred electron. In principle, one can distinguish between *accepting modes*, which change their equilibrium configuration if the electronic charge density changes, and *promoting modes*. The latter enter the transfer integral, Eq. (7.7), and thus may accelerate the ET. (We note that in general this distinction is not always clear; that is, accepting modes may act simultaneously as promoting modes and vice versa.)

Including the vibrational DOFs, $\{R_u\} \equiv R$, along the lines of Section 2.5 (note that we use the index u instead of n as in Chapter 2 to avoid confusion with the site indices), the electron–vibrational Hamiltonian of the DA becomes

$$H_{\mathrm{DBA}} = \sum_m \left(T_{\mathrm{nuc}} + U_m(R) \right) |\varphi_m\rangle\langle\varphi_m| + \sum_{m,n} V_{mn}(R)|\varphi_m\rangle\langle\varphi_n|, \tag{7.23}$$

where we have introduced potential energy surface (PES) that relate to those state with the excess electron localized at site m:

$$U_m(R) = E_m(R) + V_{\mathrm{nuc\text{-}nuc}}(R). \tag{7.24}$$

Here, we have neglected the dependence of the basis φ_m on the vibrational coordinates. This reminds on the Born–Oppenheimer approximation and specifically assumes that there is no ET triggered by the nonadiabaticity operator Θ_{mn} defined in Eq. (2.17). This assumption is motivated by the localization of the wave functions $\varphi_m(\boldsymbol{r})$ at the various units of the DA complex (its diabatic character).

The dependence on the nuclear coordinates can be made more specific by introducing PESs, which depend on normal mode coordinates $\{q_\xi\} \equiv q$ (see Section 2.5.1). In this case it is advantageous to choose a particular electronic state to define a reference configuration of the nuclei. We take the electronic ground state of the neutral DA complex for that purpose, that is the state where the excess electron is absent. This state is supposed to be characterized by the PES $U_g(R)$ having the equilibrium configuration at $\{R_u^{(g)}\} \equiv R^{(g)}$. Next, we carry out an expansion of $U_g(R)$ around $R^{(g)}$ up to the second order with respect to the deviations $\Delta R_u^{(g)} = R_u - R_u^{(g)}$ and obtain after introducing normal-mode coordinates a Hamiltonian as given in Eq. (2.43).

Using the same normal-mode transformation also for the electronic states with an excess electron and following Section 2.5.1, one arrives at a particular model for the PES of the DA system. The PESs are parabolic, their minima are shifted with respect to each other in the space of the normal-mode coordinates, and they have different energetic offsets (see Figure 7.13). If necessary, they can additionally be characterized by vibrational frequencies depending on the site index m. The related vibrational Hamiltonian reads

$$H_m(q) = T_{\mathrm{vib}} + U_m(q) = U_m^{(g)} + \frac{1}{2} \sum_\xi \left\{ p_\xi^2 + \omega_{m\xi}^2 \left(q_\xi - q_\xi^{(m)} \right)^2 \right\}. \tag{7.25}$$

In the general case, the intersite couplings V_{mn} also depend on the nuclear coordinates. Since the magnitude of V_{mn} is mainly determined by the overlap of the exponential tail of the wave functions localized at sites m and n (see Eq. (7.15)),
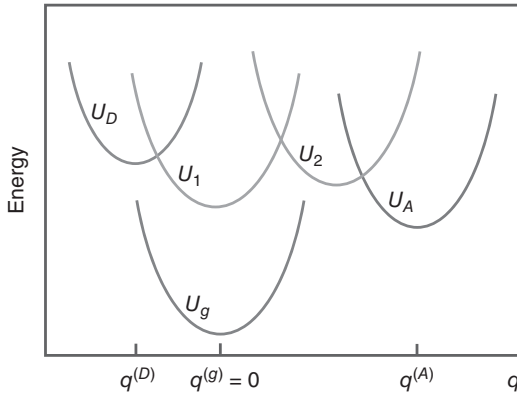
Figure 7.13 PES of the DA complex according to Eq. (7.25) versus a single normal mode coordinate $q_\xi \equiv q$ (all other coordinates with $\xi' \neq \xi$ are fixed at $q_{\xi'}^{(m)}$ for every PES U_m). While U_g is the electronic ground-state (reference) PES of the neutral complex, the PES U_m correspond to the situation where one excess electron is present at the donor ($m = D$), the acceptor ($m = A$), or at a bridge unit ($m = 1, 2, 3$, note that the position of the PES along the q-axis has nothing to do with the spatial position of the related electronic wave functions φ_m).

we expect an exponential dependence on the distance x_{mn} between the two sites:

$$V_{mn}(R) = V_{mn}^{(g)} \exp\left\{ -\beta_{mn}(x_{mn} - x_{mn}^{(g)}) \right\}. \tag{7.26}$$

The reference value $V_{mn}^{(g)}$ of the intersite couplings is reached for the reference (equilibrium) distance $x_{mn}^{(g)}$, and β_{mn} is some characteristic inverse length determined by the wave function overlap. Often, the dependence of V_{mn} on the nuclear coordinates is neglected in comparison with the onsite vibrational dynamics. We use this simplification in the following and set $V_{mn}(R) \approx V_{mn}$ (Condon approximation).

Using this model, the total Hamiltonian (7.23) becomes

$$H_{\mathrm{DBA}} = \sum_{m,n} \left\{ \delta_{mn} H_m(q) + (1 - \delta_{mn}) V_{mn} \right\} |\varphi_m\rangle\langle\varphi_n|. \tag{7.27}$$

The simplest but nontrivial version of the DA Hamiltonian, Eq. (7.27), is obtained if one neglects any bridging unit and if the vibrational frequencies are independent of the actual electronic state. We then have

$$H_{\mathrm{DA}} = H_D(q)|D\rangle\langle D| + H_A(q)|A\rangle\langle A| + V_{DA}|D\rangle\langle A| + V_{AD}|A\rangle\langle D|. \tag{7.28}$$

7.2.2.1 The Spin-Boson Model

There exists a widely used alternative notation, which employs the formal similarity of a two-level DA system, Eq. (7.28), with a spin one-half system. In analogy to the quantum mechanical treatment of the spin, we define the spin-operator components σ_x, σ_y, and σ_z as

$$\sigma_x = |D\rangle\langle A| + |A\rangle\langle D|,$$
$$\sigma_y = i\left(|D\rangle\langle A| - |A\rangle\langle D|\right),$$
$$\sigma_z = |D\rangle\langle D| - |A\rangle\langle A|. \tag{7.29}$$

Furthermore, we write the Hamiltonian (7.28) in a way similar to Section 2.5.2, where we introduced a reference vibrational Hamiltonian H_{vib} and a linear electron–vibrational coupling with dimensionless vibrational coordinates $q_\xi \sqrt{2\omega_\xi/\hbar} = C_\xi^+ + C_\xi$ and coupling constants $g_m(\xi) = -q_\xi^{(m)} \sqrt{\omega_\xi/2\hbar}$. It gives

$$
\begin{aligned}
H_{\text{DA}} = {} & U_D^{(g)} |D\rangle\langle D| + U_A^{(g)} |A\rangle\langle A| + H_{\text{vib}} \\
& + \sum_\xi \hbar\omega_\xi (C_\xi^+ + C_\xi) \left(g_D(\xi)|D\rangle\langle D| + g_A(\xi)|A\rangle\langle A| \right) \\
& + V_{DA}|D\rangle\langle A| + V_{AD}|A\rangle\langle D|.
\end{aligned}
\tag{7.30}
$$

If we introduce

$$
U_D^{(g)} = \bar{U}^{(g)} + \varepsilon/2
\tag{7.31}
$$

and

$$
U_A^{(g)} = \bar{U}^{(0)} - \varepsilon/2,
\tag{7.32}
$$

with $\bar{U}^{(0)} = (U_D^{(0)} + U_A^{(0)})/2$, $\varepsilon = U_D^{(0)} - U_A^{(0)}$, assume that the shift of the two PESs along the q_ξ-axis is symmetric ($g_D(\xi) = -g_A(\xi) = g_\xi$), and take a real-valued transfer coupling $V = V_{DA} = V_{AD}$, the Hamiltonian, (7.30) becomes

$$
H_{\text{sb}} = \bar{U}^{(0)} + H_{\text{vib}} + \frac{\varepsilon}{2}\sigma_z + \sum_\xi \hbar\omega_\xi g_\xi (C_\xi^+ + C_\xi)\sigma_z + V\sigma_x.
\tag{7.33}
$$

(Note that $|D\rangle\langle D| + |A\rangle\langle A|$ defines the completeness relation for the electronic states, which can be replaced by the unit operator.)

According to this prescription, the electronic two-state DA system has been mapped onto the problem of an effective spin one-half particle. Eq. (7.33) gives the so-called *spin-boson* Hamiltonian. The term "boson" indicates that the equilibrium vibrational energy distribution for the various normal modes follows Bose–Einstein statistics. The spin-boson model represents the archetype to study the interplay of particle (electron) transfer and vibrational motion.

7.2.2.2 Two Independent Sets of Vibrational Coordinates

In the foregoing considerations, we assumed that there exists a common set of normal mode coordinates modulating the donor as well as the acceptor electronic states. In the case of a bimolecular ET reaction, however, the electron moves between two independent molecules. Therefore, it is more appropriate to separate the sets of coordinates for the donor ($q_D \equiv \{q_{D\xi}\}$) and the acceptor ($q_A \equiv \{q_{A\xi}\}$) molecules. For simplicity, we consider the reaction scheme (7.5) without additional bridging units and introduce four different electronic states for the expansion of the Hamiltonian. They will be denoted by $|\varphi_{D-}\rangle$, $|\varphi_D\rangle$, $|\varphi_A\rangle$, and $|\varphi_{A-}\rangle$, and describe the donor with the excess electron, the neutral donor, the neutral acceptor, and the acceptor plus the excess electron, respectively. Thus, the reactant state is given by $|\varphi_{D-} \, \varphi_A\rangle$, whereas the product state is $|\varphi_D \, \varphi_{A-}\rangle$. Generalizing Eq. (7.28), the Hamiltonian for a bimolecular ET reaction follows as

$$
\begin{aligned}
H_{\text{DA}}^{(\text{bimol})} = {} & \left[H_{D-}(q_D) + H_A(q_A) \right] |\varphi_{D-} \, \varphi_A\rangle\langle\varphi_{D-} \, \varphi_A| \\
& + \left(H_D(q_D) + H_{A-}(q_A) \right) |\varphi_D \, \varphi_{A-}\rangle\langle\varphi_D \, \varphi_{A-}| \\
& + \left(V_{DA}|\varphi_{D-} \, \varphi_A\rangle\langle\varphi_D \, \varphi_{A-}| + \text{h.c.} \right).
\end{aligned}
\tag{7.34}
$$

All PESs are of the type entering Eq. (7.25), but here, we have four sets of equilibrium configurations $\{q_{m\xi}^{(0)}\}$, with $m = D^-, D, A, A^-$ and four corresponding values of $U_m^{(0)}$. Additionally, there could be intermolecular coordinates that describe variations of the distance between D and A. Such motions would in particular influence the transfer coupling V_{DA}.

7.2.3 Electron–Vibrational State Representation of the Hamiltonian

For further applications it is useful to give a representation of the DA Hamiltonian using the complete diabatic electron–vibrational basis defined by the states (cf. Section 2.6)

$$|\mu\rangle \equiv |mM\rangle \equiv |\chi_{mM}\rangle|\varphi_m\rangle. \tag{7.35}$$

The harmonic oscillator vibrational states $|\chi_{mM}\rangle$ that belong to the electronic states $|\varphi_m\rangle$ are the eigenstates of the vibrational Hamiltonian, Eq. (7.25),

$$H_m|\chi_{mM}\rangle = E_{mM}|\chi_{mM}\rangle. \tag{7.36}$$

The corresponding eigenvalues

$$E_{mM} = U_m^{(0)} + \sum_{\xi} \hbar\omega_{m\xi}(M_\xi + 1/2) \tag{7.37}$$

give the energy spectrum of the normal-mode oscillators. According to the introduction of normal-mode vibrations, the state vector $|\chi_{mM}\rangle$ factorizes into products corresponding to the different normal modes with mode index ξ

$$|\chi_{mM}\rangle = \prod_{\xi}|\chi_{mM_\xi}\rangle . \tag{7.38}$$

The Hamiltonian (7.27) can be expanded in the diabatic electron–vibrational basis as follows:

$$H_{\mathrm{DBA}} = \sum_{\mu\nu} \left(\delta_{\mu\nu}E_\mu + (1 - \delta_{mn})V_{\mu\nu}\right)|\mu\rangle\langle\nu|. \tag{7.39}$$

If the transfer integral V_{mn} is coordinate independent, the coupling matrix element follows as $V_{\mu\nu} = V_{mn}\langle\chi_{mM}|\chi_{nN}\rangle$, where $\langle\chi_{mM}|\chi_{nN}\rangle$ is the overlap integral of the vibrational wave functions belonging to different sites (Franck–Condon factor).[7]

The total DA system described by the Hamiltonian (7.39) can be viewed as a set of multilevel systems with energy spectrum E_μ and mutual level coupling $V_{\mu\nu}$. A similar system has already been considered in Section 3.4.5 from a more formal point of view. There, we calculated the total transition rate for the transfer of occupation probability from site m to site n. Here, we expect a similar relation for the description of ET reactions. Under what precise conditions this rate formula is valid will be discussed in detail in the following section.

---

7) Obviously, this approximation is identical to the Condon approximation introduced for computing the absorption spectrum in Chapter 5.

7.3   Regimes of Electron Transfer

In the forthcoming discussion, we concentrate on a simple model of a DA complex, neglecting any further bridging units. The corresponding Hamiltonian was introduced in Eq. (7.28), where the diabatic donor and acceptor electronic states have been abbreviated by $|D\rangle \equiv |\varphi_D\rangle$ and $|A\rangle \equiv |\varphi_A\rangle$, respectively (see also Figure 7.14). For the time being it will be convenient to consider the vibrational DOFs in the classical limit.

It is obvious from the previous section that one of the crucial parameters of ET theory should be the intersite coupling. For the electronic two-state model, it is a simple task to consider this coupling exactly, which means to change to the *adiabatic* representation as an alternative to the diabatic representation. Therefore, we start our discussion by introducing this representation. It is obtained after diagonalization of the Hamiltonian, (7.28). According to the results for a two-level system (see Section 2.8.2) and the fact that the vibrational kinetic energies are not affected,[8] we obtain the two adiabatic PESs U_+ and U_- as (compare Section 2.6)

$$U_\pm(q) = \frac{1}{2}\left(U_D(q) + U_A(q) \pm \sqrt{(U_D(q) - U_A(q))^2 + 4|V_{DA}|^2} \right). \qquad (7.40)$$

These adiabatic PESs together with the diabatic PESs are plotted in Figure 7.14 versus a single coordinate q. The crossing point q^* of the two diabatic PESs is defined by $U_D(q^*) = U_A(q^*)$. According to Eq. (7.40), there is a splitting of the adiabatic PESs by $2|V_{DA}|$ at the crossing point of the diabatic PESs. The difference between adiabatic and diabatic curves becomes smaller if q deviates from q^* and both PESs coincide for $|q - q^*| \gg 0$. Clearly, the shape of the adiabatic PES is much more complicated if two or more vibrational coordinates are involved.

Which type of representation is more appropriate depends on the problem under discussion. To give some guidance using *qualitative* arguments, we introduce two characteristic times. A time typical for electronic quantum motion is

$$t_{el} = \frac{\hbar}{|V_{AD}|}. \qquad (7.41)$$

Figure 7.14 Donor and acceptor PESs versus a single reaction coordinate. The diabatic (full line) as well as adiabatic curves (dashed line) are shown. There is a splitting between the adiabatic curves, which has a magnitude of $2|V_{DA}|$ at the crossing point q^*.

---
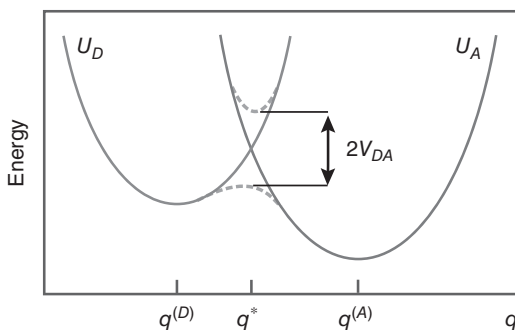
8) The nuclear kinetic energy operators enter as $T_{nuc}|D\rangle\langle D| + T_{nuc}|A\rangle\langle A|$. According to the completeness relation for the electronic states, this is identical to T_{nuc}, which demonstrates that the kinetic energy part remains unaffected by the transformation.

This quantity is proportional to the time the electronic wave function needs to move from the donor site to the acceptor site if the respective energy levels are degenerated (cf. the discussion of the two-level system dynamics in Section 3.12). Degeneracy of the electronic levels occurs if one fixes the vibrational configuration at the crossing point q^*. Provided that the vibrational motion is not effected by strong damping, the characteristic time of the vibrational motion is given by the vibrational frequency[9]

$$t_{vib} = \frac{2\pi}{\omega_{vib}}. \tag{7.42}$$

Let us first assume $t_{el} \ll t_{vib}$. In this case, the electron will move many times between the donor and acceptor before any change in the nuclear configuration occurs. This is the same situation we used in Section 2.3 to motivate the introduction of the Born–Oppenheimer (adiabatic) approximation. We expect that the electronic states will be delocalized over the whole DA complex. The electron is in an *adiabatic* state, and if one is interested in a time scale much larger than t_{el}, it becomes advantageous to change from the localized diabatic to the delocalized adiabatic representation. In particular, any vibrational motion has to be described within the adiabatic PES. Note that in the case that the vibrational motion triggers electronic transitions, a quantum mechanical treatment including the nonadiabaticity operator may be required.

If the energetic difference between the lower and the upper adiabatic PESs is large enough, one has the situation shown in Figure 7.4b where the motion along the reaction coordinate is subject to a double-well potential. Now, we can specify Figure 7.4b noting that for adiabatic ET the formal reaction coordinate can be identified with some – possibly collective – vibrational coordinates coupled to the ET. Therefore, adiabatic ET has to be understood as the rearrangement of the vibrational DOFs from their reactant configuration (minimum of diabatic donor PES) to the product configuration (minimum of diabatic acceptor PES). This rearrangement is connected with a barrier crossing, and we expect for the ET rate an expression of the standard Arrhenius type

$$k_{ET} \propto e^{-E_{act}/k_B T}, \tag{7.43}$$

with the respective activation energy E_{act}.[10]

The opposite situation is encountered if $t_{el} \gg t_{vib}$, that is if the vibrational motion is much faster than the electronic one. This reaction type is called *nonadiabatic* ET. (This should not be confused with the "nonadiabatic" coupling.) The initial and final states of the nonadiabatic ET reaction are spatially rather localized, and the motion of the reaction coordinate through the crossing region is so fast that the electronic wave function has not enough time to move completely from the donor to the

---

9) Usually, molecular systems will have vibrational modes with different vibrational frequencies. Then, ω_{vib} represents a mean frequency. Clearly, if the various frequencies are quite different, the introduction of a mean frequency is meaningless. Instead, one can use different groups of frequencies (high- and low-frequency vibrations, etc.). Of course, particular relations valid for one type of frequencies may be invalid for the other type.
10) The use of the term activation *energy* becomes inadequate if there is a macroscopic number of nuclear DOFs involved. For example, in the case of ET in polar solvents entropic effects enter the description, and one has to replace the activation energy by the activation *free energy*.

acceptor. Only a small fraction of the electronic probability density will reach the acceptor state for each passage of the crossing region.[11]

Since the coupling V_{DA} is small, it is possible to describe the ET carrying out a perturbation expansion with respect to V_{DA}, where the diabatic states represent the zeroth-order states. In the lowest order of perturbation theory (Golden Rule formula), ET occurs if the donor and acceptor levels are degenerated, that is in the crossing region of the two PESs. The transfer rate becomes proportional to $|V_{DA}|^2$, but it also depends on the probability at which the crossing region on the donor PES U_D is reached by the vibrational coordinates. Accordingly, we expect the following expression for the ET rate:

$$k_{ET} \propto |V_{DA}|^2 \, e^{-E_{act}/k_B T}. \tag{7.44}$$

Following Figure 7.14, E_{act} denotes the activation energy needed to reach the crossing region starting at the minimum position of the donor PES; hence, we have $E_{act} = U_D(q^*) - U_D(q^{(D)})$. Of course, this activation energy is different from the one appearing in the case of the adiabatic ET since the latter has been introduced with respect to the barrier in the lower adiabatic PES U_-, Eq. (7.40).

Although the two types of ET introduced so far are the result of very different values of the two characteristic times t_{el} and t_{vib}, the adiabatic as well as the nonadiabatic ET can cover a wide range of time scales up to milliseconds or even slower. On the other hand, if there is a strong DA coupling, ET reactions can proceed ultrafast (in the picosecond to femtosecond range). This situation is usually encountered in photoinduced ET reactions (Section 7.9). Here, experimental observation requires to use ultrafast preparation and detection schemes as well (cf. discussion in Chapter 6).

The foregoing discussion was based on the characteristic times for the electronic and vibrational motion. Alternatively, one can introduce characteristic energies. Let us concentrate on the model of an excess electron. If the excess electron is absent, the minimum position of the PES U_0 is given by $q_\xi = 0$. If the excess electron is introduced into the complex and its wave function is localized at the state $m = D, A$, then the *localization* energy

$$E_{loc} = \frac{1}{2} \sum_\xi \omega_\xi^2 q_\xi^{(m) \, 2} \tag{7.45}$$

is gained. By contrast, if the vibrational coordinates are fixed at the crossing point such that the electronic wave function becomes delocalized, the system may gain the *delocalization* energy (according to the energetic splitting between the D and A levels)

$$E_{del} = |V_{AD}|. \tag{7.46}$$

---

11) It should be noted here that we use the term "electronic probability density" instead of "electron," indicating that quantum mechanics only fixes the change of the wave function in the course of the time propagation. It is meaningless to ask how fast or slow the electron itself moves within the ET reaction. The reader should also note the similarity between the nonadiabatic ET and the electronic transition occurring in a linear absorption experiment. There, the weak transfer coupling of ET is replaced by the weak external electromagnetic field, both realizing an interstate coupling (cf. discussion in Chapter 6).

According to the definition of the characteristic energies, we can conclude that nonadiabatic ET occurs if $E_{loc} \gg E_{del}$. If it is energetically more favorable for the electron to be in a delocalized state ($E_{loc} \ll E_{del}$), the ET is adiabatic.

Let us return to ET rate formulas whose limiting cases, the adiabatic and the nonadiabatic ET, were estimated above. Both ET rates have been characterized by formulas of type

$$k_{ET} = \nu e^{-E_{act}/k_B T}. \tag{7.47}$$

This rate includes the activation energy for barrier crossing and the quantity ν. The latter has the dimension of a frequency and is usually called *frequency factor*. In the case of adiabatic ET, the inverse of the frequency factor is simply given by the time it takes to move along the reaction coordinate to the top of the barrier. A more detailed inspection shows that this reasoning is not correct for every type of adiabatic ET. For instance, consider a DA complex dissolved in a polar solvent. Here, the transferred electron may be strongly coupled to the solvent, and the motion of the reaction coordinate of the ET is overdamped. The rate will be mainly determined by the way the reaction coordinate reaches the crossing point. In particular, the frequency factor ν becomes proportional to $1/\tau_{rel}$, the inverse of the solvent relaxation time. This type of ET is often called *solvent-controlled*. If the nuclear coordinates (and solvent DOFs) that are coupled to the ET reaction move in such a manner that the reaction coordinate is only weakly perturbed, the motion is called *uniform*. If, however, there is a strong perturbation, the motion on the respective PES becomes irregular *diffusion*like.

This example shows that it is important to understand how one can formulate a theory for ET reactions that is valid not only for the two described limiting cases but also in the intermediate regime. To bridge the gap between the nonadiabatic ET and the adiabatic ET with uniform reaction coordinate dynamics, *Landau-Zener* theory is appropriate as will be explained in the following section.

The classical consideration of the vibrational motion assumes for the ET a thermal activation of the vibrational DOFs to reach the crossing region. If the temperature decreases such that $k_B T \ll E_{act}$, ET has to proceed via tunneling through the barrier between the donor and acceptor nuclear equilibrium configurations. This so-called *nuclear tunneling* case can be found in nonadiabatic as well as adiabatic ET reactions. It requires a quantum mechanical treatment of the vibrational coordinates.

In the case of nonadiabatic ET, one can use the Hamiltonian, Eq. (7.39), with energy levels E_{mM}. Considering a DA complex without bridge units and neglecting the coupling to any environment, the system of the two sets of energy spectra, E_{DM} and E_{AN}, represents a closed quantum system, and reversible quantum dynamics has to be expected in this multilevel systems (cf. Figure 7.15). In the presence of an environment, one has an open system, and every electron–vibrational state $|mM\rangle$ has a *finite* lifetime τ_{mM}. For simplicity, we assume the existence of a single representative lifetime τ_{rel} for the following discussion. If $\tau_{rel} < t_{vib}$ and t_{el}, a fast relaxation occurs
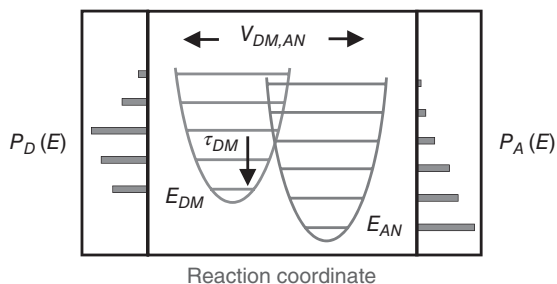
Figure 7.15 Ultrafast ET in a system of two coupled PESs with donor, E_{DM}, and acceptor, E_{AN}, vibrational levels as well as coupling matrix elements $V_{DM,AN}$. Left scheme: population P_D of the donor levels after optical excitation (cf. Figure 6.12), right scheme: population P_A of the acceptor levels after ET and relaxation. (If both spectra are degenerated, a direct transfer from a selected level E_{DM} to a level E_{AN} becomes possible, probably connected with a backtransfer. If degeneracy is absent, a set of different levels is coupled simultaneously.)

before any ET takes place,[12] and a description based on transition rates is suitable. This will be the case for the nonadiabatic ET discussed in Section 7.4.

If the lifetime of the electron–vibrational states is larger than the characteristic times t_{vib} and t_{el}, only a weak disturbance of wavelike nuclear motions in the course of the ET appears. This is typical for photoinduced ET where vibrational coherences at the donor and acceptor states can be observed on a subpicosecond time scale (see Section 7.9).

7.3.1 Landau–Zener Theory of Electron Transfer

To characterize the general aspects of the ET in a DA complex, we introduce a widely used *classical* treatment, developed by Landau and independently by Zener. Originally, Landau considered the scattering between two atoms, whereas Zener focused on the electronic levels of a diatomic molecule. In both cases, level coupling has been considered under the condition that the level separation is changed by an external perturbation. This approach is easily mapped onto the description of ET in a DA complex. The advantage is that one can derive an analytical formula for the transfer rate that is valid for any value of the coupling V_{DA} spanning the range between adiabatic and nonadiabatic ET. The actual derivation makes use of the diabatic representation.

In order to deal with the ET reaction in a DA complex according to Landau and Zener, one has to choose a *classical* description for a single vibrational coordinate. To obtain the ET rate, we let the vibrational coordinate start to move on the donor PES far away from the crossing point q^* with the acceptor PES. If the coordinate

---

12) Note that we have to guarantee that the coupling to the particular environment is not too strong. If $1/\tau_{rel} \gg \omega_{vib}$, the energy levels E_{mM} become meaningless since in this case of strong coupling, a separate definition of the diabatic energy spectrum E_{mM} cannot be justified.

moves through the crossing region, we will determine the probability that the electron will be transferred to the acceptor state as well as the probability for remaining at the donor state.

The corresponding Hamiltonian of the DA complex was introduced in Eq. (7.28). The vibrational Hamiltonian $H_m(q)$ ($m = D, A$) includes the donor and acceptor PESs $U_D(q)$ and $U_A(q)$, respectively. Both depend on the single vibrational coordinate q and may in principle have an arbitrary shape. Since the crossing point q^* between the PESs is crucial for the transfer, we expand both PESs around q^*

$$U_m(q) = U^* - F_m(q^*)\Delta q. \tag{7.48}$$

Here,

$$F_m(q^*) = -\left.\frac{\partial U_m(q)}{\partial q}\right|_{q=q^*} \tag{7.49}$$

denotes the force the vibrational coordinate experiences at the crossing point when the electron is in state $m = D, A$. Furthermore, we introduced $\Delta q = q - q^*$, and U^* abbreviates $U_D(q^*) = U_A(q^*)$ (cf. Figure 7.16).

The time dependence of the coordinate q (or Δq) is unknown so far. Since we expect the ET reaction to take place at the curve crossing around $\Delta q \approx 0$, we set $\Delta q \approx v^* t$, where v^* is the yet unknown velocity at the crossing point. It represents a parameter of the theory that should be estimated. By virtue of these approximations, the Hamiltonian becomes formally time dependent

$$H_{DA} = T_{vib} + U^* + H_0(t) + \hat{V}. \tag{7.50}$$

The classical part $T_{vib} + U^*$ is of less interest for the following; the time-dependent part reads

$$H_0(t) = -F_D \, v^* t \, |D\rangle\langle D| - F_A \, v^* t \, |A\rangle\langle A|. \tag{7.51}$$

Further, the interstate coupling is comprised in

$$\hat{V} = V_{DA}|D\rangle\langle A| + \text{h.c.} \tag{7.52}$$

The reactant state of the transfer corresponds to $t = -\infty$ ($\Delta q = -\infty$), whereas the product state is characterized by $t = \infty$ ($\Delta q = \infty$, see Figure 7.16).

In a first step, we calculate the asymptotic value of the survival probability of the electron for remaining at the donor, $P_D \equiv P_D(t = \infty)$. This quantity follows as the square of the transition amplitude (compare Section 3.3.1)

$$P_D = |\langle D|U(\infty, -\infty)|D\rangle|^2, \tag{7.53}$$
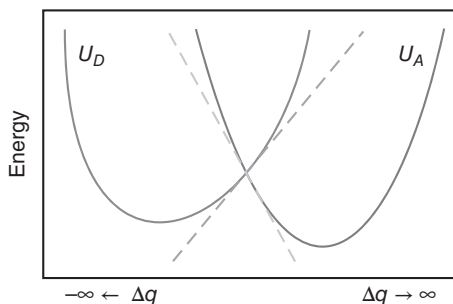
Figure 7.16 The coupled PES of a DA complex versus a single reaction coordinate. According to the treatment in the Landau–Zener theory, the PESs are approximated by straight lines around the crossing point. The asymptotic regions $\Delta q \to \pm\infty$ are also indicated.

where the time-evolution operator $U(t, t')$ is given by the Hamiltonian $H_0(t) + \hat{V}$, Eq. (7.50). Interestingly, the present model allows to calculate this transition amplitude exactly, as demonstrated in detail in the supplementary Section 7.10.1. Here, we only quote the result for the donor survival probability:

$$P_D = e^{-\Gamma}. \tag{7.54}$$

It depends on the so-called Massey parameter, which is defined as

$$\Gamma = \frac{2\pi}{\hbar v^*} \frac{|V_{DA}|^2}{|F_D - F_A|}. \tag{7.55}$$

Although it is of interest to have an expression for the survival probability P_D, we aim to get the ET rate k_{DA} based on our knowledge of P_D. The ET rate can be defined by the redistribution of probability density between the donor and acceptor within the characteristic time interval $t_{\text{vib}} = 2\pi/\omega_{\text{vib}}$. This time interval is a good estimate for the time the vibrational coordinate needs to go from the region around the minimum of the donor PES to that around the minimum of the acceptor PES and back. Considering the coordinate Δq, this vibrational motion formally corresponds to the motion between the two asymptotic values $\pm\infty$, that is to the transition from $\Delta q = -\infty$ to $\Delta q = \infty$ and back to $\Delta q = -\infty$ (cf. Figure 7.16). Determining the rate for a single transition event from the donor to the acceptor within the time interval t_{vib}, one has to account for two alternative ways: Either one goes from $\Delta q = -\infty$ to $\Delta q = \infty$ and a transition to the acceptor takes place; then, on the way back to $\Delta q = -\infty$, the system has to remain at the acceptor state. Or, the system remains at the donor state during the motion from $\Delta q = -\infty$ to $\Delta q = \infty$, but on the way back, when passing the crossing region, it moves to the acceptor state.

To calculate the ET rate for the first pathway, we note that the probability for going to the acceptor as the coordinate moves from $\Delta q = -\infty$ to $\Delta q = \infty$ is $1 - P_D$. Due to the symmetry of the problem, the probability to make no transition on the way back to $\Delta q = -\infty$ is identical to P_D. In conclusion, we obtain the change in the probability within a single oscillation period as $(1 - P_D)P_D$. In the second case of realizing the ET, the system remains with probability P_D in the donor state as the coordinate moves from $\Delta q = -\infty$ to $\Delta q = \infty$. On the way back, a transition to the acceptor state occurs with probability $1 - P_D$. This is indeed the same result as for the first transition pathway. Therefore, we obtain the transition rate as

$$k_{DA} = \frac{\omega_{\text{vib}}}{2\pi} \; 2(1 - P_D)P_D \equiv \frac{\omega_{\text{vib}}}{\pi} \; e^{-\Gamma} \; \left(1 - e^{-\Gamma}\right). \tag{7.56}$$

The expression is valid for *every* value of V_{DA}, thus covering the case of adiabatic as well as nonadiabatic ET. For large Γ (and hence large V_{DA}), we obtain the rate for adiabatic ET[13)]

$$k_{DA}^{(\text{adia})} = \frac{\omega_{\text{vib}}}{\pi} \; e^{-\Gamma}, \tag{7.57}$$

while for small Γ, the nonadiabatic limit follows:

$$k_{DA}^{(\text{nonad})} = \frac{2\omega_{\text{vib}}}{\hbar v^*} \frac{|V_{DA}|^2}{|F_D - F_A|}, \tag{7.58}$$

---

13) Obviously, the limit $V_{DA} \to \infty$ is meaningless, since for this case k_{DA} vanishes.

with a rate proportional to the square of the electronic coupling. For the intermediate regime that rate has to be calculated according to Eq. (7.56).

Introducing the Landau–Zener length,

$$l_{\mathrm{LZ}} = \frac{2\pi |V_{DA}|}{|F_D - F_A|}, \tag{7.59}$$

the Massey parameter becomes

$$\Gamma = l_{\mathrm{LZ}} \frac{|V_{DA}|}{\hbar v^*}. \tag{7.60}$$

The Landau–Zener length can be understood as the distance from the crossing point where the difference $U_D - U_A$ in the potential energy equals the magnitude of the electronic coupling V_{DA}.[14] Therefore, it gives an estimate for those Δq values up to which the coupling V_{DA} has some influence on the transfer dynamics.

Let us consider a liquid phase situation next. Here, ET reactions can be characterized by introducing a mean free path length l_{f} for the reaction coordinate. It corresponds to the average distance between two collision events of the reaction coordinate with solvent molecules. If $l_{\mathrm{f}} \gg l_{\mathrm{LZ}}$, the reaction coordinate can be considered to carry out a ballistic motion (or uniform motion) on the time scale of the ET with only minor influence of collisions with the solvent molecules. In the opposite case $l_{\mathrm{f}} \ll l_{\mathrm{LZ}}$, the motion is diffusive on the time scale of the ET. Of course, in both cases, the ET can take place either in the adiabatic or nonadiabatic regime, depending on the actual value of Γ. This situation is visualized in Figure 7.17.
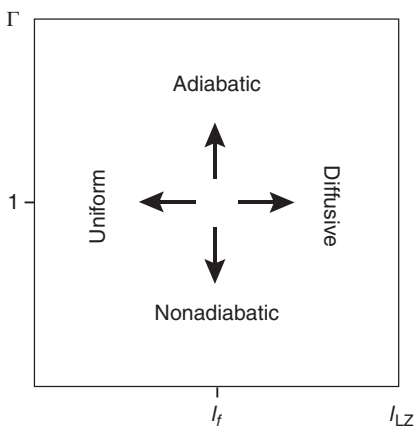
Figure 7.17 Schematic representation of the different ET regions. The horizontal axis distinguishes between the uniform and diffusive motion of the reaction coordinate by plotting the Landau–Zener length l_{LZ}, Eq. (7.59), in relation to a given mean free path length l_{f}. Along the vertical axis, adiabatic and nonadiabatic transfer is differentiated using the Massey parameter Γ defined in Eq. (7.60).

---

14) To show this, let us consider the expression $U_D(q^* + \Delta q) - U_A(q^* + \Delta q)$, which measures the potential energy difference between the case where the electron is at the donor and the case where it is at the acceptor. Expanding this expression with respect to the deviation Δq from the crossing point of both PESs, we estimate the PES difference as $|F_D - F_A| \, |\Delta q|$. Using now Eq. (7.59), we may write $|(F_D - F_A)| l_{\mathrm{LZ}} = 2\pi |V_{\mathrm{DA}}|$, which justifies the given explanation of the Landau-Zener length.

7.4 Nonadiabatic Electron Transfer in a Donor–Acceptor Complex

The concept of nonadiabatic ET was introduced in the preceding section as a charge transition process for which the vibrational motion is much faster than the motion of the transferred electron. The type of rate equation we have to expect can be found in Eq. (7.44). In what follows, we consider this important type of ET reaction in more detail. The interest in nonadiabatic ET reactions stems from the fact that bridge-mediated long-range ET usually proceeds in this limit. This more complex type of ET will be dealt with in Section 7.5. Here, we concentrate on nonadiabatic ET in a simple DA complex.

Since for nonadiabatic ET we have to account for the transfer coupling between the donor and the acceptor in the lowest order of perturbation theory, we are in the position to write down the general rate formula (valid at any temperature) using the results of Chapter 6, which deals with transitions between different electronic states. There, it has been shown that the computation of the transition rate can be reduced to the determination of a properly defined spectral density. Once this quantity is obtained (which requires the harmonic oscillator approximation for the related PES), the transfer rate can be calculated for all temperatures. In addition, vibrational modes with frequencies extending over a broad range can be incorporated. However, to provide an overview of the various approaches that can be found in the literature, we discuss different limiting cases of nonadiabatic ET. Thus, we approach the most general description of ET dynamics step by step, starting our considerations with the high-temperature limit.

7.4.1 High-temperature Case

The high-temperature limit is applicable if the relation $k_B T \gg \hbar\omega_\xi$ holds for all vibrational modes ξ. In such a situation, it is possible to describe the vibrational dynamics in the framework of classical physics. If the classical description is not possible for all types of vibrations, one has to study the subset of the high-frequency quantum modes by means of quantum mechanics (see the following section).

To derive the rate expression for the ET process, we consider the case of an excess electron in the DA complex. Then, the appropriate Hamiltonian is given by Eq. (7.28), where the PES $U_m(q)$ ($q \equiv \{q_\xi\}$) for the electron at the donor or acceptor site ($m = D, A$) follows from Eq. (7.25). Since we consider classical vibrational dynamics, the Hamiltonian H_m is replaced by the Hamiltonian functions $H_m(q(t), p(t))$ defined via the time-dependent vibrational momenta and coordinates for a given electronic state. As was demonstrated in Section 3.13, the incorporation of classical dynamics into the quantum dynamical description of transfer process is conveniently done using the Wigner representation (cf. Section 3.4.4). Its application to reaction rates is outlined in the supplementary Section 7.10.3. In what follows, we give a discussion of the rate $k_{ET} \equiv k_{DA}$ for the ET from the donor to the acceptor, which is based on more simpler arguments.

Since the vibrational coordinates are described classically, the ET system reduces to a simple electronic two-level DA system. But the two-level system is characterized by a time-dependent modulation of the energetic position of the two states due to the classical vibrational motion. Furthermore, in typical experimental situations, only an average with respect to a large number of identical DA complexes is of interest. This average can be replaced by an ensemble average with respect to the thermal equilibrium distribution function $f(q, p)$ (cf. Section 3.86), which represents the probability distribution for the vibrational DOFs in the reactant state. Applying the reasoning that leads to the Golden Rule of quantum mechanics, we arrive at a formula for the rate similar to Eq. (3.86) (however, the summation with respect to the quantum levels has been replaced by an integration over all vibrational coordinates and momenta). Since $H_D(q, p)$ and $H_A(q, p)$ enter the δ-function part of the Golden Rule formula, the kinetic energy contributions compensate each other. The average with respect to the momenta can be carried out leading to the coordinate distribution function

$$f(q) = \frac{1}{\mathcal{Z}} e^{-U_D(q)/k_B T},$$ (7.61)

and the following rate expression is obtained:

$$k_{ET} = \frac{2\pi}{\hbar} \int dq \, f(q) |V_{DA}|^2 \delta \left(U_D(q) - U_A(q) \right).$$ (7.62)

This formula gives the ET rate as the transition rate between the initial electronic state with energy $U_D(q)$ and the final state with energy $U_A(q)$ averaged with respect to all possible configurations of the vibrational coordinates. The averaging is weighted by the thermal distribution, Eq. (7.61). Therefore, Eq. (7.62) implies that there is no change of the vibrational kinetic energy during ET. In the supplementary Section 7.10.3, we give a justification for the present treatment (as well as a possible extension), and Section 7.4.3 demonstrates that the high-temperature case can be obtained as a certain limit of a rate expression valid for any temperature.

If parabolic PESs are used, an analytical expression for the ET rate can be obtained. Let us start with the simple case of a single coordinate q oscillating with frequency ω_{vib}. Note that we also will neglect any dependence of the transfer integral V_{DA} on this coordinate (Condon-like approximation). We obtain for the argument of the delta function in Eq. (7.62)

$$U_D(q) - U_A(q) = U_D^{(0)} - U_A^{(0)} + \frac{\omega_{vib}^2}{2} \left(\left(q - q^{(D)} \right)^2 - \left(q - q^{(A)} \right)^2 \right)$$

$$= \Delta E - \omega_{vib}^2 (q^{(D)} - q^{(A)}) q + \frac{\omega_{vib}^2}{2} (q^{(D)2} - q^{(A)2}).$$ (7.63)

Here, we introduced the energetic difference between the donor and acceptor PESs

$$\Delta E = U_D^{(0)} - U_A^{(0)},$$ (7.64)

which is frequently called the *driving force* of the ET reaction. The argument of the delta function in (7.62) is linear with respect to q and vanishes at

$$q^* = \frac{\Delta E + \frac{\omega_{vib}^2}{2} \left(q^{(D)2} - q^{(A)2} \right)}{\omega_{vib}^2 (q^{(D)} - q^{(A)})}.$$ (7.65)

Figure 7.18 Potential energy surfaces for a DA complex in harmonic approximation. The definition of the driving force ΔE and the reorganization energy E_λ are indicated.
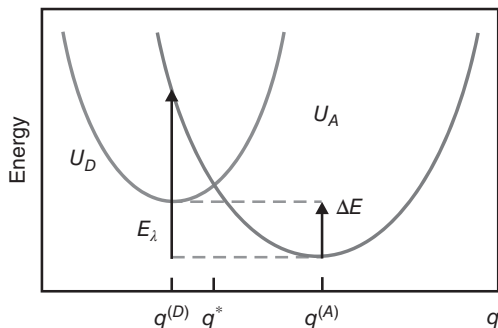
This particular value of q defines the crossing point of both PESs (Figure 7.18). The thermal distribution introduced in Eq. (7.61) reads

$$f(q) = \sqrt{\frac{\omega_{\text{vib}}^2}{2\pi k_{\text{B}}T}} \exp\left\{ -\frac{\omega_{\text{vib}}^2(q - q^{(D)})^2}{2k_{\text{B}}T} \right\}, \tag{7.66}$$

and performing the q-integration results in

$$k_{\text{ET}} = \frac{2\pi}{\hbar} \frac{|V_{DA}|^2}{\sqrt{2\pi k_{\text{B}}T\omega_{\text{vib}}^2\left(q^{(D)} - q^{(A)}\right)^2}} \exp\left\{ -\frac{\omega_{\text{vib}}^2\left(q^* - q^{(D)}\right)^2}{2k_{\text{B}}T} \right\}. \tag{7.67}$$

The obtained rate formula is of the type of Eq. (7.44). It represents the activation law for reaching the crossing point $q = q^*$ between the donor and the acceptor PESs. The activation energy is given by

$$E_{\text{act}} = \frac{1}{2}\, \omega_{\text{vib}}^2\left(q^* - q^{(D)}\right)^2. \tag{7.68}$$

This expression can be rewritten to give

$$E_{\text{act}} = \frac{(\Delta E - E_\lambda)^2}{4E_\lambda}. \tag{7.69}$$

The quantity

$$E_\lambda = \frac{\omega_{\text{vib}}^2}{2}\left(q^{(A)} - q^{(D)}\right)^2 \tag{7.70}$$

is the potential energy of the vibrational coordinate, which corresponds to the following situation: Initially, the electron is at the donor, and the vibrational coordinate has the value $q = q^{(D)}$. Then, a sudden change in the electronic state occurs (see Figure 7.18). In order to reorganize the vibrational coordinate (nuclear configuration) to the new equilibrium value $q^{(A)}$, the energy E_λ has to be removed from the system. Therefore, this energy is usually called *reorganization energy* (cf. the discussion of the reaction path Hamiltonian in Chapter 2). If the ET reaction proceeds in a solvent, the change in the electronic charge density in the DA complex is accompanied by a rearrangement of the solvent polarization field. Thus, the name *polarization energy* is also common for E_λ.[15]

15) A detailed account on the formulation of nonadiabatic ET in polar solvents can be found in May and Kühn [5].

The rate expression that follows upon introducing E_λ is named after R. A. Marcus, who pioneered the theory of ET reactions starting in the 1950s. It reads

$$k_{ET} = |V_{DA}|^2 \sqrt{\frac{\pi}{\hbar^2 k_B T E_\lambda}} \exp\left\{ -\frac{(\Delta E - E_\lambda)^2}{4 E_\lambda k_B T} \right\}. \tag{7.71}$$

Before discussing this result in detail, we note that the same expression is valid if we consider not a single but a large number of vibrational coordinates for the donor and acceptor PESs as introduced in Eq. (7.25). The only change concerns the reorganization energy, which has to be generalized from Eq. (7.70) to the case of many vibrational DOFs according to (details can be found in the supplementary Section 7.10.2)[16]

$$E_\lambda = \sum_\xi \frac{\omega_\xi^2}{2} \left(q_\xi^{(D)} - q_\xi^{(A)} \right)^2. \tag{7.72}$$

It is the main advantage of the Marcus formula that it allows one to describe the complex vibrational dynamics accompanying the electronic transition by a small number of parameters, namely the transfer coupling V_{DA}, the driving force ΔE, and the reorganization energy E_λ.[17] In particular, the introduction of the reorganization energy reduces the complicated influence of many intra- and intermolecular nuclear DOFs (or the polarization in the case of a polar solvent) to a single number.

Since the Marcus formula includes only three unknown quantities, a straightforward fit of experimental ET data often becomes possible, particularly if the temperature dependence of the rate is measured. Usually, one plots $\log k_{ET}$ versus $1/T$ in the so-called *Arrhenius plot*. Doing experiments on ET reactions in DA complexes dissolved in a polar solvent, the reorganization energy can be varied using solvents with different polarity. A controllable change in ΔE and V_{DA} is also possible altering the details of the chemical structure of the complex (cf. Figure 7.20).

Equation (7.71) describes the ET reaction proceeding from the donor to the acceptor. The rate of the backtransfer from the acceptor to the donor can be easily derived in the used model of donor and acceptor PESs with identical parabolic shapes. It is only necessary to interchange the donor and acceptor indices, leading to a change in the sign of ΔE. We get

$$k_{AD} = k_{DA}(-\Delta E) = e^{-\Delta E/k_B T} k_{DA}(\Delta E). \tag{7.73}$$

The ratio of the forward and backward rates is given by $\exp\{\Delta E/k_B T\}$; that is, the validity of the detailed balance condition is guaranteed.

Let us consider the ET rate in dependence on the driving force ΔE of the reaction at a given value of V_{DA} and E_λ. The situation already displayed in Figure 7.18 is called the *normal region* of ET. Starting in this ET region and increasing ΔE moves q^* to the left until the activation energy becomes zero for $\Delta E = E_\lambda$ (Figure 7.19). This is

---

16) If the shapes of the two coupled PESs differ, that is if the vibrational frequencies become electronic state dependent, a generalization of Eq. (7.71) can be derived as shown in Casado-Pascual et al. [6].
17) If the number of vibrational DOFs is macroscopic, the energy difference of the PES minima has to be replaced by the free energy difference.

Figure 7.19 The normal region (a), the activationless case (b), and the inverted region (c) of ET in a DA complex.
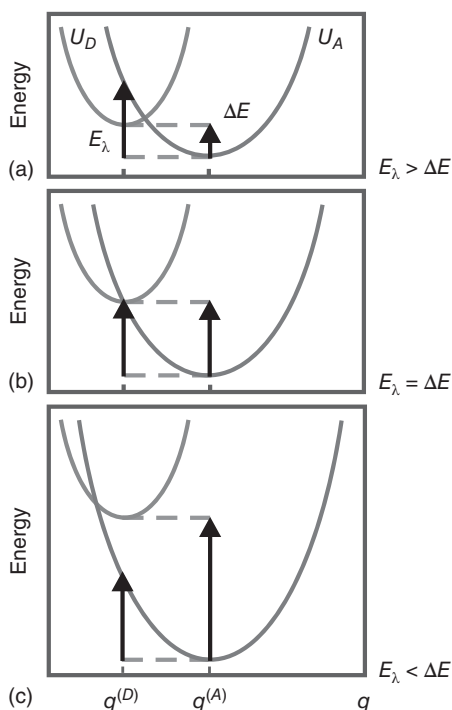
the *activationless case*. This regime of ET is observed in the experiment if the rate becomes independent of temperature. Increasing ΔE further, the activation energy increases again. This is the so-called *inverted region*. Looking at Figure 7.19c one may notice the possible strong overlap of vibrational wave functions corresponding to the presence of the transferred electron at the donor and the acceptor. Hence, in the inverted region, nuclear tunneling may become important instead of the thermally activated transfer studied so far.

ET in the inverted region has been originally proposed by R. A. Marcus in the 1950s, but it could be verified experimentally only in the late 1980s. Figure 7.20 shows how one enters the inverted region by changing systematically the acceptor compound such that ΔE is increased.

7.4.2 High-temperature Case: Two Independent Sets of Vibrational Coordinates

In the foregoing section, we applied a model that assumed a common set of vibrational coordinates $q \equiv \{q_\xi\}$ for both the reactant and the product states. This is typical for unimolecular reactions. Next, let us consider a bimolecular ET reaction proceeding in solution where the separate donor and acceptor molecules form an encounter complex to trigger ET, cf. Figure 7.2. Here, it is more appropriate to use a separate set of vibrational coordinates $q_D \equiv \{q_{D\xi}\}$ for the donor molecule and $q_A \equiv \{q_{A\xi}\}$ for the acceptor molecule as discussed in Section 7.2.2.2. Of course,
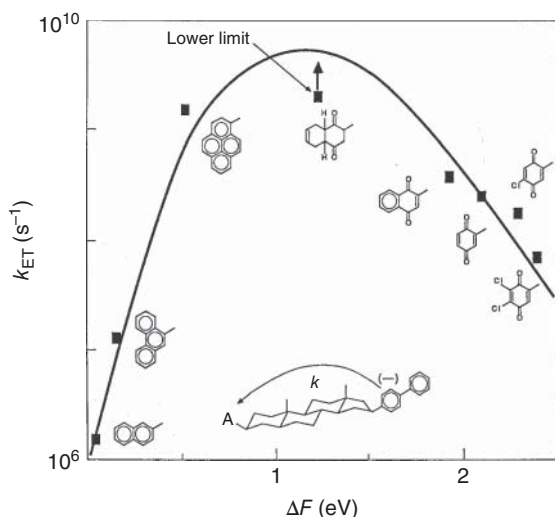
Figure 7.20 ET rate versus driving force of the reaction for a DA complex showing transfer in the inverted region. A steroid spacer (androstane) links a 4-biphenylyl donor group with different acceptors (shown below the curve). An excess electron has been attached to the donor by means of a pulsed electron beam. The complex was dissolved in methyltetrahydrofuran. The full curve has been computed from Eq. (7.104) using known parameters for the specific system (Reproduced with permission from Closs and Miller [7]/ American Association for the Advancement of Science).

if solvent contributions become important, the two separate sets of vibrational coordinates have to be supplemented by an additional third set of common coordinates. The same holds true if coordinates modulating the DA intermolecular distance are of importance.

Having distinct sets of coordinates for the donor and acceptor requires a separate description of the initial and final states of the donor and the acceptor. We consider Scheme (7.5) to be valid; that is, the reactant state is $|\phi_{D-}, \phi_A\rangle$ with PESs U_{D-} and U_A, and the product state is $|\phi_D, \phi_{A-}\rangle$ with PESs U_D and U_{A-} (cf. Figure 7.21 and Section (7.2.2.2) for the notation).
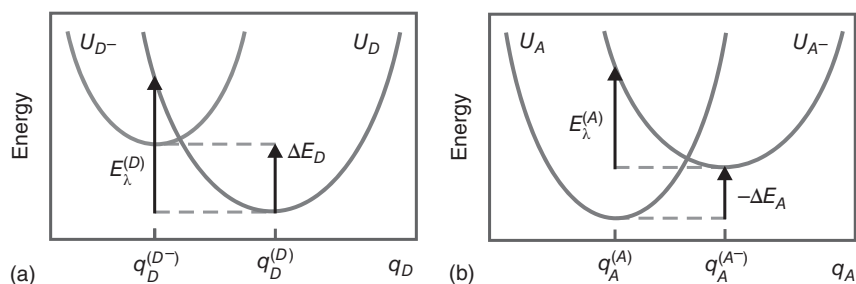
Figure 7.21 PES for the case of independent vibrational coordinates of the donor and the acceptor parts. (a) PES of the negatively charged and neutral donor and (b) the respective PESs of the acceptor. Related reorganization energies and driving forces (for $\hbar\omega = 0$) are also shown.

The ET rate equation (7.62) is easily generalized to the present case and reads (note that $\int dq_D \, dq_A$ is a shorthand notation for the multidimensional integration)

$$k_{\mathrm{ET}}^{(\mathrm{bimol})} = \frac{2\pi}{\hbar} |V_{DA}|^2 \int dq_D \, dq_A \, f_{D^-}(q_D) f_A(q_A)$$
$$\times \delta \left([U_{D^-}(q_D) + U_A(q_A)] - [U_D(q_D) + U_{A^-}(q_A)] \right). \tag{7.74}$$

Since there is a separation into vibrational coordinates belonging to the donor and the acceptor, the energy conserving delta function in the rate formula can be split up into a donor part and an acceptor part. This is achieved by introducing an additional frequency integral according to

$$\delta \left([U_{D^-}(q_D) + U_A(q_A)] - [U_D(q_D) + U_{A^-}(q_A)] \right)$$
$$= \int d\hbar\omega \, \delta \left(U_{D^-}(q_D) - \hbar\omega - U_D(q_D) \right)$$
$$\times \delta \left(U_A(q_A) + \hbar\omega - U_{A^-}(q_A) \right). \tag{7.75}$$

Let us define the auxiliary functions

$$d(\omega) = \int dq_D \, f_{D^-}(q_D) \, \delta \left(U_{D^-}(q_D) - \hbar\omega - U_D(q_D) \right) \tag{7.76}$$

and

$$a(\omega) = \int dq_A \, f_A(q_A) \, \delta \left(U_A(q_A) + \hbar\omega - U_A^-(q_A) \right). \tag{7.77}$$

Then, the rate follows as a frequency overlap of the two auxiliary functions

$$k_{\mathrm{ET}}^{(\mathrm{bimol})} = \frac{2\pi}{\hbar} |V_{DA}|^2 \int d\hbar\omega \, d(\omega) a(\omega). \tag{7.78}$$

Inspecting the argument of the delta functions in Eqs. (7.76) and (7.77), one can give a physically appealing interpretation. The function $d(\omega)$ can be understood as the frequency-resolved strength of the detachment process where the excess electron is removed from the donor. In the same manner, we understand $a(\omega)$ as the spectrum for the attachment of the excess electron at the acceptor.[18]

Using the results of the preceding section, we are able to derive explicit expressions for the auxiliary functions. We obtain

$$d(\omega) = \frac{1}{\sqrt{4\pi k_{\mathrm{B}} T E_\lambda^{(D)}}} \exp \left\{ -\frac{\left(\Delta E_D - E_\lambda^{(D)} \right)^2}{4 E_\lambda^{(D)} k_{\mathrm{B}} T} \right\} \tag{7.79}$$

and

$$a(\omega) = \frac{1}{\sqrt{4\pi k_{\mathrm{B}} T E_\lambda^{(A)}}} \exp \left\{ -\frac{\left(\Delta E_A - E_\lambda^{(A)} \right)^2}{4 E_\lambda^{(A)} k_{\mathrm{B}} T} \right\}. \tag{7.80}$$

---

18) We will encounter such a type of rate formula again in Chapter 9 when studying the transfer of intramolecular excitation energy.

The two newly introduced driving forces read

$$\Delta E_D = U_{D^-}^{(0)} - U_D^{(0)} - \hbar\omega \tag{7.81}$$

and

$$\Delta E_A = U_A^{(0)} + \hbar\omega - U_{A^-}^{(0)}. \tag{7.82}$$

The reorganization energies are obtained as

$$E_\lambda^{(D)} = \sum_\xi \frac{\omega_\xi^2}{2} \left(q_\xi^{(D^-)} - q_\xi^{(D)} \right)^2 \tag{7.83}$$

and

$$E_\lambda^{(A)} = \sum_\xi \frac{\omega_\xi^2}{2} \left(q_\xi^{(A)} - q_\xi^{(A^-)} \right)^2. \tag{7.84}$$

The frequency integration in the rate formula (7.78) can be performed straightforwardly. Again, one obtains the Marcus-type expression equation (7.71) but with the driving force given by the electronic energy difference of the reactant and the product states:

$$\Delta E = U_{D^-}^{(0)} - U_D^{(0)} + U_A^{(0)} - U_{A^-}^{(0)}. \tag{7.85}$$

The reorganization energy follows as the sum of the energies of the donor and the acceptor:

$$E_\lambda = E_\lambda^{(D)} + E_\lambda^{(A)}. \tag{7.86}$$

7.4.3 Low-temperature Case: Nuclear Tunneling

We now return to the case of a common set of vibrational coordinates for the donor and acceptor. Additionally, we suppose that $k_B T < \hbar\omega_\xi$ holds for all vibrational DOFs participating in the ET reaction. Hence, a quantum mechanical description becomes necessary. In this situation, the appropriate DA Hamiltonian is given by Eq. (7.39) (neglecting any bridge units).

As in the case of the classical description of the nuclear motion discussed so far, we consider ET reactions that proceed in an ensemble of identical DA complexes. The initial state is characterized by the vibrational energy levels E_{DM}, and the levels E_{AN} belong to the final acceptor states. How to obtain the rate of the total probability transfer from the donor state to the acceptor state has been discussed in Section 3.3 and in another context in Section 3.4.5. Again, we remind the reader that the time $\tau_{\rm rel}$ characterizing vibrational relaxation in the donor or the acceptor state has to be much shorter than all other characteristic times ($t_{\rm el}$ and $t_{\rm vib}$, see Eqs. (7.41) and (7.42), cf. discussion at the end of Section 7.3). Adapting these earlier results to the present situation, we obtain the rate of nonadiabatic ET as

$$k_{\rm ET} = \frac{2\pi}{\hbar} \sum_{M,N} f_{DM} |V_{DM,AN}|^2 \delta(E_{DM} - E_{AN}). \tag{7.87}$$

This Golden Rule formula describes the coupling of the initial manifold of states with that of the final states via a certain interaction matrix element. A thermal averaging of all initial vibrational states is carried out, and the rate contains the sum with respect to all final vibrational states. Neglecting the dependence of the electronic transfer integrals V_{DA} on the nuclear DOFs, $V_{DM,AN}$ splits up into the purely electronic transfer coupling V_{DA} and the Franck–Condon overlap integral $\langle \chi_{DM} | \chi_{AN} \rangle$.

As stated in Section 6.2, there is a formal similarity between the nonadiabatic ET from the donor to the acceptor and the optically induced electronic transition from the ground state to a particular excited electronic state of some molecule. This analogy suggests the introduction of the combined thermally averaged and Franck–Condon-weighted density of states, $\mathcal{D}$, such that for the present case the ET rate becomes

$$k_{\mathrm{ET}} = \frac{2\pi}{\hbar} |V_{DA}|^2 \mathcal{D}(\Delta E/\hbar). \tag{7.88}$$

The density of states reads

$$\mathcal{D}(\omega) = \sum_{M,N} f_{DM} |\langle \chi_{DM} | \chi_{AN} \rangle|^2 \delta \left(\hbar\omega + \sum_\xi \hbar\omega_\xi (M_\xi - N_\xi) \right). \tag{7.89}$$

It has to be taken at the driving force ΔE introduced in Eq. (7.71) to get k_{ET}. Following the considerations in Section 6.2.3, we can rewrite $\mathcal{D}$ via a time integral as

$$\mathcal{D}(\Delta E/\hbar) = \frac{1}{2\pi\hbar} e^{-G(0)} \int dt \, e^{i\Delta Et/\hbar + G(t)}, \tag{7.90}$$

with[19]

$$G(t) = \sum_\xi \left(g_D(\xi) - g_A(\xi) \right)^2 \left(e^{-i\omega_\xi t}(1 + n(\omega_\xi)) + e^{i\omega_\xi t} n(\omega_\xi) \right). \tag{7.91}$$

The function $G(t)$ was introduced in Section 6.2.3. It is of a universal character and appears whenever transitions among different electronic levels are accompanied by the rearrangement of nuclear coordinates that have been mapped on a set of independent harmonic oscillators (normal mode vibrations).

If the number of different vibrational modes becomes large, it is advisable to introduce a special type of *spectral density* responsible for the ET reaction in a DA complex (different types of spectral densities were already discussed in Sections 3.7.3 and 6.2.4). For the present application, we write in analogy to the case of nonadiabatic transitions (cf. Eq. (6.36))

$$J_{DA}(\omega) = \sum_\xi \left(g_D(\xi) - g_A(\xi) \right)^2 \delta(\omega - \omega_\xi). \tag{7.92}$$

If we write $\kappa_\xi = (g_D(\xi) - g_A(\xi))^2 \equiv \kappa(\omega_\xi)$, we get the more transparent form of the spectral density $J_{DA}(\omega) = \kappa(\omega)\mathcal{N}(\omega)$. Here, we used the oscillator DOS defined as $\mathcal{N}(\omega) = \sum_\xi \delta(\omega - \omega_\xi)$. This reminds us one of the fact that the spectral density can

---

19) Here, $g_m(\xi), m = D, A$ are dimensionless displacements of the vibrational coordinates q_ξ and have been defined in Eq. (2.66).

be interpreted as the density of oscillator states weighted by the electron–vibrational coupling constant (cf. Section 3.7.3).

The reorganization energy equation (7.70) can be expressed via the spectral density as

$$\int_0^\infty d\omega \, \omega J_{DA}(\omega) = \sum_\xi \omega_\xi \big(g_D(\xi) - g_A(\xi)\big)^2 = \frac{E_\lambda}{\hbar}. \tag{7.93}$$

The introduction of the spectral density enables us to write (see Eq. (6.37))

$$G(t) = \int_0^\infty d\omega \, \big(e^{-i\omega t}(1 + n(\omega)) + e^{i\omega t} n(\omega)\big) J_{DA}(\omega). \tag{7.94}$$

At this point, it is useful to clarify what approximations will lead to the rate formula of the high-temperature limit derived in Section 7.4.1. To this end, we note that irrespective of the actual frequency dependence, the spectral density rapidly goes to zero beyond a certain cut-off frequency ω_c. Hence, in the high-temperature limit, we have $k_B T \gg \hbar\omega_c$. This enables us to introduce for all frequencies less than ω_c the approximation $1 + 2n(\omega) \approx 2k_B T/\hbar\omega \gg 1$.

To utilize this inequality next, we separate the function $G(t)$ into its real and imaginary parts:

$$G(t) = \int_0^\infty d\omega \, \cos(\omega t) \, (1 + 2n(\omega)) \, J_{DA}(\omega) - i \int_0^\infty d\omega \, \sin(\omega t) J_{DA}(\omega). \tag{7.95}$$

If $\omega_c |t| \ll \pi/2$, the term $\exp\{G(t) - G(0)\}$ in Eq. (7.90) rapidly approaches zero since the expression $\cos(\omega t) - 1$, which appears in the exponent, is negative. But for $\omega_c |t| > \pi/2$, the different contributions to the time integral may interfere destructively. Consequently, it is possible to approximate $G(t)$ in the exponent by the leading expansion terms of the sine and cosine functions. (This is known as the short-time expansion and identical with the slow fluctuation limit introduced in Section 6.2.4.) Using the definition equation (7.92) of the spectral density gives

$$G(t) \approx -\int_0^\infty d\omega \, \frac{(\omega t)^2}{2} \, 2\frac{k_B T}{\hbar\omega} J_{DA}(\omega) - i \int_0^\infty d\omega \, \omega t J_{DA}(\omega). \tag{7.96}$$

Both frequency integrals define the reorganization energy according to Eq. (7.93), and the combined DOS determining the ET rate follows as

$$\mathcal{D}(\Delta E/\hbar) = \int_{-\infty}^{+\infty} \frac{dt}{2\pi\hbar} \, \exp\left\{ i\frac{(\Delta E - E_\lambda)t}{\hbar} \right\} \, \exp\left\{ -\frac{k_B T E_\lambda t^2}{\hbar^2} \right\}. \tag{7.97}$$

The remaining integral is easily calculated as

$$\mathcal{D}(\Delta E/\hbar) = \frac{1}{\sqrt{4\pi k_B T E_\lambda}} \exp\left\{ -\frac{(\Delta E - E_\lambda)^2}{4 E_\lambda k_B T} \right\}. \tag{7.98}$$

If inserted into expression (7.88), the classical (high-temperature) limit of the consequent quantum description of nonadiabatic ET reactions reproduces the Marcus formula, Eq. (7.71).

In principle, the concept of the spectral density enables us to describe nonadiabatic ET also for vibrational modes differing strongly in their frequencies. For example, it is typical for the ET in dissolved DA complexes that low-frequency solvent modes as well as high-frequency intramolecular vibrations are involved in the ET reaction. Therefore, one has to split up the spectral density into a solvent part $J_{sol}(\omega)$ and an intramolecular part $J_{intra}(\omega)$. For simplicity, we assume that $J_{sol}(\omega)$ is different from zero only in the low-frequency region (the cut-off frequency for collective solvent modes typically amounts to values less than $100\,\mathrm{cm}^{-1}$). This makes a classical description of the solvent modes possible. Further, it is reasonable to suppose that there is no overlap with $J_{intra}(\omega)$. The ET rate expressed in terms of these spectral densities will be given in Section 7.4.5. First, however, in the following section we introduce a model for this situation that is more common in the literature.

7.4.4 The Mixed Quantum–Classical Case

Let us consider the case where the ET is coupled to high-frequency intramolecular (quantum) modes and low-frequency (classical) modes, for example those of a solvent. Then, the high-frequency modes are conveniently taken into account using the electron–vibrational representation of the Hamiltonian given in Eq. (7.39). The solvent modes, on the other hand, are described using classical mechanics. Assuming a decoupling of both types of DOFs leads us to a combination of the Hamiltonian equation (7.27) (where the vibrational Hamiltonian H_m is interpreted as a classical Hamiltonian function) with the Hamiltonian equation (7.39) given in the electron–vibrational representation. The respective vibrational energies E_μ are supplemented by the vibrational Hamiltonian function $H_m(q)$ of low-frequency normal modes $q \equiv \{q_\xi\}$. Accordingly, the complete DA Hamiltonian can be written as

$$H_{DA} = \sum_{\mu\nu} \left(\delta_{\mu\nu} \left(E_\mu + H_m(q) \right) + (1 - \delta_{mn})V_{\mu\nu} \right) |\mu\rangle\langle\nu|. \tag{7.99}$$

The PESs $U_D(q)$ and $U_A(q)$ related to H_D and H_A, respectively, are defined as in Eq. (7.25) but with $U_m^{(0)} = 0$. A more general expression would be obtained if the PESs, and thus the related Hamilton function, differed for different vibrational states $|\chi_{mM}\rangle$. But we assume that there is no considerable rearrangement of the solvent if the vibrational state of the intramolecular modes changes.

Using this model one can generalize the ET rate, Eq. (7.62), to the case where transitions from a manifold of donor states $|\varphi_D\rangle|\chi_{DM}\rangle$ to many acceptor states $|\varphi_A\rangle|\chi_{AN}\rangle$ are included. The ET rate for this mixed case follows as

$$k_{ET} = \frac{2\pi}{\hbar} \sum_{M,N} \int dq \, f_{DM} f_D(q) |V_{DM,AN}|^2 \delta \left(E_{DM} + U_D(q) - E_{AN} - U_A(q) \right).$$

$$\tag{7.100}$$

Here, f_{DM} is the quantum mechanical distribution for the vibrational states at the donor. The rate can be determined similarly as in Section 7.4.1, leading to the following multichannel generalization of the Marcus formula (7.71):

$$k_{ET} = \sum_{M,N} f_{DM} \, k_{DM \to AN}, \tag{7.101}$$

with

$$k_{DM \to AN} = \sqrt{\frac{\pi}{\hbar^2 k_B T E_\lambda}} |V_{DM,AN}|^2 \exp\left\{ -\frac{(\Delta E_{DM,AN} - E_\lambda)^2}{4 E_\lambda k_B T} \right\}. \tag{7.102}$$

Each transfer channel from the initial vibrational level E_{DM} to the final level E_{AN} contributes its own ET rate $k_{DM \to AN}$. The reorganization energy is identical with that in Eq. (7.70), but the driving forces appear in the generalized form

$$\Delta E_{DM,AN} = E_{DM} - E_{AN}, \tag{7.103}$$

which accounts for the different initial and final states of the high-frequency mode.

The rate expression simplifies if we note that usually the energy of the high-frequency vibrational quanta exceeds the thermal energy even at room temperature. Therefore, only the vibrational ground state of this mode is occupied in the reactant state. We will concentrate on a single high-frequency normal mode, that is $E_{AN} = E_A + \hbar\omega_{\text{intra}}(N + \frac{1}{2})$ (Figure 7.22), and get the rate as

$$k_{ET} = \sqrt{\frac{\pi}{\hbar^2 k_B T E_\lambda}} |V_{DA}|^2 \sum_{N=0}^{\infty} |\langle \chi_{D0} | \chi_{AN} \rangle|^2 \exp\left\{ -\frac{(\Delta E - \hbar\omega_{\text{intra}} N - E_\lambda)^2}{4 E_\lambda k_B T} \right\}. \tag{7.104}$$

Here, the reference driving force $\Delta E \equiv E_{D0} - E_{A0}$ has been introduced; its actual value is reduced by $\hbar\omega_{\text{intra}} N$. Often, Eq. (7.104) for the ET rate is written using a
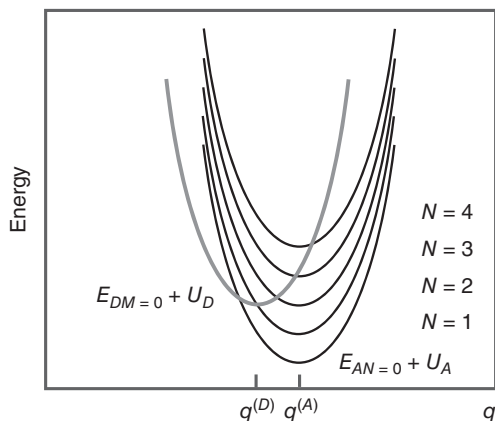
Figure 7.22 PESs for the ET in the case of a single high-frequency intramolecular vibration and a low-frequency solvent coordinate q. According to the assumption $\hbar\omega_{\text{intra}} \gg k_B T$, a single solvent coordinate PES $E_{DM=0} + U_D(q)$ has been drawn for the reactant state. The various product state solvent coordinate PESs $E_{AN} + U_A(q)$ ($E_{AN} = E_A + \hbar\omega_{\text{intra}} N$, $N = 0, \ldots, 4$) which can be reached in the course of the reaction are also shown. The product state PES with $N = 0$ corresponds to the ET in the inverted region.

more explicit expression for the Franck–Condon factor $|\langle \chi_{D0}|\chi_{AN}\rangle|^2$. Making use of the derivations given in Section 2.5.2 (cf. Eq. (2.79)) and replacing the shift g_{intra} of the PES of the intramolecular vibration by $\sqrt{E_\lambda^{(intra)}/\hbar\omega_{intra}}$, one easily obtains

$$|\langle \chi_{D0}|\chi_{AN}\rangle|^2 = \frac{1}{N!}\left(\frac{E_\lambda^{(intra)}}{\hbar\omega_{intra}}\right)^N \exp\left\{-\frac{E_\lambda^{(intra)}}{\hbar\omega_{intra}}\right\}. \tag{7.105}$$

Figure 7.22 shows the various PESs involved in the ET reaction in the mixed quantum–classical case. The product state PES with $N = 0$ corresponds to the ET in the inverted region. But the character of the ET changes to the normal region with increasing vibrational quantum number N (the PES with $N = 1$ nearly corresponds to the activationless case). The presence of the intramolecular vibrations opens additional channels for the ET reaction. Since the $N = 0$ state refers to the inverted region, the PES with $N > 0$ may result in a reduction in the activation energy for the solvent coordinate, and even the activationless case contributes to the total rate. Assuming that already the $N = 0$ PES is in the normal region, the activation energy for the solvent coordinate increases for those PESs with $N > 0$. Therefore, the rate will be dominated by the transition into the $N = 0$ state of the acceptor.

7.4.5 Description of the Mixed Quantum–Classical Case by a Spectral Density

Next, we make use of the spectral density introduced in Eq. (7.92) to calculate the ET rate, Eq. (7.88). Specifically, we show how one can calculate the ET rate derived in the foregoing section for the presence of a single high-frequency intramolecular vibration and low-frequency solvent vibrations. We set

$$J_{DA}(\omega) = J_{intra}(\omega) + J_{sol}(\omega). \tag{7.106}$$

The high-frequency contribution reads

$$J_{intra}(\omega) = j_{intra}\delta(\omega - \omega_{intra}). \tag{7.107}$$

The prefactor is given by $j_{intra} = E_\lambda^{(intra)}/\hbar\omega_{intra}$, that is as the ratio of the related reorganization energy and the energy of a vibrational quantum, which can be easily verified using Eq. (7.93). A widely used form of a solvent spectral density is given by the Debye type (with Debye frequency ω_D, cf. also Section 6.2.4)

$$J_{sol}(\omega) = \Theta(\omega) j_{sol} \frac{1}{\omega} \frac{1}{\omega^2 + \omega_D^2}. \tag{7.108}$$

Here, we can identify $j_{sol} = 2E_\lambda^{(sol)}\omega_D/\pi\hbar$.

According to the partitioning of the spectral density, we can split up the function $G(t)$, Eq. (7.94), into the solvent and intramolecular contribution $G_{sol}(t)$ and $G_{intra}(t)$, respectively. Using for $G_{intra}(t)$ Eq. (7.94) and assuming that $\hbar\omega_{intra} \gg k_B T$, one can write $G_{intra}(t) \approx e^{-i\omega_{intra}t}j_{intra}$. We insert $G_{sol}(t)$ and $G_{intra}(t)$ into Eq. (7.90) and afterward expand the expression $\exp\{G_{intra}(t)\}$ with respect to $\exp\{-i\omega_{intra}t\}$. It yields

$$\mathcal{D}(\Delta E/\hbar) = e^{-j_{intra}}\sum_{N=0}^{\infty}\frac{j_{intra}^N}{N!}\mathcal{D}_{sol}(\Delta E/\hbar - N\omega_{intra}). \tag{7.109}$$

The solvent contribution to the DOS is similar to Eq. (7.90) but with $\Delta E/\hbar - N\omega_{\text{intra}}$ instead of $\Delta E/\hbar$, reflecting the presence of the high-frequency vibrational mode.

If we take $\mathcal{D}_{\text{sol}}$ in the slow fluctuation limit, Eq. (6.55) or Eq. (7.98), we can write (note that $T_{\text{fluc}} = \hbar/\sqrt{2k_{\text{B}}TE_{\lambda}^{(\text{sol})}}$ in Eq. (6.55))

$$\mathcal{D}_{\text{sol}}(\omega) = \frac{1}{\sqrt{4\pi k_{\text{B}}TE_{\lambda}^{(\text{sol})}}} \; \exp\left\{-\frac{(\hbar\omega)^2}{4k_{\text{B}}TE_{\lambda}^{(\text{sol})}}\right\}. \tag{7.110}$$

Since $j_{\text{intra}} = E_{\lambda}^{(\text{intra})}/\hbar\omega_{\text{intra}}$, we have reproduced Eq. (7.104).

7.5 Bridge-Mediated Electron Transfer

In many cases the simple picture of a direct transfer of an electron from the donor site to the acceptor site does not apply. The reaction may proceed across bridging units between the donor and the acceptor (cf. Section 7.1). In cases where the donor and the acceptor are connected by a rather rigid polymer strand, the bridging units can be considered as a linear arrangement of identical sites; an example is given in Figure 7.23. A less homogeneous bridge structure is encountered in the ET system of the bacterial photosynthetic reaction center shown in Figure 7.3. Considering ET in proteins, the bridge becomes a three-dimensional network of LUMOs (of the amino acid residues) connecting the donor and the acceptor.

Bridge-mediated ET may take place via two different mechanisms: the superexchange ET or the sequential (hopping) transfer (cf. Figure 7.8). In the first case, the bridge units support a delocalization of the donor state wave function (Figure 7.24a). This delocalization will essentially modify the (electronic) coupling between the donor and the acceptor, which can be expressed by introducing an *effective* DA transfer integral. Since an extended electronic wave function is formed, a definite phase relation between the electronic states of the different bridge units as well as the bridge and the donor exists. According to this picture, superexchange ET is intimately connected to the presence of electronic *coherences*. Due to the off-resonance conditions between the donor and the bridge levels, small energetic fluctuations of the levels due to a weak coupling to vibrational modes should have a minor effect. However, a *strong* vibrational modulation of the energy levels of the bridge units, or of the transfer coupling between them, might prevent the formation of a delocalized electronic wave function.

A delocalized wave function, and thus coherences in the ET, can also be found if the bridge states are in near resonance to the donor and acceptor levels as is the case in Figure 7.8b. But this requires that the time scale for electronic motion is comparable to or even faster than the characteristic vibrational relaxation times. As mentioned above, the vibrational modulation of the electronic states and their mutual coupling can become predominant such that an extended wave function cannot be formed. The electron jumps between bridge levels, and one has a *sequential* ET, as shown in Figure 7.24b. We expect that in the case of fast vibrational relaxation, $\tau_{\text{rel}} \ll t_{\text{el}}$, this type of ET can be described by a set of rate equations (cf. Section 3.4.5), which includes various ET rates connecting different bridging sites (Section 7.4).

(a)

(b)
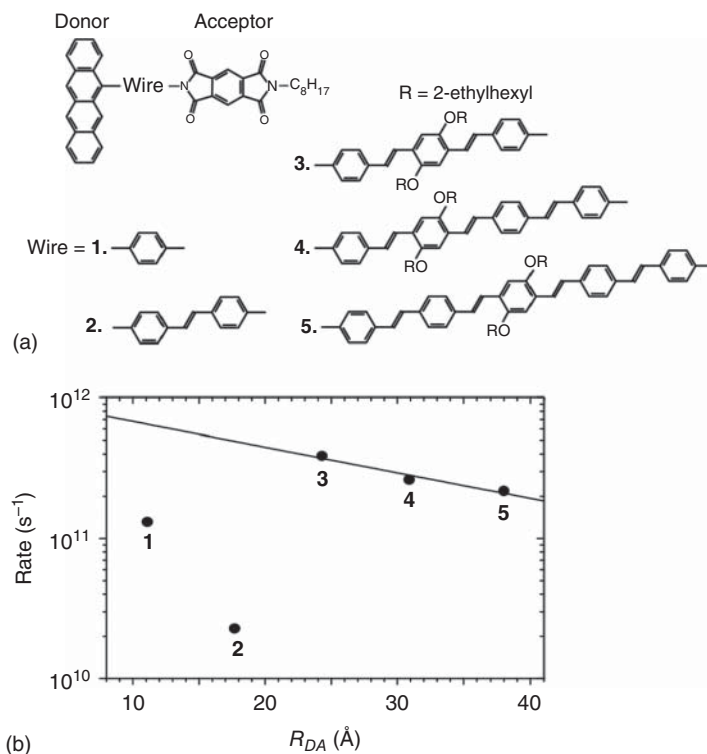
Figure 7.23 Bridge-mediated ET using a molecular wire of *p*-phenylenevinylene oligomers. The donor is given by tetracene, and the acceptor by pyromellitimide. The five different types of wires together with the donor and acceptor are shown in (a) (donor acceptor distances R_{DA} for wire **1** up to **5** are 11.1, 17.7, 24.3, 30.9, and 38.0 Å). The distance dependence of the transfer rate is shown in (b) (Reproduced with permission from Davis et al. [8]/Springer Nature).

Figure 7.24 Bridge-mediated ET between a donor and an acceptor level. (a) A scheme of the superexchange ET where the initial state wave function (shaded area) extends over the whole bridge. For the sequential ET (b), the electronic wave function is localized on the various sites during the transfer.
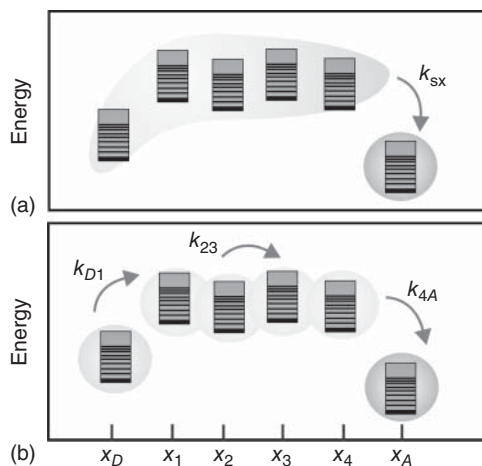
In the subsequent discussion of bridge-mediated ET, we concentrate on the superexchange mechanism. Usually, the transfer coupling between the various units is not so strong, and the ET takes place in the nonadiabatic regime. Since superexchange ET is of the through-bond type (cf. Section 7.1), the incorporation of intermediate units increases the rate compared to the case where no bridging units are present. In this latter through-space type of reactions, the ET rate is proportional to the square of the transfer integral and therefore determined by the tails of the overlapping donor and acceptor wave functions (cf. Eq. (7.26)). It will be the aim of the following consideration to understand how the intermediate bridge molecules influence the ET rate.

The appropriate Hamiltonian for the present case has already been introduced in Eq. (7.27). In order to have a clear identification of the donor and acceptor levels, we set $|\varphi_D\rangle = |D\rangle$ as well as $|\varphi_A\rangle = |A\rangle$ and get

$$H_{\text{DBA}} = H_D|D\rangle\langle D| + \sum_m \left(V_{Dm}|D\rangle\langle\varphi_m| + \text{h.c.}\right)$$

$$+ H_A|A\rangle\langle A| + \sum_m \left(V_{Am}|A\rangle\langle\varphi_m| + \text{h.c.}\right) + H_{\text{bridge}}. \qquad (7.111)$$

The bridge Hamiltonian H_{bridge} is identical to expression (7.27) with the summation restricted to the bridge sites, $m = 1, \dots, N_{\text{B}}$. Note that in the most general way, the model should include that the donor and acceptor levels may couple to every level of the bridge via the transfer integrals V_{Dm} and V_{Am}. However, because of its smallness, a direct donor–acceptor coupling is ignored.

7.5.1 The Superexchange Mechanism

To discuss the way a molecular bridge mediates the ET from the donor to the acceptor, we first consider the case of a single bridging unit. For such a situation, the bridge Hamiltonian is written as $H_{\text{bridge}} = H_B|B\rangle\langle B|$. We set $|B\rangle \equiv |\varphi_1\rangle$, and the related vibrational Hamiltonian has been denoted as H_{B}. Furthermore, two transfer integrals, V_{DB} and V_{AB}, appear that couple the bridge to the donor and the acceptor, respectively.

Let us first derive the bridge-mediated effective transfer integral without the consideration of vibrational contributions. The delocalization of the donor wave function induced by the bridge can be estimated by perturbation theory. The lowest order correction to the donor state $|D\rangle$ following from the coupling to the bridge is given by

$$|\Delta D\rangle = \frac{V_{DB}^*}{E_D - E_B}\, |B\rangle. \qquad (7.112)$$

In the nonadiabatic scheme of ET (cf. the qualitative discussion in Section 7.3), the rate is calculated via the Golden Rule formula. According to Section 3.3, we need the square of the effective coupling matrix element $V_{DA}^{(\text{eff})}$ between the modified donor state[20] $|D\rangle + |\Delta D\rangle$ and the acceptor state $|A\rangle$. The coupling is obtained as

$$V_{DA}^{(\text{eff})} = \left(\langle D| + \frac{V_{DB}}{E_D - E_B}\langle B|\right) \times V_{BA}|B\rangle\langle A| \times |A\rangle = \frac{V_{DB}V_{BA}}{E_D - E_B}. \qquad (7.113)$$

---

20) Note that the proper normalization of the state $|D\rangle + |\Delta D\rangle$ can be neglected since it is of higher order in the respective transfer integrals.

The formula holds as long as $|E_D - E_B|$ is nonzero and larger than $\sqrt{|V_{DB}V_{BA}|}$. This simple calculation can easily be extended by incorporating the vibrational levels of the DBA system. Now, the correction of the electron vibrational donor state $|D\rangle|\chi_{DM}\rangle$ follows as

$$|\Delta D\rangle|\chi_{DM}\rangle = \sum_K \frac{V_{DB}^*\langle\chi_{DM}|\chi_{BK}\rangle^*}{E_{DM} - E_{BK}} |B\rangle|\chi_{BK}\rangle. \tag{7.114}$$

As in Section 7.2.3, we assumed that the coupling matrix elements are independent of the vibrational coordinates. Additionally, we introduced the electron–vibrational energies, Eq. (7.37). Then, the effective DA coupling, Eq. (7.113), is generalized to the following expression:

$$
\begin{aligned}
V_{DM,AN}^{(\text{eff})} &= \left(\langle D|\langle\chi_{DM}| + \sum_K \frac{V_{DB}\langle\chi_{DM}|\chi_{BK}\rangle}{E_{DM} - E_{BK}} \langle B|\langle\chi_{BK}| \right) V_{BA}|B\rangle\langle A| \times |A\rangle|\chi_{AN}\rangle \\
&= \sum_K \frac{V_{DB}V_{BA}\langle\chi_{DM}|\chi_{BK}\rangle\langle\chi_{BK}|\chi_{AN}\rangle}{E_{DM} - E_{BK}}.
\end{aligned} \tag{7.115}
$$

Since it directly connects the manifold of vibrational states of the donor with that of the acceptor, we can introduce it into formula (7.87) to get the superexchange ET rate as

$$k_{\text{ET}}^{(\text{sx})} = \frac{2\pi}{\hbar} \sum_{M,N} f_{DM} \mid V_{DM,AN}^{(\text{eff})}\mid^2 \delta(E_{DM} - E_{AN}). \tag{7.116}$$

The rate expression itself has been discussed at length in Section 7.4.3. What is mainly of interest here is the structure of the effective coupling matrix element, Eq. (7.115). Again, the energy denominator should not become equal to zero and should be larger than the square root of the numerator to justify the perturbation theory. However, the inclusion of vibrational levels may lead to the case $E_{DM} = E_{BK}$. But if the electronic levels E_D and E_A are energetically rather different, this case leads to very small vibrational overlap integrals $\langle\chi_{DM}|\chi_{BK}\rangle$ and $\langle\chi_{BK}|\chi_{AN}\rangle$, and the smallness of $V_{DM,AN}^{(\text{eff})}$ is guaranteed. Following this reasoning, we may conclude that only terms with $E_{BK} \gg E_{DM}$ contribute to $V_{DM,AN}^{(\text{eff})}$. Hence, it often suffices to replace the denominator by the pure electronic energy difference $E_D - E_B$. The completeness relation for the bridge vibrational states finally results in the effective coupling, Eq. (7.113), and we may set in Eq. (7.116) $V_{DM,AN}^{(\text{eff})} \approx V_{DA}^{(\text{eff})}\langle\chi_{DM}|\chi_{AN}\rangle$ to get

$$k_{\text{ET}}^{(\text{sx})} = \frac{2\pi}{\hbar} |V_{DA}^{(\text{eff})}|^2 \mathcal{D}(\Delta E_{DA}/\hbar). \tag{7.117}$$

The combined density of states $\mathcal{D}$ depends on the driving force ΔE_{DA} of the donor–acceptor transition (as well as the vibrational overlap integrals $\langle\chi_{DM}|\chi_{AN}\rangle$) and has been introduced in Eq. (7.89). The expressions for the superexchange-mediated effective donor–acceptor coupling are widely used in the literature. But the derivation given so far reveals the shortcomings of the approach. First, it is only valid if the bridge levels are energetically well separated from the donor as well as the acceptor levels. And second, any vibrational relaxation of the transferred electron in the bridge is neglected. Therefore, it is instructive to embed the description of superexchange ET in a more general treatment. This is

based on a consequent perturbation expansion with respect to the transfer integral and will be outlined in Section 7.6. First, however, we derive expressions for the superexchange ET rate if the bridge is of a more complex structure than discussed so far.

7.5.2 Electron Transfer Through Arbitrary Large Bridges

Having discussed bridge- mediated ET for the simple case where the whole bridge is given by a single-electronic level, the more general case of a larger number of bridge units will be described now (Figure 7.25). There are two possibilities to deal with this case. First, one can extend the perturbational scheme of the foregoing section. This would be possible if the transfer couplings V_{mn} among the bridge levels are sufficiently small. However, one may also be confronted with the situation that all these couplings are large (although the coupling of the bridge levels to the donor and the acceptor remains small to justify the description of the ET as a nonadiabatic process). In this latter case, one may change from the description of the bridge levels by localized states (diabatic states) to a description by delocalized adiabatic states.

7.5.2.1 Case of Small Intrabridge Transfer Integrals

For the sake of clarity, let us consider a linear arrangement of bridge molecules with nearest-neighbor transfer coupling only. This represents a rather realistic model of a molecular bridge realized by a polymer strand (Figure 7.23). Moreover, we will not take into account vibrational levels when determining the effective transfer coupling; that is, we follow the arguments of the foregoing section, which lead us to a description in terms of electronic levels and electronic transfer integrals only. Then, the superexchange mechanism of ET through the bridge is described as follows. We first assume that the state $|D \dots N_B - 1\rangle$ of the DBA system is known, where the electron is delocalized across all bridge units except the last one. Then, an
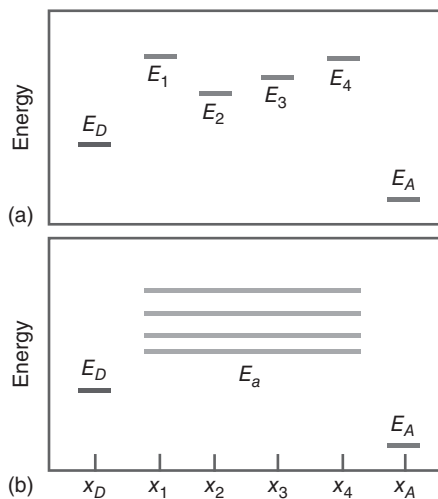
Figure 7.25 Bridge-mediated ET between a donor and an acceptor level.
(a) ET through the bridge is realized by the individual levels of the bridge units;
(b) ET is mediated by the band E_a of bridge eigenstates.

effective DA coupling $V_{DA}^{(\text{eff})}$ is obtained in a way demonstrated in the forgoing section since the last bridge level remains as the single intermediate level:

$$V_{DA}^{(\text{eff})} = \frac{V_{D,N_{\text{B}}}^{(\text{eff})} V_{N_{\text{B}},A}}{E_D - E_{N_{\text{B}}}}. \tag{7.118}$$

The formula contains the effective coupling $V_{D,N_{\text{B}}}^{(\text{eff})}$ between the state $|D \ldots N_{\text{B}} - 1\rangle$, where the electron is delocalized up to the bridge unit $N_{\text{B}} - 1$, and the last unit N_{B} of the bridge. To determine $V_{D,N_{\text{B}}}^{(\text{eff})}$, we introduce the similar effective coupling $V_{D,N_{\text{B}}-1}^{(\text{eff})}$, which now describes the interaction between the state $|D \ldots N_{\text{B}} - 2\rangle$, where the electron is delocalized up to the bridge unit $N_{\text{B}} - 2$, and the bridge unit $N_{\text{B}} - 1$. We obtain

$$V_{D,N_{\text{B}}}^{(\text{eff})} = \frac{V_{D,N_{\text{B}}-1}^{(\text{eff})} V_{N_{\text{B}}-1,N_{\text{B}}}}{E_D - E_{N_{\text{B}}-1}}. \tag{7.119}$$

In the same way, we may compute $V_{D,N_{\text{B}}-1}^{(\text{eff})}$. If this procedure is repeated until the donor level is reached, the effective donor–acceptor coupling follows as

$$V_{DA}^{(\text{eff})} = \frac{V_{D1}}{E_D - E_1} \frac{V_{12}}{E_D - E_2} \cdots \frac{V_{N_{\text{B}}-1,N_{\text{B}}}}{E_D - E_{N_{\text{B}}}} V_{N_{\text{B}},A}. \tag{7.120}$$

Introducing this expression into Eq. (7.117), we obtain the superexchange ET rate for cases where the transfer coupling within the bridge is weak enough to be handled by perturbation theory.

To further characterize this special situation, we compute the dependence of $k_{\text{ET}}^{(\text{sx})}$ on the number N_{B} of bridge units. We assume identical bridge units characterized by the energy E_{B} and the nearest-neighbor coupling V_{B} (cf. Figure 7.8). The effective coupling, Eq. (7.118), follows as $V_{DA}^{(\text{eff})}(N_{\text{B}}) = V_{DA}^{(\text{eff})}(1) \zeta^{N_{\text{B}}-1}$. Here, we introduced $V_{DA}^{(\text{eff})}(1) = V_{D1} V_{N_{\text{B}}A}/(E_D - E_B)$, which can be interpreted as the effective superexchange coupling for the case of a single bridge unit. The parameter $\zeta = V_B/(E_D - E_B)$ describes the decrease in the coupling with increasing number of bridge units. The decrease in the total rate follows an exponential law: $k_{\text{ET}}^{(\text{sx})}(N_{\text{B}}) \propto \zeta^{2(N_{\text{B}}-1)}$.

7.5.2.2 Case of Large Intrabridge Transfer Integrals

If the intrabridge transfer integrals are large, the situation is best described by introducing the eigenstates of the bridge Hamiltonian. Again, we assume that there is a large energetic distance of all bridge levels to the donor as well as to acceptor level, and we also neglect any vibrational levels of the bridge. Then, the bridge eigenstates ϕ_a and eigenenergies E_a (cf. Figure 7.25) can be obtained by diagonalization of the electronic part of the bridge Hamiltonian. The eigenstates are written as an expansion with respect to the localized bridge states: $|\phi_a\rangle = \sum_m c_a(m)|\varphi_m\rangle$. In general, the coefficients $c_a(m)$ have to be determined numerically; for certain model bridge systems, an analytical solution might exist as well (see below). Expressed in the basis of its eigenstates, the electronic part of the bridge Hamiltonian becomes

$$H_{\text{el}}^{(\text{bridge})} = \sum_a E_a |\phi_a\rangle\langle\phi_a|. \tag{7.121}$$

Since the intersite couplings are transformed to $(X = D, A)$

$$V_{Xa} = \sum_m V_{Xm} c_a(m), \tag{7.122}$$

Equation (7.27) can be written as

$$H_{el}^{(DBA)} = \sum_{X=D,A} \left\{ H_X |X\rangle\langle X| + \sum_a \left(V_{Xa} |X\rangle\langle\phi_a| + \text{h.c.} \right) \right\} + H_{el}^{(bridge)}. \tag{7.123}$$

Now, we are in the position to derive the bridge-mediated effective transfer integral. Although there is not a single intermediate bridge level as discussed in Section 7.5.1, but a whole set of levels labeled by a, we can follow the reasoning of this section since all bridge levels couple independently to the donor and the acceptor. In generalizing Eq. (7.113), the effective DA coupling follows as

$$V_{DA}^{(eff)} = \sum_a \frac{V_{Da} V_{aA}}{E_D - E_a}. \tag{7.124}$$

If inserted into Eq. (7.117), the superexchange ET rate in the case of a strong transfer coupling in the bridge is obtained. Since the effective coupling enters the rate as $|V_{DA}^{(eff)}|^2$, mixed expressions appear where the donor and the acceptor couple to different bridge states.[21]

To compute the bridge-length dependence of the ET rate, we consider the model of a regular bridge with common energy levels E_B and nearest-neighbor couplings V_B. The bridge energies E_a read $E_B + 2V_B \cos(a)$ where the quantum number is $a = \pi j/(N_B + 1)$, with $j = 1, \dots, N_B$ (cf. Section 2.8.3). The expansion coefficients $c_a(m)$ follow as $\sqrt{2/(N_B + 1)} \sin(am)$. We obtain the coupling matrix elements, Eq. (7.122), between the donor and the various bridge levels as $V_{Da} = V_{D1} \sqrt{2/(N_B + 1)} \times \sin(\pi j/[N_B + 1])$ and between the bridge levels and the acceptor as $V_{Aa} = V_{AN_B} \sqrt{2/(N_B + 1)} \times \sin(\pi j N_B/[N_B + 1])$. Then, the bridge-mediated effective DA coupling, Eq. (7.124), can be calculated:

$$V_{DA}^{(eff)}(N_B) = V_{DA}^{(eff)}(1) \left(\frac{1 - \sqrt{1 - 4\zeta^2}}{2\zeta} \right)^{N_B - 1}. \tag{7.125}$$

The effective superexchange coupling in the case of a single bridge unit $V_{DA}^{(eff)}(1) = V_{D1} V_{N_B A} /(E_D - E_B)$ and the ratio $\zeta = V_B/(E_D - E_B)$ have been already introduced in relation to Eq. (7.120). (In the present case of large intrabridge transfer integrals, the latter quantity may reach values of 0.1 and larger, whereas in the case of weak intrabridge transfer integrals, ζ remains a small quantity.)

To compare bridge-mediated ET with the direct through-space transfer, let us recall that the through-space ET rate would become proportional to $|V_{DA}^{(0)}|^2 \exp\{-2\beta x_{DA}\}$ (cf. Eq. (7.26), x_{DA} denotes the DA distance, and $V_{DA}^{(0)}$ is a reference value of V_{DA} taken at a reference distance). In the same way, we may write $V_{DA}^{(eff)}(1) = V_{DA}^{(0,eff)}(1) \exp(-2\beta x_{D1}) \exp(-2\beta x_{N_B A})$. The distance between the donor and the left

---

21) Particular dephasing mechanisms may remove the relevance of mixed expressions. Then, every bridge level contributes independently to the rate.

bridge terminal is given by x_{D1}, and $x_{N_B A}$ denotes the distance of the right bridge terminal to the acceptor (see also Figure 7.8). For simplicity, we assumed all transfer integrals to vary with the same constant β. The expression $V_{DA}^{(0,\text{eff})}(1)$ is the reference value of the effective coupling. The superexchange mechanism can increase the ET rate drastically. Compared with the through-space ET rate, the small factor $\exp\{-2\beta x_B\}$ ($x_B = x_{DA} - x_{D1} - x_{N_B A}$ is the bridge length) has been replaced by $|V_{DA}^{(0,\text{eff})}(1)|^2$ multiplied by ζ^{N_B-1} (case of weak intrabridge transfer integrals) or multiplied by the square of the second factor on the right-hand side of Eq. (7.125). In both cases, values larger than $\exp\{-2\beta x_B\} \approx 10^{-9}$ are possible ($\beta \approx 1 \text{ Å}^{-1}$ and $x_B = 20 \text{ Å}$).

7.6 Nonequilibrium Quantum Statistical Description of Electron Transfer

In this section, we generalize the treatment of ET reactions presented so far. The approach will enable us to fully include the vibrational DOFs into the bridge-mediated ET as well as to go beyond the nonadiabatic limit. To achieve this goal, a nonequilibrium quantum statistical description will be utilized as introduced in Section 3.14. There, the ubiquitous system–reservoir Hamiltonian has been rearranged in a manner that is most suitable for the following considerations. First, it has been expanded with respect to the eigenstates of the system part. Following from this, the resulting matrix elements of the system–reservoir coupling separate into diagonal and off-diagonal elements. The former enter the zeroth-order Hamiltonian H_0, whereas the latter form the perturbation $\hat{V}$. Then, applying a particular projection operator approach, one can derive rate equations for the populations of the system eigenstates containing rate expressions that are given as a complete perturbational expansion with respect to $\hat{V}$.

It is already obvious from this short explanation that such an approach will be capable of providing a unified description of ET reactions. If we identify the system states of the general approach of Section 3.14 with the diabatic electronic states $|\varphi_m\rangle$ and the vibrational DOFs of the ET system with the reservoir coordinates of Section 3.14, we may derive general expressions for the ET rates $k_{m \to n}$. These describe all transitions in the system including nonadiabatic processes as well as processes that are of higher order in the interstate couplings V_{mn}, among them the superexchange ET rates.

To establish the relation with the approach of Section 3.14, we separate the ET Hamiltonian, Eq. (7.27), according to $H_{\text{DBA}} = H_0 + \hat{V}$ with

$$H_0 = \sum_m H_m(q)|\varphi_m\rangle\langle\varphi_m| \tag{7.126}$$

and (remember the convention $V_{mm} = 0$)

$$\hat{V} = \sum_{m,n} V_{mn}|\varphi_m\rangle\langle\varphi_n|. \tag{7.127}$$

As shown in Section 3.14, the approach has to be based on the general projection superoperator $\mathcal{P}$, Eq. (3.457), here, however, defined by the diabatic states $|\varphi_m\rangle$

instead of the states $|a\rangle$.[22)] The formalism leads to rate equations for the diabatic state populations P_m and, simultaneously, to transition rates $k_{m \to n}$. A power expansion of the latter with respect to the interstate couplings V_{mn} can be deduced from the recursion relation, Eq. (3.503). The following section should give the reader an impression of the usefulness of this technique.

7.6.1 Unified Description of Electron Transfer in a Donor–Bridge–Acceptor System

As explained in Section 7.5, the determination of rates for bridge-mediated ET requires the consideration of higher order contributions with respect to the interstate coupling. Here, we may account for the simultaneous influence of the ordinary nonadiabatic transition rates between the neighboring states and, for example, the superexchange rates describing a direct transition from the donor to the acceptor (or vice versa). We remind the reader that both cases correspond to weak intrabridge transfer integrals as discussed first in Section 7.5.2. The superexchange rates would follow from Eq. (3.503) as $K_{AD}^{(2N_B+2)}(\omega = 0)$, whereas the rates connecting the neighboring states are second-order rates $k_{m \to m \pm 1}$, introduced in Eq. (3.511). Of course, all other types of rates have to be examined concerning their relevance for the whole ET reaction too.

To keep the matter simple, we deal in what follows with a three-site system of a donor, a single-bridge unit, and an acceptor state ($m = D, B, A$). As in Section 7.5.2, we consider the transfer integrals V_{DB} and V_{BA} but neglect the direct coupling V_{DA}. In this three-site system, we have to account for the rates $k_{D \to B}$, $k_{B \to A}$, and $k_{D \to A}$ as well as for the reverse ones. If expanded with respect to the transfer coupling, the first two start with second-order rates (nonadiabatic rates $k_{D \to B}^{(2)}$ and $k_{B \to A}^{(2)}$; cf. Section 7.4). The lowest order contribution to the rate $k_{D \to A}$ would be of the fourth order in V_{mn} and can be obtained from Eq. (3.521) by identifying a with the donor state quantum number and b with that of the acceptor (the rate separates in a nonfactorizable fourth-order part and into a product of two second-order rate expressions). Both types of rates will be used to solve the respective set of rate equations, that is second-order rates for the nearest neighbor transitions ($k_{D \to B}$, $k_{B \to D}$, $k_{B \to A}$, and $k_{A \to B}$) and fourth-order rates for the donor–acceptor transition ($k_{D \to A}$ and $k_{A \to D}$). Details of the derivation and specification of the second- and fourth-order rates can be found in the supplementary Sections 7.10.3 and 7.10.4, respectively.

Having discussed the different approximations for the rate expressions, we present the rate equations referring to the simple DBA system:

$$\frac{\partial}{\partial t} P_D(t) = -\left(k_{D \to B} + k_{D \to A}\right) P_D(t) + k_{B \to D} P_B(t) + k_{A \to D} P_A(t),$$

$$\frac{\partial}{\partial t} P_B(t) = -\left(k_{B \to D} + k_{B \to A}\right) P_B(t) + k_{D \to B} P_D(t) + k_{A \to B} P_A(t),$$

$$\frac{\partial}{\partial t} P_A(t) = -\left(k_{A \to B} + k_{A \to D}\right) P_A(t) + k_{B \to A} P_B(t) + k_{D \to A} P_D(t). \tag{7.128}$$

---

22) The action of $\mathcal{P}$ on an arbitrary operator $\hat{O}$ can be written as $\mathcal{P}\hat{O} = \sum_m \text{tr}\{\hat{\Pi}_m \hat{O}\}\hat{\Pi}_m \hat{R}_m$ with the vibrational equilibrium density operator $\hat{R}_m$ of the diabatic state φ_m and the projection operator $\hat{\Pi}_m = |\varphi_m\rangle\langle\varphi_m|$.

As the initial condition, we set up $P_m(0) = \delta_{mD}$. A standard way to solve such differential equations is to make the ansatz $P_m(t) = \exp(-Kt)$. In the present case, one obtains two rates K that are nonzero, and one that is equal to zero. The first two are simply computed using the conservation of total probability (for example, P_B can be replaced by $1 - P_D - P_A$). Once the resulting two inhomogeneous rate equations have been solved, the rates K read:

$$K_\pm = \frac{1}{2}\left(a + b \pm \sqrt{(a-b)^2 + c}\right), \tag{7.129}$$

with $a = k_{D\to B} + k_{B\to D} + k_{D\to A}$, $b = k_{A\to B} + k_{B\to A} + k_{A\to D}$, and $c = 4(k_{D\to A} - k_{B\to A})(k_{A\to D} - k_{B\to D})$. It is apparent from these formulas that the rates characterizing the basic nearest-neighbor hopping transitions and the superexchange transitions are strongly mixed. Only in a special case do they enter the total rate as independent contributions. This special case is characterized by rates $k_{B\to D}$ and $k_{B\to A}$ describing the outflow of charge from the bridge, which are much larger than all other rates. The inequality would be realized for a DBA system with the bridge level being positioned highly above the donor and the acceptor levels ($E_B - E_D, E_B - E_A, \gg E_D - E_A$). For such a situation, the thermally activated transfer into the bridge level is much smaller than the transfer out of the bridge. Introducing an expansion of the rates $K_\pm$ around the leading contribution $k_{B\to D} + k_{B\to A}$, one obtains $K_+ \approx k_{B\to D} + k_{B\to A}$ and

$$K_- \equiv K_{ET} = k_{D\to A} + k_{A\to D} + \frac{k_{D\to B}k_{B\to A} + k_{A\to B}k_{B\to D}}{k_{B\to D} + k_{B\to A}}. \tag{7.130}$$

The rate K_+ is responsible for a fast transfer process, but at the same time it only causes a small deviation from the initial charge distribution. The actual but slower ET is characterized by the rate K_{ET}. This overall donor–acceptor transfer rate contains the superexchange forward and backward rates in its first and second terms, respectively. The third term comprises the sequential transfer from the donor to the bridge unit and, afterward, to the acceptor as well as the reverse part of this transition. In this way, K_{ET} accounts for the superexchange and the sequential mechanism of ET by two independent contributions.

Although Eq. (7.130) has been derived for a single bridge unit only, it is well suited to describe the change in the measured ET rate when increasing the number of bridge units. Such an increase becomes possible when the total bridge is given by a polymer strand whose length can be easily varied. Prominent examples are strands of amino acids (cf. Figure 7.26a) as well DNA fragments. We briefly justify the use of Eq. (7.130) to compute the ET rate for a case where all bridge units are identical (use of a so called homopolymer as a bridge). Provided that the bridge-internal hopping transitions are much faster than the transitions into and out of the bridge, one can assume that a bridge-internal equilibrium distribution with $P_m(t) = P_B(t)/N_B$ has been established. The relation supposes that the bridge units can also be described by diabatic states with population P_m. The quantity $P_B(t)$ is the total bridge population $\sum_m P_m(t)$, and m runs over all bridge units (from 1 to N_B). It follows a reduction on the multitude of rate equations for the bridge populations to a single one governing the total bridge population. Such an equation is similar to the second one of Eqs. (7.128) but with the rates $k_{D\to B}$ and $k_{B\to A}$ (as well as the reverse ones) replaced by

(a)

(b)
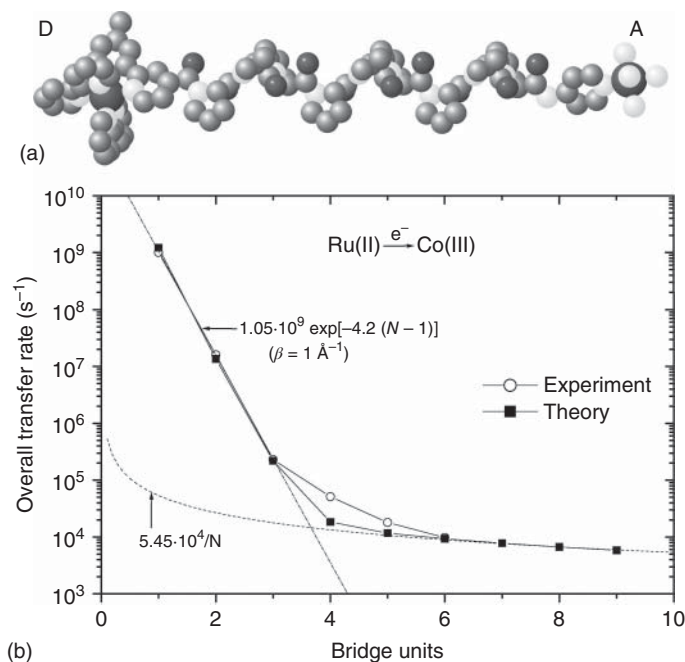
Figure 7.26 Length dependence of the overall ET rate at room temperature for the donor–bridge–acceptor complex shown in (a) ([(bpy) $_2$Ru(II)L $^\cdot$(Pro) $_n$Co(III)(NH$_3$) $_5$] $^{3+}$, carbon atoms are shown in gray, nitrogen in weak gray, and oxygen as well as the ruthenium and cobalt atoms in black). (b) Comparison of experimental data (open circles), after Isied et al. [9], and theoretical computations (full squares). The thin dotted lines show an estimate of the bridge number dependence of the rate if it is dominated by the superexchange mechanism or the sequential one (Reproduced with permission from Petrov and May [10]/American Chemical Society).

rates divided by the number of bridge units N_B. Of course, the rates $k_{D\to A}$ and $k_{A\to D}$ have to be computed with effective transfer couplings $V_{DA}^{(eff)}$ like that of Eq. (7.120).

If we again assume that the rates $k_{B\to D}$ and $k_{B\to A}$ are much larger than all other rates, we can describe the bridge length dependence of the rate by Eq. (7.130). In this case, the two basic mechanisms of bridge-mediated ET enter the total rate by separate terms, and we expect that one of the two might dominate the other for a given number of bridge units. Figure 7.26b displays such a behavior via the length dependence of the overall ET rate in the DBA complex [(bpy)$_2$Ru(II)L$^\cdot$(Pro)$_n$Co(III)(NH$_3$)$_5$]$^{3+}$. The donor is given by a ruthenium, and the acceptor by a cobalt complex, whereas an oligopeptide of the amino acid proline connects the donor and the acceptor. The oligopeptide forms a linear bridge, which has the advantage to be relatively stiff (when compared with other oligopeptides). As demonstrated by Figure 7.26b, the ET is mainly determined by the superexchange mechanisms if the bridge is short. If its length is increased, a small transition region follows. ET in long bridges ends in a region where the sequential mechanism of bridge-mediated ET characterizes the length dependence of the rate.

7.6.2 Transition to the Adiabatic Electron Transfer

Finally, we would like to return to the two-site system of a simple DA complex and briefly sketch how to go beyond the second-order approximation with respect to the DA transfer integral, that is to leave the regime of nonadiabatic ET. A number of higher order approximations have been derived in the literature. Considering the high-temperature limit, a typical expression for the rate reads

$$k_{\mathrm{ET}}^{(\mathrm{adia})} = \frac{k_{\mathrm{ET}}^{(\mathrm{nonad})}}{1 + \delta_{\mathrm{adia}}}, \tag{7.131}$$

where $k_{\mathrm{ET}}^{(\mathrm{nonad})}$ is the rate of nonadiabatic transfer given in Eq. (7.71) (Marcus-type formula). The adiabatic correction obtained, for example for the ET in polar solvents, is given by

$$\delta_{\mathrm{adia}} = 4\pi \frac{|V_{\mathrm{DA}}|^2 \tau_{\mathrm{long}}}{\hbar E_\lambda}. \tag{7.132}$$

Here, τ_{long} is the so-called longitudinal relaxation time of the solvent, and E_λ denotes the reorganization energy. For a very small transfer coupling, the nonadiabatic rate expression is recovered, whereas for a large $|V_{\mathrm{DA}}|$, the rate becomes independent of the coupling. In this manner, expression (7.131) interpolates between the two limiting cases of adiabatic and nonadiabatic ET.

An interpolation formula of this kind can also be generated using the so-called *Pade* approximation. We note that an equation similar to Eq. (3.503) allows to deduce an expansion of the ET rate like $k_{DA} = |V_{DA}|^2 C^{(2)}(\omega = 0) - |V_{DA}|^4 C^{(4)}(\omega = 0) + \dots$. Here, the $C^{(N)}$ are Fourier-transformed N-time correlation functions of the type encountered in Eq. (3.521). The Pade approximation leads to a rate expression of infinite order in V_{DA} but restricted to the two types, $C^{(2)}$ and $C^{(4)}$, of correlation functions. Such a resummation of the rate reads $k_{DA} = |V_{DA}|^2 C^{(2)}(\omega = 0)/[1 + |V_{DA}|^2 C^{(4)}(\omega = 0)/C^{(2)}(\omega = 0)]$. The expression produces a reasonable approximation for the adiabatic case where it becomes independent of the transfer integral.

7.7 Heterogeneous Electron Transfer

ET taking place between a molecule and a solid state system is a particular charge transmission process named HET (cf. Figure 7.9). The formation of a positively or negatively charged molecule in the course of HET is an important aspect when discussing the energetics of HET. To get some insight into this energetics, let us consider the transfer of a single electron from a metal electrode into a molecule that has been in a neutral state. This reactant state of the molecule should have the energy E_0 (the number 0 describes the fact that the molecule is in its neutral state). The energy E_1 is that of the molecular product state (an anion; the number 1 indicates the presence of a single excess electron). The prerequisite for such a charging reaction of the molecule is that the energy difference $E_1 - E_0$ corresponds to an available energy

in the metal electrode. As a macroscopic system its change in energy per change in the electron number is given by the chemical potential μ. If the relation $\mu > E_1 - E_0$ is fulfilled, the HET reaction of the type shown in Figure 7.9a becomes possible. Since the energy difference $E_1 - E_0$ can be roughly estimated by E_{LUMO} (Koopmans theorem), Figure 7.9 reflects the correct energetics of this reaction. In the contrary case, $\mu < E_1 - E_0$, no charge transfer is possible.[23]

Considering arbitrary charging states of a molecule with energy E_N and N excess electrons (the case $N < 0$ corresponds to missing electrons, that is cationic states of the molecule), the injection of a single electron may proceed if $\mu > E_{N+1} - E_N$. This relation generalizes the above given one for the transition from the neutral to the singly negatively charged molecule. Accordingly, transfer of an electron from the metal to the singly positively charged molecule is possible if $\mu > E_0 - E_{-1}$. The positively charged state of the molecule remains stable provided that $\mu < E_0 - E_{-1}$. This case corresponds to the charge injection processes of Figure 7.9b,c. Although not indicated explicitly, Figure 7.9b presumes that the energy of the neutral molecule with one electron excited into the LUMO minus the energy of the molecule with one electron missing in the HOMO is larger than μ. Moreover, the energy of the molecule with the filled HOMO minus the energy of the molecule with one electron missing in the HOMO should be larger than μ in Figure 7.9c.

In general, the energetic relation for charging and discharge has to be extended by the Coulomb interaction of the charged molecule with the metal electrons (if a charge is positioned close to the metal surface, the electrons forming the Fermi sea become polarized, inducing an attractive force to the molecule). Here and in what follows we do not study this coupling in an explicit manner but assume that the molecular levels have been defined by including this additional Coulomb interaction.

7.7.1 Nonadiabatic Charge Injection into the Solid State Described in a Single-Electron Model

The model explained in what follows is based again on a single-electron description, as already introduced in Section 7.2. Therefore, it covers the case of HET to a metal as well as to a semiconductor. The continuous energy of the conduction band of the metal or semiconductor is labeled

$$E_{\boldsymbol{k}} = \hbar \varepsilon_{\boldsymbol{k}} \tag{7.133}$$

and counted by the Bloch vectors $\boldsymbol{k}$ (this description corresponds to bulk states of the solid; the energies are spin degenerated). While in the case of a semiconductor all these conduction band states are empty, they are partly occupied in the case of the metal. This occupation is temperature dependent and regulated by the Fermi distribution of electrons (μ is the chemical potential of the metal):

$$f_{\text{F}}(E_{\boldsymbol{k}} - \mu) = \frac{1}{e^{(\hbar \varepsilon_{\boldsymbol{k}} - \mu)/k_{\text{B}}T} + 1}. \tag{7.134}$$

---

23) Note that Figure 7.9 corresponds to the zero temperature case where occupied and empty states of the lead electrode are separated by the Fermi energy E_{F}.

At low temperature, this expression can be approximated by a unit-step function describing the total population of levels below the Fermi energy E_{F} and empty levels above.

The flexibility to start with a common model valid for the case of HET related to a metal or a semiconductor surface is caused by the single-electron description where we have to decide separately regarding the population of the solid-state band levels after the computation of basic transition rates. In the present section, those should be of the nonadiabatic type; that is, the transfer coupling can be accounted for in the lowest order of perturbation theory (see Section 7.4).

We first consider charge injection from a molecular level into a solid-state energy band. The latter is described by the single-electron band energies $\hbar\varepsilon_{\boldsymbol{k}}$ and states $\varphi_{\boldsymbol{k}}$, while the neutral molecule has the energy $\hbar\varepsilon_0$ and the state φ_0. Ignoring molecular vibrations, charge injection becomes possible if $\hbar\varepsilon_0 = \hbar\varepsilon_{\boldsymbol{k}}$ is fulfilled; that is, the single-electron molecular level is degenerated with the band continuum. This equation replaces the general relation $E_0 > E_{-1} + \mu$ discussed for a metal in the foregoing section. We account for molecular vibrations by extending the band energies by the vibrational Hamiltonian $\mathcal{H}_{-1}$ referring to molecular cation and by adding the vibrational Hamiltonian $\mathcal{H}_0$ to $E_0 = \hbar\varepsilon_0$.[24] Related vibrational energies and states are denoted as $\hbar\omega_{0\mu}$ and $\hbar\omega_{-1\nu}$ as well as $\chi_{0\mu}$ and $\chi_{-1\nu}$, respectively. The injected electron also has to be characterized by its spin. We assume that the charge transfer is independent of the spin and neglect this internal electronic DOF. However, the derived rate has to be multiplied by 2, noting that the probability per time to have a transition event is realized by a spin-up as well as a spin-down electron.

For this model, the overall Hamiltonian of the considered HET reads

$$H_{\mathrm{HET}} = \left(E_0 + \mathcal{H}_0\right)|\varphi_0\rangle\langle\varphi_0| + \sum_{\boldsymbol{k}} \left(E_{\boldsymbol{k}} + \mathcal{H}_{-1}\right)|\varphi_{\boldsymbol{k}}\rangle\langle\varphi_{\boldsymbol{k}}|$$
$$+ \sum_{\boldsymbol{k}} \left(V_{\boldsymbol{k}}|\varphi_{\boldsymbol{k}}\rangle\langle\varphi_0| + \mathrm{H.c.}\right), \tag{7.135}$$

where $V_{\boldsymbol{k}}$ is the respective transfer coupling. The solid-state band energies are of particular interest if one would like to study how atomic details of the solid-state surface affect the HET reaction. For the following discussion, it is useful to introduce a notation that directly accounts for the continuous distribution of electronic energy levels in the solid-state system. The corresponding DOS of the band states reads (if necessary, the electron spin can be accounted for by a prefactor of 2)

$$\mathcal{N}(\Omega) = \sum_{\boldsymbol{k}} \delta(\Omega - \varepsilon_{\boldsymbol{k}}). \tag{7.136}$$

Consequently, we may write down for an arbitrary function with $F_{\boldsymbol{k}} \equiv F(\varepsilon_{\boldsymbol{k}})$ the relation

$$\sum_{\boldsymbol{k}} F_{\boldsymbol{k}} = \int d\Omega \, \mathcal{N}(\Omega) F(\Omega). \tag{7.137}$$

---

24) An account for solid-state vibrations, so-called phonons, is possible in the same way but is not included here because of the dominating strength of electron–vibrational coupling in the molecule.

This will be used later to replace the summation with respect to bulk band states by an energy integral. In this manner, one may account for an arbitrary form of the solid-state electronic states by introducing a corresponding DOS.

Because of the presumed nonadiabatic character of the HET reaction, we can make use of the rate formula, Eq. (7.88). The related transfer rate for electron injection into the solid state then takes the form

$$k_{0 \to \boldsymbol{k}} = \frac{2\pi}{\hbar} |V_{\boldsymbol{k}}|^2 D_{0 \to -1}(\varepsilon_0 - \varepsilon_{\boldsymbol{k}}). \tag{7.138}$$

This standard expression we met several times before (see, for example Sections 3.4.5, 3.7, and 6.2). The function $D_{0 \to -1}(\omega)$ describes the thermal-averaged and Franck-Condon-weighted overlap between the vibrational state of the molecule before and after charge injection. It can be expressed via the correlation function of the considered transition that reads ($\hat{R}_0$ is the vibrational equilibrium statistical operator of the neutral molecule)

$$D_{0 \to -1}(\omega) = \frac{1}{2\pi\hbar} \int dt\, e^{i\omega t} \mathrm{tr}_{\mathrm{vib}}\{\hat{R}_0 e^{i\mathcal{H}_0 t/\hbar} e^{-i\mathcal{H}_{-1} t/\hbar}\}. \tag{7.139}$$

The overall rate of HET has to account for the manifold of acceptor states in the solid and the possibility that a certain subset is already populated. Accordingly, the rate has to be written as

$$k_{\mathrm{HET}} = \sum_{\boldsymbol{k}} \left(1 - f_{\mathrm{F}}(\hbar\varepsilon_{\boldsymbol{k}} - \mu)\right) k_{0 \to \boldsymbol{k}}. \tag{7.140}$$

This formula describes nonadiabatic HET into the conduction band of a metal including the occupied states of the Fermi sea as taken into consideration by the Fermi distribution (the term $1 - f_{\mathrm{F}}$ ensures that transfer only takes place into empty band levels). When considering charge injection into a semiconductor conduction band, the Fermi distribution has to be removed since injection appears into unoccupied band state.

We assume that the $\boldsymbol{k}$-dependence of the transfer coupling can be replaced by a direct dependence on $\varepsilon_{\boldsymbol{k}}$. This enables us to write $k(\Omega)$ instead of $k_{0 \to \boldsymbol{k}}$. Using the DOS, Eq. (7.136), as well as Eq. (7.137), we arrive at

$$k_{\mathrm{HET}} = \int d\Omega\, \mathcal{N}(\Omega) \left(1 - f_{\mathrm{F}}(\hbar\Omega - \mu)\right) \frac{2\pi}{\hbar} |V(\Omega)|^2 D_{0 \to -1}(\varepsilon_0 - \Omega). \tag{7.141}$$

It is suitable to introduce the molecule–solid coupling function

$$\Gamma(\Omega) = \mathcal{N}(\Omega) \frac{|V(\Omega)|^2}{\hbar^2} \equiv \frac{1}{\hbar^2} \sum_{\boldsymbol{k}} |V_{\boldsymbol{k}}|^2 \delta(\Omega - \varepsilon_{\boldsymbol{k}}), \tag{7.142}$$

which represents a particular type of spectral density, as indicated on the right-hand side where we moved back to a $\boldsymbol{k}$-summation. Accordingly, the rate can be written as

$$k_{\mathrm{HET}} = \int d\Omega\, \left(1 - f_{\mathrm{F}}(\hbar\Omega - \mu)\right) \Gamma(\Omega) 2\pi\hbar D_{0 \to -1}(\varepsilon_0 - \Omega). \tag{7.143}$$

For a given temperature, the ratio between the thermal and vibrational excitation energy is determined by the concrete form of the vibrational correlation function

entering $\mathcal{D}_{0 \to -1}$ (cf. discussion in Sections 7.4.1 and 7.4.3). And the position of the molecular energy E_0 in relation to the band edge determines the particular influence of the DOS. If E_0 lies deep in the band, the DOS may only change slightly in the energy (frequency) interval where $\mathcal{D}_{0 \to -1}$ is different from zero. Then, one usually introduces the *wide-band limit* and replaces the DOS and the transfer coupling by their mean and frequency-independent values $\bar{\mathcal{N}}$ and $\bar{V}$, respectively, resulting in

$$\Gamma = \bar{\mathcal{N}} \frac{|\bar{V}|^2}{\hbar^2}. \tag{7.144}$$

As a consequence, Eq. (7.143) reduces to a frequency integral of $\mathcal{D}_{0 \to -1}$ taken with respect to a region where band states are empty. This indicates that, in contrast to ordinary ET, here the transfer coupling has been replaced by an expression that includes $\sqrt{\bar{\mathcal{N}} \Delta\Omega}$ (the latter quantity $\Delta\Omega$ determines the frequency range that contributes to Eq. (7.143)). While the single transfer coupling into a particular state might be small, the overall rate is increased by the factor $\bar{\mathcal{N}} \Delta\Omega$.

7.7.1.1 Low-temperature Case

From Eqs. (7.87) and (7.89), we may deduce a representation of $\mathcal{D}_{0 \to -1}$, which includes the corresponding vibrational energies and wave functions. If adapted to the present case, we have ($f_{0\mu}$ denotes the vibrational energy distribution of the uncharged molecule)

$$\mathcal{D}_{0 \to -1}(\varepsilon_0 - \Omega) = \frac{1}{\hbar} \sum_{\mu, \nu} f_{0\mu} |\langle \chi_{0\mu} | \chi_{-1\nu} \rangle|^2 \delta(\varepsilon_0 - \Omega + \omega_{0\mu} - \omega_{-1\nu}). \tag{7.145}$$

This turns the rate formula, Eq. (7.143), into

$$k_{\text{HET}} = 2\pi \sum_{\mu, \nu} f_{0\mu} |\langle \chi_{0\mu} | \chi_{-1\nu} \rangle|^2 \left(1 - f_{\text{F}}(\hbar[\varepsilon_0 + \omega_{0\mu} - \omega_{-1\nu}] - \mu) \right)$$
$$\times \Gamma(\varepsilon_0 + \omega_{0\mu} - \omega_{-1\nu}). \tag{7.146}$$

At $T = 0$, we may replace $1 - f_{\text{F}}$ by the unit step function, and f_{0M} is reduced to a vibrational ground state population only. In the case of a single dominant vibrational coordinate (with vibrational frequency ω_{vib}) and in the wide band limit, Eq. (7.144), it yields (note the replacement of μ by the Fermi energy E_{F})

$$k_{\text{HET}} = 2\pi \Gamma \sum_{\nu} |\langle \chi_{0\mu=0} | \chi_{-1\nu} \rangle|^2 \theta(E_0 - E_{\text{F}} - \hbar\omega_{-1\nu}). \tag{7.147}$$

Charge injection into the solid state starts to take place if E_0 reaches E_{F}. In this case, the charged molecule stays in its vibrational ground state. If the nuclear rearrangement upon charging the molecule is large, the vibrational overlap expression $\langle \chi_{0\mu=0} | \chi_{-1\nu} \rangle$ becomes small, as does the overall rate. Excited vibrational states of the charged molecule are populated if E_0 overcomes the Fermi energy and equals one of the energies $E_{\text{F}} + \hbar\omega_{-1\nu}$. Now, different transition channels for charging might be open, and the transition rate may be increased by this fact as well as by a possibly larger vibrational overlap.

7.7.1.2 High-temperature Case

According to Eq. (7.98), which constitutes the Marcus formula of ET, we get the correlation function $D_{0\to-1}$ as

$$D_{0\to-1}(\varepsilon_0 - \Omega) = \frac{1}{2\pi\hbar}\sqrt{\frac{\pi\hbar}{k_B T \lambda_{0,-1}}}\exp\left\{-\frac{(\varepsilon_0 - \Omega - \lambda_{0,-1})^2}{4\lambda_{0,-1}k_B T/\hbar}\right\}. \qquad (7.148)$$

The reorganization energy upon charging of the molecule is denoted as $\hbar\lambda_{0,-1}$. The HET rate, Eq. (7.143), follows as (note the use of a frequency-independent coupling Γ)

$$k_{HET} = \Gamma\sqrt{\frac{\pi\hbar}{k_B T \lambda_{0,-1}}}\int d\Omega\,\left(1 - f_F(\hbar\Omega - \mu)\right)\exp\left\{-\frac{(\varepsilon_0 - \Omega - \lambda_{0,-1})^2}{4\lambda_{0,-1}k_B T/\hbar}\right\}. \tag{7.149}$$

Here, the position of $\hbar(\varepsilon_0 - \lambda_{0,-1})$ relative to the Fermi energy determines the magnitude of the rate.

7.7.1.3 HET-induced Lifetime

The coupling of molecular levels to the solid-state band continuum gives rise to finite lifetime of the former. It is calculated in what follows for a photoinduced charge injection from an excited state φ_{0e} (e labels the excited electronic state) of the uncharged molecule into the conduction band of a semiconductor (cf. Figure 7.9d). This example avoids the consideration of effects related to a possible occupation of the band continuum, as it would be necessary in the case of a metal. The computation of the decay rate related to the lifetime of the molecular level will be achieved by the inspection of the population $P_{0e\mu}$ of the initially excited electron–vibrational state $\chi_{0e\mu}\varphi_{0e}$. The Hamiltonian appropriate for these considerations is given in Eq. (7.135), where the neutral molecular state has to be specified as the excited electronic state φ_{0e}, and by a corresponding vibrational Hamiltonian $\mathcal{H}_{0e}$. To simplify the notation, the electronic state index e is suppressed in what follows. Accordingly, we have to compute

$$P_{0\mu}(t) = |\langle\chi_{0\mu}|\langle\varphi_0|e^{-iHt/\hbar}|\varphi_0\rangle|\chi_{0\mu}\rangle|^2. \tag{7.150}$$

For the determination of this expression, the methodology introduced in Section 3.3.3 is utilized. It is based on the replacement of the time-evolution operator by the related Green's operator (cf. Eq. (3.92)). Therefore, the initial state population is written as

$$P_{0\mu}(t) = |\int\frac{d\omega}{2\pi i}e^{-i\omega t}\langle\chi_{0\mu}|\langle\varphi_0|\hat{G}_0(\omega)|\varphi_0\rangle|\chi_{0\mu}\rangle|^2. \tag{7.151}$$

The Green's operator $\hat{G}_0$ reduced to the electronic state of the neutral molecule takes the form already given in Eq. (3.111). The only extension necessary here is the inclusion of the vibrational Hamiltonians $\mathcal{H}_0$ and $\mathcal{H}_{-1}$. We get (introducing $\hat{\Pi}_0 = |\varphi_0\rangle\langle\varphi_0|$ projecting on the electronic state of the neutral molecule):

$$\hat{G}_0(\omega) = \frac{\hat{\Pi}_0}{\omega - \varepsilon_0 - \mathcal{H}_0/\hbar - \hat{\Sigma}(\omega) + i\epsilon}, \tag{7.152}$$

where the self-energy operator, Eq. (3.110), now takes the form

$$\hat{\Sigma}(\omega) = \frac{1}{\hbar^2} \sum_{k} \frac{|V_k|^2}{\omega - \varepsilon_k - \mathcal{H}_{-1}/\hbar + i\epsilon} \hat{\Pi}_0. \tag{7.153}$$

In order to compute the time dependence of the initial state population according to Eq. (7.151), we set up an equation for the reduced Green's operator matrix elements

$$G_{0\mu,0\mu}(\omega) = \langle \chi_{0\mu}|\langle \varphi_0|\hat{G}_0(\omega)|\varphi_0\rangle|\chi_{0\mu}\rangle. \tag{7.154}$$

Noting Eq. (7.152), we first move the inverse operator to the left-hand side and form matrix elements as in the foregoing equation. In a second step, the product of $\omega - \varepsilon_0 - \mathcal{H}_0/\hbar - \hat{\Sigma}$ and $\hat{G}_0$ is turned into products of matrix elements by inserting the completeness relation $\hat{\Pi}_0 \times \sum_{v}|\chi_{0v}\rangle\langle\chi_{0v}|$. It follows that

$$(\omega - \varepsilon_0 - \omega_{0\mu})G_{0\mu,0\mu}(\omega) - \sum_{v}\Sigma_{0\mu,0v}(\omega)G_{0v,0\mu}(\omega) = 1, \tag{7.155}$$

where we introduced

$$\Sigma_{0\mu,0v}(\omega) = \langle \chi_{0\mu}|\langle \varphi_0|\hat{\Sigma}(\omega)|\varphi_0\rangle|\chi_{0v}\rangle. \tag{7.156}$$

To compute the matrix elements of the self-energy operator, which includes the vibrational Hamiltonian $\mathcal{H}_1$, we insert twice the vibrational completeness relation $\sum_{\kappa}|\chi_{-1\kappa}\rangle\langle\chi_{-1\kappa}|$ defined by the eigenfunctions of $\mathcal{H}_{-1}$. We arrive at

$$\Sigma_{0\mu,0v}(\omega) = \sum_{\kappa}\langle \chi_{0\mu}|\chi_{-1\kappa}\rangle\Sigma(\omega - \omega_{-1\kappa})\langle\chi_{-1\kappa}|\chi_{0v}\rangle. \tag{7.157}$$

The self-energy, $\Sigma(\omega)$, reads (note the combination of ω with the vibrational frequencies $\omega_{-1\kappa}$ and the introduction of the DOS):

$$\Sigma(\omega) = \frac{1}{\hbar^2} \sum_{k} \frac{|V_k|^2}{\omega - \varepsilon_k + i\epsilon} \equiv \frac{1}{\hbar^2} \int d\Omega \frac{\mathcal{N}(\Omega)|V(\Omega)|^2}{\omega - \Omega + i\epsilon}. \tag{7.158}$$

The matrix $\Sigma_{0\mu,0v}$, Eq. (7.157), is determined by the vibrational overlap expressions $\langle\chi_{0\mu}|\chi_{-1\kappa}\rangle$ and $\langle\chi_{-1\kappa}|\chi_{0v}\rangle$ relating the states of the neutral molecule to those of the singly charged one.

There are two limiting cases resulting in a simple expression for $G_{0\mu,0v}(\omega)$ onto which we will concentrate in the following. First, let us assume that the reorganization energy for the charge transfer is small. Then, we may conclude that $\langle\chi_{0\mu}|\chi_{-1\kappa}\rangle \approx \delta_{\mu\kappa}$ and $\langle\chi_{-1\kappa}|\chi_{0v}\rangle \approx \delta_{\kappa v}$. The self-energy matrix, Eq. (7.157), reduces to $\delta_{\mu v}\Sigma(\omega)$. Second, the same result is obtained if the wide-band limit is taken. In this case, we directly arrive at

$$G_{0\mu,0\mu}(\omega) = \frac{1}{\omega - \varepsilon_0 - \omega_{0\mu} + i\pi\Gamma}, \tag{7.159}$$

with Γ according to Eq. (7.144). If inserted into Eq. (7.151) for the initial state population, we use the integration procedure outlined in Section 3.3.1 and obtain

$$P_{0\mu}(t) = \theta(t)e^{-2\pi\Gamma t}. \tag{7.160}$$

The initial state population decays exponentially in time with the decay rate (inverse lifetime) $2\pi\Gamma$.

7.7.2 Ultrafast Photoinduced HET from a Molecule into a Semiconductor. A Case Study

The present section concentrates on the HET scheme shown in Figure 7.9d, but for a molecule–solid coupling strong enough to lead out of the regime of nonadiabatic transfer. These considerations complete the discussion of the foregoing section where the decay of an excited state of the molecule into the semiconductor conduction band continuum has been described. Because of the assumed strong transfer coupling, the HET rate, Eq. (7.141), cannot be used. A complete dynamic description of the electron–vibrational motion becomes necessary. A similar case of ultrafast photoinduced donor–acceptor ET will be discussed in Section 7.9. Here, however, we do not use the density matrix approach but compute the time-dependent wave function of the system. It is the specificity of the TiO_2 dye system introduced in Section 7.1 (see also Figure 7.10) that HET takes place as an ultrafast process; that is, charge injection proceeds on a time scale below 100 fs. To follow such HET requires an optical triggering and subsequent observation by femtosecond laser pulses (cf. discussion of pump–probe spectroscopy in Section 4.3.6). The rapidness of the process also justifies the neglect of any dissipation in the theory described below.

To account for the optical excitation process, the model used in Section 7.7.1 and condensed in the Hamiltonian, (7.135) has to be generalized. We replace the molecular part $H_{mol} = (E_0 + \mathcal{H}_0)|\varphi_0\rangle\langle\varphi_0|$ by an expression including the electronic ground state of the molecule as well as its excited state together with an optical coupling between both ($a = g, e$ refers to the molecular electronic ground and first excited states, respectively):

$$H_{mol}(t) = \sum_a \left(E_{0a} + \mathcal{H}_{0a}\right)|\varphi_{0a}\rangle\langle\varphi_{0a}| - \mathbf{E}(t)\left(\mathbf{d}_{eg}|\varphi_{0e}\rangle\langle\varphi_{0g}| + \text{H.c.}\right). \quad (7.161)$$

This Hamiltonian becomes explicitly time dependent since the optical initiation of ultrafast HET is incorporated by the electric field part $\mathbf{E}(t)$ of the exciting laser pulse ($\mathbf{d}_{eg}$ denotes the transition dipole moment).

To study the photoinduced dynamics, the total wave function is expanded with respect to the complete electron–vibrational states:

$$|\Psi(t)\rangle = \sum_{a,\mu} A_{a\mu}(t)|\chi_{0a\mu}\varphi_{0a}\rangle + \sum_{\mathbf{k},\mu} A_{\mathbf{k}\mu}(t)|\chi_{-1\mu}\varphi_{\mathbf{k}}\rangle. \quad (7.162)$$

The expansion uses the electronic as well as the vibrational states of the molecule before and after charge injection, that is $\chi_{0a\mu}$ and $\chi_{-1\mu}$, respectively. It was assumed that the vibrational states of the molecular cation, $\chi_{-1\mu}$, are independent of the actual electronic band state.

If the total wave function, Eq. (7.162), is inserted into the corresponding time-dependent Schrödinger equation, the related equations of motion for the expansion coefficients are easily obtained. To account for the band continuum, a change from the $\mathbf{k}$-vectors to a continuous energy $\hbar\Omega$ again is advisable. Therefore, the $A_{\mathbf{k}\mu}(t)$ are replaced by the $A_{\mu}(\Omega; t)$.[25] The total populations of the different

25) To handle the continuous frequency dependence, the $A_{\mu}(\Omega; t)$ are expanded with respect to a set of basis functions (orthogonal polynomials, for example), which are defined in the region of the
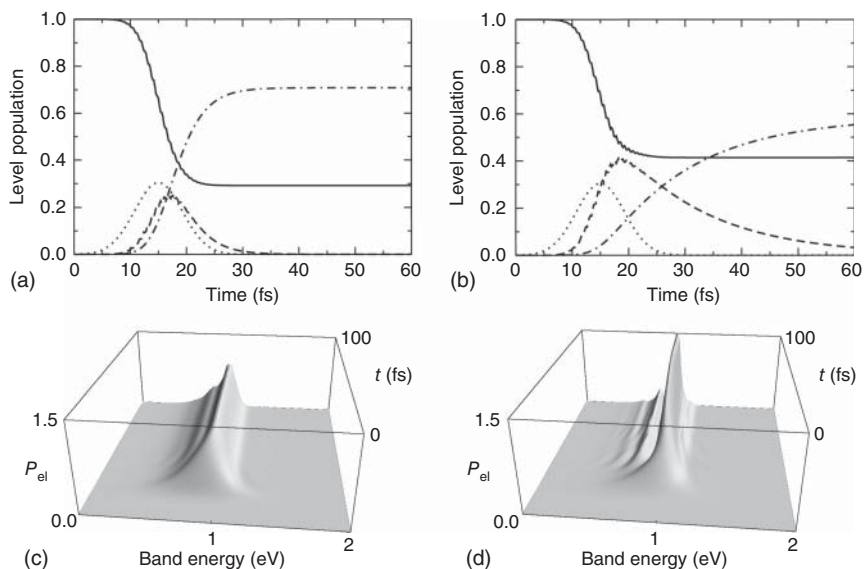
Figure 7.27 HET between perylene attached by different bridge anchor groups to a TiO_2 surface initiated by a 20 fs laser pulse (cf. also Figure 7.10). (a, c) Carboxylic acid bridge corresponding to the strong transfer coupling and (b, d) propionic acid bridge constituting a less-strong transfer coupling. Shown are the total populations of the perylene electronic ground state (full line), the excited state (dashed line), and the TiO_2 conduction band continuum (chain dotted line, the dotted line displays the exciting laser pulse envelope). The energetic distributions of the injected electron versus the conduction band energy (from the lower band edge at zero energy up to 2 eV) are drawn in (c) and (d) (Reproduced with permission from Wang et al. [11]/Springer Nature).

electronic states involved follow as $P_a(t) = \sum_\mu |A_{a\mu}(t)|^2$ for the neutral molecular states and $P_{\text{band}}(t) = \sum_{k,\mu} |A_{k\mu}(t)|^2 \equiv \int d\Omega \, \mathcal{N}(\Omega) \sum_\mu |A_\mu(\Omega;t)|^2$ for the probability that the charge injection took place. The expression $\sum_\mu |A_\mu(\Omega;t)|^2$ gives the continuous distribution $P_{\text{el}}(\Omega;t)$ of the injected electron across the conduction band. Some results for perylene attached to the semiconductor TiO_2 are presented in Figure 7.27.

7.7.3 Nonadiabatic Electron Transfer from the Solid State into the Molecule

Charge injection from a metal into a molecular level is considered in what follows. The reaction will again be described in a single-electron picture using solid-state band energies and states as well as states and energies of the neutral and singly negatively charged molecule. The basic relation for possible charge injection into the molecule again reads $E_0 = E_k$. To achieve HET, the relevant part of the band

---

conduction band from the lower to the upper band edge along the energy axis. An appropriate truncation of the infinite set of functions renders the problem tractable. Other forms of discretization are also possible.

continuum has to be populated by electrons; that is, E_0 has to be below the Fermi energy (the general relation for this case reads $E_1 < E_0 + \mu$).

In analogy to the foregoing section, the overall Hamiltonian of the considered HET reads (the positively charged state of the molecule is only replaced by the negatively charged one)

$$
\begin{aligned}
H_{\text{HET}} = \sum_{\boldsymbol{k}} & \left(E_{\boldsymbol{k}} + \mathcal{H}_0\right) |\varphi_{\boldsymbol{k}}\rangle\langle\varphi_{\boldsymbol{k}}| + \left(E_1 + \mathcal{H}_1\right) |\varphi_1\rangle\langle\varphi_1| \\
& + \sum_{\boldsymbol{k}} \left(V_{\boldsymbol{k}}|\varphi_1\rangle\langle\varphi_{\boldsymbol{k}}| + \text{H.c.}\right).
\end{aligned}
\tag{7.163}
$$

The same manipulations as in the case of charge injection into the solid state result here in the following overall rate:

$$
k_{\text{HET}} = \int d\Omega \, f_{\text{F}}(\hbar\Omega - \mu)\Gamma(\Omega)2\pi\hbar D_{0\rightarrow 1}(\varepsilon_0 - \Omega).
\tag{7.164}
$$

The Fermi distribution ensures transitions from occupied band states, and the combined DOS,

$$
D_{0\rightarrow 1}(\omega) = \frac{1}{2\pi\hbar} \int dt \, e^{i\omega t}\text{tr}_{\text{vib}}\{\hat{R}_0 e^{i\mathcal{H}_0 t/\hbar}e^{-i\mathcal{H}_1 t/\hbar}\},
\tag{7.165}
$$

relates vibrational motion in the neutral molecular state to that in the singly negatively charged state.

7.8 Charge Transmission Through Single Molecules

Charge transmission through single molecules is studied in terms of the current induced by an applied voltage (Figure 7.28). This is in contrast to the traditional ET
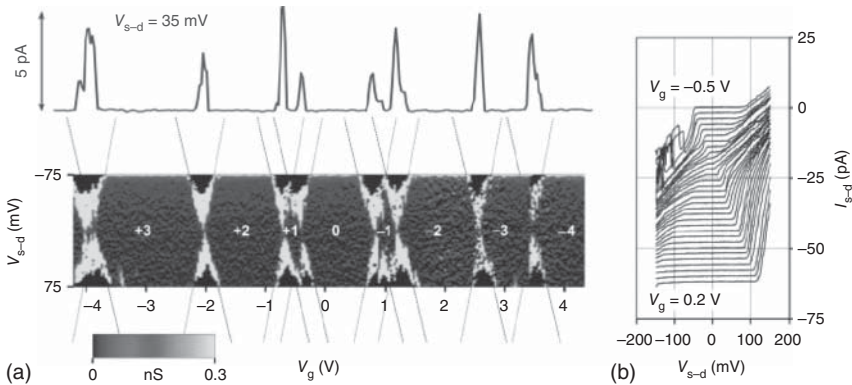
Figure 7.28 (a) IV characteristics of the single-molecule transistor of Figure 7.11. Shown are the measurements (at $T = 4.2$ K) of the differential conductance $dI_{\text{s-d}}/dV_{\text{s-d}}$ (derivative of the source–drain current $I_{\text{s-d}}$ with respect to the source–drain voltage $V_{\text{s-d}}$) as a function of $V_{\text{s-d}}$ as well as the gate potential V_{g} (the various numbers indicate the different charging states; the full line at the top of the figure shows a typical $I_{\text{s-d}} - V_{\text{g}}$ trace).
(b) Current–voltage characteristics ($I_{\text{s-d}} - V_{\text{s-d}}$ curves) at different V_{g}s are drawn in the bottom right panel (curves are shifted vertically for clarity, Reproduced with permission from Kubatkin et al. [4]/Springer Nature).

in molecular DA complexes or the HET reactions discussed in the foregoing section, where the focus is on the decay rates of state populations. Nevertheless, the whole methodology of ET theory can be applied, as will be demonstrated in this section. In order to calculate the electric current I passing through a single molecule, we recall that I is defined as the amount of charge ΔQ that moves per time interval Δt through a cross section of the given conductor, that is $I = \Delta Q/\Delta t$. Focusing on the current from the left electrode into the molecule, we may write $I_L = -|e|\partial N_L/\partial t$, where the number of electrons in the left electrode has been denoted as N_L (note that the electron charge is counted negative, and we wrote $-|e|$ instead of e). If $\partial N_L/\partial t < 0$, then negative charge flows from the left electrode through the molecule into the right electrode, but the electric current becomes positive: $I_L > 0$.[26)] ET from one lead to the other may proceed via transitions that are of the nonadiabatic type (cf. Sections 7.7.1 and 7.7.3). If the molecule–lead coupling is weak enough, charge injection from the lead into the molecule is followed by a relaxation of the charged molecule. Afterward, charge outflow into the lead may appear. This type of charge transmission has been called *inelastic* or, alternatively, *sequential* transfer (Figure 7.29). In the contrary case of strong molecule–lead coupling, charge transmission can be considered as an elastic scattering process of an electron (moving, for example from the left to the right) at the molecule. This is the *elastic* or *direct* transmission process, which resembles the superexchange DA ET (cf. Section 7.1).[27)]

To obtain the IV characteristics, two points have to be considered. First, how do the properties of the molecule (electronic levels, nuclear equilibrium configurations, vibrational frequencies, etc.) change if it is attached to nanoelectrodes. Second, how is the change in the electrostatic potential $\phi(\boldsymbol{r})$ across the molecule influenced by its actual charge distribution. With respect to the properties of the molecule, we assume that all elements of the respective Hamiltonian introduced below account for this effect. To get the correct change of the applied voltage across the molecule electronic structure, calculations are required including the presence of the external electrostatic potential $\phi(\boldsymbol{r})$. On the one hand, the actual values of $\phi(\boldsymbol{r})$ have to be computed from Poisson's equation, where the charge density is given by the single-electron density deduced from the electronic wave function of the molecule (Eq. (2.9)). On the other hand, the electronic wave function has to adjust to the presence of the external potential. Such a coupled problem needs a self-consistent solution with the boundary conditions $\phi(\boldsymbol{r}_L) = 0$ and $\phi(\boldsymbol{r}_R) = V$ ($\boldsymbol{r}_L$ and $\boldsymbol{r}_R$ label positions at the left and the right lead surfaces, respectively). This choice corresponds to a situation where the

---

26) A typical value of the current through a single molecule amounts to 1 nA. We can estimate the residence time of a single electron in the molecule as $\Delta t = |e|/I = 1.6 \times 10^{-19}$ As$/10^{-9}$ A $\approx 10^{-10}$ s $= 100$ ps.

27) Sequential and direct charge transmission can be distinguished more quantitatively by relating the lifetime τ_{life} of an extra electron at the molecule to the time τ_{rel} of intramolecular relaxation. The transmission is of the sequential type if $\tau_{\text{rel}} < \tau_{\text{life}}$ and in the reverse case of the direct type. In the foregoing Section 7.7 on HET, we learned that τ_{life} can be deduced from the molecule solid coupling function Γ, Eq. (7.142), as $\tau_{\text{life}} = 1/\Gamma$. If $\hbar\Gamma$ lies in the range of some 10 meV, the lifetime is in the range below 0.1 ps, just being below typical values of τ_{rel}. Thus, such large Γ values indicate that we are in the regime of direct transfer.
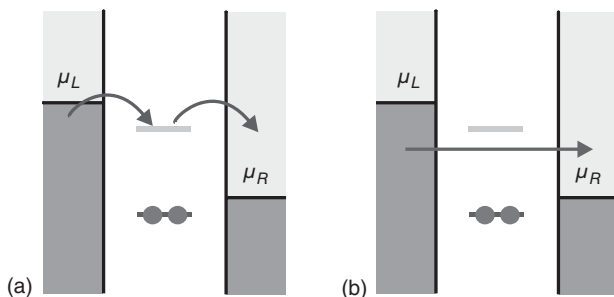
Figure 7.29 Charge transmission through a single molecule represented in a HOMO–LUMO scheme. The charge comes from the left electrode (with chemical potential μ_L) and moves to the right electrode (with chemical potential μ_R). Sequential (inelastic) transmission is drawn in (a) (an electron hops into the molecule, relaxation follows, and afterward it hops to the right electrode). Direct (elastic) transmission is presented in (b) (the electron moving from the left to the right undergoes an elastic scattering process at the molecular level).

chemical potential of the left lead stays constant but that of the right lead has been shifted by $-|e|V$.

For the present needs, this approach is simplified by neglecting the change in the electrostatic potential due to the presence of the molecule. We use $\phi(\mathbf{r}) = Vx/d$, that is the potential change in the absence of the molecule (the two leads at distance d are positioned parallel to the y–z plane of the used coordinate system). If, furthermore, it is assumed that the molecular energy levels are changed by the potential present at the center between both leads (at $x = d/2$), they have to be shifted by the energy $-|e|V/2$. Alternatively, such a configuration can be accounted for if we keep the molecular levels unchanged but move the chemical potentials up and down by half of the applied voltage:

$$\mu_L = \mu_0 + |e|V/2 \tag{7.166}$$

and

$$\mu_R = \mu_0 - |e|V/2. \tag{7.167}$$

This choice is known as the case of a *symmetrically applied voltage*. The chemical potential in the absence of an applied voltage is μ_0. It has been taken identically for both leads. Because of its simplicity, we exclusively use this scheme in the following equation. If μ_L and μ_R, as shown in Figure 7.29, are changed in this way, a current starts to flow from left to right if μ_L overcomes the LUMO level and μ_R stays below. If μ_R is positioned below the HOMO level, a current is formed by first moving an electron out of the molecule into the right lead and afterward injecting another one from the left lead. This charge transmission is often viewed as *hole* transport, with a missing electron moving from the right to the left lead.

In recent years, the theoretical description of the current flow through single molecules has been developed to a high degree of sophistication (see Further Reading). The present description will be in line with the given theory of HET, again utilizing an effective single-electron description. For simplicity, we additionally

assume that the current through the molecule only includes the formation of singly negatively charged molecular states ($E_{0-1} \ll \mu_0$).

Focusing again on two electrodes (left and right) to which the single molecule is attached and across which a voltage is applied, the Hamiltonian, Eq. (7.163), discussed in relation to HET reactions (Section 7.7.3), can be applied but has to include the coupling to two metal surfaces

$$H = \sum_{X,\mathbf{k}} \left(E_{X\mathbf{k}} + \mathcal{H}_0\right) |\varphi_{X\mathbf{k}}\rangle\langle\varphi_{X\mathbf{k}}| + \left(E_1 + \mathcal{H}_1\right) |\varphi_1\rangle\langle\varphi_1|$$
$$+ \sum_{X,\mathbf{k}} \left(V_{X\mathbf{k}}|\varphi_1\rangle\langle\varphi_{X\mathbf{k}}| + \text{h.c.}\right). \tag{7.168}$$

The index $X = L, R$ counts the left and the right metal surfaces (nanoelectrodes), which might have a different band structure but are considered here as identical (for all other ingredients, see the explanations related to Eq. (7.163)). We also formulate a spin-independent theory, finally multiplying all rates by the factor 2 (this implies that all molecular levels considered are spin degenerated). Although unifying descriptions exist, we derive in the following section separate current formulas based either on a sequential (inelastic) or a direct (elastic) charge transmission scheme.

7.8.1 Inelastic Charge Transmission

Inelastic charge transmission proceeds via charge injection from one lead resulting in a singly negatively charged molecule and afterward in a charge flow from the molecule into empty states of the other lead (cf. Figure 7.29). Discharge and charging of the molecule can be characterized by rates of HET derived in the foregoing Sections 7.7.1 and 7.7.3, respectively. The related stationary current will be deduced as the steady-state solution of the respective rate equations. Those determine the single-electron state populations $P_{X\mathbf{k}}$, which belong to the lead X's electronic states ($X = L, R$) and the population P_1 of the charged molecule. They read

$$\frac{\partial}{\partial t}P_{X\mathbf{k}}(t) = -k_{X\mathbf{k}\to 1}P_{X\mathbf{k}}(t) + k_{1\to X\mathbf{k}}P_1(t) \tag{7.169}$$

as well as

$$\frac{\partial}{\partial t}P_1(t) = -\sum_{X,\mathbf{k}}(k_{1\to X\mathbf{k}}P_1(t) - k_{X\mathbf{k}\to 1}P_{X\mathbf{k}}(t). \tag{7.170}$$

The charging rates $k_{X\mathbf{k}\to 1}$ are identical to the expression equation (7.164) and the $k_{1\to X\mathbf{k}}$ describing discharge with Eq. (7.138).

The current from electrode $X = L, R$ into the molecule equals the negative change of charge in the respective lead; that is, we may write (the factor 2 accounts for the electron spin, see above)

$$I_X = -2|e|\frac{\partial}{\partial t}\sum_{\mathbf{k}}P_{X\mathbf{k}}(t). \tag{7.171}$$

At steady-state conditions, we get $I = I_L = -I_R$; the current from the left electrode coincides with the negative current from the right electrode. To get a finite current, the time derivative of the total lead population $\sum_{\mathbf{k}}P_{X\mathbf{k}}$ should differ from zero. This is

in contrast to the standard use of rate equations given so far. There, closed systems have been considered. The total system population always stays constant. If a steady state is reached, the state populations become time independent. The assumption of a nonzero time derivative of the populations indicates that the rate equations refer (implicitly) to an open system where a constant number of electrons in the leads are guaranteed due to their connection to an external reservoir. As a consequence, we may calculate the stationary current, for example from

$$I = I_L = 2|e| \sum_{\boldsymbol{k}} \left(k_{L\boldsymbol{k} \to 1} P_{L\boldsymbol{k}} - k_{1 \to L\boldsymbol{k}} P_1 \right). \tag{7.172}$$

Since the left lead state populations $P_{L\boldsymbol{k}}$ are those of a macroscopic system, they should stay in thermal equilibrium, although electrons leave and enter the molecule (as a consequence of a stationary current through it). Therefore, $P_{L\boldsymbol{k}}$ is replaced by the Fermi distribution, Eq. (7.134), specified to the left lead and the actually applied voltage. Moreover, the net current through the molecule results in a stationary population P_1. It can be determined from the balance equation

$$P_1 \sum_{X,\boldsymbol{k}} k_{1 \to X\boldsymbol{k}} = \sum_{X,\boldsymbol{k}} k_{X\boldsymbol{k} \to 1} P_{X\boldsymbol{k}}. \tag{7.173}$$

The right-hand side is easily calculated by again replacing the $P_{X\boldsymbol{k}}$ by the corresponding Fermi distributions. It results in charging rates $k_{X \to 1}$ of the type given in Eq. (7.164). The expression on the left-hand side of Eq. (7.173), however, is incomplete. As discussed in relation to the HET reactions in Section 7.7, the used single-electron theory does not account for the population of band states of the lead where charge is injected. Therefore, the rates $k_{1 \to X\boldsymbol{k}}$ have to be completed by $1 - f_F(\hbar\varepsilon_{X\boldsymbol{k}} - \mu_X)$. This results in rates $k_{1 \to X}$ of discharge of the molecule similar to those introduced in Eq. (7.140). A simple solution of Eq. (7.173) follows: $P_1 = (k_{L \to 1} + k_{R \to 1})/(k_{1 \to L} + k_{1 \to R})$, being the ratio of the net charge outflow from the molecule and the net charge injection.

According to the given reasoning, the stationary current, Eq. (7.172), in its dependence on the applied voltage V follows as

$$I(V) = 2|e|(k_{L \to 1} - k_{1 \to L} P_1) = 2|e| \frac{k_{L \to 1} k_{1 \to R} - k_{R \to 1} k_{1 \to L}}{k_{1 \to L} + k_{1 \to R}}. \tag{7.174}$$

The expression contains contributions from the left to right current proportional to $k_{L \to 1} k_{1 \to R}$ and the corresponding contributions from the backward right to the left current proportional to $k_{R \to 1} k_{1 \to L}$. Just this combination of rates reflects the sequential character of the discussed transmission scheme (be aware of the similarity of the current expression with the sequential part of the bridge-mediated transfer as presented in Section 7.6.1, Eq. (7.130)).

7.8.1.1 An Example

To have a stable junction, the measurement of molecular IV characteristics is favorably done at low temperatures. Therefore, we specify the transition rates $k_{X \to 1}$ and $k_{1 \to X}$ to this case and, additionally, assume the dominance of a single vibrational coordinate that carries out harmonic vibrations. In the wide-band limit

of the molecule–lead interaction and for a symmetrically applied voltage, it follows that

$$k_{X \to 1} = 2\pi\Gamma \sum_v |\langle \chi_{0\mu=0} | \chi_{1v} \rangle|^2 f_F(\hbar[\varepsilon_1 + \omega_{vib} v] - \mu_X) \tag{7.175}$$

and

$$k_{1 \to X} = 2\pi\Gamma \sum_v |\langle \chi_{1\mu=0} | \chi_{0v} \rangle|^2 \left(1 - f_F(\hbar[\varepsilon_1 - \omega_{vib} v] - \mu_X)\right). \tag{7.176}$$

Charging of the molecule and thus current formation for a positive voltage (current from left to right) becomes possible if $\hbar\varepsilon_1 - \mu_0 = |e|V/2$ (recall Eq. (7.166)); that is, the vibrational ground state of the charged molecule is populated. If $\hbar(\varepsilon_1 - \omega_{vib}) - \mu_0 = |e|V/2$, a second transmission channel is opened with the first excited vibrational state of the charged molecule also occupied. Higher excited vibrational states follow if the applied voltage is further increased. How the different channels contribute is mainly regulated by the Frank–Condon factors $|\langle \chi_{0\mu=0} | \chi_{1v} \rangle|^2$. A large nuclear rearrangement of the molecule upon charging suppresses those channels connected with the low-lying excited vibrational state (this has been named the *Franck–Condon blockade*). Discharge of the molecule, in the present case of $V > 0$ via the rate $k_{1 \to R}$, proceeds if $\hbar\varepsilon_1 - \mu_0 = v\hbar\omega_{vib} - |e|V/2$. This goes along with the charging process explained earlier. The IV characteristics include steps whenever a new transmission channel due to excited vibrational states is opened.

Figure 7.30 displays measurements where it has been argued that the charge transmission proceeds in this sequential way. The IV characteristics, however, do not display distinct steps. The strong molecule–lead coupling smears out these steps, and vibrational contributions are only clearly visible if the second derivative of the current with respect to the voltage is drawn.

7.8.2 Elastic Charge Transmission

Next, charge transmission will be described as an elastic scattering process of electrons at the single molecule. This approach incorporates cases with large molecule–lead couplings where the nonadiabatic transition rates used in the preceding section are not valid. To achieve a clear view on the specificity of the scattering approach, we neglect any inelastic contributions due to the participation of molecular vibrations (this is done by removing the vibrational Hamiltonians $\mathcal{H}_0$ and $\mathcal{H}_1$ from Eq. (7.168)).

First, we determine the transition rate $k_{L\boldsymbol{k} \to R\boldsymbol{q}}$ describing an elastic scattering process of an electron, coming from the left lead and moving to the right, at the molecule. Using the detailed calculations given in the supplementary Section 7.10.5, one obtains the following expression for the transition rate (the rate of the reverse transition is obtained by an interchange of $L\boldsymbol{k}$ and $R\boldsymbol{q}$):

$$k_{L\boldsymbol{k} \to R\boldsymbol{q}} = \frac{2\pi}{\hbar^4} \delta(\varepsilon_{R\boldsymbol{q}} - \varepsilon_{L\boldsymbol{k}}) |V_R(\varepsilon_{L\boldsymbol{k}}) \langle \varphi_1 | \hat{G}(\varepsilon_{L\boldsymbol{k}}) | \varphi_1 \rangle V_L^*(\varepsilon_{L\boldsymbol{k}})|^2. \tag{7.177}$$
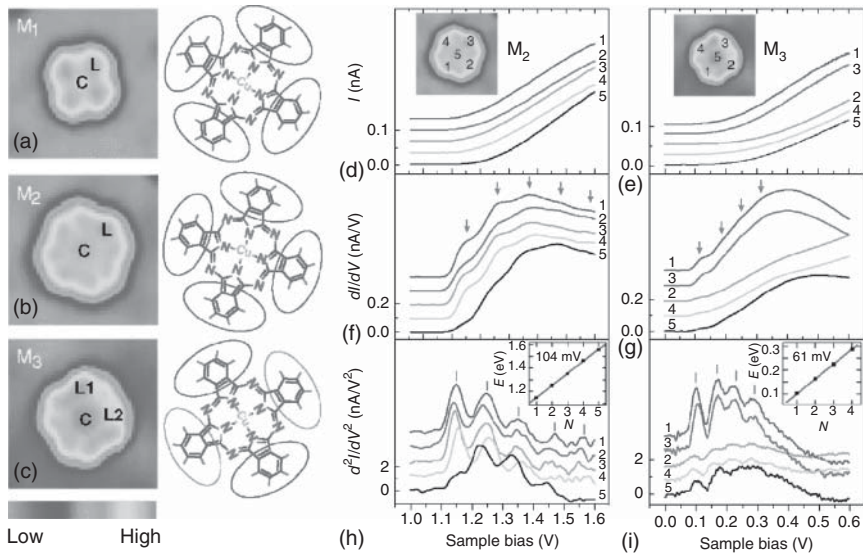
Figure 7.30 Vibrational contributions in the IV characteristics of a single copper phthalocyanine molecule contacted by the tip of a scanning tunneling microscope (STM) and an NiAl(110) surface with an ultrathin Al_2O_3 film separating the molecule from the metal surface. (a–c) STM scans of different arrangements of the molecule at the NiAl(110) surface (the different contact points of the STM tip are indicated, scan size 37 Å times 37 Å) and the related molecular structures in the respective positions; (d, e) measured currents versus applied voltage taken at the different contact points as well as their first (f, g) and second (h, i) derivatives with respect to the applied voltage. The distinct equidistant peaks in the latter are related to vibrations associated with the deformations of the inner ring of the phthalocyanine macrocycle (h) and vibrations involving the out-of-plane motions of the isoindole atoms (i) (Reproduced with permission from Qiu et al. [12]/American Physical Society).

The presence of the δ-function indicates the elastic character of the scattering process, and we again assumed that the $\mathbf{k}$-vector dependency of the molecule–lead couplings can be replaced by the direct dependence on the band energies. $\hat{G}$ is the Fourier-transformed Green's operator defined by the time evolution operator, Eq. (7.253), of the molecule–lead system (see also Section 3.3.3). It appears in a matrix element taken with the single-electronic state that characterizes the singly charged molecule.

The current related to the charge transmission from the left to the right electrode follows as

$$I_{L \to R} = 2|e| \sum_{\mathbf{k},\mathbf{q}} f_{\mathrm{F}}(\hbar\varepsilon_{L\mathbf{k}} - \mu_L) \left[1 - f_{\mathrm{F}}(\hbar\varepsilon_{R\mathbf{q}} - \mu_R)\right] k_{L\mathbf{k} \to R\mathbf{q}}. \tag{7.178}$$

Changing from the $\mathbf{k}$-vector dependence to a continuous frequency dependence ($\varepsilon_{L\mathbf{k}} \to \Omega$ and $\varepsilon_{R\mathbf{q}} \to \bar{\Omega}$), we write this expression as

$$I_{L \to R} = \frac{|e|}{2\pi} \int d\Omega \, f_{\mathrm{F}}(\hbar\Omega - \mu_L) \, \mathcal{T}_{L \to R}(\Omega) \left[1 - f_{\mathrm{F}}(\hbar\Omega - \mu_R)\right]. \tag{7.179}$$

The double frequency integration is reduced to a single one because of the δ-function in the rate. Further, we define the transmission function for electrons moving from the left to the right lead (note also the introduction of a DOS, Eq. (7.136), for each electrode)

$$\mathcal{T}_{L\to R}(\Omega) = \frac{4\pi^2}{\hbar^4}\mathcal{N}_R(\Omega)\mid V_R(\Omega)\langle\varphi_1|\hat{G}(\Omega)|\varphi_1\rangle V_L^*(\Omega)|^2 \mathcal{N}_L(\Omega). \tag{7.180}$$

We evaluate the absolute square and get

$$\mathcal{T}_{L\to R}(\Omega) = 4\pi^2\Gamma_R(\Omega)\langle\varphi_1|\hat{G}(\Omega)|\varphi_1\rangle\Gamma_L(\Omega)\langle\varphi_1|\hat{G}^+(\Omega)|\varphi_1\rangle, \tag{7.181}$$

where the definition of the molecule–lead coupling function equation (7.142) has been used (note the specification to the left and the right electrodes). The operator version $\hat{\Gamma}_X = \Gamma_X|\varphi_1\rangle\langle\varphi_1|$ of the coupling function gives an appealing form for $\mathcal{T}_{L\to R}$:

$$\mathcal{T}_{L\to R}(\Omega) = 4\pi^2 \text{tr}_{\text{mol}}\{\hat{\Gamma}_R(\Omega)\hat{G}(\Omega)\hat{\Gamma}_L(\Omega)\hat{G}^+(\Omega)\}$$
$$\equiv 4\pi^2 \text{tr}_{\text{mol}}\{\hat{\Gamma}_L(\Omega)\hat{G}^+(\Omega)\hat{\Gamma}_R(\Omega)\hat{G}(\Omega)\}. \tag{7.182}$$

The trace is restricted here to the single-state φ_1 referring to the singly-charged molecule. However, the expression stays valid if more molecular states are involved. Therefore, we introduced a labeling by the index *mol*. Since the Green's operators $\hat{G}^+$ and $\hat{G}$ are embedded in the molecule–lead coupling operators, we may change to the reduced version:

$$\hat{G}_{\text{mol}}(\Omega) = \hat{\Pi}_{\text{mol}}\hat{G}(\Omega)\hat{\Pi}_{\text{mol}}. \tag{7.183}$$

The quantity $\hat{\Pi}_{\text{mol}}$ projects on the states of the singly-charged molecule (here simply identical with $|\varphi_1\rangle\langle\varphi_1|$). We obtain

$$\mathcal{T}_{L\to R}(\Omega) = 4\pi^2 \text{tr}_{\text{mol}}\{\hat{\Gamma}_L(\Omega)\hat{G}_{\text{mol}}^+(\Omega)\hat{\Gamma}_R(\Omega)\hat{G}_{\text{mol}}(\Omega)\}, \tag{7.184}$$

and for the reverse transition from the right to the left electrode,

$$\mathcal{T}_{R\to L}(\Omega) = 4\pi^2 \text{tr}_{\text{mol}}\{\hat{\Gamma}_R(\Omega)\hat{G}_{\text{mol}}^+(\Omega)\hat{\Gamma}_L(\Omega)\hat{G}_{\text{mol}}(\Omega)\}$$
$$\equiv 4\pi^2 \text{tr}_{\text{mol}}\{\hat{\Gamma}_L(\Omega)\hat{G}_{\text{mol}}(\Omega)\hat{\Gamma}_R(\Omega)\hat{G}_{\text{mol}}^+(\Omega)\}. \tag{7.185}$$

If the coupling operators to the leads coincide, both transmission functions become identical ($\mathcal{T}_{L\to R} = \mathcal{T}_{R\to L} \equiv \mathcal{T}$).

The total stationary current follows as

$$I(V) = I_{L\to R} - I_{R\to L} = \frac{|e|}{\pi}\int d\Omega\left(f_{\text{F}}(\hbar\Omega - \mu_L)\left[1 - f_{\text{F}}(\hbar\Omega - \mu_R)\right]\mathcal{T}_{L\to R}(\Omega)\right.$$
$$\left. - f_{\text{F}}(\hbar\Omega - \mu_R)\left[1 - f_{\text{F}}(\hbar\Omega - \mu_L)\right]\mathcal{T}_{R\to L}(\Omega)\right). \tag{7.186}$$

The current formula simplifies in the case of the identical molecule–lead couplings

$$I(V) = \frac{|e|}{\pi}\int d\Omega\left(f_{\text{F}}(\hbar\Omega - \mu_L) - f_{\text{F}}(\hbar\Omega - \mu_R)\right)\mathcal{T}(\Omega). \tag{7.187}$$

The expression can be used to calculate the IV characteristics of a particular molecule attached to two nanoelectrodes. The transmission function regulates the contribution of a particular transmission channel determined by a scattered electron with energy $\hbar\Omega$. All possible channels are accounted for by the Ω-integration.

The difference in the Fermi function establishes a "transmission window" where current flow becomes possible. The lead electronic states enter only in an implicit way via the coupling operators as well as the related self-energies.

We demonstrate this by computing a concrete expression for the Green's operator $\hat{G}_{\text{mol}}(\Omega)$, Eq. (7.183), reduced to the states of the charged molecule. The general methodology is given in Section 3.3.3. We note Eq. (3.111) for the reduced Green's operator and obtain here

$$\hat{G}_{\text{mol}}(\Omega) = \frac{\hat{\Pi}_{\text{mol}}}{\Omega - \varepsilon_1 - \hat{\Sigma}(\Omega) + i\epsilon}. \tag{7.188}$$

The self-energy operator $\hat{\Sigma}$ separates into a contribution from the left and the right leads $\hat{\Sigma} = \hat{\Sigma}_L + \hat{\Sigma}_R$. According to Eq. (3.110), we have

$$\hat{\Sigma}_X(\Omega) = \frac{1}{\hbar^2} \sum_{\boldsymbol{k}} \frac{|V_{X\boldsymbol{k}}|^2}{\Omega - \varepsilon_{\boldsymbol{k}} + i\epsilon} \hat{\Pi}_{\text{mol}} \equiv \frac{1}{\hbar^2} \int d\bar{\Omega} \frac{\mathcal{N}_X(\bar{\Omega})|V_X(\bar{\Omega})|^2}{\Omega - \bar{\Omega} + i\epsilon} \hat{\Pi}_{\text{mol}}. \tag{7.189}$$

Obviously, the molecule–lead coupling operators $\hat{\Gamma}_X$ can be deduced from the anti-Hermitian part according to $\hat{\Gamma}_X = i/2\pi \times (\hat{\Sigma}_X - \hat{\Sigma}_X^+)$ (cf. Eq. (3.112)). The appearance of $\hat{\Sigma}$ in the denominator of $\hat{G}_{\text{mol}}$ recalls the fact that the molecule–lead coupling has been accounted for beyond any perturbation expansion (which guarantees the validity of the approach also for a strong coupling of the molecule to the leads).

Before presenting an explicit expression for the current, we compute the resistance at $T = 0$ following from Eq. (7.187). Noting the $T = 0$ relation $f_{\text{F}}(\hbar\Omega - \mu_L) - f_{\text{F}}(\hbar\Omega - \mu_R) = \theta(\mu_L - \hbar\Omega) - \theta(\mu_R - \hbar\Omega)$, the current follows as

$$I(V) = \frac{|e|}{\pi} \int\limits_{E_{\text{F}}/\hbar - |e|V/2\hbar}^{E_{\text{F}}/\hbar + |e|V/2\hbar} d\Omega \, \mathcal{T}(\Omega). \tag{7.190}$$

One easily computes the differential conductivity (inverse differential resistance) as the derivative of the current with respect to the voltage $g(V) = dI(V)/dV$. The conductivity ($V = 0$) follows as

$$g(V = 0) = \frac{|e|^2}{\pi\hbar} \mathcal{T}(E_{\text{F}}/\hbar), \tag{7.191}$$

where $\pi\hbar/|e|^2 = h/2|e|^2$ is known as the "quantum of resistance" (how it determines the actual conductivity is determined by the value of the transmission function at the Fermi energy).

7.8.2.1 An Example

We return to the case where the charged molecule is characterized by the single-level φ_1 with energy E_1. Moreover, identical leads are assumed. Then, Eq. (7.187) for the current can be used. When calculating the molecule–lead self-energy, we neglect the hermitian part, thus ignoring a possible shift of the molecular energy E_1 by its coupling to the leads. The imaginary part (the molecule–lead coupling function) is taken in the wide band limit, Eq. (7.144), leading to a common and frequency-independent Γ. The transmission function entering Eq. (7.187) reads

$$\mathcal{T}(\Omega) = \frac{4\pi^2\Gamma^2}{(\Omega - \varepsilon_1)^2 + 4\pi^2\Gamma^2}. \tag{7.192}$$

If the energy of the lead electron to be scattered is near the energy of the charged molecule, then $\mathcal{T}(\Omega)$ reaches values near unity. Otherwise, it is of minor importance. The broadening of the molecular energy E_1, and thus of the transmission peak, is regulated by the molecule–lead coupling (the magnitude of the latter is not restricted within this description). The current formula, Eq. (7.187), accounts for all energies $\hbar\Omega$ that fit into the "transmission window." Assuming $E_1 > E_F$, the current stays small as long as $E_1 - E_F > |e|V/2$. If the applied voltage is increase to fit the condition $E_1 - E_F \approx |e|V/2$, the current may increase abruptly but changes only a little bit if V is further increased. The respective computations that focus on the transmission function of an aromatic molecule are presented in Figure 7.31.

7.8.2.2 Inclusion of Vibrational Levels

We extend the considerations of the previous section to the inclusion of vibrational DOFs of the molecule (attached again to a left and a right lead). Although the electron transmission through the molecule will be considered in the framework of the
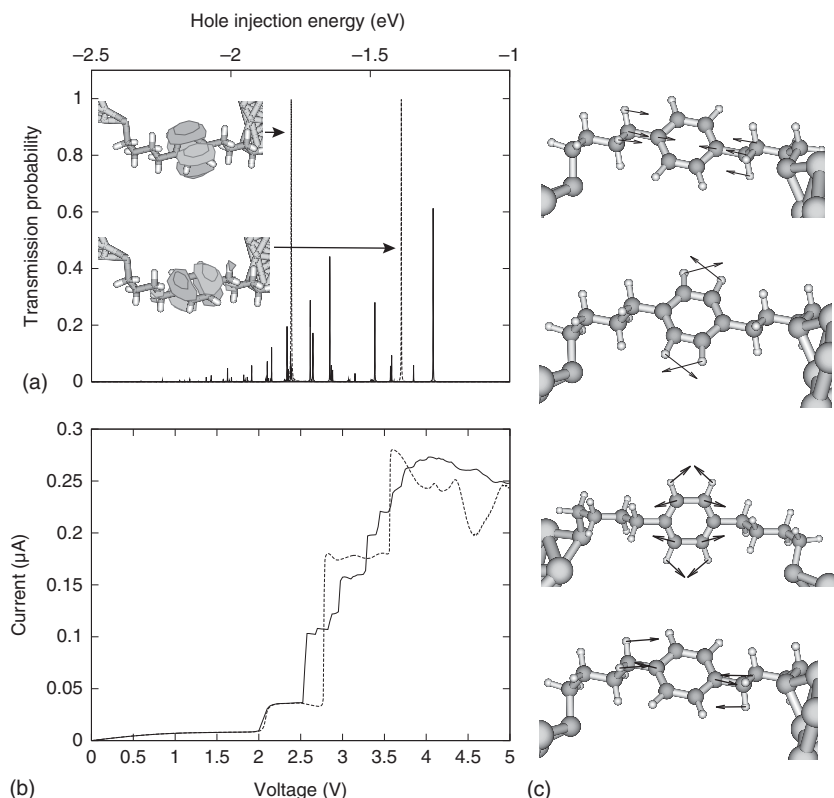
Figure 7.31 Vibrational contributions to the charge transmission through a benzene-di(ethanethiolate) molecule attached to two pyramidal gold contacts. (a) Total transmission probability (at $V = 0$) as a function of the initial hole energy (relative to the Fermi energy). The two orbitals shown dominate the transmission function at the indicated peaks. (b) IV characteristics including vibrational contributions (full line) and without (dashed line). (c) The molecular normal mode vibrations included in the computations (Reproduced with permission from Benesch et al. [13]/American Chemical Society).

scattering theory, it becomes inelastic from the point of view of the transmitted electrons. What is conserved is the electron–vibrational energy. For a transition from the left to the right lead, the energy $E_{Lk} + \hbar\omega_{0\mu}$ of the initial state has to coincide with the energy $E_{Rq} + \hbar\omega_{0\mu}$ of the final state ($\hbar\omega_{0\mu}$ and $\hbar\omega_{0\nu}$ denote the related vibrational energies). Since the vibrational state may change in the course of the scattering process, the electronic energy changes too. But note that any vibrational relaxation is not included in this description.

The inclusion of vibrational contributions into the formalism used in the preceding section is rather straightforward. Instead of the transition relation (from the left to the right lead) used before, we have to consider $|\chi_{0\mu}\rangle|\varphi_{Lk}\rangle \rightarrow |\chi_{0\nu}\rangle|\varphi_{Rq}\rangle$ ($\chi_{0\mu}$ and $\chi_{0\nu}$ denote the vibrational states of the uncharged molecule). Accordingly, we arrive at

$$k_{Lk\mu \to Rq\nu} = \frac{2\pi}{\hbar^4}\delta(\bar{\Omega} + \omega_{0\nu} - \Omega - \omega_{0\mu})|V_R(\bar{\Omega})\langle\varphi_1\chi_{0\nu}|\hat{G}(\Omega + \omega_{0\mu})|\chi_{0\mu}\varphi_1\rangle V_L^*(\Omega)|^2.$$

(7.193)

The vibrational wave functions of the initial and final scattering states appear unchanged in this expression. However, the initial and final state band continuums represented by the energies $\hbar\Omega$ and $\hbar\bar{\Omega}$, respectively, are shifted by vibrational energies (the initial electronic energy is not necessarily identical to the final electronic state energy).

When calculating the left to right current, we may introduce again an expression as in Eq. (7.179), but generalized to the inclusion of inelastic contributions:

$$I_{L \to R} = \frac{|e|}{\pi}\int d\Omega d\bar{\Omega}\, f_F(\hbar\Omega - \mu_L)\,\mathcal{T}_{L \to R}(\Omega, \bar{\Omega})\,\left[1 - f_F(\hbar\bar{\Omega} - \mu_R)\right].$$

(7.194)

The formula includes independent integrations with respect to the initial and final electronic energies reflecting the inelastic character of the scattering process (the transmission function also depends on two frequency arguments). Equation (7.194) already accounts for the distribution of the initial electrons to be scattered as well as the possible population of the final states. But a similar treatment of the initial and final vibrational states becomes necessary now. The initial vibrational states are distributed due to $f_{0\mu}$. In contrast, there are no restrictions with respect to the final states. Thus, the transmission function, (7.180) has to be generalized to

$$\mathcal{T}_{L \to R}(\Omega, \bar{\Omega}) = \frac{4\pi^2}{\hbar^4}\sum_{\mu,\nu}f_{0\mu}\,\delta(\bar{\Omega} + \omega_{0\nu} - \Omega - \omega_{0\mu})$$
$$\times\mathcal{N}_R(\bar{\Omega})|V_R(\bar{\Omega})\langle\varphi_1\chi_{0\nu}|\hat{G}(\Omega + \omega_{0\mu})|\chi_{0\mu}\varphi_1\rangle V_L^*(\Omega)|^2\mathcal{N}_L(\Omega).$$

(7.195)

We again introduce the molecule–lead coupling function, (7.142) and may write

$$\mathcal{T}_{L \to R}(\Omega, \bar{\Omega}) = 4\pi^2\sum_{\mu,\nu}f_{0\mu}\delta(\bar{\Omega} + \omega_{0\nu} - \Omega - \omega_{0\mu})$$
$$\times\Gamma_R(\bar{\Omega})\,|\,\langle\varphi_1\chi_{0\nu}|\hat{G}(\Omega + \omega_{0\mu})|\chi_{0\mu}\varphi_1\rangle|^2\Gamma_L(\Omega).$$

(7.196)

To make this relation more explicit, concrete expressions for the Green's operator matrix elements $\langle\varphi_1\chi_{0\nu}|\hat{G}(\Omega + \omega_{0\mu})|\chi_{0\mu}\varphi_1\rangle$ have to be calculated. Since the

electronic matrix element with respect to the singly charged state appears, we may calculate the Green's operator $\hat{G}_1$ reduced to this state. Similar computations have already been carried out in Section 7.7.1.3 in connection with the determination of the finite electron lifetime due to a HET process. In a first step, one has to change to vibrational matrix elements that belong to vibrational states of the singly charged molecule; that is, we have to use the states $\chi_{1\kappa}$. Therefore, one introduces the vibrational completeness relation $\sum_\kappa |\chi_{1\kappa}\rangle\langle\chi_{1\kappa}|$ left and right from $\hat{G}$ in the original matrix element (in the right-hand side case, we use the vibrational quantum number λ instead of κ). It results in matrix elements $\langle\varphi_1\chi_{1\kappa}|\hat{G}_1(\Omega + \omega_{0\mu})|\chi_{0\lambda}\varphi_1\rangle$. In the wide-band limit, we may derive an explicit expression for the Green's operator matrix elements, which read in the present case

$$G_{1\kappa,1\lambda}(\Omega + \omega_{0\mu}) = \frac{\delta_{\kappa,\lambda}}{\Omega + \omega_{0\mu} - \varepsilon_1 - \omega_{1\kappa} + i\pi(\Gamma_L + \Gamma_R)}. \tag{7.197}$$

This gives for the matrix element in the transmission function

$$\langle\varphi_1\chi_{0\nu}|\hat{G}(\Omega + \omega_{0\mu})|\chi_{0\mu}\varphi_1\rangle = \sum_\kappa \frac{\langle\chi_{0\nu}|\chi_{1\kappa}\rangle\langle\chi_{1\kappa}|\chi_{0\mu}\rangle}{\Omega + \omega_{0\mu} - \varepsilon_1 - \omega_{1\kappa} + i\pi(\Gamma_L + \Gamma_R)}. \tag{7.198}$$

Focusing again on a low-temperature region, $f_{0\mu}$ has to be replaced by $\delta_{\mu,0}$, and f_F by the unit-step function. Then, the total current becomes identical to the left-right current, and we may write (note the assumption of the wide-band limit and the assumption of identical leads, that is $\Gamma_L = \Gamma_R = \Gamma$)

$$I = \frac{|e|}{\pi} \sum_N \int_{E_F - \hbar\omega_{0\nu} - |e|V/2}^{E_F + |e|V/2} d\Omega \mid \sum_\kappa \frac{2\pi\,\Gamma\langle\chi_{00}|\chi_{1\kappa}\rangle\langle\chi_{1\kappa}|\chi_{0\nu}\rangle}{\Omega - \varepsilon_1 - \omega_{1\kappa} + 2\pi i\Gamma}\mid^2. \tag{7.199}$$

In generalization of the current formula, Eq. (7.190), with the transmission function, Eq. (7.192), scattering includes excited vibrational levels of the charged molecule. Their contributions are regulated by vibrational overlap expressions between states $\chi_{1\kappa}$ of the charged molecule and states χ_{00} as well as $\chi_{0\nu}$ of the uncharged one. And the "transmission window" is determined by vibrational energies of the neutral molecular state. All these additional transmission channels should introduce a certain fine structure in the IV characteristics. The corresponding computations are displayed in Figure 7.31, where some vibrations coupling dominantly to the charging of the molecule are included. The various steps in the low-temperature IV characteristics are due to the participation of vibrational quanta.

7.9 Photoinduced Ultrafast Electron Transfer

Photoinduced ET reactions have already been introduced in Section 7.1 (cf. Figure 7.6). In what follows, we concentrate on ET processes that are so fast that in the course of the electron motion from the donor to the acceptor, no complete vibrational relaxation is possible, that is $\tau_{rel} > t_{ET}$. Since vibrational relaxation usually occurs on a picosecond (10^{-12} seconds) or sub-picosecond time scale,

ultrafast ET reactions have to proceed in the same time region. This is also valid for the time resolution of the laser pulses used to initiate ET (to prepare the excited donor state D*, see scheme (7.3)) and to observe ET. Current laser technology achieves pulse durations comparable to or even shorter than the relevant system time scales t_{ET} and τ_{rel}. The vibrational motion is partly *coherent*, and the related wave packet dynamics can be observed using nonlinear optical spectroscopy. In this way, it is possible to take snapshots of the electron–vibrational dynamics.

If the inequality $\tau_{rel} > t_{ET}$ is valid, the ET is no longer of the nonadiabatic type. In the foregoing section, we demonstrated how to go beyond the limit of nonadiabatic ET by improving the lowest order perturbation theory with respect to the transfer integral V_{DA}. An alternative would be the use of the path integral or the hierarchy equations of motion approach outlined in Section 3.10 and 3.11, respectively, that can account for arbitrary state couplings, while providing at the same time an exact treatment of the coupling to harmonic oscillator reservoirs. Here, we present a density matrix description that is numerically less demanding as compared, for instance to a path integral study. The drawback, however, is that only a few vibrational DOFs can be incorporated nonperturbatively; the majority forms a heat bath that is treated by the quantum master equation (QME) approach.

Consequently, we derive equations of motion whose solutions describe the ET in a nonperturbative manner with respect to the interaction strength V_{DA}. To do this, we introduce a density matrix approach capable of describing the time evolution of an initially defined density matrix. Thus, the limits of adiabatic and nonadiabatic ET are naturally included, and all types of electronic and vibrational coherences are accounted for. Furthermore, it is a particular advantage of this approach that one can easily include the radiation field and compute ultrafast optical spectra. In the subsequent Section 7.9.2, different prescriptions for defining ET rates starting with the time-dependent density matrix will also be discussed.

According to Scheme (7.3), the photoinduced ET considered in what follows requires the excitation of an electron from the ground state of the DA complex to the (diabatic) donor state. Therefore, the manifold of electronic states considered so far has to be supplemented by the electronic ground state of the complex (cf. Figures 7.6 and 7.32). Often, only a small number of active vibrational coordinates couple to the
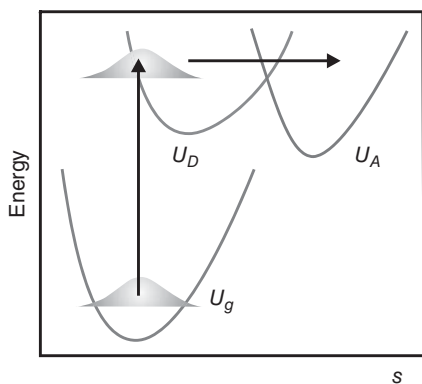
Figure 7.32 Electronic ground-state PES as well as donor and acceptor diabatic PESs (plotted along the active coordinate *s*) appropriate for photoinduced ET. If the initial state preparation becomes ultrafast, the limit of impulsive excitation can be applied, resulting in an instantaneous shift of the electronic ground state vibrational wave function to the donor PES.

external field and to the ET reaction (at least one coordinate s). All the remaining inter- and intramolecular vibrational DOFs, denoted as $Z = \{Z_\xi\}$, are incorporated in an indirect manner in the optical preparation process and the ET reaction. They are assumed to form a heat bath (uncoupled normal-mode oscillators) for the active coordinates. This assumption directly results in a separation of the complete Hamiltonian into the (active) system part H_S and the reservoir contribution H_R. (This was discussed in Chapter 3 as the basic idea behind the concept of the reduced density operator.) We write

$$H(t) = H_S(t) + H_{\text{S-R}} + H_R, \tag{7.200}$$

where the time dependence points to the inclusion of the coupling to a laser field. To derive the different parts of this Hamiltonian, we note the original form, Eq. (7.23), of the ET Hamiltonian (with bridge molecule contributions neglected here). The vibrational Hamiltonians referring to the electronic states as well as the transfer integral depend on the active as well as the reservoir coordinates. If we neglect the respective dependencies of the transfer integrals, there remain the diabatic state PES $U_m(s, Z)$. The intended system reservoir separation is achieved if we presume the following separation of the PES:

$$U_m(s, Z) = U_m(s) + W_m(s, Z) + U(Z). \tag{7.201}$$

It splits into a part $U_m(s)$ that only depends on the active coordinate, a coupling part $W_m(s, Z)$, and a part $U(Z)$. The latter expression is determined exclusively by the heat bath (reservoir) coordinates. Since it does not depend on the diabatic state index m, the coordinates Z, indeed, are not affected by the ET. $W_m(s, Z)$ depends on both types of coordinates and becomes responsible for energy dissipation from the ET system into the reservoir. The system part of Eq. (7.200) takes the form

$$H_S(t) = H_{\text{mol}} + H_F(t). \tag{7.202}$$

This Hamiltonian allows us to describe the excitation process of the donor and thus the preparation process of the ET reactant state. Note that this extends our previous considerations where the preparation process of the initial state of the excess electron had not been considered. $H_S(t)$ separates into the molecular part H_{mol} and the coupling to the external field $H_F(t)$ (described in a semiclassical approach and within the electric dipole approximation; cf. Eq. (4.18)). The molecular part comprises the vibrational Hamiltonian H_g of the electronic ground state $|\varphi_g\rangle$ and the part describing the ET reaction. We have

$$H_{\text{mol}} = H_g |\varphi_g\rangle\langle\varphi_g| + H_{\text{DA}}. \tag{7.203}$$

The system reservoir coupling part of Eq. (7.200) may be written as $\sum_m W_m(s; Z)$ $|\varphi_m\rangle\langle\varphi_m|$. We concentrate on a bilinear coupling, that is an expression that depends linearly on all system coordinates s as well as reservoir coordinates Z. For practical reasons, $H_{\text{S-R}}$ is taken as in Eq. (3.198):

$$H_{\text{S-R}} = \sum_m K_m(s)\Phi_m(Z). \tag{7.204}$$

The reservoir part reads

$$\Phi_u(Z) \equiv \Phi_m(Z) = \sum_{\xi} k_{\xi}(m) Z_{\xi}. \tag{7.205}$$

Concerning the system contribution to $H_{\text{S-R}}$, we restrict ourselves to a single harmonic reaction coordinate (vibrational frequency Ω_s and reduced mass μ_s) and obtain

$$K_m(s) = \sqrt{\frac{2\mu_s\Omega_s}{\hbar}} (s - s^{(m)}) |\varphi_m\rangle\langle\varphi_m|. \tag{7.206}$$

The used system–reservoir coupling depends on the electronic state and increases with the deviation of the system coordinate s from its equilibrium position $s^{(m)}$. (Note that we introduced $K_m(s)$ as a dimensionless quantity (cf. discussion in Section 5.3.5.) The spectral density $J_{mn}(\omega)$ referring to the given system–reservoir coupling can be obtained in analogy to Eq. (3.294) (but here with an additional dependence on the electronic quantum numbers m and n).

Before introducing the density matrix, we specify the preparation process of the reactant state. A general description of the optical preparation of an excited electronic state has already been given in Section 6.5. We follow this scheme here and assume an exclusive population of the donor state (Figure 7.32). Obviously, for large values of V_{DA}, a certain combination of donor and acceptor levels will be populated, and the description in terms of adiabatic states becomes more convenient. Additionally, it is assumed that the pulse duration τ is short compared to the time scales of vibrational motion as well as ET (limit of impulsive excitation, cf. Section 6.5). As shown in Section 6.5, this enables us to eliminate the nuclear dynamics on the electronic ground state PES from the considerations. The optically prepared initial state for the ET reaction is obtained as (cf. Eq. (6.110))

$$\hat{\rho}(t_0) = \frac{1}{\hbar^2} |\boldsymbol{d}_{Dg}\boldsymbol{E}(t_p)\tau|^2 \ \hat{R}_m |D\rangle\langle D|. \tag{7.207}$$

Here, $\boldsymbol{E}(t_p)$ is the electric field strength at pulse maximum t_p, and τ denotes the corresponding pulse duration. We emphasize that, as a result of the impulsive excitation, the vibrational state in the electronic ground state represented by the ground state vibrational equilibrium density operator $\hat{R}_m$ has been instantaneously transferred onto the donor diabatic electronic state. At low temperatures, this corresponds to the projection of the ground state vibrational wave function onto the donor state as shown in Figure 7.32. Again, although Eq. (7.207) contains the vibrational statistical operator of the electronic ground state, the dynamics within the electronic ground state could be eliminated. Equation (7.207) gives the initial value for the density matrix, which is exclusively defined with respect to the electronic DA levels. If the underlying time scale separation is not possible, it is necessary to incorporate the coupled dynamics of the ground and excited states into the equations of motion.

Having specified the total Hamiltonian (7.200), we are in a position to use the density matrix theory, introduced in Section 3.8. However, our molecular Hamiltonian (the H_{DA} part) is not in diagonal form. This might become a problem insofar as a direct use of the state representation of Section 3.8.2 requires the knowledge of the

respective eigenstates (see also the similar discussion in Section 3.12 dealing with the dynamics of a two-levels system).

Suppose that these eigenstates have been calculated from

$$H_{DA}|\psi_\alpha\rangle = \mathcal{E}_\alpha|\psi_\alpha\rangle. \tag{7.208}$$

This equation defines the *adiabatic* electron–vibrational states of the DA Hamiltonian. (Although it would be possible to classify the states according to their relation to the upper and lower adiabatic PESs, Eq. (7.40), we do not introduce such a specification.) In general terms, diabatic $|\varphi_m\rangle|\chi_{mM}\rangle$ and adiabatic states are related via a linear transformation (see also Section 2.6)

$$|\psi_\alpha\rangle = \sum_{m,M} c_\alpha(mM) \, |\varphi_m\rangle|\chi_{mM}\rangle. \tag{7.209}$$

Once the adiabatic states and energies are known, it is possible to introduce the density matrix in the adiabatic state representation,

$$\rho_{\alpha\beta}(t) = \langle\psi_\alpha|\hat\rho(t)|\psi_\beta\rangle, \tag{7.210}$$

and to derive the respective equations of motion (see Section 3.8.2). Such an approach is most appropriate for the case of strong interstate coupling V_{DA}. In particular, V_{DA} is nonperturbatively incorporated into the description of dissipative processes via the Redfield tensor, Eq. (3.345).

Alternatively, one can define the density matrix in the diabatic state representation,

$$\rho_{\mu\nu}(t) \equiv \rho_{mM,nN}(t) = \langle\chi_{mM}|\langle\varphi_m|\hat\rho(t)|\varphi_n\rangle|\chi_{nN}\rangle, \tag{7.211}$$

where it is straightforward to compute the diabatic electronic state populations:

$$P_m(t) = \text{tr}_{vib}\{\langle\varphi_m|\hat\rho(t)|\varphi_m\rangle\} = \sum_M \rho_{mM,mM}(t), \tag{7.212}$$

which can be directly related to the ET rate (for details, see Section 7.9.2). To characterize the dynamics of the vibrational mode accompanying the ET reaction, one can use the probability distribution

$$P(s,t) = \langle s|\text{tr}_{el}\{\hat\rho(t)\}|s\rangle = \sum_{m,M,N} \chi_{mM}(s)\rho_{mM,mN}(t)\chi^*_{mN}(s), \tag{7.213}$$

which replaces the square of the vibrational wave function in the case of dissipative dynamics. For further use, we also give the internal energy of the DA electron–vibrational system (for the notation, also compare Section 7.2.3):

$$E_{int}(t) = \sum_{\mu\nu} \left(\delta_{\mu\nu}E_\mu + (1 - \delta_{mn})V_{\mu\nu}\right)\rho_{\mu\nu}(t). \tag{7.214}$$

Equations (7.212)–(7.214) demonstrate that observables of interest can be determined using the density matrix in the diabatic state representation. Finally, we would like to point out that the diabatic state representation can be used in the case of strong interstate coupling too. However, one has to make sure that the Redfield tensor is calculated using the eigenstates (adiabatic states) of H_{DA}. The last point is of less importance if V_{DA} is small. In this case, dissipation can often be simulated using the diabatic states. This issue will be addressed in more detail in the following section.

7.9.1 Quantum Master Equation for Electron Transfer Reactions

In what follows, we IndexQuantum master equation for electron transfer reactionsconsider photoinduced ultrafast ET in the limit where the dissipation of electron–vibrational energy can be described within the Markov approximation. The applicability of this approximation is not straightforward and deserves some comments (cf. discussion in Section 3.6.1). Let us assume that the Markov approximation is valid in the absence of an external field. It is obvious that the situation would not change if the system interacts with an optical pulse that is long compared to τ_{mem} (the characteristic time during which the memory function, describing dissipation, decays; cf. Section 3.6.1). Also, in the limit of impulsive excitation, we would expect that the Markov approximation is still valid (the initial state preparation is short compared to any other characteristic time of the system). However, if the pulse duration is comparable to τ_{mem}, the external driving introduces a new characteristic time, and no time scale separation is possible. As a consequence, the theoretical description based on the QME in the Markov approximation (as presented below) becomes invalid.

In the following discussion, we focus on the limit of impulsive excitation and assume the validity of the Markov approximation. We consider the representation of the QME in the diabatic basis. Using $\omega_{\mu\nu} = (E_\mu - E_\nu)/\hbar$, we have

$$\frac{\partial}{\partial t}\rho_{\mu\nu}(t) = -i\omega_{\mu\nu}\rho_{\mu\nu}(t) - \frac{i}{\hbar}\sum_\kappa \left(V_{\mu\kappa}\rho_{\kappa\nu}(t) - V_{\kappa\nu}\rho_{\mu\kappa}(t)\right) + \left(\frac{\partial\rho_{\mu\nu}(t)}{\partial t}\right)_{\text{diss}}.$$

$$(7.215)$$

To obtain the dissipative part of the density matrix equation, we cannot directly use the general Formulas given in Eq. (3.345), since the diabatic representation is not an energy representation. Therefore, we start with the QME in the notation of Eq. (3.265), which does not refer to any specific representation. The indices u and v used in Eq. (3.267) can be directly identified with the electronic state index. Taking the system part of the interaction operator, $K_m(s)$, from Eq. (7.206), we obtain for the respective diabatic state matrix elements

$$\langle\chi_{kK}|\langle\varphi_k|K_m(s)|\varphi_l\rangle|\chi_{lL}\rangle = \delta_{km}\delta_{lm}\left(\delta_{K,L-1}\sqrt{L} + \delta_{K,L+1}\sqrt{L+1}\right).$$

$$(7.216)$$

The operator $\Lambda_u \equiv \Lambda_m$ (cf. Eq. (3.264))

$$\Lambda_m = \sum_n \int_0^\infty d\tau\, C_{mn}(\tau)U_{\text{DA}}(\tau)K_n U_{\text{DA}}^+(\tau)$$

$$(7.217)$$

contains time-evolution operators defined by the complete DA complex Hamiltonian H_{DA}. To calculate the diabatic matrix elements of $U_{\text{DA}}(\tau)K_n U_{\text{DA}}^+(\tau)$, we first use the adiabatic states $|\psi_\alpha\rangle$ introduced in Eq. (7.208) and obtain

$$\langle\psi_\alpha|U_{\text{DA}}(\tau)K_n U_{\text{DA}}^+(\tau)|\psi_\beta\rangle = e^{-i\omega_{\alpha\beta}\tau}\langle\psi_\alpha|K_n|\psi_\beta\rangle.$$

$$(7.218)$$

The adiabatic matrix element can be expressed by the diabatic elements, Eq. (7.216), using Eq. (7.209) as

$$
\langle \psi_\alpha | K_n | \psi_\beta \rangle = \sum_{k',K'} \sum_{l',L'} c_\alpha^*(k'K') c_\beta(l'L') \langle \chi_{k'K'} | \langle \varphi_{k'} | K_n | \varphi_{l'} \rangle | \chi_{l'L'} \rangle
$$

$$
\equiv \sum_{K',L'} c_\alpha^*(nK') c_\beta(nL') \langle \chi_{nK'} | \langle \varphi_n | K_n | \varphi_n \rangle | \chi_{nL'} \rangle. \tag{7.219}
$$

As in the general treatment of Section 3.8.2, we omit the imaginary contribution to the Redfield tensor. This is achieved in the present notation by replacing the half-sided Fourier transform of the correlation function $C_{mn}(\tau)$, appearing in Eq. (7.217), by half of its complete Fourier transform, that is by $C_{mn}(\omega)/2$. Then, the diabatic matrix elements of the Λ-operator, Eq. (7.217), read

$$
\langle \chi_{kK} | \langle \varphi_k | \Lambda_m | \varphi_l \rangle | \chi_{lL} \rangle = \frac{1}{2} \sum_n \sum_{\alpha,\beta} C_{mn}(-\omega_{\alpha\beta}) c_\alpha(kK) c_\beta^*(lL) \langle \psi_\alpha | K_n | \psi_\beta \rangle
$$

$$
= \frac{1}{2} \sum_n \sum_{\alpha,\beta} \left(1 + n(\omega_{\beta\alpha}) \right) \left(J_{mn}(\omega_{\beta\alpha}) - J_{mn}(\omega_{\alpha\beta}) \right)
$$

$$
\times c_\alpha(kK) c_\beta^*(lL) \langle \psi_\alpha | K_n | \psi_\beta \rangle. \tag{7.220}
$$

Introducing this expression, together with the matrix elements of $K_m(s)$, into the dissipative part of Eq. (7.215) gives the full density matrix equation in the diabatic representation. This equation is exact with respect to the transfer integral V_{DA}. Consequently, ET for any value of V_{DA} can be studied covering the range from the adiabatic ET to the nonadiabatic ET. In contrast, possible values of the coupling strength to the reservoir are limited by the second-order perturbational treatment. However, this restriction is not crucial as long as the total system is properly separated into a relevant system and a reservoir.

The density matrix equations of motion, if expanded with respect to the adiabatic states, will give the canonical equilibrium distribution as a stationary solution (cf. Section 3.8.2). Therefore, the density matrix in the diabatic representation reads

$$
\rho_{mM,nN}(t \to \infty) = \sum_\alpha c_\alpha(mM) c_\alpha^*(nN) \frac{e^{-\mathcal{E}_\alpha/k_B T}}{\sum_\beta e^{-\mathcal{E}_\beta/k_B T}}. \tag{7.221}
$$

As a consequence of the diabatic representation, the density matrix contains nonzero off-diagonal elements in thermal equilibrium.

For a weak coupling V_{DA}, it is possible to consider the relaxation within the diabatic states, thus choosing the dissipative part in the zeroth-order approximation with respect to the transfer integral. This has the advantage that there is no need for diagonalizing the system Hamiltonian.

We do not give the complete Redfield tensor but consider the vibrational energy relaxation rates that can be derived from the general formula (3.350) in the limit of $V_{DA} = 0$:

$$
k_{mM \to nN} = \frac{1}{\hbar^2} \delta_{mn} \frac{2\mu_s \Omega_s}{\hbar} |\langle \chi_{mM} | (s - s^{(m)}) | \chi_{mN} \rangle|^2 C_{mm}(\omega_{mM,mN})
$$

$$
= \delta_{mn} \left[\delta_{M+1,N}(M+1) n(\Omega_s) + \delta_{M-1,N} M \left(1 + n(\Omega_s) \right) \right] \Omega_s^2 J_{mm}(\Omega_s). \tag{7.222}
$$

Note that all constants have been included in the definition of the spectral density. In contrast to Eq. (7.220), only electronic diagonal contributions of the spectral density given at a single frequency Ω_s enter the rate formula. The inverse lifetime of state $|\mu\rangle$ follows as[28]

$$\frac{1}{\tau_{mM}} = \sum_N k_{mM \to mN} = \left[(M+1) n(\Omega_s) + M \left(1 + n(\Omega_s) \right) \right] \, \Omega_s^2 \, J_{mm}(\Omega_s).$$

(7.223)

This expression leads to the dephasing rate $\gamma_{mM,nN} = 1/2\tau_{mM} + 1/2\tau_{nN}$ (cf. Eq. (3.353)). Figure 7.33 gives some examples for ultrafast ET reactions by showing the probability distribution, Eq. (7.213), of the vibrational coordinate at different instants of the time evolution. The vertical position indicates the actual value of the internal energy, Eq. (7.214). As a consequence of energy dissipation, the
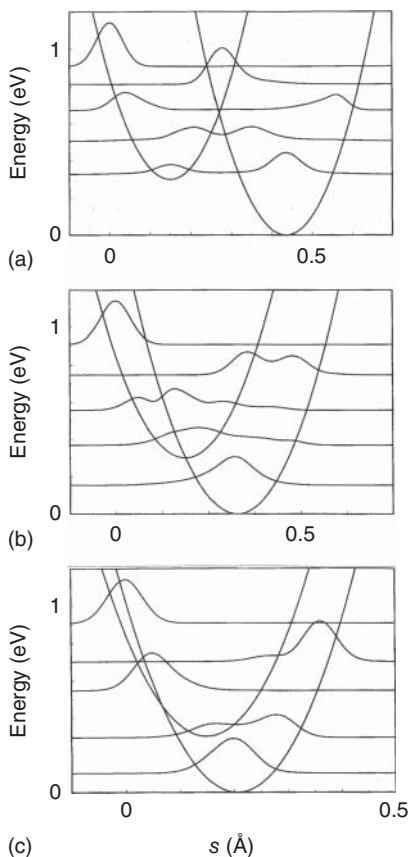
Figure 7.33 Probability distribution of the vibrational coordinate, Eq. (7.213), in the system of a coupled donor and acceptor PESs ($\hbar\Omega_s = |V_{DA}|^2 = 100$ meV, $\hbar J_{mm}(\Omega_s) = 10$ meV, $k_B T \ll \hbar\Omega_s$). The position of the probability distribution with respect to the energy axis corresponds to the actual internal energy, Eq. (7.214), at different time steps of the propagation ((a) $t = 0, 20, 40, 100,$ and 500 fs, (b) $t = 0, 20, 50, 100,$ and 500 fs, and (c) $t = 0, 20, 45, 115,$ and 500 fs, (from top)). The chosen configurations of both PESs correspond to the different types of ET reactions discussed in Section 7.4.1 ((a) normal region of ET reactions, (b) activationless case, and (c) ET in the inverted region).

---

28) The inverse lifetime of the vibrational ground $1/\tau_{m0}$ becomes proportional to $n(\Omega_s)$. Because of this fact, the bilinear system–reservoir coupling as applied here results in a long vibrational ground state lifetime. The inverse lifetime leads to dephasing rates $\gamma_{mM,nN} = 1/2\tau_{mM} + 1/2\tau_{nN} + \gamma_{mM,nN}^{(pd)}$, which may also be small if the vibrational ground state is involved and no pure dephasing $\gamma_{mM,nN}^{(pd)}$ is present (cf. Eq. (3.353)).

vibrational wave packet performs a damped motion within the coupled PESs. As an initial state, the vibrational ground state probability distribution displaced into the donor PES has been taken. Moving to Figure 7.33a from the left to the crossing point of both PESs, the wave packet splits up into two parts. This results from a partial reflection in the region around the crossing point. Destructive as well as constructive interference of both parts of the wave packet follows. In Figures 7.33b (activationless case of ET, cf. Section 7.4.1) and 7.33c (inverted case), this behavior is not so clear. The relaxation down to the vibrational ground state of the acceptor PES is most pronounced in Figure 7.33c.

The derived formulas (with or without the inclusion of V_{DA} in the dissipative part) give a solid basis for the simulation of ultrafast photoinduced ET reactions. And, if compared with more involved approaches, they are sufficiently accurate in the appropriate limit (cf. Figure 7.34). Complemented by the study of the response to additional radiation fields, the given density matrix approach allows to describe different nonlinear optical experiments. In fact, one can directly include the external fields into the density matrix equations. An alternative description is given by a perturbation expansion with respect to external fields. This leads to nonlinear response functions characterizing the molecular system (cf. Chapter 4). However, as a consequence of the expansion with respect to the electric field strength, one is practically limited to low-order processes. The outlined density matrix approach, however, provides the tools to study effects depending on the field intensity as well, such as the dynamical Stark effect.
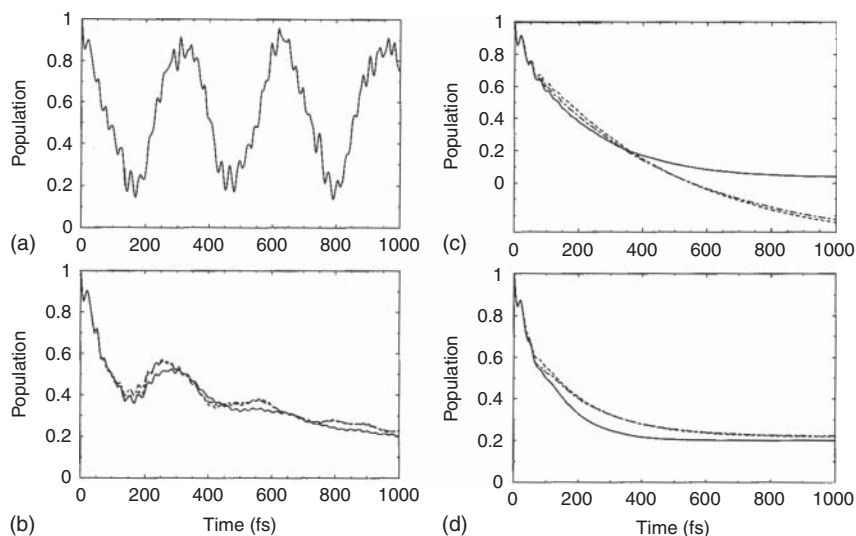
Figure 7.34 Population P_2 of the acceptor in a system of a coupled donor and acceptor PESs similar to Figure 7.33a ($T = 0$: panels (a–c), $T = 300$ K: panel (d), spectral density according to Eq. (3.301), $j_0 = 0$: panel (a), $j_0 = 0.2/\pi$: panel (b), and $j_0 = 1/\pi$: panels (c, d)). Dashed lines: solution of Eq. (7.215), dotted-dashed line: use of a time-dependent version of the Redfield tensor, and full line: results of computations based on the description of the reservoir modes by a multiconfiguration version of the approach discussed in Section 3.5.3 (Reproduced with permission from Egorova et al. [14]/American Institute of Physics).

Finally, we point out that in cases where there is no prominent vibrational mode with particular strong coupling, all vibrational DOFs can be treated as a reservoir. The system Hamiltonian includes the electronic DOFs only, and the system–reservoir coupling is of the type discussed in Section 3.12.2. The QME is formulated in terms of the electronic states, either diabatic or adiabatic, depending on the strength of the interstate coupling. An example showing the photoinduced ET dynamics of a molecular triad is given in Figure 7.35.
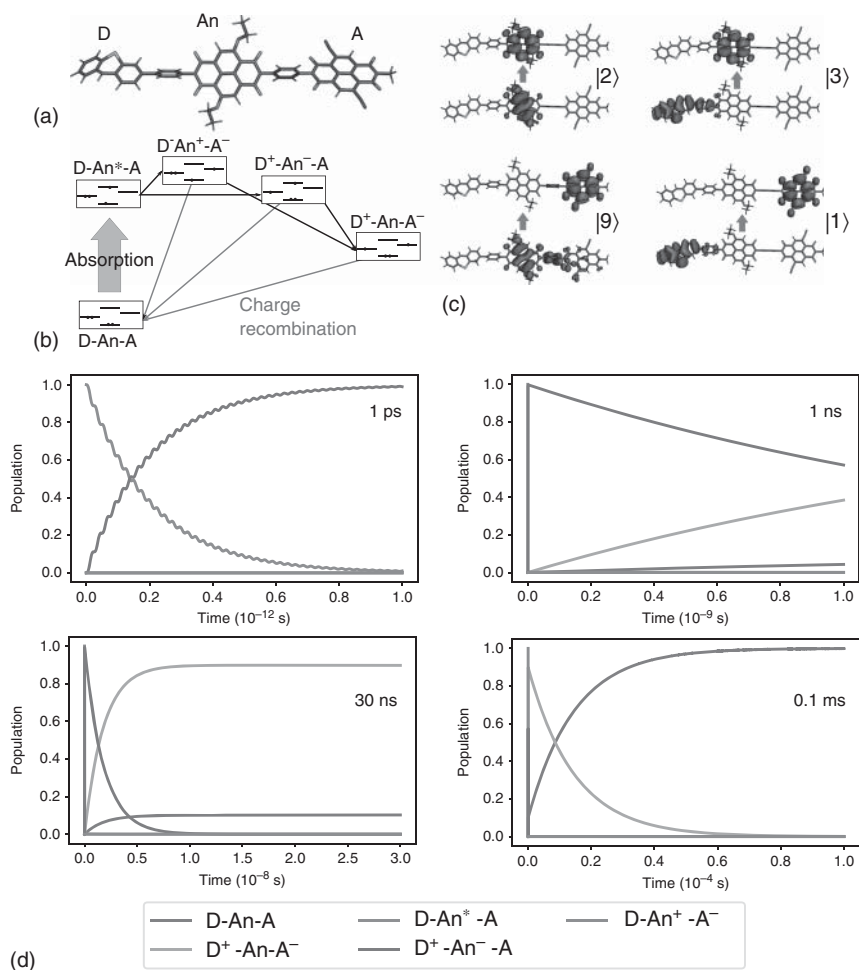
Figure 7.35 Photoinduced ET in a molecular triad (a). Upon excitation of the antenna (An), ET is triggered, yielding either D-An$^+$-A$^-$ or D$^+$-An$^-$-A, which converts into D$^+$-An-A$^-$ before charge recombination to the ground state (b). (c) The HOMO–LUMO transitions for the adiabatic case that have been used to construct a generalized Mulliken–Hush parametrization of the ET Hamiltonian. (d) Population dynamics on different time scales (as indicated), obtained from the solution of the Redfield equations. The system–bath coupling parameters were calculated using a normal mode expansion of the PESs, cf. Section 7.2.3, treating all modes as part of the bath (figure courtesy of T. Hansen, for more details, see Storm et al. [15].)

7.9.2 Rate Expressions

In the previous section, photoinduced ET has been described via the time-dependent density matrix. In order to establish the connection with the considerations of Sections 7.5 and 7.6, we concentrate on the question of how to introduce transfer rates within the present approach.

According to the general type of rate equations (3.2), we expect an exponential decay, for example for the donor state population, $P_D(t) \propto \exp\{-k_{ET}t\}$. Although such a behavior is unlikely at early times (here, it could be oscillatory and multiexponential), it is reasonable to expect it after all coherences have decayed. Therefore, one can define the ET rate k_{ET} as

$$k_{ET} = -\lim_{t \to \infty} \frac{1}{t} \ln P_D(t), \tag{7.224}$$

where the donor state population is obtained from the solution of the general density matrix equations (7.215). The deviation from an exponential decay at early times reflects an initial time dependence of k_{ET}.

Alternatively, one can introduce a transfer rate via the inverse of the mean lifetime of the electron at the donor state as

$$k_{ET} = \left(\int_0^\infty dt \, P_D(t) \right)^{-1}. \tag{7.225}$$

Finally, in the nonadiabatic limit, it is also possible to compute an explicit expression for k_{ET}. The derivation is similar to that of Section 3.4.5, which resulted in the Golden Rule formula. In correspondence to Eq. (3.173), we start with an equation of motion for the diagonal density matrix elements $\rho_{\mu\mu}$. We get the same type of equation as in Section 3.4.5, but supplemented by relaxation contributions $-\sum_\nu (k_{\mu\nu}\rho_{\mu\mu} - k_{\nu\mu}\rho_{\nu\nu})$. In Eq. (3.174), for the off-diagonal part, the transition frequency $\omega_{\mu\nu}$ has to include dephasing rates γ_μ, resulting in the replacement of $\omega_{\mu\nu}$ by the complex transition frequency $\tilde{\omega}_{\mu\nu} = \omega_{\mu\nu} - i(\gamma_\mu + \gamma_\nu)$. Then, one can follow the reasoning in Section 3.4.5 up to Eq. (3.182) taking into account, however, the coupling to a thermal reservoir.

If the rates $k_{\mu\nu}$ are large, the theory describes fast relaxation within the two diabatic states. This point had to be introduced as an additional assumption in the derivation of Section 3.4.5. Here, the approach automatically gives the thermalization introduced via the assumptions in Eq. (3.172). Taking Eq. (3.182), the only difference is the appearance of complex transition frequencies, leading to a "broadened" delta function. Thus, we have the final rate

$$k_{ET} \equiv k_{DA} = \frac{2\pi |V_{DA}|^2}{\hbar^2} \sum_{M,N} f(E_{DM}) |\langle \chi_{DM} | \chi_{AN} \rangle|^2 \frac{(\gamma_{DM} + \gamma_{AN})/\pi}{\omega_{DM,AN}^2 + (\gamma_{DM} + \gamma_{AN})^2}. \tag{7.226}$$

The expression describes nonadiabatic ET from the different vibrational donor levels E_{DM} to the final acceptor levels, broadened by $\hbar\gamma_{DM}$ and $\hbar\gamma_{AN}$, respectively. A thermal averaging and weighting by the respective Franck–Condon factors is also incorporated.

7.10 Supplement

7.10.1 Landau–Zener Transition Amplitude

The description of the ET reaction in a DA complex according to Landau and Zener can be reduced to the calculation of a particular transition amplitude as explained in Section 7.3.1. Here, we show how to compute the transition amplitude, Eq. (7.53). In a first step, the time-evolution operator is split up into a part U_0 defined by H_0 and a remaining S-operator related to the transfer coupling $\hat{V}$. Reversing the general treatment given in Section 3.2.2, the Hamiltonian defining U_0 is time dependent. Nevertheless, it can be calculated analytically. Let us consider this operator in more detail:

$$U_0(t, \bar{t}) = \hat{T} \exp \left\{ -\frac{i}{\hbar} \int_{\bar{t}}^{t} d\tau \; H_0(\tau) \right\}. \tag{7.227}$$

The two parts forming H_0 and proportional to $|D\rangle\langle D|$ and to $|A\rangle\langle A|$, however, commute with each other, and the time-evolution operator can easily be calculated as

$$U_0(t, \bar{t}) = \exp\left(i(v^* F_D)(t^2 - \bar{t}^2)/2\hbar \right) |D\rangle\langle D| + \exp\left(i(v^* F_A)(t^2 - \bar{t}^2)/2\hbar \right) |A\rangle\langle A|. \tag{7.228}$$

If we want to calculate the S-operator, the interaction representation $\hat{V}^{(I)}$ of the interstate coupling has to be determined. It reads

$$\hat{V}^{(I)}(t, \bar{t}) = \exp\left(iv^*(F_A - F_D)(t^2 - \bar{t}^2)/2\hbar \right) V_{DA} |D\rangle\langle A| + \text{c.c..} \tag{7.229}$$

Therefore, the transition amplitude can be written as

$$A_{DD} = \langle D| U_0(\infty, -\infty) S(\infty, -\infty) |D\rangle = \langle D| S(\infty, -\infty) |D\rangle. \tag{7.230}$$

The part related to U_0 can be eliminated from the matrix element, since it reduces to 1 in the limits $t \to \infty$ and $\bar{t} \to -\infty$. It remains to calculate the S-operator matrix element. This will be done by expanding the S-operator with respect to the interstate coupling. It gives (cf. Section 3.2.2)

$$\langle D| S(\infty, -\infty) |D\rangle = \sum_{n=0}^{\infty} \left(\frac{i}{\hbar} \right)^n \int_{-\infty}^{+\infty} dt_n \int_{-\infty}^{t_n} dt_{n-1} \; \ldots \; \int_{-\infty}^{t_2} dt_1$$
$$\times \langle D| \hat{V}^{(I)}(t_n, -\infty) \, \hat{V}^{(I)}(t_{n-1}, -\infty) \ldots \hat{V}^{(I)}(t_1, -\infty) |D\rangle. \tag{7.231}$$

The matrix element corresponds to n jumps of the electron between the donor and the acceptor levels starting at the donor level but also ending there. Consequently,

the number of jumps must be even. Taking into account the concrete structure of the interstate coupling, Eq. (7.229), we can write

$$\langle D|S(\infty, -\infty)|D\rangle = \sum_{n=0}^{\infty} \left(\frac{|V_{DA}|}{i\hbar} \right)^{2n} \int_{-\infty}^{+\infty} dt_{2n} \int_{-\infty}^{t_{2n}} dt_{2n-1} \dots \int_{-\infty}^{t_2} dt_1$$

$$\times \lim_{\tau \to -\infty} \exp\left\{ \frac{i}{\hbar} \frac{v^*(F_A - F_D)}{2} \left((t_{2n}^2 - \tau^2) - (t_{2n-1}^2 - \tau^2) \right) \right.$$

$$\left. \pm \dots -(t_1^2 - \tau^2)) \right\}. \tag{7.232}$$

The contributions proportional to τ^2 cancel, and we introduce new time variables $(\tau_1, \dots, \tau_n)$ and $(T_1, \dots, T_n)$ which replace the set $(t_1, \dots, t_{2n})$. This is done such that the Jacobian of this transformation remains unchanged. We set $\tau_1 = t_1$, $\tau_m = t_1 + \sum_{j=1}^{m-1}(t_{2j+1} - t_{2j})$ for $2 \leq m \leq n$, and $T_m = t_{2m} - t_{2m-1}$ for $1 \leq m \leq n$. For the transition amplitude, we obtain

$$\langle D|S(\infty, -\infty)|D\rangle = \sum_{n=0}^{\infty} (-1)^n \left(\frac{V_{DA}|}{\hbar} \right)^{2n} \int_{-\infty}^{+\infty} d\tau_1 \int_{\tau_1}^{\infty} d\tau_2 \dots$$

$$\times \dots \int_{\tau_{n-1}}^{\infty} d\tau_n \int_{0}^{\infty} dT_1 \dots dT_n$$

$$\times \exp\left\{ \frac{i}{\hbar} \frac{v^*(F_A - F_D)}{2} \left(2\sum_{m=1}^{n} \tau_m T_m + \left[\sum_{m=1}^{n} T_m \right]^2 \right) \right\}. \tag{7.233}$$

Any interchange of the variables τ_m does not alter the total integral. Therefore, we can extend all τ_m-integrations to $-\infty$. Doing so, it is necessary to introduce the prefactor $1/n!$ The remaining integrals can be calculated, and we have

$$\langle D|S(\infty, -\infty)|D\rangle = \sum_{n=0}^{\infty} (-1)^n |V_{DA}/\hbar|^{2n} \frac{1}{n!} \left(\frac{\pi\hbar}{v^*|F_A - F_D|} \right)^n = e^{-\Gamma/2}, \tag{7.234}$$

with

$$\Gamma = \frac{2\pi}{\hbar v^*} \frac{|V_{DA}|^2}{|F_D - F_A|}. \tag{7.235}$$

This result has been used in Section 7.3.1.

7.10.2 The Multimode Marcus Formula

In what follows, we explain in some detail how to derive the Marcus formula, Eq. (7.71), in the case of many vibrational DOFs leading to the multimode reorganization energy, Eq. (7.72). To achieve this goal, we start again with formula (7.62) for the ET rate. However, to tackle the rate calculation it is advantageous to replace

the delta function by its respective Fourier integral. We obtain (notice that $q = \{q_\xi\}$ and the introduction of the partition function $\mathcal{Z}$)

$$k_{\text{ET}} = \frac{|V_{DA}|^2}{\hbar^2 \mathcal{Z}} \int\limits_{-\infty}^{+\infty} dt \int dq \, \exp\left\{ -\frac{U_D(q) - U_D^{(0)}}{k_B T} + \frac{it}{\hbar}[U_D(q) - U_A(q)] \right\}. \tag{7.236}$$

In a first step, one calculates the integrals with respect to the vibrational coordinates. Due to the replacement of the delta function by a Fourier integral, the multiple coordinate integral factorizes into a product of simple integrals. These can be reduced to integrals with respect to Gaussian functions. We obtain

$$\int dq \, \exp\left\{ -\frac{U_D(q) - U_D^{(0)}}{k_B T} + \frac{i}{\hbar} t[U_D(q) - U_A(q)] \right\}$$

$$= \left(\prod_\xi \sqrt{\frac{2\pi k_B T}{\omega_\xi^2}} \right) \exp\left\{ -\frac{k_B T}{\hbar^2}[U_A(q_D) - U_A^{(0)}] \, t^2 \right\}$$

$$\times \exp\left\{ \frac{i}{\hbar} \left[U_D(0) - U_A(0) - \sum_\xi \omega_\xi^2 (q_\xi^{(D)} - q_\xi^{(A)}) q_\xi^{(D)} \right] t \right\}. \tag{7.237}$$

The expression $U_A(q_D) - U_A^{(0)}$ can be identified as the reorganization energy, Eq. (7.72). The remaining time integral again is of Gaussian type and can easily be performed. A proper collection of all constants finally yields the multimode Marcus-type formula, Eq. (7.71).

7.10.3 Second-order Electron Transfer Rate

The rate that is of second order with respect to the transfer coupling describes nonadiabatic ET and is computed in Sections 7.4. Here, we give an alternative view on the high-temperature version of this rate. It is based on a mixed quantum–classical description of ET, with the vibrational dynamics accompanying the ET considered in the framework of classical mechanics. In this way, the treatment will justify the ansatz we used in Section 7.4.1 (cf. also Section 6.3.3). Furthermore, this approach will be applied when calculating higher order transfer rates in the supplementary Section 7.10.4.

The mixed quantum–classical description starts from the frequency-dependent rate expression, Eq. (3.505), connecting here diabatic states φ_m and φ_n. The intended approximation can be easily introduced if the vibrational part of the trace expression in Eq. (3.505) is transformed into the Wigner representation (cf. Section 3.4.4). In order to do this, we define the operator

$$\hat{\sigma}_m(t) = \mathcal{U}_0(t)\mathcal{L}_V \hat{W}_m = U_0(t) \left(\mathcal{L}_V \hat{R}_m \hat{\Pi}_m \right) U_0^+(t), \tag{7.238}$$

where $\mathcal{U}_0(t)\ldots = U_0(t)\ldots U_0^+(t)$ defines the time evolution based on the Hamiltonian H_0, Eq. (7.126). We further introduced the Liouvillian $\mathcal{L}_V$ of the transfer coupling, Eq. (7.127). Finally, $\hat{\Pi}_m$ denotes the projector on φ_m, and $\hat{R}_m$ is the

corresponding vibrational equilibrium statistical operator. The trace expression of Eq. (3.505) adopted to the present notation follows as

$$\text{tr}_{\text{vib}}\{\langle\varphi_n|\mathcal{L}_V\hat{\sigma}_m(t)\}|\varphi_n\rangle\} = \frac{1}{\hbar}\sum_k \left(V_{nk}\langle\varphi_k|\text{tr}_{\text{vib}}\{\hat{\sigma}_m(t)\}|\varphi_n\rangle\right.$$
$$\left. -(k\leftrightarrow n)\right). \tag{7.239}$$

The advantage of introducing $\hat{\sigma}_m$ is related to the fact that its equation of motion is easily derived, and that it can be transformed into the Wigner representation without further difficulties. We note that

$$\text{tr}_{\text{vib}}\{\hat{\sigma}_m(t)\} = \int dq\,\langle q|\hat{\sigma}_m(t)|q\rangle \equiv \int dx\frac{dp}{(2\pi\hbar)^{\mathcal{N}}}\,\hat{\sigma}_m(x,p;t). \tag{7.240}$$

In the first part of this equation, we specialized the trace using the complete set of vibrational coordinate operator eigenstates $|q\rangle \equiv |\{q_\xi\}\rangle$. Then, in the second part, this particular choice of the trace has been transformed from the coordinate representation of $\hat{\sigma}_m$ to the Wigner representation. The transformation of $\langle q|\hat{\sigma}_m(t)|q\rangle$ corresponds to a partial Wigner transformation as introduced in Section 6.3.3. $\hat{\sigma}_m(x,p;t)$ depends on the set of $\mathcal{N}$ classical vibrational coordinates $x = \{x_\xi\}$ and vibrational momenta $p = \{p_\xi\}$ but remains an operator in the electronic state space (the integrations in Eq. (7.240) abbreviate $\mathcal{N}$-fold integrals with respect to the vibrational coordinates and momenta). According to Eq. (7.238), we obtain the initial value

$$\hat{\sigma}_m(x,p;t=0) = \frac{1}{\hbar}f_m(x,p)\sum_k \left(V_{km}|\varphi_k\rangle\langle\varphi_m| - (k\leftrightarrow m)\right). \tag{7.241}$$

As a result of the Wigner representation, the equilibrium statistical operator $\hat{R}_m$ has been replaced by the equilibrium distribution $f_m(x,p)$ of the vibrational coordinates and momenta.

Having introduced the (partial) Wigner representation of $\hat{\sigma}_m(t)$, we can directly obtain an equation of motion for $\hat{\sigma}_m(x,p;t)$ in the mixed quantum–classical limit. It reads (note the appearance of commutators and anticommutators)

$$\frac{\partial}{\partial t}\hat{\sigma}_m(x,p;t) = -\frac{i}{\hbar}\left[H_0,\hat{\sigma}_m\right]_- + \frac{1}{2}\sum_\xi \left\{\left[\frac{\partial H_0}{\partial x_\xi},\frac{\partial\hat{\sigma}_m}{\partial p_\xi}\right]_+ - \left[\frac{\partial H_0}{\partial p_\xi},\frac{\partial\hat{\sigma}_m}{\partial x_\xi}\right]_+\right\}. \tag{7.242}$$

As it is the case for $\hat{\sigma}_m$, the Hamiltonian H_0 derived from Eq (7.126) also depends on the classical coordinates and momenta but remains an operator in the electronic state space. Let us neglect the second term on the right-hand side. Then, it is easy to solve the remaining equation. After taking electronic matrix elements, it follows that

$$\langle\varphi_k|\hat{\sigma}_m(x,p;t)|\varphi_l\rangle = \langle\varphi_k|U_0(t)\hat{\sigma}_m(x,p;t=0)U_0^+(t)|\varphi_l\rangle$$
$$= \frac{1}{\hbar}(\delta_{ml}V_{km} - \delta_{mk}V_{ml})f_m(x,p)\,\exp\left(-\frac{i}{\hbar}[U_k - U_l]t\right). \tag{7.243}$$

Since the vibrational kinetic energy is independent of the actual electronic state, the action of the time-evolution operators U_0 and U_0^+ present in the first part of this

equation reduces to $\exp(-i[U_k - U_l]t/\hbar)$. The latter expression carries the only time dependence of Eq. (7.243). There is no direct time dependence of the coordinates and momenta, and their distribution remains fixed at the initial equilibrium distribution $f_m(x, p)$. Because of this special property of the solution, Eq. (7.243), of Eq. (7.242), it is called a *static* approximation (cf. Section 6.3.3).[29]

To finally get the (frequency-independent) nonadiabatic rate according to Eq. (3.505), we have to insert Eq. (7.243) into Eq. (7.239). It follows for the rate that

$$k_{m \to n}^{(2)} = \frac{|V_{mn}|^2}{\hbar^2} \int dt \int dx \frac{dp}{(2\pi\hbar)^{\mathcal{N}}} f_m(x, p) \exp\left(-\frac{i}{\hbar}(U_m - U_n)t\right). \quad (7.244)$$

Two types of integrations contained in this formula can be carried out. The momentum integration simply reduces $f_m(x, p)$ to the coordinate distribution function $f_m(x)$, Eq. (7.61), and the time integral can be computed resulting in $\delta(U_m - U_n)$. Thus, we arrive at a type of ET rate as given in Eq. (7.62). With this result, we justify the ansatz taken to start with Eq. (7.62) and to compute the ET rate in the high-temperature limit. As shown, the static approximation of Eq. (7.242) results in the δ-function, which guarantees ET at the crossing of the PES. To go beyond the static approximation is equivalent to a consideration of ET outside the PES crossing points.

The given derivation puts the obtained rate expression into an alternative frame indicating, in particular, how MD simulations for the vibrational coordinates may be used to compute transition rates. Furthermore, the adopted static approximation offers an easy way to compute higher order rates, as demonstrated in the following section.

7.10.4 Fourth-order Donor–Acceptor Transition Rate

In what follows, the details are given for the calculation of the fourth-order rate, $k_{D \to A}^{(4)}$, which describes a direct transition from the donor via a single bridge molecule to the acceptor. Fourth-order rates that describe the transfer of the neighboring sites will be briefly mentioned at the end of this section. In calculating this rate, we follow the approach given in the preceding section, which takes advantage of changing to the Wigner representation and applying a static approximation for the classical vibrational dynamics.

In a first step, we write the nonfactorized trace expression of the fourth-order rate, Eq. (3.520), as

$$\text{tr}\{\hat{\Pi}_A \mathcal{L}_V \mathcal{U}_0(t_3) \mathcal{L}_V \mathcal{U}_0(t_2) \mathcal{L}_V \mathcal{U}_0(t_1) \mathcal{L}_V \hat{R}_D \hat{\Pi}_D\} = \text{tr}_{\text{vib}}\{\langle \varphi_A | \mathcal{L}_V \hat{\sigma}_D^{(3)}(t_3)\} | \varphi_A \rangle\}. \quad (7.245)$$

To change to the Wigner representation of the operator expressions under the trace, we defined, in analogy to Eq. (7.238), the operator

$$\hat{\sigma}_D^{(3)}(t_3) = \mathcal{U}_0(t_3) \mathcal{L}_V \hat{\sigma}_D^{(2)}(t_2). \quad (7.246)$$

---

29) To account for the derivatives in Eq. (7.242) becomes more involved. A discussion can be found in Casado–Pascual et al. [16].

The newly introduced operator $\hat{\sigma}_D^{(2)}(t_2)$ is defined in the same way but with $\hat{\sigma}_D^{(1)}(t_1)$ on the right-hand side. The expression for $\hat{\sigma}_D^{(1)}(t_1)$ coincides with Eq. (7.238) but with m replaced by D. The initial value of $\hat{\sigma}_D^{(1)}(t_1)$ is given by $\mathcal{L}_V \hat{R}_D \hat{\Pi}_D$. Since one operator determines the initial value of the following one, a sequential computation of the total rate becomes possible. The related electronic matrix elements will be selected according to the three pathways of Figure 3.14.

Let us start with the Wigner representation $\hat{\sigma}_D^{(1)}(x, p; t_1)$ of $\hat{\sigma}_D^{(1)}(t_1)$ (cf. Eq. (7.240)), which is a partial representation taken with respect to the vibrational DOFs. The combination of the various electronic matrix elements of $\hat{\sigma}_D^{(1)}(x, p; t_1)$ needed to get the rate will be constructed in using the Liouville space pathway scheme of Figure 3.14 (the state labeling 1, 2, and 3 used in Section 3.14.6 have to be replaced by D, B, and A, respectively). In any case, the coordinate and momentum dependence is exclusively given by the equilibrium distribution $f_D(x, p)$. The determination of $\hat{\sigma}_D^{(1)}(x, p; t_1)$ in the static approximation follows, similar to Eq. (7.243). The arbitrary electronic matrix element $\langle \varphi_m | \hat{\sigma}_D^{(1)}(x, p; t_1) | \varphi_n \rangle$ reads as $\exp(-i(U_m - U_n)t_1/\hbar) \langle \varphi_m | \mathcal{L}_V \hat{R}_D \hat{\Pi}_D | \varphi_n \rangle$. If we carry out the single-side Fourier-transformation (with t from 0 to ∞), we end up with $\hbar \langle \varphi_m | \mathcal{L}_V \hat{R}_D \hat{\Pi}_D | \varphi_n \rangle / \Delta_{mn}$. The energy denominator is determined by the PESs U_m and U_n and has the form $\Delta_{mn}(x) = \hbar\omega + i\epsilon - [U_m(x) - U_n(x)]$ (with $\epsilon \to +0$).

To get the contribution of $\hat{\sigma}_D^{(2)}(t_2)$ to the total rate, we proceed similarly as in the case of $\hat{\sigma}_D^{(1)}(t_1)$. The initial value for $\hat{\sigma}_D^{(2)}(t_2)$ is given by the solution constructed for $\hat{\sigma}_D^{(1)}(t_1)$ and the action of $\mathcal{L}_V$. The electronic matrix elements of the static solution for the Wigner representation $\hat{\sigma}_D^{(2)}(x, p; t_2)$ read $\hbar \langle \varphi_m | \hat{\sigma}_D^{(2)}(x, p; t_2 = 0) | \varphi_n \rangle / \Delta_{mn}$. In the same way, the contribution of $\hat{\sigma}_D^{(2)}(t_2)$ to the rate can also be calculated. Then, all three single contributions have to be collected to obtain the rate expression.

We order the rate according to the different pathways given in Figure 3.14 and start with the computation of the contribution due to pathway I. It is the sequence of transitions starting at $W_{DD}^{(eq)}$ and moving across $W_{BD}^{(1)}$, $W_{AD}^{(2)}$, and $W_{AB}^{(3)}$ to arrive at $W_{AA}^{(3)}$. Since only the thermal distribution function depends on the vibrational momenta, the whole expression can be reduced to a multiple coordinate integral together with the coordinate distribution function $f_D(x)$. It follows that

$$L_{AD}^{(4,I)}(\omega) = -\frac{i}{\hbar} \int dx \left\{ \frac{V_{AB}}{\Delta_{AD}(x)} \frac{V_{BD} f_D(x)}{\Delta_{BD}(x)} \frac{V_{DB}}{\Delta_{AB}(x)} V_{BA} \right.$$
$$\left. + V_{AB} \frac{V_{BD}}{\Delta_{BA}(x)} \frac{f_D(x) V_{DB}}{\Delta_{DB}(x)} \frac{V_{BA}}{\Delta_{DA}(x)} \right\}. \tag{7.247}$$

Pathway I of Figure 3.14 can be directly identified by the different factors in the first term on the right-hand side (the second term on the right-hand side corresponds to the equivalent pathway, which finally results in a complex conjugated expression). The second factor $\sim V_{BD}$ originates from $\hat{\sigma}_D^{(1)}$, and the first factor $\sim V_{AB}$ from $\hat{\sigma}_D^{(2)}$. The third factor $\sim V_{DB}$ follows from $\hat{\sigma}_D^{(3)}$, and the fourth factor is the result of the final action of $\mathcal{L}_V$.

According to the described scheme, one can also calculate the contributions due to pathways II and III. If combined with the factorized part of the total rate (cf. Eq. (3.521)), one obtains the difference of the full frequency-dependent rate and the contribution due to the Liouville space pathway I. It reads

$$K_{AD}^{(4)}(\omega) - L_{AD}^{(4,\mathrm{I})}(\omega) = \frac{|V_{DB}V_{BA}|^2}{\hbar(\hbar\omega + i\epsilon)} \int dx\,dy \ \left(-i\delta(x-y) + f_B(y)\right) f_D(x)$$

$$\times \left(\frac{1}{\Delta_{BD}(x)} + \frac{1}{\Delta_{DB}(x)}\right)\left(\frac{1}{\Delta_{AB}(y)} + \frac{1}{\Delta_{BA}(y)}\right). \quad (7.248)$$

To achieve this combination, we introduced a second integration with respect to the vibrational coordinates (abbreviated by y). The term $\sim \delta(x-y)$ with $\delta(x-y) \equiv \prod_\xi \delta(x_\xi - y_\xi)$ refers to the pathway II's and III's contributions, while the factorized part of the rate is given by the term proportional to the bridge molecule vibrational coordinate distribution $f_B(y)$ (note the similarity of the present expression to some of the terms in Eq. (3.533), which describes a fourth-order transition in a three-level system as discussed in Section 3.14.6.1). The prefactor $1/(\hbar\omega + i\epsilon)$ stems from $1/\Delta_{BB}$, which is obtained when one follows pathways II and III; it directly appears in the factorized part of the fourth-order rate as well. If common denominators are introduced in the two last brackets, the resulting expression becomes proportional to ω^2. As a consequence, $K_{AD}^{(4)} - L_{AD}^{(4,\mathrm{I})}$ is proportional to ω and vanishes in the $\omega = 0$-limit. In this limit, the whole rate reads as

$$k_{D\to A}^{(4)} = L_{AD}^{(4,\mathrm{I})}(\omega = 0). \quad (7.249)$$

The expression will be specified for the case $\Delta E_{BD}, \Delta E_{BA} \gg \Delta E_{DA} > 0$ (note $\Delta E_{mn} = E_m - E_n$). If we ignore the vibrational coordinate dependence of the transition energies to the bridge state, we obtain

$$k_{D\to A}^{(4)} = \frac{2\pi}{\hbar} \frac{|V_{DB}V_{BA}|^2}{\Delta E_{BD}\Delta E_{BA}} \int dx\, f_D(x)\delta(U_D(x) - U_A(x))$$

$$= \frac{2\pi}{\hbar}|V_{DA}^{(\mathrm{eff})}|^2 \mathcal{D}_{DA}(\Delta E_{DA}/\hbar), \quad (7.250)$$

with

$$|V_{DA}^{(\mathrm{eff})}|^2 = \frac{|V_{DB}V_{BA}|^2}{\Delta E_{BD}\Delta E_{BA}} \quad (7.251)$$

and with the combined DOS $\mathcal{D}_{DA}$ used in Section 7.4.3. We already encountered the effective bridge–molecule-mediated coupling $V_{DA}^{(\mathrm{eff})}$ in Eq. (7.117). It describes the superexchange mechanism of ET. Here, we obtained a symmetric expression that contains ΔE_{BD} as well as ΔE_{BA}. Nevertheless, the structure of the effective coupling, Eq. (7.251), justifies the assignment of the rate $L_{AD}^{(4,\mathrm{I})}$ (and the related pathway of Figure 3.14) to the superexchange mechanism.

However, $k_{D\to A}^{(4)}$ is determined by the superexchange mechanism alone, only in the framework of the static approximation. Fourth-order rates such as $k_{D\to B}^{(4)}$ and $k_{B\to A}^{(4)}$ (which give a higher order correction to the nonadiabatic transition rates) also vanish for the static approximation. If we go beyond the static approximation, pathways II and III of Figure 3.14 as well as $k_{D\to B}^{(4)}$ and $k_{B\to A}^{(4)}$ contribute too.

7.10.5 Rate of Elastic Charge Transmission Through a Single Molecule

To describe elastic charge transmission through a single molecule, as was done in Section 7.8.2, we give here a detailed derivation of the corresponding transition rate $k_{L\boldsymbol{k}\to R\boldsymbol{q}}$. It describes the transition of the electron from the left to the right lead $|\varphi_{L\boldsymbol{k}}\rangle \to |\varphi_{R\boldsymbol{q}}\rangle$ with the scattering center given by the molecule. The basic quantity for the following considerations is the transition amplitude

$$A_{L\boldsymbol{k}\to R\boldsymbol{q}}(t,\bar{t}) = \langle \varphi_{R\boldsymbol{q}}|U(t-\bar{t})|\varphi_{L\boldsymbol{k}}\rangle. \tag{7.252}$$

It is defined by the time-evolution operator

$$U(t-\bar{t}) = \exp\left(-\frac{i}{\hbar}H(t-\bar{t})\right), \tag{7.253}$$

where H is the overall Hamiltonian, Eq. (7.168). The transition amplitude has to be computed in the limits $t \to \infty$ and $\bar{t} \to -\infty$. To achieve the infinite time limit and to finally determine the transition rate $k_{L\boldsymbol{k}\to R\boldsymbol{q}}$, the S-matrix formalism will be applied (cf. Section 3.2.2). Since the S-operator will be defined by the operator V, which corresponds to the electrode–molecule interaction of Eq. (7.168), the approach allows us to replace the overall time-evolution operator by a quantity that is reduced to the state space of the charged molecule.

In contrast to Eq. (3.38), we introduce the S-operator as[30]

$$U(t-\bar{t}) = U_0(t)\tilde{S}(t,\bar{t})U_0^+(\bar{t}). \tag{7.254}$$

The zero-order time evolution with its Hamiltonian H_0 is obtained from H, Eq. (7.168), by neglecting the molecule–lead coupling V. It reads

$$U_0(t-\bar{t}) = \exp\left(-\frac{i}{\hbar}H_0(t-\bar{t})\right). \tag{7.255}$$

The S-operator takes the form

$$\tilde{S}(t,\bar{t}) = \hat{T}\exp\left(-\frac{i}{\hbar}\int_{\bar{t}}^{t} d\tau\, e^{-\epsilon|\tau|}U_0^+(\tau)VU_0(\tau)\right). \tag{7.256}$$

To ensure an asymptotic vanishing of the coupling potential, the factor $\exp(-\epsilon|\tau|)$ with $\epsilon \to +0$ has been introduced.[31] We abbreviate

$$V(\tau) = e^{-\epsilon|\tau|}U_0^+(\tau)VU_0(\tau). \tag{7.257}$$

The S-operator obeys

$$\tilde{S}(t,\bar{t}) = 1 - \frac{i}{\hbar}\int_{\bar{t}}^{t} d\tau\, V(\tau)\tilde{S}(\tau,\bar{t}) \tag{7.258}$$

---

30) The version used here is obtained if in Eq. (3.46) the coupling Hamiltonian in the interaction representation $V^{(I)}(\tau) = U_0^+(\tau - t_0)VU_0(\tau - t_0)$ is written as $U_0(t_0)U_0^+(\tau)VU_0(\tau)U_0^+(t_0)$. Removing $U_0(t_0)$ and $U_0^+(t_0)$ from the exponential using the related power expansion, $S(t,t_0) = U_0(t_0)\tilde{S}(t,t_0)U_0^+(t_0)$ follows.
31) This procedure avoids the introduction of scattering states referring to the full Hamiltonian $H_0 + V$. In the infinite time limit before and after the scattering event, the free states $\varphi_{L\boldsymbol{k}}$ and $\varphi_{R\boldsymbol{q}}$ are identical with the scattering states.

as well as

$$\tilde{S}(t,\bar{t}) = 1 - \frac{i}{\hbar} \int\limits_{\bar{t}}^{t} d\tau \; \tilde{S}(t,\tau)V(\tau). \tag{7.259}$$

If this latter relation is inserted into the former one, it follows for $\tilde{S}$

$$\tilde{S}(t,\bar{t}) = 1 - \frac{i}{\hbar} \int\limits_{\bar{t}}^{t} d\tau \; V(\tau) - \frac{1}{\hbar^2} \int\limits_{\bar{t}}^{t} d\tau_1 \int\limits_{\bar{t}}^{\tau_1} d\tau_2 \; V(\tau_1)\tilde{S}(\tau_1,\tau_2)V(\tau_2). \tag{7.260}$$

With this expression, one can rewrite the matrix elements constituting the transition amplitude, Eq. (7.252). If we insert the derived equation for $\tilde{S}$, there only remains the term with V appearing two times explicitly (note the introduction of the unit step function):

$$A_{Lk \to Rq}(t,\bar{t}) = -\frac{1}{\hbar^2} \int\limits_{\bar{t}}^{t} d\tau_1 d\tau_2$$
$$\times \langle \varphi_{Rq} | U_0(t)V(\tau_1)\theta(\tau_1 - \tau_2)\tilde{S}(\tau_1,\tau_2)V(\tau_2)U_0^+(\bar{t}) | \varphi_{Lk} \rangle. \tag{7.261}$$

We replace $\tilde{S}$ by U by inverting Eq. (7.254) and introduce the Green's operator $\hat{G}(\tau) = -i\theta(\tau)U(\tau)$ (cf. Section 3.3.3). This yields

$$A_{Lk \to Rq}(t,\bar{t}) = -\frac{i}{\hbar^2} \int\limits_{\bar{t}}^{t} d\tau_1 d\tau_2$$
$$\times \langle \varphi_{Rq} | U_0(t - \tau_1)e^{-\epsilon|\tau_1|}V\hat{G}(\tau_1 - \tau_2)Ve^{-\epsilon|\tau_2|}VU_0^+(\bar{t} - \tau_2) | \varphi_{Lk} \rangle. \tag{7.262}$$

After introducing the continuous energies $\hbar\Omega$ and $\hbar\bar{\Omega}$ of the initial and final states of the scattering process, respectively, as well as the coupling matrix elements of the molecule lead interaction V, it follows that

$$A_{Lk \to Rq}(t,\bar{t}) = -\frac{i}{\hbar^2} \int\limits_{\bar{t}}^{t} d\tau_1 d\tau_2$$
$$\times e^{-i\bar{\Omega}(t-\tau_1)-\epsilon|\tau_1|}V_R(\bar{\Omega})\langle \varphi_1 | \hat{G}(\tau_1 - \tau_2) | \varphi_1 \rangle V_L^*(\Omega)e^{i\Omega(\bar{t}-\tau_2)-\epsilon|\tau_2|}. \tag{7.263}$$

As required, a matrix element with respect to the state of the charged molecule is obtained. In a final step, the Green's operator $\hat{G}(\tau_1 - \tau_2)$ is replaced by its Fourier-transformed version $\hat{G}(\omega)$ via a Fourier integral:

$$A_{Lk \to Rq}(t,\bar{t}) = -\frac{i}{2\pi\hbar^2} \int d\omega \; V_R(\bar{\Omega})\langle \varphi_1 | \hat{G}(\omega) | \varphi_1 \rangle V_L^*(\Omega)$$
$$\times \int\limits_{\bar{t}}^{t} d\tau_1 d\tau_2 \; e^{-i\bar{\Omega}t}e^{i(\bar{\Omega}-\omega)\tau_1-\epsilon|\tau_1|}e^{-i(\Omega-\omega)\tau_2-\epsilon|\tau_2|}e^{i\Omega\bar{t}}. \tag{7.264}$$

Next, the limit $t, \bar{t} \to \infty$ (or $t = \tau/2$, $\bar{t} = -\tau/2$ with $\tau \to \infty$) is taken together with $\epsilon \to +0$. One arrives at

$$A_{Lk \to Rq}(\infty, -\infty) = -\frac{2\pi i}{\hbar^2} \lim_{\tau \to \infty} e^{-i(\bar{\Omega} + \Omega)\tau/2}$$

$$\times \int d\omega \, \delta(\bar{\Omega} - \omega) \delta(\Omega - \omega) V_R(\bar{\Omega}) \langle \varphi_1 | \hat{G}(\omega) | \varphi_1 \rangle V_L^*(\Omega).$$

$$(7.265)$$

After carrying out the ω-integration, the absolute square of the transition amplitude (the population of the final scattering states) takes the form

$$|A_{Lk \to Rq}(\infty, -\infty)|^2 = \delta^2(\bar{\Omega} - \Omega) \frac{(2\pi)^2}{\hbar^4} | V_R(\Omega) \langle \varphi_1 | \hat{G}(\Omega) | \varphi_1 \rangle V_L^*(\Omega)|^2.$$

$$(7.266)$$

The δ-function ensures that the energy of the final state $\hbar\bar{\Omega}$ coincides with the energy of the initial state $\hbar\Omega$ (the relative orientation of the wave vector of the incoming and outgoing electrons remains arbitrary). The highly divergent square of the δ-function can be removed when calculating the rate as the transfer of probability per time. In order to do this, we first note

$$(2\pi\delta(\omega))^2 = \left(\lim_{\tau \to \infty} \int_{-\tau/2}^{\tau/2} dt e^{i\omega t} \right)^2 = \lim_{\tau \to \infty} \left(\frac{2\sin(\omega\tau/2)}{\omega} \right)^2 \qquad (7.267)$$

$$= \lim_{\tau \to \infty} 2\pi\tau \frac{\sin^2(\omega\tau/2)}{\pi\omega^2\tau/2} = \lim_{\tau \to \infty} 2\pi\tau \delta(\omega). \qquad (7.268)$$

If inserted into Eq. (7.266), we can compute the population per time. It follows the rate as given in Eq. (7.177).

References

1 A. Neubauer et al., J. Phys. Chem. Lett. **5**, 1355 (2014).

2 B. Pelado et al., Chem. Eur. J. **21**, 5814 (2015).

3 B. Brueggemann et al., Phys. Rev. Lett. **97**, 208301 (2006).

4 S. Kubatkin et al., Nature **425**, 698 (2003).

5 V. May and O. Kühn, *Charge and Energy Transfer Dynamics in Molecular Systems*, 3rd Edition, (Wiley-VCH, Weinheim, 2011).

6 J. Casado-Pascual et al., Chem. Phys. Lett. **360**, 333 (2002).

7 G. L. Closs and J. R. Miller, Science **240**, 440 (1988).

8 W. B. Davis et al., Nature **396**, 60 (1998).

9 S. S. Isied et al., Chem. Rev., **92**, 381 (1992).

10 E. G. Petrov and V. May, J. Phys. Chem. A **105**, 10176 (2001).

11 O. Kühn and L. Wöste (eds.), *Springer Series in Chemical Physics* Vol. **87** (Springer-Verlag, 2007), p. 437.

12 X. H. Qiu et al., Phys. Rev. Lett. **92**, 206102 (2004).

13 C. Benesch et al., J. Phys. Chem. **112**, 9880 (2008).

14 D. Egorova et al., J. Chem. Phys. **119**, 2761 (2003).

15 F. E. Storm et al., PhysChemChemPhys **21**, 17366 (2019).

16 J. Casado-Pascual et al., J. Chem. Phys. **118**, 291 (2003).

Further Reading

- Classic works on Marcus theory:
  R. A. Marcus, J. Chem. Phys. **24**, 966 (1956).
  R. A. Marcus and N. Sutin, Biochim. Biophys. Acta **200**, 811 (1985).
- Review articles and books on electron transfer:
  F. Di Giacomo, *Introduction to Marcus Theory of Electron Transfer Reactions*, (World Scientific, Singapore, 2019).
  S. Fukuzumi, *Electron Transfer: Mechanisms and Applications*, (Wiley, Weinheim, 2020).
  H. Oberhofer, K. Reuter, and J. Blumberger, *Charge Transport in Molecular Materials: An Assessment of Computational Methods*, Chem. Rev. **117**, 10319 (2017).
- Review on dye sensitized solar cells:
  A. B. Muñoz-García, I. Benesperi, G. Boschloo, J. J. Concepcion, J. H. Delcamp, E. A. Gibson, G. J. Meyer, M. Pavone, H. Pettersson, A. Hagfeldt, and M. Freitag, Chem. Soc. Rev. **50**, 12450 (2021).
- Review articles and books on *Molecular Electronics*:
  J. C. Cuevas and E. Scheer, *Molecular Electronics: An Introduction to Theory and Experiment* (2nd Edition), (World Scientific, Singapore, 2017).
  N. Xin, J. Guan, C. Zhou, X. Chen, C. Gu, Y. Li, M. A. Ratner, A. Nitzan, J. F. Stoddart, and X. Guo, *Concepts in the Design and Engineering of Single-Molecule Electronic Devices*. Nat. Rev. Phys. **1**, 211 (2019).
- Review on trajectory-based methods for photoinduced ET dynamics:
  R. Long, O. V. Prezhdo, and W. Fang, *Nonadiabatic Charge Dynamics in Novel Solar Cell Materials*, Wiley Interdiscip. Rev. Comput. Mol. Sci. **7**, e1305 (2017).

8

Proton Transfer

We discuss fundamental aspects of the theory of proton transfer across inter- or intramolecular hydrogen bonds in gas as well as in condensed phase. Since the strength of the hydrogen bond depends on the distance between the proton donor and acceptor entities, vibrational motions modifying the latter are strongly coupled to the proton transfer. We give a classification of such vibrational modes and elaborate on their effect on quantum mechanical proton tunneling.

A central observation is that often the proton dynamics can be adiabatically separated from the slow motions of the environmental degrees of freedom. This suggests a close analogy to the treatment of coupled electronic–nuclear dynamics presented in Chapters 2, 6, and 7. Similar to the case of electron transfer, proton transfer can occur in the adiabatic as well as in the nonadiabatic limit. The former requires the proton wave function to adjust instantaneously to any change in the environmental configuration, whereas the latter assumes that the proton dynamics is slow compared to the typical relaxation times for the environment.

Since proton transfer reactions usually take place in the condensed phase, we discuss the application of approximate quantum and quantum–classical hybrid methods to the solution of the nuclear Schrödinger equation in some detail. A powerful tool in this respect is provided by the surface hopping method, which allows to treat nonadiabatic transitions between the adiabatic proton states while retaining the classical nature of the environment. This is indispensable in the nonadiabatic limit where proton transfer takes place via tunneling between different diabatic states. In the limit of weak coupling, the introduction of diabatic proton states allows to express transfer rates in close analogy to the case of electron transfer. Finally, we briefly address some aspects of proton-coupled electron transfer.

8.1 Introduction

As a second type of charge transfer, we consider the proton transfer (PT) in intra- and intermolecular hydrogen bonds as shown in Figure 8.1. At first glance, one
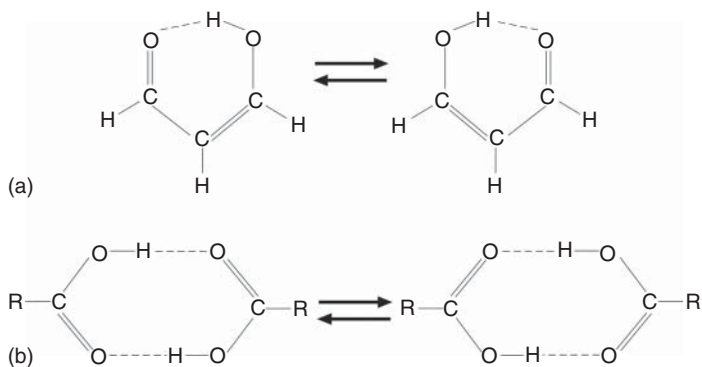
Figure 8.1 (a) Single PT in malonaldehyde, which is one of the standard examples for an intramolecular PT system with strong coupling between the proton motion and heavy atom vibration. In particular, the O—O wagging vibration modulates the reaction barrier for isomerization. (b) Double PT across the intermolecular hydrogen bonds in carboxylic acid dimers (typical examples for R are R—H or R—CH$_3$).

might wonder why dealing with the transfer of a positive charge to that of a negative charge (electron transfer, ET) has been discussed in quite some detail before. And indeed, there are many similarities between ET and PT, for example in the interaction with a polar environment. However, there are also some features that are unique to PT. After all, protons are much heavier than electrons, and therefore, their wave function will be much more localized in space. On the other hand, the proton is still a quantum particle. This means that its motion has to be treated quantum mechanically, and PT is influenced not only by zero-point energy effects but also by quantum tunneling even at room temperature. Further, the simultaneous motion of several protons may be subject to strong correlation effects. As an example, we have shown the intermolecular double PT in carboxylic acid dimers in Figure 8.1b. Here, an important question is related to the type of transfer, that is, the double PT can proceed either step-wise or concerted. For larger systems with many hydrogen bonds such as water clusters, the correlated motion of several protons may lead to interesting collective phenomena.

Many intriguing possibilities in PT studies are opened by the fact that there are four isotopes of hydrogen with mass ratios higher than for any other element of the periodic table. This gives rise to the so-called *kinetic isotope effect*, that is the dependence of transfer rates on the isotopic species. This effect can be used, for instance to investigate the relative importance of tunneling for the transfer process.

Finally, PT transfer is often strongly coupled to *specific* low-frequency (heavy atom) modes of its immediate surroundings. A standard example in this respect is malonaldehyde shown in Figure 8.1a. Here, the intramolecular O—O wagging vibration has a strong influence on the reaction barrier and therefore on the isomerization reaction shown in Figure 8.1a. The interplay between quantum mechanical tunneling and the strong coupling to low-frequency skeleton modes

in PT reactions has some interesting consequences for the tunneling splittings or the related tunneling transfer rates. Some ideas in this respect will be discussed in Section 8.2.3.

PT has an enormous importance for many processes in biology and chemistry. We have already discussed the initial ET steps of photosynthesis in Chapter 7. Subsequent to the ET, a PT across the membrane occurs, and the concerted action of ET and PT ultimately establishes the storage of solar energy in terms of a trans-membrane electrochemical potential. This is one example for a *proton pump*. A second one is given, for instance by the transmembrane protein bacteriorhodopsin that encapsulates a chain of water molecules (water wire) through which a proton can be transferred (Figure 8.2). The transfer of excess protons in water networks, as well as PT processes taking place in ice, has also attracted a lot of attention. In particular, PT on ice surfaces is believed to have some importance for the ozone depletion in the stratosphere. PT is often a key event in enzyme catalysis, where it leads to activation of the proton donor after PT has been triggered, for instance by polar residues in the protein surroundings. Indeed, often PT and ET reactions

(a) (b)
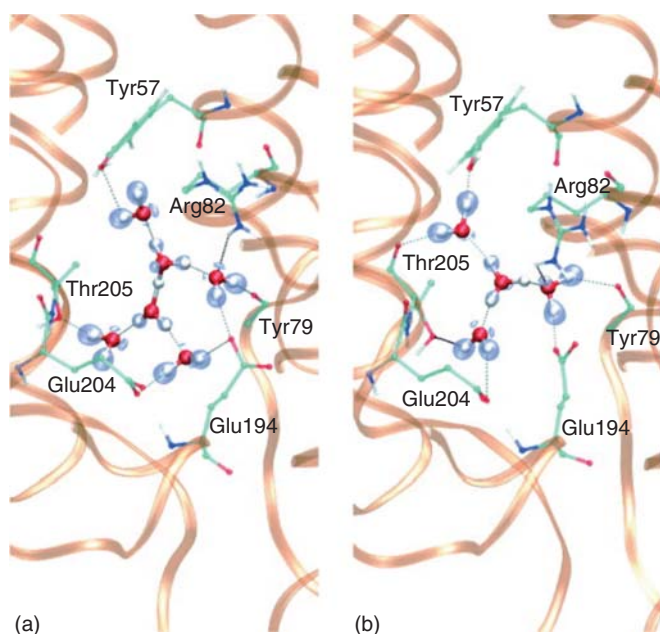
Figure 8.2 Protonated water networks in bacteriorhodopsin encompass different transient binding motifs during PT such as the solvated Zundel ((a), center) and Eigen (b) type. In the Zundel cation, $H_5O_2^+$, the hydrogen bond is symmetric; that is, the proton is shared by the two terminal water molecules. In the Eigen cation, $H_3O^+ \cdot (H_2O)_3$, the proton is localized at the solvated hydronium core H_3O^+. The simulation has been performed using a QM/MM method (Eq. (2.138)) at $T = 300$ K. Further shown are some important residues as well as the protein backbone. Hydrogen bonds are visualized by thin broken lines (Reproduced with permission from Rousseau et al. [1]/John Wiley & Sons).

are strongly coupled to each other and occur simultaneously in the so-called proton-coupled electron transfer (PCET) reactions (Section 8.6).

Traditionally, hydrogen bonds are characterized by means of their stationary infrared (IR) spectra. While this allows a general characterization, for instance in terms of the strength of the hydrogen bond (Section 8.2.1), it was shown that ultrafast IR spectroscopy allows to uncover the details of such spectra in the condensed phase. An example is given in Figure 8.3: In Figure 8.3c,d, IR pump–probe signals are displayed for different laser frequencies across the broad absorption band of phthalic acid monomethyl ester in the OH-stretching region. The analysis of the oscillations in the signal provided evidence for a mechanism where the laser excites a superposition of states involving a low-frequency mode that modulates the O–H–O distance (cf. Section 4.3.6). In the linear absorption spectrum (Figure 8.3a) these transitions are hidden under a broad band.

Two-dimensional IR spectroscopy can be applied to study the PT reactions by observing cross-peaks due to chemical exchange (cf. Section 4.3.7). A prominent example is the PT from a hydronium ion (H_3O^+) to a hydrogen-bonded water molecule yielding again a hydronium ion. This process is important, for instance for explaining the rapid diffusion of protons in water by means of the Grotthuss mechanism. Here, the newly formed hydronium will pass a proton (not necessarily the same) to another water molecule and so on. In Figure 8.4, the results of a two-dimensional IR investigation of the elementary PT step are shown. The actual IR probe is the hydrogen bonding to a nearby CN group. Analysis in combination with molecular dynamics simulations gave a PT time of about 1.6 ps.

While the dynamics observed with IR spectroscopy occurs in the electronic ground state, photochemical reactions involving PT in excited electronic states have also been studied extensively. The sudden change in the electronic state leads to a strong modification of the charge distribution within the hydrogen bond (acidity/basicity), thus giving rise to a large driving force for PT, which occurs on a time scale below 100 fs. This transfer can be strongly coupled to intramolecular vibrational modes of the molecular skeleton, and indeed, signatures of multidimensional coherent nuclear wave packet motion have been observed for a number of excited state PT reactions (Figure 8.5). Ultrafast excited state PT can also occur simultaneously with nonadiabatic transitions at conical intersections. This type of photochemical reaction has been found to play a role in the photoprotection of nucleic acid base pairs.

The theoretical description of PT often rests on the large mass difference between the proton and the heavier atoms being involved in the reaction. This makes it possible to introduce a *second Born–Oppenheimer separation* after the electronic problem has been split off as shown in Section 2.3. As with ET, PT can then be characterized as being in the *adiabatic* or in the *nonadiabatic* limit (or in between). If the proton motion is fast, and the proton is able to adjust *instantaneously* to the actual configuration of the environmental DOFs, a description in terms of adiabatic proton states and a corresponding delocalized wave function is appropriate (Section 8.3). The PT rate may become proportional to some frequency factor characterizing the shape of the adiabatic reaction barrier. On the other hand,
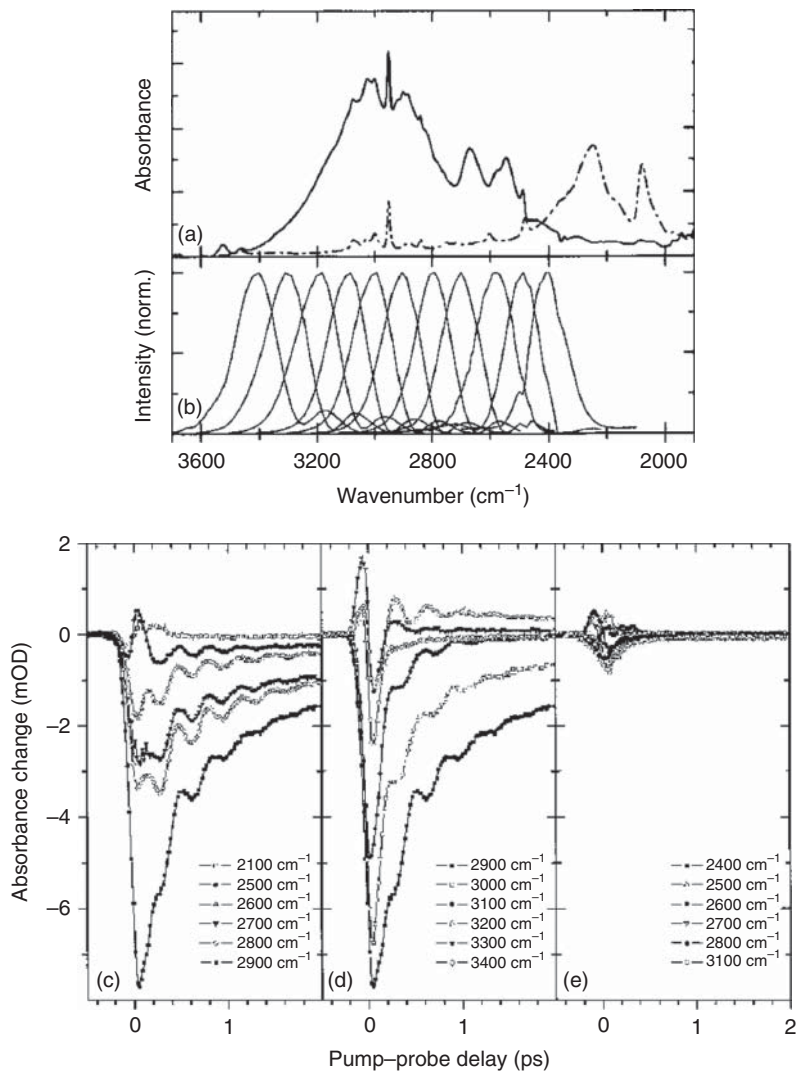
Figure 8.3 Coherent oscillations in a hydrogen bond after ultrashort IR pulse excitation. (a) Linear absorption spectrum of phthalic acid monomethyl ester (solid line, cf. also the lower part of Figure 8.7) and its deuterated form (dashed line) in solution (C_2Cl_4). (b) IR pump pulse intensity profiles for the different excitation conditions leading to the pump–probe signals, which are shown as a function of the delay time between the pulses in (c) and (d). The oscillatory component of the signal can be attributed to the excitation of a wave packet with respect to a low-frequency mode ($100\ cm^{-1}$) which couples strongly to the OH stretching vibration. The decay of the signal is due to relaxation and dephasing processes introduced by the interaction with the solvent. (e) The signal that comes solely from the solvent (Reproduced with permission from Madsen et al. [2]/The Chemical Society of Japan).
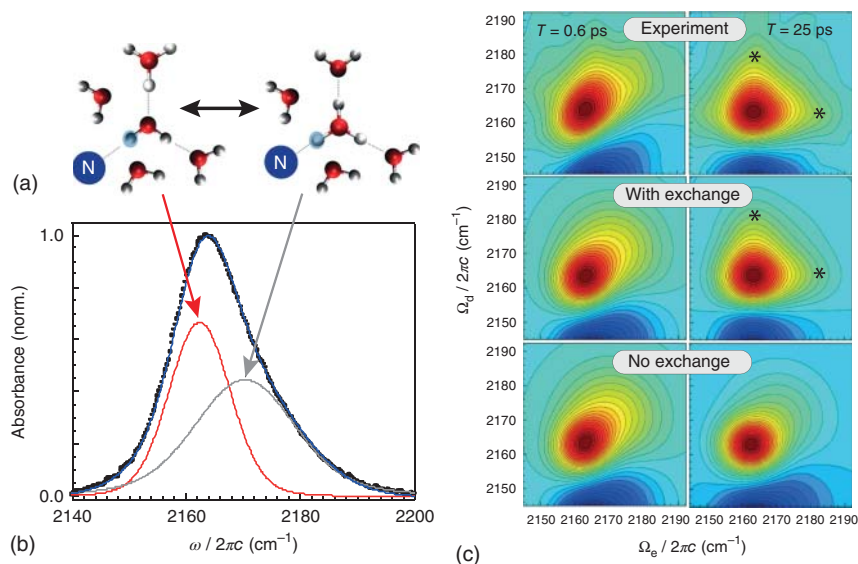
Figure 8.4 Two-dimensional IR spectroscopy monitoring PT between water and hydronium bonded to methyl thiocyanate (MeSCN) in HCl solution. (a) Equilibrium between MeSCN, hydrogen-bonded to H_2O and H_3O^+. The reaction proceeds by shifting a proton to a neighboring water molecule. (b) The two species can be distinguished by their different contributions to the IR absorption spectrum in the range of the CN stretching vibration as indicated. (c) In 2D IR spectra, this forward and backward PT is observed as the appearance of cross-peaks (asterisks) with increasing population time (chemical exchange, cf. Section 4.3.7). The top row is experimental data at two population times. The middle and bottom rows are calculated data with and without inclusion of chemical exchange, respectively (figure courtesy of M. D. Fayer, for more details see Yuan et al. [3]).

in the nonadiabatic limit, the proton motion is much slower than the characteristic time scales for the environment (Section 8.4). The PES is conveniently described in terms of weakly interacting diabatic proton states, and the transfer occurs via tunneling. As with the case of ET, the related transfer rates will be proportional to the square of the coupling matrix elements (cf. Section 7.44). In both cases, the surrounding solvent has an important influence, for it may stabilize reactants and products but also provide the fluctuating force that triggers the transfer event.

Quantum effects are of considerable importance for the proton motion. However, only if the dynamics can be reduced to a reasonably small number of DOFs will PT be amenable to wave packet propagation methods, as outlined in Section 8.5.1. On the other hand, for real condensed phase environments, solvent and low-frequency intramolecular modes have to be treated classically within a quantum–classical hybrid approach (cf. Section 3.13). Here, a unified description of the different regimes of PT is provided by the *surface hopping* method, which combines classical trajectories with quantum transitions (Sections 3.13.2 and 8.5.2).
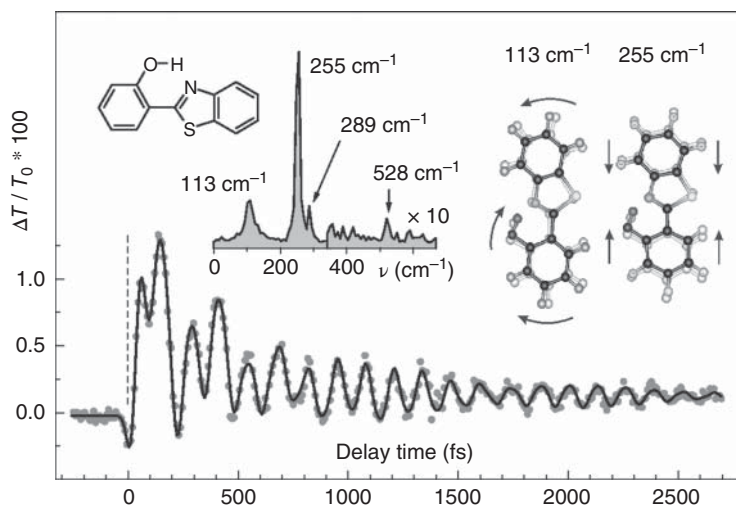
Figure 8.5 Infrared transient transmission change due to stimulated emission of 2-(2-hydroxyphenyl)benzothiazole (upper left) detected at 500 nm after ultrafast excitation at 340 nm. PT takes place as a wave packet motion from the enol (shown here) to the keto ($-O\cdots H-N-$) form in about 50 fs. The reaction coordinate is dominated by a low-frequency bending-type mode at 113 cm^{-1}, which modulates the hydrogen bond such that the donor–acceptor ($O\cdots N$) distance is reduced (right part). In the keto-form several modes are coherently excited as seen from the Fourier transform of the oscillatory signal. Most notable is a symmetric mode at 255 cm^{-1}. The normal mode displacements shown in the right correspond to the enol configuration of the electronic ground state. Their character is assumed to change not appreciably in the excited electronic state (figure courtesy of S. Lochbrunner, for more details see also Lochbrunner and Riedle [4]).

In the following section, we elaborate on the discussion of the properties of hydrogen bonds. Further, we introduce the Hamiltonian for a PT complex that sets the stage for the subsequent discussions of the different dynamics regimes.

8.2 Proton Transfer Hamiltonian

8.2.1 Hydrogen Bonds

In Section 2.3, the coupled motion of electronic and nuclear DOFs was treated by making use of their adiabatic separability. This resulted in PESs for the nuclear motion corresponding to the various adiabatic electronic states. As a consequence of nonadiabatic couplings, electronic transitions between different adiabatic states are possible, especially in the vicinity of avoided crossings. For the following discussion, we assume that the electronic problem has been solved, and the adiabatic PES is known. We restrict our considerations to the electronic ground state only, although the concepts in principle apply to any other electronic state as long as nonadiabatic couplings can be neglected.

Considering the motion of the proton within the hydrogen-bonded complex, we note that in general it is not a bare proton that is transferred, but part of the electronic charge is dragged with the proton. This makes the distinction between PT and "hydrogen atom" transfer sometimes ambiguous. There is also some electronic charge flow in the donor and acceptor groups that goes in the direction opposite to that of the PT. This leads to a large variation in the molecule's dipole moment, which is a characteristic feature of PT. Consequently, the hydrogen bond is highly polarizable, and a polar solvent or charged residues in a protein environment can be expected to have a large influence on PT.

The PES $U(R)$ will be a function of some PT coordinate(s), *all* other nuclear coordinates of the PT complex, and the environmental coordinates. Of course, such a high-dimensional PES cannot be obtained on an *ab initio* level of quantum chemistry. This level of theory is usually reserved for a small subset of *relevant* coordinates only, while the majority of DOFs is treated approximately (see below). The most important coordinates are, of course, those that are directly related to the proton motion. For simplicity, let us consider a linear hydrogen-bonded complex as shown in Figure 8.6b. The hydrogen bond is formed between a proton donor, X–H, and a proton acceptor, Y. Here, X and Y may represent parts of the same molecule (*intramolecular hydrogen bond*) or of different molecules (*intermolecular hydrogen bond*). In the case of a linear hydrogen bond as shown in Figure 8.6b, the PT (reaction) coordinate s can be chosen as the difference between the X–H distance, d_{XH}, and the H–Y distance, d_{HY}, that is $s = d_{XH} - d_{HY}$.

The minimum requirement for a PES of the simple system shown in Figure 8.6b would include, besides the PT coordinate s, the information about the distance $d_{XH} + d_{HY}$ between the donor and the acceptor fragments. Depending on the complexity of X and Y, an *ab initio* calculation of a two-dimensional PES $U(s, d_{XH} + d_{HY})$ may be possible, for instance using the methods introduced in Section 2.5.3.

Before incorporating possible environmental DOFs of a solvent or a protein, let us briefly discuss some general features of the hydrogen-bonded complex shown in Figure 8.6b. First of all, hydrogen bonds may be characterized by the fact that proton donor X–H and acceptor Y retain their integrity in the complex. While the X–H bond is covalent, the hydrogen bond H$\cdots$Y is of a noncovalent character. A widely accepted point of view is that often the hydrogen bond has the characteristics of a strong van der Waals interaction. At long distances d_{HY}, this comprises electrostatic, dispersion, and induction contributions. At short distances, repulsive exchange interactions between the overlapping electron densities of X–H and Y dominate. The process of hydrogen bond formation comes along with a decrease in the DA distance $d_{XH} + d_{HY}$ and an increase in the X–H bond length d_{XH}. The latter effect weakens the X–H bond.

The strength of hydrogen bonding depends on the properties of the donor and acceptor entities, that is in particular on their electronegativity. However, it is also a function of the separation, $d_{XH} + d_{HY}$, between the donor and acceptor that may be imposed by external means. We can distinguish between *weak* and *strong* hydrogen bonds.[1] For weak hydrogen bonds, the DA distance is relatively large (>3 Å),

---

[1] Note that this classification scheme is not rigorously defined in the literature and may vary in dependence on the properties being used for characterizing the strength of the hydrogen bond.
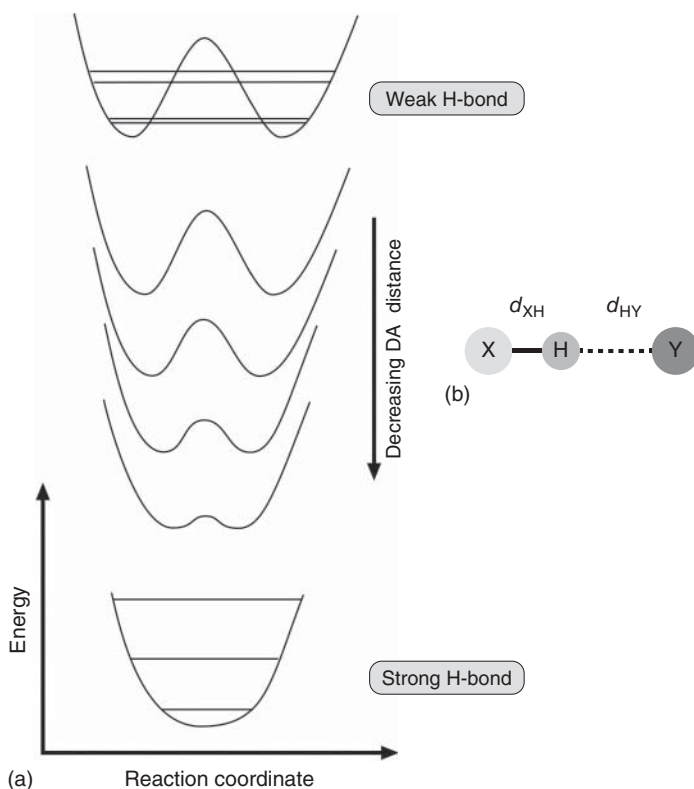
Figure 8.6 (a) Potential energy profile along a PT reaction coordinate, for example $s = d_{XH} - d_{HY}$ in the case of a linear hydrogen bond (as sketched in (b)), in dependence on the donor–acceptor (DA) distance $d_{XH} + d_{HY}$. (The symmetric situation plotted here may correspond to the case X = Y.) Compounds characterized by a large distance form weak hydrogen bonds, while strong hydrogen bonds typically involve a small DA distance. The strength of the hydrogen bond and the exact shape of the potential, of course, depend on the donor and acceptor entities.

and the potential energy profile for moving the proton along the reaction coordinate s between X and Y shows the typical double-minimum behavior plotted in Figure 8.6a (top). The barrier will be high enough to allow for several proton states to be energetically below its top.

This situation might be characteristic of intramolecular hydrogen bonds, where the DA distance is more or less fixed by the rigid molecular frame. On the other hand, intermolecular hydrogen bonds are often much stronger, especially in ions. Here, the larger structural flexibility allows for relatively short distances between the donor and acceptor. Thus, the barrier along the PT coordinate s is rather low if existent at all. This is sketched in Figure 8.6a (bottom). In between these two extreme situations, we have medium-strong hydrogen bonds with moderate barrier heights.

Weak and strong hydrogen bonds may also be distinguished by the extent to which they modify the IR absorption spectra of the X–H stretching vibration. Upon forming a weak hydrogen bond, the frequency of the X–H stretching vibration

moves by about 100–300 cm^{-1} to lower frequencies due to the bond lengthening. In addition, the IR X–H absorption band is broadened. This broadening is a consequence of the larger anharmonicity of the PES in the region of the X–H vibration, which may come along with a pronounced coupling to low-frequency modes of the complex. A strong hydrogen bond, on the other hand, is characterized by a much larger red shift and a more considerable broadening of the absorption line. A comparison between the spectra of a free OH-stretching vibration and OH vibrations in inter- and intramolecular hydrogen bonds is shown in Figure 8.7. The interdependence of the hydrogen bond strength and length allows for the establishment of empirical relations between the hydrogen bond length and the X–H transition frequency as shown in Figure 8.8.

In what follows, we discuss the effect of the coupling between the PT coordinate and the intramolecular modes first. The interaction with environmental DOFs will be included in Section 8.2.4. The separate consideration of intramolecular modes is motivated by their distinct influence in case of strong coupling, for instance on the hydrogen bond geometry. The effect of the environment can often be characterized as leading to phase and energy relaxation or, in the case of polar environments, to a stabilization of a specific configuration of the hydrogen bond. Of course, such a separation is not always obvious, for instance for intermolecular PT in a protein environment. Here, the motion of the protein in principle may influence the PT distance as well.
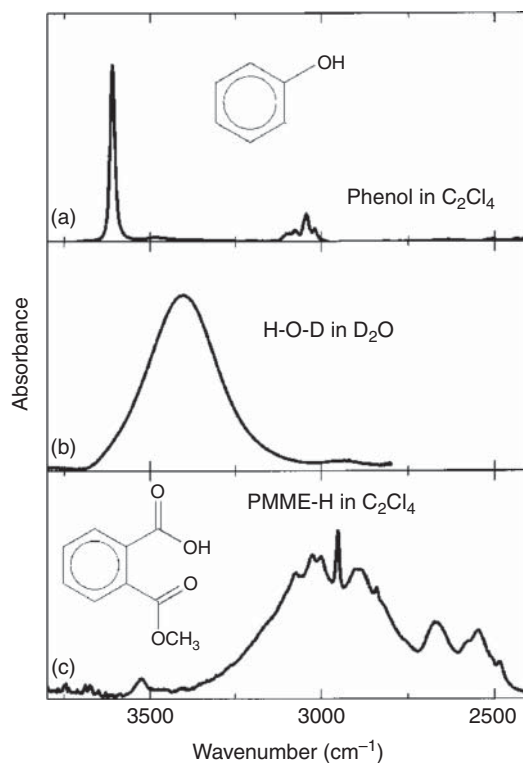
Figure 8.7 Infrared absorption spectra show clear signatures of hydrogen bond formation. Compared to the narrow line of a free OH-stretching vibration (a), the absorption band shifts to lower frequencies and broadens considerably if a condensed phase situation is considered such as the OH vibration in deuterated water (b). The absorption may also develop a peculiar substructure as shown for an intramolecular hydrogen bond (c) (Reproduced with permission from Madsen et al. [2]/The Chemical Society of Japan).
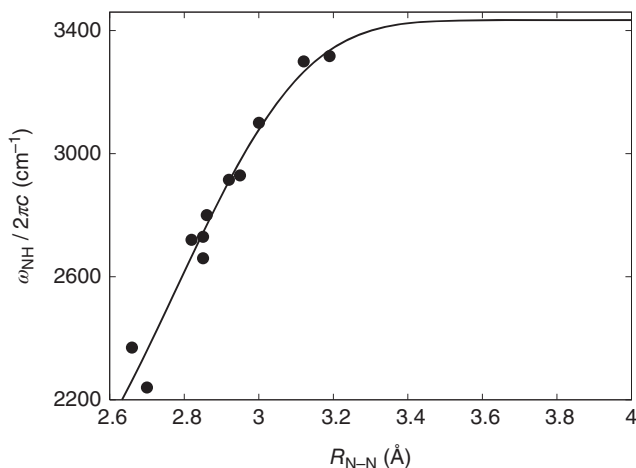
Figure 8.8 Empirical correlation between the N–H stretching frequency and the N···N hydrogen bond distance, R_{N-N}, obtained from experimental data on the crystal structures for systems containing intermolecular N–H···H hydrogen bonds and the respective infrared absorption spectra (figure courtesy of Y. Yan, data taken from Novak [5]).

8.2.2 Reaction Surface Hamiltonian for Intramolecular Proton Transfer

We discuss the PES for the intramolecular DOFs of a system as that in Figure 8.6b. Note that malonaldehyde, shown in Figure 8.1, would be a particular example for such a system. Suppose that $q = \{q_\xi\}$ comprises all the so-called heavy atom vibrational coordinates of the total X–H···Y complex that have a strong influence on the PT insofar as they modulate, for instance the distance $d_{XH} + d_{HY}$. Further, we assume that these modes can be treated in harmonic approximation. This scenario has already been discussed in Section 2.5.3, where we derived a suitable reaction surface Hamiltonian, Eq. (2.86); an example for a PT reaction is shown in Figure 2.10. If we neglect the dependence of the force constant matrix on the proton coordinate, the reaction surface Hamiltonian can be written as

$$H = T_s + U(s) + \sum_\xi \left[\frac{p_\xi^2}{2} + \frac{\omega_\xi^2}{2} q_\xi^2 - F(s)q_\xi \right]. \tag{8.1}$$

Here, the T_s is the kinetic energy operator for the proton motion, and $U(s)$ is the respective potential as obtained, for example from a quantum chemistry calculation of the adiabatic electronic ground state energy in dependence on the proton position (cf. Eq. (2.19)). The last term in Eq. (8.1) describes the coupling between the PT coordinate and the heavy atom modes. Note that for a coordinate-independent force constant matrix, these modes are not coupled by the motion of the proton (cf. Eq. (2.86)).

   The principal effect of the coupling term on the PT dynamics can be highlighted by considering two typical cases, that is a linear coupling, $F(s) = c_1 s$ and a quadratic coupling, $F(s) = c_2 s^2$. In Figure 8.9, we show some schematic PESs for both situations in the case of a single heavy atom mode. A linear coupling apparently is not
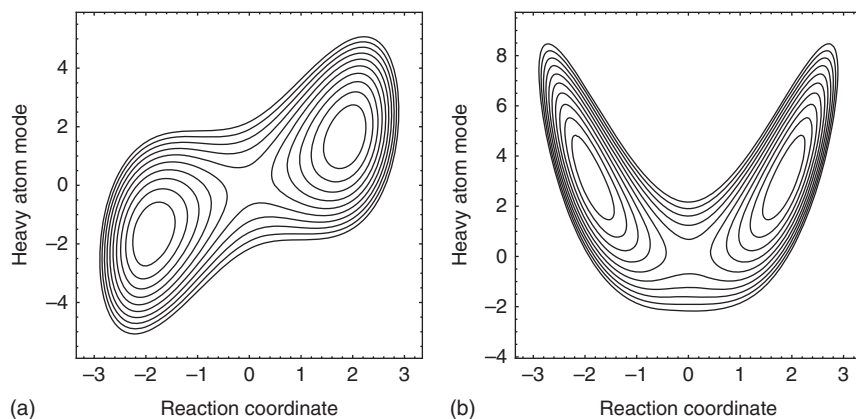
Figure 8.9 Schematic view of two-dimensional PES for linear (a) and quadratic (b) coupling between the PT coordinate (reaction coordinate) and a harmonic heavy atom mode (coordinates are given in arbitrary units). For a specific example, see Figure 8.11.

favorable to PT since it effectively increases the distance between the donor and acceptor, and therefore, according to Figure 8.6a, the barrier for PT will be increased. A mode that is quadratically coupled, however, can reduce the barrier for PT dramatically. In fact, if we follow the minimum energy path on the two-dimensional PES in Figure 8.9b, we find that at the saddle point (transition state) the heavy atom mode is compressed. This type of mode is frequently also called *promoting* or *gating* mode. In fact, gating modes will often be of DA stretching type.[2] A prominent example for a promoting mode is the O–O wagging vibration in malonaldehyde (cf. Figure 8.1). We note in passing that the principal behavior discussed in Figure 8.6a can be viewed as representing cuts through the two-dimensional PES of Figure 8.9. In the following section, we elaborate on the influence of intramolecular modes on the quantum tunneling of the proton, which is expressed in terms of the spectroscopically accessible tunneling splitting.

8.2.3 Tunneling Splittings

Quantum tunneling of the proton through the reaction barrier is one of the most characteristic features in particular for PT in symmetric potentials. Proton tunneling can be viewed in time and energy domains. Consider, for example the case of a one-dimensional reaction coordinate shown in Figure 8.10 and focus on the two lowest eigenstates. If we neglect the higher excited states for the moment, we have essentially recovered the two-level system discussed in Section 2.8.2 (cf. Figure 2.16). There the coupling between two localized states was shown to give rise to a splitting of the respective eigenstates into a doublet containing a symmetric "+" and an antisymmetric "−" state (with respect to the symmetry center at $s = 0$). In the present case, the appearance of a splitting ΔE_0 can be viewed as a consequence

---

2) There is a third kind of coupling mode which is called *squeezing* type. Here, only the frequency changes upon PT. Such modes are often related to out-of-plane motions of planar molecules.
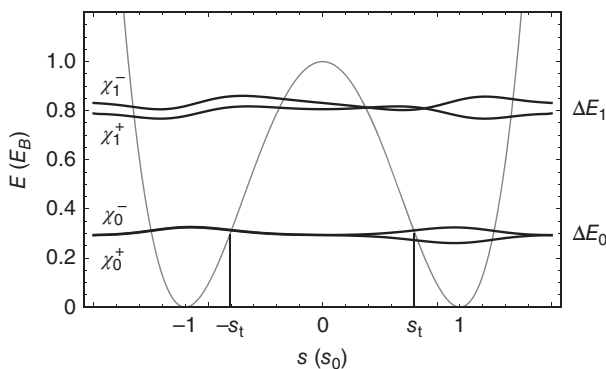
Figure 8.10 One-dimensional potential energy curve along a PT coordinate s with the four lowest eigenfunctions. There are two tunneling doublets ($\pm$) below the barrier with the splitting given by ΔE_0 and ΔE_1. The turning points for the classical motion within each potential well are labeled by $\pm s_t$ for the lowest pair of states. (Energy is given in units of barrier height, E_B, and coordinate in units of its value at minimum s_0.)

of the coupling between two almost localized states (in the left and right well) due to the wave function overlap in the barrier region. The eigenfunctions in Figure 8.10 are then the symmetric and antisymmetric combinations of these local states.

An alternative view is provided by a time-domain approach. Let us take a state that is localized in one of the minima (that is, a superposition of the two lowest eigenstates shown in Figure 8.10) as an initial wave packet. This wave packet will oscillate between the two wells; that is, it will tunnel through the potential barrier. Adopting the results of Section 3.12, the oscillation period is given by $2\pi\hbar/\Delta E_0$ (cf. Eq. (3.413)).

In what follows, we focus on the (energy-domain) tunneling splitting, which is experimentally accessible, for example by high-resolution vibration–rotation spectroscopy. In particular, we address the question: how the tunneling splitting is influenced by the coupling to intramolecular modes? However, let us start with the one-dimensional case shown in Figure 8.10. An expression for the splitting can be obtained from the standard quasi-classical Wentzel–Kramers–Brillouin theory, which gives

$$\Delta E_0 = \frac{\hbar\omega}{\pi} \exp\left\{ -\frac{1}{\hbar} \int_{-s_t}^{s_t} ds \sqrt{2m_{\text{proton}}(E - U(s))} \right\}. \tag{8.2}$$

Here, ω is a characteristic frequency in the left/right well, E is the energy of the localized left/right states, and $\pm s_t$ are the turning points for the classical motion at that energy. From Eq. (8.2) it is obvious that the tunneling splitting is rather sensitive to the details of the PES and in particular to the energetic separation between the considered state and the top of the barrier as well as to the tunneling distance $2s_t$. Thus, the splitting increases for excited states as shown in Figure 8.10. From the dynamics perspective, this implies that, for instance an initially prepared localized wave packet on the left side of the barrier will be transferred faster with increasing energy.

So far, we have considered a one-dimensional situation. However, from Figure 8.9 it is clear that PT in principle is a multidimensional process, and an accurate treatment has to take into account the coupling, for example to the heavy atom vibrations of the immediate surrounding. Due to the exponential dependence of the tunneling splitting on the details of the overlapping wave functions in the classically forbidden region, the calculation of tunneling splittings can be considered as a critical test of the accuracy of theoretical methods. This holds in particular as tunneling splittings can be rather accurately measured, for example with gas-phase high-resolution spectroscopy.

To discuss the multidimensionality in the context of tunneling splittings, Herring's formula is most suitable. The starting point is the exact pair of wave functions for a certain doublet characterized by the quantum numbers v, that is $\chi_v^\pm(s, q)$. These functions are solutions of the stationary Schrödinger equations (using mass-weighted coordinates, V is the total potential energy operator)

$$\nabla^2 \chi_v^+(s, q) = \frac{2}{\hbar^2}(V(s, q) - E_v^+)\chi_v^+(s, q), \tag{8.3}$$

$$\nabla^2 \chi_v^-(s, q) = \frac{2}{\hbar^2}(V(s, q) - E_v^-)\chi_v^-(s, q). \tag{8.4}$$

Multiplication of Eq. (8.3) [(8.4)] by $\chi_v^-(s, q)$ [$\chi_v^+(s, q)$] from the left, integrating the resulting expression over the half-space $s > 0$, and subtracting the results yield using Green's theorem

$$\frac{2}{\hbar^2}(E_v^- - E_v^+)\int\limits_{s>0} ds \int dq \chi_v^+(s, q)\chi_v^-(s, q)$$

$$= \int\limits_{s=0} dq \left[\chi_v^+(s, q)\frac{\partial}{\partial s}\chi_v^-(s, q) - \chi_v^-(s, q)\frac{\partial}{\partial s}\chi_v^+(s, q)\right]. \tag{8.5}$$

Next, we assume that there are some functions, $\chi_v^{(L/R)}(s, q)$, localized in the left/right wells such that

$$\chi_v^\pm(s, q) = \frac{1}{\sqrt{2}}\left[\chi_v^{(R)}(s, q) \pm \chi_v^{(L)}(s, q)\right]. \tag{8.6}$$

Inserting this expression into Eq. (8.5), and assuming that for $s > 0$ the integrals over $\chi_v^{(L)}\chi_v^{(L)}$ and $\chi_v^{(L)}\chi_v^{(R)}$ are negligible, gives for the tunneling splitting

$$(E_v^- - E_v^+) = \hbar^2 \int\limits_{s=0} dq \left[\chi_v^{(L)}(s, q)\frac{\partial}{\partial s}\chi_v^{(R)}(s, q) - \chi_v^{(R)}(s, q)\frac{\partial}{\partial s}\chi_v^{(L)}(s, q)\right]. \tag{8.7}$$

This expression highlights the fact that the tunneling splitting is determined by the properties of the wave functions on the symmetry plane defined by $s = 0$.

Let us discuss the effect of linear coupling (antisymmetric) and promoting (symmetric) modes on the tunneling splitting. In Figure 8.11, we give an example of a four-dimensional reaction surface calculation (Eq. (2.86)) for the PT in a derivative of tropolone (for the reaction scheme, see Figure 8.11a). The potential
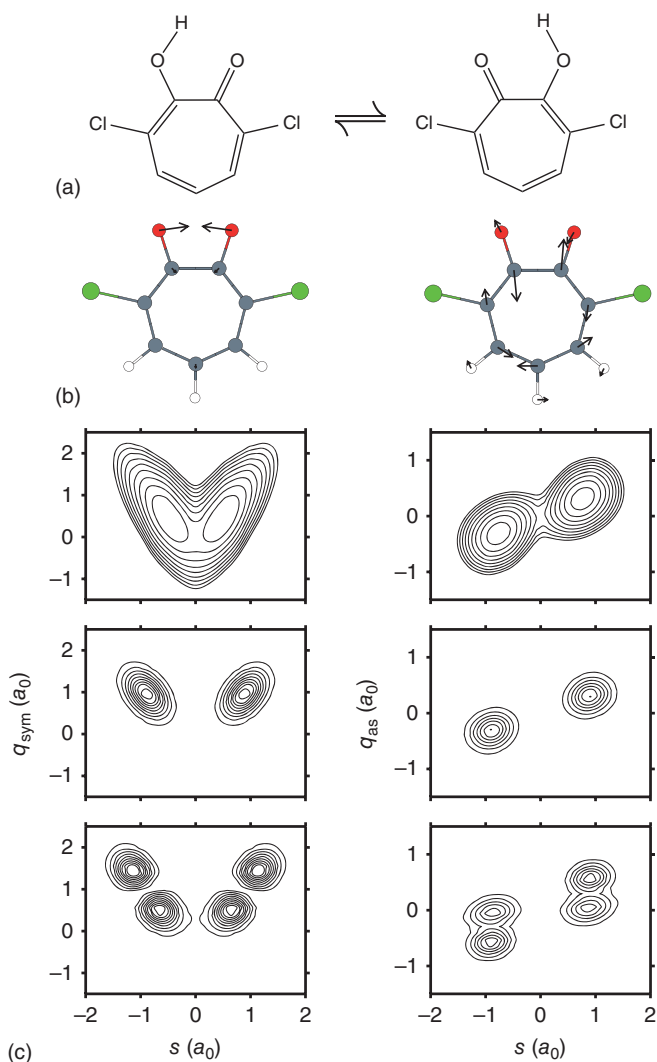
Figure 8.11 PES and eigenfunctions of (in-plane) PT in 3,7-dichlorotropolone (panel a). The two-dimensional projections of the PES (first row of (c)) and the related probability densities (second and third rows of (c)) correspond to some eigenfunctions of a four-dimensional *ab initio* quantum chemical Cartesian reaction surface Hamiltonian, Eq. (2.86). The influence of a symmetric (left column) and an antisymmetric (right column) normal mode (displacement vectors in (b)) is shown. The results have been obtained for the case that the proton moves on a straight line (s) orthogonal to the C_2 symmetry axis going through the transition state. The ground state tunneling splitting is 3 cm^{-1} (upper eigenfunctions). For the excitation of the symmetric/antisymmetric mode (lower left/lower right), the splitting amounts to 17/4 cm^{-1} (figure courtesy of K. Giese).

includes the two coordinates for the motion of the proton in the plane of the molecule as well as a symmetrically and an antisymmetrically coupled skeleton normal mode (for the normal mode displacement vectors, see Figure 8.11b). We have also plotted two-dimensional projections of the full four-dimensional potential as well as the selected eigenfunctions in Figure 8.11c.

Let us first consider the effect of a promoting type (symmetric coupling) mode. Already from Figure 8.9 it is clear that a symmetric coupling leads to an effective reduction in the barrier. In the left row of Figure 8.11 it is seen that the overall bending of the two-dimensional potential is reflected in the ground state wave functions. Thus, the overlap on the symmetry plane will be increased, and the tunneling splitting is larger as compared to the case of no coupling to this mode. Upon excitation of the symmetric mode only (not to be confused with the excited doublet in Figure 8.10), the wave function overlap increases further, as does the splitting in the excited doublet.

The situation is more complicated for the linear (antisymmetric) coupling mode shown in the right row of Figure 8.11. From the projection of the ground state wave function on the PT coordinate s and the antisymmetric coordinate q_{as}, it is seen that the presence of an antisymmetric mode may reduce the tunneling splitting since the left and right parts of the ground state wave function are shifted in opposite directions. In principle, one would expect such a behavior also for the excited states with respect to this mode (lower right panel in Figure 8.11). However, for the excited state wave functions, a comparison with the ground state already indicates that the details of the overlap on the symmetry plane will strongly depend on the position of the nodes along the oscillator coordinate in the left and right wells. Therefore, in principle, it is possible that the magnitude of the tunnel splitting even may oscillate when going to higher excited states due to the interference between the localized wave functions that overlap on the symmetry plane and give rise to the tunneling splitting.

8.2.4 The Proton Transfer Hamiltonian in the Condensed Phase

Having discussed the influence of intramolecular modes that are immediately coupled to the PT coordinate, let us next include the interaction with some environmental DOFs such as a solvent. In principle, one should distinguish between intramolecular and environmental coordinates in the following discussion. This would be particularly important if some intramolecular modes have a distinct effect on the PT coordinate such that they cannot be treated on the same level of approximation as the remaining environment. For simplicity, however, we do not make this distinction and comprise all DOFs (intramolecular and environment) into the coordinate $Z = \{Z_\xi\}$. The total Hamiltonian can then be written as follows:

$$H = H_{proton}(s) + H_R(Z) + V(s, Z). \tag{8.8}$$

Here, the Hamiltonian of the PT coordinate $H_{proton}(s)$ is given by the first two terms in Eq. (8.1) (notice that in general s can be a three-dimensional vector), $H_R(Z)$ is the Hamiltonian for the environment (solvent or protein plus intramolecular

modes), and $V(s, Z)$ comprises the interaction between the PT coordinate and the environment. Notice that Eq. (8.8) has the form of a system-bath Hamiltonian (cf. Eq. (3.3)); in the spirit of Chapter 3, the proton coordinate can be considered as being the relevant system, while the remaining coordinates Z form the reservoir.

The interaction potential $V(s, Z)$ can be partitioned into a short- and a long-range part. Often, it is reasonable to assume that the short-range part will be dominated by the interaction of the solvent with the intramolecular modes, since the respective donor and acceptor groups might shield the proton from direct collisions with the solvent. The long-range Coulomb interaction, however, influences the PT directly, since the latter is often accompanied by a large change in the dipole moment. In fact, a polar solvent is very likely to stabilize one of the two configurations found in the gas-phase double-well potential. This is typical, for instance for hydrogen-bonded acid–base complexes, where the ionic form may be stabilized in polar solution.

In practical condensed phase calculations, the environmental DOFs are normally treated by classical mechanics. On the other hand, it is often necessary to describe the proton quantum mechanically. The Hamiltonian $H_{\text{proton}}(s)$ may be obtained, for instance by performing gas-phase quantum chemical calculations for an appropriately chosen reference system that contains the PT coordinate. The interaction $V(s; Z)$ then may enter via effective pair (for example, Lennard-Jones) and Coulomb potentials. One of the essential ingredients here is a detailed model for the charge distribution along the PT coordinate. Besides this atomistic view, one can also introduce the solvent by means of a continuum model (cf. Section 2.7.1).

In what follows, we consider two different ways of rewriting the Hamiltonian (8.8) such that it becomes suitable for treating PT in the adiabatic and nonadiabatic limits.

8.2.4.1 Adiabatic Representation

The Born–Oppenheimer separation of electronic and nuclear motions provided the key to electronic and vibrational spectra and dynamics (cf. Chapter 2). In fact, the small mass of the proton makes it tempting to separate its motion from the slow dynamics of its environment (for example, intramolecular heavy atom modes and collective protein modes). Assuming that the set $\{Z_\xi\}$ of coordinates and the proton coordinate s are adiabatically separable, it is reasonable to define an *adiabatic* proton wave function as the solution of the following Schrödinger equation for fixed values of the environmental coordinates Z:

$$\left(H_{\text{proton}}(s) + V(s, Z)\right) \chi_A(s, Z) = E_A(Z)\chi_A(s, Z). \tag{8.9}$$

Here, the eigenenergies $E_A(Z)$ $(A = 0, 1, 2, \ldots)$ and the wave function $\chi_A(s, Z)$ depend parametrically on the coordinates Z in analogy to the parametric dependence of the electronic energies on the nuclear coordinates discussed in Chapter 2. Given the adiabatic basis functions $|\chi_A\rangle$, the total nuclear wave function can be expanded as follows:

$$\phi(s, Z) = \sum_A \Xi_A(Z) \, \chi_A(s, Z). \tag{8.10}$$

Stressing the analogy with the electronic–nuclear situation discussed in Section 2.3, the $\Xi_A(Z)$ can be considered as the wave functions for the motion of the
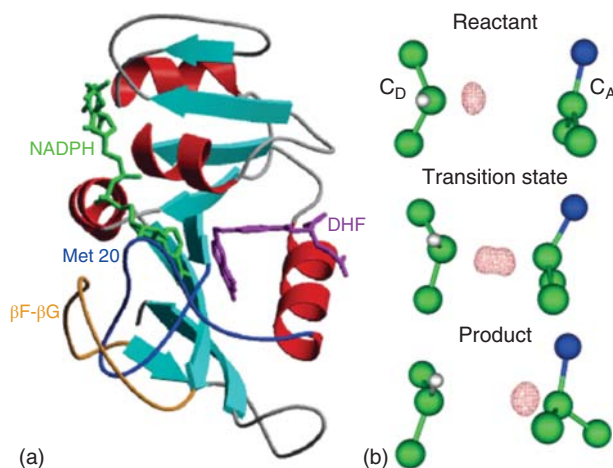
Figure 8.12 Quantum–classical hybrid treatment of the hydride (H⁻) transfer reaction catalyzed by the enzyme dihydrofolate reductase. In the three-dimensional structure (for *Escherichia coli* (a)), the nicotinamide adenine dinucleotide phosphate (NADPH) cofactors to the (protonated) 7,8-dihydrofolate (DHF) are labeled. The hydride transfer takes place from the donor carbon (C_D) of the NADPH to the acceptor carbon (C_A) of DHF. In (b), adiabatic wave functions are plotted for the hydride at three representative configurations of the environmental (DHF substrate, NADPH cofactor, protein, solvating water molecules) coordinates along the reaction path. The immediate surroundings of the donor and acceptor sites are also shown (figure courtesy of S. Hammes–Schiffer; for more details, see also Agarwal et al. [6]).

slow (environmental) DOFs in the proton adiabatic state $|\chi_A\rangle$. The corresponding equations for their determination follow in analogy to Eq. (2.18) and will not be repeated here.

It should be pointed out that for a condensed phase environment a classical treatment of the reservoir coordinates Z will be necessary using, for example the quantum–classical hybrid methods discussed in Section 3.13. In Figure 8.12, we show an example for an adiabatic proton wave function in a classical environment. Three snapshots are plotted along the reaction path of a hydride (H⁻) transfer reaction catalyzed by an enzyme.

8.2.4.2 Diabatic Representation

The diabatic representation is convenient if the proton wave function is rather localized at the donor or the acceptor site of the hydrogen bond. This will be the case for systems with a rather high barrier (weak hydrogen bonds). Following the strategy discussed in Section 2.6, we define diabatic proton states for the reactant and the product configuration according to some properly chosen Hamiltonian $H_R(s,Z)$ and $H_P(s,Z)$, respectively. This means that we have to solve the eigenvalue problem

$$H_{R/P}(s,Z)\chi_{j_R/j_P}(s,Z) = E_{j_R/j_P}(Z)\chi_{j_R/j_P}(s,Z). \tag{8.11}$$

Here, $E_{j_R/j_P}(Z)$ define the diabatic PESs for the motion of the environmental DOFs in the reactant/product state. The total PT Hamiltonian in the diabatic representation can then be written as

$$H = \sum_{j=(j_R,j_P)} \sum_{j'=(j'_R,j'_P)} \left[\delta_{jj'} \left(E_j(Z) + H_R(Z) \right) + (1 - \delta_{jj'})V_{jj'}(Z) \right] |\chi_{j'}\rangle\langle\chi_j|. \qquad (8.12)$$

Here, the diabatic state coupling $V_{jj'}(Z)$ is given by (cf. Eq. (8.9))

$$V_{jj'}(Z) = \int ds \; \chi_j^*(s,Z)[H_{\text{proton}}(s) + V(s,Z) - H_R(s,Z) - H_P(s,Z)]\chi_{j'}(s,Z). \qquad (8.13)$$

The diabatic basis can be used for the expansion of the total wave function:

$$\phi(s,Z) = \sum_{j=(j_R,j_P)} \Xi_j(Z) \; \chi_j(s,Z). \qquad (8.14)$$

The analogy between the present treatment and that of the electron–vibrational problem discussed in Chapters 2, 6, and 7 is apparent. In the spirit of the diabatic representation introduced in Section 2.6, the diabatic Hamiltonians $H_{R/P}(s,Z)$ will be conveniently chosen such that the coupling is only in the potential energy operator (static coupling).

8.3 Adiabatic Proton Transfer

The regime of adiabatic PT is characteristic of relatively strong hydrogen bonds. In this situation, the potential energy curve often has only a rather low barrier. The heavy atom coordinates will move so slowly that the proton can respond "instantaneously" to any change in Z. Thus, its wave functions $\chi_A(s,Z)$ as a solution of the Schrödinger equation (8.9) will always correspond to the potential, which follows from the actual configuration of Z (see Figures 8.12 and 8.13).

In order to explore some general features of the potential energy curve for adiabatic PT, let us consider the situation of a reactant state with equilibrated heavy atom coordinates as shown in the left panel of Figure 8.13. The potential obtained by varying the PT coordinate but keeping the heavy atom coordinates in $V(s,Z)$ *fixed* will be asymmetric. On the other hand, any displacement of the heavy atom coordinates will influence the potential for PT. Suppose that we have moved the heavy atom configuration such that it corresponds to some symmetric transition state. Then, the potential for PT will be symmetric (upper panel of Figure 8.13) with the lowest eigenstate along the proton coordinate being possibly above the top of the barrier. If we promote the heavy atom coordinates to their equilibrated product configuration, the PT potential will become asymmetric again but with the more stable configuration being on the product side (right panel of Figure 8.13). For the asymmetric reactant and product states, it is reasonable to assume that the proton wave function will be rather localized in these states. In the symmetric case, however, it may be delocalized with respect to the PT coordinate s.
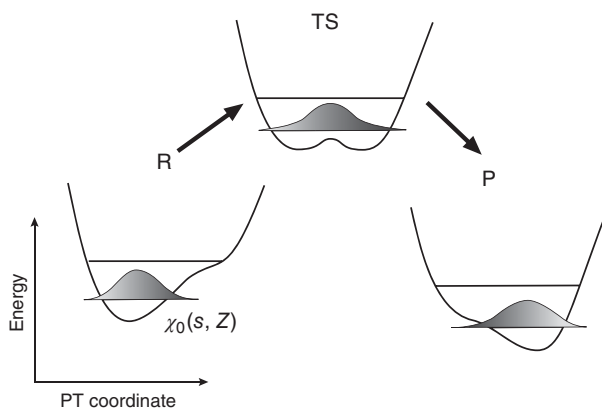
Figure 8.13 Schematic view of the potential energy curve for PT in the adiabatic regime. Here, the proton wave function, $\chi_0(s, Z)$, adjusts instantaneously to the actual configuration Z of its environment. The three different panels correspond to environmental DOFs "frozen" at their reactant (R), transition (TS), and product (P) configuration (from left to right). The proton is always in its lowest eigenstate (for an application, see Figure 8.12).

Suppose that the system was initially in the lowest proton eigenstate $\chi_0(s, Z)$ corresponding to the reactant configuration of Z. From the discussion above it is clear that it requires some *fluctuations* of the heavy atom coordinates in order to move the system from the reactant to the product state. In practice, it can be either the fluctuation of the dipole moments of the solvent or the fluctuation of some strongly coupled mode. Looking at Figure 8.13, we notice that adiabatic PT corresponds to the situation where the proton remains in its lowest eigenstate when the heavy atom coordinates move toward the product configuration.

In principle, we have separated our total system into a relevant and an environmental part (cf. Eq. (8.8)). This would suggest to use the methods of nonequilibrium quantum statistics, introduced in Chapter 3. In particular, one could straightforwardly write down a QME for the time evolution of the reduced proton density matrix. This would require to make some assumptions concerning the spectral density of the environment or to do some classical simulation of the spectral density as outlined in Section 5.3. In fact, there might be cases where such a treatment is justified. However, in general, the interaction with the surroundings *cannot* be treated using perturbation theory. This already becomes obvious by inspecting the schematic PES shown in Figure 8.13.

Therefore, a realistic modeling of PT in solution can only be achieved by resorting to the quantum–classical hybrid approach; the proton coordinate is treated quantum mechanically, and the environment classically. We note in passing that there may be situations where some of the strongly coupled modes must be treated quantum mechanically as well. This can occur especially for coupled intramolecular modes whose frequency may exceed $k_B T$ at the given temperature.

According to Section 3.13, the hybrid approach requires to solve the coupled set of Eqs. (3.438) and (3.439). In the present case of adiabatic dynamics, the simultaneous solution of the time-dependent Schrödinger equation is not necessary.

Since the classical particles are assumed to move very slowly, it suffices to solve the time-independent Schrödinger equation for fixed positions of the heavy atoms. Thus, the hybrid approach can be cast into the following scheme: Given some configuration of the environment, $Z(t)$, the *stationary* Schrödinger equation (8.9) is solved numerically. This defines, for instance the "instantaneous" adiabatic ground state proton wave function $\chi_0(s, Z(t))$ (for an example, see Figure 8.12).

This wave function is used to calculate the mean-field force F_ξ on the environmental DOFs, which is given by (cf. Eq. (3.441))

$$
\begin{aligned}
F_\xi &= -\frac{\partial}{\partial Z_\xi} \int ds\ \chi_0^*(s, Z(t)) V(s, Z(t)) \chi_0(s, Z(t)) \\
&= -\left\langle \chi_0 \left| \frac{\partial V}{\partial Z_\xi} \right| \chi_0 \right\rangle.
\end{aligned}
\tag{8.15}
$$

The expression (8.15) is a special case of the *Hellmann–Feynman theorem*, and F_ξ is the Hellmann–Feynman force.[3] This force is now used to propagate the classical DOFs by one time step according to the canonical equations:

$$
\begin{aligned}
\frac{\partial Z_\xi}{\partial t} &= \frac{\partial}{\partial P_\xi} H_R(Z), \\
\frac{\partial P_\xi}{\partial t} &= -\frac{\partial}{\partial Z_\xi} H_R(Z) + F_\xi.
\end{aligned}
\tag{8.16}
$$

From the new positions obtained in this way, a new interaction potential $V(s, Z)$ is calculated, and the stationary Schrödinger equation for the proton wave function is solved again. This procedure is continued until some desired final time. We emphasize that, in contrast to the general situation discussed in Section 3.13, the adiabatic limit does not require a simultaneous self-consistent solution of the time-dependent Schrödinger equation and Newton's equations of motion. This is due to the fact that the problem is decoupled by fixing the classical coordinates on the time scale of the motion of the quantum ones.

The results of such a simulation can be used to obtain, for instance reaction rates. Let us consider the situation of a PT system where the position of the barrier along the PT coordinate is at $s = s^*$. Then, the probability P_R that the proton is in the reactant configuration can be calculated from the adiabatic ground state proton wave function as follows:

$$
P_R(Z(t)) = \int_{-\infty}^{s^*} ds\, |\chi_0(s, Z(t))|^2.
\tag{8.17}
$$

This probability will be a function of time, since the adiabatic proton wave function depends on the actual configuration of the classical coordinates, $Z(t)$. The probability P_R will approach unity in the reactant state and zero after a complete transition to the product state occurred. In Figure 8.14, we show P_R for a model PT reaction as described in the figure caption. Here, the interaction with the solvent is rather

---

3) The Hellmann–Feynman theorem states that given the Schrödinger equation $H(Z)|\chi(Z)\rangle = E(Z)|\chi(Z)\rangle$, with Z being a parameter, it holds that $\partial E(Z)/\partial Z = \langle \chi(Z)|\partial H(Z)/\partial Z|\chi(Z)\rangle$, which can be proven using the chain rule.
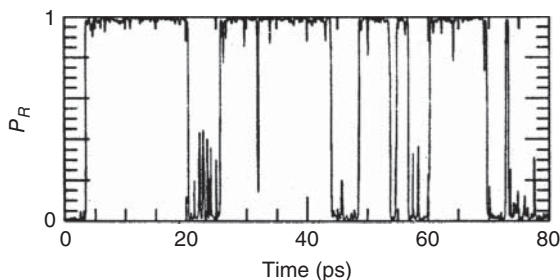
Figure 8.14 The probability for the proton to be in the reactant configuration is shown for an adiabatic PT situation. The model system is a strongly bonded $XH^+ - X$ complex immersed in a polar aprotic diatomic solvent (Reproduced with permission from Borgis et al. [7]/American Chemical Society).

strong such that the proton is most of the time stabilized either on the reactant or the product side. Large fluctuations of the solvent dipoles, however, cause occasional transitions between the two configurations; that is, the reaction barrier is crossed. From the knowledge of the time dependence of the reactant state population, one can in principle obtain the transition rate by simple counting the reactive barrier crossings in Figure 8.14 during a long-time quantum–classical propagation or by averaging over an initial distribution for the classical system.

8.4 Nonadiabatic Proton Transfer

Whenever we have a situation where the hydrogen bond is rather weak, the concepts of adiabatic PT discussed in the previous section can no longer be applied. Here, the reaction barrier will be rather high, and consequently, the splitting between the two lowest eigenstates is small. Thus, the different adiabatic states come close to each other, and nonadiabatic transitions become rather likely at normal temperatures (cf. Figure 8.6a). On the other hand, the transfer time will be long compared with the typical relaxation time scales for the environment. We have already seen in Chapter 7 that this situation is most conveniently described using a *diabatic* representation of the Hamiltonian as given by Eq. (8.12). We focus on a situation of a protonic two-state system. This may be appropriate at temperatures low enough such that the second pair of vibrational states (in an only modestly asymmetric PT potential, cf. Figure 8.6) is thermally not occupied. The two states will be labeled as $j = (R, P)$.

Since we have assumed that the conditions for nonadiabatic PT are fulfilled, we can straightforwardly write down the rate for transitions between the diabatic reactant and the product states using the Golden Rule expression of Eq. (3.86). Suppose that the stationary Schrödinger equation for the environmental DOFs

$$[E_j(Z) + H_R(Z)] \, \Xi_{j,N}(Z) = E_{j,N} \, \Xi_{j,N}(Z), \quad j = (R, P) \tag{8.18}$$

has been solved, the Golden Rule transition rate reads

$$k_{R \to P} = \frac{2\pi}{\hbar} \sum_M f_{R,M} \sum_N |\langle \Xi_{R,M} | V_{RP} | \Xi_{P,N} \rangle|^2 \delta(E_{R,M} - E_{P,N}). \tag{8.19}$$

Here, the $N = \{N_\xi\}$ comprises the quantum numbers for the environmental DOFs Z in the reactant and product diabatic states. Of course, expression (8.19) is only of limited value since calculating the eigenstates of the environment is in the general case impossible. However, as in the case of ET, one can obtain an analytical expression for the limit of a harmonic oscillator environment. We are not going to repeat the derivations given in Section 7.4, which can easily be adapted to the present situation.

For PT reactions, however, it may often be necessary to include a coordinate dependence of the diabatic state coupling, that is to go beyond the Condon approximation, which has been used in the treatment of nonadiabatic ET. This is basically due to the intramolecular promoting modes, which may have a drastic influence on the PT rate. Note that this influence will be even more pronounced in the nonadiabatic regime, where the tunneling coupling is rather small. Compared to the dominant effect of possible promoting modes, the dependence of the diabatic coupling on the solvent coordinates is often neglected. For the actual form of this dependence, it is reasonable to assume a form similar to that used for ET in Eq. (7.26). Note, however, that the parameter β, which characterizes the wave function overlap, is much larger for PT than for ET since the proton wave functions will be more localized.

In the case of a coordinate-dependent state coupling, and also for more general (not harmonic) environments, it is necessary to return to the definition of the transfer rate in terms of correlation functions as given in Eq. (3.184). Adapting Eq. (3.184) to the present situation, the PT rate can be written as

$$k_{R \to P} = \frac{1}{2\hbar} \mathrm{Re} \int\limits_0^\infty dt \, \mathrm{tr}_R \left\{ \hat{R}_R e^{iH_R^{(0)}t/\hbar} V_{RP}(Z) e^{-iH_P^{(0)}t/\hbar} V_{PR}(Z) \right\}. \qquad (8.20)$$

Here, we used the shorthand notation $H_{R/P}^{(0)} = E_{R/P}(Z) + H_R(Z)$; $\hat{R}_R$ is the statistical operator for the reactant state, and the trace is also performed with respect to the reactant states. Equation (8.20) can be transformed into a more convenient form using the operator identity

$$e^{-iH_P^{(0)}t/\hbar} = e^{iH_R^{(0)}t/\hbar} \, \hat{T} \exp\left\{ -\frac{i}{\hbar} \int\limits_0^t dt' \, e^{iH_R^{(0)}t'/\hbar} (H_P^{(0)} - H_R^{(0)}) e^{-iH_R^{(0)}t'/\hbar} \right\}. \qquad (8.21)$$

Introducing the time-dependent energy gap between the reactant and product state configurations as

$$\Delta H^{(\mathrm{I})}(t) = e^{iH_R^{(0)}t/\hbar} \, (H_P^{(0)} - H_R^{(0)}) \, e^{-iH_R^{(0)}t/\hbar}, \qquad (8.22)$$

we can rewrite Eq. (8.20) as

$$k_{R \to P} = \frac{1}{2\hbar} \, \mathrm{Re} \int\limits_0^\infty dt \, \mathrm{tr}_R \left\{ \hat{R}_R \, V_{RP}^{(\mathrm{I})}(Z, t) \, \hat{T} \exp\left\{ -\frac{i}{\hbar} \int\limits_0^t dt' \Delta H^{(\mathrm{I})}(t') \right\} V_{PR}^{(\mathrm{I})}(Z, 0) \right\}, \qquad (8.23)$$

where the interaction representation of $V_{RP}(Z)$ is with respect to $H_R^{(0)}$. In the context of linear optical spectroscopy of molecular systems, expressions of the type (8.23)

have been shown to be amenable to a classical treatment (cf. Section 6.3.3). This requires to replace the quantum dynamics of the environment, which is introduced via $V_{RP}^{(I)}(Z, t)$ and $\Delta H^{(I)}(t)$, by classical dynamics on the diabatic reactant state potential energy surface, or more specifically, $V_{RP}^{(I)}(Z, t)$ is replaced by $V_{RP}(Z(t))$ and $\Delta H^{(I)}(t)$ by $\Delta H(Z(t))$. This reminds on the dynamical classical limit (DCL) limit discussed in Section 6.3.3. Here, the time dependence of the coordinates is governed by the equations of motion of classical mechanics. In addition, the time-ordered exponential in Eq. (8.23) can be replaced by an ordinary exponential in the classical approximation. Finally, the thermal averaging in Eq. (8.23) has to be performed with respect to some classical thermal distribution function for the reactant state as detailed in Section 3.13.

8.5 The Intermediate Regime: From Quantum to Quantum–Classical Hybrid Methods

The Golden Rule description in the previous section was based on the assumption of weak hydrogen bonding. In other words, the energetic separation between the two lowest vibrational states of the PT coordinate (tunnel splitting) has to be small. One consequence is that the adiabatic approximation is no longer justified, and transitions between different proton states occur. In the previous section, this has been described using coupled diabatic proton states.

In Section 8.2, we already mentioned that the actual barrier height and therefore the tunneling splitting is subject to strong modifications in the presence of a fluctuating environment. Thus, unless hydrogen bonding is really strong, there may be no clear separation between the adiabatic regime and some intermediate, or even the nonadiabatic, regime. In this case, one has to use an alternative formulation that is suited for all regimes and in particular incorporates transitions between adiabatic proton states.

In principle, one could apply the QME approach discussed in Chapter 3 and treat the quantum dynamics of the relevant system under the influence of the dissipative environment. We have already mentioned, however, that the consideration of only a single relevant coordinate, that is the proton coordinate, may not be sufficient, and it might be necessary to include, for instance several modes of the environment into the relevant system in order to allow for a perturbative treatment of the system–environment coupling. But, in practice, the propagation of RDMs in more than three dimensions requires a considerable numerical effort. As an alternative, one could use the nonperturbative methods discussed in Sections 3.10 and 3.11. Incorporating, for example weakly damped promoting modes into the reservoir will be computationally demanding as well.

In what follows, we first discuss a fully quantum mechanical wave packet method in Section 8.5.1 before focusing on a quantum–classical hybrid approach in Section 8.5.2.

8.5.1 Multidimensional Wave Packet Dynamics

Suppose that it is sufficient to restrict the dynamics to the PT coordinate and a finite number of nuclear coordinates. Let us further assume that the Hamiltonian is available in the reaction surface form given by Eq. (8.1), that is with some (intramolecular) oscillator modes q_ξ. The simplest possible wave function would have the form of a Hartree product (cf. Eq. (3.50)):

$$\phi(s, q, t) = a(t)\chi(s, t) \prod_\xi \Xi_\xi(q_\xi, t). \tag{8.24}$$

In Section 3.2, we have shown how one can obtain a set of separate equations of motion for the wave functions of the different DOFs using the time-dependent Dirac–Frenkel variational principle. Applied to the present case, one finds the Schrödinger equation for the reaction coordinate

$$i\hbar \frac{\partial}{\partial t}\chi(s, t) = \left[T_s + U_{\text{SCF}}(s, t)\right]\chi(s, t), \tag{8.25}$$

where the effective potential

$$U_{\text{SCF}}(s, t) = U(s) + \sum_\xi \left[\frac{1}{2}\omega_\xi^2 \langle \Xi_\xi(t)|q_\xi^2|\Xi_\xi(t)\rangle - F_\xi(s)\langle \Xi_\xi(t)|q_\xi|\Xi_\xi(t)\rangle\right] \tag{8.26}$$

has been introduced. It contains the time-dependent mean-field potential due to the interaction with the oscillator modes. For the latter, we obtain the equations of motion

$$i\hbar \frac{\partial}{\partial t}\Xi_\xi(q_\xi, t) = \left[T_\xi + \frac{1}{2}\omega_\xi^2 q_\xi^2 - F_\xi(t)q_\xi\right]\Xi_\xi(q_\xi, t). \tag{8.27}$$

Here, we define the time-dependent linear driving forces for the oscillator dynamics $F_\xi(t) = \langle \chi(t)|F_\xi(s)|\chi(t)\rangle$. This quantity contains an average with respect to the proton coordinate; that is, it describes the mean-field interaction for the oscillator modes. Furthermore, notice that Eq. (8.27) corresponds to a harmonic oscillator with time-dependent driving force. Therefore, if the reservoir is initially in the ground state and described by an uncorrelated Gaussian wave packet, the dynamics, which is initiated by the interaction with the proton coordinate, is that of a Gaussian wave packet with a time-dependent mean value. Since the dynamics of both subsystems is determined by simultaneous solution of Eqs. (8.25) and (8.27), this approach is called *time-dependent self-consistent field method*.

The approach outlined so far is rather appealing for it allows to treat a fair number of DOFs on a quantum mechanical level. It may provide a reasonable description for hydrogen bond motion in the vicinity of a minimum on the PES or for strong hydrogen bonds. On the other hand, for PT reactions between the reactant and product potential wells, it is likely to fail. The reason lies in the mean-field character of the coupling. To illustrate this, suppose that we are interested in the force that acts on some oscillator coordinate if the proton is in its vibrational ground state $\chi_0(s)$. For a symmetric double minimum potential, the ground state wave function will obey $\chi_0(s) = \chi_0(-s)$ (cf. Figure 8.10). Hence, given an antisymmetric coupling such as $F_\xi(s) \propto s$ (cf. Figure 8.9a), the mean force will vanish. Although this is an extreme

example, it becomes clear that upon PT, the force on the oscillator modes may change considerably such that for a rather delocalized proton wave packet details of this coupling are averaged out, leading to a qualitatively wrong behavior.

A recipe for including correlations beyond the mean-field approximation even for rather large systems is most easily appreciated if we return to the diabatic picture of some general system-bath Hamiltonian as given by Eq. (8.12).[4] Having defined the diabatic proton states for the reactant and product, we can use the so-called *coupled-channel* approach. To this end, let us expand the time-dependent total wave function in terms of the stationary *diabatic* proton states as follows (cf. Eq. (8.14)):

$$\phi(s, Z; t) = \sum_{j=(j_R j_P)} \Xi_j(Z; t) \chi_j(s, Z). \tag{8.28}$$

Inserting this ansatz into the time-dependent Schrödinger equation with the Hamiltonian in Eq. (8.12), one obtains the coupled-channel equation for the time-dependent wave function of the environment, $\Xi_{j=(j_R j_P)}(Z; t)$,

$$i\hbar \frac{\partial}{\partial t} \Xi_j(Z; t) = \left(E_j(Z) + H_R(Z) \right) \Xi_j(Z; t) + \sum_{j' \neq j} V_{jj'}(Z) \, \Xi_{j'}(Z; t). \tag{8.29}$$

Given a diabatic Hamiltonian as in Eq. (8.12), this equation is in principle exact. However, unless the number of environmental DOFs can be restricted to just a few, the numerical effort for solving the coupled-channel equations is prohibitive. Therefore, it is customary to neglect correlations between different environmental coordinates and assume that the wave function for the different diabatic states of the proton, $\Xi_j(Z; t)$, can be factorized as follows[5]:

$$\Xi_j(Z; t) = \prod_k \Xi_j(Z_\xi; t). \tag{8.30}$$

Using this factorization ansatz and employing again the Dirac–Frenkel time-dependent variational principle (cf. Eq. (3.47)), one obtains the following equation for the wave function $\Xi_j(Z_\xi; t)$:

$$i\hbar \frac{\partial}{\partial t} \Xi_j(Z_\xi; t) = \sum_{j'} H_{jj'}^{(\text{eff})}(Z_\xi; t) \, \Xi_{j'}(Z_\xi; t). \tag{8.31}$$

We can identify this as a *mean-field* approach; that is, the time evolution of the wave function for the environmental DOF Z_ξ is determined by the averaged potential of all other DOF $Z_{\xi' \neq \xi}$. The effective time-dependent Hamiltonian entering Eq. (8.31) is given by

$$H_{jj'}^{(\text{eff})}(Z_\xi; t) = \int d\tilde{Z} \, \Xi_j^*(\tilde{Z}; t) \left[\delta_{jj'} \left(E_j(Z) + H_R(Z) \right) + (1 - \delta_{jj'}) V_{jj'}(Z) \right] \Xi_{j'}(\tilde{Z}; t). \tag{8.32}$$

---

4) It is rather straightforward to map this general Hamiltonian onto the specific reaction surface Hamiltonian for an oscillator reservoir.
5) Note that the following treatment is not unique to PT; that is, it can be applied to the electron–vibrational dynamics as well.

Here, we introduce $\tilde{Z}$ as the shorthand notation for all coordinates Z except Z_ξ. Further, we have used

$$\Xi_j(\tilde{Z}; t) = \prod_{\xi' \neq \xi} \Xi_j(Z_{\xi'}; t). \tag{8.33}$$

This approximate treatment allows to consider much larger environments but neglects any correlation effects in the dynamics of different environmental DOFs. However, in contrast to the time-dependent self-consistent field approach, the force acting on the reservoir particles depends on the diabatic state of the reaction coordinate.

Whenever only a few DOFs have to be considered, one can resort to numerically exact methods that allow to account for all relevant correlations.[6] Here, the most versatile approach is the multiconfiguration time-dependent Hartree method discussed in Section 3.2.3. In Figure 8.15, we show the results of MCTDH wave packet propagations of PT along a chain of four water molecules. The model includes the proton coordinates r_i as well as the hydrogen bond length R_i (Figure 8.15a). In Figure 8.15b, the probability density for an excess proton that is initially inserted into the left most unit of the chain is shown for the central unit as a function of time for the fully correlated seven-dimensional wave packet. Initially, the proton is in the reactant well of this potential (the form of the PES is similar to that shown in Figure 8.9a). After 100 fs, the wave packet has moved into the barrier region, where the proton is shared between the two oxygen atoms, to proceed into the product region. In Figure 8.15c, a simulation is shown where the heavy atom coordinates R_i are treated by a single Hartree product only. Clearly, the mean-field nature of this description has a dramatic influence on the wave packet that appears to be considerably less structured during its evolution.

8.5.2 Surface Hopping

Due to the complexity of the environment, however, one often wants to retain its classical description. From Eq. (8.28), it is obvious that in general the total system is in a superposition state with respect to the diabatic proton states. This introduces some conceptual difficulty since the classical environment cannot be in such a state; that is, it cannot experience the forces due to *both* diabatic proton states at the *same* time. One possibility to solve this problem approximately is to average the forces on the classical DOFs with respect to the quantum states. However, this will only be a good approximation if these forces are not very different in the two quantum states, which is often not the case.

An alternative and simple classical approach incorporating quantum transitions is given by the *surface hopping* method, introduced in Section 3.13.2. Here, the classical propagation of the environmental DOFs is combined with certain prescriptions for quantum transitions in the quantum subsystem.

---

6) Note that depending on the importance of correlations and on the representation of the Hamiltonian (for example, harmonic oscillator based), hundreds of DOFs can be treated at reasonable numerical costs.
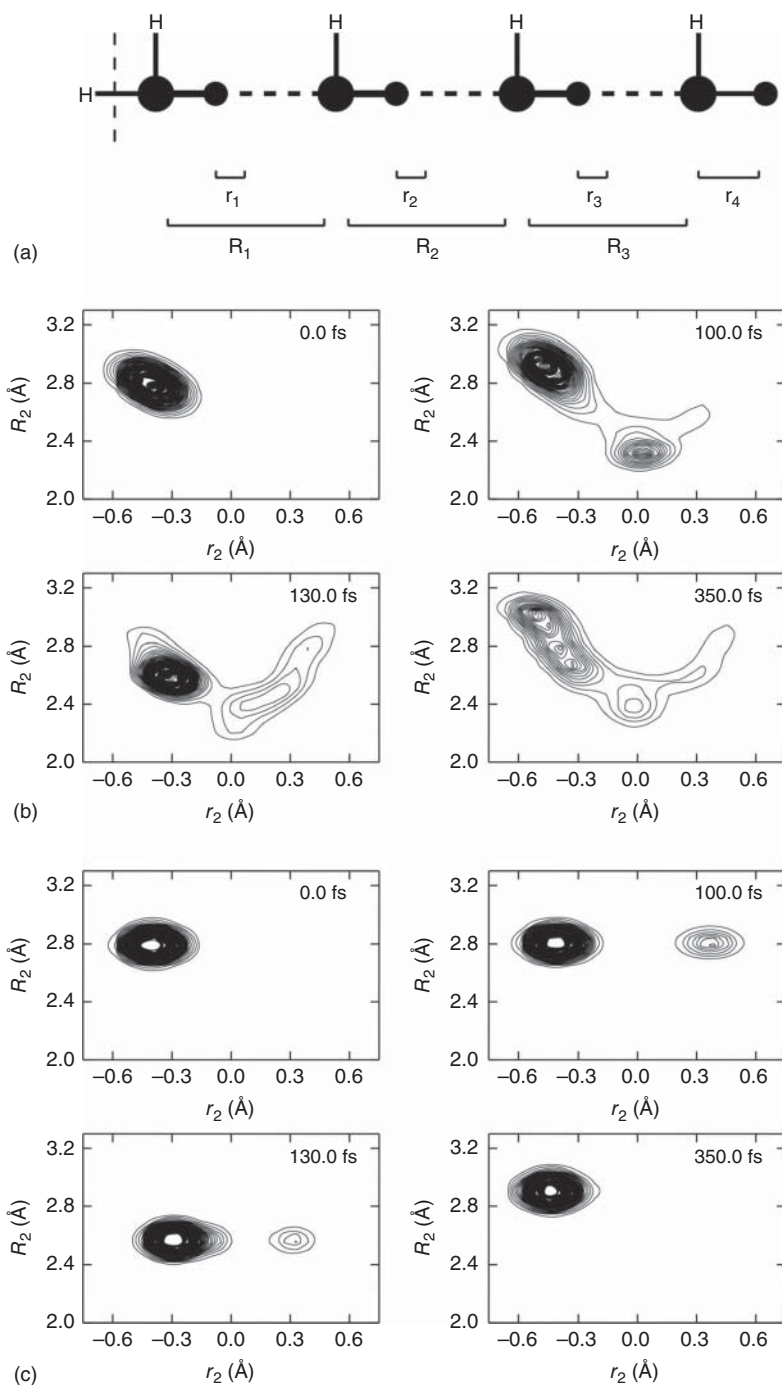
Figure 8.15 Wave packet dynamics of a seven-dimensional quantum model mimicking excess PT in a water chain (a). (b) and (c) Probability densities for two selected coordinates for the exact case and for an approximation where the heavy atom coordinates are treated by a single Hartree product (Reproduced with permission from Vendrell and Meyer [8]/American Institute of Physics).

For the simulation of PT reactions, one employs the instantaneous *adiabatic* proton states, which have to be determined according to Eq. (8.9) for each time step. The proton wave function at any time step can then be expanded in terms of this instantaneous adiabatic basis set according to[7]

$$\chi(s, Z; t) = \sum_A c_A(t) \, \chi_A(s, Z(t)). \tag{8.34}$$

Inserting this expression into the time-dependent Schrödinger equation with the Hamiltonian given by Eq. (8.9), one obtains the following set of equations:

$$\frac{\partial}{\partial t} c_A = -\frac{i}{\hbar} E_A \, (Z) c_A - \sum_\xi \frac{\partial Z_\xi}{\partial t} \sum_{A'} c_{A'} \left\langle \chi_A \left| \frac{\partial}{\partial Z_\xi} \, \chi_{A'} \right. \right\rangle. \tag{8.35}$$

The last factor on the right-hand side can be identified with the nonadiabatic coupling matrix (cf. Eq. (3.449)). The quantum–classical propagation then proceeds as explained in Section 3.13.2. The surface hopping method gives a means to calculate, for instance the transitions rates without referring to any particular limit of PT.[8] Since the proton coordinate is treated quantum mechanically, the effects of tunneling and zero-point motion are naturally included. It should be emphasized again that the incorporation of nonadiabatic transitions relies on some ad hoc stochastic model that, however, uses information about the probability distribution with respect to the proton states.

In the enzymatic catalysis example given in Figure 8.12, the surface hopping method was used to address the influence of quantum effects for hydride (H^-) transfer. Nonadiabatic transitions were found to have only a minor effect on the rate for this process.

8.6 Proton-coupled Electron Transfer

PCET will be discussed in a scheme involving electron donor/acceptor D_{el}/A_{el} and proton donor/acceptor D_p/A_p configurations. In the latter case, the protonated donor will be labeled $D_p^+ = D_p - H^+$ and likewise for the acceptor. In principle, one can distinguish between concerted and sequential PCET. In the case of concerted PCET, PT and ET occur simultaneously and without a stable intermediate, that is[9]

$$[D_{el}^- A_{el}][D_p^+ A_p] \; \rightarrow \; [D_{el} A_{el}^-][D_p A_p^+], \tag{8.36}$$

---

7) Note that in general any suitable basis set can be used, but this would require to calculate matrix elements of the proton Hamiltonian on the right-hand side of Eq. (8.35).

8) This can be done, for instance by partitioning the possible values of the PT coordinate into the reactant and product side configuration. Based on the expectation value of the PT coordinate for a given classical trajectory, it can be decided whether a reactive transition between the reactant and the product configuration occurred.

9) Notice that in cases where electron and proton share the donor and acceptor, one obtains hydrogen atom transfer.

whereas in sequential PCET, either ET precedes PT

$$[D_{el}^- A_{el}][D_p^+ A_p] \; \rightarrow \; [D_{el} A_{el}^-][D_p^+ A_p] \; \rightarrow \; [D_{el} A_{el}^-][D_p A_p^+] \tag{8.37}$$

or vice versa

$$[D_{el}^- A_{el}][D_p^+ A_p] \; \rightarrow \; [D_{el}^- A_{el}][D_p A_p^+] \; \rightarrow \; [D_{el} A_{el}^-][D_p A_p^+]. \tag{8.38}$$
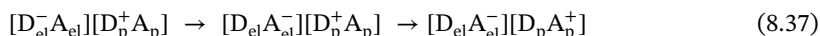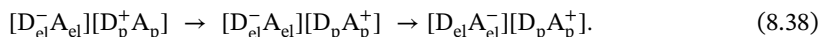
Concerted PCET often proceeds in the nonadiabatic limit, that is as a transition between localized electron–proton states triggered by thermal fluctuations of a reaction coordinate (such as a collective solvent coordinate).[10] In this case, it can be described adapting the Golden rule expression developed in the context of ET, Eq. (7.101). Figure 8.16 illustrates the situation, which has a close analogy to the case of ET shown in Figure 7.22. In the diabatic reactant state, $[D_{el}^- A_{el}][D_p^+ A_p]$, the electronic DOFs are in the respective ground state, $|\phi_D\rangle$, whereas the proton state is $|\chi_{DM}\rangle$. At the same time, the reaction coordinate is in its reactant configuration. In the product state, $[D_{el} A_{el}^-][D_p A_p^+]$, the situation is analogous, with electronic ground state $|\phi_A\rangle$ and proton state $|\chi_{AN}\rangle$.

When calculating the rate, k_{PCET}, according to Eq. (7.101), one has to be aware of the fact that in general the diabatic state coupling will depend on the distance between the proton donor and acceptor. According to Figure 8.6, even the shapes of the local potential and thus the proton wave function may depend on this distance. As outlined in Section 8.4, such cases can be treated using a correlation function approach.

Sequential PCET can proceed via two pathways, Eqs. (8.37) and (8.38). In particular, for enzymatic reactions, it is found that the energy of the intermediate state is
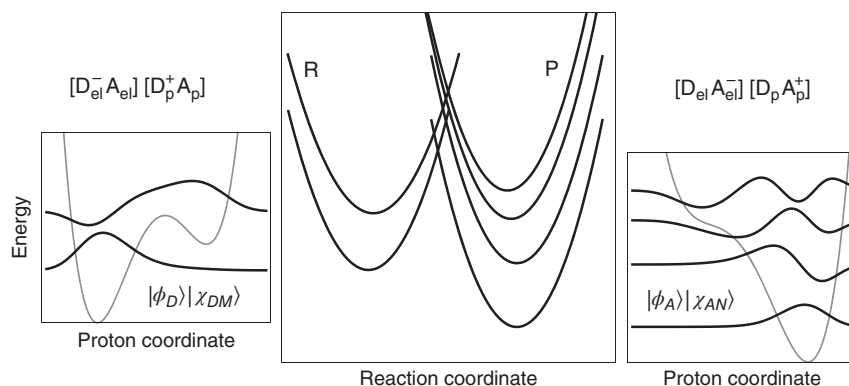
Figure 8.16 Potential energy curves for nonadiabatic PCET according to Eq. (8.36). On the left and right sides, the potential for local proton motion is shown together with proton wave functions. In the center, the diabatic reactant and product potentials of the reaction coordinate (collective solvent coordinate) are given that correspond to particular local proton states as indicated by their energetic positions (cf. Figure 7.22).

10) Note that within the nonadiabatic limit for the PCET reaction, one can further differentiate according to the ratio of time scales for electron and proton tunneling. For instance, a reaction can be electronically adiabatic with respect to the proton motion if the electronic time scale is much shorter than that of the proton.

higher than that of the initial state, and only the second reaction step proceeds energetically downhill. Hence, forward as well as backward rates have to be considered for the first reaction step. The appropriate system of coupled rate equations can be obtained in analogy to the case of donor–bridge–acceptor ET, Eq. (7.128). The rates for the individual ET and PT steps follow from the respective theories for PT and ET discussed in the present and the previous chapters, respectively.

References

1 R. Rousseau et al., Angew. Chem. Int. Ed. **43**, 4804 (2004).

2 D. Madsen et al., Bull. Chem. Soc. Jpn. **75**, 909 (2002).

3 R. Yuan et al., ACS Cent. Sci. **5**, 1269 (2019).

4 S. Lochbrunner and E. Riedle, J. Chem. Phys. **112**, 10699 (2000).

5 A. Novak, Struct. Bond. **18**, 177 (1974).

6 P. K. Agarwal et al., J. Phys. Chem. B **106**, 3283 (2002).

7 D. Borgis et al., J. Phys. Chem. **96**, 3188 (1992).

8 O. Vendrell and H.-D. Meyer, J. Chem. Phys. **122**, 104505 (2005).

Further Reading

- Overview of different aspects of proton transfer:
  J. T. Hynes, J. P. Klinman, H.-H. Limbach, and R. L. Schowen (eds.), *Hydrogen Transfer Reactions*, (Wiley–VCH, Weinheim, 2006).
- Overview of excited state proton transfer:
  K.-L. Han and G.-J. Gao (eds.), *Hydrogen Bonding and Transfer in the Excited State*, (John Wiley & Sons, Chichester, 2010).
- Overview of isotope effects:
  A. Kohen and H.-H. Limbach (eds.), *Isotope Effects in Chemistry and Biology*, (Taylor and Francis, Boca Raton, FL, 2006).
- Review on multidimensional quantum dynamics and spectroscopy of hydrogen bonds:
  K. Giese, M. Petković, H. Naundorf, and O. Kühn, Phys. Rep. **430**, 211 (2006).
- Reviews on proton-coupled electron transfer and applications:
  S. Hammes–Schiffer and A. A. Stuchebrukhov, Chem. Rev. **110**, 6939 (2010).
  D. G. Nocera, J. Am. Chem. Soc. **144**, 1069 (2022).

9

Excitation Energy Transfer

The transfer of electronic excitation energy within a molecular aggregate will be considered. The construction of the respective Hamiltonian is explained in detail. We will discuss the coupling of electronic excitations between different molecules, which causes excitation energy delocalization and transfer, as well as the interaction with the various types of vibrational degrees of freedom. Attention is focused on the so-called Frenkel exciton model, where the moving excitation energy is completely described as an intramolecular excitation, and no charge transfer between different molecules occurs. Excitation energy transfer in a situation of weak and strong dissipation is described. The latter case directly leads to the well-established Förster theory for incoherent excitation energy hopping. It is shown that the Förster transfer rate can be expressed in terms of the emission and absorption spectra of the donor molecule and the acceptor molecule, respectively. Next, we demonstrate how optical absorption spectra are influenced by the formation of Frenkel exciton states. Finally, excitation energy transfer is discussed in terms of photon exchange, and the formation of charge-transfer excitons and the process of exciton–exciton annihilation are described.

9.1 Introduction

Let us start with the consideration of the electronic excitation energy transfer (EET) between two molecules according to the general scheme

$$D^* + A \longrightarrow D + A^* \tag{9.1}$$

The excitation energy donor is labeled by D, and the excitation energy acceptor A. The starting point is a situation where the donor molecule has been excited (D^*), for instance, by absorption of a photon, and the acceptor molecule is in its ground state (A). Then, the Coulomb interaction between these molecules leads to a reaction where the donor molecule is deexcited, and the electrostatic energy is transferred to the acceptor molecule, which becomes excited. Figure 9.1 displays this process in a HOMO–LUMO scheme. Since the deexcitation of the donor molecule recalls spontaneous photon emission (fluorescence, see Section 6.4), the described process of EET is often also named *fluorescence resonance energy*
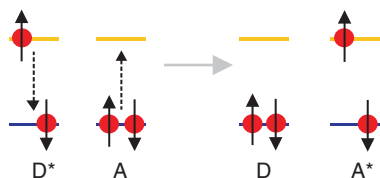
Figure 9.1 Excitation energy transfer between an energy donor molecule D and an acceptor molecule A. A HOMO–LUMO scheme has been used for both molecules. D is initially in the excited state in which one electron has been promoted from the HOMO to the LUMO. In the final state, D is in its ground state, and A is excited. The Coulomb interaction triggers the exchange of excitation energy. If the excited donor is in the singlet spin state, the electron spin of the LUMO electron may point upward and that of the HOMO electron downward or vice versa. Such a spin configuration is also reached for the excited acceptor after excitation energy transfer.
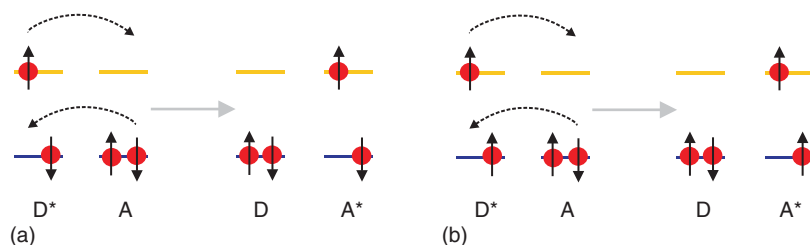
Figure 9.2 Excitation energy transfer between an energy donor molecule D and an acceptor molecule A viewed as a two-electron-exchange process. Both molecules are described in a HOMO–LUMO scheme (inverse spin orientation in D* and A* is also possible). (a) Singlet–singlet transfer and (b) triplet–triplet transfer.

transfer (FRET, the term "resonance" expresses the requirement that the energy of the initial and final EET states should coincide). The product state can also be reached via an electron-exchange mechanism between the donor and the acceptor molecules (see Figure 9.2). The electron in the LUMO of D moves to the LUMO of A, and the hole in the HOMO of D is filled by an electron of the HOMO of A. The latter process requires that the wave functions of D and A overlap, while the former process (without electron exchange) may take place even if both molecules are spatially well separated.

If the coupling responsible for EET becomes sufficiently large, the quantum mechanical state $|D^*A\rangle$ that corresponds to the initial state of the EET and the state $|DA^*\rangle$ that describes the result of the EET may form a superposition state $c_1|D^*A\rangle + c_2|DA^*\rangle$. If generalized to an arbitrary set of molecules, this state is known as the *Frenkel exciton*. To distinguish the Frenkel exciton from other types of excitons, it can be considered as an electron–hole pair with both particles residing at the same molecule (the missing single electron in the HOMO of an excited molecule is considered the hole).

Frenkel excitons are encountered in associated and noncovalently bound complexes. Examples are molecular crystals of aromatic compounds such as benzene and naphthalene and rare gases in the solid phase. Another important class of
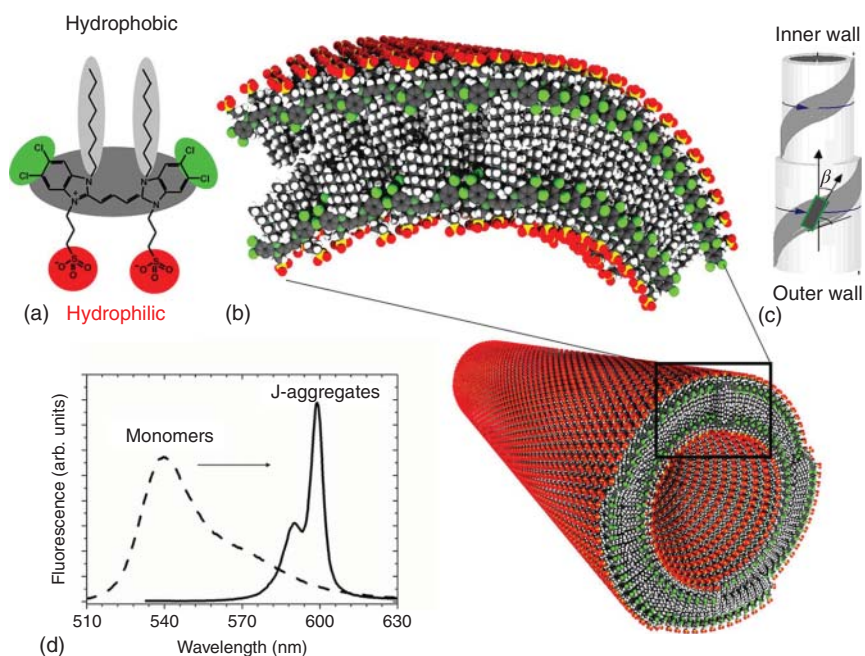
Figure 9.3 Cylindrical J-aggregate of an amphiphilic dye molecule. (a) Monomer cyanine unit. (b) Schematic of self-assembled double-walled nanotube. (c) Schematic drawing of monomer transition dipoles at angles β with respect to the long axis of the tube. (d) Monomer and aggregate fluorescence spectra; the two peaks in the latter case correspond to the inner and outer ring excitons (reprinted by permission from Eisele et al. [1], copyright Springer Nature (2009)).

Frenkel exciton systems are dye aggregates (for instance, cyanine dyes). Upon aggregation, which occurs in solution or in thin solid films, the dyes form rod-like arrangements consisting of several hundred molecules (see Figure 9.3). In the past decades biological *multichromophore complexes* also attracted broad interest. The light-harvesting complexes of natural photosynthetic antenna systems represent fascinating examples where the concept of Frenkel excitons can be applied. Much effort has been devoted to the study of both the primary steps of photosynthesis, that is directed EET in the antenna (solar energy collection) and charge transfer in the reaction center (connected with charge separation). A schematic view of an antenna system consisting of several so-called pigment–protein complex is shown in Figure 9.4. In particular, the Fenna–Matthews–Olson (FMO) complex (panels (b) and (c)) has attracted considerable attention. It transfers excitation energy between the chlorosome antenna and the reaction center. Since its atomic structure is known for a long time, it has become a model system for theoretical and spectroscopic studies. Figure 9.4d shows two-dimensional spectra of the FMO complex at a temperature of 77 K for two different population times (the room temperature linear absorption spectrum can be found in Figure 9.21b). For short delay times, the spectrum is essentially elongated along the diagonal line, resembling the linear absorption spectrum. With increasing delay time, exciton relaxation proceeds
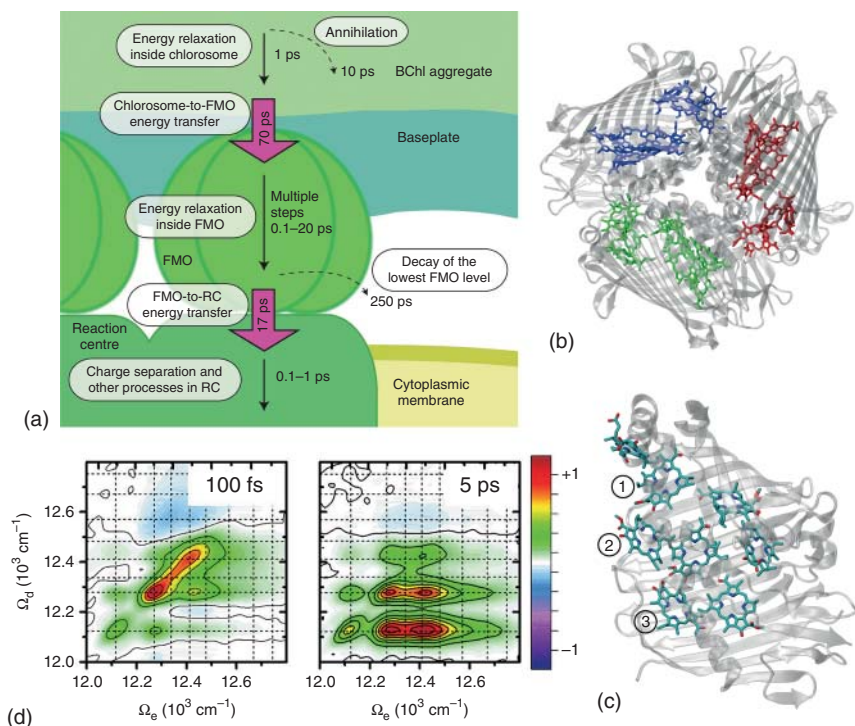
Figure 9.4 (a) Time scales of energy flow and charge separation in the photosynthetic apparatus of the green sulfur bacterium *Chlorobaculum tepidum* consisting of an assembly of light-harvesting complexes, a chlorosome, Fenna–Matthews–Olson (FMO) proteins, and reaction centers (RCs). The actual time scales have been obtained using two-dimensional electronic spectroscopy. (b) Structure of the FMO trimer complex, which serves as an energy transporter between the chlorosome and the RC (see panel (a)). (c) Arrangement of bacteriochlorophyll (BChl) *a* molecules in a monomeric unit of FMO trimer. EET is often assumed to be initiated at site 1 and to proceed toward site 3. (d) Two-dimensional electronic spectra at $T = 77$ K for two population times (100 fs and 5 ps); the dashed lines indicate the excitonic transition energies (panel (a) reprinted with permission from Dostál [2], copyright Springer Nature (2016); panels (b, c) courtesy of A. A. Ahmed; panel (d) courtesy of E. Thyrhaug and D. Zigmantas; for more information, see also Thyrhaug et al. [3]).

toward the lowest excited state of the complex. This gives rise to peaks below the diagonal due to ground state bleaching and stimulated emission processes (cf. Section 4.3.7). Fitting such spectra provides access to energy relaxation rates. For a quantum dynamical simulation of EET in the FMO complex, see Figure 9.18.

Finally, we point to organic–inorganic hybrid systems where molecules are attached to semiconducting nanoparticles (quantum dots, see Figure 9.5), and EET takes place between the nanoparticle and the molecule. The theoretical and experimental investigation of the behavior of excitons in molecular aggregates has a long history. Already in the 1930s, G. Scheibe and E. E. Jelley observed characteristic changes of optical absorption bands upon changing conditions such as to – in modern terms – promote supramolecular self-aggregation. The spectrum changes from a broad monomeric absorption band to a comparatively sharp and
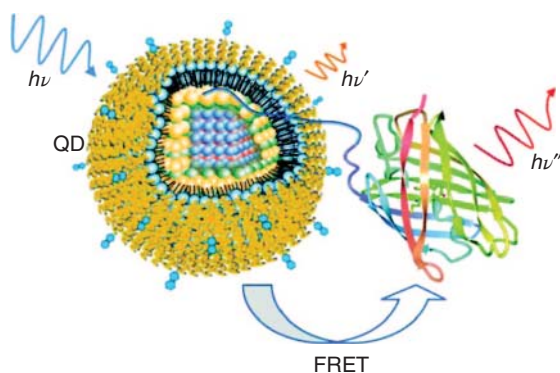
Figure 9.5 Fluorescence resonance energy transfer (FRET) between a CdSe/ZnS core–shell quantum dot (coated with a lipid layer) and a fluorescent protein (similar to the so-called green fluorescent protein). Both are connected via a polyhistidine chain. Upon excitation of the quantum dot, energy is nonradiatively transferred to the fluorescent protein, and sensitized emission is observed (reprinted with permission from Dennis and Bao [4], copyright 2008 American Chemical Society).

shifted aggregate absorption band (and likewise for emission of the so-called J-aggregates as is shown in Figure 9.3). This effect will be discussed in more detail in Section 9.7. Early theoretical contributions by T. Förster and D. L. Dexter were based on an incoherent rate equation approach. The variety of phenomena highlighted in recent discussions ranges from cooperative radiative decay (superradiance), quantum coherent dynamics, and disorder-induced localization to nonlinear effects such as exciton–exciton annihilation and multiexciton state formation. This is paralleled by a large number of theoretical investigations focusing on exciton transport in molecular systems beyond the rate limit. Historically, a prominent role was played by the *Haken–Strobl–Reineker* model, which describes the influence of the environment on the exciton motion in terms of a stochastic process. Recent efforts focus on density matrix theories that treat the environment in an quantum statistical way and that go beyond limitations set by the perturbation theory with respect to the exciton–environment coupling (for instance, the HEOM approach outlined in Section 3.11).

The case opposite to the Frenkel exciton, where electron and hole are separated by a distance much larger than the spacing between the neighboring molecules, is called a *Wannier–Mott exciton*. It occurs in systems with strong binding forces between constituent molecules or atoms such as covalently bound semiconductors.[1] The *charge-transfer exciton*, an intermediate form, is also frequently discussed. Here, electron and hole reside on molecules that are not too far apart. This type of exciton appears if the wave functions of the involved molecules are sufficiently overlapping, as is necessary for an electron-transfer reaction (cf. Chapter 7). Charge-transfer excitons can be found, for example, in polymeric chains formed by silicon compounds (polysilanes) or polythiophene assemblies and also in molecular crystals.

---

1) Frenkel and Wannier–Mott excitons are usually characterized by the electron–hole binding energy, which is on the order of 1 eV and 10 meV, respectively. Within a simple H-atom picture of electron–hole interaction, this difference can be rationalized in terms of the dielectric shielding of the Coulomb interaction, which is much larger in inorganic than in organic materials.

This chapter focuses on the description of EET and Frenkel excitons in molecular aggregates. The term "aggregate" is used to characterize a molecular system that consists of noncovalently bound molecules, which will also be called monomers. Occasionally, we also use the term "chromophore complex". The electronic excitation energy in an aggregate can move as an exciton over the whole system at least in principle.[2] The initial state relevant for the transfer process is often created by means of photon absorption resonant to the corresponding $S_0 \rightarrow S_1$ transitions of the interacting monomers. In general, the excited state is a superposition of monomer states, that is it may contain contributions of all monomers. In terms of the corresponding wave functions, this implies a delocalization over the whole aggregate. The degree of delocalization and the type of motion initiated by the external field (cf. Figure 9.6) depend crucially on the interaction between the exciton system and
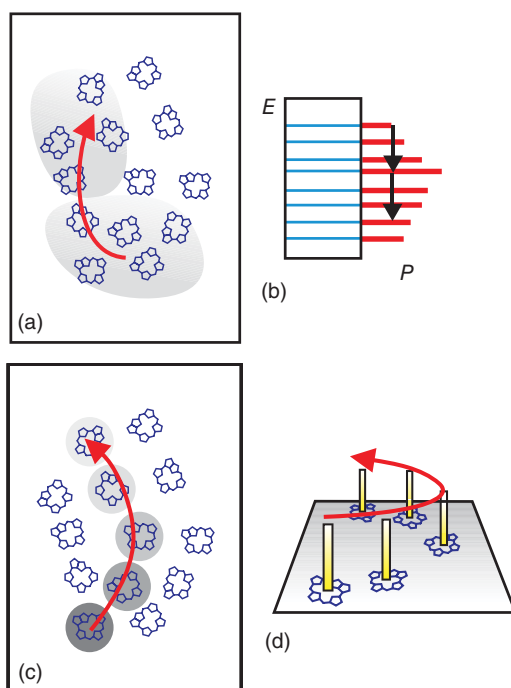
Figure 9.6 Schematic illustration of exciton motion in a chromophore complex of pheophorbide-a molecules. (a) Coherent limit where the shaded area symbolizes the exciton wave packet extending over several monomers. (b) Coherent motion appears via wave packet formation within the energy spectrum of delocalized exciton states. Here, the horizontal sticks indicate the probability P that a certain exciton state is involved in the wave packet. The probability distribution changes due to energy relaxation as indicated by the arrows. (c) Incoherent limit where the excitation hops from molecule to molecule (at a certain time, the excitation is present at different molecules with a certain probability corresponding to the gray scale). (d) The molecules can often be described as an electronic two-level systems (upper and lower ends of the vertical sticks) with the excitation of the upper level moving along a particular path (indicated by the arrow).

---

2) Since in the experiment any regular structure of the aggregate is disturbed by external influences, exciton motion is restricted to smaller parts of the whole aggregate (see below).

the environmental DOFs such as intramolecular nuclear motions. As already discussed in connection with the electron-transfer reactions (cf. Section 7.3), the ratio between the characteristic times of intramolecular (vibrational) relaxation and intermolecular transitions determines the particular way the EET proceeds. Two limiting cases can be distinguished. If the intramolecular relaxation is slow (compared with the intermolecular transfer), then the excitation may move as a delocalized wave packet through the aggregate (cf. Figure 9.6a,b), that is the EET is a *coherent* transfer process. In the opposite case, the excitation remains localized as shown in Figure 9.6c,d, and the EET is called *incoherent*. A more detailed discussion will be given in Section 9.4.

First, we outline in Section 9.2 some fundamentals of exciton theory, introducing the single- and the two-exciton states, and discussing the coupling to vibrational DOFs. Although we introduce the higher excited aggregate states, which contain two (or even more) excitations (cf. Figure 9.9), only the related phenomenon of exciton–exciton annihilation will be discussed in the supplementary Section 9.9. The techniques to describe the different regimes of exciton dynamics are presented in Sections 9.5 and 9.6. The optical properties of different types of aggregates are described in Section 9.7.

9.2 The Aggregate Hamiltonian

Let us consider a molecular aggregate consisting of N_{mon} molecules (monomers) arranged in an arbitrary geometry and with the center of mass of the mth molecule located at $\boldsymbol{X}_m$. The aggregate Hamiltonian H_{agg} is separated into intra- and intermolecular contributions:

$$H_{\mathrm{agg}} = \sum_m H_m + \frac{1}{2}\sum_{m,n} V_{mn}. \tag{9.2}$$

The intramolecular contributions H_m describe individual molecules and are identical with the expression of H_{mol} in Eq. (2.97). They depend on the electronic coordinates of molecule m abbreviated by r_m as well as on the respective nuclear coordinates denoted by R_m. Since we have in mind an expansion with respect to the electronic states of the monomers, we first separate the Hamiltonians H_m into the nuclear kinetic energy operators T_m and the remaining Hamiltonians $H_m^{(\mathrm{el})}$, which define the respective electronic states; that is, we write

$$H_m = T_m + H_m^{(\mathrm{el})}. \tag{9.3}$$

All types of intermolecular Coulomb interactions are included in V_{mn}: the intermolecular electron–electron interaction $V_{mn}^{(\mathrm{el-el})}$, the intermolecular coupling among the nuclei $V_{mn}^{(\mathrm{nuc-nuc})}$, and the electron–nuclei coupling $V_{mn}^{(\mathrm{el-nuc})}$ (between the electrons of molecule m with the nuclei of molecule n) as well as the coupling $V_{mn}^{(\mathrm{nuc-el})}$, where electrons and nuclei have been interchanged.

The present chapter is devoted to EET where electron delocalization across different molecules is unimportant. Therefore, we expand the aggregate Hamiltonian, Eq. (9.2), in terms of the adiabatic electronic states, $\varphi_{ma}(r_m; R_m)$, of the individual

molecules m. This facilitates a classification of transfer processes with respect to intramolecular electronic excitations. The label a counts the actual electronic state (S_0, S_1, etc.). These states are defined via the stationary Schrödinger equation for a given monomer (cf. Eq. (2.12))

$$H_m^{(\text{el})}(R_m)\varphi_{ma}(r_m; R_m) = U_{ma}(R_m)\varphi_{ma}(r_m; R_m). \tag{9.4}$$

The U_{ma} are the corresponding monomer PESs. Note that states belonging to different monomers are not orthogonal.[3]

Next, we construct an expansion basis for the electronic states of the total aggregate. This will be done in analogy to the treatment presented in Section 2.4. First, we define the Hartree product ansatz (see Eq. (2.25)),

$$\phi_A^{(\text{HP})}(r; R) = \prod_{m=1}^{N_{\text{mon}}} \varphi_{ma_m}(r_m; R_m), \tag{9.5}$$

with A covering the whole set of monomer quantum numbers a_m and describing the electronic configuration of the *total* aggregate (r and R abbreviate the total aggregate electronic and nuclear coordinates, respectively).

In a second step, we generate an antisymmetric wave function (see Eq. (2.26)):

$$\phi_A^{(\text{AS})}(r; R) = \frac{1}{\sqrt{N_{\text{p}}!}} \sum_{\text{perm}} (-1)^p \mathcal{P}\left[\phi_A^{(\text{HP})}(r; R)\right]. \tag{9.6}$$

Here, $\mathcal{P}$ generates a permutation of electron coordinates of different monomers in the aggregate, and p counts the number, N_{p}, of permutations.[4]

In contrast to the Hartree–Fock procedure of Section 2.4, however, for simplicity, the monomer wave functions $|\varphi_{ma_m}\rangle$ are assumed to be known and not the subject to a variational procedure. We note again that the functions equation (9.6) are neither orthogonal nor normalized. This becomes particularly obvious upon expanding the Schrödinger equation for the aggregate electronic state $|\psi\rangle$ with respect to the basis equation (9.6). We write

$$\psi(r; R) = \sum_A C_A \phi_A^{(\text{AS})}(r; R) \tag{9.7}$$

and obtain

$$\sum_B \left(\left\langle \phi_A^{(\text{AS})} | H_{\text{agg}} | \phi_B^{(\text{AS})} \right\rangle - E \left\langle \phi_A^{(\text{AS})} | \phi_B^{(\text{AS})} \right\rangle \right) = 0. \tag{9.8}$$

As an example, let us consider a simple aggregate consisting of two monomers (*molecular dimer*). At the moment, it suffices to concentrate on the electronic part $V_{12}^{(\text{el–el})}$ of the intermolecular interaction. Then, one recovers matrix elements of the Coulomb interaction, which describe the direct and the exchange contributions

---

3) The present use of nonorthogonal monomer states is similar to the treatment of bridge-mediated electron transfer in a DA complex discussed in Section 7.2.1.

4) The number N_{p} of necessary permutations is obtained as $(\sum_m N_m)!/\prod_m(N_m!)$, where N_m denotes the number of electrons of the monomer m.

(cf. Coulomb and exchange operator in Eqs. (2.29) and (2.30)). For the dimer, we have

$$
\left\langle \phi^{(AS)}_{a_1 a_2} \middle| V^{(el-el)}_{12} \middle| \phi^{(AS)}_{b_1 b_2} \right\rangle
$$

$$
= \int dr_1 dr_2 \frac{1}{\sqrt{N_p!}} \sum_{\text{perm}} (-1)^p P \varphi^*_{1a_1}(r_1; R_1) \varphi^*_{2a_2}(r_2; R_2)
$$

$$
\times V^{(el-el)}_{12} \frac{1}{\sqrt{N_p!}} \sum_{\text{perm}} (-1)^{p'} P' \varphi_{2b_2}(r_2; R_2) \varphi_{1b_1}(r_1; R_1)
$$

$$
\equiv J^{(el-el)}_{12}(a_1 a_2, b_2 b_1) - K^{(el-el)}_{12}(a_1 a_2, b_2 b_1). \tag{9.9}
$$

The direct Coulomb interaction J_{12} is given by a single term. But the exchange part $K^{(el-el)}_{12}(a_1 a_2, b_2 b_1)$ contains different contributions, depending on the number of electrons that have been interchanged between the two monomers. The case where only a single electron has been exchanged between certain molecular orbitals is given in Eq. (9.227). A closer inspection of Eq. (9.227) reveals that the spatial overlap between the two molecular orbitals, which belong to monomers 1 and 2, is responsible for the exchange contribution (cf. Figure 9.2). Such a wave function overlap decreases exponentially with increasing intermolecular distance. Usually, for distances larger than few angstroms, one can neglect the exchange contributions to the interaction energy.

In the following discussion, we concentrate on aggregates where the mutual distances between the molecules are large enough to neglect the intermolecular exchange terms. This means that we can use the Hartree product ansatz (9.5) for the electronic wave function of the aggregate. As a consequence of the neglect of intermolecular wave function overlap, we can assume $\langle \varphi_{ma} | \varphi_{nb} \rangle = \delta_{ma,nb}$; thus, the states $\phi^{(HP)}_A$ form an orthogonal basis. The expansion of the Hamiltonian equation (9.2)

$$
H_{\text{agg}} = \sum_{A,B} \langle \phi^{(HP)}_A | H_{\text{agg}} | \phi^{(HP)}_B \rangle \times |\phi^{(HP)}_A \rangle \langle \phi^{(HP)}_B | \tag{9.10}
$$

results in the following matrix elements:

$$
\langle \phi^{(HP)}_A | H_{\text{agg}} | \phi^{(HP)}_B \rangle = \sum_m \langle \phi^{(HP)}_A | H_m | \phi^{(HP)}_B \rangle + \frac{1}{2} \sum_{m,n} \langle \phi^{(HP)}_A | V_{mn} | \phi^{(HP)}_B \rangle
$$

$$
= \sum_m \langle \varphi_{ma_m} | H_m | \varphi_{mb_m} \rangle \prod_{k \neq m} \delta_{a_k b_k}
$$

$$
+ \frac{1}{2} \sum_{m,n} \langle \varphi_{ma_m} \varphi_{na_n} | V_{mn} | \varphi_{nb_n} \varphi_{mb_m} \rangle \prod_{k \neq m,n} \delta_{a_k b_k}. \tag{9.11}
$$

We abbreviate the monomer Hamiltonian by

$$
H_m(ab) = \langle \varphi_{ma} | H_m | \varphi_{mb} \rangle, \tag{9.12}
$$

and the Coulomb matrix element by

$$
J_{mn}(ab, cd) \equiv \langle \varphi_{ma} \varphi_{nb} | V_{mn} | \varphi_{nc} \varphi_{md} \rangle. \tag{9.13}
$$

Accordingly, the overall aggregate Hamiltonian takes the form

$$H_{\text{agg}} = \sum_m \sum_{a,b} H_m(ab)|\varphi_{ma}\rangle\langle\varphi_{mb}|$$
$$+ \frac{1}{2}\sum_{m,n}\sum_{a,b,c,d} J_{mn}(ab,cd)|\varphi_{ma}\varphi_{nb}\rangle\langle\varphi_{nc}\varphi_{md}|. \tag{9.14}$$

The quantity $|\varphi_{ma}\varphi_{nb}\rangle\langle\varphi_{nc}\varphi_{md}|$ has to be understood as the product of the transition operators $|\varphi_{ma}\rangle\langle\varphi_{md}|$ and $|\varphi_{nb}\rangle\langle\varphi_{nc}|$. Moreover, the expression implies that H_{agg} acts in the state space spanned by the states $\phi^{\text{HP}}_{\{a\}}$, Eq. (9.5), but avoids a notation where $|\varphi_{ma}\rangle\langle\varphi_{mb}|$ and $|\varphi_{ma}\varphi_{nb}\rangle\langle\varphi_{nc}\varphi_{md}|$ act on the unit operator $\mathbf{1} = \sum_A |\phi^{\text{(HP)}}_A\rangle\langle\phi^{\text{(HP)}}_A|$ of the electronic state space. However, any use of H_{agg} has to be understood in this way.

Let us inspect the different types of matrix elements involved in H_{agg}, Eq. (9.14). Those of the monomer Hamiltonians read in more detail

$$H_m(ab) = \delta_{ab}(T_m + U_{ma}) + (1 - \delta_{ab})\hat{\Theta}_{mab}, \tag{9.15}$$

with the operator $\hat{\Theta}_{mab}$ of nonadiabatic coupling, Eq. (2.17), and the PES that covers the diagonal part of the nonadiabatic coupling operator (see Eq. (9.4)). The matrix elements of the Coulomb interaction are analyzed in the following section.

9.2.1 The Intermolecular Coulomb Interaction

We specify Eq. (9.13) by noting the separation of the intermolecular Coulomb coupling in electronic and nuclear contributions. The respective matrix elements of Eq. (9.13) can be written as

$$J_{mn}(ab,cd) \equiv \int dr_m dr_n\ \varphi^*_{ma}(r_m)\varphi^*_{nb}(r_n)V^{\text{(el-el)}}_{mn}(r_m,r_n)\varphi_{nc}(r_n)\varphi_{md}(r_m)$$
$$+ \delta_{bc}\int dr_m\varphi^*_{ma}(r_m)V^{\text{(el-nuc)}}_{mn}(r_m,R_n)\varphi_{md}(r_m)$$
$$+ \delta_{ad}\int dr_n\varphi^*_{nb}(r_n)V^{\text{(nuc-el)}}_{mn}(R_m,r_n)\varphi_{nc}(r_n)$$
$$+ \delta_{ad}\delta_{bc}V^{\text{(nuc-nuc)}}_{mn}. \tag{9.16}$$

To further simplify the matrix elements, we take into consideration the antisymmetric character of the electronic wave functions. For example, focusing on the r_m integral in the electron–electron interaction part, we may write

$$\int dr_m\ \varphi^*_{ma}(r_m)V^{\text{(el-el)}}_{mn}(r_m,r_n)\varphi_{md}(r_m)$$
$$= \int dr_m \sum_{i\in m}\sum_{j\in n}\frac{e^2}{|\boldsymbol{r}_{mi}-\boldsymbol{r}_{nj}|}\varphi^*_{ma}(\boldsymbol{r}_{m1},\dots,\boldsymbol{r}_{mN})\varphi_{md}(\boldsymbol{r}_{m1},\dots,\boldsymbol{r}_{mN}). \tag{9.17}$$

Here, the index $i(j)$ refers to the electrons at monomer $m(n)$ with respective coordinates $\boldsymbol{r}_{mi}$ ($\boldsymbol{r}_{nj}$). Next, the electron coordinate summation is rewritten, replacing the actual coordinate $\boldsymbol{r}_{mi}$ by $\boldsymbol{r}_{m1}$. Then, the antisymmetry of φ^*_{ma} and φ_{md} allows us to shift $\boldsymbol{r}_{m1}$ again to the first position in the electronic wave functions. The $\boldsymbol{r}_{m2}$- to

$\boldsymbol{r}_{mN}$-integration only affects the wave function product, and we are motivated to introduce

$$\varrho_{ab}^{(m)}(\boldsymbol{x}) = eN_m \int dr_m \delta(\boldsymbol{x} - \boldsymbol{r}_{m1})\varphi_{ma}^*(r_m)\varphi_{mb}(r_m). \tag{9.18}$$

The δ-function guarantees that the integration covers all electronic coordinates of monomer m except the electronic coordinate $\boldsymbol{r}_{m1}$, which is replaced by the new variable $\boldsymbol{x}$. If Eq. (9.18) is considered when $a = b$, the quantity $\varrho_{aa}^{(m)}(\boldsymbol{x})$ gives the electronic charge density in the electronic state φ_{ma} of molecule m. If $a \neq b$, the so-called *transition charge density* $\varrho_{ab}^{(m)}$ is obtained connecting the electronic states φ_{ma} and φ_{mb} (see Figure 9.7).

For the further treatment of the matrix elements, Eq. (9.16), we rearrange the Coulomb potentials and introduce densities according to Eq. (9.18). This results in a twofold coordinate integration,

$$\begin{aligned}
J_{mn}(ab, cd) = \int d^3\boldsymbol{x}d^3\boldsymbol{x}' \; \frac{\varrho_{ad}^{(m)}(\boldsymbol{x})\varrho_{bc}^{(n)}(\boldsymbol{x}')}{|\boldsymbol{x} - \boldsymbol{x}'|} \\
- \delta_{bc} \int d^3\boldsymbol{x} \sum_{\nu \in n} \frac{\varrho_{ad}^{(m)}(\boldsymbol{x}) \, eZ_\nu}{|\boldsymbol{x} - \boldsymbol{R}_\nu|} - \delta_{ad} \int d^3\boldsymbol{x}' \sum_{\mu \in m} \frac{eZ_\mu \, \varrho_{bc}^{(n)}(\boldsymbol{x}')}{|\boldsymbol{R}_\mu - \boldsymbol{x}'|} \\
+ \delta_{ad}\delta_{cb}V^{(\text{nuc-nuc})}.
\end{aligned} \tag{9.19}$$

This expression further simplifies if we introduce the molecular charge density where electrons as well as nuclei contribute

$$n_{ab}^{(m)}(\boldsymbol{x}) = \varrho_{ab}^{(m)}(\boldsymbol{x}) - \delta_{ab} \sum_{\mu \in m} eZ_\mu \delta(\boldsymbol{x} - \boldsymbol{R}_\mu). \tag{9.20}$$

Now, Eq. (9.19) turns into the form

$$J_{mn}(ab, cd) = \int d^3\boldsymbol{x}d^3\boldsymbol{x}' \; \frac{n_{ad}^{(m)}(\boldsymbol{x})n_{bc}^{(n)}(\boldsymbol{x}')}{|\boldsymbol{x} - \boldsymbol{x}'|}. \tag{9.21}$$
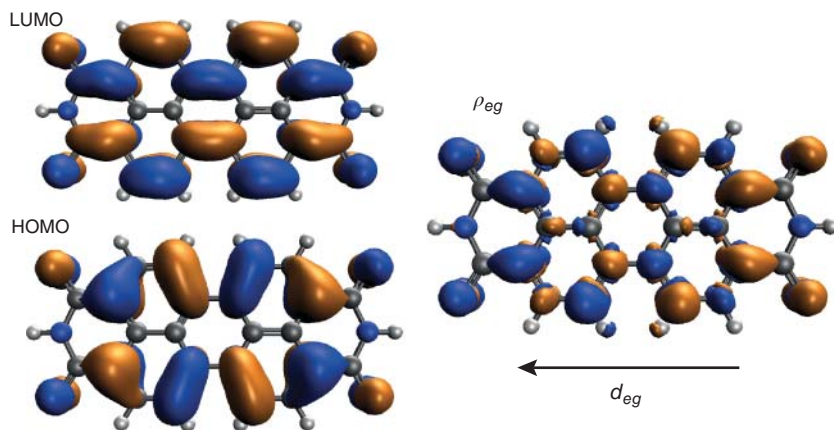
Figure 9.7 Transition density ρ_{eg} (Eq. (9.18)) for the S_0 to S_1 transition of perylene bisimide, which is well described by a HOMO to LUMO transition. Also shown is the transition dipole vector, which follows from Eq. (9.27).

The Coulomb matrix elements can be computed via simple spatial integrals with respect to the charge density of molecules m and n. The introduced molecular charge density $n_{aa}^{(m)}$ indicates the amount of unbalanced charge distribution in the neutral molecule due to the continuous spatial distribution of the negative electron charge and the localized positive charge of the nuclei. The neutrality of the molecule (zero total charge) is guaranteed by the property $\int d^3x \, n_{aa}^{(m)}(x) = 0$. If $a \neq b$, then the molecular charge density reduces to the electronic transition density.

There exists an approximation of Eq. (9.21), which is of great practical value. Here, the continuous charge distribution is replaced by *atomic centered partial charges q_μ*:

$$J_{mn}(ab, cd) = \sum_{\mu, \nu} \frac{q_{m\mu}(ad) q_{n\nu}(bc)}{|\boldsymbol{R}_{m\mu} - \boldsymbol{R}_{n\nu}|} \ . \tag{9.22}$$

The $\boldsymbol{R}_{m\mu}$ and $\boldsymbol{R}_{n\nu}$ give the spatial positions of all atoms of molecules m and n, respectively, and the $q_{m\mu}(ad)$ and $q_{n\nu}(bc)$ are the related partial charges.[5] The electronic quantum numbers indicate whether they belong to transition charges ($a \neq d$ and $b \neq c$) or not.

9.2.1.1 Dipole–Dipole Coupling

One cannot invoke any further approximation if the electron–nuclei densities in Eq. (9.21) have a spatial extension that is comparable to the distance between monomers. However, if the intermolecular distance is large compared to the extension of the densities, there is no need to account for all the details of the latter. To construct an approximate expression for the Coulomb matrix elements, we will carry out a treatment similar to that of Section 2.7.1, where it is shown how to remove the short-range part of the Coulomb interaction by employing a multipole expansion. To this end, the Coulomb matrix element, Eq. (9.21), is written in terms of coordinates related to the center of masses, $\boldsymbol{X}_m$ and $\boldsymbol{X}_n$, of a pair of monomers. We further introduce the intermolecular distance $\boldsymbol{X}_{mn} = \boldsymbol{X}_m - \boldsymbol{X}_n$ and replace $1/|x - x'|$ in Eq. (9.21) by $1/|\boldsymbol{X}_{mn} + x - x'|$. In a next step, the multipole expansion in powers of $|x - x'|/|\boldsymbol{X}_{mn}|$ is performed up to the second-order term (cf. Section 2.7.1). Under the assumption that the intermolecular distance is large compared to the extension of the monomer densities at m and n, typical values of x and x' are small compared to $|\boldsymbol{X}_{mn}|$.

We abbreviate $\boldsymbol{X}_{mn} = \boldsymbol{X}$ and $x - x' = \boldsymbol{r}$ and obtain

$$\frac{1}{|\boldsymbol{X} + \boldsymbol{r}|} \approx \frac{1}{|\boldsymbol{X}|} + \boldsymbol{r}\nabla_X \frac{1}{|\boldsymbol{X}|} + \frac{1}{2} (\boldsymbol{r}\nabla_X)(\boldsymbol{r}\nabla_X) \frac{1}{|\boldsymbol{X}|}. \tag{9.23}$$

The two types of derivatives read in detail

$$\boldsymbol{r}\nabla_X \frac{1}{|\boldsymbol{X}|} = -\frac{\boldsymbol{r}\boldsymbol{X}}{|\boldsymbol{X}|^3} \tag{9.24}$$

and

$$\frac{1}{2}(\boldsymbol{r}\nabla_X)(\boldsymbol{r}\nabla_X) \frac{1}{|\boldsymbol{X}|} = -\frac{\boldsymbol{r}^2}{2|\boldsymbol{X}|^3} + \frac{3(\boldsymbol{r}\boldsymbol{X})^2}{2|\boldsymbol{X}|^5}. \tag{9.25}$$

---

5) These partial charges can be obtained, for instance, by fitting the electrostatic field near monomer m or n as shown by Madjet et al. [5].

If we insert the obtained approximation into Eq. (9.21), the zero- and the first-order contributions vanish due to charge neutrality (there remain x- or x'-integrals of the density resulting in zero contributions). Looking at the second-order terms, only those contribute that simultaneously contain an x- and an x'-dependence:

$$J_{mn}(ab, cd) \approx \int d^3x \, d^3x' \; n_{ad}^{(m)}(x + X_m) n_{bc}^{(n)}(x' + X_n)$$
$$\times \left(-\frac{xx'}{|X_{mn}|^3} - \frac{3(xX_{mn})(x'X_{mn})}{|X_{mn}|^5} \right). \tag{9.26}$$

We note the general definition of the molecular dipole moment, which is independent of the actual choice of X_m; that is, we can set $X_m = 0$ and obtain

$$d_{mab} = \int d^3x \, x n_{ab}^{(m)}(x) = \int d^3x \, x \varrho_{ab}^{(m)}(x) - \delta_{ab} \sum_{\mu \in m} eZ_\mu R_\mu \tag{9.27}$$

and arrive at the Coulomb matrix element in *dipole–dipole approximation*

$$J_{mn}(ab, cd) \approx \frac{d_{mad} d_{nbc}}{|X_{mn}|^3} - 3 \frac{(X_{mn} d_{mad})(X_{mn} d_{nbc})}{|X_{mn}|^5}. \tag{9.28}$$

Often, it is underlined that *point dipoles* are used to compute the interaction.[6] Figure 9.8 shows a comparison between the full Coulomb coupling (including the exchange contribution) and the dipole approximation for a DA pair in different alignments. From Figure 9.8c, it is seen that as expected the dipole approximation breaks down for small DA distances.

9.2.2 The Two-level Model

In this section, we specify the Hamiltonian, Eq. (9.14), for a situation where, besides the electronic ground state, S_0, only the first excited singlet state, S_1, of the different molecules is involved in the EET. Such a restriction is possible, for example, if a single S_1 state is initially excited, and if the S_1 states of all other molecules have approximately the same transition energy. The incorporation of further states such as higher excited singlet states or triplet states is straightforward.

9.2.2.1 Classification of the Coulomb Interactions

We consider the matrix elements of the Coulomb interaction, $J_{mn}(ab, cd)$. According to the two-level assumption, all electronic quantum numbers can take only two values, corresponding to the ground state S_0 ($a = g$) and the excited state S_1 ($a = e$). In Table 9.1, we summarize the physical processes described by the different matrix elements and the combinations of electronic state indices they correspond to. In row I, all matrix elements are listed that describe the electrostatic interaction between charge densities located at monomers m and n. Row II of Table 9.1 contains

---

6) A so-called extended dipole is introduced if the negative and positive charges are represented independently by their center of mass, and if the resulting two spatially separated point charges are used to define a dipole moment.
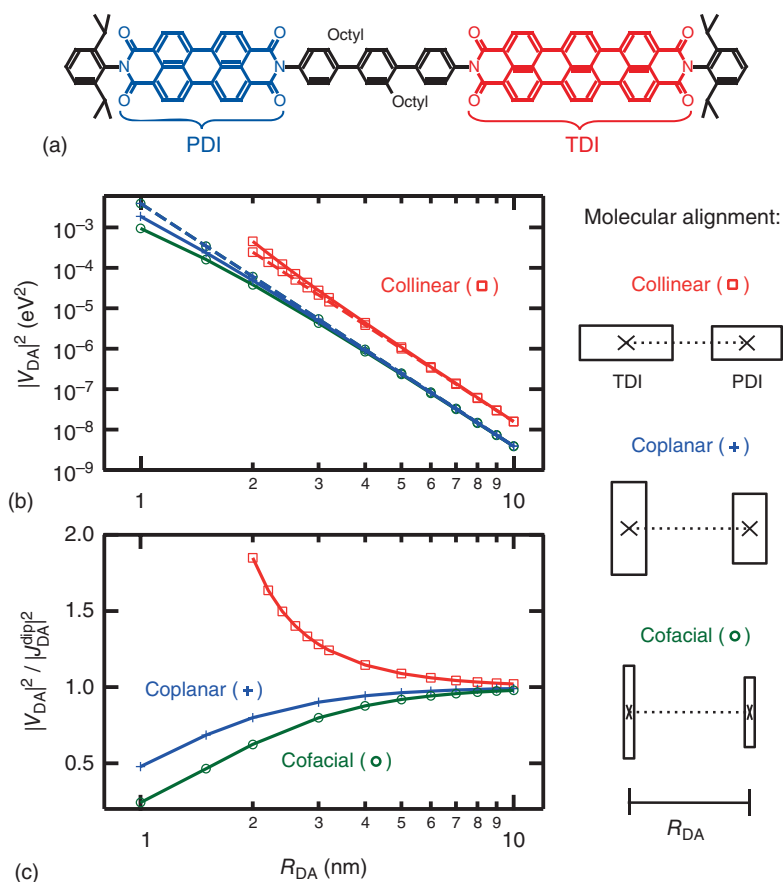
Figure 9.8 (a) Rylene diimide dyad with a perylene diimide (PDI) donor and a terrylene diimide (TDI) acceptor. (b) Distance dependence of the full Coulomb coupling V_{DA} (solid line, including the exchange contribution) and the dipole approximation J_{DA}^{dip} (dashed line) for different molecular alignments (S_0-S_1 transitions, the oligophenylene bridge was not included; note the logarithmic scale). (c) Ratio between full Coulomb and dipole–dipole coupling (reprinted with permission from Fückel et al. [6]; copyright (2008) American Institute of Physics).

those matrix elements that are responsible for the interaction of the transition from g to e (or reverse) at monomer m with the charge density either of the state g or e at monomer n. Next, we have those matrix elements that cause the motion of the excitation energy between different monomer sites in the aggregate (row III). They describe the transition of monomer m from the ground to the excited state, while the reverse process takes place at monomer n. This situation is sketched in Figure 9.1. Finally, the last row IV contains the processes of simultaneous excitation or deexcitation of both monomers.

If the deviation of $n_{aa}^{(m)}$ and $n_{bb}^{(n)}$ from zero is small enough (locally balanced charge distributions in the monomers), the contributions of both quantities can be neglected, and the matrix elements of types $J_{mn}(ab, bd)$ and $J_{mn}(ab, ca)$ vanish.

Table 9.1 Classification of the Coulomb interaction matrix elements in Eq. (9.16) for electronic two-level systems (note that J_{mn} is symmetric with respect to the site indices).

	Matrix element	Interaction process
(I)	$J_{mn}(gg, gg)$	Between charges
	$J_{mn}(ee, ee)$	at monomers m and n
	$J_{mn}(ge, eg)$	
	$J_{mn}(eg, ge)$	
(II)	$J_{mn}(eg, gg)$	Between transitions at
	$J_{mn}(gg, ge)$	monomer m with charges at n
	$J_{mn}(ge, ee)$	
	$J_{mn}(ee, eg)$	
(III)	$J_{mn}(eg, eg)$	Between $S_0 \rightarrow S_1$ transition at monomer m
	$J_{mn}(ge, ge)$	and $S_1 \rightarrow S_0$ transition at n (and reverse)
(IV)	$J_{mn}(ee, gg)$	Simultaneous excitation and deexcitation
	$J_{mn}(gg, ee)$	of monomers m and n

The whole set of Coulomb matrix elements, Eq. (9.21), reduces to the matrix element of row III:

$$J_{mn}(eg, eg) \equiv J_{mn} = \int d^3x d^3x' \ \frac{\varrho_{eg}^{(m)}(\boldsymbol{x})\varrho_{ge}^{(n)}(\boldsymbol{x}')}{|\boldsymbol{x} - \boldsymbol{x}'|}. \tag{9.29}$$

It is responsible for EET among different monomers and is usually called *excitonic coupling*. The electronic transition densities give a measure for the degree of *local* wave function overlap between the electronic ground state and the excited state of monomer m.

To present the excitonic coupling in dipole–dipole approximation, we note that the dipole moments, Eq. (9.27), $\boldsymbol{d}_{meg} \equiv \boldsymbol{d}_m$ reduce to electronic transition dipole moments. Thus, the matrix element of Eq. (9.28) can be cast into the form

$$J_{mn} = \kappa_{mn} \frac{|\boldsymbol{d}_m||\boldsymbol{d}_n^*|}{|\boldsymbol{X}_{mn}|^3}. \tag{9.30}$$

Here, we introduced the orientation factor

$$\kappa_{mn} = \boldsymbol{n}_m \ \boldsymbol{n}_n - 3(\boldsymbol{e}_{mn} \ \boldsymbol{n}_m)(\boldsymbol{e}_{mn} \ \boldsymbol{n}_n), \tag{9.31}$$

where $\boldsymbol{n}_m$, $\boldsymbol{n}_n$, and $\boldsymbol{e}_{mn}$ are the unit vectors pointing in the directions of the transition dipole moments $\boldsymbol{d}_m$, $\boldsymbol{d}_n$, and the distance vector $\boldsymbol{X}_{mn}$, respectively. As already stated, this approximate form of the Coulomb interaction is applicable if the spatial extension of both transition densities appearing in Eq. (9.29) is small compared to the intermolecular distance $|\boldsymbol{X}_{mn}|$.

9.2.3 Single and Double Excitations of the Aggregate

The aggregate Hamiltonian equation (9.14) includes all possible excitations of the molecular aggregate, with the majority never being observable in the experiment. Therefore, it is advantageous to classify the total wave function according to the number of excited molecules, N^*, starting with the ground state and including elementary single and double excitation states. In what follows this will be explained for the case of the two-level model. This is particularly useful when studying optical properties of aggregates where the number of excited molecules can be related to the number of photons absorbed by a single aggregate. The following considerations complement those of the foregoing section by introducing this ordering scheme. According to possible nonbalanced charge distributions in the ground and excited states of the various molecules, there appear different intermolecular electrostatic interactions. However, in most of the exciton literature these couplings are not considered. In passing, we note that such electrostatic couplings can also be introduced between the molecules of the aggregate and those forming the environment (a solvent, for example).

The quantum mechanical electronic state of the aggregate $\phi_A^{(\mathrm{HP})}$ contains the subset of N^* excited molecules and the subset of $N_{\mathrm{mon}} - N^*$ molecules in the ground state. The superposition of all states with fixed N^* can be used as an ansatz for the N^*-exciton eigenstate of the Hamiltonian (9.14). Multiexciton states play an important role for the nonlinear optical properties of molecular aggregates. As an example, we consider single-exciton states ($N^* = 1$) as well as two-exciton states ($N^* = 2$, cf. Figure 9.9). The single-exciton state can be reached from the aggregate ground state via an optical excitation process that involves the absorption of a single photon. A subsequent absorption step may lead from the single- to the two-exciton state (excited state absorption).
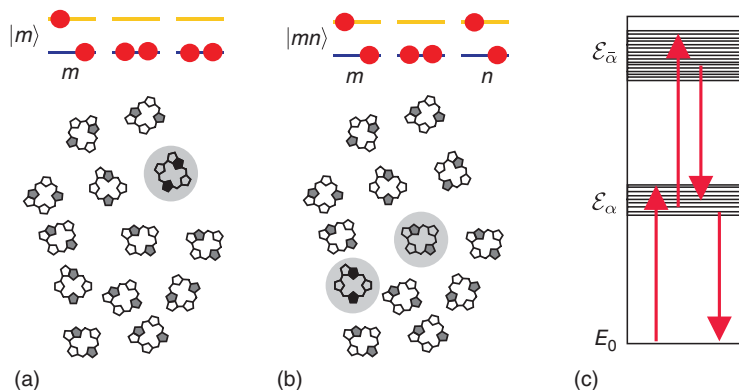
Figure 9.9 Schematic illustration of the presence of a singly excited state (a), Eq. (9.34), and a doubly excited state (b), Eq. (9.35), in the type of chromophore complex introduced in Figure 9.6. (c) Energy-level scheme of delocalized aggregate states including the 8 one-exciton states, Eq. (9.67), with energies $E(\alpha)$ and the 28 two-exciton states, Eq. (9.70), with energies $E(\bar{\alpha})$. Optical excitation as well as nonradiative excited state decay is labeled by arrows.

The classification with respect to the number of excited molecules is easily achieved by the following rearrangement of the electronic aggregate state completeness relation:

$$\sum_A |\phi_A^{(HP)}\rangle\langle\phi_A^{(HP)}| = |0\rangle\langle0| + \sum_m |m\rangle\langle m| + \sum_{m,n>m} |mn\rangle\langle mn| + \cdots \quad (9.32)$$

The first term contains the aggregate ground state wave function

$$|0\rangle = \prod_m |\varphi_{mg}\rangle. \quad (9.33)$$

The presence of a single excitation in the aggregate is accounted for by the second term according to (cf. Figure 9.9)

$$|m\rangle = |\varphi_{me}\rangle\prod_{n\neq m} |\varphi_{ng}\rangle. \quad (9.34)$$

The third term in Eq. (9.32) corresponds to the presence of two excitations in the aggregate (Figure 9.9, the expression does not exist for $m = n$ due to the Pauli principle):

$$|mn\rangle = |\varphi_{me}\rangle|\varphi_{ne}\rangle\prod_{k\neq m,n} |\varphi_{kg}\rangle. \quad (9.35)$$

The restriction with respect to the m- and n-summation introduced in Eq. (9.32) avoids double counting of twofold excited states. Higher excitations can be considered in the same manner but are of less importance for the interpretation of the majority of experiments.

The introduced ordering of states results in the following separation of the total Hamiltonian:

$$H_{agg} = H_{agg}^{(0)} + H_{agg}^{(1)} + H_{agg}^{(2)} + H_{agg}^{(od)}, \quad (9.36)$$

with the ground state contribution

$$H_{agg}^{(0)} = \mathcal{H}_0|0\rangle\langle0|, \quad (9.37)$$

the part describing the presence of a single excitation

$$H_{agg}^{(1)} = \sum_{m,n}\mathcal{H}_{mn}|m\rangle\langle n|, \quad (9.38)$$

and the two excitation contribution

$$H_{agg}^{(2)} = \sum_{k,l>k}\sum_{m,n>m}\mathcal{H}_{kl,mn}|kl\rangle\langle mn|. \quad (9.39)$$

Off-diagonal contributions (for example $H_{agg}^{(10)}$) are all included in $H_{agg}^{(od)}$. They may include terms describing optical transition due to the presence of a radiation field. In contrast to the diagonal contributions, they do not conserve the number of excitations.[7] The quantities $\mathcal{H}_0$, $\mathcal{H}_{mn}$, and $\mathcal{H}_{kl,mn}$ represent vibrational Hamiltonians, partially with matrix character, and are derived next.

---

7) Note that there is an alternative representation of the exciton Hamiltonian in terms of creation and annihilation operators defined in within second quantization. For details, see Section 9.10.1.

9.2.3.1 The Ground State Matrix Element

From the matrix element, Eq. (9.11), of the overall aggregate Hamiltonian, we obtain (all electronic quantum numbers refer to the electronic ground state)

$$\mathcal{H}_0 \equiv \langle 0|H_{\mathrm{agg}}|0\rangle = \sum_m H_{mg} + \frac{1}{2}\sum_{m,n} J_{mn}(gg, gg). \tag{9.40}$$

The matrix element can be understood as an aggregate vibrational Hamiltonian separating into the overall nuclear kinetic energy $T_{\mathrm{nuc}} = \sum_m T_m$ and a PES

$$\mathcal{U}_0(R) = \sum_m U_{mg}(R_m) + \frac{1}{2}\sum_{m,n} J_{mn}(gg, gg)(R_m, R_n). \tag{9.41}$$

This PES is formed by the contributions of the monomers as well as by the mutual electrostatic (Coulomb) interaction among the different molecules. (The latter contribution vanishes if we can replace all molecular charge densities $n_{gg}^{(m)}$ by zero.)

9.2.3.2 The Single Excited State Matrix Elements

For computing matrix elements of the type $\langle k|H_{\mathrm{agg}}|l\rangle$, the index k may be equal or unequal to l. We start with the first case and obtain, using Eq. (9.11),

$$\langle k|H_{\mathrm{agg}}|k\rangle = H_{ke} + \sum_{m\neq k} H_{mg} + \frac{1}{2}\sum_n J_{kn}(eg, ge) + \frac{1}{2}\sum_m J_{mk}(ge, eg)$$
$$+ \frac{1}{2}\sum_{m,n\neq k} J_{mn}(gg, gg). \tag{9.42}$$

The contributions due to the vibrational Hamiltonians are directly obtained by considering $a_m = e$ for $m = k$ and $a_m = g$ otherwise in Eq. (9.11). The matrix elements of Eq. (9.11) concerning V_{mn} take into consideration that $m \neq n$; therefore, we have to deal with the cases $m = k$ ($a_m = e$) but $n \neq k$; $n = k$ but $m \neq k$; and $m, n \neq k$. If the charge distribution of electrons and nuclei is well balanced in both molecules, the Coulomb interactions J_{kn}, J_{mk}, and J_{mn} do not contribute. Changing to the off-diagonal parts of the matrix element, that is the case $l \neq k$, we arrive at

$$\langle k|H_{\mathrm{agg}}|l\rangle = \frac{1}{2}J_{kl}(eg, eg) + \frac{1}{2}J_{lk}(ge, ge), \tag{9.43}$$

where the monomer Hamiltonians in $\sum_m H_m$ do not contribute. If $m = k$ ($m = l$), then $\delta_{a_l b_l}$ ($\delta_{a_k b_k}$) appear (see the product of δ-symbols in Eq. (9.11)) and are equal to zero. If $m \neq k$ and $m \neq l$, the two expressions $\delta_{a_l b_l}$ and $\delta_{a_k b_k}$ vanish simultaneously. From the coupling Hamiltonian, only two nonvanishing contributions remain and correspond to $m = k$, $n = l$ and $m = l$, $n = k$.

The single-excitation matrix elements of the aggregate Hamiltonian can be cast into the following form:

$$\mathcal{H}_{mn} = \langle m|H_{\mathrm{agg}}|n\rangle = \delta_{mn}[T_{\mathrm{nuc}} + \mathcal{U}_0(R)] + \mathcal{U}_{mn}(R), \tag{9.44}$$

with the PES matrix

$$\mathcal{U}_{mn}(R) = \delta_{mn}U_{meg}(R) + [1 - \delta_{mn}]J_{mn}(eg, eg; R_m, R_n), \tag{9.45}$$

and with

$$U_{meg}(R) = U_{me}(R_m) - U_{mg}(R_m)$$
$$+ \sum_{k \neq m} \left(J_{mk}(eg, ge; R_m, R_k) - J_{mk}(gg, gg; R_m, R_k) \right). \tag{9.46}$$

This expression defines the PES of the mth molecule's excitation. It includes the Coulomb interaction with all other molecules if the mth molecule is in its ground state as well as in its first excited state. The Coulomb matrix elements may strongly affect the PES for those cases where the distances and mutual orientations among the molecules change. If this is not the case, however, the J_{mk} introduce a constant energy shift to U_{me} as well as U_{mg}.

9.2.3.3 The Double Excited State Matrix Elements

The matrix elements to be discussed are of the type $\langle kl|H_{\text{agg}}|k'l'\rangle$. We start with the contributions due to the monomer Hamiltonians and get

$$\langle kl| \sum_m H_m |k'l'\rangle = \delta_{kk'}\delta_{ll'} \left(H_{ke} + H_{le} + \sum_{m \neq k,l} H_{mg} \right). \tag{9.47}$$

The two Kronecker δ-functions are expected since we consider a monomer matrix element with one of the two excited state wave functions producing an overlap expression, for example $\langle \varphi_{le}|\varphi_{la}\rangle$ (the case $k = l'$ and $l = k'$ is impossible since $k < l$ and $k' < l'$).

The discussion of the matrix element with respect to the intermolecular Coulomb interaction, V_{mn}, requires more attention. We distinguish the cases where the indices k and l from the bra part of the matrix elements do or do not coincide with m and n of the Coulomb potential (note the replacement of $1/2 \sum_{m,n} V_{mn}$ by $\sum_{m,n>m} V_{mn}$). We first treat the case $m = k$ and $n = l$ and obtain

$$\langle kl|V_{kl}|k'l'\rangle = \delta_{kk'}\delta_{ll'}J_{kl}(ee, ee). \tag{9.48}$$

Next, we consider $m = k$ and $n \neq l$

$$\langle kl| \sum_{n \neq l} V_{kn}|k'l'\rangle = \delta_{kk'}\delta_{ll'} \sum_{n \neq l} J_{kn}(eg, ge) + \delta_{lk'}J_{kl'}(eg, eg). \tag{9.49}$$

The first and the second terms on the right-hand side follow from the case $l = l'$. However, one may also consider the case $l = k'$, which leads to the third term on the right-hand side. The case $k = l'$ does not contribute. In the same manner, we can treat the case $m \neq k$ and $n = l$, that is

$$\langle kl| \sum_{m \neq k} V_{ml}|k'l'\rangle = \delta_{kk'}\delta_{ll'} \sum_{m \neq k} J_{ml}(ge, eg) + \delta_{kl'}J_{k'l}(ge, ge). \tag{9.50}$$

Finally, we get

$$\langle kl| \sum_{m \neq k} \sum_{n \neq l} V_{mn}|k'l'\rangle = \delta_{kk'}\delta_{ll'} \sum_{m \neq k} \sum_{n \neq l} J_{mn}(gg, gg). \tag{9.51}$$

Collecting all terms, we obtained the following expression for the matrix element (remember $m < n$ and $k < l$)):

$$\mathcal{H}_{mn,kl} = \langle mn|H_{\text{agg}}|kl \rangle = \delta_{mk}\delta_{nl}[T_{\text{nuc}} + \mathcal{U}_0(R)] + \mathcal{U}_{mn,kl}(R), \tag{9.52}$$

with the PES matrix

$$\mathcal{U}_{mn,kl}(R) = \delta_{mk}\delta_{nl}\, U_{mn,eg}(R) + \delta_{nk}\, J_{ml}(eg,eg;R_m,R_l)$$
$$+ \delta_{ml}\, J_{nk}(eg,eg;R_k,R_n), \tag{9.53}$$

and with

$$U_{mn,eg}(R) = U_{me}(R_m) - U_{mg}(R_m) + U_{ne}(R_n) - U_{ng}(R_n)$$
$$+ J_{mn}(ee,ee;R_m,R_n) - J_{mn}(gg,gg;R_m,R_n)$$
$$+ \sum_{k \neq m,n} \big(J_{mk}(eg,ge;R_m,R_k) - J_{mk}(gg,gg;R_m,R_k)$$
$$+ J_{nk}(eg,ge;R_n,R_k) - J_{nk}(gg,gg;R_n,R_k)\big). \tag{9.54}$$

When considering double excitations of the aggregate, the new Coulomb matrix element $J_{mn}(ee,ee)$ describes the interaction between both excited molecules. The remaining Coulomb matrix elements refer to the coupling to the charge distributions of those molecules staying in the electronic ground state.

9.2.3.4 Off-Diagonal Matrix Elements and Coupling to the Radiation Field

We start with considering the matrix element between a singly excited state and the aggregate ground state and obtain

$$\langle k|H_{\text{agg}}|0 \rangle = \Theta_{keg} + \sum_m J_{km}(eg,gg). \tag{9.55}$$

The expression is determined by the nonadiabatic coupling operator of molecule k and the Coulomb matrix element accounting for the interaction of an excitation at molecule k with the electronic ground state charge distribution of all other molecules. The next type of matrix element we have to calculate is that between the doubly excited aggregate state and the ground state

$$\langle kl|H_{\text{agg}}|0 \rangle = J_{kl}(ee,gg). \tag{9.56}$$

It remains to compute the matrix elements coupling the singly excited state to the doubly excited state

$$\langle kl|H_{\text{agg}}|k' \rangle = \delta_{kk'}\left(\Theta_{leg} + J_{kl}(ee,ge) + \sum_{m \neq k} J_{ml}(ge,gg)\right)$$
$$+ \delta_{lk'}\left(\Theta_{keg} + J_{kl}(ee,eg) + \sum_{n \neq l} J_{kn}(eg,gg)\right). \tag{9.57}$$

All these matrix elements are of less interest when considering the stationary states of the aggregate since they only offer nonresonant contributions. However, they determine the processes where the degree of aggregate excitation changes (see Section 9.9).

9.2.3.5 Neglect of Intermolecular Electrostatic Coupling

For further use, we specify the results of the foregoing section to the commonly used case where the molecular charge densities n_{gg}^m and n_{ee}^m, referring to the electronic ground state and the first excited state, respectively, can be neglected. Then, the ground state contribution, Eq. (9.37), to the aggregate Hamiltonian takes the form

$$H_{\text{agg}}^{(0)} = \sum_m H_{mg} |0\rangle\langle 0|. \tag{9.58}$$

For the singly excited state part, Eq. (9.38), we get

$$H_{\text{agg}}^{(1)} = \sum_m \left(H_{me} + \sum_{n \neq m} H_{ng} \right) |m\rangle\langle m| + \sum_{m,n} J_{mn} |m\rangle\langle n|. \tag{9.59}$$

In the same way, one can specify the Hamiltonian of the doubly excited aggregate states.

9.2.4 Introduction of Delocalized Exciton States

Frenkel exciton states will be introduced as a superposition of the local excited states $|m\rangle$, Eq. (9.34), and in the case of two-exciton states by introducing a superposition of the doubly excited states, Eq. (9.35) (cf. Figure 9.9). In order to do this we consider the case where all atoms of the molecules forming the aggregate carry out only small vibrations around a fixed structure and undergo only small rearrangements upon electronic excitation. This fixed structure is characterized by the equilibrium nuclear coordinates R_0 of the aggregate electronic ground state. For such a situation, it is customary to replace the nuclear coordinates by their equilibrium values and to arrive at pure electronic Hamiltonians for the ground and excited states of the aggregate. Moreover, we again assume that electrostatic couplings among the molecules are of minor importance (the molecular charge densities, Eq. (9.20), should vanish).

For the electronic ground state, we have

$$E_0 = \sum_m E_{mg}. \tag{9.60}$$

The energies E_{mg} follow from the PES U_{mg} taken at the nuclear equilibrium configuration. The Hamiltonian for the singly excited state reads

$$H_{\text{agg}}^{(1)} = \sum_{m,n} (\delta_{mn} E_0 + E_{mn}) |m\rangle\langle n|. \tag{9.61}$$

It includes the energy matrix

$$E_{mn} = \delta_{mn} E_m + [1 - \delta_{mn}] J_{mn}(eg, eg). \tag{9.62}$$

The so-called *site energies* are deduced from Eq. (9.46) as[8]

$$E_m = U_{me}(R_0) - U_{mg}(R_0). \tag{9.63}$$

---

8) They are also often called *Franck–Condon transition energies*, since in a scheme where the energy has been drawn versus nuclear coordinates, E_m corresponds to a vertical energy difference starting at the ground state PES equilibrium value.

In the same way, we obtain the Hamiltonian of the doubly excited aggregate state:

$$H_{\text{agg}}^{(2)} = \sum_{m,n>m} \sum_{k,l>k} E_{mn,kl} |mn\rangle\langle kl|, \tag{9.64}$$

with

$$E_{mn,kl} = \delta_{mk}\delta_{nl}(E_m + E_n) + \delta_{nk}J_{ml} + \delta_{ml}J_{kn}. \tag{9.65}$$

In the present model, there is no coupling between the aggregate ground state and the singly and doubly excited states. Therefore, we may solve separate eigenvalue equations for singly and doubly excited states. To remove the unimportant ground state energy, we set in this section $E_0 = 0$. In the case of a single excitation, the eigenvalue equation reads

$$H_{\text{agg}}^{(1)} |\alpha\rangle = \mathcal{E}_\alpha |\alpha\rangle. \tag{9.66}$$

To construct the solutions to this equation, we expand the eigenstate $|\alpha\rangle$ with respect to the complete basis of singly excited states:

$$|\alpha\rangle = \sum_m c_\alpha(m)|m\rangle. \tag{9.67}$$

This expansion highlights the Frenkel exciton as a superposition of excited states of the individual molecules. Introducing this expansion into Eq. (9.66) and multiplying it by $\langle n|$ from the left yields

$$\mathcal{E}_\alpha c_\alpha(n) = \sum_m \langle n|H_{\text{agg}}^{(1)}|m\rangle c_\alpha(m) = E_n c_\alpha(n) + \sum_m J_{nm} c_\alpha(m). \tag{9.68}$$

The state $|\alpha\rangle$ is called the *exciton state*, and $\mathcal{E}_\alpha$ is the exciton energy (to underline the singly excited character of this state, it is often named one-exciton state); there exist N_{mon} one-exciton states. An expansion of $H_{\text{agg}}^{(1)}$ with respect to the exciton states leads to the *exciton Hamiltonian*

$$H_{\text{ex}} = \sum_\alpha \mathcal{E}_\alpha |\alpha\rangle\langle\alpha|. \tag{9.69}$$

To determine the eigenstates corresponding to the presence of two excitations in the considered aggregate, we have to solve the eigenvalue equation (note the replacement of α by $\tilde{\alpha}$):

$$H_{\text{el}}^{(2)} |\tilde{\alpha}\rangle = \mathcal{E}_{\tilde{\alpha}} |\tilde{\alpha}\rangle. \tag{9.70}$$

The *two-exciton* states are expanded as

$$|\tilde{\alpha}\rangle = \sum_{m,n>m} c_{\tilde{\alpha}}(mn)|mn\rangle, \tag{9.71}$$

with the expansion coefficients following from (remember $E_0 = 0$ and the definition of E_m and E_n)

$$\mathcal{E}_{\tilde{\alpha}} c_{\tilde{\alpha}}(mn) = (E_m + E_n)c_\alpha(mn) + \sum_k \left(J_{mk} c_{\tilde{\alpha}}(nk) + J_{kn} c_{\tilde{\alpha}}(km) \right). \tag{9.72}$$

Note that there are $N_{\text{mon}}(N_{\text{mon}} - 1)/2$ possible two-exciton states. The two-exciton state Hamiltonian can be written similar to Eq. (9.69). Before turning to the consideration of the exciton–vibrational coupling, two examples of such single- and two-exciton spectra are discussed for which analytical expressions are available.

9.2.4.1 The Molecular Heterodimer

As the simplest example, we consider the so-called heterodimer, which consists of two monomers with different excitation energies E_1 and E_2 and a coupling $J = J_{12}$. The eigenvalue problem for the two coupled two-level molecules has already been solved in Section 2.8.2. The one-exciton eigenvalues are given by

$$\mathcal{E}_{\alpha=\pm} = \frac{E_1 + E_2}{2} \pm \frac{1}{2} \sqrt{(E_1 - E_2)^2 + 4|J|^2}. \tag{9.73}$$

For the details of the corresponding eigenfunctions, refer Section 2.8.2. Here, we set the arbitrary phase factors appearing in the solution of the two-level problem equal to 1 and write

$$|+\rangle = \frac{1}{\sqrt{1+\eta^2}} \left(\eta|1\rangle + e^{-i \arg(J)}|2\rangle \right)$$

$$|-\rangle = \frac{1}{\sqrt{1+\eta^2}} \left(|1\rangle - \eta e^{-i \arg(J)}|2\rangle \right). \tag{9.74}$$

The parameter η (cf. Eq. (2.164)) is equal to zero for $J = 0$ and otherwise, given by

$$\eta = \frac{1}{2|J|} \left| E_1 - E_2 + \sqrt{(E_1 - E_2)^2 + 4|J|^2} \right|. \tag{9.75}$$

Equation (9.74) illustrates the delocalization of the wave function over the dimer. The two-exciton state in a molecular dimer, $|mn\rangle$, already extends over both monomers; that is, a meaningful delocalized superposition state cannot be formed. For the eigenenergy, we have $\mathcal{E}_{\tilde{\alpha}} = E_1 + E_2$.

9.2.4.2 The Finite Molecular Chain and the Molecular Ring

Next, we consider an aggregate that consists of a linear arrangement of N_{mon} identical molecules with $S_0 \rightarrow S_1$ excitation energies $E_m = E_{\text{exc}}$ and nearest-neighbor dipole–dipole coupling J. The neglect of long-range dipole–dipole interactions is justified in cases where the distance between the monomers is not too small (note that according to Eq. (9.30), $J_{m,m+1} = 2^3 J_{m,m+2}$). Such regular structures can be found in systems that show a rodlike arrangement of the molecules after aggregation.

The determination of the energy spectrum of a finite linear chain has already been explained in Section 2.8.3. In the present notation, we obtain

$$\mathcal{E}_\alpha = E_{\text{exc}} + 2J \cos(\alpha), \tag{9.76}$$

with $\alpha = \pi j/(N_{\text{mon}} + 1)$ ($j = 1, \ldots, N_{\text{mon}}$). The wave function expansion coefficients read

$$c_\alpha(m) = \sqrt{\frac{2}{N_{\text{mon}} + 1}} \sin(\alpha m). \tag{9.77}$$

This result is confronted with that obtained for a regular molecular ring, a system which was discussed already in Section 2.8.3. We again consider identical molecules with excitation energy E_{exc} and nearest-neighbor dipole–dipole coupling J but now in a ring-like spatial arrangement. Here, Eq. (9.76) remains valid but with $\alpha = 2\pi j/N_{\text{mon}}$ ($j = 0, \ldots, N_{\text{mon}} - 1$) and

$$c_\alpha(m) = \frac{1}{\sqrt{N_{\text{mon}}}} e^{i\alpha m}. \tag{9.78}$$

Note that, due to the periodicity of the aggregate, the sine function in Eq. (9.77) has been replaced by a complex exponential. Moreover, we get the site-independent probability distribution $|c_\alpha(m)|^2 = 1/N_{mon}$ for the molecular ring, which is different from the probability distribution following for the regular chain.

The two-exciton states for the linear chain can also be constructed.[9] The respective eigenvalues read

$$\mathcal{E}_{\tilde{\alpha}} = 2E_{exc} + 4J\left(\cos(\alpha) + \cos(\beta)\right), \tag{9.79}$$

with $\alpha = \pi j/N_{mon}$ and $\beta = \pi j'/N_{mon}$ $(j, j' = 1, 3, \ldots, 2N_{mon} - 1)$ and similar for β (note that for this particular case, the quantum number $\tilde{\alpha}$ is given by the pair α and β). The expansion coefficients of the related eigenstates are obtained as

$$c_{\tilde{\alpha}}(mn) = \frac{\text{sgn}(m-n)}{N_{mon}} e^{i(\alpha m + \beta n)}, \tag{9.80}$$

where $\text{sgn}(m-n) = (1 - \delta_{mn})(m-n)/|m-n|$.

Apparently, for a more complex structure of the aggregate, excitonic spectra are only obtainable by numerical means.

9.3 Exciton–Vibrational Interaction

The aggregate Hamiltonian introduced in Section 9.2.3 depends on the nuclear coordinates. We can distinguish between intramolecular coordinates of a certain monomer, intermolecular coordinates giving the relative position and orientation between monomers, and environmental coordinates, for instance, of a surrounding solvent or protein scaffold. The coupling between electronic excitations and nuclear DOFs enters the Hamiltonian, Eq. (9.36), in two ways: via the monomer vibrational Hamiltonian H_{ma} $(a = e, g)$ and the intermolecular Coulomb couplings J_{mn}. Recalling the dipole approximation, Eq. (9.30), the latter quantities mainly depend on the distances X_{mn} between molecules m and n as well as their mutual orientations. Below, we focus on the influence of nuclear DOFs on single-exciton states for a two-level description of each monomer only.

For illustration, we start with a description that is directly based on a diagonalization of the single excitation Hamiltonian $H_{agg}^{(1)}$, Eqs. (9.38) and (9.44). This results in exciton levels already described in Section 9.2.4, but here in a more general way because we account for the parametrical dependence on all nuclear coordinates of the aggregate. Therefore, instead of Eq. (9.67), we write

$$|\Phi_\alpha(R)\rangle = \sum_m c_\alpha(m; R)|m\rangle, \tag{9.81}$$

where the exciton expansion coefficients as well as the exciton energies $\mathcal{E}_\alpha(R)$ depend on the nuclear coordinates (analogous to the case of molecular states in Section 2.13). Therefore, the states introduced via Eq. (9.81) are often called

---

9) See, for instance, Mukamel [7].

adiabatic exciton states.[10] Incorporating nonadiabatic couplings among different exciton states, we obtain the aggregate Hamiltonian as

$$H_{\mathrm{agg}}^{(1)} = \sum_{\alpha,\beta} (\delta_{\alpha\beta}[T_{\mathrm{nuc}} + U_\alpha(R)] + [1 - \delta_{\alpha\beta}]\hat{\Theta}_{\alpha\beta}) |\Phi_\alpha\rangle\langle\Phi_\beta|. \tag{9.82}$$

Here, $U_\alpha(R) = \mathcal{E}_\alpha(R) + \hat{\Theta}_{\alpha\alpha}(R)$ represents the PES for exciton state $|\Phi_\alpha\rangle$.

This approach appears to be rather attractive since it considers exciton formation as well as the effect of the nuclear coordinates without any approximation. However, for practical computations, it is usually impossible to proceed in such a strict manner. The introduction of adiabatic excitons results in a complicated coordinate dependence of state vectors and PES, and nonadiabatic effects have to be considered as well. Both difficulties can be hardly tackled within a quantum description of nuclear motion for realistic aggregates.

In order to proceed, the different dependences of the vibrational Hamiltonian $\mathcal{H}_{mn}$, Eq. (9.44), on the nuclear coordinates will be specified as follows: First, only intramolecular vibrations are considered. This case applies when the molecules in the aggregate are rather weakly coupled and, thus, can be characterized by independent vibrational coordinates. Provided that the intramolecular DOFs, possibly supplement by DOFs of the immediate surrounding, form a dense spectrum of states, this situation is usually characterized by a system–reservoir model where each monomer couples to its own reservoir. Further, it is assumed that reservoir DOFs of different monomers are uncorrelated. Second, a description of all coordinates by respective normal-mode vibrations is given, which applies to situations of closely packed systems. This case might include contributions of the environment as well. In terms of a system–reservoir description, this implies that all electronic transitions (system) couple to the same reservoir DOFs. In a third variant, we consider an intermediate situation where electronic transitions are coupled to intramolecular DOFs, which in turn interact with environmental DOFs. The description by aggregate normal mode vibrations is finally transferred to a coupling to delocalized exciton states. In what follows, we for simplicity neglect electrostatic contributions and use Eqs. (9.58) and (9.59).

9.3.1 Exclusive Coupling to Intramolecular Vibrations

Concentrating on an exclusive consideration of intramolecular vibrations, all single molecule PESs U_{ma} only depend on the respective set R_m of intramolecular nuclear coordinates (possibly supplement by DOFs of the immediate surrounding). Although the Coulomb matrix elements J_{mn} may be modulated by their nuclear coordinate dependence, we neglect this effect in what follows. This is justified for small amplitude intramolecular motions that do change neither the intermolecular distance nor the transition density appreciably. Often, the intramolecular nuclear motions are described within harmonic approximation, that is by introducing

---

10) If the $|\Phi_\alpha\rangle$ introduced here are taken at the nuclear configuration of the aggregate ground state, they turn into the $|\alpha\rangle$, Eq. (9.67).

intramolecular normal-mode coordinates $q_{m\xi}$. In this case, the monomeric vibrational ground state Hamiltonian in Eq. (9.58) takes the form

$$H_{mg} = \frac{1}{2}\sum_{\xi}\left\{p_{m\xi}^2 + \omega_{m\xi}^2 q_{m\xi}^2\right\}. \tag{9.83}$$

Here, we have set the energy at the reference geometry equal to zero (cf. Eq. (2.43)). The diagonal part of the singly excited state Hamiltonian $H_{\text{agg}}^{(1)}$, Eq. (9.59), can be written as (q denotes all normal-mode coordinates of the aggregate, and $\{q_{m\xi}\}$ the set of coordinate for monomer m)

$$H_{me} + \sum_{n\neq m}H_{ng} = T_{\text{vib}} + U_m(q). \tag{9.84}$$

Here, T_{vib} is the normal-mode kinetic energy of all monomers. The PES referring to a singly excited state takes the form

$$U_m(q) = U_{me}(\{q_{m\xi}\}) + \sum_{n\neq m}U_{ng}(\{q_{n\xi}\}). \tag{9.85}$$

The ground state normal-mode PES, $U_{ng}(\{q_{n\xi}\})$, is given by the second term in Eq. (9.83). An approximation to the excited state PES can be obtained by a first-order Taylor expansion of the energy gap between the ground and the excited states (cf. Eq. (9.46) expressed in normal-mode coordinates using $R_m(\{q_{m\xi}\})$),

$$U_{meg}(\{q_{m\xi}\}) \approx E_m + \sum_{\xi}\left(\frac{\partial U_{meg}(\{q_{m\xi}\})}{\partial q_{m\xi}}\right)_{\{q_{m\xi}=0\}} \times q_{m\xi}, \tag{9.86}$$

with $E_m = U_{meg}(\{q_{m\xi}=0\})$ being the electronic site energy of monomer m.

It is common to introduce dimensionless normal mode coordinates according to $Q_{m\xi} = \sqrt{2\omega_{m\xi}/\hbar}\,q_{m\xi}$ as well as the dimensionless coupling constant

$$g_m(\xi) = \left(\frac{\partial U_{meg}(Q_{m\xi})}{\partial Q_{m\xi}}\right)_{\{Q_{m\xi}=0\}} \times \frac{1}{\hbar\omega_{m\xi}}. \tag{9.87}$$

It can be related to the Huang–Rhys factor (cf. Section 6.2.3). Thus, Eq. (9.86) becomes

$$U_{meg}(\{Q_{m\xi}\}) \approx E_m + \sum_{\xi}\hbar\omega_{m\xi}g_m(\xi)Q_{m\xi}. \tag{9.88}$$

Within the first-order Taylor expansion, the PES for a single excited state in Eq. (9.85) takes the form

$$U_m(Q) = E_m - \sum_{\xi\in m}\hbar\omega_{\xi}g_m^2(\xi) + \sum_{\xi\in m}\frac{\hbar\omega_{m\xi}}{4}\left(Q_{m\xi} + 2g_m(\xi)\right)^2$$
$$+ \sum_{n\neq m}\sum_{\xi\in n}\frac{\hbar\omega_{n\xi}}{4}Q_{n\xi}^2. \tag{9.89}$$

Note that this PES describes the local excitation as a linearly shifted oscillator mode in analogy to the discussion in Sections 2.5.1, 6.2.3, and 7.2.2. Further, we point to the similarity with the description of bimolecular ET in terms of independent sets of vibrational coordinates discussed in Section 7.4.2. The second term on the
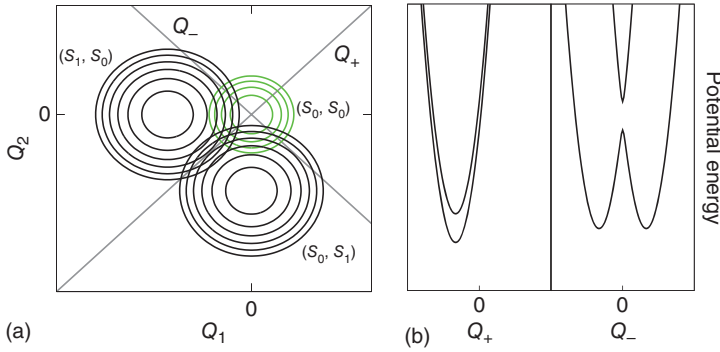
Figure 9.10 (a) PESs according to the model of Eq. (9.89) for a dimer with one mode per monomer Q_m. Each monomer is described by two electronic states, that is S_0 and S_1. Shown are the harmonic PESs for the ground state (S_0, S_0) and the two singly excited states (S_1, S_0) and (S_0, S_1). (b) Including the Coulomb coupling J_{12}, one obtains excitonic PESs (cf. Eq. (9.82)), here plotted along the symmetric, Q_+, and antisymmetric, Q_-, cuts as indicated in (a).

right-hand side is the reorganization energy, $E_\lambda^{(m)} = \sum_\xi \hbar\omega_\xi g_m^2(\xi)$, of the intramolecular modes at monomer m.

The PES is shown for a dimer with one mode per monomer and electronic states S_0 and S_1 in Figure 9.10a. Starting from the parabolic ground state PES with electronic configuration (S_0, S_0), the excited state PES is shifted either along mode Q_1 (S_1, S_0) or mode Q_2 (S_0, S_1). The respective excitonic PESs are given in Figure 9.10b (cf. Eq. (9.82)). The resulting exciton–vibrational Hamiltonian for the model of linearly coupled intramolecular vibrations, which describes the motion of a single excitation in the aggregate under the influence of the nuclear DOFs, reads

$$H_{\text{agg}}^{(1)} = H_{\text{ex}} + H_{\text{vib}} + H_{\text{ex–vib}}. \tag{9.90}$$

It contains the electronic (excitonic) part

$$H_{\text{ex}} = \sum_{m,n} \left(\delta_{mn} E_m + J_{mn} \right) |m\rangle\langle n|, \tag{9.91}$$

the vibrational part $(P_{m\xi} = \sqrt{2/\hbar\omega_{m\xi}}\; p_{m\xi})^{[11]}$

$$H_{\text{vib}} = \sum_m \sum_{\xi\in m} \frac{\hbar\omega_{m\xi}}{4} (P_{m\xi}^2 + Q_{m\xi}^2) \sum_n |n\rangle\langle n|, \tag{9.92}$$

and the exciton–vibrational coupling

$$H_{\text{ex–vib}} = \sum_m \sum_{\xi\in m} \hbar\omega_{m\xi} g_m(\xi) Q_{m\xi} |m\rangle\langle m|. \tag{9.93}$$

This form of $H_{\text{agg}}^{(1)}$ is also known as the Holstein Hamiltonian. Provided that the intramolecular modes form a dense spectrum, this Hamiltonian describes a system–reservoir model where each monomer couples to its own reservoir. This description

---

11) The projector $\sum_n |n\rangle\langle n|$ ensures that the vibrational Hamiltonian acts in the state space of single excitations of the aggregate.

will be utilized, for instance, in Section 9.5 where a system is studied with molecules well separated from each other, and where the intermolecular vibrations have only a minor influence on the EET.

9.3.2 Coupling to Aggregate Normal Mode Vibrations

The model of Section 9.3.1 is readily adjusted to the situation where all nuclear DOFs of the aggregate and the surrounding medium are treated as a *single* set of normal modes $Q = \{Q_\xi\}$; that is, the modes are not monomer specific and thus are not labeled by the site index. This model would be appropriate in situations, for example, with tightly packed aggregates that feature delocalized normal modes. Formally, this model is analogous to the treatment of ET by a common set of nuclear coordinates in Section 7.2.2.

For this model, the dimensionless coupling constant in Eq. (9.87) changes to

$$g_m(\xi) = \left(\frac{\partial U_{meg}(Q_\xi)}{\partial Q_\xi} \right)_{\{Q_\xi = 0\}} \times \frac{1}{\hbar\omega_\xi}. \tag{9.94}$$

To account for the modification of the excitonic coupling by vibrational motions, which now include variations in the intermolecular distance, we introduce the equilibrium value $J_{mn}^{(0)}$ for the coupling between molecule m and n. Performing an expansion with respect to $\{Q_\xi\}$ around the equilibrium configuration, we get in first order[12]

$$J_{mn} \approx J_{mn}^{(0)} + \sum_\xi \left(\frac{\partial J_{mn}}{\partial Q_\xi} \right)_{Q_\xi = 0} \times Q_\xi = J_{mn}^{(0)} + \sum_\xi \hbar\omega_\xi \tilde{g}_{mn}(\xi) Q_\xi, \tag{9.95}$$

where we defined the coupling matrix $\tilde{g}_{mn}(\xi)$. The monomer coupling $g_m(\xi)$ can be combined with $\tilde{g}_{mn}(\xi)$ to the *exciton–vibrational coupling matrix*

$$g_{mn}(\xi) = \delta_{mn} g_m(\xi) + (1 - \delta_{mn}) \tilde{g}_{mn}(\xi). \tag{9.96}$$

The resulting exciton–vibrational Hamiltonian for this model can be written as in Eq. (9.90) but now with the excitonic part

$$H_{\text{ex}} = \sum_{m,n} \left(\delta_{mn} E_m + J_{mn}^{(0)} \right) |m\rangle\langle n|, \tag{9.97}$$

the vibrational part

$$H_{\text{vib}} = \sum_\xi \frac{\hbar\omega_\xi}{4} (P_\xi^2 + Q_\xi^2) \sum_m |m\rangle\langle m|, \tag{9.98}$$

and the exciton–vibrational coupling

$$H_{\text{ex–vib}} = \sum_{m,n} \sum_\xi \hbar\omega_\xi g_{mn}(\xi) Q_\xi |m\rangle\langle n|. \tag{9.99}$$

In the limit of a dense spectrum of modes, this Hamiltonian describes a system–reservoir model where all monomers couple to the same reservoir.

---

12) Note that, in principle, this type of approximation would also be possible if it is necessary to include the effect of variations of the transition densities due to intramolecular mode vibrations. Further, it should be emphasized that restricting ourselves to small amplitude vibrations limits the applicability of Eq. (9.95).

9.3.3 Differentiating Between Intramolecular and Reservoir Normal Mode Vibrations

The models introduced in the two foregoing sections treat all vibrational DOFs on the same footing. However, often, it is necessary to distinguish between intra- and intermolecular DOFs. For instance, typical chromophores often show a Franck–Condon progression with respect to some high-frequency intramolecular vibrations. Due to the interaction with the environment, the individual transitions are broadened. Recalling the discussion of Section 6.2, such a situation could be described by a (multimode) Brownian oscillator model. In the present case, the intramolecular modes, $Q_{m\xi}$, take the role of the active coordinates, whereas intermolecular modes, Z_i (for instance, solvent and protein), form the reservoir.[13] The model assumes that system and reservoir modes have been obtained by separate diagonalization such that there is a coupling that is in lowest order bilinear in the two coordinates (cf. Section 5.4 and Eq. (6.58)). Using the results of Section 9.3.1, the resulting system–reservoir Hamiltonian for the description of a single excitation in the aggregate has the standard form $H = H_{\mathrm{S}} + H_{\mathrm{R}} + H_{\mathrm{S\text{-}R}}$, with

$$H_{\mathrm{S}} = \sum_{m,n} \left(\delta_{mn}(T_{\mathrm{vib}} + U_m(Q)) + J_{mn} \right) |m\rangle\langle n|, \tag{9.100}$$

where $U_m(Q)$ is given by Eq. (9.89). The system–reservoir interaction is of Caldeira–Leggett form

$$H_{\mathrm{S\text{-}R}} = \sum_{m,i} \sum_{\xi \in m} c_{mi}(\xi) Q_{m\xi} Z_i |m\rangle\langle m|, \tag{9.101}$$

where $c_{mi}(\xi)$ is the coupling constant. Finally, the reservoir corresponds to a harmonic oscillator Hamiltonian equation (9.98) with coordinates Z_i.

9.3.4 Exciton–Vibrational Hamiltonian and Excitonic Potential Energy Surfaces

The aggregate Hamiltonian $H_{\mathrm{agg}}^{(1)}$, Eq. (9.90) (or likewise Eq. (9.90)), corresponds to a diabatic representation in terms of the coupling between different monomers. Often, it is rewritten in terms of the eigenstates of the exciton Hamiltonian, Eq. (9.91), that is the *exciton states*, using the expansion, Eq. (9.67). Since these eigenstates have been defined for a fixed nuclear configuration, they form a crude adiabatic basis in contrast to Eq. (9.81) (cf. Section 2.6).

Assuming the same separation of $H_{\mathrm{agg}}^{(1)}$ as in Eq. (9.90), we obtain the excitonic part H_{ex} as in Eq. (9.69), and the exciton–vibrational coupling reads

$$H_{\mathrm{ex\text{-}vib}} = \sum_{\alpha,\beta} \sum_{\xi} \hbar\omega_\xi g_{\alpha\beta}(\xi) Q_\xi |\alpha\rangle\langle\beta|. \tag{9.102}$$

The exciton–vibrational coupling matrix is given by

$$g_{\alpha\beta}(\xi) = \sum_{m,n} c_\alpha^*(m) g_{mn}(\xi) c_\beta(n). \tag{9.103}$$

---

13) Note that the actual partitioning depends on the situation at hand. For instance, modes of the immediate surrounding of the molecule could be taken as part of the set $Q_{m\xi}$. On the other hand, in particular, low-frequency modes of the molecule could be included into the reservoir.

The vibrational part remains unaffected; only $\sum_m |m\rangle\langle m|$ has to be replaced by $\sum_\alpha |\alpha\rangle\langle\alpha|$.

If diagonal elements of $g_{\alpha\beta}(\xi)$ are much larger than the off-diagonal ones, one can introduce a notation of $H_{\text{agg}}^{(1)}$, leading to a certain type of PES (cf. Eq. (9.82)). To this end, we take the potential energy part $\sum_\xi \hbar\omega_\xi Q_\xi^2/4$ of H_{vib} and combine it with the term $\propto Q_\xi$ of Eq. (9.102) to define the (shifted) *excitonic* PES

$$U_\alpha(Q) = \mathcal{E}_\alpha - \sum_\xi \hbar\omega_\xi g_{\alpha\alpha}^2(\xi) + \sum_\xi \frac{\hbar\omega_\xi}{4}\big(Q_\xi + 2g_{\alpha\alpha}(\xi)\big)^2. \tag{9.104}$$

The energy shift $\sum_\xi \hbar\omega_\xi g_{\alpha\alpha}^2(\xi)$ is the reorganization energy $E_\lambda^{(\alpha)}$ of the exciton state $|\alpha\rangle$. Then, the exciton representation of the aggregate Hamiltonian is obtained as

$$H_{\text{agg}}^{(1)} = \sum_{\alpha,\beta} \left(\delta_{\alpha\beta} \left\{ T_{\text{vib}} + U_\alpha(Q) \right\} \right.$$
$$\left. + (1 - \delta_{\alpha\beta})\sum_\xi \hbar\omega_\xi g_{\alpha\beta}(\xi)Q_\xi \right) |\alpha\rangle\langle\beta|. \tag{9.105}$$

This expression is similar to that of Eq. (9.82); however, the vibrational coordinate dependence is simple, and instead of nonadiabatic couplings, here, a type of static normal mode coordinate dependent coupling appears. It should be noted that Eq. (9.105) resembles the linear vibronic coupling model introduced in Section 6.6.2.[14]

9.4 Regimes of Excitation Energy Transfer

Similar to the case of electron-transfer reactions in Chapter 7, the actual type of excitation energy dynamics is determined by the relation between two time scales. The intramolecular vibrational relaxation time, τ_{rel}, determines the time that the nuclear vibrations of each molecule need to return to thermal equilibrium after the electronic transition takes place. The transfer time, τ_{trans}, is given by the inverse of the characteristic interaction energy between two molecules. It is the time the excitation energy needs to move between monomers, neglecting any additional perturbations. The different regimes of EET are sketched in Figure 9.11 in dependence on the intra- and intermolecular interaction strengths.

If $\tau_{\text{rel}} \ll \tau_{\text{trans}}$, it is impossible to form a wave function involving different molecules. Intramolecular relaxation introduces fast dephasing, and we are in the regime of *incoherent transfer* labeled by I in Figure 9.11. The excitation energy motion proceeds diffusively, similar to the *random walk* known from statistical

---

14) If the nuclear coordinates of the PES appearing in Eq. (9.82) are expanded around their equilibrium configuration, one obtains something similar to but not identical with the excitonic PES introduced in Eq. (9.104). In the latter case, the full exciton–vibrational Hamiltonian is diagonalized at each configuration of the nuclear coordinates, cf. Figure 9.10b.

Figure 9.11 Schematic representation of different EET regimes. The strength of intermolecular interactions increases along the horizontal axis, and that of intramolecular couplings along the vertical axis. Förster transfer as described in Section 9.5 is typical for region I, whereas the density matrix description given in Section 9.6 can be applied in region II. In the intermediate region III, delocalized exciton formation and exciton–vibrational coupling have to be dealt with on an equal footing.
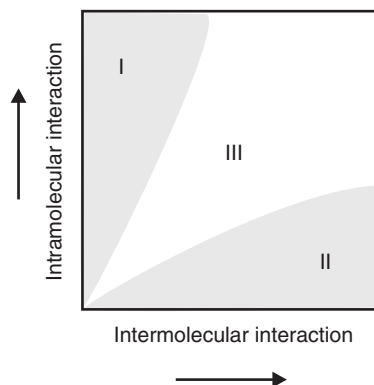
physics (see Figure 9.6c,d). This type of transfer is characterized by a probability $P_m(t)$ for the excitation energy to be at molecule m but not by a wave function extending over different molecules. Incoherent EET will be discussed in Section 9.5.

If, on the other hand, $\tau_{\text{trans}} \ll \tau_{\text{rel}}$, excitation energy can move almost freely from molecule to molecule according to the corresponding Schrödinger equation. The exciton propagates through the aggregate as a quantum mechanical wave packet (see Figure 9.6a,b). Since such a type of motion requires fixed phase relations between excited state wave functions of different molecules, it is called *coherent transfer*. (In Chapter 3, we discuss that this type of motion is typical for closed quantum systems not subject to the influence of environmental perturbations.) The corresponding region of coherent motion is indicated as region II in Figure 9.11, and the related theoretical description uses the density matrix $\rho_{mn}(t)$, here in local state (site) representation or, alternatively, in the exciton representation $\rho_{\alpha\beta}(t)$ (see Section 9.6).

Clearly, there are regions between the coherent and the incoherent types ($\tau_{\text{rel}} \approx \tau_{\text{trans}}$). This motion is called *partially coherent* exciton transfer (region II in Figure 9.11), but notice that such a characterization of the intermediate region of transfer processes is often not straightforward. In general, a concurrence of the different types of motion within the same aggregate is possible. For example, if there are two groups of closely packed molecules in the aggregate, EET within each group may be coherent (or partially coherent), but between the groups the EET could take place as a hopping process (cf. Section 9.6.4). Moreover, moving in region III of Figure 9.11 to the upper right corner, both basic couplings become large. This region characterizes qualitatively a type of EET motion where the excitation is delocalized but connected with a noticeable displacement of the vibrational DOFs (we refer to the similarity with the ultrafast ET described in Section 7.9). This regime where nonperturbative and non-Markovian effects play a dominant role requires adequate methods such as the HEOM approach introduced in Section 3.11.

The given discussion also applies if extended to doubly excited aggregate states (two-exciton states). However, two-exciton dynamics are outside the scope of the following discussion.

9.4.1 Quantum Statistical Approaches to Excitation Energy Transfer

The basic quantity for the following theoretical description of EET dynamics in molecular aggregates is the density operator reduced to the electronic (excitonic) DOF:

$$\hat{\rho}(t) = \text{tr}_{\text{vib}}\{\hat{W}(t)\}. \tag{9.106}$$

$\hat{W}(t)$ is the total nonequilibrium statistical operator of the complete set of all involved electrons and nuclei of the different molecules forming the aggregate as well as of a particular environment. When starting with such a density operator, one sets the focus on the electronic (excitonic) dynamics with all vibrational contributions accounted for as a thermal environment and averaged out via $\text{tr}_{\text{vib}}\{\dots\}$. This choice is to be preferred when considering aggregates where the spatial arrangement of the various molecules does not undergo large changes on the time scale of EET. The actual method for simulating EET depends on the particular regime as indicated in Figure 9.11. One may carry out perturbation theory with respect to either the excitonic coupling or the exciton–vibrational coupling.

The case where the excitonic coupling represents only a weak perturbation and intramolecular couplings dominate will be discussed first in Section 9.5 (case of fast intramolecular relaxation as compared to the transfer time). It will lead us to what is known as the *Förster theory* of EET. Here, the formation of delocalized exciton states can be neglected, and EET has to be considered as incoherent (see Figure 9.6c,d). From our general discussion in Chapter 3, we know that incoherent quantum particle motion is adequately described by rate equations for the state occupation probabilities

$$P_m(t) = \langle m|\hat{\rho}(t)|m\rangle. \tag{9.107}$$

Before utilizing the general rate equation approach of Section 3.14, we calculate the EET rate using the Golden Rule approach of quantum mechanics.

If EET is dominated by excitonic couplings, it can be described via transitions among delocalized exciton states (cf. Figure 9.6a,b) using the exciton level populations

$$P_\alpha(t) = \langle \alpha|\hat{\rho}(t)|\alpha\rangle. \tag{9.108}$$

Corresponding transition rates can be calculated in second order with respect to the exciton–vibrational coupling in a standard Golden Rule scheme (a more general approach would make use of excitonic PES). Such a second-order description of the exciton–vibrational coupling is also possible in a density matrix theory based on

$$\rho_{\alpha\beta}(t) = \langle \alpha|\hat{\rho}(t)|\beta\rangle. \tag{9.109}$$

Within this theory, rates responsible for population redistribution as well as coherence change appear. The appropriate theoretical tool is introduced in Section 3.5.6. We identify the electronic excitations (limited to the singly excited electronic states of the aggregate) with the *relevant* system in the sense of Chapter 3. The vibrational DOFs of the aggregate are considered as the reservoir (heat bath) responsible for electronic energy dissipation and dephasing of the coherent exciton motion.

The adequate description of the exciton dynamics is given by the QME approach of Section 3.6.

Of course, it is straightforward, for example, to calculate the probability $P_m(t)$ that the molecule m is excited at time t from the density matrix in the representation of delocalized exciton states. Using the expansion coefficients $c_\alpha(m)$ introduced in Eq. (9.67), it follows that

$$P_m(t) = \sum_{\alpha,\beta} c_\alpha(m) c_\beta^*(m) \rho_{\alpha\beta}(t). \tag{9.110}$$

In principle, one may also choose directly the site representation of the density operator in terms of the localized basis set $|m\rangle$ defined in Eq. (9.34). This gives the reduced density matrix

$$\rho_{mn}(t) = \langle m | \hat{\rho}(t) | n \rangle. \tag{9.111}$$

Since the Förster transfer is realized as a hopping process between different sites, it is reasonable to assume that a site representation is well suited for establishing the link between Förster theory and the density matrix approach. However, this would only be possible for the case of weak electron–vibrational coupling where Förster rate may become similar to the second-order rate expression used in the density matrix approach.

There is a further aspect of the density matrix approach on EET dynamics that particularly favors it for the study of optical properties. This statement is related to the fact that the definition equation (9.109) can be easily extended to include the ground state $|0\rangle$ as well as the states $|mn\rangle$, Eq. (9.35), with two excitations in the aggregate (or the two-exciton state, Eq. (9.71)). Accordingly, one may compute off-diagonal density matrix elements such as $\langle \alpha | \hat{\rho}(t) | 0 \rangle$. The latter is proportional to the polarization between the ground state and the one-exciton state $|\alpha\rangle$ and allows to directly include the coupling to the radiation field (written as in Eq. (4.18)) into the density matrix equation. Then, as described in Section 4.3, there is no need to introduce any linear or nonlinear response function characterizing the exciton system. Instead, the density matrix obtained at a finite strength of the radiation field offers a direct access to nonlinear spectra.

9.5 Transfer Dynamics in the Case of Weak Excitonic Coupling: Förster Theory

In this section, we will be concerned with the regime of incoherent transfer where a localized excitation jumps from molecule to molecule. Therefore, the rates $k_{m\to n}$ of EET from molecule m to molecule n will be calculated. According to Section 3.14, the $k_{m\to n}$ should enter rate equations

$$\frac{\partial}{\partial t} P_m(t) = -\sum_n k_{m\to n} P_m(t) + \sum_n k_{n\to m} P_n(t), \tag{9.112}$$

which determine the probabilities P_m to find molecule m in its excited state. First, we consider the case where these rates are proportional to the square of the

intermolecular Coulomb interaction. The Golden Rule formula derived in Section 3.4.5 is used to compute the rate. A more general description, by utilizing the rate theory of Section 3.14, is presented afterward.

9.5.1 The Transfer Rate

The EET rate will be detailed for a system of two molecules that are not necessarily identical (heterodimer). In analogy to the discussion of electron transfer, the heterodimer will be called a DA complex (the monomer index m will be $m = D$ or $m = A$, cf. Figure 9.12). First, we concentrate on the case of two *independent* sets of vibrational coordinates, defined for either the donor or the acceptor part of the dimer (cf. Section 7.4.2, where a similar situation has been discussed for the electron transfer). This case is of particular importance if intramolecular vibrations of the donor and acceptor molecules dominate the transfer. The assumption that the energy spectrum of each molecule m is only determined by its *own* set of coordinates R_m is particularly reasonable at large intermolecular distances (>10 Å).

In order to describe the EET in such a DA complex, we introduce wave functions for both molecules as $\Psi_{maM}(r_m; R_m) = \varphi_{ma}(r_m; R_m)\chi_{maM}(R_m)$ ($m = D, A$; $a = g, e \equiv S_0, S_1$). Here, r_m stands for the electronic coordinates of molecule m, and R_m for those of the corresponding nuclei. The $S_0 \to S_1$ transition energies are given by $E_{meM} - E_{mgN}$.

According to Figure 9.12, the transfer proceeds via deexcitation of the donor and the simultaneous excitation of the acceptor. This results in the following general transfer rate:

$$k_{\text{EET}} = \frac{2\pi}{\hbar} \sum_{M_D,N_D} \sum_{M_A,N_A} f_{DeM_D} f_{AgN_A}$$
$$\times |\langle \Psi_{DeM_D} \Psi_{AgN_A} | V_{\text{DA}} | \Psi_{AeM_A} \Psi_{DgN_D} \rangle|^2$$
$$\times \delta(E_{DeM_D} + E_{AgN_A} - E_{AeM_A} - E_{DgN_D}). \tag{9.113}$$
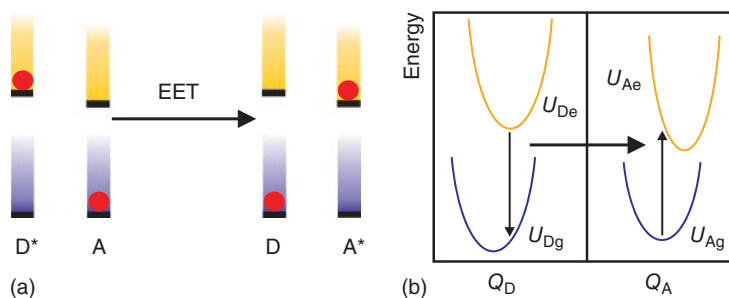
Figure 9.12 EET in a DA pair. (a) Both molecules are represented by electronic two-level systems with related vibrational manifolds. The gray spheres indicate the type of excitation, left part: initial state with the excited donor (D*) and the deexcited acceptor (A), right part: final state with the deexcited donor (D) and the excited acceptor (A*). (b) Related PES drawn versus a vibrational coordinate of the donor (Q_D) and the acceptor (Q_A); cf. two-dimensional representation of PESs in Figure 9.10.

The initial vibrational equilibrium in the donor and acceptor is described by the distribution functions f_{DeM_D} and f_{AgN_A}, respectively. The matrix element of the complete DA Coulomb interaction V_{DA} has already been discussed in Section 9.2.2. Since the DA distance should exceed ~10 Å, intermolecular wave function overlap is of no importance, and we neglected the exchange contributions. Assuming that the resulting Coulomb matrix element J_{DA} does not depend on the nuclear coordinates (Condon approximation), we obtain

$$\langle \Psi_{DeM_D} \Psi_{AgN_A} | V_{DA} | \Psi_{AeM_A} \Psi_{DgN_D} \rangle = J_{DA} \langle \chi_{DeM_D} | \chi_{DgN_D} \rangle$$
$$\times \langle \chi_{AgN_A} | \chi_{AeM_A} \rangle, \qquad (9.114)$$

which depends on the Franck–Condon-type overlap integrals. If the overall matrix element is inserted into Eq. (9.113), the following expression is obtained:

$$k_{\mathrm{EET}} = \frac{2\pi}{\hbar} |J_{DA}|^2 \mathcal{D}_{\mathrm{EET}}. \qquad (9.115)$$

Here, we introduce the combined density of states (DOS) referring to the EET process:

$$\mathcal{D}_{\mathrm{EET}} = \sum_{M_D, N_D} \sum_{M_A, N_A} f_{DeM_D} f_{AgN_A}$$
$$\times |\langle \chi_{DeM_D} | \chi_{DgN_D} \rangle|^2 |\langle \chi_{AgN_A} | \chi_{AeM_A} \rangle|^2$$
$$\times \delta(E_{DeM_D} + E_{AgN_A} - E_{AeM_A} - E_{DgN_D}). \qquad (9.116)$$

Taking all assumptions together, we notice that we have recovered the model that had been derived in the context of electron-transfer reactions in Section 7.4.2, where it is shown that in the case of two independent sets of vibrational coordinates, the energy conservation for the transfer reaction contained in the δ-function of the Golden Rule formula could be separated into two parts. This separation will also be applied in the present case. In order to obtain this appealing form of the transfer rate, we rewrite the δ-function in Eq. (9.116) as

$$\delta(E_{DeM_D} + E_{AgN_A} - E_{AeM_A} - E_{DgN_D}) = \int dE \, \delta(E_{DeM_D} - E_{DgN_D} - E)$$
$$\times \delta(E + E_{AgN_A} - E_{AeM_A}). \qquad (9.117)$$

Here, the first δ-function on the right-hand side accounts for the donor emission. The energy, $E = \hbar\omega$, that is set free in this process is used to excite the acceptor. Introducing a product of two δ-functions leads to the following compact expression for the combined DOS (note the change to the frequency argument):

$$\mathcal{D}_{\mathrm{EET}} = \hbar \int d\omega \, \mathcal{D}_D^{(\mathrm{em})}(\omega) \mathcal{D}_A^{(\mathrm{abs})}(\omega), \qquad (9.118)$$

where we introduce the combined DOS for the donor deexcitation (excitation energy emission)

$$D_D^{(\mathrm{em})}(\omega) = \sum_{M_D, N_D} f_{DeM_D} |\langle \chi_{DeM_D} | \chi_{DgN_D} \rangle|^2 \, \delta(E_{DeM_D} - E_{DgN_D} - \hbar\omega), \qquad (9.119)$$

and for the acceptor excitation (absorption of excitation energy)

$$
\mathcal{D}_A^{(abs)}(\omega) = \sum_{M_A, N_A} f_{AgN_A} |\langle \chi_{AgN_A} | \chi_{AeM_A} \rangle|^2 \, \delta(E_{AgN_A} - E_{AeM_A} + \hbar\omega). \tag{9.120}
$$

Since the EET combined DOS, Eq. (9.118), follows as the frequency integral of the overlap expression given by the donor and acceptor DOS, $\mathcal{D}_{EET}$ is often called *spectral overlap expression*.

9.5.2 The Förster Rate

From Figure 9.12, it is clear that the process of EET can *formally* be viewed as the combined process of optical recombination at the donor and simultaneous optical absorption at the acceptor. The Förster approach is built upon this analogy. Hence, the transfer rate will be expressed in terms of the $S_1 \rightarrow S_0$ donor emission spectrum and the $S_0 \rightarrow S_1$ acceptor absorption spectrum. If the electronic coupling J_{DA} is taken in the dipole–dipole approximation, Eq. (9.30), we may replace $\mathcal{D}_D^{(em)}$ by the donor emission spectrum as well as $\mathcal{D}_A^{(abs)}$ by the acceptor absorption spectrum and arrive at the *Förster formula* of EET.

According to Eq. (9.119), the donor emission spectrum can be written as (cf. Section 4.4 and Eq. (6.88))

$$
I_D(\omega) = \frac{4\omega^3}{3c^3} |\boldsymbol{d}_D|^2 \mathcal{D}_D^{(em)}(\omega). \tag{9.121}
$$

The acceptor absorption coefficient is (see Eq. (9.120), Section 4.2.1, and Eq. (6.14))

$$
\alpha_A(\omega) = \frac{4\pi^2 \omega N_{mon}}{3c} |\boldsymbol{d}_A|^2 \mathcal{D}_A^{(abs)}(\omega). \tag{9.122}
$$

Using Eqs. (9.115)–(9.122), we obtain the Förster formula that expresses the EET rate in terms of the *spectral overlap* between the monomeric emission and the absorption spectra (cf. Figure 9.13):

$$
k_{EET} = \frac{9c^4 \kappa_{DA}^2}{8\pi n_{agg} |\boldsymbol{X}_{DA}|^6} \int\limits_0^\infty \frac{d\omega}{\omega^4} \, I_D(\omega) \, \alpha_A(\omega). \tag{9.123}
$$

The orientation factor κ_{DA} is given by Eq. (9.31), and $|\boldsymbol{X}_{DA}|$ is the DA distance. The rate, Eq. (9.123), decreases like the inverse sixth power of the donor–acceptor distance. The distance, R_F, for which the transfer rate is equal to the radiative decay rate of the donor,

$$
k_{EET}(R_F) = \frac{1}{\tau_{phot}^{(D)}} = \int\limits_0^\infty d\omega I_D(\omega), \tag{9.124}
$$

is called the *Förster radius*. In Table 9.2, we have listed Förster radii for some typical biological DA systems. In terms of the Förster radius, the transfer rate is

$$
k_{EET} = \frac{1}{\tau_{phot}^{(D)}} \left(\frac{R_F}{|\boldsymbol{X}_{DA}|} \right)^6. \tag{9.125}
$$
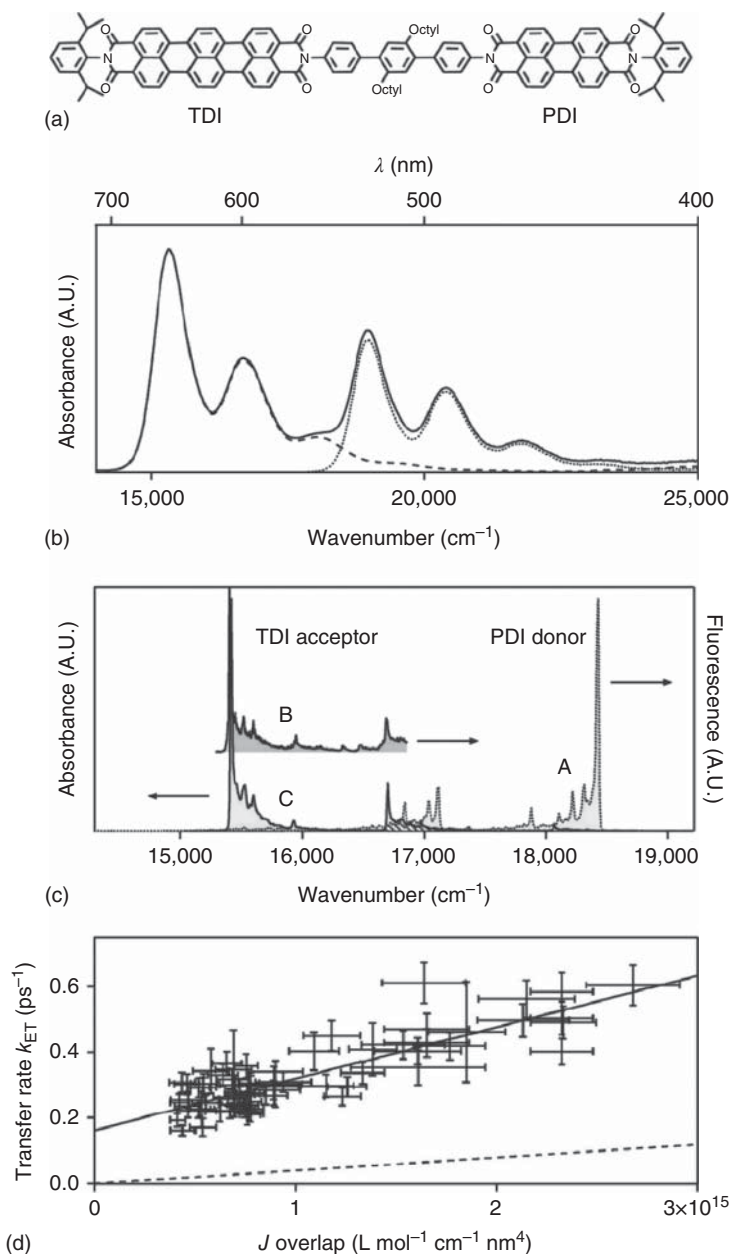
Figure 9.13 EET in a donor (PDI) acceptor (TDI) pair (chemical structure – (a)) characterized by single molecule spectroscopy. (b) Ensemble averaged room temperature absorption spectra (dotted curve: donor, dashed curve: acceptor). (c) Single donor fluorescence emission spectrum (A, 1.4 K), single acceptor fluorescence excitation spectrum (B, 20 K) with spectral overlap (C). (d) Experimentally determined EET rates versus spectral overlap, which indicate a linear interrelation following equation (9.123) (the various data are deduced from measurements on different single pairs) (reprinted with permission from Métivier et al. [8]; copyright (2007) American Physical Society).

Table 9.2 Förster radii for typical biological donor–acceptor systems.

Donor	Acceptor	R_F [nm]
Chl a	Chl a	8–9
Chl b	Chl a	10
β-Carotene	Chl a	5

Source: data taken from van Grondelle [9]

The absolute value of the Förster rate is determined by the donor emission and the acceptor absorption coefficient. As a note in caution, we would like to emphasize that although the idea of the combination of an optical emission and absorption process has been used to derive the Förster rate, the transfer does *not* involve the exchange of a photon. The interaction equation (9.9) or (9.16) is of pure Coulomb type. The term photon can only be used if the coupling between the donor and the acceptor molecules includes retarded (transverse) contributions of the radiation field (see the detailed discussion in Section 9.10.2).

The intuitive and experimentally accessible form of the transfer rate has led to a wide use of Förster theory. It allows to estimate the EET rate by separately measuring the donor emission spectrum as well as the acceptor absorption spectrum. It should be noted, however, that Eq. (9.123) is strictly valid only for homogeneously broadened spectra. Moreover, molecular systems where the dipole–dipole coupling is of the order or even larger than the homogeneous line width cannot be described using the incoherent Förster approach, which is based on the Pauli master equation. This situation requires the solution of the density matrix equation, taking into account the coherent exciton dynamics. Before discussing this in Section 9.6 some variants of the excitation transfer processes discussed so far will be considered.

9.5.3 Nonequilibrium Quantum Statistical Description of Förster Transfer

In the following equations, we apply the technique introduced in Section 3.14 to derive the rate equations for EET. Therefore, we extend our considerations from a single DA pair to an aggregate with an arbitrary number of molecules. Since we are aiming at a nonequilibrium quantum statistical description of Förster transfer, we are interested in transfer rates derived via a perturbation series with respect to the excitonic coupling J_{mn}, whereas the coupling to the vibrational coordinates is treated exactly.

We can directly translate the treatment of Section 3.14 if we neglect the nuclear coordinate dependence of the excitonic coupling in the single-excitation Hamiltonian, $H_{agg}^{(1)}$. For the following considerations, it is essential to use the version of this Hamiltonian given in Eq. (9.59), where intermolecular electrostatic couplings due to (permanent) molecular charge densities have been neglected.[15] This Hamiltonian

---

15) A more detailed inspection shows that it would be sufficient for the following considerations to neglect the modulation of this coupling due to its nuclear coordinate dependence.

has to be split up according to Section 3.14 into a zeroth-order part H_0 and a perturbation $\hat{V}$. According to Eq. (9.59), the zeroth-order part takes the form

$$H_0 = \sum_m \left(H_{me} + \sum_{n \neq m} H_{ng} \right) |m\rangle\langle m|, \tag{9.126}$$

and the excitonic coupling defines the perturbation

$$\hat{V} = \sum_{m,n} J_{mn} |m\rangle\langle n|. \tag{9.127}$$

We obtain a rate equation such as Eq. (9.112) for the probability P_m that the mth molecule has been excited. The corresponding transition rate (of second order with respect to J_{mn}) can be deduced from the general formulas of Section 3.14.5 and becomes, of course, identical to Eq. (9.115). The combined DOS $\mathcal{D}_{\mathrm{EET}}$, written here for a transition from molecule m to molecule n, however, takes the form

$$\mathcal{D}_{mn} = \frac{1}{2\pi\hbar} \int dt \, \mathrm{tr}_{\mathrm{vib}}\{\hat{R}_m \hat{U}_m^+(t)\hat{U}_n(t)\} \equiv \frac{1}{2\pi\hbar} \int dt \, C_{m \to n}(t). \tag{9.128}$$

In the second part of this expression we introduced the correlation function $C_{m \to n}(t)$, replacing the vibrational trace expression of the first part. The $\hat{U}_m(t)$ denote the time-evolution operators[16] describing nuclear motions according to the vibrational Hamiltonians $H_{me} + \sum_{k \neq m} H_{kg}$ entering H_0, Eq. (9.126). As demonstrated in Section 9.3.1, the complete vibrational Hamiltonian can be decomposed into local vibrational Hamiltonians corresponding either to the ground or to the excited electronic level. Accordingly, the vibrational equilibrium statistical operator in Eq. (9.128) takes the following form: $\hat{R}_m = \hat{R}_{me}\prod_{n \neq m}\hat{R}_{ng}$. In a similar manner, the time-evolution operator is obtained as $\hat{U}_m(t) = \hat{U}_{me}(t)\prod_{n \neq m}\hat{U}_{ng}(t)$. As a result, the correlation function in Eq. (9.128) reads

$$C_{m \to n}(t) = \mathrm{tr}_m\{\hat{R}_{me}\hat{U}_{me}^+(t)\hat{U}_{mg}(t)\}\mathrm{tr}_n\{\hat{R}_{ng}\hat{U}_{ng}^+(t)\hat{U}_{ne}(t)\}$$
$$\times \prod_{k \neq m,n} \mathrm{tr}_k\{\hat{R}_{kg}\hat{U}_{kg}^+(t)\hat{U}_{kg}(t)\}. \tag{9.129}$$

Since the trace of $\hat{R}_{kg}$ is normalized to unity, all monomer correlation functions in the k-product are equal to 1 as well, and those for molecules m and n are abbreviated as

$$C_{m\ e \to g}(t) = \mathrm{tr}_m\{\hat{R}_{me}\hat{U}_{me}^+(t)\hat{U}_{mg}(t)\} \tag{9.130}$$

and

$$C_{n\ g \to e}(t) = \mathrm{tr}_n\{\hat{R}_{ng}\hat{U}_{ng}^+(t)\hat{U}_{ne}(t)\}. \tag{9.131}$$

These correlation functions, when Fourier transformed, can be used to express the combined DOSs entering the EET rate (Sections 6.2.2 and 6.4). We arrive at (see Eq. (6.90), the transition frequencies have not been indicated explicitly)

---

16) To distinguish the notation of the time-evolution operators from that of the PES, we write the former with an additional hat in this section.

$D_m^{(\text{em})}(\omega) = C_{m\ e\to g}(-\omega)/2\pi\hbar$ and (see Eq. (6.19)) $D_n^{(\text{abs})}(\omega) = C_{n\ g\to e}(\omega)/2\pi\hbar$. Accordingly, the combined DOS, Eq. (9.128), can be written as

$$D_{mn} = \frac{1}{2\pi\hbar} \int dt\ C_{m\ e\to g}(t) C_{n\ g\to e}(t)$$

$$\equiv \frac{1}{(2\pi)^2\hbar} \int d\omega\ C_{m\ e\to g}(-\omega) C_{n\ g\to e}(\omega). \tag{9.132}$$

Let us discuss the result using simple models for the monomer correlation functions $C_{m\ e\to g}$ and $C_{n\ g\to e}$, which have been introduced in Section 6.2.6, where we used the Debye spectral density, Eq. (6.51), and distinguished between the case of slow and fast nuclear motion (the vibrational time scale T_{vib} is compared to the time scale of the energy gap fluctuations $T_{\text{fluc}} = \hbar/\sqrt{k_B T S_{eg}}$). Neglecting for a moment the site index (and introducing general electronic quantum numbers a and b), the first case results in

$$C_{a\to b}^{(\text{slow})}(t) = \exp\left(i(\omega_{ab} - S_{ab}/2\hbar)t - k_B T S_{ab} t^2/2\hbar^2\right), \tag{9.133}$$

and the second one (case of fast nuclear motion) in

$$C_{a\to b}^{(\text{fast})}(t) = \exp\left(i\omega_{ab}t - |t|/\tau_{ab}\right). \tag{9.134}$$

The transition frequency ω_{ab} is specified by the minima of the two PES $(U_a^{(0)} - U_b^{(0)})/\hbar$, and the Stokes shift S_{ab} of the transition is equal to twice of the respective reorganization energy. The dephasing time τ_{ab} is determined by a representative vibrational frequency $\omega_{\text{vib}} = \omega_D$ as

$$\hbar/\tau_{ab} = k_B T S_{ab}/\hbar\omega_{\text{vib}}. \tag{9.135}$$

While a computation of the correlation function equation (9.129) is conveniently carried out in the time domain, an interpretation should be given in terms of the released and absorbed excitation energy, that is after Fourier transformation into the frequency domain. Therefore, we give here the Fourier-transformed monomer correlation functions

$$C_{e\to g}^{(\text{slow})}(-\omega) = \sqrt{\frac{2\pi\hbar^2}{k_B T S_{eg}}} \exp\left\{-\frac{\left(\hbar[\omega - \omega_{eg}] + S_{eg}/2\right)^2}{2k_B T S_{eg}}\right\}, \tag{9.136}$$

$$C_{g\to e}^{(\text{slow})}(\omega) = \sqrt{\frac{2\pi\hbar^2}{k_B T S_{eg}}} \exp\left\{-\frac{\left(\hbar[\omega - \omega_{eg}] - S_{eg}/2\right)^2}{2k_B T S_{eg}}\right\}, \tag{9.137}$$

and

$$C_{e\to g}^{(\text{fast})}(-\omega) = C_{g\to e}^{(\text{fast})}(\omega) = \frac{2/\tau_{eg}}{(\omega - \omega_{eg})^2 + 1/\tau_{eg}^2}. \tag{9.138}$$

Next, we present for both cases the DOS. The case of slow nuclear motion leads to ($\omega_{mn} = \omega_{meg} - \omega_{neg}$, $S_{mn} = S_{meg} + S_{neg}$)

$$D_{mn}^{(\text{slow})} = \frac{1}{\sqrt{2\pi k_B T S_{mn}}} \exp\left\{-\frac{\left(\hbar\omega_{mn} - S_{mn}/2\right)^2}{2k_B T S_{mn}}\right\}. \tag{9.139}$$
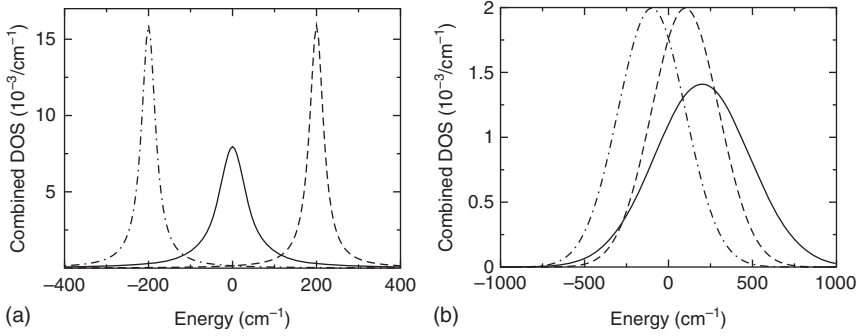
Figure 9.14 Combined DOS for DA EET ($m = D$, $n = A$). Solid lines: $\mathcal{D}_{\text{EET}} \equiv \mathcal{D}_{\text{DA}}$, Eq. (9.132); dashed lines: $\mathcal{D}_D^{(\text{em})}$, Eq. (9.119); dash-dotted lines: $\mathcal{D}_A^{(\text{abs})}$, Eq. (9.120). $\mathcal{D}_{\text{DA}}$ is drawn versus energy detuning $\hbar(\omega_D - \omega_A)$ and $\mathcal{D}_D^{(\text{em})}$ as well as $\mathcal{D}_A^{(\text{abs})}$ versus $\hbar\omega - \hbar\omega_0$ with $\hbar\omega_D = \hbar\omega_0 + 200\,\text{cm}^{-1}$ and $\hbar\omega_A = \hbar\omega_0 - 200\,\text{cm}^{-1}$ ($k_B T = 200\,\text{cm}^{-1}$). (a) Model of fast nuclear motion, $S_D = S_A = 50\,\text{cm}^{-1}$, $\hbar\omega_{\text{vib}}^{(D)} = \hbar\omega_{\text{vib}}^{(A)} = 500\,\text{cm}^{-1}$); (b) Model of slow nuclear motion ($S_D = S_A = 200\,\text{cm}^{-1}$).

In the case of fast nuclear motion, we arrive at

$$\mathcal{D}_{mn}^{(\text{fast})} = \frac{\Gamma_{mn}/\pi}{(\hbar\omega_{mn})^2 + \Gamma_{mn}^2}, \tag{9.140}$$

with

$$\Gamma_{mn} = k_B T \left(\frac{S_{meg}}{\hbar\omega_{\text{vib}}^{(m)}} + \frac{S_{neg}}{\hbar\omega_{\text{vib}}^{(n)}} \right). \tag{9.141}$$

In Figure 9.14, we plotted $\mathcal{D}_{\text{EET}}$ for both limiting cases together with $\mathcal{D}_D^{(\text{em})}$ and $\mathcal{D}_A^{(\text{abs})}$. Be aware of the fact that the model of a fast nuclear motion results in rate expressions independent of temperature. Thus, this rate does not fulfill the principle of detailed balance.

Finally, we contrast Förster and Redfield theories for the case of weak excitonic coupling. Förster theory assumes that EET proceeds from a vibrationally relaxed state of the donor-excited state PES. That is, upon vertical excitation of the donor, it will take a certain time for the thus-prepared nonequilibrium distribution to equilibrate. This can be compared with Redfield theory, which assumes that the reservoir is always in equilibrium but according to the electronic ground state. In addition, the Markov approximation requires that the actual EET be slow compared to the reservoir relaxation time scale. Taking, for example, the Debye spectral density, Eq. (6.51) (or (3.302)), the time scale of the reservoir relaxation (vibrational motion) is given by ω_D^{-1}. The deviation from equilibrium upon excitation is characterized by the reorganization energy (skipping again the site index) $E_\lambda = S_{eg}/2$.

In Figure 9.15, we compare the Förster and the Redfield EET rates (the specific expression is given in Eq. (9.169)) for a heterodimer. In addition, the exact result according to a HEOM propagation is given. In all cases the relaxation time is fixed ($\omega_D^{-1} = 100\,\text{fs}$), and the reorganization energy is varied. For small reorganization energy, the three methods give comparable results since in the limit of weak
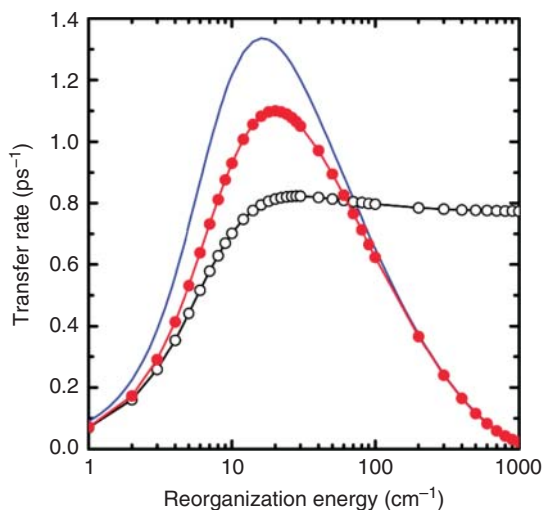
Figure 9.15 Transfer rates for a DA heterodimer ($\hbar(\omega_D - \omega_A) = 100\,\text{cm}^{-1}$) coupled to a reservoir that is described by a Debye spectral density, Eq. (3.302). Rates are shown in dependence on the reorganization energy (E_λ, Eq. (3.296)) for $\omega_D^{-1} = 100\,\text{fs}$. The excitonic coupling is $J_{DA} = 20\,\text{cm}^{-1}$. Closed circles: exact results using the HEOM approach (cf. Section 3.11), solid line: Förster theory, and open circles: Redfield theory (reprinted with permission from Ishizaki and Fleming [10], copyright American Institute of Physics (2009)).

excitonic and system–reservoir coupling, perturbation theory and Markov approximation are reasonable. For large reorganization energies, the perturbation theory with respect to the system–reservoir coupling breaks down, and Redfield theory predicts a behavior that is qualitatively wrong. In fact, increasing E_λ, one reaches the slow modulation limit, and for a fixed DA detuning, the rate should decrease toward zero, cf. Eq. (9.139).

9.5.3.1 Case of Common Vibrational Coordinates

The preceding considerations of EET focused on the case where the donor and the acceptor molecules are exclusively characterized by their own (intramolecular) vibrations. Such a description is appropriate if the distance between the molecules is large. If they are positioned not too far apart from each other, they may share common vibrational coordinates mainly related to the actual environment. We will study the effect of such common modes on EET here. A modulation of the excitonic coupling, which would also be possible in the case of smaller intermolecular distances, is described in Section 9.5.3.2.

The model has already been introduced in Section 9.3.2 (case of common reservoirs). The combined DOS of the type introduced in Eq. (9.128) determines the EET rate. However, the trace formula as well as the time evolution operators cannot be factorized into monomer contributions. It will be convenient to use the time-evolution operator $\hat{U}_m(t) = \exp(-i\mathcal{H}_m t/\hbar)$ with the Hamiltonian

$$\mathcal{H}_m = \hbar\omega_m + H_{\text{vib}}^{(m)}. \tag{9.142}$$

The energy $\hbar\omega_m$ follows as $E_m - E_\lambda^{(m)}$, with the reorganization energy $E_\lambda^{(m)} = \sum_\xi \hbar\omega_\xi g_m^2(\xi)$. The Hamiltonian $H_{\text{vib}}^{(m)} = \sum_\xi \frac{\hbar\omega_\xi}{4}(P_\xi^2 + (Q_\xi + 2g_m(\xi))^2)$ describes the normal-mode vibrational dynamics if molecule m is in its excited state. Then, the correlation function introduced in Eq. (9.128) reads ($\omega_{mn} = \omega_m - \omega_n$):

$$C_{m\to n}(t) = e^{i\omega_{mn}t}\text{tr}_{\text{vib}}\{\hat{R}_m e^{iH_{\text{vib}}^{(m)}t/\hbar}e^{-iH_{\text{vib}}^{(n)}t/\hbar}\}. \tag{9.143}$$

Concerning its general structure, the formula coincides with Eq. (6.19), where the combined DOS corresponds to linear absorption. Thus, we can directly use the results of Section 6.2.3, where the DOS has been specified to a model of displaced harmonic PES (in the same manner, we could directly compute the low-temperature version of nonadiabatic electron transfer in Section 7.4.3). According to Eq. (6.23), we can write the correlation function, Eq. (9.143), as

$$C_{m\to n}(t) = e^{i\omega_{mn}t - G_{mn}(0) + G_{mn}(t)}. \tag{9.144}$$

The $G_{mn}(t)$ are similar to Eq. (6.24). After defining the spectral density

$$j_{mn}(\omega) = \sum_\xi (g_m(\xi) - g_n(\xi))^2 \, \delta(\omega - \omega_\xi), \tag{9.145}$$

they read

$$G_{mn}(t) = \int d\omega \, e^{-i\omega t}(1 + n(\omega)) \left[j_{mn}(\omega) - j_{mn}(-\omega)\right]. \tag{9.146}$$

The dimensionless exciton–vibrational coupling constants have been introduced in Eq. (9.87). The related rate expression follows as

$$k_{m\to n} = \frac{|J_{mn}|^2}{\hbar^2}e^{-G_{mn}(0)}\int dt \, e^{i\omega_{mn}t + G_{mn}(t)}. \tag{9.147}$$

It provides an expression that is directly related to a spectral density. As in Section 9.5.3, we may consider the limiting case of slow and fast nuclear motion, with the resulting combined DOS being formally identical to those of Eqs. (9.139) and (9.140), respectively. However, the Stokes shift as well as the dephasing times represent global quantities that do not separate into monomer contributions. For illustration, we only consider the approximation of slow nuclear motion (see also the derivation of the high-temperature limit of ET in Section 7.4.3). According to Eq. (7.98), we reproduce $D_{mn}^{(\text{slow})}$, Eq. (9.139), however, with the common reorganization energy $E_\lambda \equiv S_{mn}/2 = \hbar \int_0^\infty d\omega \, \omega j_{mn}(\omega)$.

It is interesting to expand the EET rate, Eq. (9.147), in lowest order with respect to the exciton–vibrational coupling. We calculate the time integral in Eq. (9.147) with $\exp G_{mn}(t) \approx 1 + G_{mn}(t)$ and obtain (note that in principle the prefactor $\exp[-G_{mn}(0)]$ has to be expanded as well)

$$k_{m\to n} = \frac{|J_{mn}|^2}{\hbar^2}e^{-G_{mn}(0)} \left(2\pi\delta(\omega_{mn}) + G_{mn}(\omega_{mn})\right). \tag{9.148}$$

The rate diverges for $\omega_{mn} = 0$, otherwise it becomes proportional to $G_{mn}(\omega_{mn}) = 2\pi[1 + n(\omega_{mn})] [j_{mn}(\omega_{mn}) - j_{mn}(-\omega_{mn})]$, an expression, which we will discuss again later in Section 9.6.3. In the following section, we demonstrate for a similar case that the divergence can be removed by the inclusion of intramolecular vibrations.

9.5.3.2 Case of Vibrational Modulation of the Excitonic Coupling

In what follows we consider the case of EET in systems with an intermolecular distance less than the Förster radius. Such a situation is characterized not only by the participation of intermolecular (aggregate normal mode) vibrations but also by vibrational modulations of the excitonic coupling J_{mn}. This may result from distance fluctuations of the coupled molecules, a change in their mutual orientation, or even from a dependence of the transition density on the intramolecular normal-mode displacement. Such a modulation has already been introduced in Eq. (9.95). To compute a respective EET rate, we use the aggregate Hamiltonian, Eq. (9.90), but with the simplifying assumption of a coupling to vibrational coordinates, Eq. (9.93), which has been reduced to site off-diagonal contributions only (the coupling due to the $g_m(\xi)$, Eq. (9.87), is neglected). Now, the transition rates read (see Section 3.14.5, Eq. (3.512))

$$k_{m \to n} = \int dt\, e^{i\omega_{mn}t} \tilde{C}_{m \to n}(t), \tag{9.149}$$

with the new type of correlation functions

$$\tilde{C}_{m \to n}(t) = \frac{1}{\hbar^2} \mathrm{tr}_{\mathrm{vib}} \{ \hat{R}_{\mathrm{vib}} \hat{U}_{\mathrm{vib}}^+(t) J_{mn}(q) \hat{U}_{\mathrm{vib}}(t) J_{nm}(q) \}, \tag{9.150}$$

which accounts for the normal-mode dependence of the excitonic coupling. Since we removed the excitation (site) energies $\hbar\omega_m$ and $\hbar\omega_n$ from the time-evolution operators (leading to the transition frequencies ω_{mn}), time evolution is caused by nondisplaced normal mode oscillator Hamiltonians (the $\hat{R}_m$ have been replaced by $\hat{R}_{\mathrm{vib}}$ describing nondisplaced vibrational equilibrium). Using Eq. (9.95), which assumes a linear dependence on the normal-mode coordinate, we get

$$\tilde{C}_{m \to n}(t) = \frac{|J_{mn}^{(0)}|^2}{\hbar^2} + \sum_{\xi} |\omega_{\xi} \tilde{g}_{mn}(\xi)|^2 \mathrm{tr}_{\mathrm{vib}} \{ \hat{R}_{\mathrm{vib}} Q_{\xi}(t) Q_{\xi} \}$$

$$= \frac{|J_{mn}^{(0)}|^2}{\hbar^2} + \sum_{\xi} |\omega_{\xi} \tilde{g}_{mn}(\xi)|^2 \left(e^{-i\omega_{\xi}t}[1 + n(\omega_{\xi})] + e^{i\omega_{\xi}t} n(\omega_{\xi}) \right). \tag{9.151}$$

A similar expression has already been computed in Section 3.7.2 (note that a single coordinate operator Q_{ξ} does not contribute, and that the quadratic expression becomes diagonal with respect to the normal-mode index ξ). We introduce the spectral density

$$\tilde{j}_{kl,mn}(\omega) = \sum_{\xi} \tilde{g}_{kl}(\xi) \tilde{g}_{mn}(\xi) \delta(\omega - \omega_{\xi}) \tag{9.152}$$

and, assuming $\omega_{mn} \neq 0$, arrive at the following rate expression:

$$k_{m \to n} = \int dt\, e^{i\omega_{mn}t} \int d\omega\, \omega^2 \left(e^{-i\omega t}[1 + n(\omega)] + e^{i\omega t} n(\omega) \right) \tilde{j}_{mn,nm}(\omega)$$

$$= 2\pi \omega_{mn}^2 \left(1 + n(\omega_{mn}) \right) [\tilde{j}_{mn,nm}(\omega_{mn}) - \tilde{j}_{mn,nm}(-\omega_{mn})]. \tag{9.153}$$

Since $\omega_{mn} \neq 0$, there is no contribution proportional to $\delta(\omega_{mn})$, and EET is characterized by the spectral density due to the vibrational modulation of the excitonic

coupling. This rate expression would be of interest if the excitation energies of donor and acceptor are out of resonance (the spectral overlap is small).

The divergence for $\omega_{mn} = 0$ does not appear in the model of Section 9.3.3, which comprises intramolecular and aggregate normal-mode vibrations. Using this model (but neglecting the diagonal part of the coupling to the normal-mode vibrations), the rate can be deduced from a type of correlation function as introduced in Eq. (9.150). However, it has to be multiplied with the combination $C_{m\ e \to g}(t) C_{n\ g \to e}(t)$ of monomer correlation functions already used in Eq. (9.132). We generalize the latter formula by the inclusion of an additional frequency argument to arrive at $\mathcal{D}_{mn}(\omega) = 1/2\pi\hbar \times \int dt \exp(i\omega t) C_{m\ e \to g}(t) C_{n\ g \to e}(t)$ and write the EET rate as

$$k_{m \to n} = \frac{|J_{mn}^{(0)}|^2}{\hbar^2} \mathcal{D}_{mn}(0)$$

$$+ 2\pi\hbar \int d\omega\, \omega^2 \tilde{j}_{mn,nm}(\omega) \left([1 + n(\omega)] \mathcal{D}_{mn}(-\omega) + n(\omega) \mathcal{D}_{mn}(\omega) \right). \quad (9.154)$$

It results in a Förster-like expression, Eq. (9.115), but corrected by transitions that are assisted by a single normal-mode vibrational quantum. According to Eq. (9.153), it is clear that this rate expression would be of particular value if the DA spectral overlap given by $\mathcal{D}_{mn}(0)$ is small, but the aggregate normal-mode vibrations cover frequency ranges ω where $\mathcal{D}_{mn}(\pm\omega)$ takes large enough values.

9.6 Transfer Dynamics in the Case of Strong Excitonic Coupling

In Section 9.4.1, we characterized the case of strong excitonic coupling as one where it is most appropriate to consider all quantities of interest in the exciton representation. The corresponding Hamiltonian (referring to the singly excited aggregate state and the inclusion of aggregate normal-mode vibrations) is introduced in Section 9.3.4. To characterize the corresponding exciton dynamics, we may compute the populations P_α of exciton levels, Eq. (9.108), as well as work with the respective exciton density matrix $\rho_{\alpha\beta}(t)$, Eq. (9.109). In the present section, we do this by carrying out a perturbation theory with respect to the exciton–vibrational coupling, introduced in Eq. (9.102). Of course, EET rates in the exciton representation are included in the corresponding density matrix theory formulated in the framework of the QME introduced in Section 3. Therefore, it would not be necessary to develop a separate rate theory. Nevertheless, for completeness and further reference, we briefly present such a rate equation approach in Section 9.6.1. The full density matrix theory is formulated afterward.

9.6.1 Rate Equations for Exciton Dynamics

When focusing on a rate theory description of exciton dynamics with rates of the second order with respect to the exciton–vibrational coupling, Eq. (9.102), we expect

the following type of equations:

$$\frac{\partial}{\partial t} P_\alpha(t) = -\sum_\beta \left(k_{\alpha \to \beta} P_\alpha(t) - k_{\beta \to \alpha} P_\beta(t) \right). \tag{9.155}$$

The rates have to be calculated from

$$k_{\alpha \to \beta} = \int dt \, e^{i\Omega_{\alpha\beta} t} C_{\alpha \to \beta}(t). \tag{9.156}$$

The transition frequencies are defined by the exciton energies as $\Omega_{\alpha\beta} = (\mathcal{E}_\alpha - \mathcal{E}_\beta)/\hbar$, and the correlation function reads

$$C_{\alpha \to \beta}(t) = \frac{1}{\hbar^2} \mathrm{tr}_{\mathrm{vib}} \{ \hat{R}_{\mathrm{vib}} \hat{U}_{\mathrm{vib}}^+(t) \hat{V}_{\alpha\beta} \hat{U}_{\mathrm{vib}}(t) \hat{V}_{\beta\alpha} \}. \tag{9.157}$$

The vibrational dynamics are characterized by the Hamiltonian H_{vib} of unshifted normal mode vibrations of the aggregate, which results in the equilibrium statistical operator and the time-evolution operator $\hat{R}_{\mathrm{vib}}$ and $\hat{U}_{\mathrm{vib}}(t)$, respectively. The coupling operators $\hat{V}_{\alpha\beta}$ are given by $\sum_\xi \hbar \omega_\xi g_{\alpha\beta}(\xi) Q_\xi$. The computation of $\hat{U}_{\mathrm{vib}}^+(t) \hat{V}_{\alpha\beta} \hat{U}_{\mathrm{vib}}(t)$ simply results in time-dependent normal-mode oscillator operators, and the correlation function can be determined in analogy to Eq. (9.151):

$$C_{\alpha \to \beta}(t) = \int d\omega \, \omega^2 e^{-i\omega t} (1 + n(\omega)) \left(j_{\alpha\beta,\beta\alpha}(\omega) - j_{\alpha\beta,\beta\alpha}(-\omega) \right). \tag{9.158}$$

This results in the following transition rate:

$$k_{\alpha \to \beta} = 2\pi \Omega_{\alpha\beta}^2 \left([1 + n(\Omega_{\alpha\beta})] j_{\alpha\beta,\beta\alpha}(\Omega_{\alpha\beta}) + n(\Omega_{\beta\alpha}) j_{\alpha\beta,\beta\alpha}(\Omega_{\beta\alpha}) \right). \tag{9.159}$$

The spectral density has been defined in the general form

$$j_{\alpha\beta,\gamma\delta}(\omega) = \sum_\xi g_{\alpha\beta}(\xi) g_{\gamma\delta}(\xi) \delta(\omega - \omega_\xi). \tag{9.160}$$

According to Eq. (9.159), transitions between different exciton states are accompanied by the absorption or emission of a single normal mode oscillator quantum. The spectral density $j_{\alpha\beta,\beta\alpha}$ taken at the exciton transition frequency regulates the strength of such transitions.

9.6.2 Density Matrix Equations for Exciton Dynamics

The foregoing section used exciton state populations to characterize EET, which is only possible if coherences among different levels described by off-diagonal elements of the exciton density matrix $\rho_{\alpha\beta}$ are of no importance. If we consider, however, an ultrafast optical preparation of a singly excited aggregate state, these coherences will appear. In analogy to the optical preparation of an excited electronic state discussed in Section 6.5, an *excitonic* wave packet is formed.[17] Just such a case we have in mind when introducing the exciton density matrix description of EET even though the coupling to the radiation field will not be included in what follows.

---

17) If instantaneous optical excitation is assumed, the resulting superposition state is of the type $|A\rangle = \sum_\alpha C_\alpha |\alpha\rangle$. Accordingly, an excitonic wave packet evolves in time as already discussed in Section 3.2.1. Obviously, the initial value of the exciton density matrix reads $\rho_{\alpha\beta}(t_0) = \langle \alpha| \, |A\rangle\langle A| \, |\beta\rangle \equiv C_\alpha C_\beta^*$; that is, in principle, all off-diagonal elements contribute.

The desired density matrix theory is easily obtained by translating the general approach of Section 3.8 to Frenkel excitons in molecular aggregates. To this end, we take H_{ex} from Eq. (9.69) as the system Hamiltonian H_S. The reservoir Hamiltonian H_R is given by the vibrational Hamiltonian H_{vib}, Eq. (9.98). Finally, the system–reservoir coupling H_{S-R} is identified as the exciton–vibrational coupling, Eq. (9.102). To use the general formulas of Section 3.8.2 (where any memory effects due to the coupling to the reservoir are neglected), we have to rewrite H_{ex-vib} in the form of Eq. (3.198). In the present case, the summation in Eq. (3.198) is carried out with respect to the index $u = (\alpha, \beta)$ combining the two possible exciton indices. Therefore, the system part of the interaction Hamiltonian is $K_u = |\alpha\rangle\langle\beta|$, and the reservoir part is $\Phi_u = \sum_\xi \hbar\omega_\xi g_{\alpha\beta}(\xi)Q_\xi$. This identification enables us to write down the reservoir correlation function equation (3.247) as (see also Section 3.8.4)

$$C_{\alpha\beta,\gamma\delta}(t) = \sum_\xi \omega_\xi^2 g_{\alpha\beta}(\xi)g_{\gamma\delta}(\xi)\left[[1 + n(\omega_\xi)]e^{-i\omega_\xi t} + n(\omega_\xi)e^{i\omega_\xi t}\right]. \tag{9.161}$$

(The equilibrium correlation function of the dimensionless normal-mode coordinates was calculated in Section 3.7.2.) Let us use the most simple variant of the density matrix theory introduced in Section 3.8.3 (Bloch approximation), which neglects all elements of the relaxation matrix that cannot be written in terms of energy relaxation and dephasing rates. This decouples the equation of motion for the population- and coherence-type density matrix elements, and we obtain the following equations of motion:

$$\frac{\partial}{\partial t}\rho_{\alpha\beta} = -i\Omega_{\alpha\beta}\rho_{\alpha\beta}$$
$$-\delta_{\alpha\beta}\sum_\kappa \left(k_{\alpha\to\kappa}\rho_{\alpha\alpha} - k_{\kappa\to\alpha}\rho_{\kappa\kappa}\right) - (1 - \delta_{\alpha\beta})(\gamma_\alpha + \gamma_\beta)\rho_{\alpha\beta}. \tag{9.162}$$

Since the basis $|\alpha\rangle$ diagonalizes the single-exciton Hamiltonian H_{ex}, the coherent part on the right-hand side contains only the transition frequencies between the exciton eigenstates, $\Omega_{\alpha\beta}$. The transition rates have been already introduced in Eq. (9.159) (they are identical to $2\Gamma_{\alpha\beta,\beta\alpha}(\Omega_{\alpha\beta})$, a quantity defined in its general form already in Eq. (3.342)). The corresponding dephasing rates are

$$\gamma_\alpha = \frac{1}{2}\sum_\beta k_{\alpha\to\beta}. \tag{9.163}$$

Assuming that the exciton–vibrational coupling matrix factorizes, $g_{\alpha\beta}(\xi) = g_{\alpha\beta} \times g(\xi)$, the relaxation rates are given by

$$k_{\alpha\to\beta} = 2\pi|g_{\alpha\beta}|^2\Omega_{\alpha\beta}^2\left[1 + n(\Omega_{\alpha\beta})\right]\left[j(\Omega_{\alpha\beta}) - j(-\Omega_{\alpha\beta})\right]. \tag{9.164}$$

By construction, the stationary limit of the equations of motion for the single-exciton reduced density matrix is given by

$$\rho_{\alpha\beta}(\infty) = \delta_{\alpha\beta}\frac{e^{-\mathcal{E}_\alpha/k_B T}}{\sum_{\alpha'}e^{-E_{\alpha'}/k_B T}}. \tag{9.165}$$

Since the excitonic coupling has been accounted for in the determination of the relaxation rates in Eq. (9.164), it is guaranteed that the energy relaxation rates fulfill the principle of detailed balance with respect to the exciton eigenstates

$k_{\alpha\to\beta}/k_{\beta\to\alpha} = \exp\{-[\mathcal{E}_\alpha - \mathcal{E}_\beta]/k_B T\}$. Accordingly, the system will relax to the correct equilibrium distribution (Eq. (9.165)) after initial preparation in a nonequilibrium state.[18]

Finally, it should be mentioned that the assumption of a linear exciton–vibrational coupling that neglects pure dephasing, for instance, leads to a relaxation matrix according to which coherences between degenerate eigenstates ($\Omega_{\alpha\beta} = 0$) are not subject to dephasing processes. Therefore, the equations of motion (9.162) might not be appropriate for the description of highly symmetric aggregates having degenerate exciton eigenenergies such as regular molecular rings. In realistic systems, however, static distributions of monomer transition energies and dipole–dipole interactions are likely to remove any degeneracy, thus justifying the use of Eq. (9.162).

To illustrate the dynamics in the eigenstate representation, we show in Figure 9.16 the numerical solution of Eq. (9.162) for a regular chain-like aggregate with seven monomers. For simplicity, we restrict ourselves to situations where a factorization of the exciton–vibrational coupling matrix is justified (cf. Section 3.7.3). In this case, the dissipative influence of the aggregate's vibrational modes can be described by a single, exciton state independent, spectral density

$$j(\omega) = \sum_\xi g^2(\xi)\delta(\omega - \omega_\xi). \tag{9.166}$$

In the example, we used the model spectral density type $j(\omega) = \theta(\omega)\exp\{-\omega/\omega_c\}$ / $2\omega_c^3$. Here, ω_c is a cutoff frequency (cf. discussion in Section 3.7.3). First, we plotted in Figure 9.16a the transition amplitudes (oscillator strengths of the respective transitions) defined in Eq. (9.200) together with the positions of all eigenstates. Being in H-aggregate configuration, the energetically highest exciton state has by far the largest transition amplitude. This allows us to assume that an external field can prepare the system in this particular state. With the highest state being initially excited with probability of 1, the subsequent dynamics shows a relaxation toward the equilibrium distribution (9.165). The latter will be different for two different temperatures (Figure 9.16c,d). The relaxation proceeds via emission and absorption of single vibrational quanta. The relaxation rates relevant for the initial excited state are shown in Figure 9.16b for the two temperatures.

9.6.3 Site Representation

To study EET in real space, even though delocalized states have been formed, we may use the theory of the foregoing section but change from the exciton density matrix to the local site population using Eq. (9.110). It would also be of interest to directly set up an equation of motion for the density matrix ρ_{mn} in site representation. This would automatically lead to a formulation of the dissipative part in terms of localized states instead of exciton states. We will find that this approach has some shortcomings since it neglects contributions of the excitonic coupling to dissipation.

---

18) Note, however, that Eq. (9.165) neglects the effect of exciton–vibrational coupling on the total equilibrium density. This is justified in the assumed weak coupling limit.
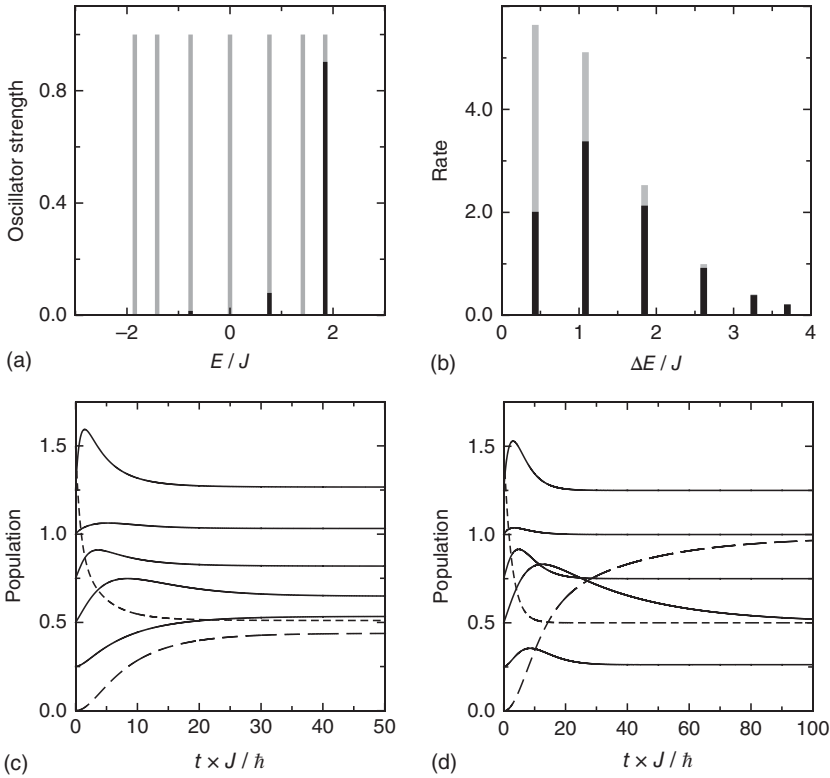
Figure 9.16 Dissipative dynamics in a regular chain-like aggregate of seven molecules with nearest-neighbor coupling of strength J ($J_{mn}/J = \delta_{m,n+1} + \delta_{m,n-1}$): (a) position of the energy levels (gray bars) as well as oscillator strengths (solid bars), (b) transition rates from the state of highest energy to all states of lower energy (given at the respective energy gap) for $1/k_B T = J$ (gray) and $1/k_B T = 10J$ (solid). The two lower panels show the population dynamics $\rho_{\alpha\alpha}(t) = P_\alpha(t)$ for $1/k_B T = J$ (c) and $1/k_B T = 10J$ (d). Initially, the state of highest energy has been populated. The curves are offset with increasing energy (short dashes: highest state, long dashes: lowest state). For the spectral density, we have chosen $j(\omega) = \theta(\omega) \exp\{-\omega/\omega_c\}/2\omega_c^3$ with a cutoff frequency $\hbar\omega_c = 0.5J$. The coupling matrix has been set to $g_{mn} = 0.5J_{mn}$.

We do not present the details of the derivation of density matrix equations but refer the reader to the rather similar discussion in Section 9.6.2.

In what follows, we again assume the validity of the Bloch model and arrive at the following density matrix equations:

$$
\frac{\partial}{\partial t} \rho_{mn} = -i\omega_{mn}\rho_{mn} - \frac{i}{\hbar} \sum_l (j_{ml}\rho_{ln} - j_{ln}\rho_{ml})
$$

$$
- \delta_{mn} \sum_l (k_{m\to l}\rho_{mm} - k_{l\to m}\rho_{ll}) - (1 - \delta_{mn})(\gamma_m + \gamma_n)\rho_{mn}. \tag{9.167}
$$

The transition rates are introduced in Eq. (9.153) in terms of the related spectral densities, Eq. (9.152), which, however, appear here directly within the framework of the QME approach (note the general notation here with $g_{mn}(\xi)$, Eq. (9.96), instead

of $\tilde{g}_{mn}(\xi)$). Obviously, $k_{m \to n}$ is only different from zero if the coupling to the vibrational modes is *off-diagonal* in the site index m. This requires that $g_{mn}(\xi) \neq 0$ for $m \neq n$. Since the off-diagonal elements of $g_{mn}(\xi)$ derive from the modulation of the excitonic coupling (cf. Eq. (9.95)), this is in accordance with the mentioned transfer character of energy relaxation. The transition rates define the dephasing rates as (cf. Eq. (3.352))

$$\gamma_m = \frac{1}{2} \sum_n k_{m \to n}. \tag{9.168}$$

Let us discuss the density matrix equations (9.167). The coherent contribution to the right-hand side (first line), which derives from the matrix elements of H_{ex}, Eq. (9.91), indicates that the motion of a single exciton in the aggregate is enforced by the excitonic coupling. This means that an exciton initially localized at a single molecule or over a small number of molecules will move through the aggregate like a wave packet. This motion is reversible and results from a nonperturbative consideration of the excitonic coupling. The dissipative part on the right-hand side of Eq. (9.167) (second line) is responsible for irreversibility. In particular, we have energy relaxation that affects the occupation probabilities, $\rho_{mm}(t) = P_m(t)$, and dephasing of the single-exciton coherences described by $\rho_{mn}(t)$. For an aggregate having identical monomer transition energies, such as the regular chain discussed in Section 9.2.4, the occupation probabilities at thermal equilibrium should be equal for all monomers. However, an initial preparation of an exciton at a particular molecule will result in a coherent motion over the whole aggregate since $\omega_{mn} = 0$ leads to vanishing energy relaxation rates (cf. Eq. (9.153)). This contradiction is due to the restriction to a *linear* exciton–vibrational interaction. In particular, the incorporation of pure dephasing contributions would result in a proper equilibration. Nevertheless, the theory in its present form is appropriate for situations where some irregularity of the monomeric $S_0 \to S_1$ transitions is present. But this irregularity leading to a localization of the exciton states is already required to justify the neglect of the dipole–dipole interaction when calculating the relaxation rates.

In order to illustrate the dynamics according to Eq. (9.167), we consider the linear chain model of Figure 9.16 but now for the case of different site energies. The energy relaxation rates in the site representation become

$$k_{m \to n} = 2\pi \omega_{mn}^2 |g_{mn}|^2 \left[1 + n(\omega_{mn}) \right] \left[j(\omega_{mn}) - j(\omega_{nm}) \right]. \tag{9.169}$$

In Figure 9.17, we have plotted the population dynamics for two different system–reservoir coupling strengths. The behavior of $P_m(t)$ reflects the interplay between coherent exciton transfer due to the coupling between the sites and the energy relaxation and dephasing due to the exciton–vibrational coupling. Increasing the strength of the latter results in a gradual disappearance of the oscillatory behavior of the site populations.

In order to examine the manner in which the present density matrix theory includes hopping-like Förster transfer as a limiting case, we derive the respective hopping transfer rate $k_{m \to n}$. We notice that Förster theory implies a weak Coulomb interaction, and the transfer dynamics can be categorized as being in the
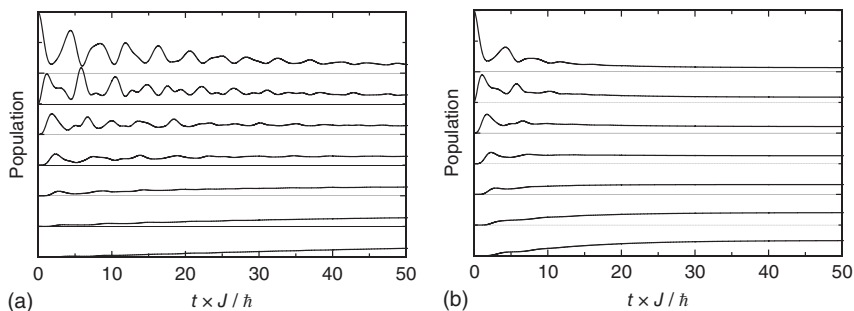
Figure 9.17 Dissipative exciton dynamics according to Eq. (9.167) for a linear aggregate of seven monomers (model of Figure 9.16 but with an energetic offset of J between the neighboring site energies). The initial state has been chosen as $P_m(t=0) = \delta_{m1}$, and the temperature is $1/k_B T = J$. For the system–reservoir coupling, we used $g_{mn} = 0.1J_{mn}$ (a) and $g_{mn} = 0.2J_{mn}$ (b). (For visual clarity, the curves have been vertically offset according to the energetic ordering of the sites where the initially populated site is highest in energy.)

nonadiabatic limit according to the terminology introduced for electron transfer in Section 7.3. Stressing the similarity to the case of electron transfer, we can adopt the results of Section 7.9.2, where the nonadiabatic electron-transfer rate has been derived from density matrix theory (Eq. (7.226)). In the present case, the nonadiabatic rate for exciton (hopping) transfer is given by

$$k_{m \to n} = \frac{2\pi}{\hbar^2} |J_{mn}|^2 \frac{(\gamma_m + \gamma_n)/\pi}{\left(\omega_{mn}^2 + (\gamma_m + \gamma_n)^2\right)}. \tag{9.170}$$

This formula contains a broadening of the transition with frequency ω_{mn}, which is of a Lorentzian type. It resembles the rate expression introduced in Section 9.5.3 with the related combined DOS, Eq. (9.140), derived for the case of fast nuclear motion. However, the dephasing rates γ_m and γ_n are derived in the lowest order of perturbation theory, while those appearing in Eq. (9.140) include the Stokes shift and thus completely account for nuclear rearrangement beyond any perturbational treatment.

9.6.4 Excitation Energy Transfer Among Different Aggregates

As demonstrated in Section 9.5, Förster theory is based on the assumption of the motion of excitations that are localized on a single monomer of the aggregate. A generalization of this case appears if two aggregates that are characterized by strong internal Coulomb interaction are weakly coupled. This is the case where the excitonic coupling enters nonperturbatively as well as perturbatively into the description.

For the derivation of the transfer rate, one can closely follow the argument of Section 9.5.1. However, the initial and the final states of the transitions are not those of a single monomer but of the whole aggregate. To see how this modifies the rate, let us first consider the coupling matrix (cf. Eq. (9.29)). We neglect as in Eq. (9.114) the dependence of the electronic matrix elements on the vibrational coordinates and

discuss the transition from the exciton levels $|D\alpha\rangle$ of the donor aggregate to the exciton levels $|A\beta\rangle$ of the acceptor aggregate. If we expand the exciton states according to Eq. (9.67), we obtain

$$
\begin{aligned}
J_{D\alpha,A\beta} &= \langle D\alpha, A0 | V_{\mathrm{DA}}^{(\mathrm{el-el})} | A\beta, D0 \rangle \\
&= \sum_{m,n} c_{D\alpha}^*(m) \langle Dm, A0 | V_{mn}^{(\mathrm{el-el})} | An, D0 \rangle c_{A\beta}(n) \\
&= \sum_{m,n} c_{D\alpha}^*(m) c_{A\beta}(n) J_{Dm,An}.
\end{aligned}
\tag{9.171}
$$

The interaggregate coupling is build up by the couplings $J_{Dm,An}$ between the monomers m of the donor aggregate and the monomers n of the acceptor aggregate. Since both expansion coefficients are proportional to $1/\sqrt{N_{\mathrm{mon}}}$, where N_{mon} denotes the (assumed) identical number of monomers in both aggregates, a rough estimate of the coupling matrix elements gives $N_{\mathrm{mon}}\bar{J}$ ($\bar{J}$ is a representative mean value of the various J_{mn}). Hence, we have to expect a certain enhancement of the EET rate in relation to the ordinary Förster transfer if the transitions take place between delocalized states of two separated aggregates. The transition rate can be written as

$$
\begin{aligned}
k_{D\alpha \to A\beta} &= \frac{2\pi}{\hbar} \, |J_{D\alpha,A\beta}|^2 \\
&\times \sum_{M,N} f(\mathcal{E}_{D\alpha M}) |\langle \chi_{D\alpha M} | \chi_{A\beta N} \rangle|^2 \delta(\mathcal{E}_{D\alpha M} - \mathcal{E}_{A\beta N}).
\end{aligned}
\tag{9.172}
$$

Obviously, a similar expression as Eq. (9.123) for the total rate $k_{\mathrm{DA}} = \sum_{\alpha,\beta} k_{D\alpha \to A\beta}$ can be derived, where the emission and absorption spectra now belong to the whole donor and acceptor aggregates, respectively.

9.6.5 Exciton Transfer in the Case of Strong Exciton–Vibrational Coupling

As already underlined in Section 9.3, the adiabatic exciton Hamiltonian, Eq. (9.82), would be an appropriate model to discuss exciton–vibrational coupling as well as excitonic coupling beyond any perturbation theory, at least in principle. Accordingly, one has to carry out an expansion of the PES up to the second order with respect to the deviation from the equilibrium position. Then, the introduction of normal-mode vibrations leads to excitonic PES as introduced in Eq. (9.104). Nonadiabatic couplings $\hat{\Theta}_{\alpha\beta}$ will appear, which induce transitions between the different PES. One obtains the lowest order transition rate between different exciton levels as

$$
k_{\alpha \to \beta} = \frac{2\pi}{\hbar} \sum_{M,N} f(\mathcal{E}_{\alpha M}) |\langle \chi_{\alpha M} | \hat{\Theta}_{\alpha\beta} | \chi_{\beta N} \rangle|^2 \delta(\mathcal{E}_{\alpha M} - \mathcal{E}_{\beta N}),
\tag{9.173}
$$

where the excitonic energies include the set of vibrational quantum numbers M or N. It should be emphasized that this rate expression can be understood as a rate for an internal conversion process between delocalized excitonic aggregate states. The given rate expression, Eq. (9.173), however, has only formal significance since the vibrational states are hardly obtainable for realistic systems.

Alternatively, one could start with $H_{\mathrm{agg}}^{(1)}$, Eq. (9.105), which resembles the diabatic picture. Now, the off-diagonal part of the exciton–vibrational coupling, Eq. (9.102),

becomes responsible for transitions. It may represent a weak perturbation if different exciton states are localized on different parts of the aggregate (cf. Eq. (9.103)). In this case, we may follow the general rate theory of Section 3.14.5, Eq. (3.512), and write the rate as

$$k_{\alpha \to \beta} = \int dt \, e^{i\tilde{\Omega}_{\alpha\beta} t} C_{\alpha \to \beta}(t). \tag{9.174}$$

The transition frequencies $\tilde{\Omega}_{\alpha\beta} = \tilde{\Omega}_\alpha - \tilde{\Omega}_\beta$ are defined by the shifted exciton energies $\hbar\tilde{\Omega}_\alpha = \mathcal{E}_\alpha - \sum_\xi \hbar\omega_\xi g_{\alpha\alpha}^2(\xi)$ introduced in Eq. (9.104), and the correlation functions take the form

$$C_{\alpha \to \beta}(t) = \frac{1}{\hbar^2} \mathrm{tr}_{\mathrm{vib}} \{\hat{R}_\alpha \hat{U}_\alpha^+(t) \hat{V}_{\alpha\beta} \hat{U}_\beta(t) \hat{V}_{\beta\alpha}\}. \tag{9.175}$$

$\hat{R}_\alpha$ characterizes vibrational equilibrium in the excitonic PES referring to state $|\alpha\rangle$, and the time-evolution operators are defined by the vibrational Hamiltonians $T_{\mathrm{vib}} + \sum_\xi \hbar\omega_\xi (Q_\xi + 2g_{\alpha\alpha}(\xi))^2/4$, which are easily deduced from Eq. (9.105). Consequently, the coupling operators $\hat{V}_{\alpha\beta}$ ($\alpha \neq \beta$) are equal to $\sum_\xi \hbar\omega_\xi g_{\alpha\beta}(\xi) Q_\xi$. This approach results in rate equations of the type already introduced in Eq. (9.155), of course, with the rates, Eq. (9.174), replacing those defined in Eq. (9.156).[19]

In the following equation, we outline a different approach to the calculation of the rate.[20] In a generalization of the previous considerations, the rate now combines a displacement of the different PES to each other and a coordinate dependence of the coupling. In the derivation of $C_{\alpha \to \beta}$, we utilize the displacement operator

$$D_\alpha = \exp \left\{ -\sum_\xi g_{\alpha\alpha}(\xi) \left(C_\xi - C_\xi^+ \right) \right\}, \tag{9.176}$$

which has been originally introduced in Section 2.5.2 and extensively used in Section 6.7.1. Noting, for example, $\hat{U}_\alpha^+(t) = D_\alpha^+ \hat{U}_{\mathrm{vib}}^+(t) D_\alpha$, with $\hat{U}_{\mathrm{vib}}^+(t) = \exp(iH_{\mathrm{vib}} t/\hbar)$ and $H_{\mathrm{vib}} = \sum_\xi \hbar\omega_\xi C_\xi^+ C_\xi$ (in a slight modification of Eq. (9.92)), we may write (be aware of a similar replacement for $\hat{R}_\alpha$)

$$C_{\alpha \to \beta}(t) = \frac{1}{\hbar^2} \mathrm{tr}_{\mathrm{vib}} \{D_\alpha^+ \hat{R}_{\mathrm{vib}} \hat{U}_{\mathrm{vib}}^+(t) D_\alpha \hat{V}_{\alpha\beta} D_\beta^+ \hat{U}_{\mathrm{vib}}(t) D_\beta \hat{V}_{\beta\alpha}\}$$
$$= \frac{1}{\hbar^2} \mathrm{tr}_{\mathrm{vib}} \{\hat{R}_{\mathrm{vib}} \hat{U}_{\mathrm{vib}}^+(t) D_\alpha \hat{V}_{\alpha\beta} D_\alpha^+ D_\alpha D_\beta^+ \hat{U}_{\mathrm{vib}}(t) D_\beta D_\alpha^+ D_\alpha \hat{V}_{\beta\alpha} D_\alpha^+\}. \tag{9.177}$$

Next, we use Eq. (2.72) and arrive at

$$D_\alpha \hat{V}_{\alpha\beta} D_\alpha^+ = \sum_\xi \hbar\omega_\xi g_{\alpha\beta}(\xi) \left(Q_\xi - 2g_{\alpha\alpha}(\xi) \right) = \hat{V}_{\alpha\beta} - 2E_\lambda(\alpha\beta), \tag{9.178}$$

where we introduce the expression

$$E_\lambda(\alpha\beta) = \sum_\xi \hbar\omega_\xi g_{\alpha\beta}(\xi) g_{\alpha\alpha}(\xi). \tag{9.179}$$

---

19) The approach is known in the literature as the *modified Redfield theory* (cf. Section 3.8.2). However, this name is misleading since it represents the rate theory governing populations and not the complete exciton density matrix as it is the case in the original Redfield theory.

20) For more details, see also Renger and Marcus [11].

This resembles the reorganization energy appearing in Eq. (9.104). Note further that $D_\alpha \hat{V}_{\beta\alpha} D_\alpha^+$ is the Hermitian conjugate of Eq. (9.178).

For the following discussion, we rewrite the correlation function as

$$C_{\alpha \to \beta}(t) = \frac{4|E_\lambda(\alpha\beta)|^2}{\hbar^2}$$
$$\times \text{tr}_{\text{vib}} \{\hat{R}_{\text{vib}} \hat{U}_{\text{vib}}^+(t) \left(1 - \hat{K}_{\alpha\beta}\right) D_{\alpha\beta} \hat{U}_{\text{vib}}(t) D_{\alpha\beta}^+ \left(1 - \hat{K}_{\beta\alpha}\right)\}. \tag{9.180}$$

Here, we introduce

$$\hat{K}_{\alpha\beta} = \hat{V}_{\alpha\beta}/E_\lambda(\alpha\beta), \qquad \hat{K}_{\beta\alpha} = \hat{V}_{\beta\alpha}/E_\lambda^*(\alpha\beta) \tag{9.181}$$

and

$$D_{\alpha\beta} = D_\alpha D_\beta^+ \equiv \exp \left\{ \sum_\xi [g_{\alpha\alpha}(\xi) - g_{\beta\beta}(\xi)] \left(C_\xi - C_\xi^+\right) \right\}. \tag{9.182}$$

Moreover, we may formally remove the action of the vibrational time-evolution operators by setting $\hat{U}_{\text{vib}}^+(t) \left(1 - \hat{K}_{\alpha\beta}\right) D_{\alpha\beta} \hat{U}_{\text{vib}}(t) = \left(1 - \hat{K}_{\alpha\beta}(t)\right) D_{\alpha\beta}(t)$, with $\hat{K}_{\alpha\beta}(t) = \hat{U}_{\text{vib}}^+(t)\hat{K}_{\alpha\beta}\hat{U}_{\text{vib}}(t)$ and $D_{\alpha\beta}(t) = \hat{U}_{\text{vib}}^+(t)D_{\alpha\beta}\hat{U}_{\text{vib}}(t)$. Both time-dependent quantities are easily calculated since they depend on C_ξ and C_ξ^+, which have to be replaced by the time-dependent variants $C_\xi \exp(-i\omega_\xi t)$ and $C_\xi^+ \exp(i\omega_\xi t)$, respectively.

In order to carry out a computational procedure similar to Section 6.7.1, we generalize the correlation function to the expression

$$\tilde{C}_{\alpha \to \beta}(t; x, y) = \frac{4|E_\lambda(\alpha\beta)|^2}{\hbar^2}$$
$$\times \text{tr}_{\text{vib}} \left\{ \hat{R}_{\text{vib}} \exp\left(-x\hat{K}_{\alpha\beta}(t)\right) D_{\alpha\beta}(t) D_{\alpha\beta}^+ \exp\left(-y\hat{K}_{\beta\alpha}\right) \right\}. \tag{9.183}$$

A first-order expansion with respect to x and y followed by the choice $x = y = 1$ reproduces the original correlation function. However, the present form allows for the computation of the trace. There are always normal-mode oscillator operators in the exponent, which can be rearranged properly as already demonstrated in Section 6.7.1. Accordingly, the overall vibrational trace $T(t)$ contained in $\tilde{C}_{\alpha \to \beta}$ factorizes as $\prod_\xi T_\xi(t)$. Carrying out the calculation of the particular $T_\xi(t)$ similar to Section 6.7.1, one finally arrives at the following expression for the correlation functions entering the rate equation (9.174):

$$C_{\alpha \to \beta}(t) = e^{\Phi_{\alpha\beta}(t)} \left\{ \left[\lambda_{\alpha\beta} - \Lambda_{\alpha\beta}(t)\right]^2 + C_{\alpha \to \beta}^{(2)}(t) \right\}. \tag{9.184}$$

This includes

$$\Phi_{\alpha\beta}(t) = \int d\omega \, (e^{-i\omega t} - 1)(1 + n(\omega))$$
$$\times \left(j_{\alpha\alpha,\alpha\alpha}(\omega) - 2j_{\alpha\alpha,\beta\beta}(\omega) + j_{\beta\beta,\beta\beta}(\omega) - (\omega \to -\omega)\right), \tag{9.185}$$

the reorganization energy type expression

$$\lambda_{\alpha\beta} = \int d\omega \, \omega \left(j_{\alpha\alpha,\alpha\beta}(\omega) + j_{\alpha\beta,\beta\beta}(\omega)\right), \tag{9.186}$$

and the auxiliary function

$$\Lambda_{\alpha\beta}(t) = \int d\omega \, \omega e^{-i\omega t} \left(1 + n(\omega)\right)$$
$$\times \left(j_{\alpha\alpha,\alpha\beta}(\omega) - j_{\alpha\beta,\beta\beta}(\omega) - (\omega \to -\omega)\right). \tag{9.187}$$

The correlation function $C_{\alpha\to\beta}^{(2)}(t)$ also appearing in Eq. (9.184) is of second order in the off-diagonal exciton–vibrational coupling and identical to the quantity introduced in Eq. (9.158). The spectral densities appearing in all expressions have been introduced in Eq. (9.160). Since $\exp[\Phi_{\alpha\beta}(t)]$ mainly determines the rate, it is obvious that this expression goes beyond any perturbation theory with respect to the exciton–vibrational coupling. In the limit $g_{\alpha\alpha} = 0$, the rate expression reduces to what has been derived in Section 9.6.1 (only $C_{\alpha\beta}^{(2)}(t)$ remains nonzero).

9.6.6 Nonperturbative and Non-Markovian Exciton Dynamics

With the development of nonperturbative quantum dynamics methods such as HEOM (cf. Section 3.11), dissipative EET of Frenkel excitons became one of the main applications. The numerical effort related to a HEOM propagation of the exciton density matrix is strongly connected to the form of the spectral density and the temperature. Recall that the essential step in the derivation of the HEOM method presented in Section 3.11 has been a representation of the reservoir correlation function in terms of a sum of exponential functions. According to Section 3.7.3, such an expansion is possible for typical spectral density models. However, each term of the expansion will increase the dimension of the hierarchy index array and thus the numerical effort. Therefore, the method is particularly well suited for the description of the high-temperature limit where the Matsubara summation can be neglected. Still, spectral densities with a multipeak structure, which could be fit, for instance, to a sum of Brownian oscillator spectral densities, provide a challenge. The structured environment of electronic excitations in pigment–protein complexes such as those of photosynthesis features rather complex spectral densities. As an example, Figure 9.18b shows the experimentally determined spectral density for the S_0–S_1 electronic excitation of bacteriochlorophyll (BChl) *a* monomer in the FMO complex, cf. Figure 9.4.

To cope with structured spectral densities, wave function-based methods such as multilayer MCTDH (cf. Section 3.2.3) provide a feasible alternative. To this end, one assumes the validity of the exciton–vibrational coupling model introduced in Section 9.3.1. The Hamiltonian is given by Eq. (9.90); that is, each electronic transition couples to local vibrational DOFs according to a spectral density such as the one shown in Figure 9.18b. This requires to discretize the spectral density into a certain number of modes. Then, the state vector can be expanded into the basis of single excitation states according to[21]

$$|\Psi(Q, t)\rangle = \sum_m |\chi_m(Q, t)\rangle |m\rangle. \tag{9.188}$$

---

21) Note the analogy to the linear vibronic coupling model introduced for the description of ultrafast internal conversion in Section 6.6.2. In the present case, there is no dependence of the Coulomb coupling on the normal-mode coordinates, and the normal modes are monomer specific.
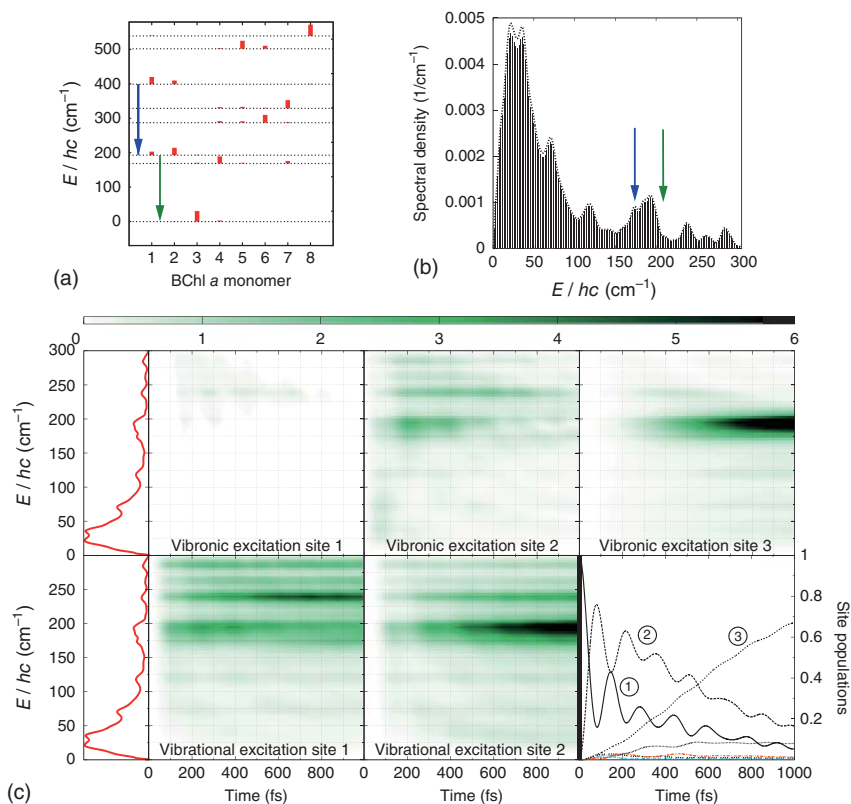
Figure 9.18 EET in the FMO complex (cf. Figure 9.4). (a) One-exciton eigenenergies and their decomposition into contributions from the different BChl *a* monomers (bars – $|c_\alpha(m)|^2$ in Eq. (9.69)). (b) Experimental spectral density and its discretization into 74 modes (arrows show transition energies according to panel (a)). (c) Distribution of vibrational (Eq. (9.190)) and vibronic (Eq. (9.191)) energies as well as population dynamics (Eq. (9.189)) after initial excitation of site $m = 1$ (sites 4–8 are only marginally populated; the spectral density is shown for guidance in the left panel) (For more details, see also Schulze et al. [12]).

Given N_{mon} monomers and N_{vib} modes per monomer, Q comprises the $N_{\text{mon}} \times N_{\text{vib}}$ normal-mode coordinates the wave packet depends on. The time-dependent Schrödinger equation with the Hamiltonian in Eq. (9.90) can be solved using the method outlined in Section 3.2.3.

As an example, we show a simulation of EET in the FMO complex in Figure 9.18. The complex consists of eight monomers (cf. Figure 9.4). Its one-exciton eigenstates are characterized in Figure 9.18a according to their decomposition equation (9.67). Figure 9.18b shows the spectral density together with its discretization. The system is initially prepared in site $m = 1$, and the population dynamics

$$P_m(t) = \langle \chi_m(Q, t) | \chi_m(Q, t) \rangle \tag{9.189}$$

reflects the strong coupling between sites $m = 1$ and 2 by exhibiting a quantum beat behavior, similar to the generic coupled two-level system in Figure 3.8. Site 3 is

gradually occupied. Note that in the photosynthetic apparatus of this green sulfur bacterium, site 3 is connected to the pathway to the reaction center, which reflects the purpose of the FMO complex to transmit energy from the chlorosome antenna to the reaction center (cf. Figure 9.4). Due to the high-dimensional vibrational space (ca. 600 modes) one observes a decay of population toward site 3 without any recurrence.

One advantage of such propagations is the availability of the full wave packet, which allows to extract information about the dynamics of the vibrational DOFs. Figure 9.18c shows the distribution of vibrational and vibronic excitations during the dynamics for different sites. The vibrational excitation in the electronic ground state at site m can be defined as the expectation value of the operator

$$H_m^{\mathrm{vib}} = \sum_{\xi \in m} \frac{\hbar \omega_{m\xi}}{4} (P_{m\xi}^2 + Q_{m\xi}^2)(1 - |m\rangle\langle m|). \tag{9.190}$$

It gives the vibrational energy irrespective of which site of the aggregate is electronically excited. The vibronic excitation (that is, the vibrational excitation in the locally excited electronic state) of a particular site m can be defined as the expectation value of

$$H_m^{\mathrm{vibro}} = \sum_{\xi \in m} \frac{\hbar \omega_{m\xi}}{4} (P_{m\xi}^2 + Q_{m\xi}^2 + 4\hbar \omega_{m\xi} g_m(\xi) Q_{m\xi})|m\rangle\langle m|. \tag{9.191}$$

In Figure 9.18c, the expectation values of theses operators are spectrally resolved and plotted together with the spectral density. The behavior can be explained using the simple DA picture shown in Figure 9.12. Assuming an initial vertical excitation of the wave packet from the ground state, this wave packet will move until the donor is deexcited. Upon deexcitation, the wave packet is projected back onto the ground state PES where it is displaced with respect to the equilibrium position. The extent of displacement depends on the relation between the vibrational frequency and the inverse of the Coulomb coupling causing the EET ($1/\tau_{\mathrm{trans}}$). This is the reason for the threshold behavior of vibrational excitation seen in Figure 9.18c. The structured vibronic excitation is a resonance effect. According to Figure 9.18a,b, the electronic energy difference matches certain regions of the spectral density around 180–200 cm^{-1}. In these regions, one finds vibronic excitations at sites 2 and 3; that is, the EET is assisted by vibronic excitation. The participation of vibrational DOFs thus establishes the resonance for efficient EET. Finally, we emphasize that these results correspond to the limit of zero temperature. Finite temperature effects can be included in the MCTDH propagation using, for instance, the thermofield method outlined in Section 3.15.1.

9.7 Optical Properties of Aggregates

Having considered a variety of EET processes, we now turn to the stationary linear absorption coefficient of a molecular aggregate as one of the basic spectroscopic quantities. Of particular interest will be its relation to the energy spectrum of the

single-exciton Hamiltonian introduced in Section 9.2. Following the discussions given in Chapter 6 and in particular in Section 6.2.1, we expect an expression for the absorption coefficient to be similar to Eq. (6.13); that is, there should be an absorption line for every possible transition from the ground to some excited exciton–vibrational state. To be more precise, the initial state is defined by the Hamiltonian $H_{\text{agg}}^{(0)}$, Eq. (9.37). The final states of the transition are obtained from the eigenstates of the single-excited state Hamiltonian $H_{\text{agg}}^{(1)}$, Eq. (9.38). Unlike the initial states, a general expression for the final states cannot be derived in a simple way. This is due to the fact that one would have to account for arbitrarily strong exciton–vibrational and Coulomb coupling at the same time. If there are many vibrational modes, an exact treatment becomes impossible. Therefore, some reasonable approximations will be discussed in what follows.

If we neglect any contribution of the exciton–vibrational coupling to the absorption spectrum, we obtain a sequence of sharp lines positioned at frequencies that coincide with $\mathcal{E}_\alpha/\hbar$. This provides a reference for further discussions. Including the exciton–vibrational coupling, we expect a broadening of the lines as already discussed in Section 6.3.2. Let us start with a short derivation of the absorption coefficient $\alpha(\omega)$ for an ensemble of aggregates using the general expression equation (4.46), which defines $\alpha(\omega)$ via the dipole–dipole correlation function $C_{\text{d–d}}(t)$, Eq. (4.42).

In the present case, the dipole operator comprises the contributions $\hat{\mu}_m$, Eq. (9.27), of all molecules in the aggregate according to $\hat{\mu} = \sum_m \hat{\mu}_m$. This expression is valid for optical transitions into all excited states as well as for transitions between different excited states (for instance, one- to two-exciton states). For the present purposes, however, it is sufficient to restrict the model to transitions into the single exciton state (corresponding to a S_0–S_1 transition). Further, we note that when computing $\alpha(\omega)$, the volume density of molecules appearing in Eq. (4.46) has to be replaced by that of the aggregates n_{agg}. We do not present the total absorption coefficient formula again but focus on the dipole–dipole correlation function for an ensemble of aggregates randomly oriented in the sample. Noting the structure of the equilibrium statistical operator $\hat{W}_{\text{eq}} = \hat{R}_0 |0\rangle\langle 0|$, where $\hat{R}_0$ describes vibrational equilibrium in the aggregate ground state, we immediately arrive at

$$C_{\text{d–d}}(t) = \text{tr}_{\text{vib}} \left\{ \hat{R}_0 \langle 0| U_{\text{agg}}^+(t) \hat{\mu} U_{\text{agg}}(t) \hat{\mu} |0\rangle \right\}. \tag{9.192}$$

Since the aggregate ground state projector $|0\rangle\langle 0|$ reduces the electronic part of the trace to the electronic ground state matrix element, there only remains a trace with respect to all involved vibrational DOFs. Also, be aware of the neglect of the so-called antiresonant contributions (the second term in the dipole operator commutator does not appear, and any contribution in the negative frequency range is absent in the absorption).

The further treatment of the dipole–dipole correlation function depends on the way we represent the dipole operator $\hat{\mu}$. If we use the notation with the monomer dipole operators $\hat{\mu}_m$ and restrict ourselves to the first excited state only, we may write

$$\hat{\mu} = \sum_m \hat{\mu}_m \equiv \sum_m \boldsymbol{d}_m |m\rangle\langle 0| + \text{h.c.}, \tag{9.193}$$

where $\boldsymbol{d}_m$ is the transition matrix element of the two-level model of Section 9.2.2 already used in Eq. (9.30). The dipole–dipole correlation functions reads

$$C_{\text{d-d}}(t) = \sum_{m,n} \text{tr}_{\text{vib}}\{\hat{R}_0 \langle 0|e^{iH_{\text{agg}}^{(0)}t/\hbar}|0\rangle d_m^+ \langle m|e^{-iH_{\text{agg}}^{(1)}t/\hbar}|n\rangle d_n\}. \qquad (9.194)$$

Here, d_n, for example, denotes the projection of the vectorial matrix element $\boldsymbol{d}_n$ on the polarization direction of the external field. $\langle 0| \exp(iH_{\text{agg}}^{(0)}t/\hbar)|0\rangle$ can be replaced by $\exp(i\mathcal{H}_0 t/\hbar)$, with $\mathcal{H}_0$, according to Eq. (9.37). If the Condon approximation is taken, we may move the transition dipole matrix elements out of the vibrational trace.

Alternatively, we may use the exciton representation of the dipole operator

$$\hat{\mu} = \sum_{\alpha} \boldsymbol{d}_{\alpha}|\alpha\rangle\langle 0| + \text{h.c.}, \qquad (9.195)$$

where the transition matrix elements are given by

$$\boldsymbol{d}_{\alpha} = \langle\alpha|\sum_m \hat{\mu}_m|0\rangle = \sum_m c_{\alpha}^*(m)\boldsymbol{d}_m. \qquad (9.196)$$

Now, we get the dipole–dipole correlation function in Condon approximation as

$$C_{\text{d-d}}(t) = \sum_{\alpha,\beta} d_{\alpha}^* d_{\beta} \text{tr}_{\text{vib}}\{\hat{R}_0 e^{i\mathcal{H}_0 t/\hbar}\langle\alpha|e^{-iH_{\text{agg}}^{(1)}t/\hbar}|\beta\rangle\}. \qquad (9.197)$$

While the singly excited state time-evolution operator connects different exciton states $|\alpha\rangle$ and $|\beta\rangle$, it connects different locally excited states in the site representation of the dipole–dipole correlation function, Eq. (9.194). Tackling these contributions represents the central difficulty in calculating the absorption. Here, the ratio of the excitonic coupling and the coupling to the vibrations decides which representation is more appropriate for a perturbative treatment.

9.7.1 Case of No Exciton–Vibrational Coupling

In this simple reference case, we use the exciton representation, Eq. (9.197), of the dipole–dipole correlation function. A neglect of vibrational contributions gives

$$C_{\text{d-d}}(t) = \sum_{\alpha} |d_{\alpha}|^2 e^{-i\mathcal{E}_{\alpha}t/\hbar}. \qquad (9.198)$$

This result is obtained because in the present approximation, $H_{\text{agg}}^{(1)}$ becomes diagonal with respect to the exciton states. The absorption coefficient takes the form (the prefactor $1/3$ follows from the orientation averaging, cf. Chapter 6)

$$\alpha(\omega) = \frac{4\pi^2 \omega n_{\text{agg}}}{3c} \sum_{\alpha} |\boldsymbol{d}_{\alpha}|^2 \delta(\hbar\omega - \mathcal{E}_{\alpha}). \qquad (9.199)$$

The strength for transitions from the ground state into the single-exciton state $|\alpha\rangle$ is determined by the respective transition dipole moment, Eq. (9.196), where the expansion coefficients $c_{\alpha}(m)$ give the contribution of the mth molecule to the single-exciton eigenstate $|\alpha\rangle$. In order to characterize this quantity, we compute the

oscillator strength. For a collection of molecules with identical transition dipole moments (same magnitude and same spatial orientation), $\boldsymbol{d}_m = \boldsymbol{d}$, it reads

$$O_\alpha = \frac{|\boldsymbol{d}_\alpha|^2}{|\boldsymbol{d}|^2} = \left| \sum_m c_\alpha(m) \right|^2. \qquad (9.200)$$

As a consequence of the neglect of environmental influences, the external field can in principle excite exciton states that are delocalized over the whole aggregate.

To illustrate the given formulas, let us first consider a molecular dimer whose energy levels are introduced in Section 9.2.4. The oscillator strength defined in Eq. (9.200) for transitions into the symmetric and antisymmetric eigenstates is (for η see Eq. 9.75)

$$O_\pm = \frac{|1 \pm \eta \exp(\pm i \; \arg(J))|^2}{1 + \eta^2}. \qquad (9.201)$$

In Figure 9.19, we show the distribution of oscillator strength in the dimer absorption spectrum for the degenerate case, $E_1 = E_2 = E_0$ ($\mathcal{E}_\pm = E_0 \pm |J|$), in dependence on the geometry of the transition dipole moments. The sign of the dipole–dipole coupling can be positive or negative, as indicated for two extreme cases in Figure 9.19. For dipoles pointing in the same direction giving rise to a collective dipole, this implies that the energy shift observed in the spectrum with respect to the monomer is positive for $J > 0$ and negative for $J < 0$ and of magnitude $|J|$. According to Eq. (9.74), the transition is into the symmetric state, that is $|+\rangle$ for $J > 0$ or $|-\rangle$ for $J < 0$. In molecular aggregates, this energy shift can be observed upon aggregation. Depending on whether the absorption band shifts to longer or shorter wavelengths, aggregates are classified as J- or H-aggregates, respectively.

If there is some detuning between the monomer transition energies ($E_1 \neq E_2$), which can be caused by different local environments for the two otherwise identical molecules (static disorder), both eigenstates will carry oscillator strength. In the limit where $|E_1 - E_2| \gg |J|$, the absorption spectrum becomes monomeric, and the eigenstates are localized at the corresponding molecules.

Figure 9.19 Dependence of the amplitudes for transitions between the ground state and the two excited eigenstates of a molecular dimer on the mutual arrangement of the monomeric transition dipole moments (depicted by the arrows). In the degenerate dimer, the oscillator strength, Eq. (9.201), is solely located in the symmetric state combination of the local states, which is below/above the monomer energy for $J < 0/J > 0$.

Next, let us consider an aggregate consisting of a linear arrangement of N_{mon} identical molecules as introduced in Section 9.2.4. If we consider the absorption spectrum, we note that the single-exciton state $\mathcal{E}_0 = E_0 + 2J$ will have the lowest (highest) energy for a J-(H-)aggregate. It also has the largest transition amplitude for optical absorption. The respective oscillator strengths, Eq. (9.200), are given by

$$O_\alpha = \frac{1 - (-1)^j}{2} \cot^2 \left(\frac{\pi}{2} \frac{j}{N_{mon} + 1} \right). \tag{9.202}$$

The expression for O_α shows that nearly all the oscillator strength is contained in a single exciton state ($j = 1$, cf. part of Figure 9.16). As an example of a linear chain-type aggregate, we show the absorption spectrum of 5,5′,6,6′-tetrachloro-1,1′-diethyl-3,3′-di(4-sulfobutyl)-benzimidazolcarbocyanine (TDBC) in Figure 9.20. It is a J-aggregate, and the excitonic interaction induces a shift of the absorption band to longer wavelengths upon aggregation.

9.7.1.1 Static Disorder

An important factor determining the width of absorption lines of artificially prepared or naturally occurring aggregates is static disorder. In this section, we outline an approach that takes the effect of energetic and structural disorder into account. The formulation is rather general and can be applied to the much simpler case of single molecules in solution as well.

As has already been discussed in Section 6.2, a change in the energy-level structure, for example, from aggregate to aggregate leads to an additional broadening of the absorption, which is measured on a sample containing a large number of aggregates. In general, one can characterize such a behavior by a set of parameters $y \equiv \{y_j\}$, which enter the Hamiltonian and describe a specific energetic and structural situation in the aggregate. The parameters y will be additionally labeled by A,

Figure 9.20 Molecular structure of the dye TDBC (5,5′,6,6′-tetrachloro-1,1′-diethyl-3,3′-di (4-sulfobutyl)-benzimidazol-carbocyanine) forming J-aggregates, together with the room temperature monomer absorption (in methanol) and the J-band (in water) (reprinted with permission from Moll et al. [13]; copyright (1995) American Institute of Physics).
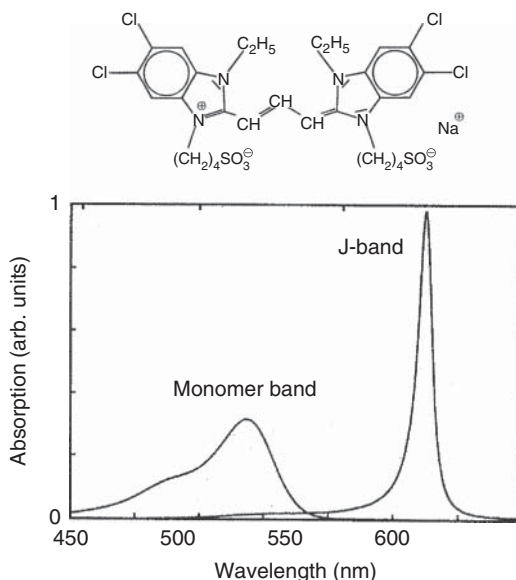
which counts all aggregates contained in the sample volume V. This indicates that the set y varies from aggregate to aggregate. Accordingly, every aggregate will have its own absorption cross section $\sigma = \sigma(\omega; y_A)$. The cross section is delivered by the absorption coefficient as $\sigma = \alpha/n_{\text{agg}}$, and we may write

$$\alpha_{\text{inh}}(\omega) = \frac{1}{V} \sum_{A \in V} \sigma(\omega; y_A). \tag{9.203}$$

The inhomogeneous broadening can be described as an averaging with respect to different realizations of the aggregate's structure and energy spectrum. This is called a *configurational average*. If there exists a large number of different realizations, one can change from the summation to the integration with respect to the different parameters y_j

$$\alpha_{\text{inh}}(\omega) = \int dy \, \mathcal{F}(y) \sigma(\omega; y). \tag{9.204}$$

The integration extends over the whole set of parameters. The appropriate normalized distribution function $\mathcal{F}(y)$ can formally be introduced as

$$\mathcal{F}(y) = \frac{1}{V} \sum_{A \in V} \prod_j \delta(y_j - y_{Aj}). \tag{9.205}$$

For specific applications, $\mathcal{F}(y)$ is taken to be a continuous function of the parameters y_j.

In what follows, we consider the simple case where disorder can be described by Gaussian distributions of the various exciton levels around certain mean values $\overline{\mathcal{E}}_\alpha$. In fact, the Gaussian form of the distribution function can be justified from the central limit theorem of probability theory. We set

$$\mathcal{F}(y) \to \mathcal{F}(y \equiv \{\mathcal{E}_\alpha\}) = n_{\text{agg}} \prod_\alpha \mathcal{F}_\alpha(\mathcal{E}_\alpha - \overline{\mathcal{E}}_\alpha), \tag{9.206}$$

with

$$\mathcal{F}_\alpha(E) = \frac{1}{\sqrt{2\pi\Delta_\alpha^2}} \exp\left\{ -\frac{E^2}{2\Delta_\alpha^2} \right\}. \tag{9.207}$$

Here, Δ_α is the width of the Gaussian distribution for the state $|\alpha\rangle$. Taking the cross section according to Eq. (9.199), the inhomogeneously broadened absorption spectrum is obtained as

$$\alpha_{\text{inh}}(\omega) = \int d\mathcal{E} \, \mathcal{F}(\mathcal{E}) \sigma(\omega; \mathcal{E}) = \frac{4\pi^2 \omega n_{\text{agg}}}{3c} \sum_\alpha |\boldsymbol{d}_\alpha|^2 \, \mathcal{F}_\alpha(\hbar\omega - \overline{\mathcal{E}}_\alpha). \tag{9.208}$$

In this simple case, the distribution of microscopic parameters directly determines the line shape of the inhomogeneously broadened spectrum. In order to connect the broadening to the actual structure of the monomers or aggregates, atomistic simulations have to be carried out. Figure 9.21a shows the simulation results for the distribution of BChl site energies of a monomer of the FMO protein (cf. Figure 9.4), which fit nicely to Gaussian distributions. Figure 9.21b shows a simulation of the absorption spectrum including exciton–vibrational coupling which is responsible for homogeneous broadening. The way to calculate these spectra is briefly explained in Section 9.7.2.

(a)

(b)
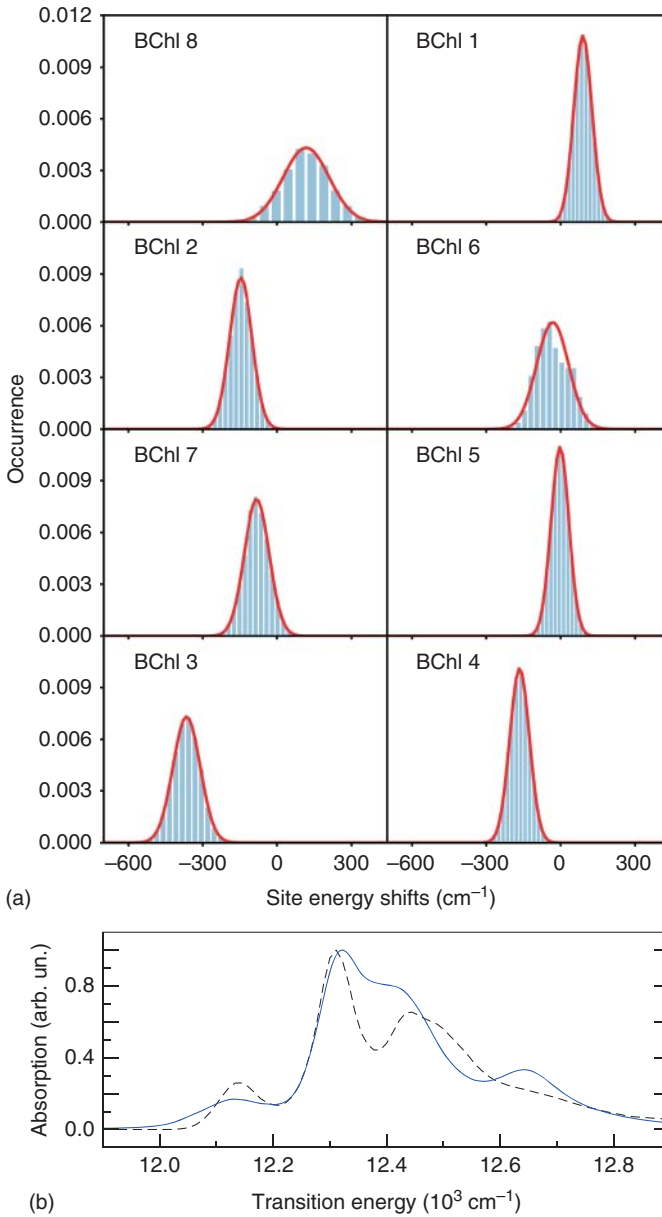
Figure 9.21 (a) Distribution of site energy shifts relative to an experimentally determined transition energy ($E_0 = 1256 \, \text{cm}^{-1}$) for the eight BChl monomers of one subunit of the FMO protein (cf. Figure 9.4). They were obtained from Monte Carlo sampling of protein conformations. The distributions are fitted to a Gaussian function (line, Eq. (9.207)). (b) Linear absorption of the FMO protein at $T = 4$ K (solid line: theory, dashed line: experiment) including static disorder as well as exciton–vibrational coupling according to Section 9.7.2.3 (Figure courtesy of T. Renger, for more details see Chaillet et al. [14]).

9.7.2 Inclusion of Exciton–Vibrational Coupling

As in the case of EET rate computations presented in the foregoing sections, we distinguish between weak and strong exciton–vibrational coupling. For the former case, we use an approach based on the density matrix theory of Section 9.6.2. The description of a situation where exciton–vibrational coupling is strong and cannot be accounted for by perturbation theory will be based on the concept of excitonic PES, Section 9.3.4, and resembles the rate computation of Section 9.6.5 called modified Redfield theory. However, we start our discussion of exciton–vibrational coupling by introducing the so-called *n*-particle expansion in Section 9.7.2.1. It provides a clear eigenstate picture of the effect of this interaction but is restricted to cases of small aggregates coupled to a few modes only. These modes are treated explicitly and can be considered as part of the relevant system.

9.7.2.1 The *n*-Particle Expansion

In what follows, we outline an approach that can describe the exciton–vibrational coupling Hamiltonian in Eq. (9.90) in a numerically exact manner. Practical applications, however, will be restricted to a few monomers and vibrational DOFs. It is based on the introduction of an exciton–vibrational basis, which is diabatic with respect to the excitonic coupling. In Section 7.2.3, we introduce a diabatic electron–vibrational basis to treat electron-transfer dynamics. In the present case of Eq. (9.90), this basis has to be modified to account for the local vibrational modes that couple to the single excitation states (again, we use the two-level model for illustration). Specifically, the ground and the excited states, Eqs. (9.33) and (9.34), respectively, have to be supplemented by the respective vibrational wave functions describing the local normal modes in the actual electronic states.

For illustration, we assume that there is only one vibrational mode per monomer described by the vibrational state $|\chi_{m_a M}\rangle = |M_{a_m}\rangle$.[22] Hence, in the electronic ground state of the aggregate, the wave function reads

$$|0M\rangle = |0\rangle|M\rangle = \prod_m |\varphi_{mg}\rangle|M_{g_m}\rangle. \tag{9.209}$$

Here, M comprises the set of quantum numbers $\{M_{g_1}, \ldots, M_{g_{N_{mon}}}\}$. The single-excited state is written as (cf. Eq. (2.52))

$$|mM\rangle = |m\rangle|M\rangle = |\varphi_{me}\rangle|M_{e_m}\rangle \prod_{n \neq m} |\varphi_{ng}\rangle|M_{g_n}\rangle, \tag{9.210}$$

with $M = \{M_{g_1}, \ldots, M_{e_m}, \ldots, M_{g_N}\}$. Notice that here it is assumed that $|M_{e_m}\rangle$ are the eigenfunctions of the shifted oscillator in the local excited state $|\varphi_{me}\rangle$. The representation of the exciton–vibrational Hamiltonian, Eq. (9.90), in this basis can be performed in analogy to the case of ET (cf. Section 7.2.3). Thereby, one can invoke again the Condon approximation; that is, the matrix elements of the excitonic

---

22) The extension to an arbitrary number of modes per monomer is straightforward due to the product character of the normal-mode oscillator eigenfunction, cf. Eq. (2.46).

coupling are $J_{mn}\langle M|N\rangle$. The vibrational overlap integrals follow in analogy to Eq. (9.114) as

$$\langle M|N\rangle = \langle M_{e_m}|N_{g_m}\rangle\langle M_{g_n}|N_{e_n}\rangle \prod_{k\neq m,n} \delta_{M_{g_k},N_{g_k}} \; . \tag{9.211}$$

Here, the local Frank–Condon factors enter, which can be calculated according to Eq. (2.79). Notice that there is no restriction on the vibrational quantum numbers, and the occupation of the vibrational states will be determined by the detuning of the electronic states of the monomers as well as the shift of the ground and excited state PESs with respect to each other (reorganization energy), cf. Figure 9.18. The situation is sketched in Figure 9.22a for a trimer aggregate. In order to limit the possible excitation space with respect to the electronic ground state vibrations, one introduces the n-particle expansion. In the one-particle expansion shown in Figure 9.22b, the vibrational quantum numbers corresponding to the electronic ground state PESs

Figure 9.22 Schematic of the exact (a), one-particle (b), and two-particle (c) representations of the exciton–vibrational wave function for a trimer aggregate with one vibrational mode per monomer. The vibrational states that are included are shown with black lines.

Exact representation

(a)

One-particle approximation

(b)

Two-particle approximation

(c)   Monomer ⟶

Excited state PES
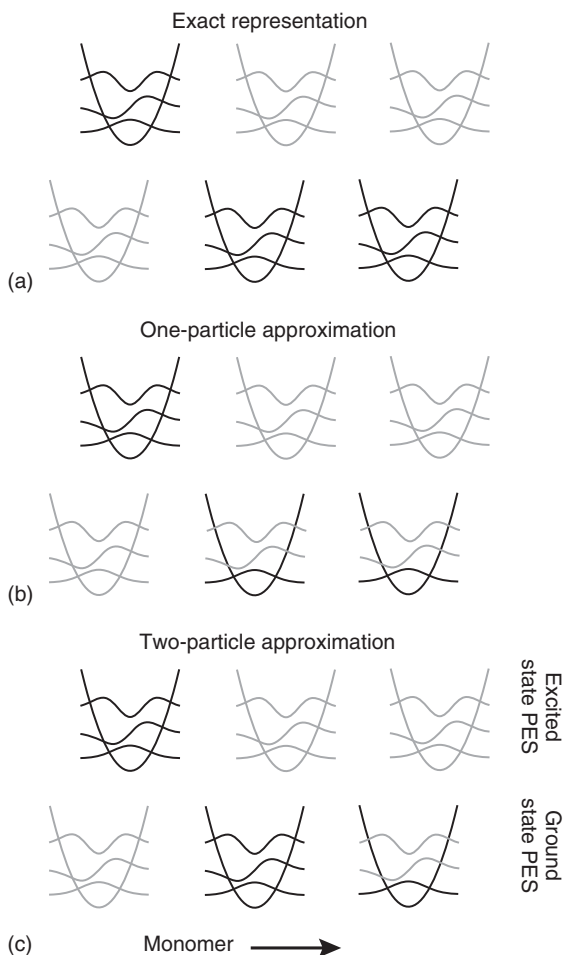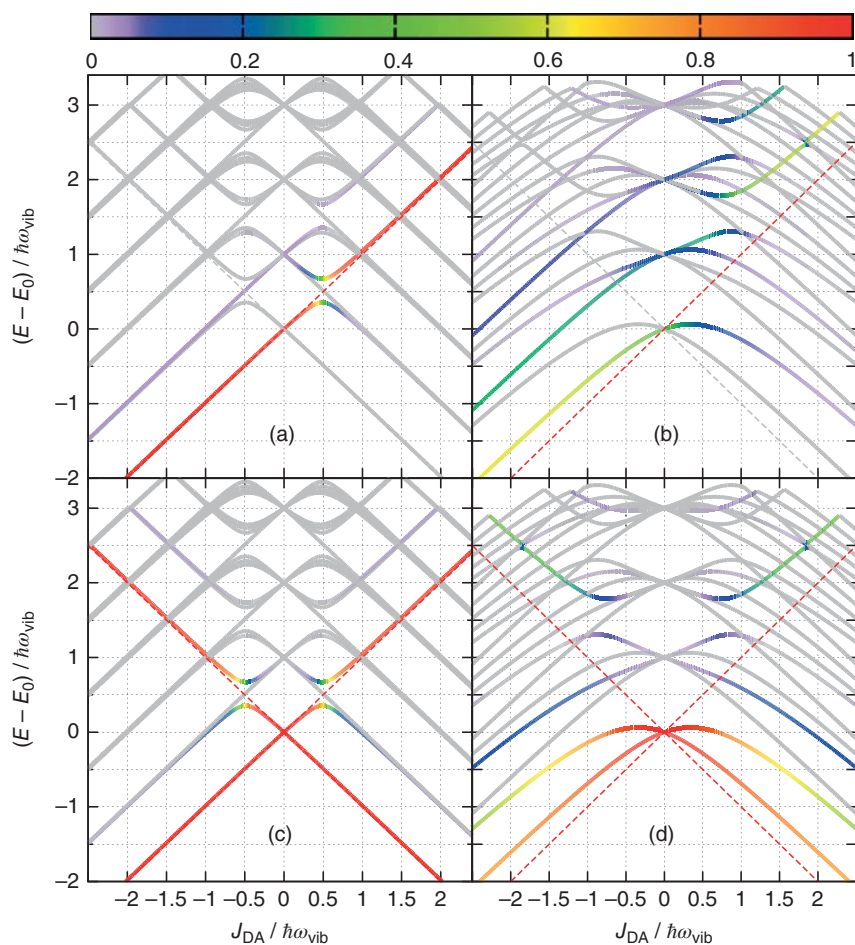
Ground state PES

Figure 9.23 Oscillator strengths for transitions from the electronic and vibrational ground state of a molecular dimer ($E_0 = E_D = E_A$, one vibrational mode per monomer) into the one-exciton–vibrational eigenstates in dependence on the excitonic coupling J_{DA} and for reorganization energies of $E_\lambda/\hbar\omega_{vib} = 0.05$ (a) and 1.0 (b). Panels (c) and (d) show the electronic contributions to the transitions in panels (a) and (b), respectively. The dashed lines correspond to the energies of the pure electronic model equation (9.73) (for more details, see also Schröter et al. [15]).

are restricted to zero. In the two-particle expansion, the vibrational quantum numbers of one electronic ground state PES are unrestricted, and pairs of all ground state PESs with the considered excited states are taken into account (one case is given in Figure 9.22c).

In Figure 9.23, properties of the one-exciton–vibrational eigenstates of a molecular homodimer are shown in dependence on the excitonic coupling. Figure 9.23a,b gives the oscillator strength for transitions from the electron–vibrational ground state of the aggregate to these eigenstates for two different exciton–vibrational coupling strengths as expressed by the reorganization energy, that is $E_\lambda/\hbar\omega_{vib} = 0.05$

(a) and $E_\lambda/\hbar\omega_{\text{vib}} = 1.0$ (b). For $J_{\text{DA}} = 0$, one has the monomer Franck–Condon progression. Increasing J_{DA} shifts the eigenstates, and for certain parameter values avoided level crossings are observed. Note that the level structure is symmetric with respect to $J_{\text{DA}} = 0$, but the oscillator strengths are not. In order to analyze their behavior, Figure 9.23c,d shows the corresponding electronic character of the transitions, which is defined as the expectation value of the projection operator $\sum_{m=D,A} |mM\rangle\langle Mm|$ for $M = \{0, 0\}$. In the case of the small reorganization energy (Figure 9.23a,c), the results resemble those of the pure electronic dimer (energy levels given as dashed lines); that is, for $J_{\text{DA}} < 0$, all oscillator strength is concentrated in the lowest state, and for $J_{\text{DA}} > 0$, it follows the state with dominant electronic character. In the case of the large reorganization energy (Figure 9.23b,d), the mixing between electronic and vibrational states leads to a redistribution of oscillator strength over a number of transitions. Still, the H- and J-like shifts of the spectra are discernible.

Finally, we note that the present model can be supplemented by a coupling to a reservoir as discussed in Section 9.3.3. This would give the possibility to include the effect of dephasing that causes line broadening. In Sections 9.7.2.2 and 9.7.2.3, however, we introduce line broadening using a correlation function approach that does not require knowledge about exciton–vibrational eigenstates.

9.7.2.2 Weak Exciton–Vibrational Coupling

If the exciton–vibrational coupling is sufficiently weak, we may compute the absorption coefficient following the procedure of Section 6.3.2. There, the coupling of a monomer to a thermal environment was taken into account perturbatively. This situation is similar to the case of weak exciton–vibrational coupling, as already discussed in Section 9.6. To calculate the absorption coefficient, we start with Eq. (6.68), where the dipole–dipole correlation function $C_{\text{d-d}}(t)$ is determined by a density operator propagation. If we translate the notation of Section 9.6 to the present case, we obtain Eq. (6.69) in the following form:

$$C_{\text{d-d}}(t) = \sum_\alpha \left(\boldsymbol{d}_\alpha^* \langle\alpha|\hat{\sigma}(t)|0\rangle + \boldsymbol{d}_\alpha \langle 0|\hat{\sigma}(t)|\alpha\rangle \right). \tag{9.212}$$

Instead of a single excited state as in Eq. (6.69), we have here the set of exciton levels (the trace with respect to the vibrational states does not appear since those DOFs form the dissipative environment). The density operator $\hat{\sigma}(t)$ follows from the propagation of the initial state $\hat{\sigma}(0) = [\hat{\mu}, |0\rangle\langle 0|]_-$. Taking into account the density matrix equations introduced in Section 9.6.2 (but generalized here to the off-diagonal type of functions $\rho_{\alpha 0}$) and the dephasing rates, Eq. (9.163), we obtain the absorption spectrum in analogy to Eq. (6.72) as

$$\alpha(\omega) = \frac{4\pi\omega n_{\text{agg}}}{3\hbar c} \sum_\alpha |\boldsymbol{d}_\alpha|^2 \frac{\gamma_\alpha}{(\omega - \omega_{\alpha 0})^2 + \gamma_\alpha^2}. \tag{9.213}$$

This formula is apparently a generalization of Eq. (9.199) with the transitions into the exciton states at frequencies $\omega_{\alpha 0}$, broadened by the dephasing rates γ_α. This broadening is determined by the spectral density entering Eq. (9.164). The different values

of $J(\omega_{\alpha\beta})$ at different transition frequencies lead to different values of the dephasing rates (cf. also Figure 3.6) and thus spectral widths.

9.7.2.3 Strong Exciton–Vibrational Coupling

The concept of excitonic PES introduced in Section 9.3.4 allows to calculate the absorption spectrum beyond the simple approximation introduced in Section 9.7.2.2. In order to illustrate the use of excitonic PES and their residual coupling to each other condensed in the Hamiltonian $H_{\mathrm{agg}}^{(1)}$, Eq. (9.105), we start by introducing the assumption that the vibrationally induced coupling among different PESs is sufficiently small and can be neglected. Then, $H_{\mathrm{agg}}^{(1)}$ becomes diagonal with respect to the exciton states, and the dipole–dipole correlation function, Eq. (9.197), simplifies to

$$C_{\mathrm{d-d}}(t) = \sum_{\alpha} |d_{\alpha}|^2 \mathrm{tr}_{\mathrm{vib}} \{\hat{R}_0 e^{i\mathcal{H}_0 t/\hbar} e^{i[T_{\mathrm{vib}} + U_{\alpha}(q)]t/\hbar}\}. \tag{9.214}$$

Here, $\mathcal{H}_0 = \sum_m H_{mg}$, with H_{mg} being a harmonic oscillator Hamiltonian (e.g. Eq. (9.83)). Since the excitonic PESs are given by displaced parabolas, we can apply the formula derived in Section 6.2.3 for every exciton level and get

$$C_{\mathrm{d-d}}(t) = \sum_{\alpha} |d_{\alpha}|^2 e^{-i\tilde{\Omega}_{\alpha} t - G_{\alpha}(0) + G_{\alpha}(t)}. \tag{9.215}$$

We used exciton frequencies $\tilde{\Omega}_{\alpha}$ that have already been introduced in relation to the rate expression, Eq. (9.174), and that include the reorganization energy $E_{\lambda}^{(\alpha)} = \sum_{\xi} \hbar\omega_{\xi} g_{\alpha\alpha}^2(\xi) \equiv \hbar \int d\omega\, \omega j_{\alpha\alpha,\alpha\alpha}(\omega)$ referring to a particular excitonic PES. The spectral density depending fourfold on the exciton quantum numbers has been defined in Eq. (9.160). The line shape function takes the form

$$G_{\alpha}(t) = \int d\omega\, e^{-i\omega t}[1 + n(\omega)][j_{\alpha\alpha,\alpha\alpha}(\omega) - j_{\alpha\alpha,\alpha\alpha}(-\omega)]. \tag{9.216}$$

The neglect of the interexciton state coupling produces an absorption coefficient where every excitonic PES contributes independently. In a next step, one can account for the vibrationally induced interexciton level coupling. The following calculations are again based on Eq. (9.197) for the dipole–dipole correlation function; however, as demonstrated below, it is sufficient to use the separation equation (9.90) for $H_{\mathrm{agg}}^{(1)}$. The exciton–vibrational coupling, Eq. (9.102), does not separate into a diagonal and off-diagonal part and acts as the total perturbation. As a result, we separate the time-evolution operator referring to the singly excited aggregate state as (cf. Sections 3.2.2, 6.2.2, and 6.2.5)

$$e^{-iH_{\mathrm{agg}}^{(1)} t/\hbar} = U_1^{(0)}(t) S_1(t,0), \tag{9.217}$$

with

$$U_1^{(0)}(t) = e^{-i(H_{\mathrm{ex}} + H_{\mathrm{vib}})t/\hbar}, \tag{9.218}$$

and with

$$S_1(t,0) = \hat{T} \exp\left(-\frac{i}{\hbar} \int_0^t dt_1\, U_1^{(0)+}(t_1) H_{\mathrm{ex-vib}} U_1^{(0)}(t_1)\right). \tag{9.219}$$

The exciton Hamiltonian H_{ex} has been defined in Eq. (9.69), and H_{vib} is given in Eq. (9.92) but with $\sum_\alpha |\alpha\rangle\langle\alpha|$ replacing $\sum_m |m\rangle\langle m|$. The dipole–dipole correlation function reads

$$C_{d-d}(t) = \sum_{\alpha,\beta} d_\alpha^* d_\beta e^{-i\mathcal{E}_\alpha t/\hbar} \text{tr}_{vib}\{\hat{R}_0 \langle\alpha|S_1(t,0)|\beta\rangle\}. \tag{9.220}$$

The vibrational trace expression cannot be calculated exactly but is perfectly suited for the cumulant approximation introduced in Section 6.2.5. Let us focus on that part where $\alpha = \beta$ and take the ansatz (cf. Eq. (4.80)):

$$\text{tr}_{vib}\{\hat{R}_0 \langle\alpha|S_1(t,0)|\alpha\rangle\} = e^{\Gamma_\alpha(t)}. \tag{9.221}$$

Expanding S_1, Eq. (9.219), up to the second order in H_{ex-vib}, we notice that the first-order contribution does not contribute ($\text{tr}_{vib}\{\hat{R}_0 Q_\xi\}$ vanishes identically). Then, the second-order term can be identified with the second-order term of $\Gamma_\alpha^{(2)}(t)$ of $\Gamma_\alpha(t)$:

$$\Gamma_\alpha^{(2)} = -\frac{1}{\hbar^2} \int_0^t dt_1 \int_0^{t_1} dt_2$$
$$\times \text{tr}_{vib}\{\hat{R}_0 \langle\alpha|U_1^{(0)+}(t_1) H_{ex-vib} U_1^{(0)}(t_1) U_1^{(0)+}(t_2) H_{ex-vib} U_1^{(0)}(t_2)|\alpha\rangle\}. \tag{9.222}$$

The exciton part of this expression results in terms that oscillate with excitonic transition frequencies $\Omega_{\alpha\beta} = (\mathcal{E}_\alpha - \mathcal{E}_\beta)/\hbar$. The vibrational trace leads to the correlation function $\text{tr}_{vib}\{\hat{R}_0 Q_\xi(t_1 - t_2) Q_\xi\}$ already used previously (cf. Section 9.6). After carrying out the double time integration, we arrive at

$$\Gamma_\alpha^{(2)}(t) = \sum_\beta \gamma_{\alpha\beta}(t), \tag{9.223}$$

with

$$\gamma_{\alpha\beta}(t) = \int d\omega \, \frac{\omega^2}{(\Omega_{\alpha\beta} - \omega)^2} \left(e^{i(\Omega_{\alpha\beta} - \omega)t} - 1 - i(\Omega_{\alpha\beta} - \omega)t \right)$$
$$\times [1 + n(\omega)][j_{\alpha\beta,\beta\alpha}(\omega) - j_{\alpha\beta,\beta\alpha}(-\omega)]. \tag{9.224}$$

The expression has been written using the spectral density, Eq. (9.160). We extract the term $\beta = \alpha$ from the summation and get

$$\Gamma_{\alpha\alpha}^{(2)}(t) = iE_\lambda^{(\alpha)} t/\hbar - G_\alpha(0) + G_\alpha(t) - \sum_{\beta \neq \alpha} \gamma_{\alpha\beta}(t), \tag{9.225}$$

where $E_\lambda^{(\alpha)}$ is as introduced in Section 9.6.5 and G_α in Eq. (9.216). Finally, arrive at the dipole–dipole correlation function:

$$C_{d-d}(t) = \sum_\alpha |d_\alpha|^2 e^{-i\bar{\Omega}_\alpha t - G_\alpha(0) + G_\alpha(t) - \sum_{\beta \neq \alpha} \gamma_{\alpha\beta}(t)}. \tag{9.226}$$

This expression generalizes Eq. (9.215) to the inclusion of off-diagonal parts of the exciton vibrational coupling. The results of an exemplary simulation are shown in Figure 9.21.

9.8 Excitation Energy Transfer Including Charge-transfer States

9.8.1 Excitation Energy Transfer Via Two-electron Exchange

In the preceding part of this chapter, we have not taken into account the charge transfer that accompanies EET. This type of EET, caused by the Coulomb interaction, occurs not only for short distances but also for distances of some 10 nm. For short distances, electronic wave function overlap becomes possible, and electron-exchange contributions may be of importance. If they contribute in a significant way, the EET is called a *Dexter transfer* (in extension of the Förster transfer, discussed in Section 9.5). Due to the close proximity of the donor and the acceptor molecules, the excitonic coupling has to include the electron-exchange contributions as introduced in Eq. (9.9). To highlight such contributions, we restrict Eq. (9.9) to the electronic ground and the first excited states and to the contribution caused by a single-electron exchange between the donor and acceptor

$$
\langle \phi_{Dg,Ae}^{(AS)} | V_{DA}^{(el-el)} | \phi_{Ag,De}^{(AS)} \rangle
$$

$$
= \int dr_D dr_A \frac{1}{\sqrt{2}} \left(\varphi_{Dg}^*(r_D', \boldsymbol{r}_D) \varphi_{Ae}^*(r_A', \boldsymbol{r}_A) - \varphi_{Dg}^*(r_D', \boldsymbol{r}_A) \varphi_{Ae}^*(r_A', \boldsymbol{r}_D) \right)
$$

$$
\times V_{DA}^{(el-el)} \frac{1}{\sqrt{2}} \left(\varphi_{Ag}(r_A', \boldsymbol{r}_A) \varphi_{De}(r_D', \boldsymbol{r}_D) - \varphi_{Ag}(r_A', \boldsymbol{r}_D) \varphi_{De}(r_D', \boldsymbol{r}_A) \right). \quad (9.227)
$$

Here, the total set of electron coordinates has been separated into coordinates for a single electron at the donor and acceptor, that is $\boldsymbol{r}_D$ and $\boldsymbol{r}_A$ that are subject to exchange, and the remaining coordinates r_D' and r_A'. The corresponding exchange corrections to the excitonic coupling are based on expressions such as $\varphi_{Dg}^*(r_D', \boldsymbol{r}_D) \varphi_{Ae}^*(r_A', \boldsymbol{r}_A) \ \varphi_{Ag}(r_A', \boldsymbol{r}_D) \varphi_{De}(r_D', \boldsymbol{r}_A)$. The dependence of $\varphi_{Ag}(r_A', \boldsymbol{r}_D)$ on $\boldsymbol{r}_D$ and the dependence of $\varphi_{De}(r_D', \boldsymbol{r}_A)$ on $\boldsymbol{r}_A$ indicate the need for a sufficiently strong spatial overlap of the wave functions in order to have some noticeable contributions.

The exchange contributions discussed so far only introduce corrections to the excitonic coupling. A new transfer mechanism, however, is obtained if one views EET as a two-electron-transfer (2ET) process (see Figure 9.2). The detailed scheme of 2ET-assisted EET as given in Figure 9.24 indicates that new intermediate states are involved. Moreover, the transfer may proceed as a *sequential* as well as a *concerted* two-electron transition. The new states are the so-called *charge-transfer states* (ionic states; Figure 9.24). The state $|D^+A^-\rangle = |\varphi_D^+ \varphi_A^-\rangle$ occurs when the excited electron moves from the donor LUMO to the acceptor LUMO. The $|D^-A^+\rangle = |\varphi_D^- \varphi_A^+\rangle$ state involves ET from the acceptor HOMO to the donor HOMO.[23] The latter process

---

23) Related energies of the two charge-transfer states can be estimated as follows. Considering $E_{D^+A^-}$ the energy to remove an electron from the donor can be roughly estimated by the ionization potential $W_D > 0$. Electron affinity of the acceptor $A_A > 0$ is a measure for the energy release when capturing a single excess electron. So far, we may write $E_{D^+A^-} \approx E_{DA} + W_D - A_A$. Moreover, the formation of a charge-transfer state generates Coulomb interaction energy in the most simple case given as e^2/X_{DA} (the donor acceptor distance is denoted by X_{DA}). This energy has to be added to $E_{D^+A^-}$ for electron–hole pair formation: $E_{D^+A^-} \approx E_{DA} + W_D - A_A + e^2/x_{DA}$. In the same manner, we get $E_{D^-A^+} \approx E_{DA} + W_A - A_D + e^2/X_{DA}$.
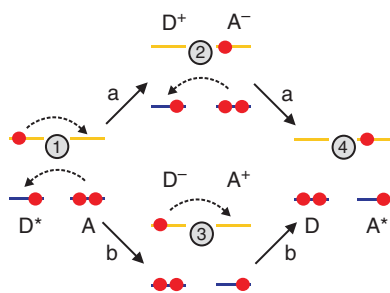
Figure 9.24 HOMO–LUMO scheme of EET based on a two-electron exchange via charge-transfer (ionic) states. The upper middle panel shows the intermediate state where the LUMO electron of the donor has been transferred to the acceptor LUMO to leave a molecular cation D^+ and to form a molecular anion A^-. Subsequent ET from the acceptor HOMO to the donor HOMO results in the final state (EET pathway "a"). This two-electron-exchange process competes with the process displayed by the lower middle panel where HOMO–HOMO ET precedes the LUMO–LUMO transition (EET pathway "b"; also note the labeling of the four states involved by 1–4).

can be understood alternatively as a hole transfer from the donor to the acceptor. Consequently, EET may proceed according to

$$|D^*A\rangle \to |D^+A^-\rangle \to |DA^*\rangle, \tag{9.228}$$

where DA hole transfer follows DA ET. This first pathway of EET is labeled by "a" in Figure 9.24. The second pathway labeled by "b" in Figure 9.24 reads

$$|D^*A\rangle \to |D^-A^+\rangle \to |DA^*\rangle. \tag{9.229}$$
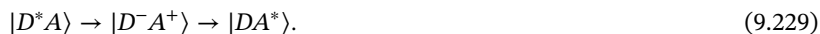
Here, DA hole transfer precedes DA ET.

Having identified these two basic processes for DA EET, we focus on some of the details next. An important question concerns the issue of whether one has a sequential process with a real population of the intermediate charge-transfer states or a concerted process where the charge-transfer states only act as virtual intermediate states. We also have to clarify how to account for the two different pathways of 2ET. It is already clear at this point that the 2ET-assisted EET would be of increasing importance for the overall transition if the energetic positions of the intermediate states get closer to that of the initial and final states. We also underline that 2ET-assisted EET competes with the direct process if singlet–singlet transfer is concerned, but 2ET-assisted transfer is the only possibility in the case of triplet–triplet transfer (cf. Figure 9.2).

The transition $|D^*A\rangle \to |D^+A^-\rangle$ reminds on the process of photoinduced DA ET discussed earlier in Section 7.1, and the transition $|D^+A^-\rangle \to |DA^*\rangle$ is reminiscent to photoinduced DA hole transfer. As a consequence, it is reasonable to model 2ET-assisted EET using the same description as in Section 7.2. Therefore, we introduce PESs that refer to the different states, namely U_{D^*A} and $U_{D^+A^-}$ in the case of ET (see Figure 9.25). The PESs are defined with respect to a common set of vibrational coordinates (cf. also Section 9.3.2). For the hole transfer, we have the PESs $U_{D^+A^-}$ and U_{DA^*}. To specify the second EET pathway, the PES $U_{D^+A^-}$ is replaced by $U_{D^-A^+}$.
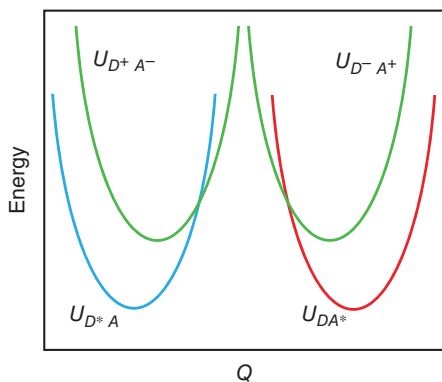
Figure 9.25 PES of the DA complex undergoing 2ET-assisted EET. The present symmetric scheme assumes the need of additional excitation energy when forming the two possible charge-transfer states. Largest nuclear reorganization has been assumed when moving between the neutral states. Less nuclear rearrangement is necessary for changing between the ionic states.

The related transfer couplings are denoted as $V(D^+A^-, D^*A)$ and $V(DA^*, D^+A^-)$ as well as $V(D^-A^+, D^*A)$ and $V(DA^*, D^-A^+)$. Also, similar to ET discussed in Chapter 7, we can distinguish between the strong and the weak coupling cases (adiabatic and nonadiabatic ET, respectively). As already indicated, we consider the latter case and expect standard nonadiabatic ET rates for the different electron and hole transfer processes. Concentrating on pathway "a" of Figure 9.24, we need to obtain the rates $k_{D^*A \to D^+A^-}$ and $k_{D^+A^- \to DA^*}$. EET, however, should also be possible as a direct one-step process with a rate $k_{D^*A \to DA^*}$ that includes the charge-transfer states as virtual intermediate states. Obviously, this would be a fourth-order rate with respect to the transfer coupling. A detailed analysis based on the fourth-order rate theory of Section 3.14.6 will be given in what follows.

As already indicated in Figure 9.24, we label the involved states $|m\rangle$ with $m = 1, \dots, 4$ ($|D^*A\rangle = |1\rangle$, $|D^+A^-\rangle = |2\rangle$, $|D^-A^+\rangle = |3\rangle$, and $|DA^*\rangle = |4\rangle$). Next, we specify the Hamiltonian describing 2ET-assisted EET by carrying out an expansion with respect to the states of interest. Moreover, we separate the Hamiltonian into a zeroth-order part and a perturbation

$$H = H_0 + \hat{V}. \tag{9.230}$$

The zeroth-order part is written as

$$H_0 = \sum_m H_m |m\rangle\langle m|, \tag{9.231}$$

where the vibrational Hamiltonians H_m cover the kinetic energy operator of the vibrational coordinates and the corresponding PES U_m. The coupling part of H takes the form

$$\hat{V} = \sum_{m,n} V_{mn} |m\rangle\langle n|. \tag{9.232}$$

V_{14} (V_{41}) can be identified with the excitonic coupling equation (9.29), resulting in a second-order transition rate. Concerning the inclusion of V_{14} and the computation of the Förster-type rate $k_{1 \to 4}^{(F)}$, we refer to Section 9.5. Here, we focus on the contribution of the remaining V_{mn}, which are V_{12}, V_{13}, V_{24}, and V_{34}, as well as the complex-conjugated expressions. Further, we invoke the Condon approximation;

that is, we assume that the transfer couplings V_{mn} are independent of the vibrational coordinates.

According to Eq. (7.88), the second-order rates of the sequential transitions can be written as $k_{m \to n} = 2\pi\hbar |V_{mn}|^2/\hbar \times \mathcal{D}_{m \to n}(\hbar\varepsilon_{mn})$, with $\hbar\varepsilon_{mn}$ being the driving force of the transition entering the combined DOS $\mathcal{D}_{m \to n}$. The rate of direct transfer $k_{1 \to 4}$ requires some additional effort. We expect the following form:

$$k_{1 \to 4} = k_{1 \to 4}^{(F)} + k_{1 \to 4}^{(2ET)}, \qquad (9.233)$$

where $k_{1 \to 4}^{(F)}$ denotes the standard Förster-type EET, Eq. (9.115) (if necessary corrected by exchange contributions), and $k_{1 \to 4}^{(2ET)}$ is the rate of 2ET-assisted EET. An explicit expression for this rate is derived in Section 9.10.3 for a Lindblad-type dissipation model.

In line with this reasoning, we expect to obtain rate equations for the state populations P_m, which take the form (cf. Eq. (7.128) describing bridge-mediated ET):

$$\frac{d}{dt}P_1 = - \left(k_{1 \to 4} + k_{1 \to 2} + k_{1 \to 3} \right) P_1 + k_{4 \to 1}P_4 + k_{2 \to 1}P_2 + k_{3 \to 1}P_3, \qquad (9.234)$$

$$\frac{d}{dt}P_2 = - \left(k_{2 \to 1} + k_{2 \to 4} \right) P_2 + k_{1 \to 2}P_1 + k_{4 \to 2}P_4, \qquad (9.235)$$

$$\frac{d}{dt}P_3 = - \left(k_{3 \to 1} + k_{3 \to 4} \right) P_3 + k_{1 \to 3}P_1 + k_{4 \to 3}P_4, \qquad (9.236)$$

and

$$\frac{d}{dt}P_4 = - \left(k_{4 \to 1} + k_{4 \to 2} + k_{4 \to 3} \right) P_4 + k_{1 \to 4}P_1 + k_{2 \to 4}P_2 + k_{3 \to 4}P_3. \qquad (9.237)$$

Before focusing on the respective higher order rate theory, we shortly comment on a particular regime of EET (be aware of the similarity to bridge-mediated ET as discussed in Section 7.6.1). If the formation of the two intermediate states (labeled by 2 and 3) is less probable, that is if the transition rates to these states are much smaller than those out of these states ($k_{1 \to 2}, k_{1 \to 3}, k_{4 \to 2}, k_{4 \to 3} \ll k_{2 \to 1}, k_{3 \to 1}, k_{2 \to 4}, k_{3 \to 4}$), the populations P_2 and P_3 would remain small in the course of the EET. At the same time, the solution of the rate equations for P_2 and P_3 is dominated by the rates of probability outflow from the states 2 and 3. Accordingly, a solution of these rate equations becomes possible by neglecting the time derivatives $\partial P_2/\partial t$ and $\partial P_3/\partial t$, and EET can be characterized by a single rate whose forward part reads

$$K_{EET}^{(fw)} = k_{1 \to 4} + \frac{k_{1 \to 2}k_{2 \to 4}}{k_{2 \to 1} + k_{2 \to 4}} + \frac{k_{1 \to 3}k_{3 \to 4}}{k_{3 \to 1} + k_{3 \to 4}}. \qquad (9.238)$$

An effective rate of the sequential transfer (second and third terms on the right-hand side) is added to the rate of direct transfer. Therefore, both mechanisms can be compared, which is not possible in such an easy way in a more general case.

9.8.2 Charge-transfer Excitons and Charge Separation

In Section 9.8.1, the charge-separated (CS) (ionic) states have been considered as intermediate states in 2ET-assisted EET, which was described as an incoherent rate process. However, charge-transfer states are of importance beyond 2ET-assisted

EET. For instance, in typical bulk heterojunction organic solar cells, excitons are generated in polymer assemblies (such as polythiophene) interfacing a region with electron acceptor molecules (for instance, fullerene). Excitons in the polymer part can be of intramolecular (that is, electron and hole are on the same polymer) and intermolecular types (here, electron and hole are on different polymers). The latter excitation where electron and hole reside on different monomers, not too far apart, can give rise to, possibly delocalized, *charge-transfer excitons* (cf. Section 9.1). In principle, the Coulomb interactions between Frenkel and charge-transfer excitations may lead to states of mixed character. At the interface to the acceptor molecules, charge separation takes place; that is, the Frenkel/charge-transfer exciton state dissociates. This is prerequisite for generating free charges that can propagate to the electrodes.

In order to describe the local and nonlocal single excitation states of an aggregate, the ansatz, Eq. (9.5), has to include ionic states as well.[24] Thus, the basis in Eq. (9.34) can be extended according to

$$|m_e n_h\rangle = \delta_{mn}|m\rangle + (1 - \delta_{mn})|\varphi_m^-\rangle|\varphi_n^+\rangle \prod_{m,n\neq k} |\varphi_{kg}\rangle. \tag{9.239}$$

The second term describes electron and hole on sites m and n, respectively, with the monomers being in the corresponding ionic states φ_m^- and φ_n^+. All other monomers are in their electronic ground states. Using this basis, the exciton Hamiltonian equation (9.91) has to be supplemented by a charge-transfer part

$$H_{\text{CT}} = \sum_{m\neq n} \sum_{k\neq l} \left[\delta_{mk}\delta_{nl}E_{m_e n_h} + V_{m_e n_h, k_e l_h} \right] |m_e n_h\rangle\langle k_e l_h| \tag{9.240}$$

and a coupling between Frenkel and charge-transfer excitons

$$V_{\text{ex--CT}} = \sum_{m,n} \sum_{k,l} (1 - \delta_{mk}) \left[\delta_{mn}(1 - \delta_{kl}) + \delta_{kl}(1 - \delta_{mn}) \right]$$
$$\times V_{m_e n_h, k_e l_h} |m_e n_h\rangle\langle k_e l_h|. \tag{9.241}$$

Here, $E_{m_e n_h}$ is the energy of the charge-transfer state, and $V_{m_e n_h, k_e l_h}$ is the coupling between electron–hole pairs. It can be written in analogy to Eq. (9.19) if the transition densities include charge-transfer excitations. These electronic Hamiltonians can be supplemented by the contributions from electron–vibrational interaction using the various strategies outlined in Section 9.3.

In Figure 9.26, results of a multilayer MCTDH simulation (cf. Section 9.6.6) are shown for a model of the charge separation at a polythiophene–fullerene heterojunction. The model consists of stacked polythiophene polymers and fullerene molecules, which are comprised into a single effective acceptor site (Figure 9.26a). Exciton–vibrational coupling is accounted for using the model of Section 9.3.1. Among the nonlocal charge-transfer excitation states, those where the electron is fixed at the acceptor site are considered as CS states. If the separation exceeds eight units, the charge is taken as a free carrier. Figure 9.26b,c shows the time-dependent

---

24) In a more rigorous formulation, one should include exchange effects due to wave function overlap as well; that is, one should start with the ansatz equation (9.6).
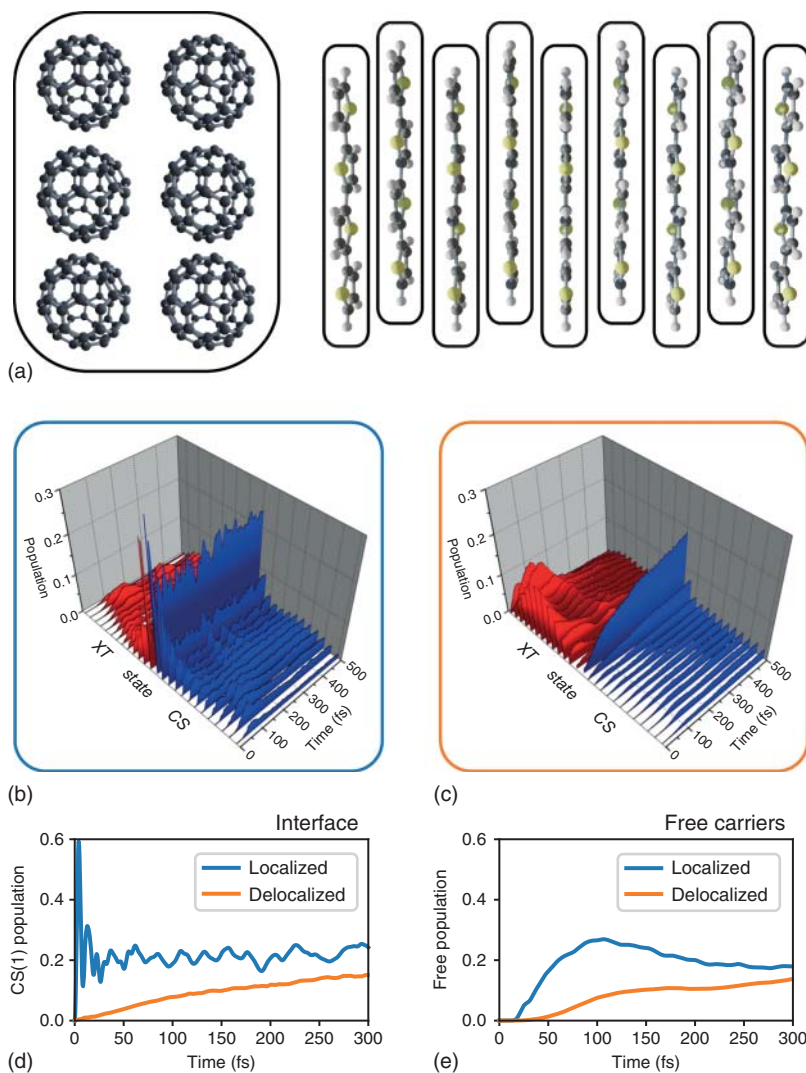
Figure 9.26 Exciton dynamics and dissociation in a model of a polythiophene–fullerene heterojunction (a); the fullerenes are combined in one effective acceptor. There are 13 Frenkel exciton (XT) and 13 charge separated (CS) states. In the latter, the electron is fixed at the acceptor. (b) and (c) The population dynamics of XT and CS states starting from a localized Frenkel exciton at the interface or else from a delocalized bright exciton in the donor domain. (d) Population of the interfacial charge-transfer state (CS_1) and (e) free carrier population (integrated over CS_n for $n = 8, \ldots, 13$) for both the initial conditions (Figure courtesy of I. Burghardt, for more details, see Polkehn et al. [16]).

population of Frenkel- and CS states for an initial excitation of the local XT state at the interface and the high energy bright exciton state of the polythiophene donor domain, respectively. Charge-transfer exciton states are not taken into account. The results in Figure 9.26b–e point to the strong influence of the initial state on the initial dynamics of charge separation.

9.9 Exciton–Exciton Annihilation

The Förster transfer considered in Section 9.5 concentrates on the description of a single excitation in the aggregate. This is appropriate whenever the light intensity used to excite the aggregate is low enough to justify the restriction on a singly excited state. However, upon increasing the light intensity, one may study states where different molecules of the aggregate are excited simultaneously. This opens a new relaxation channel, that is *exciton–exciton annihilation*, as will be discussed in what follows.

Exciton–exciton annihilation is usually characterized as a two-step process (cf. Figure 9.27). First, two excitations being in the S_1-state of the molecules have to move close to each other so that their excitation energy can be used to create a higher excited S_n-state ($n > 1$) at one molecule (Figure 9.27a,b). This step leaves behind the other molecule in the S_0 ground state and is usually called exciton fusion.
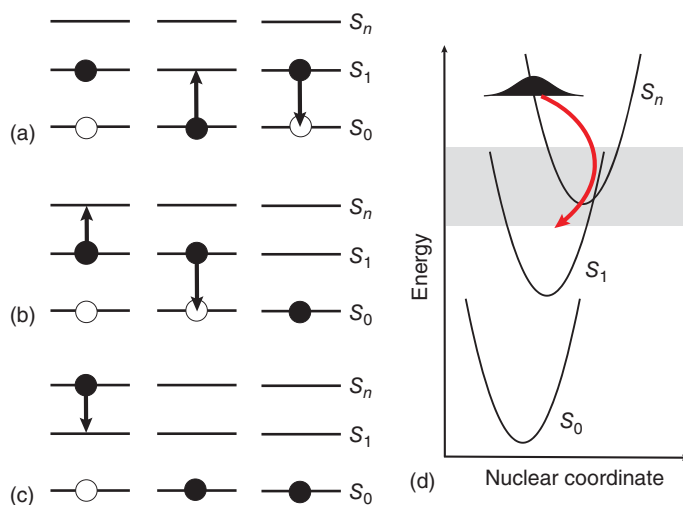
Figure 9.27 Scheme of exciton–exciton annihilation in a molecular trimer with nearest neighbor exciton coupling. (a) EET results in a state with two excitations at the neighboring molecules. (b) Exciton fusion leaves one molecule in a higher excited state (S_n), whereas the other one returns to the ground state. (c, d) Nonadiabatic internal conversion dynamics causes an $S_n \rightarrow S_1$ transition. Thus, one electronic excitation state has been transformed into vibrational excitation. The gray-shaded area in panel (d) indicates that there may be more electronic states in between S_n and S_1.

In a second step, an ultrafast internal conversion process returns the molecule, from the higher excited S_n-state back to the S_1-state. The whole process can be represented by the following scheme:

$$M_1(S_1) + M_2(S_1) \xrightarrow{\text{fusion}} M_1(S_n) + M_2(S_0) \xrightarrow{\text{IC}} M_1(S_1) + M_2(S_0) \tag{9.242}$$
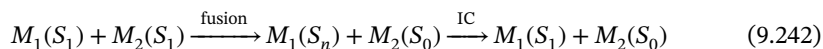
Exciton–exciton annihilation is often described by the phenomenological rate equation

$$\frac{dn(\boldsymbol{r},t)}{dt} = -\gamma_{\mathrm{d}} n(\boldsymbol{r},t) - \gamma_{\mathrm{a}} n(\boldsymbol{r},t)^2, \tag{9.243}$$

with the exciton density $n(\boldsymbol{r},t)$ at the spatial position $\boldsymbol{r}$, the intrinsic decay rate of a single exciton γ_{d} (for instance, due to photon emission), and the annihilation rate γ_{a}. Such a macroscopic description is valid for larger aggregates (and organic semiconductors) characterized by exciton diffusion. An example is given in Figure 9.28.

A consequent microscopic description has to consider the detailed dynamics of exciton–exciton annihilation as shown in Figure 9.27. That is, the theoretical formulation needs to use a three-level model for every molecule of the aggregate and has to account for, at least, two-exciton states. The process of internal conversion has to be considered too.

If the excitations that undergo the annihilation process are not completely localized, the description has to be done using delocalized single- and two-exciton states. In the opposite case, it will be sufficient to calculate the annihilation rate for the transition from localized states. Both cases will be considered in Section 9.9.2. In Section 9.9.1, we briefly comment on a model for two-exciton states if a double excitation of the individual molecules into an S_n-state has been incorporated.
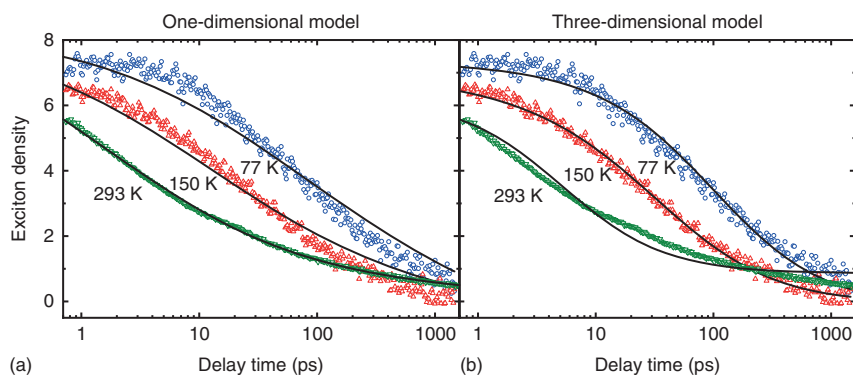
Figure 9.28 Time dependence of exciton density (fraction of excited molecules in a pump–probe experiment) in perylene bisimide aggregates at different temperatures. The experimental data (dots) are fit to Eq. (9.243) employing one-dimensional (a) and three-dimensional (b) diffusion models. From the agreement between theory and experiment, it could be concluded that exciton dynamics changes from one- to three-dimensional diffusion with decreasing temperature (Figure courtesy of S. Wolter, for more details see Wolter et al. [17]).

9.9.1 Three-level Description of the Molecules in the Aggregate

Instead of the two-level model used so far for the description of the individual monomers of the aggregate, we additionally incorporate a third state $|\varphi_{mf}\rangle$ that corresponds to a higher S_n-level (cf. Figure 9.27). The related energy is denoted by ϵ_{mf}, with the energetic position determined by the relation $\epsilon_{mf} - \epsilon_{me} \approx \epsilon_{me} - \epsilon_{mg}$. This accounts for the fact that the process of exciton fusion in Figure 9.27b requires a resonance between the participating transitions. Moreover, it is assumed that there exists a nonvanishing transition dipole matrix element $\tilde{\boldsymbol{d}}_m = \langle \varphi_{mf}|\hat{\mu}|\varphi_{me}\rangle$ that connects the S_1 state with the higher excited state (the matrix elements for the direct transition $S_0 \rightarrow S_n$, $\langle \varphi_{mf}|\hat{\mu}|\varphi_{mg}\rangle$, are set equal to zero).

As a result, a new class of Coulomb coupling matrix elements arises in addition to those introduced in Section 9.2.2. To keep the model simple, we assume that electrostatic couplings among molecules due to a nonvanishing molecular charge density, Eq. (9.20), do not contribute. Having only the coupling matrix elements $J_{mn}(eg, eg)$ in the two-level model, Eq. (9.21), tells us that the new types $J_{mn}(fe, fe)$ and $J_{mn}(fg, ee)$ (as well as the complex-conjugated expressions) must also be considered. The first one describes EET between the S_1 and the S_n states (molecule m undergoes the transition $S_1 \rightarrow S_n$, while the reverse process takes place in molecule n). The second type of matrix element characterizes the excitation of molecule m and the deexcitation of molecule n, both being initially in the S_1 state (see also Figure 9.27). Therefore, the general Hamiltonian, Eq. (9.14), valid for a multilevel description of each molecule in the aggregate, becomes

$$
\begin{aligned}
H_{\text{agg}} = &\sum_m \sum_{a=g,e,f} H_{ma}|\varphi_{ma}\rangle\langle\varphi_{ma}| \\
&+ \sum_{m,n} \left(J_{mn}(eg,eg)|\varphi_{me}\varphi_{ng}\rangle\langle\varphi_{ne}\varphi_{mg}| + J_{mn}(fe,fe)|\varphi_{mf}\varphi_{ne}\rangle\langle\varphi_{nf}\varphi_{me}| \right. \\
&+ \left. J_{mn}(fg,ee)|\varphi_{mf}\varphi_{ng}\rangle\langle\varphi_{ne}\varphi_{me}| + \text{h.c.} \right).
\end{aligned}
\tag{9.244}
$$

The off-diagonal part of the monomer Hamiltonian, Eq. (9.15), responsible for nonadiabatic transitions is treated separately. We introduce

$$
H_{\text{na}} = \sum_m \Theta_m(ef)|\varphi_{me}\rangle\langle\varphi_{mf}| + \text{h.c.},
\tag{9.245}
$$

which describes nonadiabatic coupling between the S_n and the S_1 states (cf. Eqs. (2.97) and (6.111)).[25] A similar expression had already been used in Section 6.6 to describe the internal conversion process.

In a next step, we introduce the two-exciton state by extending the derivations given in Section 9.2.4. Instead of Eq. (9.71), the two-exciton state is now written as (the quantum numbers $\tilde{\alpha}$ refer exclusively to the two-exciton states)

$$
|\tilde{\alpha}\rangle = \sum_{m,n} c_{\tilde{\alpha}}(m,n)|me, ne\rangle + \sum_m c_{\tilde{\alpha}}(m)|mf\rangle.
\tag{9.246}
$$

This state covers two S_1 excitations at molecules m and n (cf. Eq. (9.35) and note the additional label "e") as well as higher excitation at the mth molecule. The latter state

---

25) Note that, in practice, $S_n \neq S_2$; that is, there will be a certain number of excited states in between S_1 and S_n as indicated by the shaded area in Figure 9.27d.

is similar to that introduced in Eq. (9.34) but with φ_{me} replaced by φ_{mf} (note the label "f" here). The extensions introduced in this section will be used to discuss different types of exciton–exciton annihilation rates in Section 9.9.2.

9.9.2 The Rate of Exciton–Exciton Annihilation

Let us start with the consideration of exciton–exciton annihilation in the limit of delocalized exciton states. In this case, one can directly utilize the results obtained for internal conversion in Section 6.6, but now the reactant state is given by the two-exciton state $|\tilde{\alpha}\rangle$, and the product state by the single-exciton state $|\beta\rangle$. The rate follows as

$$k_{\tilde{\alpha}\to\beta} = \frac{2\pi}{\hbar}|\Theta(\tilde{\alpha},\beta)|^2 \mathcal{D}(\tilde{\alpha},\beta;(\mathcal{E}_{\tilde{\alpha}} - \mathcal{E}_\beta)/\hbar), \tag{9.247}$$

where the DOS can be defined in analogy to Eq. (6.113) or (6.115) but based on the PES of the single- and two-exciton states. The coupling matrix elements $\Theta(\tilde{\alpha},\beta)$ are given by the exciton representation of the nonadiabatic coupling, Eq. (9.245):

$$\Theta(\tilde{\alpha},\beta) = \langle\tilde{\alpha}|H_{\mathrm{na}}|\beta\rangle = \sum_m \Theta_m(fe)c_{\tilde{\alpha}}^*(mf)c_\beta(me). \tag{9.248}$$

Let us assume that all molecules in the aggregate are identical and characterized by the same nonadiabatic coupling $\Theta_m(fe)$. Furthermore, we replace the DOS in Eq. (9.247) by a quantity referring to the local internal conversion processes. Then, we obtain

$$k_{\tilde{\alpha}\to\beta} = \left|\sum_m c_{\tilde{\alpha}}^*(mf)c_\beta(me)\right|^2 k_{f\to e}^{(\mathrm{IC})}. \tag{9.249}$$

Here, $k_{f\to e}^{(\mathrm{IC})}$ is the rate of internal conversion, which, according to our assumption, is identical for all molecules of the aggregate. The exciton–exciton annihilation, therefore, can be described by this local internal conversion rate, weighted, however, by the square of an overlap expression. This expression incorporates the overlap of the probability amplitudes $c_{\tilde{\alpha}}^*(mf)$ and $c_\beta(me)$ for having a double and single excitation, respectively, at site m. In this description, the first step of exciton–exciton annihilation, namely, exciton fusion, is masked by the two-exciton state, in particular by the nonvanishing expansion coefficient $c_{\tilde{\alpha}}(mf)$ measuring the probability to have a double excitation at a single molecule.

If the annihilation process proceeds via localized states as indicated in Scheme (9.242) and Figure 9.27, one has to start with the doubly excited state $|me, ne\rangle$. It is transferred to the intermediate state $|mf\rangle$ of a higher excited single molecule, and the product state is simply given by the single excited state $|me\rangle$ at molecule m. This scheme recalls bridge-mediated ET reactions as discussed in Section 7.5. There, the transfer from the initial donor state through the intermediate bridge states into the final acceptor state could take place as a direct transition (superexchange transfer) or as a stepwise process going from the donor to the bridge and then to the acceptor (sequential transfer). The latter appears if vibrational relaxation in the intermediate state (the bridge states) interrupts the direct transfer from the donor to the acceptor. One can expect similar conditions in the case of exciton–exciton annihilation.

Let us consider, for instance, the two-step annihilation process. It is characterized by the rate $k_{me,ne\rightarrow mf}$ describing the creation of the higher excited state at molecule m and the rate $k_{mf\rightarrow me}$ characterizing the internal conversion at molecule m. The first rate is computed with the Coulomb matrix element $J_{mn}(fg, ee)$ as the perturbation, and the second rate is simply the rate of internal conversion $k_{f\rightarrow e}^{(IC)}$. Both should enter rate equations for the various state populations with the solution characterizing the two-step annihilation process. But similar to the introduction of the superexchange process in Section 7.5, one may also describe the annihilation as a process without intermediate state relaxation.

9.10 Supplement

9.10.1 Second Quantization Notation of the Aggregate Hamiltonian

Frequently, second quantization is used to express the aggregate Hamiltonian in terms of exciton creation and annihilation operators. In what follows, the introduction of these operators will be sketched for the aggregate Hamiltonian, Eq. (9.14), describing a two-level model. Further, we assume that the charge densities of molecules m and n are locally neutral, that is the Coulomb interaction is reduced to the excitonic coupling, Eq. (9.29) (for notational convenience, we use $J_{mm} = 0$). Then, neglecting off-diagonal parts of the monomer Hamiltonian (we set $H_m(aa) = H_{ma}$), we arrive at

$$H_{\text{agg}} = \sum_m \sum_{a=g,e} H_{ma}|\varphi_{ma}\rangle\langle\varphi_{ma}| + \sum_{m,n} J_{mn}|\varphi_{me}\varphi_{ng}\rangle\langle\varphi_{ne}\varphi_{mg}|. \tag{9.250}$$

As a further simplification, we fix the nuclear coordinates at their values corresponding to the aggregate ground state ($R \rightarrow R_0$, nuclear kinetic energy equal to zero). If we replace the PES U_{ma} in Eq. (9.15) by the corresponding energies

$$E_{ma} = U_{ma}(R_0), \tag{9.251}$$

we obtain the electronic part of the aggregate Hamiltonian as

$$H_{\text{agg}}^{(\text{el})} = \sum_m \sum_{a=g,e} E_{ma}|\varphi_{ma}\rangle\langle\varphi_{ma}| + \sum_{mn} J_{mn}|\varphi_{me}\varphi_{ng}\rangle\langle\varphi_{ne}\varphi_{mg}|. \tag{9.252}$$

Next, we introduce creation and annihilation operators as follows:

$$B_m^+ = |\varphi_{me}\rangle\langle\varphi_{mg}|, \qquad B_m = |\varphi_{mg}\rangle\langle\varphi_{me}|. \tag{9.253}$$

This results in

$$H_{\text{agg}}^{(\text{el})} = E_0 + \sum_m E_m B_m^+ B_m + \sum_{m,n} J_{mn} B_m^+ B_n. \tag{9.254}$$

The first term on the right-hand side denotes the electronic aggregate ground state energy

$$E_0 = \sum_m E_{mg}. \tag{9.255}$$

The excitation energy of molecule m

$$E_m = E_{me} - E_{mg} \tag{9.256}$$

is the site energy. The operators are of the Pauli type, obeying the commutation relations

$$\left[B_m^+, B_n\right]_+ = \delta_{mn} + (1 - \delta_{mn})2B_m^+B_n \tag{9.257}$$

and

$$\left[B_m^+, B_n^+\right]_+ = (1 - \delta_{mn})2B_m^+B_n^+. \tag{9.258}$$

The relation $[B_m^+, B_m]_+ = |\varphi_{mg}\rangle\langle\varphi_{mg}| + |\varphi_{me}\rangle\langle\varphi_{me}|$ can be interpreted as the completeness relation for the electronic state space of the mth molecule; that is, it can be set equal to unity. This relation has been used to derive Eq. (9.254) from Eq. (9.252). For $m = n$, the excitations behave like Fermions, and two of them cannot occupy the same molecular state.

9.10.2 Photon-mediated Long-range Excitation Energy Transfer

In the framework of the Förster theory presented in Section 9.5, EET has been characterized by the overlap of the donor emission spectrum and the acceptor absorption spectrum. This way of formulating the rate suggests an interpretation of the transfer as a process where a photon is emitted by the donor and afterward absorbed by the acceptor. However, the use of the donor–acceptor Coulomb interaction V_{DA}, Eq. (9.113), to compute the rate indicates that the Förster transfer cannot be simply viewed as a *photon-mediated* EET process. The present section is devoted to clarify this issue. To this end, a theory of EET is formulated that is based on the general electromagnetic interaction between the donor and the acceptor. It will include the Förster theory in the limit of small DA distances. The value of this approach is not a revision of the Förster theory, but it will provide a more basic classification including some corrections valid for large DA distances.

In order to prepare for the following discussion, we briefly review some basics of matter radiation interaction (see also the discussion in Chapter 4 and especially Section 4.4). First, we recall that within the Coulomb gauge, the vector potential $\boldsymbol{A}$ represents a transversal field that couples to the molecular system via the so-called minimal coupling Hamiltonian, Eq. (4.8), where the momenta of the charged particles are replaced by $\boldsymbol{p}_j - \boldsymbol{A}(\boldsymbol{r}_j)q_j/c$.

After quantization of the transversal vector potential according to Eq. (4.127), the full electromagnetic interaction among electrons and nuclei is mediated by the short-ranged instantaneous Coulomb interaction and the long-range retarded exchange of transversal photons. This already indicates that the Förster theory represents the short-range contribution of the complete interaction, which includes long-range transversal photon exchange too.

When formulating a comprehensive theory of DA EET, it is advisable to move from the minimal coupling Hamiltonian to the so-called multipolar Hamiltonian by applying a canonical transformation (Power–Zienau transformation). Carrying out

the latter requires a rather cumbersome procedure that includes the representation of all molecules by charges as well as polarization and magnetization densities. The transformation becomes much easier if one can restrict the description of the donor and acceptor to their transition dipole moments $\boldsymbol{d}_D$ and $\boldsymbol{d}_A$, respectively. It amounts to carrying out a unitary transformation as Eq. (4.10), with the classical vector potential being replaced by the quantum mechanical expression. Both molecules are assumed to be locally neutral, and higher multipoles are of minor importance. Then, the complete electromagnetic interaction is reduced to an interaction between transition dipoles and can be accounted for by the *dipolar coupling Hamiltonian*:

$$H_{\text{int}} = \sum_{m=D,A} \sum_{\lambda,\boldsymbol{k}} \left(\boldsymbol{g}_{\lambda\boldsymbol{k}}(\boldsymbol{X}_m)\hat{a}_{\lambda\boldsymbol{k}} + \text{h.c.}\right) \left(\boldsymbol{d}_m|\varphi_{me}\rangle\langle\varphi_{mg}| + \text{h.c.}\right). \tag{9.259}$$

The coupling constant entering this expression takes the form (compare Eq. (4.129))

$$\boldsymbol{g}_{\lambda\boldsymbol{k}}(\boldsymbol{x}) = i\sqrt{\frac{2\pi\hbar\omega_{\boldsymbol{k}}}{L^3}}e^{i\boldsymbol{k}\boldsymbol{x}}\boldsymbol{n}_{\lambda\boldsymbol{k}}. \tag{9.260}$$

H_{int} describes photon emission and absorption by the donor (positioned at $\boldsymbol{X}_D$) and the acceptor (positioned at $\boldsymbol{X}_A$). It takes place via an exclusive coupling to the transition dipole moments $\boldsymbol{d}_D$ of the donor and $\boldsymbol{d}_A$ of the acceptor. The Hamiltonian for the photon field is given by Eq. (4.128), where the zero-point energy contribution is of no interest here and can be neglected. The introduction of the model is completed by fixing the Hamiltonian of the DA complex. We focus on the dimer limit of the aggregate Hamiltonian equation (9.36) by taking the ground state contribution, Eq. (9.37), and the parts referring to the singly and doubly excited states, Eqs. (9.38) and (9.39), respectively, but neglecting any intermolecular Coulomb coupling. This yields

$$H_{\text{agg}} = \mathcal{H}_0|0\rangle\langle0| + \sum_{m=D,A} \mathcal{H}_m|m\rangle\langle m| + \mathcal{H}_{\text{DA}}|DA\rangle\langle DA|. \tag{9.261}$$

The introduced states $|0\rangle$, $|m\rangle$, and $|DA\rangle$ are the dimer variants of those defined in Eqs. (9.33), (9.34), and (9.35), respectively. The new Hamiltonians exclusively account for intramolecular vibrational dynamics and read: $\mathcal{H}_0 = H_{Dg} + H_{Ag}$, $\mathcal{H}_D = H_{De} + H_{Ag}$, $\mathcal{H}_A = H_{Dg} + H_{Ae}$, and $\mathcal{H}_{\text{DA}} = H_{De} + H_{Ae}$ (recall that the H_{ma} denote monomer vibrational Hamiltonians). Note that we have included the simultaneous excitation of the donor as well as the acceptor; the relevance of this will become clear below.

Equation (9.259) represents the complete electromagnetic coupling between the donor and the acceptor, provided their involved internal charge distributions can be approximated by transition dipole moments (between the ground and the first excited states). Therefore, any rate calculation based on this coupling expression should comprise the Förster rate. However, there appear some differences with respect to the Golden Rule formulation of the Förster rate given in Section 9.5.2. First, when including the quantized radiation field into the rate calculations, the Hilbert space has to be extended by photon contributions. And second, the rate represents a fourth-order transition rate including intermediate states. Figure 9.29 illustrates the two-step character of the process: donor deexcitation does not directly

Figure 9.29 Photon-mediated EET in a DA complex. Both molecules are represented by an electronic two-level system with related vibrational manifolds and are coupled to the continuum of photon states (P). Two intermediate states contribute to the transition. Upper pathway: donor deexcitation initiates photon emission into the continuum of single photon states (P*), followed by photon absorption due to the acceptor. Lower pathway: photon emission and acceptor excitation appears before donor deexcitation.
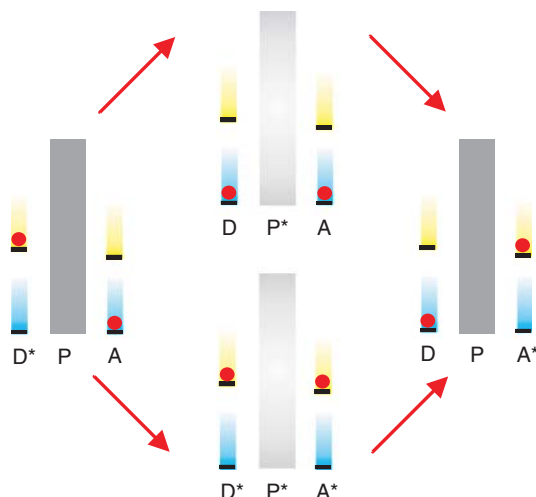
lead to an acceptor excitation, but first sets free a photon. Only in a second step, the photon is absorbed by the acceptor, moving the latter into its excited state (upper transition pathway in Figure 9.29). The related transition rate will be of second order with respect to the donor–photon coupling and also of second order with respect to the acceptor–photon coupling; that is, the overall rate is of fourth order with respect to the dipolar coupling, Eq. (9.259). When calculating the rate, we will also meet the counterintuitive two-step transition (lower transition pathway in Figure 9.29) where photon emission and acceptor excitation take place before donor deexcitation (formally such an additional process appears since the molecule–photon coupling, Eq. (9.259), comprises simultaneous photon creation and annihilation). It is just this process that requires the inclusion of the doubly excited state $|DA\rangle$ (the relevance of this is related to the time-energy uncertainty of quantum mechanics as discussed below).

9.10.2.1 Preparatory Considerations for the Rate Computation

As explained in Section 9.10.2 and displayed in Figure 9.29, the rate of photon-mediated EET will be of fourth order with respect to the photon–molecule interaction equation (9.259). Therefore, we will utilize the general rate theory introduced in Section 3.14. Within this approach, Eq. (3.522) gives the fourth-order rate corrected by a product of two second-order rates. As discussed there, the latter correct the fourth-order rates with respect to a sequential transition from the initial to the intermediate state and, afterward, from the intermediate to the final state. In the case of a simple three-level system, this factorized contribution completely compensates particular fourth-order contributions, which have been characterized by the so-called Liouville space pathways (LSPs) of types II and III (see Figure 3.14). In what follows we will make use of the fact that, reproducing the Förster rate of EET in a particular limit, we can concentrate on the LSP of type I. It gives the direct (coherent) transition with a virtual intermediate state population only; all other contributions cancel with the product of second-order rates.

According to Eqs. (3.522)–(3.524), the rate of *photon-mediated* EET takes the form (dropping the LSP pathway index I)

$$k_{D\to A}^{(pm)} = 2\mathrm{Re} \int_0^\infty dt_3 \, dt_2 \, dt_1 \, C_{AD}(t_3, t_2, t_1).$$
(9.262)

To calculate the correlation function, we identify the statistical operator of state 1 in Eq. (3.522), with $\hat{W}_D$ describing the excited donor and the absence of any photon (photon vacuum $|vac\rangle$). Consequently, it takes the form $\hat{W}_D = \hat{R}_D|D\rangle\langle D| \times |vac\rangle\langle vac|$, where $\hat{R}_D = \hat{R}_{De}\hat{R}_{Ag}$ characterizes the vibrational equilibrium in the excited donor and the unexcited acceptor. Second, the state 3 in Eq. (3.523) corresponds to the final state of the transition with the unexcited donor, the excited acceptor, and, again, the photon vacuum. Noting all these specifications, we obtain

$$C_{AD}(t_3, t_2, t_1) = \frac{1}{\hbar^4}\mathrm{tr}_{vib}\{\langle A|\langle - \text{vac} \, U(t_3 + t_2)H_{int}U(t_1)H_{int}\hat{W}_D$$
$$\times U^+(t_1 + t_2)H_{int}U^+(t_3)H_{int}|vac\rangle|A\rangle\}.$$
(9.263)

The original trace, which also covers electronic and photonic contributions, has already been reduced to a trace with respect to the vibrational DOFs, whereas electronic and photonic contributions are specified by the matrix element $\langle A|\langle vac| \dots |vac\rangle|A\rangle$. The time-evolution operators are defined by the sum of the zeroth-order Hamiltonians H_{phot}, Eq. (4.128) and H_{agg}, Eq. (9.261); they factorize into a photon part and into monomer contributions. The included electron–photon matrix element separates into two matrix elements, which will be calculated first. We have

$$\langle A|\langle vac|U(t_3 + t_2)H_{int}U(t_1)H_{int}|vac\rangle|D\rangle$$
$$= U_A(t_3 + t_2) \times \langle A|\langle vac|U_{phot}(t_3 + t_2)H_{int}U_{agg}(t_1)U_{phot}(t_1)H_{int}|vac\rangle|D\rangle. \quad (9.264)$$

Remember that U_A is defined by $\mathcal{H}_A$, U_{phot} by H_{phot}, and U_{agg} by the complete DA complex Hamiltonian, Eq. (9.261). The general expression of the latter has to be taken here since the transition from the excited donor state to the excited acceptor state (from the right to the left part of the matrix element) may proceed in two ways: via the unexcited DA pair as well as via the state of a simultaneous DA excitation (cf. Figure 9.29). Therefore, we may replace $U_{agg}(t_1)$ by $U_0(t_1)|0\rangle\langle 0| + U_{DA}(t_1)|DA\rangle\langle DA|$.

When calculating the photon state matrix element of Eq. (9.264), one meets the photon correlation function (the hat remains on the tensorial character of this function; note also $\boldsymbol{X}_{AD} = \boldsymbol{X}_A - \boldsymbol{X}_D$):

$$\hat{C}_{phot}(\boldsymbol{X}_{AD}, t) = \langle vac|\sum_{\lambda,\boldsymbol{k}} \left(\boldsymbol{g}_{\lambda\boldsymbol{k}}(\boldsymbol{X}_A)a_{\lambda\boldsymbol{k}} + h.c.\right) U_{phot}(t)$$
$$\times \sum_{\kappa,\boldsymbol{q}} \left(\boldsymbol{g}_{\kappa\boldsymbol{q}}(\boldsymbol{X}_D)a_{\kappa\boldsymbol{q}} + h.c.\right) |vac\rangle$$
$$= \frac{2\pi\hbar}{V}\sum_{\lambda,\boldsymbol{k}} \boldsymbol{n}_{\lambda\boldsymbol{k}} \otimes \boldsymbol{n}_{\lambda\boldsymbol{k}} \, \omega_{\boldsymbol{k}} \, e^{i(\boldsymbol{k}\boldsymbol{x}-\omega_{\boldsymbol{k}}t)}.$$
(9.265)

The second part of this formula follows immediately since an average has to be taken with respect to the photon vacuum only ($\otimes$ is the tensorial product). Apparently, Eq. (9.264) turns into the form

$$\langle A | \langle -\!\!- \text{vac}\, U(t_3 + t_2)H_{\text{int}}U(t_1)H_{\text{int}}|\text{vac}\rangle|D\rangle$$
$$= U_A(t_3 + t_2) \times \left(U_0(t_1) + U_{DA}(t_3 + t_2)\right) [\boldsymbol{d}_A \hat{C}_{\text{phot}}(\boldsymbol{X}_{\text{AD}}, t_1)\boldsymbol{d}_D^*]. \tag{9.266}$$

The combination of the transition dipole matrix elements with the photon correlation function indicates that the Condon-approximation has been incorporated. The notation $[\boldsymbol{d}_A \hat{C}\boldsymbol{d}_D^*]$ implies a scalar multiplication of $\boldsymbol{d}_A$, with $\boldsymbol{n}_{\lambda\boldsymbol{k}}$ appearing left in the second part of Eq. (9.265), and of $\boldsymbol{d}_D^*$, with $\boldsymbol{n}_{\lambda\boldsymbol{k}}$ appearing on the right. In the same way, we may compute the second electron–photon matrix element in Eq. (9.263) to arrive at (note the negative time argument in the photon correlation function, which is caused by the appearance of U_{phot}^+)

$$\langle D | \langle \text{vac} | U^+(t_1 + t_2)H_{\text{int}}U^+(t_3)H_{\text{int}}|\text{vac}\rangle|A\rangle$$
$$= U_D^+(t_1 + t_2) \times \left(U_0^+(t_3) + U_{DA}^+(t_3)\right) [\boldsymbol{d}_D \hat{C}_{\text{phot}}(\boldsymbol{X}_{\text{DA}}, -t_3)\boldsymbol{d}_A^*]. \tag{9.267}$$

Introducing both electron–photon matrix elements into the correlation function, Eq. (9.263), one ends up with four new correlation functions. The expression $\text{tr}_{\text{vib}}\{\hat{R}_D U_D^+(t_1 + t_2)U_0^+(t_3)U_A(t_3 + t_2)U_0(t_1)\}$ corresponds to the EET process with the unexcited DA pair as the intermediate state (upper pathway in Figure 9.29). Being aware of the separate vibrational coordinates for the donor and the acceptor, this three-time correlation function factorizes into $C_{De\rightarrow g}(t_1 + t_2)C_{Ag\rightarrow e}(t_3 + t_2)$ (see Eqs. (9.130) and (9.131), respectively). In contrast, the correlation function $\text{tr}_{\text{vib}}\{\hat{R}_D U_D^+(t_1 + t_2)U_{AD}^+(t_3)U_A(t_3 + t_2)U_{DA}(t_1)\}$ results from the presence of the doubly excited pair as an intermediate state (lower pathway in Figure 9.29). It reduces to $C_{De\rightarrow g}(t_2 + t_3)C_{Ag\rightarrow e}(t_1 + t_2)$. The interference of both transition paths leads to two mixed terms. So, we finally arrive at

$$C_{\text{AD}}(t_1, t_2, t_3) = \frac{|d_D d_A|^2}{\hbar^4} \left(C_{De\rightarrow g}(t_1 + t_2)C_{Ag\rightarrow e}(t_3 + t_2) \right.$$
$$+ C_{De\rightarrow g}(t_1 + t_2 + t_3)C_{Ag\rightarrow e}(t_2)$$
$$+ C_{De\rightarrow g}(t_2)C_{Ag\rightarrow e}(t_1 + t_2 + t_3)$$
$$+ \left. C_{De\rightarrow g}(t_2 + t_3)C_{Ag\rightarrow e}(t_1 + t_2) \right)$$
$$\times [\boldsymbol{n}_A \hat{C}_{\text{phot}}(\boldsymbol{X}_{\text{AD}}, t_1)\boldsymbol{n}_D][\boldsymbol{n}_D \hat{C}_{\text{phot}}(\boldsymbol{X}_{\text{DA}}, -t_3)\boldsymbol{n}_A], \tag{9.268}$$

where the mixed contributions are at the second and third positions of the right-hand side. Recall the notation $\boldsymbol{d}_m = d_m \boldsymbol{n}_m$, where d_m represents the absolute value of the transition dipole moment, and $\boldsymbol{n}_m$ is the corresponding unit vector.

9.10.2.2 Photon Correlation Functions

Before proceeding with the rate computation, we have to further analyze the photon correlation function, Eq. (9.265), with the focus on its Fourier-transformed version (with respect to its time argument). To carry out the $\lambda\boldsymbol{k}$-summation, we first note that $\sum_\lambda \boldsymbol{n}_{\lambda\boldsymbol{k}} \otimes \boldsymbol{n}_{\lambda\boldsymbol{k}} = 1 - \boldsymbol{k} \otimes \boldsymbol{k}/|\boldsymbol{k}|^2$. This equation represents a rearrangement of

the expansion of an arbitrary vector field with respect to the basis of two transversal vectors (for a given partial wave with wave vector $\boldsymbol{k}$) as well as the longitudinal vector $\boldsymbol{k}/|\boldsymbol{k}|$. Secondly, $\boldsymbol{k}$-vectors inside the $\boldsymbol{k}$-summation are replaced by the action of the nabla operator. We get

$$\hat{C}_{\text{phot}}(\boldsymbol{x}, t) = \left[-\nabla^2 + \nabla \otimes \nabla \right] \zeta_{\text{phot}}(x, t). \tag{9.269}$$

The newly introduced function ζ_{phot} only depends on $x = |\boldsymbol{x}|$ and is given as (note $k = |\boldsymbol{k}|$, the change to a $\boldsymbol{k}$-integration, and the introduction of spherical coordinates):

$$\zeta_{\text{phot}}(x, t) = \frac{\hbar c}{4\pi^2} \int \frac{d^3\boldsymbol{k}}{|\boldsymbol{k}|} \, e^{i(\boldsymbol{k}\boldsymbol{x} - \omega_k t)} = \frac{\hbar c}{\pi} \int_0^\infty dk \frac{\sin(kx)}{x} e^{-ickt}. \tag{9.270}$$

The Fourier transform simply follows as ($\theta(\omega)$ is the unit step function)

$$\zeta_{\text{phot}}(x, \omega) = \theta(\omega) 2\hbar \frac{\sin(\omega x/c)}{x}. \tag{9.271}$$

Calculating the photon-mediated EET rate, we also need the retarded correlation function

$$\hat{C}_{\text{phot}}^{(\text{ret})}(\boldsymbol{x}, t) = \theta(t) \hat{C}_{\text{phot}}(\boldsymbol{x}, t). \tag{9.272}$$

A Fourier transformation leads to (be aware that $\hat{C}_{\text{phot}}(\boldsymbol{x}, t) = \hat{C}_{\text{phot}}^*(\boldsymbol{x}, -t)$)

$$\hat{C}_{\text{phot}}^{(\text{ret})}(\boldsymbol{x}, \omega) = -\int \frac{d\overline{\omega}}{2\pi i} \frac{\hat{C}_{\text{phot}}(\boldsymbol{x}, \overline{\omega})}{\omega - \overline{\omega} + i\varepsilon}. \tag{9.273}$$

In order to derive a concrete expression for $\hat{C}_{\text{phot}}^{(\text{ret})}(\boldsymbol{x}, \omega)$, one may directly compute the Fourier transform of $\zeta_{\text{phot}}^{(\text{ret})}(x, t) = \theta(t)\zeta_{\text{phot}}(x, t)$ at positive and negative frequency arguments, ending up with expressions that include the integral cosine and sine functions. To arrive at the rate of photon-mediated EET, we only need the combination of the retarded photon correlation function at positive and negative frequencies (see Section 9.10.2.3). This combination can be calculated by adding both parts and also directly without a separate determination at positive and negative frequencies. In any case, one arrives at the following simple form (note the introduction of $K = \omega/c$):

$$\frac{1}{\hbar} \left(\zeta_{\text{phot}}^{(\text{ret})}(x, \omega) + \zeta_{\text{phot}}^{(\text{ret})}(x, -\omega) \right) = (\theta(\omega) - \theta(-\omega)) \frac{\sin(Kx)}{x} - i \frac{\cos(Kx)}{x}. \tag{9.274}$$

The application of the nabla operators according to Eq. (9.269) results in an expression for a particular combination of retarded photon correlation functions.

9.10.2.3 The Rate of Photon-mediated Excitation Energy Transfer

Having the explicit structure of the photon correlation function at hand, we may use Eq. (9.268) to compute the rate $k_{D \to A}^{(\text{pm})}$ according to Eq. (9.262). It is advisable to

introduce Fourier-transformed molecular correlation functions $C_{De \to g}$ and $C_{Ag \to e}$ as well as Fourier-transformed retarded photon correlation function $\hat{C}^{(\text{ret})}$:

$$
\begin{aligned}
k_{D \to A}^{(\text{pm})} = \frac{|d_D d_A|^2}{\hbar^4} \int \frac{d\omega d\overline{\omega}}{(2\pi)^2} \; C_{De \to g}(-\omega) \Bigg\{ & \frac{-i}{\omega - \overline{\omega} - i\varepsilon} \\
& \times \left([\boldsymbol{n}_D \hat{C}_{\text{phot}}^{(\text{ret})*}(\boldsymbol{X}_{\text{DA}}, \omega) \boldsymbol{n}_A] + [\boldsymbol{n}_D \hat{C}_{\text{phot}}^{(\text{ret})*}(\boldsymbol{X}_{\text{DA}}, -\overline{\omega}) \boldsymbol{n}_A] \right) \\
& \times \left([\boldsymbol{n}_A \hat{C}_{\text{phot}}^{(\text{ret})}(\boldsymbol{X}_{\text{AD}}, \overline{\omega}) \boldsymbol{n}_D] + [\boldsymbol{n}_A \hat{C}_{\text{phot}}^{(\text{ret})}(\boldsymbol{X}_{\text{AD}}, -\omega) \boldsymbol{n}_D] \right) \\
& + \text{c.c.} \Bigg\} \; C_{Ag \to e}(\overline{\omega}).
\end{aligned}
\tag{9.275}
$$

In contrast to Eqs. (9.115) and (9.132) describing ordinary Förster-type EET, here the retarded photon correlation functions are responsible for mediating the EET (be aware of the two-fold frequency integration). The combination of the part proportional to $\hat{C}^{(\text{ret})*}(\boldsymbol{X}_{\text{DA}}, \omega)$ with that proportional to $\hat{C}^{(\text{ret})}(\boldsymbol{X}_{\text{AD}}, \overline{\omega})$ corresponds to the intuitive photon-mediated transfer process shown as the upper pathway in Figure 9.29. The total rate follows via the inclusion of the lower pathway of Figure 9.29 and a mixture of both.

The expression simplifies considerably if we note that the photon correlation function changes only slightly across the frequency range, where $C_{De \to g}(\omega)$ and $C_{Ag \to e}(\omega)$ deviate from zero. Characterizing this range by a mean frequency ω_0, we obtain ($X_{\text{DA}} = |\boldsymbol{X}_{\text{DA}}|$)

$$
k_{D \to A}^{(\text{pm})} = \frac{2\pi}{\hbar} |d_D d_A|^2 |\mathcal{A}(x_{\text{DA}}, \omega_0)|^2 \mathcal{D}_{\text{DA}}.
\tag{9.276}
$$

The combined DOS $\mathcal{D}_{\text{DA}} \equiv \mathcal{D}_{\text{EET}}$ has been defined in Eq. (9.132), and the newly defined function $\mathcal{A}$ (photon transition amplitude) is determined by the retarded correlation functions. According to Eq. (9.269), the latter can be expressed by $\zeta_{\text{phot}}^{(\text{ret})}$ introduced in Section 9.10.2.2. It follows that

$$
\begin{aligned}
\mathcal{A}(x_{\text{DA}}, \omega_0) &= \frac{1}{\hbar} \left(-[\boldsymbol{n}_D \boldsymbol{n}_A] \nabla^2 + [\boldsymbol{n}_D \nabla][\boldsymbol{n}_A \nabla] \right) \\
& \quad \times \left(\zeta_{\text{phot}}^{(\text{ret})}(X_{\text{DA}}, \omega_0) + \zeta_{\text{phot}}^{(\text{ret})}(X_{\text{DA}}, -\omega_0) \right) \\
&= K_0^3 \left[\frac{\kappa_{\text{DA}}}{(K_0 X_{\text{DA}})^2} - \frac{i \overline{\kappa}_{\text{DA}}}{K_0 X_{\text{DA}}} + \frac{i \kappa_{\text{DA}}}{(K_0 X_{\text{DA}})^3} \right] e^{i K_0 X_{\text{DA}}}.
\end{aligned}
\tag{9.277}
$$

To obtain the second equality, we used Eq. (9.274) and carried out the various derivatives. Also, notice the introduction of $K_0 = \omega_0 / c$, which determines the inverse wavelength of the exchanged photon. The orientation factor κ_{DA} has already been introduced in Eq. (9.31). The other factor reads

$$
\overline{\kappa}_{\text{DA}} = [\boldsymbol{n}_D \boldsymbol{n}_A] - [\boldsymbol{n}_D \boldsymbol{e}_{\text{DA}}][\boldsymbol{n}_A \boldsymbol{e}_{\text{DA}}].
\tag{9.278}
$$

If $K_0 X_{\text{DA}} \ll 1$, that is if the DA distance is much smaller than the photon wavelength, the rate $k_{D \to A}^{(\text{pm})}$, Eq. (9.276), reduces to the Förster-type expression, Eq. (9.123) (it depends on $1/X_{\text{DA}}^6$). In the present context, one may state that Förster-type EET is dominated by a *virtual photon exchange*. In the opposite case, $K_0 X_{\text{DA}} \gg 1$, the rate accounts for real photon emission by the donor and photon absorption by

the acceptor (here, it decreases with the inverse square of the DA distance; see also the discussion below). If one ignores the counterintuitive photon-mediated process (lower pathway in Figure 9.29), the transition amplitude also includes sine and cosine functions. In particular, one cannot reproduce the Förster-type rate for short DA distances. This has to be expected since the energy-time uncertainty works most effectively at short distances, that is at short "photon flight times" (strong contribution by the counterintuitive process). Interestingly, the elaborated combination of the two transition pathways reproduces the simple picture of a Coulomb interaction between the donor and the acceptor.

9.10.2.4 Some Estimates

To estimate the rate of photon-mediated EET, we use Eq. (9.276), together with the expression for the spectral overlap based on fast nuclear motion (cf. Section 9.5.3 and Figure 9.14). The rate, Eq. (9.276), is written as

$$k_{D \to A}^{(pm)} = \frac{2\pi}{\hbar} |d_D d_A|^2 \left(\frac{\kappa_{DA}^2}{X_{DA}^6} + \frac{K_0^2 \kappa_{DA}(\kappa_{DA} - 2\overline{\kappa}_{DA})}{X_{DA}^4} + \frac{K_0^4 \overline{\kappa}_{DA}^2}{X_{DA}^2} \right) \mathcal{D}_{DA}. \quad (9.279)$$

Figure 9.30 shows the rate versus the DA distance X_{DA}. The acceptor molecule has been chosen to be identical to the donor, so we set $\hbar\omega_D = \hbar\omega_A = \hbar\omega_0$ (the transition dipole moments are perpendicular to the line connecting the donor and the acceptor, that is $\kappa_{DA} = \overline{\kappa}_{DA} = 1$). For distances less than 20 nm, the photon-mediated transfer agrees completely with the Förster rate, and any dependence on the choice of $\hbar\omega_0$ vanishes. The extreme smallness of the Förster rate for the largest distance of 500 nm is compensated for, when using the general rate due to photon-mediated transfer. Its distance dependence is dominated by the $1/X_{DA}^2$ term and increases according to the fourth power of ω_0. Such a behavior indicates that the EET appears mainly as a
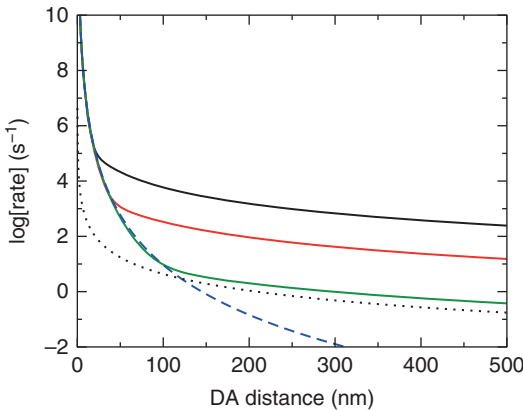
Figure 9.30 Transfer rates of photon-mediated EET versus DA distance and for different DA excitation energies (transition dipole moments are perpendicular to the line connecting the donor and the acceptor and amount to 5D, $\mathcal{D}_{DA}$ according to Eq. (9.140), $\Gamma_{DA} = 40$ meV). Solid lines: rate of photon-mediated EET, $\hbar\omega_0 = \hbar\omega_D = \hbar\omega_A = 10$, 5, *and* 2 eV (from above to below); dashed line: Förster rate; dotted line: photon-mediated transfer for the case $\kappa = 0$ and $\overline{\kappa} = 2/3$ ($\hbar\omega_0 = 2$ eV).

photon emission by the donor and a subsequent photon absorption by the acceptor (this view of a real photon exchange just confirms that the rate becomes proportional to ω_0^4/X_{DA}^2).

The presented theory of photon-mediated EET seems rather appealing. However, the very low transfer rates for intermolecular distances beyond 200 nm, where distinct deviations from the Förster theory are observable in Figure 9.30, preclude its application to standard molecular systems. For the largest molecular excitation energy used (10 eV), however, the transfer time (inverse rate) stays in the millisecond region for such a large DA separation. Of course, the choice of 10 eV is not very realistic for S_0–S_1 transitions in typical organic dyes (but values of about 4.5 eV are of importance for exciton formation and EET in DNA strands). On the other hand, for a DA geometry where the orientation factor κ, Eq. (9.278), equals zero, the Förster rate vanishes, and the photon-mediated transfer rate is determined exclusively by the long-range term $\sim 1/X_{DA}^2$ (case where $[\boldsymbol{n}_D\boldsymbol{n}_A] = 3[\boldsymbol{n}_D\boldsymbol{n}][\boldsymbol{n}_A\boldsymbol{n}]$ and $\boldsymbol{n}_D \parallel \boldsymbol{n}_A$, resulting in $\kappa = 0$ and $\overline{\kappa} = 2/3$). The transfer time stays in the millisecond region for distances less than 10 nm, and thus EET may occur.

9.10.3 Fourth-order Rate of Two-electron-transfer-assisted EET

General rate equations for state populations have been introduced in Section 3.14 with the special feature that the transition rates are of arbitrary order with respect to the interstate couplings. According to Eq. (3.522), the fourth-order rate, which is of interest here, takes the form

$$k_{m\to n}^{(2ET)} = \int\limits_0^\infty dt_3 \, dt_2 \, dt_1 \, \left\{ \left(C_{m\to n}(t_3, t_2, t_1) + \text{c.c.} \right) \right.$$
$$\left. - \sum_k \left(C_{m\to k}(t_1) + \text{c.c.} \right) \left(C_{k\to n}(t_3) + \text{c.c.} \right) \right\}. \quad (9.280)$$

A possible factorization of the three-time correlation function into two single-time correlation functions is compensated by the last term on the right-hand side, which just includes products of two of such single-time correlation functions. The three-time correlation function separates into three parts corresponding to three different so-called Liouville space pathways (LSP, see Section 3.14.6)

$$C_{m\to n}(t_3, t_2, t_1) = C_{m\to n}^{(I)}(t_3, t_2, t_1) + C_{m\to n}^{(II)}(t_3, t_2, t_1) + C_{m\to n}^{(III)}(t_3, t_2, t_1). \quad (9.281)$$

These different LSP contributions have already been given in Eqs. (3.524)–(3.526). The LSP I contribution is responsible for a direct transition across the intermediate states (often called superexchange transfer). Sequential transitions including intermediate state relaxation are covered by the LSP II and III contribution.

To get concrete rate expressions, one has to rely on certain approximations with respect to the type and the dynamics of the vibrational coordinates. The simplest approximation, which will be used in what follows for the rate computation, is based on the replacement of all vibrational coordinates by a thermal environment, which only causes dephasing among different electronic states (be aware of the similarity

to the case of fast nuclear motion introduced in Section 6.2.4 and already used in Section 9.5.3 to characterize Förster-type EET). In such a case, the vibrational Hamiltonians H_m are replaced by electronic energies $\hbar\varepsilon_m$, and the effect of the vibrational coordinates is accounted for by a particular form of dissipation entering the equation of motion of the density operator $\hat{\rho}$ reduced to the electronic DOF. This type of dissipation (Lindblad type) has been already discussed in Chapter 3, Eq. (3.363) and reads here

$$-\mathcal{D}\hat{\rho}(t) = -\frac{1}{2}\sum_m \gamma_m \left([\hat{\Pi}_m, \hat{\rho}(t)]_+ - 2\hat{\Pi}_m\hat{\rho}(t)\hat{\Pi}_m\right). \tag{9.282}$$

The dissipative superoperator $\mathcal{D}$ includes the projection operators $\hat{\Pi}_m = |m\rangle\langle m|$ and introduces dephasing of the off-diagonal elements of the density matrix ρ_{mn} with dephasing rates γ_m but does not affect the diagonal matrix elements. The resulting time evolution of the density matrix reads

$$\begin{aligned}\rho_{mn}(t) &= \langle m|\mathcal{U}(t-t_0)\hat{\rho}(t_0)|n\rangle \\ &= \left(\delta_{mn} + (1-\delta_{mn})e^{-i[\tilde{\varepsilon}_m - \tilde{\varepsilon}_n^*](t-t_0)}\right)\hat{\rho}_{mn}(t_0).\end{aligned} \tag{9.283}$$

The time-evolution superoperator is denoted by $\mathcal{U}$, $\hat{\rho}_{mn}(t_0)$ is the initial value of the density matrix, and we introduced $\tilde{\varepsilon}_m = \varepsilon_m - i\gamma_m/2$.

Since we changed from electron–vibrational dynamics to electron motion only, while including dissipation due to the presence of an environment, we cannot directly use Eqs. (3.524)–(3.526) specifying the different LSP correlation functions. Instead, we need to change to new correlation functions, which include a dissipative time propagation described by the time-evolution superoperator $\mathcal{U}(t)$, introduced in Eq. (9.283). Therefore, we have to go back to Eq. (3.521) in order to derive the "dissipative" variant of the LSP correlation functions. Here, the initial density operator $\hat{W}_{D^*A} = \hat{W}_1$ is specified as $|1\rangle\langle 1|$ (note the absence of a vibrational equilibrium statistical operator). Accordingly, the three-time correlation functions read

$$C_{1\to 4}^{(\mathrm{I})}(t_3, t_2, t_1) = \frac{1}{\hbar^4}\mathrm{tr}_{\mathrm{vib}}\left\{\langle 4|\mathcal{U}(t_3)\left\{\mathcal{U}(t_2)\left(\hat{V}\mathcal{U}(t_1)\left[\hat{V}|1\rangle\langle 1|\right]\right)\hat{V}\right\}\hat{V}|4\rangle\right\}, \tag{9.284}$$

$$C_{1\to 4}^{(\mathrm{II})}(t_3, t_2, t_1) = \frac{1}{\hbar^4}\mathrm{tr}_{\mathrm{vib}}\left\{\langle 4|\mathcal{U}(t_3)\left\{\hat{V}\mathcal{U}(t_2)\left(\mathcal{U}(t_1)\left[\hat{V}|1\rangle\langle 1|\right]\hat{V}\right)\right\}\hat{V}|4\rangle\right\}, \tag{9.285}$$

and

$$C_{1\to 4}^{(\mathrm{III})}(t_3, t_2, t_1) = \frac{1}{\hbar^4}\mathrm{tr}_{\mathrm{vib}}\left\{\langle 4|\hat{V}\mathcal{U}(t_3)\left\{\mathcal{U}(t_2)\left(\mathcal{U}(t_1)\left[\hat{V}|1\rangle\langle 1|\right]\hat{V}\right)\hat{V}\right\}|4\rangle\right\}. \tag{9.286}$$

The time propagation of $\hat{V}|1\rangle\langle 1|$ has to be performed according to Eq. (9.283). When considering the action of $\mathcal{U}(t)$, it must be restricted to the operator expression in the bracket to the right of $\mathcal{U}(t)$. For example, the notation $\mathcal{U}(t_1)\left[\hat{V}|1\rangle\langle 1|\right]\hat{V}$ means that first $\mathcal{U}(t_1)\left[\hat{V}|1\rangle\langle 1|\right]$ has to be calculated and afterward $\hat{V}$ is multiplied from the right. A detailed computation gives the following expression for the correlation

function, which corresponds to LSP I (cf. also Eq. (3.530); the back transfer correlation function simply followed by an interchange of "1" and "4")

$$C_{1\to 4}^{(I)}(t_3, t_2, t_1) = \frac{1}{\hbar^4} V_{42} V_{21} V_{12} V_{24} e^{i[\bar{\varepsilon}_1^* - \bar{\varepsilon}_2]t_1 + i[\bar{\varepsilon}_1^* - \bar{\varepsilon}_4]t_2 + i[\bar{\varepsilon}_2^* - \bar{\varepsilon}_4]t_3}$$

$$+ \frac{1}{\hbar^4} V_{42} V_{21} V_{13} V_{34} e^{i[\bar{\varepsilon}_1^* - \bar{\varepsilon}_2]t_1 + i[\bar{\varepsilon}_1^* - \bar{\varepsilon}_4]t_2 + i[\bar{\varepsilon}_3^* - \bar{\varepsilon}_4]t_3}$$

$$+ \frac{1}{\hbar^4} V_{43} V_{31} V_{12} V_{24} e^{i[\bar{\varepsilon}_1^* - \bar{\varepsilon}_3]t_1 + i[\bar{\varepsilon}_1^* - \bar{\varepsilon}_4]t_2 + i[\bar{\varepsilon}_2^* - \bar{\varepsilon}_4]t_3}$$

$$+ \frac{1}{\hbar^4} V_{43} V_{31} V_{13} V_{34} e^{i[\bar{\varepsilon}_1^* - \bar{\varepsilon}_3]t_1 + i[\bar{\varepsilon}_1^* - \bar{\varepsilon}_4]t_2 + i[\bar{\varepsilon}_3^* - \bar{\varepsilon}_4]t_3}. \tag{9.287}$$

A closer inspection shows that the first term on the right-hand side refers to the EET along pathway "a" of Figure 9.24 (only the charge-transfer state 2 is involved). EET pathway "b" is represented by the last term on the right-hand side. The second and the third terms involve an interference of EET reaction paths "a" and "b." According to the general structure of the LSP I correlation function, the two mentioned contributions are analogous to the superexchange mechanism in ET theory. The intermediate charge-transfer state 2 or 3 is only populated virtually. The 2ET necessary here to achieve the EET appears as a uniform process. In the same way, one may compute the LSP II and III correlation functions. They are partly compensated by the product of two single-time correlation functions, which according to the present model take the simple form $C_{m\to n}(t) = |V_{mn}/\hbar|^2 \exp(-i[\varepsilon_m - \varepsilon_n^*]t)$.

The final fourth-order rate expression follows after carrying out the triple time integral in Eq. (9.280). We separate the rate into one part corresponding to the LSP I and a second part with contributions from the LSP II and III. The first part is denoted by $k_{1\to 4}^{(sx)}$. The second contribution to the total rate follows from those parts of the LSP II and III correlation functions, which have not been compensated for by the product of second-order correlation functions. In the present description the separate rate contributions of the pathways "a" and "b" to $C_{1\to 4}^{(II)}$ as well as $C_{1\to 4}^{(II)}$ are completely compensated for. Only the EET "a"–"b" interference terms contribute. The related rate is denoted as $k_{1\to 4}^{(if)}$ and enters the total rate according to

$$k_{1\to 4}^{(2ET)} = k_{1\to 4}^{(sx)} + k_{1\to 4}^{(if)}. \tag{9.288}$$

We introduce transition frequencies $\varepsilon_{mn} = \varepsilon_m - \varepsilon_n$ and the level broadening $\gamma_{mn} = (\gamma_m + \gamma_n)/2$ and obtain the superexchange part as

$$k_{1\to 4}^{(sx)} = \frac{2}{\hbar^4} \text{Im} \left\{ \frac{1}{\varepsilon_{14} + i\gamma_{14}} \left[\frac{|V_{12} V_{24}|^2}{[\varepsilon_{12} + i\gamma_{12}][\varepsilon_{24} + i\gamma_{24}]} \right. \right.$$

$$+ \frac{V_{42} V_{21} V_{13} V_{34}}{[\varepsilon_{12} + i\gamma_{12}][\varepsilon_{34} + i\gamma_{34}]} + \frac{V_{43} V_{31} V_{12} V_{24}}{[\varepsilon_{13} + i\gamma_{13}][\varepsilon_{24} + i\gamma_{24}]}$$

$$\left. \left. + \frac{|V_{13} V_{34}|^2}{[\varepsilon_{13} + i\gamma_{13}][\varepsilon_{34} + i\gamma_{34}]} \right] \right\}. \tag{9.289}$$

The first term on the right-hand side corresponds to an EET process that is exclusively based on the reaction pathway "a." Pathway "b" contributes to the fourth term on the right-hand side, and an interference of both is contained in the second and the third terms. If the initial- and final state energies are nearly identical, but those of the

charge-transfer states are well separated ($|\varepsilon_{14}| \ll |\varepsilon_{12}|, |\varepsilon_{13}|$), the rate, Eq. (9.289), is reduced to (note also $\varepsilon_{21} \approx \varepsilon_{24}$ and $\varepsilon_{31} \approx \varepsilon_{34}$)

$$k_{1 \to 4}^{(\text{sx})} = \frac{1}{\hbar^4} \left| \frac{V_{12} V_{24}}{\varepsilon_{21}} + \frac{V_{13} V_{34}}{\varepsilon_{31}} \right|^2 \frac{2 \gamma_{14}}{\varepsilon_{14}^2 + \gamma_{14}^2}. \tag{9.290}$$

The EET is mediated by an effective coupling known from ET theory (see Chapter 7, Eq. (7.113)). Here, however, it covers contributions from two EET pathways. The rate, which includes the EET pathway interference contributions stemming from $C^{(\text{II})}$ and $C^{(\text{III})}$, takes the form

$$\begin{aligned}
k_{1 \to 4}^{(\text{if})} = \frac{2}{\hbar^4} \text{Im} \Bigg\{ & \frac{V_{42} V_{21} V_{13} V_{34}}{[\varepsilon_{12} + i\gamma_{12}][\varepsilon_{32} + i\gamma_{32}][\varepsilon_{34} + i\gamma_{34}]} \\
& + \frac{V_{43} V_{31} V_{12} V_{24}}{[\varepsilon_{13} + i\gamma_{13}][\varepsilon_{23} + i\gamma_{23}][\varepsilon_{24} + i\gamma_{24}]} \\
& + \frac{V_{42} V_{21} V_{13} V_{34}}{[\varepsilon_{12} + i\gamma_{12}][\varepsilon_{32} + i\gamma_{32}][\varepsilon_{42} + i\gamma_{42}]} \\
& + \frac{V_{43} V_{31} V_{12} V_{24}}{[\varepsilon_{13} + i\gamma_{13}][\varepsilon_{23} + i\gamma_{23}][\varepsilon_{43} + i\gamma_{43}]} \Bigg\}.
\end{aligned} \tag{9.291}$$

The first and the second terms on the right-hand side follow from $C^{(\text{II})}$, while the third and the fourth terms are due to $C^{(\text{III})}$. The corresponding second-order rates are

$$k_{m \to n} = \frac{1}{\hbar^2} |V_{mn}|^2 \frac{2 \gamma_{mn}}{\varepsilon_{mn}^2 + \gamma_{mn}^2}. \tag{9.292}$$

Figure 9.31 illustrates the derived rate expressions for a model where the donor is identical to the acceptor (homodimer, $\varepsilon_1 = \varepsilon_4$, note also $\varepsilon_2 = \varepsilon_3$) and where all
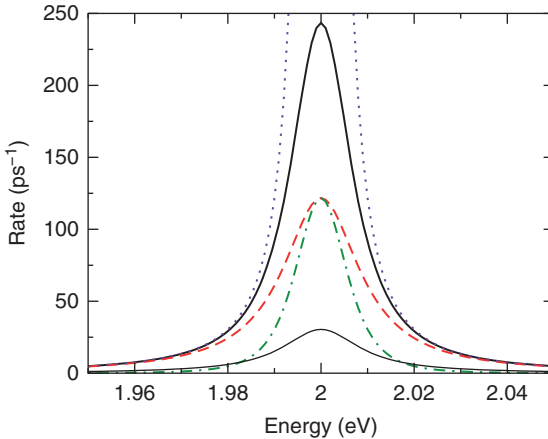
Figure 9.31 2ET-assisted EET in a DA complex (identical molecules; use of the electronic state dephasing model; all charge-transfer couplings as well as dephasing rates are 10 meV). Shown are different rates versus the energy of the charge-transfer states ($\hbar\varepsilon_2 = \hbar\varepsilon_3$, $\hbar\varepsilon_1 = \hbar\varepsilon_4 = 2$ eV). Full line: $k_{1 \to 4}^{(\text{tot})}$, dashed line: rate $k_{1 \to 4}^{(\text{sx})}$, dotted line: $k_{1 \to 4}^{(\text{sx})}$ in the approximate form of Eq. (9.290), dashed-dotted line: $k_{1 \to 4}^{(\text{if})}$, and thin full line: all types of second-order rates $k_{m \to n}$.

transfer couplings and dephasing rates coincide. While the approximate rate for $k_{1\to4}^{(sx)}$, Eq. (9.290), diverges at $\varepsilon_1 = \varepsilon_2$, all other rates stay finite. Near resonance, the total fourth-order rate is formed roughly in equal parts by $k_{1\to4}^{(sx)}$ and $k_{1\to4}^{(if)}$. Second-order rates are somewhat smaller. However, the large values of the rate indicate that in this energy range, the assumption of nonadiabatic transfer would no longer be valid.

Changing to a charge-transfer state energy that is up to $1\,\mathrm{eV}$ higher than $\hbar\varepsilon_1$, the rate $k_{1\to4}^{(if)}$ is of minor importance, and the approximate form of $k_{1\to4}^{(sx)}$ coincides with the exact one as well as the total fourth-order rate. In this energy range where $\varepsilon_2 \gg \varepsilon_1$, EET becomes single exponential with the overall forward rate $K_{EET}^{(fw)}$ introduced in Eq. (9.238), and $K_{EET}^{(fw)}$ is dominated by the fourth-order rate. Therefore, 2ET-assisted EET proceeds in this parameter range as a concerted transition. To compare quantitatively ordinary EET with this 2ET-assisted version (note Eq. (9.233) for the total rate), we recall the variant of the Förster-type rate, Eq. (9.115), fixed by the combined DOS, Eq. (9.140). This results in a rate expression similar to that given in Eq. (9.292). However, the transfer coupling has to be replaced by the excitonic coupling J_{mn}. If we assume identical dephasing rates, the comparison can be reduced to one of the coupling matrix elements. Since Figure 9.8 shows values in the $100\,\mathrm{meV}$ range at the closest intermolecular distance, the assumption of a larger transfer coupling than the $10\,\mathrm{meV}$ used in Figure 9.31 indicates that 2ET-assisted EET may become comparable to Förster-type EET.

Finally, we recall the fact that the used model of interelectronic state dephasing overestimates the rates (which also do not satisfy the detailed balance condition). More realistic calculations are, however, outside the scope of the present discussion. Nevertheless, the given description of 2ET-assisted EET offers a broader view on possible transfer mechanisms and illustrates the application of fourth-order rate theory.

References

1 D. M. Eisele et al., Nat. Nanotechnol. **4**, 658 (2009).

2 J. Dostál et al., Nat. Chem. **8**, 705 (2016).

3 E. Thyrhaug et al., J. Phys. Chem. Lett. **7**, 1653 (2016).

4 A. M. Dennis and G. Bao, Nano Lett. **8**, 1439 (2008).

5 M. E. Madjet et al., J. Phys. Chem. B **110**, 17268 (2006).

6 B. Fückel et al., J. Chem. Phys. **128**, 074505 (2008).

7 S. Mukamel, *Principles of Nonlinear Optical Spectroscopy*, (Oxford University Press, 1995).

8 R. Métivier et al., Phys. Rev. Lett. **98**, 047802 (2007).

9 R. van Grondelle, Biochem. Biophys. Acta **811**, 147 (1985).

10 A. Ishizaki and G. R. Fleming, J. Chem. Phys. **130**, 234111 (2009).

11 Th. Renger and R. A. Marcus, J. Chem. Phys. **107**, 107 (2003).

12 J. Schulze et al., J. Chem. Phys. **144**, 185101 (2016).

13 J. Moll et al., J. Chem. Phys. **102**, 6362 (1995).

14 M. L. Chaillet et al., J. Phys. Chem. Lett. **11**, 10306 (2020).

15 M. Schröter, S. D. Ivanov, J. Schulze, S. P. Polyutov, Y. Yan, T. Pullerits, and O. Kühn, Phys. Rep. **567**, 1 (2015).

16 M. Polkehn et al., J. Phys. B **51**, 014003 (2018).

17 S. Wolter et al., J. Phys. B **50**, 18405 (2017).

Further Reading

- Exciton theory:

  V. A. Agranovich, *Excitations in Organic Solids*, (Oxford University Press, Oxford, 2009).

  L. Valkunas, D. Abramavicius, and T. Mančal, *Molecular Excitation Dynamics and Relaxation*, (Wiley-VCH, Weinheim, 2013).

- Computational Chemistry in exciton theory:

  C. Curutchet and B. Mennucci, Chem. Rev. **117**, 294 (2017).

- Exciton–vibrational dynamics

  N. J. Hestand and F. C. Spano, Chem. Rev. **118**, 7069 (2018).

  M. Schröter, S.D. Ivanov, J. Schulze, S.P. Polyutov, Y. Yan, T. Pullerits, and O. Kühn, Phys. Rep. **567**, 1 (2015).

- Förster theory and its extensions:

  M. Şener, J. Strümpfer, J. Hsin, D. Chandler, S. Scheuring, C. N. Hunter, and K. Schulten, ChemPhysChem **12**, 518 (2011).

- Excitons in photosynthesis and organic materials:

  R. E. Blankenship, *Molecular Mechanisms of Photosynthesis*, (Wiley, Hoboken, NJ, 2021).

  J.-L. Brédas, E. H. Sargent, and G. D. Scholes, Nat. Mater. **16**, 35 (2016).

- Ultrafast spectroscopy of excitonic systems:

  D. Abramavicius, B. Palmieri, D. V. Voronine, F. Sanda, and S. Mukamel, Chem. Rev. **109**, 2350 (2009).

515

Index

WILEY END USER LICENSE AGREEMENT

Go to www.wiley.com/go/eula to access Wiley's ebook EULA.